INTERNATIONAL JOURNAL OF MODERN ENGINEERING RESEARCH (IJMER)

ISSN : 2249-6645

Volume 3 - Issue 2

Web : www.ijmer.com
Email : ijmer.editor@gmail.com

International Journal of Modern Engineering Research (IJMER)

Editorial Board

International Journal of Modern Engineering Research (IJMER)
www.ijmer.com Vol.3, Issue.2, Mar-Apr. 2013 pp-604-610 ISSN: 2249-6645

The Strategy of Energyas A Good Opportunity for Protection of the Environment in the Republic Of Kosovo

Vehebi Sofiu, [1] Amantina Pervizaj, [2] Bekim Selimi, [3] Edmond Erxhepi[4]
1, International Postgraduate School" Jozef Stefan", Ljubljana, Slovenia
2, 3, 4, South East European University "UEJL", Tetovo-Macedonia

Abstract: *The power supply system in Kosovo is mainly thermal and is one of the only potential opportunities to become possible exploitation of this natural resource including the fossil burnings as the biggest pollutant of the environment with CO_2. Also, the strategic position that Kosovo possesses makes possible the completion of fossil energy with pure renewable energy, enabling energizing opportunities of energy suppliers and consumers, district heating pipelines, heating of storage facilities and electricity transmission lines both in cities and region. Production and distribution of energy has taken an increasingly significant rolein the energy market and has become a regional indispensability. In this strategy is presented a model for structural and operational optimization of development which is presented as a model of efficiency for the production and consumption of the electricity, heating, transport of fuels in production plants, water transport in district heating pipelines and accumulation of heating. The problem is formulated as comprehensive unfulfilled problem in terms of not achieving the objectives in the short-term and medium-term strategic plan that in front of itself presented the Republic of Kosovo. The strategic solution provides structural development, ie.which are predicted for them to have their units of production, heating transportation linesand warehouses for storage of coals which should be built upon a construction of a new power plant, as well as their spaces to be together with the designing parameters for plants and district heating pipelines of the Pristina city. Such a model enables an integration of all suppliers, consumers of all categories and coordination with relevant authorities in order to form a common view of different situations as a basis for decision-making based on a regional energy policies drafted according to projects with the guidelines of treaties to the communities of energy signed as a member.*

Keywords: *Energy strategy, protection of environment, energy systems, optimization;*

I. Introduction

Review of Energy Strategyis based on theprogrammeandthe decisions of the Government of Kosovo, thedocument of the medium-term sectorial policies, as well as a number of relevant studies and analyzes. Particular attention is paid to the compatibilityof this strategywith the *acquis*of the European Union, these mandatory *acquis*for Kosovowithin the membershipof the Energy Community Treaty.The Kosovo Energy Strategyalso aimsthe effective managementof the existing energy resourcesand environment protection. It focuses on increasing the security of supplyaccording to European standards and the diversification of energy sources. This strategy aims to stimulate the rational use of energyand increase the efficiency of its use, the use of renewable energy sources, the introduction of new technologiesthat do not irreparably damage the environment while respecting the applicationof internationally accepted environmental standards.This strategy involves a 10-year period, representing a clear documentthat is developedbased on relevant documents and studies. Measures for the implementationof the revised strategy include the medium-term up to 2015, and the long-term until 2025. Goals and measures set out in this documentconstitute a clear visionfor some key aspectsof high interestfor the developmentof the energy sectorduring the decade 2009-2025 [1].

Plicies, legal framework and institutions of the energy sector

Develpment of policies, organization, regulation and managementof the energy sectorin the Republic of Kosovo are conducted through a set of lawsthat are generallyin lines with the directives of the European Union (BE) for energy, while sector institutions including government, regulatoryand energy enterprisesfor all possibilities of exploitationof natural energy resourcesinclude and those subsidized ones.

II. Legal framework

Laws, regulationsand below highlighted decisionsof the Governmentconstitute the legal basisfor the organization and managementof the Kosovo Energy Sector:
Law on Energy No. 2004/8;
Law on Energy Regulator No. 2004/9;
Law on Electricity No. 2004/10;
Law on Spational Planning No. 2003/4;
Regulation on Mines and Minerals No. 2005/3;
Regulation for the Independent Commissionof Mines and Minerals No. 2005/2, respectivelyLaw on Amnedment of the Regulationon the Establishment of the ICMM;
Law on Environmental Protection No. 2003/9;
Law on Trade of Petroleumand its Derivatives No. 2004/5;
Law on Scientific Research Activities No. 2004/42;

Regulation for the Long-term Allocation of the Real Estate of Social-owned Property, managed by municipalities in Kosovo No. 2005/13;
Law on Foreign Investment No. 02/2005;
Government's Decision to restructure KECJ.S.C., No. 06/2005;
Government's Decisionfor unbundling of KECJ.S.C., No. 04/36, 2008;
Government's Decisionon the Establishment of the Companyfor Distribution and Supply of Electricity No. 03/38, 2008; and its privatization through private tender No. 03/38, 2008 and No. 08/39;
Law on Public Enterprises No. 03/2008;
Government's Decisionon ownership policyof the CentralPENo. 11/39 and No. 13/39;
Law on competition No. 36/2004; and
Government's Decisionon the possibilityof energy project developmentof the Hydro Power Plant Zhur, No. 02/40 2008 [2].

KOSOVO ENERGY CORPORATION is the Kosovo public companywhichis included into its ownershipand operates with the assets of generation,supply and distributionof electricity in the phase of privatization and lignite mining. From 1999 until late 2006,is managed by international staff while from January in 2007 was followed by technical assistance, also from a foreign company. However, such technical assistance, along with local management, by the end of 2008 failed to make KECfinancially viabledue to the low rate of collectionand large losses, since 2009the Kosovo Energy Corporationis governed by local managementand this made possible to be a financially stable company making progress for every yearin all fields (production, collection rate, losses)from production to energy distribution[2].

TRANSMISSION SYSTEM OPERATOR(KOSTT J.S.C.)was founded in 2006, in accordance with theunblunding provisionsof the Law on Energyand conditions of theEnergy Community Tr**e**aty. KOSTT j.s.c.is a public owned company, responsible for the operation, planning, maintenanceand developmentof the transmission networkand its interconnectionswith neighbouring power systems, in order to maintain securityof supply in Kosovo. In addition, KOSTT j.s.c. is responsible for the functioning and operationof the wholesale electricity marketin Kosovo. The main source of incomes for KOSTT j.s.c. comes in the form of transfer paymentpaid by KECj.s.c. as defined by ERO.In the strategic planthe system operator isin the modernization of contemporary technologies of power lines and facilities[2].

III. Production of lignite and electricity

Electricity sector in Kosovois dominated bythermal productionof KECj.s.c., a vertically integrated system, with the exception of the transmission systemthat is not a part of KECj.s.c. KECj.s.c. is consisted of two lignite minesin Bardh and Mirash, two thermal power plantswith lignite burning Kosovo A and B, with the overall effective capacity of 740-1000 MW (with an installed capacity of 1878 MW), from the distribution network, and from supplywhich is in the stage of privatizationin May 2013[3].

IV. Production of lignite

In the long runlignite will remain the main fuelfor production of electricity in Kosovo. The reserves of lignite in Kosovoare found in two major basins, labeled as "Kosova" and "Dukagjini". Geological lignite reserves are estimated to be about 14 billion tons (this includes all categories of reserves)[4].

V. Generation of electricity

The assets of generation in tabele 1, distribution and lignite miningare operated byenergy sector of the public company of KECj.s.c. KECj.s.c. suffers from major financial, technical, personnel (number of employees)and managerial problems. Most of the generating capacity of KECj.s.c. is in two thermal power plants of – Kosovo A and Kosovo B. Technically installed capacity of two thermal power plants, despite their long-standing approximately 24-46 years, would be able to meet consumption demands for basic electricity, but, due to the degradationand lack of investmentin the lignite sector and the thermal power plants in Kosovoduring 1990-1999 period, then, deficient maintenance, and no indispensable and timely rehabilitation, technical readiness andperformance of generating units, despite the continuously identified growthup to 2008 are below the level of installed parameters. Table 5summarizes the data for thermo-electro-existing generating capacities in Kosovo.Kosovooperates only about 43MW of installed capacityin hydro power plants, though it possesses more hydro potentials[5].

Tabele 1: Energy generation's in Kosovo

Block of the thermal power plant	Capacity of block of the thermal power plant MWh			Type of fuel	Starting year of the work (long-standing)
	installed	Threshold	Net available		
TC KOSOVO A					
Block A1	65	58	0	LIGNIT/FIRED OIL	1962
Block A2	125	113	0	LIGNIT/FIRED OIL	1964(44)
Block A3	200	182	110-120	LIGNIT/FIRED OIL	1970(38)
Block A4	200	182	110-120	LIGNIT/FIRED OIL	1971(38)
Block A5	200	187	125-130	LIGNIT/FIRED OIL	1975(33)
TC KOSOVO B					
Block B1	339	309	240-260	Lignit-Mazut	1983(25)
Block B2	339	309	200-280	Lignit-Mazut	1984(24)

VI. Transmission of electricity

The transmission system is managed bythe Transmission System and Market Operator (KOSTT j.s.c.). Kosovo is a contracting party to regional Energy Communityand is connected to the regional system through interconnections with Serbia, Macedonia, Montenegroand Albania.The overall length of transmission lines (400 kV, 220 kV and 110 kV) is 1,187 km. Most of the transmission lines are put back in operation, after the overwar repairs, while some of the substationsare still in bad technical situation. Transmission network of 400 kV and 220 kV of Kosovois an integral part of regional interconnection sistem figure 1[6].

Figure 1: Managed sistem in Kosovo

VII. Protection of the environment

Protection of the environmentis in the legal mandateof the Ministry of Environment and Spatial Planning(MESP). However,this strategy should be dealtwith the environmentfrom the energy sector standpoint. Emission of current gases, dust anddischarge of contaminated watersfrom existing thermal power plants, due to outdated technologiesand improper operation of equipment and plants are above the levels permitted by relevant Directives of the European Union (EU).

The Final Reportof the Strategic Environmental and Social Assesment (SESA) was completed in November 2008, after consultation with experts and the public. This report, in the strategic level, involves issues and environmental and social impacts associated with the existing situation and development of energy sector and lignite in the wider region of planned New Mine. The report of SESA explores and examinesthe results of strategic solutionsthat the Government of Kosovo and investorsin the futureshould undertake in the context of improving the situationand developmentof the project of New Kosovo. The most significant development optionsfrom environmental and social perspectivesare analyzedand related to construction location of the TPP of New Kosovo, scheme and dynamics of mine development, the size of TPP's blocks, selection of technology, and the development pace of the projectin relation tothe demand of output power level and the remaining operational lifeof existing thermal power plants, especially of TPP of Kosovo A.

VIII. Project of 'New Kosovo

In order to have a sustainable development of the energy sector, the Kosovo government is planning the involvementof expertise and private capital from abroad. The World Bank is supporting Kosovo in its effortsto attract investmentfor the development of the project of "New Kosovo", throughTechnical Assistance Project of Lignite Energy

(TAPLE). This effort is also supported by the EUthrough the Funding of Study Options, as well as other technical studies that are in the function of TAPLE. The project of "New Kosovo" anticipatesthe construction of a newthermal power plant in two phases. The first phase includes the capacity of 1000 MW and the second phase, later, with the same capacity of 1000 MW. For these units will be developedthe relevant mining of lignite and development of installed capacity up to 2000 MW.The main objectives of TAPLE are: (a) the Government's supportin strengthening the policy, legal and regulatory frameworkthat enable new investments in the energy sector; and (b) the Government's supportto attract qualified private investorsfor the construction of the new thermal power plant with lignite, based on high principles of environmental and social sustainability[3].

IX. Regional and European integrations

Kosovo is strongly committedto European integrations. The energy sector of integration process takes place on two fronts: (I) participation in the Energy Community, and (II) integration process in Europein the framework of theTracking Mechanismfor the Stabilization and Association.

X. Energy Community Treaty

Kosovo is a signitoryto the Treatyof Energy Community Establishment (ECT) of Southeastern Europe, which entered into force in June 2006. In this context, the Government of Kosovo is substantially committedto develop the energy sectorin accordance with the requirements of the ECT. This Treaty obligesan implementation of 'Acquis Communnitaire' of theEUby each Contractory Partyaccording to a timetablefor the implementation of the required reforms.

European Integration Process for Kosovo

The Tracking Mechanism of Stabilization and Association (TMSA) is designed to provide Kosovo the expertise andthe political leadershipof the European Commission, in order to assist the Kosovo authoritiesto take advantages of various instruments of the Stabilization and Association process.

Table 2: Two scenariosof the GDP's rate of growth [%] for the period 2009-2018

Scenario	2009-2010	2011-2014	2015-2018
Medium	3.20	3.10	3.00
High	6.20	5.29	5.00

Regular meetings are heldto assess the progress made in Kosovoin terms of political, economic and institutional reformsin accordance withconditioned Stabilization and Association Processof the EU. The European Commission regularly monitors progress in the Stabilization and Association Process in Kosovo by STM.European Partnership and its Plan of Action (EPPA) presents a framework for monitoring progressthat Kosovo is making a year-on-yearin terms of the European Community. The Institutions of Kosovo are strongly committedto the implementation ofEPPA which on one hand providesall steps for reformand on the other handdirects the assistance of the European Community to Kosovo.

XI. Anticipation of energy demand

In the context of plans for economic developmentof the countryand anticipation of energy demandsas more realistic are supposed two scenarios of rate of growth of the Gross Domestic Products (GDP) for the period 2009-2018 as shown in Table 2.

Anticipation of electricity production in Kosovofor the period 2009-2018

During the entire period 1999-2008, the annual output of electricityfrom local sourceswas below the level of demand. The current levelof the local annual production of electricityis about 4300 – 4600 GWh.Electricity production forecastfor 2009-2018 period is based on the production of electricity from thermal power plants of Kosovo B, Kosovo A, hydro power plant of Ujman, the existing and the new distributive hydro power plants, HPP of Zhur and from productionof the "New Kosovo" thermal power plant. Coverage of demand for electricityis expected to achieve the following:

Production of electricityin thermal power plant of Kosovo A with operating Blocks A3, A4 and A5. The implementation of the European Directivefor Large Plants burnings, the units of the HPP of Kosova A will be de-commissionedby the end of 2015.

Production of electricity in thermal power plant of Kosovo B with operating blocks of B1 and B2. In 2016 and 2017 are expected to be carried out and realizedthe revitalzation projects to meet environmental demandsrequired by the European Directivefor Large Plants burnings. Then, these blocks will be able to continue commercial operating even 15 years after the revitalization, respectively by 2030.

Electricity productionin Hydro power plant of Ujman, which with maintenance and revitalizationwill be into commercial operationin the long run period.

Electricity production from distributive hydro power plants.

Electricity generationfrom hydro power plantin Zhur, which is expected to be builtby 2015 and put into commercial operation by 2016.

Electricity productionin the new blocksof the TPP of New Kosovo is expected that the first generating block to be put into commercial operationby 2016.

In the period 2010-2018 will be built and put into operationmore than 16 small hydro power plantswith total installed capacitygreater than 60 MW. Meanwhile,will be rehabilitatedand put into use and the small existing hydro power plants.

For a certain period in futureuntil the activation of the TPP of New Kosovo, coverage of the electricity balance will be achieved through import.

Based on the above receptions, for the period 2009-2018,the production of electricityfrom local generation plants is expected to be as shown inthe following Table 3[4]

Tabele 3: Prediction of electricity production [GWh]

	2009	2010	2011	2012	2013	2014	2015	2016	2017	2018
TPP of Kosovo A	1300	1300	1300	1450	1450	950	500	0	0	0
TPP of Kosovo B	3300	3300	3300	3300	3300	3300	3300	2500	2500	3400
TPP ofNew Kosovo	0	0	0	0	0	0	1750	5500	7500	7500
HPP of Ujman	79	79	79	79	79	79	79	79	79	79
HPP of Zhur	0	0	0	0	0	0	398	398	398	398
DistributiveHPP	42	100	125	150	175	200	210	225	240	250
Total	4721	4779	4804	4979	5004	4529	6237	8702	10717	11627

Electricity supply of Kosovo for the period 2009 – 2018

Supply of electricity in the period 2009 – 2018 will be conducted throughdomestic production and importswhich will be needed by the end of 2015. In 2016 is expected to put in operationthe first blockin the thermal power plant of New kosovoand definitely there will be no need for imports. Amount of electricity importdepends on the control of its consumption, mostlyfrom the elimination of commercial losses. Demands according to above described scenariosand the estimated production of electricityfor the period 2009–2018 are summarized in Tabele 4[5].

Tabele 4: Supply of electricity in the period 2009 – 2018

	2009	2010	2011	2012	2013	2014	2015	2016	2017	2018
Demand [GWh]										
SMK	4994	5226	5418	5621	5834	6059	6295	6500	6715	6939
SLK	5299	5514	5713	5929	6164	6422	6662	6898	7153	7431
Production	4721	4779	4804	4979	5004	4529	6237	8702	10717	11627
Balance [GWh]										
For SMK	-273	-447	-614	-642	-830	-1530	-58	2202	4902	4688
For SLK	-578	-735	-909	-950	-1160	-1893	-425	1804	4464	4196

Supply of thermal power plantswith lignitefor the period 2009-2018

Demands for ligniteto supply the existing thermal power plantsand the TPP of New Kosovo (for the fist phase up to 1000 MW) are shown in Table 5.

In these demands of coalare not includedthe market demandsfor the crude and dried coal[5].

Tabele 5: Demands for coal in tonnes

Year	TPP A	TPP B	TPPNew Kosovo	Market	Total
2009	2405	4785	0	50	7240
2010	2405	4785	0	70	7260
2011	2405	4785	0	100	7290
2012	2683	4785	0	110	7578
2013	2683	4785	0	120	7588
2014	1758	4785	0	130	6673
2015	925	4785	1925	150	7785
2016	0	3625	6050	160	9835
2017	0	3625	8250	170	12046
2018	0	4585	8250	180	13015

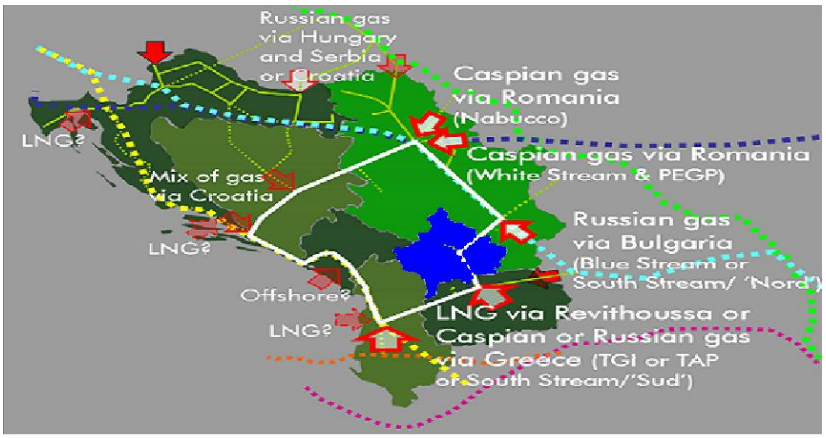

Figure 2: Ring of natural mas to Western Balkans

XII. Energy efficiency to be applied

Under the provisions of the Energy Community Treaty, Kosovo is committedto increase the share of energy obtained from renewable sourcesin its generation portfolio. The government has set a target for Kosovo, which is an achievement of energy proportionfrom renewable sources from 7% till 2016. Energy efficiency is an important additional toolfor achievement of this goal. Also, with this will reducethe release of gases of greenhouse effect, consumers will reduce their energy bills, as well as demand in general, at least in relative terms. It is clear thatincrease in the energy sharefrom renewable sourcesis important for Kosovoin terms of diversification of energy sourcesand almost complete dependencefrom generating capacitieswith lignite burnings.

Fulfillment of anticipationsfor the production of energyfromRESrepresents a long-term objectivethat relates to compliancewith theobligations ofECT. Increased EE and use ofRESwill contribute to the realizationof three of the country's energy policy goals: support for overall economic growth, increased security of energy supplyand environmental protection[7].

XIII. Measures to be taken

In order to implement the aforementioned policies and measures, the Government will:

In 2009, preparethe National Action Planfor Energy Efficiency, as defined by the 'Task Force' on Energy Efficiency of ECT;

Transpose the EU Directivefor Energy Servicesin the law and local regulationsduring the period 2009-2010;

Meet the existing legal and regulatory frameworksfor energy efficiencyand renewable sourcesin compliance with the requirements of theECT, including the Law on Energy Efficiencywhich will establish the Agency for Energy Efficiencyand Energy Efficiency Fundand Renewable Sources;

Define and adopta strategy for heating sector, based on the studyof heating market in Kosovo (2007), including the option of connectingthe central heating systemof Pristinawith the thermal power plant of Kosovo B;

Review existing policiesand adopt incentivesthat will support the developmentof renewable sources sector;

Cede with concessionthe construction of the hydro power plant of Zhur, after being subjected toacceptable feasibility studies, environmental and social security measuresand go through the public consultation process;

Identify and evaluate, during 2009 and 2010, other small existing hydro-potentials in Kosovo;

By the end of 2011, cede under concessionbuilding of all small identified hydro power plants to private investorsand that will be identified during 2009-2010 through a transparent and competitive tendering process;

Zhvillojë dhe fuqizojë, deri në fund të vitit 2009, masat stimuluese fiskale për promovimin e efiçiencës së energjisë dhe teknologjive të energjisë së ripërtërishme;

By the end of 2010, develop a comprehensive programmefor the promotion of private investmentsin energy efficiency projectsand renewable energy; and

Ratify the Convention Framework of the UN on Climate Changeand the Kyoto Protocol as soon as possible[8].

European Integrations and International Cooperation

European integrations, as a top priorityof the Government of Kosovoin the energy sector, will continue to be implemented through:

Tracking Mechanism Processfor Stabilization and Associationwith EU (STM),

Participation in the Energy Community Treaty (ECT), and

Development of Bilateral Cooperation.

MEM will continue to coordinateworkfor well-being of activitiesof the energy sectorwithin the implementationof the Tracking Mechanisms Process for Stabilization and Association with the EU. Annual reports of the European Community for Kosovo pay special attention to the energy sector. They identify progress and challenges for the future. These challenges

will be constantly in the focus of institutional work of the energy sector. MEM will continue to take appropriate measuresso for each challengeto prepare a concreteplan of measures and undertake proper activitiesto overcome it[9].

Development of local institutional capacities

Capacity development of policy-making, regulatory and managerialrepresents an another significant challenge for Kosovothat relates and directly affectsthe implementation of this Revised Energy Strategy. The Government each year will allocate funds from its budget for the development of human capacities, as well as will encourage and supportthe energy and mining regulatory entities to act in the same way. But the only support of budget will not be sufficient, so it's required and expectedthat in the framework of cooperationwith international donorsto provide supportfor human capacity devlopmentin the field of policy-making, economic regulation of energy sectorand management of energy companies. This assistance has not missed until now, but it should be increasedbecause the challenges facing the energy sector currently are larger.

Development of research capacitiesand application of new technologiesis another fieldwhere attention and support are required. The Government is committed in this respectand will support scientific research institutionsand universitiesin the best focus of their workin the development of research capacities, introduction of new technologiesand their application in Kosovo[10].

Measures for the implementaion of the Energy Strategy

Implementaion programme of Energy Strategy (IPES) for the period 2009-2018will include:

Those measures and projects (revised as needed) that have not been financed and implementedduring the period 2006-2012 and are considered as priorityand required by this revised energy strategy;

Measures and new projectsthat have been identified and includedin this revised energy strategyfor the short-term and the medium-term;

Concrete proposalsrelated to manner of fundingfor each measure, programme, or project involved in it (including funding under the MTEF during 2009-2012, or by concrete donors); and

A measure forinstitutionalizationof local inter-institutional cooperationfor the implementation of the IPES during 2009-2012. IPES during 2009-2012will consider in particularand the projects presentedin the Donors Conference for Kosovo, held in Brusselson 11 July 2008. IPESin advance will consult with MEF and the main donorsin order to achieve its better funding for the three years 2009-2012. Coordinate the preparation of IPES during 2009-2012will be made by MEM during the periodfrom February to March 2012. IPES during 2010-2012is presented for approvalby the Government of Kosovo and completed as a wholeand was adopted by theAssembly of Kosovo[11].

XIV. CONCLUSION

Based on the priority listrelated to electricity production opportunities, and, in conformity with the European directives on renewable energy, Kosovo includes 20% of it regarding to climatic and geographic conditions. Today, for this reason, Kosovo has its natural coal resource which makes up over 97 % of electricity productionwith the outdated and amortized equipments that, in general, are the biggest polluters with CO_2in Kosovo. In general,in order to reduce the emmissionsaccording to EU standard, in the thermal power plants of Kosovo are installed filters and protective equipmentfor the purpose of CO_2reduction which probably is one of the shortcomings that the the Kosovo thermal power plants are being faced with. These evasions can be achieved putting into operation and the other resources of the renewable energy being efficient with exploitation of natural resources. From these possibilities can be clearly seen that the number of advantages with benefits significantly exceed the number of deficiencies in relation to the requirements of developing technologies protecting the living environment from climate changeon the occasion of the global warmingand measures taken by the effects of greenhouse gases, putting in use the management and monitoringof the types of efficient energy.In general, the legal and regulatory infrastructure for renewable energy sourcesin the Republic of Kosovois unified as that of the Uuropean Union, according to relevant directives of the Law on Energy Efficiencythat has been put in use by the European Union for RESand their further institutional development until 2020according to the parity 20+20+20, and at the same time this is the strategic goal of the Republic of Kosovo aimed to energy and technology development.

LITERATURE

[1] *www.eere.energy.gov*
[2] Legjislacioni, Kuvendi i Republikës së Kosovës
[3] Ministria e Energjisë dhe Minierave, Qeveria e Republikës së Kosovës
[4] *www.altenergymag.com/emagazine/2012*
[5] *www.kek-energy.com*
[6] *www.kosst.com*
[7] U.S.Department of Energy, Energy efficiency & renewable energy,Amerika,
[8] http://www.nrel.gov/learning/re_basics.html
[9] Komisioni Evropian, Sektori i energjisë
[10] Seanx Liu;"Civil and Enviromental Engineering",University of California at Berkley
[11] Jeams ; „Civil and Enviro,ental enginnering",University of Nevada at Lasvegas

International Journal of Modern Engineering Research (IJMER)
www.ijmer.com Vol.3, Issue.2, March-April. 2013 pp-611-617 ISSN: 2249-6645

Wireless Sensor Networks in Intelligent Transportation Systems

Ondrej Karpis
Department of technical cybernetics, University of Zilina, Slovakia

Abstract: *One of the main goals of intelligent transportation systems (ITS) is economical profit in the form of fuel consumption reduction, efficient use of existing infrastructure, pollution reduction and so on. Certainly, the economical goal is not the only one. Increasing mobility, safety and passenger comfort are other very strong motivations for implementation of ITS in practice. The paper analyzes the possibilities of exploitation the technology of wireless sensor networks (WSN) in ITS. Detailed description of sensor node designed for sensing intensity of magnetic field and acceleration is provided. As an example, the proposed sensor is used to sense the speed of moving vehicles and to classify the vehicles according their estimated length.*

Keywords: *Intelligent Transportation System, Sensor Node, Wireless Sensor Network*

I. INTRODUCTION

Transportation is inseparably linked to the life of every person, whether in the form of passenger transport or material transport. The amount of transported people and goods continues to grow and with it the economic importance of transport. With around € 533 billion in Gross Value Added (GVA) at basic prices, the transport and storage services sector (including postal and courier activities) accounted for about 5.1 % (4.6 % in 2008) of total GVA in the EU-27 in 2009 [1]. It should be noted, however, that this figure only includes the GVA of companies whose main activity is the provision of transport (and transport-related) services and that own account transport operations are not included. The transport services sector employed around 10.6 million persons, i.e. 5 % of the total workforce. In 2010, private households in the EU spent € 904 billion (13 %) of their total consumption on transport-related items, e.g. to purchase vehicles, to buy fuel for cars or tickets for bus, train, plane and so on. Referring to above mentioned information, transportation sector represents one of core ones in the EU. In general, meaningful activities in transportation field have positive influence on economy growing as well as decreasing of unemployment. Unfortunately, growing number of vehicles and traffic volume in any transportation mode, e.g. road, railway, aerospace, marine one, has implied increasing of traffic accidents, congestion and environmental problems. In order to solve these problems, international organizations, governmental authorities, industry corporations have been putting effort into supporting of applying electronics, information and communication technologies in the field of transportation, so that intelligent transport systems became reality. The economic impact of the ITS industry is significant. U.S. ITS market revenues are estimated for about $48 billion in present days and exceed those for electronic computers, motion picture and video products, direct mail advertising, or internet advertising. U.S. private sector ITS market revenues are expected to climb to $67 billion by CY 2015 [2].

Economical profit represents one of core motivation factors of research and development (R&D) activities in the field of ITS. Certainly, it is not the only one. Increasing transport safety, traffic flow fluidity, environment protection and In 2010, 31 030 persons were killed in road accidents and 62 passengers lost their lives in railway sector in EU. Statistically, the most dangerous transportation mode is the road one. Table 1 presents number of road fatalities in several countries of the world. At this moment comparison of the countries statistics is not a goal. In general, it is possible to state that there are too many road fatalities per year even in the most developed countries.

Table 1. Transport safety – road fatalities

Year 2010	**EU-27**	**USA**	**JAPAN**	**CHINA**	**RUSSIA**
Total number of road fatalities	31 030	32 885	4 863	70 000	26 600
Per million inhabitants	62	106	38	52	186

Effectiveness of the transport could be evaluated on the basis of various criteria, e.g. cost of journey, coming in time, delay on the way and so on. Principally, passengers or goods are transported via selected transport mode (road, air, railway, etc.) to arrive to destination with minimal delay, i.e. to avoid congestions on the way, and expenses.

Table 2 shows volume of passenger transport in selected world countries. Analyzing the data, it is possible to state that road transportation mode is dominant one concerning passengers transport. It is valid globally. Core problem of the mobility represents road traffic congestions. Improving mobility effectiveness will be depended on fluidity of traffic flows. ITS technologies could significantly help to increase road throughput. Certainly, extension of existing infrastructure and selection of proper transport mode increases effectiveness of the mobility as well. Concerning freight transport, multimodal goods distribution allows very effective utilizing of complex transportation infrastructure. This strategy can increase the probability of congestion avoiding significantly.

Table 2. Passenger transport in pkm
(Passenger-kilometer: a unit of measure: 1 passenger transported a distance of 1 kilometer)

	EU-27 2010	USA 2009	JAPAN 2010	CHINA 2010	RUSSIA 2010
Passenger car	4738	5828	766	1491	
Bus + trolley-bus + coach	510	490	87		148
Railway	404	40	393	876	139
Tram + metro	90	18			49
Waterborne	38	0.6	4.3	7.2	0.9
Air (domestic)	524	888	74	403	147

Ecology programs are focused on decreasing of environmental pollution, reduction of massive consumption of fossil fuels. Emission is dominantly related to road transportation. Protection of environment must be principally based on the development of new "zero emission" fuels for cars, replacing fossil fuels motors by electro/hybrid motors, managing traffic flows fluidity in compliance with avoiding congestions, providing relevant and real time traffic information to driver, supporting Eco-driving mode and so on.

Comfort could be characterized by following factors: vehicle`s technologies perform complicated operations instead of driver; real-time as well as value-added information are available to the driver for in-time and correct decision making.

Referring to above mentioned information, it is possible to conclude that implementation of Intelligent transport systems is reasonable and have positive influence on mobility safety, ecology as well as economies. It is now undisputed that intelligent transportation system brings significant benefits to users and operators of transport infrastructure. Getting information about the current state of transport infrastructure and transport parameters is essential for effective management of traffic on the roads. One promising means of obtaining the necessary information is a wireless sensor network, which is able to obtain relevant data from spatially distributed sources. WSN is composed of simple, inexpensive elements (nodes) that are able to capture the necessary data, to pre-process them and to transfer them to the center using wireless transmission paths. The center is able to handle the data and to implement appropriate intervention action, or it can provide the data to the operator or users of the transport system. Today we meet the fact that WSNs are becoming an integral subsystem of each ITS.

II. WIRELESS SENSOR NETWORKS

Development and successful deployment of WSNs depend on advances in different areas such as: low-power electronics, micro-electro-mechanical system (MEMS) components, new reliable sensors, power sources with high energy density, devices with ability to generate energy from the environment and new RF communication standards. The most promising application areas of WSNs are:

- Transport,
- Medicine,
- Monitoring and protection of the environment,
- Military,
- Guarding, protecting and tracking,
- Industry and many more.

WSN can be applied wherever we encounter spatially distributed information sources. An interesting application area of the WSN is the traffic. It is clear that monitoring and managing the traffic requires information sources that are geographically dispersed over a large area. A comprehensive overview about the state of transport can be obtained only on the basis of information obtained from a large number of properly deployed sensors. Therefore, the monitoring and management of the traffic naturally tends to the applications of sensor networks. Currently, the most frequently used WSN applications in the field of transport applications are: monitoring of traffic and dynamic routing [3], [4], monitoring and management of parking lots [5], [6], adaptive control of intersections [7], [8].

Successful deployment of WSN in different applications depends on parameters of the sensor nodes. The most important parameters are:

- The processing power and memory capacity of the sensor,
- Low power consumption/long lifetime,
- Production cost,
- Security,
- Fault tolerance and other.

Note that it is impossible to develop a universal node that is optimal in terms of all the above requirements as some of these requirements are contradictory: large computing power at minimal cost and power consumption; long life without operator intervention at small dimensions of the energy source; sufficient speed of communication within a limited frequency band, low transmission power and low sensitivity of the receiver (Transmit power and the receiver sensitivity is

closely related to the consumption of communication units.). For these reasons, parameters of the resultant sensor node represent kind of a compromise between the requirements of applications and capabilities of current technology.

III. SENSOR NODE STRUCTURE

Despite the variety of application areas the basic structure of the node is the same. Each sensor node must be able to perform three basic functions: data collection, data preprocessing, and data transmission. Each function is provided by another subsystem. In addition to these three basic subsystems we need power subsystem to provide energy to all other subsystems.

3.1. Data collection subsystem

Data collection subsystem is application depended and consists of sensor elements sensing relevant signal values in compliance with defined aim. The diversity of application areas cause that it is difficult to define universal properties and parameters of data collection subsystem. Any application requires a little bit specific approach from subsystem design point of view. The data collection subsystems are mostly focused on: temperature, pressure, humidity, acoustic noise level, lighting conditions, biological and chemical agents, vehicle movement, the presence/absence of the object etc.

Basic functions of the data collection subsystem are:

- Sensing of selected signals by proper sensors and transforming of measured signals to ones which are suitable for additional processing (most often electrical voltage).
- Adjusting of signal level in such way that dynamic range of A/D converters is utilized in the best manner.
- Filtration of the additive inherent and interfered noise from the signal. The useful part of the signal should not be distorted.
- Filtration in order to limit the frequency spectrum of the signal so it is in compliance with selected sampling period (ant aliasing filter).

Besides presented basic functions additive functions are often provided by the subsystem e.g. periodic evaluation of the signal level and activating the processor if the measured signal reaches predefined threshold value.

As the data collection subsystem is application depended it is often realized as a compact module connected to the sensor node via a set of connectors. For its construction are used modern electronic elements, especially sensors, operational amplifiers, amplifiers with programmable gain, comparators and other microelectronic components.

3.2. Data processing subsystem

The role of data processing subsystem depends on how the WSN process the data. If the network is decentralized each node must have sufficient processing power to process all relevant data and to calculate results. In the case of centralized network structure the node just collects data and sends them to the central unit for further processing. However, usually it is impossible to transmit all the measured data as the data transmission is very energy intensive. Therefore, we try to minimize the volume of transmitted data. It is important to realize essential part of the data processing directly at the point of its origin - in a sensor node. Data transmitted to other network nodes should contain just information essential for problem solving. Basic data preprocessing algorithms thus relates to the methods of information content extracting (compression). Another possibility is to use collaborative signal processing algorithms. These algorithms use the smart distribution of data processing between the different network nodes in order to increase overall computing power of the network while minimizing the total energy consumption.

Basic functions of processing subsystem are: digital processing of measured signal values, controlling of individual modules of the sensor node, securing of transmitted data and potentially another additive functions required by particular application. It is possible to use different devices as the core of the processing subsystem: ASIC, FPGA or universal microcontrollers. All requirements related to technical solution is necessary to consider during selection of proper unit core. Nowadays, microcontrollers (MCU) are mostly used as a control system of sensor node. It is clear that it is very important to carefully consider required computing performance because increasing of it will increase energy consumption. In current solutions are used mainly 32-bit processors StrongARM with energy consumption of 0.3W@1.5V/200MHz in active state, different MCUs from 32-bit Atmel ARM7 90mW@3.3V/48MHz, through 16-bit MCUs TI MSP430F5437 1mW@3.0V/8MHz to 8-bit Atmel ATmega644 0.72 mW@1.8V/1MHz. Note that mentioned data has only informative character. In case of selection of proper type of MCU is necessary to take into account significantly more parameters (capacity of program memory, data memory, integrated peripheries, circuit architecture, availability of development tools and many other factors).

3.3. Communication subsystem

Communication subsystem provides ability of wireless communication – fundamental property of a wireless network. Communication capability of WNS nodes are in most practical cases limited by communication range and data rate. It is important to remember that increasing of communication range requires increasing of transmit power/receiver sensitivity, i.e. energy consumption is increased as well. Above mentioned conclusions result from Friis transmission equation:

$$\frac{P_R}{P_T} = G_T G_R \left(\frac{\lambda}{4\pi d} \right)^2 \quad (1)$$

where G_T and G_R are the antenna gain of the transmitting and receiving antennas, respectively, λ is wavelength, d is the distance, P_R is power available at the receive antenna terminals and P_T is power delivered to transmit antenna. The factor in parentheses is the so-called free-space path loss. The antenna gains are with respect to isotropic, and the wavelength and distance units must be the same. The formula is valid only is the antennas are in unobstructed free space and the bandwidth is narrow enough that a single value for the wavelength can be assumed.

Increasing of communication range of individual sensor node increases interference among network elements so that it has negative influence on total throughput of the network. This is the reason why the most common communication range is between 10 and 300 m, for transmit power 0 to 10 dBm and receiver sensitivities -90 to -102 dBm. The transceivers operate the most often in frequency bands: ISM 443 MHz, 886/916MHz and 2.4 GHz. Note that limitation of communication distance has no influence on the ability of the network to exchange information between two remote nodes as the multi-hop message routing techniques are used [9].

As communication subsystem can be used commercial module produced by companies NXP, AUREL, MaxStream, RF Digital Corporation, etc. The second option is to design proprietary radio unit satisfying requirements of the application. Let us notice that in each case it is necessary to respect limits defined by European normalization and state telecommunication authorities.

3.4. Power subsystem

For every WSN application is important period of network operation without maintenance. Energizing of sensor nodes by electrical energy is critical problem. To solve the problem it is possible to choose from one of following energy sources:

- Primary batteries,
- Rechargeable batteries,
- Energy harvesting (collecting energy from surrounding environment),
- Combination of rechargeable batteries and energy harvesting.

During energy resource selection process it is necessary to evaluate parameters limiting range of applicability. One of such parameters is self-discharging that could be in case of some types of batteries even 30 % per month. Another important parameter is the range of operation temperatures, number of charging cycles, etc. For the purpose of planned long term service-less operation of the network (i.e. longer than 6 months) most favorite energizing is based on using primary lithium batteries, potentially with the system of energy harvesting and super-capacitor.

Figure 1 shows basic structure of sensor node consisting from above mentioned four subsystems.

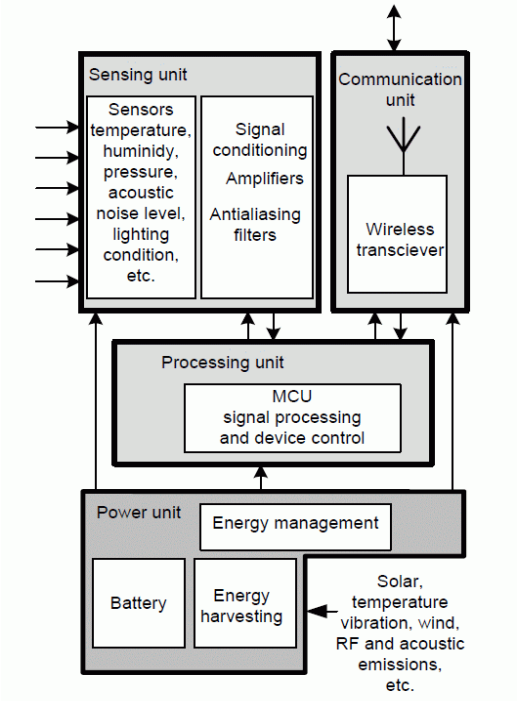

Figure 1. Node structure

IV. NODE FOR ROAD TRAFFIC MONITORING

At University of Zilina, Department of technical cybernetics, we developed a node prototype for monitoring the traffic. As the node is not dedicated for commercial utilizing, questions related to energy severity, reliability and cost of product were not prioritized at the time of sensor node design. Monitoring of the traffic is based on a magnetometer. As the cars consist mainly from a metal, they influence magnetic field of Earth and the changes can be sensed by a magnetometer even from relatively large distance from the car.

The node is based on a low-power 32-bit microcontroller STM32F100RB. The MCU is based on the ARM-Cortex M3 core. It has two types of memory: SRAM with capacity of 8 kB and Flash memory with capacity of 128 kB. Microcontroller integrates many standard peripherals supporting extension of application possibilities. Memory subsystem is extended by micro SD card that allows saving of big amount of data content for off-line evaluation. MCU´s power management unit supports several energy saving modes. Sensing part of the node consists from the sensor LSM303 containing 3-axis magnetometer with a 3-axis accelerometer. Magnetometer sensitivity is adjustable in range from ± 1.3 Gauss to ± 8.1 Gauss. Accelerometer range is possible to adjust in interval from ± 2 g to ± 8 g. The communication subsystem can be based on module RFM70 or XBee. Module RFM70 enables communication over short distances in the ISM 2.4 GHz band with data rates up to 2 Mbps. XBee module uses the same ISM band and has better communication range but slower data rate (up to 250 kbps) than RFM70. Motherboard dimensions are 49 x 33 mm (Fig. 2).

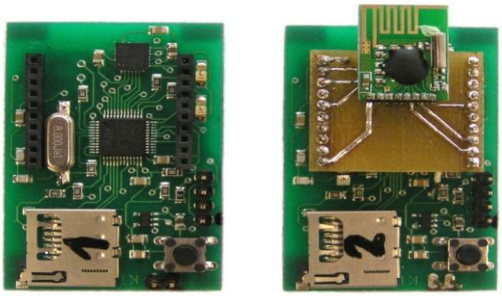

Figure 2. Node prototype – without and with RFM70 module

Data collecting center of the WSN is based on a personal computer equipped with a special USB adapter that enables communication with both mentioned communication modules.

Power unit allows using primary or rechargeable cells or super capacitors recharged by solar cells [10], [11]. Under development is a new super capacitor charging system using a thermo generator?

V. EXPERIMENT

Sensor nodes basic testing was realized as follows. Two nodes were placed on the verge of the road with spacing of 2 m. One module transmitted the measured data and the second module stored both measurements to the SD card. The sampling frequency was 220 Hz (highest supported by the magnetometer) and sensitivity was set to ± 1.3 gauss. The measurement took 18 minutes. During the measurement the vehicles were recorded by a camera. Analysis of the camera recording has provided the number and type of vehicles: 131 passenger cars, 4 vans, 4 trucks, 2 buses and a bicycle - altogether 142 vehicles. Very good sensitivity of the magnetometer is confirmed by the fact that it was able to detect even a bicycle.

Figure 3 shows data acquired from both sensors during a 8 second interval. Let us notice that sensor 2 is located 2 m ahead of sensor 1. Time difference between measured signals is depended on localization of sensor elements, speed of passing vehicle and orientation of vehicle movement. Average speed of vehicle passing the sensors can be calculated on the basis of the evaluation of time difference between corresponding changes of magnetic induction measured by sensors 1 and 2. The first part of the record belongs to a vehicle going in the right direction and the second part to a vehicle in the opposite direction. Evaluating shift between records is very useful for eliminating false-positives.

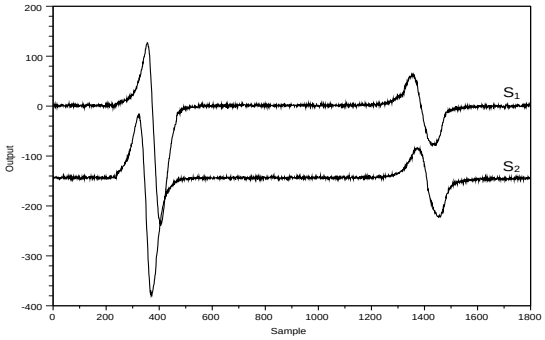

Figure 3. Different direction of vehicle movement

For each vehicle we can determine its speed. Assuming a uniform speed of the vehicle, the relation for vehicle speed is:

$$v = d * Fs / s \quad (2)$$

Where *Fs* is the sampling frequency, *s* is the shift between the measurements calculated using correlation and *d* is the distance between the sensors. Using the calculated speed of vehicle we can estimate its length *l*, which is proportionally dependent on the length of the vehicle record (*N*) by the relation:

$$l = N * v / Fs \quad (3)$$

In Fig. 4 are depicted the lengths of all detected vehicles. It is well possible to distinguish between two groups of vehicles: smaller (personal) and larger vehicles (vans, trucks and buses). The reason why the calculated length of some passenger cars is unusually large has not yet been determined. However, we must remember that the calculated length is not the length of the vehicle but rather the length the magnetic profile of the vehicle. As such, it is very dependent on the material from which is the car made.

Presented measurements illustrate usability of sensor nodes with magnetic induction sensing for monitoring of traffic flow parameters. Influences of the second sensed parameter (vibration) were not involved in the test. More measurements can be found in [12].

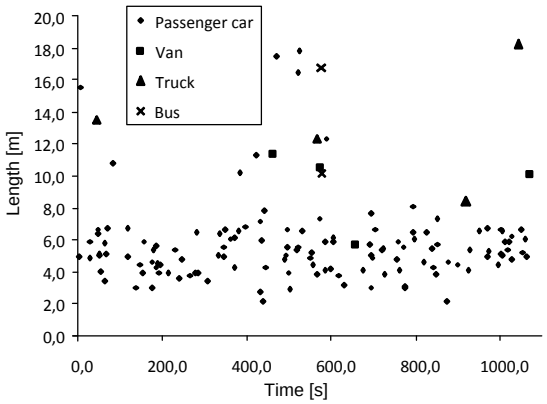

Figure 4. Estimated lengths of all vehicles

Future research activities will be focused on building of a whole WSN and online evaluating of measured signals. Our ultimate goal is to get enough information to adaptive control of intersections.

VI. CONCLUSION

Problematic of intelligent transport systems is subject of interest of many authorities, institutions as well as commercial corporations in present days. The paper shortly introduces basic attributes of transportation processes from safety, effectiveness, environmental and comfort point of views. Referring to key technologies using in transportation applications: sensing, data processing, data transmission etc., problematic of wireless sensor networks is presented in the paper as well. It is possible to state that both of research areas (ITS and WSN) are using principally comparable technologies for data collection, processing and transmission. It means that WSN technologies are well applicable in the field of intelligent transportation systems. Certainly, selection of applications must correlate with specific WSN characteristics. Finally, it is possible to state that implementation of wireless autonomous devices in the field of intelligent transportation systems has very good perspective.

VII. ACKNOWLEDGEMENT

This contribution/publication is the result of the project implementation:
Centre of excellence for systems and services of intelligent transport II,
ITMS 26220120050 supported by the Research & Development Operational Programme funded by the ERDF.

REFERENCES

[1] European Commission, EU Transport in figures. Statistical pocketbook, 2012
[2] The Intelligent Transportation Society of America, Sizing the U.S. and North American intelligent transportation systems market: Market data analysis of its revenues and employment, August 2011
[3] J. Micek, J. Kapitulik, Wireless sensor networks in road transportation applications, Proceedings of MEMSTECH, Polyana-Svalyava, Ukraine, 2011, 114-119
[4] E.F. Nakamura et al., A reactive role assignment for data routing in event-based wireless sensor networks, Computer Networks, 53(12), 2009, 1980-1996
[5] V.K. Boda, A. Nisipuri, I. Howitt, Design considerations for a wireless sensor network for locating parking spaces, Proceedings of the SoutheastCon, Charlotte, NC, 2007, 698-703
[6] V.W.S. Tang, Y. Zheng, J. Cao, An intelligent car park management system based on wireless sensor networks, Proceedings of 1st International Symposium on Pervasive Computing and Applications, 2006, 65-70
[7] M. Tubaishat, Y. Shang, H. Shi, Adaptive traffic light control with wireless sensor networks, Proceedings of IEEE Consumer Communications and Networking Conference, 2007, 187-191
[8] Y. Wen, J.L. Pan, J.F. Le, Survey on application of wireless sensor networks for traffic monitoring. Proceedings of International Conference on Transportation Engineering, Chengdu, China, 2007, 2079-2084
[9] K. Akkaya, M. Younis, A Survey on routing protocols for wireless sensor networks. Ad Hoc Networks, 3(3), 2005, 325-349
[10] J. Micek, J. Kapitulik, WSN sensor node for monitoring protected areas, Proceedings of FedCSIS, Wroclaw, Poland, 2012, 803-807
[11] M.Kochlan, P.Sevcik, Supercapacitor power unit for an event-driven wireless sensor node, Proceedings of FedCSIS, Wroclaw, Poland, 2012, 791-796
[12] O. Karpis, Sensor for Vehicles Classification, Proceedings of FedCSIS, Wroclaw, Poland, 2012, 785-789

International Journal of Modern Engineering Research (IJMER)
www.ijmer.com Vol.3, Issue.2, March-April. 2013 pp-618-621 ISSN: 2249-6645

Methods of Research into Privacy in Housing

Alireza Daneshpour, [1] Mohamed Rashid Embi[2]
[12]*Faculty of Built Environment, University Teknologi Malaysia*

Abstract: *Systematic research through residents' attitudes, preferences, etc. in dwellings has become the dominant mode of environmental research into building design. Most of these works have been directed at the evaluation of buildings in terms of user satisfaction. Some have proposed, developed and applied procedures for identifying the factors contributing to resident satisfaction in dwellings. Others critically question the extent of the usefulness and appropriateness of the theoretical and methodological ground of this approach. The aim of this paper is to identify an appropriate approach for measuring and evaluating amount of privacy in apartments. The method which used is review of documents related to our issue and the technique which applied in this way is content analysis. The results shows that research into privacy, for the sake of adequacy, must treat people as subjects as well as objects. For research into privacy in man-environment transactions, or for understanding privacy needs and satisfaction with design neither the people itself nor the setting alone are sufficient. It seems that the congruence model is a particularly appropriate approach for studying privacy in design.*

Keywords: *congruence model, housing, dwellings, privacy*

I. INTRODUCTION

Social science research methods entered architectural practice for the first time in the 1950s. More recently questions have been raised about the philosophical bases of social science procedures which, following the positivist conception relied on the natural sciences for a methodological model. As Studer (1972) noted: "Science no longer seeks truth but useful and reasonable ways of organizing experience." [1] The problem is not new, but its recent emergence from a wider critique of the sciences in general is the result of some radical changes in the scholastic world (Studer 1972, Stevens 1988). This critique must be borne in mind in designing research on architectural issues today, yet the research techniques used still rely on this tradition because they have yielded many important insights. [2]

Theorists on culture remain divided on how best to define culture and what aspects of it to emphasize. A common view in contemporary social science is that culture consists primarily of thoughts, moods, feelings, beliefs and values. The human world has been divided in two: objective social structure on the one hand, subjective thoughts and perceptions on the other and the cultural part is defined as the most fluid, constrained and least variable category of non-behavior. Over the past quarter century, four approaches to the study of culture largely outside the mainstream of social science have been pursued with growing interest. These approaches have been oriented primarily toward the realms of meaning, symbolism, language and discourse. The first is phenomenology; the second, cultural anthropology; the third structuralism; and the fourth critical theory. In contrast to the previous classical approach which emphasizes the subjective moods and intentions of the actor each has come increasingly to stress the more observable objective shared aspects of culture and to seek patterns among them. In other words culture is understood as a behavioral phenomenon instead of having only subjective meanings. In this sense the study of culture includes the meaning of symbols, Conditions, patterns and rules of use which render the symbols meaningfu1.[3] Although this study will conduct some investigation into abstract cultural meanings most of it will rely on the latest approach. i.e. the objective one.

The problem is that the positivist account of science assumes that science produces objective, value-free, reliable facts and knowledge about the world. Phenomenology, on the other hand, holds that these attributes seem dubious or at least simplistic. Phenomenology is to a large degree characterized by uncertainty. Yet phenomenology has its problems too. Still we can learn much from its argument.

The phenomenological movement has recently penetrated architectural thought and received a wide following. Phenomenology 'calls for a return to the foundations of meaning and experience'. [2] Unlike positivism, it considers people more as 'active producers of meaning, than as simply passive hearers'. Rather than an emphasis on and search for causality and precise explanation. Characteristic of positivism, phenomenology deals with the search for meanings and its goal understands.

The phenomenological critique of science attacks certain throughout processes used in the positivist conception of science. Among these is the role of quantification. Though phenomenology as a movement has quite recently entered architectural circles, the role of quantification had already been discussed and criticized by a number of writers.

Several authors, by elaborating the significance and complexity of human experience of and in the environment, have attacked the notion of quantifiability, characteristic of much psychological research in architecture. Quantifiability assumes that all significant and or relevant factors in human experience can be measured in purely quantitative terms' (Daley 1968). The opposite view holds that quantification, by rendering the human condition measurable, can distort, misdescribe, and do violence to experience and thereby lead to erroneous assumptions or trivial conclusions (Daley 1968, Stevens 1988). A third view maintains that quantification, at least in the present state of architectural research could be premature. [4] Attempts at quantification have tended to make numbers, concepts and calculative techniques look 'more real than the phenomena they represent' .He further argued that interest in the quantifiable has led to the neglect of many significant qualitative aspects of reality that do not easily lend themselves to quantification [2]. This is especially true of the experience

of privacy [5].The research method used in this study strives to proceed with the qualitative qualities of built form but recognizes the utility of quantification.

There are generally two orientations to the study and evaluation of the physical environment: phenomenological, which deals with the environment as it is experienced; and objective, which analyses the environment as it is believed to be [6, 7]. Accordingly two different approaches toward the treatment of building users have been used. Canter noted that one approach deals with people as subjects whose experience is of interest, and the other considers people as objects, in which case their behavior is of concern [8]. Arthur Patterson and Romedi Passini, as well as Canter, consider both approaches necessary and stress the employment of a combined approach in which both behavioral as well as attitudinal measures are used .Canter suggested that relating both behavior and attitudes to the attributes of the physical setting can lead to the generation of meaningful, useful and valid information which may potentially promote the understanding of the building-user interface [8].

For the study of privacy, especially in buildings, views similar to these have been proposed by a number of researchers and writers [9, 5, 10]. Treating people merely as objects has been particularly criticized. It has been argued that the satisfaction of people with their privacy in dwellings also requires the measurement of the psychological performance of a building, the evaluation of which is bound to depend on and take consideration of the experience and judgment of the individual [10]. It has been emphasized that research into privacy, for the sake of adequacy, must treat people as subjects as well as objects [5].

Systematic research through residents' attitudes, preferences, etc. in dwellings has become the dominant mode of environmental research into building design. Most of these works have been directed at the evaluation of buildings in terms of user satisfaction. Some have proposed, developed and applied procedures for identifying the factors contributing to resident satisfaction in dwellings [11]. Others critically question the extent of the usefulness and appropriateness of the theoretical and methodological ground of this approach. Donnelly, among others, examines some aspects of housing appraisals which are based on the 'user satisfaction' approach [4]. He points, among other things in such studies, to the neglect of many variables of the social world in which people live. Lee believes 'user satisfaction' alone is not a very useful measure and it provides a low level of explanation [12]. He emphasizes the advantages of an approach which incorporates the above with 'compatibility studies'. The latter studies are concerned with the establishment of a comfortable match between user requirements and design. A similar view has been proposed by Rapaport. He states that a major finding emerging from man-environment studies stresses that it is the subjective environment of the person which affects behavior. And that this subjective world is not independent of the objective environment or real world. For an objective environment to be responsive to and supportive of behavior, Rapoport argues for congruence between the 'subjective' and 'objective' environments. The concept of congruence is an important one for this study and merits some discussion here [13].

II. PEC MODEL

The model of person-environment compatibility, otherwise known as person-environment congruence or fit (PEC), has been applied in a number of recent studies into man-environment relations (Kaplan 1983). A literature review indicates that research into privacy in housing design needs to go beyond the testing and mere description of privacy of the individual or of the environment taken separately. For research into privacy in man-environment transactions, or for understanding privacy needs and satisfaction with design neither the people itself nor the setting alone are sufficient. The congruence model is a particularly appropriate approach for studying privacy in design. Indeed, Kiyak has proposed the application of a model of person-environment congruence for the study of privacy. In Kiyak work the fit between the individual's desire for privacy and the privacy provided by the physical setting is the main concern. In the other hand what is important is not the lack of opportunities for physical privacy itself; rather it is the lack of congruence between privacy needs and the provision of privacy by the setting. Privacy needs can range from low to high degrees, while the setting of it may vary accordingly. The lack of such a fit and its impact on people is important, especially in residential settings, where neither the environment nor the people residing in it can readily change and adapt to any significant extent. Kiyak's research was based on the use of this congruence concept in an empirical study of privacy.[14]

Kiyak examined person-environment fit between the preference for privacy and the availability of privacy among institutionalized elderly in housing units in long-term care facilities. His analysis and results suggested some positive correlation between user satisfaction and this congruence model. According to him while the setting provided residents with high degrees of physical privacy, those whose desire for privacy was low perceived the setting as too high in privacy and turned out to be less satisfied with the privacy of the setting than those whose desire for privacy was high, who were more satisfied than the former group. Also he found that a situation which provided slightly higher degrees of privacy relative to what was wanted appeared more acceptable to people than a situation which offered some degrees lower than desired. He concluded that optimum satisfaction was associated with a more or less congruent state between privacy wanted and privacy provided by the setting. He stated that when the gap between the latter two is wide, it may influence the individual's well-being in that setting.

However Kiyak's study did not relate design aspects to privacy situations. This is because his approach in the main followed Marshall's (1972) and was one of a behavior-oriented nature rather than a design-directed one. Marshall's (1972) approach was that of measuring preferred and achieved privacy by evaluating the attitudes of a sample population towards privacy in housing (Marshall 1972). Kiyak's (1978) work nevertheless provided some general impression of the relationship between the overall design and privacy needs of the elderly. User satisfaction was not just explained simply by design characteristics; rather the degree of fit between people and their environment was more important for their well-being. His

proposed congruence model between desired and achieved privacy is a useful strategy to evaluating designs in terms of privacy and its relation to well-being and hence it is utilized in this study.[15]

Canter (1970) argued that most user surveys tend to produce information about individual differences in response to aspects of given buildings. Such studies, he said, though of value in their own right, fail to examine systematically or show how differences in design features and architectural elements make for differences in responses. This suggests that comparative studies for evaluating aspect of buildings derived from different design solutions might be a useful methodological consideration. Appraising different dwellings through a comparative study has often been considered advantageous [8]. For example Altman and Chemers (1984) emphasised the adoption of a comparative perspective in man-environment studies. This study adopts a comparative approach to three design solutions in a setting in which privacy is a paramount consideration.[16]

Recently literature has tended to stress the uncertain basis of much of the scientific methodology in architectural research and practice. Questions have been raised as to the validity and reliability of many of the methods and techniques used, and how useful the data these produce are (Bechtel 1970, Lozar 1974, Patterson and Passini 1974, Stevens 1988(1-20)).[17,18,19] Science is said to be largely characterized by an inductive process of inquiry, an integral part of which is always uncertainty (Jenks 1988). Issues in housing, especially, appear complex enough to preclude any simplistic certainties. "However soundly based or apparently 'good' research or theories may seem, there will always be an element of doubt and uncertainty"[20]

III. CONCLUSION

Environmental studies in architecture have extensively borrowed their research methods and measurement techniques from the social sciences. There has been a considerable increase in recent decades in the number of such studies employing inhabitant or user surveys, especially in housing design. Despite some recently articulated concerns about such research in architecture, this type of research has yielded the most informative results to date. The concerns expressed in the critiques mentioned above do, nevertheless, need to be borne in mind in understanding the strengths and limitations of the methods used here. Research into privacy, for the sake of adequacy, must treat people as subjects as well as objects. For research into privacy in man-environment transactions, or for understanding privacy needs and satisfaction with design neither the people itself nor the setting alone are sufficient. It seems that the congruence model is a particularly appropriate approach for studying privacy in design.

IV. ACKNOWLEDGEMENTS

The work is financed by International doctoral fellowship (IDF) provided by University Teknologi Malaysia and the Ministry of Higher Education of Malaysia.

REFERENCES

[1] Studer, R.G., Environmental Decision Making: The Organization of Spatial Stimuli, in Environment and the Social Sciences: Perspectives and Applications, J.F. Wohlwill and D.H. Carson, Editors. 1972: Washington D. C. American Psychological Association, Inc., D.C. p. 279 - 292.
[2] Stevens, G., Architectural Science in Retreat? The New Anti-Science Movement in Architecture. Architectural Science Review, 1988. **31**(4): p. 145- 152.
[3] Wuthnow. R and others. Cultural Analysis. Routledge and Kegan Paul. U.S.A. 1984. PP. 3-7, 247
[4] Donnelly, D., Are We Satisfied with 'housing satisfaction'? Built Environment, 1980. **6**(1): p. 29- 34.
[5] Fischer, C.T., Privacy as a profile of authentic consciousness. Humanitas, 1975. **11**(1): p. 27- 43.
[6] Roshansky, H.M., W.H. Ittelson, and L.G. Rivlin, the Influence of the Physical Environment on Behavior: Some Basic Assumptions, in Environmental Psychology: Man and His Physical Setting, H. M.Proshansky, W.H. Ittelson, and L.G. Rivlin, Editors. 1970, Holt, Rinehart and Winston: New York. p. 27-36.
[7] Lang, J., Creating Architectural Theory: The Role of the Behavioral Sciences in Environmental Design. 1987, Van Nostard Reinhold Company, New York.
[8] Canter, D.V., Should We Treat Building Users as Subjects or Objects?, in Architectural Psychology, D.V. Canter, Editor. 1970, RIBA Publications: London. p. 11 – 12
[9] Hill, A.R., Visibility and Privacy, in Architectural Psychology, D.V. Canter, Editor. 1970, RIBA Publications: London. P.39 -43.
[10] Hath out, S.M., Privacy in Housing Design: Environmental Study in Urban Housing Study of the Hulme Area, Manchester, 1979, University of Manchester. p. 155.
[11] Francescato, G., Evaluating Residents' Satisfaction in Housing for Low and Moderate Income Families: A Multimethod Approach, in EDRA 5: Part 5. Methods and Measures, C.C. Lozar, Editor. 1974: Environmental Design Research Association Inc. p. 285 - 295
[12] Lee, T.R., Do We Need A Theory?, in Architectural Psychology, D.V. Canter, Editor. 1970, RIBA Publications: London. p. 18- 25.
[13] Rapoport, A., Neighborhood Heterogeneity or Homogeneity. Architecture and Comportment/Architecture and Behavior, 1980/81(1): p. 75 - 76

[14] Kiyak, H.A., A Multidimensional Perspective on Privacy Preferences or Institutionalized Elderly, in EDRA 9: New Directions in Environmental Design Research, W.E. Rogers and W.H. Ittelson, Editors. 1978, Environmental Design Research Association: Tempe, Arizona. p. 79 - 91.
[15] Marshall, N.J., Privacy and Environment. Human Ecology, 1972. **1**(2): p. 93 - 110.
[16] Altman, I. and M.M. Chemers, Culture and Environment. 1984, Cambridge University Press, Monterey, California.
[17] Bechtel, R.B., Human Movement and Architecture, in Environmental Psychology: Man and His Physical Setting, H.M.P.W.H. Ittelson and L.G. Rivlin, Editors. 1970, Holt, Rinehart and Winston, Inc.: New York. p. 642- 645.
[18] Lozar, C.C., Methods and Measures, in EnRA 5. Part 5: Methods and Measures, C.C. Lozar, Editor. 1974: Environmental Design Research Association Inc. p. 169 and 211 - 220.
[19] Patterson, A. and P. Romedi, The Evaluation of Physical Settings: To Measure Attitudes, Behavior or Both?, in EDRA 5; Part 5: Methods and Measures, C.C. Lozar, Editor. 1974: Environmental Design Research Association Inc. p. 161 - 176.
[20] Jenks, M., Housing Problems and the Dangers of Certainty', in Rehumanizing Housing, N. Teymur, T.A. Markus, and T. Woolley, Editors. 1988, Butterworths: London. p. 53 - 60.

International Journal of Modern Engineering Research (IJMER)
www.ijmer.com Vol.3, Issue.2, March-April. 2013 pp-622-625 ISSN: 2249-6645

Automatic Detection of Unsafe Dynamic Component Loadings in Multi-Terminals by Using IP Address

Gnanasoundari.A, [1] Dr.S. Tamilarasi[2]
[1]*Final Year Student, M.Tech CSE Department, Dr.M.G.R.Educational and Research Institute University, Tamil Nadu, India*
[2]*Professor of CSE and IT Department, Dr.M.G.R.Educational And Research Institute University, Tamil Nadu, India*

Abstract: *The mechanism widely used for an improved system of modularity and flexibility is Dynamic loading of software components. Dynamic loading can be hijacked by placing an arbitrary file with the specified name in a directory searched before resolving the target component, thereby making the system more vulnerable. The vulnerable components are important to be deducted.*
In this paper an automated technique to detect vulnerable and unsafe dynamic component loadings are presented. Analysis has two phases:
1) Online phase – by applying dynamic binary instrumentation to collect runtime information on component loading.
2) Offline phase – to analyze the collected information to detect vulnerable component loadings.
This technique is implemented in networked system of Microsoft Windows and UNIX using system IP address and it can deduct unsafe components and stopped. Our evaluation results show that unsafe component loading is prevalent in software on both OS platforms, and it is more severe on Microsoft Windows.

Keywords: *Full path, Filename, Online Phase, Offline phase*

I. Introduction

Dynamic loading allows an application the flexibility to dynamically link a component and use its exported functionalities. Benefits include modularity and generic interfaces for third-party software such as plug-ins. It also helps to isolate software bugs as bug fixes of a shared library can be incorporated easily. With these advantages, dynamic loading is widely used in designing and implementing software.

Important stage in dynamic loading is component resolution by locating the correct component for use at runtime. Two resolution methods are used in Operating systems by either specifying the *full path* or the filename of the target component. Using *full path*, operating systems simply locate the target from the given full path. With filename, operating systems resolve the target by searching a sequence of directories, determined by the runtime directory search order, to find the first occurrence of the component.

Operating systems might provide mechanisms to protect system resources. For example, Microsoft Windows supports Windows Resource Protection (WRP) to avoid system files from being replaced. However, these do not prevent loading of a malicious component located in a directory searched before the directory where the intended component resides.

In case an attacker sends a victim an archive file containing a document for a vulnerable program (e.g., a Word document) and a malicious DLL. If the victim opens the document after extracting the archive file, the vulnerable program will load the malicious DLL, which leads to remote code execution.

II. Unsafe Component Loading

This section describes dynamic loading of components, types of unsafe loadings and remote attack for vulnerable dynamic loading.

2.1 Dynamic Loading of Components

Software components often use functionalities exported by other components such as shared libraries at runtime. This operation is generally involves in three phases: **resolution, loading, and usage**. Specifically, an application resolves the needed target components, loads them, and utilizes the desired functions provided by them.

Component interoperation can be achieved through dynamic loading provided by operating systems or runtime environments. For instance, the **LoadLibrary** and **dlopen** system calls are used for dynamic loading on Microsoft Windows and Unix-like operating systems, respectively. Dynamic loading is mostly executed in two steps: **component resolution** and **chained component loading**.

2.1.1 Component Resolution

To resolve a target component, it is required to specify it correctly. Operating systems provide two types of target component specifications: **full path** and **filename**. For full path specification, operating systems resolve a target component based on the provided full path. For filename specification, operating systems obtain the full path of the target component from the provided file name and a dynamically determined sequence of search directories. Specifically, an operating system iterates through the directories until it finds a file with the specified file name, which is the resolved component. For example, suppose that a target component is specified as audmigplugin.dll and the directory search order is given as

C:\Program Files\iTunes; C:\Windows\System32; ...; $PATH on Microsoft Windows. If the first directory containing a file with the name audmigplugin.dll is C:\Windows\System32, the resolved full path is determined by this directory.

2.1.2 Chained Component Loading:

In dynamic loading, the full path of the target component is determined by its specification through the resolution process and the component is incorporated into the host software if it is not already loaded. During the process of incorporation the target component, the component's load-time dependent components are also loaded.

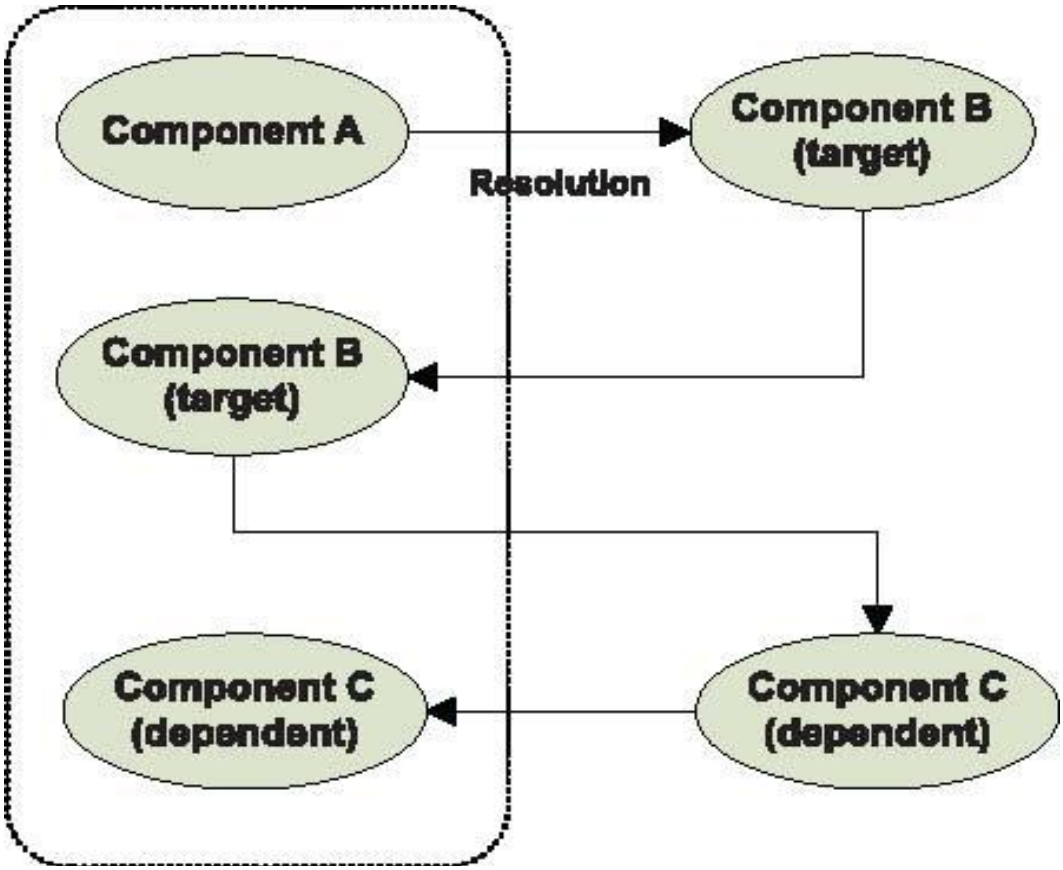

Fig. a. Dynamic component loading procedure

Fig. a, demonstrates the general procedure of dynamic loading. Suppose component B is loaded by component A. B's dependent components (component C) are also loaded. We can usually obtain information on B's dependent components from B's file description. This process of chained component loading is repeated until all dependent components are loaded.

2.2 Unsafe Component Resolution

Despite dynamic loading is a critical step in software execution, it also has an inherent security implication. Particularly, a loaded target component is only determined by the specified file name. This can lead to the loading of unintended or even malicious components and thus may allow arbitrary code execution. Two types of unsafe component resolution are classified, **resolution failure** and **unsafe resolution**, and illustrated their conditions in Table 1.

TABLE 1: Conditions for Detecting Unsafe Component Loadings

Type	**Conditions**
Resolution failure	• Target component not found
Unsafe resolution	• the target component specified by its file name,
	• the resolution is determined by iteratively searching a sequence of directories, and
	• There exists another directory searched before the one containing the target component.

III. Detection of Unsafe Components in Network System

Fig 2 - ARCHITECTURE DIAGRAM

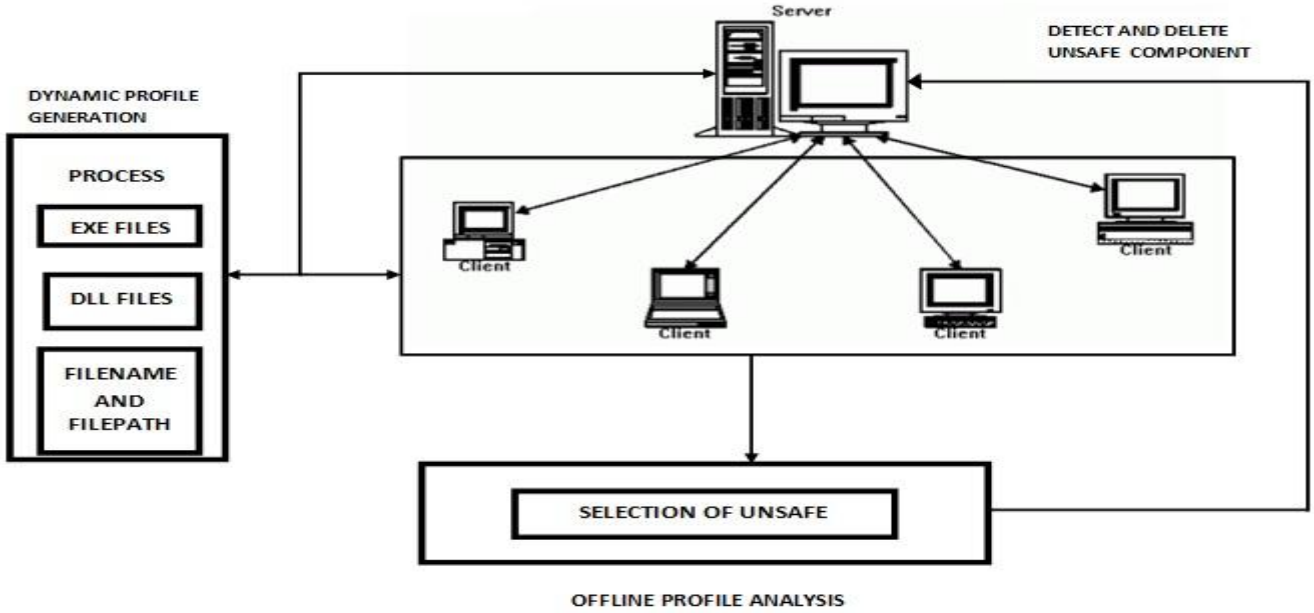

Fig. 2 shows the high-level overview of our analysis process, which is composed of two phases: dynamic profile generation and offline profile analysis.

3.1 Dynamic Profile Generation

We dynamically applied the binary executable analysis to capture a sequence of system level actions for dynamic loading of components. During the instrumented program execution, we collect three types of information: **system calls invoked for dynamic loading, image loading,** and **process and thread identifiers**. The collected information is stored as a profile for the instrumented application and is analyzed in the offline profile analysis phase.

The dynamic profile generated information extracted from the Client side to monitor the server by using the IP address. The server can monitor the dynamic loading to detection unsafe components and stop the vulnerable host.

3.2 Offline Profile Analysis

Firstly, we extract each component loading from the profile. First group a sequence of actions in the profile by process and thread identifiers as the actions performed by different threads may be interleaved due to context switching. This grouping separates the sequences of dynamic loadings performed by different threads. Then, we divide the sequence for each thread into subsequence of actions, one for each distinct dynamic loading. This can be achieved by using the first invoked system call for dynamic loading as a delimiter. Next, we obtain a list of groups, each of which contains a sequence of actions for loading a component at runtime. This gives the possible control flows in the dynamic loading procedure. Note that each group contains loading actions for both the target component and the load-time dependent components

Algorithm 1. OfflineProfileAnalysis
Input: S (a sequence of actions for a dynamic loading) Auxiliary functions:
Target Spec(S): return target specification of S
DirSearchOrder(S): return directory search order used
In S
ImgLoad(S): return the image loadings in S
Resolution Failure(S): return the resolution failures in S
Chained Loading(S): return actions for the chained
Loadings in S IsUnsafeResolution (filename, resolved path, search_dirs): check whether the resolution is unsafe
1: img_loads ImgLoad(S)
2: failed resolutions Resolution Failure(S)
3: if jimg_loadsj¼¼0 then
4: if jfailed_resolutionsj¼¼1 then
5: Report this loading as a resolution failure
6: end if
7: else
8: spec Target Spec(S)
9: dirs DirSearchOrder(S)
10: if spec is the filename specification then
11: resolved path img_loads [0].resolved path // retrieve the first load
12: if IsUnsafeResolution (spec, resolved_path, dirs) then

13: Report this loading as an unsafe resolution
14: end if
15: end if
16: chained loads Chained Loading(S)
17: for each load in chained loads do
18: OfflineProfileAnalysis (each load)
19: end for
20: end if

IV. Discussion and Conclusion

In this paper, we have described the analysis technique to detect unsafe dynamic component loadings in networked systems by using IP address. Our technique works in two phases. It first generates profiles to record a sequence of component loading behaviours at runtime using dynamic binary instrumentation. It then analyzes the profiles to detect two types of unsafe component loadings: resolution failures and unsafe resolutions. To assess our technique, we implemented tools to detect unsafe component loadings on Microsoft Windows and Linux. Our evaluation shows that unsafe component loadings are prevalent on both platforms and more severe on Windows platforms from a security perspective.

References

[1] "About Windows Resource Protection," http://msdn.microsoft. Com/en- us/library/aa382503 (VS.85).aspx, 2011.
[2] "Windows DLL Exploits Boom; Hackers Post Attacks for 40-Plus Apps," http://www.computerworld.com/s/article/9181918/ Windows_DLL_exploits_boom_hackers_post_attacks_for_40_ plus_apps, 2011.
[3] "Hacking Toolkit Publishes DLL Hijacking Exploit," http:// www.computerworld.com/s/article/9181513/Hacking_toolkit_ publishes_DLL_hijacking_exploit, 2011.
[4] T. Kwon and Z. Su, "Automatic Detection of Unsafe Component Loadings," Proc. 19th Int'l Symp. Software Testing and Analysis, pp. 107-118, 2010.
[5] "Zero-Day Windows Bug Problem Worse than First Thought, Says Expert," http://www.computerworld.com/s/article/9180978/ Zero_day_Windows_bug_pro blem_worse_than_first_thought_ says_expert, 2011.
[6] "Update: 40 Windows Apps Contain Critical Bug, Says Researcher," http://www.computerworld.com/s/article/9180901/ Update_40_Windows_apps_contain_critical_bug_says_ researcher, 2011.
[7] "Researcher Told Microsoft of Windows Apps Zero-Day Bugs 6 Months Ago," http://www.computerworld.com/s/article/ print/9181358/Researcher_told_Mi crosoft_of_Windows_apps_ zero_ day_bugs_6_months_ago, 2011.
[8] "Exploiting DLL Hijacking Flaws," http://blog.metasploit.com/ 2010/08/exploiting-dll-hijacking-flaws.html, 2011.
[9] "Microsoft Releases Tool to Block DLL Load Hijacking Attacks," http://www.computerworld.com/s/article/print/9181518/ Microsoft_releases_tool_to_block_DLL_load_hijacking_attacks, 2011.
[10] "About the Security Content of Safari 3.1.2 for Windows," http:// support.apple.com/kb/HT2092, 2011.
[11] "IE's Unsafe DLL Loading," http://www.milw0rm.com/ exploits/2929, 2011.
[12] "Microsoft Security Bull. MS09-014," http://www.microsoft. com/TechNet/security/Bulletin/MS09-014.mspx, 2011.
[13] "Microsoft Security Bull. MS09-015," http://www.microsoft. com/TechNet/security/Bulletin/MS09-015.mspx, 2011.
[14] B. Cornelissen, A. Zaidman, A. van Deursen, L. Moonen, and R. Koschke, "A Systematic Survey of Program Comprehension through Dynamic Analysis," IEEE Trans. Software Eng., vol. 35, no. 5, pp. 684-702, Sept./Oct. 2009.
[15] C.-K. Luk, R. Cohn, R. Muth, H. Patil, A. Klauser, G. Lowney, S. Wallace, V.J. Reddi, and K. Hazelwood, "Pin: Building Customized Program Analysis Tools with Dynamic Instrumentation,"Proc. ACM SIGPLAN Conf. Programming Language Design and Implementation, pp. 190-200, 2005.

International Journal of Modern Engineering Research (IJMER)
www.ijmer.com Vol.3, Issue.2, March-April. 2013 pp-626-632 ISSN: 2249-6645

Energy and Exergy Analysis of Extraction cum Back Pressure Steam Turbine

A.H.Rana[1], J.R.Mehta[2]
[1]*M.E.Mech (Scholar), Mechanical Engineering Department, Faculty of Technology and Engineering, The M.S.Unirsity of Baroda, Vadodara, Gujarat (India).*
[2]*Asst.Professor, Mechanical Engineering Department, Faculty of Technology and Engineering, The M.S.Unirsity of Baroda, Vadodara, Gujarat (India).*

Abstract: *Power is very vital factor for development of any society. Coal shares major chunk of fuels used to produce power in thermal power plants in India. Coal reserves are limited and present coal consumption rate is in increasing trend to fulfill the power demand. Therefore energy efficiency and energy conservation are of prime importance. Moreover, fossil fuel based power plant has significant negative environmental impacts. Energy and exergy analysis are used to analyze the performance of thermal systems. Energy analysis deals with quantity aspect whereas exergy analysis deals with quality aspect in addition to quantity. Exergy analysis focuses on magnitude and true location of energy loss. In this analysis, energy efficiency, exergy destruction, exergy efficiency and turbine heat rate are evaluated at 70 % and 85 % maximum continuous rating (MCR) of steam turbine. Analysis shows that operating turbine at 85 % MCR attract heat rate improvement by 17.01 kJ / kWh, which reduces CO_2 emission by 26.89 kg/h, SO_2 emission by 26.89 kg/h and ash generation by 41.47 kg/ day.*

Keywords: *Energy, Efficiency, Exergy, Exergy destruction, Power plant, Emission*

I. INTRODUCTION

Steam power plants supply 57 % of total power demand in India. Coal is the major source of energy in these power plants. The conversion efficiency from coal to electricity in steam power plants is low and combustion of coal has heavy negative impact on environment [1]. Efficiency enhancement of coal to electric power generation is major challenge against steam power plants. Thus, inefficient use of coal not only wastes resources but creates environmental pollution issues such as CO_2, SO_2 and NO_x emissions.

Energy conservation study is many times focused on energy efficiency. The first law of thermodynamics is used to analyze the energy utilization. First law analysis doesn't use the quality aspect of energy. Exergy is the consequent of second law of thermodynamics. It is a property that enables us to determine the useful work potential in a given amount of energy at reference environmental state. A thorough understanding of exergy can provide insights into the efficiency, environmental impact and sustainability of energy systems. Exergy analysis is now widely used in design, simulation and performance evaluation of thermal and thermo-chemical systems [2, 3].

Cogeneration turbine systems, which produce heat at useful temperatures at the expense of reduced electrical power, have higher efficiencies than conventional steam turbine systems. The correct merit of cogeneration systems should be determined with the help of exergy analysis because energy analysis tends to overstate performance.

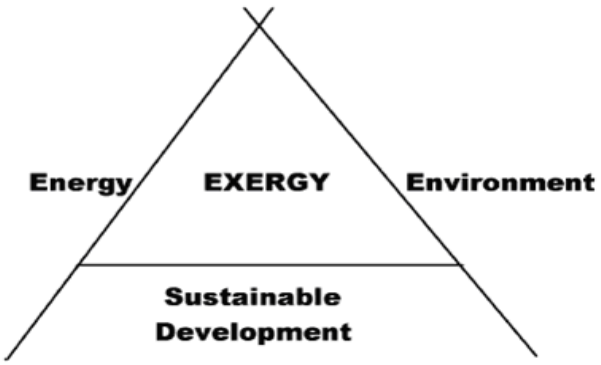

Fig.1 Interdisciplinary triangle covered by exergy analysis [4]

In the steam turbine under study, steam is first expanded from inlet pressure to extraction pressure in seven stages. The extracted high pressure and exhausted low pressure steam is being used in process heating of soda ash manufacturing. Remaining steam expands up to exhaust pressure. Steam turbine system is usually analyzed by energy analysis which uses first law analysis but better understanding is attained when a more complete thermodynamic view is taken, which utilises ***the second law of thermodynamics in conjunction with energy analysis, via exergy methods*** [5].

This study is focused on energy and exergy analysis of 20.6 MW Extraction cum Back Pressure Steam Turbine. Energy efficiency, exergy destruction and exergy efficiency are worked out at two different load conditions such as 70 % and 85 % of MCR. The turbine heat rate is also evaluated for both load conditions. The effect of turbine heat rate improvement on coal consumption and environment pollution such as CO_2 and SO_2 emissions are also discussed.

II. Methodology

This section presents equations for energy and exergy analysis. It also presents schematic diagram (Fig.2) and experimental data (Tab. I).

1. Energy and second law efficiency (exergy efficiency) relations

The expressions of energy and exergy efficiencies for the extraction cum back pressure steam turbine (cogeneration) are based on the following definitions [6].

$$\eta_{I} = (\text{Actual Power Develop by Turbine Shaft}) / (\dot{E}_{in} - \dot{E}_{out}) \quad (1)$$

$$\eta_{II} = \Psi_{Power} / (\Psi_{in} - \Psi_{out}) = \Psi_{power} / [\dot{m}_i (h_i - T_o s_i) - (\dot{m}_o (h_o - T_o s_o)] \quad (2)$$

2. The reference environment

Exergy is always evaluated with respect to a reference environment. The reference environment is in stable equilibrium, acts as an infinite system and is a sink or source for heat and materials. It experiences only internal reversible processes, in which its intensive properties (i.e. temperature T_0, pressure P_0) remains constant. In this analysis surrounding temperature and pressure are taken as T_0=34^{0}C (307 K) and P_0=101.325 kPa as based on weather and climate condition at Bhavnagar, Gujarat (India).

3. Data of Steam Turbine

Data for study is taken at 70 and 85 % MCR of Extraction cum Back Pressure Steam Turbine working at Nirma Ltd., Bhavnagar, Gujarat. The boiler of this power plant is fired by coal blend having lignite (70%) + Indonesian coal (30%) and coal firing rate is 10.5 kg/s. The ultimate analysis of coal blend is as follows: C - 44.65 %, N - 1.21 %, H - 3.06 %, O - 10.8 %, S - 1.87 %, Ash - 10.5 %, Moisture - 27.78 % and GCV of coal is 4226 kcal/kg (17664.68 kJ/kg).

TABLE I

EXPERIMENTAL DATA OF STEAM TURBINE

Sr. No.	Particular	Unit	Value at 70 % MCR	Value at 85 % MCR
1	Main Steam Flow	kg/s	40.75	43.05
2	Main Steam Pressure	kg/cm^2	104.9	107
3	Main Steam Temperature	^{o}C	492	497
4	Enthalpy of Inlet Steam	kJ/kg	3347.3	3357.7
5	Entropy of Inlet Steam	kJ/kg K	6.54	6.54
6	HP Extraction Flow	kg/s	22.47	18.33
7	HP Extraction Temperature	^{o}C	360.5	360
8	HP Extraction Pressure	kg/cm^2	34.48	34
9	Enthalpy of HP Ext. Steam	kJ/kg	3129.3	3129.1
10	Entropy of Inlet HP Ext.Steam	kJ / kg K	6.68	6.69
11	LP Extraction Flow	kg/s	18.28	24.72
12	LP Extraction Temperature	^{o}C	126	125
13	LP Extraction Pressure	kg/cm^2	1.6	1.72
14	Enthalpy of LP Exh. Steam	kJ / kg	2716.8	2712
15	Entropy of Inlet LP Exh. Steam	kJ / kg K	7.03	7.07
16	Generator Power	kW	13875	17100

Assumptions:

1. There is no steam loss across steam turbine.
2. Gear box efficiency as per the manufacturer is 98.40 %
3. Generator efficiency as per the manufacturer is 98.03 %
4. High pressure extracted steam and low pressure exhaust steam from turbine is utilised in process heating of soda ash manufacturing.

4. STEAM TURBINE MAIN SPECIFICATIONS

Manufacturer: Hang Zhou Steam Turbine Co. Limited, China
Model & Type: EHNG 50/40/50
Nominal Rating: 20600 kW
Nominal Speed: 5022 rpm
Normal first bled steam pressure: 35 bar
Normal first bled steam temperature: 366^0C
Normal exhaust steam pressure: 2.5 bar
Normal exhaust steam temperature: 133^0C
Number of stages: (1+23) / (Impulse + Reaction)
Governor manufacturer: Wood Ward
Governor type: Electric & Hydraulic

5. SCHEMATIC DIAGRAM OF STEAM TURBINE

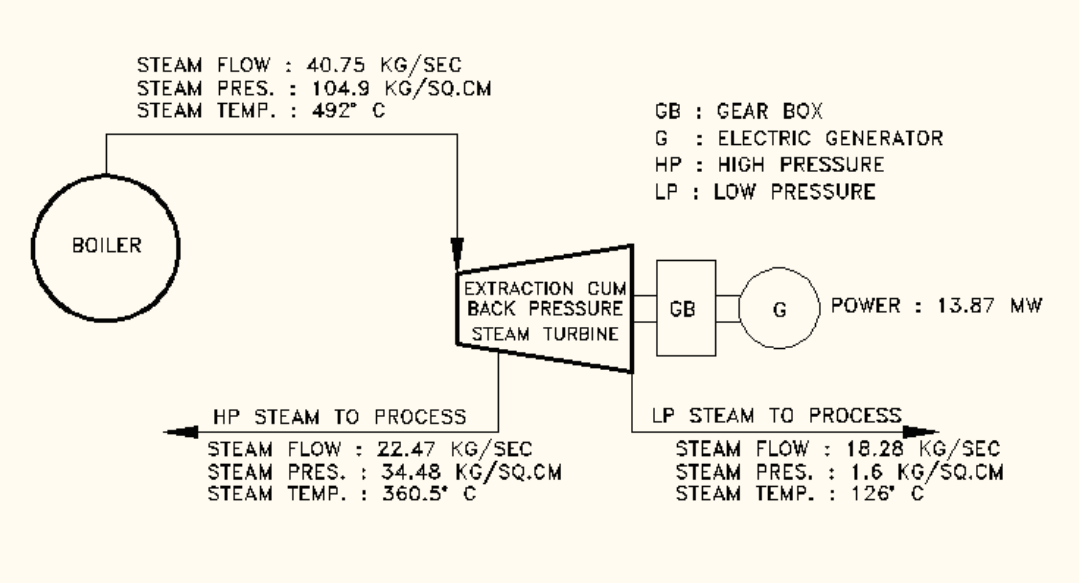

Fig.2 Process Flow Diagram of Steam Turbine

III. Analysis

A. ENERGY ANALYSIS FOR 70 % MCR

1. Energy input is equal to product of mass of steam into turbine and its enthalpy at entry.

$$\dot{E}_i = \dot{m}_i \times h_i \quad (3)$$
$$= 40.75 \text{ kg/s} \times 3347.3 \text{ kJ/kg}$$
$$= 136402.475 \text{ kJ/s.}$$

2. Energy output is sum of heat extracted and heat exhausted.

$$\dot{E}_o = (\dot{m}_{ext} \times h_{ext}) + (\dot{m}_{exh} \times h_{exh}) \quad (4)$$
$$= (22.47 \text{ kg/s} \times 3129.3 \text{ kJ/kg}) + (18.28 \text{ kg/s} \times 2716.8 \text{ kJ/kg})$$
$$= 119978.480 \text{ kJ/s.}$$

3. Work done is equal to the energy in steam at entry to turbine minus that at exit.

$$W.D = \dot{E}_i - \dot{E}_o \quad (5)$$
$$= 136402.475 \text{ kJ/s} - 119978.480 \text{ kJ/s}$$
$$= 16424.00 \text{ kW.}$$

4. Actual Power Develop by Turbine Shaft :

$$P = \text{Generator Power} \times \eta^{-1}_{gearbox} \times \eta^{-1}_{generator} \quad (6)$$
$$= 13875 \text{ kW} \times (0.984)^{-1} \times (0.9803)^{-1}$$
$$= 14380 \text{ kW.}$$

5. Energy Efficiency (1st Law efficiency) of Turbine :

η_I = (Actual Power Develop by Turbine Shaft) / ($\dot{E}_{in}$ - $\dot{E}_{out}$) (7)
= 14380 kW / (136402.475 kJ/s-119978.480 kJ/s)
= 87.56 %.

6. Heat Rate of Turbine [7] :

HR = Net Heat Input / Turbine Power (8)
= ($\dot{E}_i$ - $\dot{E}_o$) x 3600 s / 14380 kWh
= (136402.475 kJ/s - 119978.480 kJ/s) x 3600 / 14380 kWh
= 4111.71 kJ/kWh.

B. EXERGY ANALYSIS FOR 70 % MCR

1. Exergy Input :

$\Psi_{in} = \dot{m}_s (h_s - T_0 s_s)$ (9)
= 40.75 kg/s x [3374.3 kJ/s - (307 K x 6.54 kJ/kg K)]
= 55685.690 kJ/s.

2. Exergy Out :

$\Psi_{out} = \dot{m}_{ext} (h_{ext} - T_0 S_{ext}) + \dot{m}_{exh} (h_{exh} - T_0 S_{exh})$ (10)
= 22.47 kg/s x [3129.3 kJ/s - (307 K x 6.68 kJ/kg K)] +18.28 kg/s x [2716.8 kJ/s - (307 K x 7.03 kJ/kg K)]
= 34445.819 kJ/s.

3. Exergy Destruction in Turbine :

$\Psi_{des} = \Psi_{in} - \Psi_{out} - \Psi_{power}$ (11)
= 55685.690 kJ/s – 34445.819 kJ/s – 14380 kW
= 6859.87 kJ/s.

4. Exergy Efficiency (2nd Law efficiency) of Cogeneration Turbine :

$\eta_{II} = \Psi_{power} / (\Psi_{in} - \Psi_{out})$ (12)
= 14380 kW / (55685.690 kJ/s -34445.819 kJ/s)
= 67.70 %

C. ENERGY ANALYSIS FOR 85 % MCR

1. Energy input is equal to product of mass of steam into turbine and its enthalpy at entry.

$\dot{E}_i = \dot{m}_i \times h_i$ (13)
= 43.05 kg/s x 3357.7 kJ/kg
= 144548.985 kJ/s.

2. Energy output is sum of heat extracted and heat exhausted.

$\dot{E}_o = (\dot{m}_{ext} \times h_{ext}) + (\dot{m}_{exh} \times h_{exh})$ (14)
= (18.33 kg/s x 3129.1 kJ/kg) + (24.72 kg/s x 2712 kJ/kg)
= 124397.043 kJ/s.

3. Work done is equal to the energy in steam at entry to turbine minus that at exit.

W.D = $\dot{E}_i - \dot{E}_o$ (15)
= 144548.985 kJ/s -124397.043 kJ/s
= 20151.942 kW.

4. Actual Power Develop by Turbine Shaft :

P = Generator power x $\eta^{-1}_{gearbox}$ x $\eta^{-1}_{generator}$ (16)
= 17100 kW x $(0.984)^{-1}$ x $(0.9803)^{-1}$

= 17720 kW.

5. Energy Efficiency (1st Law efficiency) of Turbine :

η_I = (Actual Power Develop by Turbine Shaft) / ($\dot{E}_{in}$ - $\dot{E}_{out}$) (17)
= 17720 kW / (144548.985 kJ/s- 124397.043 kJ/s)
= 87.94 %.

6. Heat Rate of Turbine :

HR = Net Heat Input / Turbine Power (18)
= ($\dot{E}_i$ - $\dot{E}_o$) x 3600 / 17720 kWh
= (144548.985 kJ/s - 124397.043 kJ/s) x 3600 / 17720 kWh
= 4094.07 kJ/kWh.

D. EXERGY ANALYSIS FOR 85 % MCR

1. Exergy Input :

$\Psi_{in} = \dot{m}_s (h_s - T_0 s_s)$ (19)
= 43.05 kg/s x [3357.7 kJ/s - (307 K x 6.54 kJ/kg K)]
= 58114.05 kJ/s.

2. Exergy Out :

$\Psi_{out} = \dot{m}_{ext} (h_{ext} - T_0 s_{ext}) + \dot{m}_{exh} (h_{exh} - T_0 s_{exh})$ (20)
= 18.33 kg/s x [3129.1 kJ/s-(307 K x 6.69 kJ/kg K)] + 24.72 kg/s x [2712 kJ/s -(307 K x 7.07 kJ/kg K)]
= 33095.82 kJ/s.

3. Exergy Destruction in Turbine :

$\Psi_{des} = \Psi_{in} - \Psi_{out} - \Psi_{power}$ (21)
= 58114.05 kJ/s - 33095.81 kJ/s - 17720 kW
= 7298.24 kJ/s.

4. Exergy Efficiency (2nd Law efficiency) of Cogeneration Turbine :

η_{II} = Ψ_{power} / (Ψ_{in} - Ψ_{out}) (22)
= 17720 kW / (58114.05 kJ/s -33095.82 kJ/s)
= 70.83 %.

E. CO_2 AND SO_2 EMISSION REDUCTION BY TURBINE HEAT RATE IMPROVEMENT

1. Coal Saving = HR Improvement x Generator Power / GCV (23)
= 17.01 kJ/ kWh x 17100 kW / 17664.68 kJ/kg
= 16.46 kg/h.

2. Combustion Equation : $C + O_2 = CO_2$ (24)

3. 1 kg Carbon Generates 3.66 kg of CO_2 [8]

4. CO_2 Emission Reduction =3.66 x Carbon percentage in coal x Coal saving (25)
= 3.66 x 0.4465 x 16.46 kg/h
= 26.89 kg/h

5. 1 kg Sulphur Generates 2 kg of SO_2 [9]

6. SO_2 Emission Reduction = 2 x Sulphur percentage in coal x Coal saving (26)
= 2 x 0.0187 x 16.46 kg/h
= 0.62 kg/h.

F. ASH GENERATION REDUCTION BY TURBINE HEAT RATE IMPROVEMENT

1. Ash Generation Reduction = Coal saving x Ash percentage in coal (27)
= 16.46 kg/h x 0.105 = 1.72 kg/h x 24 h/day = 41.47 kg/day

IV. Result And Discussion

TABLE II
EXPERIMENTAL RESULTS

Sr. No	20.6 MW Extraction Cum Back Pressure Steam Turbine		
	Particulars	**Value at 70 % MCR**	**Value at 85 % MCR**
1	Energy Efficiency (%)	87.56	87.94
2	Exergy Destruction (kJ/s)	6859.87	7298.24
3	Heat input (kJ/s)	136402.475	144548.985
4	Useful heat output (kJ/s)	119978.480	124397.043
5	Turbine Work output (Kw)	14380	17720
3	Exergy Efficiency (%)	67.70	70.83
4	Heat Rate (kJ/kWh)	4111.71	4094.07
5	CO_2 emission reduction	26.89 kg/h	
6	SO_2 emission reduction	0.62 kg/h	
7	Ash generation reduction	41.47 kg/day	

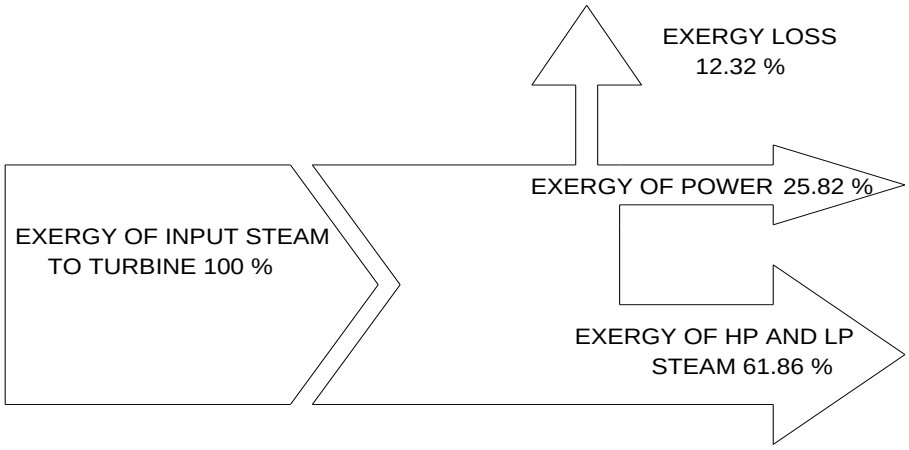

Fig.3 Grassman diagram for exergy flow through Steam Turbine at 70 % MCR

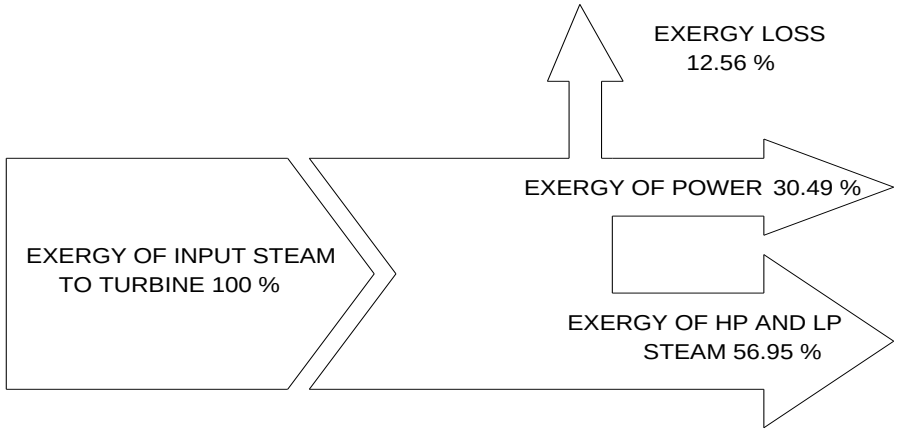

Fig.4 Grassman diagram for exergy flow through Steam Turbine at 85 % MCR

- **Experimental results show that as power load on steam turbine increases from 70 % to 85 % MCR**,

1. Turbine's energy and exergy efficiency increases by 0.38 % and 3.13 %.
2. The exergy destruction is increased by 438.34 kJ/s due to steam turbine irreversibilities and lower exergy output of HP and L.P.Steam.
3. The exergy efficiency is remarkably lower than energy efficiency in both the cases. This is mainly due to thermal product, which is higher than electrical power, is delivered at a lower temperature.
4. There is an improvement observed in turbine heat rate by 17.01 kJ/kWh.
5. Coal saving achieved due to heat rate improvement is 395 kg/day.
6. Ash handling plant load is reduced by 41.47 kg/day. This improves life of plant because ash is highly erosive in nature. It creates mechanical wear during handling.
7. Heat rate improvement lead to CO_2 emission reduction by 26.89 kg/h and SO_2 emission reduction by 0.62 kg/h.

V. Conclusion

Turbine exergy efficiency is lower than its energy efficiency as utilization of heat is at lower temperature than inlet. Turbine exergy loss is 12.32 % and 12.56 % at 70 % and 85 % MCR. When Turbine MCR is increased from 70 to 85%, coal consumption is reduced by 16.46 kg/h and ash handling plant load is reduced by 41.47 kg/day. CO_2 emission is reduced by 26.89 kg/h, while SO_2 emission is reduced by 0.62 kg/h. Thus, it is more advantageous to run turbine at higher MCR.

VI. Acknowledgment

The support for this work provided by Shri G.J Adroja, Shri D.G.Jakhade, Shri L.M.Mavani, Shri D.R.Fondekar, Shri K.N.Pandya and Shri H V Mendpara of The Nirma Ltd, Kalatalav, Bhavnagar, Gujarat (India) is gratefully acknowledged.

Nomenclature

$\dot{E}_i$ - Energy in [kJ/s], $\dot{E}_{out}$ - Energy out [kJ/s], Ψ_{in} - Exergy in [kJ/s], Ψ_{out} - Exergy out [kJ/s], Ψ_{des} - Exergy destruction [kJ/s] Ψ_{power} - Exergy of power [kJ/s], $\dot{m}$ - Mass flow rate [kg/s], h - Specific enthalpy [kJ/kg], s - Specific entropy [kJ/kg K], P -Turbine actual power [kW], T_0 -Atmospheric temperature [K], P_0 -Atmospheric pressure [kPa] , i - Inlet, o – Outlet, η_I - Energy efficiency [%], η_{II} - Exergy efficiency [%], HR- Heat rate [kJ/kWh], ext - steam extraction, exh - steam exhaust,

MCR - Maximum continuous rating, GCV - Gross calorific value [kJ/kg], C – Carbon, H – Hydrogen , O – Oxygen, N – Nitrogen, S – Sulphur, SO_2 - Sulphur dioxide, CO_2 - Carbon dioxide, NO_x - Nitrogen oxide, HP – High pressure, LP – Low pressure.

References

Web Page:

[1] Ministry of Power, Govt. of India, Web site,www.powermin.nic.in/Indian_electricity_scenario. (Accessed on 7 December 2012)

Journal Papers:

[2] Ganapathy T, Alagumurthi N, Gakkhar RP, Murugesan K. Exergy analysis of operating lignite fired thermal power plant. Journal of Engineering Science and Technology Review 2009; 2:123–30.

[3] Kanoglu, M, Dincer, I, Rosen, M A., 2007, "Understanding energy and exergy efficiencies for improved energy management in power plants". Energy Policy 35, 3967–3978.

[4] Rosen, M.A., Dincer I.2001.Exergy as the confluence of energy, environment and sustainable development .Exergy, an International Journal 1(1), 3-13.

[6] Sanjay Y., Singh O., and Prasad B.N., 2007, "Energy and Exergy Analysis of Steam Cooled Reheat Gas Steam Combined Cycle," Applied Thermal Engineering, 27, pp. 2779-2790.

Chapters in Books:

[5] I.Dincer and M.Rosen,"Energy, Exergy and Sustainable Development", Elsevier, 2007, Chap- 12,257-265

[7] Bureau of Energy Efficiency, Ministry of Power Govt. of India, Energy Auditor guide book volume- 4,2005,Chap-3,45-53.

[8] P Chattopadhyay,"Boiler Operation Engineering", 2nd edition, McGraw-Hill, 2000, Chap-10,314.

[9] N.C.Pandya and NC.S.Shah, "Heat Engines", 9th edition, Charotar Publishing House, Anand, 1990, Chap-13,594.

International Journal of Modern Engineering Research (IJMER)
www.ijmer.com Vol.3, Issue.2, March-April. 2013 pp-633-636 ISSN: 2249-6645

Modal Analysis of Adhesively Bonded Joints of Different Materials

Y. B. Patil, [1] R. B. Barjibhe[2]
[1]S.S.G.B.C.O.E. & T; Department of Mechanical Engineering, Bhusawal-425203, North Maharashtra University, Maharashtra, India
[2]Faculty of S.S.G.B.C.O.E. & T; Department of Mechanical Engineering, Bhusawal-425203, North Maharashtra University, Maharashtra, India

Abstract: *It is important to study the modal analysis (natural frequency and mode shape) of the single lap adhesive joint to understand the dynamic nature of the systems, and also in design and control. In this work modal analysis of bonded beams with a single lap epoxy adhesive joint of plates are investigated. The three specimen are used which consist of Al-Al plates, Cu-Cu plates and Ms-Ms plates. ANSYS 11.0 finite element software is use for modal analysis of single lap adhesive joint. The results show that the natural frequencies are directly proportional to the Young's modulus and Density ratio.*

I. Introduction

In the 1940s, adhesive bonding become importance in structural bonding in aircraft industry. The subject of adhesives became even more interesting to scientists when the application of synthetic resins as adhesives for wood, rubber, glass and metals were discovered. Adhesive bonding as an alternative method of joining materials together has many advantages over the more conventional joining methods such as fusion and spot welding, bolting and riveting. Adhesive bonding is gaining more and more interest due to the increasing demand for joining similar or dissimilar structural components, mostly within the framework of designing light weight structures. The current trends are to use viscoelastic material in the joints for passive vibration control in the structures subjected to dynamic loading. These components are often subjected to dynamic loading, which may cause initiation and propagation of failure in the joint. In order to ensure the reliability of these structures, their dynamic response and its variation in the bonded area must be understood.

In adhesive joint the major function of adhesive is to transmit loads from one member of joint to another. It allows a more uniform stress distribution than is obtained by another mechanical joining process such as welding, bolting, riveting, etc. Thus, adhesive often permit the fabrication of structures that are mechanical equivalent or superior to conventional assembles and furthermore cost and weight benefits. The conventional joining process increase the weight of the structure by adding extra material such as bolt, screws, extra filler material. If you want to joint two plate by bolting then hole is created in the plate which result in stress concentration or if you joint by weld then there is localized heating of the component take place which alter its mechanical properties. In adhesive joining process you do not need to create the hole in the plate or there is no localized heating take place. Thus adhesive bonding gaining more importance in joining process where you have to avoid stress concentration and avoid localized heating. In addition adhesive can produce joints with high strength, rigidity, dimensional precision in the light metals, such as aluminum and magnesium, which may be weakened or distorted by welding. Adhesive can also prevent electrochemical corrosion between dissimilar metals.

II. Adhesive Bond

2.1Adhesive Bonding:

Adhesive bonding is a material joining process in which an adhesive, placed between the adherend surfaces, solidifies to produce an adhesive bond (Figure1). When we bond components together the adhesive first thoroughly wets the surface and fills the gap between, then it solidifies. When solidification is completed the bond can withstand the stresses of use. The strongest adhesives solidify through chemical reaction and have a pronounced affinity for the joint surfaces. Adhesives come in several forms thin liquids, thick pastes, films, powders, pre-applied on tapes, or solids that must be melted. Adhesive can be designed with a wide range of strengths, all the way from weak temporary adhesives for holding papers in place to high strength structural systems that bond cars and airplanes. Now a day's adhesive compete with mechanical fastening systems such as nuts, bolts, and rivets, or welding and soldering.

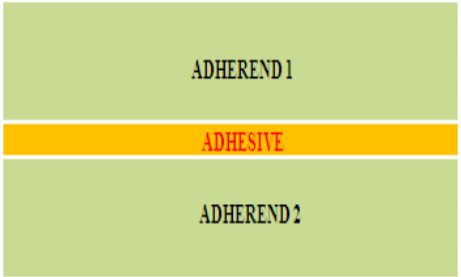

Figure 1: Adhesive Bond.

2.2. Epoxy adhesive:

Epoxy adhesives consist of an epoxy resin plus a hardener. Upon cure, epoxies typically form tough, rigid thermo-set polymers with high adhesion to a wide variety of substrates and superior environmental resistance. When using a one-part heat-cure system, the resin and a latent hardener are supplied already mixed and typically need to be stored refrigerated or frozen. By heating the system, the latent hardener is activated causing cure to initiate. The epoxy will normally start to cure rapidly at temperatures of 100 to 125°C (212 to 257°F) and cure times of 30 to 60 minutes are typical. Heat curing also generally improves bond strengths, thermal resistance and chemical resistance. When using a two-part system, the resin and hardener are packaged separately and are mixed just prior to use. This allows more active hardeners to be used so that the two-part epoxies will rapidly cure at ambient conditions.

III. Problem Definition

Natural, free vibration is a manifestation of the oscillatory behavior in mechanical systems, as a result of repetitive interchange of kinetic and potential energies among components in the system. Proper design and control are crucial in maintaining high performance level and production efficiency, and prolonging the useful life of machinery, structures, and industrial processes. Before designing or controlling an engineering system for good vibratory performance, it is important to understand, represent (model), and analyze the vibratory characteristic of the system.

An engineering system, when given an initial disturbance and allowed to execute free vibrations without a subsequent forcing excitation, will tend to do so at a particular "preferred" frequency and maintaining a particular "preferred: geometric shape. This frequency is termed a "natural frequency" of the system, and the corresponding shape of the moving parts of the system is termed a "mode shape". Any arbitrary motion of a vibrating system can be represented in terms of its natural frequencies and mode shapes. The subject of modal analysis primarily concerns determination of natural frequencies and mode shapes of a dynamic system. Once the modes are determined, they can be used in understanding the dynamic nature of the systems, and also in design and control. Therefore modal analysis is extremely important in vibration engineering.

Vibration testing is useful in a variety of stages in the development and utilization of a product. In the design and development stage, vibration testing can be use to design, develop, and verify the performance of individual components of a complex system before the overall system is assembled and evaluated.

IV. Methodology

In this work modal analysis of bonded beams with a single lap epoxy adhesive joint of plates are investigated. The three specimen are used which consist of Al-Al plates, Cu-Cu plates and Ms-Ms plates. The two sets of adherends use are aluminium plates of dimension 140 mm long, 38 mm wide, 5mm thickness; copper plates of dimension 140 mm long, 38 mm wide, 5mm thickness and mild steel plates of dimension 140 mm long, 38 mm wide, 5mm thickness. The araldite epoxies adhesive is use which consists of hardener and strainer. Both hardener and resin mixed with equal volume to form the adhesive paste which is use for preparation of specimen.

V. Modal Analysis

If the structural vibration is of concern in the absence of time-dependent external loads, a modal analysis is performed. Modal analysis determines the vibration characteristics of structure or machine components while it is being designed. The vibration characteristics (natural frequencies and mode shapes) are important in the design of the structure for dynamic loading conditions.

5.1Result and Discussion:

In this work modal analysis of bonded beams with a single lap epoxy adhesive joint of plates are investigated. The three specimen are used which consist of Al-Al plates, Cu-Cu plates and Ms-Ms plates. For present study the overlap length of 15mm is use for single lap adhesive joint. The Modal analysis had been done by using ANSYS 11.0 FEA software. The first five natural frequencies corresponding to different materials of single lap epoxy adhesive joints are shown in Table 1. The comparisons of frequency with respect to mode shapes are shown by Figure2.

Table 1: Comparative Table of Single Lap Adhesive Joint

Frequency Hz			
Mode shape	Cu-Cu	Al-Al	Ms-Ms
First	42.062	59.002	58.203
Second	260.68	366.40	358.80
Third	299.55	422.32	415.41
Fourth	553.95	788.39	783.35
Fifth	734.11	1029.3	1016.5

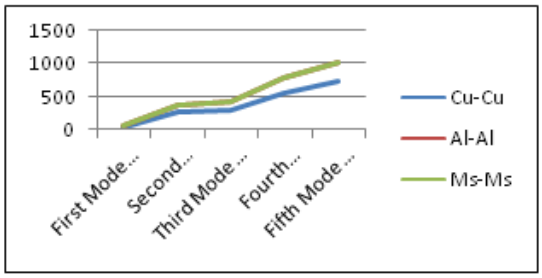

Figure2 Comparison of Frequency With Respect To Mode

The result show that natural frequencies are changing as the materials are changing of single lap adhesive joint. The result shows that the natural frequencies are depend on Young's modulus (E) and Density (ρ) ratio. The Young's modulus (E) and Density (ρ) ratio of Al-Al single lap adhesive joint is 0.025. The Young's modulus (E) and Density (ρ) ratio of Cu-Cu single lap adhesive joint is 0.013. The Young's modulus (E) and Density (ρ) ratio of Ms-Ms single lap adhesive joint is 0.025. As the ratio of the Young's modulus (E) and Density (ρ) of Al-Al single lap adhesive joint and Ms-Ms single lap adhesive joint are same therefore their natural frequencies are nearby same which is shown by Table 1 and Figure2. The Young's modulus (E) and Density (ρ) ratio of Cu-Cu single lap adhesive joint is different from Al-Al single lap adhesive joint and Ms-Ms single lap adhesive joint therefore the natural frequencies of Cu-Cu single lap adhesive joint are different than the Al-Al single lap adhesive joint and Ms-Ms single lap adhesive joint. The Fig.3- 5 shows the mode shapes for different material of single lap adhesive joint. The inspection of mode shapes shows that most of the mode shapes are similar for different material of single lap adhesive joint.

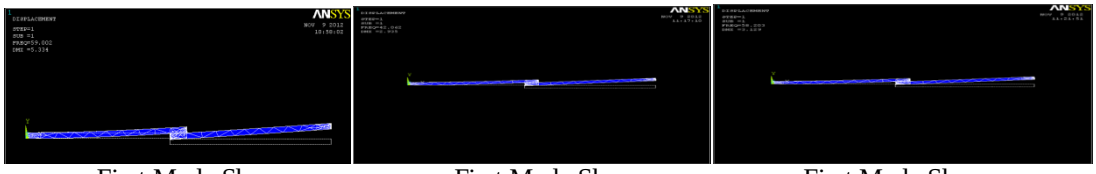

First Mode Shape First Mode Shape First Mode Shape

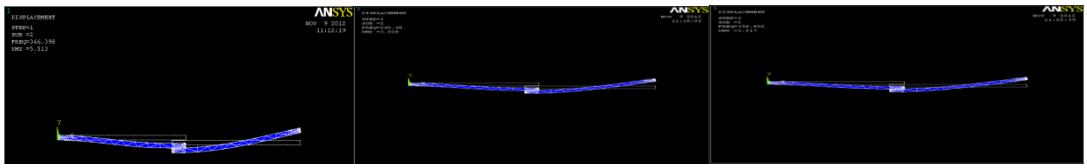

Second Mode Shape Second Mode Shape Second Mode Shape

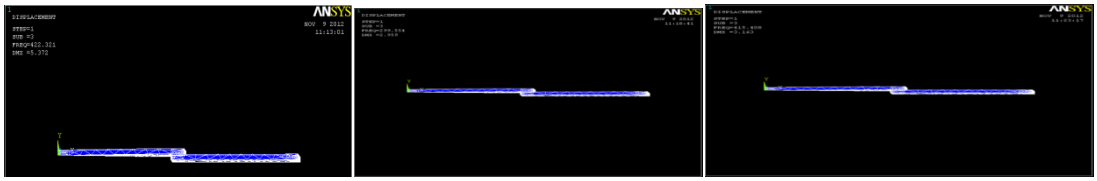

Third Mode Shape Third Mode Shape Third Mode Shape

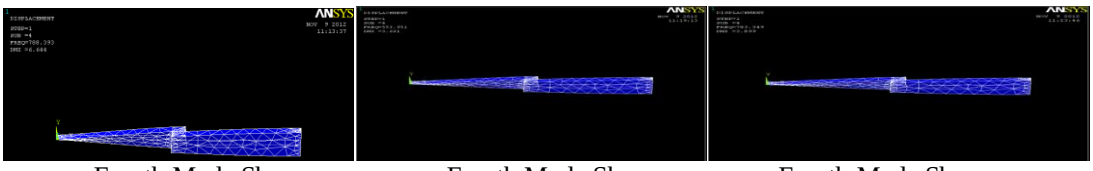

Fourth Mode Shape Fourth Mode Shape Fourth Mode Shape

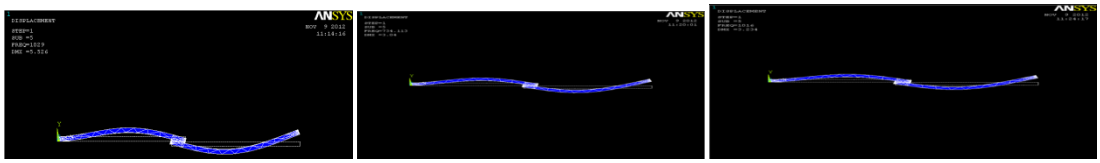

Fifth Mode Shape Fifth Mode Shape Fifth Mode Shape

Figure 3 Mode Shapes of Al-Al Single Lap Adhesive Joint.

Figure 4 Mode Shapes of Cu-Cu Single Lap Adhesive Joint.

Figure5 Mode Shapes of Ms-Ms Single Lap Adhesive Joint.

VI. Conclusion

Adhesive bonding as an alternative method of joining materials together has many advantages over the more conventional joining methods such as welding, bolting and riveting. For example, adhesives can be used to bond dissimilar materials, adhesive joints have a high stiffness to weight ratio and the stress distribution within the joint is much improved. Corrosion and vibration stress associated with mechanical fasteners and welds can be reduced or eliminated by forming continuous adhesive joint. It is important to study the modal analysis (natural frequency and mode shape) of the single lap adhesive joint to understand the dynamic nature of the systems, and also in design and control. The results show that the natural frequencies are directly proportional to the Young's modulus and Density ratio. If this ratio is increasing the natural frequencies are increasing for respective mode shapes.

The natural frequencies and mode a shape gives designer/engineers an idea of how the design will respond to different types of dynamic loads. This allows to designer/engineer to change the design to avoid resonant vibrations or to vibrate at a specified frequency. Also helps in calculating solution controls (time steps, etc.) for other dynamic analyses. It is conclude that the FEA of dynamic response of the bonded beams with a single lap joint will help future applications of adhesive bonding by allowing different parameters to be selected to give as large as a process window as possible for bonded beams vibration analysis.

References

[1] Xiaocong He, "Numerical and experimental investigations of the dynamic response of bonded beams with a single-lap joint", International Journal of Adhesion and Adhesive, vol. 37, pp 79-85, 2012
[2] R.A.Deshmukh, S.A. Sonawane, " Vibration analysis of adhesively bonded lap joint", Proc. of Int. Conf. on Advances in Robotics, Mechanical Engineering and Design, pp 27-29, 2011.
[3] Recep Gunesa, M Kemal Apalaka, Mustafa Yildirim and Ismail Ozkes, " Free vibration analysis of adhesively bonded single lap joints with wide and narrow functionally graded plates", Journal on Composite Structures, vol. 92, pp 1-17, 2010.
[4] M.A. De Rosa, M. Lippiello, M.J. Maurizi, H.D. Martin, "Free vibration of elastically restrained cantilever tapered beams with concentrated viscous damping and mass", Journal of Mechanics Research Communications, vol. 37, pp 261–264, 2010.
[5] A. Vaziri, H Nayeb-Hashemi, H.R. Hamidzadeh, "Experimental and Analytical Investigations of the Dynamic Response of Adhesively Bonded Single Lap Joints", Journal of Vibration and Acoustics, vol. 126, pp. 84-91, 2004.
[6] A. Vaziri, H.R. Hamidzadeh, H Nayeb-Hashemi, " Dynamic response of adhesively bonded single-lap joints with a void subjected to harmonic peeling loads", Proc Instn Mech Engrs, vol. 215, pp 199-206, 2001.
[7] A. Vaziri, H. Nayeb-Hashemi, "Dynamic response of a repaired composite beam with an adhesively bonded patch under a harmonic peeling load", International Journal of Adhesion & Adhesives, vol. 26, pp 314–324, 2006.
[8] Sadettin Orhan, "Analysis of free and forced vibration of a cracked cantilever beam", NDT&E International, vol. 40, pp 443-450, 2007.
[9] Recep Gunesa, M. Kemal Apalaka,_, Mustafa Yildirim, "The free vibration analysis and optimal design of an adhesively bonded functionally graded single lap joint", International Journal of Mechanical Sciences, vol. 49, pp 479–499, 2007.
[10] M Kemal Apalak, Recep Ekici and Mustafa Yildirim, " Free vibration analysis and optimal design of an adhesively bonded double containment cantilever joint", vol. 67, pp 797-806, 2008.
[11] M. Lucic, A. Stoic, J. Kopac, "Investigation of aluminum single lap adhesively bonded joints", Journal of Achievements in Materials and Manufacturing Engineering, vol. 15, pp 79-87, 2006.
[12] X. He, S.O. Oyadiji, "Influence of adhesive characteristics on the transverse free vibration of single lap-jointed cantilevered beams", Journal of Materials Processing Technology, vol. 119, pp 366-373, 2001.
[13] M.A. Ansarifar, J. Zhang, J. Baker, A. Bell, R.J. Ellis, "Bonding properties of rubber to steel, aluminium and nylon 6,6", International Journal of Adhesion & Adhesives, vol. 21, pp 369–380, 2001.
[14] A. Baldan, "Adhesion phenomena in bonded joints", International Journal of Adhesion & Adhesives, vol. 38, pp 95–116, 2012.

International Journal of Modern Engineering Research (IJMER)
www.ijmer.com Vol.3, Issue.2, March-April. 2013 pp-637-641 ISSN: 2249-6645

Effect of Case Hardening Treatment on the Structure and Properties of Automobile Gears

Swapnil R. Nimbhorkar, [1] Prof.B.D.Deshmukh[2]
[1]*M.Tech 2nd yr. (Prod.Engg), Yeshwantrao Cavan College of Engineering, Nagpur*
[2]*Head of the department, Yeshwantrao Chavan College of Engineering, Nagpur*

***Abstract*:** *As my research concerned it is basically concentrate on "To study the effect of case hardening treatment on the structure and properties of automobile gears, which consist of carburizing process which is a case hardening process." Case hardening is the process of hardening the surface of metal, often low carbon steel by infusing elements into the metal surface forming a hard, wear resistance skin but preserving a tough and ductile applied to gears, ball bearings, railway wheels. Comparative study of the following gears viz. grade of EN353, SAE8620 and 20MNCR5 are done in my research. The basic study in my research is Procedural study, Micro structure study, testing of hardness gradient of automobile gears.*

Keywords: *Hardness gradient, gears, defects, case depth, Defect, Microstructure,*

I. Introduction

As we know there is a little bit of steel in everybody life. Steel has many practical applications in every aspects of life. Steel with favourable properties are the best among the goods. The steel is being divided as low carbon steel, high carbon steel, medium carbon steel, high carbon steel on the basis of carbon content. Low carbon steel has carbon content of 0.15% to 0.45%. Low carbon steel is the most common form of steel as it's provides material properties that are acceptable for many applications. It is neither externally brittle nor ductile due to its lower carbon content. It has lower tensile strength and malleable. Steel with low carbon steel has properties similar to iron. As the carbon content increases, the metal becomes harder and stronger but less ductile and more difficult to weld.

The process heat treatment is carried out first by heating the metal and then cooling it in water, oil and brine water. The purpose of heat treatment is to soften the metal, to change the grain size, to modify the structure of the material and relive the stress set up in the material. The various heat treatment process are annealing, normalizing, hardening, austempering, martempering, tempering and surface hardening. Case hardening is the process of hardening the surface of metal, often low carbon steel by infusing elements into the metal surface forming a hard, wear resistance skin but preserving a tough and ductile applied to gears, ball bearings, railway wheels. Comparative study of the following gears viz. grade of EN353, SAE8620 and 20MNCR5 are done in my research. The basic study in my research is Procedural study, Micro structure study, testing of hardness gradient of automobile gears.

II. Need Of Case Hardening Treatment

-In order to improve both the wear resistance and the fatigue strength of steel components under dynamic and thermal stresses.
-Makes the surface layer known as the case significantly harder than the residual material known as the core.
-Case hardness depth or the thickness of the hardened layer, is an important quality attribute of the case hardening process.

III. Purpose of Research Study

As there are various types of material are used for manufacturing of automobile gears viz.EN353, SAE8620, 20MNCR5. These material have different properties such as toughness, hardness, wear resistance, ductility etc. These properties are vary according to parameter of case hardening treatment on the temperature variation.

In order to improve the properties of these materials, we have to reduce the defect present in it at root level so that Gears will give the best performance while driving the vehicles.
There are various defects present in automobile gears and with this following parameter we can reduce them.

IV. Procedural Study

Heat treatment Procedure for EN353 Gear-

- CARBURISING:-
- Pack, salt or gas carburize at 910˚C, holding for sufficient time to develop the required case depth and carbon content.
- Slow cool from carburizing temperature and re-heat to 870˚C, hold until temperature is uniform throughout the section, quench as required in water, oil or air cool.

TEMPERING:

- Re-heat to 780˚C - 820˚C, hold until temperature is uniform throughout the section, and quench in oil.
- Temper immediately while still hand warm.
- Heat to 150˚C - 200˚C as required.
- Soak for 1 - 2 hours per 25mm of section, and cool in still air.

Heat treatment procedure for 20MnCr5 Gear:

- Carburizing process-Heating Gear up to 880^0 c
- Cycle Time – According to Case Depth required.
- Hardening Temp. -Drop Down to 850^0 c
- Oil Quenching
- Tempering-210^0C
- Hardness Testing
  -

Heat treatment procedure for SAE8620 Gear

- CARBURISING
- Pack, salt or gas carburize at 900˚C holding for sufficient time to develop the required case depth and carbon content.
- Slow cool from carburizing temperature and re-heat to 840˚C, hold until temperature is uniform throughout the section, quench as required in water, oil or air cool.

TEMPERING:

- Re-heat to 780˚C -820˚C, hold until temperature is uniform throughout the section, and quench in oil.
- Temper immediately while still hand warm.
- Heat to 150˚C -200˚C as required.
- Soak for1-2 hours per 25mm of section, and cool in still air.

V. Microstructure Study

Inclusion rating test

EN353 Gear

Inclusion type	Sulphide type (A)		Alumina type (B)		Silicate type (C)		Oxide type (D)	
	Thin	Heavy	Thin	Heavy	Thin	Heavy	Thin	Heavy
Rating	.5	.5	.5	0	.5	0	.5	.5

20MNCR5 Gear

Inclusion type	Sulphide type (A)		Alumina type (B)		Silicate type (C)		Oxide type (D)	
	Thin	Heavy	Thin	Heavy	Thin	Heavy	Thin	Heavy
Rating	.5	.5	.5	.5	.5	0	1	1

SAE8620Gear

Inclusion type	Sulphide type (A)		Alumina type (B)		Silicate type (C)		Oxide type (D)	
	Thin	Heavy	Thin	Heavy	Thin	Heavy	Thin	Heavy
Rating	.5	.5	.5	.5	0	0	.5	.5

- Inclusion ratings are within the desired limit of EN353, 20MNCR5, SAE8620 Grade

VI. Metallurgical Analysis of Gear

EN353 GEAR

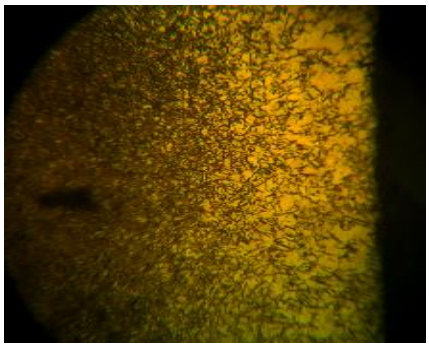

4 % Nital etched sample shows carburizing case depth Upto 0.6 mm at 500X magnification range.

20MNCR5 GEAR

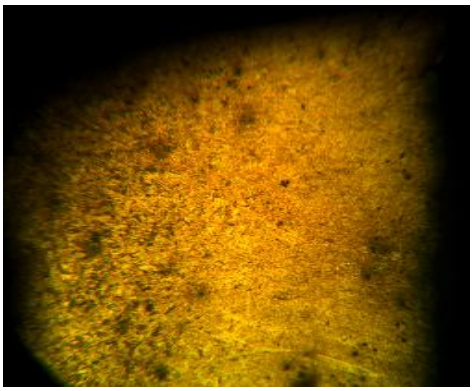

4 % Nital etched sample shows carburizing case depth Upto 0.8 mm at 500X magnification range.

SAE8620 GEAR

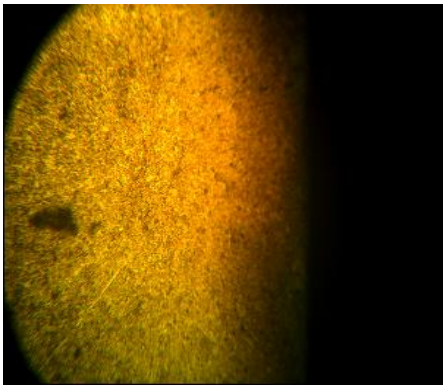

4 % Nital etched sample shows carburizing case depth Upto 0.7 mm at 500X magnification range.

- Microscopic examination relieved the fact that there exists the amount of retained austenite along with the martensite.

VII. Testing Of Hardness Gradient

Micro-Vickers hardness test:

Sr No.	Sample ID	Distance	Hardness in VPN
1	EN353 GEAR	0.2	652
		0.3	636
		0.4	578
		0.5	533
		0.6	436

- Hardness gradient values shows in EN353 Grade sudden drop at the case depth 0.6mm.This is due to less amount of chromium.

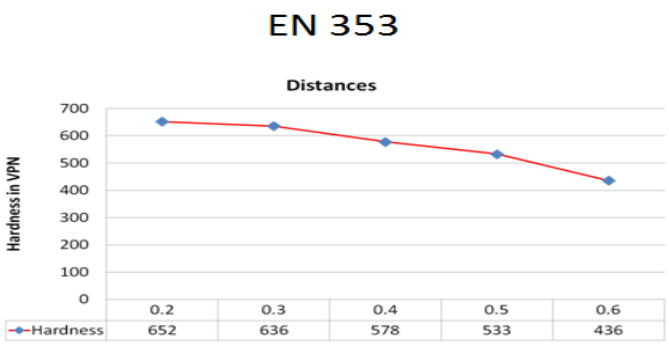

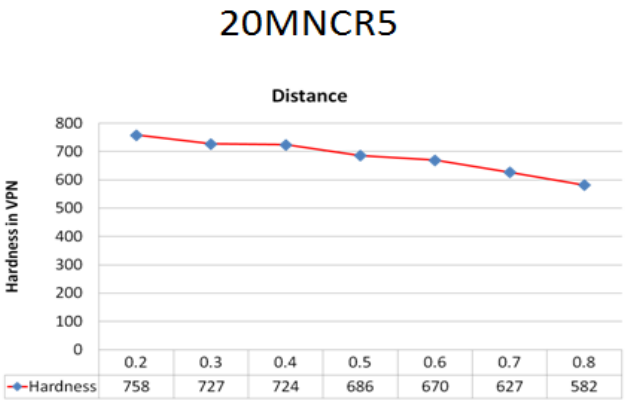

Sr No.	Sample ID	Distance	Hardness in VPN
1	20MNCR5 Gear	0.2	758
		0.3	727
		0.4	724
		0.5	686
		0.6	670
		0.7	627
		0.8	582

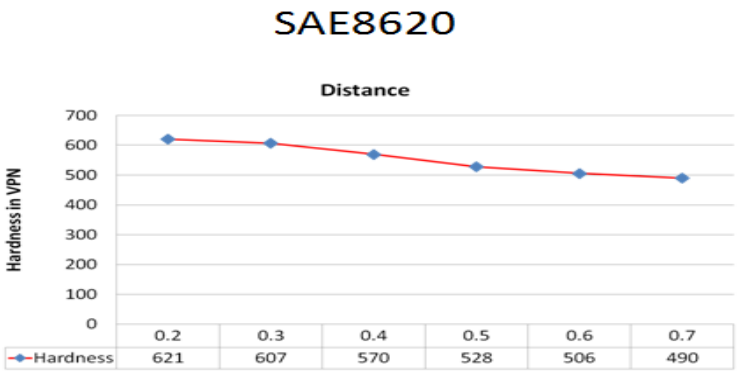

Sr No.	Sample ID	Distance	Hardness in VPN
1	SAE8620 Gear	0.2	621
		0.3	607
		0.4	570
		0.5	528
		0.6	506
		0.7	490

VIII. Conclusion

- Inclusion ratings are within the desired limit of EN353, 20MNCR5, SAE8620 Grade.
- Microscopic examination relieved the fact that there exists the amount of retained austenite along with the martensite.
- Retained austenite in EN353 is more thanSAE8620, 20MNCR5 due to higher hardening temperature.
- Hardness gradient values shows in EN353 Grade sudden drop at the case depth0.6mm. This may be due to less amount of chromium.

Referance

[1] R. Martin, J. Seabra, L. Magalhaes., Micropitting of Austempered Ductile Iron Gears: Bioderadable ester vs. mineral oil. Mechanica Experimental, 2006, vol.13, pg 55-65.
[2] Fatai Olufemi Aramide, Simeon Ademola Ibitoye. Effects of carburization time and temperature on the mechanical properties of carburize M.S. using activated carbon as carburizer. Material Research, vol.12, No. 4, 483-487, 2009.
[3] K. Palaniradja, N. Alagumurthi, V. Soundararajan. Optimization of process Variables in gas carburizing process: A taguchi study with experimental investigation on SAE 8620 and AISI 3310 steels. Turkish J. Eng. Env. Sci. 29, 2005, 279-284.
[4] K. Palaniradja, N. Alagumurthi, V. Soundararajan. Thermal and metallurgical effects associated with gas carburized and induction hardened components. The Open Materials Science Journal, 2010, 4, 74-91.
[5] Sven Bentsen, Theodora Marcu, Alexander Klekvkin. Carburizing of low-alloyed chromium materials- An Overview. Presented at PM2008 in Washington, USA on June 9, 2008.
[6] Anand Verma, Konchady Gopinath. Impact strength comparison with carburization depth variation for gear steel by instrumented charpy, izod and Brugger tests. International Journal of Applied Science & Engineering, 2011, 9,1:13-18.
[7] A.M. Freborg, B.L. Ferguson, Z. Li. Engine heat treatment for stronger aerospace gears. Gear Solution, July 2006.
[8] C.P. Kern, Dr. J.A. Wright, Dr. J.T. Sebastian. QuesTek innovation and solar atmospherers explain the mfg. and processing of a new class of vacuum-carburized gear steels with very high hardenability. Gear Solution. Jan 2012.
[9] Dr. Volker Heuer, Dr. Klaus Loeser, Gunther Schmitt. Recent developments allow the integration of heat treatment into the gear mfg. line and to synchronize heat treatment with gear machining.Gear Solution. July 2011.
[10] By Kelly T. Jones, P.E., Michael R. Newsome and Matthew D. Carter, P.E Gas Carburizing vs .Contour Induction Hardening in Bevel Gear machining.Gear Solution. July 2011.

International Journal of Modern Engineering Research (IJMER)
www.ijmer.com Vol.3, Issue.2, March-April. 2013 pp-642-646 ISSN: 2249-6645

Computational Investigation Of Elastic Properties Of Nitride Compounds

Abbès Beloufa,[1] Zouaoui Bensaad,[2] Bel-Abbes Soudini,[3] Nadir Sekkal,[4] Abdellah Bensaad,[5] Hamza Abid[6]

[12356]*University of Sidi Bel Abbès, 22000 Sidi Bel Abbès, Algeria,*
[4]*Département de Physique-Chimie, ENST, BP 1523, El M'Naouer, 31000 Oran, Algeria*

Abstract: *An investigation into the elastic properties of the In GaN compound under high pressure and high temperature was conducted using first-principles calculations based on density functional theory. For the calculation of the elastic properties we have used the Vinet EOS theory of state based on the augmented plane wave (APW) and quantum statistical methods. In this work we have used the all-electron full-potential linear muffin tin orbital (FP-LMTO) method augmented by a plane-wave basis (PLW) to calculate the total energies as well as the basic ground state properties. Exchange-correlation has been accounted for within LDA using the exchange-correlation potential calculated by Vosko et al. and Perdew et al. The results of the calculated properties for the considered compound are discussed and compared to the theoretical works as well as to the experimental data. We have also applied this computational method to InGaN alloys to check its transferability to predict the linear optical and thermodynamic properties from those of their parent compounds.*

Keywords: *Elastics Properties, (In, Al, Ga) N, equation of state, LMTO methods.*

I. Introduction

III-nitride semiconductors have been realized for many commercial light emitters and detectors in short wavelength regime over the last decade. The InGaN semiconductors alloy is of considerable importance for short and medium wavelength optoelectronics and photonics. InGaN is used as tremendous impact on many important systems technologies [1], [2].

In the last few years a lot of progress has been made in developing ab initio methods to compute the total energy, electronic structure and elastic properties of molecules, clusters and solid state systems. The elastic constants of the materials at high pressures are essential in order to predict and understand material response, strength, mechanical stability and phase transitions. The accurate measurement of these quantities is a difficult task due to difficult experimental conditions at high pressure. With the advances in ab initio methods, it is possible to compute a systematic study of the elastic properties as well as electronic and optical properties of materials at elevated pressure conditions. InGaN system crystallizes in the cubic zincblende and wurtzite structures at ambient pressure. It is clear that pressure and temperature are certainly critical parameters for the structural stabilities, and electronic and optical properties. The aim of this present work therefore is to explore the influence of these effects on the electronic and optical properties of the InGaN system and to show their direct consequence on the optoelectronic devices.

The most important technical details of our calculations are discussed in Computational method. The core of the article appears in the results and discussion, where the results are presented and analyzed. The article ends with a short exposition of the main results in tables.

II. Computational Method

In the present work, the calculations were performed in two steps using different approaches based on the local density approximation LDA from the density functional theory using the parameterization of *Vosko et al* [3] and also of Perdew et al [4]. We use the Savrasov version of the full potential linear muffin-tin orbital (FP-LMTO) method augmented with a plane wave basis (PLW) [5]. The non overlapping muffin tin spheres potential is expanded in spherical harmonics inside the spheres and Fourier transformed in the interstitial regions.

In this work, the orbital $3d^{10}$, $4s^2$, $4p^1$ of Ga, $4d^{10}$, $5s^2$, $5p^1$ of In, $2s^2$, $2p^3$ of N , and $3s^2$, $3p^1$ of Al are all included into the self-consistent treatment, i.e viewed as valence electrons. We use for GaN, AlN and AlN the value 8 for the parameter RMK_{max} which determines the matrix size, where K_{max} is the PW cut-off and *R*M ($R_{Ga,}$ R_N are Muffin-tin radius equal to 8 for the Ga and N atoms, respectively with RGa = 1.*59* and *R*N=1.87), for the ternary alloys (example: InGaN, AlGaN) the value (R_N are muffin-tin radius equal to 8,75 au for the Ga and N atoms, respectively with *R*Ga = 2.*08*, *R*In = 2.*08* and *R*N = 1.71).

In order to overcome the complexity of the EOS, the common practice is that the temperature of the substance is raised first and then the substance is compressed along the isotherm of interest. The relevant equations are called the thermal and isothermal EOSs, respectively [6, 7]. The thermal EOS is used to calculate the volume at atmospheric pressure and temperature *T*, compressed along the isotherm of interest *V*0, *T*. It is also necessary to know the temperature effect on the bulk modulus, B0 (T). Using the values of the volume and the bulk modulus at the corresponding temperature the isothermal EOS calculates the effect of pressure by incorporating the first and second derivates of the bulk modulus, $(\partial B/\partial P)_T$ *and* $(\partial^2 B/\partial P^2)_T$, at the given temperature.

The indium gallium nitride (InGaN) semiconductor materials have received much attention in the past few years due to their important applications in the blue-green light emitting diodes (LED) and the short wavelength laser diodes [8,9].The phase behaviour, structural parameters, bulk modulus, its pressure derivative and the equilibrium lattice parameters have been obtained by fitting Birch-Murnaghan EOS [10].

The elastic constants of the materials at high pressures are essential in order to predict and understand material response, strength, mechanical stability and phase transitions.

The EOS of a III-V can be described in a general form as a functional relationship between the pressure, volume, and temperature as

$$P(V,T) = P_{St}(V,300) + P_{th}(V,T) \quad (1)$$

Where $P(V,T)$ represents the pressure and volume V and temperature T, $P_{St}(V,300)$ and $P_{th}(V,T)$ represent the static pressure at volume V and 300K, and the thermal pressure at volume V and temperature T, respectively.

The modification has been incorporated such that the Vinet EOS becomes consistent with the extreme compression behaviour of solids predicted from the quantum statistical models [11.12] which can be formulated as follow:

$$P = 3B_0 \times K^{\frac{-5}{3}} \times G \times \exp\left[\frac{3}{2}\left(B_0^{'} - 3\right) \times G + \left(Y - \frac{3}{2}\right) \times G^2\right] \quad (2)$$

Where $K = \frac{V}{V_0}$, $G = \left(1 - K^{\frac{1}{3}}\right)$ and

$$Y = \left(\frac{3}{8}\left(B_0^{'} - 1\right)\left(B_0^{'} + 3\right) + \frac{3}{2}B_0 B_0^{''} + \frac{1}{3}\right)$$

Here B_0, $B_0^{'}$ and $B_0^{''}$ are respectively the values of isothermal bulk modulus *B* and its pressure derivatives (dB/dP) and $(d^2B/dP^2)_V$. The value of T_0 is 300K.

III. Results and Discussion

The theoretical ground-state parameters B_0, $B_0^{'}$ and B_0 $B_0^{''}$ of $In_{0.5}Ga_{0.}$ Are obtained and listed in Table I,

V (bohr3)	B_0(GPa)	B_0'	$-B_0.B_0$''
763.93	72.21	4.9813	18,34062
763.99	72.13	4.9956	18,56807
764.50	71.56	5.0606	19,22574
766.58	69.74	5.2216	20,335
769.20	67.64	5.3936	21,3526
771.90	65.52	5.5718	22,38563
775.14	63.15	5.7735	23,49767
778.54	60.71	5.9899	24,64583
782.10	58.21	6.2236	25,8616
785.89	55.60	6.4789	27,14525
789.77	52.97	6.7527	28,50215
794.33	50.04	7.0700	29,96375

Table 1. Elastic parameters of Cubic $In_{0.5}Ga_{0.5}N$

Figure 1 illustrates curve of the $-B_0.B_0$''calculated as a function of pressure derivatives bulk modulus B_0' according to Eq (2). An expression for the isothermal bulk modulus B_T is obtained by differentiating the Vinet EOS (Eq (2).

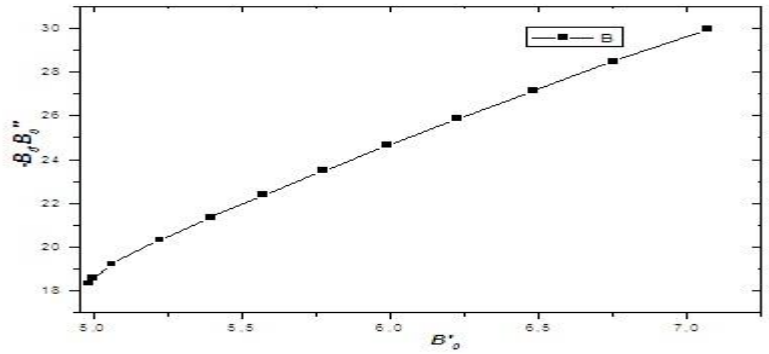

Figure 1. Relationship between B'_0 and B_0B_0''

To analyze the structural properties, the equilibrium lattice parameters are calculated within the method seen previously using the habitual minimization procedure. The total energy was calculated for different values of the lattice constant, and the ground state corresponds to the lowest value of the total energy. Fig. 2 shows the total energy as a function of volume for In0.5Ga0.5N, AlN and InN in the zincblende (8 atoms). The curves were obtained by calculating the total energy E at many different volumes around equilibrium and by fitting the calculated values to the Murnaghan/Birch [10] equation of state. In order to make easier the comparison of our results, we have plotted the E-V diagram for the zincblende phase.

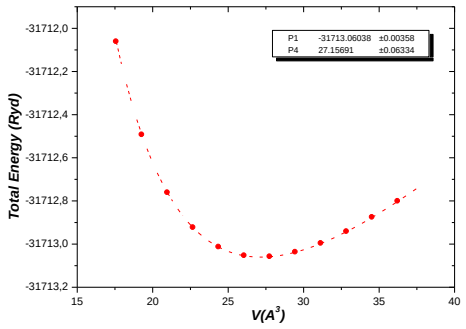

Figure 2. Calculated total energy versus relative volume for $In_{0.5}Ga_{0.5}N$

The results of the site-projected partial density of states are shown in Fig. 3. There is not just one way to perform this atom and orbital decomposition, so the results should be interpreted qualitatively. The lower valence bands ranging from 2.51 to -3.50 eV has significant contribution from Ga-d orbitals.

The intermediate subband between -4.4 and -2 eV, originates from In/Ga-s orbitals. The higher-energy set of valence bands can be further divided into two subbands. The lower-energy subband from -4.6 to -0.6 eV is originates from In/Ga/N-p band. The higher-energy subband from -2.4eV up to Fermi level (EF) are consists of N/s and In/Ga-p states. The conduction band running from 0.5 eV consists of admixture of Sb- s/p/, In-s/p/d and Ga-s/p states. From the partial density of states one can see that there exist a strong hybridization between Ga-p and Ga-s between -4 eV up to E_F.

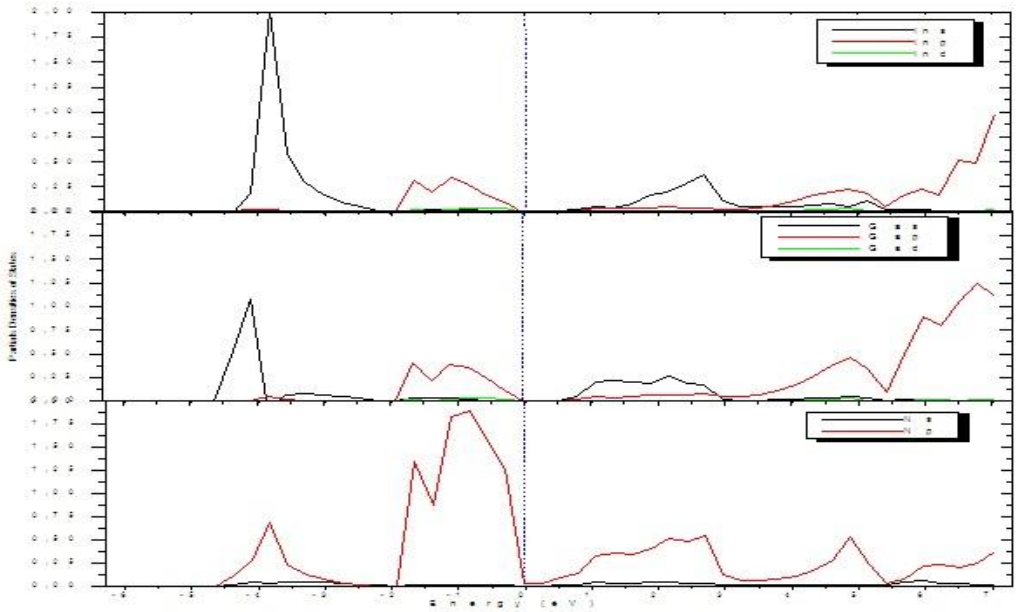

Figure 3. Partial densities of states of Cubic $In_{0.5}Ga_{0.5}N$.

The results of the fit of our *Pressure-Volume-Temperature (P-V-T)* data to the thermal pressure EOS are summarized in Table 3. Figure 4 shows the *P-V-T* data from both the experiments and calculations carried out in our study. The values of $\alpha B_T(V_0,T)=\frac{\partial P}{\partial T}$ where $\alpha=\frac{1}{V}\left(\frac{\partial V}{\partial T}\right)$ was 0.00244236. This result is in general agreement with previous studies [13, 14and 15].

A Vinet EOS fitted to the room temperature data fielded an isothermal bulk modulus of *BT0* = 67.64GPa and a pressure derivative of *BT0'* = 5.3936. The high-temperature data from the first-principles calculations were fitted to the thermal pressure EOS. The resulting calculated parameter of the thermal pressure αBT *(V0, T)* was 2.44 x 10-3 (GPa/K).
To assess the influence of different EOSs, we calculated the parameters from our pressure volume
data using different EOSs. The difference in parameters is significant. As InGaN is unstable at pressures lower than 25 GPa [16,17 and 18].

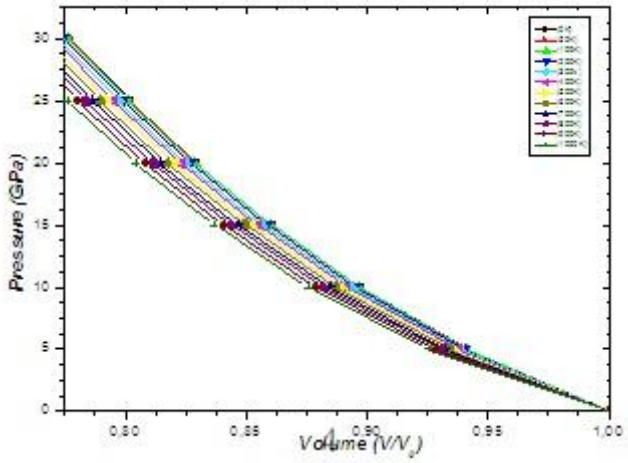

Figure 4. Pressure-volume data for $In_{0.5}Ga_{0.5}N$. The circles and diamonds denote the volumes from the first-principle calculations at temperatures from 0 to 1000 K.

Parameters For V_0 at 0GPa and 300K	Values
V_0(Bohr)^3	769.20
B_{T0}(GPa)	67.64
B'_{T0} (GPa)	5.3936
$\alpha B_T(V_0,T)=\frac{\partial P}{\partial T}$ (GPa/K)	0.002442360

Table 2. The thermoelastic parameters of Cubic $In_{0.5}Ga_{0.5}N$

We calculate the elastic properties of InN, GaN and InGaN by computing the components of the stress tensor for small strains, using the method developed recently by Charpin [19, 20]. It is well known that a cubic crystal has only three independent elastic constant C11, C12 and C44. So a set of three equations is needed to determine all the constants, which means that three types of strain must be applied to the starting crystal. The first type involves calculating the elastic modulus (C11 + 2C12), which are related to the bulk modulus *B:*

$$B=\frac{1}{3}(C_{11}+2C_{12}) \qquad (3)$$

The elastic constants of the cubic materials are shown in Table 3. we compare our main finding of zincblende AlN and GaN, this table also shows the elastic constants obtained from first-principles LAPW computations and calculations works [21,22,23,24]. The accuracy of the elastic constants C11, C12 and C44 is remarkably good.
For comparison, the first-principles results also differ from the calculations works by less than 3%,.

	GaN[25]	GaN	AlN[25]	AlN	InN[25]	InN	InGaN[26,27]	InGaN
C11(Gpa)	293	277	304	311	187	170	240	233.5
C12(Gpa)	159	162	160	155	125	131	159.5	145
C44(Gpa)	155	171	193	200	86	93	120.5	133

Table 3. Elastic parameters of Cubic $In_{0.5}Ga_{0.5}N$

IV. Conclusion

Full potential linear muffin-tin orbital method (FP-LMTO) within the density functional theory has been applied to study the electronic and thermal properties of ternary alloys InGaN in cubic phase using the density functional theory with LDA. The local density approximation has been used with and without generalized gradient correction based on exchange-correlation energy optimization. The calculated energy allowed us to investigate several structural properties such as lattice

parameter, bulk modulus and its pressure derivative. Our calculated lattice parameter is found to be in reasonable agreement with other theoretical works.

The numerically calculated values showed generally reasonable agreement with the available experimental and other calculations for the electronic and thermal properties only (Dos, three independent elastic constant C11, C12 and C44…).

The results obtained for the P-V-T relationships in the present study give information regarding higher order thermodynamic likes the isothermal P-V relationship which yields the bulk modulus. It is found from the results that bulk modulus increases with the increase in pressure whereas it decreases with the increase in temperatures. The additional advantages of the EOS are that the expression is simple and allows calculating some required variables.

V. Acknowledgements

The authors thank also S.Y.Savrasov for his Mindlab software freely available for research. This work has been supported by the University of Sidi-bel-Abbes (Algeria) and by the Algerian national research project CNEPRU under number J0202120060047.

References

[1] S. Nakamura, T. Mokai, M. Senoh, Jpn. Appl. Phys. 30, 1998 (1991).
[2] S. Nakamura, M. Senoh, N. Iwasa, and S. Nagahama, "High-power InGaN single-quantum-well-structure blue and violet light-emitting diodes," Appl. Phys. Lett., vol. 67, pp. 1868–1870, Sept. 1995.
[3] S. Nakamura, "A bright future for blue/green LED's," IEEE Circuits Devices, pp. 19–23, May 1995.
[4] S.H.Vosko, L.Wilk and M.Nussair, Can. J. Phys. 58 (1980) 1200.
[5] J. P. Perdew, S. Burke, M. Ernzerhof, Phys. Rev. Lett. 77 (1996) 3865.
[6] S.Y.Savrasov, Phys Rev B 54 (1996) 16470
[7] T. S. Duffy and Y. Wang, Rev. Mineral. Geochem. 37, 425 1998.
[8] S. Nakamura and G. Fasol, The Blue Laser Diode, Springer-Verlag, Heidelberg, 1997.
[9] G.B. String fellow and M. Georage Craford, High Brightness Light Emitting Diodes-Semi-conducteurs and Semimetals Volume 48, Academic Press, San Diego, California, USA, 1997.
[10] F.D.Murnaghan, Proc. Natl. Acad. Sci. USA 30 (1944) 5390.
[11] R. J. Angel, Rev. Mineral. Geochem. 41, 35 2000.
[12] Kalitkin N N&Kuz'mina LV, Sov Phys-solid state, 13 v (1972) 1938.
[13] Holzapfel W B, High Pressure Res, 16 (1981) 81.
[14] Fei Y, Ricolleau A, Frank M, Mibe K, Shen G and Prakapenka V 2007 Proc. Natl. Acad. Sci.104 9182
[15] Ono S, Brodholt J P, Alfè D, Alfredsson M and Price G D 2008 J. Appl. Phys. 103 023510
[16] J.B. Li, Hui Yang, L.X. Zheng, D.P. Xu, Y.T. Wang // MRS Internet J. Nitride Semicond. Res.
4S1, G3.25 (1999).
[17] M. Marques, L.K. Teles, L.M.R. Scolfaro, and J.R. Leite // Appl. Phys. Lett. 83(5) (2003).
[18] G. Franssen, T. Suski, P. Perlin, H. Teisseyre, A. Khachapuridze, L. H. Dmowski, J. A. Plesiewicz, A. Kaminska, M. Kurouchi, Y. Nanishi, H. Lu, and W. Schaff, Appl. Phys. Lett. 89, (2006) 121915.
[19] Ueda Y, Matsui M, Yokoyama A, Tange T and Funakoshi K 2008 J. Appl. Phys. 103 113513
[20] T. Charpin, A package for calculating elastic tensors of cubic phases using WIEN2k, in User's Guide of WIEN2k, An Augmented-Plane-Wave + Local Orbitals Program for Calculating Crystal Properties, P. Blaha, K. Schwarz, G.K.H. Madsen, D. Kvasnicka and J.Luitz, Techn Wien, Austria), 2001. ISBN 3-9501031-1-2.
[21] M.B. Kanoun, A.E. Mera
[22] F. Grosse and J. Neugebauer, Phys. Rev B 63, 085207 (2001).
[23] K. Karch, J.-M. Wagner, and F. Bechstedt Phys. Rev. B 57, 7043 (1998).
[24 K. Shimada, T. Sota, and K. Suzuki, J Appl. Phys. 84, 4951 (1998).
[25] K. Kim, W. R. L. Lambrecht, and B. Segall, Phys. Rev. B 53, 16 310 (1996).
[26] A. Vertikov, I. Ozden, A. V. Nurmik ko "Investigation of excess carrier diffusion in nitride semi-conducteurs with near-field optical microscopy" Appl. Phys. Lett. 74, 850, (1999).
[27] D. Cherns, S. J. Henley, F. A. Ponce "Edge and screw dislocations as nonradiative centers in InGaN/GaN quantum well luminescence" Appl. Phys. Lett., 78, 2691 (2001).
[28] I. Vurgaftman, J. R. Meyer "Band parameters for nitrogen-containing semi-conducteurs" J. Appl. Phys.94, 3675 (2003).
[29] S. P. Łepkowski, J. A. Majewski, and G. Jurczak, Phys. Rev. B 72, 245201 2005_.

International Journal of Modern Engineering Research (IJMER)
www.ijmer.com Vol.3, Issue.2, March-April. 2013 pp-647-651 ISSN: 2249-6645

Statistical Optimization for Generalised Fuzzy Number

Sk. Khadar Babu [1], Rajesh Anand.B [2], Madhusudhan Reddy.K [3], M.V.Ramanaiah [4], Karthikeyan.K[5]

[135] *School of Advanced Sciences, VIT University, Vellore – 632 014.*
[24]*S.V. University, Tirupathi 517 502.*

***Abstract*:** *In this paper an attempt has been made to propose a method based on Pascal triangular graded mean representation to solve the two-objective fuzzy assignment problem under fuzzy environment. In this, costs and times are to be fuzzy variables. And we apply statistical interpretation for new approach to solve the fuzzy assignment problem. Here we take the coefficients of fuzzy numbers from Pascal triangles and develop a new procedure to solve fuzzy assignment problem. Given through the numerical example*

Keywords: *Assignment problem, Triangular Fuzzy number, Pascal triangular graded mean representation.*

I. Introduction

Assignment problem is a common problem in the real system. For this problem in deterministic environment, a lot of models and algorithms have been presented up to now. In recent years, many researchers began to investigate this kind of problem under the uncertain environment .Tadei and Ricciardi [13] given the solutions of the multilevel assignment problems. Bogomolnaia.A and Moulin.A (1&2) given a new solution for random assignment problem and developed a procedure for a simple assignment problem with unique solution. The another uncertainty in the real world is fuzziness. In order to deal with fuzziness, Zadeh [14] gave an information about the the fuzzy set theory in 1965. For the assignment problem, it may be also considered under the fuzzy environment, which causes the research of fuzzy assignment problem. Constructive bounds and exact expectation of the random assignment problem was discussed by Coppersmith and Sorkin (4). Lin and Wen [7] framed and designed a labeling algorithm for it. Ridwan [8] did a simple preference based traffic assignment problem in fuzzy approach. A multi-criteria fuzzy assignment method was introduced by Belacela and Boulasselb (3).

In a linear programming problem, the assignment problem is a particular case to assign the different jobs to different workers. It has been discussed with the situation in which jobs are to be assigned to a persons for execution. The assignment problem is derived in terms of Linear programming formulation was given by D. Konig [5]. Let a number of *n* jobs be given that must be performed by *m* workers, where the costs and the times depend on the specific assignments. Each job must be assigned one worker and each worker has to perform one and only one job so that the total cost and the total time is minimized after all the jobs are completed. S.Muruganandam et.al given a special procedure to solve the two-objective assignment problem through the graded mean integration representation. The Hungarian method [6], which is the most popular, a very convenient and efficient iterative procedure for solving an assignment problem.

Based on the uncertainity, in decision-making, we always treat some parameters as uncertain variables, which cannot obtain their concrete values. In this paper, we consider a two objective assignment problem under fuzzy environment in which the costs and the times are supposed to be fuzzy variables. This paper is organized as follows: In section 2, we construct the mathematical model for the problem. In section3, the methodology is introduced. In section 4, a statistical implementations are given. In section 5, a numerical example is given and in section 6, we give a conclusion for our problem.

II. Mathematical Model

Assume there are *n* jobs and *m* workers. For the convenience of description, the notations *i* = 1, 2, …….*m* and *j* = 1, 2,……..*n* are used to denote the indexes of the different workers and jobs. The purpose of the two objective assignment problem in this paper is *n* jobs and *m* workers, so that the total cost and the total time is minimized after all the jobs are completed. If worker *i* has ability to undertake some jobs and we think that he will probably produce much less profit or consume very long time, in such conditions worker *i* may be deprived of opportunity to undertake these jobs.

In the process of decision making, if job *j* is assigned to worker *i*, then the corresponding costs and consumed times, denoted by $\tilde{c}_{ij}$ and $\tilde{t}_{ij}$, *i* = 1,2,3,……..*m* , *j* = 1,2,3……*n*, respectively. Generally, the optimal plan is made before the jobs are completed, thus it is impossible for us to know the concrete values of $\tilde{c}_{ij}$ and $\tilde{t}_{ij}$ in advance. In order to obtain a decision, $\tilde{c}_{ij}$ and $\tilde{t}_{ij}$ (*i* = 1,2,3,……..*m* , *j* = 1,2,3……*n*) have been given. Then the cost matrix and the consumed time matrix may be denoted by

$$\tilde{C}=(\tilde{c}_{ij})_{nxn}=\begin{pmatrix}\bar{c}_{11} & \bar{c}_{12} & . & . & . & \bar{c}_{1n}\\ \bar{c}_{21} & \bar{c}_{22} & . & . & . & \bar{c}_{2n}\\ . & . & . & . & . & .\\ . & . & . & . & . & .\\ . & . & . & . & . & .\\ \bar{c}_{m1} & \bar{c}_{m2} & . & . & . & \bar{c}_{mn}\end{pmatrix} \qquad \tilde{T}=(\tilde{t}_{ij})_{nxn}=\begin{pmatrix}\bar{t}_{11} & \bar{t}_{12} & . & . & . & \bar{t}_{1n}\\ \bar{t}_{21} & \bar{t}_{22} & . & . & . & \bar{t}_{2n}\\ . & . & . & . & . & .\\ . & . & . & . & . & .\\ . & . & . & . & . & .\\ \bar{t}_{m1} & \bar{t}_{m2} & . & . & . & \bar{t}_{mn}\end{pmatrix}$$

In order to model the above fuzzy assignment problem, the following variables are employed:

$$x_{ij}=\begin{cases}1 & if\ worker\ i\ is\ to\ assigned\ to\ job\ j\\ 0 & otherwise\end{cases}$$

Where $i = 1,2,\ldots\ldots\ldots,m,$ $j = 1,2,\ldots\ldots\ldots\ldots\ldots,n$

The two objective fuzzy assignment problem can now be stated as equation:

Minimize $\sum_{i=1}^{m}\sum_{j=1}^{n}\tilde{c}_{ij}\bar{x}_{ij}$

Maximize $\sum_{i=1}^{m}\sum_{j=1}^{n}\tilde{t}_{ij}\bar{x}_{ij}$

Subject to $\sum_{i=1}^{m}\bar{x}_{ij}=1 \quad j = 1, 2, 3\ldots\ldots\ldots\ldots m$

$\sum_{i=1}^{n}\bar{x}_{ij}=1 \quad i = 1, 2, 3\ldots\ldots\ldots\ldots n$

$\bar{x}_{ij} = 0$ or 1

Since the elements of the cost matrix and the consumed time matrix are fuzzy variables, it follows that the total cost and the total consumed time are also fuzzy variables. In order to optimize the objective, we introduce the methodology in the next section.

III. Methodology

3.1 Triangular Fuzzy Number

A fuzzy number A is a triangular fuzzy number denoted by (a_1, a_2, a_3) and its membership function $\mu_A(x)$ is given below:

$$\mu_A(x)=\begin{cases}\dfrac{x-a_1}{a_2-a_1}, & a_1 < x < a_2\\ \dfrac{x-a_3}{a_2-a_3}, & a_2 < x < a_3\end{cases}$$

3.2 Triangular Fuzzy Number

Chen [9] has been introduced function principle for fuzzy arithmetical operations. We shall use this principle as the operation of addition, multiplication, subtraction and division of fuzzy numbers.

Suppose $\tilde{a}=(a_1,a_2,a_3)$ and $\tilde{b}=(b_1,b_2,b_3)$ are two triangular fuzzy numbers. Then

(i) $\tilde{a}+\tilde{b}=(a_1,a_2,a_3)+(b_1,b_2,b_3)=(a_1+b_1,a_2+b_2,a_3+b_3)$

(ii) $\tilde{a}-\tilde{b}=(a_1,a_2,a_3)-(b_1,b_2,b_3)=(a_1-b_1,a_2-b_2,a_3-b_3)$

(iii) The multiplication of $\tilde{a}$ and $\tilde{b}$ is $\tilde{a}\times\tilde{b}=(c_1,c_2,c_3)$ where $T=\{a_1b_2,a_1b_3,a_3b_1,a_3b_3\}$

$C_1=\min T$, $C_2=a_2b_2$, $C_1=\max T$.

If $a_1, a_2, a_3, b_1, b_2, b_3$ are non-zero positive real numbers, then

$$\tilde{a}\times\tilde{b}=(a_1,a_2,a_3)\times(b_1,b_2,b_3)=(a_1b_1,a_2b_2,a_3b_3)$$

(iv) $\frac{1}{\tilde{b}} = \tilde{b}^{-1} = \left(\frac{1}{b_3}, \frac{1}{b_2}, \frac{1}{b_1}\right)$ Where b_1, *b2, b3are* all non-zero positive real numbers, then the division of $\tilde{a}$ and $\tilde{b}$ is

$$\frac{\tilde{a}}{\tilde{b}} = \left(\frac{a_1}{b_1}, \frac{a_2}{b_2}, \frac{a_3}{b_1}\right)$$

(v) Let $k \in R$. Then for $k(a_1, a_2, a_3) = (ka_1, ka_2, ka_3)$ for $k \geq 0$.

3.3 Graded Mean Integration Representation Method

Chen and Hseih [10, 11, 12] propose graded mean integration representation for representing generalized fuzzy number. Then S.Muruganandam described for generalized fuzzy number.

Suppose L^{-1} and R^{-1} are inverse functions of functions *L* and *R*, respectively and the graded mean h-level of generalized fuzzy number is $A=(a_1, a_2, a_3, a_4 : w)$ is $h[L^{-1}(h)+R^{-1}]/2$. Then the defuzzified value P (A) by graded mean integration representation of generalized fuzzy number based on the integral value of graded mean *h* - level is

$$P(A) = \frac{\int_0^h [\frac{L^{-1}(h)+R^{-1}(h)}{2}]\, dh}{\int_0^w h\, dh}$$

Where *h* is between 0 and *w*, $0 < w \leq 1$.

If $A=(a_1, a_2, a_3)$ is a triangular fuzzy number. Chen and Hsieh [10, 11, 12] already find the general formulae of the representation of generalized triangular fuzzy number as follows:

$$\text{P(A)} = \frac{1}{2} \frac{\int_0^1 \int h[a_1 + h(a_2 - a_1) - h(a_3 - a_2)]dh}{\int_0^1 hdh} \quad ; \text{P(A)} = \frac{a_1 + 4a_2 + a_3}{6}$$

3.4. Pascal triangular graded mean approach

Chen and Hsieh [10,11,12] proposed graded mean integration representation for representing generalized fuzzy number and S.Muruganandam etal described one more graded mean representation for generalized fuzzy number. This is useful to obtain the solution of the generalized fuzzy variables for assignment problem. But, the present approach is very simple way of analyzing multi objective fuzzy variables for assignment problem then we apply Hungarian method we get the optimum solution. Here, we apply simple statistical tests to analyze and compare the above two methods. This approach is also applicable for multi-objective fuzzy assignment problem. But , this procedure is simply taken from the following Pascal triangles. These are useful to take the coefficients of fuzzy variables are Pascal triangular numbers and we just add and divided by the total of Pascal numbers, then we call it as Pascal's triangular probability approach. This is also the alternative procure for graded mean representation.

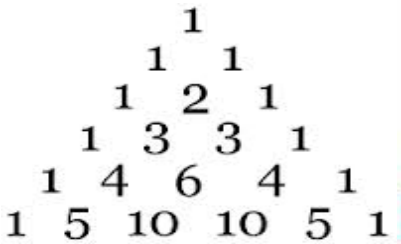

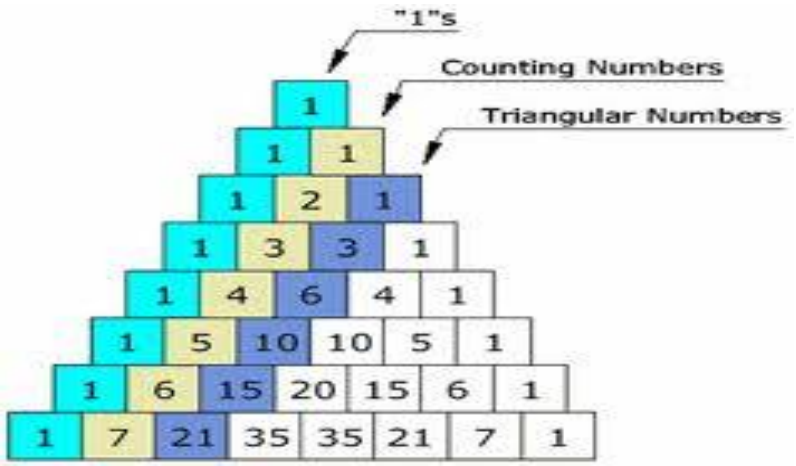

Let the are two triangular fuzzy numbers then we can take the coefficient of fuzzy numbers as pascal triangular type and apply the simple probability approach.

Let the $\tilde{a}=(a_1,a_2,a_3)$ and $\tilde{b}=(b_1,b_2,b_3)$ are two triangular fuzzy numbers then we can take the coefficient of fuzzy numbers from pascal's triangles and apply the simple probability approach then we get the following formula:

$$P(A)=\frac{a_1+2a_2+a_3}{4}$$

The coefficients of a_1, a_2, a3 are 1, 2, 1. This approach can be extended for n dimensional Pascal Traingular fuzzy order also.

IV. Statistical Implementations

4.1 For Seducers F-Test

Let us assume X is for getting values from Graded integration mean method and Y be the Variable is for getting values from Pascal Triangle approach. Then obtain variances of the both variables and find F calculated value and then compare with F table values at 5% level of significance. If F cal (Value) > F tab (Value), then we reject hypothesis (Ho) otherwise we do not.

4.2 For Student t-test

Apply t-test for the above two variables X and Y then Calculate t value and compare to t table value at 5% level of significance. If calculated t > t- table value, we reject hypothesis (Ho) otherwise we do not reject Ho.

5. Results and Discussions

In this section, we give a some simple results and discussions though the following numerical example to show the efficiency of the methodology. The cost and time matrix are given in triangular fuzzy numbers.

$$\tilde{C}=\begin{pmatrix}(11,12,14) & (7,9,10) & (12,14,16)\\ (5,7,9) & (8,10,12) & (7,10,12)\\ (10,12,15) & (6,9,11) & (4,6,9)\end{pmatrix}$$

$$\tilde{T}=\begin{pmatrix}(6,9,10) & (1,3,5) & (3,6,8)\\ (2,4,6) & (7,9,11) & (5,7,9)\\ (4,6,8) & (6,8,10) & (2,5,6)\end{pmatrix}$$

$$\tilde{C}+\tilde{T}=\begin{pmatrix}(17,21,24) & (8,12,15) & (15,20,24)\\ (7,11,15) & (15,19,23) & (12,17,21)\\ (14,18,23) & (12,17,21) & (6,11,15)\end{pmatrix}$$

Applying the graded mean integration representation for defuzzification

$$P(A)=\frac{a_1+4a_2+a_3}{6}$$

$$C+T=\begin{pmatrix}21 & 12 & 20\\ 11 & 19 & 17\\ 18 & 17 & 11\end{pmatrix}$$

By Pascal triangular approach

$$P(A)=\frac{a_1+2a_2+a_3}{4}$$

5.1 Statistical interpretation

For F –Test : Let we stated the hypothesis

Ho: There is no significance difference between the variances of the above two variables

X : 20.83 11.83 19.83 11 19 16.83 18.16 16.83 10.83

Y : 20.75 11.75 19.75 11 19 16.75 18.25 16.75 10.75

Variance(X) = 15.2518 ; Variance(Y) = 15.2969 and Fcal Value = 1.0029:F tab Value =3.44(at 5%level of significance); F cal value is very least, so we do not reject hypothesis.

For t-test : Let the Hypothesis

Ho: There is no significance difference between the means of the two variables.

Mean of X is 16.1267 and Mean of Y is 16.0833 and t-cal Value = 0.0222 ,t-tab Value is 2.120 then we reject Hypothesis.

Based on statistical tests, mean and variances are the same ,then we say that these two grouped values are came from the normal population. And for the solution of these two methods are comparatively same. Therefore, this approach is alternative for the previous one.

Applying the Hungarian method, the solution is

$$\begin{pmatrix} 21 & 12^{*} & 20 \\ 11^{*} & 19 & 17 \\ 18 & 17 & 11^{*} \end{pmatrix}$$

Optimal allocation:

Therefore, the optimum feasible solution is 12+11+11=34.

V. Conclusion

This measure is more applicable for generalized fuzzy number by comparing graded mean average method and it is also useful to solve the assignment problem by Hungarian method. For statistical tests, there is no significance difference between the two methods. By comparison, Pascal triangular method is also applicable for fuzzy assignment problem. It is also applicable to solve the multi-objective fuzzy assignment problems also.

Based on statistical tests, mean and variances are the same, then we say that these two grouped values are came from the normal population. And for the solution of these two methods are comparatively same. Therefore, this approach is alternative for the previous one.

References

[1] Bogomolnaia A., and MoulinA.,(2001), A New solution to the Random Assignment Problem, Journal of Economic Theory, **100**: 295-328.
[2] Bogomolnaia A., and Moulin H., (2002), A Simple Random Assignment problem with a Unique Solution, Economic Theory, 19: 623 – 636.
[3] Belacela N., and Boulasselb M.R., (2001), Multicriteria Fuzzy Assignment Method: A Useful Tool to Assist Medical Diagnosis, Artificial Intelligence in Medicine, 21: 201 – 207.
[4] Coppersmith D., and Sorkin G.B (1999), Constructive Bounds and Exact Expectation for the Random Assignment Problem, Random Structure and Algorithm, 15(2): 113 – 144.
[5] Gillett Billy E., (2000), Introduction to Operations Research – A Computer Oriented Algorithmic Approach, Tata Mc-Graw Hill, New Delhi.
[6] Kuhn H.W., (1956), the Hungarian Method for the Assignment Problem, Naval Res. Logist. Quart. 2: 254 – 258.
[7] Lic C.J., and Wen U.P., (2004), a Labeling Algorithm for the Fuzzy Assignment Problem, Fuzzy Sets and Systems. 142: 373 – 391.
[8] Ridwan M., (2004), Fuzzy preference Based Traffic Assignment Problem, Transportation Res. Part C, 12:209 – 233.
[9] Shan-Huo Chen,(1985), Operations on Fuzzy Numbers with Functions Principle, Tamkang J. Management Sci., 6(1): 13 – 25.
[10] Shan-Huo Chen, and Chih Hsun Hsieh, (2000), Graded Mean Integration Representation of Generalized Fuzzy Number, Proceeding of Conference of Taiwan Fuzzy system Association, Taiwan.
[11] Shan-Huo Chen and Chin Hsun Hseih, (2000), Graded Mean Integration Representation of Generalized Fuzzy Number journal of the chunese Fuzzy System Association, Taiwan, 5(2): 1-7.
[12] Shan-Huo chen, and Chin Hsun Hseih,(2000), Representation, Ranking, Distance and Similarity of L-R Type Fuzzy Number and Application, Australia Journal of Intelligent Information Processing Systems, Australia, 6(4): 217 – 229.
[13] Tadei R., and Nicoletta Ricciard:X., (1999), The Dynamic Multilevel Assignment Problem as a Stochastic External Process, European Journal of Operational Research 117: 264 – 274.
[14] Zadeh L A., (1965), Fuzzy Sets, Inform. Control, 8: 338 – 353.

International Journal of Modern Engineering Research (IJMER)
www.ijmer.com Vol.3, Issue.2, March-April. 2013 pp-652-658 ISSN: 2249-6645

Indium Arsenide on Insulator Mosfets to Increase Carrier Mobility

Kamrul Hassan, [1] Manan Chowdhury, [2] Mohammad Atif Bin Shafi, [3] Md. Takdirul Islam[4]
[1 4]*Department of EEE, Chittagong University of Engineering & Technology (CUET), Bangladesh*
[23]*Department of EEE, East West University (EWU), Bangladesh*

Abstract: *Silicon-on-insulator (SOI) MOSFET is one of the modern state of the art transistor in which a semiconductor layer like silicon is formed above an insulator layer on a semiconductor substrate. In SOI MOSFET, there is much more advantages over bulk silicon MOSFET such as high speed operation, low power consumption, small short channel effects. Over the past several years, the inherent scaling limitations of silicon (Si) electron devices have fuelled the exploration of alternative semiconductors, with high carrier mobility, to further enhance device performance. In particular, compound semiconductors heterogeneously integrated on Si substrates have been actively studied: such devices combine the high mobility of III–V semiconductors and the well established, low-cost processing of Si technology. This integration, however, presents significant challenges. Conventionally, heteroepitaxial growth of complex multilayer's on Si has been explored but besides complexity, high defect densities and junction leakage currents present limitations in this approach. Motivated by this challenge, we use a three surface potentials (gate oxide-silicon film interface, silicon-film-buried oxide interface and buried oxide-substrate interface) based compact model to study a fully depleted SOI and XOI MOSFETs. We have simulated the surface potentials, surface charge density, gate capacitance, drain current, transconductance and unity gain frequency of SOI and XOI MOSFETs. The different output characteristics show a better performance for InAs. We have got high drain current, transconductance and unity gain frequency of XOI MOSFET. On the other hand, we got very low (negative) threshold voltage for XOI MOSFET. So, by using XOI MOSFET, we can get high speed operation and amplification, low power consumption than SOI MOSFET as well as bulk silicon MOSFET.*

Keywords: *FD SOI MOSFET, In AS multilayter, Strong inversion, Poisson's equation, Surface potential based model, Transconductance*

I. INTRODUCTION

The SOI technology is introduced to overcome the limits of bulk or conventional Si MOSFETs. Among the problems are that the carrier mobility is decreasing due to impurity scattering, the gate tunneling current is increasing as the gate insulator becomes thinner, and the p-n junction leakage is increasing as the junction becomes shallower. These trends make the conventional scaling less and less feasible. As a result, the operating voltage is set higher than the expected value of a scaled-down device to achieve the desired speed performance and therefore the power dissipation goes high [2]. SOI CMOS offers a higher integration density than bulk CMOS. This high density results mainly from the absence of wells in SOI technology. SOI CMOS devices can be isolated by reach through oxidation, while bulk devices normally use junction isolation. SOI wafers can be processed in standard bulk silicon processing lines. As the feature size scaled down in modern IC technology, the source drain junction depth needs to be reduced to suppress short channel effects. In bulk silicon devices, such reduction may bring an unwanted interaction between the silicon and the metal such as metal punching through the junction. If the device is built on an SOI wafer, the source drain junction sits directly on dielectric layer (BOX) and no leakage occurs even the metal punches through the junction [3]. We considered epitaxial transfer method for the integration of ultrathin layers of single-crystal InAs on Si/ SiO2 substrates. As a parallel with silicon-on-insulator (SOI) technology14, we use 'XOI' to represent our compound semiconductor on-insulator platform.[12] Through experiments and simulation, the electrical properties of InAs XOI transistors are explored, elucidating the critical role of quantum confinement in the transport properties of ultrathin XOI layers. Importantly, a high-quality InAs/dielectric interface is obtained by the use of a novel thermally grown interfacial InAsOx layer (1 nm thick). The fabricated field-effect transistors exhibit a peak transconductance of 1.6mSmm21 at a drain–source voltage of 0.5 V, with an on/off current ratio of greater than 10,000.

II. ADOPTED TECHNIQUE

The main objective of our work is performance comparison between InAs-on-Insulator and Silicon-on-Insulator MOSFETs using a compact model. First of all, we follow a model as discussed in Ref. [9] which uses three surface potentials. However, before proceed to our objective, we want to verify our model with the results of Ref. [9]. After verifying the model, we want to change the channel material to InAs by replacing Si and then to compare the performance. For fair comparison the device dimensions, doping densities will be assumed same. Then after calculating surface potential, using this we want to compare the C-V characteristics and the drain current. From the I_D-V_{GS} curve, we can calculate the threshold voltage, on and off current ratio of the MOSFET. Then we also want to observe the difference between transconductance and unity gain frequency of InAs-on-Insulator and Silicon-on-Insulator MOSFET.

III. MODEL

3.1 Ideal Surface Potential Model

To obtain a closed-form analytical approximation for potentials at the three surfaces of the FDSOI MOSFET, namely front oxide–silicon film surface φ_{sf} , buried oxide–silicon film interface φ_{sb} , and buried oxide–substrate interface φ_{sbulk} . For this purpose, three different equations are obtained by solving the 1-D Poisson equation in vertical direction and applying the boundary conditions at different surfaces [9]. The 1-D Poisson equation of an FD-SOI MOSFET, shown in Figure 2-1, can be written as:

$$\frac{\partial^2\varphi(y)}{\partial y^2} = -\frac{1}{\varepsilon_{Si}}(p(y) - n(y) - N_{ch}) \quad \text{..... (1)}$$

Where $\varphi(y)$ is the potential, ε_{Si} is the dielectric constant of silicon, $p(y)$ and $n(y)$ are the hole and electron concentrations, respectively and N_{ch} is the doping in the silicon layer [9].

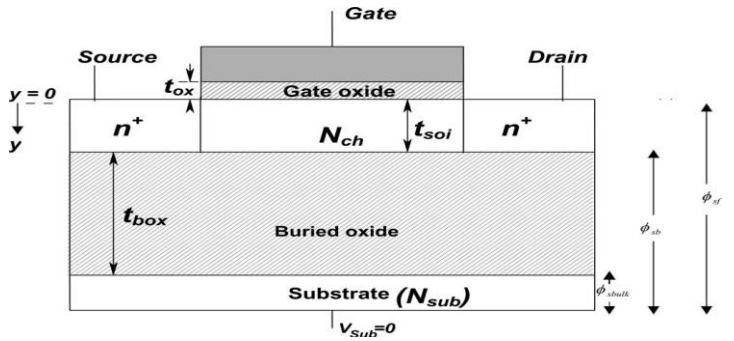

Fig .1. Cross-sectional view of the FD SOI MOSFET [9]

Equation (1) can be further expressed as

$$\frac{\partial^2\varphi(y)}{\partial y^2} = -\frac{qN_{ch}}{\varepsilon_{Si}}\left\{\left[\exp\left(-\frac{\varphi(y)}{\varphi_t}\right)-1\right] - \exp\left(-\frac{2\varphi_F + V_{CB}}{\varphi_t}\right)\left[\exp\left(\frac{\varphi(y)}{\varphi_t}\right)-1\right]\right\} \quad \text{.... (2)}$$

Where φ_F is the Fermi potential, φ_t is the thermal voltage, and V_{CB} is the channel floating body potential, which varies from V_{SB} at source to $V_{SB}+V_{DS}$ at drain [9]. Multiplying both sides of Eq. (2) by $2\frac{\partial\varphi(y)}{\partial y}$ and then integrating from buried oxide–silicon film interface φ_{sb} to front oxide–silicon film surface φ_{sf} considering boundary conditions we get,

$$(V_g - \varphi_{sf})^2 - \frac{C_{box}^2}{C_{ox}^2}(\varphi_{sbulk} - \varphi_{sb})^2 = -\gamma^2\left\{\begin{array}{l} -\varphi_t\left[\exp\left(-\frac{\varphi_{sf}}{\varphi_t}\right) - \exp\left(-\frac{\varphi_{sb}}{\varphi_t}\right)\right] \\ -(\varphi_{sf} - \varphi_{sb}) - \exp\left(-\frac{2\varphi_F + V_{CB}}{\varphi_t}\right) \\ \left(\varphi_t\left[\exp\left(\frac{\varphi_{sf}}{\varphi_t}\right) - \exp\left(\frac{\varphi_{sb}}{\varphi_t}\right)\right] - (\varphi_{sf} - \varphi_{sb})\right) \end{array}\right\} \quad \text{.....(3)}$$

$$\varphi_{sf} - \varphi_{sb} = \alpha + (\varphi_{sb} - \varphi_{sbulk})\frac{C_{box}}{C_{soi}} \quad \text{..... (4)}$$

$$\varphi_{sb} = \varphi_{sbulk} + \gamma_{bulk}\sqrt{\varphi_{sbulk}} \quad \text{..... (5)}$$

Where, $\gamma_{bulk} = \frac{\sqrt{2qN_{sb}\varepsilon_{Si}}}{C_{box}}$, $\alpha = \frac{qN_{ch}t_{soi}^2}{2\varepsilon_{Si}}$, $C_{soi} = \frac{\varepsilon_{ox}}{t_{soi}}$ and $C_{box} = \frac{\varepsilon_{ox}}{t_{box}}$.

Equations (3), (4) and (5) together describe the exact Poisson equation for an FDSOI MOSFET and are obtained without any approximation except the assumptions that the back silicon surface and the substrate region never go into inversion and that the device always remains in FD condition. These equations can be solved iteratively to get the exact values of all three surface potentials [9].

3.2 Drain Current Model

The surface potential nor the depletion charge density changes much after strong inversion. The central assumption of the charge-sheet model for the depletion charge density,

$$Q_d = -qN_aW_d = -\sqrt{2\varepsilon_{Si}qN_a\varphi_{sf}} \quad \text{..... (6)}$$

Can be extended to beyond strong inversion. Since the total silicon charge density Q_s is given by

$$V_{GS} = V_{FB} + \varphi_{sf} - \frac{Q_s}{C_{ox}} \quad \text{..... (7)}$$

Now Eq. (6) allows the inversion charge density to be expressed as

$$Q_i = Q_s - Q_d = -C_{ox}\left(V_{GS} - V_{FB} - \varphi_{sf}\right) + \sqrt{2\varepsilon_{Si}qN_a\varphi_{sf}} \quad \text{..... (8)}$$

It should be noted that the charge sheet model does not literally assume all the inversion charge is located at the silicon surface with a zero depth.

The variable in the drain current integral, $I_{ds} = \mu_{eff}\frac{W}{L}\int_0^{V_{DS}}(-Q_i(V))dV$ ..... (9)

Can be transformed from V to φ_{sf}, $I_{ds} = \mu_{eff}\frac{W}{L}\int_{\varphi_{ss}}^{\varphi_{sd}}\left(-Q_i\left(\varphi_{sf}\right)\right)\frac{dV}{d\varphi_{sf}}d\varphi_{sf}$ ..... (10)

Where φ_{ss}, φ_{sd} are the values of the surface potential at the source and the drain ends of the channel

3.3 Surface Electric Field and Surface Charge

Conventionally, the electrostatic potential is defined in terms of the intrinsic Fermi level,

$$\varphi_i = -\frac{E_i}{q} \quad \text{..... (11)}$$

There is a negative sign because E_i is defined as electron energy while φ_i is defined for a positive charge. The electric field E_s which is defined as the electrostatic force per unit charge is to the negative gradient of φ .

$$E_s = -\frac{d\varphi}{dy} \quad \text{..... (12)}$$

Now we can write Poisson's equation as $\frac{d^2\varphi}{dy^2} = -\frac{dE_s}{dy} = -\frac{\rho_{net}(y)}{\varepsilon_{Si}}$ ..... (13)

Where $\rho_{net}(y)$ is the net charge density per unit volume at y, and ε_{Si} is the permittivity of silicon equal to $11.7\varepsilon_0$. Here ε_0 = 8.85 x 10^{-14} F/cm is the vacuum permittivity [11].

Another form of Poisson's equation is Gauss's law, which is obtained by integrating Eq. (13)

$$E_s = \frac{1}{\varepsilon_{Si}}\int \rho_{net}(y)dy = \frac{Q_s}{\varepsilon_{Si}} \quad \text{..... (14)}$$

Where Q_s is the integrated charge density per unit area. Now the surface charge can be obtain from Eq. (7) if φ_{sf} is known

$$Q_S = -C_{ox}(V_{GS} - V_{FB} - \varphi_{sf}) \quad \text{..... (15)}$$

Therefore the surface electric field becomes [11]

$$E_S = -\frac{C_{ox}}{\varepsilon_{Si}}(V_{GS} - V_{FB} - \varphi_{sf}) \quad \text{..... (16)}$$

3.4 Capacitances of MOS Structure

We now consider the capacitances of a MOS structure. In most cases, MOS capacitances are defined as small-signal differential of charge with respect to voltage or potential. The total MOS capacitance per unit area is [11]

$$C_g = \frac{d(-Q_s)}{dV_g} \quad \text{..... (31)}$$

By substituting the value of Q_s, we get

$$C_g = C_{ox}\left\{\frac{\rho(\varphi_{sf})^{\frac{1}{2}}}{\rho(\varphi_{sf})^{\frac{1}{2}} + k_o\frac{q}{kT}\left(1 + \frac{n_i^2}{N_A^2}e^{\frac{q\varphi_{sf}}{kT}}\right)}\right\} \quad \text{..... (32)}$$

Where $\rho(\varphi_{sf}) = \frac{q}{kT}\varphi_{sf} + \frac{n_i^2}{N_A^2}e^{\frac{q\varphi_{sf}}{kT}}$

IV. PERFORMANCE IMPROVEMENT FOR XOI MOSFET WITH RESPECT TO SOI

The three surface potential based compact model is used to generate the surface potentials and then the front surface potential is used to calculate the I-V and C-V curves for performance comparison between the SOI and XOI MOSFETs. The different parameters used for the InAs XOI MOSFET are shown in Table 1. These parameters have been used in Ref. [12]. For fair comparison, the same device dimensions and doping densities are assumed for the SOI MOSFET.

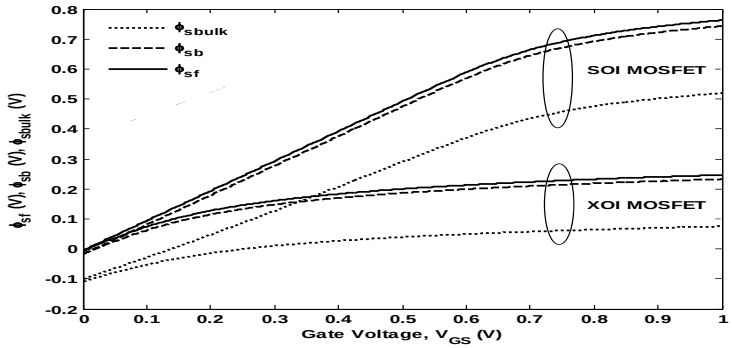

Figure. 2. Different surface potentials versus gate voltage curve

Figure 1-2 shows the variation of surface potentials φ_{sf} , φ_{sb} and φ_{sbulk} versus the gate voltage of SOI and XOI MOSFETs for a front oxide thickness of 7 nm, buried oxide thickness of 50 nm and silicon film thickness of 15 nm. Here, the surface potential curves of XOI MOSFET are saturated quicker than SOI MOSFET. We have got small saturation value of front surface potential because a large potential drops across the gate oxide and a smaller voltage drops across the channel thickness of XOI MOSFET.

Table 1: Simulation parameters of SOI and XOI MOSFETs [12]

Subject	SOI	XOI
Flat Band voltage, V_{fb}	-0.2 V	-0.2V
Electron concentration in channel, N_{ch}	4×10^{16} cm^{-3}	4×10^{16} cm^{-3}
Electron concentration in substrate, N_{sub}	1×10^{15} cm^{-3}	1×10^{15} cm^{-3}
Intrinsic concentration, n_i	1.5×10^{10} cm^{-3}	1×10^{15} cm^{-3}
Gate Oxide thickness, t_{ox}	7 nm	7 nm
Buried Oxide thickness, t_{box}	50 nm	50 nm
Channel Thickness, t_{soi}	15 nm	15 nm
Vacuum Permittivity, ε_o	8.854×10^{-12} F/m	8.854×10^{-12} F/m
Relative permittivity of silicon dioxide, $\varepsilon_{r,ox}$	3.9	3.9
Relative permittivity of Zirconium dioxide, ε_r	20	20
Electron mobility, μ_e	650 cm^2/V-s	1300 cm^2/V-s
Channel Length, L	500 nm	500 nm

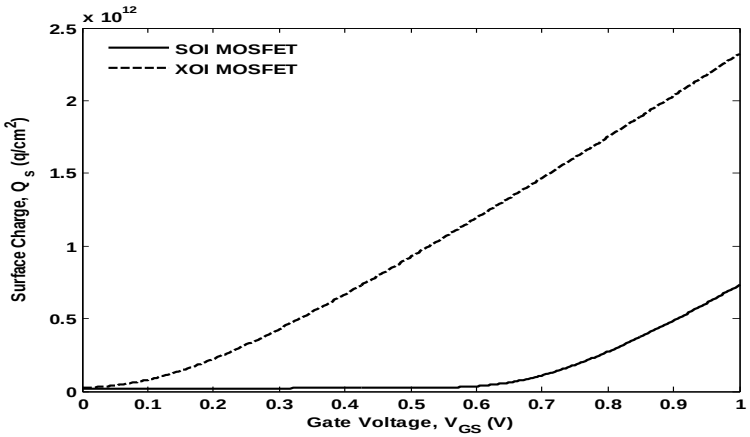

Figure. IV. Surface charge versus gate voltage curve

Figure 1-3 shows the surface charge density versus gate voltage curve between SOI and XOI MOSFETs. There are two regions of the curve. The flattened region represents the weak inversion region and the rising part is the strong inversion region. Since the inversion charge density increases rapidly with an increase in gate voltage as we have seen in the Figure 3-4. It occurs like that the surface potential changes with gate voltage and the electron concentration increases rapidly with very small changes in surface potential. We have observed, for XOI MOSFET the surface charge curve reaches in strong inversion region earlier than SOI MOSFET. For this, the surface potentials of XOI MOSFET saturated earlier than SOI MOSFET.

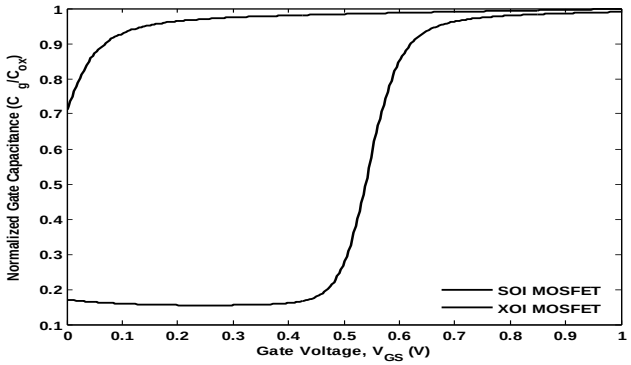

Figure.4. Gate capacitance versus gate voltage curve

For SOI MOSFET at first the curve is flat and the capacitance value is small because the FET turns on at $V_{GS} \approx$ 0.45 V. After the FET is turned on, the capacitance rapidly increases with gate bias and saturates to C_{ox} at strong inversion. The gate capacitance of the XOI FET quickly saturates to C_{ox} because the XOI FET turns on at a very small gate bias.

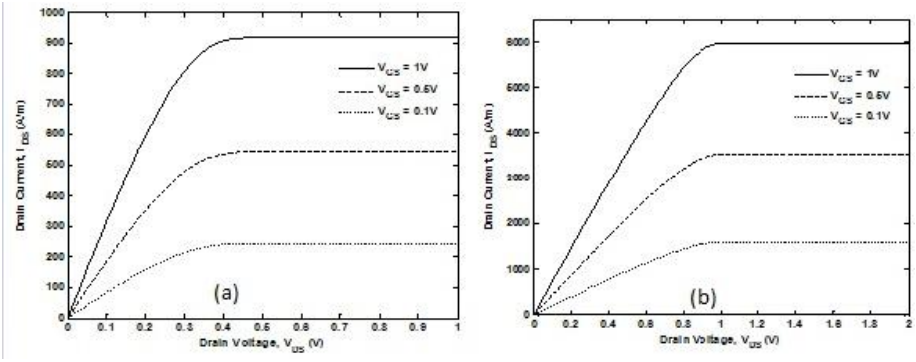

Figure. 1. $I_D - V_{DS}$ Characteristics curves of SOI and XOI MOSFETs

Figure 1-5(a) and (b) show $I_D - V_{DS}$ characteristics curves of SOI and XOI MOSFETs respectively for different gate voltages. When V_{GS} changes, the I_D versus V_{DS} curve will change. We saw that, if V_{GS} increases, the initial slope of I_D versus V_{DS} increases. The drain current in saturation is virtually independent of V_{DS} and the MOSFET acts as a current source.

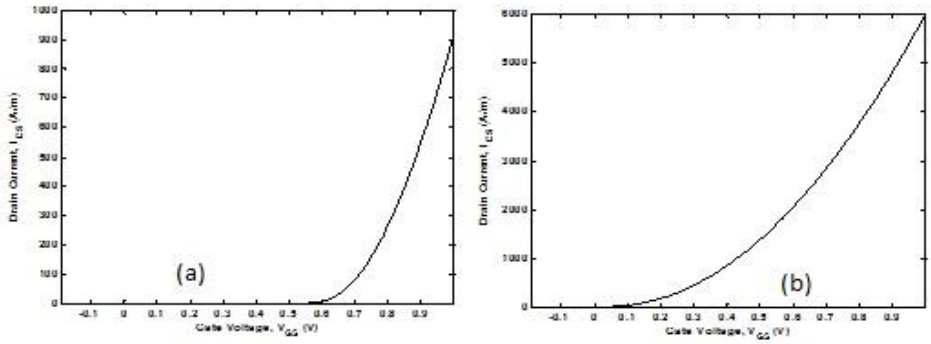

Figure. 6. Gate capacitance versus gate voltage curve

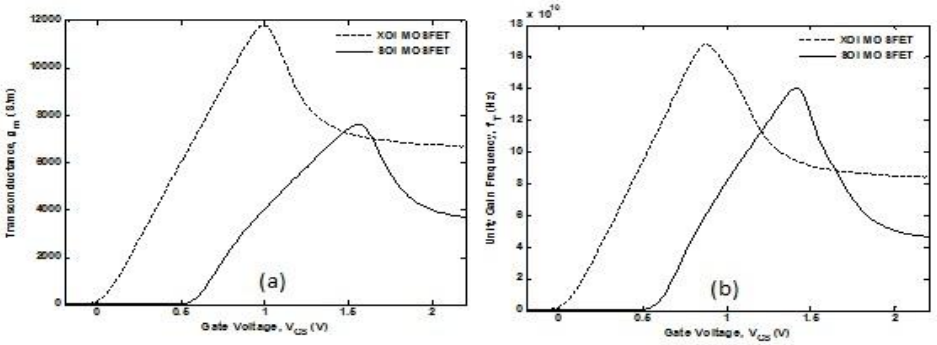

Figure.7. Gate capacitance versus gate voltage curve

Figure 1-6 shows the transconductance versus gate voltage characteristics curve for SOI and XOI MOSFETs for V_{DS} = 0.5 V and L = 500 nm. The MOSFET transconductance is defined as the change in drain current with respect to the corresponding change in gate voltage. The transconductance increase linearly with V_{DS} but is independent of V_{GS} in the saturation region. The transconductance is also a function of the geometry of the device as well as of carrier mobility and threshold voltage. For XOI MOSFET, transconductance is around 1.2 times higher than that of SOI MOSFET. This is because the carrier mobility of InAs is higher than that of Si.

Figure 1-7 shows the unity gain frequency versus gate voltage characteristics curve of XOI and SOI MOSFETs. The unity gain frequency of a MOSFET (f_T) is defined as the frequency at which the short-circuit current-gain (i_d / i_g) of the common-source amplifier becomes unity. f_T is also called the transition frequency. f_T gives an idea of the high-frequency behavior of the MOSFET. In XOI MOSFET, unity gain frequency f_T is 1.2 times higher than SOI MOSFET. Higher f_T means higher transconductance and lower internal MOSFET capacitances which means better amplification. So, by using XOI MOSFET, we can amplify signal more than SOI MOSFET.

V. CONCLUSION

From the simulation results, we observe that, for the same device dimensions and doping densities of the SOI and XOI MOSFETs, we got around 6 times higher drive current, around 1.5 times higher transconductance and around 1.2 times higher unity gain frequency. On the other hand, we got very low (negative) threshold voltage for XOI MOSFET. After the analysis, we see that, to overcome the limitations of bulk silicon MOSFET, we can use SOI MOSFET which can be solved the scaling problems. And over SOI MOSFET, XOI MOSFET has better performance because of high carrier mobility of compound semiconductors such as III-V semiconductors. So, by using XOI MOSFET, we can get high speed operation and amplification, low power consumption than SOI MOSFET as well as bulk silicon MOSFET.

REFERENCES

[1] Narayana Murty Kodeti, "White paper on Silicon-on-insulator (SOI) implementation", Infotech Enterprises Ltd., pp. 3-8, June 2009
[2] Takayasu Sakurai, Akira Matsuzawa, and Takakuni Douseki, "Fully depleted SOI CMOS circuits and technology for ultra-low power applications", First edition, Springer, ch. 1, pp. 1-19, 2006
[3] John Z. Ren, "Low voltage SOI MOSFET with suppressed floating body effects", Master of Applied Science thesis paper, University of Toronto, pp. 9-17, 1999
[4] Aatish Kumar, V. Ramgopal Rao and Prof. Rakesh Lal, "Simulation and characterization of SOI MOSFETs", Dual degree project report, Indian Institute of Technology, Mumbai, pp. 49-50, 2001
[5] http://en.wikipedia.org/wiki/SiliconOnInsulator
[6] Zhou Xing, Lim Khee Yong, "A general approach to compact threshold voltage formulation based on 2D numerical simulation and experimental correlation for deep submicron ULSI technology development", IEEE Transactions on Electron Devices, vol. 47, pp. 214-221, January 2000
[7] Neil H. E. Weste, Kamran Eshraghian, "Principles of CMOS VLSI Design", Second edition, Addison Wesley, ch. 2, pp. 27-35, October 1994
[8] Haldun Haznedar, "Digital Microelectronics", First edition, Benjamin-Cummings publication company, ch. 5, pp. 174-181, January 1991
[9] Pradeep Agarwal, Govind Saraswat, and M. Jagadesh Kumar, "Compact surface potential model for FD SOI MOSFET considering substrate depletion region", IEEE Transactions on Electron Devices, vol. 55, no. 3, pp. 789-795, March 2008
[10] J. R. Brews, "A charge-sheet model of the MOSFET," Solid State Electron., vol. 21, pp. 345-346, 1978
[11] Yuan Taur, Tak H. Ning, "Fundamentals of modern VLSI devices," Second edition, Cambridge University Press, ch. 2-3, pp. 52-90, 2009
[12] Hyunhyub Ko, Kuniharu Takei, Rehan Kapadia, Steven Cguang, Hui Fang, Paul W. Leu, Kartik Ganapathi, Elena Plis, Ha Sul Kim, Szu-Ying Cgen, Morten Madsen, Alexandra C. Ford, Yu-Lun Chueh, Sanjay Krishna, Sayeef Salahuddin & Ali Javey, " Ultrathin compound semiconductor on insulator layers for high-performance nanoscale transistors", Nature, vol. 468, pp. 286-289, November, 2010
[13] Takayasu Sakurai, Akira Matsuzawa, and Takakuni Douseki, "Fully depleted SOI CMOS circuits and technology for ultra-low power applications", First edition, Springer, ch. 8, pp. 372-373, 2006
[14] Dieter K. Schrodera and Jeff A. Babcock, "Negative bias temperature instability: road to cross in deep submicron silicon semiconductor manufacturing", Applied Physics Reviews- Focus Review, pp. 5-6, July 2003

Simulink Modeling of Novel Hybrid H-Bridge Inverter for Smart Grid Application

Ch.Venkateswra rao, [1] S.S.Tulasiram, [2] Arun Kumar Rath[3]
[1](PHD scholar, Department of EEE, JNTUK, Kakinad, India)
[2](Professor in Department of EEE, JNTUH, Hyderabad, AP India)
[3](Asst. Professor in Department of EEE, GIET, Gunupur, India)

Abstract: *Hybrid H- bridge inverter. The proposed novel cascaded Hybrid H-bridge produces higher voltage levels with less number this paper presents a single-phase multistring Multi-level photovoltaic (PV) inverter topology for Micro grid-connected PV systems with a novel of devices. This will reduce the number of gate drives and protection circuits requirement, this inurn reduces the cost increase the reliability. Design Procedure for various components of single Hybrid H- bridge cell is given. A cascaded Grid connected PV topology is proposed. Finally a Matlab/Simulink based model is developed and simulation results are presented.*

Keywords:*PVCell, Hybridge H-bridge, Multi-lebel phovoltaic(PV) inverter, Matalab/Simulink, Micro grid-connected PV System;*

I. Introduction

Natural quantity available, it has been spotlighted as the future energy sources of promising potentiality, due As the PV system is clean and large enough in the to the stable supply of the energy and alternative method of responding to the problem of the earth environment followed by the increase of the demand for the electric power supply. Solar-electric-energy demand has grown consistently by 20%–25% per annum over the past 20 years, which is mainly due to the decreasing costs and prices. This decline has been driven by the following: 1) an increasing efficiency of solar cells; 2) manufacturing-technology improvements; and 3) economies of scale [2]. A PV inverter, which is an important element in the PV system, is used to convert dc power from the solar modules into ac power to be fed into the grid. A general overview of different types of PV inverters is given in [3] and [4].

In recent years, multilevel converters have shown some significant advantages over traditional two-level converters, especially for high power and high voltage applications. In addition to their superior output voltage quality, they can also reduce voltage stress across switching devices. Since the output voltages have multiple levels, lower d*v/dt is achieved, which greatly alleviates electromagnetic* interference problems due to high frequency switching. Over the years most research work has focused on converters with three to five voltage levels, although topologies with very high number of voltage levels were also proposed. In general, the more voltage levels a converter has the less harmonic and better power quality it provides. However, the increase in converter complexity and number of switching devices is a major concern for multilevel converter. There are several topologies available, being the Neutral Point Clamped [5], Flying Capacitor [6] and Cascaded H bridge inverter [7] the most studied and used. In recent years many variations and combinations of these topologies have been reported, one of them is the cascaded H-bridge [7-10].

II. High Power Converters Classifications

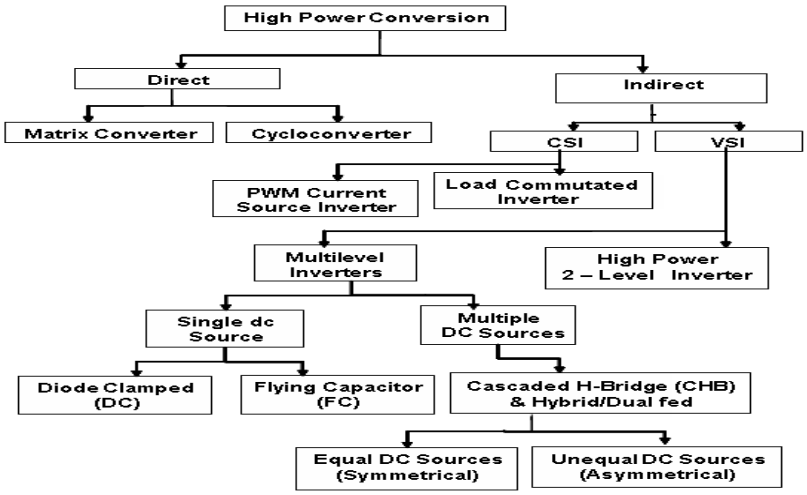

Figure 1 Classification of High power Converters

Fig.1 shows the classification of high power converters. Out of all converters Cascaded bridge configuration is more popular. Cascaded bridge configuration is again classified into 2 types 1) Cascaded Half Bridge 2) Cascaded Full Bridge or Cascaded H-Bridge. In this paper a novel cascaded hybrid H- Bridge topology is proposed for PV application.

A Half H-Bridge

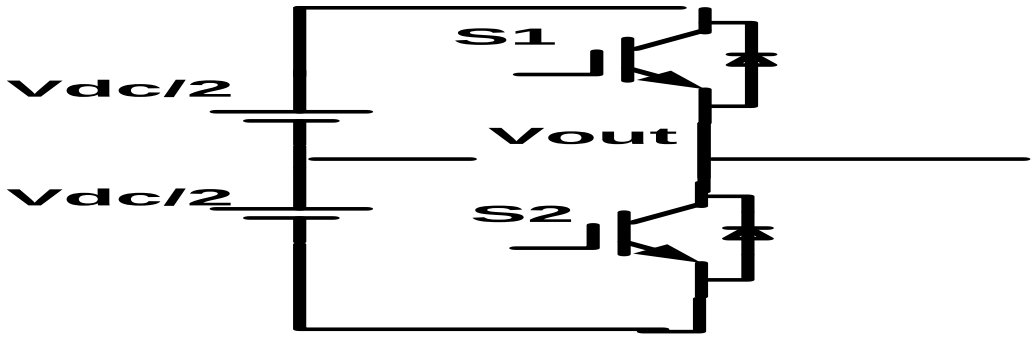

Figure 2 Half Bridge

Fig.2 shows the Half H-Bridge Configuration. By using single Half H-Bridge we can get 2 voltage levels. The switching table is given in Table 1

Table 1. Switching table for Half Bridge

Switches Turn ON	Voltage Level
S2	Vdc/2
S1	-Vdc/2

B Full H-Bridge

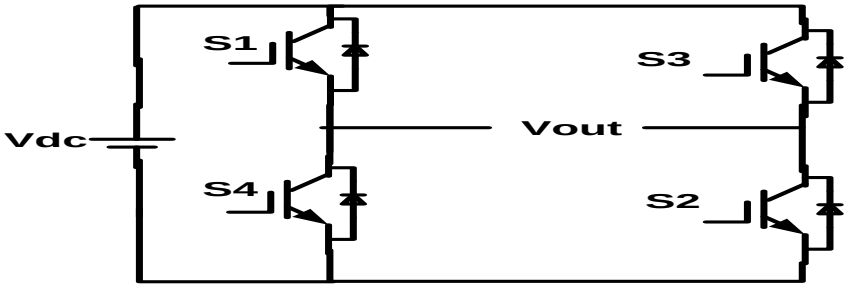

Figure. 3 Full H-Bridges

Fig.3 shows the Full H-Bridge Configuration. By using single H-Bridge we can get 3 voltage levels. The number output voltage levels of cascaded Full H-Bridge are given by 2n+1 and voltage step of each level is given by Vdc/n. Where n is number of H-bridges connected in cascaded. The switching table is given in Table2

C Hybrid H-Bridge

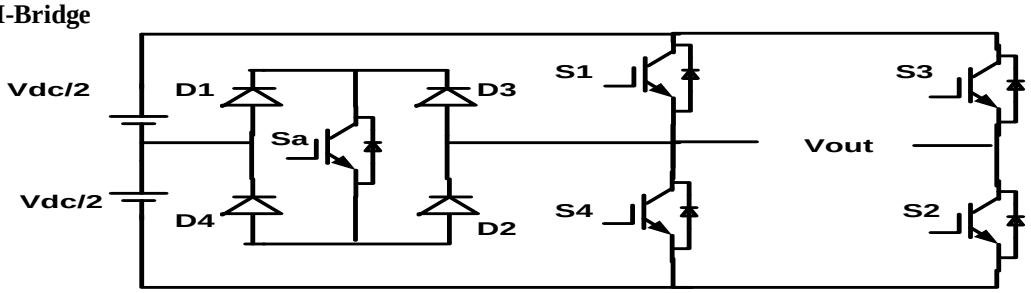

Table 2. Switching tabe Full Bridge

Switches Turn ON	Voltage Level
S1,S2	Vdc
S3,S4	-Vdc
S4,D2	0

Figure. 4 Hybrid H-Bridges

Fig. 4 shows the Hybrid H-Bridge configuration. By using single Hybrid H-Bridge we can get 5 voltage levels. The number output voltage levels of cascaded Hybrid H-Bridge are given by 4n+1 and voltage step of each level is given by Vdc/2n. Where n is number of H-bridges connected in cascaded. The switching table of Hybrid H-Bridge is given in Table 3.

Table 3. Switching table for Hybrid H-Bridge

Switches Turn On	Voltage Level
Sa, S2	Vdc/2
S1,S2	Vdc
S4,D2	0
Sa,S3	-Vdc/2
S3,S4	-Vdc

D Cascaded Hybrid H-Bridge

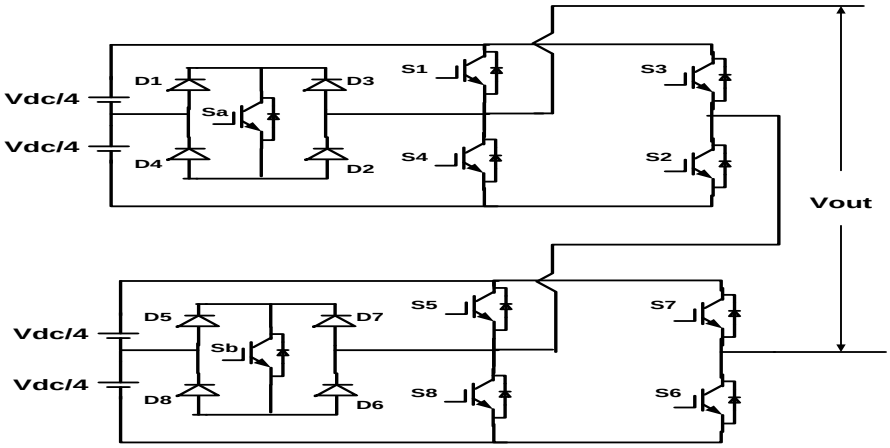

Figure 5. Cascaded Hybrid H-Bridges

The proposed CHHB uses less number of switches to produce more voltage levels. This will reduce Gate Drivers and protection circuit requirement thus it reduce cost and complexity of the circuit. For example for 9 level output the proposed converter uses 10 switches but cascaded H- Bridge converter uses 12 switches. This difference increases as the number of output voltage levels increases

Table 4 Switching table for Cascaded Hybrid H-Bridge

Switches Turn On	Voltage Level
Sa,S2,S8,D6	Vdc/4
S1.S2,S8,D6	2Vdc/4
S1,S2,Sb,S6	3Vdc/4
S1,S2,S5,S6	Vdc
S4,D2,S8,D6	0
Sa,S3,S8,D6	-Vdc/4
S3,S4,S8,D6	-2Vdc/4
S3,S4,Sb,S7	-3Vdc/4
S3,S4,S7,S8	-Vdc

III. DESIGN OF PROPOSED NOVEL HYBRID H-BRIDGE INVERTER

A. Device Current

The IGBT and DIODE currents can be obtained from the load current by multiplying with the corresponding duty cycles. Duty cycle, $d = ½(1+Km\sin\omega t)$

Where, m = modulation index K = +1 for IGBT, -1 for Diode.

$$i_{ph} = \sqrt{2}\, I\, \sin(\omega t - ø)$$

Where i = RMS value of the load (output) current,

Ø = Phase angle between load voltage and current.

Then the device current can be written as follows.

$$\therefore\ i_{device} = \frac{\sqrt{2}}{2} I \sin(\omega t - ø) * (1 + km\ \sin \omega t)$$

The average value of the device current over a cycle is calculated as

$$i_{avg} = \frac{1}{2\pi}\int_{ø}^{\pi+ø} \frac{\sqrt{2}}{2} I \sin(\omega t - ø) * (1 + k\, m sin\omega t) d\omega t$$

$$= \sqrt{2}\, I \left[\frac{1}{2\pi} + \frac{K\, m}{8} \cos ø\right]$$

The device RMS current can be written as

$$i_{rms} = \sqrt{\int_{ø}^{\pi+ø} \frac{1}{2\pi} \left(\sqrt{2}\, I \sin(\omega t - ø)\right)^2 * \frac{1}{2} * \left((1 + k\, m sin\omega t) d\omega t\right)} = \sqrt{2}\, I \sqrt{\left[\frac{1}{8} + \frac{K\, m}{3\pi} \cos ø\right]}$$

B. IGBT Loss Calculation

IGBT loss can be calculated by the sum of switching loss and conduction loss. Where conduction loss can be calculated by,

$$P_{on\,(IGBT)} = V_{ceo} * I_{avg\,(igbt)} + I^2_{rms\,(igbt)} * r_{ceo}$$

$$I_{avg\,(igbt)} = \sqrt{2}\, I \left[\frac{1}{2\pi} + \frac{m}{8} \cos ø\right]$$

$$I_{rms\,(igbt)} = \sqrt{2}\, I \sqrt{\left[\frac{1}{8} + \frac{m}{3\pi} \cos ø\right]}$$

Values of V_{ceo} and r_{ceo} at any junction temperature can be obtained from the output characteristics (Ic vs. Vce) of the IGBT as shown in Fig .6.

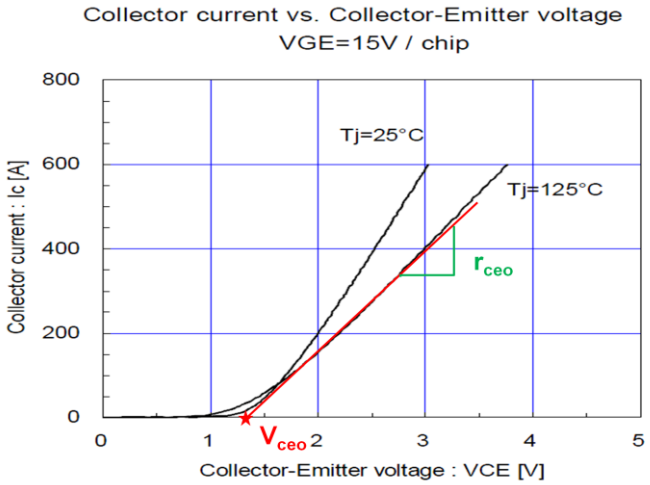

Figure 6 IGBT output characteristics

The switching losses are the sum of all turn-on and turn-off energies at the switching events

$$E_{sw} = E_{on} + E_{off} = a + b\, I + c\, I^2$$

Assuming the linear dependence, switching energy $E_{sw} = (a + b\, I + c\, I^2) * \frac{V_{DC}}{V_{nom}}$

Here V_{DC} is the actual DC-Link voltage and V_{nom} is the DC-Link Voltage at which E_{sw} is given. Switching losses are calculated by summing up the switching energies.

$$P_{sw} = \frac{1}{T_o} \sum_n E_{sw}\,(i)$$

Here 'n' depends on the switching frequency.

$$P_{sw} = \frac{1}{T_o} \sum_n (a + b\, I + c\, I^2)$$

$$= \frac{1}{T_o} \left[\frac{a}{2} + \frac{b\, I}{\pi} + \frac{c\, I^2}{4}\right]$$

After considering the DC-Link voltage variations switching losses of the IGBT can be written as follows.

$$P_{sw\,(IGBT)} = f_{sw} \left[\frac{a}{2} + \frac{b\, I}{\pi} + \frac{c\, I^2}{4}\right] * \frac{V_{DC}}{V_{nom}}$$

So, the sum of conduction and switching losses gives the total losses.

$$P_{T\,(IGBT)} = P_{on\,(IGBT)} + P_{sw\,(IGBT)}$$

C. Diode Loss Calculation

The DIODE switching losses consists of its reverse recovery losses and the turn-on losses are negligible.

$$E_{rec} = a + b\,I + c\,I^2$$

$$P_{sw\,(DIODE)} = f_{sw}\left[\frac{a}{2} + \frac{b\,I}{\pi} + \frac{c\,I^2}{4}\right] * \frac{V_{DC}}{V_{nom}}$$

So, the sum of conduction and switching losses gives the total DIODE looses.

$$P_{T\,(DIODE)} = P_{on\,(DIODE)} + P_{sw\,(DIODE)}$$

The total loss per one switch (IGBT+DIODE) is the sum of one IGBT and DIODE loss.

$$P_T = P_{T\,(IGBT)} + P_{T\,(DIODE)}$$

D. Thermal Calculations

The junction temperatures of the IGBT and DIODE are calculated based on the device power losses and thermal resistances. The thermal resistance equivalent circuit for a module is shown in Fig 7. In this design the thermal calculations are started with heat sink temperature as the reference temperature. So, the case temperature from the model can be written as follows.

$$T_c = P_T\,R_{th(c-h)} + T_h$$

Here $R_{th(c-h)}$ = Thermal resistance between case and heat sink

P_T = Total Power Loss (IGBT+DIODE)

IGBT junction temperature is the sum of the case temperature and temperature raise due to the power losses in the IGBT.

$$T_{j\,(IGBT)} = P_{T(IGBT)}\,R_{th(j-c)IGBT} + T_c$$

DIODE junction temperature is the sum of the case temperature and temperature raise due to the power losses in the DIODE.

junction temperatures. In order to make the calculated values close to the actual values,

$$T_{j\,(DIODE)} = P_{T(DIODE)}\,R_{th(j-c)DIODE} + T_c$$

The above calculations are done based on the average power losses computed over a cycle. So, the corresponding thermal calculation gives the average junction temperatures. In order to make the calculated values close to the actual values,

transient temperature values are to be added to the average junction temperatures.

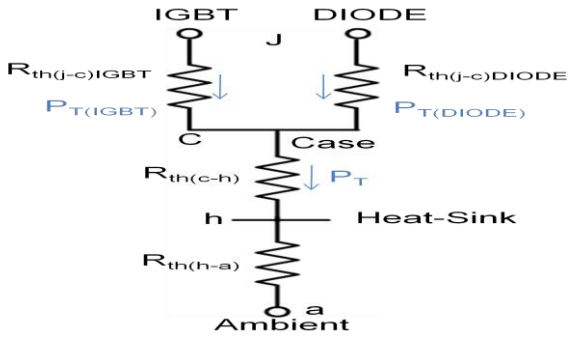

Figure. 7 Thermal resistance equivalent circuit

E. DC-Capacitor Selection

The required capacitance for each cell depends on the allowable ripple voltage and the load current. The rms ripple current flowing into the capacitor can be written as follows and the ripple current frequency is double the load current frequency (Hybrid H-Bridge).

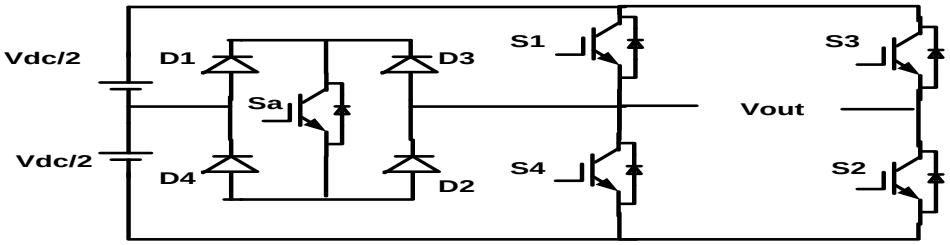

Figure. 8 Hybrid H- Bridge converter

$$I_c = -\frac{I}{V_{dc}}\frac{1}{2}\left(|U_{ac}| * K + I\omega L\right)\sin(2\omega t)$$

Since the value of 'L' is very small, the above equation can be written as below.

$$I_c = -\frac{I}{V_{dc}}\frac{1}{2}\left(|U_{ac}| * K\right)\sin(2\omega t)$$

$$I_C = -K\frac{1}{2}\frac{|U_{ac}|}{V_{dc}} * \sin(2\omega t) = -K\frac{m}{2}\sin(2\omega t)$$

Here 'm' is the modulation index.

$$\text{Here } I_{cp} = C\frac{du_{pp}}{dt}$$

$$\frac{m}{2} I\sqrt{2} = \mathrm{C}\, 2\omega * \Delta V\ V_{dc}$$

$$\mathrm{C} = \frac{m}{4\omega}\frac{1}{\Delta V\, V_{dc}}\sqrt{2}\, I$$

IV. PROPOSED PV SYSTEM

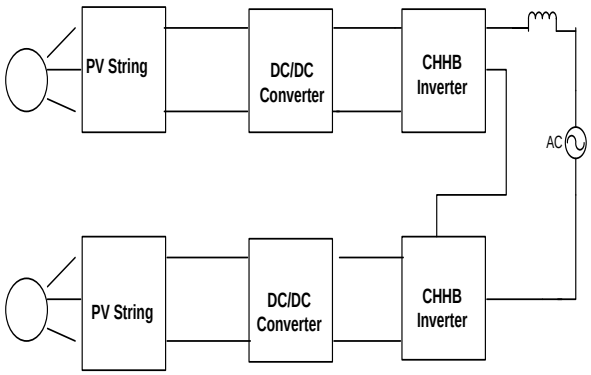

Figure. 9. Grid Connected PV System

The general block diagram of PV system is shown here. The PV string converters solar radiation into DC.Here we are using DC/DC Boost converter to increase the output voltage. The output inverter converts DC into AC and feeding into the grid. The proposed system uses small PV array cascading to produce higher voltage output. This system reduces overall cost and complexity. The Fig.8 shows the proposed PV configuration.

V. SIMULINK MODELING AND SIMULATION RESULTS

Fig. 10 Shows the Matlab/Simulink model of complete PV system. It consists of PV array block, DC/DC converter Block, Hybrid H-Bridge Block.

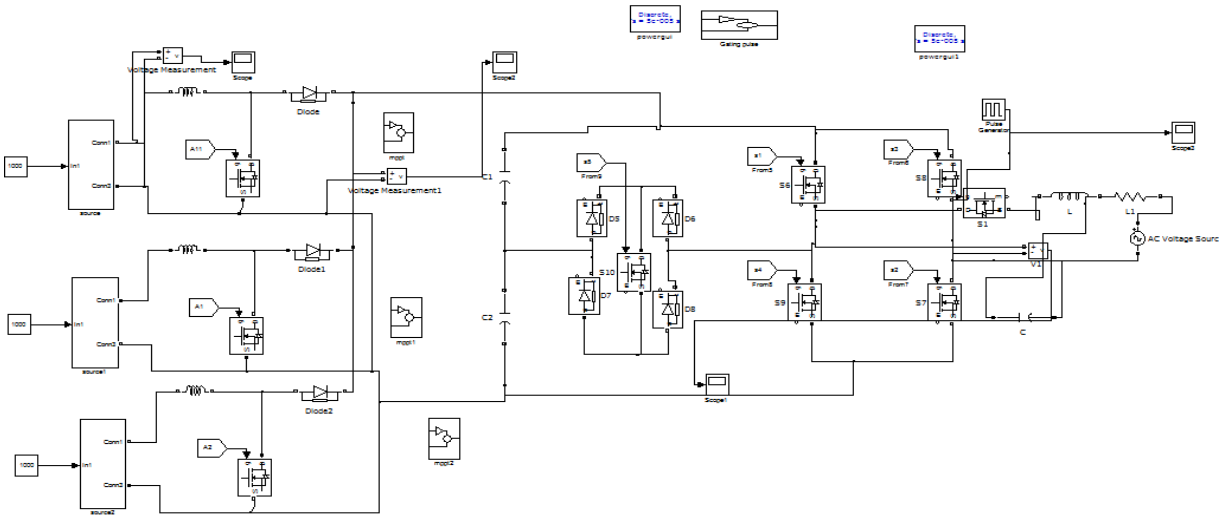

Figure. 10 Matlab/Simulink model of Hybrid H-bridge

Fig. 11 shows the inverter input DC voltage and Multilevel AC output voltage. Fig. 12 Shows the five level output of the Hybrid H-Bridge. Fig.13 shows the grid voltage and current wave forms.

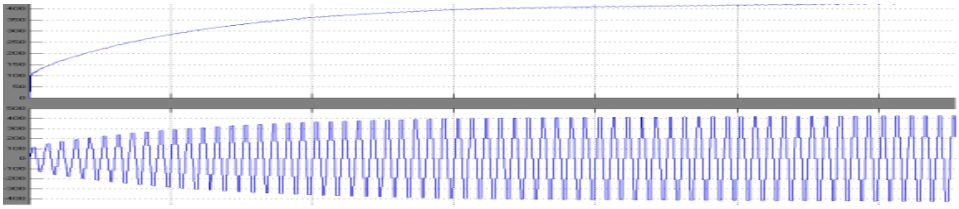

Figure.11 Inverter Input and Output

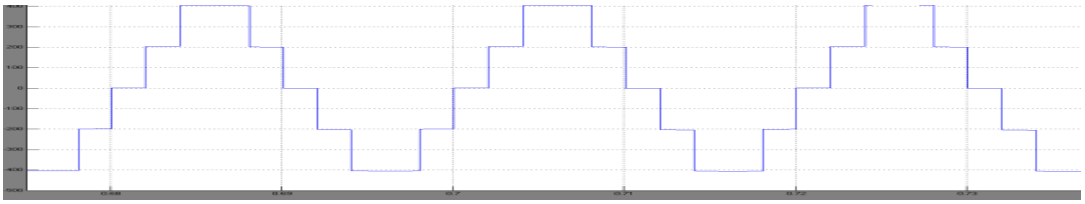

Figure12. Five level output of Hybrid H-bridge

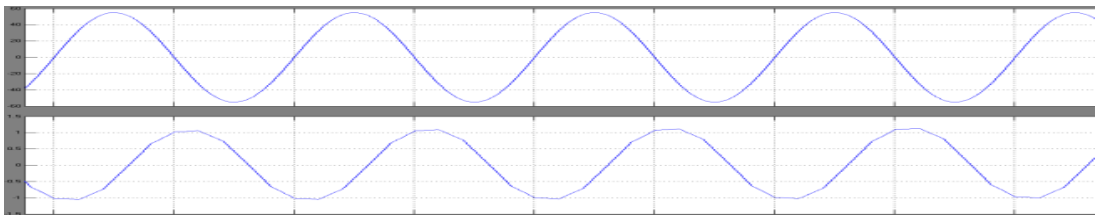

Figure13 Gr**id voltage and Grid current**

VI. CONCLUSION

This paper presents a single-phase multistring Multi-level photovoltaic (PV) inverter topology for grid-connected PV systems with a novel hybrid H- bridge inverter. The proposed novel cascaded Hybrid H-bridge produces higher voltage levels with less number of devices. This will reduce the number of gate drivers and protection circuits requirement, this inurn reduces the cost increase the reliability. Design Procedure for various components of single Hybrid H- bridge cell is given. A cascaded Grid connected PV topology is proposed. Finally a Matlab/Simulink based model is developed and simulation results are presented.

REFERENCES

[1] grid connected inverter for photovoltaic solar power generation system," in Proc. IEEE PowerCon, Oct. 2002, vol. 1, pp. 570–573.
[2] J. M. Carrasco, L. G. Franquelo, J. T. Bialasiewicz, E. Galvan, R. C. PortilloGuisado, M. A. M. Prats, J. I. Leon, and N.Moreno-Alfonso, "Power-electronic systems for the grid integration of renewable energy s[1] N. A. Rahim and S. Mekhilef, "Implementation of three-phase ources: A survey," IEEE Trans. Ind. Electron., vol. 53, no. 4, pp. 1002–1016, Aug. 2006.
[3] S. B. Kjaer, J. K. Pedersen, and F. Blaabjerg, "A review of single-phase grid connected inverters for photovoltaic modules," IEEE Trans. Ind. Appl., vol. 41, no. 5, pp. 1292–1306, Sep./Oct. 2005.
[4] S. Daher, J. Schmid, and F. L.M. Antunes, "Multilevel inverter topologies for stand-alone PV systems," IEEE Trans. Ind. Electron., vol. 55, no. 7, pp. 2703–2712, Jul. 2008.
[5] M. Meinhardt and G. Cramer, "Past, present and future of grid-connected photovoltaic- and hybrid-power-systems," in Proc. IEEE-PES Summer Meeting, Jul. 2000, vol. 2, pp. 1283–1288.
[6] S. Kouro, J. Rebolledo, and J. Rodriguez, "Reduced switching-frequency modulation algorithm for high-power multilevel inverters," IEEE Trans.Ind. Electron., vol. 54, no. 5, pp. 2894–2901, Oct. 2007.
[7] S. J. Park, F. S. Kang, M. H. Lee, and C. U. Kim, "A new single-phase five level PWM inverter employing a deadbeat control scheme," IEEE Trans. Power Electron., vol. 18, no. 18, pp. 831–843, May 2003.
[8] L. M. Tolbert and T. G. Habetler, "Novel multilevel inverter carrier-based PWM method," IEEE Trans. Ind. Appl., vol. 35, no. 5, pp. 1098–1107, Sep./Oct. 1999.
[9] Y. Liu, H. Hong, and A. Q. Huang, "Real-time calculation of switching angles minimizing THD for multilevel inverters with step modulation," IEEE Trans. Ind. Electron., vol. 56, no. 2, pp. 285–293, Feb. 2009.
[10] N. S. Choi, J. G. Cho, and G. H. Cho, "A general circuit topology of multilevel inverter," in Proc. IEEE 22th Annu. PESC, Jun. 24–27, 1991, pp. 96–103.
[9] L.M.Tolber, T.G.Habetler, "Novel Multilevel inverter Carrier based PWM Method," IEEE Ind.Appli., vol.35. Pp.1098-1107. Sep/Oct 1999.
[10] Holmes, D. G. and Lipo, T. A., Pulse width modulation for power converters: principles and practice, IEEE.
[11] T.H.Barton, "Pulse Width Modulation Waveforms – The Bessel Approximatilon", IEEE-IAS Conference Record,

Authors Profile

Ch. Venkateswara Rao receieved his M.Tech degree from JNTUK, kakinada and U.G from IE (India), Kolkata) in the year 1993. A life member in ISTE and IAENG. This Author won first prize in Energy conservations Award for the year 2009. He is currently working as a professor in the department of EEE in Gandhi Institute. of Engineering and Technology, Gunupur, Odisha He guided many.UG & PG Projects. He is having overall Industrial &Teaching experience of 18 years. His major Research interests are Energy Conservation and Smart Grid technologies.

S STulsiram working as a Professor in the Department of EEE in JNTUH, Hyd. He has 30 years of Teaching experience. He is former Head of the department of EEE, JNTUCE, Kakinada. The Author has Published many papers in International & National Journals/ Conferences. His research interests are Power Systems, High Voltage Engineering & smart grid technologies.

Arun Kumar Rath received his M. Tech Degree in Power Electronics and Drives from GIET, Gunupur under BPUT and UG from BPUT. A life time member of ISTE and also a life time member of SESI & IAENG. He working as a Asst. professor in EEE Department at Gandhi institute of engineering & Technology. He is having overall more thane 9 years experiences in Industrial and teaching fields. His interest areas are Power system engineering and Power Electronics & smart grid technologies.

International Journal of Modern Engineering Research (IJMER)
www.ijmer.com Vol.3, Issue.2, March-April. 2013 pp-667-673 ISSN: 2249-6645

Characteristics of Grade 60 and Grade 72.5 Re-bars in Pakistan

Shahida Manzoor, [1] Dr. Shuaib Ahmad[2]
12Department of Civil Engineering, NED University of Engineering & Technology, Pakistan

Abstract: *In Pakistan, quality assurance of re-bars is practically non-existent and there is no generally accepted testing method for testing of re-bars. Steel re-bars of Grade 60 are exclusively used in Pakistan; however production of high strength re-bars has recently started. In this study, thirty samples of steel re-bars of Grade 60 and thirty samples of Grade 72.5 were tested using ASTM standard testing protocol to obtain the stress-strain curves and comparisons were made between the experimental results of Grade 60 and Grade 72.5 re-bars. It can be concluded that Grade 72.5 steel shows less deformation capacity as compared to Grade 60 steel. For Grade 60 re-bars, the yield strengths of all individual re-bars were much higher than the prescribed minimum yield strength, i.e. 60 ksi. For the Grade 72.5 re- bars, about 50 % of the re-bars did not reach the prescribed minimum yield strength of 72.5 ksi.*

The experimental curves were then compared with an idealized stress-strain curve developed by using a fractional equation. It is recommended that instead of producing Grade 72.5 ksi reinforcing bars, the traditional ASTM Grade 75 reinforcing bars be produced.

Keywords: *idealized curve, standardize, stress strain curve, Tension tests*

1. Lecturer, Department of civil engineering, NED University of Engineering &Technology.
2. Professor, Department of civil engineering, NED University of Engineering &Technology.

I. INTRODUCTION

There are number of standards which cover the testing of re-bars in Pakistan. These include; ASTM Standards [1], BS Standards [2], ISO Standards [3] and PS Standard [4]. Pakistan Standards and Quality Control Authority (PSQCA) has adopted a slightly revised/modified version of BS 4449-2005 [2] standard and this standard is PS-1612-2007 [4]. The contents of PS-1612-2007 [4] are essentially the same as BS 4449-2005 [2]. For quality assurance, some agencies prefer to use portions of ASTM A615 [1] test standards and portions of BS 4449-1997 or BS 4449-2005 test standards. The use of portions of one standard and portions of the other standards is not technically correct and should not be permitted. A summary of the review of the standards [1-4] is presented in Table 1.

In Pakistan, steel bars are manufactured using variety of sources. Steel re-bars manufactured from ship scrap materials are likely not to exhibit adequate deformation capacity or ductility. This study was initiated to develop a standard testing protocol to be adopted in Pakistan for standardized testing of re-bars in Pakistan. Evaluation of testing protocol at facility of one re-bar manufacturer and one academic institution was conducted. With slight modification, the testing protocol at NED University of Engineering and technology (NEDUET) Materials Testing Laboratory was made in conformance with ASTM A615 Standard [1]. It is recommended that one internationally recognized test standard should be adopted and used in Pakistan for the testing and quality assurance of re-bars.

Using ASTM A615 [1] testing protocol, thirty samples of #5 bars, (16 mm) of Grade 60 re-bars and thirty samples of #5 bars, (16 mm) Grade 72.5 re-bars were tested and stress-strain curves were obtained. Grade 72.5 re-bars shows less deformation capacity as compared to Grade 60 re-bar steel. The experimental results were compared with idealized analytical stress-strain curve of Grade 60 (420 MPa) and Grade 72.5 (500 MPa) reinforcing bars developed by Ahmad [6, 10]. It is recommended that instead of producing Grade 72.5 ksi reinforcing bars, the traditional ASTM Grade 75 reinforcing bars be produced.

II. EXPERIMENTAL PROGRAM

In the preliminary study, an evaluation of testing protocol at facility of one manufacturer and one academic institution was conducted. For conformance with ASTM A615 Standard [1], a slight modification (adjustment in the rate of loading), was made in the testing protocol at NEDUET Materials Testing Laboratory.

Using the ASTM A615 Standard [1] and ASTM A370 [5] testing procedure, tension tests were performed for 60 samples of deformed steel re-bars. The size of bars was taken as #5 (16 mm). Thirty samples were of Grade 60 (420 MPa) rebars and thirty samples were of high strength, Grade 72.5 (500 MPa) re-bars. These tests were performed in the Material testing laboratory of NEDUET. A Universal Testing Machine of 50 tons capacity and an Extensometer were used for the tests. All the samples were cut for the required length of about 24 in (600 mm).

The tests were performed at two rates of loading, 10 mm/min (0.4 in/min) up to one half of the yield point and then rate of loading was reduced to 1.5 mm/min. (1/16 in/min) up to or near yielding. This rate of loading was maintained until the yield point, after which the rate of loading was increased to 10 mm/min (0.4 in/min) until rupture of the specimen (ASTM testing method A 370 [5]).

2.1 Results

Test results of tension tests on Grade 60 #5 (16 mm) re-bars are shown in **Table 2** and it can be observed that all of the bars show yield strength much higher than the prescribed minimum yield strength, i.e. 60 ksi. The average yield value of 30 samples is 77.2 ksi which is substantially higher than specified yield strength of 60 ksi. Stress-strain curves for 30 samples of Grade 60 #5 (16 mm) re-bars are shown in **Figure 1.**

Test results of tension tests on Grade 72.5 deformed bars #5 (16 mm) are shown in **Table 3** and it can be observed that about 50 % of the bars do not reach the prescribed minimum yield strength of 72.5 ksi. The average yield value of 30 samples is 72.7 ksi which is just above the specified yield strength of 72.5 ksi. Stress-strain curves for 30 samples of Grade 72.5 re-bars are shown in **Figure 2.**

2.1.1 Control points of stress-strain curve and Idealized stress-strain Curves

For the development of idealized analytical stress-strain curve of steel re-bars, five (5) control points are used. **Figure 3** shows the control points for an experimental stress strain curve. Using the coordinates of the control points, calibrated by Ahmad [6, 10] for about 2000 samples and the fractional equation developed by Ahmad [6, 10], idealized stress-strain curves for Grade 60 re-bars and Grade 72.5 re-bars are developed. These idealized analytical stress-strain curves are compared with the experimental stress-strain curves.

2.1.2 Average Experimental stress strain curve

The control points from test results of thirty samples of Grade 60 and thirty samples of Grade 72.5 re-bar (High strength) were averaged and the average values of the control points were obtained. **Table 4** shows the average values of the experimental control points for Grade 60 re-bars of #5(16 mm) and **Table 5** shows the average values of the experimental control points for Grade 72.5 re-bars of #5(16 mm).

Figure 4 shows the average stress-strain curve of Grade 60 #5 bars using control points of **Table 4** and **Figure 5** shows the average stress-strain curve of Grade 72.5 #5 bars using control points of **Table 5**.

2.1.3 Comparison of Average Experimental and Idealized stress strain curves

The comparison of experimental average and idealized analytical stress strain curve of Grade 60 re-bars (**Figure 6)** shows that ultimate tensile stress in the idealized stress strain curve is higher than that obtained experimentally. The deformation capacity of the re-bars tested is adequate with a strain of 0.218 %. The strain capacity in the idealized curve is 0.15 %.

The comparison of experimental average and idealized analytical stress strain curve of Grade 72.5 re-bars **(Figure7)** shows that ultimate tensile stress in the idealized stress strain curve is higher than that obtained experimentally. The deformation capacity of the re-bars tested is adequate with a strain of 0.133 %. The strain capacity in the idealized curve is 0.125 %.

III. Conclusions and Recomendations

On the basis of the results, the following conclusions can be drawn:

1. The deformation capacity of Grade 72.5 re-bars is less as compared to that of Grade 60 re-bars.
2. For Grade 60 re-bars, the yield strengths of all individual re-bars were much higher than the prescribed minimum yield strength of 60 ksi and the average yield value of 30 samples is 77.2 ksi which is substantially higher than specified yield strength of 60 ksi.
3. For the Grade 72.5 re- bars, about 50 % of the re-bars did not reach the prescribed minimum yield strength of 72.5 ksi and the average yield value of 30 samples is 72.7 ksi which is just above the specified yield strength of 72.5 ksi.

The following recommendations are made:

1. One internationally recognized standard, preferably ASTM A615 should be adopted and used in Pakistan for the testing and quality assurance of re-bars
2. Instead of Grade 72.5 re bars, Grade 75 re-bars as per ASTM A615 should be manufactured in Pakistan.

Table 1: Comparison of Existing Standards

No.	Item	ASTM A615 [1]	BS 4449-2005[2]	ISO 6935-2:2007(E)[3]
1	**Scope**	Covers both deformed and plain carbon steel bars. Standard is for grade 40 (280 MPa), grade 60 (420 MPa) and grade 75 (520 MPa)	Covers only deformed bars of grade 72.5 (500 MPa)	This Standard contains technical requirements for ten grades of ribbed (deformed) steel bars from grade 43(300 MPa) to grade 72 (500 MPa) strengths and different ductility levels.
2	**Manufacture**	Standard specifically requires the use of electric furnace, basic oxygen or open hearth process	The manufacturing process is at the discretion of the manufacturer, but it should be reported to the purchaser.	The manufacturing process is at the discretion of the manufacturer.
3	**Chemical composition**	Phosphorous content should not exceed 0.06%.	It states that values of individual elements, namely Carbon, Sulphur, Phosphorous, Nitrogen and Copper should not exceed certain limits. A value of Carbon equivalent content should also be calculated and checked against values given in Table 2 (BS 4449-2005 **[2])**	It is same as BS 4449-2005 [2].
4	**Tensile Requirement**	Elongation of 8 in (200mm) gauge length is tested and checked in percentage of original length and compared with the elongations given in Table 2 (ASTM A615 [1]. For grade 40(280 MPa) and 60(420 MPa), yield point is taken at a strain of 0.5 % and for grade 75(520 MPa) steel, yield point is taken at a strain of 0.35%.	It states that ratio of tensile /yield strength and total elongations must be in accordance with Table 4 BS 4449-2005 [2]). Determine yield strength from 0.2% proof strength if a yield phenomenon is not present.	It is similar to BS 4449-2005[2] except that it includes more grades for bars.
5	**Bending requirement**	The angle of bend should be 180° unless otherwise specified. Test is performed at room temperature. Rate of bending is not specified.	It is bent up to 90°, aged and then bent back to 20°. Test temperature is 10°-35° and rate of bending is 60 °/s.	The test piece is tested for bending over a mandrel to an angle 160° to 180°. Test temperature and rate of bending are same as BS 4449 [2]
6	**permissible variation in weight(mass)**	Only 6% variation is allowed.	±4.5% on nominal diameter greater than 0.32 inch(8mm) and ±6% on nominal diameter of bar less than 0.32in(8mm).	Permissible deviation is ±4% to ±8%, depending upon the diameter of the bar.
7	**Gauge Length of specimen**	8 inch (200mm).	5 x diameter of bar	5 x diameter of bar

Table 2: Test results of tension tests on Grade 60 deformed bars #5 (16 mm) re-bars

Tests	f_y	ε_y	f_{sh}	ε_{sh}	f_u	ε_u	f_r	ε_r
1	74.10	0.0025	77.25	0.0189	92.23	0.101	60.77	0.160
2	75.50	0.0031	76.64	0.0197	91.28	0.106	60.95	0.207
3	79.93	0.0025	82.20	0.0246	98.81	0.116	75.71	0.235
4	85.24	0.0028	87.60	0.0237	105.62	0.134	78.03	0.270
5	80.90	0.0030	81.70	0.0155	97.79	0.120	67.20	0.230
6	74.50	0.0024	78.20	0.0600	93.90	0.148	59.90	0.503
7	77.92	0.0026	77.75	0.0217	93.51	0.118	61.90	0.225
8	77.88	0.0030	77.00	0.0180	92.90	0.151	63.94	0.277
9	74.82	0.0027	79.14	0.0420	96.33	0.150	69.65	0.230
10	79.26	0.0030	80.37	0.0260	92.68	0.132	66.84	0.219
11	70.76	0.0027	70.92	0.0147	86.33	0.139	54.20	0.254
12	74.50	0.0025	76.80	0.0167	91.29	0.122	54.30	0.216
13	76.47	0.0027	77.17	0.0250	93.59	0.170	69.40	0.317
14	77.42	0.0023	78.86	0.0660	95.46	0.144	71.64	0.453
15	79.44	0.0029	79.82	0.0147	95.71	0.133	66.22	0.246
16	71.98	0.0023	81.04	0.0170	95.27	0.097	63.55	0.172
17	76.45	0.0024	82.48	0.0175	95.74	0.093	60.32	0.144
18	76.31	0.0027	81.40	0.0176	95.19	0.098	67.30	0.160
19	74.41	0.0025	81.43	0.0177	90.62	0.031	63.27	0.187
20	79.58	0.0029	77.98	0.0177	95.70	0.112	62.88	0.164
21	77.55	0.0027	81.44	0.0178	94.77	0.103	61.26	0.158
22	74.85	0.0026	78.68	0.0173	95.00	0.106	63.54	0.190
23	78.78	0.0026	84.78	0.0174	98.54	0.085	77.96	0.132
24	82.60	0.0029	83.20	0.0176	98.68	0.074	70.07	0.182
25	81.31	0.0035	83.20	0.0176	99.63	0.117	65.50	0.178
26	77.61	0.0027	81.52	0.0177	99.00	0.093	67.50	0.156
27	79.81	0.0027	83.72	0.0177	99.12	0.117	62.28	0.194
28	79.58	0.0027	81.90	0.0178	99.46	0.098	65.10	0.155
29	73.10	0.0027	77.74	0.0178	88.25	0.108	53.87	0.191
30	74.10	0.0027	79.55	0.0176	90.45	0.102	60.80	0.157
Average	**77.22**	**0.00271**	**80.04933**	**0.022367**	**95.095**	**0.113897**	**64.86167**	**0.21873**

f_y =yield point, ε_y =yield point strain, f_{sh} =stress at onset of strain hardening, ε_{sh} = strain at onset of strain hardening, f_u=ultimate tensile strength, ε_u =strain at ultimate, f_r =stress at fracture point, ε_r = strain at fracture point

Table 3: Test results of tension tests on Grade 72.5 deformed bars #5 (16 mm) re-bars

Tests	f_y	ε_y	f_{sh}	ε_{sh}	f_u	ε_u	f_r	ε_r
1	70.97	0.0022	71.22	0.002	82.65	0.106	57.50	0.130
2	73.60	0.0025	76.91	0.024	90.93	0.073	60.65	0.106
3	70.48	0.0024	71.53	0.025	82.77	0.123	47.57	0.194
4	68.73	0.0024	68.65	0.023	81.65	0.140	76.76	0.221
5	70.45	0.0020	75.46	0.014	83.42	0.111	56.45	0.183
6	69.85	0.0023	75.40	0.015	83.60	0.116	56.33	0.170
7	71.96	0.0025	78.40	0.017	84.34	0.094	57.00	0.143
8	73.61	0.0022	73.50	0.011	84.56	0.137	60.48	0.218
9	69.73	0.0016	71.53	0.007	82.59	0.110	70.28	0.134
10	74.82	0.0024	75.24	0.004	91.22	0.163	75.68	0.265
11	75.40	0.0024	75.90	0.027	91.92	0.156	62.70	0.314
12	78.91	0.0024	84.94	0.011	92.28	0.089	63.13	0.136
13	73.34	0.0023	74.74	0.008	89.63	0.112	71.40	0.150
14	71.90	0.0020	76.78	0.009	87.86	0.118	57.20	0.112
15	74.97	0.0023	80.00	0.010	91.00	0.098	57.20	0.172
16	75.35	0.0023	81.48	0.010	90.61	0.099	60.80	0.158
17	73.30	0.0020	84.41	0.003	90.20	0.060	60.60	0.090
18	76.66	0.0024	85.78	0.003	92.47	0.060	58.26	0.087
19	69.43	0.0020	78.08	0.003	82.34	0.048	56.26	0.076
20	68.27	0.0015	78.36	0.003	81.73	0.053	55.18	0.076
21	75.55	0.0020	84.32	0.003	91.20	0.049	60.20	0.078
22	72.27	0.0020	78.21	0.003	83.75	0.053	56.96	0.078
23	73.83	0.0020	82.45	0.003	90.30	0.060	62.73	0.087
24	73.41	0.0020	82.35	0.003	90.47	0.053	60.00	0.084
25	75.38	0.0020	84.25	0.003	90.70	0.050	61.50	0.084
26	73.14	0.0020	73.54	0.003	84.70	0.050	55.96	0.074
27	73.84	0.0020	79.92	0.003	84.74	0.050	56.23	0.071
28	72.20	0.0020	80.67	0.003	88.65	0.066	60.60	0.090
29	69.50	0.0023	73.37	0.003	81.00	0.071	55.27	0.099
30	71.48	0.0020	77.36	0.003	83.90	0.077	57.72	0.106
Average	**72.7443**	**0.002144**	**77.83**	**0.008**	**86.906**	**0.088**	**60.29**	**0.132873**

f_y =yield point, ε_y =yield point strain, f_{sh} =stress at onset of strain hardening, ε_{sh} = strain at onset of strain hardening, f_u=ultimate tensile strength, ε_u =strain at ultimate, f_r =stress at fracture point, ε_r = strain at fracture point

Table 4: Average experimental control points for Grade 60 re-bars of #5(16 mm)

Point	Stress (ksi)	Strain (in/in)
1.Origin	**0**	**0**
2.Yield point f_y	77.22	0.00271
3. Onset of Strain hardening f_{sh}	80.05	0.02240
4. Ultimate Point f_u	95.10	0.11400
5. Fracture point f_r	64.86	0.21800

Table 5: Average experimental control points for Grade 72.5 re-bars of #5(16 mm)

Point	Stress (ksi)	Strain (in/in)
1.Origin	**0**	**0**
2.Yield point f_y	72.74	0.00214
3. Onset of Strain hardening f_{sh}	77.83	0.00840
4. Ultimate Point f_u	86.28	0.08800
5. Fracture point f_r	60.28	0.13300

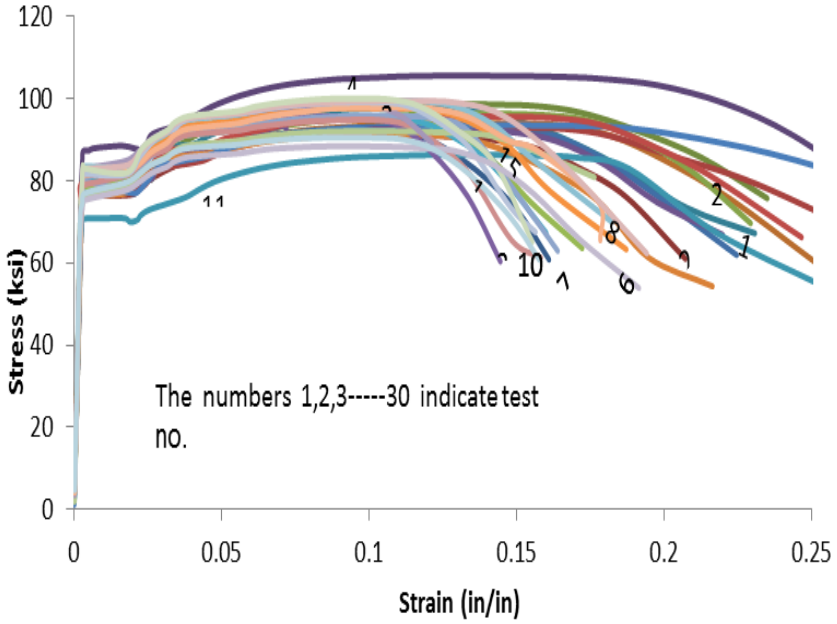

Fig. 1: Stress-strain curves for 30 samples of Grade 60 #5 (16 mm) re-bars

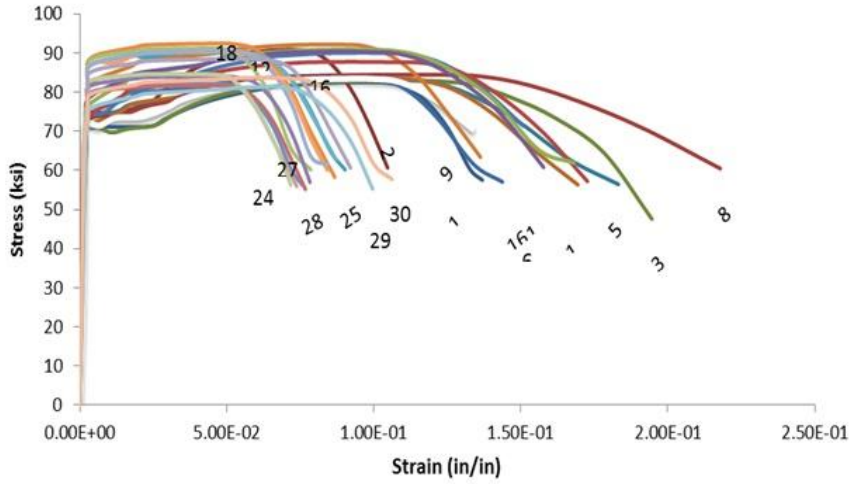

Fig. 2: Stress-strain curves for 30 samples of Grade 72.5 re-bars

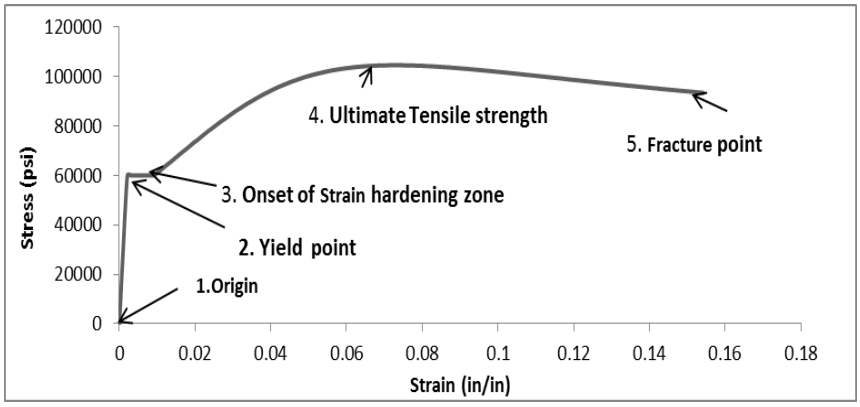

Fig. 3: Control points for an experimental average stress strain curve and idealized stress-strain

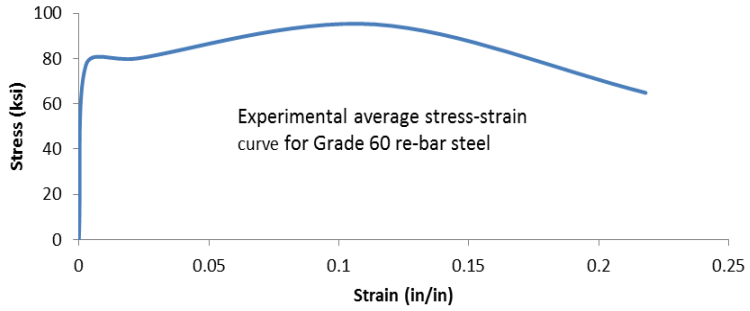

Fig.4: Experimental average stress-strain curve of Grade 60 #5 bars using control points of Table 4

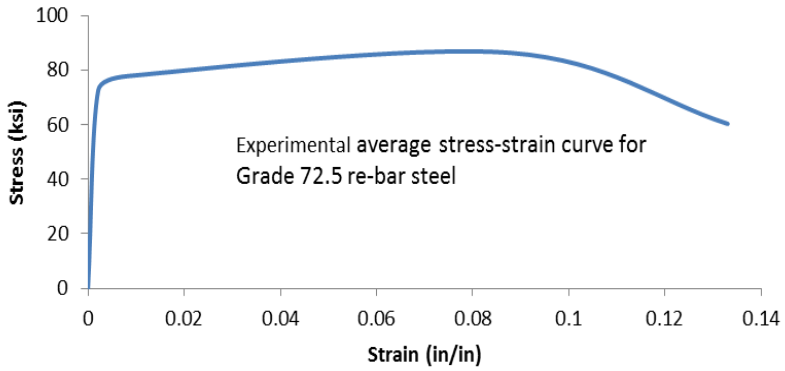

Fig. 5: Experimental average stress-strain curve of Grade 72.5 #5 bars using control points of Table 5

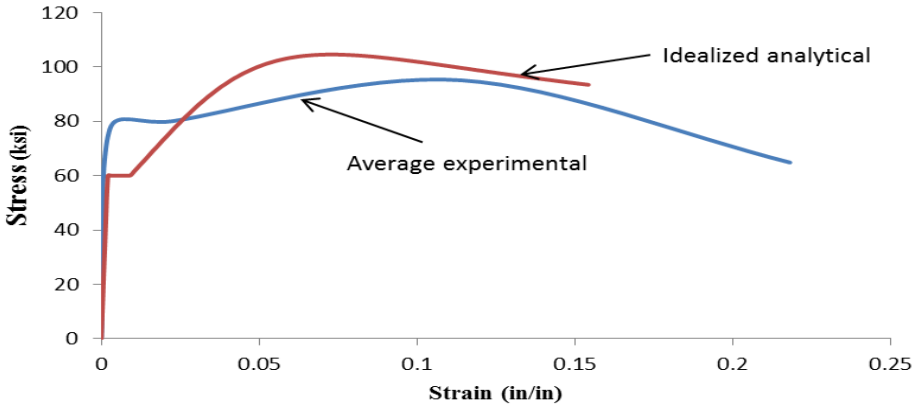

Fig. 6: Comparison of experimental average and idealized analytical stress-strain curve of Grade 60 re-bar

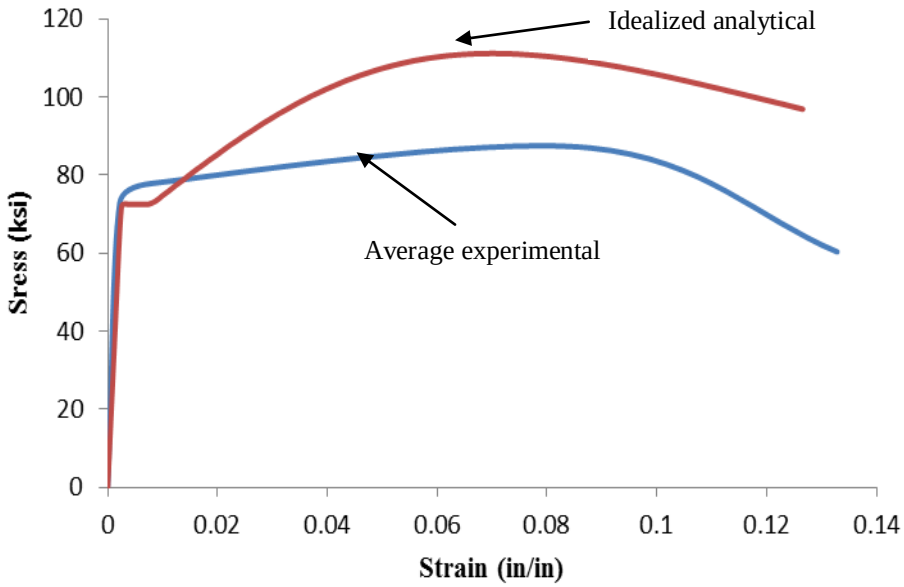

Fig. 7: Comparison of experimental average and idealized analytical stress-strain curve of Grade 72.5 re-bar

References

[1]. ASTM Standard A615/A 615M-04a, Standard Specification for Deformed and Plain Carbon Steel Bars for Concrete Reinforcement, 2006
[2]. British Standard BS 4449, Steel for the reinforcement of concrete-Weld-able reinforcing steel-Bar, coil and de-coiled product-Specification, 2005[8]. International Standard ISO 6935-2:2007 (E), Steel for reinforcement of concrete Part 2: Ribbed bars, 2007
[3] International Standards ISO 6935-2:2007 (E), Steel for reinforcement of concrete Part 2: Ribbed bars, 2007
[4]. Pakistan Standard PS 1612-2007 (R), ICS No.77.140.06, Steel for the reinforcement of concrete-Weld-able reinforcing steel-Bar, coil and de-coiled product-Specification, Pakistan Standards and Quality Control Authority, 2007
[5]. ASTM Standard A370, Standard Specification for Deformed and Plain Carbon Steel Bars for Concrete Reinforcement, 2006
[6]. Ahmad, S. H., and Shah, S. P., "Complete Stress-Strain Curve of Concrete and Nonlinear Design," Proceedings of CSCE-ASCE ACI-CES International Symposium of Nonlinear Design of Concrete Structures, Waterloo, August 1979.
[7]. Ahmad, S. H., and Shah, S. P., "Complete Triaxial Stress-Strain Curves for Concrete," Journal, Structural Division, ASCE, Vol. 108, No. ST4, April 1982, pp. 728-742
[8]. Ahmad, S. H., and Shah, S. P., "Stress-Strain Curves of Confined Concrete," Journal, American Concrete Institute, Vol. 79, November-December 1982, pp. 484-490
[9]. Ahmad, S. H., and Shah, S. P., "Behavior of Hoop Confined Concrete Under High Strain Rates," Journal, American Concrete Institute, Vol. 82, No. 5, September-October 1985, pp. 634-647
[10]. Ahmad, S. H., and Shah, S. P., "Structural Properties of High Strength Concrete and its Implications of Precast and Pre stressed Concrete," Journal of Pre stressed Concrete Institute, Vol. 30, No. 6, November-December 1985, pp. 92-119.

International Journal of Modern Engineering Research (IJMER)
www.ijmer.com Vol.3, Issue.2, March-April. 2013 pp-674-677 ISSN: 2249-6645

Effect of Turbo charging On Volumetric Efficiency in an Insulated Di Diesel Engine For Improved Performance

S.Sunil Kumar Reddy, [1] Dr. V. Pandurangadu, [2] S.P.Akbar Hussain[3]
[13]*Associate Professor, Mechanical Department, N.B.K.R.I.S.T, Vidyanagar, Nellore, A.P*
[2]*Professor, Mechanical Department, Jawaharlal Nehru Technological University, Anantapur. A.P*

Abstract: *The world's rapidly dwindling petroleum supplies, their raising cost and the growing danger of environmental pollution from these fuels have led to an intensive search for an alternative fuels with concerned efforts to conserve the oil reserves. Among all the fuels, tested alcohol is proved best alternatives to the petroleum fuels because all these are derived from indigenous sources and are renewable. However, with the alcohols higher latent heat of vaporization and lower cetane number, the Insulated engine (IE) is used for the combustion in the diesel engines. The higher temperature in the combustion chamber decreases the ignition delay and aids combustion but drops the volumetric efficiency. The degree of degradation of volumetric efficiency depends on the temperatures in the combustion chamber and it further increases the frictional horsepower due to thinning of lubricant.*

Therefore, for improving the thermal efficiency of insulated engine, the volumetric efficiency drop is compensated by turbo charging in the present experimental work. This gave the better performance with reduction in smoke. With the turbo, charging the intake boost pressure is raised and its effect on the engine performance is also studied.

I. Introduction

In the diesel engines for about 30% of the total energy is lost to the cooling water. This lost energy can be recovered in the form of useful energy by expanding gases in the turbines. But due to lower temperature in the combustion chambers, the fuels which have high calorific value cannot be burned. This can be achieved with an insulated engine due to the availability of higher temperature at the time of fuel injection. The heat available due to insulation can be effectively used for vaporizing alcohols. Some important advantages of the insulated engines are improved fuel economy, reduced HC and CO emission, reduced noise due to lower rate of pressure rise and higher energy in the exhaust gases [2 & 3]. However, one of the main problems in the insulated engines is the drop in volumetric efficiency. This further decrease the density of air entering the cylinder because of high wall temperatures of the insulated engine. The degree of degradation of volumetric efficiency depends on the degree of insulation.

In the present work for compensating the decrease in volumetric efficiency a single cylinder insulated DI diesel engine is turbocharged to different inlet pressures depending upon the load and the performance of the insulated engine under turbocharging condition is investigated.

II. Experimental Details

The single cylinder, four strokes 3.68 KW Kirloskar, water-cooled DI diesel engine with a bore of 80 mm and stroke of 110 mm and a compression ratio of 16.5:1 is used for the experiment. The engine load is applied with eddy current dynamometer. For the reduction of heat to the cooling water, an air gap insulated piston and liner and ceramic-coated cylinder head and valve (BP9) is used for this experimental investigation. The emissions are measured with exhaust analyzer. The air gap insulated piston and the experimental set up used for the experiment is as shown in the Fig.1 & 2 respectively

Fig. 1: Photographic view of Aluminum piston Crown with an air-gap insulation

Fig. 2. Experimental set up of Insulated Engine Test Rig

III. Turbocharging Equipment

To pressurize the inlet air, internally powered turbocharging equipment with closed loop lubrication is fabricated. The schematic diagram of the turbocharging equipment is shown in Fig: 3. in the turbocharging the high temperature exhaust gases are expanded in a low-pressure turbine for the power generation and this is further coupled to motor of the compressor [4, 5]. This compressor compresses the inlet air and supplies to the engine at slightly higher pressure. By controlling the inlet air, the engine is turbocharged at different inlet pressures.

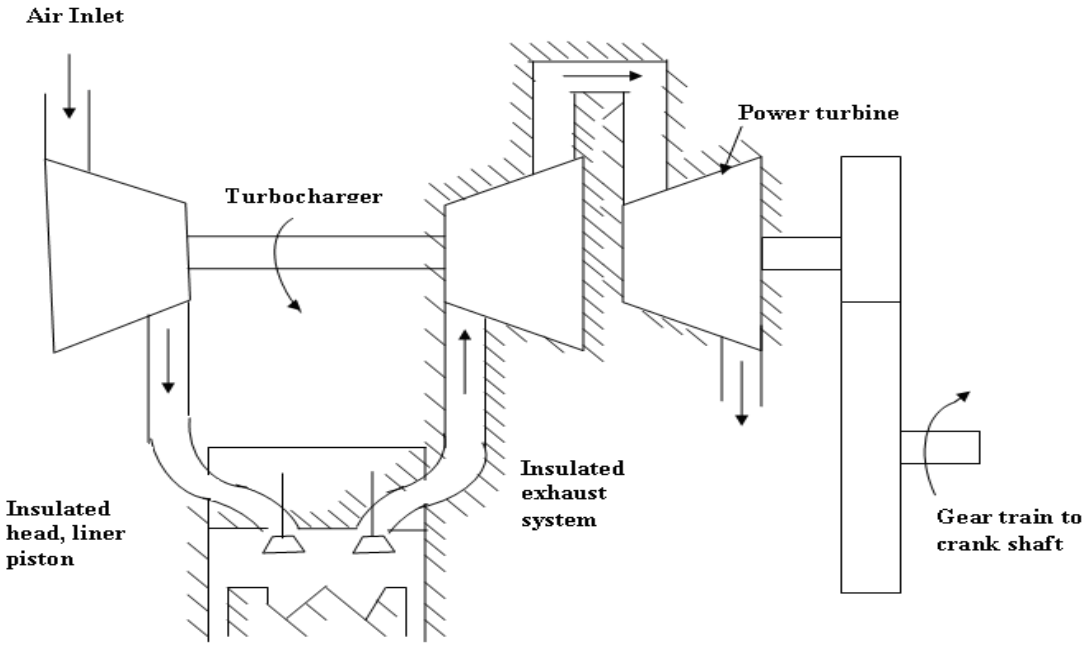

Fig. 3 Turbocharged Insulated Diesel Engine

IV. Results and Discussions

Initially the tests are performed at a constant speed of 1500 rpm with constant injection timing (29^0 bTDC) in a normal diesel engine. All the performance parameters and emissions are measured. For the insulated engine, due to higher operating temperatures and further lower ignition delays with insulation in the combustion chamber, the injection timing of 27 ^{0}bTDC is found to give the optimum performance. So all the tests are performed in the insulated engine with alcohol as fuel at the above optimum injection timing.. For testing the engine under turbocharging conditions, the specially fabricated turbocharging equipment is used.

Effect of Insulation on the Volumetric Efficiency

The volumetric efficiency drop mainly depends on the cylinder temperatures in an insulated engine, which in turns depends upon the type and degree of insulation employed. In the present work air-gap insulation both for the piston and liner and PSZ coating for the cylinder head and valve have been incorporated. Fig: 4 shows the variation of the volumetric efficiency drop of the insulated alcohol engine compared with normal diesel engine (NE). The volumetric efficiency drop of an insulated engine is about 10% compared to normal engine at rated load.

Effect of Turbocharging on the Volumetric Efficiency

The variation of volumetric efficiency with power output with intake boost pressure is shown in Fig: 5. With the increase of boost pressure more air is available for the combustion which further increases the combustion efficiency. At higher boost pressures excess air doesn't improve the combustion efficiency [5]. So it is concluded that 790 mm of Hg is the optimum boost pressure at which the drop in volumetric efficiency is compensated with turbocharger.

Because of the increased backpressure with turbocharging conditions, the inlet boost pressures are higher for compensating the volumetric efficiency drop in normal engine. It requires nearly 4% of intake boost pressure under turbocharging conditions for compensating the maximum efficiency drop of 10% in the normal engine. Comparison of percentage of boost pressure required for volumetric efficiency compensation with power output is shown in Fig: 6.

Brake Thermal Efficiency

The variation of brake thermal efficiency with power output for turbocharged condition is shown in Fig:7. When the engine is turbocharged with volumetric efficiency compensation thermal efficiency is improved continuously with load. The maximum improvement is about 4.3% over insulated engine. The improvement in thermal efficiency under turbocharging

conditions is marginal due to following reasons: (1) In the present work inlet boost pressures in turbocharging are moderate, because they were selected on the basis of volumetric efficiency compensation. At higher pressures still higher thermal efficiency could be obtained. (2) Higher frictional losses due to increase in gas pressures. (3) The engine had stability problem at higher intake pressures.

V. Combustion Parameters

With the turbo charging more air will be available for the combustion and this will change the combustion parameters. The effect of turbocharging on the engine performance is shown in the following figures.

Peak Pressure

The peak pressure variation of turbocharging with power output is shown in Fig:8. The peak pressures of normal engine, Insulated engine and turbocharged Insulated engines are compared in the same figure. It is observed that the peak pressures are higher with turbocharged engine and is about 82 bar at the rated load.

Ignition Delay

The variation of ignition delay with power output for turbocharging conditions is shown in Fig: 9. With the turbocharging more amount of air enters into the chamber which increases the combustion process and reduces the ignition delay. But at higher loads due to the high latent heat of alcohol, the ignition delay is slightly increased [6]. It is concluded that there is a reduction of 6.2^0 CA for the turbocharged insulated engine compared to normal engine at rated load. So it will be beneficial to increase the turbocharging pressures in order to have a shorter ignition delays.

Exhaust Temperature and Emissions

The increase in the exhaust temperatures are 20^0C to 50^0C with turbocharging. Fig: 10 shows the variation of exhaust temperatures with power output. This is due to the increase of mass flow rate of air, reduction in the ignition delay and hotter combustion chamber which further increases the combustion process.

Fig: 11 shows the variation of exhaust smoke number with power output for turbocharging condition. It is concluded from the same figure that there is a significant reduction in smoke level in turbocharged engine compared to normal engine at rated load condition due to complete combustion.

VI. Conclusions

The following conclusions are drawn based on the experimental investigations on an insulated diesel engine under turbocharging conditions:

1. The increase in the in take boost pressure improves the brake thermal efficiency of the engine.
2. For the compensation of drop in volumetric efficiency of the insulated engine 4% intake boost pressure is required for turbocharging.
3. Though the higher temperatures are available in the combustion chamber due to insulation, the increase in exhaust gas temperature is marginal. This is attributed to the higher latent heat of vaporization of alcohol.
4. As the alcohol contains oxygen and more air is available in the turbocharging for combustion, the ignition delay is reduced.
5. Due to the complete combustion of alcohol at higher temperatures the smoke emissions are also marginal.

References

[1] R.D.Barnes, - Effect of a supplementary fuel in turbo charged diesel engine- SAE 750469, 1975
[2] R.Kamo and W.Bryzik," Adiabatic Turbocompound Engine Performance Prediction", SAE 1978, paper 780068.
[3] R. Kamo, et al," Cummins- TARADCOM Adiabatic Turbocompound Engine program", SAE 1981, Paper 810070.
[4] Michael C. Brands," Vehicle Testing of Cummins Turbocompound Diesel Engine", SAE 1981, Paper 810073.
[5] N.Sivarama Prasad Rao, S.Jabez Dhinagar, B.Nagalingam and K.V.Gopalakrishnan, "Compensating the Volumetric Efficiency drop of an adiabatic diesel engine for improved performance", Third International Conference on I.C. Engines, IIT, Chennai, Vol.II, pp 288-299, 1986.
[6] Ozer Can, smet Çelikten and Nazım Usta," Effects of ethanol addition on performance and emissions of a turbocharged indirect injection Diesel engine running at different injection pressures ", SAE Technical paper,2004.
[7] Arunachalam M , "Investigations on the performance of a diesel engine with ceramic thermal barrier coating on parts of the combustion chamber surface", Proc. of the QIP short term course on recent developments in I.C. engines, IIT, Madras,1988
[8] Sutor P, Bryzik W, "Laboratory Development and Engine Performance of New High–Temperature Diesel Engine Lubricants", SAE Technical Paper 890145
[9] Wang J C," High temperature Liquid Lubricant Development-Part Ii: Bench Test Development", SAE Paper No. 932843.
[10] Wallance F J et al, "Thermally insulated diesel engine", Proc. Of the Institution of Mech. Engrs., vol 198A, No.: 5, PP 97-105.2000

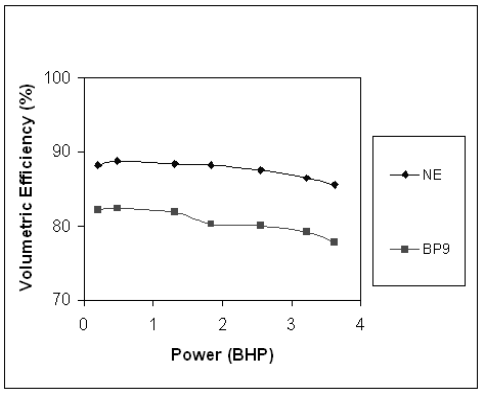

Fig: 4 Variation of Volumetric Efficiency with Power Output

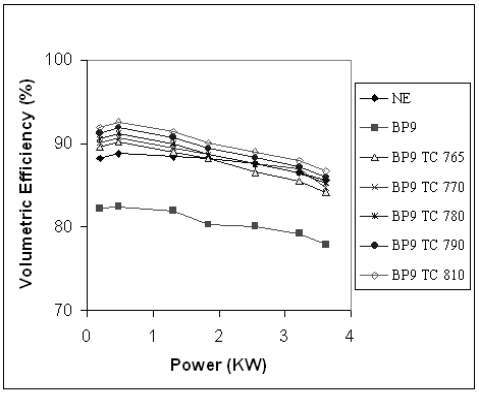

Fig: 5 Variation of Volumetric Efficiency with Turbocharging

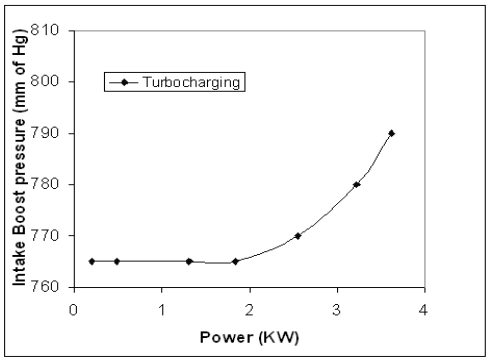

Fig: 6 Comparison of Intake Boost Pressure Required for Volumetric Efficiency Compensation with Power Output in Turbocharging

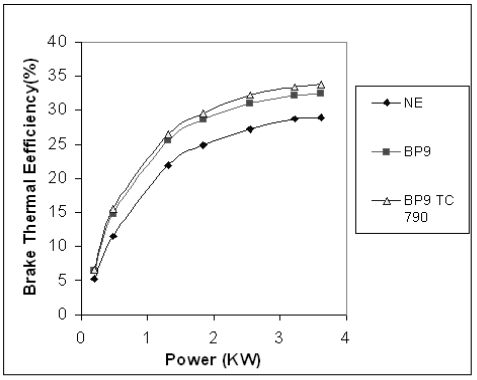

Fig: 7 Comparison of Brake thermal Efficiency with Power Output for Volumetric Efficiency Compensation with Turbocharging

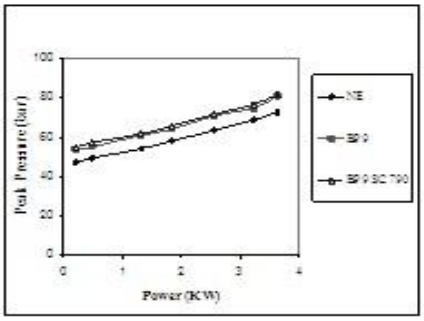

Fig: 8 Comparison of Peak Pressure with Power Output for Volumetric Efficiency Compensation with Turbocharging

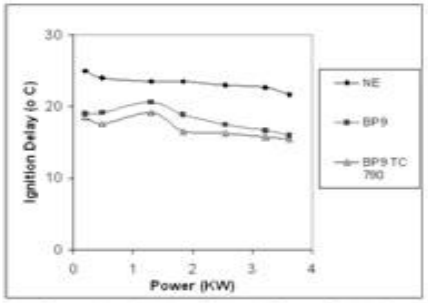

Fig: 9 Comparison of Ignition Delay with Power Output for Volumetric Efficiency Compensation with Turbocharging

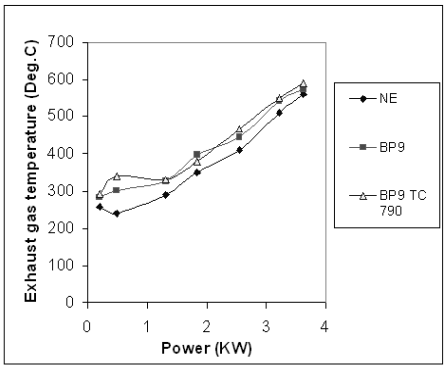

Fig: 10 Comparison of Exhaust Gas Temperature with Power Output for Volumetric Efficiency Compensation with Turbocharging

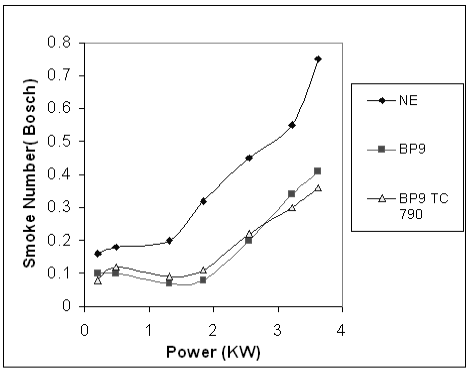

Fig: 11 Comparison of Smoke Emissions with Power Output for Volumetric Efficiency Compensation with Turbocharging

International Journal of Modern Engineering Research (IJMER)
www.ijmer.com Vol.3, Issue.2, March-April. 2013 pp-678-684 ISSN: 2249-6645

Changing Dynamics of Land Use in Residential Neighbourhood of Vani Vilasa Mohalla¸ Mysore

Dr. B. Shankar[1], D.Vidhya[2]
[1]*Associate Professor, Institute of Development Studies, University of Mysore, Mysore*
[2]*Consultant in Urban and Regional Planning, Bangalore*

Abstract**:** *Large cities have experienced rapid spatial growth because of higher growth rates of urban population. Land is an important resource for spatial expansion and accommodating various activities within the residential areas of the city. Therefore, there is an increase in land use change in residential areas by the local and planning authorities and they are allowing changes in making streets as commercial streets for socio-economic benefits. Many streets in residential areas have altered into commercial, public and semi public activities and apartments. Thus, the residential areas are affected greatly in terms of increasing density and overloading the existing infrastructure facilities by changing dynamics of land use. With a result of this, the residential areas are transforming into mixed land use. The City of Mysore is a large city and an emerging metropolitan city in the State of Karnataka. Vani Vilasa Mohalla, is a residential neighbourhood it is one among many residential areas which was developed before Independence. The neighbourhood is experiencing rapid land use transformation. The paper presents the changing dynamics of land use for emerging mixed land use in a residential neighbourhood of Vani Vilasa Puram, Mysore and proposes planning strategies for mixed land use.*

Keywords: *Changing Dynamics, Land Use, Diversity, Neighbourhood, Mixed Land Use.*

I. Introduction

In recent years, large cities have experienced rapid growth and majority of these cities are facing uncontrolled developments at the densely populated areas and changing of residential land use into mixed land use. Land use changes are increasingly known as the consequence of actors and factors' interactions (Bakker and van Doorn 2009). These conversions and their consequences are obvious and it has been becoming a disaster around the city areas. The relationships between population increase, economic developments and land use change have generated much of the research interests. In the 1960s and 70s mixed use re-emerged, as a tool for urban revitalization, in large-scale projects referred to among the development community as mixed-use developments. It is presumed that mixed land uses yields socio-economic benefits and therefore has a positive effect on housing and commercial values.

Land use is an important tool for Master Plan and land, which is allotted for residential area and is designed as per zoning and subdivision regulations for satisfying the concept of neighbourhood designs. Over a period of time City Corporations and Urban Development Authorities allow change in making street as Commercial Street due to increase pressure for commercial activities. With a result of this, many streets in the residential areas altered to commercial, public and semi public activity and also apartments and there is increase in land use changes over the years. Thus, the residential areas are affected by the changing dynamics of land use by increasing the density of the area. It looks like a mixed land use driven in the residential area which is violation to zoning regulation. It has also mounted pressure on existing infrastructure like water supply, traffic and transportation, sewerage etc. Very recently, these changes have been recognised by introducing the concept of mixed land use in residential areas in many of Indian Master Plans namely Delhi¸ Mumbai, Bangalore etc. The City of Mysore is experiencing changing dynamics in residential areas which need to be recognized and addressed properly by the Planning Authority in its development control regulations.

II. Background of Mysore

Mysore is the second largest city in the State of Karnataka and it had a population of 887,446 as per 2011 provisional census figures and it increased from 7, 85, 800 in 2001. The name of Mysore was derived from mahisha (a demon). Formerly, the city was the state capital and head quarters of the Princely State of Mysore. It is situated at a distance 140kms from Bangalore, on the southern part of Karnataka State at 12° 18' North latitude and 76° 12' East longitude, and at an altitude of 770 mts above mean sea level. The city lies in a saucer shaped basin flanked by Chamundi hills on the south-east and a raised platform near Hinakal village on the west. The city has a salubrious climate and the temperature varies from 12° C to 35° C. It has an average annual rainfall of about 798mm. The city spreads across an area of 128.42sq.kms. The literacy rate is 82.8 percent.

III. Land Use Of Mysore

The general land use pattern of Mysore city owes its origin to its past. The old city is predominantly the central business district, which scattered around the palace and it is also the heart of the city. The land use for different periods from 1966 to 2009 is given in table 1.

Table 1 Land Use for the Period from 1966 to2009

Land Use	1966		1997		2009	
	Area in Hectares	% age	Area in Hectares	% age	Area in Hectares	% age
Residential	2997.57	40.40	3057.30	42.60	6747.52	47.75
Commercial	211.25	2.41	182.23	3.00	467.04	3.30
Industrial	614.32	13.49	1021.01	8.73	1281.63	9.07
Parks and Open Spaces	625.25	5.49	415.77	8.9	765.36	5.42
Public and Semi-Public	1230.67	11.32	856.45	17.49	1517.34	10.74
Traffic and Transportation	911.77	20.22	1530.73	12.95	3238.01	22.91
Public utility	23.87	0.49	37.26	0.34	-	-
Water sheet	37.23	2.41	182.68	0.53	-	-
Agricultural	384.45	3.77	285.34	5.46	6747.52	47.75
Total	7036.38	100	7568.77	100	14131.97	100

Source: Mysore Urban Development Authority, Mysore

IV. Spatial Growth of Mysore City

The spatial expansion in four different periods is given in the following fig.1

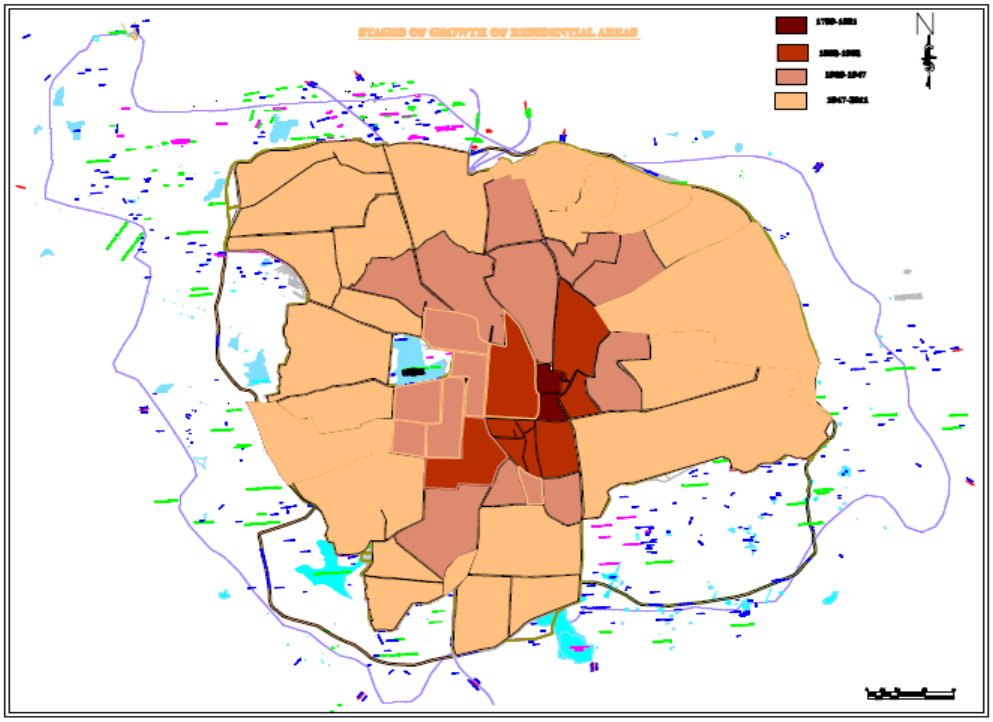

Fig. 1 Residential Growth in Different Periods

The residential areas which were developed in different periods are as as follows:

Growth of Residential Areas	Period
Nazarbad, old and new Agrahara, Santhepet, Sivarampet, Mandi, Lashkasr, Devaraj, Chama raja, Fort, Irangere Mohallas	1799-1890
Lakshmi Puram, ,jalpuri,Ediga,K.R Mohalla, Chamundipuram, Ashokapuram, Agraharas, Chatanahalli, DoddaHolegeri, Bannimantap,	1900-1915
Krishnamurthy puram, Jayanagar, Vanivilas puram, Gokulam and Padavarahalli, Yadavagiri, Narasimhraja Mohalla, Saraswathipuram	1915-1935
Jayalakshipuram, Brindavan extension, Mahadevapura, Kesare, Kuvempunagar, Kurubarahalli, Gayathripuram, Bannimantap	1947 to date

V. Background of Vani Vilasa Mohalla

Vani Vilasa Mohalla is one of the oldest residential neighbourhoods developed during Maharaja's period before the Independence India. The neighbourhood was developed in the name of Maharani Kempa Nanjammani Vani Vilasa Sannidhana, was the wife of Chamaraja Wodeyar IX. During 19th century, the city continued to grow, congestion and haphazard growth began. By the end of this century, the town had become old fashioned with narrow and crooked lanes, devoid of ventilation, drainage and lung space and having congested blocks of pot tilled and dingy houses.

In the year 1930, the Maharja and Yuvaraja gave some donation to the City Improvement Trust Board to construct houses for poor and middle class families. By 1934, the Board acquired and demolished about 5,000 houses in highly congested areas at a cost of Rs. 3.5 million. As many as 37 neighbourhoods, of which prominent ones are Vanivilas Mohalla, Gokulam, Lakshmipuram, and many more residential neighbourhood layouts, were laid out. Vani Vilasa Mohalla had 3874 population in 1991 increased to 5116 in 2001 and 6787 in 2011. Number of houses also increased from 1003 in 1997 to 1357 and 2011.

Table 2. Demographic and Housing Details of Vani Vilasa Mohalla

	1991	2001	2011
Population	3874	5116	6787
Male	1930	2550	3380
Female	1944	2566	3407
No of Houses	1003	1137	1357
Road length	21.5	21.5	24.4

Sources: 1.Mysore Urban Development Authority and 2. Mysore City Corporation

VI. Neighborhood Concept Vanivilasa Mohalla

The neighbourhood was designed for minimum population of 5,000 to 6,000 populations. The focal point was the elementary school which is centrally located on a common or green space, along with other institutions that have service areas coincident with the neighbourhood boundaries. The radius of the neighbourhood was maximum of one quarter mile thus precluding a walk of more than that distance for any elementary school child. Major collector streets and sub-arterial road are located at the edge residential neighbourhoods. Interior street patterns was designed on grid-iron pattern and constructed with light duty surfacing so as to encourage a quiet, safe and low volume traffic movement and preservation of the residential atmosphere and shopping districts was sited at the edge of neighbourhoods preferably at major street intersections.

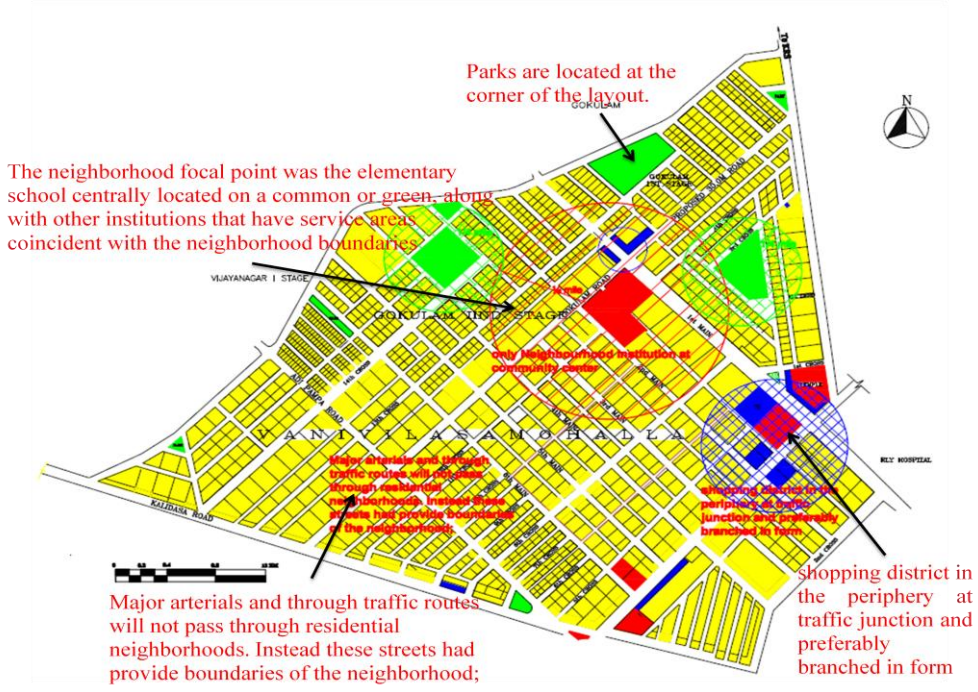

Fig.2 Neighbourhood Concept of VV Mohalla

Residential Neighbourhood layout plan was prepared during 1934 as per the City Improvement Trust Board norms. Terrain conditions were flat with gentle slope towards north east direction and south east is most elevated. The dimension of site areas were 60'x40', 100'x120', 120'x180' and these plots were designed to meet the requirements of high income group people. Now, these bigger plots have great land values for promotion of real estate rates in this neighbourhood. A separate conservancy lane has been provided for disposal of night soil and these spaces are being misused and abused by neighbouring residents in many instances. Parks are provided at the corner of layout many of the waste part of the land is being used for parks. Many institutions, specialized hospital, hotels are being located in this area.

VII. Land Use Pattern Of Vani Vilasa Mohalla

The residential neighbourhood has an extent of 134 hectares. The prominent uses in this area are residential (55.75 %) followed by traffic and transportation (29.12%), parks and open spaces (5.41%), public and semi-public (5.2%) and commercial (4.2%).

Table 3: Land Use of VV Mohalla in Different Periods

	1960		2009		2012	
Use	Area in hectares	% of land use	Area in hectares	% of land use	Area in hectares	% of land use
Residential	74.70	55.75	64.7	48.3	63.4	47.3
Commercial	6.05	4.52	11.2	8.33	11.4	8.54
Public and semi public	7.0	5.20	9.55	7.13	10.6	7.94
Park and open space	7.25	5.41	8.32	6.21	8.33	6.20
Traffic and transportation	39.02	29.12	40.2	30.0	40.2	30.0
Total	134	100	134.	100	134.	100

VIII. Land Use Analysis

The total area covered under residential use is 63.40 hectares. This works out to 47.32**%** of the total built up area. The net residential density of population, works out to be 5711 persons per sq kms as per 2001 census. The residential use has decreased from 64.73 hectares to 63.40 hectares from 2009 to 2012 and from 74.40 to 64.73 from 1960 to 2009 respectively. The area under commercial use is 11.44 hectares. The areas allowed for commercial activities are retail business, whole-sale business, ware-houses, shopping mall, cinema theatres, hotels etc., commercial use has increased from 6.05 hectares to 11.44 hectares from 1960 to 2012. The area under public and semi-public uses accounts for 5.20%. This includes the land utilized for public offices, educational institutions and hospitals. Many educational institutions are located in this area, from primary school to post graduation level. An area of 8.33 hectares is under parks and open spaces use, forming 6.20 per cent of the total developed area which is less than planning standards of 12-15%. The area under traffic and transportation is 40.22 hectares, which accounts for 30 percent of the total built-up area.

IX. Housing Typologies

By 1934, the City Improvement Trust Board developed about 570 sites and 100 model houses around which the development was encouraged at a cost of Rs. 350,000. The model houses were built with country tiled roof with brick and mud wall during 1931-37. The sites formed in Vani Vilasa Mohalla by the Board and provided at reduced rates of 15 or 7 paise per square meter instead of 30 paise. By 1950, the housing typology changed to Mangalore tiled and 1970 to terraced house.

Table.4 Housing Typology in Vanivilasa Mohalla

year	1934	1950	1970	2011
Country Tiled brick and mud wall	150	184	102	72
Mangalore tiled with brick walls	57	190	248	310
Terraced with brick	----	57	235	851
Vacant sites	413	219	185	47

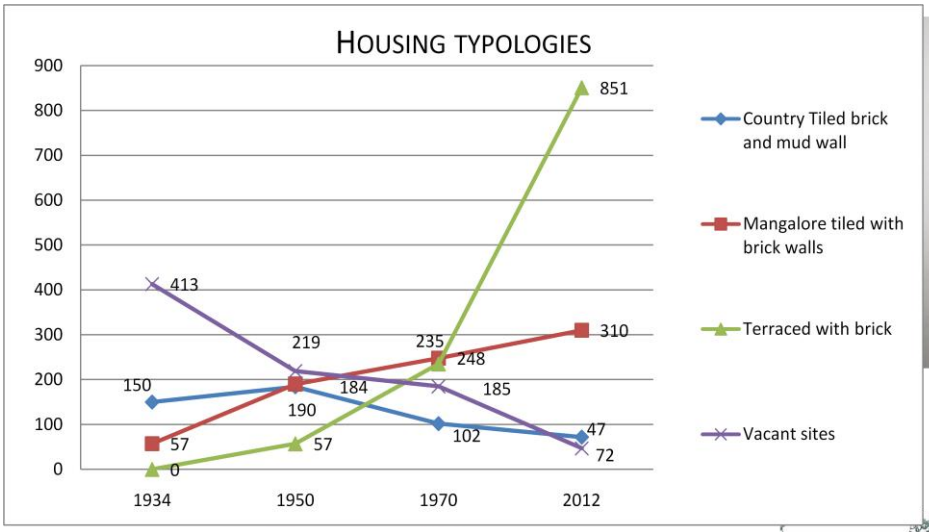

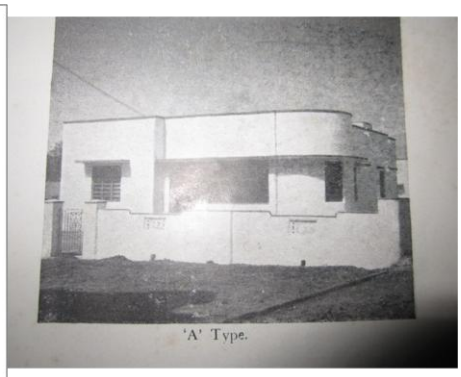

Model house constructed in 1934

Mangalore tiled with brick walls

X. Hirschmann- Herfindahl Model

Hirschmann-Herfindahl model is employed to identify the diversity of change in land use. In this model, it is assumed that households will be living in a mixed urban environment. In this situation employment is an indicator for land use, which suggests that not just the number of jobs, but also the composition of total employment in terms of different economic activities matters for mixed land use. Therefore, it has been defined a diversity index so as to be able to examine the impact of a mixture of employment and housing on property values. Let $_{Hh}$ denote the number of households in a neighbourhood of house *h* and E_{gh} the number of employees in sector *g*. The diversity index for house is the inverse of the Hirschmann- Herfindahl index. In other words P_{gh} and P_{Hh} represent respectively employment and household shares of the sum of employment and households. If activities in the neighbourhood of the house under consideration are fully concentrated in one sector, or when only households occupy in this neighbourhood of house, we find and this index increases as activities in this neighbourhood become more diverse.

$$D_h = 1/\left(\sum_{\forall g}\left(P_{gh}^2\right) + P_{Hh}^2\right), \text{ where } P_{gh} = E_{gh}/\left(H_h + \sum_{\forall g}\left(E_{gh}\right)\right) \text{ and } P_{Hh} = H_h/\left(H_h + \sum_{\forall g}\left(E_{gh}\right)\right).$$

Data sets of Vani Vilas Mohalla

P_{gh} = *1117/ (6787+*$\sum_{\forall g}$ *(1117))*

= *1117/ (6787+3351)*

P_{gh} =*0.110*

Type	No of shops	Average no of employees	Total no of employees
Hotels	18	10	180
Retail shops	162	3	486
Super market	2	15	30
Service station	8	5	40
Banks	7	15	105
others	92	3	276
		Total	1117

$$P_{Hh} = H_h / \left(H_h + \sum_{\forall g}\left(E_{gh}\right)\right).$$

$P_{Hh} = 6787/(6787+ \sum ¥g(1117))$

$=6787/(6787+3351)$

$P_{Hh} = 0.64$

The diversity index for house is the inverse of the Hirschmann Herfindahl index:

$$D_h = 1 / \left(\sum_{\forall g}\left(P_{gh}^2\right) + P_{Hh}^2\right),$$

$D_h = 1/(\sum_{¥g}(0.110 \ \ )+ 0.640 \ \ )$

$= 1/(\sum_{¥g}(0.012)+ 0.47)$

$= 1/(0.0459+0.40)$

$=1/0.435$

$D_h = 2.50$

If activities in the neighbourhood are fully concentrated in one area, or when only households occupy in the neighbourhood of house *h*, then the value of D_h=1 and this index increases as activities in this neighbourhood become more diverse. Vani Vilasa Mohalla neighbourhood has the value of DH = 2.50 and this indicates that the activities are diverse in this neighbourhood.

XI. Issues

The major phenomenon of developed residential area is mixed land use pattern and it is difficult to get alter. The commercial activities have intruded into residential areas especially all along major roads. In case of Jaipur, the city was planned to introduce mixed residential and non residential activities. The zonal-development plans identified the various use zones/activities to be permitted in various parts of the proposed mixed land use area. The mixed use in the same building like residential cum commercial or residential cum institutional or residential cum services industry could be permitted as per the Land use Zoning Code. Whereas in case of Bangalore, Mixed land used was proposed in Master Plan and the honourable High Court of Karnataka directed the authorities to disallow fresh construction of non-residential nature in areas classified as residential in the Revised Master plan 2015. Hence, there is a potential scope to address the diverse neighbourhood of mixed land use due to changing dynamics of land uses in residential areas in the Karnataka Town and Country Planning Act through suitably amendments.

XII. Planning Strategies

The mixed use has positive and negative socio-economic and environmental impacts. Therefore, formulation of a balanced policy of mixed use considering its environmental impact and the socio-economic is need of an hour. Non-residential activity on residential premises should be permitted selectively and carefully, taking into consideration community needs, environmental impact and provision for safe and easy traffic circulation and adequate parking. Mixed Use streets to be identified based on traffic/parking studies. For identification of mixed use streets in zonal regulations, mixed use may be permitted on ground floor, in residential plots facing streets/road of minimum 15.0 or 18.0 meters. Only selective commercial/ non-residential activity should be allowed in the residential premises by considering the needs of the residents, environmental concerns, secure and painless traffic movement and ample of parking space. Permissible use of land includes the retail shops, convenience stores and any other specific use or professional activity not considered harmful for the society. The front setback should be used only for parking purpose. The premises to be entered only from the service lane, but, the direct entry from the main road to be avoided. The planned nature of the residential area to be preserved

XIII. Conclusion

The City of Mysore is experiencing changing dynamics in residential areas. Vani Vilasa Mohalla is the one of the oldest residential layout developed during Maharaja's period, before the Independence India. The diversity index for house is

the inverse of the Hirschmann- Herfindahl index and in this neighbourhood D_h =2.50 this indicates activities are diverse in this neighbourhood, Vani Vilasa Mohalla has been developing into mixed land use pattern and is difficult to get alter. A well developed policy would set the tone for harmonised development of existing residential areas in to mixed land area.

References

[1]. Aurand, A. (2010). Density, Housing Types and Mixed Land Use: Smart Tools for Affordable Housing? Urban Studies 47(5): 1015-1036.
[2]. Britaldo, S. S., C. C. Gustavo, L. P. Cassio, 2001. DINAMICA – A Stochastic Cellular Automata Model Designed to Simulate the Landscape Dynamics in an Amazonian Colonization Frontier. Ecological Modeling. 154: Pp 217-235.
[3]. Wang, Y., and Zhang, X., 2001. A Dynamic Modeling Approach to Simulating Socioeconomic Effects on Landscape Changes. Ecological Modelling. 140: Pp. 141-162.
[4]. Verburg, P. H., W. Soepboer, A. Veldkamp, R.Limpiada, V. Espaldon, S. S. A. Mastura,2002. Modeling the Spatial Dynamics of Regional Land Use: The CLUE-S Model, Environnemental Management. 30 (3): Pp. 391–405.
[5]. Ligtenberg, A., A. K. Bregt, R. V. Lammeren, 2001. Multi Actor Based Land Use Modeling: Spatial Planning Using Agents. Land Use and Urban Planning. 56: Pp. 21-33.
[6]. Briassoulis, E., 2000. Analysis of Land Use Change: Theoretical and Modeling Approaches. In The Web Book of the Regional Science. S. Loveridge (Ed.). West Virginia University, Regional Research Institute, Morgantown, WV.
[7]. Burnell, J.D. (1985). Industrial Land Use, Externalities, and Residential Location. Urban Studies, 22(5): 399-408.
[8]. Cao, T.V. And Cory, D. (1981). Mixed Land Uses, Land-Use Externalities, and Residential Property Values: A Re-Evaluation. Annals of Regional Science 16, 1-24.
[9]. Cervero, R. (1989). Jobs-Housing Balance And Regional Mobility, Planning. University Of North Carolina. Batty, M. (2007), 'Model Cities', Town Planning Review, 78(2): 125-178.
[10]. Post. R. B. (1 964) Criteria for Theories of Urban Spatial Structure: An Evaluation of Current Research M.A. Thesis. Chape1 Hill: Department Of City And Regional Studies
[11]. Xiang W-N, Clarke K C, 2003, "The Use of Scenarios in Land-Use Planning" Environment and Planning B: Planning And Design 30(6) 885 – 909

BIOGRAPHIES

Dr. B. Shankar received the B.E. degree in Civil Engineering in 1984, M.U.R.P degree in Urban and Regional Planning in 1989 and Ph.D degree in Urban and Regional Planning in 1997 from the University of Mysore, Mysore. He is working as Associate Professor in Urban and Regional Planning at the Institute of Development Studies, University of Mysore, Mysore. His research interests to include Urban Planning, Land Use Planning, Urban Poverty, Community Development, Heritage Conservation, and Planning Legislation.

D.Vidhya received the B.E. degree in Civil Engineering from Shri Jayachamarajendra College of Engineering and M.Tech in Urban and Regional Planning from the University of Mysore, Mysore. Presently, she is freelance consultant in the field of Urban and Regional Planning, Bangalore. Her research interests to include mixed land use, land use planning and infrastructure development.

International Journal of Modern Engineering Research (IJMER)
www.ijmer.com Vol.3, Issue.2, March-April. 2013 pp-685-691 ISSN: 2249-6645

Effect of Shape of Cross-section and Its Performance for Concrete Filled Steel Fluted Columns

Dr. B.R Niranjan, [1] Eramma. H[2]
[1](*Professor, Civil Engg Department, UVCE/ Bangalore University, India)*
[2](*Research Scholar, Civil Engg Department, UVCE/ Bangalore University, India)*

Abstract: *An attempt has been made to use this composite structural member as a column with a modification of flutes on the steel tube which enhances the aesthetics and development area of sheet by which the moment of inertia gets increased by about 17 to 40 % for rectangular flutes and 9 to 23 % for triangular flutes. Confining concrete by providing triangular and rectangular shape fluted steel tube has been investigated by a well planned experimental work on twenty six concrete filled steel fluted columns (CFSFC). The parameters chosen for the study are (i) Geometry of the specimen - Triangular fluted columns (TFC) and rectangular fluted columns (RFC) (ii) Different L/D ratios (size of the columns) (iii) Longitudinal reinforcement. Three series of specimens having different L/D ratios, 2500mm long have been tested with M20 grade of self compacting concrete (SCC). It is observed that the load resistance is better in rectangular fluted columns as compared to the triangular fluted columns by 1.31 %, 1.05 % and 9.92% respectively for L/D ratio of 15, 20 and 25. The moment of inertia gets increased by about17% to 40% for RFC and 9% to 23% for TFC.*

Keywords: *CFSFC, CFST, RFC, TFC, SCC, Composite Column.*

I. INTRODUCTION

CFST column technology evolved for the past forty years. Significant research has been made to understand the behaviour of CFST columns taking advantage of confinement avoiding the necessity of form work. Better resistance of loads by columns for axial strength has been achieved by confining concrete by steel tubes. It has been envisaged to study strength, stiffness and buckling characteristics by providing flutes to steel sheet of columns which enhances aesthesis of columns. Also, fluted columns enhances the strength and also stiffness as the surface area of steel sheet and moment of inertia of the column increases. The advantage of steel members having high tensile strength and ductility and concrete members having better compressive strength have been better made use as a composite member. Additional longitudinal reinforcement in the columns makes the columns still stronger. Hence, it has been envisaged to check whether such a columns would act as a slender column. Most of the researchers [(1-18)] have considered the effect of geometric properties like shape, l/d ratio, t/d ratio, boundary conditions, strength of materials and the loading conditions. It has been found that generally the failure occurs by either local buckling or yield failure. It has been found that Euro code gives a better design method which yields values nearer to experimental values. Studies performed on different L/D ratios with small eccentricities have yielded that the degree of confinement offered by a thin walled circular steel tube to the internal concrete is dependent on the load conditions. Other parameters that have been considered by many researchers are different loading conditions like earthquake load, repetitive load, impact load etc.

II. PREPARATION OF SPECIMEN FOR STEEL SHEET

Mild steel sheet with thickness 0.8 mm has been pressed in a mill to obtain five triangular flute with 10 mm at apex of triangle uniformly along the length. These sheets were given a tubular shape and tacked along the edges at an interval of 250 mm along the length of the column. The number and the size of the flutes remained same irrespective of the diameter of the column i.e., for different L/D ratios as shown in Fig 2.1. The moment of inertia gets increased by about 17% to 40 % for rectangular fluted columns and 9% to 23 % for triangular fluted columns are as shown in Table II**.** The development length of the width of each of these columns with different L/D ratios as compared to a circular column of the same diameter is 14, 18 and 22% for triangular fluted columns and 24, 29 and 34 % for rectangular fluted columns for L/D ratios of 15, 20 and 25 respectively as shown in Table III. Reinforcement cage is then placed inside these fluted tubes taking care to maintain the necessary cover. The five types of columns have been shown in Fig 2.2 and Fig 2.3 respectively. Though regular ties have not been used, however four ties have been provided at equal distances to keep the reinforcement in position. Self Compacting Concrete of design mix M_{20} designed as per Nan Su method[(15)] and tested for conformity as per IS specifications is poured into the fluted steel tube. These columns were cured for 28 days by frequently pouring water over top of the column. Pilot specimens cured in a similar manner were tested to know the basic properties and are entered in Table I. The transformed area and experimental load details are shown in Table IV.

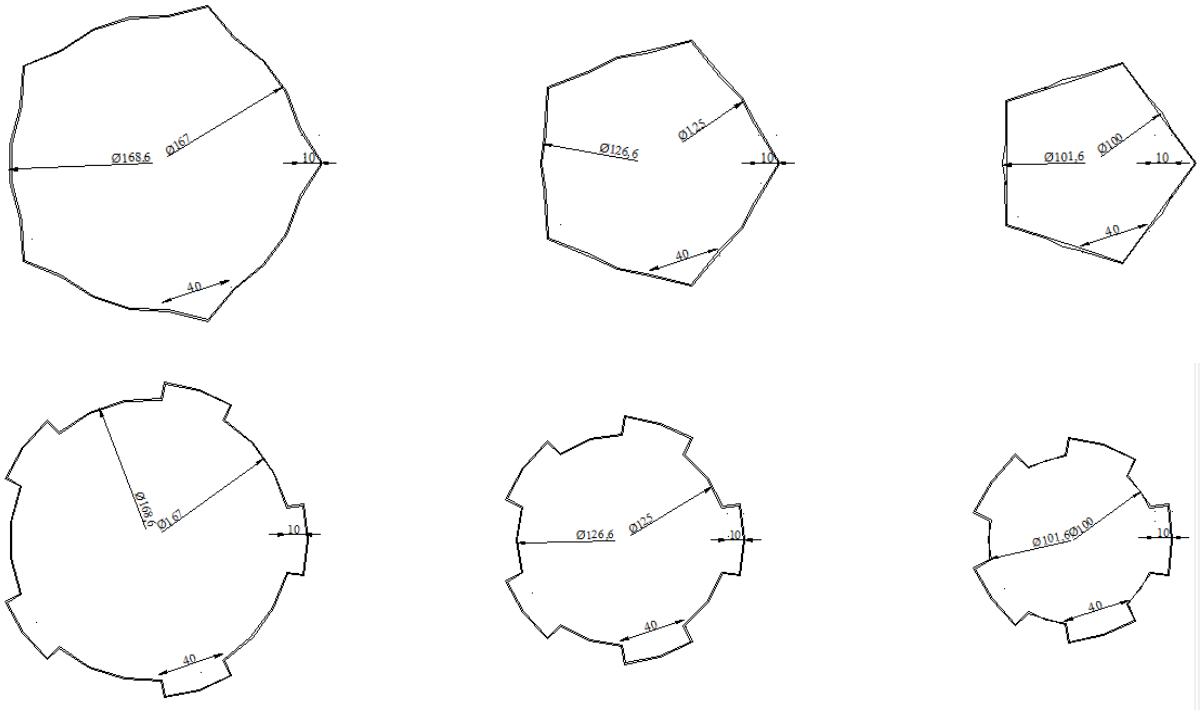

Fig 2.1 Cross section of TFC & RFC with L/D ratio of 15, 20 & 25.

III. EXPERIMENTAL SETUP

The tests were conducted using a 2000 kN capacity hydraulic jack placing the specimen in the testing machine as shown in Fig. 3.1 & 3.2. The bearing surfaces of the testing machine and the bearing plates were wiped clean and any loose sand or other material removed from the surface of the specimen. Which were to be in contact with the bearing plates. The specimen was placed between the bearing plates in such a manner that the upper bearing plate was directly in line with the lower plate and the bearing plates extend at least 25 mm from each end of the specimen. The columns were placed restraining rotation at both ends. Care was taken to ensure that truly axial load was transformed to each of the columns. This was achieved by using plumb bob and a Theodolite.

3.1 INSTRUMENTS

Foil strain gauge (8mm x 8mm) 350 + 0.5 Ω were employed to measure the strains at the centre of the steel tube and centre of the reinforcement (core) of the specimens. Three numbers 50 mm dial test indicators with a least count of 0.01 mm one for axial and the other two for lateral were used to measure axial and lateral deformations upon loading as shown in Fig 3.2 Apart from these instruments plumb bob and linear scales have been used.

3.2 RESULTS AND DISCUSSION

Behaviour of the columns have been studied to understand deformation characteristics in the axial direction and in the transverse direction. Strains have been measured on the steel sheet in two perpendicular directions. Generally, the columns have shown linear behaviour up to about one third of the total load that is about 250 kN axial compressive load. It was envisaged to study the buckling characteristic because of the less width to length of column. But, none of the columns have shown buckling, near the mid portion of the column. The confinement of the column is so large and even the columns without the longitudinal reinforcement and L/D ratio of 25 have not shown any buckling. All the columns have failed near supports of column showing local buckling. Behaviour of each column and its characteristics has been explained in subsequent articles. Among various number of reinforcements, the ultimate load has been found to be maximum for L/D ratio of 15 to be in 4 number of reinforcements and in L/D ratio of 20 and 25 it is for 3 number of reinforcements for triangular fluted columns and the ultimate load has been found to be maximum for L/D ratio of 15, 20 and 25 to be in 4 number of reinforcements for rectangular fluted columns as shown in Fig.3.3(a) and Fig 3. 3(b) respectively.

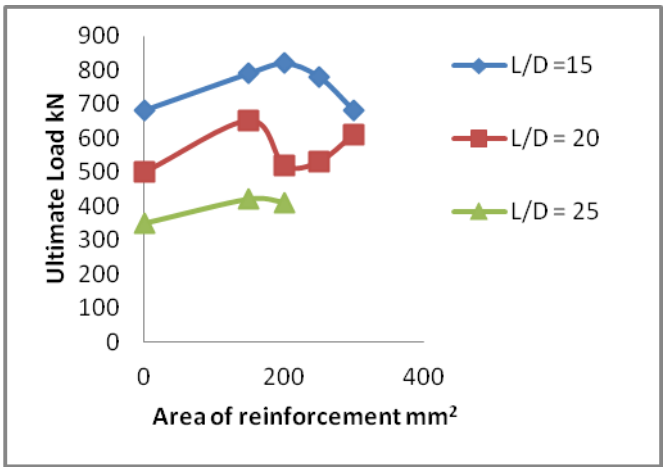

Fig 3.3(a) Triangular Fluted Column

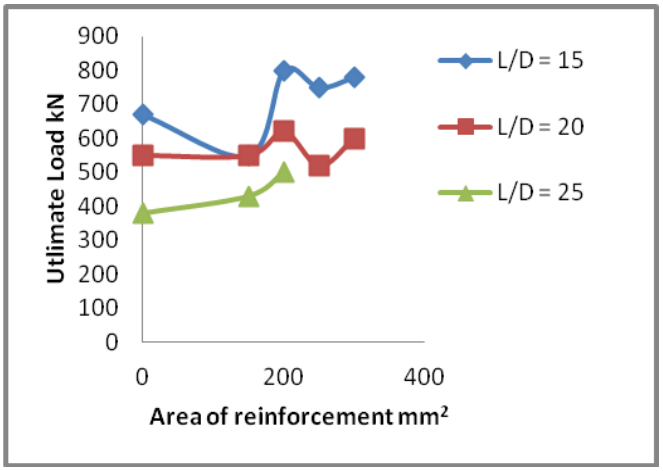

Fig 3.3(b). Rectangular Fluted Column

Fig 3.3 Ultimate load v/s Area of reinforcement

3.3 EQUATIONS

Calculation of Equivalent Moment of Inertia for composite column

$I_e = I_c + I_{ess} + I_{est}$

Where I_e = Equivalent moment of inertia
I_c =Moment of inertia of concrete
I_{ess} = Equivalent moment of inertia of steel sheet
I_{est} = Equivalent moment of inertia of reinforcement

3.3.1 Rectangular Fluted Column

MI about x-x axis

$I_{xx} = I_{\text{circle}} + I_{\text{rectangle flute}}$

$$I_{xx} = \left(\frac{\pi\ (R^4 - r^4)}{4} + A\ \bar{y}^2\right) + \left(\frac{d\ b^3}{12} + A\ \bar{y}^2\right)$$

MI about y-y axis

$I_{yy} = I_{\text{circle}} + I_{\text{rectangle flute}}$

$$I_{yy} = \left(\frac{\pi\ (R^4 - r^4)}{4} + A\ \bar{x}^2\right) + \left(\frac{d\ b^3}{12} + A\ \bar{x}^2\right)$$

3.3.2 Triangular Fluted Column

MI about x-x axis

$I_{xx} = I_{\text{circle}} + I_{\text{triangle flute}}$

$$I_{xx} = \left(\frac{\pi\ r^4}{4} + A\,\bar{y}^2\right) + \left(\frac{b\ h^3}{36} + A\ \bar{y}^2\right)$$

MI about y-y axis

$I_{yy} = I_{\text{circle}} + I_{\text{triangle flute}}$

$$I_{yy} = \left(\frac{\pi \ r^4}{4} + A\,\bar{x}^2\right) + \left(\frac{h\,b^3}{36} + A\ \bar{x}^2\right)$$

3.4 Calculation of equivalent Area

$A_t = A_c + m_1 A_{st} + m_2 A_{ss}$

Where A_t = Area of transformed section
A_c = Area of concrete
A_{st} = Area of reinforcement steel
A_{ss} = Area of steel sheet

Modular ratio

$$m_1 = \frac{Est}{Ec}$$

$$m_2 = \frac{Ess}{Ec}$$

Where E_c = Young's Modulus of Concrete
E_{ss} = Young's Modulus of` Steel Sheet
E_{st} = Young's Modulus of reinforcement

I. FIGURES AND TABLES

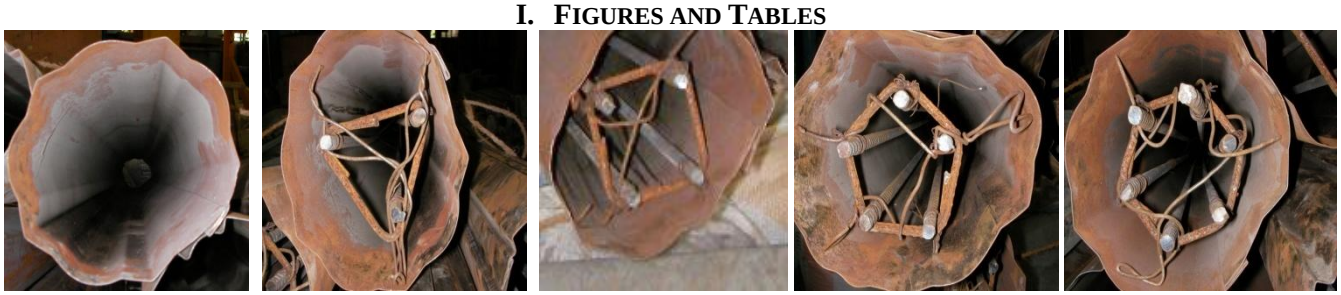

No Reinforcement 3#8 4#8 5#8 6#8

Fig 2.2. Triangular fluted columns with and without reinforcement

No Reinforcement 3#8 4#8 5#8 6#8

Fig 2.3. Rectangular fluted columns with and without reinforcement

Fig 3.1 Experimental Setup

Fig.3.2 Dial Test Indicators laterally & axially

Table I. Details of testing of the materials from experimental results

SL No	Materials	Poission's ratio (μ)	Modulus of Elasticity (E) N/mm^2	Remarks
1	Concrete	0.16	0.223 x 10^5	Split tensile strength test
2	Reinforcement	0.28	0.21 x 10^5	Tensile test
3	Steel Sheet	0.26	0.723 x 10^5	Tension coupon test

Table II Comparison results of Equivalent Moment of Inertia of Fluted column, Non fluted internal diameter column and Non fluted external diameter column.

Sl No	Specimen	Equivalent Moment of Inertia mm^4 (with flutes)	Eq Moment of Inertia mm^4(without flutes considering internal dia)	Eq Moment of Inertia mm^4(without flutes considering external dia)	% increase (internal dia+with flutes)	% decrease (external dia – with flutes)
1	TFC-L/D 15	41.96 x 10^6	38.18 x 10^6	60.01 x 10^6	9.00	30.07
2	TFC-L/D 20	14.18 x 10^6	11.98 x 10^6	21.69 x 10^6	15.51	34.62
3	TFC-L/D 25	6.36 x 10^6	4.90 x 10^6	10.17x 10^6	22.95	37.46
4	RFC-L/D 15	46.23 x 10^6	38.18 x 10^6	60.01 x 10^6	17.41	22.96
5	RFC-L/D 20	16.76 x 10^6	11.98 x 10^6	21.69 x 10^6	28.52	22.72
6	RFC-L/D 25	8.15 x 10^6	4.90 x 10^6	10.17 x 10^6	39.87	19.86

Table III: Development Length of the Columns

Name of the Specimens	Development Length mm		% Increase
	Without Flutes(Internal Diameter)	With Flutes(Internal Diameter +Flutes)	
CFSFC-TFC-L/D 15	524.65	611.10	14.14
CFSFC-TFC-L/D 20	392.69	479.11	18.03
CFSFC-TFC-L/D 25	314.15	400.60	21.58
CFSFC-RFC-L/D 15	524.65	687.50	23.68
CFSFC-RFC-L/D 20	392.69	555.51	29.31
CFSFC-RFC-L/D 25	314.15	477.00	34.14

Table IV. Area of cross section of columns

Specimen Name Column-L/D-No Rein	A_t (Equivalent) mm^2 TFC	A_t (Equivalent) mm^2 RFC	% increases	Experimental Load kN		% increase
				TFC	RFC	
C-15-0	24338.14	25538.01	4.70	680	670	1.49
C-15-3	25776.68	26976.54	4.45	790	550*	43.63
C-15-4	26256.25	27456.12	4.37	820	800	2.50
C-15-5	26735.73	27935.60	4.30	780	750	4.00
C-15-6	27215.30	28415.17	4.22	680	780	12.82
C-20-0	14360.84	15560.71	7.71	500	550	9.09
C-20-3	15799.37	16999.24	7.06	650	550	18.18
C-20-4	16278.95	17478.82	6.86	520	620	16.12
C-20-5	16758.43	17958.30	6.86	530	520	1.92
C-20-6	17238.00	18437.87	6.51	610	600	1.66
C-25-0	9737.53	10937.39	10.92	350	380	7.89
C-25-3	11176.06	12375.92	9.70	420	430	2.32
C-25-4	11655.64	12855.50	9.33	410	500	18.00

* Without arc weld column. First experiment test specimen the sheet is opened up, immediately put arc weld for remaining columns, then the strength of the columns has been increases.

IV. CONCLUSION

- The moment of inertia gets increased by about 17%, 29% & 40% for RFC and 9%, 16% & 23% for TFC for L/D ratio of 15, 20 & 25 respectively.
- The development length i.e., width of the sheet of these triangular fluted columns increases for different L/D ratios of 15, 20 and 25 by 14%, 18% and 22% as compared to a circular column of the same diameter and the same for rectangular fluted columns will be 24%, 29% and 34%
- The cross section area gets increased by about 4.40%, 7% & 9.98% for L/D ratio of 15, 20 and 25 respectively for rectangular fluted columns as compared to triangular fluted columns.
- It is observed that the load resistance is better marginally in the case of rectangular fluted columns as compared to the triangular fluted columns by 1.31 %, 1.05 % and 9.92 % respectively for L/D ratio of 15, 20 and 25.
- Among various number of reinforcements, the ultimate load has been found to be maximum for L/D ratio of 15 to be in 4 number of reinforcements and in L/D ratio of 20 and 25 it is for 3 number of reinforcements for triangular fluted columns and the ultimate load has been found to be maximum for L/D ratio of 15, 20 and 25 to be in 4 number of reinforcements for rectangular fluted columns.
- The study has shown that for an L/D ratio 25, no buckling has been observed even without longitudinal reinforcement. All the columns failed by local buckling.

V. ACKNOWLEDGEMENTS

The authors wish to thank the authorities of Bangalore University for giving an opportunity to conduct the experiments in the Structural Engineering Laboratory of Faculty of Engineering-Civil.

REFERENCES

Journal Papers:

[1] O'Shea. MD & Bridge. RQ, 1997, "Local buckling of thin–walled circular steel sections with or without internal restraint" Journal of Constructional Steel Research, vol. 41, issues 2-3, Feb-March 1997 pp. 137-157.

[2] O'Shea, MD &, Bridge RQ 2000, "Design of circular thin-walled concrete filled steel tubes " Journal of Structural Engineering, ASCE, Proc. 126, 1295-1303.

[3] Brian Uy, 2001, "Local and post-local buckling of fabricated steel and composite cross sections", Journal of Structural Engineering, ASCE, Vol. 127, no. 6, pp.666-677.

[4] Brian Uy et al, 2003, "Strength of Concrete Filled Steel Box Columns Incorporating Interaction Buckling", Journal of Structural Engineering, ASCE, Vol 129 pp. 626-639.
[5] Bridge, RQ, et al, 1995, " Local buckling of square thin-walled steel tubes with concrete infill". In: Proceedings of the international conference on structural stability and design, pp 307-14
[6] Artiomas Kuranovas et al, 2007, "Behavior of hollow concrete-filled steel tubular composite elements", Journal of Civil Engineering and Management 2007, Vol XIII, No 2, 131–141
[7] Ben Young, Ehab Ellobody, 2006, "Experimental investigation of concrete-filled cold-formed high strength stainless tube columns", Journal of Constructional Steel Research, 62 (2006) pp 484-492.
[8] Bradford, MA, et al, 2001, "Slenderness limits for CHS sections", In: Ninth International Symposium on tubular Structures, Dusseldorf, pp 377-81.
[9] Fam, A, et al, 2004, "Concrete-filled steel tubes subjected to axial compression and lateral cyclic loads", Journal of Structural Engineering, ASCE, vol. 130, no. 4, pp. 631-640.
[10] Giakoumelis. G & Lam. D, 2004, "Axial capacity of circular concrete-filled tube columns", Journal of Constructional Steel Research, vol. 60, pp. 1049-1068
[11] Liang QQ, et al, 2004, "Local and post-local buckling of double skin composite panels", Proceedings of the Institute of Civil Engineers Structures and Buildings, vol. 156, no 2, pp 111-19**.**
[12] Liang QQ, et al, 2006a, "Local buckling of steel plates in concrete -filled thin-walled steel tubular beam-columns", Journal of Constructional Steel Research, accepted 26 May 2006a.
[13] Lin-Hai Han, e al, 2007, "Behaviors of concrete-filled steel tubular members subjected to combined loading", THIN-WALLED STRUCTURES 45 (2007) pp 600-619.
[14] Lin-Hai Han, et al, 2004, "Concrete-filled double skin (SHS outer and CHS INNER) steel tubular beam-columns. THIN-WALLED STRUCTURES 42 (2004) PP 1329-1355.
[15] Nan Su, et al, 2001, "A simple mix design method for self – compacting concrete" Cement and Concrete Research 31 (2001) 1799 – 1807.
[16] Shanmugam N.E., Lakshmi. B , 2001,"State of the art report on steel-concrete composite columns". Journal of Constructional Steel Research 57 (2001) pp 1041-1080.
[17] Subramanian.S & Chattopadhyay, 2002. "Experiments for mix proportioning of self-compacting concrete", The Indian Concrete Journal, January 2002 pp 13-19.
[18] Uy, B 1998, "Local and post-local buckling of concrete filled steel welded box columns", Journal of Constructional Steel Research, vol. 47, pp 47-52.

Books:

[19] Dayaratnam. P, Limit state design of reinforced concrete structures, 2004
[20] Sinha S.N, Reinforced Concrete Design, First Revised Edition, Tata McGraw Hill publishing company limited.
[21] Dr.Prakash Rao D.S, Strength of materials, A practical approachVolume1, University press (India) Limited Publications.
[22] LIN. T.Y., & NED H. BURNS "Design of prestressed concrete structures " Third Edition 1982, JOHN WILEY & SONS, Inc.,
[23] Shetty, M.S., "Concrete Technology" Theory and Practice, First Multicolour Illustrative Revised Edition 2006**.**

International Journal of Modern Engineering Research (IJMER)
www.ijmer.com Vol.3, Issue.2, March-April. 2013 pp-692-697 ISSN: 2249-6645

Strategies for Reinvigorating the Urban Heart of Mysore

Dr. B. Shankar, [1] M.C.Shashikumar[2]
[1]*Associate Professor in Urban and Regional Planning, Institute of Development Studies, University of Mysore Mysore,*
[2]*Joint Director of Town Planning, Government of Karnataka, Mysore Division, Mysore*

Abstract: *Reinvigoration of urban heart is an increasingly important for planning of large cities. Cities work better when they are diverse and livable, with a mix of land uses, high population densities and lively streets with magnificent urban built form, architectural buildings and urban design elements. Therefore, it is necessary to conserve the central area for regaining the past glory. Reinvigoration is a deliberate, planned and overall effort to change the urban built environment by adopting comprehensive approach and large scale modification of existing city central area for serving the present and future generations. Mysore is an historical, cultural and planned city in India and it has a strong urban heart with well defined boundaries. The paper presents the structure and issues of urban heart of Mysore and proposes strategies for reinvigoration.*

Keywords: *Reinvigoration, Urban Heart, Strategy, Heritage City*

I. Introduction

The core areas of Indian cities are experiencing rapid changes in land use, high density of developments, traffic congestion, haphazard developments, land speculation, urban decay, dilapidated buildings, insanitary conditions, over loading on the existing infrastructure and many more. Cities' effort enhanced when they are rejuvenated their built and urban forms. It is commonly accepted that reinvigoration of urban heart is an important component of urban renewal for planning of cities. Reinvigoration is a deliberate, planned and overall effort to change the urban built environment by adopting comprehensive urban renewal programmes. Conservation, rehabilitation and redevelopment are the three components of urban reinvigoration, which are interrelated. In this paper an attempt has been made to highlight the significance of city core and propose strategies for reinvigoration of urban heart of Mysore.

II. Background of Mysore

Mysore is the second largest city in Karnataka State. The city had a population of 887,446 as per 2011 provisional census figures and increased from 7, 85, 800 in 2001. It is situated at 140 km from Bengaluru. Mysore has many architectural buildings, which were built in the beginning of twentieth century during Maharaja's regime. Mysore is an educational, commercial and administrative heritage and tourist centre. The city is famous for if cultural festival namely *Dasara.* The city has more concentrated wealth of beauty spots and is rich in picturesque and historic and other kinds of interest. The streets in the city have been laid out on broad and generous lanes with pedestrian walks on either side. The skyline of the city with the clock tower, statues, vista and the palace domes against the background of Chamundi hills presents a beautiful townscape.

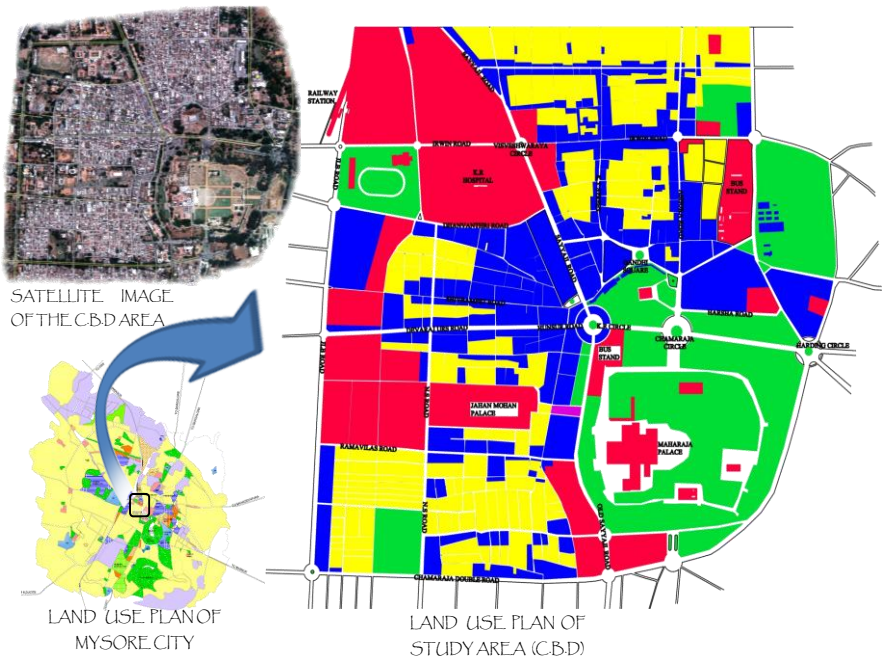

Fig.1 Urban Heart of Mysore

III. Urban Heart of Mysore

The present structure of Mysore city is a product of history, early directive planning of Mysore City Improvement Trust Board (MCITB) in 1903, and recently the dominant market forces and ineffective planning. Now, central area of the city is more than 100 years old, but the city had the charm of princely capital. In addition, because of the slow growth rate and rigid land market controlled solely by the state agency, it could until recently hold together a coherent and comfortably compact form and structure. Recent developments however, are trying to rupture as it the seams. The essential elements which define Mysore central area are Palace, business, commercial and administrative centre. The central area is also the cultural center with art gallery etc. The respect and reverence they inspire in the people of Mysore are so deep-rooted that any development which will lessen the physical and visual importance of these elements will not be accepted. The central area covers an area of 281.70 hectares and comprises of all types of land use. The height and form of the buildings are different in the areas of commercial, residential and varies from public buildings. The inner parts of the city especially the older areas are in greater demand for commercial use. Until recently, the business and commercial activity of the city was conducted in old low-rise buildings. This was a beginning to change, and old buildings got pulled down and new structures which have come up have a little regard to the bulk density regulations, setbacks, lung spaces or even the character or architectural quality of the buildings. The city is beginning to loose the sense of the place. The blending of the manmade structures with the natural features of balanced treatment of architectural composition has given the city a rare and captivating beauty. The statues, clock towers and fountains have been beautifully designed in different styles and erected within carefully planned open space.

There are quite a number of beautiful houses built in the old traditional styles rising up to three floors with sufficient open space all around. The streets in the city have been laid out on broad and generous lanes with pedestrian walks on either side. This presents to the visitors, some of the most attractive vistas. The Albert-Victor Road, which has a parkway beautifully laid within the Curzon Park and hugging the palace gate and the Fort, is worth visiting to appreciate the beauty of Mysore city. The skyline of the city with the clock tower, statues and the palace domes against the background of Chamundi Hills present a beautiful townscape. Public buildings have maintained beautiful gardens within their premises enhance the appearance of the city. Trees planted on either side of some roads form an avenue. Mysore thus has the distinction of being developed on a grand scale into a planned city and a centre of tourism. The junction like K.R.Circle, Nehru Circle, and Vishweshvaraiah Circle form the good rotaries in the circulation pattern. The buildings around these circles are also designed with circular façade brings harmony and feeling of the place.

Mysore Urban Development authority has identified planning district number one as intensively populated area in master plan and Mysore City Corporation has considered this road as inner-ring road which forms the boundary for urban heart. The boundary of the urban heart is follows: east by Bangalore Nilagiri road; west by JLB road; north by Sawday road and south by Chamaraja double road. The city centre is having more heritage building, recreation centres, public buildings, market places, educational institutions, commercial streets and buildings, hotels and lodging, bus terminals and railway stations. The people's movement is towards heart of city for their daily needs. At present the city is losing its past glory owning to absence of any comprehensive vision for safeguarding its built heritage. Also, the city centre is losing its charm as the roads are narrow and congested due to increase in vehicles. The urban heart of Mysore is changing rapidly in land use and in appearance as well as. As the city grows in size, the importance of the heart of the city assumes more and more the function of shopping and style. The limited space, narrow streets, old houses and traffic of all types of vehicles are in striking contrast to the environment of the heart of city.

IV. Land Use Pattern

Urban areas contain a complex interaction of land uses and activities. Newer cities with strong planning controls may have fairly well defined residential, shopping or industrial areas. Elsewhere a great mix of land uses may be existed side-by-side, sometimes in conditions of extreme conflict. Different land uses place differing demands upon the city network.

Table 1: Land Use of Mysore City

Land use	1976(ODP)		1986 (CDP)		1997(RCDP)	
	Area in hectares	% to total	Area in hectares	% to total	Area in hectares	% to total
Residential	81.07	28.78	74.25	26.36	67.14	23.83
Commercial	31.55	11.2	40.87	14.51	48.59	17.24
Industrial	4.65	1.65	6.79	2.41	6.00	2.21
Parks and open space	21.94	7.79	17.01	6.04	17.05	6.12
public and semi public	48.76	17.31	67.58	23.99	67.58	23.99
Traffic and transportation	68.42	24.29	75.13	26.67	75.14	26.67
Total	281.7	100	281.7	100	281.70	100

Source: Mysore Urban Development Authority, Mysore.

Table 2: Existing land Use- 2009

Land use	Area in hectares	%
Residential	62.25	22.09
Commercial	52.88	18.77
Industrial	6.6	2.34
Parks and open space	17.25	6.15
Public and semi public	67.58	23.98
Traffic and transportation	75.14	26.67
Total	281.7	100.00

Source: Primary survey conducted by researchers

Residential land use in the central area is 62.25 hectares which constitute about 22.09% of total area. The residential areas are older and most of the residences are found to be older than 100 to 150 years. At present, commercial land use in this district is about 52.88 hectares which constitutes 18.77% of the total area. The district has more commercial activities compared to any other district in the city. The area occupied by palace is about 8% of the total area. Administrative and government offices, educational institutions have been classified as public and semipublic land use in the planning district one. The total area under public and semipublic is 67.58 hectares and constitutes about 23.98% of the urban heart. In the central area, parks and open spaces constitute about 6.15% covering an area of 17.25 hectares. Parks are much concentrated around the palace, moat around the fort are being later maintained as parks. Parks like Curzon Park and People's parks are located in the central part of the city where large numbers of people spend their leisure. These parks serve as a place for relaxing the visitors in the central area and it is observed that often, vendors and hawkers occupy these areas. A portion of open space in front of Town hall has given a magnificent look to the building. Industries in the central area occupy 6.0 hectares and they constitute 2.21% of the total area.

V. Architectural Characters

The heritage buildings of Mysore can be classified as Indo – Sarcenic, traditional Hindu, Greco-Roman, Gothic and the European classical styles based on their architectural features,

A. Indo Sarcenic.

Amba Vilas Palace is an Indo-saracenic building and its styling was an occasional departure from the long-lasting vogue of the European, they yet have a compelling presence in the city's remarkable heritage of architecture.

Fig.2 Ambavilas Palace

Mixtures of Hindu and Muslim characteristics of architecture are found in the building and some of the Islamic architectural influences found namely Islamic pointed and cup shaped arch opening found in the verandahs, projecting minarets near the entrance porticos, big bulbous domes in the centre and in the corners of the building on their roof level. Also, architectural features are found in curvilinear chatris, banana and lotus stem brackets attached to the column capitals including motifs of the Hindu gods and goddess in studiously created niches. The interiors of the some of the buildings have colonnaded court yards with Hindu style architectural motifs on the column brackets and doors of the palaces are carved with figures of Hindu gods and goddesses.

B. European Classical Architecture

Lalitha Mahal Palace is the best example of European Classical style of architecture. The buildings of this style can be seen with extensive use of Lonic and Corinthian columns supporting their structures. The elevations of these buildings are treated with thick bands of cornices, finaled parapets and rediments containing Hindu gods and goddesses.

Fig.3. Lalitha Mahal Palace

Other buildings which have influenced this style of architecture are the Wesley and the Philomenas church, University Educational buildings like the Uvaraja's and Maharaja's degree colleges and many more buildings.

C. Traditional Hindu Style

The Jaganmohan Palace is example of predominantly Hindu traditional style. All temples in Mysore exhibit the traditional Hindu style of architecture. Each temple has a Garbhagruha, Sukanasi, Navaranga and Mukhamantapa. The agrahara houses are examples of traditional style with a simple but functional structure placed shoulder to shoulder with shared masonry walls.

Fig. 4 Jagan Mohan Palace

D. Greco-Roman Architecture.

In these structures a Vatican dome rising on a drum (Circular, Octagonal etc.) dominates the elevation. The column styles could be Tuscan, Ionic and Corinthian; arched and plastered colonnades form the two wings. Greek deities define the tier and the balustraded parapet bends are an agreeable addition to a rich composition. The Deputy Commissioner's Office (Dewan's Kacheri) Chaluvamba Park and the Krishna raja Hospital are classic examples.

Fig.5 K.R. Hospital

Gothic architecture

The Philomena Church is a best example for its gothic architectural influence and tall towers or spheres at the entrance of this church; all the openings are supported by gothic arches.

Fig.5: St. Philomena Church

Spires or long tapering roof-like elongated pyramids that are commonly found in churches are the typical characteristics of gothic style. The main hall or nave with multiple molded columns culminates in stately arches which guide the eye to the vaults. The altar is set against arched screens of stone works which are in harmony with the arched vertical lines and tapering vaults of the structure.

VI. Tourism

The city combines beauty with diversity, situated in the southern tip of the state and it enjoys a salubrious climate for tourist attractions. There are many tourists' spots worthy of being seen, which are land marks and they are situated within five kilometers radius from the city centre. The world famous Mysore Palace, Jagan Mohan Palace, Art Gallery, Chamundi Hill, Chamarajendra Zoological Gardens, St.Philomen's Church, Railway Museum, Lalith Mahal Palace, Karanji Lake etc. Around Mysore many important historical buildings and tourists places which attracts tourists and they are, Brindavan Gardens, Ranganathittu, Bird Sanctury, Somanathapura, Srirangapattna, Gommatagiri, Balamuri, Nanjangud etc.

Table 3: Tourist inflow (lakhs)

	2004- 2005	2005-2006	2006-2007	2007-2008	2008-2009
Palace	20.19	21.51	25.26	24.10	25.80
Art Gallery	2.29	2.42	2.48	2.45	2.51
Zoo	15.96	15.30	16.45	16.53	16.85

Source: Tourism office, Mysore.

VII. Problems of Urban Heart

Mysore being a monumental city has unique architectural features which creates a beautiful townscape. New buildings, which are coming up recently like Restaurants, community halls, cinema theatres are not to suit this city's architecture and are disturbing the whole architectural circle have broken the skyline by the domes where the new buildings are cutting straight. This created the contrast between Palace i.e., on Sri Harsha Road and B.N.Road. Because of more commercial threshold in this zone, the height of the buildings has increased. There is a shift in residential to commercial near Bus stand and Railway station. It is also observed that parking facilities are provided in the basement of newly constructed buildings. Palace is the central place in heart of the city and it attracts the highest number of tourists. City bus-stand is operating just beside the palace in the moat area. Absence of organized parking place in and around the heritage buildings and diversified image of the facades around the heritage area including commercial hoardings hanging all around the area are some of the problems faced by the urban heart. Most of the structures are very older and in bad condition. Many structures are fit for demolition on the commercial streets i.e., on Sayyaji Rao Road, Ashoka Raod, Irwin Road etc.

VIII. SWOT Analysis

STRENGTHS	WEAKNESSES
The heritage city continues to attract increased number of visitors every year. The slow and measured way of life adds to the charm of this royal city. Brindavan Gardens, Rangana Thittu Bird Sanctuary, Srirangapattana, Melkote, Somanathapura, Talakadu etc, located nearby are added tourist attractions. The traditional products of Mysore viz., Mysore Silk, Sandal oil, Handicrafts, Mysore Mallige (Jasmine) etc. are of great commercial importance.	Land developments on all sides have encroached upon the lung space. Huge commercial constructions are coming up by pulling down the heritage structures.
OPPORTUNITIES	**THREATS**
Reinvigoration of central area is expected to give a face-lift to the entire city of Mysore. Improved tourist infrastructure would provide tremendous commercial opportunities. IT and BT sectors would attract visitors from all over the globe. There would be more market for the traditional products of Mysore	Large scale speculative land purchase will add to the existing suffocation. The existing facilities and civic amenities may not be sufficient for the increasing tourist inflow.

IX. Planning Strategies for Reinvigoration

Mysore has a strong historical core and neither it has scope to expand horizontally; nor it can expand vertically because of height of the building cannot be higher than the Palace's height. Central area of the city needs to be developed promoting actively as a viable place to live, work, shop and visit. It should be the business, financial and cultural centre. It also needs to offer a strong local and regional presence and be a place that local people are proud of and visitors can enjoy and it is to be made environmentally attractive, economically viable, and attractive and liveliness. It is high time to take up conserve measures in the central area to regain the past glory through reinvigorating the urban heart of Mysore and is as follows:

a) All the monuments should be identified, graded and taken for conservation.
b) The precincts have to be identified and they have to be developed within their envelops
c) A separate regulations to be developed for inner city core or urban heart
d) The projects should be initiated which would therefore aim at decongesting the old city areas, like Santepet, Gandhi square, Devaraja Market.
e) Action may be taken to introduce rapid transit and efficient public transport systems. One way to keep city centre alive is good planning.
f) Discourage new large constructions in the core city area, and force all new development in dedicated zones around the periphery.
g) Floor Space Index (FSI) in the core city could be pegged at a suitably low level, while higher FSI permitted in the periphery.
h) Larger development fees or betterment charges could be levied in the central area.
i) Pro-actively develop fully self-sustained enclaves (industrial, commercial, or residential) on the periphery, so that there is no incentive for development to move to the core.
j) Providing basic facilities, street beautification and proper maintenance around heritage buildings has to be taken up by planning authority and incorporate these suggestions while preparing land use plan and also forecasting the future need.
k) Residential should is not be allowed for change of land use to avoid mixed land use, where the occupants are free from traffic disturbance.
l) Architectural control to be imposed around Palace on the Sayyaji Rao Road, K.R.Circle, Ashoka Road.
m) Public and semi public places are retained and are regulated not to grow further.
n) Strict enforcement of zoning regulation and building Bye-law to congestion.

X. Conclusions

Reinvigoration of urban heart is an increasingly important component of city planning system. The Mysore is known as cultural and historical capital and its central area is known for its heritage religious and architectural buildings. It is losing harmony among buildings, streets and open spaces visual apparent. The central area is over crowded with all the economic and administrative activities coupled by environmental degradation and pressure on existing infrastructure. Therefore, it is high time to conserve the central area to regain the past glory through reinvigorating the urban heart of Mysore.

References

[1] Niamh Moore (1999), Rejuvenating docklands: the Irish context, Irish Geography, vol. 32 (2).
[2] ITPI New Delhi, Journal volume-6, number 1 (January- March, 2009) article "Revitalizing Chitar Oli: A Street with Tradition.
[3] Ashotosh Joshi. (2007), "Regeneration of Indian Historic Cities", The Journal of the Indian institute of Architecture, volume 72, issue 12, pp.20-22.
[4] Kevin lynch (1994), "The Image of the City", MIT Press, Cambridge.
[5] Johan Rannels (1956), "The core of the city" Columbia University press, New York.
[6] Regeneration of Brevery site in http://www.vaux Co.uk
[7] Regenerating Derby, in www.qaresearch.co.uk
[8] Ian Bond Conservation (2003) urban landscape character Analysis.
[9] City centre master plan Bellingham, Washington August-2002.
[10] Conservation Area Review Background paper, www.nort-herts.gov.uk.
[11] Conservation Area Review Appraisals English heritage 2005, www.helm.org.uk.
[12] A Guide to planning in conservation areas (2004) Stroud District Council, www.stroud.gov.uk.

BIOGRAPHIES

Dr. B. Shankar received the B.E. degree in Civil Engineering in 1984, M.U.R.P degree in Urban and Regional Planning in 1989 and Ph.D degree in Urban and Regional Planning in 1997 from the University of Mysore, Mysore. He is working as Associate Professor in Urban and Regional Planning at the Institute of Development Studies, University of Mysore, Mysore. His research interests to include Urban Planning, Land Use Planning, Heritage Conservation, and Planning Legislation.

M. C. Shashi Kumar received B.E. degree in Civil Engineering and M.Tech in Urban and Regional Planning from the University of Mysore, Mysore in 2010. Presently, he is working as Joint Director of Town Planning, Department of Town Planning, Mysore Division, Government of Karnataka. His research interests to include Heritage Conservation.

International Journal of Modern Engineering Research (IJMER)
www.ijmer.com Vol.3, Issue.2, March-April. 2013 pp-698-703 ISSN: 2249-6645

Creating Awareness for Heritage Conservation in the City of Mysore: Issues and Policies

Dr. B. Shankar, [1] Dr. Chidambara Swamy[2]
[1]*Associate Professor in Urban and Regional Planning, Institute of Development Studies, University of Mysore*
[2]*Professor and Head, Department of Architecture, Adhiyamaan College of Engineering, Hosur*

Abstract: *Heritage awareness is a crucial part of any heritage conservation and management. The creation of awareness is time-consuming and it requires commitment and local support. It is often the most recognizable component of a heritage management. One of the most effective ways to build and maintain respect for community's heritage is through a selection of activities that raise public awareness and increase appreciation. The success of heritage conservation initiatives depends on the understanding and participation of the local community. The City of Mysore is one of the prominent historical, cultural and heritage cities in India. The city has been identified as a heritage city for conservation by the State and Central Governments. The awareness programmes have also been launched under Jawarharlal Nehru National Urban Renewal Mission by City Corporation in collaboration with Heritage Commissioner's office. The paper focuses on the efforts made by various agencies for creating awareness for heritage conservation and proposes policy measures for creating effective heritage awareness in the city of Mysore.*

Key Words: Heritage, Culture, Conservation, Awareness and Policies

I. Background

Heritage awareness is an important component of conservation. One of the basic causes for damage of heritage is due to lack of awareness to the public at large and non involvement of people in the process of conservation as well. The Constitution of India prescribed under the *fundamental duties* that the protection of heritage is one of the important duties of each and every Citizen of India, but the efforts made by the local authorities and agencies are not significant. The society's responsibility is to conserve the heritage that was created in the past. The local people need to take part in the process of conservation. Therefore, it is high time that greater emphasis to be laid down for creating awareness to the public including people at large.

II. Heritage Awareness in Mysore

The Department of Archeology, Museums and Heritage, Heritage Commissioners office, Mysore City Corporation and Tourism Department have taken a leading role for creating awareness on heritage by involving stakeholders of Mysore. The Mysore Heritage Area Experts Committee for preservation and protection of heritage areas has listed 201 heritage buildings. Heritage commissioner's office has given guidelines and suggestions to keep the vicinity of heritage buildings clean and tidy and it has fixed "signage boards" with brief description (Shilaphalaka) which are placed near the heritage buildings.

The workshops, seminars, photo exhibitions of heritage buildings/structures and visit to heritage areas are being conducted for tourists, officials, publics, and school and college students. A small booklet on heritage of Mysore was published. Awareness programmes for tour guides and training programme on conservation and maintenance of heritage buildings for various government department officials were also organized by heritage commissioner's office. For creating awareness among school and college students, *heritage clubs* were started in the year 2007. Photo exhibition on monuments and buildings were organized in the premises of Exhibition Authority during Dasara celebrations. Besides, dance, dramas, cultural activities, essay writing, debate, painting/sketches and Janapada programmes were also conducted. Heritage walk is being introduced to create awareness among the public throughout the year. The public, tourists, different departmental official, schools and college students, NGOs, hospitality people, travel agencies and other concerned peoples were involved extensively. The other details of heritage structures along the path are printed and are given to all participants to create better awareness and knowledge on built heritage of the city. T-shirts, caps, embossed with landmark buildings are also given to participants. The heritage walk (see fig.1) has been designed as people initiative, where they shall be equally involved in making the project a success.

Many voluntary agencies namely Dr. Reddy Foundation and 'Royal Heritage Walk' have been conducting activities related to heritage walk in the city. Many foreign tourists have participated in the heritage walk. Post graduate students of arts, history and tourism department's students of the University of Mysore and private colleges are also participating in the heritage walk and they are working towards creating awareness on heritage assets.

Fig.1: Route Map of Heritage Walk

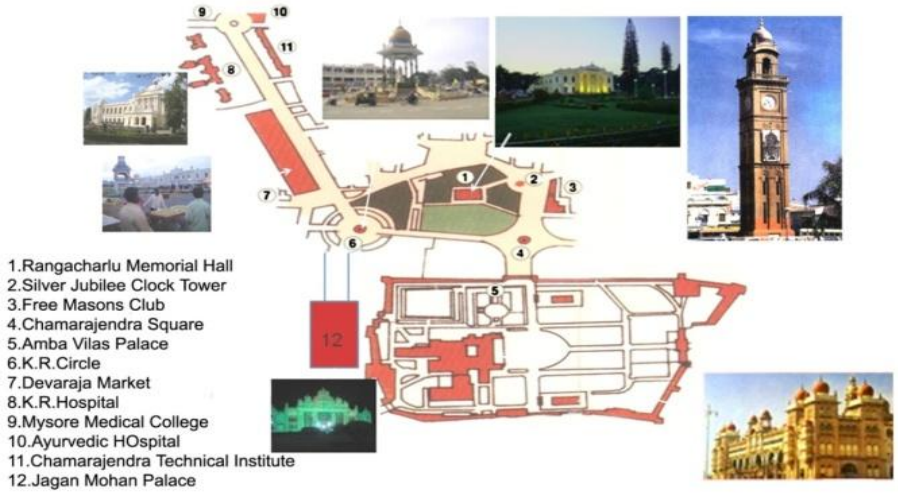

A. Initiatives of Heritage Walk by IHCN: The Indian Heritage Cities Network Foundation (IHCN) has established its centre at Mysore in May 2011 for boosting the heritage conservation activities in the city. It has organized four-day third biennial conference in Mysore during May 2011 and the conference was funded by UNESCO, New Delhi, in collaboration with the Government of Karnataka, Karnataka Urban Infrastructure Development Finance Corporation and Mysore City Corporation. The conference deliberated on various aspects of heritage cities and its conservation. "Heritage Walk" to historic core areas was organized to the conference delegates.


Begin with Town Hall Premises


Town Hall


Clock Tower


Chamaraja Circle


Dufferin Clock Tower.


IHCN Particpants

Fig.2 Heritage Walk at Different Places

III. SWOT Analysis

STRENGTHS	WEAKNESSES
1. Awareness programmes viz. heritage walk, workshops and competition: debate, essay writing, painting, etc., initiated by Heritage Commissioners' Office. 2. A special component of heritage conservation is being planned under JNNURM project. 3. Networking of Institutions – Philanthropist/Charitable Institution, heritage clubs, IHCN, UNESCO, NGOs, schools and colleges.	1. There is no significant effort for developing effective IEC materials for creating awareness. 2. No specific information to the public authorities or public for management of heritage assets including alterations and demolitions. 3. There is no wide publicity drives. 4. No mechanism for participation of people or owners of private buildings/ stakeholders.
OPPORTUNITIES	**THREATS**
1. Setting up of Heritage Cell for planning, management, and control and resource mobilization. 2. Scope for framing of Heritage Polices and IEC under JNNURM Tool Kit. 3. Tourist Development Plan of State Government to boost heritage and culture.	1. Private owners and businessmen resist/ oppose for maintaining the assets owned by them. 2. Relocation of City Bus and Sub-urban terminals for pedestranisation in the heritage core and restricting vehicles.

IV. Issues and Options

The awareness programmes are being conducted by the city authorities by involving public and stakeholders, which has achieved a reasonable success in Mysore city. Still a large mass of people and owners of the heritage buildings and authorities have to realize holistically the need and importance of safeguarding this valuable rich heritage of Mysore. In spite of these little efforts, many valuable heritage buildings are demolished; building elements disfigured; encroachments and incompatible developments have come around the heritage buildings; structural problems continued and heritage buildings are not maintained in the heritage area of Mysore. The awareness programmes are required to be conducted more regularly and consistently involving all sections of the society, especially owners of the heritage buildings, officials of the development authority and people living in and around the heritage areas/buildings. Already identified heritage walk path is limited to certain streets and the extension of path to other important heritage buildings namely Jagan Mohan Palace in the vicinity of heritage core to be explored. The heritage path proposed by the heritage commissioner's office is lacking with public amenities, street furniture, tourist information route map, professionally trained subject guide and few heritage buildings are in bad condition and facing structural problems.

- Heritage path proposed by heritage commissioner's office is lacking with basic amenities, street furniture, separate heritage-track and information maps.
- Present heritage walk includes only buildings surrounding the palace, even though large number of architecturally important buildings concentrated in other part of the city.
- Heritage buildings are in bad condition and few are in dilapidated condition requires urgent conservation, preservation and adoptive re-use measures.
- Lack of awareness to both officials and owners of the private buildings leads to demolition and built transformations.
- Commercial activities in the core area attract large volume of traffic and informal sector people.
- Private owners of the heritage buildings lack conservation knowledge due to this many buildings are demolished or altered without showing concern to the existing architecture.

The main objectives need to create awareness are to;

- Encourage and promote awareness on traditional built forms of the city.
- Create better awareness regarding heritage resources.
- Co-ordinate efforts of different disciplines, stakeholders and authorities.
- Mobilize finance and resources for restoration and support participatory action programmes.
- All the listed heritage buildings are to be placed with special plaque (Shilapalaka) at the entrances to enhance the identity and inculcate a sense of pride and belonging among the neighborhoods.

Fig. 3: Shilapalaka and Sign board Installed in Front of Building

- Create awareness among the general public towards the importance of safeguarding heritage assets.
- Heritage walk needs to be promoted more intensively by involving professionals, institutions, associations, volunteers, tourists, agencies, community organizations, NGOs and all stakeholders.
- The dilapidated heritage buildings to be given wide publicity for undertaking conservation and restoration measures by the owners of the property.
- Public private partnership initiatives to be encouraged on similar lines of Infosys Foundation, which has extended financial support for conservation and restoration of Jayalaxmi Vilas Mansion and other heritage buildings of the University of Mysore. Similar initiatives from private and other stakeholders are to be promoted and encouraged for conservation and restoration of dilapidated or damaged heritage buildings in the city.
- Best way to maintain the building is to put them for some use. The damaged or ruined heritage buildings to be restored to original character and put them under adaptive re-use and compatible uses like, tourist oriented activities, museums, tourist information centers, tourist hotel, arts and craft centre, etc.
- Adaptive reuse of building to be encouraged in consultation with management or owners of building as done in the case of Lalitha Mahal Palace and Jayalaxmi Mansion illustrated below:

a) Hotel Lalitha Mahal *Palace* has been under adaptive re-use and converted the palace into five-star hotel by suitably modifying to suit the function without affecting the structure and character of the building.

a. Jayalaxmi *Vilas Mansion*, located in the University campus has been conserved under public private partnership initiatives from Infosys foundation by successfully accommodating folklore museum and research centre without affecting the existing architecture.

- Devaraja market, Gun house, Lawnsdowne building, Janatha bazaar, Free mansions club are in dilapidated condition and they located very close to the Palace and tourist zone needs immediate attention of restoration by involving private and other agencies' support. Similarly, many heritage buildings, particularly private residential heritage buildings in the city are in need of restoration and adoptive re-use.
- Mysore City Corporation has constituted Heritage Cell to create awareness among citizens and to develop a comprehensive plan for the conservation of Mysore city. Many awareness and conservation programmes have to be taken up immediately.
- Specialized training programmes need to be organized for conservation professionals. The efforts of community groups and individuals need to be supported to ensure heritage conservation.
- Conservation aspects to be included in curriculum of schools and colleges to bring more awareness among younger generations.
- Heritage artifact, viz. sandal wood artifact, sandal soap, silk saris, sandal wood garlands, traditional Mysore paintings, etc, needs more publicity to showcase the wealth and diversity of the art and architecture of Mysore.
- Light and sound shows showcasing Mysore city's history, culture, art and architecture was started in May 2011 and organized inside the palace premises for public and tourists to highlight and to create better awareness on Mysore heritage. Similar kind of programmes needs to be encouraged with the help of public and private partnership to boost tourism.
- Association of old heritage property owners need to be formed to encourage conservation and restoration of their structures and also to help them in getting financial assistance, property tax exemption, resolving legal issues, etc. towards safeguarding built heritage of Mysore.
- Create more awareness through educational and publicity programs and involve local community in developing tourism and heritage management.
- Public participation has to be seen as an important tool in the process of urban conservation. People have to be involved at the initial stages to achieve a self sustenance and continuity.

A. Stakeholders Participation

The following agencies have involved in creating heritage awareness in the city and are (a)INTACH (b) MHATF (c) Voluntary Organizations (d) ADB and (e) JNNURM. Besides the agencies that were participated in awareness are listed below:

- **Government Authorities:** Department of Archeology, Museums and Heritage, Mysore City Corporation and Mysore Urban Development Authority.
- **Public Authorities:** Tourism department, Lake development authority, Horticulture department, Public works department, Electricity department, University of Mysore, Hospitals, KUIDFC, Police and Law-Order Department, Information and Broadcasting Department and Other public Offices
- **Private Agencies:** Hotels, Travel agencies, Private Property Owners.
- **Tourists:** Domestic, National, and International
- **Institutions:** Education department, Schools and colleges, CAVA: Traditional Arts and crafts, paintings, Arts and cultural department. (Rangayana, folklore, Sanskrit, etc.)., Department of Kannada and Culture, Folklore and Museums, Yoga Music and dance.(Private)
- NGOs: INTACH, IHCN, UNESCO, Heritage clubs, Voluntary organizations,
- **Service Providers:** Hotels, Travel Agencies, Tonga's and Tourists Guides

V. Proposed Heritage Policies for Creating Awareness

The existing programmes are not adequate and are to be conducted rigorously rather an on a piece meal approach, It needs to be given more professional touch to bring more systematic awareness involving various professionals, agencies and stakeholders in the field. Following new initiatives are proposed;

A. **Restructuring of Heritage Walks:** The existing heritage walk path proposed by heritage commissioner's office to be continued by including Jagan Mohan Palace and may be named as Royal walk or heritage walk-1. The newly proposed heritage walk may be named as Nature walk or Heritage walk-2 mainly covering Mysore university educational institutions located in university campus including Kukkarahalli Lake environs. The proposed walk starts from Maharaja's college centenary hall by covering the following buildings namely Maharaja's College, Yuvarajas College, Oriental research institute, Maharaja's Junior college, Maharanis College, Deputy Commissioner's office, Crawford hall, Kukkarahalli Lake and heritage walk may conclude at Jayalaakasmi Vilas Mansion.

B. **Freedom Walk:** Freedom Walk be organized in heritage areas on all national level festivals like, Independence day, Republic day and birth days of important National leaders like Gandhiji, Vivekananda, Nethaji Subhas Chandra Bose, Mysore Maharajas, Dewans of Mysore, Freedom fighters etc., so that people will gather in large numbers to celebrate these events and also understand and respect, pay homage.

C. **Street Plays:** Street plays with participants of the local community and eminent personalities from the area to be organized by involving institutions like Rangayana, CAVA and other institutions on a common platform to understand the issues related to tangible heritage in the city.

D. **Children's Books:** Books depicting the history of Mysore city, Mysore Maharajas' and important events like Mysore Dasara and brief history of city monuments should be published in simple language for understanding and creating interest among the children.

E. **Heritage Products:** Mysore is famous for sandalwood, silk and Mysore paintings. Various products and artifacts made out of sandalwood, Mysore sandal soap, silk saris, Mysore Turban, popularly known as Mysore Peta, sandalwood garlands etc', are very popular in the country. These products' exhibition cum sale to be organized in the core heritage zone and this will benefit both tourists and locals and also the revenue generates from this can be utilized for the heritage development.

F. **Elected Representative's Involvement:** The involvement of politicians in their respective areas to be ensured in all the citizen forums, ward sabha, ward committee and other formal and informal organizations of the city corporation, They need to be involved at all stages of development and heritage related activities namely cultural and other important events of the city.

G. **Museum cum Information Centre:** At present tourists who are visiting the city are finding difficulties in getting first hand information on various aspects of the heritage city. Many of the valuable arts, crafts, paintings and heritage buildings of the city are slowly disappearing due to urban expansion and city's growth. Opening an information centre and museum to showcase city's rich heritage in the heritage area will benefit both tourists and locals.

H. **Light and Sound Shows:** Present illumination of Palace on holidays and Sundays to be continued to attract tourists and general public to the heritage area. Light and sound shows pertaining to history, culture and architecture of Mysore city to be organized in palace premises (Just started on may- 2011) to create more attraction and interest among the tourists and public (similar activity happening in red fort Delhi). These programmes are to be performed during the Dasara season and summer seasons continuously and general holidays as well. This will spread the message of history of Mysore very fast to all concerned tourists of different destinations and attract more tourists to the city.

I. **Tonga Tour***:* During Mysore Maharajas Period Tonga ride has been very popular among the tourists as well as local people. Over a period of time due to city's fast growth, and modern development automobiles dominated the city streets and Tongas are reduced. The age old Tonga vehicles are to be decorated and re-introduced in the heritage area. The pedestrianizing the area around main Palace needs to be undertaken to facilitate the visits to heritage buildings (heritage walk area) to synchronize with Tonga riding. Tonga riders can be trained as guides and given identity cards, taking people for guided tours to the important heritage areas. Maps and photographs of the places are to be displayed in tongas. Also, pollution free vehicles may be promoted for environmental friendliness for which tourism department has to take necessary steps for initiation of this programme.

J. **Heritage City News paper:** Heritage and tourism department along with citizens group can jointly bring out news paper exclusively discussing the issues related to heritage city and public awareness. This will spread the message of heritage awareness to more people in short period of time. The Hindu, Times of India and Star of Mysore are already publishing city heritage issues on regular basis in addition to Sunday's special editions.

K. **Training Administrators:** Knowledge, skills and attitudes on heritage to be provided to the officials, who work in various departments related to heritage in Mysore city. Proper education and awareness programmes to these officials can go a long way in protecting and preserving the rich built heritage. The training programmes are to be organized in the State Institute of Urban Development (SIUD) and District Training Institute, Mysore regularly as a specialization to promote efficient heritage management. Lectures and demonstration programmes on different aspects of built, cultural heritage and conservation and management be introduced. Mysore Heritage Cell may take a leading initiative in conducting this programme.

L. **Festivals:** Mysore Dasara is a very popular and world famous attracts tourists. In order to ensure community participation to raise the level of awareness and sense of belonging about the heritage, festivals like Mysore Dasara, cultural festivals, World Heritage Day and heritage week may be organized every year. Cultural events, photo exhibition, drawing, paintings and essay competitions, lecture series and other related activities can be a part of the events to create more awareness on heritage to children and public.

M. **Heritage Awards:** Heritage awards to be initiated to encourage people, individual, organizations, schools and media to take part in the competitions. "Mysore Heritage Awards" to be instituted for recognizing the efforts of conservation of heritage areas/buildings in Mysore. This should be an annual feature and award to be decided by a panel consisting of many eminent personalities and this event can be organized on 18th April of every year to celebrate World Heritage Day. The other suggested awards namely best maintained residential heritage building award, best maintained public building award, heritage school award, news paper award covering maximum number of heritage issues, heritage reporter award for best reporting heritage issues and life time contribution award.

N. **Promotion of Heritage in Education:** Heritage educational programmes are successful only when the local community comes forward to support and initiate heritage related activities. This is possible when the local people to whom the very heritage belongs understands its values, takes pride and establish a sense of belonging. Social and cultural festivals play a greater role in generating awareness and mobilize communities. Community meetings, audio, visual shows, exhibitions, street plays, annual celebrations, cultural walks books and publications are all of effective means of cultural education.

The National Commission on Urbanization and Model Building Bye-laws of Government of India has recommended that there is a need for incorporating the conservation principles into the basic curricula of architecture, engineering and town planning. In order to create awareness of the value of heritage, suitably designed courses has to be included in the curricula of schools and colleges. Motivations and training of technical personnel in these lines will help in spreading the message of heritage conservation. Education and awareness programmes therefore are the most significant tool to achieve continued relationship with the past.

VI. Conclusions

Though, there is enough scope to include the heritage subject in the preparation of master plans under section 12(1)(f) of the KTCP Act and to contain separate heritage regulations, the present regulations are not adequate to meet the challenges of heritage areas. There is need to evolve detailed regulations for delineating heritage zones, and Development Control Regulations on lines of Hampi World Heritage Regulations for proper planning and conservation heritage areas in the City of Mysore. Further, efforts are required to create greater awareness among the people to include Information Education Communication, heritage walk, freedom walk, street plays, light and sound shows, Tonga tour, heritage festivals, heritage awards, heritage news paper for promoting effective management and conservation of heritage area.

References

[1]. Shankar B. and Chidambara Swamy, "Policy Measures for Improving the Imageability in the City of Mysore", International Journal of Modern Engineering Research (IJMER), Vol.2, Issue.2, Mar-Apr 2012 pp-134-138 ISSN: 2249-6645.
[2]. Chidambara Swamy and Dr. B. Shankar, Conservation Strategies for Heritage City: Mysore, Vol.3, No.5, International Journal on Recent Trends in Engineering and Technology (IJRTET), ISSN 2158-5563, May 2010.
[3]. Chidambara Swamy and Dr. B. Shankar, Reprising the Eternal Glory of Udaipur: Issues and Strategies for Heritage Conservation, Vol. 54, World Academy of Science and Engineering, Technology (WASET), June-2009
[4]. Government of India, Heritage Tool Kit for Preparation of City Development Plan under JNNURM, Ministry of Urban Development, New Delhi, November 2006.
[5]. Kamataka Town and Country Planning Act. 1961. Department of Town Planning. Govt. of Karnataka, 2006.
[6]. Report on JNNURM by STUP Consultants Pvt. Ltd. for Department of Tourism, Karnataka on Heritage and Urban renewal of Heritage core under J.N.NURM Scheme detailed
[7]. Thakur, Nalini (1997), "Rich Past, Dismal Present", Indian Architect and Builder, July.
[8]. Thapar, B.K. (1989), "Reflections: On the Role of INTACH in India's Conservation Movement", Architecture + Design, Nov-Dec.
[9]. Urs Nanjaraja (2007), Mysore: Noorinnooru Varshgala Hinde, Abhiruchi Prakashana, Mysore.
[10]. Shankar B., "Inclusive Urban Planning: Challenges and Strategies of Karnataka State", Poster Paper, IDES_CPS, Civil Engineering Series-Advances in Civil Engineering ACE, Ed., pp-11-15, 2011, New York.
[11]. Shankar B. and Uma S., "Conservation Strategies for Srirangapatna Town: Evaluation of Heritage Buildings", International Journal of Modern Engineering Research (IJMER), Vol.2, Issue.2, Mar-Apr 2012 pp-160-164

BIOGRAPHIES

Dr. B. Shankar received the B.E. degree in Civil Engineering in 1984, M.U.R.P degree in Urban and Regional Planning in 1989 and Ph.D degree in Urban and Regional Planning in 1997 from the University of Mysore, Mysore. He is working as Associate Professor in Urban and Regional Planning at the Institute of Development Studies, University of Mysore, Mysore. His research interests to include Urban Planning, Urban Poverty, Community Development, and Heritage Conservation.

Dr. Chidambara Swamy received the Bachelor degree in Architecture in 1994 and M.U.R.P degree in Urban and Regional Planning in 1999 from the University of Mysore, Mysore. He is working as the Professor and Head, Department of Architecture, Adhiyamaan College of Engineering-Hosur. His research interest includes, heritage planning and conservation, city planning.

International Journal of Modern Engineering Research (IJMER)
www.ijmer.com Vol.3, Issue.2, March-April. 2013 pp-704-708 ISSN: 2249-6645

Control System for Manipulation of Services in Ubiquitous Environment

Mario I. García Antonio, [1] José A. Cruz Tolentino, [2] Victor Gómez, [3]
Alejandro Jarillo-Silva, [4] Luis A. González Rojas, [5]
Amando Alejandro Ruíz Figueroa[6]

[123456]*Universidad de la Sierra Sur, St. Guillermo Rojas Mijangos S/N, Oaxaca, México. Department of Information Technology, Sierra Sur University, Oaxaca, México*

Abstract: *The ubiquitous computing are to guide a the creation of intelligent space, where of users already not interaction with a only the computation system but on with different computer system at a time and not necessarily a user is aware of this interaction. Recent research describes computer systems where the user accesses the services of a ubiquitous environment through mobile devices. The problem with these systems is the lack of full control over physical objects (e.g. doors, windows, heating systems, etc). In this paper, we propose the incorporation of a control system that allows manipulation of physical objects in ubiquitous environments by developing a communication protocol based on the standard USB 2.0*

Keywords: *communication protocol, control system, ubiquitous environment.*

I. INTRODUCTION

Since the last years, a computer revolution is changing the way of acting in society. It is going to the era in which a user controlling a PC, to the era where the user uses the same time several electronics platforms to access the information when you require it. This notion of Mark Weiser viewable in the year 1988 in his article "The Computer for the 21st Century" in which he noted "the most profound technologies are those that disappear ... weave themselves into everyday life until they become indistinguishable" [8]. This approach gave rise to what is now know as ubiquitous computing.

The notion of ubiquitous computing wager a to create intelligence environments where the technology are invisible of user, does present only where are need and easily a most interaction natural and easy. This conception proposes develop computer system that together with the use of mobile devices to communicate via wireless networks, same as in recent years has increased in popularity [4].

For achieve this invisibility, systems should be as free possible to the administration of human beings. In this way is especially difficult develop systems where mobile devices involving dynamically connect and disconnect from a network, if they require explicit configuration to work together and the management overhead outweighs any possible benefit.

Service discovery has been a major achievement in the area of ubiquitous computing by allowing the user through their mobile device to quickly find the services of an environment.

Once the user finds such services initiates an interaction with these. This interaction is based on the handling of service independently of the user location in the environment. Services will not necessarily be computer services, physical services may also exist. (E.g. control to open and close windows, doors, on or off lighting, ventilation, etc).

So, this way controlling a physical service involves knowing their status (e.g. on or off on a ventilator) and the transition can be made from one state to another. Include manipulation of physical services in a ubiquitous environment means developing a component that is responsible for managing the physical service and their status. In this way, include a control system in a ubiquitous environment will be able to bring the system from an initial state to a final state in a finite time [3].

To include a control system to a ubiquitous system should be a protocol that allows this communication.

Therefore, the development of this paper is to include control system architecture of a ubiquitous environment and the protocol to achieve the manipulation of a physical service.

II. HEADINGS

The distribution of this article is divided into 4 sections, section III describes the related **work** on service discovery systems, section IV presents the **proposed** control system and communication protocol, and section V presents **conclusions and future work** arising from this research.

III. RELATED WORK

Currently, the technological headway allow develop systems be geared to paradigm of ubiquitous computing. The building of ubiquitous environment provide of ways and means for that the users discover the services of an environment. The discovery is the process in which a network entity (client) is reported spontaneously from the availability of services or devices available on a network (resource), i.e., is a mechanism to dynamically refer to a network

resource for the customer to contact the resource [4].

A key part of a ubiquitous environment are the different areas, which are autonomous and independent, i.e., manage their own resources and services to exchange information with other areas [11]. Users who interact in these areas are considered nomadic user, because they acquire specific functions of the current environmental context.

Within a ubiquitous environment is required that the user can access and manipulate nomadic services offered by each area using mobile devices in this context mobile users have a wide range of mobile devices which is considered as heterogeneous devices [13].

Thus, market-leading companies in information technology have developed technologies for service discovery, as in the case of SSDP (Simple Service Discovery Protocol) [5] used by Microsoft, Intel, Sony and Samsung which supports a simple form of search in which customers specify the resource. Jini Network Technology [7] developed by Sun Microsystem's is a network technology to create a service infrastructure to adapt to change. Also, Bluetooth Special Interest Group (Bluetooth SDP) [15] is a protocol that defines the characteristics of services available for learning that are given to a device. These technologies allow service discovery. Therefore, creating service discovery systems involves using some components of these technologies.

B. SEDINU SYSTEM

Similarly, parallel research centers working in the construction of service discovery systems, such is the case SEDINU system (Service Discovery for Nomadic Users) [10]. A service discovery system where the user through their mobile device acquires information of hardware and software services provided by the areas of environment.

The feature that distinguishes this system is that it is intended to be a framework for building ubiquitous environments.

This system consists of three sites; Site A, Site B and Site C. See Figure 1.

The Site A, houses the module Application Tiny SEDINU responsible for showing the user the services available from the current autonomous area through their mobile device, the Site B, which contains the module Location Detector responsible for sending the current user coordinate system RBACSoft (Software - Role Based Access Control), who determines the current autonomous area where the user is located. And finally, the Site C consists of two modules, the module Service Manager and module Ad hoc Creator including system RBACSoft [10]. Thus, when the user accesses the environment, the system SEDINU provides user services through their mobile device. Thus, the host service interacts directly with the system to acquire information RBACSoft a database containing information on available services.

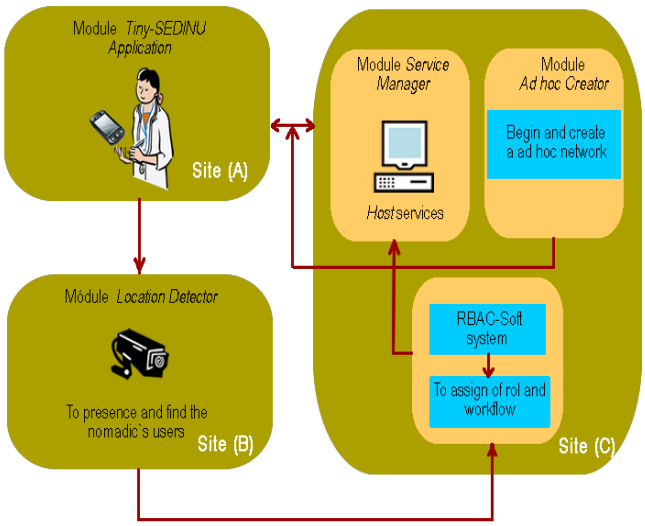

Figure. 1: Architecture of distribution SEDINU system

RBACSoft system has an important role within this system, besides providing information to the mobile device of services available includes a database for each of the autonomous areas of a ubiquitous environment. Therefore, our proposal is to add a control system and communication protocol to achieve this system for the manipulation of physical services in a ubiquitous environment.

IV. PROPOSAL

The development of our proposal consists of a new architecture in the development of ubiquitous environments by modifying the structure of the database RBACSoft component of SEDINU system and includes a control system to achieve the goal of manipulating a physical service.

This inclusion is to modify the structure of the database RBACSoft and add the following Add the entity Sistema_Control with the attributes idF_idAreaN1, idF_idobjetos, idF_idsistcontrol. Thus, it will log tuples a control system in the database corresponding to the autonomous area. Similarly, establishing the relationship cardinality of the entity AreaN1 with the entity Sistema_Control making it possible to lace a control system with each of the autonomous areas of a ubiquitous environment.

Similarly, to modify the entity RecursosA_N1 adding the attribute idsistcontrol join with attribute estado, ensure which these attributes: a control system can manipulate one or more physical elements in one or more autonomous areas and that a physical element can only be controlled by a control system.

Finally, add the entity Estados with attributes id_estado, nom_estado and idF_objetos. This with to store information of the states that each object can to have.

Thus adding control system architecture of an environment ubiquitous gives rise to a new structure of the database. See Figure 2. With this structured is possible to include a control system environment ubiquitous.

It should bear in mind that the building of a control system together the interaction of various components. (e.g. sensors, actuators, plants, etc). The interaction of these components will in order to bring the system form an initial state until a finite state, in a finite time [3].

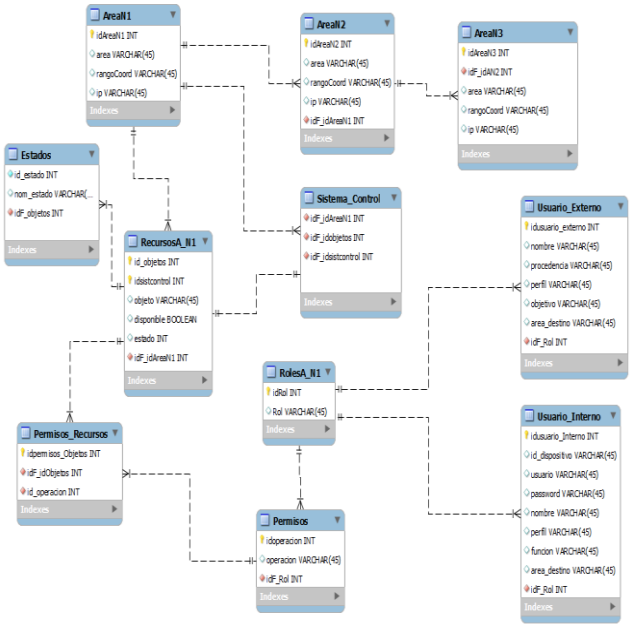

Figure. 2: Structure of database

A adding a control system is necessary to establish the communication between the services host, and a system control. We implement this communication with the standard USB 2.0 [2].

The communication using standard USB 2.0 is a viable option for establish this communication. The use of this standard is a accesible solution when you need to communicate to a computer with and external device (e.g. mouse, keyboard, printer, digital camera, store devices as hard disk). The using of this interface also allows control systems that handle specific functions (e.g. communication with a microcontroller).

Other feature with has this standard is the speed of transmission of the information, being of 480 Mbps, a considerable speed for manipulating a physical service in seconds. In addition to the USB 2.0 ports has automatic detection and configuration plug and play, being this possible without installing additional software or restart the computer to recognize USB [2].

The standard USB 2.0 deliver of advantages of send and received information a through of endpoints, when a device USB is connected at system, the system will recognize and configure it, the device is organized as a set of endpoints. Then the system sets all communication routes through pipes necessary between the host and each endpoint available in the configuration [6].

The use of endpoints ensures that the data sent from the control system to the host guarantees data delivery to the addressee and the package will be free of errors. Taking place that during the execution of protocolo rules the resulting information will be consistency in both components.

For to establish communication between the host services and control system there is a need to build a communication protocolo between two components, being essential to know the time when the user indicates manipulate a physical service and the time when has finished execution this action

The need of establish protocols for communication is fundamental for communication between machines and network devices, because the machines, though intelligent, are not human being that can run a task with a single instruction to tell the machine . Therefore, the need to build fast rules and protocols with strict procedures for deal with

any eventuality [12].

Thus, a control system consequence of great importance in the design of a ubiquitous environment. The following Figure 3 shows the inclusion of a control system in RBACSoft system. The Figure 3 describes the following process: User from your device **mobile** first authenticates with the **server** of current autonomous area, then, the **server** depending on the function and purpose of the nomadic user determines the task to be performed in the area. Subsequently, this information is stored in the **database**, after establishing the connection to the database, and establishing connection with the **control system** vía USB 2.0 standard and it is therefore possible to manipulate the **physical element** that is controlled by control system.

Once to include this component in the architecture of RBACsoft, the flow begin in the host services requesting the registration database of physical object, once acquire this information, then, host sends the data to the control system asking to change the object state.

For protocol, the host acquires information of registration from database, once that acquire sends a notification a control system for manipulate the element. The control system executes the action verifying its availability. Then, it returns a notification to the host and it will request an updated record in the database. If not run the action is notified to the host and does not update the record. Figure 4 presents the outline of this communication protocol.

One of the considerations of implementation of this communication protocol is to hold together the integrity of the database with current state of the object. This ensures that changes made to the database do not cause loss of consistency [14]. And, therefore, hold together in the control system with the database.

The design of this new architecture in the RBACsoft system consist to achieve the manipulation of physical service in a environment ubiquitous will allow on the user to have full control of physical elements from environment.

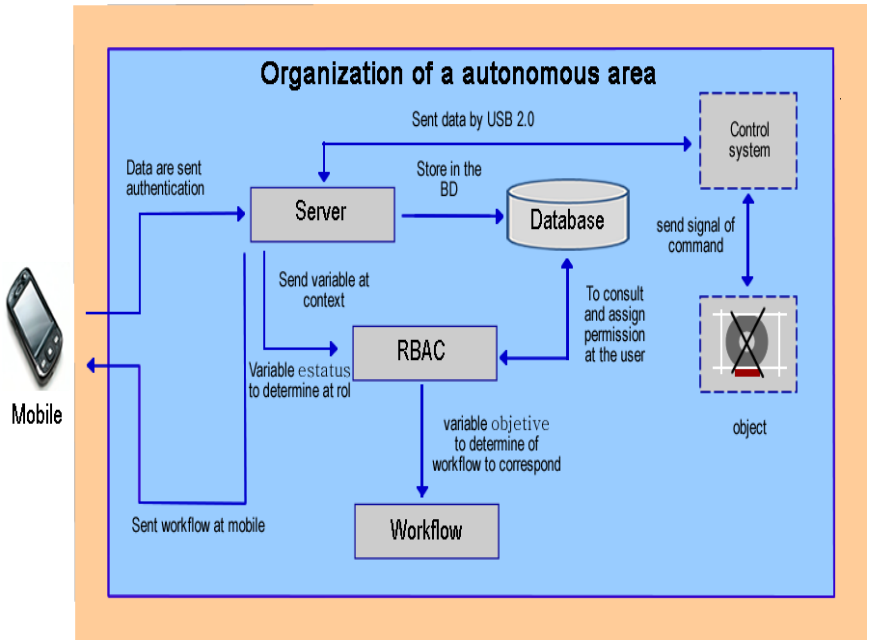

Figure. 4: Communication protocol.

V. CONCLUSION AND FUTURE WORK

We present the inclusion of a control system specifically RBACSoft system, since the information it provides is information acquired by SEDINU to display information to the user through their mobile devices. In the develop of this protocol lack the recognition of different physical devices in the control system, the test was implement with a physical device and working successfully. Other of the way research is develop a access concurrent of various mobile devices accessing on a same control system. Therefore, migrate our USB 2.0 protocol at USB 3.0, as a feature from USB 3.0 is the increment the speed of the information a changing of the 480 Mbps at 4,8Gbps. Finally, to make standard our protocol a fundamental component in the develop of ubiquitous environment of specifically manipulation of physical services

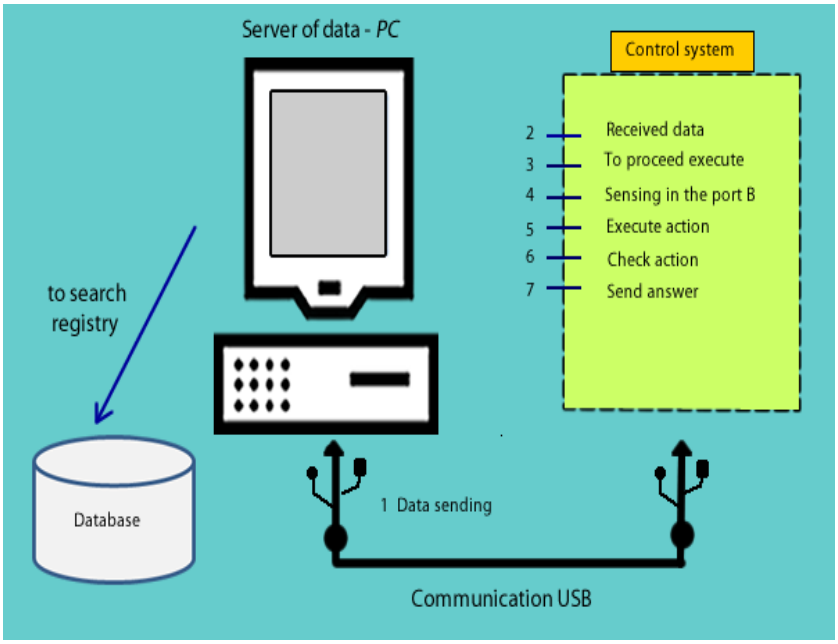

Figure. 3: Control system in RBACsoft system

REFERENCES

[1] USB Implementers Forum, I. C. o. U. t. (2003). Universal Serial Bus Revision 2.0 Specification [cited: february-16-2012] available in: http://www.usb.org/developers/docs/.
[2] Axelson, J. (2005). Usb complete: Everything you need to develop custom usb peripherals. Madison, WI 53704: Editorial Lakeview Research LLC.
[3] Ogata, K. (1998). Ingeniería de control moderna. Naucalpan de Juárez, Edo. De México: Editorial Prentice-Hall.
[4] W, Keith Edwards. (April-June 2006), Discovery Systems in Ubiquitous Computing. PERVASIVE computing, pp. 70-77, Published by the IEEE CS and IEEE ComSoc.
[5] M. Jeronimo and J. Weast, UPnP Design by Example: A Software DeveloperŠs Guide to Universal Plug and Play, Intel Press, May 2003. [6] OEM., S. T. (2003). Soporte Técnico OEM, Fujitsu España. Marzo de 2003 [cited: february-16-2012] available in: http://www.fujitsu.com/downloads/EU/es/soporte/discosduros/- UnpaseoporUSB-2.pdf
[7] S. Oaks and H. Wong, Jini in a Nutshell: A Desktop Quick Reference, Reilly & Associates, Inc., Sebastopol, CA, USA, March 2000.
[8] Weiser, M. (January-March 2002), the Computer for the 21st Century. Scientific American, Sept., 1991, pp. 94-104, reprinted in IEEE Pervasive Computing, pp. 19-25.
[9] Navarrete, M. (2010). Administración de fujos de trabajo organizados en áreas autónomas para entornos ubicuos. Master thesis, Depto. de Computación, Centro de Investigación y de Estudios Avanzados del Instituto Politécnico Nacional, Unidad Zacatenco, México. D.F.
[10] Gómez. V., Decouchant. D., Mendoza. S. and Rodríguez, J. (2009). Nomadic user interaction/ cooperation within autonomous areas. In Pro- ceedings of the 15th Collabo- ration Researchers International Workshop on Groupware, 32-40.
[11] Andrew, T. (1996). Sistemas operativos distribuidos. México: Editorial Prentice Hall.
[12] Herrera, E. (2005). Tecnologías y redes de transmisión de datos. México: Editorial Limusa.
[13] Kindberg, T. Barton, John. A Web-Based Nomadic Computing System.Copyright Hewlett-Packard Company 2000, 1- 14
[14] Silberschatz, A. (2002). Fundamentos de bases de datos. España: Editorial McGraw-Hill Inc.
[15] C.Chang, P. K. Sahoo and S. Lee, Ş A Location-Aware Routing Protocol for the Bluetooth ScatternetŤ , Wireless Personal Communications, vol. 40, num. 1, pp. 117-135, January 2007.
Note that the proceedings title is set in italic

International Journal of Modern Engineering Research (IJMER)
www.ijmer.com Vol.3, Issue.2, March-April. 2013 pp-709-714 ISSN: 2249-6645

Influence of curing regime on strength development of grade C60 concrete

A.E. Abalaka, [1] O. G. Okoli[2]
[1]*Department of Building, Federal University of Technology, Minna, Nigeria*
[2]*Department of Building, Ahmadu Bello University, Zaria, Nigeria*

Abstract: Compressive strength of grade C60 concrete cubes cured in water and ambient air (uncured) were determined at 3, 7, 14, 28 and 90days. At 90 days, uncured specimens recorded strength reduction of 15.50% compared to control. Furthermore, cubes of the same grade of concrete were cured for limited durations in water and then removed and subsequently stored in air, and their compressive strength determined at 28 and 90 days. At test age of 28days, cubes that were water cured for only 3days recorded maximum compressive strength of 74.15N/mm^2. However at 90 days, cubes that were water cured for only 28 days recorded the maximum compressive strength of 77.58N/mm^2. The sorptivity and coefficient of water absorption did show improved pore structures and reduced permeability as water curing days increased.

Keywords: Curing, hydration, compressive strength.

1. Introduction

Proper curing of concrete is important in ensuring that concrete structures meet expected performance criteria with reduced maintenance costs. Curing of concrete is the process used for promoting the hydration of cement and consists of the control of temperature and of the moisture movement from and into the concrete, and it is generally accepted that concrete has to be sufficiently cured to provide optimum performance (Khatri *et al*., 1977; Tasdemir, 2003). The aim is to keep the concrete saturated or as nearly saturated as possible until the originally water-filled space in the fresh cement paste has been filled to the desired extent by the products of cement hydration (Mamlouk and Zaniewski, 2011; Neville, 1981; Taylor, 2000; Stark, 2011). For hydration to proceed, it is important to saturate calcium silicate hydrate (C-S-H) gels with water. This water is usually provided externally by curing or internally using water saturated porous aggregates. Proper curing reduces the rate of moisture loss and provides a continuous source of moisture required for the hydration that reduces the porosity and provides a fine pore size distribution in concrete (Alamri, 1988). Though cement hydration produces many solid hydration products, the major hydration product responsible for compressive strength of concrete is a rigid C-S-H gel. Though the atomic structure of C-S-H gel, the nature of its formation, and its molecular bonding is not certain, studies suggest that the gel has a complex amorphous composition (Harris *et al*., 2002; Murray *et al*., 2010) that is mainly responsible for the compressive strength development in concrete. The work of Masoero *et al*. (2012) shows that CSH particles form at very diverse sizes and the diversity in the size of the nanoscale units leads to a denser, disorderly packing of the particles, which corresponds to stronger cement paste.

Though it is known that the growth of CSH gels and other solid hydration products in concrete is promoted by curing, studies have shown that the strength of concrete and microscopic pore structures are also affected by the degree of hydration. The study by Nassif *et al*. (2005) using high performance concrete show higher elastic modulus for specimens that were cured using burlap compared to air-dry cured specimens.

The work of Soroka and Baum (1994) showed that at 28 days, compressive strength of concrete cube specimens continuously wet cured was 40% higher than those uncured and at 90days, specimens continuously moisture cured had compressive strength 20% higher than those of uncured cubes. Alizadeh *et al*. (2008) reported compressive strength increases of concrete cubes cured in water compared to air cured cubes at 7 and 28 days using Portland cement at cement content of 400kg/m^3: importantly, compressive strength increases were reported to be more significant after 1, 3 and 6 days of moisture curing than 27days, though strength increase was recorded at 27 days. At specimen ages of 7 and 28 days there were no significant compressive strength difference between 6 and 27days of wet curing; this appears to suggest that the first 6 days of wet curing was more important in compressive strength increase over air curing.

The work of Parrott (1992) on the effects of 1, 3, and 28 days initial moisture curing on the permeability of concrete subjected to drying for 6 and 18 months at 60% RH shows that the permeability of concrete samples subjected to 3 days curing was about one-sixth of the samples cured for only one day. Similarly, the permeability of concrete subjected to 28 days initial curing was one quarter of the permeability of samples cured for only 3 days.

In another study by Shafiq and Cabrera (2004), ordinary Portland cement (OPC) concrete dry cured had total porosity 5-10% higher than wet cured samples at 28 days. Similarly, the coefficients of oxygen and water permeability of air dried samples were 2-19 times higher than coefficients obtained for water cured samples.

Hydration of cement is a long term process which requires water and proper temperature; longer curing duration results in increased hydration and strength. Since cement hydration is a long term process that can continue beyond 30 years (Wood, 1991), in practical concrete production this process cannot continue indefinitely for years, the important factor is how long the curing process should last to ensure that concrete reaches acceptable level of performance.

In this study, the compressive strength, tensile strength and durability properties of grade C60 were measured. The curing regime adopted was such that samples were cured for limited period of time and then stored on the laboratory floor (uncured) to determine the effect of limited water curing on concrete.

2. Materials and Method

A commercial brand of OPC (type 1) in Nigeria was used for this study. The compositions of the OPC used are given in Table 1.

Crushed granite of 20mm maximum size with specific gravity of 2.63 was used as coarse aggregates; natural river bed quartzite sand with specific gravity of 2.73 was used as fine aggregates. The results of the sieve analysis of the aggregates are given in Table 2. The particle size distribution of the fine aggregates correspond to zone 2 sand by the BS 882: 1983 classification. The concrete mix proportions used are given in Table 3.

The concrete was mixed in a tilting drum mixer for 3 minutes, and manually compacted in two layers in 100mm steel moulds. A chloride free lignosulphonate based plasticizer (Fosroc Conplast P505) complying with BS EN 934 standard was used to increase the slump of the concrete mix. After 24hrs in the moulds, the cubes were de-molded and cured in water in compliance to BS 1881. P111:1997 standard.

The study was done in two stages: The stage I study was to determine the separate effects of continuous water curing and open air storing conditions on compressive strength at ages of 3, 7, 14 and 28days; concrete cubes cured in water were used as control for this first stage. The cubes that were cured in water were removed at the ages 3,7,14, 28 and 90 days, excess surface water wiped off and the compressive strength determined. The cubes that were stored on the laboratory floor were tested at the ages of 3,7,14, 28 and 90 days and their compressive strength determined. In the technical term of curing, the cubes that were stored in the open air in the laboratory would be considered as uncured specimens.

In the stage II, concrete cube specimens cured in water for limited durations of 1, 2, 3, 4, 5, 6, 7, 14 and 28 days were removed from the curing tank and then stored on laboratory floor and their compressive strength was determined at test ages. The age of test was inclusive of the continuous wet curing duration. The chosen regime was such that cubes that were cured in water for 1 day for example, were removed from the curing tank at that age and then stored on the laboratory floor for another 27 days and the compressive strength determined at the age of 28 days. The relative wet curing durations of these specimens at 28 days are shown in Figure1. At 90 days, the compressive strength of the cubes that were cured for limited durations and that of the cubes continuously cured in water were determined. Figure 2 shows the relative durations of water and air curing days of the cubes at 90 days. The split tensile strength of cylinders (150mm×300mm), sorptivity and coefficient of water absorption of the cubes were determined at 90 days. The average daytime temperature recorded was 23^{o}C at an average daily relative humidity of 44%.

The compressive strength of the cubes were determined in compliance to BS 1881: part 4:1970 standard using *ELE ADR 3000* digital compression machine at a loading rate of 3.00kN/s; split tensile strength of concrete cylinders were determined in compliance to BS 1881: Part 117: 1983 standard using the same machine at a loading rate of 2.10kN/s.
Three samples were tested for each parameter investigated and the results are averages of three specimen tests.

Table 1. Composition of OPC by XRF

SiO_2	Al_2O_3	Fe_2O_3	CaO	MgO	SO_3	K_2O
24.79%	6.35%	0.92%	58.50%	2.87%	4.91%	0.80%
Na_2O	**Mn_2O_3**	**P_2O_5**	**TiO_2**	**Cl-**	**SR**	**AR**
0.65%	0.0%	0.15%	0.06%	0%	3.41	6.88

SR: silica ratio=SiO_2/ (Al_2O_3+Fe_2O_3), AR=alumina ratio= Al_2O_3/Fe_2O_3

Table 2. Particle size distribution of aggregates as percentage by weight passing sieve sizes

	Sieve size (mm)							
	20	**10**	**5**	**2.36**	**1.18**	**0.60**	**0.30**	**0.15**
Fine aggregates	-	-	92.4	81.6	61	38.3	14.5	5.3
Coarse aggregates	95.00	40.62	0.80	-	-	-	-	-

Table 3. Concrete mix proportions

Cement content	Sand	Coarse aggregates	Free w/c ratio
400kg/m^3	512.4kg/m^3	1317.6kg/m^3	0.30

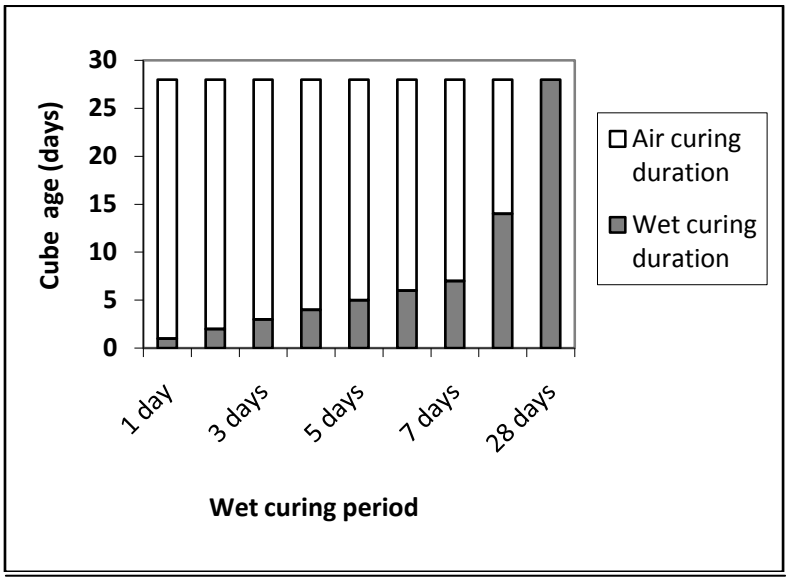

Figure 1. Relative proportions of specimen curing periods at 28 days for stage II study.

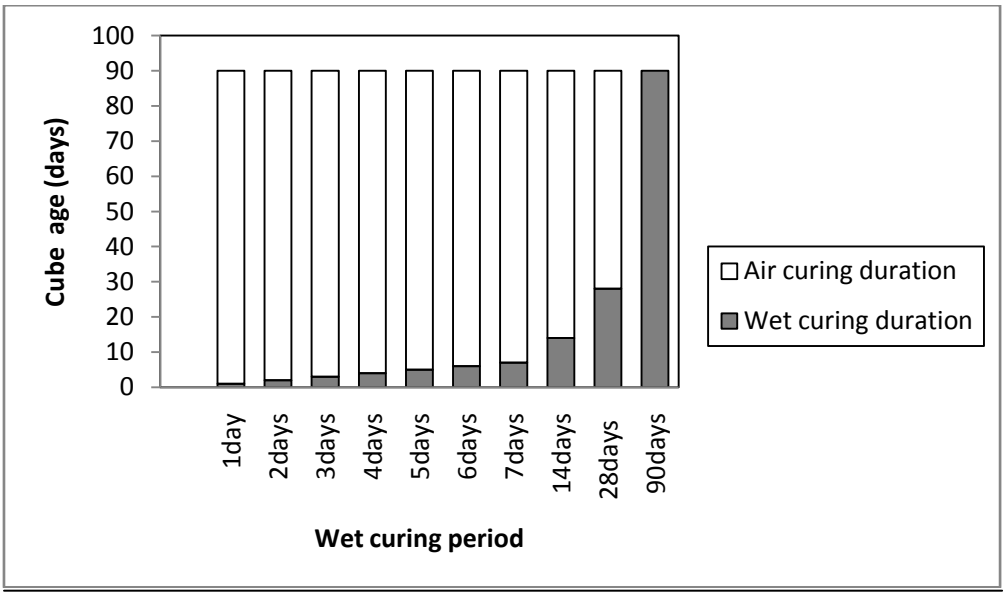

Figure 2. Relative proportions of specimen curing periods at 90days for stage II study.

2.1. Coefficient of water absorption

Coefficient of water absorption is a measure of permeability of concrete (Ganesan, 2008; Giannotti da Silva *et al*., 2008). This is determined by measuring water uptake in dry concrete in a time of 1 hour. The concrete specimens were heated in an oven at 98^{o}C until a constant weight was attained at ten days and the cubes were allowed to cool gradually to room temperature for 24hrs. Four sides of 100mm cube samples were sealed with 1mm thick silicone sealant to a height of 30mm to allow water absorption on only one surface of the cube. The samples were immersed to a depth of 10mm in water as shown in Fig. 3. After immersion in water for one hour, the cubes were taken out and the wet surface was wiped of excess water and weighed. The coefficient of water absorption of the specimens at 90 days was calculated from the formula,

$K_a = \left[\frac{Q}{A}\right]^2 \times \frac{1}{t}$, where K_a is the coefficient of water absorption (m^2/s), Q is the quantity of water absorbed (m^3) by the oven dry specimen in the time (t), t=3600 seconds and A is the surface area (m^2) through which water was absorbed (Ganesan *et al*., 2008).

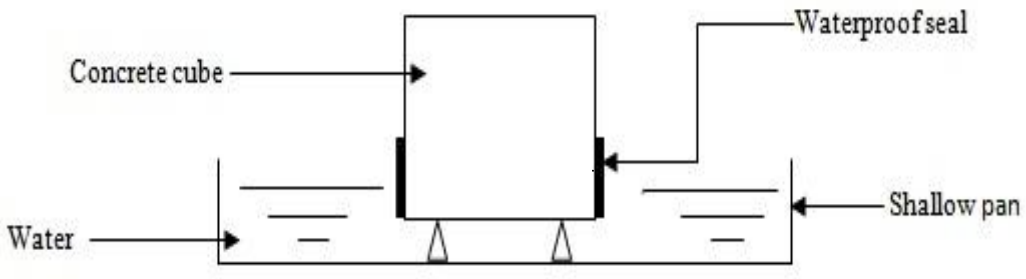

Figure 3. Coefficient of water absorption and sorptivity test

2.2. Sorptivity

Sorptivity is a measure of the capillary forces exerted by the pore structure causing fluids to be drawn into the body of the material (Ganesan *et al*., 2008; Hall, 1989). The concrete specimens were heated in an oven at 98°C until a constant weight was attained at ten days and then allowed to cool to room temperature for 24hrs. The sides of the cubes were coated with silicone sealant to allow the flow of water on only one surface of the cube specimen. The cube specimens were immersed to a depth of 10mm in water on only one surface. The initial mass of the cube was taken at time 0 and at time intervals of 1, 2, 4, 8, 10, 20, 30, 60 and 90 minutes, the samples were removed from water and excess water blotted off and the sample weighed. It was then placed back in water and the process repeated at the same selected time intervals. The sorptivity value of the specimens at 90 days were calculated using the formula,

$i = S/\sqrt{t}$, where i is the cumulative water absorption per unit area of the surface (m^3/m^2); S is the sorptivity ($m/\sqrt{t}$) and t is the elapsed time (s) (Stanish *et al*., 1997).

3. Results

The results of compressive, split tensile strength tests on the concrete specimens at different ages for air cured (uncured) and water cured specimens are given in Tales 4 and 5. The results of coefficient of water absorption and sorptivity tests on water cured and uncured specimens at 90 days are also shown in the same Tables. The results in Tables 4 and 5 represent the stage I data.

Table 4. Effects of water curing on concrete for stage I study

Plasticizer (l/m^3)	**Slump (mm)**	**Wet curing** Compressive strength (N/mm^2)					Sorptivity s ($m \times \sqrt{t}$)	Coefficient of water absorption **Ka** (m^2/s) $\times 10^{-8}$	Tensile strength (N/mm^2)
		3days	**7days**	**14days**	**28days**	**90days**	**90days**	**90days**	**90days**
5.0	5	54.30	54.58	63.65	66.25	72.15	0.810	1.406	4.817

Table 5. Effects of air curing on concrete for stage I study

Plasticizer (l/m^3)	**Slump (mm)**	**Air curing** Compressive strength (N/mm^2)					Sorptivity s ($m \times \sqrt{t}$)	Coefficient of water absorption **Ka** (m^2/s) $\times 10^{-8}$	Tensile strength (N/mm^2)
		3days	**7days**	**14days**	**28days**	**90days**	**90days**	**90days**	**90days**
5.0	5	49.21	53.56	54.92	60.55	60.93	1.244	4.933	4.198

The results of the stage II study are given in Table 6. The compressive strength of 61.63N/mm^2 represents the results of cube tests on specimens that were cured in water for only 1day, removed at the end of one day and stored in the

laboratory for another 27days and tested on that day. The compressive strength of 62.22N/mm^2 represents the result of the same set of cubes that were previously cured in water for only 1 day, but stored in air and tested at the age of 90days. The split tensile test, sorptivity and coefficient of water absorption tests on specimens at the age of 90 days are given in Table 6.

Table 6. Effect of limited wet curing duration on compressive strength of concrete for stage II study

		Wet curing duration									
		1day	**2days**	**3days**	**4days**	**5days**	**6days**	**7days**	**14days**	**28days**	**90days**
	Test age										
Compressive strength (N/mm^2)	**28days**	61.63	60.77	74.15	65.09	68.57	64.88	66.13	72.99	64.57	-
	90days	62.22	62.67	74.94	69.90	70.58	71.10	67.75	73.32	77.58	72.15
Tensile strength (N/mm^2)	**90days**	4.083	4.831	4.729	4.994	4.173	4.884	4.951	4.474	5.471	4.817
Sorptivity s $(m \times \sqrt{t})$	**90days**	0.893	0.891	0.891	0.884	0.887	0.884	0.884	0.884	0.880	0.810
Coefficient of water Absorption **Ka** (m^2/s) $\times 10^{-8}$	**90days**	2.259	1.968	1.875	1.870	1.865	1.765	1.755	1.631	1.575	1.406

4. Discussion

The results of compressive strength tests for the stage I study on water cured and uncured cubes in Tales 4 and 5 show substantial strength reductions for the uncured specimens compared to the water cured specimens at all the ages tested. The compressive strength loss of uncured cubes compared to water cured cubes was highest at 15.50% at the age of 90 days. Similarly, tensile strength of uncured cylinders was 12.85% less than the water cured cylinders at 90 days. The increases in compressive strength and tensile strength as a result of water curing recorded are due to the increased hydration of cement, promoted by curing. It is well known that increased hydration promotes the growth of calcium silicate hydrate (CSH) gels that are mainly responsible for the high compressive strength of concrete. The values of the coefficient of water absorption and sorptivity measurements of the cubes show a more compact microstructure of the concrete as a result of increased hydration. The sorptivity of uncured cubes was 53.58% higher than that of water cured cubes at 90 days. In a similar manner, the coefficient of water absorption of uncured cubes was 250.85% higher than that of water cured cubes. During cement hydration, other solid hydration products are formed in addition to CSH gels, and since curing promotes the formation more of these products, a more compact concrete results from water curing.

The results in Table 6 show the effects of limited water curing on mechanical properties of concrete for the stage II study at 28 and 90days. The maximum compressive strength value of 74.15N/mm^2 was recorded at only 3 days of wet curing and test age of 28 days. The results of stage I tests and stage II tests can be compared since the specimens are from the same grade of concrete. For example, the compressive strength of cubes cured for only 1day and tested at 28 days (61.63N/mm^2) shown in Table 6(stage II study) was slightly higher than that of cubes air cured for 90 days (60.93N/mm^2) representing stage I study shown in Table 5. Similarly, the values of the sorptivity of cubes cured in water for only 1day (stage II) was 26.61% less than that of uncured cubes of the same age(stage I study). The coefficient of water absorption of cubes cured for only 1day in water was 46.19% less than that of uncured cubes of the same age. These results show the significant compressive strength and microstructure improvement resulting from only 1day of moisture curing of concrete compared to uncured concrete at test age of 90 days.

At the age of 90 days, the maximum compressive strength recorded was at 28 days of limited water curing. The results indicate that limited curing saturates the concrete microscopic pores, and thus after cessation of curing, water was still available for hydration. The extent to which this water was available was determined by the degree of saturation, which in turn depends on the duration of limited curing. It is known that the degree of hydration of cement is dependent on the vapour pressure. The work of Powers (1947) shows that the degree of hydration is negligible at a vapour pressure below 0.3 of the saturation pressure and low hydration occurs at a vapour pressure of 0.8 of the saturation pressure. Spears (1983) opined that cement hydration does not improve when cured at relative humidity below 80%. Water curing by immersion of the cubes produces saturation pressure that promotes maximum hydration.

Increase in tensile strength of the concrete cylinders that were subjected to limited curing over uncured cylinders was recorded from 2 days and above.

The sorptivity and coefficient of water absorption of the cubes showed reduction in values as the wet curing duration period increased. The results show that though the cubes were removed from water, solid hydration products that improved the microstructure of the concrete were developed.

Though the compressive strength of cubes cured in water for only 1 day was 13.76% less than that cured continuously in water at 90 days, it is none the less 2.12% higher than that of uncured cubes of the same age (stage I study).

5. Conclusions

The results have shown that when concrete is subjected to limited early water curing, cement hydration would continue even when it is stopped. This would result in increase in compressive strength of the concrete and improved microstructure of the concrete compared to uncured concrete. Improvement in tensile strength of cylinders subjected to limited curing periods over uncured cylinders started from 2 days of limited water curing. The results have shown that the first six days of water curing was very significant in compressive strength development of concrete.

References

[1] BSI (1970). Methods of testing concrete for strength. BS 1881: Part 4. BSI. London. UK.
[2] BSI (1983). Splitting tensile (indirect) strength of cylindrical concrete specimens.BS 1881: Part 117. London.
[3] BSI (1983). Specification for aggregates from natural sources for concrete. BS 822. BSI. London. UK.
[4] BSI (1997). Methods of normal curing of test specimens. (20 degree C method). BS 1881. P111. BSI. London. UK.
[5] BSI (2001). Admixtures for concrete, mortar and grout. Concrete admixtures. Definitions, requirements, conformity, marking and labeling. BS EN 934-2:2001. BSI. London. UK.
[6] Ganesan K, Rajagopal K, Thangavel K. (2008). Rice husk ash blended cement: assessment of optimal level of replacement for strength and permeability properties of concrete. Construction and Building Materials. Vol. 22(8), p.1675-1683.
[7] Giannotti da Silva F, Liborio J. B. L, Helene P. (2008). Improvement of physical and chemical properties of concrete with Brazilian silica rice husk (SRH), Revista Ingeniería de Construcción Vol. 23:(1)., pp.18-25. Available at http://www.scielo.cl/pdf/ric/v23n1/art02.pdf
[8] Hall C (1989). Water sorptivity of mortars and concretes: a review. Magazine of Concrete Research. Vol. 41(14), p. 51-61.
[9] Harris A.W., Manning M.C., Tearle W.M., Tweed C.J. (2002). Testing of models of the dissolution of cements—leaching of synthetic CSH gels. Cement and Concrete Research. Vol. 32, p. 731–746.
[10] Khatri R.P, Sirivivatnanon V, Yu L.K. (1977). Effect of curing on water permeability of concretes prepared with normal Portland cement and with slag and silica fume. Magazine of Concrete Research. Vol.49 (180), p. 167–172.
[11] Masoero E, Del Gado E, Pellenq R.J, Ulm F.J, and Yip S. 2012. Nanostructure and nanomechanics of cement: polydisperse colloidal packing. Physical Review Letters. Vol 109(15). P, 155503-06.
[12] Nassif H. H., Najm H., Suksawang N. (2005) Effect of pozzolanic materials and curing methods on the elastic modulus of HPC. Cement and Concrete Composites. Vol. 27, p. 661–670.
[13] Neville A. M. (1981). Properties of concrete. Third edition. Longman scientific & technical. England, pp 307-318.
[14] Parrott L. J. (1992). Factors influencing relative humidity in concrete. Magazine of Concrete Research. Vol. 43, p.45–52.
[15] Powers T.C. (1947). A discussion of cement hydration in relation to the curing of concrete. Proceedings of highway research board. Vol.27, p. 177-88.
[16] Shafiq N., Cabrera J.G. (2004). Effects of initial curing condition on the fluid transport properties in OPC and fly ash blended cement concrete. Cement and Concrete Composites. Vol. 26, p. 381–387.
[17] Spears R.E (1983). The 80 percent solution to inadequate curing problems. Concrete international. Vol. 5, p. 15-18.
Stanish KD, Hooton RD, Thomas MDA (1997). Testing the chloride penetration resistance of concrete: a literature review, [19] FHWA contract DTFH61 1997, Department of civil engineering, University of Toronto, Canada. pp 19-22.
[18] Stark J (2011). Recent advances in the field of cement hydration and microstructure analysis. Cement and Concrete Research. Vol. 41, p. 666-678.
[19] Tasdemir C. (2003). Combined effects of mineral admixtures and curing conditions on the sorptivity coefficient of concrete. Cement and Concrete Research. Vol. 33, p. 1637-1642.
[20] Taylor G.D. (2000). Materials in construction, an introduction. Third edition. Pearson education limited. England. U.K, pp 50-51.
[21] Wood S.L. (1991). Evaluation of the long-term properties of concrete, ACI Materials Jour ush_reddy@yahoo.comnal. Vol. 88 (6), p, 630– 643

International Journal of Modern Engineering Research (IJMER)
www.ijmer.com Vol.3, Issue.2, March-April. 2013 pp-715-720 ISSN: 2249-6645

Performance Analysis of OFDM System Using PAPR Reduction Techniques

K.Ram Mohan Rao[1], T.Sravanti [2]
[1](Asst Professor, Dept of ECE, Sri Indu College of Engineering and Technology, Hyderabad, AP, India)
[2](Research scholar, Dept of ECE, University College of Engineering, Osmania University, Hyderabad, AP, India)

Abstract: Orthogonal Frequency division Multiplexing (OFDM) is an efficient method of data transmission for high speed communication systems. However, the main drawback of OFDM system is the high Peak to Average Power Ratio (PAPR) of the transmitted signals. OFDM consist of large number of independent subcarriers, as a result of which the amplitude of such a signal can have high peak values. Coding, phase rotation and clipping are among many PAPR reduction schemes that have been proposed to overcome this problem. Here two different PAPR reduction methods e.g. partial transmit sequence (PTS) and selective mapping (SLM) are used to reduce PAPR. Significant reduction in PAPR has been achieved using these techniques. The performances of the three methods are then compared.

Index Terms: Orthogonal frequency division multiplexing (OFDM), peak-to-average power ratio (PAPR), and PAPR reduction techniques

I. Introduction

Orthogonal frequency division multiplexing (OFDM) is a multicarrier modulation (MCM) technique which seems to be an attractive candidate for fourth generation (4G) wireless communication systems. OFDM offer high spectral efficiency, immune to the multipath delay, low inter-symbol interference (ISI), immunity to frequency selective fading and high power efficiency. Due to these merits OFDM is chosen as high data rate communication systems such as Digital Video Broadcasting (DVB) and based mobile worldwide interoperability for microwave access (mobile Wi-MAX). However OFDM system suffers from serious problem of high PAPR. In OFDM system output is superposition of multiple sub-carriers. In this case some instantaneous power output might increase greatly and become far higher than the mean power of system. To transmit signals with such high PAPR, it requires power amplifiers with very high power scope. These kinds of amplifiers are very expensive and have low efficiency-cost. If the peak power is too high, it could be out of the scope of the linear power amplifier. This gives rise to non-linear distortion which changes the superposition of the signal spectrum resulting in performance degradation. If no measure is taken to reduce the high PAPR, OFDM system could face serious restriction for practical applications [1]-[4]. PAPR can be described by its complementary cumulative distribution function (CCDF). In this probabilistic approach certain schemes have been proposed by researchers. These include clipping, coding and signal scrambling techniques. Under the heading of signal scrambling and distortion techniques there are three schemes included. Which is Partial transmit sequence (PTS) and Selected Mapping (SLM) and proposed companding. Although some techniques of PAPR reduction have been summarized in [5], it is still indeed needed to give a comprehensive review including some motivations of PAPR reductions, such as power saving, and to compare some typical methods of PAPR reduction through theoretical analysis and simulation results directly. An effective PAPR reduction technique should be given the best trade-off between the capacity of PAPR reduction and transmission power, data rate loss, implementation complexity and Bit-Error-Ratio (BER) performance etc.

In this paper, firstly the distribution of PAPR based on the characteristics of the OFDM signals are investigated then typical PAPR reduction techniques are analyzed.

II. OFDM Signal Characteristics

An OFDM symbol is made of sub-carriers modulated by constellations mapping. This mapping can be achieved from phase-shift keying (PSK) or quadrature amplitude modulation (QAM). For an OFDM system with N sub-carriers, the high-speed binary serial input stream is denoted as $\{a_i\}$.After serial to parallel (S/P) conversion and constellation mapping, a new parallel signal sequence $\{d_0,d_1,.....d_i.....d_{N-1}\}$is obtained, d_i is a discrete complex valued signal[6]. Here, $d_i \in \{\pm 1\}$ when BPSK mapping is adopted. When QPSK mapping is used, $d_i \in \{\pm 1, \pm i\}$.Each element of parallel signal sequence is supplied to N orthogonal sub-carriers $\{e^{j2\pi f0t}, e^{j2\pi f1t} \dots e^{j2\pi fN\text{-}1t}\}$ for modulation, respectively. Finally, modulated signals are added together to form an OFDM symbol. Use of discrete Fourier transform simplifies the OFDM system structure. The complex envelope of the transmitted OFDM signals can be written as

$$x(t) = \frac{1}{\sqrt{N}} \sum_{K=0}^{N-1} X_K \; e^{j2\pi f_k t}, \; 0 \le t \le NT \qquad (1)$$

Signals with large N become Gaussian distributed with Probability Density Function (PDF) is given by [5].

$$P_r\{x(t)\} = \frac{1}{\sqrt{2\pi}\sigma} e^{-\frac{[x(t)]^2}{2\sigma^2}} \qquad (2)$$

Where σ is the variance of x(t).

III. PAPR (Peak-To-Average Power Ratio)

In general, the PAPR [3] of OFDM signals x (t) is defined as the ratio between the maximum instantaneous power and its average power

$$PAPR[X(t)] = \frac{P_{PEAK}}{P_{AVERAGE}} = 10\ \log_{10} \frac{\max[|X(n)|^2]}{E[|X_n|^2]} \quad (3)$$

Where P_{PEAK} represents peak output power, $P_{AVERAGE}$ means average output power. E[·] denotes the expected value, x_n represents the transmitted OFDM signals which are obtained by taking IFFT operation on modulated input symbols Xk [7]. x_n is expressed as:]

$$x_n = \frac{1}{\sqrt{N}} \sum_{K=0}^{N-1} X_k\, W_N^{nk} \quad (4)$$

The instantaneous output of an OFDM system often has large fluctuations compared to traditional single-carrier systems. This requires that system devices, such as power amplifiers, A/D converters and D/A converters, must have large linear dynamic ranges. If this is not satisfied, a series of undesirable interference is encountered when the peak signal goes into the non-linear region of devices at the transmitter, such as high out of band radiation and inter-modulation distortion. PAPR reduction techniques are therefore of great importance for OFDM systems. Also due to the large fluctuations in power output the HPA (high power amplifier) should have large dynamic range. This results in poor power efficiency.

IV. PAPR(Peak-To-Average Power Ratio) Reduction Techniques

Several PAPR reduction techniques have been proposed in the literature [6]. These techniques are divided into two groups - signal scrambling techniques and signal distortion techniques which are given below:

a) Signal Scrambling Techniques

- Block Coding Techniques
- Block Coding Scheme with Error Correction
- Selected Mapping (SLM)
- Partial Transmit Sequence (PTS)
- Interleaving Technique
- Tone Reservation (TR)
- Tone Injection (TI)

b) Signal Distortion Techniques

- Peak Windowing
- Envelope Scaling
- Peak Reduction Carrier
- Clipping and Filtering

One of the most pragmatic and easiest approaches is clipping and filtering which can snip the signal at the transmitter is to eliminate the appearance of high peaks above a certain level. But due to non-linear distortion introduced by this process, orthogonality [8] is destroyed to some extent which results in In-band noise and Out-band noise. In-band noise cannot be removed by filtering, it decreases the bit error rate (BER). Out-band noise reduces the bandwidth efficiency but frequency domain filtering [7] can be employed to minimize the out-band power. Although filtering has a good effect on noise suppression, it may cause peak re-growth. To overcome this drawback, the whole process is repeated several times until a desired situation is achieved. Here, two signal scrambling techniques are used to overcome these problems.

1. Selection Mapping Technique (SLM)

The CCDF of the original signal sequence PAPR above threshold PAPR0 is written as $Pr\{PAPR > PAPR_0\}$ Thus for K statistical independent signal waveforms, CCDF can be written as $[Pr\{PAPR > PAPR_0\}]^R$ so the probability of PAPR exceed the same threshold. The probability of PAPR larger than a threshold Z can be written as

$$P(PAPR < Z) = F(Z)^N = (1 - \exp(-Z))^N \quad (5)$$

Assuming that M-OFDM symbols carry the same information and that they are statistically independent of each other. In this case, the probability of PAPR greater than Z is equals to the product of each independent probability. This process can be written as

$$P(\ PAPR_{LOW} > Z) = (P\{PAPR > Z\})^M = \left((1 - \exp(-Z))^N\right)^M \quad (6)$$

In selection mapping method, firstly M statistically independent sequences which represent the same information are generated, and next, the resulting M statistically independent data blocks

$S_m=[S_{m,0}, S_{m,1}, S_{m,N-1}]^T$, for m=1,2,...,M are then forwarded into IFFT operation simultaneously. $x_m=[x_1,x_2,x_3]^T$ in discrete time-domain are acquired and then the PAPR of these M vectors are calculated separately. Eventually, the sequences x with the smallest PAPR is selected for final serial transmission. Figure 1 shows the basic block diagram of selection mapping technique for suppressing the high PAPR.

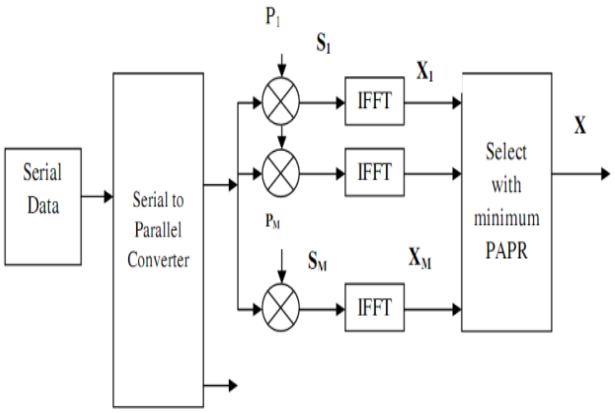

Figure 1. The Block Diagram of Selected Mapping Technique

2. Partial Transmit Sequence (PTS)

Partial Transmit Sequence (PTS) algorithm is a technique for improving the statistics of a multi-carrier signal. The basic idea of partial transmit sequences algorithm is to divide the original OFDM sequence [9] into several sub-sequences and for each sub-sequences multiplied by different weights until an optimum value is chosen.

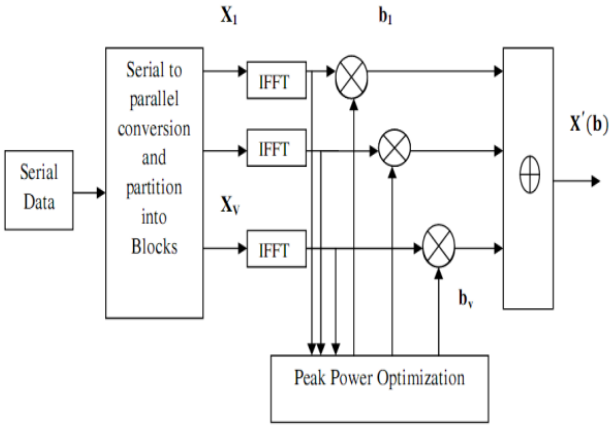

Figure 2. The Block diagram of PTS Technique

Figure 2 [10] is the block diagram of PTS technique. From the left side of diagram, the data information in frequency domain X is separated into V non-overlapping sub-blocks and each sub block vectors has the same size N. So for each and every sub-block it contains N/V nonzero elements and set the rest part to zero. Assume that these sub-blocks have the same size and no gap between each other. The sub-block vector is given by

$$X = \sum_{v=1}^{V} b_v X_v \quad (7)$$

where $b_v=e^{j\varphi v}(\varphi_v \in[0,2\pi])\{v=1,2,X_v\}$ is a weighting factor been used for phase rotation. The signal in time domain is obtained by applying IFFT operation [11] on, that is

$$\hat{x} = \text{IFFT}(X) = \sum_{v=1}^{V} b_v \ \text{IFFT}(X_v) = \sum_{v=1}^{V} b_v X_v \quad (8)$$

For the optimum result one of the suitable factor from combination b = [b1,b2,….b_v] is selected and the combination is given by

$$b = [b_1, b_2, \dots b_v] = argmin_{(b_1,b_2,\dots b_v)}(max_{1\leq n\leq N}|\sum_{v=1}^{V} b_v X_v|^2) \quad (9)$$

Where arg min [(·)] is the condition that minimize the output value of function.

3. Proposed Companded Technique

OBI is the spectral leakage into alien channels. Quantification of the OBI caused by companding requires the knowledge of the power spectral density (PSD) of the companded signal. Unfortunately analytical expression of the PSD is in general mathematically intractable, because of the nonlinear companding transform involved. Here we take an alternative approach to estimate the OBI. Let (x) be a nonlinear companding function, and (t) = sin(ωt) be the input to the compander. The companded signal (t) is:

$$y(t) = f[x(t)] = f[\sin(\omega t)] \quad (10)$$

Since (t) is a periodic function with the same period as (t), (t) can then be expanded into the following Fourier series:

$$y(t) = \sum_{k=-\infty}^{+\infty} c(k)e^{j\omega t}, \quad (11)$$

Where the coefficients (k) is calculated as:

$$c(k) = c(-k)\frac{1}{T}\int_0^T y(t)e^{-j\omega t}\ dt, \quad (12)$$

Notice that the input x in this case is a pure sinusoidal signal, any (k) ≠ 0 for $|k| > 1$ is the OBI produced by the nonlinear companding process. Therefore, to minimize the OBI, (k) must approach to zero fast enough as k increases. It has been shown that (k) · k−(m+1) tends to zero if $y(t)$ and its derivative up to the m-th order are continuous [8], or in other words, $c(k)$ converges at the rate of $\mathbf{k^{-(m+1)}}$ **.** Given an arbitrary number n, the n-th order derivative of (t), $d^n y/dt^n$ is a function of $d^i f(x)/dx^i$, (i = 1, 2, · · · , n), as well as sin(ωt) and cos(ωt), i.e.:

$$\frac{d^n y}{dt^n} = g\left(\frac{d^n f(x)}{dt^n}, \frac{d^{n-1} f(x)}{dt^{n-1}}, \dots, \frac{df(x)}{dx}, \sin(wt), \cos(wt)\right) \quad (13)$$

sin(ωt) and and cos(ωt) are continuous functions, $d^n y/dt^n$ is continuous if and only if $d^i f(x)/dx^i$ are continuous. Based on this observation we can conclude:

Companding introduces minimum amount of OBI if the companding function (x) *is infinitely differentiable*.

The functions that meet the above condition are the smooth functions.

We now propose a new companding algorithm using a smooth function, namely the airy special function. The companding function is as follows

$$f(x) = \beta.sign(x).[airy(0) - airy(\alpha.|x|)] \quad (14)$$

Where airy (·) is the airy function of the first kind. α is the parameter that controls the degree of companding (and ultimately PAPR). β is the factor adjusting the average output power of the compander to the same level as the average input power:

$$\beta = \sqrt{\frac{E[|x|^2]}{E[|airy\ (0) - airy\ (\alpha.|x|)|^2]}} \quad (15)$$

Where E[·] denotes the expectation.

The decompanding function is the inverse of (x):

$$f^{-1}(x) = \frac{1}{\alpha}.sign(x).airy^{-1}[airy(0) - \frac{|x|}{\beta}] \quad (16)$$

Where the superscript -1 represents the inverse operation. Notice that the input to the decompander is a quantized signal with finite set of values.

We can therefore numerically pre- compute $f^{-1}(x)$ and use table look-up to perform the decompanding in practice.

V. Simulation Results

Figure 4 shows the CCDF as a function of PAPR distribution when SLM method is used with 64 numbers of subcarrier. M takes the value of 1 (without adopting SLM method), 2, 4, 8 and 16. It is seen in Figure 4 that with increase of branch number M, PAPR's CCDF gets smaller.

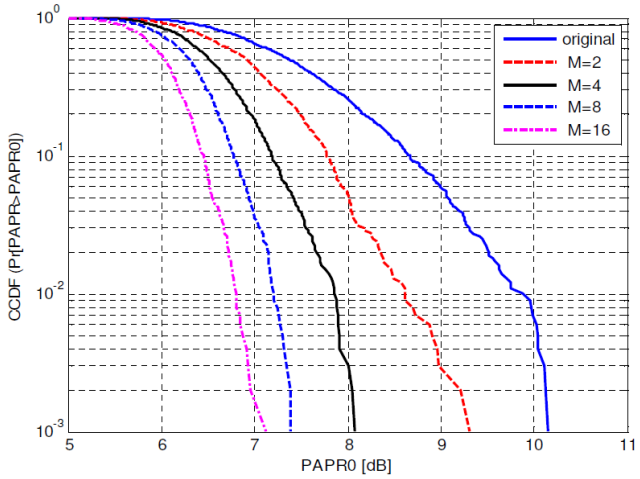

Figure. 4. PAPR's CCDF using SLM method with N=64

Now discussed the simulation result for PTS technique, there are varying parameters which impact the PAPR reduction performance these are: 1) The number of sub-blocks V, which influences the complexity strongly; 2) The number of possible phase value W, which impacts the
complexity; and 3) The sub-block partition schemes. Here, only one parameter is considered that is sub-block size V=4.

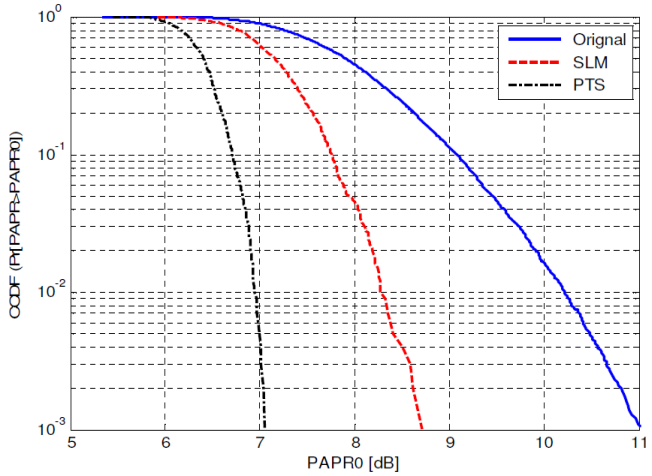

Figure 5. PAPR's CCDF using SLM and PTS method with N=64

Figure.6 depicts the CCDF of the three companding schemes. The new algorithm is roughly 1.5dB inferior to the exponential, but surpasses the μ-law by 2dB

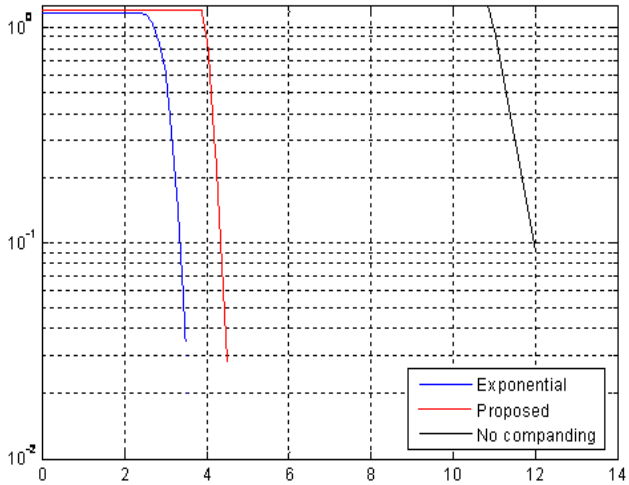

Figure.6.Complementary cumulative distribution function of original and companded signals

From the above figures it is clear that new proposed companded technique provides a better PAPR reduction performance than compared to PTS method and SLM method

VI. Conclusion

OFDM is a very attractive technique for wireless communications due to its spectrum efficiency and channel robustness. One of the serious drawbacks of OFDM systems is that the composite transmit signal can exhibit a very high PAPR when the input sequences are highly correlated. In this paper, several important aspects are described as well as mathematical analysis is provided, including the distribution of the PAPR used in OFDM systems. Three typical signal scrambling and distortion techniques, SLM, PTS and Companding are investigated to reduce PAPR, all of which have the potential to provide substantial reduction in PAPR. Proposed Companding method performs better than PTS method and SLM method in reducing PAPR.

References

[1] Y.Wu and W. Y. Zou, "Orthogonal frequency division multiplexing: A multi-carrier modulation scheme," IEEE Trans. Consumer Electronics, vol. 41, no. 3, pp. 392–399, Aug. 1995.
[2] E. Telatar, "Capacity of multi-antenna Gaussian channels," European Transactions on Telecommunications, vol. 10, no 3, Dec 1999.
[3] Foschini G J, Gans M J, "On limits of wireless communication in a fading environment when using multiple antennas," Wireless Personal Communication, vol. 6.
[4] Shinsuke Hara, Ramjee, "Principle and history of MCM/OFDM," in Multicarrier techniques for 4G mobile communication, Artech House.
[5] KUANG Yu-jun, TENG Yong, "A new symbol synchronization scheme for cyclic prefix based systems," The Journal of China Universities of Posts and Telecommunications.
[6] Peled A, Ruiz A, "Frequency domain data transmission using reduced computational complexity algorithms," Acoustics, Speech, and Signal Processing, IEEE International Conference.
[7] Cooper, G.R, Nettleton, R.W, "A spread spectrum technique for high capacity mobile communications," IEEE Transaction on Vehicular Technology, Nov 1978, vol. 27.
[8] H. Sampath, et al., "A fouth-generation MIMO-OFDM broadband wireless system: design, performance and field trial results," IEEE Communication Magazine, Sep 2002, vol. 40, no 9.
[9] Oh-Ju Kwon and Yeong-Ho Ha, "Multi-carrier PAP reduction method using sub-optimal PTS with threshold," IEEE Transactions on Broadcasting, June. 2003, vol. 49.
[10] Jayalath, A.D.S, Tellainbura, C, "Side Information in PAR Reduced PTS-OFDM Signals," Proceedings 14th IEEE Conference on Personal, Indoor and Mobile Radio Communications, Sept. 2003, vol.1.
[11] I. N. Bronshtein, K. A. Semendyayev, G. Musiol, and H. Muehlig, Handbook of Mathematics, 5th ed. New York: Springer, 2007, p. 422.

AUTHORS PROFILE

K.Ram Mohan Rao obtained B.Tech degree in Electronics and Communication Engineering from JNTU, Hyderabad, India and M.Tech degree in Digital Electronics and Communication Systems from JNTU, Hyderabad, India. He is working as an Assistant Professor in the Department of Electronics and Communication Engineering, Sri Indu College of Engineering and Technology, Hyderabad, India. His research interests include digital Communication, Image Processing and wireless communications

T.Sravanti obtained B.Tech degree in Electronics and Communication Engineering from JNTU, Hyderabad, India. and M.Tech degree in Digital Electronics and Communication Systems from JNTU,Hyderabad, India.. She is working as an Assistant Professor in the Department of Electronics and Communication Engineering, Jagruti Institute of Engineering and Technology, Hyderabad, India. She is pursuing her Ph.D. in the Department of Electronics and Communication Engineering, University College of Engineering Hyderabad, Osmania University. Her research interests include digital Communication, computer networks, Signal Processing, wireless communications, cellular and mobile networks.

International Journal of Modern Engineering Research (IJMER)
www.ijmer.com Vol.3, Issue.2, March-April. 2013 pp-721-724 ISSN: 2249-6645

A Mining Approach for Web Engineering In Respect Of Business Intelligence Application

Tapan Nayak, [1] Prof. B Lakshma Reddy[2]
[1]*Department of Computer Science, CMJ University, Shillong, Meghalaya, INDIA*
[2]*Department of Computer Science, Garden City College, Bangalore, INDIA*

Abstract: *Using mining approach in Engineering process of Web Applications is a complex problem, due to the variety of languages and technologies that are contemporary used to realize them. Indeed, the benefits that can be obtained are remarkable: the presence of documentation at different abstraction levels will help the execution of maintenance interventions, migration and reengineering processes, reducing their costs and risks and improving their effectiveness. The main objective of this paper is to identify the application of web engineering process from mining techniques for a intelligence application. In this paper, all aspects are studied that are basically required for web mining and web engineering process. Since the last few decades, there has been an immense increase in use of World Wide Web (WWW) for a wide and variety of web based business applications. The web based intelligent application plays a leading role in e-commerce business applications. As a consequence, there is a need to improve Intelligence of Web Engineering Applications in the context of Business and IT industry. To achieve this objective web engineering process must be able to identify some useful insights for business intelligence. The proposed research work attempts to initiate Business Intelligence from Web Based Applications. The issues of research work are uniformly accommodated in five steps which are provided in this paper.*

Keywords: *Web Engineering, Web Mining, Web site Errors, Web Development, Web Crisis*

I. INTRODUCTION

Although the development of Web based applications may seem easy, it is often more complex and challenging than many of us think. . Two key attributes distinguish web-based systems development from traditional software development: rapid growth of the requirements of Web-based systems and the continual change of their information content. Web Applications are evolutionary. For many web applications, it's not possible to specify fully what they should or will contain at the start of their development, because their structure and functionality will evolve over time. Hence, Web based system development is not a one-time event as currently perceived and practiced by many web developers; it is, instead, an iterative process with a long life cycle.

1.1 Motivation

Reasons for mining approach for web engineering on business application

- **Interfacing**. An overall web architecture describing how the network and the various servers such as web servers, applications servers, and database servers interact and application can be used when a system is required to interface to another system and how both systems would negotiate is to be established.
- **Commercial espionage**. Learning about an enemy's or competitor's latest research by stealing or capturing a prototype and dismantling it. It may result in development of similar product.
- **Usability and User-Centered Designs.** Effective Web site design requires attention to usability. Web-based systems need to be designed for easy navigation and customer attractive, User-centered design methods for Web sites is presented in , while presents a User-Centric Approach to Modeling Web Information Systems.
- **Improve documentation shortcomings** Using, the web log file contains information about the user IP address, the requested page, time of request, the volume of the requested page, its referrer, and other useful information. Web log file is the main source of data analysis in web mining. Web log file contains data about requested URL, time and date of request, method used.
- **Obsolescence.** Application Integrated circuits often seem to have been designed on obsolete, proprietary systems, which means that the only way to incorporate the functionality into new technology is to web-engineer the existing chip and then re-design it.
- **Software Modernization**. Web mining is the usage of data mining techniques to extract interesting information from web data. Patterns extracted from applying web mining techniques on web data can be used to maintain websites by improving their usability.
- **Product Security Analysis.** To examine how a product works, what are specifications of its components, estimate costs and identify potential patent infringement. Acquiring sensitive data by disassembling and analysing the design of a system component.
- **Academic/learning purposes.** The essence of Web engineering is to successfully manage the diversity and complexity of Web application development and hence, avoid potential failures, which can have serious implications. It is a proactive approach to building Web applications.

II. RELATED WORK

The rapid growth of the Internet, Intranets, Extranets, and the World Wide Web has already had a significant impact on business, industry and commerce, sports, finance, education, government and entertainment sectors, and our personal and working life. Many legacy information and database systems are being migrated to the Internet and the Web environments. A Web based business application software model of the system describes various components of the system and how they are linked for mining techniques used for extracting relevant information.. The application architecture model shows that, a map of various information and functional modules. An information module may provide the same information to all the users or provide customized or personalized information to each user. Functional modules such as login page, registration pages, web forms for data collections and the shopping carts used in e-commerce systems – collect and process the users input. Specific requirements for look and feel consistency of information, scalability, maintainability and quality control mechanisms determine the software architecture [4].

The primary cause of Web system failures are the flawed design and development process and poor management of their development. The emerging Web engineering discipline deals with the process of developing Web-based systems and applications.. To tackle the above mentioned problems, Web engineers are increasingly applying Data Mining algorithms to various Webs engineering process. For instance, mining algorithms can be applied to trace the patterns in which a user browses the Web pages and group together those Web pages making the retrieval of the information fast, thus increasing the responsiveness. Web development is a process, not simply a one-time event. Thus, Web Engineering deals with all aspects of Web-based systems development, starting from conception and development to implementation, performance evaluation, and continual maintenance. Web Engineering, therefore, covers a range of areas: requirements elicitation and analysis; Web system modeling; Web architecture; Web system design; Web page design; scripting/coding; interface with databases, ERP systems, and other Web-based systems; Web quality; Web usability; Web security; Web system performance evaluation; Web testing; Web development methodologies; Web development process; Web metrics; and Web project management [3].

III. Mining Approach for Web Engineering

A successful Web Engineering Applications is one which can improves insights of web based business intelligence by sharing results among various modules in the process of effective decision making by using basic mining techniques as a tool. Many attributes of quality Web-based Systems such as ease of navigation, accessibility, scalability, maintainability, usability, compatibility and interoperability, security, readability, and reliability are not given due consideration during development. Many developers seem to be unaware of the real issues and challenges facing major Web based application development and its continual maintenance in respect of mining approach. Web Engineering must be a systematic discipline and quantifiable approach for development, operation and maintenance of web based business applications for a successful business. To achieve the goal of business intelligence in web based applications, one has to concentrate on various aspects of web content. A mining approach for web engineering application is necessary to study the role of various components of web application in business intelligence.

An algorithm was developed as a web mining approach which can investigate the components of web that are used in business intelligence [4]. The different phases in mining for web engineering are shown in figure 1.

I. FIGURES AND TABLES

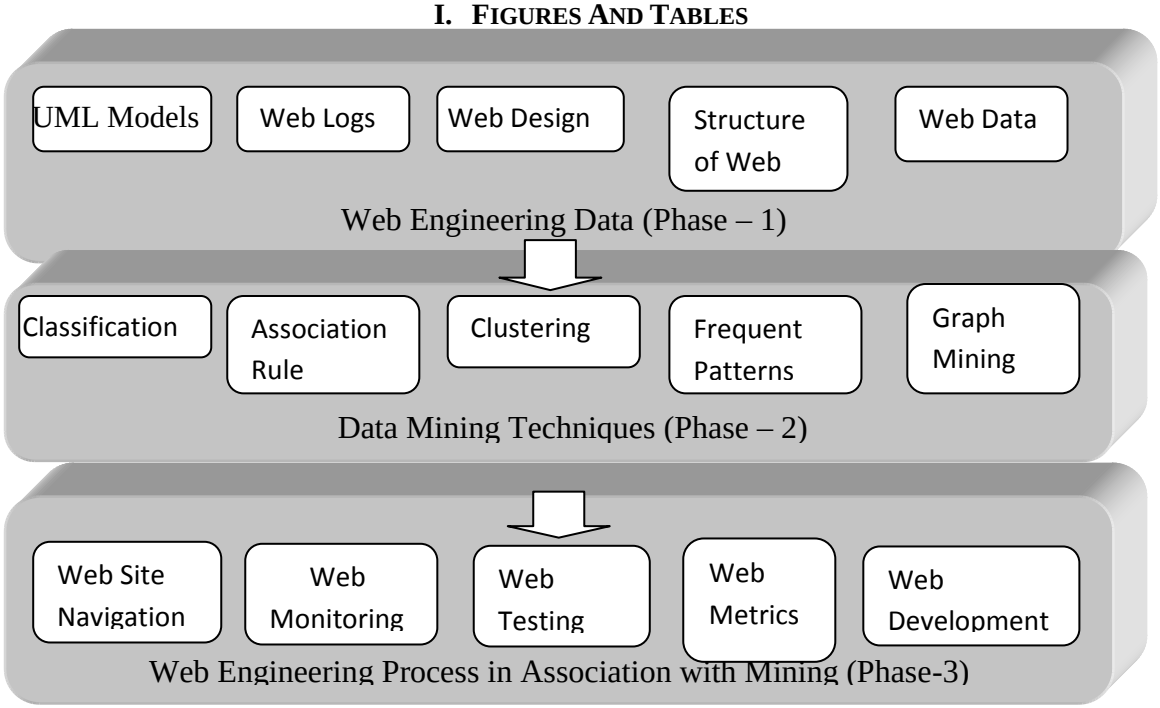

Figure 1: Phases of Mining for Web Engineering

Phases in Mining Process:
An algorithm consists of 3 phases. They are
Phase 1: Extracting Web Data from web application
Phase 2: Web Mining Approaches to extract features of web application
Phase 3: Web engineering process associated with Web Mining

Phase 1: **Extracting Web Data from web application**: An algorithm was developed using the web program in extracting the components of web such as Web site Structure, Web site Error Reports, Web site objects used in web design, and contents of Web log. The Web Program retrieves all necessary web data elements using a standard set of web tools. These tools include Web site Extractor, Web page Analyzer, W3C HTML Validator, Power Mapper, and Web log Expert. The overall structure of the algorithm is shown in figure 2.

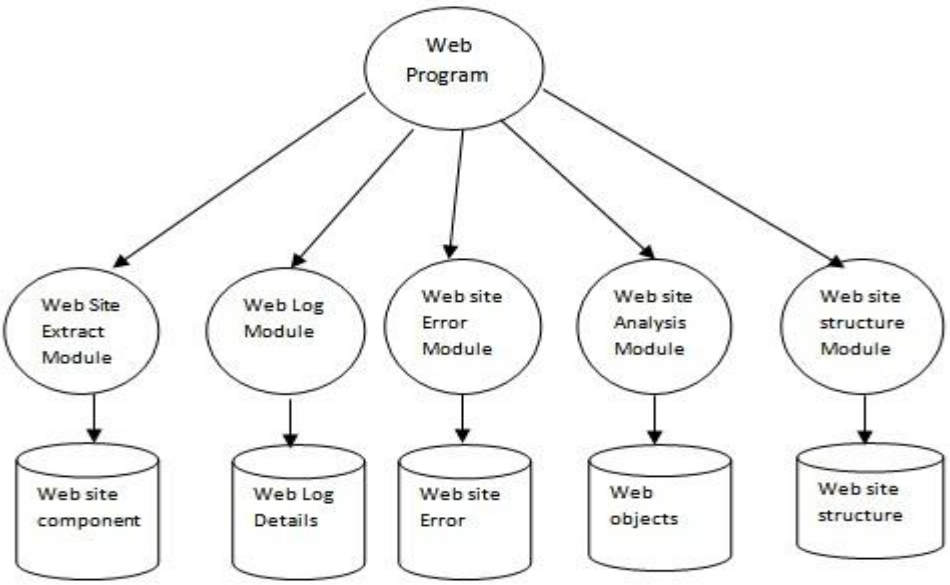

Figure 2: Architecture of Algorithm

Phase 2: Web mining techniques to extract features of web application:

Web mining is the usage of data mining techniques to extract interesting information from web data. Patterns extracted from applying web mining techniques on web data can be used to maintain websites by improving their usability. The patterns can also be used to study user behaviour and interests, facilitate support and services introduced to the website navigator, improve the structure of the website, and facilitate personalization and adaptive websites. After extracting web engineering data, various web mining techniques are applied on data base which consists of web information.

1. Association Rule Mining:

In ARM a couple set of association rules are applied on elements of web site structure to identify relationships among various modules of web engineering application. Association rule mining is finding all association rules with support and confidence values that are greater than or equal a user-specified minsup and minconf respectively. In general, the process of extracting interesting association rules consists of two major steps.
Step 1: The first step is finding all item sets that satisfy minsup (known as Frequent-Item set generation).
Step 2: The second step, is generating all association rules that satisfy min conf using item sets generated in the first step. After generating frequent item sets, association rules that are greater than or equal to min conf are generated. Those rules are called interesting association rules. Those rules can be invested in many different applications. One of those applications is improving the structure of the company's website that the mined database belongs to. This is done during the website's design phase by creating links between items that seem to be sold together, or highlight those links if they are already exist, and/or create index pages which are pages that have direct links to some products that may be of interest for some group of customers. All paragraphs must be indented. All paragraphs must be justified, i.e. both left-justified and right-justified.

2) Classification:

Classification is dividing an existing set of events or transactions into other predefined sets or classes based on some characteristics. In web usage mining, classification is used to group users into predefined groups with respect to their navigation patterns in order to develop profiles of users belonging to a particular class or category. A web mining strategy for web personalization based on a novel pattern recognition strategy which analysis and classifies users taking into account both user provided data and navigational behaviour of the users.

3) Clustering:

Clustering is the process of partitioning a given population of events or items into sets of similar elements, so that items within a cluster have high similarity in comparison to one another, but are very dissimilar to items in other clusters. In web usage mining there are two main interesting clusters to be discovered: usage clusters and pages clusters [4]. The authors in [5] present an approach to cluster web pages to obtain high quality clusters of web pages and use those clusters to produce index pages, where index pages are web pages that have direct links to pages that may be of interest of some group of website navigators. In [5] clustering techniques are applied to web log file to discover those subsets of web pages that need to be connected and to improve the already connected pages.

Phase 3: Web Engineering Process associated with web mining

The basic knowledge of Web Mining techniques that are applied on Web data produce various process related to Web Engineering frame work. These process associated with web services, web architectures, web configuration management data, web application classification, web testing, requirements elicitation and analysis; Web system modeling; Web architecture; Web system design; web communities, Website Navigation, Web page design; Web quality; Web usability; Web security; Web system performance evaluation; Web testing; Web development methodologies; Web development process; Web metrics; and Web project management [6]. These services are very much essential in any type of web application. Patterns extracted from applying web mining techniques on web data can be used to maintain websites by improving their usability through simplifying user navigation and information accessibility and improving the content and the structure of the website in a way that meets the requirements of both website owner and user which will consequently increase the overall profit of the business or the industry that the maintained website belongs to [8].

IV. CONCLUSION

This paper presents a development structure of a mining module for web engineering and also describes tool architecture to extract phases from existing web engineering structure, but also with the more challenging mining content. Here an attempt is made to find all areas involved in mining process. Further the work can be extended to find services of web mining process required for web engineering.

REFERENCES

[1] Ajith Abraham, "Business Intelligence from Web Usage Mining", Department of Computer Science, Oklahoma State University, USA.
[2] Anupam Joshi and Pranam Kolari, "Web Engineering Column: Web Mining: Research and Practice", IEEE Computing and Science and Engineering, July/August 2004 pp. 49-53.
[3] Athula Ginge and San Murugesan, "Web Engineering: A Methodology for Developing Scalable, Maintainable Web Applications", Cutter IT Journal, Vol.14, No.7, July 2001, Page. 24-35.
[4] G sreedhar, Dr. A A Chari, Dr. V V Venkata Ramana, " A Qualitative and Quantitative Frame work for effective Web Site Design", IJCA, Vol 2, May 2010, PP 48-56.
[5] Jiawei Han, Kevin Chen-Chuan Chang, "Data Mining for Web Intelligence", IEEE Computer November, 2002 pp. 64-70
[6] Martha Koutri and Sophia Daskalaki. "Improving Web Site Usability through a Clustering Approach", In Proceedings of the 10th International Conference on Human-Computer Interaction HCI, Crete, Greece, 2003, PP. 11-19.
[7] Tao Xie, Jian Pei, Ahmed E. Hassan "Mining Software Engineering Data", 29th International Conference on Software Engineering, 2007, IEEE.
[8] Wingyan Chung "Designing Web-based Business Intelligence Systems: A Framework and Case Studies: In DESRIST", February 24-25, California CA USA 2006, pp. 147 – 171.
[9] M V Kamal, "Mining for web engineering-business intelligence application case study", IJESS, Vol2, Issue 6 (June 2012).
[10] Nayak, ""Reverse Engineering: Methodologies for Web Applications" IJSWS 12-209, Vol. 2, Issue, 1, pp.39-44, August-November, 2012",
[11] San Murugesan, Yogesh Deshpande "Web Engineering: A New Discipline for Development of Web-based Systems".
[12] Scharl, A., A Conceptual, User-Centric Approach to Modeling Web Information Systems , Proc Australian Web Conference (Ausweb99), Ballina, Australia, April 1999.
[13] Detroyer, O.M.F., and C.J. Leune, WSDM: A User-Centered Design Methods for Web Sites, Proc. WWW7Conference, Brisbane, 1998.

International Journal of Modern Engineering Research (IJMER)
www.ijmer.com Vol.3, Issue.2, March-April. 2013 pp-725-735 ISSN: 2249-6645

The effect of chemical reaction on an unsteady MHD free convection flow past an infinite vertical porous plate with variable suction

K. Sarada, [1] B. Shanker[2]

[1]*Lecturer in Mathematics, Vivekananda Govt. Degree College, Vidyanagar, Hyderabad, 500010, Andhra Pradesh, India*
[2]*Professor, Department of Mathematics, University College of Science, Osmania University, Hyderabad, 500007, Andhra Pradesh, India*

Abstract: *The effect of chemical reaction on an unsteady magneto hydrodynamic flow past an infinite vertical porous plate with variable suction and heat convective mass transfer, where the plate temperature oscillates with the same frequency as that of variable suction velocity. The non – linear partial differential equations governing the flow have been solved numerically using finite difference method. The flow phenomenon has been characterized with the help of flow parameters such as velocity, temperature and concentration profiles for different parameters such as thermal Grashof number (Grashof number for heat transfer)* (Gr) *, solutal Grashof number (Grashof number for mass transfer)* (Gc) *, Prandtl number* $(\Pr)$*, Schmidt number* (Sc) *, Hartmann number* (M) *, Permeability parameter* (K) *and Chemical reaction parameter* (k_r)*, The velocity, temperature and concentration profiles are shown through graphically and Skin – friction, Nusselt number and Schmidt number are shown through tabular forms.*

Key Words: *Chemical reaction, Unsteady, MHD, Free convection flow, Porous medium, Infinite vertical porous plate, Finite difference method.*

Nomenclature

A	Variable suction parameter
B_o	Magnetic field component along $y'-$ axis
C_p	Specific heat at constant pressure
Gr	Grashof number
Gc	Modified Grashof number
g	Acceleration of gravity
K'	The permeability of medium
K	The permeability parameter
M	Hartmann number
$\Pr$	Prandtl number
Sc	Schmidt number
k_r	Chemical reaction parameter
D	Chemical molecular diffusivity
T'	Temperature of fluid near the plate
T'_w	Temperature of the fluid far away of the fluid from the plate
T'_∞	Temperature of the fluid at infinity
C	Concentration of the fluid
C'	Concentration of fluid near the plate
C'_w	Concentration of the fluid far away of the fluid from the plate
C'_∞	Concentration of the fluid at infinity
t'	Time in x', y' coordinate system
t	Time in dimensionless co – ordinates
u'	Velocity component in $x'-$ direction
v'	Velocity component in $y'-$ direction
u	Dimensionless velocity component in $x'-$ direction
Nu	Nusselt number

Sh Sherwood number
R_{e_x} Reynold's number
x', y' Co – ordinate system
x, y Dimensionless coordinates
v_o Mean suction velocity

Greek symbols

β Coefficient of volume expansion for heat transfer
β^* Coefficient of volume expansion for mass transfer
ε Smallest positive constant
K_T Thermal conductivity of the fluid
σ Electrical conductivity of the fluid
ν Kinematic viscosity
θ Non – dimensional temperature
ρ Density of the fluid
τ Skin – friction
μ Viscosity, Ns/m^2

I. Introduction

Combined heat and mass transfer problems with chemical reaction are of importance in many processes and have, therefore, received a considerable amount of attention in recent years. In processes such as drying, evaporation at the surface of a water body, energy transfer in a wet cooling tower and the flow in a desert cooler, heat and mass transfer occur simultaneously. Possible applications of this type of flow can be found in many industries. For example, in the power industry, among the methods of generating electric power is one in which electrical energy is extracted directly from a moving conducting fluid. Many practical diffusive operations involve the molecular diffusion of a species in the presence of chemical reaction within or at the boundary. There are two types of reactions, homogeneous reaction and heterogeneous reaction. A homogeneous reaction is one that occurs uniformly throughout a given phase. The species generation in a homogeneous reaction is analogous to internal source of heat generation. In contrast, a heterogeneous reaction takes place in a restricted region or within the boundary of a phase. It can therefore be treated as a boundary condition similar to the constant heat flux condition in heat transfer. The study of heat and mass transfer with chemical reaction is of great practical importance to engineers and scientists because of its almost universal occurrence in many branches of science and engineering. The flow of a fluid past a wedge is of fundamental importance since this type of flow constitutes a general and wide class of flows in which the free stream velocity is proportional to a power of the length coordinate measured from the stagnation point. In many transport processes in nature and in industrial applications in which heat and mass transfer is a consequence of buoyancy effects caused by diffusion of heat and chemical species. The study of such processes is useful for improving a number of chemical technologies, such as polymer production and food processing. In nature, the presence of pure air or water is impossible. Some foreign mass may be present either naturally or mixed with the air or water. The present trend in the field of chemical reaction with viscosity analysis is to give a mathematical model for the system to predict the reactor performance. A large amount of research work has been reported in this field. In particular, the study of chemical reaction, heat and mass transfer is of considerable importance in chemical and hydrometallurgical industries. Chemical reaction can be codified as either heterogeneous or homogeneous processes. This depends on whether they occur at an interface or as a single phase volume reaction.

Both free and forced convection boundary layer flows with Soret and Dufour have been addressed by Abreu *et al.* [1]. Afify [2] carried out an analysis to study free convective heat and mass transfer of an incompressible, electrically conducting fluid over a stretching sheet in the presence of suction and injection with thermal diffusion and diffusion thermo effects. Beg *et al.* [3] have also analyzed the chemical reaction rate effects on steady buoyancy – driven dissipative micropolar free convective heat and mass transfer in a Darcian porous regime. Beg *et al.* [4] have also studied numerically both viscous heating and Joule (Ohmic) dissipation effects on transient Hartmann – Couette convective flow in a Darcian porous medium channel also including Hall current and ion – slip effects. Chaudhary *et al.* [5] studied the effect of free convection effects on magnetohydrodynamic flow past an infinite vertical accelerated plate embedded in porous media with constant heat flux by using Laplace transform technique for finding the analytical solutions. Chin *et al.* [6] obtained numerical results for the steady mixed convection boundary layer flow over a vertical impermeable surface embedded in a porous medium when the viscosity of the fluid varies inversely as a linear function of the temperature. Das and Mitra [7] discussed the unsteady mixed convective MHD flow and mass transfer past an accelerated infinite vertical plate with suction. Recently, Das and his co – workers [8] analyzed the effect of mass transfer on MHD flow and heat transfer past a vertical porous plate through a porous medium under oscillatory suction and heat source. Das *et al.* [9] investigated numerically the unsteady free convective MHD flow past an accelerated vertical plate with suction and heat flux. Das and his associates [10] estimated the mass transfer effects on unsteady flow past an accelerated vertical

porous plate with suction employing finite difference analysis. Gireesh kumar *et al.* [11] investigated effects of chemical reaction and mass transfer on MHD unsteady free convection flow past an infinite vertical plate with constant suction and heat sink.

Hayat *et al*. [12] analyzed a mathematical model in order to study the heat and mass transfer characteristics in mixed convection boundary layer flow about a linearly stretching vertical surface in a porous medium filled with a visco – elastic fluid, by taking into account the diffusion thermo and thermal diffusion effects. Ibrahim *et al.* [13] studied the effects of chemical reaction and radiation absorption on transient hydromagnetic natural convection flow with wall transpiration and heat source. The unsteady free convective MHD flow with heat transfer past a semi – infinite vertical porous moving plate with variable suction has been studied by Kim [14]. Effects of chemical reaction on free convection flow of a polar fluid through a porous medium in the presence of internal heat generation are examined by Patil and Kulkarni [15]. Several studies have also described thermal radiation effects on convection flows in porous media. MHD convective flow of a micropolar fluid past a continuously moving vertical porous plate in the presence of heat generation/absorption was studied by Rahman and Sattar [16]. Sarangi and Jose [17] studied the unsteady free convective MHD flow and mass transfer past a vertical porous plate with variable temperature. The effect of temperature dependent viscosity and thermal conductivity on unsteady MHD convective heat transfer past a semi – infinite vertical porous plate has studied Seddek and Salama [18]. Seddeek *et al.* [19] more recently reported on the effect of chemical reaction and variable viscosity on hydromagnetic mixed convection heat and mass transfer for Hiemenz flow through a Darcian porous media in the presence of radiation and magnetic field. Seethamahalakshmi *et al.* [20] discussed the effects of Soret on an unsteady magnetohydrodynamic free convection flow past an infinite vertical porous plate with variable suction. The unsteady free convection flow of a viscous incompressible fluid past an infinite vertical plate with constant heat flux is considered on taking into account viscous dissipative heat, under the influence of a transverse magnetic field studied by Srihari *et al* [21].

The object of the present paper is to analyze the chemical reaction effect on an unsteady magneto hydrodynamic free convection flow past an infinite vertical plate by taking variable suction into account. The governing equations are transformed by using unsteady similarity transformation and the resultant dimensionless equations are solved by using the finite difference method. The effects of various governing parameters on the velocity, temperature, concentration, skin – friction coefficient, Nusselt number and Sherwood number are shown in figures and tables and discussed in detail. From computational point of view it is identified and proved beyond all doubts that the finite difference method is more economical in arriving at the solution and the results obtained are good agreement with the results of Seethamahalakshmi *et al*. [20] in some special cases.

II. Mathematical Analysis

Consider the unsteady magneto hydrodynamic flow past an infinite vertical porous plate with variable suction and heat convective mass transfer, where the plate temperature oscillates with the same frequency as that of variable suction velocity in presence of chemical reaction.

We made the following assumptions.

1. In Cartesian coordinate system, let $x'-$axis is taken to be along the plate and the $y'-$axis normal to the plate. Since the plate is considered infinite in $x'-$direction, hence all physical quantities will be independent of $x'-$direction.
2. The wall is maintained at constant temperature (T_w') and concentration (C_w') higher than the ambient temperature (T_∞') and concentration (C_∞') respectively.
3. Let the components of velocity along x' and y' axes be u' and v' which are chosen in the upward direction along the plate and normal to the plate respectively.
4. A uniform magnetic field of magnitude B_o is applied normal to the plate. The transverse applied magnetic field and magnetic Reynold's number are assumed to be very small, so that the induced magnetic field is negligible.
5. The polarization effects are assumed to be negligible and hence the electric field is also negligible.
6. The homogeneous chemical reaction of first order with rate constant between the diffusing species and the fluid is assumed.
7. The concentration of the diffusing species in the binary mixture is assumed to be very small in comparison with the other chemical species, which are present and hence Soret and Dufour effects are negligible.
8. The Hall Effect of magneto hydrodynamics and magnetic dissipation (Joule heating of the fluid) are neglected.

Hence the governing equations of the problem are:

$$\frac{\partial \rho'}{\partial t'}+\frac{\partial(\rho' u')}{\partial x'}+\frac{\partial(\rho' u')}{\partial y'}=0 \tag{1}$$

$$\rho'\left(\frac{\partial u'}{\partial t'}+u'\frac{\partial u'}{\partial x'}+v'\frac{\partial u'}{\partial y'}\right)=-\frac{\partial \rho'}{\partial x'}+\rho' g\beta(T'-T_\infty')+\rho' g\beta^*(C'-C_\infty')+\frac{\partial}{\partial x'}\left(2\mu\frac{\partial u'}{\partial x'}\right)+$$
$$\frac{\partial}{\partial y'}\left\{\mu\left(\frac{\partial u'}{\partial y'}+\frac{\partial v'}{\partial x'}\right)\right\}-\frac{\mu}{K'}u'-\sigma B_o^2 u' \tag{2}$$

$$\rho' C_p' \left(\frac{\partial T'}{\partial t'} + u' \frac{\partial T'}{\partial x'} + v' \frac{\partial T'}{\partial y'} \right) = K_T \left(\frac{\partial^2 T'}{\partial x'^2} + \frac{\partial^2 T'}{\partial y'^2} \right) \quad (3$$

$$\rho' \left(\frac{\partial C'}{\partial t'} + u' \frac{\partial C'}{\partial x'} + v' \frac{\partial C'}{\partial y'} \right) = \rho' D \left(\frac{\partial^2 C'}{\partial x'^2} + \frac{\partial^2 C'}{\partial y'^2} \right) - K_r \left(C' - C_\infty' \right) \quad (4)$$

Here, the status of an equation of state is that of equation $\rho' =$ constant. This means that the density variations produced by the pressure, temperature and concentration variations are sufficiently small to be unimportant. Variations of all fluid properties other than the variations of density except in so far as they give rise to a body force, are ignored completely (Boussinesq approximation). All the physical variables are functions of y' and t' only as the plate are infinite. It is also assumed that the variation of expansion coefficient is negligibly small and the pressure and influence of the pressure on the density are negligible. Within the framework of above assumptions the governing equations reduce to Continuity Equation:

$$\frac{\partial v'}{\partial y'} = 0 \quad (5)$$

Momentum Equation:

$$\frac{\partial u'}{\partial t'} + v' \frac{\partial u'}{\partial y'} = g\beta \left(T' - T_\infty' \right) + g\beta^* \left(C' - C_\infty' \right) + \nu \frac{\partial^2 u'}{\partial y'^2} - \left(\frac{\sigma B_o^2}{\rho} + \frac{\nu}{K'} \right) u' \quad (6)$$

Energy Equation:

$$\frac{\partial T'}{\partial t'} + v' \frac{\partial T'}{\partial y'} = \frac{K_T}{\rho' C_p'} \frac{\partial^2 T'}{\partial y'^2} \quad (7)$$

Species Diffusion Equation:

$$\frac{\partial C'}{\partial t'} + v' \frac{\partial C'}{\partial y'} = D \frac{\partial^2 C'}{\partial y'^2} - K_r \left(C' - C_\infty' \right) \quad (8)$$

And the corresponding boundary conditions are

$$\left. \begin{array}{l} t' \le 0 : u' = 0,\ T' = T_\infty',\ C' = C_\infty' \quad for\ all\ y' \\ t' > 0 : \begin{cases} u' = 0,\ T' = T_w' = 1 + \varepsilon e^{i\omega' t'},\ C' = C_w' \quad at\ y' = 0 \\ u' \to 0,\ T' \to T_\infty',\ C' \to C_\infty' \quad as\ y' \to \infty \end{cases} \end{array} \right\} \quad (9)$$

From the continuity equation, it can be seen that v' is either a constant or a function of time. So, assuming suction velocity to be oscillatory about a non – zero constant mean, one can write $v' = -v_o \left(1 + \varepsilon A e^{i\omega' t'} \right)$ (10)

Where ε, A are small such that $\varepsilon A << 1$. The negative sign indicates that the suction velocity is directed towards the plate. In order to write the governing equations and the boundary conditions in dimensional following non – dimensional quantities are introduced.

$$\left. \begin{array}{l} y = \frac{y' v_o}{\nu},\ t = \frac{t' v_o}{\nu},\ u = \frac{u'}{v_o},\ v = \frac{v'}{v_o},\ \theta = \frac{T' - T_\infty'}{T_w' - T_\infty'},\ C = \frac{C' - C_\infty'}{C_w' - C_\infty'},\ Gr = \frac{g\beta\nu \left(T_w' - T_\infty' \right)}{v_o^3},\ Sc = \frac{\nu}{D}, \\ Gc = \frac{g\beta^* \nu \left(C_w' - C_\infty' \right)}{v_o^3},\ \Pr = \frac{\mu C_p}{K_T},\ M = \left(\frac{\sigma B_o^2}{\rho} \right) \frac{\nu}{v_o^2},\ K = \frac{K' v_o^2}{\nu^2},\ k_r = \frac{K_r \nu}{v_o^2},\ \omega = \frac{4\nu\omega'}{v_o'^2} \end{array} \right\} \quad (11)$$

Hence, using the above non – dimensional quantities, the equations (6) – (9) in the non – dimensional form can be written as

$$\frac{1}{4} \frac{\partial u}{\partial t} - \left(1 + \varepsilon A e^{i\omega t} \right) \frac{\partial u}{\partial y} = \frac{\partial^2 u}{\partial y^2} + (Gr)\theta + (Gc)C - \left(M + \frac{1}{K} \right) u \quad (12)$$

$$\frac{1}{4}\frac{\partial\theta}{\partial t}-\left(1+\varepsilon Ae^{i\omega t}\right)\frac{\partial\theta}{\partial y}=\frac{1}{\Pr}\frac{\partial^2\theta}{\partial y^2} \tag{13}$$

$$\frac{1}{4}\frac{\partial C}{\partial t}-\left(1+\varepsilon Ae^{i\omega t}\right)\frac{\partial C}{\partial y}=\frac{1}{Sc}\frac{\partial^2 C}{\partial y^2}-k_r C \tag{14}$$

And the corresponding boundary conditions are

$$\left.\begin{array}{l} t\le 0:\ u=0,\ \theta=0,\ C=0\ \ for\ \ all\ \ y \\ t>0:\begin{cases} u=0,\ \theta=1+\varepsilon e^{i\omega t},\ C=1\ \ at\ \ y=0 \\ u\to 0,\ \theta\to 0,\ C\to 0\ \ as\ \ y\to\infty \end{cases} \end{array}\right\} \tag{15}$$

All the physical parameters are defined in the nomenclature.

It is now important to calculate the physical quantities of primary interest, which are the local wall shear stress, the local surface heat and mass flux. Given the velocity field in the boundary layer, we can now calculate the local wall shear stress (i.e., skin – friction) is given by and in dimensionless form, we obtain Knowing the temperature field, it is interesting to study the effect of the free convection and radiation on the rate of heat transfer. This is given by which is written in dimensionless form as

$$\tau=\frac{\tau_w}{\rho u_w^2},\ \tau_w=\left[\mu\frac{\partial u}{\partial y}\right]_{y'=0}=\rho v_o^2 u'(0)=\left[\frac{\partial u}{\partial y}\right]_{y=0} \tag{16}$$

The dimensionless local surface heat flux (i.e., Nusselt number) is obtained as

$$N_u(x')=-\left[\frac{x'}{(T_w'-T_\infty')}\frac{\partial T'}{\partial y'}\right]_{y'=0}\quad \text{Then } Nu=\frac{N_u(x')}{R_{e_x}}=-\left[\frac{\partial\theta}{\partial y}\right]_{y=0} \tag{17}$$

The definition of the local mass flux and the local Sherwood number are respectively given by with the help of these equations, one can write

$$S_h(x')=-\left[\frac{x'}{(C_w'-C_\infty')}\frac{\partial C'}{\partial y'}\right]_{y'=0}\quad \text{Then } Sh=\frac{S_h(x')}{R_{e_x}}=-\left[\frac{\partial C}{\partial y}\right]_{y=0} \tag{18}$$

Where $R_{e_x}=-\dfrac{v_o x'}{\nu}$ the Reynold is's number.

III. Method of solution

Equations (12) – (14) are coupled non – linear partial differential equations and are solved by using initial and boundary conditions (15). However, exact or approximate solutions are not possible for this set of equations. And hence we solve these equations by an implicit finite difference method of Crank – Nicolson type for a numerical solution. The equivalent finite difference scheme of equations (12) – (14) is as follows:

$$\frac{1}{4}\left(\frac{u_{i,\,j+1}-u_{i,\,j}}{\Delta t}\right)-B\left(\frac{u_{i+1,\,j}-u_{i,\,j}}{\Delta y}\right)=\frac{1}{2}\left(\frac{u_{i-1,\,j+1}-2u_{i,\,j+1}+u_{i+1,\,j+1}}{(\Delta y)^2}+\frac{u_{i-1,\,j}-2u_{i,\,j}+u_{i+1,\,j}}{(\Delta y)^2}\right)$$
$$-\frac{1}{2}\left(M+\frac{1}{K}\right)\left(\frac{u_{i,\,j+1}+u_{i,\,j}}{\Delta y}\right)+\frac{1}{2}(Gr)\left(\frac{\theta_{i,\,j+1}+\theta_{i,\,j}}{\Delta y}\right)+\frac{1}{2}(Gc)\left(\frac{C_{i,\,j+1}+C_{i,\,j}}{\Delta y}\right) \tag{19}$$

$$\frac{1}{4}\left(\frac{\theta_{i,\,j+1}-\theta_{i,\,j}}{\Delta t}\right)-B\left(\frac{\theta_{i+1,\,j}-\theta_{i,\,j}}{\Delta y}\right)=\frac{1}{2\Pr}\left(\frac{\theta_{i-1,\,j+1}-2\theta_{i,\,j+1}+\theta_{i+1,\,j+1}}{(\Delta y)^2}+\frac{\theta_{i-1,\,j}-2\theta_{i,\,j}+\theta_{i+1,\,j}}{(\Delta y)^2}\right) \tag{20}$$

$$\frac{1}{4}\left(\frac{C_{i,\,j+1}-C_{i,\,j}}{\Delta t}\right)-B\left(\frac{C_{i+1,\,j}-C_{i,\,j}}{\Delta y}\right)=\frac{1}{2Sc}\left(\frac{u_{i-1,\,j+1}-2u_{i,\,j+1}+u_{i+1,\,j+1}}{(\Delta y)^2}+\frac{u_{i-1,\,j}-2u_{i,\,j}+u_{i+1,\,j}}{(\Delta y)^2}\right)$$
$$-\frac{1}{2}(k_r)\left(\frac{C_{i,\,j+1}+C_{i,\,j}}{\Delta y}\right) \tag{21}$$

Here the suffix i corresponds to y and j corresponds to t. Also $B = 1 + \varepsilon A e^{i\omega t}$, $\Delta t = t_{j+1} - t_j$ and $\Delta y = y_{i+1} - y_i$

The complete solution of the discrete equations (19) – (21) proceeds as follows:

Step – (1): Knowing the values of C, θ and u at a time $t = j$, calculate C and θ at a time $t = j+1$ using equations (20) and (21) and solving tri – diagonal linear system of equations.

Step – (2): Knowing the values of θ and C at time $t = j$, solve the equation (19) (*via* tri – diagonal matrix inversion) to obtain u at a time $t = j+1$.

We can repeat steps (1) and (2) to proceed from $t = 0$ to the desired time value.

The implicit Crank – Nicolson method is a second order method $\left(o\left(\Delta t^2\right)\right)$ in time and has no restrictions on space and time – steps, Δy and Δt, *i.e.*, the method is unconditionally stable. The finite differences scheme used, involves the values of the function at the six grid points. A linear combination of the "future" points is equal to another linear combination of the "present" points. To find the future values of the function, one must solve a system of linear equations, whose matrix has a tri – diagonal form.

The computations were carried out for $Gr = 1.0, Gc = 1.0, \Pr = 0.71$ (Air), $Sc = 0.22$ (Hydrogen), $M = 1.0$, $K = 1.0, A = 1.0, \varepsilon = 0.001, \omega t = \frac{\pi}{4}, k_r = 1.0$, $t = 1.0$ and $\Delta y = 0.1, \Delta t = 0.001$ and the procedure is repeated till $y =$ 4. In order to check the accuracy of numerical results, the present study is compared with the available theoretical solution of Seethamahalakshmi *et al*. [20] and they are found to be in good agreement.

IV. Results and Discussions

In the preceding sections, the problem of chemical reaction effects on an unsteady MHD free convection flow past an infinite vertical porous plate with constant suction was formulated and the dimensionless governing equations were solved by means of a finite difference method. In the present study we adopted the following default parameter values of finite difference computations: $Gr = 1.0$, $Gc = 1.0$, $\Pr = 0.71$ (Air), $Sc = 0.22$ (Hydrogen), $M = 1.0$, $K = 1.0$, $A = 1.0$, $\varepsilon = 0.001, \omega t = \frac{\pi}{4}$, $k_r = 1.0$ and $t = 1.0$. All graphs therefore correspond to these values unless specifically indicated on the appropriate graph.

The influence of thermal Grashof number, Gr, on the velocity is shown in Figure (1). The thermal Grashof number signifies the relative effect of the thermal buoyancy force to the viscous hydrodynamic force. The flow is accelerated due to the enhancement in buoyancy force corresponding to an increase in the thermal Grashof number. The positive values of Gr correspond to cooling of the plate by natural convection. Heat is therefore conducted away from the vertical plate into the fluid which increases the temperature and thereby enhances the buoyancy force. In addition, it is seen that the peak values of the velocity increases rapidly near the plate as thermal Grashof number increases and then decays smoothly to the free stream velocity. Figure (2) presents typical velocity profiles in the boundary layer for various values of the solutal Grashof number, Gc. The solutal Grashof number Gc defines the ratio of the species buoyancy force to the viscous hydrodynamic force. It is noticed that the velocity increases with increasing values of the solutal Grashof number.

Figures (3) and (8) show the behavior of velocity and temperature profiles for different values Prandtl number. The numerical results show that the effect of increasing values of Prandtl number results in a decreasing velocity. It is observed that an increase in the Prandtl number results a decrease of the thermal boundary layer thickness and in general lower average temperature within the boundary layer. The reason is that smaller values of $\Pr$ are equivalent to increase in the thermal conductivity of the fluid and therefore, heat is able to diffuse away from the heated surface more rapidly for higher values of $\Pr$. Hence in the case of smaller Prandtl number as the thermal boundary later is thicker and the rate of heat transfer is reduced. The effect of Schmidt number Sc on the velocity and concentration are shown in figures (4) and (9). As the Schmidt number increases, the velocity and concentration decreases. This causes the concentration buoyancy effects to decrease yielding a reduction in the fluid velocity. Reductions in the velocity and concentration distributions are accompanied by simultaneous reductions in the velocity and concentration boundary layers.

The effect of Hartmann number, M on the velocity is shown in figure (5). The velocity decreases with an increase in the Hartmann number. It is because that the application of transverse magnetic field will result a resistive type force (Lorentz force) similar to drag force which tends to resist the fluid flow and thus reducing its velocity. Also, the boundary layer thickness decreases with an increase in the Hartmann number. Figure (6) shows the effect of the permeability of the porous medium parameter, K on the velocity distribution. As shown, the velocity is increasing with the increasing dimensionless porous medium parameter. The effect of the dimensionless porous medium K becomes smaller as K increase. Physically, this result can be achieved when the holes of the porous medium may be neglected. Figures (7) and (10), illustrate the behavior velocity and concentration for different values of chemical reaction parameter, k_r. It is observed that an increase in leads to a decrease in both the values of velocity and concentration. A distinct velocity escalation occurs

near the wall after which profiles decay smoothly to the stationary value in free stream. Chemical reaction therefore boosts momentum transfer, i.e., accelerates the flow.

The profiles for skin – friction (τ) due to velocity under the effects of Grashof number (Gr), Modified Grashof number (Gc), Prandtl number $(\Pr)$, Schmidt number (Sc), Hartmann number (M), Permeability parameter (K) and Chemical reaction parameter (k_r) are presented in the table – 1 respectively. We observe from this table – 1, the skin – friction (τ) increases under the effects of Grashof number (Gr), Modified Grashof number (Gc) and Permeability parameter (K). And decreases under the effects of Prandtl number $(\Pr)$, Schmidt number (Sc), Hartmann number (M) and Chemical reaction parameter (k_r)

Table – 1: Skin – friction results (τ) for the values of Gr, Gc, $\Pr$, Sc, M, K and k_r

Gr	Gc	$\Pr$	Sc	M	K	k_r	τ
1.0	1.0	0.71	0.22	1.0	1.0	1.0	5.8411
2.0	1.0	0.71	0.22	1.0	1.0	1.0	8.9829
1.0	2.0	0.71	0.22	1.0	1.0	1.0	8.5404
1.0	1.0	7.00	0.22	1.0	1.0	1.0	4.4432
1.0	1.0	0.71	0.30	1.0	1.0	1.0	5.7113
1.0	1.0	0.71	0.22	2.0	1.0	1.0	4.5870
1.0	1.0	0.71	0.22	1.0	2.0	1.0	6.8033
1.0	1.0	0.71	0.22	1.0	1.0	2.0	5.5172

Table – 2: Rate of heat transfer (Nu) values for different values of $\Pr$ and Rate of mass transfer (Sh) values for different values of Sc and k_r

$\Pr$	Nu	Sc	k_r	Sh
0.71	7.7337	0.22	1.0	6.7401
7.00	4.9322	0.30	1.0	6.4490
		0.22	2.0	6.0074

The profiles for Nusselt number (Nu) due to temperature profile under the effect of Prandtl number $(\Pr)$is presented in the table – 2. From this table we observe that, the Nusselt number (Nu) due to temperature profiles decreases under the effect of Prandtl number $(\Pr)$. The profiles for Sherwood number (Sh) due to concentration profiles under the effect of Schmidt number (Sc) and Chemical reaction parameter (k_r) are presented in the table – 2. We see from this table the Sherwood number (Sh) due to concentration profiles decreases under the effects of Schmidt number (Sc) and Chemical reaction parameter (k_r).

Table – 3: Comparison of present Skin – friction results (τ) with the Skin – friction results (τ^*) obtained by Seethamahalakshmi *et al*. [20] for different values of Gr, Gc, $\Pr$, Sc, M and K

Gr	Gc	$\Pr$	Sc	M	K	τ	τ^*
1.0	1.0	0.71	0.22	1.0	1.0	4.5517	4.5508
2.0	1.0	0.71	0.22	1.0	1.0	6.2941	6.2931
1.0	2.0	0.71	0.22	1.0	1.0	6.5403	6.5397
1.0	1.0	7.00	0.22	1.0	1.0	3.9954	3.9922
1.0	1.0	0.71	0.30	1.0	1.0	4.2225	4.2216
1.0	1.0	0.71	0.22	2.0	1.0	3.8467	3.8449
1.0	1.0	0.71	0.22	1.0	2.0	4.9277	4.9260

In order to ascertain the accuracy of the numerical results, the present results are compared with the previous results of Seethamahalakshmi *et al*. [20] for Gr = Gc = 1.0, $\Pr$ = 0.71, Sc = 0.22, M = 1.0 and K = 1.0 in table – 3. They are found to be in an excellent agreement.

V. Conclusions

In this paper, the chemical reaction effects on an unsteady MHD free convection flow past an infinite vertical porous plate with variable suction was considered. The non – dimensional governing equations are solved with the help of finite difference method. The conclusions of the study are as follows:

1. The velocity increases with the increase in thermal Grashof number, solutal Grashof number and Permeability parameter.
2. The velocity decreases with an increase in the Hartmann number.
3. An increase in the Prandtl number decreases the velocity and temperature.
4. The velocity as well as concentration decreases with an increase in the Schmidt number.
5. The velocity as well as concentration decreases with an increase in the chemical reaction parameter.
6. The skin – friction increases with the increase in thermal Grashof number, solutal Grashof number and Permeability parameter.
7. The skin – friction decreases with an increase in the Hartmann number, Prandtl number, Schmidt number and Chemical reaction parameter.
8. An increase in the Prandtl number decreases the Nusselt number.
9. The Sherwood number decreases with an increase in the Schmidt number and Chemical reaction parameter.
10. On comparing the skin – friction (τ) results with the skin – friction (τ^*) results of Seethamahalakshmi *et al*. [20] it can be seen that they agree very well.

References

[1] Abreu, C. R. A., Alfradique, M. F. And Silva Telles, A., 2006. Boundary layer flows with Dufour and Soret effects: I: Forced and natural convection, Chemical Engineering Science, Vol. 61, Np. 13, pp. 4282 – 4289.

[2] Afify, A. A., 2009. Similarity solution in MHD: Effects of thermal diffusion and diffusion thermo on free convective heat and mass transfer over a stretching surface considering suction or injection, Communications in Nonlinear Science and Numerical Simulation, Vol. 14, No. 5, pp. 2202 – 2214.

[3] Beg, O. A., Bhargava, R., Rawat, S., Takhar, H. S. and Beg, T. A., 2007. A study of buoyancy – driven dissipative micropolar free convection heat and mass transfer in a Darcian porous medium with chemical reaction, Nonlinear Analysis: Modeling and Control J., Vol. 12, No. 2, pp. 157 – 180.

[4] Beg, O. A., Zueco, J. and Takhar, H. S., 2009. Unsteady magnetohydrodynamic Hartmann – Couette flow and heat transfer in a Darcian channel with Hall current, ion slip, viscous and Joule heating effects: network numerical solutions, Communications Nonlinear Science Numerical Simulation, Vol. 14, No. 4, pp. 1082 – 1097.

[5] Chaudhary, R. C., Goyal, M. C., Jain, A., 2009. Free convection effects on MHD flow past an infinite vertical accelerated plate embedded in porous media with constant heat flux, Matematicas Ensenanza Universitaria, Vol. 17, No. 2, pp. 73 – 82.

[6] Chin, K. E., Nazar, R., Arifin, N. M. and Pop, I., 2007. Effect of variable viscosity on mixed convection boundary layer flow over a vertical surface embedded in a porous medium, International Communications in Heat and Mass Transfer, Vol. 34, No. 4, pp. 464 – 473.

[7] Das, S. S. And Mitra, M., 2009. Unsteady mixed convective MHD flow and mass transfer past an accelerated infinite vertical plate with suction, Ind. J. Sci. Tech., Vol. 2, No. 5, pp. 18 – 22.

[8] Das, S. S., Satapathy, A., Das, J. K. and Panda, J. P., 2009. Mass transfer effects on MHD flow and heat transfer past a vertical porous plate through a porous medium under oscillatory suction and heat source, Int. J. Heat Mass Transfer, Vol. 52, pp. 5962 – 5969.

[9] Das, S. S., Satapathy, A., Das, J. K. and Sahoo, S. K., 2007. Numerical solution of unsteady free convective MHD flow past an accelerated vertical plate with suction and heat flux, J. Ultra Sci. Phys. Sci., Vol. 19, No. 1, pp. 105 – 112.

[10] Das, S. S., Sahoo, S. K. and Dash, G. C., 2006. Numerical solution of mass transfer effects on an unsteady flow past an accelerated vertical porous plate with suction, Bull. Malays. Math. Sci. Soc., Vol. 29, No. 1, pp. 33 – 42.

[11] Gireesh kumar, J., Satyanarayana, P. V. and Ramakrishna, S., 2009. Effects of chemical reaction and mass transfer on MHD unsteady free convection flow past an infinite vertical plate with constant suction and heat sink, J .Ultra Scientist, Vol. 21, No. 3, pp. 12 – 28.

[12] Hayat, T., Mustafa, M. and Pop, I., 2010. Heat and mass transfer for Soret and Dufour effects on mixed convection boundary layer flow over a stretching vertical surface in a porous medium filled with a visco – elastic fluid, Communications in Nonlinear Science and Numerical Simulation, Vol. 15, No. 5, pp. 1183 – 1196

[13] Ibrahim, F. S., Elaiw, A. M. and Bakr, A. A., 2008. Effect of the chemical reaction and radiation absorption on the unsteady MHD free convection flow past a semi infinite vertical permeable moving plate with heat source and suction, Communications Nonlinear Science Numerical Simulation, Vol. 13, No. 6, pp. 1056 – 1066.

[14] Kim, Y. J., 2008. Unsteady MHD convective heat transfer past a semi – infinite vertical porous moving plate with variable suction, Int. J. Engg. Sci., Vol. 38, pp. 833 – 845.

[15] Patil, P. M. and Kulkarni, P. S., 2008, Effects of chemical reaction on free convection flow of a polar fluid through a porous medium in the presence of internal heat generation, International Journal of Thermal Sciences, Vol. 47, pp. 1043 – 1053.

[16] Rahman, M. M. and Sattar, M. A., 2006. MHD convective flow of a micropolar fluid past a continuously moving vertical porous plate in the presence of heat generation/absorption, J. Heat Transfer, Vol. 17, pp 85 – 90.

[17] Sarangi, K. C. and Jose, C. B., 2005. Unsteady free convective MHD flow and mass transfer past a vertical porous plate with variable temperature, Bull. Cal. Math. Soc., Vol. 97, No. 2, pp. 137 – 146.

[18] Seddeek, M. A. and Salama, F. A., 2007. The effect of temperature dependent viscosity and thermal conductivity on unsteady MHD convective heat transfer past a semi – infinite vertical porous plate, J. computational Materials Sci., Vol. 40, pp. 186 – 192.

[19] Seddeek, M. A., Darwish, A. A. and Abdelmeguid, M. S., 2007. Effects of chemical reaction and variable viscosity on hydromagnetic mixed convection heat and mass transfer for Hiemenz flow through porous media with radiation, Communications in Nonlinear Science and Numerical Simulation, Vol. 12, No. 2, pp. 195 – 213.

[20] Seethamahalakshmi, Prasad, B. D. C. N. and Ramana Reddy, G. V., 2012. MHD free convective mass transfer flow past an infinite vertical porous plate with variable suction and Soret effect, Asian Journal of Current Engineering and Maths, Vol. 1, No. 2, pp. 49 – 55.

[21] Srihari, K., Anand Rao, J. and Kishan, N., 2006. MHD free convection flow of an incompressible viscous dissipative fluid in an infinite vertical oscillating plate with constant heat flux, Jl. Energy, Heat and Mass Transfer, Vol. 28, pp. 19 – 28.

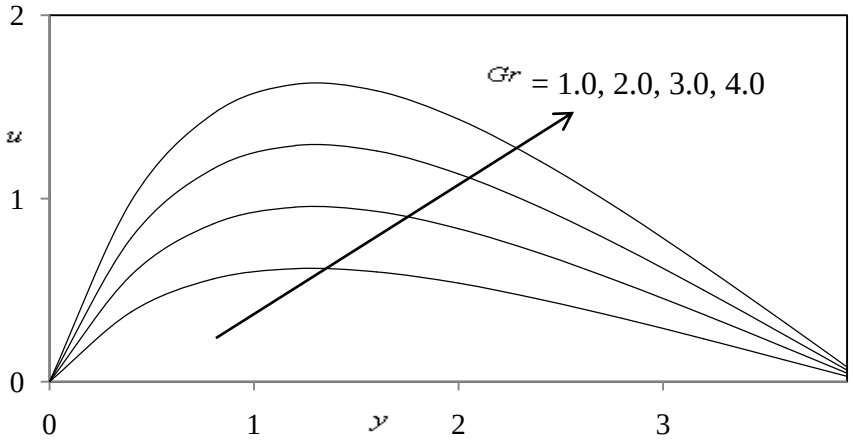

Figure 1. Velocity profiles for different values of Gr

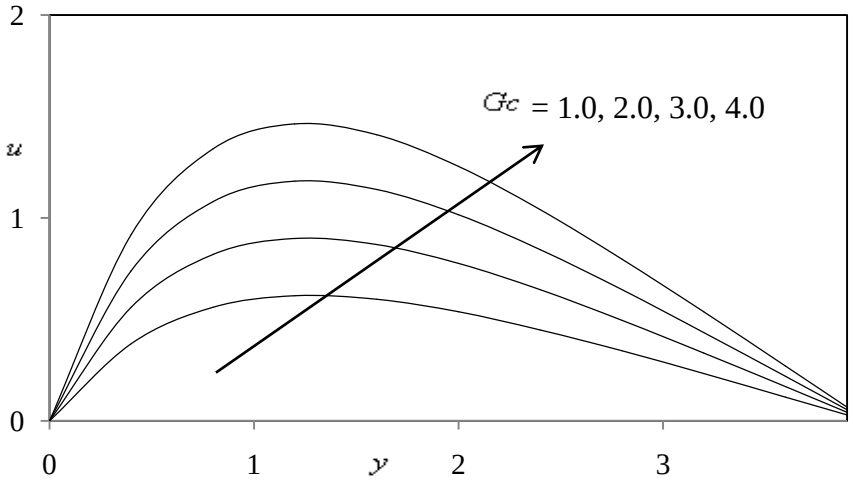

Figure 2. Velocity profiles for different values of Gc

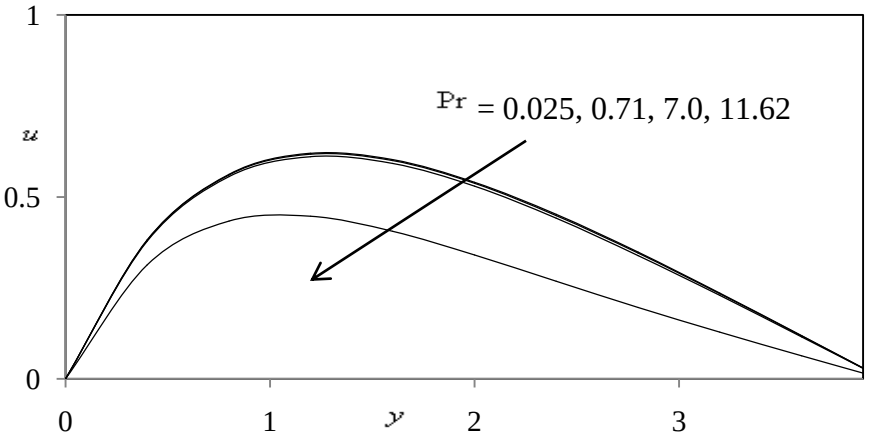

Figure 3. Velocity profiles for different values of Pr

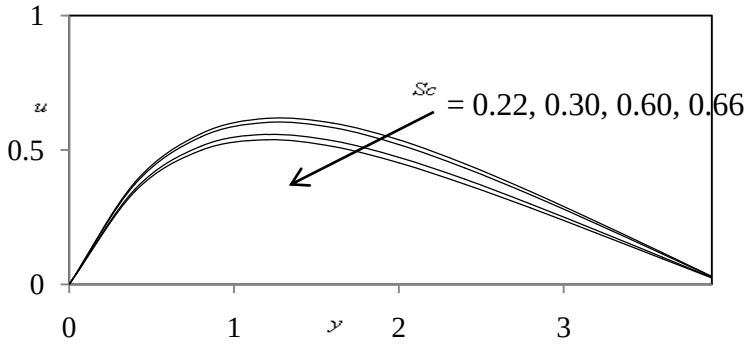

Figure 4. Velocity profiles for different values of Sc

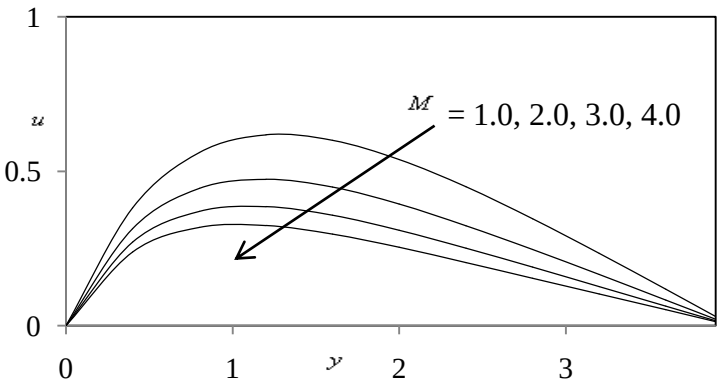

Figure 5. Velocity profiles for different values of M

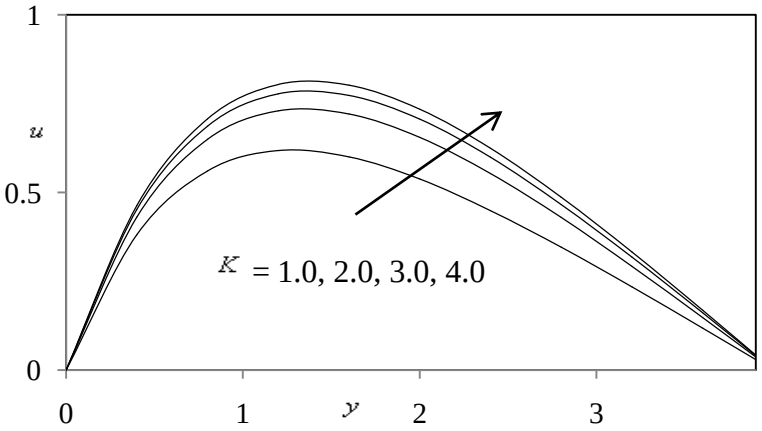

Figure 6. Velocity profiles for different values of K

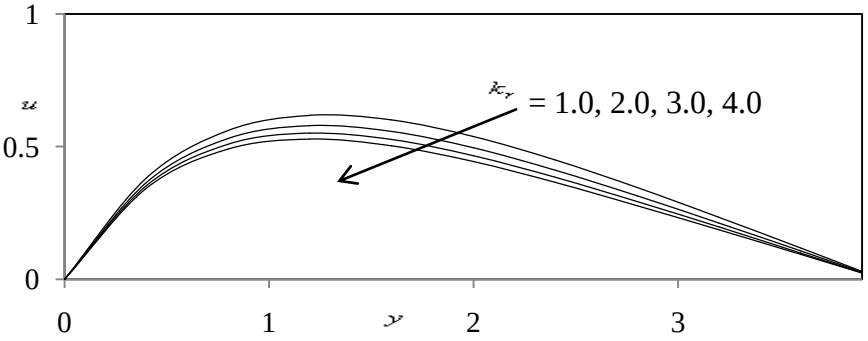

Figure 7. Velocity profiles for different values of k_r

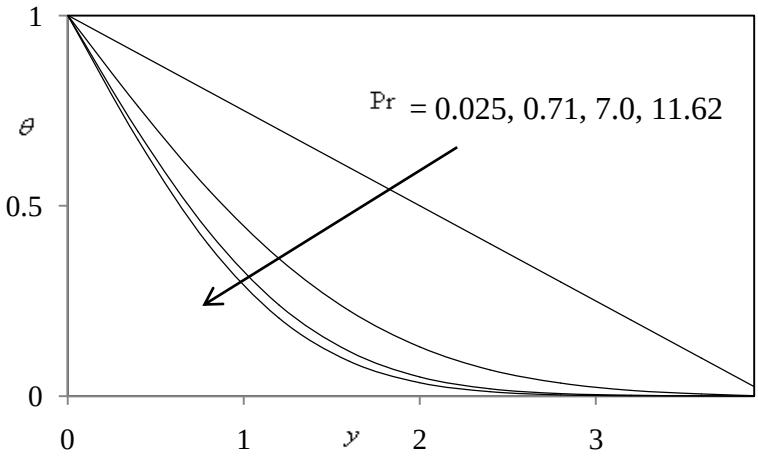

Figure 8. Temperature profiles for different values of Pr

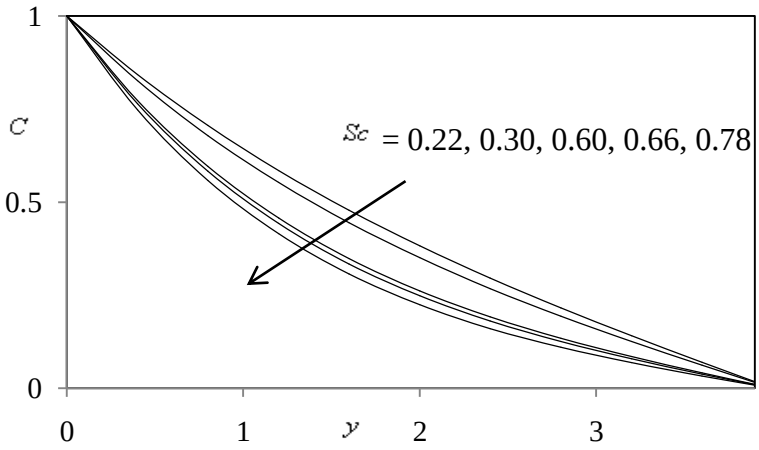

Figure 9. Concentration profiles for different values of Sc

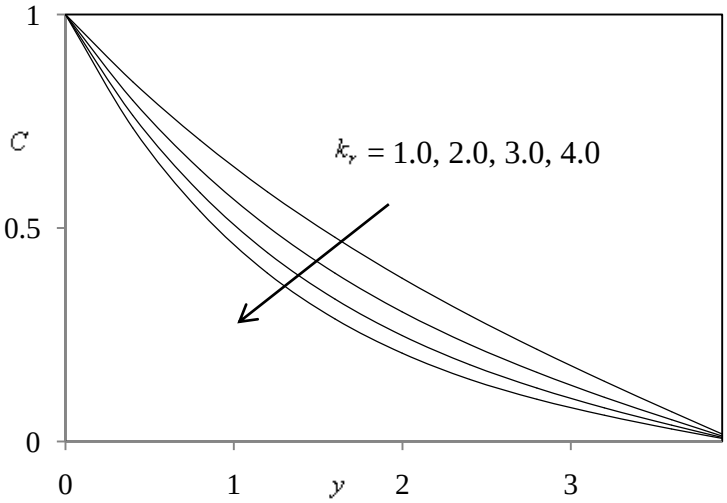

Figure 10. Concentration profiles for different values of k_r

International Journal of Modern Engineering Research (IJMER)
www.ijmer.com Vol.3, Issue.2, March-April. 2013 pp-736-738 ISSN: 2249-6645

Study and Minimization of Surface Defects on Bars and Wire Rod Originated in Continuous Cast Billets

Dinesh Dekate, [1] Prof. B.D. Deshmukh, [2] Sarang Khedkar[3]
[123]*(Department of Mechanical Engineering, Yashawantrao Chavan College of Engineering, Nagpur, India)*

Abstract: *In order to minimize surface defects in long products, their origin needs to be assessed .To this purpose a methodology was developed, that includes metallographic studies on bars and wire rod using several reagents. A description is made of the different steps involved in this method, including the use of etchants to determine the former position of the defect in the billet, it is also discussed the interpretation given to internal oxidation, scale inside the defect, decarburization, and other metallographic features. A discussion of pin holes and transverse cracks on billet is made, taking into accounts its aspect and metallographic features on billet, the evolution during reheating and rolling and the final aspect and metallographic features on bar/wire rod. Root causes of these defects and solutions recommended are analyzed for each case.*

Keywords: *Continuous Casting, Billet Casting, Cast Defects, Rolling, Surface Defects*.

I. INTRODUCTION

Casting of carbon steel billets for commercial products usually implies silicon and manganese oxidation, and is mostly carried out with metering nozzle and powder lubrication. Under these conditions, surface defects are often detected in rolled products.

So, finding of the defect in the rolled products is helpful in keeping control of casting conditions. A methodology is used to reached this aim was developed at Mahalaxmi TMT steel plant along the time, as troubleshooting work for several plants was carried out. The paper is based on experience made by own while troubleshooting defect problems in carbon steel long products at several rolling mills.

II. METHODOLOGY TO DETERMINE THE ORIGIN OF DEFECTS

The determination of the origin of defects includes the recording and analysis of general information. It is important to know the frequency of defect, position in same corner or face of the billet, position in bar or wire rod. It is also relevant an exhaustive study of the general appearance of the defect by naked eye or with magnifying glass. After that, the observation of polished samples, generally transverse cuts of the rolled products or of the billet and microscopic study at higher magnification, etching with reagents give insight defects features. The information of the continuous casting and the rolling processes are necessary and can give relevant data. Sometimes it could be important to design the follow up of heats in the metal shop and rolling mill processes. The general criteria are summarized in Table 1.

TABLE I

Tasks	Information
General information	Frequency, position, in one of the strands or in one of the faces of the billet, position in wire rod, influence of some steel grade, etc.
Microscopic study	With the necked eye or helped with magnifying glass, polished sample observation, transverse cuts in rolled products & billets, etching with reagents.
Process information	Routine data from Rolling Mill & Steel Melting Shop(CCM)
Own Background	Search for similar defects in own reports and from other plants like Nilesh steel Jalana.
Physical simulation	Generally it has only academic interest or for preventing the problem from repetition in the future.

III. METALLOGRAPHIC OBSERVATIONS

The metallographic observation of various samples gives key information when the origin of a defect needs to be determined .often; it is not possible to find out the origin of defect with just observation of transverse cuts under microscope, without an idea of the general aspect of the defect. In Table 2 different techniques for the study of the defects and the information that can be taken from them, regarding to the origin of defects are monitored.

TABLE II: Study of defect and information regarding origin

Observation type	Information obtained
With naked eye or with magnifying glass	Oxygen Penetration (pin holes) due to internal oxidation after cutting billet samples, location on billet corner and mid way cracks.
As polished	Micro inclusions, Irregular solidification structure
Etching by HCL	Decarburization, segregation

IV. DEFECT ANALYZED

4.1. PIN HOLES:

Pin holes are observed often for semi-killed steels cast with casting powder. It can give a place to defects in the final product if there is an important number in a small area or if they penetrate deep in the billet.

4.1.1 APPEARANCE IN BILLET:

Figure 1 and 2 shows pin holes in billet surface after continuous casting forming a deep penetration of 50 mm repeating on each strand.

Fig I: Aspect of pin holes on the surface of a billet cast with casting powder observed by magnifying glass

Fig II: Aspect of pin holes on the surface of a billet cast with casting powder observed by naked eye.

The pin hole have a characteristic look showing in Figure I and Figure II which is due to development of scale and certain degree of decarburization.

4.1.2 ASPECT DURING ROLLING:

Figure III shows the defect on rolled bar of the billet having deep pin hole

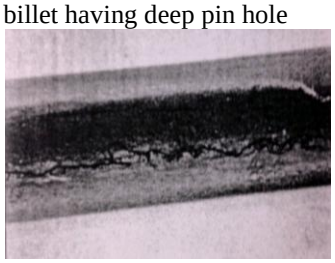

Fig III: Defect on rolled bar the billet having deep pin hole.

Most pin holes on surface of billet disappears during reheating due to scale formation, but the deeper pin holes are yet observed necked eye on the billet after reheating, they are difficult to rolled.

4.1.3 CAUSES AND SOLUTIONS.

Formation of pinholes is mostly related to evolution of gases resulting from casting powder decomposition during casting and can be enhanced by high oxygen activity in the liquid steel. Normal figures for lubrication rate are 20 to 30 gm/min, depending on powder properties, billet size and casting speed .To minimize pinhole formation it is important not only to check if lubrication rate is within the usual range, but also verify if the powder distribution in the transverse section is homogeneous. Good distribution of casting powder is very important and to avoid excessive use of lubrication in corners.

4.2 TRANSVERSE CRACKS:

Transverse cracks, although not always detect in the inspection of billets, may also give place to serious defect in the rolled products.

4.2.1 APPEARANCE IN BILLET

Figure IV and Figure V shows the aspect of transverse cracks in continuous casted billets observed by magnifying glass and by HCL etching closed to a surface, the cracks are looks as if it has been formed at high temperature, probably in the mould.

Fig IV: Transverse cracks on observed by magnifying glass

Fig V: Transverse cracks on observed after etching with HCL

4.2.2 ASPECT DURING ROLLING:

Transverse cracks during rolling gave place to V defects which is shown in Figure VI.

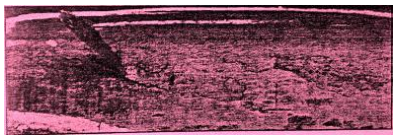

Fig VI: Evolution of transverse cracks during rolling, forming V defect

In transverse cut, they display a change in the direction for high reduction ratios.

4.2.3 CAUSES AND SOLUTIONS

Transverse cracks can form in the mould or during strengthening. When they are located in any corner, they are likely to be formed due to tensile effort related to sticking, this can be worsen by deep oscillation marks When the cracks are present only in the corner belonging to inner radius, they could be formed by tensile efforts during strengthening. This is common when corner temperature is within low ductility range. A sound approach to solve the problem is to set proper secondary cooling to avoid the dangerous temperature range in the corners during strengthening.

V. CONCLUSION

A methodology to study effects in carbon steel long products was developed at Sidhabali Ispat Chandrapur and Vinas Rolling Mill Hingna, Nagpur (India) while troubleshooting defect problems for iron and steel industry- Mahalaxmi TMT, Wardha, India.

For the study of defects many lab technique were developed that allow having different tools when the step where the defect was originated is to be determined. This way, it is much easier to take action in the plant in order to minimize a given defect.

This is exemplified with two defects commonly encountered when billets are cast with casting powder as lubricant: Pinholes and transverse cracks.

VI. ACKNOWLEDGEMENTS

The authors are thankful to Mr. C. R. DAD (CEO) Mahalaxmi TMT Deoli, Wardha, for their assistance with the trials, support and valuable discussions.

REFERENCES

Journal Papers:

[1] I.A.Bakshi , J.L. Brendzy ,N.Walkar, I.V. Shrivastava and J.K.Brimakombe “Iron making and steel making “No 11993, 54 – 62.
[2] J.L.Brendzy, I.A.Bakshi, N.Walkar, I.V. Shrivastava and J.K.Brimakombe “Iron making and steel making” No 11993, 63 – 74.
[3] Brian G. Thomas, “Detection of Quality Problems in Continuous Casting of Steel" No 1206 Nov 2010, 29-45
[4] L. Reda, C. Genzano, J. Madias. “Electric Furnace Conference Proceedings” 2001, 771-780.
[5] J. K. Brimacombe, I. V. Samarasekera. “Course on Continuous Casting of Billets, Blooms and Slabs”. IAS, San Nicolas, Argentina, November 1994, 22-25.

Books:

[6] Dr.R.H. Tupkary and V.R.Tupkary. “Modern Steel Making” 40-60.

International Journal of Modern Engineering Research (IJMER)
www.ijmer.com Vol.3, Issue.2, March-April. 2013 pp-739-746 ISSN: 2249-6645

Flow Physics Analysis of Three-Bucket Helical Savonius Rotor at 90^0 Twist Angle Using CFD

Pinku Debnath, [1] Rajat Gupta[2]
[12]*Mechanical Engineering, / National Institute of Technology, Silchar, India*

Abstract: *In this research work the flow behavior was analyzed, which affect the power coefficient as well as torque coefficient of a helical Savonius rotor is investigated by means of commercial code CFD. Conventional three bladed Savonius rotors have high coefficient of static torque at certain rotor angles and negative coefficient of static torque at certain rotor angle. In order to increase the efficiency of all rotor angles the system a helical Savonius rotor with a twist of certain proposed degree is introduced. A three-dimensional model of* 90^0 *twist three blades helical Savonius rotor at* 0^0, 60^0, 120^0 *and* 150^0 *rotor angle has been constructed by using the software gambit of the Fluent 6.3 package. The contours of static pressure and velocity magnitude around the rotor blades area at horizontal iso-plane is obtained from the CFD simulation. High performance was obtained at advanced bucket in upstream air flow at* 60^0 *rotor angle and maximum positive static pressure obtained at* 150^0 *rotor angle, which affect the positive coefficient of static torque.*

Keywords: *Helical Savonius rotor, rotor angle, CFD analysis, velocity contour, and static pressure contour.*

I. INTRODUCTION

The Savonius rotor is a vertical axis wind turbine (VAWT) originally invented by a Finnish engineer Sigurd J. Savonius in 1922 [1]. N. Fulisawa observed the relation between rotor performance and flow characteristics field around a Savonius rotor by using a laser light sheet and a CCD camera with a shutter speed of 0.002s [2]. Nobuyuki Fujisawa measured the flow fields in an around Savonius rotors at various overlap ratios with particle imaging velocimetry technology and comparison analysis is conducted between a vertical-axis spiral rotor and a conventional Savonius rotor by using CFD technology [3]. The flow field around a Savonius rotor, which is closely related to the torque and the power performance of the rotor, has been investigated by many researchers to clarify the power mechanism of the rotor. Most investigations have been experimental studies with flow visualization techniques, such as tufts [4, 5]. The flow physics of the rotor with overlap variation 12.37% to 25.87% were analysed with the help of velocity and pressure contours of the rotor. From this analysis the overlap of 19.87% was the optimum overlap condition at which pressure and velocity differences across the rotor were the highest for which maximum power extraction by the rotor would be possible at that overlap condition [6]. The combination of Darrieus and Savonius rotors thus exhibits high starting torque and high power coefficient. Keeping the above points they have made to study the flow physics of a combined three-bucket Darrieus and Savonius rotor using Fluent 6.0. They have considered four overlap conditions between 10.87% to 25.87% for the Savonius part of the combined rotor and observed highest relative speed and highest pressure of the combined rotor near its top at 15.37% overlap condition [7]. M.A.Kamoji et al. [8] performed the static torque coefficients at all the rotor angles for helical Savonius rotors are positive. However, for conventional Savonius rotor, there are several rotor angles at which static torque coefficient is negative. Conventional Savonius rotor configurations with steady two-dimensional RANS CFD simulations were also conducted by Gupta et al. in which static torque predictions for a Savonius rotor with external flow Control demonstrated good agreement with the corresponding experimental wind tunnel results [9]. Gupta et al. [10] has also been observed that the aerodynamic performance and optimum overlap of the combined rotor are strongly controlled by the flow physics of the individual rotors. Katsuya I et al. [11] simulated numerically the flow over a two-bucket Savonius rotor by solving 2D finite volume equations using an upwind scheme for unstructured mesh. The result shows good matching with the experimental values of power coefficient, aerodynamic coefficients. M., Manzoor Hussain, Mehdi et al. [12] conducted the enhancement of efficiency by modifying the blades configuration from straight semicircular to a twisted semi circular one. Wind flow analysis was done over each configuration of the rotor with the blade twist ranging from 5^0 to 60^0 in a steps of 5^0. Maximum efficiency is obtained 33.85% at 45^0 twist angle, when compared to 25.6% without twist. A fully automatic optimization finally takes place, the commercial tool Gambit for geometry and grid generation (including quality check) and the industrial CFD code ANSYS-Fluent to compute the flow field around the Savonius rotor [13].

II. DESCRIPTION OF PHYSICAL MODEL

In the present research work, the performance of a three-bucket helical Savonius rotor with semicircular profiles buckets at 90° twist angle as shown in Figure- 1 was analyzed. The operation of the rotor is simulated with the variation in rotor angle at0^0, 60^0, 120^0 and 150^0. The diameter of the rotor has a value of 24cm, while the value of the rotor height is 40cm. The thickness of the buckets is 3 mm.

III. DETAILS OF COMPUTATIONAL DOMAIN

The three dimensional computational domain of three-bladed helical Savonius rotor along with the boundary conditions is shown in the Figure- 2. The computational domain resembles was 60cm x 60cm in cross-section. Wind speed was considered on the inlet face ABCD, outflow was considered on the outlet face EFGH, symmetry condition was considered for the side walls of the computational domain and blades are consider as rotating wall. The computational domain was adopted of the unstructured hexahedral mesh and the moving mesh techniques in Figure- 3. The computations were initially carried out with various levels of refinement of mesh which is done in gambit of the Fluent 6.3 package. The number of cells and nodes involved in meshing of the rotor with various levels are given in Table 1. The grid independent limit computational mesh (Masson eta al., 1997) [14] was obtained by changing the resolution of mesh at all important areas of the rotor which is shown in the Figure- 4.

3.1 Computational Domain Discretization Method:

The continuity equation, Newton's second law, the conservation of momentum equation (N-S equation) and realizable k-ε turbulence model are numerically solved by the commercial software FLUENT 6.3. Finite Volume Method is used for discretizing a differential equation and computes the static pressure and velocity fields of the flow on the rotor buckets. Applying the discretizing techniques the computational domain divided into a finite number of elementary control volumes. The sequential algorithm, Semi-Implicit Method for Pressure-Linked Equation (SIMPLE), was used for solving all the scalar variables with the k-ε turbulence model. The finite volume discretization transforms the differential equations governing the flow in a linear system of algebraic equations that is iteratively solved.

3.2 Mathematical Formulation:

In the present study, the results were obtained by applying the Finite Volume Method to solve the conservation equations of the turbulent air flow on the helical Savonius rotor, which allows the calculation of the performance of the rotor. Among these conservation equations, there is the mass balance equation. The Eq. (1) with indicial notation represents the mass balance, where ρ is the density, $\vec{V}$ is the velocity vector and value of $\vec{S}_m$ is zero for steady-state flow.

$$\frac{\partial \rho}{\partial t} + \nabla . (\rho \vec{V}) = \vec{S}_m = 0 \qquad (1)$$

The momentum equation must be solved along with the mass balance equation. The Eq. (2) represents the momentum equation, where ρ is the density, $\vec{V}$ is the velocity vector, p is the static pressure, and $\bar{\bar{\tau}}$ is the stress tensor (described below), and $\rho\vec{g}$ and $\vec{F}$ are the gravitational body force and external body forces (e.g., that arise from interaction with the dispersed phase), respectively.

$$\frac{\partial}{\partial t}(\rho \vec{V}) + \nabla . (\rho \vec{V} \vec{V}) = - \nabla p + \nabla . \bar{\bar{\tau}} + \rho \vec{g} + \vec{F} \qquad (2)$$

The stress tensor is given by

$$\bar{\bar{\tau}} = \mu [(\nabla . \vec{V} + \nabla . \vec{V}^T) - \frac{2}{3} \nabla . \vec{V} I] \qquad (3)$$

Where μ is the molecular viscosity, I is the unit tensor, and the second term on the right hand side is the effect of volume dilation.

3.3 Turbulence Model:

The realizable k-ε turbulence model provides superior performance for flows involving rotation, boundary layers under strong adverse pressure gradients, separation, and recirculation. The modeled transport equations for k and ε in the realizable k-ε model are:

$$\frac{\partial (\rho k)}{\partial t} + \frac{\partial (\rho k u_j)}{\partial x_j} = \frac{\partial}{\partial x_j} [(\mu + \frac{\mu_t}{\sigma_k}) \frac{\partial k}{\partial x_j}] + G_k + G_b - \rho_\varepsilon - Y_M + S_k \qquad (4)$$

and

$$\frac{\partial (\rho \varepsilon)}{\partial t} + \frac{\partial (\rho \varepsilon u_i)}{\partial x_i} = \frac{\partial}{\partial x_j} [(\mu + \frac{\mu_t}{\sigma_\varepsilon}) \frac{\partial \varepsilon}{\partial x_j}] + \rho C_1 S_\varepsilon - \rho C_2 \frac{\varepsilon^2}{k + \sqrt{v\varepsilon}} + C_{1\varepsilon} \frac{\varepsilon}{k} C_{3\varepsilon} G_b + S_\varepsilon \qquad (5)$$

Where

C_1 = max [0.43.$\frac{\eta}{\eta+5}$], $\eta = S.\frac{k}{\varepsilon}$ and $S = \sqrt{2S_{ij}S_{ij}}$

In these equations, G_k represents the generation of turbulence kinetic energy due to the mean velocity gradients. G_b is the generation of turbulence kinetic energy due to buoyancy. Y_M represents the contribution of the fluctuating dilatation in compressible turbulence to the overall dissipation rate. C_2 And $C_{1\varepsilon}$ are constants. σ_k and σ_ε are the turbulent Prandtl numbers for *k* and ε , respectively S_k and S_ε are user-defined source terms [15].

IV. FIGURES AND TABLES

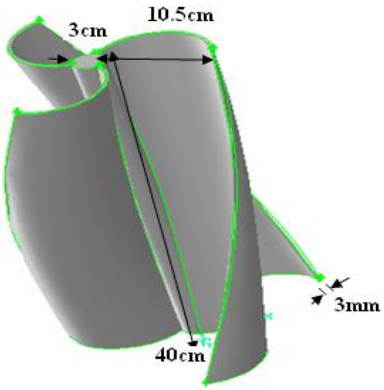

Figure 1: Physical model of 90° twist three bucket helical Savonius rotor

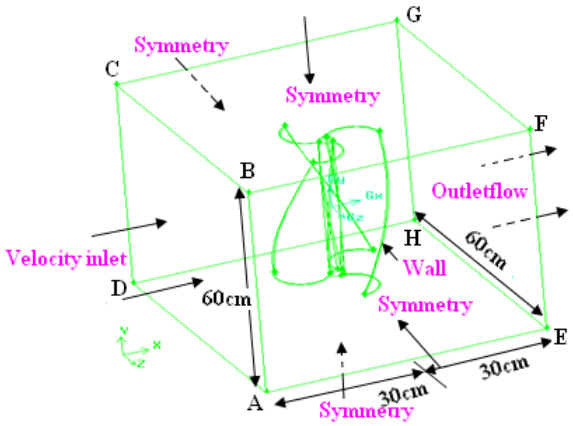

Figure 2: Computational domain and boundary condition

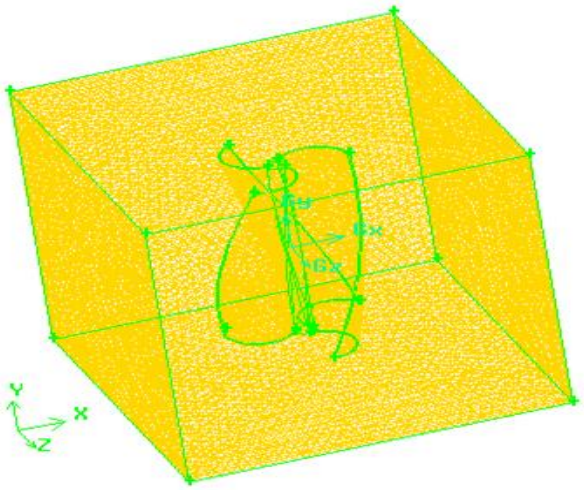

Figure 3: Computational mesh of 90° twist helical Savonius rotor

Table 1: Details of refinement levels of the 3-buckets helical Savonius rotor

Refinement Level	No. of Nodes	No. of Elements
1	34226	179994
2	35619	188283
3	37039	195053
4	44244	215022
5	48459	258595
6	50430	267086

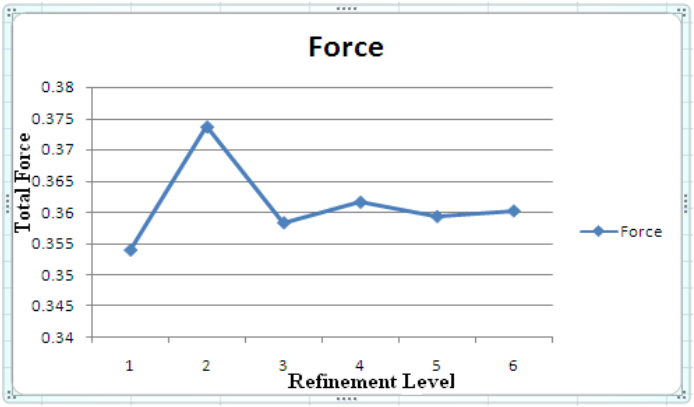

Figure 4: Variation of total force with respect to refinement level

V. RESULTS AND DISCUSSION

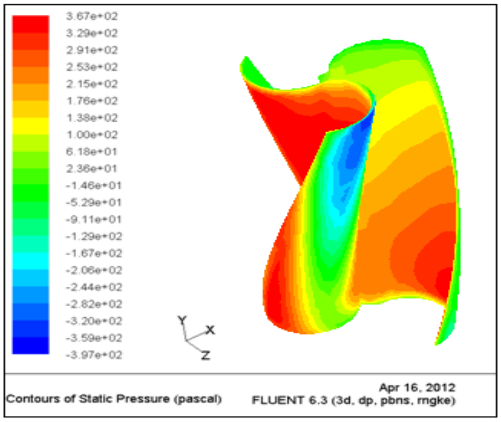

Figure 4(a): Static pressure magnitude contour for 0^0 rotor angle

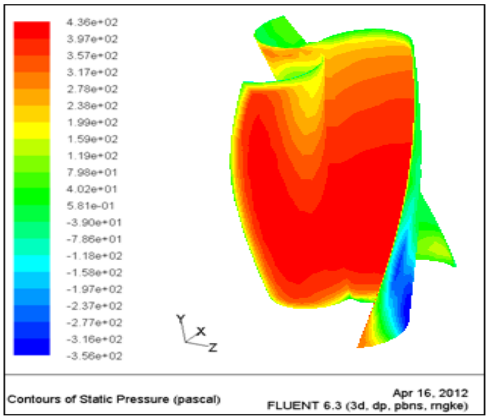

Figure 4(b): Static pressure magnitude contour for 60^0 rotor angle

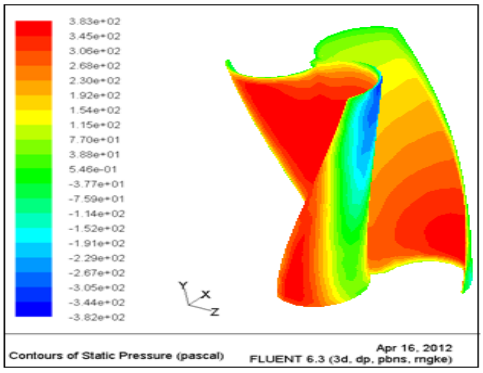

Figure 4(c): Static pressure magnitude contour for 120^0 rotor angle

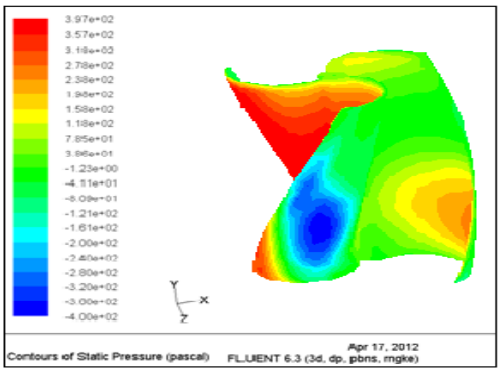

Figure 4(d): Static pressure magnitude contour for 150^0 rotor angle

The helical Savonius rotor with three bladed 90^0 twist angle, the contour plot analysis at 0^0, 60^0, 120^0 and 150^0 rotor angle for one revolution of the rotor, the contour plot analysis gives an idea about the flow physics of a wind rotor and its power generation mechanism. In the present study, relative velocity magnitude (velocity of the rotor relative to wind) and static pressure contours are analyzed. Fig- 5(a) to Fig- 5(d) show the velocity contours of the three-bucket helical Savonius rotor for different rotor angle conditions of 0^0, 60^0, 120^0 and 150^0. The velocity magnitude contour shows that the maximum velocity magnitudes near the chord end of advance bucket and decrease downstream side of the rotor. For 0^0 rotor angle velocity obtained 2.98×10^1 m/sec to 1.49m/sec, for 60^0 rotor angle 2.86×10^1 m/sec to 1.43m/sec, for 120^0 rotor angle 2.98×10^1 m/sec to 1.49m/sec and at 150^0 rotor angle 2.95×10^1 m/sec to 1.47m/sec at XZ iso-plane. Fig- 4 (a) to Fig- 4 (d) show the static pressure flow separation near to the bucket wall and Fig- 6 (a) to Fig- 6 (d) show the static pressure contours of the rotor for the aforesaid rotor angle conditions. These pressure contours show a decrease of static pressure from the upstream side to the downstream side across the rotor, which results in useful for evaluate the performance of rotor. At 0^0 rotor angle Fig- 6(a), static pressure decreases from 3.67×10^2 Pascal to -3.97×10^2 Pascal from upstream side to downstream side. At 60^0 rotor angle Fig- 6(b), static pressure decreases from 4.36×10^2 Pascal to -3.56×10^2 Pascal from upstream side to downstream side. At 120^0 rotor angle Fig- 6(c), static pressure decreases from 3.83×10^2 Pascal to -3.82×10^2 Pascal from advanced bucket to downstream bucket. At 150^0 rotor angle Fig- 6(d), static pressure decreases from 3.97×10^2 Pascal to -4.004×10^2 Pascal from upstream bucket to downstream bucket at XZ iso-plane.

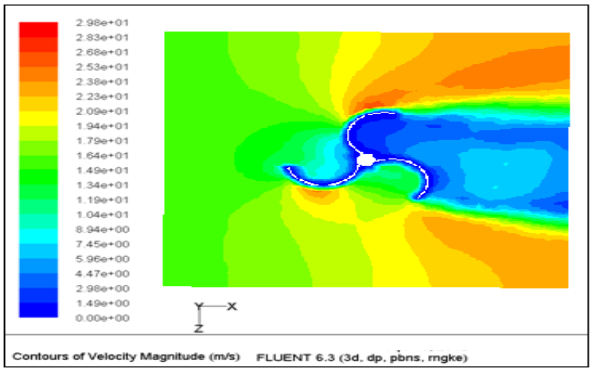

Figure 5 (a): Velocity contour of 0^0 rotor angle at XZ iso-plane

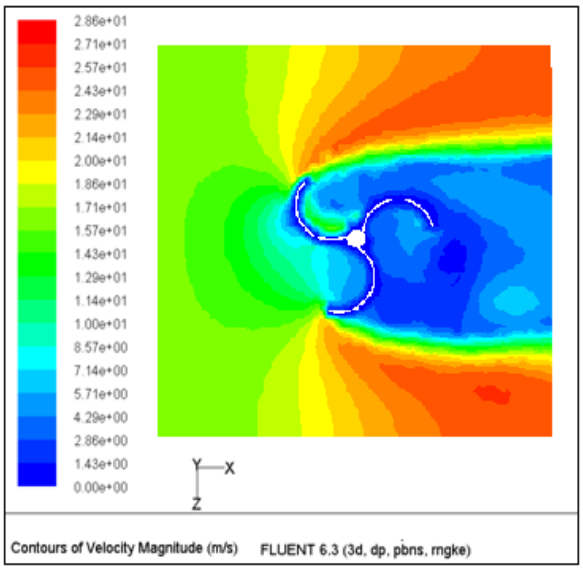

Figure 5 (b): Velocity contour of 60^0 rotor angle at XZ iso-plane

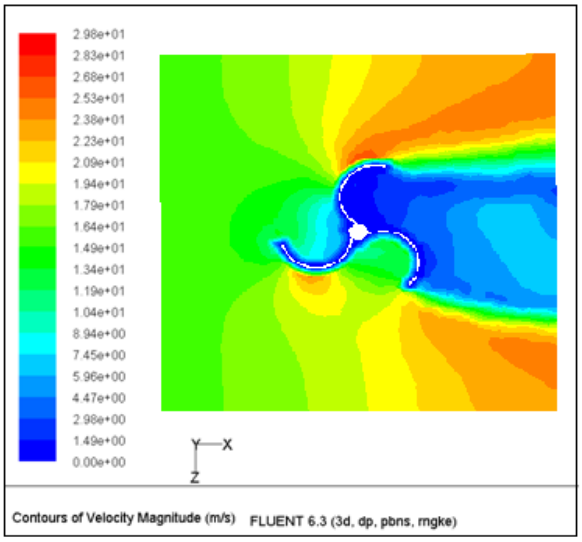

Figure 5 (c): Velocity contour of 120^0 rotor angle at XZ iso-plane

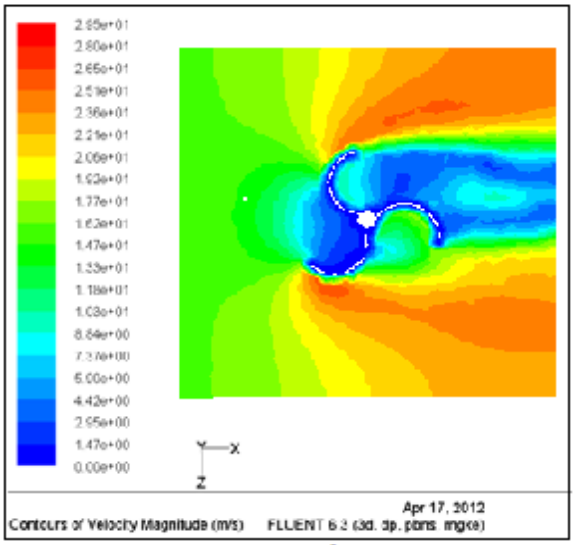

Figure 5 (d): Velocity contour of 150^0 rotor angle at XZ iso-plane

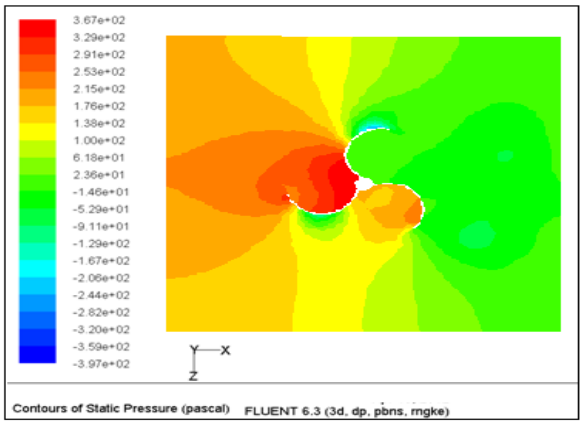

Figure 6 (a): Static pressure contour of 0^0 rotor angle at XZ iso-plane

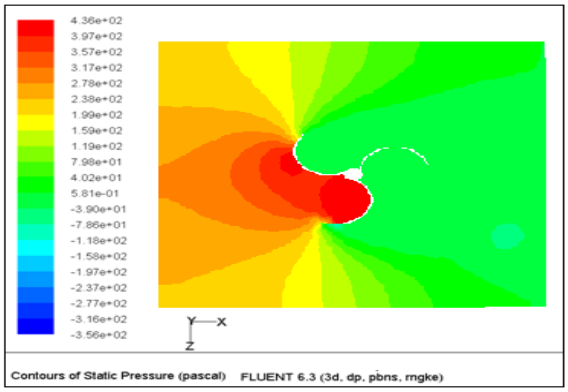

Figure 6 (b): Static pressure contour of 60^0 rotor angle at XZ iso-plane

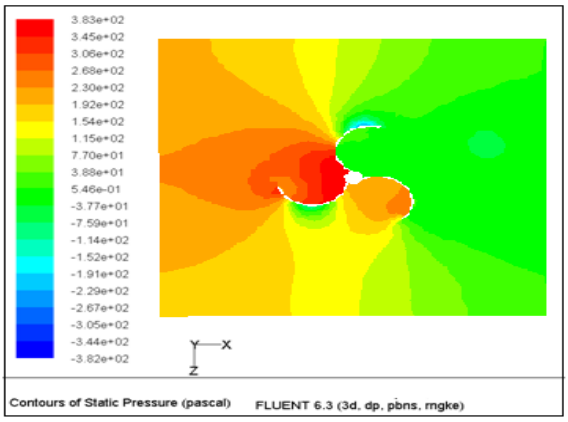

Figure 6 (c): Static pressure contour of 120^0 rotor angle at XZ iso-plane

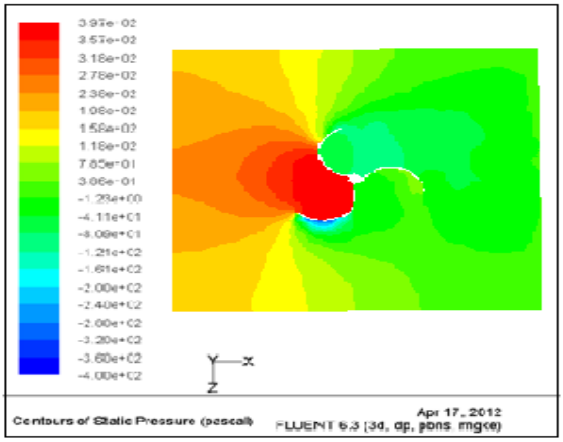

Figure 6 (d): Static pressure contour of 150^0 rotor angle at XZ iso-plane

VI. CONCLUSION

Flow physics analysis clearly shows that the static pressure decreases from the upstream side to the downstream side across the rotor, which results in useful lift for the rotor. So the maximum static pressure obtained near to the advanced bucket at 0^0, 60^0, 120^0 and 150^0 rotor angle are 367 Pascal, 436 Pascal, 383 Pascal and 397 Pascal. Again for velocity contour analysis the maximum velocity obtained near to the advanced bucket chord at 0^0, 60^0, 120^0 and 150^0 rotor angle are 22.3 m/sec, 25.7m/sec, 23.8m/sec and 23.6m/sec. So it can conclude, there is no sharp increase static pressure between rotor angles of 60^0 to 120^0. At 60^0 rotor angle maximum static pressure and velocity magnitude obtained 436 Pascal and 25.7m/sec which is marginally higher compare to other rotor angles, would ensure improved aerodynamic torque of the rotor as a whole during of the power stroke in one revolution of rotor. Flow physics analysis also shows the effect of positive static torque at variation of rotor angle. For 90° twist three buckets helical Savonius rotor at 150° rotor angle maximum positive static pressure distributions near the chord ends is obtained 3.97×10^2 Pascal to 3.06×10^{-1} Pascal from upstream side to downstream side which gives the positive static torque. So it can be concluded from flow physics analysis that three bucket 90^0 twist angle helical Savonius rotor at 60^0 rotor angle maximum lift force during power stroke was evaluated and maximum positive static torque was evaluated at 150^0 rotor angle.

REFERENCES

[1] Savonious, S. J., 1931.The Savonius rotor and its applications. Mech Eng. 53(5), pp 333-338.
[2] N.Fujisawa and F.Gotoh, "Visualization study of the flow in and around a Savonius rotor," Experiments in Fluids, vol. 12, pp 407 412, 1992.
[3] Nobuyuki Fujisawa,"Velocity measure- ments and numerical calculations of flow fields in and around Savonius rotors," Journal of Wind Engineering and Industrial Aerodynamics, vol. 59, pp 39-50, 1996.
[4] G. Bergeles and N. Athanassiadis, On the flow field around a Savonius rotor, Wind Eng. 6 (1982) 140-148.
[5] G.J. Bowden and S.A. McAleese, The properties of isolated and coupled Savonius rotors, Wind Eng. 8 (1984) 271- 288.
[6] R. Gupta , K.K. Sharma, "Flow Physics of a Three-Bucket Savonius Rotor using Computational Fluid Dynamics (CFD)" International Journal of Research in Mechanical Engineering and Technology, Vol. 1, Issue 1, Oct. 2011.
[7] R. Gupta, K.K. Sharma, "Flow physics of a combined darrieus-savonius rotor using computational fluid dynamics (CFD)" International Research Journal of Engineering Science, Technology and Innovation Vol. 1(1) pp. 1-13, April, 2012
[8] M.A. Kamoji, S.B.Kedare and S.V. Prabhu, "Performance tests on helical Savonius rotors," Renewable Energy, vol. 34, pp. 521-529, 2009.
[9] Gupta R, Debnath B, Das R. CFD analysis of a two-bucket Savonius rotor using Fluent package. In: Proc. of the European Wind Energy Conference, 2009.
[10] Gupta R, Biswas A (2011). "CFD Analysis of Flow Physics and Aerodynamic Performance of a Combined Three-bucket Savonius and Three-bladed Darrieus Turbine". Int. J. Green Energy. 8: 209–233.
[11] Katsuya, I.; Toshio, S. "Simulation of flow around rotating Savonius turbines". Proceedings the sixth National Symposium on Computational Fluid Dynamics, 2001,pp 691-694.
[12] M.,Manzoor Hussain: Mehdi,S. Nawazish: Reddy, P. Ram: "CFD analysis of low speed vertical axis wind turbine with twisted blades" International Journal of Applied Engineering Research: January,2008: Volume 3: Issue 1.
[13] Fluent Inc., Fluent Version 6.3 User's guide, Lebanon, New Hampshire, USA; 2006.
[14] Masson C, Ammara I, Paraschivoiu I (1997). "An aerodynamic method for the analysis of isolated horizontal-axis wind turbines". Int. J. Rotating Mach.vol. 3, pp 21-32.
[15] FLUENT Inc. "Fluent 6.0 documentation: user's guide" (2005).

International Journal of Modern Engineering Research (IJMER)
www.ijmer.com Vol.3, Issue.2, March-April. 2013 pp-747-751 ISSN: 2249-6645

Sustainability Index Measurement of Energy Efficient Skyscrapers: Present Indian Perspective

Shankha Pratim Bhattacharya, [1] Sonam Singh[2]
[1](Department of Architecture and Regional Planning, IIT Kharagpur, India)
[2](Architecture Division, Aakriti Architects, Kolkata, India)

Abstract: *During last century development of skyscraper have been rapidly increasing worldwide. The present fifth generation skyscrapers are influenced by the energy conservation and sustainable strategies. This paper brings out the list of such techniques and design principles used in tall building. A comprehensive literature study has been made to classify and characterize the innovative sustainable techniques. A comparative analysis is worked out in a weighted scale for the classified sustainable and energy conservation technologies and design principles. During analysis, present techno-socio-economic Indian scenario is given prime importance. Final phase of the paper measures the sustainability index of the above said technology and principles. This index and the ranking ultimately reveal that the passive design criteria with some selective energy generation techniques are the key features of modern sustainable skyscrapers in India.*

Keywords: *Energy generation, Facade design, Passive system, Skyscrapers, Sustainability index*

I. INTRODUCTION

Over the passage of time a considerable amount of changes and reforms in design of building and the use of building material are identified. The change in building design with respect to its space and volume is mainly due to the socio-economic shift. The new structural materials and the innovative use of building materials also imparted to the change in building vocabulary. The high cost of land price and the advancement in the field of structural engineering initiated to adopt vertical development in the core urban areas. Over the past hundred years the high-rise building has also undergone an array of development. The parametric changes in design and practices of tall building are influenced by various factors like, development of new material and technology, regulatory changes by civil bodies, change in demography in urban areas and modern economic and commercial impact to the society.

Generally, Skyscrapers are not considered as an ecological building. The Skyscrapers require more energy and material resources to build, to operate and eventually, to demolish. Tall buildings require high strength structural material to withstand the heavy superstructure and lateral loads. It requires greater energy demands to transport and pump materials to the upper floors. Until we have an economically viable alternative built form, the skyscraper as a building type will continue to be built particularly to meet the demands of urban and city growth and increasing rural-to-urban migration. UN report, in the year 2010 estimated that, urban population will exceed rural population within next twenty years. Sixty percent of the world population will live in urban areas by 2030. These changes will be clearly visible in Asian countries along with India, where the economy is increasing rapidly. In modern context the climate change and global warming are the burning issues. It is a fact that, the built environment made a significant contribution on the global green house effect. UNEP environmental programme, 2007 found that, the building materials and its present system are accountable for 30-40 percent of the primary energy used in the world [1].

So as a whole, particularly from the building type point of view, skyscrapers can never be considered as an eco-friendly building as it has certain negative environmental impact. But a positive improvement has been noticed regarding the thermal performance and the energy efficiency of the high rise buildings since their birth (1885) [2].

II. ENERGY GENERATION IN HIGH RISE BUILDINGS

Historically, the development of high rise building can be clustered into five energy generations. These five generations are separated by each other with a connecting event. Four such connecting events are recognised as (i) Introduction of 1916 New York zoning law, (ii) Innovation and use of curtain wall as building façade, 1951 and (iii) The energy crises in 1970s. (iv) Rise of an environmental consciousness in 1997 [3].

After the zoning law was implemented, the bulky nature of first generation building became slender to incorporate the vertical setback. The energy requirement for heating and air-conditioning increases proportionally with the increase of building surface area [4] the third generation buildings maximized the use of single-glazed dark colour curtain glass wall at their building facade. Rectangular dark glass facade buildings (known as black skyscrapers) quickly became popular around the world, regardless of building's site location and climatological considerations. The use of dark curtain wall increases the building's primary energy consumption in two folds. The black skyscrapers fully rely on HVAC system and have increased dependence on artificial lighting; hence increased energy consumption. The popularity of the single-glazed curtain wall facade high rise building construction was abruptly interrupted by the energy crises that evoked in 1973 and 1979. The mass people gradually became conscious of using energy in buildings. Many developed nations brought in building energy performance codes, forcing a widespread switch to double-glazing. The construction of single-glazed curtail wall was strongly criticized. The black skyscrapers in general became increasingly unpopular and the construction of black skyscrapers in American cities drastically went down.

Finally, the first significant tall building reflecting new environmentally conscious principles was the Commerzbank in Frankfurt (1997) by Norman Foster. The building is also considered the first 'ecological' skyscraper due to its use of sky gardens and energy-saving technologies [5]. It includes a full height central atrium to provide natural light and ventilation, open to sky gardens in various vertical levels, air movement through operable windows and water based ceiling cooling system.

An environmental consciousness started playing a role in all over the world. Many climate sensitive and energy efficient design features are introduced in the built environment to reduce the energy consumption. But all the features may not be feasible to incorporate in the Indian high rise building perspective. A comprehensive literature survey produces a list of the energy conservation features applicable to buildings and that are discussed in the next chapter.

III. SUSTAINABLE FEATURES OF MODERN HIGH RISE BUILDINGS

Built in 1956, Frank Lloyd Wright's Price Tower in Oklahoma shows many features and was in future rationalized as sustainable one. Some literature would of course, claim that the early work of Geoffrey Bowa in Sri Lanka (Mahaweli office tower, Colombo, 1976), Charles Correa in India (Kanchenjunga Apartments, Bombay, 1983), or Harry Seidler in Australasia (Riverside Centre, Brisbane, 1986) are more indicative of the first prototypes for eco-skyscrapers [6]. The majority of the tall building presently constructed tries to follow some typical requirement of sustainability. The practice of the sustainable features and technologies has many bifurcations. In this present study, the sustainability and the energy conservation approach are grouped into five classifications: Façade Design, Passive System, Generation of Electricity, Visual Comfort and Renewable System. Based on the literature review and application in the modern buildings for last thirty years, the sustainable and energy conservation technologies and design principles are listed under the five groups as below:

III.1 Façade Design

1. A typically designed facade allows for natural ventilation for over half the year through **operable windows**. This system can be adopted for low rise building of height maximum 20 floors.
2. **Balconies and overhangs** usually provide sufficient amount of shading to the direct solar radiation. But very few high rise building incorporates the shading devices into its façade due to monotony in building elevation. The portion of the building without any shading devices is rendered with high-quality solar glass panels which minimize solar gain.
3. **High performance curtain wall** reduces solar heat gain through low-emissivity (low-e) glass.
4. **Internally ventilated double wall system** keeps the interior thermal environment under control.
5. Façade on the sides of maximum heat gain (eastern and western) is made of **triple glazed glass** which insulates the building's interior.

III.2 Passive System

1. A **central atrium** can be designed to provide natural lighting and ventilation to internal office spaces. A temperature gradient can be set up to execute ventilation due to stack effect. But in sufficiently high buildings natural stack effect must be supported by mechanical ventilation.
2. **Buffer spaces** should be created between the external outdoor and internal air conditioned spaces. Buffer zone reduces the conductive solar heat gain. [For example, buffer space can be of car park deck, entrance lobby, service floor, storage areas]
3. A local **evaporative cooling** is well executed by the reflection pools at building entrance. The efficiency of the evaporative cooling will enhance if the building is placed at upstream side of the breeze passing the pool.
4. Extensive **site landscaping** reduces the direct solar reflection.
5. A **water-based cooling system** has been designed for chilled ceilings. A radiant cooling ceiling system is designed to circulate cool air in the office floors. Perimeter "chilled beams" are provided in the ceiling level instead of normal air-conditioning and ventilation duct. These perimeter chilled beams carry the cold water (approximately 14^0 C) through concealed copper pipes. Floor-by-floor air handling units provide more even, efficient, and healthy cooling and fresh air.
6. An **inverted design concept**, where the maximum opening are given in the interior courtyard side.

III.3 Generation of Energy

1. **Wind turbine** can be set up in certain vertical level to generate electricity. The aerodynamic shape of the building envelop with typical floor plan become the key feature to enhance the air draft. The wing-like towers assist to accelerate the wind velocity and create pressure differences. The funnel condition allows sufficient air flow that imparts to the electricity generation.
2. **Small wind turbines** of the size of a window, sometimes designed and placed in strategic maximum wind locations to generate local level of back-up power.
3. **Photovoltaic cells** can be employed in the building façade to generate electricity.
4. Installation of **Building Integrated Photovoltaic cells**. Building integrated photovoltaic (BIPV) are the photovoltaic material that are used to replace conventional building material (such as cladding tiles or roof tiles) in parts of the building envelope such as roof, wall and skylight. They are increasingly being incorporated into the construction of new buildings as an ancillary source of electrical power.

III.4 Visual Comfort

1. Open to sky, large gardens can be accommodated in differential vertical levels to increase the natural light quantity in interiors. These are known as **Sky Courts**. Sky courts at different intermediate levels allow occupants to enjoy greenery, as well as creating a passive cooling.
2. **Spiral vegetation** and landscaping planter boxes can be designed **along with the ramp**. The continuous vegetated areas occupy a surface area of productive biomass. The planting contributes to the ambient cooling of the façades through evaporation and transpiration. The landscaped ramp results in a built form with a vertical landscape.
3. **Energy-efficient, high-efficacy, lighting** with zonal control minimize the electrical load. Road and amenity lighting are also designed with solar-powered.
4. **Day light responsive controls**: maximizing the use of natural light by the use of lighting controls that respond to daylight, integrated into the system of the blinds.

III.5 Renewable System

1. **Twofold drainage system** is designed to separate the waste and soil water. The water treatment also allows the gray water recycling.
2. **Recycle of rain water** through a sophisticated rain water capture system can be designed so that, it can be aimed for nearly zero storm water discharged to city sewer system.
3. **Dual-flush for the closets** and **electronic taps** controls the flow of excess water use.
4. **High efficient office equipment**: Sophisticated equipment that yield water and power conservation.
5. **Using recycled / industrial byproduct** as prime building materials.

These sustainable and energy conservation technologies and design features are further assessed through selected sustainable parameters and discussed in subsequent paragraphs.

IV. MEASUREMENT OF SUSTAINABLE INDEX AND DISCUSSIONS

The features of sustainable and energy conservation technology and design are finally assessed through five sustainable parameters. This point system assessment ultimately measures the suitability index. The index will rank the applicability of the features (mentioned in previous chapter) in Indian condition. Following five sustainability index measurement parameters (appeared as P1 to P6 in Table1) are considered during comparative analysis:

1. Energy Saving Potential (it is based on the relative amount of energy conservation in the tropical climate of India)
2. Impact on environment (It includes the direct and indirect impact on the environment in a long term basis. It also takes account of the embodied energy of the used material)
3. Application and Technical Feasibility (many features may not be readily applicable and may require technological or engineering up-gradation. Sometimes some of the features are not feasible to adopt in socio-economic circumstances)
4. Degree of Maintenance (it takes the regular and extent of required maintenance affair of the adopted technology)
5. Initial Cost (it gives the capital investment on the installation of energy conservation technological features)
6. Return on Investment (it estimates the return period and the amount of yearly return on the capital investment)

Point (1 to 5) is awarded to each of the parameters for entire features. Better potential and appropriateness of the technology with respect to the parameter is given lower points. Whereas the higher point of any parameter indicates the relatively adverse scenario. Around twenty modern eco-skyscrapers of fifth energy generation are thoroughly studied as a part of the case study. The point is given to each category according to the latest literature survey and the review articles along with the explanation and narration given by the prime electronic media. The approach to the adopted technology and the suitability in the Indian environment is considered. Both in terms of technological feasibility and socio-economic structure of present Indian scenario is taken care of. Two statistical properties, the “mean” and the “range” of the overall point marking are considered to finalize the sustainable index measurement. As the minimum value of the “mean” recognize the best fitted performance and the minimum “range” gives more confidence for adoptability, the product of the two is calculated. The minimum value of the product signifies the best suitability. Sustainable index (SI) can finally represent in mathematical form as:

$$\mathrm{SI} = \left(P_{avg}\right) \times \left[\left(P_{\max}\right) - \left(P_{\min}\right)\right]$$

Table1. Sustainability Index Analysis and Measurement

Sustainability & Energy Conservation Features		Sustainability Index Measurement Parameters							
Façade Design		**P-1**	**P-2**	**P-3**	**P-4**	**P-5**	**P-6**	**SI**	**Rank**
1	Operable Windows	4	1	3	1	1	4	**7.00**	**1**
2	Balconies & Overhangs	5	1	3	2	2	3	**10.67**	**4**
3	High Performance Curtain Wall	1	3	4	3	4	2	**8.50**	**2**
4	Internally Ventilated Double Wall System	1	4	5	4	5	1	**13.33**	**5**
5	Triple Glazed Glass	1	4	4	3	4	2	**9.00**	**3**
Passive System		**P-1**	**P-2**	**P-3**	**P-4**	**P-5**	**P-6**	**SI**	**Rank**
1	Central Atrium	3	1	2	2	2	3	**4.33**	**1**
2	Buffer Spaces	4	1	3	2	3	2	**7.50**	**3**
3	Evaporative Cooling	2	1	3	2	2	4	**7.00**	**2**
4	Site Landscaping	3	1	2	3	3	4	**8.00**	**4**
5	Water-based Cooling System	1	2	3	3	5	1	**10.00**	**5**
6	Inverted Design Concept	3	1	3	2	2	4	**7.50**	**3**
Generation of Energy		**P-1**	**P-2**	**P-3**	**P-4**	**P-5**	**P-6**	**SI**	**Rank**
1	Wind Turbine	1	3	5	4	5	2	**13.33**	**4**
2	Small Wind Turbines	3	3	3	3	4	2	**6.00**	**1**
3	Photovoltaic Cells	1	1	3	2	4	2	**6.50**	**2**
4	Building Integrated Photovoltaic Cells	2	1	4	2	5	1	**10.00**	**3**
Visual Comfort		**P-1**	**P-2**	**P-3**	**P-4**	**P-5**	**P-6**	**SI**	**Rank**
1	Sky Courts	2	1	4	3	3	3	**8.00**	**3**
2	Spiral Vegetation	3	1	3	2	2	4	**7.50**	**2**
3	Energy-Efficient, High-Efficacy, Lighting	1	2	2	2	4	1	**6.00**	**1**
4	Day Light Responsive Controls	1	3	3	3	5	2	**11.33**	**4**
Renewable System		**P-1**	**P-2**	**P-3**	**P-4**	**P-5**	**P-6**	**SI**	**Rank**
1	Twofold Drainage System	3	2	4	4	4	2	**6.33**	**3**
2	Recycle of Rain Water	2	1	2	3	3	3	**4.67**	**2**
3	Dual-flush for the Closets	3	3	5	4	4	2	**10.50**	**4**
4	High Efficient Office Equipment	2	3	4	5	5	1	**13.33**	**5**
5	Using Recycled / Industrial By-product	2	1	3	1	1	1	**3.00**	**1**

The Table 1 shows the complete analysis and the rank of the sustainable and energy conservation technologies and design features for Indian condition.

The final outcome of the analysis can be categorized into three parts.

(i) The traditional solar passive design features like central atrium with stack effect, buffer spaces, facade treatment with overhang are best suitable to control over the thermal heat gain (and to minimize the cooling load) of the building.

(ii) Miniature form of wind turbine and the photovoltaic cell along with energy efficient artificial lighting can be well fitted for Indian condition high rise building. A spiral split level interior garden concept can also be adopted for visual comfort.

(iii) Using recycled material and a comprehensive rain water harvesting scheme can be adopted in buildings.

V. CONCLUSION

The climatic change and global warming have presently become a burning issue worldwide. The requirement of environmental sustainability and further reduction in primary energy demand in buildings was noticed in late twentieth century buildings. In the present study, the sustainability index is measured for some selected energy conservation technology and design principles. The judgment was carried out in Indian context. The analysis finally reveals that the traditional solar passive design principles with a building surface solar and wind energy generation technology could be the appropriate solution at present. Using recycled and industrial by-product material with rain water capturing system will enhance the overall sustainability of the Indian tall building.

REFERENCES

[1] UNEP, Buildings and Climate Change: Status, Challenges and Opportunities, Nairobi, United Nations Environmental Programme, 2007.
[2] R.G. Stein, Observations on Energy Use in Buildings, Journal of Architectural Education, 30 (3), 1977, 36-41.
[3] P. Oldfield, D. Trabucco, and A. Wood, Five energy generations of tall buildings: an historical analysis of energy consumption in high-rise buildings, The Journal of Architecture, 14 (5), 2009, 591-613.
[4] D. Arnold, Air Conditioning in Office Buildings after World War II, ASHRAE Journal, 1999,33–41.
[5] A. Wood, Sustainability: A New High-Rise Vernacular, the Structural Design of Tall and Special Buildings, 16, 2007, 401-410.
[6] K. Yeang, and R. Powell, Designing the Eco-Skyscrapers: Premises for Tall Building Design, The Structural Design of Tall and Special Buildings, 16, 2007, 411-427.

International Journal of Modern Engineering Research (IJMER)
www.ijmer.com Vol.3, Issue.2, March-April. 2013 pp-752-758 ISSN: 2249-6645

Design and Fabrication of Solar R/C Model Aircraft

Prof. Alpesh Mehta, [1] Chirag Joshi, [2] Kuldeepsinh Solanki, [3] Shreekant Yadav[4]

[1]*Assistant Professor of Mechanical Engineering, Government Engineering College, Godhra, Gujarat, India*
[2,3,4]*Students of 8th Semester Mechanical Engineering, Government Engineering College, Godhra, Gujarat, India*

Abstract: *The Generally domain Aircraft uses conventional fuel. These fuel having limited life, high cost and pollutant. So there is great demand of use of non-exhaustible unlimited source of energy like solar energy. Solar aircraft is one of the ways to utilize solar energy. A few manned and unmanned solar powered aircraft have been developed and flown in the last 30 years. Solar aircraft uses solar panel to collect the solar radiation for immediate use but it also store the remaining part for the night flight. This experiment intended to stimulate research on renewable energy sources for aviation. The basic challenges for a solar powered aircraft are Geographical area of operation, payload, Energy collection and utilization, and design parameter. This research runs over an extensive period of time, which will provide us with sufficient opportunities to do research and create designs. Assuming we will be able to make accurate calculations, our expectations are that we will actually produce an aircraft capable of flying on solar power. A simulated Remote Control (RC) model size solar airplane allowed to vary altitude proves to be capable of flying multiple day-night cycles at medium and high latitudes during summer. Still, it should be noted that the plane we manufactured is a prototype only. We gathered enormous amounts of knowledge. For if development continues, solar powered aircraft might truly be used in future for different types of aerial monitoring and unmanned flights.*

Keywords: *Aircraft, Bernoulli's principle, Reynolds number, solar energy, Solar cells*

I. INTRODUCTION

The Energy comes in different forms. Light is a form of energy. Sun is source of energy called "sunlight". Sunshine is free and never gets used up. Also, there is a lot of it. The sunlight that heats the Earth in an hour has more energy than the people of the world use in a year. A little device called a solar cell can make electricity right from sunlight. The dream of flight powered only by the sun's energy or sunlight has long motivated scientists and hobbyists. A solar aircraft is one which collects energy from the sun by means of photovoltaic solar cells. The energy may be used to drive electric motor to power the aircraft. Such airplanes store excess solar energy in batteries for night use.

Also there are rapidly increasing traffic problems in world and in our country also, so it is required to go for such small solar aircrafts which can be used for transporting goods or materials between places at short distance. Using solar panels there is more space due to escape of engines and turbines.

In 1783, dream of flying became reality "Historians credit France's Montgolfier brothers with the first pioneering balloon flight". Next revolution was in 1903, when Orville and Wilbur Wright made their 'Flyer 1' and flew 36 meters with their plane. Flyer 1 was a petrol engine, just like later aircraft. Nowadays, aviation accounts for three percent of all CO2-emissions produced by mankind. This doesn't seem much, but more important is that profit of commercial aviation strongly relies on the oil price. Due to high prices of crude oil lately, profits of commercial aviation have been diminished and aviation industry is now looking for alternative energy sources to propel modern-day aircraft. Options that are being considered are bio fuels, hydrogen and ethanol. An option which is rarely considered is solar energy, an option we wanted to investigate.

II. HISTORY

The Solar Impulse is a project with the construction of an initial prototype with a 61-metre wingspan, referred to by its registration number "HB-SIA". It is the research of four years and studies, calculations and simulations. Its mission is to verify the working hypotheses in practice and to validate the selected construction technologies and procedures. On 24 July, 2012, it has taken-off at 05:01am with flight duration of 13hours 29mins and average speed of 34 kts. It has an average altitude of 3596 meters without any fuel. However there are many projects based on solar system which were tried and: Characteristics of various solar-powered airplanes are in table below.

[15]Table 1: History

Model	Year	Solar Cells	Energy (W)	Weight (lbs)	Wingspan (ft)	Altitude (ft)	Battery	Control
Sunrise I	1974	1000	450	26	32	20,000	N/A	Remote
Sunrise II	1975	4480	600	4	32	75,000	N/A	Remote
Solar Challenger	1980	16,128	2600	200	47	12,000	N/A	Remote
HALSOL *	1983	N/A	N/A	N/A	98	N/A	N/A	Remote
Pathfinder	1993	Silicon	7,500	560	98	50,500	N/A	Remote
Pathfinder-Plus	1998	Silicon	12,500	700	121	80,201	N/A	Remote
Centurion	1998	Silicon	12,500	1,900	206	100,000	N/A	Remote
Helios	1999	62,120	12,500	2,048	247	100,000	LiPo	Remote
Sunseeker I	1986	N/A	N/A	N/A	N/A	N/A	NiCd	Pilot
Sunseeker II	2002	N/A	N/A	N/A	N/A	N/A	LiPo	Pilot
SoLong	2005	76	225	25	15.6	26,250	LiPo	Remote
Sky-Sailor	2004	216	90	2.5	3.2	6,500	LiPo	Remote
Zephyr	2007	N/A	1,500	66	59	60,000	LiPo	Remote
Solar Impulse	2007	12,000	6,000	3307	200	27,887	LiPo	Pilot

III. PROJECT WORK

3.1PRINCIPLE OF OPERATION

Our basic principle is to use solar power by means of aircraft. And this thing can be done by solar panels which is composed by solar cells connected in a certain configuration, cover the whole surface of wing. With help of sun irradiance and inclination of the rays this panels converts radiative energy into electric energy. This electric energy is used to charge battery which drives electric motor. Maximum amount of power is obtained from the solar panels. Propeller which is mounted on motor shaft produces thrust continuously. Because of this, aircraft is moved and force is produced on wing by dynamic effect of air which opposes the downward Force of weight. During the night, the only energy available comes from the battery. There is a transmitter and receiver, which are used to send and receive signals from a control panel. The receiver, located inside the plane, will send signals to elements called servos. They can move the rudder, ailerons and elevator. Besides, the receiver also controls the engine throttle.

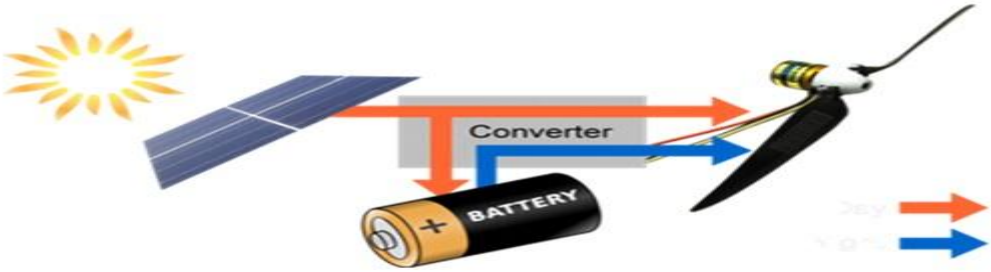

Figure 1: Basic principle of operation

3.2 Design

Table 2: Parameters

Mass(gm) = 650	Wing chord(cm) = 15.04	Tail span(cm) = 31.46
Wing loading = 0.456	Coefficient of lift = 0.373	Tail root chord(cm) = 9.64
Wing area(cm^2) = 1425	Angle of attack = 4.2	Tail tip chord(cm) = 4.34
Aspect Ratio = 6.3	Tail area(cm^2) = 220	Tail moment arm(cm) = 43.94
Wing span(cm) = 94.74	Aspect ratio of tail = 4.5	Volume ratio = 45.106
Reynolds no. = $3*10^6$	L/D ratio = 64.9	Pitch moment = -0.002

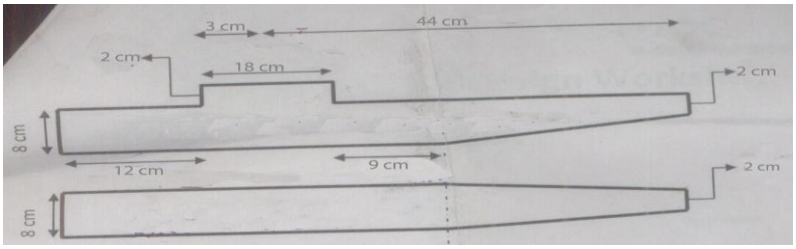

Figure 2: Fuselage Design

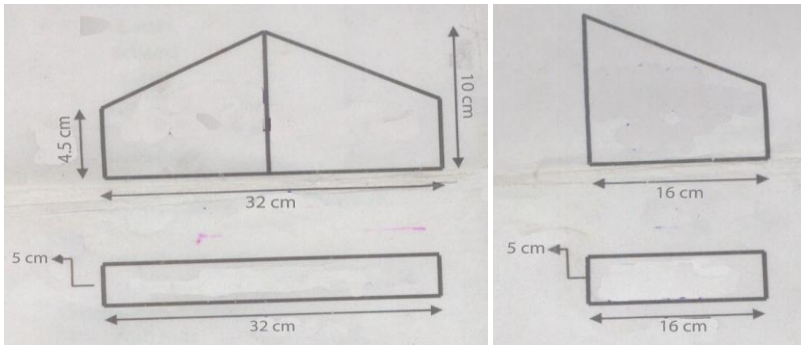

Figure 3: Elevator and Rudder Design

3.3 Aerofoil selection

We have used symmetrical aerofoil because the wings will be hand fabricated and developing a cambered airfoil will be difficult. That means there will be no camber. We have selected NACA aerofoil of 4 digit i.e., NACA 0015, where 0 camber and 15% thickness to chord length ratio. The 'NACA' aerofoils are shapes for aircraft wing developed by the National Advisory Committee for Aeronautics (NACA).

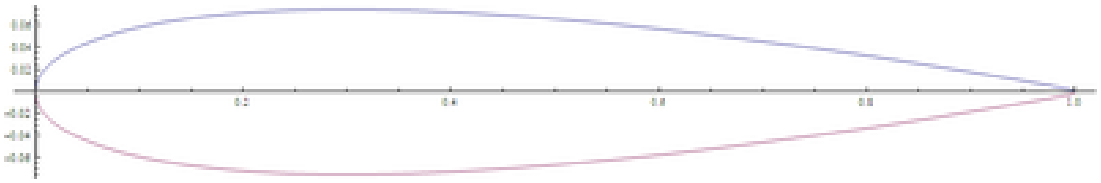

Figure 4: NACA0015 Aerofoil

By choosing proper Angle of attack we use software by which different parameters are generated. We also use FoilSim- a simulator for aerofoil. With this software we investigate how an aircraft wing produces lift and drag by changing the values of different factors that produce aerodynamic forces.
After many, such type of iterations and simulations we select aerofoil for our model.

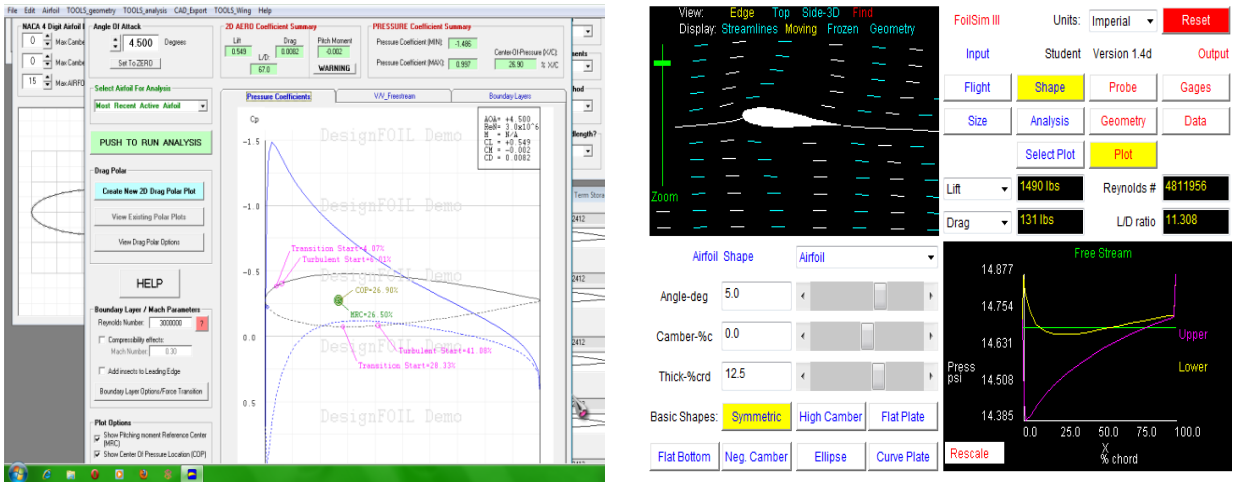

Figure 5: Aerofoil analysis

3.4 Solar cells

The solar cells should provide enough power during flight to extend flying range drastically or even power the aircraft entirely. Just as with all materials used on our plane, mass is a crucial element, so the solar cells can't be too heavy. Cells are often being integrated in glass, something that would contribute far too much weight. Three solar cell types are in current use. They include amorphous solar cells, monocrystalline solar cells, and multicrystalline solar cells. Each type has its advantages and disadvantages that make it suited to specific applications. For the purposes of Solar Power Industries, multicystalline solar cells represent the greatest efficiency for manufacturing and the greatest value to the customer.
Amorphous cells have been used for a long time in products like solar powered calculators, and garden lamps. The entire panel consists of one piece, making individual solar cells less identifiable. This has long been the least efficient solar cell type, but they have begun to improve to the point where they may become a viable alternative to crystalline solar cells. Theoretically, monocrystalline cells are the most efficient cell type, but in practice poly-crystalline cells produce nearly the

same energy output. Moreover, since monocrystalline silicon crystals form circular cross-sections, more silicon is wasted when squaring the wafer than when manufacturing multicrystalline cells since they naturally produce square cross-sections. SPI focuses solely on the production of polycrystalline solar cells because of these advantages.

We are going to use solar monocrystalline silicon cells, each 150 microns thick and chosen for their lightness, flexibility and efficiency. Monocrystalline wafers produce the highest efficiency Photovoltaic Solar Cell or the most power output. But, usually will cost more than multicrystalline cells for the same power output.

3.5 Plots and Pro-E design

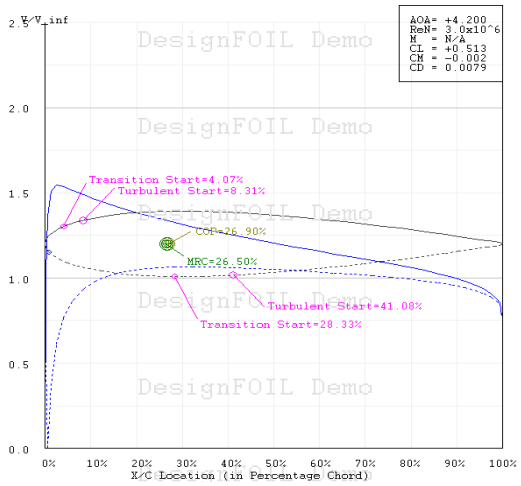

Figure 6: V/V Freestream

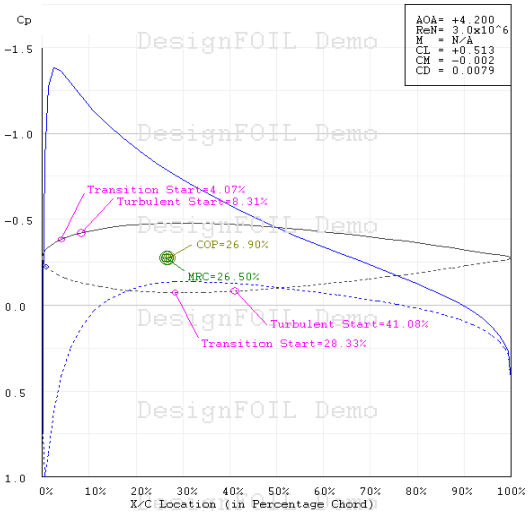

Figure 7: Pressure Coefficients

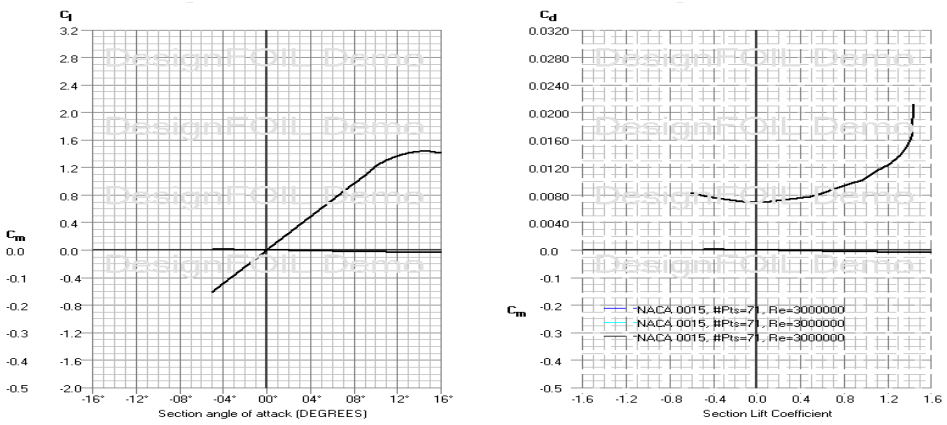

Figure 8: NACA Plot

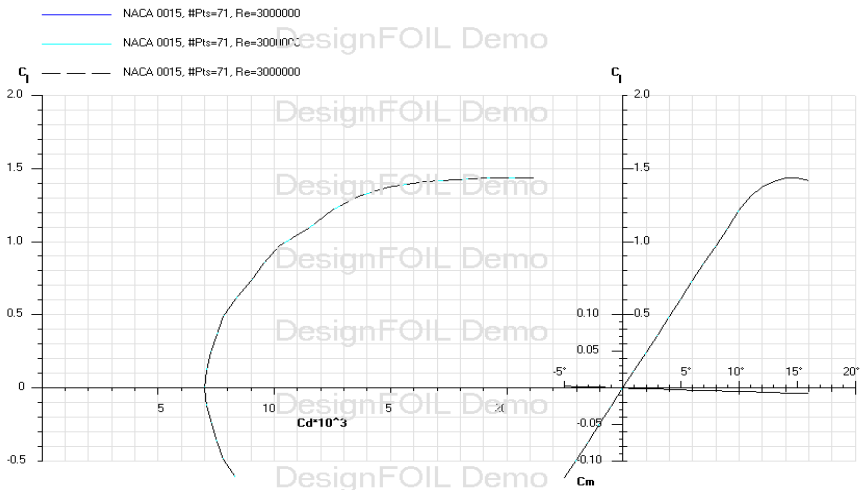

Figure 9: EPPLER Plot

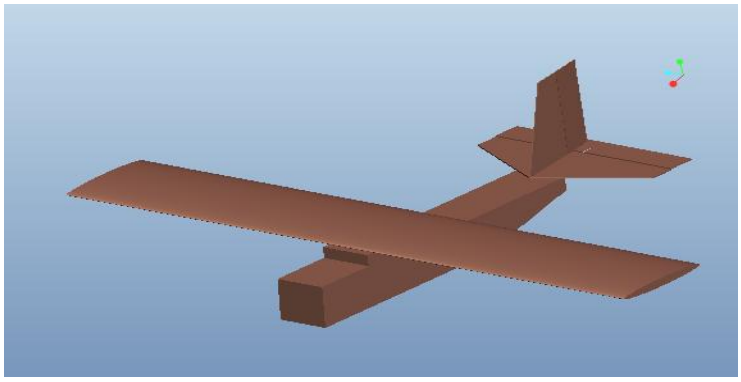

Figure 10: Pro-E model

3.6 Electrical Parts selection

Brushless outrunner motor is a recent type. These motors have the rotor "outside" as part of a rotating outer case while the stator is located inside the rotor. This arrangement gives much higher torque than the conventional brushless motors, which means that the "outrunners" are able to drive larger and more efficient propellers without the need of gearboxes.

As we want to carry weight of about 650gm, this is not so heavy so we decide to choose brushless outrunner motor. The dimensions of motor are shown in figure. The motor has max pull of about 890gm.
It has 1000rpm/v with max power of 210watt.

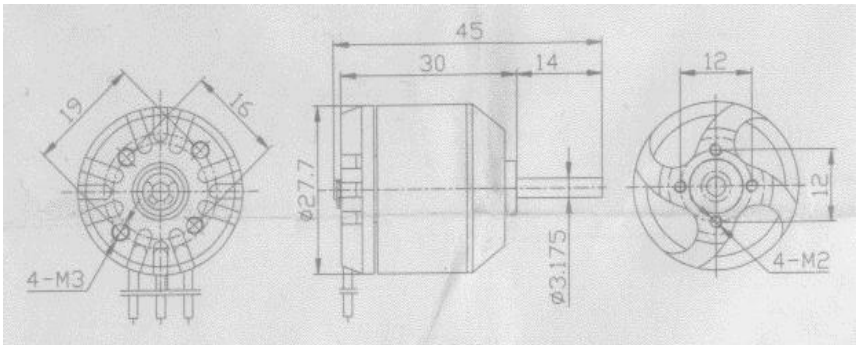

Figure 11: Motor dimension

A common way to control the electric motor's speed is by using an Electronic Speed Controller (ESC). An electronic speed controller specially designed for the brushless motors, which converts the battery's DC voltage into three pulsed voltage lines that are 120^{o} out of phase. The Electronic Speed Controller is based on Pulse Width Modulation (PWM), which means that the motor's rpm is regulated by varying the pulses' duty-cycle according to the transmitter's throttle position.
We choose ESC with max current 25A. It has BEC and burst of 3A and 30A respectively.

Figure 12: Electronic speed control

To move elevator and rudder required torque is about 1.6 kg-cm. Also, 2.3 kg torque is required to move aileron. Here servo 1 is used for elevator and rudder while servo 2 is used to operate aileron.

Table 3: Servo 1 parameters

Weight (g)	9
Torque (kg)	1.6
Speed (Sec/60deg)	0.12

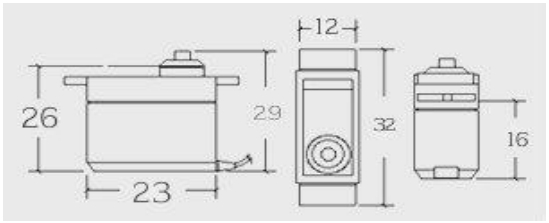

Figure 13: Servo 1 dimensions

Table 4: Servo 2 parameters

Weight (g)	25
Torque (kg)	2.3
Speed (Sec/60deg)	0.08

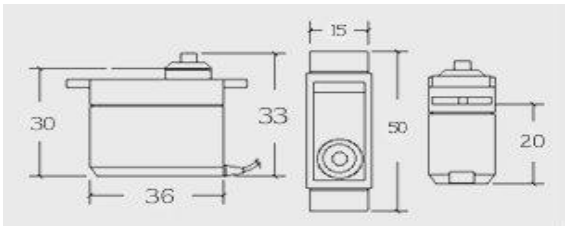

Figure 14: Servo 2 dimensions

Batteries are available in different sizes, weights, voltages and capacities C, which refer to their stored energy expressed either in amps-hour Ah or milliamps-hour mAh. A battery with a capacity of 1500mAh should deliver 1500mA during one hour before it gets totally discharged (flat). This is suitable for motor and ESC we choose.

Table 5: Battery parameters

Capacity(mAh)	1500
Config(s)	3
Discharge(c)	20
Weight(g)	146

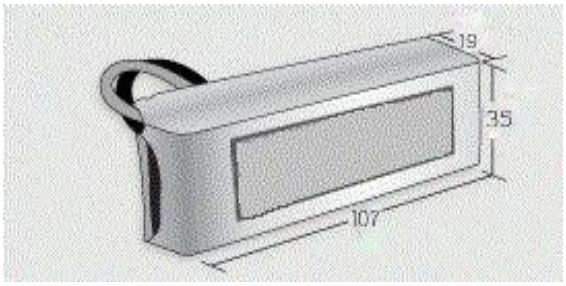

Figure 15: Battery dimensions

Also we have used clevis, control horns and like some others items to move elevators, rudders, ailerons etc.
As discussed earlier monocystaline silicon cells is used. Because of the chosen batteries and the 0.1-0.2 volts lost over the diode, solar cells we use on the airplane must have a total output of 12 volts. This would require about 20 solar cells of following type.

[20]Table 6: Solar cell parameters

Dimension	125mm×125mm±0.5mm
	Diagonal 150mm±1mm
Thickness	Final Cell: 210μm±40μm
	Silicon: 200μm±30μm

Test accuracy: Pmpp: ±1.50% rel.
Efficiency: ±0.25% abs.
Typical Temperature Coefficients:
Pmpp: -0.47%/℃,
Voltage: -0.38%/℃, Current: +0.10%/℃

weight: about 8.4 gm/cell

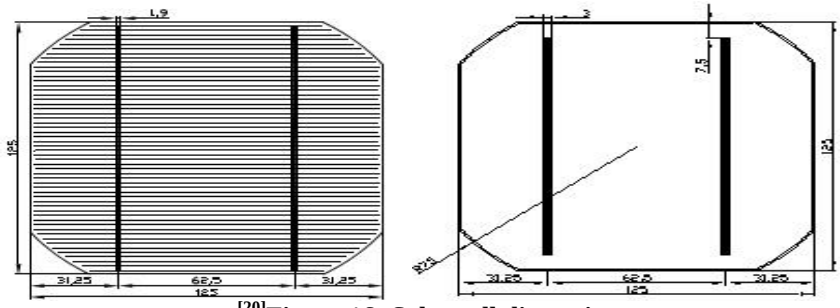

[20]Figure 16: Solar cell dimension

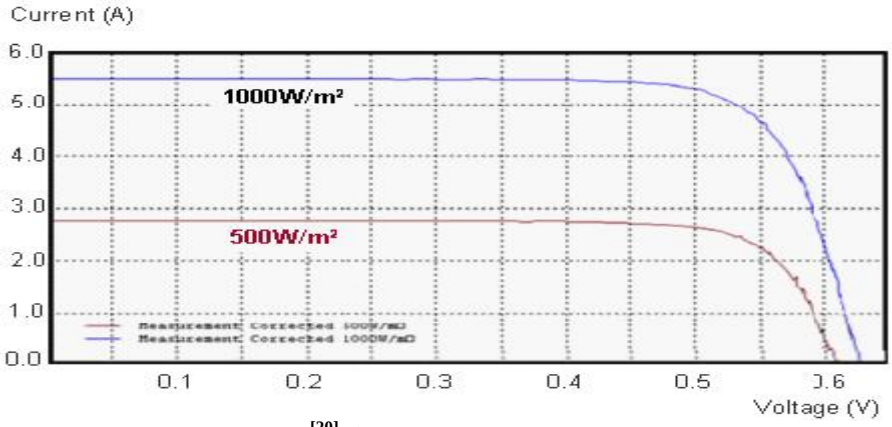

[20]Figure 17: I-V Curve

IV. CONCLUSION

In this paper all performance parameter calculations, analysis and parts selection are discussed. This type of aircraft can be used to fly day and night. Main advantage of it is use of non-conventional source of energy. As discussed in paper the dimensions and number of solar cell of specified type, we have almost made solar aircraft so now we are going to test it. After testing we will make modification as per requirement.

REFERENCES

[1] Vineet Kumar Vashishtha, Ashok kumar, Rahul makade and ShashiLata, "Solar Power the Future of Aviation Industry", International Journal of Engineering Science and Technology.

[2] Prof. Alpesh Mehta, Shreekant Yadav, Kuldeepsinh Solanki, Chirag Joshi, "SOLAR AIRCRAFT: FUTURE NEED", International Journal of Advanced Engineering Technology T/Vol.III/ Issue IV/Oct.-Dec., 2012.

[3] A. Noth, R. Siegwart, W. Engel, Version 1.1, December 2007,"Design of Solar Powered Airplanes for Continuous Flight".

[4] Moran Jack (2003), An introduction to theoretical and computational aerodynamics, Dover. P. 7. ISBN 0-486-42879-6.

[5] William H. Phillips, "Solar aircraft", U.S. Patent.

[6] Howard J. Fuller, "Solar Powered aircraft", U.S.Patent.

[7] Andrew T. Klesh and Pierre T. Kabamba, "Solar-Powered Aircraft: Energy-Optimal Path Planning and Perpetual Endurance", Journal of Guidance, Control, and Dynamics.

[8] Stefan Leutenegger, Mathieu Jabas and Roland Y. Siegwart, "Solar Airplane Conceptual Design and Performance Estimation",J Intell Robot Syst (2011) 61:545–561DOI 10.1007/s10846-010-9484-x.

[9] Noth, W. Engel and R. Siegwart, "Recent Progress on The Martian Solar Airplane Project Sky-Sailor", 9th ESA workshop on Advance Space Technologies for Robotics and Automation, 'ASTRA 2006' ESTEC, November 28-30, 2006.

[10] Adam M. Wickenheiser and EphrahimGarcia, "Conceptual Design Considerations for Microwave-and Solar-Powered Fuel-Less Aircraft", JOURNAL OF AIRCRAFT Vol. 46, No. 2, March–April 2009.

[11] Andr´eNoth, Stefan Leutenegger, Walter Engel, and Roland Siegwart, "Designing solar airplanes for continuous flight".

[12] E. N. Jacobs, K. E. Ward, & R. M. Pinkerton, 1933 The characteristic of 78 related airfoils sections from tests in the variable-density wind tunnel, NACA Report No. 460.

[13] Andr´eNoth, Walter Engel and Roland Siegwart, "Design of an Ultra-Lightweight Autonomous Solar Airplane for Continuous Flight".

[14] Hannes Ross, Member of the Solar Impulse Team, 85640 Putzbrunn, Germany, "Fly around the World with a Solar Powered Airplane".

[15] Senior Design Team 96, Solar-Powered Airplane, Southern illinois university Carbondale.

[16] Daniel P. Raymer, President, Conceptual Research Corporation, Sylmar, California, "Aircraft Design: A Conceptual Approach".

[17] John D. Anderson, Jr, third ed, "Fundamentals of aerodynamics", chep 4.

[18] Richard Hantula, science and curriculum consultant, "How Do Solar Panels Works?"

[19] "Trainer Design" (http://adamone.rchomepage.com)

[20] (http://www.fqes.demon.co.uk/cfd/naca.html#07)

[21] "Solar Panel Manufacturer in China" (http://www.shinesolarworld.com)

[22] Andy Lennon, Basics of R/C Model Aircraft Design.

International Journal of Modern Engineering Research (IJMER)
www.ijmer.com Vol.3, Issue.2, March-April. 2013 pp-759-764 ISSN: 2249-6645

On Topological $\tilde{g}$ α--WG Quotient Mappings

G.Anitha, [1] M.Mariasingam[2]
[1]Research Scholar, V.O.Chidambaram College, Tuticorin, Tamil Nadu, India
[2]Department of Mathematics, V.O.Chidambaram College, Tuticorin, Tamil Nadu, India

Abstract: *The aim of this paper is to introduce $\tilde{g}_\alpha$wg-quotient map using $\tilde{g}_\alpha$wg-closed sets and study their basic properties. We also study the relation between weak and strong form of $\tilde{g}_\alpha$wg-quotient maps. We also derive the relation between $\tilde{g}_\alpha$wg-quotient maps and $\tilde{g}_\alpha$-quotient maps and also derive the relation between the $\tilde{g}_\alpha$wg-continuous map and $\tilde{g}_\alpha$wg-quotient maps. Examples are given to illustrate the results.*

Keywords: *$\tilde{g}_\alpha$-closed sets, $\tilde{g}_\alpha$-open sets, $\tilde{g}_\alpha$wg-closed sets, $\tilde{g}_\alpha$wg-open sets.*

2000 Mathematics Subject Classification: *54C10, 54C08, 54C05*

I. Introduction

Njastad [12] introduced the concept of ~~an~~ α-sets and Mashhour et al [9] introduced α-continuous mappings in topological spaces. The topological notions of semi-open sets and semi-continuity, and preopen sets and precontinuity were introduced by Levine [5] and Mashhour et al [10] respectively. After advent of these notions, Reilly [14] and Lellis Thivagar [1] obtained many interesting and important results on α-continuity and α-irresolute mappings in topological spaces. Lellis Thivagar [1] introduced the concepts of α-quotient mappings and α*-quotient mappings in topological spaces. Jafari et al.[15] have introduced $\tilde{g}_\alpha$-closed set in topological spaces. The author [6] introduced $\tilde{g}_\alpha$-WG closed set using $\tilde{g}_\alpha$-closed set. In this paper we have introduced $\tilde{g}_\alpha$-WG quotient mappings.

II. Preliminaries

Throughout this paper (X,τ), (Y,σ) and (Z,η) (or X, Y and Z) represent non empty topological spaces on which no separation axiom is defined unless otherwise mentioned. For a subset A of a space the closure of A, interior of A and complement of A are denoted by cl(A), int(A) and A^c respectively.
We recall the following definitions which are useful in the sequel.

Definition 2.1: A subset A of a space (X, t) is called:

(i)semi-open set [5] if A⊆cl(int(A));
(ii) a α-open set [12] if A⊆ int(cl(int(A))).

The complement of semi-open set(resp.α-open set) is said to be semi closed (resp.α-closed)

Definition 2.2: A subset A of a topological space(X, τ)is called

(i)w-closed set [13] if cl(A) $\subseteq$U, whenever A $\subseteq$U and U is semi-open in (X, τ).

(ii) * g-closed set [16] if cl(A) $\subseteq$ U, whenever A $\subseteq$U and U is w-open in (X, τ).

(iii) a # g-semi closed set(# gs-closed)[17] if scl(A) $\subseteq$U, whenever A $\subseteq$U and U is * g -open in (X, τ).

(iv) a $\tilde{g}_\alpha$-closed [15] if αcl(A) $\subseteq$U, whenever A $\subseteq$U and U is # gs-open in (X, τ).

(v) a $\tilde{g}_\alpha$-Weakly generalized closed set($\tilde{g}_\alpha$wg-closed) [6] if Cl(Int(A)) $\subseteq$ U, whenever A $\subseteq$U,U is $\tilde{g}_\alpha$-open in (X, τ).

The complements of the above sets are called their respective open sets.

Definition 2.3: A function $f:(X,\tau)\to(Y,\sigma)$ is called

(i) a α-continuous [1] if f(V) is a α -closed set of (X, τ) for each closed set V of (Y, σ).
(ii)a α -irresolute [1] if f-1(V) is an α -open in (X,τ) for each α -open set V of (Y, σ).
(iii) a $\tilde{g}_\alpha$-continuous [3] if f^{-1}(V) is a $\tilde{g}_\alpha$_-closed set of (X, τ) for each closed set V of (Y, σ),
(iv)a $\tilde{g}_\alpha$_-irresolute [3] if f□1(V) is $\tilde{g}_\alpha$-open in (X, τ) for each $\tilde{g}_\alpha$-open set V of (Y, σ),
(v)$\tilde{g}_\alpha$wg - continuous [7] if f^{-1}(V) is $\tilde{g}_\alpha$wg-closed in (X, τ) for every closed set V of (Y, σ).
(vi) $\tilde{g}_\alpha$wg - irresolute [7] if f^{-1}(v) is $\tilde{g}_\alpha$wg-closed in (X, τ) for every $\tilde{g}_\alpha$wg-closed set V in (Y, σ)

Definition 2.4: A space(X, τ) is called $T_{\tilde{g}_\alpha wg}$-space [6] if every $\tilde{g}_\alpha$wg-closed set is closed.

Definition 2.5: A function $f:(X,\tau)\to(Y,\sigma)$ is said to be

(i)a $\tilde{g}_\alpha$wg -open [8]if the image of each open set in (X,τ) is $\tilde{g}_\alpha$wg -open set in (Y,σ).
(ii) a strongly $\tilde{g}_\alpha$wg -open or $((\tilde{g}_\alpha wg)^*$-open)[8] if the image of each $\tilde{g}_\alpha$wg -open set in (X,τ) is a $\tilde{g}_\alpha$wg -open in (Y,σ).

Definition 2.6: A surjective map $f:(X,\tau)\to(Y,\sigma)$ is said to be

(i) a quotient map [4] provided a subset U of (Y,σ) is open in (Y, σ) if and only if f^{-1}(U) is open in (X, τ),
(ii) An α-quotient map [1] if f is α -continuous and f^{-1}(U) is open in (X, τ) implies U is an α -open in (Y, σ)
(iii) An α^* -quotient map [1] if f is α -irresolute and f^{-1}(U) is an α -open set in (X, τ) implies U is an open set in (Y, σ).
(iv) a $\tilde{g}_\alpha$-quotient map[2] if f is $\tilde{g}_\alpha$-continuous and f^{-1}(U) is open in (X,τ) implies U is a $\tilde{g}_\alpha$-open set in (Y,σ).
(v) a strongly $\tilde{g}_\alpha$-quotient map[2], provided a set U of (Y,σ) is open in Y if and only if f^{-1}(U) is a $\tilde{g}_\alpha$-open set in (X,τ).
(vi) a $\tilde{g}_\alpha{}^*$-quotient map[2]if f is $\tilde{g}_\alpha$ -irresolute and f^{-1}(U) is an $\tilde{g}_\alpha$ -open set in (X, τ) implies U is an open set in (Y, σ).

Remark 2.7: The collection of all $\tilde{g}_\alpha$wg-closed ($\tilde{g}_\alpha$wg-open sets) are denoted by $\tilde{G}_\alpha$WG_Cl(X) and ($\tilde{G}_\alpha$WG-O(X)), respectively.

III. $\tilde{g}_\alpha$ - Weakly Generalized quotient maps.

Definition 3.1: A surjective map $f:(X,\tau)\to(Y,\sigma)$ is said to be $\tilde{g}_\alpha$wg-quotient map if f is $\tilde{g}_\alpha$wg-continuous and f^{-1}(V) is open in (X,τ) implies V is $\tilde{g}_\alpha$wg-open set in (Y,σ).

Example3.2: Let$X=\{a,b,c,d\},\tau=\{\emptyset,X,\{a\},\{a,c\},\{a,b,d\}\},Y=\{1,2,3\},\sigma=\{\emptyset,Y,\{1\},\{1,2\},\{1,3\}\}$,
$\tilde{g}_\alpha$wg$O(X)$={∅,X,{a},{a,c},{a,b},{a,d},{a,b,c},{a,b,d},{a,c,d}}, $\tilde{g}_\alpha$wgO(Y) = {∅,Y,{1},{1,2},{1,3}}
The map $f:(X,\tau)\to(Y,\sigma)$ is defined as f(a)=1, f(b)=2=f(d), f(c)=3. The map f is $\tilde{g}_\alpha$wg-quotient map.

Proposition 3.3: If a map $f:(X,\tau)\to(Y,\sigma)$ is $\tilde{g}_\alpha$wg-continuous and $\tilde{g}_\alpha$wg-open then f is $\tilde{g}_\alpha$wg-quotient map.
Proof: We only need to prove f^{-1}(V) is open in (X,τ) implies V is $\tilde{g}_\alpha$wg-open in (Y,σ). Let f^{-1}(V) is open in (X,τ). Then f(f^{-1}(V)) is $\tilde{g}_\alpha$wg-open in(Y,σ). Since f is $\tilde{g}_\alpha$wg-open. Hence V is $\tilde{g}_\alpha$wg-open in (X,τ).

IV. Strong form of $\tilde{g}_\alpha$ - Weakly Generalized quotient maps.

Definition 4.1: Let $f:(X,\tau)\to(Y,\sigma)$ be a surjective map. Then f is called strongly $\tilde{g}_\alpha$wg-quotient map provided a set U of (Y,σ) is open in Y if and only if f^{-1}(U) is $\tilde{g}_\alpha$wg-open set in (X,τ)

Example 4.2: Let $X=\{a,b,c,d\},\tau=\{\emptyset,X,\{a\},\{b,c\},\{a,b,c\}\},Y=\{1,2,3\},\sigma=\{\emptyset,Y,\{1\},\{2\},\{1,2\}\}$
$\tilde{g}_\alpha$wg$O(X)$={∅,X,{a},{b},{c},{a,c},{a,b},{b,c},{a,b,c},{a,b,d},{a,c,d}}, $\tilde{g}_\alpha$wgO(Y) = {∅,Y,{1},{2},{1,2}}
The map $f:(X,\tau)\to(Y,\sigma)$ is defined as f(a)=1, f(b)=2=f(c), f(d)=3.The map f is strongly $\tilde{g}_\alpha$wg-quotient map.

Theorem 4.3: Every strongly $\tilde{g}_\alpha$wg-quotient map is $\tilde{g}_\alpha$wg-open map.
Proof: Let $f:(X,\tau)\to(Y,\sigma)$ be a strongly $\tilde{g}_\alpha$wg $-$ $quotient\ map$. Let V be any open set in (X,τ). Since every open set is $\tilde{g}_\alpha$wg-open by theorem 3.2[6]. Hence V is $\tilde{g}_\alpha$wg-open in (X,τ). That is f^{-1}(f(V)) is $\tilde{g}_\alpha$wg-open in(X,τ). Since f is strongly $\tilde{g}_\alpha$wg-quotient, then f(V) is open in (Y,σ) and hence f(V) is $\tilde{g}_\alpha$wg-open in (Y,σ). This shows that f is $\tilde{g}_\alpha$wg-open map.

Remark 4.4: Converse need not be true

Example 4.5: Let $X=\{a,b,c,d\},\tau=\{\emptyset,X,\{a\},\{b\},\{a,b\}\},Y=\{1,2,3\},\sigma=\{\emptyset,Y,\{1\},\{2\},\{1,2\},\{1,3\}\}$, $\tilde{g}_\alpha$wg$O(X)$={∅,X,{a},{b},{a,b},{a,b,c},{a,b,d}}, $\tilde{g}_\alpha$wgO(Y) = {∅,Y,{1},{2},{1,2},{1,3}}. $f:(X,\tau)\to(Y,\sigma)$ is defined by f(a)=1=f(b), f(c)=3, f(d)=2 is a $\tilde{g}_\alpha$wg-open map but not a strongly $\tilde{g}_\alpha$wg-quotient map. Since the set {2} is open in (Y,σ) but f^{-1}({2})={d} is not $\tilde{g}_\alpha$wg-open in (X,τ).

Theorem 4.6: Every strongly $\tilde{g}_\alpha$wg-quotient map is strongly $\tilde{g}_\alpha$wg-open.
Proof: Let $f:(X,\tau)\to(Y,\sigma)$be a strongly $\tilde{g}_\alpha$wg-quotient map. Let V be a $\tilde{g}_\alpha$wg-open in (X,τ). That is f^{-1}(f(V)) is $\tilde{g}_\alpha$wg-open in(X,τ). Since f is strongly $\tilde{g}_\alpha$wg-quotient, then f(V) is open in (Y,σ) and hence f(V) is $\tilde{g}_\alpha$wg-open in (Y,σ). This shows that f is $\tilde{g}_\alpha$wg-open map.

Example4.7: Let $X=\{a,b,c\},\tau=\{\emptyset,X,\{a\},\{c\},\{a,c\}\},Y=\{1,2,3\},\sigma=\{\emptyset,Y,\{1,3\}\}$, $\tilde{g}_\alpha$wg$O(X)$={S∅,X,{a},{c},{a,c}}, $\tilde{g}_\alpha$wgO(Y) = {∅,Y,{1},{3},{1,2},{1,3},{2,3}}. The map $f:(X,\tau)\to(Y,\sigma)$ is defined as identity map. Then f is strongly $\tilde{g}_\alpha$wg-open but not strongly $\tilde{g}_\alpha$wg-quotient map. Since
f^{-1}({3})={c} is $\tilde{g}_\alpha$wg-open in (X,τ) but {3} is not open in (Y,σ).

Definition 4.8: Let $f:(X,\tau)\to(Y,\sigma)$ be a surjective map. Then f is called a $(\tilde{g}_\alpha wg)^*$ -quotient map if f is $\tilde{g}_\alpha$wg-irresolute and f^{-1}(V) is a $\tilde{g}_\alpha$wg-open set in (X,τ) implies V is open in (Y,σ).

Example 4.9: X={a,b,c,d}, τ={∅,X,{a},{b},{a,b}}, Y={1,2,3}, $\sigma=\{\emptyset,Y,\{1\},\{3\},\{1,3\}\}$
$\tilde{g}_\alpha$wg$O(X)$={∅,X,{a},{b},{a,b},{a,b,c},{a,b,d}}, $\tilde{g}_\alpha$wgO(Y) = {∅,Y,{1},{3},{1,3}}. The map $f:(X,\tau)\to(Y,\sigma)$ defined by f(a)=1, f(b)=3, f(c)=2=f(d). The map f is $(\tilde{g}_\alpha wg)^*$-quotient map.

Theorem 4.10: Every $(\tilde{g}_\alpha wg)^*$-quotient map is $\tilde{g}_\alpha$wg-irresolute.
Proof: Obviously true from the definition.

Remark 4.11: Converse need not be true.

Example 4.12: X={a,b,c,d}, $\tau=\{\emptyset,X,\{a\},\{a,c\},\{a,b,d\}\},Y=\{1,2,3\},\sigma=\{\emptyset,Y,\{1\},\{1,3\}\}$
$\tilde{g}_\alpha$wg$O(X)$={∅,X,{a},{a,c},{a,b},{a,d},{a,b,c},{a,b,d},{a,c,d}}, $\tilde{g}_\alpha$wgO(Y) = {∅,Y,{1},{1,2},{1,3}} Let $f:(X,\tau)\to(Y,\sigma)$ is defined by f({a})={1}, f({b})={2}=f({d}),f({c})={3}. The map f is $\tilde{g}_\alpha$wg-irresolute but not $(\tilde{g}_\alpha wg)^*$-quotient map Since f^{-1}({1,2})={a,b,d} is $\tilde{g}_\alpha$wg-open in (X,τ) but the set {1,2} is not open in (Y,σ).

Theorem 4.13: Every $(\tilde{g}_\alpha wg)^*$-quotient map is strongly $\tilde{g}_\alpha$wg-open map.

Proof: Let $f:(X,\tau)\to(Y,\sigma)$ be a $(\tilde{g}_\alpha wg)^*$-quotient map. Let V be $\tilde{g}_\alpha$wg-open set in (X,τ). Then f^{-1}(f(V)) is $\tilde{g}_\alpha$wg-open in (X,τ). Since f is $(\tilde{g}_\alpha wg)^*$-quotient this implies that f(V) is open in (Y,σ) and thus $\tilde{g}_\alpha$wg-open in (Y,σ) and thus f(V) is $\tilde{g}_\alpha$wg-open in (Y,σ). Hence f is strongly $\tilde{g}_\alpha$wg-open.

Remark 4.14: Converse need not be true

Example 4.15: Let X={a,b,c}, τ={$\emptyset, X, \{c\}, \{a,c\}, \{b,c\}$}, Y={1,2,3}, $\sigma=\{\emptyset, Y, \{1\}, \{2,3\}\}$,
$\tilde{g}_\alpha$wg$O(X)$={∅,X,{c}.{a,c},{b,c}}, $\tilde{g}_\alpha$wgO(Y) = {∅,Y,{1},{2},{3},{1,2},{2,3},{1,3}}
Let $f:(X,\tau)\to(Y,\sigma)$ be a identity map, f is strongly $\tilde{g}_\alpha$wg –open map but not $(\tilde{g}_\alpha wg)^*$-quotient map. since
F-1{1}={a} is $\tilde{g}_\alpha$wg-open in (Y,σ) but the set{1} is not $\tilde{g}_\alpha$wg-open set in (X,τ).

Proposition 4.16: Every $\tilde{g}_\alpha$-irresolute (α-irresolute) map is $\tilde{g}_\alpha$wg-irresolute.
Proof: Let U be $\tilde{g}_\alpha$-closed (α-closed) set in(Y,σ). Since every $\tilde{g}_\alpha$-closed (α-closed) set is $\tilde{g}_\alpha$wg-closed by theorem 3.7(by theorem 3.11)[6]. Then U is $\tilde{g}_\alpha$wg-closed in (Y,σ). Since f is $\tilde{g}_\alpha$-irresolute (α-irresolute), f^{-1}(U) is $\tilde{g}_\alpha$-closed (α-closed) in (X,τ) which is $\tilde{g}_\alpha$wg-closed in (X,τ). Hence f is $\tilde{g}_\alpha$wg-irresolute.

V. Comparisons

Proposition 5.1:
(i) Every quotient is $\tilde{g}_\alpha$wg-quotient map.
(ii) Every α-quotient map is $\tilde{g}_\alpha$wg-quotient map.
Proof: Since every continuous and α-continuous map is $\tilde{g}_\alpha$wg-continuous by theorem 2.3 1nd 2.7[7] and every open set and α-open set is $\tilde{g}_\alpha$wg-open by theorem 3.11[6]. The proof follows from the definition.

Remark 5.2: Converse of the above proposition need not be true.

Example 5.3: Let X={a,b,c,d}, $\tau=\{\emptyset, X, \{a\}, \{b\}, \{a,b\}\}, Y=\{1,2,3\}, \sigma=\{\emptyset, Y, \{1,2\}\}$
$\tilde{g}_\alpha$wg$O(X)$={∅,X,{a},{b}, {a,b}, {a,b,c},{a,b,d}}, $\tilde{g}_\alpha$wgO(Y) = {∅,Y,{1},{1,2},{1,3},{2,3}}. Let $f:(X,\tau)\to(Y,\sigma)$ is defined by f({a})={1}, f({b})={2},f({c})={3}=f({d}).The function f is $\tilde{g}_\alpha$wg-quotient but not a quotient map. Since f^{-1}{1}={a} is open in(X,τ) but the set {1} is not open in (Y, σ).

Example 5.4: Let X={a,b,c,d}, $\tau=\{\emptyset, X, \{a\}, \{b\}, \{a,b\}\}, Y=\{1,2,3\}, \sigma=\{\emptyset, Y, \{1,2\}\}$
$\tilde{g}_\alpha$wg$O(X)$={∅,X,{a},{b}, {a,b}, {a,b,c},{a,b,d}},$\alpha O(X)$= {∅,X,{a},{b}, {a,b}, {a,b,c},{a,b,d}}, $\tilde{g}_\alpha$wgO(Y) = {∅,Y,{1},{1,2},{1,3},{2,3}}, $\alpha O(Y)$= {∅,Y,{1,2}}. Let $f:(X,\tau)\to(Y,\sigma)$ is defined by f({a})={1}, f({b})={2},f({c})={3}=f({d}).The function f is $\tilde{g}_\alpha$wg-quotient but not α-quotient map. Since
f^{-1}{1}={a} is open in(X,τ) but the set {1} is not α- open in (Y, σ).

Theorem 5.5: Every $\tilde{g}_\alpha$-quotient map is $\tilde{g}_\alpha$wg-quotient map.
Proof: Let $f:(X,\tau)\to(Y,\sigma)$ be a $\tilde{g}_\alpha$-quotient map. Then f is $\tilde{g}_\alpha$-continuous function. By theorem 2.5[7] every $\tilde{g}_\alpha$-continuous function is $\tilde{g}_\alpha$wg-continuous function, then f is $\tilde{g}_\alpha$wg-continuous map. Let f^{-1}(V) is open in (Y,σ). Since every $\tilde{g}_\alpha$-open set is $\tilde{g}_\alpha$wg-open . Then V is $\tilde{g}_\alpha$wg-open in (Y,σ). Hence V is $\tilde{g}_\alpha$wg-open in (Y,σ). Hence f is $\tilde{g}_\alpha$wg-quotient map.

Remark 5.6: Converse need not be true:

Example 5.7: Let X={a,b,c,d}, $\tau=\{\emptyset, X, \{d\}, \{a,c\}, \{a,c,d\}\}$, $Y=\{1,2,3\}, \sigma=\{\emptyset, Y, \{2\}, \{3\}, \{1,3\}, \{2,3\}\}$
$\tilde{g}_\alpha$wg$O(X)$={∅,X,{a},{c},{d},{a,c},{a,d},{c,d},{a,b,d},{a,c,d},{b,c,d}}, $\tilde{g}_\alpha$O(X) = {∅,Y,{a},{c},{d},{a,c},{a,d},{c,d},{a,c,d}}. Let $f:(X,\tau)\to(Y,\sigma)$ is defined by f(a)=2, f(b)=1,f(c)=3=f(d). f is $\tilde{g}_\alpha$wg-quotient map but not $\tilde{g}_\alpha$-quotient map Since f^{-1}{1,3}={b,c,d} is $\tilde{g}_\alpha$wg-open in(X,τ) but not $\tilde{g}_\alpha$- open in (Y, σ).

Theorem 5.8: Every strongly $\tilde{g}_\alpha$wg-quotient map is $\tilde{g}_\alpha$wg-quotient.

Proof: Let V be any open set in(Y,σ). Since f is strongly $\tilde{g}_\alpha$wg-quotient, f^{-1}(V) is $\tilde{g}_\alpha$wg-open set in (X,τ). Hence f is $\tilde{g}_\alpha$wg continuous. Let f^{-1}(V) be open in (X,τ). Then f^{-1}(V) is $\tilde{g}_\alpha$wg-open in (X,τ). Since f is strongly $\tilde{g}_\alpha$wg-quotient, V is open in (Y,σ). Hence f is a $\tilde{g}_\alpha$wg quotient map.

Remark 5.9: Converse need not be true

Example 5.10: Let X= {a, b, c, d}, $\tau=\{\emptyset, X, \{a\}, \{a,c\}, \{a,b,d\}\}, Y=\{1,2,3\}, \sigma=\{\emptyset, Y, \{1\}\}$
$\tilde{g}_\alpha$wg$O(X)$={∅,X,{a},{a,c},{a,b},{a,d},{a,b,c},{a,b,d},{a,c,d}}, $\tilde{g}_\alpha$wgO(Y) = {∅,Y,{1},{1,2},{1,3}} Let $f:(X,\tau)\to(Y,\sigma)$ is defined by f({a})={1}, f({b})={3},f({c})=2=f({d}).The function f is $\tilde{g}_\alpha$wg-quotient but not strongly $\tilde{g}_\alpha$wg-quotient. Since f^{-1}{1,3}={a,b} is $\tilde{g}_\alpha$wg-open in(X,τ) but {1,3} is not open in (Y, σ).

Theorem 5.11: Every strongly $\tilde{g}_\alpha$-quotient map is strongly $\tilde{g}_\alpha wg$-quotient map.
Proof: Let $f:(X,\tau)\to(Y,\sigma)$ strongly $\tilde{g}_\alpha$-quotient map. Let V be any open set in (Y,σ). Since f is strongly $\tilde{g}_\alpha$-quotient, f^{-1}(V) is $\tilde{g}_\alpha$-open in (X,τ). Since every $\tilde{g}_\alpha$-open set is $\tilde{g}_\alpha wg$-open by theorem. Then f^{-1}(v) is $\tilde{g}_\alpha$wg-open in(X,τ). Hence f is strongly $\tilde{g}_\alpha$wg-quotient map.

Remark 5.12: Converse need not be true.

Example 5.13: Let X={a,b,c,d}, $\tau=\{\emptyset, X, \{d\}, \{a,c\}, \{a,c,d\}\}$, $Y=\{1,2,3\}, \sigma=\{\emptyset, Y, \{b\}, \{c\}, \{b,c\}, \{a,c\}\}$
$\tilde{g}_\alpha$wg$O(X)$={∅,X,{a},{c},{d},{a,c},{a,d},{c,d},{a,b,d},{a,c,d},{b,c,d}}, $\tilde{g}_\alpha$O(X) = {∅,Y,{a},{c},{d},{a,c},{a,d},{c,d},{a,c,d}}. Let $f:(X,\tau)\to(Y,\sigma)$ is defined by f({a})={b}, f({b})={a},f({c})=c=f({d}). Since f^{-1}{a,c}={b,c,d} is $\tilde{g}_\alpha$wg-open in(X,τ) but not $\tilde{g}_\alpha$- open in (Y, σ).

Theorem 5.14: Every strongly $\tilde{g}_\alpha$wg quotient map is $\tilde{g}_\alpha$wg quotient
Proof: Let V be any open set in (Y,σ). Since f is strongly $\tilde{g}_\alpha$wg quotient, $f^{-1}(V)$ is $\tilde{g}_\alpha$wg-open set in(X,τ). Hence f is $\tilde{g}_\alpha$wg-continuous. Let $f^{-1}(V)$ be open in (X,τ). Then $f^{-1}(V)$ is $\tilde{g}_\alpha$wg open in (X,τ) . Since f is strongly $\tilde{g}_\alpha$wg-quotient V is open in (Y,σ). Hence f is a $\tilde{g}_\alpha$wg-quotient map.

Remark 5.15: Converse need not be true

Example 5.16: Let X={a,b,c,d}, $\tau = \{\emptyset, X, \{a\}, \{a,c\}, \{a,b,d\}\}, Y = \{1,2,3\}, \sigma = \{\emptyset, Y, \{1\}\}$
$\tilde{g}_\alpha$wg$O(X)$={∅,X,{a},{a,c},{a,b},{a,d},{a,b,c},{a,b,d},{a,c,d}}, $\tilde{g}_\alpha$wgO(Y) = {∅,Y,{1},{1,2},{1,3}} Let $f:(X,\tau) \to (Y,\sigma)$ is defined by f({a})={1}, f({b})={3},f({c})=2=f({d}).The function f is $\tilde{g}_\alpha$wg-quotient but not strongly $\tilde{g}_\alpha$wg-quotient. Since f^{-1}{1,3}={a,b} is $\tilde{g}_\alpha$wg-open in(X,τ) but {1,3} is not open in (Y, σ).

Theorem 5.17: Every $(\tilde{g}_\alpha wg)^*$-quotient map is $\tilde{g}_\alpha$wg-quotient map.
Proof: Let f be $(\tilde{g}_\alpha wg)^*$-quotient map. Then f is $\tilde{g}_\alpha$wg-irresolute, by theorem 3.2[7] f is $\tilde{g}_\alpha$wg-continuous. Let $f^{-1}(V)$ be an open set in (X,τ). Then $f^{-1}(V)$ is a $\tilde{g}_\alpha$wg-open in(X,τ). Since f is $(\tilde{g}_\alpha wg)^*$-quotient, V is open in (Y,σ). It means V is $\tilde{g}_\alpha$wg-open in (Y,σ). Therefore f is a $\tilde{g}_\alpha$wg-quotient map.

Remark 5.18: Converse need not be true

Example 5.19: Let X={a,b,c,d}, $\tau = \{\emptyset, X, \{a\}, \{a,c\}, \{a,b,d\}\}, Y = \{1,2,3\}, \sigma = \{\emptyset, Y, \{1\}\}$
$\tilde{g}_\alpha$wg$O(X)$={∅,X,{a},{a,c},{a,b},{a,d},{a,b,c},{a,b,d},{a,c,d}}, $\tilde{g}_\alpha$wgO(Y) = {∅,Y,{1},{1,2},{1,3}} Let $f:(X,\tau) \to (Y,\sigma)$ is defined by f({a})={1}, f({b})={3},f({c})=2=f({d}).The function f is $\tilde{g}_\alpha$wg-quotient but not ($\tilde{g}_\alpha$wg)*-quotient. Since f^{-1}{1,2}={a,c,d} is $\tilde{g}_\alpha$wg-open in(X,τ) but {1,2} is not open in (Y, σ).

Theorem 5.20: Every α^*-quotient map is $(\tilde{g}_\alpha wg)^*$-quotient map.
Proof: Let f be α^*-quotient map. Then f is surjective, α-irresolute and $f^{-1}(U)$ is α-open in (X,τ) implies U is open set in(Y,σ). Then U is $\tilde{g}_\alpha wg$-open in (Y,σ). Since every α-irresolute map is $\tilde{g}_\alpha$wg-irresolute by proposition 4.16 and every α-irresolute map is α-continuous. Then $f^{-1}(U)$ is α-open which is $\tilde{g}_\alpha wg$-open in(X,τ). Since f is α^*-quotient map, U is open in (Y,σ). Hence f is $(\tilde{g}_\alpha wg)^*$-quotient map.

Remark 5.21: Converse need not be true

Example 5.22: X={a,b,c,d}, $\tau = \{\emptyset, X, \{d\}, \{a,c\}, \{a,c,d\}\}, Y = \{1,2,3\}, \sigma = \{\emptyset, Y, \{2\}, \{3\}, \{2,3\}, \{1,3\}\}$
$\tilde{g}_\alpha$wg$O(X)$={∅,X,{a},{c},{d},{a,c},{a,d},{c,d},{a,b,d},{a,c,d},{b,c,d}}, $\tilde{g}_\alpha$wgO(Y) = {∅,Y,{2},{3},{2,3},{1,3}}, $\alpha O(X)$={{d},{a,c},{a,c,d}}, αO(Y)={{2},{3},{2,3},{1,3}}. The map $f:(X,\tau) \to (Y,\sigma)$ is defined by f(a)=2, f(b)=1,f(c)=3=f(d).The function f is ($\tilde{g}_\alpha$wg)*-quotient but not $(\alpha)^*$-quotient map. Since the set {2} is α-open in (Y,σ) but f^{-1}{2}={a} is not α -open in(X,τ).

Theorem 5.23: Every $(\tilde{g}_\alpha)^*$ quotient map is $(\tilde{g}_\alpha wg)^*$-quotient map:
Proof: Let f be $(\tilde{g}_\alpha)^*$-quotient map. Then f is surjective, $\tilde{g}_\alpha$-irresolute and f(U) is $\tilde{g}_\alpha$-open in (X,τ) implies U is open in(Y,σ). Then U is $\tilde{g}_\alpha$wg-open in(Y,σ). Since every $\tilde{g}_\alpha$-irresolute map is $\tilde{g}_\alpha$wg-irresolute and every $\tilde{g}_\alpha$-irresolute map is $\tilde{g}_\alpha$-continuous. Then $f^{-1}(U)$ is $\tilde{g}_\alpha$-open set which is $\tilde{g}_\alpha$wg-open set in(X,τ). Since f is a $(\tilde{g}_\alpha)^*$-quotient map, U is open in (Y,σ). Hence f is a $(\tilde{g}_\alpha wg)^*$-quotient map.

Remark 5.24: Converse need not be true

Example 5.25: Let X={a,b,c,d}, $\tau = \{\emptyset, X, \{d\}, \{a,c\}, \{a,c,d\}\}, Y = \{1,2,3\}, \sigma = \{\emptyset, Y, \{2\}, \{3\}, \{2,3\}, \{1,3\}\}$
$\tilde{g}_\alpha$wg$O(X)$={∅,X,{a},{c},{d},{a,c},{a,d},{c,d},{a,b,d},{a,c,d},{b,c,d}}, $\tilde{g}_\alpha$wgO(Y) = {∅,Y,{2},{3},{2,3},{1,3}}, $\tilde{g}_\alpha O(X)$={{a},{d},{c},{a,c},{a,d},{c,d},{a,b,d},{a,c,d},{b,c,d}}. $\tilde{g}_\alpha$O(Y)={{2},{3},{2,3},{1,3}}. The map $f:(X,\tau) \to (Y,\sigma)$ is defined by f({a})={2}, f({b})={1},f({c})=3=f({d}).The function f is ($\tilde{g}_\alpha$wg)*-quotient but not $(\tilde{g}_\alpha)^*$-quotient map. Since the set {1,3} is $\tilde{g}_\alpha$-open in (Y,σ) but f^{-1}{1,3}={b,c,d} is not $\tilde{g}_\alpha$-open in(X,τ).

Theorem 5.26: Every $(\tilde{g}_\alpha wg)^*$-quotient map is strongly $\tilde{g}_\alpha$wg-quotient.
Proof: Let V be an open set in (Y,σ). Then it is $\tilde{g}_\alpha$wg-open in(Y,σ) since f is $(\tilde{g}_\alpha wg)^*$-quotient map. $f^{-1}(V)$ is $\tilde{g}_\alpha$wg-open in (X,τ).(Since f is $\tilde{g}_\alpha$wg-irresolute). Also V is open in(Y,σ) implies $f^{-1}(V)$ is $\tilde{g}_\alpha$wg-open in (X,τ). since f is $(\tilde{g}_\alpha wg)^*$-open V is open in(Y,σ). Hence f is strongly $\tilde{g}_\alpha$wg-quotient map.

Remark 5.27: Converse need not be true

Example 5.28: Let X={a,b,c,d}, $\tau = \{\emptyset, X, \{a\}, \{b\}, \{a,b\}, \{a,b,c\}\}, Y = \{1,2,3\}, \sigma = \{\emptyset, Y, \{1\}, \{1,2\}\}$
$\tilde{g}_\alpha$wg$O(X)$={∅,X,{a},{b},{a,b},{a,b,c},{a,b,d}}, $\tilde{g}_\alpha$wgO(Y) = {∅,Y,{1},{1,2},{1,3}} Let $f:(X,\tau) \to (Y,\sigma)$ is defined by f({a})={1}, f({b})={2}=f({c}),f({d})={3}.The function f is strongly $\tilde{g}_\alpha$wg-quotient but not a $(\tilde{g}_\alpha wg)^*$-quotient. Since the set {1,3} is $\tilde{g}_\alpha$wg-open in(Y,σ) but f^{-1}{1,3}={a,d} is not open in (X,τ).

Remark 5.29: Quotient map and α^*-quotient map are independent

Example 5.30: Let X={a,b,c,d}, $\tau = \{\emptyset, X, \{a\}, \{a,b\}\}, Y = \{1,2,3\}, \sigma = \{\emptyset, Y, \{1\}, \{1,2\}\}$
$\alpha O(X)$={∅,X,{a},{a,b},{a,c},{a,d},{a,b,c},{a,b,d},{a,c,d}}, αO(Y) = {∅,Y,{1},{1,2},{1,3}} Let $f:(X,\tau) \to (Y,\sigma)$ is defined by f(a)=1, f(b)={2},f(c)=3=f(d).The function f is quotient but not a $(\alpha)^*$-quotient. Since f^{-1}{1,3}={a,c,d} is α-open in(X,τ) but the set {1,3} is not open in (Y,σ).

Example 5.31: Let X={a,b,c,d}, $\tau = \{\emptyset, X, \{a\}, \{a,c\}, \{a,b,c\}\}, Y = \{1,2,3\}, \sigma = \{\emptyset, Y, \{1\}, \{1,2\}, \{1,3\}\}$

$\alpha O(X)$={∅,X,{a},{a,b},{a,c},{a,d},{a,b,c},{a,b,d},{a,c,d}}, αO(Y) = {∅,Y,{1},{1,2},{1,3}} Let $f:(X,\tau)\to(Y,\sigma)$ is defined by f(a)=1, f(b)={2},f(c)=3=f(d).The function f is α^* quotient but not a quotient map. Since f^{-1}{1,3}={a,c,d} is α-open in(X,τ) but the set {1,3} is not open in (Y,σ)

Remark 5.32: Quotient map and strongly $\tilde{g}_\alpha$wg-quotient map are independent.

Example 5.33: X={a,b,c,d}, $\tau=\{\emptyset,X,\{d\},\{a,c\},\{a,c,d\}\}, Y=\{1,2,3\},\sigma=\{\emptyset,Y,\{2\},\{3\},\{2,3\},\{1,3\}\}$
$\tilde{g}_\alpha wgO(X)$={∅,X,{a},{c},{d},{a,c},{a,d},{c,d},{a,b,d},{a,c,d},{b,c,d}}, $\tilde{g}_\alpha$wgO(Y) = {∅,Y,{2},{3},{2,3},{1,3}}, $\alpha O(X)$={{d},{a,c},{a,c,d}}, αO(Y)={{2},{3},{2,3},{1,3}}. The map $f:(X,\tau)\to(Y,\sigma)$ is defined by f(a)=2, f(b)=1,f(c)=3=f(d).The function f is strongly $\tilde{g}_\alpha$wg-quotient but not quotient map. Since the set {2} is open in (Y,σ) but f^{-1}{2}={a} is not open in(X,τ).

Example 5.34: X={a,b,c,d}, $\tau=\{\emptyset,X,\{a\},\{a,b\}\}, Y=\{1,2,3\},\sigma=\{\emptyset,Y,\{1\},\{1,2\}\}$
$\tilde{g}_\alpha wgO(X)$={∅,X,{a},{a,b},{a,c},{a,d},{a,b,c},{a,b,d},{a,c,d}}, $\tilde{g}_\alpha$wgO(Y) = {∅,Y,{1},{1,2},{1,3}}, The map $f:(X,\tau)\to(Y,\sigma)$ is defined by f(a)=1, f(b)=2,f(c)=3=f(d).The function f is quotient but not strongly $\tilde{g}_\alpha$wg-quotient map. Since f^{-1}({1,3} is $\tilde{g}_\alpha$wg -open in (X,τ) but the set {1,3} is not open in
(Y,σ).

Remark 5.35: From the above results we have the following diagram where A ⟶ B represent A implies B but not conversely, A ⟷ B represents A and B are independent each other.

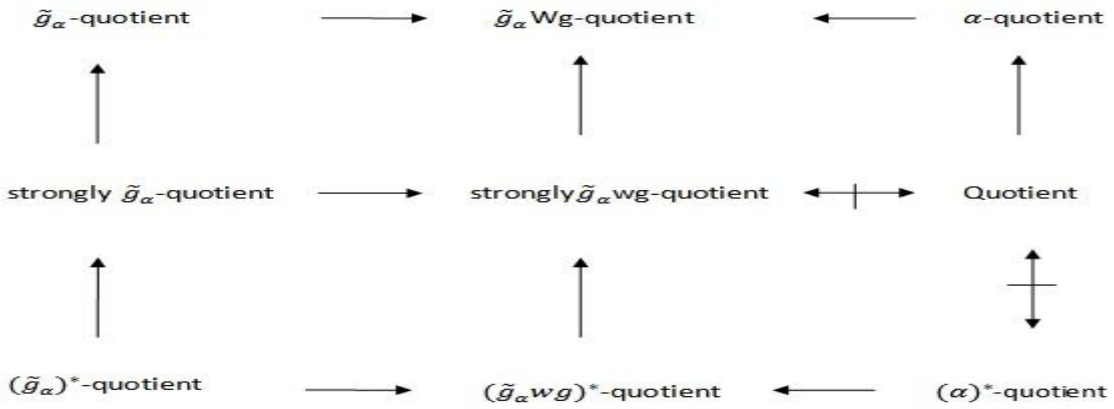

VI. Applications

Theorem 6.1: The composition of two $(\tilde{g}_\alpha wg)^*$-quotient maps is $(\tilde{g}_\alpha wg)^*$-quotient.
Proof: Let $f:(X,\tau)\to(Y,\sigma)$and $g:(Y,\sigma)\to(Z,\eta)$ be two $(\tilde{g}_\alpha wg)^*$-quotient maps. Let V be any $\tilde{g}_\alpha$wg-open set in (Z,η). Since g is $(\tilde{g}_\alpha wg)^*$-quotient, g^{-1}(V) is $\tilde{g}_\alpha$wg-open in(Y,σ) and since f is $(\tilde{g}_\alpha wg)^*$-quotient then
$(f^{-1}(g^{-1}(V)))=(g\circ f)^{-1}(V)$ is $\tilde{g}_\alpha$wg-open in(X,τ). Hence g∘f is $\tilde{g}_\alpha$wg-irresolute.

Let $(g\circ f)^{-1}(V)$ is $\tilde{g}_\alpha$wg-open in(X,τ). Then $f^{-1}(g^{-1}(V))$ is $\tilde{g}_\alpha$wg-open in(X,τ). Since f is $(\tilde{g}_\alpha wg)^*$-quotient, g^{-1}(V) is open in (Y,σ). Since g is $(\tilde{g}_\alpha wg)^*$-quotient, V is open in (Z,η). Hence g∘f is $(\tilde{g}_\alpha wg)^*$-quotient.

Proposition 6.2: If $h:(X,\tau)\to(Y,\sigma)$ is $\tilde{g}_\alpha$wg-quotient map and $g:(X,\tau)\to(Z,\eta)$ is a continuous map that is constant on each set h^{-1}(y) for y∈Y, then g induces a $\tilde{g}_\alpha$wg-continuous map $f:(Y,\sigma)\to(Z,\eta)$ *such that* $f\circ h=g$.
Proof: g is a constant on h^{-1}(y) for each y∈Y, the set g(h^{-1}(y)) is a one point set in (Z,η). If f(y) denote this point, then it is clear that f is well defined and for each $x\in X, f(h(x))=g(x)$. We claim that f is $\tilde{g}_\alpha$wg-continuous. For if we let V be any open set in (Z,η), then g^{-1}(V) is an open set in (X,τ) as g is continuous. But $g^{-1}(V)=h^{-1}(f^{-1}(V))$ is open in (X,τ). Since h is $\tilde{g}_\alpha$wg-quotient map, f^{-1}(V) is a $\tilde{g}_\alpha$wg-open in(Y,σ). Hence f is $\tilde{g}_\alpha$wg-continuous.

Proposition 6.3: If a map $f:(X,\tau)\to(Y,\sigma)$ is surjective, $\tilde{g}_\alpha$wg-continuous and $\tilde{g}_\alpha$wg-open then f is a $\tilde{g}_\alpha$wg-quotient map.
Proof: To prove f is $\tilde{g}_\alpha$wg-quotient map. We only need to prove f^{-1}(V) is open in (X,τ) implies V is $\tilde{g}_\alpha$wg-open in (Y,σ). Since f is $\tilde{g}_\alpha$wg-continuous. Let f^{-1}(V) is open in (X,τ). Then f(f^{-1}(V)) is $\tilde{g}_\alpha$wg-open set, since f is $\tilde{g}_\alpha$wg-open. Hence V is $\tilde{g}_\alpha$wg-open set. Hence V is $\tilde{g}_\alpha$wg-open set, as f is surjective, f(f^{-1}(V))=V. Thus f is a $\tilde{g}_\alpha$wg-quotient map.

Proposition 6.4: If $f:(X,\tau)\to(Y,\sigma)$be open surjective, $\tilde{g}_\alpha$wg-irresolute map, and $g:(Y,\sigma)\to(Z,\eta)$is a $\tilde{g}_\alpha$wg-quotient map then $g\circ f:(X,\tau)\to(Z,\eta)$ is $\tilde{g}_\alpha$wg-quotient map.
Proof: Let V be any open set in (Z, η). Since g is $\tilde{g}_\alpha$wg-quotient map then g^{-1}(V) is $\tilde{g}_\alpha$wg-open in (Y,σ). Since f is $\tilde{g}_\alpha$wg-irresolute, $f^{-1}(g^{-1}(V))=(g\circ f)^{-1}(V)$ is $\tilde{g}_\alpha$wg-open in (X,τ). This implies
$(g\circ f)^{-1}(V)$ is $\tilde{g}_\alpha$wg-open set in (X,τ). This shows that g∘f is $\tilde{g}_\alpha$wg-continuous map. Also assume that
$(g\circ f)^{-1}(V)$ *is open in* (X,τ). *For* $V\subseteq Z$, *that is* $(f^{-1}(g^{-1}(V))$ *is open in* (Y,σ). It follows that g^{-1}(V) is open in (Y,σ). Since f is surjective and g is $\tilde{g}_\alpha$wg-quotient map. V is $\tilde{g}_\alpha$wg-open set in(Z,η).

Proposition 6.5: Let $f:(X,\tau)\to(Y,\sigma)$be strongly $\tilde{g}_\alpha$wg-open surjective and $\tilde{g}_\alpha$wg-irresolute map and $g:(Y,\sigma)\to(Z,\eta)$ be strongly $\tilde{g}_\alpha$wg-quotient map then $g\circ f$ is a strongly $\tilde{g}_\alpha$wg-quotient map.

Proof: Let V be an open set in(Z,η). Since g is strongly $\tilde{g}_\alpha$wg-quotient, $g^{-1}(V)$ is a $\tilde{g}_\alpha$wg-open in(Y,σ). Since f is $\tilde{g}_\alpha$wg-irresolute, $f^{-1}(g^{-1}(V))$ is a $\tilde{g}_\alpha$wg-open in (X,τ) implies $(g\circ f)^{-1}(V)$ is a $\tilde{g}_\alpha$wg-open in (X,τ). Assume $(g\circ f)^{-1}(V)$ is $\tilde{g}_\alpha$wg-open in(X,τ). Then $(f^{-1}\left(g^{-1}(V)\right)$ is $\tilde{g}_\alpha$wg-open in (X,τ). Since f is strongly $\tilde{g}_\alpha$wg-open, then $f(f^{-1}(g^{-1}(V)))$ is $\tilde{g}_\alpha$wg-open in (Y,σ) which implies $g^{-1}(V)$ is $\tilde{g}_\alpha$wg-open in(Y,σ). Since g is strongly $\tilde{g}_\alpha$wg-quotient map, V is open in (Z,η). Thus g∘f is strongly $\tilde{g}_\alpha$wg-quotient map.

Theorem 6.6: Let p:$(X,\tau)\to(Y,\sigma)$be $\tilde{g}_\alpha$wg-quotient map and the spaces $(X,\tau),(Y,\sigma)$ are $T_{\tilde{g}_\alpha wg}$-spaces. f:$(Y,\sigma)\to(Z,\eta)$ is a strongly $\tilde{g}_\alpha$wg-continuous iff f∘$p:(X,\tau)\to(Z,\eta)$is a strongly $\tilde{g}_\alpha$wg-continuous.
Proof: Let f be strongly $\tilde{g}_\alpha$wg-continuous and U be any $\tilde{g}_\alpha$wg-open set in (Z,η). Then $f^{-1}(U)$ is open in (Y,σ). Since p is $\tilde{g}_\alpha$wg-quotient map, then $p^{-1}(f^{-1}(U))=(f\circ p)^{-1}(U)$ is $\tilde{g}_\alpha$wg-open in(X,τ). Since(X,τ) is $T_{\tilde{g}_\alpha wg}$-space, $p^{-1}(f^{-1}(U))$ is open in (X,τ). Thus f∘p is strongly $\tilde{g}_\alpha$wg-continuous.
Conversely, Let the composite function f∘p is strongly $\tilde{g}_\alpha$wg-continuous. Let U be any $\tilde{g}_\alpha$wg-open set in (Z,η), $p^{-1}(f^{-1}(U))$ is open in (X,τ). Since p is a $\tilde{g}_\alpha$wg-quotient map, it implies that $f^{-1}(U)$ is $\tilde{g}_\alpha$wg-open in (Y,σ). Since (Y,σ) is a $T_{\tilde{g}_\alpha wg}$-space, $f^{-1}(U)$ is open in (Y,σ). Hence f is strongly is $\tilde{g}_\alpha$wg-continuous.

Theorem 6.7: Let $f:(X,\tau)\to(Y,\sigma)$ be a surjective, strongly $\tilde{g}_\alpha$wg-open and $\tilde{g}_\alpha$wg-irresolute map and $g:(Y,\sigma)\to(Z,\eta)$ be a $(\tilde{g}_\alpha wg)^*$-quotient map, then g∘f is a $(\tilde{g}_\alpha wg)^*$-quotient map.
Proof: Let V be $\tilde{g}_\alpha$wg-open set in (Z,η). Since g is a $(\tilde{g}_\alpha wg)^*$-quotient map, $g^{-1}(V)$ is a $\tilde{g}_\alpha$wg-open set in(Y,σ), since f is $\tilde{g}_\alpha$wg-irresolute, $f^{-1}(g^{-1}(V))$ is $\tilde{g}_\alpha$wg-open in (X,τ). Then $(g\circ f)^{-1}(V)$ is $\tilde{g}_\alpha$wg-open in (X,τ). Since f is strongly $\tilde{g}_\alpha$wg-open, $f(f^{-1}(g^{-1}(V)))$ is $\tilde{g}_\alpha$wg-open in (Y,σ) which implies $g^{-1}(V)$ is a $\tilde{g}_\alpha$wg-open in (Y,σ). Since g is $(\tilde{g}_\alpha wg)^*$-quotient map then V is open in (Z,η).
Hence g∘f is a $(\tilde{g}_\alpha wg)^*$-quotient map.

Theorem 6.8: Let $f:(X,\tau)\to(Y,\sigma)$be a strongly $\tilde{g}_\alpha$wg-quotient map and $g:(Y,\sigma)\to(Z,\eta)$be a $(\tilde{g}_\alpha wg)^*$-quotient map and f is $\tilde{g}_\alpha$wg-irresolute then g∘f is $(\tilde{g}_\alpha wg)^*$-quotient map.

Proof: Let V be a $\tilde{g}_\alpha$wg-open in (Z,η). Then $g^{-1}(V)$ is $\tilde{g}_\alpha$wg-open in (Y,σ) since g is $(\tilde{g}_\alpha wg)^*$-quotient map. Since f is $\tilde{g}_\alpha$wg-irresolute map, then $f^{-1}(g^{-1}(V))$ is $\tilde{g}_\alpha$wg-open in (X,τ). ie, $(g\circ f)^{-1}(V)$ is $\tilde{g}_\alpha$wg-open in (X,τ) which shows that g∘f is $\tilde{g}_\alpha$wg –irresolute. Let $f^{-1}(g^{-1}(V))$ is $\tilde{g}_\alpha$wg-open in (X,τ). Since f is strongly $\tilde{g}_\alpha$wg-quotient map then $g^{-1}(V)$ is open in (Y,σ) which implies $g^{-1}(V)$ is $\tilde{g}_\alpha$wg-open in(Y,σ). Since g is $(\tilde{g}_\alpha wg)^*$-quotient map, V is open in (Z,η). Hence g∘f is $(\tilde{g}_\alpha wg)^*$-quotient map.

References

[1] M. Lellis Thivagar, A note on quotient Mappings, Bull. Malaysian Math. Soc. 14(1991), 21-30.
[2] M.Lellis Thivagar and Nirmala Rebecca Paul. On topological$\tilde{g}_\alpha$-quotient mappings, Journal of Advanced Studies in Topology Vol.1, 2010, 9-16.
[3] M.Lellis Thivagar and Nirmala Rebecca Paul. Remarks on $\tilde{g}_\alpha$-irresolute maps , Bol.Soc.Paran.Mat Vol.291(2011) 55-66.
[4] M.Lellis Thivagar and Nirmala Rebecca Paul, New Types of Topological mappings, International Journal of.Math.Sci and Engg.Appli., Vol No.IV(2011),43-61.
[5] Levine, N.: Semi-open sets and semi-continuity in topological spaces, Amer. Math. Monthly, 70(1963), 36-41.
[6] Maria Singam, M., Anitha, G., $\tilde{g}_\alpha$-Weakly generalized closed sets in topological spaces,, Antarctica J.Math;9(20(2012),133-142.
[7] Maria Singam, M., Anitha, G., $\tilde{g}_\alpha$-Weakly generalized continuous functions, International Journal of Mathematical Archive-2(11), 2011, 2135-2141.
[8] Maria Singam, M., Anitha, G., Contra $\tilde{g}_\alpha$-WG continuous functions, International Journal of Computer Applications-2(11), 2011, 2135-2141.
[9] Mashhour, A. S., Hasanein, I. A and El-Deeb, S. N. α-continuous and α-open mappings, Acta Math. Hungar., 41(1983), 213-218.
[10] Mashhour, A. S., Abd El-Monsef, M. E and El-Deeb, S. N. On precontinuous mappings and weak pre-continuous mappings, Proc. Math. and Phys. Soc. Egypt, 53(1982), 47-53.
[11] J. R.Munkres, Topology, A first course, Fourteenth Indian Reprint.
[12] Njastad. O, on some classes of nearly open sets, Pacific J. Math. , 15(1965), 961-970.
[13] Rajesh.N.,Lellis Thivagar.M.,Sundaram.P.,Zbigniew Duszynski.,$\tilde{g}-$semi closed sets in topological spaces, Mathematica Pannonica,18(2007),51-61.
[14] Reilly, I. L and Vamanamurthy, M. K. On α-continuity in topological spaces, Acta Math Hungar., 45(1-2)(1985), 27- 2.
[15] Saeid Jafari,M.Lellis Thivagar and Nirmala Rebecca Paul. Remarks on $\tilde{g}_\alpha$-closed sets in topological spaces, International Mathematical Forum, 5, 2010, no.24, 1167-1178.
[16] Veera Kumar M.K.R.S.Between * g closed sets and g-closed sets, Mem.Fac.Sci.Kochi Univ.Ser.App.Math.,21(2000),1-19
[17] Veera kumar M.K.R.S. $^{\#}g$ -semi closed sets in topological spaces, Antartica J.Math 2(2005), 201-222.

International Journal of Modern Engineering Research (IJMER)
www.ijmer.com Vol.3, Issue.2, March-April. 2013 pp-765-768 ISSN: 2249-6645

Multiple Response Optimizations in Drilling Using Taguchi and Grey Relational Analysis

B.Shivapragash, [1] K.Chandrasekaran, [2] C.Parthasarathy, [3] M.Samuel[4]
1 Assistant Professor, Department of mechanical engineering, PRIST University ,Trichy, Tamilnadu, India
2,3,4 Assistant Professor, Department of mechanical engineering, PRIST University ,Trichy, Tamilnadu, India

Abstract: *Composite materials are important engineering materials due to their outstanding mechanical properties. Metal matrix composite (MMCs) are one of the widely known composites because of their superior properties such as high strength, hardness, stiffness, and corrosion resistances. Al-$TiBr_2$ produces higher tool wear, poor surface roughness and minimizes the metal removal rate. The quality of the material is influenced by the cutting conditions, tool material and geometry. The present work is focusing on multiple response optimization of drilling process for composite Al-$TiBr_2$. The study provided to minimise the damage events occurring during drilling process for composite material. A statistical approach used to analyse experiment data. Taguchi method with grey relational analysis was used to optimize the machining parameters with multiple performance characteristics in drilling of MMC Al-$TiBr_2$. The results shows that the maximum feed rate, low spindle speed are the most significant factors which affect the drilling process and the performance in the drilling process can be effectively improved by using this approach.*

Keywords: *Drilling, Grey relational analysis, Metal removal rate, Surface roughness, Taguchi method*

I. Introduction

To provide cost effectiveness in manufacturing and especially machining operations, there is a continuous need to reduce tooling costs. The most well-known methods used to reduce tooling costs are various applications of more resistant tool materials, heat treatments, cutting fluids, speed and feed rates and the development of coated cutting tool [1, 2]. A composite material is a heterogeneous solid consists of two or more different materials that are mechanically or metallurgical bonded together. Each of its components retains its identity in the composite and maintains its characteristic structure and property. The composite material, however generally possesses characteristics properties, such as stiffness, strength, high temperature performance, corrosion resistance, hardness or conductivity that are not possible with the individual components by them. Analysis of these properties shows that they depend on the property of individual components; the relative amount of components; the size, shape and distribution of the discontinuous components; the degree of bonding between them and the orientation of the various components [3]. MMC have become a large leading material in composite materials, and particle reinforced aluminum MMCs have received considerable attention due to their excellent engineering properties. These materials are known as the difficult-to-machine materials, because of the hardness and abrasive nature of reinforcement element like silicon carbide (SiC) particles [4]. The application fields of MMCs include aerospace, defence and automotives [4]. Hybrid MMCs were obtained by reinforcing the matrix alloy with more than one type of reinforcements having different properties [6]. The Al-based hybrid composites, with 20% SiC Whiskers and 0, 2%, 5%, 7% SiC nano particles, were fabricated by squeeze casting route [7]. In the view of the growing engineering applications of these composites, a need for detailed and systematic study of their machining characteristics is envisaged. The efficient and economic machining of these materials is required for the desired dimensions and surface finish [8].

Nihat Tosun[9] Use The grey relational analysis for optimizing the drilling process parameters for the work piece surface roughness and the burr height is introduced. Various drilling parameters, such as feed rate, cutting speed, drill and point angles of drill were considered. An orthogonal array was used for the experimental design. Optimal machining parameters were determined by the grey relational grade obtained from the grey relational analysis for multi-performance characteristics (the surface roughness and the burr height). Experimental results have shown that the surface roughness and the burr height in the drilling process can be improved effectively through the new approach. Stein and Dornfeld [10] presented a study on the burr height, thickness, and geometry observed in the drilling of 0.91-mm diameter through holes in stainless steel 304L. They presented a proposal for using the drilling burr data as part of a process planning methodology for burr control. To minimize the burr formed during drilling, Ko and Lee [11] investigated the effect of drill geometry on burr formation. They showed that a larger point angle of drill reduced the burr size. Sakurai et al. [12] have also tried to change the cutting conditions and determined high feed rate drilling of aluminium alloy. The researchers examined cutting forces, drill wear, heat generated, chip shape, hole finish, etc. Gillespie and Blotter [13] studied experimentally the effects of drill geometry, process conditions, and material properties. They have classified the machining burrs into four types: Poisson burr, rollover burr, tear burr, and cut-off burr. Valuable review about burr in machining operation provided important information [14].Erol Kilickap [15] Modelling and optimization of burr height in drilling of Al-7075 using Taguchi method and response surface methodology. This investigation presents the use of Taguchi and response surface methodologies for minimizing the burr height and the surface roughness in drilling Al-7075. The optimization results showed that the combination of low cutting speed, low feed rate, and high point angle is necessary to minimize the burr height The study shows that the Taguchi method is suitable to solve the stated within minimum number of trials as compared with a full

factorial design. Limited research papers are available for machining of composite materials in drilling processes. So in this investigation grey relational analysis is used to multiple response optimizations on Al-$TiBr_2$ in drilling.

II. Materials And Methods

In this study, Al-$TiBr_2$ is used as the work piece material. The dimensions of this work piece material are 100×170×15 mm. The chemical composition of Al-$TiBr_2$ is given in Table 1.

Table.1.Chemical Composition of Al-TiB_2

Component	Mg	Si	Fe	Cu	Zn	Ti	Mn	Cr	Al
Amount (wt)	0.8	0.4	0.7	0.15	0.25	0.15	0.15	0.04	Balance

Grey Relational Analysis

The black box is used to indicate a system lacking interior information. Nowadays, the black is represented, as lack of information, but the white is full of information. Thus, the information that is either incomplete or undetermined is called Grey. A system having incomplete information is called Grey system. The Grey number in Grey system represents a number with less complete information. The Grey element represents an element with incomplete information. The Grey relation is the relation with incomplete information. Those three terms are the typical symbols and features for Grey system and Grey phenomenon. There are several aspects for the theory of Grey system:

1. Grey generation: This is data processing to supplement information. It is aimed to process those complicate and tedious data to gain a clear rule, which is the whitening of a sequence of numbers.
2. Grey modeling: This is done by step 1 to establish a set of Grey variation equations and Grey differential equations, which is the whitening of the model.
3. Grey prediction: By using the Grey model to conduct a qualitative prediction, this is called the whitening of development.
4. Grey decision: A decision is made under imperfect countermeasure and unclear situation, which is called the whitening of status.
5. Grey relational analysis: Quantify all influences of various factors and their relation, which is called the whitening of factor relation.
6. Grey control: Work on the data of system behavior and look for any rules of behavior development to predict future's behavior, the prediction value can be fed back into the system in order to control the system.

This study will adopt all six above- mentioned research steps to develop a vendor evaluation model based on Grey relational analysis, and apply to vendor evaluation and selection. All details will be discussed in the following sections. The Grey relational analysis uses information from the Grey system to dynamically compare each factor quantitatively. This approach is based on the level of similarity and variability among all factors to establish their relation. The relational analysis suggests how to make prediction and decision, and generate reports that make suggestions for the vendor selection. This analytical model magnifies and clarifies the Grey relation among all factors. It also provides data to support quantification and comparison analysis. In other words, the Grey relational analysis is a method to analyze the relational grade for discrete sequences. This is unlike the traditional statistics analysis handling the relation between variables. Some of its defects are: (1) it must have plenty of data; (2) data distribution must be typical; (3) a few factors are allowed and can be expressed functionally. But the Grey relational analysis requires less data and can analyze many factors that can overcome the disadvantages of statistics method.

III. Design of Experiment

The experimental layout for the machining parameters using the L_9 orthogonal array design the drilling machine is used for the in this study. The radial drilling machine was adapted to drilling process and HSS tool with dia of 0.6 mm was used. The surface roughness (SR) and material removal rate (MRR) are two essential part of a product in any drilling machining operation. The theoretical surface roughness is generally dependent on many parameters such as the tool geometry, tool material and work piece material. The array having a three control parameter and three levels are shown in table 1. This method, more essentials all of the observed values are calculated based on the maximum the better and the minimum the better. In the present study spindle speed depth of cut feed rate have been selected as design factor. While other parameter have been assumed to be constant over the Experimental domain. This Experiment focuses the observed values of MRR and SR were set to maximum, intermediate and minimum respectively. Each experimental trial was performed with three simple replications at each set value. Next, the optimization of the observed values was determined by comparing the standard analysis and grey relational analysis.

Table 2 Drilling parameters and levels

Designation	Parameters	Level 1	Level 2	Level 3
A	Spindle Speed(rpm)	1000	1500	2000
B	Feed Rate (mm/min)	0.5	1.0	1.5
C	Depth of cut (mm)	02	04	06

IV. Result and Discussion

The algorithm of grey relational analysis coupled with principal analysis to determine the optimal combinations of the cutting parameters for rough cutting process in high-speed drilling operation is described step by step as follow:

(1) Convert the experimental data into S/N values.
(2) Normalize the S/N ratio.
(3) Calculate the corresponding grey relational coefficients.
(4) Calculate the grey relational grade using principal component analysis.
(5) Select the optimal levels of cutting parameters.
(6) Conduct confirmation experiments.

Optimal combination of the cutting parameters

The performance characteristics obtained from the experimental results are initially converted into S/N ratio to search for a desirable result with the best performance and the smallest variance. Thus, metal removal rate is of higher-the-better type. As for surface roughness, it can be clearly recognized as one of lower the-better type. The experimental results are substituted into Equation 1 to calculate the S/N ratios of surface roughness and metal removal rate shown in Table 4.

$$S/N=-10\log 1/n\sum y_i^2 \quad (1)$$

Table 3 S/N ratio for MRR and SR

Trials	A	B	C	S/N ratio for MRR	S/N ratio for SR
1	1	1	1	2.73441	-10.2644
2	1	2	2	2.67078	-6.9271
3	1	3	3	2.92256	-7.2722
4	2	1	2	3.10672	-11.1501
5	2	2	3	2.8603	-9.4551
6	2	3	1	2.92256	-9.8831
7	3	1	3	3.46373	-11.9539
8	3	2	1	3.16725	-11.8879
9	3	3	2	2.47703	-10.4489

All the original sequences of S/N ratio in Table 3 are then substituted into Equation 2 to be normalized. The outcomes result is shown in Table 4 and denoted as Z_i and Z_j for reference sequence and comparability sequence respectively. In order to objectively the relative importance for each performance characteristic in grey relational analysis, principal component analysis is specially introduced here to determine the corresponding weighting values for each performance characteristic. The elements of the array for multiple performance characteristics listed in Table 5 represent the grey relational coefficient of each performance characteristic.

$$Z^*_{ij}(k) = z_{ij}(k) - \min z_{ij}(k)/\max z_{ij}(k) - \min z_{ij}(k) \quad (2)$$

Table 4 Normalized values of S/N Ratio for MRR and SR

Trial No	Normalized values of S/N Ratio Z_{ij}	
	MRR(Z_i)	SR (Z_j)
1	0.260	0.663
2	0.196	0.000
3	0.451	0.068
4	0.637	0.840
5	0.388	0.502
6	0.451	0.588
7	0.999	1.000
8	0.699	0.986
9	-0.0002	0.700

Table 5 Grey Relational Coefficients for MRR and SR

Trial No	Grey Relational Coefficient		Grey Grade
	MRR	SR	
1	0.657397	0.42959	0.543493
2	0.7183	1.0000	0.85915
3	0.525618	0.879272	0.702445
4	0.439404	0.373107	0.406256
5	0.56296	0.498552	0.530756
6	0.525618	0.459539	0.492578
7	0.333394	0.333333	0.333364
8	0.416927	0.336277	0.376602
9	1.000548	0.416457	0.708502

The response table of Taguchi method is employed here to calculate the average grey relational grade for each cutting parameter level. It is done by sorting the grey relational grades corresponding to levels of the cutting parameter in each column of the orthogonal array, and taking an average on those with the same level. Using the same method, calculations are performed for each cutting parameter level and the response table is constructed as shown in Table 6. Basically, the larger the grey relational grade is the better the corresponding multiple performance characteristic. From the response table for the grey relational grades shown in Table 05, the best combination of the cutting parameters is the set with spindle low speed, high feed rate and middle depth of cut.

Table 6 Optimum Level for Drilling Parameter

Factors		1	2	3
A	Spindle Speed	**0.701696**	0.47653	0.472823
B	Feed Rate	0.427704	0.588836	**0.634508**
C	Depth of Cut	0.470891	**0.657969**	0.522188

V. Conclusions

In this study mainly focus on material removal rate and surface roughness on Al-$TiBr_2$ in radial drilling machining with dry conditions. From the study of result in drilling is using Grey relational analysis. These following can be concluded by this present studies.

1. Optimum cutting parameters for minimization surface roughness is spindle speed set as low level (1000 rpm), feed rate set as maximum level (1.5 mm/min) and depth of cut set as middle level (6 mm).
2. Optimum cutting parameters for maximization material removal rate is spindle speed set as low level (1000 rpm), feed rate set as maximum level (1.5 mm/min) and depth of cut set as middle level (6 mm).

Reference

[1] Da Silva, F.J., Franco, S.D., Machado, A.R., Ezugwu, E.O., Souza Jr. A.M. (2006). Performance cryogenically treated HSS tools. Wear, vol. 261, no.5-6, p. 674-685,
[2] Boris Stirn, Kiha Lee, David A. Dornfeld (2001) "BURR FORMATION IN MICRO-DRILLING".
[3] KILIÇKAP E, ÇAKIR O, AKSOY M, INAN A. Study of tool wear and surface roughness in machining of homogenized SiC-p reinforced aluminium metal matrix composite. Journal of Materials Processing Technology, 2005, 165: 862-867.
[4] MOHAN B, RAJADURAI A, SATYANARAYANA K G. Electric discharge machining of Al/SiC metal matrix composites using rotary tube electrode [J]. Journal of Mater Process Technology, 2004, 153: 978-985.
[5] ZHAN Y Z, ZHANG G D. The role of graphite particles in the high temperature wear of copper hybrid composites against steel [J]. Materials and Design, 2006, 27: 79-84.
[6] ZHANG X N, GENG L, WANG G S. Fabrication of Al-based hybrid composites reinforced with SiC whiskers and SiC nano particles by squeeze casting [J]. Journal of Materials Processing Technology, 2066, 176: 146-151.
[7] GALLAB M, SKLAD M. Machining of Al/SiC metal matrix composites. Part II: Workpiece integrity [J]. Journal Mater Process, 1998, 83: 277-283.
[8]. Lin TR, Shyu RF (2000) Improvement of tool life and exit burr using variable feeds when drilling stainless steel with coated drills. Int J Adv Manuf Technol 16:308–313
[9]. Stein JM, Dornfeld DA (1997) Burr formation in drilling miniature holes. Ann CIRP 46/17:63–66
[10]. Ko SL, Lee JK (2001) Analysis of burr formation in drilling with a new-concept drill. J Mater Process Technol 113:392–398
[11]. Sakurai K, Adachi K, Kawai G, Sawai T (2000) High feed rate drilling of aluminum alloy. Mat Sci Forum 331–337:625–630
[12]. Gillespie LK, Blotter PT (1976) the formation and properties of machining burs. Transactions ASME Journal of Engineering for Industry 98:66–74
[13]. Aurich JC, Dornfeld D, Arrazola PJ, Franke V, Leitz L, Min S (2009) Burrs: analysis, control and removal. CIRP Annals Manuf Technol 58:519–542
[14]. Erol Kilickap Modelling and optimization of burr height in drilling of Al-7075 using Taguchi method and response surface methodology Springer-Verlag London Limited 2010.

International Journal of Modern Engineering Research (IJMER)
www.ijmer.com Vol.3, Issue.2, March-April. 2013 pp-769-772 ISSN: 2249-6645

Stress Analysis of a Mono-parabolic Leaf Spring–A Review

D.N.Dubey, [1] S.G.Mahakalkar[2]
*12*Department *of Mechanical Engineering, YCCE -an autonomous institute, India*

Abstract: *This work has been carried out on a mono parabolic leaf spring of a Maruti Omni Car. This paper describes design and experimental analysis of a conventional parabolic leaf and suggested composite material leaf spring .The composites used are HM and HS Carbon polymers .Finite Element analysis (FEA) is carried out at static condition of the spring model so that stress distribution can be observed for analysis of high stress zones. CAD model is prepared in Pro-E .The analysis has been observed for various loading conditions and the overall stress distribution zones have been studied. The objective is to compare the load carrying capacity, stiffness and weight savings of composite parabolic leaf spring with that of a conventional steel leaf spring .The design constraints are stresses and deflections induced during various loading conditions.*

Keywords: *Leaf springs, Composites, HS Carbon, HM Carbon, FEM Simulation, Mono-parabolic leaf springs*

I. INTRODUCTION

A leaf spring is mostly used in suspension of the wheeled vehicles. It is also referred as semi-elliptical leaf spring and forms an arc shape .The center of the arc is positioned and fixed on the on the axle. A leaf spring can either be attached directly to the frame at both ends or attached directly at one end, usually the front, with the other end attached through a shackle, a short swinging arm. The shackle takes up the tendency of the leaf spring to elongate when compressed and thus makes for softer springiness. There is almost a direct proportionality between the weight of the vehicle and its fuel consumption. This paper is mainly focused on the implementation of composite materials by replacing steel in conventional leaf springs of a suspension system. Automobile-sector is showing an increased interest in the area the introduction of the paper should explain the nature of the problem, previous work, purpose, and the contribution of the paper. The contents of each section may be provided to understand easily about the paper. of composite material-leaf springs due to their high strength to weight ratio. Therefore analysis of composite material leaf springs has become essential in showing the comparative results with conventional leaf springs.

In this analysis the conventional steel leaf spring is tested for static load condition and results are compared with a virtual model of composite material leaf spring. Leaf spring is modeled in Pro-E 5.0 CAD software and it is imported and simulated in ANSYS 10.0 for better understanding. Results of Composite Leaf Spring are compared on the basis of analysis reports produced by ANSYS software. The material used for conventional steel leaf spring is EN45 and for composite leaf spring HS Carbon and HM Carbon material is used.

II. LITERATURE SURVEY

We know that composite materials have more elastic strain energy storage capacity and high strength-to-weight ratio as compared to the conventional steel. With use of composite materials the weight of the leaf spring without any reduction on load carrying capacity and stiffness can be achieved. Therefore analysis of composite material leaf springs has become essential in showing the comparative results with conventional leaf springs.(1,2) I. Rajendran, S. Vijayarangan presented a formulation & solution technique using genetic algorithms for design optimization of composite leaf springs. . (3)By using the results of conventional leaf spring Mahmood M. Shokrieh, Davood designed and optimized composite one made from fiberglass with epoxy resin using ANSYS. Main consideration was given to the optimization of the spring geometry.(4) Mouleeswaran Senthil Kumar describes static and fatigue analysis of steel leaf spring and composite multi leaf spring made up of glass fibre reinforced polymer using life data analysis.(5)M.Venkatesan ,D .Helmen Devaraj in their work have compared the load carrying capacity of steel and composite material by giving design constraints.(6) M.Raghvedra ,Syed Altaf Hussain ,V.Pandurangadu, K.Palani Kumar have used laminated composites as a replacement to conventional steel and have studied the three composites subjected to the loads.Material properties of composite structures have been reported in many literature works .Recently emphasis is been given on mass reduction and development of alternate materials and processing technology in the vehicle equipment manufacturing industry.

III. METHODOLGY

In this paper, a comparative analysis of virtual model of conventional steel leaf spring is done with a virtual model of a composite leaf spring under static load condition. Varying loads are applied and the results have been studied for various loading condition. Two eye ends are fixed and loads have been applied at the center of the arc in upward direction .The spring is loaded maximum load of 1200N is applied to all the three materials .Further loads of 800N and 400N are applied subsequently and the values are studied .A static analysis determines stresses, strains, displacements and forces in the structure .

The parameters like material properties, loading conditions, support conditions are specified for the pre-processing analysis. The boundary conditions are applied by taking into consideration experimental loading conditions.

IV. CHARACTERISTICS OF COMPOSITES

A composite material is defined as a material composed of two or more constituents combined on a macroscopic scale by mechanical and chemical bonds. Typical composite materials are composed of inclusions suspended in a matrix. The constituents have the characteristic to retain their identities in the composite. Many composite materials offer properties which is a combination of strength and modulus that are either comparable to or better than any traditional metallic materials.

Composites have low specific gravities, the strength weight-ratio and modulus weight-ratios of these composite materials are markedly superior to those of metallic materials. As a result of so many advantages composites have emerged as a major class of structural material and are either used or being considered as substitutions for metal in many weight-critical components in aerospace, automotive and other industries. These materials also offer high internal damping which leads to better vibration energy absorption within the material and results in reduced transmission of noise land vibration to

V. SPECIFICATIONS OF CONVENTIONAL LEAF SPRINGS USED IN MARUTI OMNI

Conventional steel leaf springs are manufactured by EN45, 60Si7, EN47, 50Cr4V2, 55SiCr7 and 50CrMoCV4 etc. These materials are widely used for production of the parabolic leaf springs and conventional multi leaf springs .The material used for Maruti Omni Is EN45.

The leaf spring is used in the case study is of Maruti Omni vehicle ,for Rear Suspension .The conventional steel leaf spring used for experiment is made up of EN45. The composition of material is given below.

Grade	C%	Mn%	Si %	Cr%	Ni %	Mo %	S,P % (max)
En45	0.45 - 0.55	0.50-0.80	0.50 max	0.80 - 1.20	-	-	.050*

TABLE 1-Reference 'Book by Mahindra Ugine Steel Company Limited (MUSCO)'

VI. Specifications of Existing Leaf Spring

Design Parameters of the existing monoparabolic leaf spring include the leaf span, the weight of the spring, material selected, its camber, density of the material, Tensile strength and Young Modulus.

Parameter	Value
Material selected - steel	55Si2Mn90
Young's Modulus (E)	$2.1x10^{11}$ (N/mm2)
Spring Weight	3.5Kg
Tensile Strength	1960 (N/mm2)
Leaf Span	1025 (mm)
Camber	90.81 mm
Density	.00007850 kg/mm3

TABLE 2 - Specification of Existing Leaf Spring

VII. Simulation of Mono-Parabolic Leaf Spring Using Fem

The monoparabolic leaf spring is first modeled in Pro-E 5.0 and then exported to ANSYS where it is further meshed, constrained and loaded and simulated further. All the analysis for the composite leaf spring is done by using ANSYS 10.0. For composite materials the same parameters are used as that of the conventional leaf spring. For designing of composite leaf spring also the camber is taken 90.81 mm. The two eye ends are rolled and constraints are given. Whenever loads are applied at the eye end section it becomes is free to travel in longitudinal direction. This particular motion will help leaf spring to get flattened when the load is applied.. Produced results are very well compared with the realistic leaf spring and it's Experimental Procedure. The range of loads is applied and results are analyzed. The maximum principle stress is evaluated by software i.e. Von Mises Stress and Maximum Deflection is also observed. It is very much clear from the results produced by the ANSYS for Conventional Steel Leaf Spring, that red colored area indicated that eye end is the possible failure area for leaf spring .Meshing is a process in which geometry is discretized into nodes and elements The structure are meshed and has nodes and elements in it.

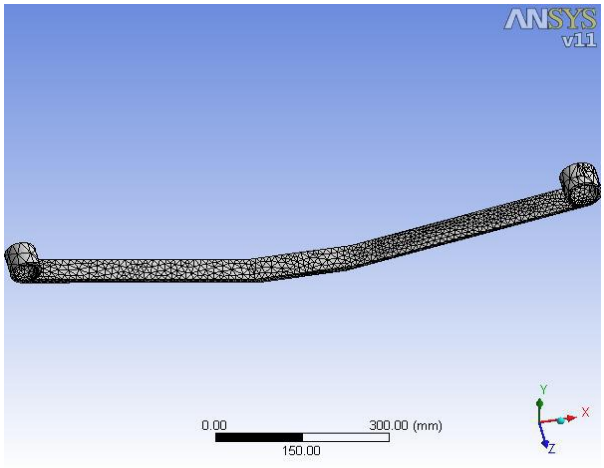

FIG1-MESHED MODEL OF LEAF SPRING

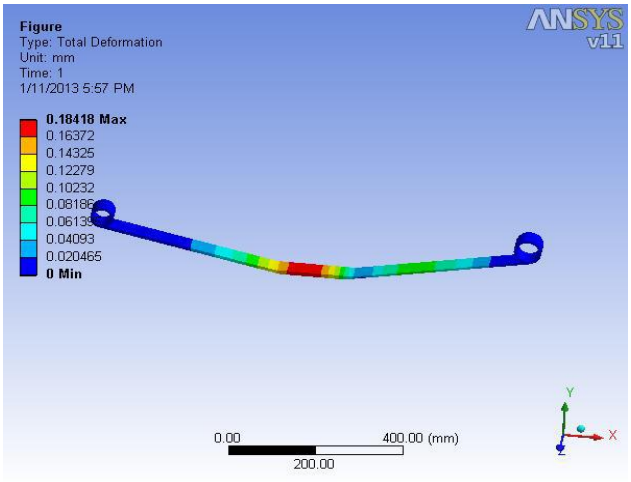

FIG2-TOTAL DEFORMATION AT 1200N FOR EN45

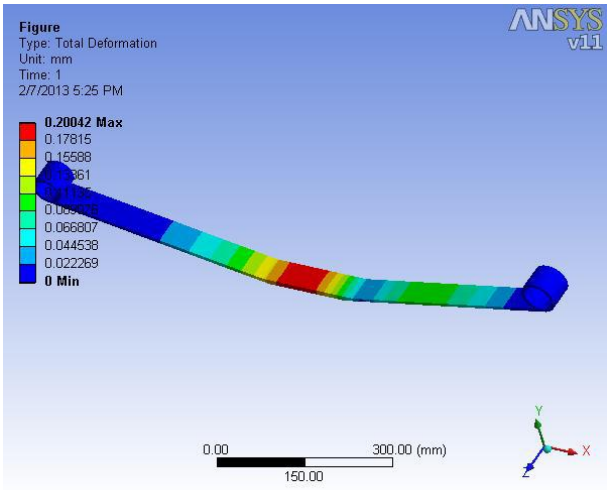

FIG3-TOTAL DEFORMATION AT 1200N FOR HM CARBON

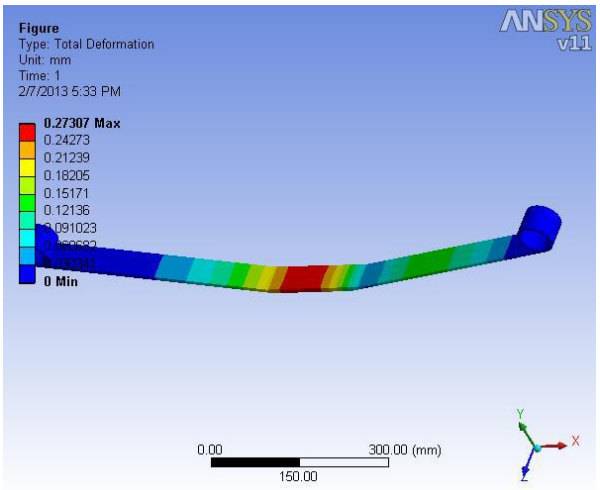

FIG4-TOTAL DEFORMATION AT 1200N FOR HS CARBON

VIII. Analysis Of Leaf Spring Using Fem

A stress analysis is performed using FEM and a comparative analysis of load and deflection of steel and the composite leaf springs is done. The total defelction in the leaf spring for three loading conditions i.e 1200N, 800N and 400 N is depicted below.

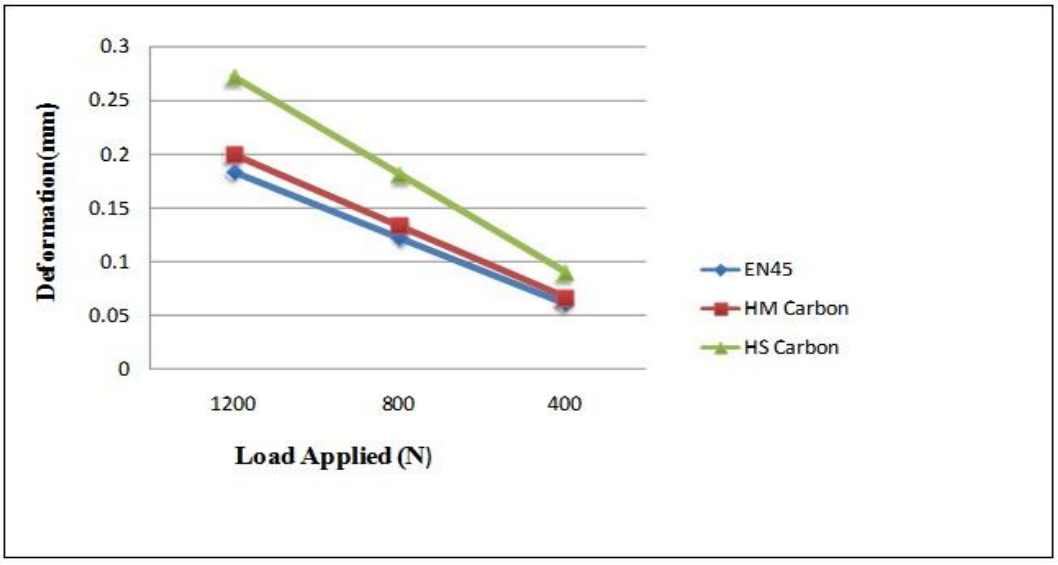

The above graph shows a comparative analysis of deformation of conventional steel used and the virtual models of HS and HM composite leaf springs.

IX. Conclusion

A comparative study has been made between carbon composite leaf spring and steel leaf spring with respect to weight and strength.The original steel leaf spring would weigh about 3.5 kgs whereas composie leaf spring would weigh 0.7314 kgs. So,we have observed that almost 65-70% of weight reduction could be achieved by using the carbon composites.At various loading conditions the composites under study show deflection as compared to conventional steel.The study has demonstrated that composite leaf springs would offer substantial weight savings.

REFERENCES

[1] "Optimal Design Of A Composite Leaf Spring Using Genetic Algorithms" By Rajendran,I.,Vijayrangan,S. Int. Jr. Of Computer and Structures 79 2001:Pp.1121-1129
[2] "Design and Analysis of a Composite Leaf Spring" by Rajendran,I.,Vijayrangan,S., Journal of Institute Of Engineers India,82,2002,180-187
[3] "Analysis and Optimization of a Composite Leaf Spring" by Mahmood M.Shokrieh, Dawood Rezaei, Int. Jr. Of Computer and Structures 60 2003:pp317-325
[4] "Analytical and Experimental Studies on Fatigue Life Prediction Of Steel and Composite Multi-leaf Spring for Light Passenger Vehicle Using Life Data Analysis" by Mouleeswaran.S .Kumar, S.Vijayrangam, ISSN 2249-6645 Materials Science. Vol.2, Issue4, July-Aug 2012 pp-1875-1879
[5] Design and Analysis Of Composite Leaf Spring In Light Vehicle" by M.Venkatesan, D.Helmen Devraj Int. Jr. Of Modern Engineering Research (IJMER) Vol.2, issue1, Jan-Feb 2012 pp-213-218
[6] "Modeling and Analysis of Laminated Composite Leaf Spring under the Static Load Condition by using FEA" by M.Raghvedra, Syed Altaf Hussain, V.Pandurangadu, K.Palani Kumar, Int. Jr. Of Modern Engineering Research (IJMER) Vol.2, issue 4, July-Aug.2012 pp-1875-1879
[7] "Mono Composite Leaf Spring for Light Weight Vehicle-Design, End Joint Analysis and Analysis and Testing" by G.S.Shiva Shankar, S.Vijayarangan, ISSN 1392-1320 Materials Science. Vol.12, No.3.2006
[8] "Automobile Leaf Springs from Composite materials" by H.A.AL-Qureshi, Journal of Material Processing Technology, 118, 2001, 58-61
[9] "Mono Composite Leaf Spring for Light Weight Vehicle Design, End Joint Analysis and Testing" by Vijayrangan.S, Gulur Siddharamanna Shiva Shankar, Material Science, 12 (3), 2006, 220-22
[10] "Analytical and Experimental studies on Fatigue life Prediction of steel leaf Soring and composite leaf multi leaf spring for Light passenger vehicles using life data analysis"by Senthil kumar and Vijayarangan, ISSN 1392 13material science Vol. 13 No.2 2007.
[11] "Mono Composite Leaf Spring for Light Weight Vehicle Design, End Joint, Analysis and Testing"by Shiva Shankar and Vijayarangan ISSN 1392 Material Science Vol. 12, No.3, 2006.
[12] "Modelling and Analysis of Composite Leaf Spring under the Static Load Condition by using FEA" by M.M.Patunkar, D.R.Dolas International Journal Of Mechanical & Industrial Engineering, Volume 1 Issue-2011

International Journal of Modern Engineering Research (IJMER)
www.ijmer.com Vol.3, Issue.2, March-April. 2013 pp-773-778 ISSN: 2249-6645

Enhancement of Power Quality in Thirty Bus System Using ZSI Based STATCOM

N. Usha, [1] M.Vijaya Kumar[2]
[1]*Research scholar, JNTUA, Anantapur, A.P, INDIA,*
[2]*Professor, Department of Electrical & Electronics Engineering, JNTUA, Anantapur, A.P, INDIA,*

Abstract: This paper presents the modeling and simulation results of Z-Source Inverter based Static Compensator (STATCOM).The thirty bus system with and without STATCOM are modeled and simulated using the MATLAB software. The present work proposes Z-Source Inverter for the control of reactive power. Z-Source inverter would ensure a constant DC voltage across the DC link during the process of voltage. The advantages of this system are reduced ripple, shoot through capability and reduced heating. Voltages and reactive power at various buses of thirty bus distribution network, with and without STATCOM are studied.

Key Words: *FACTS*, Power quality, *Reactive power, Static Synchronous Compensator (STATCOM), Z-Source Inverter (ZSI).*

I. Introduction

Electrical power quality problem is an occurrence manifested as a nonstandard voltage, current or frequency that results in a failure or a mis-operation of end user equipments. Distribution networks experience distinct change from a low to high load level everyday. With restructuring of power system and shifting trend towards distributed and dispersed generation, the issue of power quality problem is going to take newer dimensions. In developing countries like India, where the variation of power frequency and many such other determinants of power quality are themselves a serious question, it is very vital to take positive steps in this direction. The present work is to identify the prominent concern in this area and hence the measures that can enhance the quality of power are recommended.

The introduction of FACTS has given the new direction to the power system to solve the power quality problems [1]. At present, a wide range of very flexible controllers are emerging for custom power applications [2].As an important kind of FACTS devices, Static Var Compensator (SVC) is widely used in power system for shunt reactive compensation. However using Thyristor controlled reactor (TCR) and Thyristor Switched Capacitor (TSC) for reactive power generation, the thyristor controlled SVC brings harmonics and possible harmonic resonance into system. The STATCOM is a shunt connected reactive power compensation device that is capable of generating and /or absorbing reactive power. FACTS devices are routinely employed in order to enhance the power transfer capability of the otherwise under-utilized parts of the interconnected network[3,4].Out of all static FACT devices the STATCOM is the most effective device and has the potential to be exceptionally reliable with the added capability to sustain reactive current at low voltage (constant current not constant impedance), reduced land use , increased relocatability and voltage and frequency support capability(by replacing capacitors with batteries as energy storage). Although currently being applied to regulate transmission voltage to allow greater power flow in a voltage limited distribution network in the same manner as a SVC, the STATCOM has further potential. By giving an inherently faster response and greater output to a system with a depressed voltage, the STATCOM offers improved quality of supply.

II. Static Sychronous Compensator (STATCOM)

The static synchronous compensator (STATCOM) is a voltage source inverter based FACTS controller and also shunt connected reactive compensation equipment, which is capable of generating and /or absorbing reactive power. The STATCOM provides operating characteristics similar to a rotating synchronous compensator without the mechanical inertia. The STATCOM employ solid state power switching devices and provide rapid controllability of the three phase voltages, both in magnitude and phase angle.

The STATCOM mainly consists of DC voltage source behind self-commutated voltage source inverter using GTO/IGBT and coupling transformer with a leakage-reactance. The AC voltage difference across the leakage reactance produces reactive power exchange between the STATCOM and the power system, such that the AC voltage at the bus bar can be regulated to improve the voltage profile of the power system, which is the primary duty of the STATCOM. The basic objective of a VSI is to produce a sinusoidal AC voltage with minimal harmonic distortion from a DC voltage.

The principle of STATCOM operation is as follows: The AC voltage difference across the leakage reactance makes the power exchange between the STATCOM and the power system. The VSI voltage is compared with the AC bus voltage system, when the AC bus voltage magnitude is above that of the VSI magnitude; the AC system sees the STATCOM as inductance connected to its terminals. Otherwise if the VSI voltage magnitude is above that of the AC bus voltage magnitude, the AC system sees the STATCOM as capacitance connected to its terminals. If both AC system and VSI voltage magnitudes are equal, the reactive power exchange is zero. If the STATCOM has a DC source or energy storage device on its DC side, it can supply real power to the power system. This can be achieved by adjusting the phase angle of the STATCOM terminals and the phase angle of the AC power system. When phase angle of the AC power system leads the

VSI phase angle, the STATCOM absorbs the real power from the AC system, if the phase angle of the AC power system lags the VSI phase angle, the STATCOM supplies real power to AC system.

The Voltage Source Converter or Inverter (VSC or VSI) is the building block of a STATCOM and other FACTS devices. A very simple inverter produces a square voltage waveform as it switches the direct voltage source on and off. The basic objective of a VSI is to produce a sinusoidal AC voltage with minimal harmonic distortion from a DC voltage.

In the last decade commercial availability of Gate Turn Off thyristor (GTO) devices with high power handling capability, and the advancement of other types of power-semiconductor devices such as IGBT's have led to the development of controllable reactive power sources utilizing electronic switching converter technology. These technologies additionally offer considerable advantage over the existing ones in terms of space reduction and performance. The GTO thyristor enable the design of solid-state shunt reactive compensation equipment based upon switching converter technology.

This concept was used to create a flexible shunt reactive compensation device named static synchronous compensator (STATCOM) due to similar operating characteristics to that of a synchronous compensator but without the mechanical inertia. Single-line diagram of STATCOM is shown in Fig1.

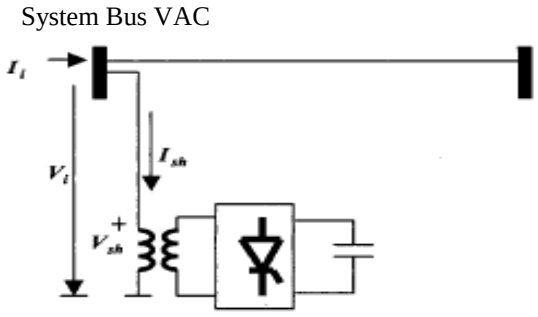

Fig.1 Single-line diagram of a STATCOM.

The advent of Flexible AC Transmission systems (FACTS) is giving rise to a new family of power electronics equipment emerging for controlling and optimizing the performance of power system, e.g. STATCOM, SSSC and UPFC. The use of voltage source inverter (VSI) has been widely accepted as the next generation of the reactive power controllers of the power system to replace the conventional VAR compensator, Such as the thyristor-switched capacitors (TSC) and thyristor controlled reactors (TCR).

III. Impedance Source Inverter (ZSI)

The main circuit of configuration of the Z-Source Inverter with load is shown in Fig2. Z-Source Inverter circuit consists of a diode rectifier, DC link circuit, and an inverter bridge. The differences are that the DC link circuit is implemented by the Z-Source network (c_1, c_2, L_1, and L_2) and small input capacitors (c_a, c_b, and c_c)are connected to the diode rectifier. Since Z-Source Inverter bridge can boost the DC capacitor (c_1, and c_2) voltage to any value above the DC value of the rectifier, a desired output voltage is always obtainable regardless of line voltage. Using the 230V load system as an example ,the DC capacitor voltage can be boosted to 350V or greater in order to produce 230 V AC output regardless of the line voltage.Theoritically ,the DC capacitor voltage can be boosted to any value above the inherent DC voltage(310-325V for a 230-V line) of the rectifier ,by using the shoot through zero switching states. When a higher voltage is needed or during voltage sags. The capacitor voltage is, however, limited by the device voltage rating in practical use.

New type of STATCOM using dynamic phasor is given by Hannan[5], Modeling and simulation of distribution STATCOM is dealt by Giroux[6].solution to power quality problem is given by Mineski[7].Analysis and implementation of thyristor based STATCOM is given by [8]&[9].Compensation of voltage sag is given by Haque[10] .Harmonics study and comparison of ZSI with traditional Inverters is given by Justus[11] and maximum boost control of Z-source is given by Peng and Shen in [12]&[13].Z-source inverter for adjustable speed drives is given by Peng[14].ZSI and Push-pull inverter based STATCOM given by Usha [15]&[16].

The authors are unaware of any literature dealing STATCOM using Z-Source Inverter based STATCOM for thirty bus distribution system. This work compares reactive power in thirty bus system at various buses with and without ZSI based STATCOM.

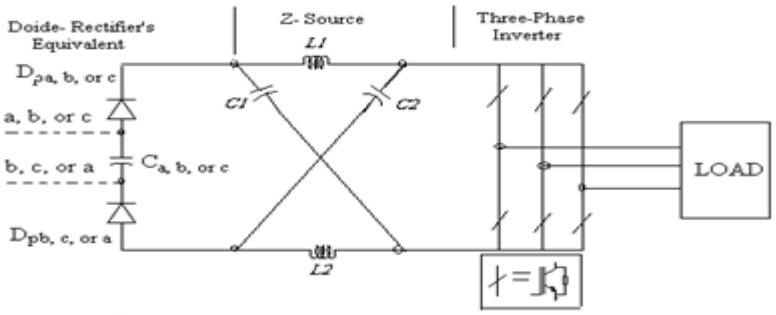

Fig.2 Main circuit configuration of Z-Source Inverter

IV. Simulation Results

A thirty bus system is considered for simulation studies. The circuit model of thirty bus system without STATCOM is shown in Fig3a. The thirty bus system is modeled and simulated using MATLAB/SIMULINK. Each line is represented by series impedance model. The shunt capacitance of the line is neglected. The voltage and reactive power at buses 11 and 25 are shown in Fig3b, 3c, 3d and Fig3e respectively.

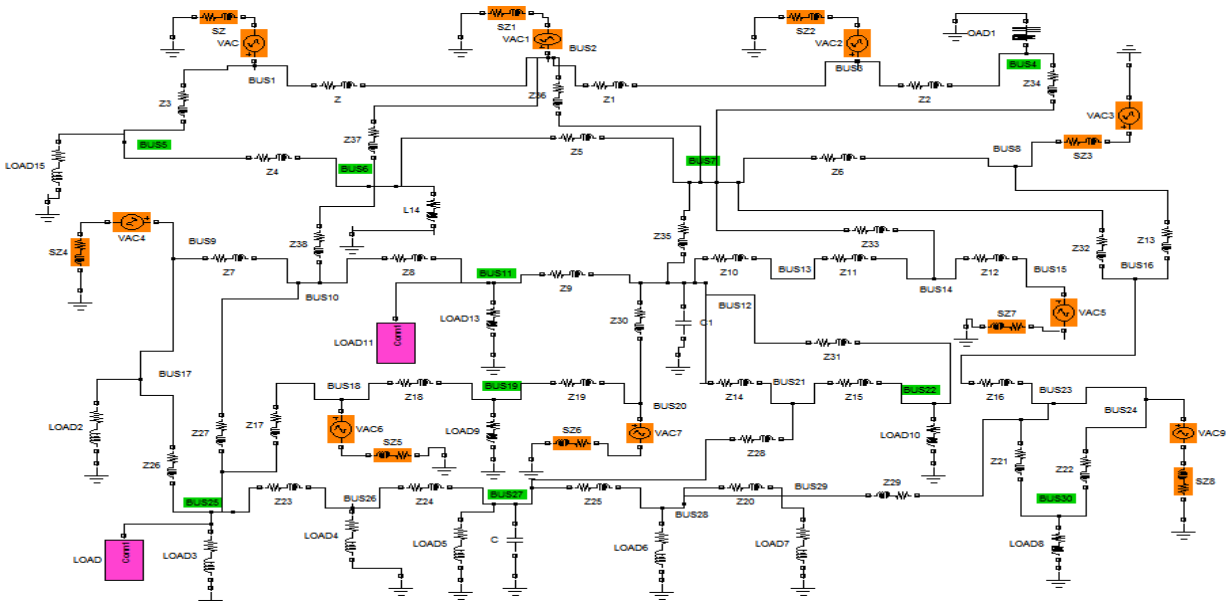

Fig3a 30 bus system without STATCOM

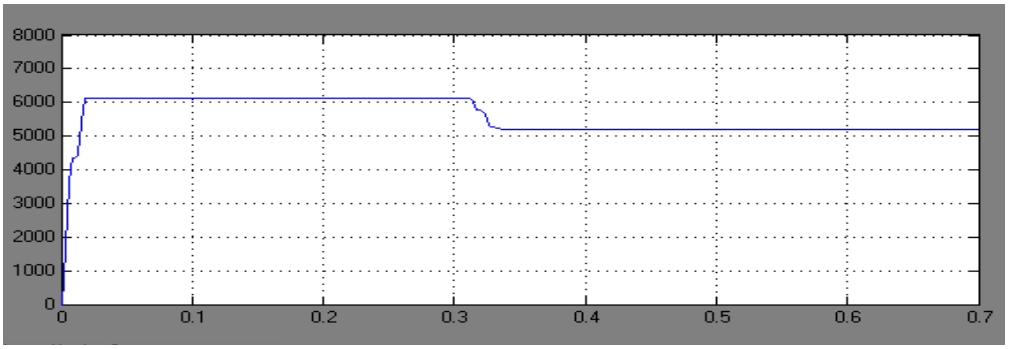

Fig 3b Voltage at bus 11

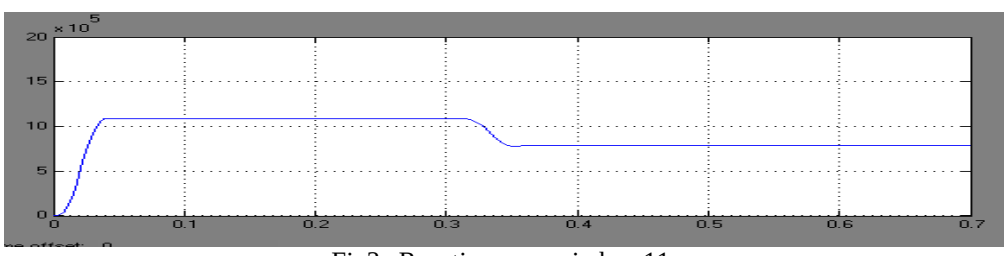

Fig3c Reactive power in bus 11

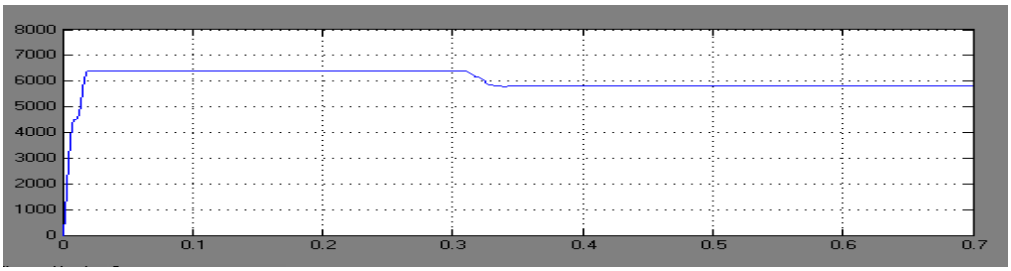

Fig3d Voltage at bus 25

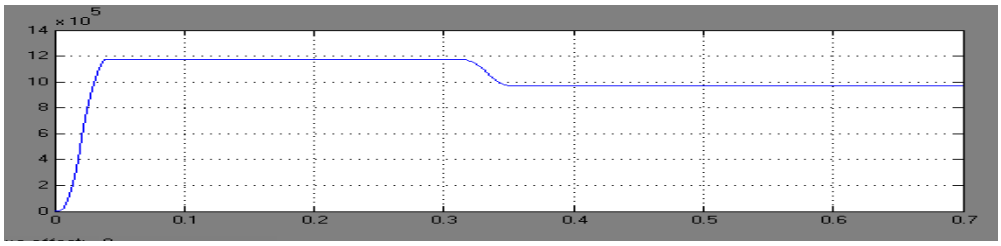

Fig3e Reactive power in bus 25

The buses 11 and 25 are identified as weak buses and STATCOMs are connected at these buses. The circuit model of thirty bus system with STATCOMs is shown in Fig4a. The voltage and reactive power at buses 11 and 25 are shown in Fig4b, 4c, 4d and Fig 4e respectively. The summary of reactive power in various buses is given in Table1.It can be seen that the reactive power increases in the buses near the STATCOMs. The increase in reactive power is due to increase in the voltage of the nearby buses. The reactive power in various buses is given in Fig4f. Hence ZSI based STATCOM gives best performance.

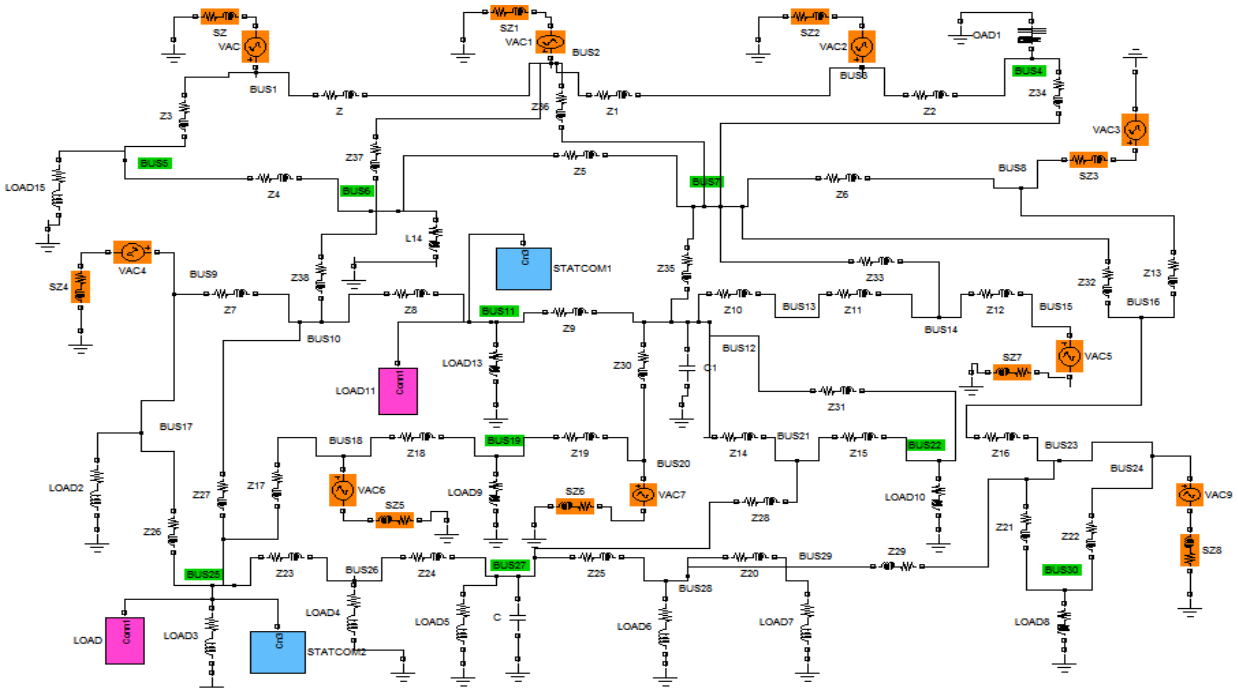

Fig4a 30 bus system with STATCOMs

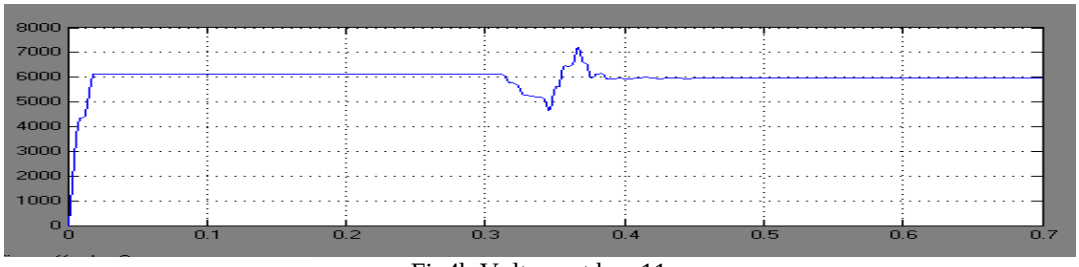

Fig4b Voltage at bus 11

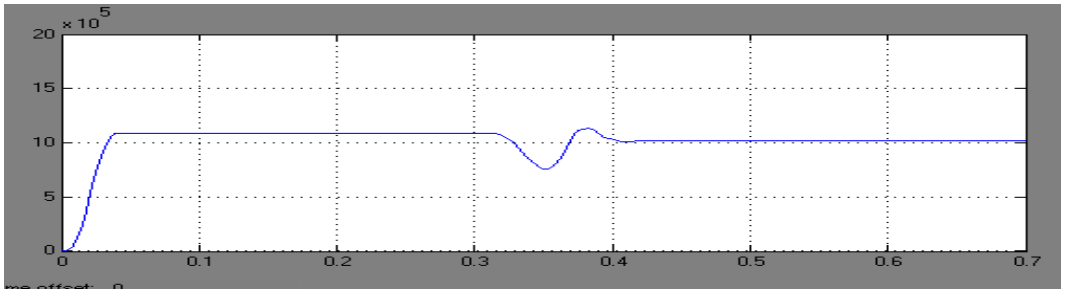

Fig4c Reactive power in bus 11

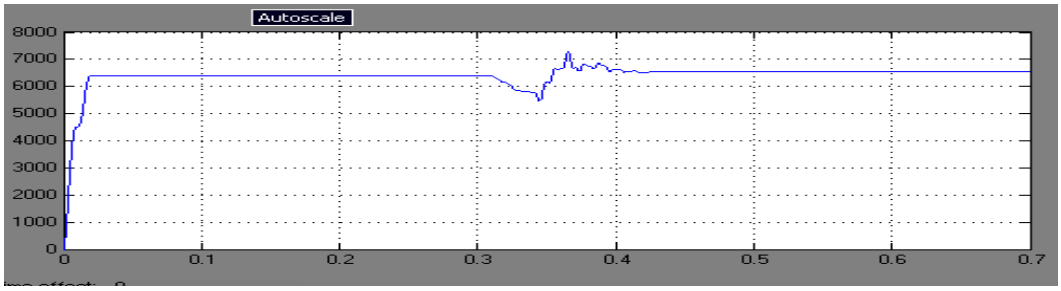

Fig 4d Voltage at bus 25

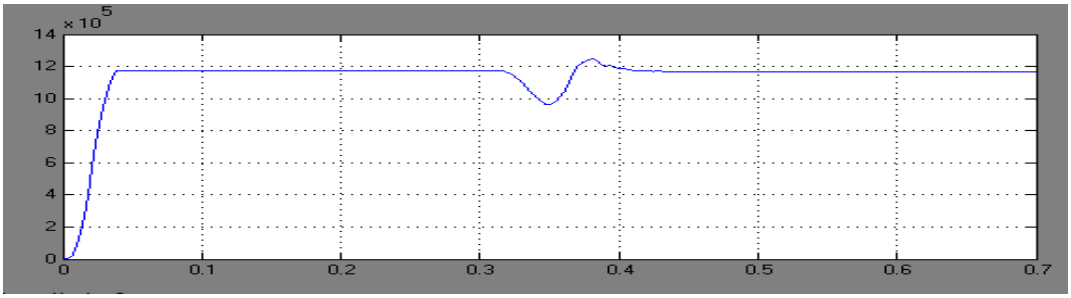

Fig 4e Reactive power in bus 25

Table-1: Summary of Reactive power with and without STATCOMs in various buses

Bus no	Reactive power without STATCOM MVAR	Reactive power with STATCOM MVAR
Bus-4	0.67	0.68
Bus-5	1.08	1.099
Bus-11	0.783	1.02
Bus-17	1.54	1.58
Bus-19	0.718	0.73
Bus-22	0.539	0.58
Bus-25	0.974	1.16
Bus-27	0.686	0.742
Bus-30	0.896	0.899

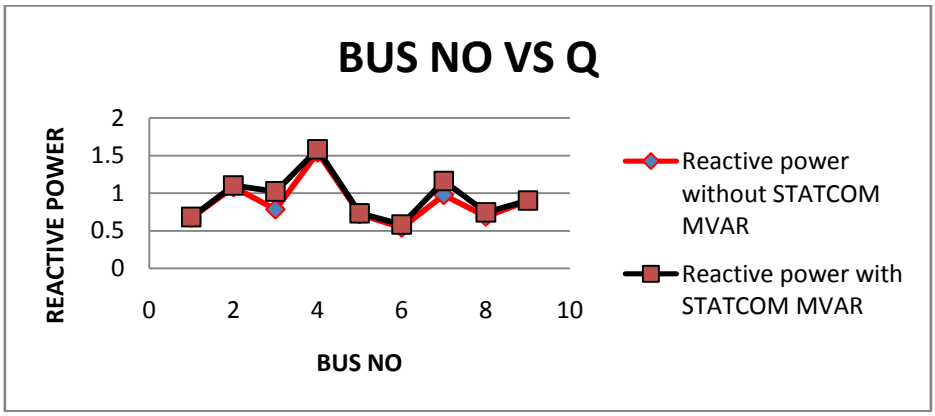

Fig 4f Reactive power in various buses

V. Conclusion

This work has explored the possibility of using Z-Source Inverter based STATCOM system. The thirty bus system is modeled and simulated using MATLAB software and results are presented. The simulation results of Thirty bus system with and without STATCOMs are presented. Simulation studies were done using single phase model of balanced three phase system. It is found that the bus voltages near the STATCOMs are improved and hence the reactive power. Overall power quality can be improved by using more STATCOMs at the load buses. The simulation results are in line with the predictions. This system has improved reliability and power quality. The scope for future work is simulation can also be done using PSCAD or PSIM. The simulation studies can be extended to 64-bus and 128-bus systems. Testing can also be done on extremely large real time power systems and also the laboratory model for STATCOM can be done using Micro-controller or DSP processor.

References

[1]. N.G.Hingorani and L.Gyugyi, understanding FACTS, Concepts and technology of Flexible AC Transmission systems, Piscataway, NJ; IEEE Press, 2000.
[2] S.Nillson, "Special application consideration for custom power systems", in proc.IEEE power Eng.Soc, winter Meeting 1999, vol.2, 1999, pp.1127-1130.
[3] "R.Mohan and R.K.Varma", Thyristor based FACTS Controllers for Electrical systems Transmission, Piscataway, NJ; IEEE Press, 2000.
[4] G.F.Reed,M.Takeda,I. Iyoda(1999), "Improved power quality solutions using advanced solid state switching and static compensation technologies",IEEE power Engineering Society Winter Meeting, Vol 2,27-31,726-734.
[5] Hannan M.A,Mohamed A.,Hussain A.,Dabbay M.,Power Quality Analysis of STATCOM using Dynamic phasor Modeling, International journal of Electrical power system Research, 79(2009),993-999.
[6] P.Giroux, G.Sybille, and H. Le-Huy, "Modeling and simulation of a distribution STATCOM using simulink's power system blockset", in proc. Annu. Conf. IEEE Industrial Electronic society, pp, 990-994.
[7] R.Mineski, R.Pawelek, I.Wasiak (2004), "Shunt compensation for power quality improvement using a STATCOM controller, modeling and simulation", IEE proc. On Generation, Transmission and Distribution, Vol.151, No.2.
[8] Jianye Chen, Shan song Zanji Wang, "Analysis and implementation of thyristor based STATCOM", 2006. International conference on power system Technology.
[9] Nitus vorahonpiput and soranchai chatratana, "STATCOM Analysis and controller design for power system voltage regulation "Transmission and distribution conference and exhibition 2005: Asia and pacific, IEEE/PES.
[10] M.H.Haque "compensation of Distribution system voltage sag by DVR and DSTATCOM", Power Tech proceedings 2001, IEEE Porto Volume: 1, sept.2001.
[11] B.Justus Rabi and Arumugam", Harmonics study and comparison of Z-Source inverter with Traditional Inverters", American journal of applied sciences2 (10):1418-1426, 2005.
[12] F.Z.Peng, M.Shen, F.Z.Peng, and Z.Qian, "Maximum boost control of the Z-source inverter", in Proc.39th IEEE Industry Applications conf., vol1, Oct.2004.
[13] M.Shen, J.Wang, A. Joseph, F.Z.Peng, L.M.Tolbert, and D.J.Adams, "Maximum constant boost control of the Z-Source Inverter", presented at the IEEE Industry Application soc.Annu.Meeting, 2004.
[14] F.Z.Peng,X.Yuan ,X.Fang and Z.Qian, "Z-Source inverter for adjustable speed drives",IEEE power Electron .Lett.,vol.1,no.2,pp.33-35, Jun.2003.
[15] N.Usha and M.Vijaya kumar "Simulation Results of eight-bus system using push-pull inverter based STATCOM" Interntional journal, JATIT, voL10, No2, Dec'2009.
[16] N.Usha and M.Vijaya kumar "comparison of VSI and ZSI based STATCOM", Interntional journal, IJERIA, vol3, No1, Feb'2010.

ABOUT THE AUTHORS

N.Usha has obtained her B. Tech degree from S.V.University and M.Tech degree from JNTU, Anantapur. She has 13 years of teaching experience. She has published three research papers at International level. She is presently a research scholar at JNTUA, Anantapur, A.P. She is working in the area of STATCOM.

Prof. M.Vijaya Kumar has obtained his B.Tech from S.V.University and M.Tech from NIT, Warangal and PhD from JNTU, Hyderabad. He has 21years of teaching experience. He has published 45 research papers at national and International level. His research area is power quality improvement in power systems.

International Journal of Modern Engineering Research (IJMER)
www.ijmer.com Vol.3, Issue.2, March-April. 2013 pp-779-784 ISSN: 2249-6645

Nox REDUCTION BY USING UREA INJECTION AND MARINE FERROMANGANESE NODULE AS SCR OF A DIESEL ENGINE FULLED WITH PONGAMIA PINNATA METHYL ESTER

S.Ghosh, [1] S.N. Chaudhuri, [2] D. Dutta[3]
[1]*Asst. Prof. Camellia School of Engineering and Technology Barasat, Kazipara, Kolkata*
[2]*Director, Kanad Institute of Engineering & Management, Mankar, Burdwan*

Abstract: *Pongamia pinata methyl ester (PPME) is chosen as alternative fuel for diesel engines. It is renewable and offer potential reduction in CO; HC and smoke emissions due to higher O_2 contents in it compared to diesel fuel but higher nitrogen oxides (NOx) emission. Nitrogen oxides (NOx) in the atmosphere cause serious environmental problems, such as photochemical oxidant, acid rain, and global warming. The removal of nitrogen oxides (NOx) from the exhaust of diesel engines is still a very challenging problem even though there have been many studies. Technologies available for NOx reductions either enhance other polluting gas emissions or increase fuel consumption.*

Injection of aqueous solutions of urea in the tail pipe of a diesel engine fuelled with Pongamia pinata methyl ester (PPME) for the reduction of oxides of nitrogen (NOx) was carried out in a four stroke, single cylinder, water cooled, constant speed diesel engine. Four observations were made for various concentration of urea solution 0%, 10%, 20%, and 30% by weight with different flow rates of urea solution as reductant by fitting Marine Ferromanganese nodule as SCR catalyst which improves the chemical reactions. 64% NOx reduction achieved with the urea flow rate 0.60 lit/hr, 30% concentration of urea solution and marine ferromanganese nodule as SCR.

Keywords: *Pongamia pinata methyl ester, Diesel engine, NOx, SCR, Marine Ferromanganese nodule.*

I. Introduction

The minimization of fuel consumption and the reduction of emissions have been two driving forces for engine development throughout the last decades. The first objective is in the financial interest of the vehicle owners. The second is imposed by legislation, sometimes also supported by excise reductions or customers' demands for clean engines.

The ongoing emission of NOx is a serious persistent environmental problem due to; it plays an important role in the atmospheric ozone destruction and global warming [1]. NOx is one of the most important precursors to the photochemical smog. Component of smog irritate eyes and throat, stir up asthmatic attacks, decrease visibility and damages plants and materials as well. By dissolving with water vapor NOx form acid rain which has direct and indirect effects both on human and plants. An SCR (Selective Catalytic Reduction) exhaust gas after treatment system which uses urea solution as a reducing agent has a high NOx reduction potential and is a well-known technique for stationary applications [2]. The idea of using urea SCR systems for the reduction of NOx emissions in diesel engines is two decades old. Since then, many applications have been developed, some of which have reached commercialization [3]. But, it is still a challenge for researchers.

There are numerous techniques for NOx removal. Selective catalytic reduction (SCR) of NOx with Urea is considered as potential technology for NOx reduction in diesel engine tail pipe emission. The main requirements for an SCR catalyst of automotive applications are high volumetric activity, stability over a extensive temperature range (180°C–650°C), and high selectivity with respect to the SCR reaction. In the last years, a main challenge was the development of catalysts with higher volumetric activity and this has been achieved by increasing the intrinsic activity of the catalyst formulation and by increasing the cell concentration of the monoliths [4]. Ammonia has been ruled out as a reducing agent, due to toxicity and handling issues, and urea appears to be the reductant of choice for most applications, stored on board in an aqueous solution. To overcome the difficulties connected with pure ammonia, urea can be hydrolyzed and decomposed to generate ammonia.

$$CO(NH_{2)2} \rightarrow NH_3 + HNCO$$
$$HNCO + H_2O \rightarrow NH_3 + CO_2$$

It seems that urea, as ammonia source, is the best choice for such applications as urea is not toxic and also can be easily transported as a high-concentration aqueous solution. As a result, NOx can be reduced with not only ammonia but also the urea itself and its decomposition by product, HNCO, as shown in reactions [5].

$$2CO(NH_2)_2 + 6NO \rightarrow 5N_2 + 2CO_2 + 4H_2O$$
$$4HNCO + 6NO \rightarrow 5N_2 + 4CO_2 + 2H_2O$$
$$4NH_3 + 4NO + O_2 \rightarrow 4N_2 + 6H_2O$$

Even though the use of urea in the reduction of NOx from the flue gas streams of power plants is a well-established method, there have not been many studies on the use of urea as a reductant in treatment of the exhaust of lean-burn engines.

Schar et al. (2003) [6] suggested an advanced controller for a urea SCR catalytic converter system for a mobile heavy-duty diesel engine. The after treatment system consists of injecting device for urea solution and a single SCR catalytic converter. Chakravarthy et al. [7] have done a comprehensive literature review on the performance of zeolite catalysts compared to vanadia catalysts, and found that zeolite catalysts generally have a higher NOx reduction efficiency of SCR with NH_3, and may have a broader temperature window for selectivity of SCR towards N_2. Secondly the optimization of the urea injection strategy under transient engine operating conditions, in order to provide the necessary amounts of NH_3 for NOx removal and at the same time minimize the amount of excess NH_3 slipping to the environment. Koebel et al. (2003) [8] presented that atomization of urea-water-solution in hot exhaust stream yields to solid or molten urea.

Birkhold et al. [9] have claimed for automotive applications, that the urea-water-solution based SCR was a promising method for control of NOx emissions. Urea-water-solution containing 32.5 wt% urea was sprayed into the hot exhaust stream, for the subsequent generation of NH_3 in the hot exhaust gas. As the evaporation and spatial distribution of the reducing agent upstream the catalyst were vital factors for the conversion of NOx, the urea dosing system has to ensure the proper preparation of the reducing agent at all operating conditions. Specific concerns with the ammonia process included the storage, handling, and delivery of the ammonia. Also, any ammonia not consumed in the process may be emitted ("ammonia slip") as a result of this process. For these and other reasons, alternative agents have been proposed over the years. Two of these that have received significant interest include cyanuric acid [$(HNCO)_3$] and urea [$(NH_2)2CO$] [10]. Koebel et al. (2000) [11] suggested the basic problems and challenges of the use of urea-SCR in mobile applications. Though urea-SCR is very effective method for removing NOx at temperatures above 250° C there was a need for removing NOx in a wide range of temperatures because of a large temperature variation of exhaust gas according to the operation condition of the engine and because of further reduction of NOx emission limits. Schaber et al. [12] suggested that molten urea evaporates to gaseous urea at temperatures above 413 K, but mainly decompose directly to NH_3 and HNCO above 425 K.Fang et al. (2003) [13] presented the effect of moisture on urea decomposition process and found that the moisture could assist the hydrolysis of HNCO only in the temperature region below the first decomposition stage (below 250^oC). The DRIFTS measurements showed that the final brown colour product formed at 450^oC could be a chemical complex of polymeric melamines with high molecular weights which might actually block the active sites on the catalyst surface. Their study showed that urea thermo-lysis exhibits two decomposition stages, involving ammonia generation and consumption respectively. Decomposition occurring after the second stage leads to the production of melamine complexes that hinder the overall performance of the catalyst. They asserted that polymeric melamine complexes can be formed both with and without the catalyst and they do not undergo further decomposition (at least up to 320^oC). Wolfgana Held et al. (1990) [14] have suggested that, the use of urea is usually regarded as safe, it is easy to transport in the vehicle in an aqueous solution, which make it also easy to dose as necessary. Copper-exchange zeolite catalysts can selectively convert nitrogen oxides over a much wider range of fuel-air ratios than nobel-metal catalysts and they achieved only 65% of NOx reduction, the urea dosage was not analyzed, also they have not given the required construction la out of engine arrangement. Also they have not explained the secondary reaction.

In this study injection of aqueous solutions of urea and Marine Ferromanganese Nodule as SCR in the tail pipe of a diesel engine fuelled with Pongamia pinata methyl ester (PPME) for the reduction of oxides of nitrogen (NOx) was carried out in a four stroke, single cylinder, water cooled, constant speed diesel engine.

- **MARINE FERROMANGANISE NODULE**

Ferromanganese Nodule which, is easily available from sea bed, is considered an economically important source of Ni, Co, Cu, Si and rare earth elements [15]. The physical and chemical properties revels that the nodules in general has high porosity, large specific surface area [16]. It has high structural stability [17]. It has also acidic and basic sites as it is chemically an assembly of oxide [18, 15]. The nodule is easily reduced at 200°C to form Fe_3O_4, MnO, Ni, Cu, Co and is oxidized by oxygen to Fe_2O_3, MnO_2, NiO, CoO [19]. The nodule catalyses the oxidation of CO, CH_4 [17], and the CO oxidation activity is better than $Pt.Al_2O_3$ catalyst [20].

- **SELECTIVE CATALYTIC REDUCTION (SCR)**

Selective catalytic reduction (SCR) is an after treatment process. A SCR system attempts to reduce oxides of nitrogen (NOx) back to harmless nitrogen and elemental oxygen that are constituents of air. It permits the NOx reduction reaction to take place in an oxidizing atmosphere. It is called "selective" because the catalytic reduction of NOx with ammonia (NH3) or urea as a reductant occurs preferentially to the oxidation of NH3 or urea with oxygen.

NOx reduction by SCR process takes place without a fuel penalty. It also allows diesel engine developers to take advantage of the trade-off between NOx and PM without fuel penalty. For mobile source applications ammonia is used as a selective reductant, in the presence of excess oxygen, to convert over 70% (up to 95%) of NO and NO_2 to nitrogen over a specified catalyst system. Different precursors of ammonia can be used; but for vehicles the most common option is a solution of urea in water carefully metered from a separate tank and injected into the exhaust system where it hydrolyzes into ammonia ahead of the SCR catalyst. Urea solution is a stable, colorless, non-flammable fluid containing 32.5% urea which is not considered as hazardous to health and does not require any special safety measures.

To determine the kind of catalyst to be used that depend on exhaust gas temperature, reduction of nitrogen oxides necessary, oxidation of SO2 and the concentration of other exhaust gas constituents.

II. EXPERIMENTAL SETUP

Injection of aqueous solutions of urea from a separate urea tank in the tail pipe of test the diesel engine fuelled with Pongamia pinata methyl ester (PPME) for the reduction of oxides of nitrogen (NOx) was carried out in a four stroke, single cylinder, water cooled, constant speed diesel engine with eddy current dynamometer. Four observations were made for the exhaust gas analysis of various concentration of urea solution 0%, 10%, 20%, and 30% by weight with different flow rates of urea solution by fitting Marine Ferromanganese nodule as oxidant catalyst. The technical specifications of the engine are given in Table I, and the schematic of the experimental setup is shown in Fig. 1. The power output of the engine was measured by an electrical dynamometer. AVL gas analyzer was used for the measurement of amounts of exhaust emissions. Digital control panel was used to collect data such as torque, water flow of engine etc. A three way control valve and needle are used to maintain the urea flow rate. Urea solution for different concentration is made before the experiment. The measurements were taken after steady state of the engine for each set of readings.

Table -1: Specification of engine

Type of engine	Four stroke single cylinder Diesel engine
Bore	87.6mm
Stroke	110mm
Compression ratio	17.5:1
Rated speed	1500
Rated power	7HP (5.2 kW)@1500rpm
Displacement volume	661.5cm^3

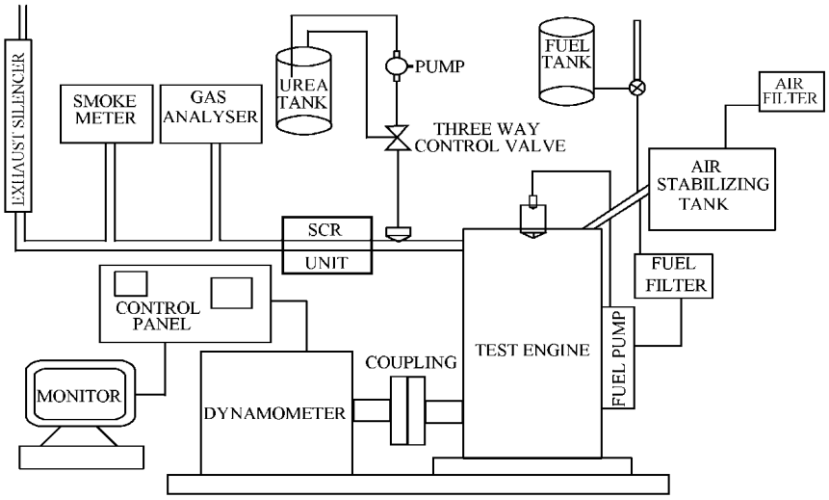

Figure 1. Schematic of Experimental Setup

III. RESULTS AND DISCUSSIONS

The output obtained from the experiment is plotted to determine the effect of the injection of urea solution at various concentration and flow rate as reductant and marine ferromanganese nodule as SCR on the NOx emission analysis of the test engine.

1. (NO_x) Emission v/s Brake power without urea and SCR

Fig. 2 shows the variations of NOx emissions with brake power of a diesel engine fuelled with Pongamia pinata methyl ester (PPME) without urea solution and SCR at constant speed of the engine. From the graph it is observed that the NOx emission increases with the increase of brake power due to high combustion temperature in the combustion chamber. This indicates that the emission of NOx is very much influenced by the cylinder gas temperature and the availability of oxygen during combustion.

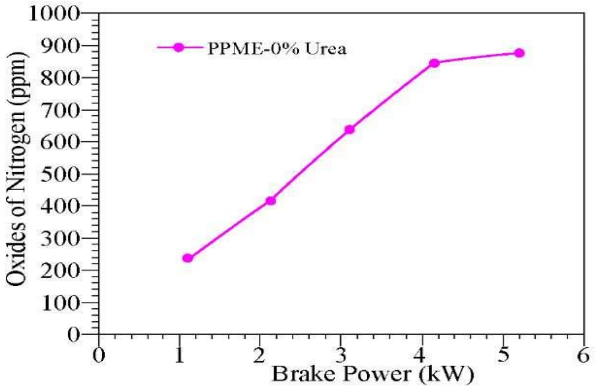

Figure 2. (NO_x) Emission v/s Brake power without urea and SCR

2. (NO_x) Emission v/s Brake power with10% urea solution without SCR

Fig. 3 shows the variations of NOx emissions with brake power of a diesel engine fuelled with Pongamia pinata methyl ester (PPME) with 10% urea solution and without SCR at constant speed of the engine. From the graph it is observed that the NOx emission decreases with the injection of 10% urea solution. It is also observed that as the urea flow rate increases NOx reduction increases due to better mixing of the exhaust gases in the tail pipe.

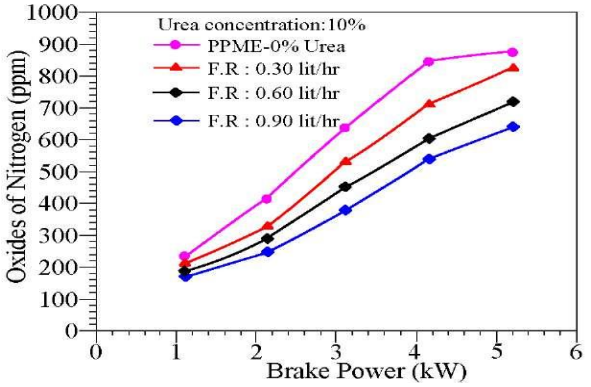

Figure 3. (NO_x) Emission v/s Brake power with10% urea solution without SCR

3. (NO_x) Emission v/s Brake power with20% urea solution without SCR

Fig. 4 shows the variations of NOx emissions with brake power of a diesel engine fuelled with Pongamia pinata methyl ester (PPME) with20% urea solution and without SCR at constant speed of the engine. From the graph it is observed that the NOx emission decreases with the increase of the concentration of the urea solution and urea injection flow rate due to further better mixing of the exhaust gases in the tail pipe.

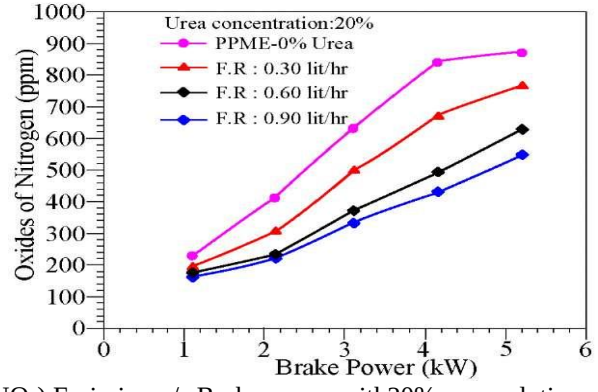

Figure 4. (NO_x) Emission v/s Brake power with20% urea solution without SCR

4. (NO_x) Emission v/s Brake power with30% urea solution without SCR

Fig. 5 shows the variations of NOx emissions with brake power of a diesel engine fuelled with Pongamia pinata methyl ester (PPME) with30% urea solution and without SCR at constant speed of the engine. From the graph it is observed that the NOx emission further decreases with the increase of the concentration of the urea solution and urea injection flow rate due to better surface contact of the exhaust gases.

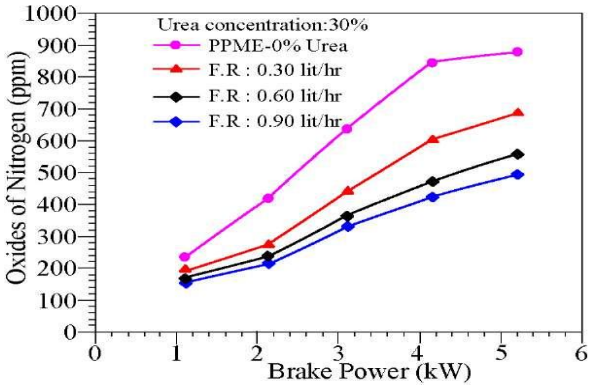

Figure 5. (NO_x) Emission v/s Brake power with30% urea solution without SCR

5. (NO_x) Emission v/s Brake power with varying urea solution concentration without SCR at constant injection flow rate

Fig. 6 shows the variations of NOx emissions with brake power of a diesel engine fuelled with Pongamia pinata methyl ester (PPME) with various concentrations of urea solution and constant flow rate 0.60 lit/hr without SCR at constant speed of the engine. From the graph it is observed that the NOx emission decreases with the increase of the concentration of the urea solution at constant urea injection flow rate.

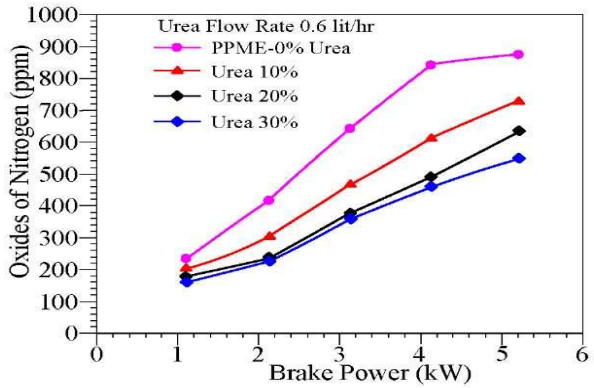

Figure 6. Oxides of Nitrogen emission (NO_x) v/s Brake power with varying urea solution concentration without SCR at constant injection flow rate

***6.* (NO_x) Emission v/s Brake power with varying concentration of urea solution at constant injection flow rate with Marine Ferromanganese Nodule as SCR.**

Fig. 7 shows the variations of NOx emissions with brake power of a diesel engine fuelled with Pongamia pinata methyl ester (PPME) with various concentrations of urea solution and constant flow rate 0.60 lit/hr with Marine Ferromanganese Nodule as SCR at constant speed of the engine. From the graph it is observed that the NOx emission decreases remarkably with the introduction of the Marine Ferromanganese Nodule as SCR in tail pipe of the engine.

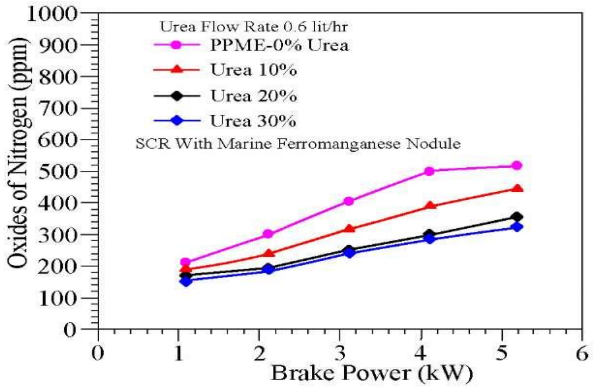

Fig. 7. (NO_x) Emission v/s Brake power with varying concentration of urea solution at constant injection flow rate (0.60 lit/hr) with Marine Ferromanganese Nodule as SCR.

IV. CONCLUSION

From the study it can be concluded that urea injection with Marine Ferromanganese Nodule as SCR in the tail pipe 64% NOx reduction achieved. Moreover, it also indicates that the catalyst used in the test engine commercially attractive as compared to noble metal catalyst.

REFERENCES

[1] Busca G., Lietti L., Ramis G., and Berti F., Chemical and mechanistic aspects of the selective catalytic reduction of NOx by ammonia over oxide catalysts: A review, Applied catalysts B: environmental, 18(1-2), 1998, 1-36
[2] H. Bosch, F. J. J. G. Janssen: Catalytic Reduction of Nitrogen Oxides: A Review on the Fundamentals and Technology, Catalysis Today, 2(369), 1988.
[3] Perry, R. A. and Siebers, D. L. Rapid reduction of nitrogen oxides in exhaust gas streams. Nature, 324, 1986, 657–658.
[4] Kleemann, M., Dissertation Nr. 13401, ETH Zurich, 1999.
[5] Hug, H. T., Mayer, A., and Hartenstein, A., SAE Technical Paper Series, 930363, Detriot, March 1–5, 1993
[6] C.M.SCHAR, C.H. Onder and H.P. Geering, M Elsener, Control of a Urea SCR catalytic Converter System for a Mobile Heavy Duty Diesel Engine , SAE Transaction, 2003010776, 2003.
[7] Chakravarthy, K., Choi, J.-S., and Daw, S. Modeling SCR on zeolite catalysts – A summary of observations on SCR kinetics based on the open literature. In Eighth DOE-CLEERS Workshop, Dearborn, Michigan, 17–19 May 2005
[8] M. Koebel and E. O. Strutz, Thermal and Hydrolytic Decomposition of Urea for Automotive Selective Catalytic Reduction Systems: Thermo chemical and Practical Aspects, Journal of Industrial and Engineering Chemistry Research, 42, 2003, 2093-2100
[9] F. Birkhold, U. Meingast, P. Wassermann, and O. Deutschmann, Modeling and simulation of the injection of urea-water-solution for automotive SCR DeNOx-systems, Applied Catalysis B: Environmental, 70, 2007, 119-127
[10] J. A. Caton and Z. Xia, The Selective Non-Catalytic Removal (SNCR) of Nitric Oxides From Engine Exhaust Streams: Comparison of Three Processes, Journal of Engineering for Gas Turbines and Power, Transactions of the ASME, 126, 2004, 234-240
[11] M. Koebel, M. Elsener, and M. Kleemann, Urea-SCR: a promising technique to reduce NOx emissions from automotive diesel engines, Catalysis Today, 59, 2000, 335–345
[12] P. M. Schaber, J. Colson, S. Higgins, D. Thielen, B. Anspach, and J. Brauer, Thermal decomposition (pyrolysis) of urea in an open reaction vessel, Thermochimica Acta, 424, 2004, 131–142
[13] H. L. Fang and H. F. M. DaCosta, Urea thermolysis and NOx reduction with and without SCR catalysts, Applied Catalysis B: Environmental, 46, 2003, 17-34
[14] Wolfgang Held, Axel Konig and Thomas Richter, Lothar Puppe, Catalytic NOx Reduction in Net Oxidizing Exhaust Gas, SAE Transsactions, 900496, 1990
[15] Mohapatra .B.K.,S.K. Mishra & R.K. Sahoo, Characteristics of marine ferromanganese concentrations at elevated temperature, Thermochimica Acta, 145, 1989, 33-49
[16] Bobonich F.M., Lazarenko V.I., Oriovskii G.N. and Solomakha V.S., Geol.Khim. Biol. Nauke, 6, 1987.
[17] Weisz P.B., Deep sea manganese nodules as oxidation catalysts, J. Catal, 10, 1968, 407
[18] Cronan, D.S., and J.S. Tooms, The geochemistry of manganese nodules and associated pelagic doposits from the Pacific and Indian Oceans, Deep-Sea Research, 1969, 335-359,
[19] Dobet C., Noville F., Crine M. and Pirard J.P., Texture of manganese nodules used as a catalyst for demetallizing and desulphurizing petroleum residua, Colloids and Surfaces, 11(1-2), 1984, 187-197
[20] Nitta M., Characteristics of manganese nodules as adsorbent and catalysts, a review, Appl. Catal., 9, 1984, 151-176

International Journal of Modern Engineering Research (IJMER)
www.ijmer.com Vol.3, Issue.2, March-April. 2013 pp-785-787 ISSN: 2249-6645

Privacy Protection Using Unobservablity and Unlink ability against Wormhole Attacks in Manet

N.Sugumar, [1] K.Jayarajan M.E, [2] R.Anbarasu, M.E[3]
[1]*Final Year M.E-CSE,*
[23] *Associate Professor Selvam College of Technology, Namakkal*

ABSTRACT: An efficient privacy-preserving routing protocol USOR that achieves content un-observability by employing anonymous key establishment based on group signature. The setup of USOR is simple: In privacy-preserving communications can largely be divided into two categories: cryptosystem-based techniques and broadcasting-based techniques. The cryptosystem-based techniques include mix-based systems and secure multiparty computation-based systems, originating from mix net and DC-net respectively. Broadcasting based schemes provide communication privacy by mixing the real messages with dummy packets so that it is infeasible for the adversaries to identify the real packets and track the message source. First, an anonymous key establishment process is performed to construct secret session keys. Then an unobservable route discovery process is executed to find a route to the destination. This process is done by establishing session keys between two nodes. After verifying the signature between themselves, the anonymous key is established between these two nodes which mean the two nodes establish this key without knowing who the other party is. It can effectively prevent replay attacks and session key disclosure attack, and meanwhile, it achieves key confirmation for established session keys. This key establishment protocol uses elliptic curve Diffie- Hellman (ECDH) key exchange to replace Diffie-Hellman key exchange, and uses group signature to replace MAC code.In this protocol, both control packets and data packets look random and indistinguishable from dummy packets for outside adversaries. Only valid nodes can distinguish routing packets and data packets from dummy traffic with inexpensive symmetric decryption.

I. Introduction

Mobile computing is human computer interaction by which a computer is expected to be transported during normal usage. Mobile computing involves mobile communication, mobile hardware, and mobile software. Communication issues include ad-hoc and infrastructure networks as well as communication properties, protocols, data formats and concrete technologies.

Many types of mobile computers have been introduced
- Wearable Computer
- Personal Digital Assistant
- Smartphone
- Carputer
- UMPC

1.2 TECHNICAL AND LIMITATIONS OF MOBILE COMPUTING

1.2.1 Range & Bandwidth:

Mobile Internet access is generally slower than direct cable connections, using technologies suchas GPRS , 3G and 4G networks. These networks are usually available within range of commercial cell phone towers. Higher speed wireless LANs are inexpensive but have very limited range.

1.2.2 Security Standards:

When working mobile, one is dependent on public networks, requiring careful use of VPN. Security is a major concern while concerning the mobile computing standards on the fleet. One can easily attack the VPN through a huge number of networks interconnected through the line.

1.2.3 Power Consumption:

When a power outlet or portable generator is not available, mobile computers must rely entirely on battery power. Combined with the compact size of many mobile devices, this often means unusually expensive batteries must be used to obtain the necessary battery life.

1.2.4 Transmission Interferences:

Weather, terrain, and the range from the nearest signal point can all interfere with signal reception. Reception in tunnels, some buildings, and rural areas is often poor.

1.2.5 Potential Health Hazards:

People who use mobile devices while driving are often distracted from driving and are thus assumed more likely to be involved in traffic accidents.[3] (While this may seem obvious, there is considerable discussion about whether banning

mobile device use while driving reduces accidents or not.[4][5]) Cell phones may interfere with sensitive medical devices. Questions concerning mobile phone radiation and health have been raised.

1.2.6 Human Interface with Device:

Screens and keyboards tend to be small, which may make them hard to use. Alternate input methods such as speech or handwriting recognition require training.

II. Related Work

2.1 Anonymous Network Model

In this module, anonymous route is discovered between the nodes this information will not leak to others.This is adopted using session key and broadcast key generation by means of Key Generation Center(KGC).This anonymous connection is established by verifying signatures of the each node.

2.2 Secure Key Generation and Route Discovery Phase

This phase is a privacy-preserving route discovery process based on the keys established in previous phase.Similar to normal route discovery process, our discovery process also comprises of route request and route reply.The route request messages flood throughout the whole network, while the route reply messages are sent backward to the source node only.This performed based on the ID-based private key of every node.

2.3 Broadcast Key Distribution

The broadcast key has been established among the nodes in the network. The key generated from the public key generated for the group.This broadcast key act like a security issue where each node should get authenticated before it enters into the network for communication.The BK will be shared among the neighbors in the zone.

2.4 Attacker Model

For the collusion attacks, USOR still offers unobservability as promised. Though information disclosure is unavoidable for colluding insiders, and the adversary knows some keys, the information that the colluding insiders can obtain is largely restricted by USOR.For preventing the Sybil attacks, the centralized key server generates group signature signing keys and ID-based keys for network nodes. Thus, it is impossible for the adversary to obtain other valid identities except the compromised ones.

2.5 Performance Evaluation

The sender computes the anonymity of RREQ packets. The sender anonymity is the obtained by calculating entropy of probability distribution of possible sender of RREQ packets.The performance has been rated by comparing the results from MASK. This results show that the error rate has been reduced.This system not only achieves anonymity, unobservability, unlinkability but also prevents from Sybil attack and collusion attack.

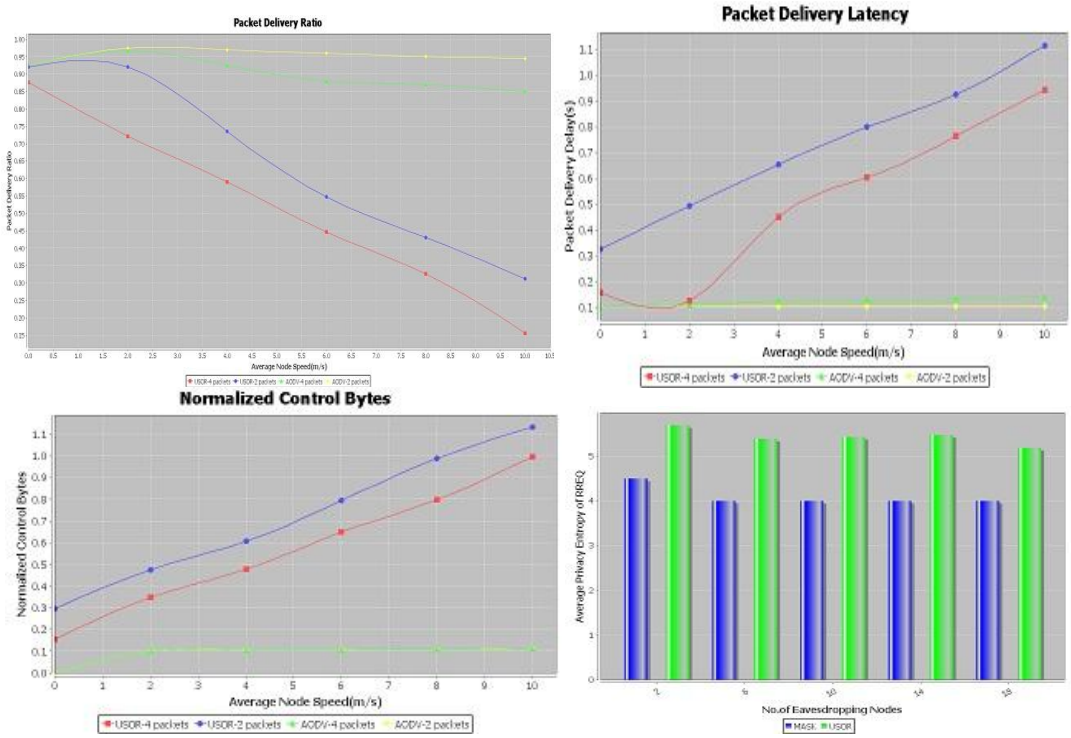

III. Conclusions

The USOR offers unobservability as promised. Though information disclosure is unavoidable for colluding insiders, and the adversary knows some keys, the information that the colluding insiders can obtain is largely restricted by USOR. In the padded USOR, all packets including RREQ, RREP packets and other control packets are padded to 128 bytes. Due to the packet padding, performance of the padded USOR is obviously downgraded, but the padded USOR still achieves satisfactory performance: more than 85% delivery success and about 250ms delivery latency. And also it not only provides strong privacy protection, it is also more resistant against attacks due to node compromise. Finally, achieves stronger privacy protection than existing schemes like MASK.

References

[1] Karim El Defrawy, Member, and Gene Tsudik, Senior Member"Privacy-preserving location-based on-demand routing in MANETs," IEEE J. Sel. Areas Column., vol. 29, no. 10, pp. 1926–1934, 2011.
[2] Andreas Pfitzmann, TU Dresden and Marit Hansen, ULD Kiel "Anonymity, Unlinkability, Undetectability, Unobservability,Pseudonymity, and Identity Management –A Consolidated Proposal for Terminology"Version v0.31 Feb. 15, 2008.
[3] Jiejun Kong, Xiaoyan Hong" ANODR: ANonymous On Demand Routing with Untraceable Routes for Mobile Ad-hoc Networks" June 1–3, 2003.
[4] Karim El Defrawy and Gene TsudiK"ALARM: Anonymous Location-Aided Routing in Suspicious MANETs"March 2007.
[5] Reshmi Maulik and Nabendu Chaki "A Study on Wormhole Attacks in MANET " ISSN 2150-7988 Volume 3 (2011) pp. 271-279.
[6] Nadher MohammedAhmed AI-Safwani"The Effect of Eavesdropping and Wormhole Attacks on Mobile Adhoc Networks"2009.
[7] Tanu Preet Singh, Shivani Dua and Vikrant Das" Energy-Efficient Routing Protocols In Mobile Ad-Hoc Networks" Volume 2, Issue 1, January 2012.
[8] Kortuem.G., Schneider. J., Preuitt.D, Thompson .T.G.C, F'ickas.S. Segall.Z. "When Peer toPeer comes Face-to-Face: Collaborative Peer-to-Peer Computing in Mobile Ad hoc Networks", 1st International Conference on Peer-to-Peer Computing, August, Linkoping, Sweden, pp. 75-91 (2001)
[9] Mangrulkar.R.S, Dr. Mohammad Atique, "Trust Based Secured Adhoc on Demand Distance Vector Routing Protocol for Mobile Adhoc Network" (2010)
[10] Marc Branchaud, Scott Flinn,"x Trust: A Scalable Trust Management Infrastructure"
[11] Menaka Pushpa.A M.E., "Trust Based Secure Routing in AODV Routing Protocol" (2009)
[12] Sridhar, S., Baskaran, R.: Conviction Scheme for Classifying Misbehaving Nodes in Mobile Ad Hoc Networks in the proceedings of CCSIT 2012 published by Springer (LNICST) 2012
[13] "TAODV: A Trusted AODV Routing protocol for Mobile ad hoc networks" (2009)

International Journal of Modern Engineering Research (IJMER)
www.ijmer.com Vol.3, Issue.2, March-April. 2013 pp-788-792 ISSN: 2249-6645

Surface Properties of the Stainless Steel X10 CrNi 18/10 after Aplication of Plasma Polishing in Electrolyte

D. Vaňa, [1] Š. Podhorský, [2] M. Hurajt, [3] V. Hanzen[4]
[1234]*Department of Welding and Foundry, Slovak Technical University, Slovakia*

Abstract: *The first part of the paper deals with surface properties of the stainless steel specimen after plasma polishing in electrolyte. The plasma polishing technology is considered as a more environmental friendly alternative to the common electrochemical polishing process (electropolish). The electrolyte solutions use no acids or toxicants, low concentrated water solutions of various salts are used instead. The surface roughness, the gloss level and the thickness of removed layer are in the focus, as well as their dependence upon the treatment time. The results are then compared to the surface properties of specimens treated by standard electrochemical polishing. The specimens of the same material, the same shape and the same surface state have been used for both polishing technologies. Finally, the differences between those polishing processes and the differences between the properties of the polished surfaces are discussed.*

Keywords: *electrolyte, plasma, polishing, stainless steel*

I. INTRODUCTION

Polishing of stainless steels is widely used, mainly in order to improve the corrosion resistance of its surface as well as to reduce the surface roughness. Polishing is the most common surface finishing operation of stainless steel products in the field of medical, pharmaceutical, food or chemical industry. The corrosion resistance improvement is not the only benefit of the polishing process, but the surface also becomes smoother and more resistant to dirt, bacteria, rot, etc. [2, 3].

Surface polishing in acids mixture under the influence of electric current, e.g. the electrochemical polishing, known as electro- polishing, is the most commonly used polishing method for surface finishing of complexly shaped industrial parts. A new polishing technology, the plasma polishing in electrolyte has been developed as an alternative to the standard electrochemical polishing. This paper deals with some properties of stainless steel surface treated by the plasma polishing process in electrolyte. Especially the surface roughness reduction, the rise of gloss level and the material removal rate are examined.

II. THE PRINCIPLE OF THE PLASMA POLISHING

The metal part, to be treated, is immersed into the electrolyte and is connected to the plus pole of the electric current supply. So the treated part is the anode. The second electrode is connected to the minus pole of the power supply. As it can be seen on the *Fig. 1*, the principal scheme of this process is similar to the electro-chemical polishing at first glance. The main differences are in the voltage value and in the chemical composition of the electrolyte. The high concentrated mixture of acids is displaced by low-concentrated water solution of chemically neutral salts. A water-steam film is forming on the entire treated surface due to high value of the voltage between electrodes. The film is electrically nonconductive and it separates the metal surface from the electrolyte. In this way the electric current is broken so the electric circuit gets disconnected. But if the voltage between the electrodes is high enough (a few hundreds of volts), the water-steam film becomes ionized due to high value of the electric field in the thin film. In this case, the electric current flows through the water-steam film in the form of glow discharge. In this way, the discharge act on the metal surface in this process. The discharge always runs toward the peaks of the surface profile in the form of thin columns since the distance between the electrodes (metal – wall of electrolyte) is here shortest. In this way the surface peak is quickly removed. When the material of the peak is removed, the column of discharge moves to another surface peak where the thickness of the water-steam layer is less. In this way the surface becomes smoother. If a proper chemical composition of the electrolyte and suitable parameters of the process are used, the treated surface becomes glossy [4].

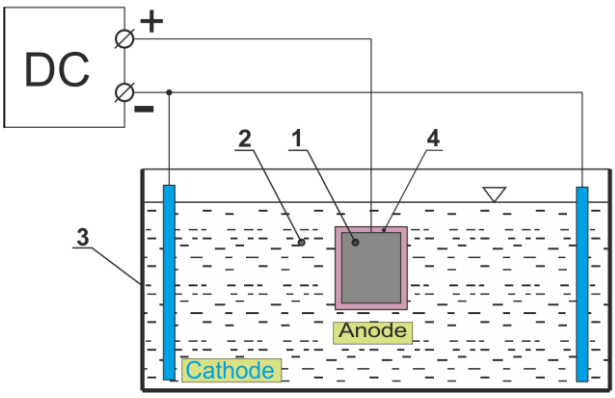

Fig. 1 The principal scheme of the process;
1 – treated specimen, 2 – electrolyte solution, 3 – work vessel, 4 – ionized water-steam film, 5 – power supply.

One of the advantages of this technology is in the possibility to treat metal parts with complex and irregular shape. Furthermore, there is no shielding effect as it is in the case of electrochemical polishing. The next advantage of the plasma polishing process is in the harmless composition of the electrolyte. The electrolytes are based on environmental friendly solution of various salts. The solutions of concentrations 4 ÷ 6% are prepared by dissolving

granulate in the water without extra demand on its quality. In the spent solution, iron is bound in the form of oxides. [2, 3].

III. THE SPECIMENS

A rolled sheet of austenitic stainless steel X10 CrNi 18/8 has been used for specimens. The specimens of dimensions 50 mm × 50 mm × 3 mm has been cut from the sheet using water jet cutter. Two holes of diameter 5 mm were drilled to fix the specimen to its holder during polishing. The surface of the specimens was not treated e.g. it was in crude (rolled) state. Due to untreated surface layer the initial (before polishing) gloss level of the specimen had the value of 7.5 GU only. Its average initial value of the surface roughness *Ra* was 1.7 μm.

IV. THE EXPERIMENTAL PROCEDURE

The experiment has been focused on the effect of plasma polishing upon the treated surface's properties. The properties have been examined are: the gloss level, the surface roughness and the layer thickness removal Δh. To know the exact material removal rate is important when precise machine parts with tight tolerances are polished. The total treatment time lasted 5 minutes and was divided into a few intervals to get the surface properties dependence on the treatment time. After each polishing step the examined properties were measured always on the same spot on the specimen. The conditions and the process parameters were kept on constant values during each plasma-polishing step. The electrolytic solution of concentration 6 % has been used at temperature 65°C and the immersion depth of the specimen was 100 mm.

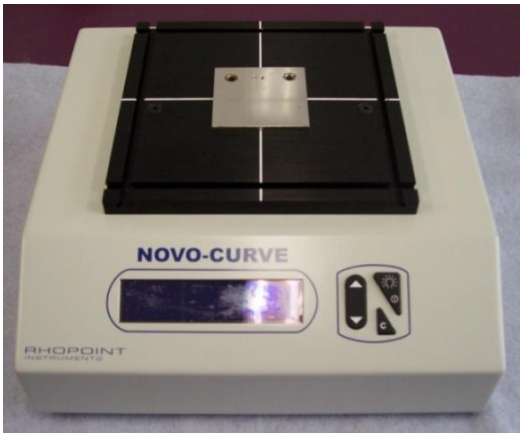

Fig. 3 The gloss level measurement on a specimen

Fig. 2 The surface roughness measurement on a specimen using surface tester TR 200

For exact gloss level assessment of the treated specimen a gloss-meter of the type Novo Curve (Rhopoint Instruments, UK) has been used. The gloss meter uses 60° measurement angle and it conforms to ASTM D523 and to ISO 2813. The gloss level has been measured at the geometric centre of the specimen (*Fig. 2*) five times and the average values of these data are in third column of the *TABLE 2*. Surface tester of type TR 200 (*Fig.3*) has been used to evaluate the surface roughness. The resolution of used surface tester is 0.01 μm and it conforms to DIN4772. The tested area was the same as in the case of the gloss level measurements. The surface roughness of *Ra* has been measured five times at the same spot, the average values are in the *TABLE 1*, as well.

The thickness h_T and the exact weight of the specimens m_T have been measured after each plasma-polishing treatment step, e.g. after the treatment time *T*, to evaluate the value of the layer thickness removal Δh_T. The value of layer thickness removal can be calculated as the difference between thickness of specimen before and after polishing. Since this value is near the resolution and accuracy of common digital micrometres, such results are not precise enough. Therefore, the material removal rate is calculated from the weight difference of the specimen before and after polishing and the value of the layer thickness removal is computed from this value using own software, developed for this specific purpose. The balance of type PB 303-S (Mettler-Toledo) with resolution 1 mg has been used. The measured values of the specimen's weight and the calculated data are given in *TABLE 1*. The layer thickness removal is the thickness of the removed material layer from one side of the treated surface, not the specimen's thickness difference. The speed of layer thickness removal $\dot{\Delta h}$ has been calculated from the value

Table 1 *Properties of the specimen #1 after each plasma-polishing step;*

T [min]	Ra_T [μm]	G_T [GU]	m_T [g]	Δh_T [μm]	$\Delta \dot{h}_T$ [μm/min]
0	1.69	8.8	55.379	—	—
0.5	1.51	32.8	55.332	1.09	2.18
1	1.38	66.4	55.270	2.53	2.53
1.5	1.23	87.4	55.222	3.64	2.43
2	1.06	98.8	55.181	4.59	2.30
2.5	1.00	137.3	55.134	5.67	2.27
3	0.98	157.7	55.087	6.76	2.20
4	0.88	205.7	55.016	8.41	2.10
5	0.78	201.7	54.935	10.28	2.06

T – time of treatment, Ra – surface roughness, G – gloss level, m –weight of the specimen, Δh – layer thickness removal, $\Delta \dot{h}_T$ – speed of layer thickness removal

of the layer thickness removal divided by the appropriate treatment time *T*. These data can be found in the last column of the *TABLE 1*.

V. THE RESULTS

Graphical representation of the obtained data is shown on *Fig. 4*. The value of surface roughness *Ra* decreases by the treatment time nonlinearly, initially it declines quickly but then this decline slows down. So the roughness falls more quickly at the beginning of the polishing process. Using regression analysis of the measured data the following relation has been found:

$$Ra = 1.68 - 0.35T + 0.036\,T^2 \quad [\mu m, min] \tag{1}$$

The gloss level of the treated surface rises almost linearly by the treating time during the first four minutes (*Fig. 4*). After the maximal value is reached, there is no evident change of the gloss level. This relation can be described in the interval 0 to 5 minutes by the following equation:

$$G = 10.8 + 39.6\,T + 8.8\,T^2 - 1.8\,T^3 \quad [GU, min] \tag{2}$$

The layer thickness removal shown in *Fig. 4* seems to be constant by the treatment time at first glance, but as it can be seen in *TABLE 1* the values slightly decrease except the first value. The following equation has been used to describe this dependence in the range of $1 \div 5$ minutes:

$$\Delta h = -0.12 + 2.52\,T - 0.09T^2 \quad [\mu m, min] \tag{3}$$

This equation is not valid in the first minute of treatment, where the value of the layer thickness removal is less. It can be explained by the fact, that the initial specimen's surface had been covered by an oxide film. Metal oxides are electrically nonconductive so it takes longer to remove them for the plasma-polishing process. A graphical presentation of the dependence of the layer thickness removal Δh_T upon the treatment time *T* is shown on the *Fig. 5*.

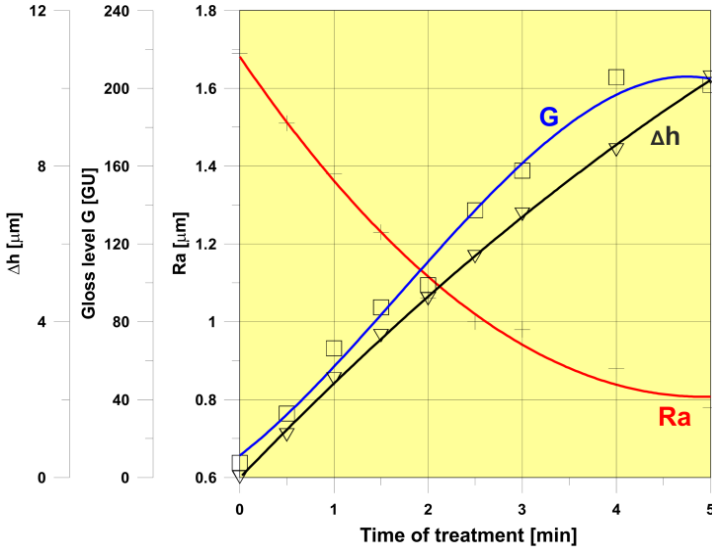

Fig. 5 Surface roughness, gloss level and layer thickness removal dependence upon the treatment time

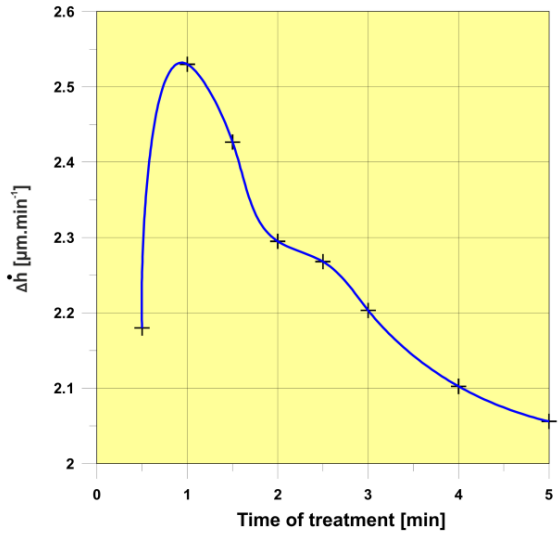

Fig. 4 Dependence of the layer thickness removal speed upon the treatment time

VI. COMPARISON TO THE STANDARD ELECTROPOLISH

The plasma-polishing technology is an alternative to the commonly used electrochemical polishing process, known simply as "electropolish". There is the question, how the surface parameters will differ if the same samples are processed by both polishing methods. Therefore a few specimens have been polished electrochemically, as well. The specimens of the same material, the same shape and the same surface state as it was in the case of plasma-polishing have been used. The electrolyte solution for electrochemical polishing consisted of 64% H_3PO_4, 13% H_2SO_4 and 23% H_2O [5, 6]. The temperature of the electrolyte has been kept during polishing at 60°C. Four specimens (specimen #2 to #5) have been processed 3 minutes, each at different value of the electric current density: 40 A.dm^{-2}, 50 A.dm^{-2}, 60 A.dm^{-2} and 72 A.dm^{-2}.

Table 2 The measured and calculated properties of the specimens before and after 3 minutes of electrochemical polishing

Specimen No.	Ra_0 [μm]	Ra_3 [μm]	ΔRa_3 [%]	G_0 [GU]	G_3 [GU]	t_0 [mm]	m_0 [g]	m_3 [g]	Δh_3 [μm]	$\Delta \dot{h}_T$ [μm/min]
2	1.67	1.46	-12.6	8.8	116.0	2.8638	55.672	55.202	10.9	3.62
3	1.87	1.50	-19.8	8.8	141.6	2.8202	54.967	55.202	12.9	4.30
4	1.86	1.45	-22.0	8.8	148.5	2.8488	55.609	54.408	14.9	4.98
5	1.75	1.28	-26.9	8.8	184.4	2.8132	54.792	54.056	17.0	5.67

The measurement procedure of the specimens' parameters and the data processing was the same as it was described for the case of plasma-polishing. The measured data can be found in the *TABLE 2*. Subscript 0 is used for values measured before polishing (processing time T = 0 min), and subscript 3 is used for values measured after 3 minute of polishing (T = 3 min). The values of the layer thickness removal Δh for each specimen, calculated from the specimens' weight difference are also in in *TABLE 2*, as well as the relative values of the surface roughness reduction *ΔRa*. The results obtained for the specimen #1, which have been treated 3 minutes by plasma-polishing process, are graphically compared to the results obtained for the next four specimens (#2 to #5), which have been treated electrochemically also 3 minutes. *Fig. 6* shows the relative surface roughness reduction *ΔRa* of the treated specimens. It is obvious, that the plasma-polishing process is much more efficient in surface flattening than the traditional electrochemical polishing process, regardless the used anodic current density. The value of *Ra* decreases by 42 % when plasma-polishing has been used, the highest decrement of *Ra* in the case of electrochemical polishing is for the highest used value of anodic current density and its value is 27 % only.

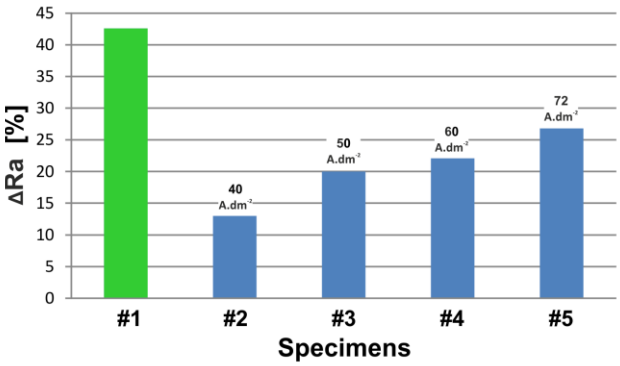

Fig. 6 Surface roughness reduction of the specimens after 3 minutes of treatment

The surface gloss levels of the specimens are compared in *Fig. 7*. As it can be seen on the figure, the reached gloss level of the polished surface is proportional to the electric current density used during electrochemical process. At its highest value (72 A.dm^{-2}) the gloss level is little higher than the gloss level of the plasma-polished specimen. The values of layer thickness removal from the specimens' surface after 3 minutes of treatment are compared at *Fig. 8*. This value is also proportional to the anodic current density in the case of electrochemical polishing as it was for the gloss level or for the surface roughness declension. As it is evident in the picture, all these values are much higher than as the value of layer thickness removal of plasma polished specimen. After 3 minutes of treatment, the plasma-polishing process removes 6.76 μm thick layer of the metal from the treated surface only.

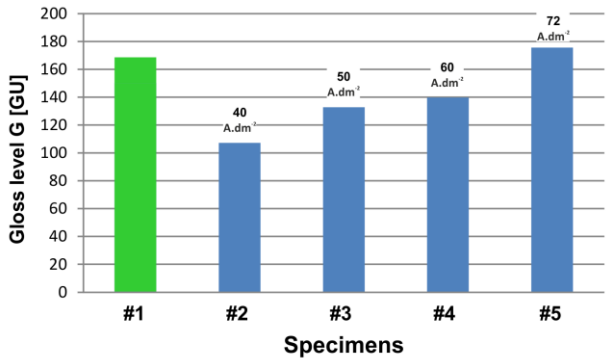

Fig. 7 Surface gloss level of the specimens reached after3 minutes of treatment

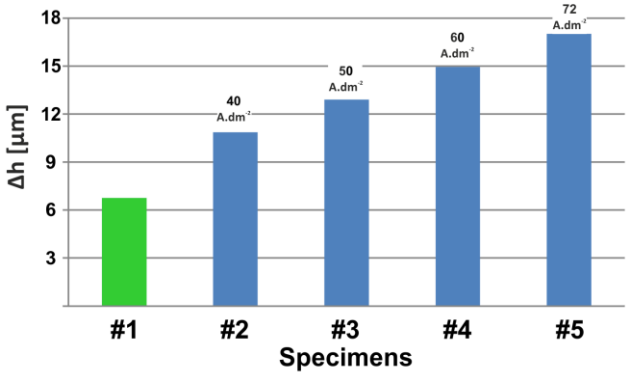

Fig. 8 The values of the layer thickness removal from the specimens' surface after 3 minutes of treatment

VII. DISCUSSION

Analysing the above results of the accomplished experiments a few conclusions can be drawn. The plasma-polishing process removes the material from the treated surface starting to remove the top of the surface profile's peaks. Even a little amount of the material has been removed when the process starts, it corresponds to a relatively high value of layer thickness removal – marked as *h1* shown in *Fig. 8*. After the tops of the surface profile peaks are disappeared and the process removes the next same amount of the material as in the previous case, e.g. *S2 = S1* on the *Fig. 8*, the thickness of this removed layer *h2* is much less as the thickness of the prior layer *h1*. Therefore the value of the layer thickness removal falls down quickly at the

beginning of the treatment and then it continually slows down probably to a constant value. The material removing progress is more complex if the treated surface is covered by a layer of oxides or any other dirt. Since this topmost layer of metal-oxides is electrically nonconductive it takes longer for plasma-polishing process to remove them. It explains the low material removal speed at the beginning of the treatment on the *Fig. 5*. As soon as the topmost layer is removed the surface roughness decreases according to above described theory.

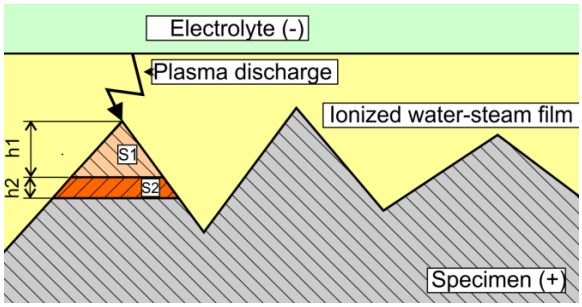

Fig. 9 Surface profile of the treated metal during plasma polishing

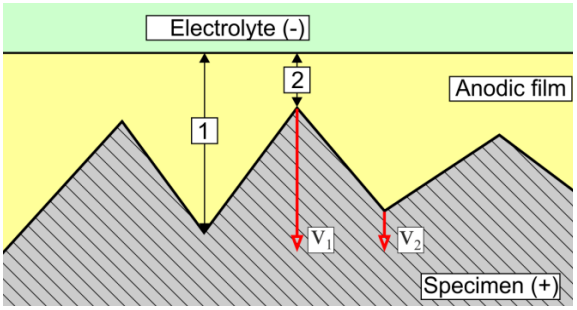

Fig. 10 Surface profile of the treated metal during electrochemical polishing

The material removal process during plasma polishing is different as it is in the case of standard electrolytic polishing, when the material from the surface is removed by anodic dissolution – *Fig. 10*. An anodic film forms on the treated surface during electrochemical polishing. The anodic film has lower electric conductivity then the surrounding electrolytic solution and the process of surface flattering is based on different velocity of anodic dissolving through this layer. Anodic dissolving is more intensive on the peaks of surface profile, where the anodic film is thinner so the electrical resistance is lower. Therefore the velocity of anodic dissolving v_1 is faster here than on the "valleys" of the surface profile – v_2. In this way, the metal is being removed not only on the peaks of the surface profile, but from whole surface although with different speed. This is the reason why it takes longer to reduce the surface roughness (*Fig. 6*) and why the thickness of layer removed from the surface is much higher (*Fig. 8*) then as it in the case of plasma-polishing, where the metal is removed mainly from the surface profile's peaks.

VIII. CONCLUSION

Surface properties of the specimens made from stainless steel X10 CrNi 18/10 have been plasma polished in electrolyte. The resulting properties of the polished surface depend on the treatment time. The gloss level rapidly increases during the first four minutes as it is described by the equation (2). The surface roughness reduction is most significant during the first four minutes, as well. The equation (1) will be useful to calculate the needful processing time when the desired value of the surface roughness is in focus. To calculate the dimension changes, for example when the precision machine parts are plasma-polished, the equation (3) can be used. All above equations can be also used for other stainless steels, although the resulting values may slightly differ.

The plasma polishing process is more efficient at surface roughness reduction than the common electrochemical polishing process. Furthermore, the value of the layer thickness removal is much less in the case of plasma polishing process. It can be supposed that this value will not depends on the spent state of the electrolytic solution such as it is in the state of electrochemical process. But this expectation must be confirmed experimentally in the next.

REFERENCES

[1] M. Murgaš, J. Solár, Š. Podhorský, I. Novotný: Boundary of possibilities of plasma-electrolytic technology at reducing of a metal surface roughness, Proc. International conference CO-MAT-TECH 2000, Bratislava, SK, 2000, 183-188.
[2] D. Vaňa, Š. Podhorský: Electrolytic-plasma polishing of stainless steel in electrolyte, IN: TEAM, Trnava, 2011, 243-246.
[3] R. Tóth, Š. Podhorský: Electrolytic-plasma cleaning and surface conditioning of casting, IN: ActaMetallurgica, 5, 1999, 192-196.
[4] Š. Podhorský, R. Šuba, R. Tóth: Metalic surfaces treated by plasma discharge in electrolyte. In: Funkčné povrchy v strojárstve 2007 v krajinách V4: Trenčín, Alexander Dubček University of Trenčín, 2007, 138-143.
[5] E. S. Lee: Machining Characteristics of the Electro polishing of Stainless Steel (STS316L). IN: Int J Adv Manuf Technol, Springer-Verlag London Limited (2000) 16, 591–599.
[6] V. Číhal, Korozivzdorné oceli a slitiny (Prague, Academia, 1999).

International Journal of Modern Engineering Research (IJMER)
www.ijmer.com Vol.3, Issue.2, March-April. 2013 pp-793-797 ISSN: 2249-6645

Spray characterization of nozzle for fire extinguisher

Varun. K. R, [1] Rajashekhar. C. R, [2] Bhaskar Dixit[3]
[12]*Student, Department of Mechanical Engineering, Sri Siddhartha University, India*
[3]*Professor, Department of Centre for Disaster Mitigation, Jain University, India*

Abstract: The development of water mist fire suppression technology has made substantial progress over the last decade. Water mist based techniques are becoming popular but the fire extinguishment products call for high initial investment. There exists a need to develop cost effective water mist generation techniques appropriate for fire suppression.

A standard portable water-CO_2 fire extinguisher nozzle is selected for study with an application density of 1.0 *l*/min/m^2.A multi-jet nozzle with opposed jet configuration is developed to get improved spray characteristics. Droplet Sauter Mean Diameters (SMD) were empirically calculated using correlations available in the literature.

The spray developed has resulted in droplets with SMD in the range of 0.3 – 0.4 mm as calculated from correlations and confirmed using experimental measurements.

Keywords: atomization, fire suppression, portable water extinguishers, spray nozzles, water spray

I. Introduction

Water is the most cost effective reagent for fire extinguishment. Water in the form of jets/sprays is used for fire suppression. Water dispensation at an optimal rate is essential to improve effectiveness of utilization and also protect the fire affected regions from the ill effects of water inundation in the post fire scenario. Several studies exist in the literature aimed at improving the utilization efficiency of water during fire suppression [1, 5, 6]. Breaking up water jets into finer particles improves surface area available for heat absorption but smaller particle mass reduces penetration of water into fire. Mist based extinguishers are available in the market which claim lower water consumption but they are prohibitively expensive and therefore their availability for use is restricted. Even to this day, the flow rates employed in Class-A fire extinguishers available in the market utilize large application densities (>1 l/min/m^2) to ensure effectiveness in extinguishment.
Therefore, there exists a scope for improvement in water utilization effectiveness of fire extinguishers.

Standard issue portable water CO_2 fire extinguisher of 9 *l* volume is selected for the present study. Water jet nozzle is replaced with a multi-jet opposed configuration.

II. Literature survey

Grant et al [1] have reviewed class a fire suppression using water sprays. State-of-the-art on quantitative characterization of water sprays, spray patterns and practical methods for measuring drop size distribution with equations and correlations are discussed. Several nozzle configurations appropriate for fire extinguishment are described. Issues associated with quenching crib fires are also discussed.

Liu and Kim [2] have discussed extinguishing mechanisms involved in the water mist systems. Factors which affect the water mist performance are highlighted.

Meenakshi and Rajora [4] have tested performance of water mist generated with a mist nozzle of diameter 0.5 mm. Ultra fine mist of size 17 microns is generated and tested on an enclosed fire.

Adiga, et al. [3] have discussed suppression effectiveness of ultra fine mist, less than 10 microns in size by simulating the fire using fluent, Computational Fluid Dynamics (CFD) software.

Sridhara and Raghunandan [6] have discussed flow visualization techniques for evaluating the spray characteristics using different lighting techniques.

Roberts [7] has discussed the measurement of droplet characteristics. This paper discusses the three stages to obtain data on droplet sizes. This paper employs still photography and also high speed video image capturing techniques for measurement.

Estes and Mudawar [8] have worked on empirical correlations for water sprays. 3W argon ion laser based Phase Doppler Particle Analyzer (PDPA) is used for spray characterization. The mean diameter used to describe a spray depends on its intended use: 'Sauter Mean Diameter' (SMD) of the droplets is normally employed. It defines a droplet which has the mean surface area and mean volume for the whole spray. It is equally relevant to the behavior of fuel in combustion problems and water sprays used in fire fighting.

$$D_{ab} = \left(\frac{\sum N_i D_i^a}{\sum N_i D_i^b} \right)^{1/(a-b)} \quad (1)$$

Sauter Mean Diameter, d_{32}, uses a=3 and b=2 in equation 1 to calculate mean diameter. The paper recommends correlation given in equation 2.

$$\frac{d_{32}}{d_0} = \left[We_{d_0}^{0.5}\, Re_{d_0}\right]^{-0.259} \quad (2)$$

Viriato Semibo, Pedro Andrade and Maria da Gra Ca Carvalho [9], have worked on numerical prediction of SMD for sprays. The paper has discussed several correlations used in atomizers. Correlation given in equation 3 is recommended for water sprays of the type used in the current work.

$$SMD = A\left[\frac{\sigma^{0.5}\mu_L}{\rho_A^{0.5}\Delta P_L}\right]^{0.5}(t\cos\theta)^{0.25} + B\left[\frac{\sigma\rho_L}{\rho_A\Delta P_L}\right]^{0.25}(t\cos\theta)^{0.75} \quad (3)$$

III. Studies on spray

1.1. Nozzle design

The nozzle is being fabricated as shown in figure. The concept of the design of the nozzle is to pass the water from one end and while the water coming from the other face is to be get atomized. In this point of view the design is made in such a way that the water is atomized in the out section of nozzle. At the out section of the nozzle which is on the closed side, six holes are drilled at some particular angle.

The nozzle used in the current work is shown in fig1. The nozzle is based on opposed jet configuration where several jets converge to a point and disperse resulting in a spray of water with finer particle size. Six angular holes of 0.7 mm diameter are drilled on a PCD of 7 mm. Hole axis inclination is such that the jets oppose each other at a distance of 15 mm resulting in an effective jet break up. Total orifice area is comparable to standard jet nozzle area of the extinguisher.

Flow rates from the nozzle is evaluated at several pressures and compared with standard nozzle. Figure 2 gives the comparison. The setup used to generate the spray is described in Figure 6.

The various tests are being conducted from the nozzle. The mass flow rate at various pressures is studied and tabulated and a graph is also plotted between pressure verses mass flow rate and compares with the theoretical calculation and at the 6bar pressure and spray characterization is studied.

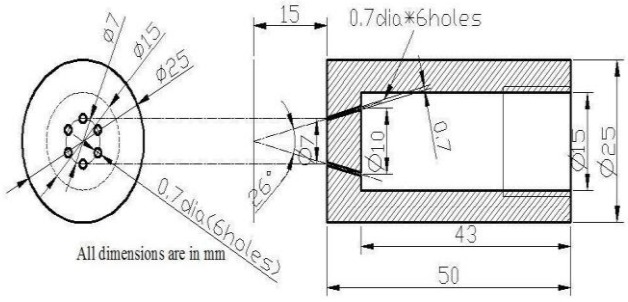

Fig. 1: Engineering drawing of opposed jet nozzle

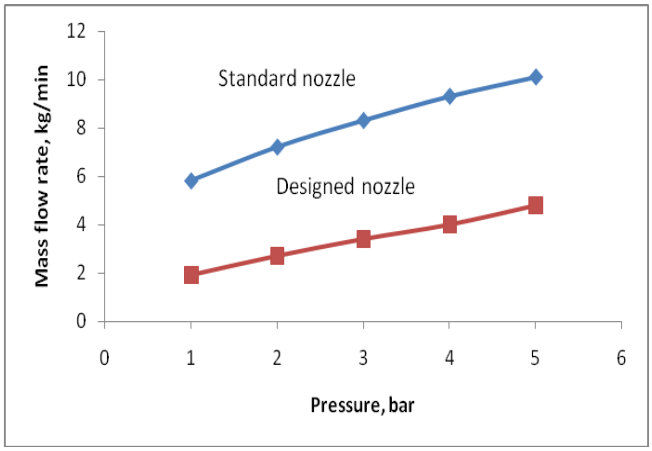

Fig. 2: Effect of pressure on mass flow rates

1.2. Effect of mass flow rate

Fig 3 gives the comparison between the theoretical and experimental mass flow rates for the opposed jet configuration nozzle.

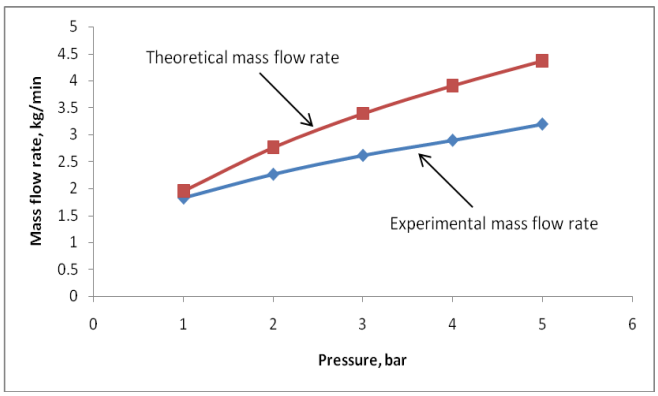

Fig 3: Effect of theoretical and experimental mass flow rate with pressure

Fig 4 shows the schematic representation of the spray, in which the cone angle, jet break up length, throw of the spray and width of the spray is measured at 6 bar pressure from the opposed jet nozzle configuration.

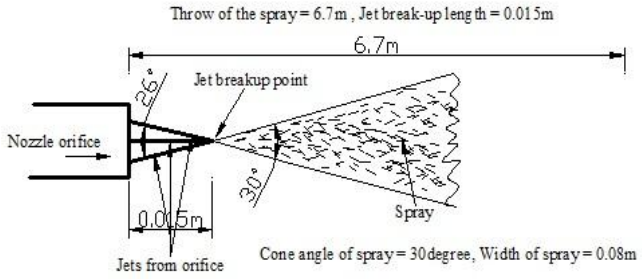

Fig 4: Spray characterization

1.3. Sauter Mean Diameter

Sauter mean diameter (SMD, d_{32} or $D[3, 2]$) is an average of particle size. It was originally developed by German scientist J. Sauter in the late 1920s. It is defined as the diameter of a sphere that has the same volume/surface area ratio as a particle of interest.

The value of d_{32} using the correlation from the equation (2), at 6bar gauge pressure, was found to be,

$$\frac{d_{32}}{d_0} = \left[We_{d_0}^{0.5}\, Re_{d_0}\right]^{-0.259}$$

$$d_{32} = 0.293\text{mm}$$

The value of the SMD calculated using the correlation from the equation 93), at 6bar gauge pressure was found to be,

$$SMD = A\left[\frac{\sigma^{0.5}\mu_L}{\rho_A^{0.5}\Delta P_L}\right]^{0.5}(t\cos\theta)^{0.25} + B\left[\frac{\sigma\rho_L}{\rho_A\Delta P_L}\right]^{0.25}(t\cos\theta)^{0.75}$$

$$SMD = 0.317\text{mm}$$

The result of the calculated SMD obtained from the equation (2) and equation (3) are almost similar.

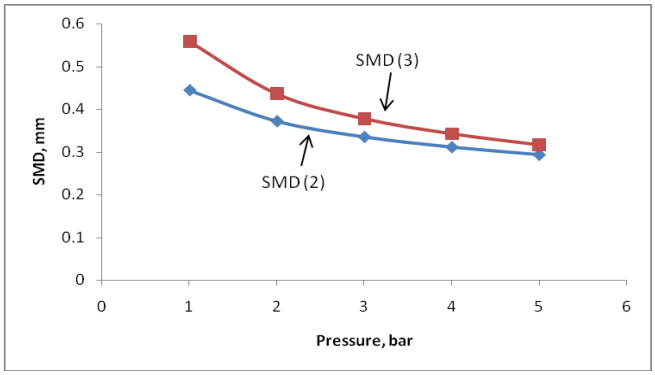

Fig. 5: Effect of Pressure on SMD

Figure 5 shows effect of pressure on predicted SMD from two different correlations. The predicted values from both correlations quantitatively agree with each other. The rate of decrease of SMD is demonstrated to be large at pressures below 3 bar and beyond 3 bar; the decrease in SMD with increase in pressure is small.

IV. Experimental set up

The Figure 6 give a schematic description of experimental set up used for testing the sprays. Regulated air supply from a two stage air compressor (300 *l*/min Free Air Delivered, 200 *l* reservoir and 12 bar pressure) is employed. Additional reservoir of 150 *l* capacity is used as buffer. Air from the reservoir is used to pressurize the 9 *l* capacity portable extinguisher chamber. Water is drawn from the bottom of cylinder and forced through the nozzle due to the pressure above water surface as indicated in Figure 6. The mass flow rate is checked for different pressures in the set up shown in fig 6.

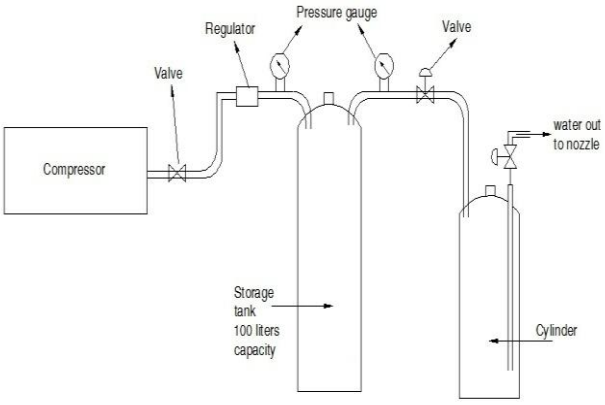

Fig. 6: Opposed jet spray generation system

V. Experimentation

The empty cylinder weight is noted before filling the water. The water is filled into the cylinder and closed tightly ensuring no leakage and weight of the cylinder is noted and tabulated. All the connections are made sequentially and ensure no leakage in any point. The compressor is connected to the air tank through the pressure gauge and pressure valve. The air tank is connected to the cylinder to pressurize the water in the cylinder through pressure gauge. The compressor is made to run till it reaches its maximum pressure and automatically stops. The pressure is released and check for any leakage in connecting points. The pressure is released and adjusted to the required pressure using the pressure valve.

Once the pressure is set in the pressure valve then the pressure is released to the cylinder. The empty bucket weight is noted. Initially the pressure is set to 2bar and amount of water collected is noted. The readings are taken for different pressures 2bar to 6bar. There are nearly five to six trials are taken at each pressure. The readings are noted and tabulated for different pressures. The graph is plotted between pressure and mass flow rate.

VI. Result and discussion

Experiments were carried out with the opposed jet nozzle. The mass flow rate were checked at different pressures from 1 bar to 6 bar and compared the performance of the opposed jet configuration nozzle with the standard nozzle used in standard water-Co_2 fire extinguisher as shown in fig 2. This shows the utilization of water in opposed jet nozzle is less compared to standard.

Fig 3 shows the comparison of the theoretical and experimental mass flow rate from nozzle. The experimental readings appears to be less compared to the theoretical, this is may be due to the losses while conducting the experiments.

The value of d_{32}, using the correlation from the equation 2, at 6 bar gauge pressure, is 0.293 mm. The value of the SMD calculated using the correlation from the equation 3, at 6 bar gauge pressure was found to be 0.317 mm.

Data from water mist systems available in the market also employ similar droplet sizes as obtained from current opposed jet nozzle.

VII. Conclusion

A spray nozzle based on opposed jet configuration has been developed suitable for use in portable water based fire extinguishers.

The spray nozzle is studied for droplet size and distribution photographically. The spray is found have an SMD in the range of 0.3 mm to 0.4 mm which is considered appropriate for use in water extinguishment of Class A fires in literature. Spray SMD is also calculated from empirical correlations. Calculated values of SMD for the spray geometry also lie in the range of 0.3 to 0.4 mm. Study of expensive 'water mist' fire extinguishers commercially available indicates use of similar water particle sizes. Studies are being carried out to examine the effect of spray penetration to ensure the effectiveness of employed application density.

References

[1] G. Grant, J. Brenton, D. Drysdale' "Fire Supression by Water Sprays", progress in energy and combustion science 26 (2000) 79-130
[2] Zhigang Liu and Andrew K. Kim "A Review of water mist fire suppression systems –fundamental studies", Journal of fire protection engineering, Vol. 10, No. 3, 2000, pp. 32-50.
[3] KC Adiga and Heather D. Willauer, Ramagopal Ananth, and Frederick W. Williams "Droplet Breakup Energies and Formation of Ultra-Fine Mist", Journal of fire protection engineering,
[4] Meenakshi Gupta, R. Rajora, "Effect of Air or Nitrogen on Fire Suppression Performance of Twin Fluid Water Mist System in an Enclosed Chamber", Proceedings of fire science and technology, FIRST Nov 3-4, 2011
[5] KC Adiga, Robert F. Hatcher Jr, Ronald S. Sheinson, Frederick W. Williams, Scott ayers, "A Computational and Experimental Study of Ultra Fine Water Mist as a Total Flooding Agent", fire safety journal 42 (2007) 150-160.
[6] SN Sridhara and BN Raghunandan, "Photographic Investigations of Jet Disintegration in Air-blast Sprays", Journal of applied fluid mechanics, vol 3, no. 2, pp 111-123, 2010
[7] GV Roberts, "An Experimental Investigation of Thermal Absorption by Water Spray", Fire and emergency planning directorate fire research and development group.
[8] Kurt a. Estes and Issam Mudawar "Correlation of Sauter Mean Diameter and Critical Heat Flux for Spray Cooling of Small Surfaces" vol,38, 16,pp. 2985-2996, 1995.
[9] Viriato Semibo, Pedro Andrade and Maria da GraCa Carvalho, "Spray Characterization: Numerical Prediction of Sauter Mean Diameter and Droplet Size Distribution" fuel vol. 75, no. 15, pp, 1707-1714, 1996.

International Journal of Modern Engineering Research (IJMER)
www.ijmer.com Vol.3, Issue.2, March-April. 2013 pp-798-808 ISSN: 2249-6645

The Mechanical Behaviour of Recycled High Density Polvethvlene

Abo El-Khair M.S, [1] Ali, A.A, [2]
[1]Assoc. Prof, MTC, Egypt
[2]Egyptian armed forces,

Abstract: *In last few years with the increasing use of polymeric materials the disposal of the used material became a serious problem. As polyethylene is one of the common used polymers in many applications it represents a significant amount of the total municipal waste of thermoplastic materials. Thus recycling process of polyethylene is a subject which needs more investigation. Hence in the present work an experimental investigation of the mechanical properties was carried out on virgin and recycled/virgin high density polyethylene (HDPE) to study the effect of three successive generations of HDPE as well as of the amount of recycled material added to the virgin one on the density, tensile, impact, and creep properties.*

The results showed that with recycling the HDPE three times, the density as well as the modulus of elasticity, the percentage elongation, the impact strength, and the recovery percentage of the HDPE decrease while the tensile strength increases. With increasing the recycled to virgin ratio of HDPE the density, the impact strength, and the recovery percentage increase while the modulus of elasticity, the percentage elongation, and the tensile strength remain almost constant.

Key Words: *Polyethylene, recycling, recovery, mechanical properties, and moulding.*

I. Introduction

Rare materials, such as gold and silver, are recycled because acquiring new supplies is expensive. Other materials may not be as expensive to replace, but they are recycled for another reasons. Recycling helps in land conservation; landfills fill up quickly and acceptable sites for new ones are difficult to find because of objections by neighbors to noise and smell. The major way to reduce the need for new sites is to recycle wastes. Also recycling a product creates less pollution than producing a new one, which reduces the number of pollution-related illnesses. From the economic point of view, recycling reduces the need for raw materials and conserves energy by reducing the need to process new material, which usually requires more energy than recycling [1]. The increased interest in plastics recycling has resulted from three important trends. First the increase of the production and use of plastics, as shown in Table 1 Second, the resin prices have increased dramatically. Third, growing concern about the quality of the environment has led to more restrictive disposal regulations. Some factors can adversely affect the quality of recycled plastics. These factors include the possible degradation of the plastic during its original life cycle and the possible addition of foreign materials to the recycled plastic during the recycling process. But the main problem remains how to sort the different types of plastics.

Table 1. Projections of materials generated in MSW stream, 1995:2010 [2]

Materials	% of total generation		
	1995	2000	2010
Paper and paper board	42.8	44.5	48.4
Food and yard wastes	23.1	22.1	19.9
Plastics	9.3	9.8	10.3
Total metals	8.1	7.8	7
Glass	5.6	4.8	3.8
Wood	3.7	3.9	4.1
Others	7.3	7.2	6.6

There are well-established processes for recycling metals and ceramics, but the recycling of plastics scrap has not developed to a comparable extent. The higher densities of metals and ceramics make it easier to separate these materials from other components of an industrial or municipals waste stream. Polymer scrap, on the other hand, is difficult to recover once it has been mixed into a waste stream [3]. So, plastics are more difficult to recycle than metal, paper, or glass. While about 35%, 40%, and 25% of Aluminum, paper, and glass products, respectively, were recycled in United States, only about 5% of plastics were recycled in 1994. Most modern automated plastic sorting systems are not capable of differentiating between many types of plastics. However, some progression is being made in these systems to separate plastics by color, density, and chemical composition. For example, X-ray sensors can distinguish PET from PVC by sensing the presence of chlorine atoms in PVC material [1].

One of the successful systems for identifying plastic containers by plastic type is "chasing arrows". It appears on the bottom of many plastic containers to promote plastic recycling. The chasing arrows enclose a number (such as 1 indicating PET, 2 indicating HDPE, 3 indicating PVC) which aids plastic sorting process, Fig. 1 [2].

Fig.1. SPI code system: Voluntary guidelines for plastic bottle and container material code system [2]

Another problem facing the process of plastics recycling is following rules of thumb which recommend recycled plastic usage, usually 25% or less by weight. These rules are very conservative, and are not based on sound experimentation [4]. It was shown in a previous study on LDPE [5], that despite the loss of the mechanical properties in the recycling process, the properties found were still greater than many other virgin thermoplastics.

Polyethylene is by far the most extensively used plastic material and accounted for 35% of the total sales in the United States in 1993. The main reason for its prime position is that, it is low in cost and has many industrial important properties: high toughness at room temperature and also at lower temperatures with sufficient strength, good flexibility over a wide range of temperatures even down to -73°C, excellent corrosion resistance, excellent insulating properties, odorless and tasteless [6]. So, HDPE is a commonly used material for containers, pipes, electrical insulation, chemical tubing, house wears, and blow-moulded bottles. More recently some other applications were introduced like cement powder plants, drainage, petrochemical plants, utility conduits and swimming pools.

The recycled HDPE can be applied in several products, such as: soft-drink bottle base caps, flowerpots, drainpipes, stadium seats, traffic barrier cones, golf bag liners, detergent bottles, and toys. The aim of the present experimental work is to study the mechanical properties namely, elasticity modulus, yield strength, percentage elongation, Charpy impact strength, creep and recovery behaviour, and density of virgin HDPE under normal conditions and to study the effect of recycled material percentage and recycling generations.

II. Experimental Work

I.1-Material and Processing:

The tested material is high density polyethylene in granulated form made in Egypt (under license of BP Chemicals). It was produced in August 2002 by SIDPEC Company for Petrochemicals and commercially named "Egyptene" with degree HD6070UA 219. First of all, a steel die, Fig. 2, was designed and manufactured to produce HDPE standard specimens in dimensions according to ASTM D638M–93 [7], for tensile specimens and ES 895-1967 [8] for impact specimens. All the specimens was injected in the " Factory of Plastic Packages for Armed Forces".

Fig.2.-The manufactured steel die

A Pattern field injection moulding machine model BSKM 45/23 shown in Fig.3 is used. The recycling processes were carried out in the same place by using a Chinese crusher model SCP-640 and a spring recycling & blending M/C model SEVB-85 as shown in Figs. 4 and 5 respectively.

Fig. 3. The injection machine

Fig. 4. The plastics crusher

Fig. 5. The recycling line machine

The following chart represents a summary of the experimental tests carried out on HDPE specimens.

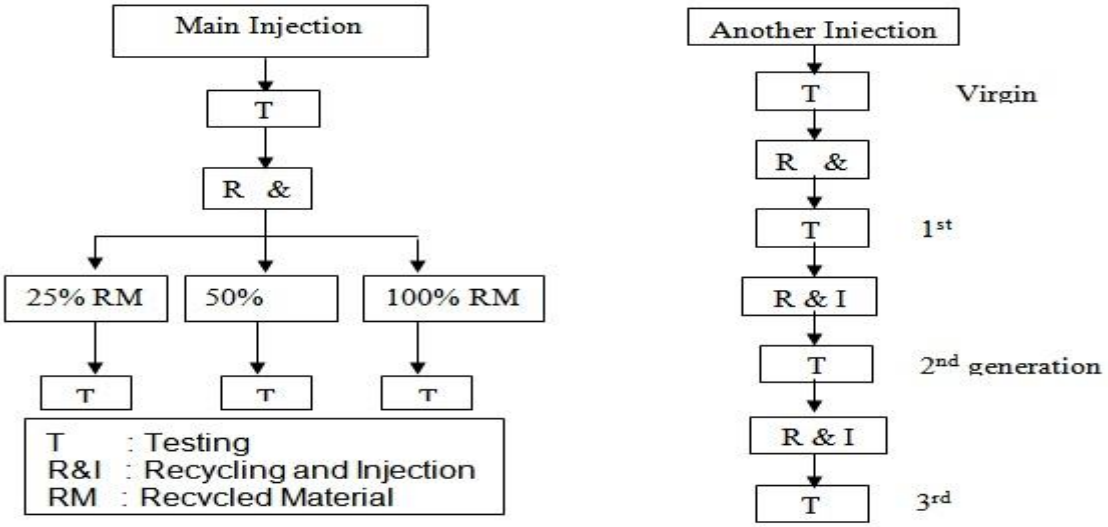

I.2-Tests Procedure

Set of mechanical tests have been performed in order to measure the change in mechanical properties of the recycled polyethylene samples taken after each recycling step, results of tests have been recorded for each sample corresponding to the number of recycling processes as presented hereinafter.

I.2.1-Tensile test

Tensile tests were carried out on universal Testing Machine Zwick Tensometer, 10 KN load cell. The cross–head speed was fixed at 50 mm/min all over the experiments. Young's modulus (MPa), yield stress (MPa), break stress (MPa), elongation at yield (%), and elongation at break (%) were recorded. Five specimens were tested in each step and the average values were considered. Tests were carried out according to ASTM standards D638M–93 [7]. All the specimens were preconditioned for 48 hours and tested in an air-conditioned atmosphere at 23 $\pm$ 2 °C and 50 $\pm$ 6 % relative humidity. The specimens' dimensions are shown in Fig. 6.

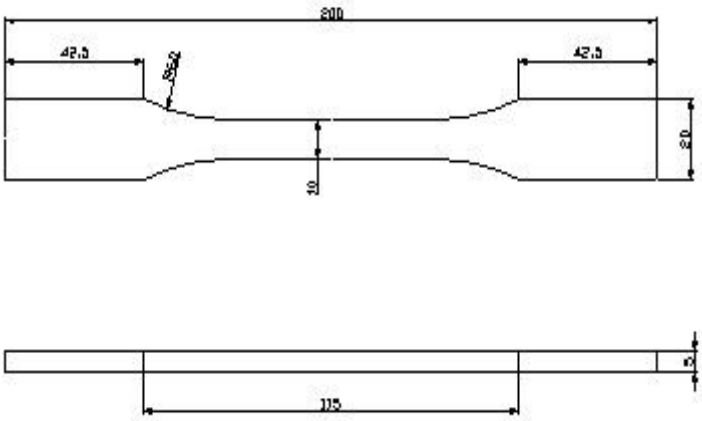

Fig. 6. Tensile test specimen

I.2.2-Impact test:

To determine the impact strength of HDPE, a Charpy pendulum impact testing machine for polymers (RKP50), was employed. The pendulum mass was 2.95 Kg and the impact velocity was 3.834 m/s with supporting span of 70 mm. The machine is computerized, so the output time–energy curve can be printed out for each specimen. Tests were carried out according to ES 895-1967 [8]. All the specimens were tested in an air-conditioned atmosphere at 23 + 2 °C and 50 + 6 % relative humidity. The impact strength was obtained in kJ/m2 by dividing the energy used in breaking the specimen by its affected area. The specimens' dimensions are shown in Fig. 7.

I.2.3-Creep test:

Plastics exhibit a similar shape of creep strain against time for constant stress and temperature as for metals. However, one distinct difference is the ability of plastics, being viscoelastic materials, to recover slowly over a

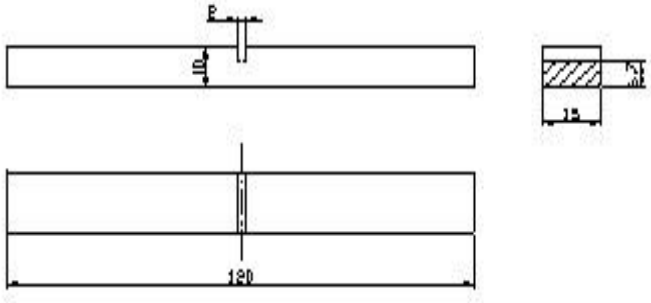

Fig.7- Impact test specimen

Period of time after the removal of the applied load. Thus the creep test was carried out to study the recovery due to the viscoelastic behaviour of HDPE by loading the specimens with constant stress of 7 MPa for 10 hours and then removing the load suddenly. The strain–time curves were plotted showing an elastic strain recovery region followed by a time dependent recovery region and a plastic permanent deformation region, as shown in Fig. 8.

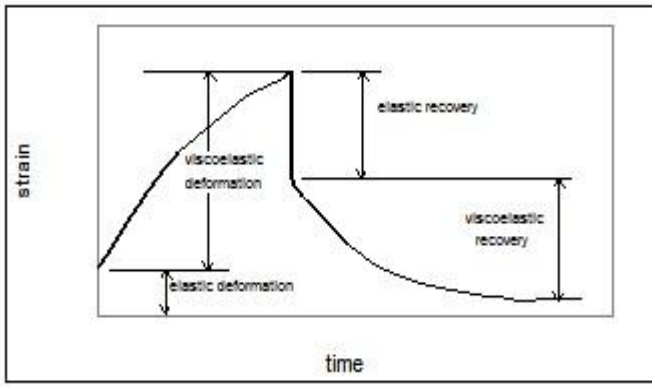

Fig. 8. Typical creep and recovery behaviour of a plastic [9]

The creep test rig, Fig. 9, consists of frame, specimen clamps, loading levers, elongation scale, and loading weights. This device can carry three specimens with different loads at the same time. The applied load at the lever end is magnified to the ratio of 10 at the specimen, Fig. 10. The same tensile test specimen configuration was used with a gauge length of 40 mm [10].

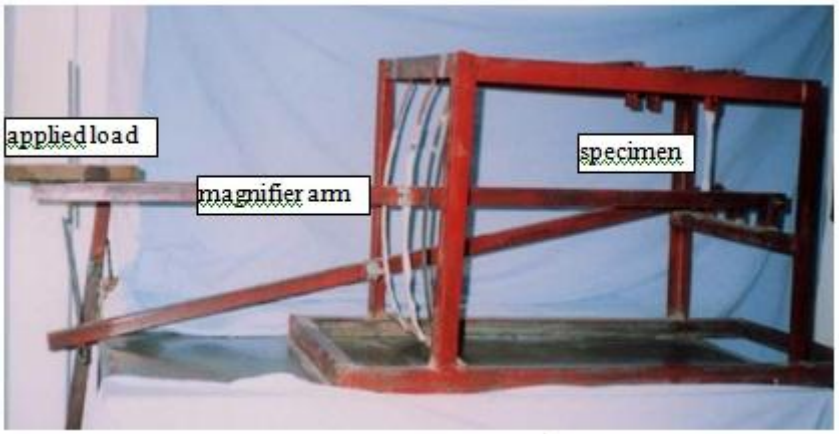

Fig. 9. The creep test rig

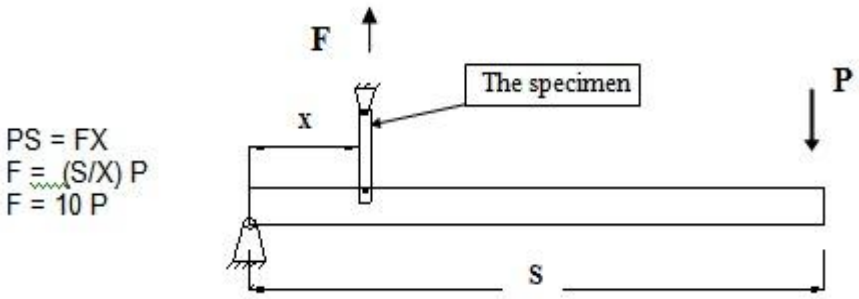

Fig. 10. Schematic drawing for loading the specimen on the creep test rig

I.2.4 Density test:

The specimen weight was recorded before each test by using an electronic balance of 1 mg sensitivity. The specimen then was submerged in oil which was poured out in a 100 cm^3 vessel graduated to 1 cm^3. The volume of the specimen was determined by subtracting the oil level record before and after submerging the specimen. The density was obtained in g/cm^3 by dividing the specimen weight by its volume. Five specimens were tested in each step and the average value was considered.

III. Results and Discussion

1.1 Effect of Recycled Material Percentage

To study the effect of the recycled material content, a main injection for virgin material was carried out and tested. The average values and conditions for this injection are tabulated in Table 2.

Table 2. Results of virgin specimens:

	Young's modulus, MPa	Yield strength, MPa	Elongation percentage, %	Impact strength, kJ/ m^2	Creep recovery behaviour,%	Density, g/cm^3
Average value	556	24.1	20	4	total 80.26 time depend- ent 62	0.945
No. of tested specimens	5			3	3	6
Test temperature, ^oC	23 ± 2				31	34
Relative humidity, %	44	48			48	48

It can be stated that the increase of recycled content increases the density of HDPE, Fig. 11. It means that the HDPE crystallinity could be raised by addition more recycled material to the virgin one. The variation of the Injection temperatures from 160 ^oC for virgin material to 180 ^oC for 100% recycled content may affect the crystallinity of HDPE and may be responsible of this behaviour.

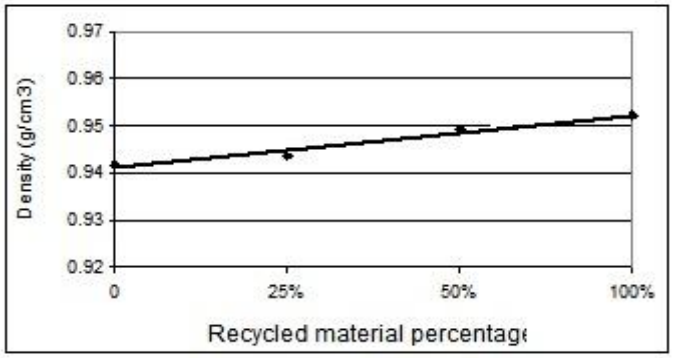

Fig. 11. Effect of recycled material percentage on the density

عدم التجانس

The variation of Young's modulus with the recycled content of HDPE is illustrated in Fig. 12. No significant effect for the recycled content on the elastic modulus. Its average value is 524 MPa. Figure 13 shows the yield strength stability with variation of recycled material content where its value is nearly 24 MPa for all ratios. The overall decrease at 100% recycled material content is about 2.5% from the virgin strength value. The resulting elongation percentage is nearly constant of about 20% with the various contents of recycled material, Fig. 14. Despite the heterogeneity between the granulates size of recycled and virgin materials due to the crushing process, no deterioration is observed in the tensile properties.

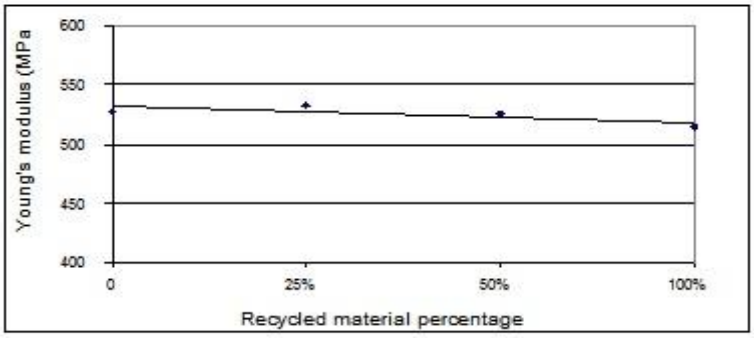

Fig. 12. Effect of recycled material percentage on the Young's modulus

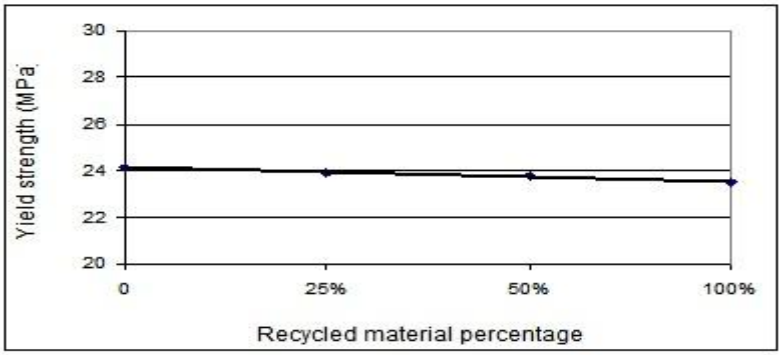

Fig. 13. Effect of recycled material percentage on the yield strength

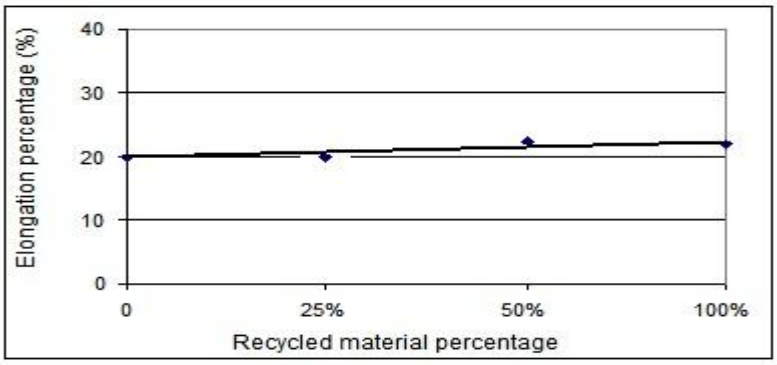

Fig. 14. Effect of recycled material percentage on the elongation percentage

The variation of the impact strength with the recycled material content is investigated and plotted in Fig. 15. The complete recycled material recorded impact strength of 3.37 times that of the virgin material. This improvement in impact performance conforms with previous study on polypropylene compounds which were carefully prepared to avoid the inclusions of impurities [11]. So, the HDPE toughness may be raised by blending with recycled material. It may be also noticed that increasing recycled material content from 25 to 50% has no significant effect on the impact strength.

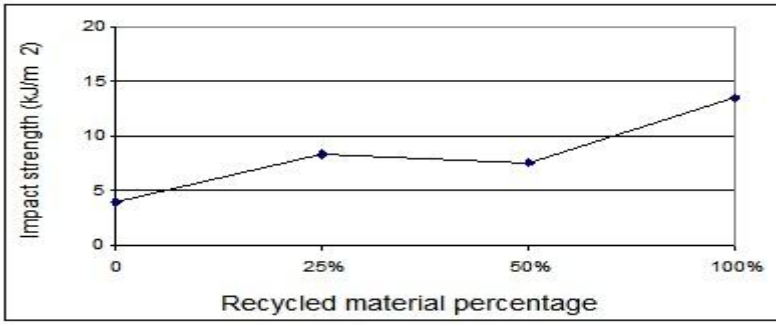

Fig. 15. Effect of recycled material percentage on the impact strength

The effect of increasing the content of the recycled material on creep properties is shown in Fig. 16. The addition of 25% recycled material decreases the maximum strain percentage by about 12% of the virgin material value. Further increase in the recycled material content results in an increase in the maximum strain percentage. This may be due to the heterogeneity between virgin and recycled HDPE granulates which may be responsible of inducing material with lower flow resistance; enhancing creep.

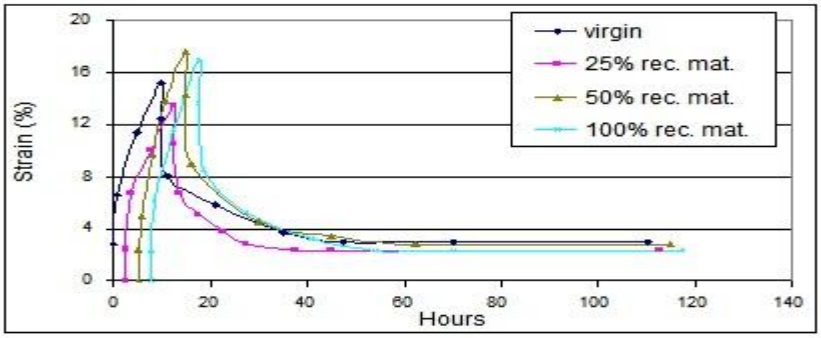

Fig. 16. Effect of recycled material percentage on the creep behaviour

The recovery behaviour means how much the loaded material returns to its original dimensions after removing the load of creep test. The recovery value of a material depends on its viscoelastic properties, the applied load, period of loading, and test conditions. As it was mentioned before, all of the tested specimens were exposed to a tensile stress of 7 MPa for 10 hours before removing the load suddenly to investigate the material behaviour according to its viscoelastic properties.

The total recovery percentage is calculated by dividing the difference between maximum and minimum strains by the maximum strain. The minimum strain is the constant strain for 60 hours; it indicates the plastic or permanent deformation. By studying Fig. 17, the percentage of total recovery increases nearly linearly with increasing the recycled material content. At 100% recycled materials the recovery percentage value exceeds that of virgin material by about 7.5%. The existence of recycled material content assists HDPE to return to its original shape.

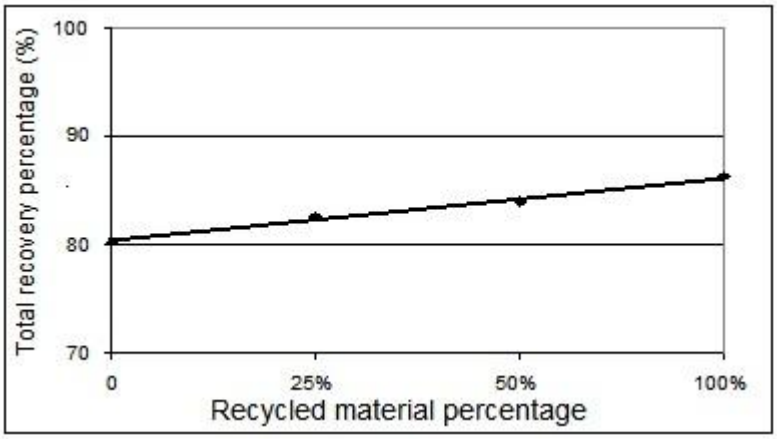

Fig. 17. Effect of recycled material percentage on the total recovery

Regards to Figs. 13 and 14, the decrease of yield strength and the increase of elongation percentage indicate improving the ductility of HDPE with increasing the recycled material content. This improving may be responsible of increasing the ability of HDPE to recover deformations.

IV. Effect Of Recycling Generations

To study the effect of the recycling generations, an independent main injection was carried out and tested before recycling. The average values and conditions for the virgin material of the second injection are tabulated in Table 3.

Table 3-Properties of virgin specimens

	Young's modulus, MPa	Yield strength, MPa	Elongation percentage, %	Impact strength, kJ/ m^2	Creep recovery behaviour,%	Density, g/cm^3
Average value	505	24.25	21.7	83	total 87.7 time depend- ent 55	0.944
No. of tested specimens	5	3	3	3	3	3
Test temp-erature, ^oC	23 ± 2				30	30
Relative humidity, %	46		48		56	52

As illustrated in Fig. 18, the higher reprocessing of HDPE the lower its density. It is expected that successive recycling operations cut the long polymer chains inducing more branched structure approaching that of low-density polyethylene [4].

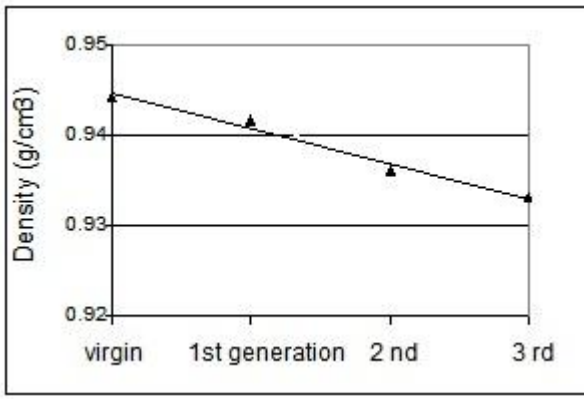

Fig. 18. Effect of recycling generations on the density

As shown in Fig. 19, the modulus of elasticity decreases during the first cycle by 10% from its virgin value and remains constant during 1^{st} to 3^{rd} generations. This effect may be explained by the decrease of the density which may cause a decrease in material crystallinity with repeating the recycling process. This trend is similar to the previous study on reinforced polyethylene [4].

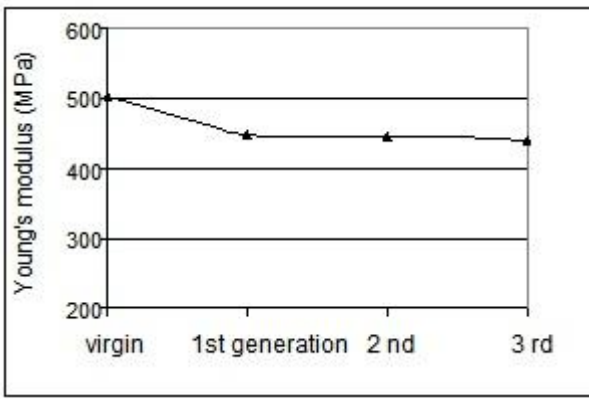

Fig. 19. Effect of recycling generations on the Young's modulus

In respect of the yield strength, Fig. 20, no significant changes were recorded and the highest recorded variation is 4% from the virgin material strength.

Figure 21 shows the elongation percentage as a function of number of generations. It remains about 21 % up to the 2nd generation. After 3rd generation a decrease to a value of 17.5% is recorded. This behaviour may be attributed to the possible degradation through the recycling process caused by main chain scissions accompanied by an increase in the molecular weight. As it is known, the chains of material with high molecular weight can be tangled easily, and therefore the flow resistance goes high producing brittle material [12].

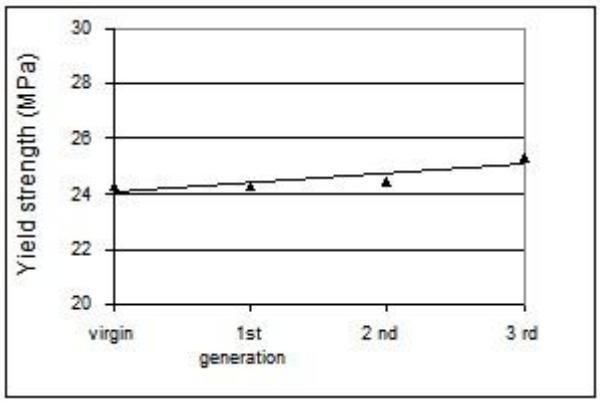

Fig. 20. Effect of recycling generations on the yield strength

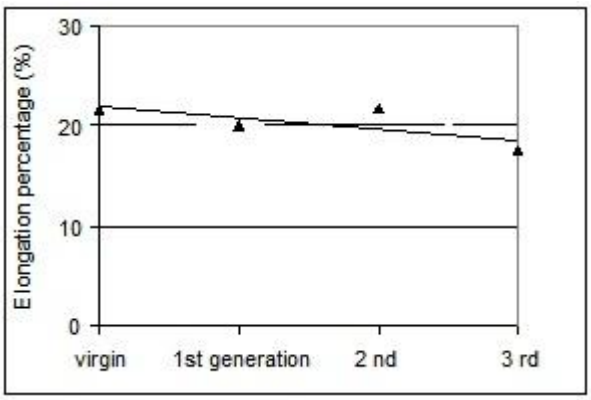

Fig. 21. Effect of recycling generations on the elongation percentage

By studying Fig. 22, the first cycle greatly affects the impact strength by reducing it to seventh part of its value before recycling. The expected change in molecular weight of the recycled HDPE together with the change in injection conditions combine to reduce the impact strength of the mouldings. As the mouldings become more brittle the effect of any impurities present will become increasingly more important and would contribute to the sharp fall-off in the impact properties [11]. This behaviour nearly approaches a previous study on LDPE [5].

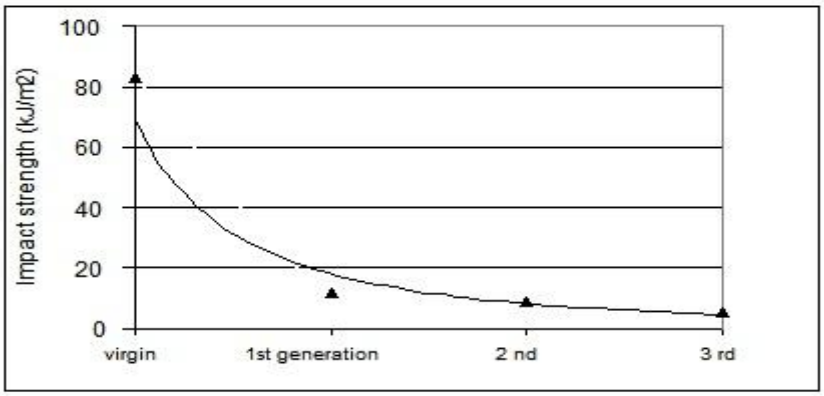

Fig. 22. Effect of recycling generations on the impact strength

The results of the recycling generations effect on the creep behaviour are obtained and plotted in Fig. 23. It can be noticed that the maximum strain percentage of the first generation was significantly affected by a drop of about 15% than that of the

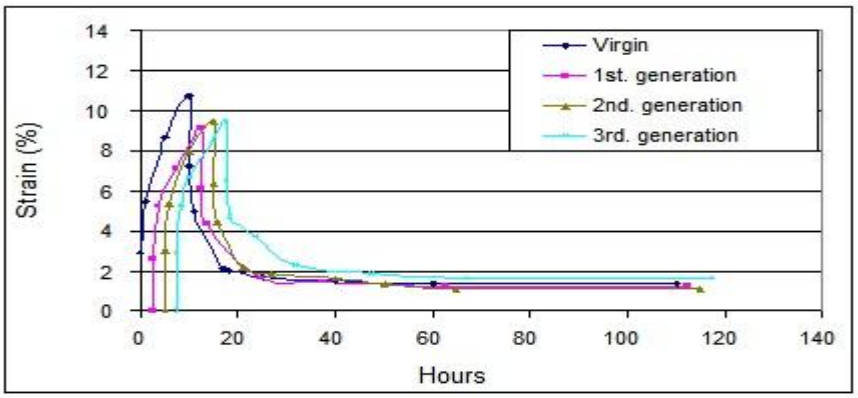

Fig. 23. Effect of recycling generations on the creep behavior

virgin material. It may be attributed to the possible degradation through the recycling process causing polymer main-chain scissions and showing restrictions to chains mobility. However, the maximum strain stabilizes from the first to the third recycling generations. Figure 24 shows that the total recovery does not show real variation with the successive generations except after the third one; a reduction of about 6% is recorded after the last cycle, which means that the material loses its ability to return to its original shape by recycling after the third time.

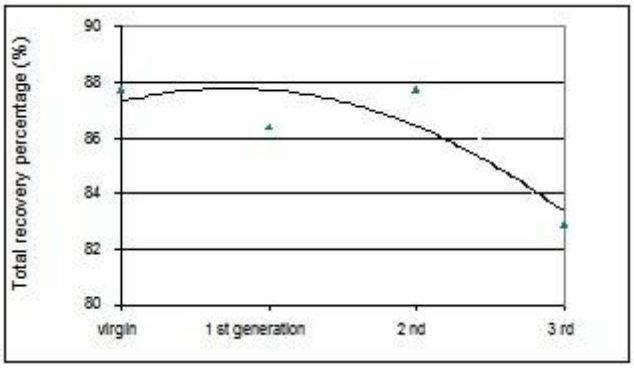

Fig. 24. Effect of recycling generations on the total recovery

V. Conclusions

From the obtained results of testing virgin, recycled, and recycled/virgin mixtures of HDPE specimens, the following conclusions can be drawn:

1- With increasing the recycling generations the density, the modulus of elasticity, the percentage elongation, the impact strength, and the recovery percentage of the HDPE decrease while the tensile strength slightly increases. This decrease in properties can be explained by cutting the long chains (during repeated recycling) inducing more branched structure with lower density and crystallinity. Also, a possible degradation through the recycling process (caused by main chain scissions) may be responsible of this behaviour.

2- HDPE tends to be more brittle at the third generation. This tendency can be attributed to the change of injection conditions together with the expected increase in the molecular weight which leads to high flow resistance.

3- The density, the impact strength, and the recovery percentage increase with increasing the recycled material content while the modulus of elasticity, the percentage elongation, and the tensile strength remain almost constant. These results can be due to the injection conditions variation, mainly the temperature, with increasing the recycled material content which may increase the crystallinity and the density. The heterogeneity between virgin and recycled HDPE granulates may be responsible of inducing material with lower flow resistance; enhancing creep properties.

The effects of recycling are summarized in the following table:

Properties vs Recycling processes	Density	Young's modulus	Yield strength	percentage elongation	Impact strength	Recovery percentage
Recycling generations	decrease	decrease	increase	decrease	decrease	Decrease
Recycled content	increase	constant	constant	constant	increase	Increase

4- HDPE properties slightly changed with recycling, in the scope of the present work, which shows that following traditional rules, which recommend a limited content of recycled material to be added to the virgin material, is not a good way in general and may be conservative and more recycled material can be added without having a significant effect on the mechanical properties of some polymers such as HDPE.
5- Any acceptable deterioration in the mechanical properties of HDPE due to recycling process may be covered by a design factor.
6- Recycled plastics as HDPE are not low performance materials. They may possess better properties than some other materials and better understanding of the recycled plastics behaviour will increase the demand for recycled materials which will help in protecting the environment and in saving the raw materials.

References

[1] Richardson, T.L., "Recycling", Microsoft, Encarta, Encyclopedia, (1999).
[2] Nabil, M., "Plastics Waste Management: Disposal, Recycling, and Reuse", Canadian Plastics Institute, Toronto, Canada, Marcel Dekker Incorporation, (1992).
[3] Corish, P.J., "Concise Encyclopedia of Polymer Processing and Applications", Pergamon Press, (1992).
[4] Harold, "Effect of Recycling on Material Properties of PET at Various Recycling Ratios and Recycling Generations", M. Sc. Thesis, University of Buertorico, (2003).
[5] Khattab, A.A. and ElZoghby, A.A., "Effect of Recycling on the Mechanical Properties of Low Density Polyethylene", Journal of Engineering and Applied Science, v 45 n4, (1998), pp. 533-547.
[6] Smith, W.F.,"Principles of Materials Science and Engineering", Second Edition, McGraw Hill, New York, (1990)
[7] ASTM Standards, "Standard Test Method for Tensile Properties of Plastics (Metric)", ASTM D638M–93, (1993).
[8] Egyptian Standards, "Determination of Impact Properties of Plastics", ES 895, (1967).
[9] Crawford, R.J., "Plastics Engineering", Third Edition, The Queen's University of Belfast, (1998).
[10] Naga, S.A.R., Raafat, M.G., Bekheet, N. and Afifi, A., "Effect of Temperature, Cross Head Speed, and Duration of Load on the Mechanical Properties of PVC Polymeric Material", Military Technical College, 8th International Conference on Eurospace Sciences and Aviation Technology, Cairo, Egypt, (1999).
[11] Derfel, W. and Michael, B., "The Effect of Recycled Plastic and Compound Additives on the Properties of an Injection–Moulded Polypropylene Co-polymer", Journal of Materials Science, v15, (1980), pp. 2843-2860.
[12] Lozano, M.J., Rodriguez, M.T., Gonzalez, E.A., and Villalpando, J., "Physical – Mechanical Properties and Morphological Study on Nylon-6 Recycling by Injection Molding", Journal of Applied Polymer Science, v 76, (2000), pp. 851-858.

International Journal of Modern Engineering Research (IJMER)
www.ijmer.com Vol.3, Issue.2, March-April. 2013 pp-809-815 ISSN: 2249-6645

Privacy Preserving On Continuous and Discrete Data Sets- A Novel Approach

Sathya Rangasamy, [1] P.Suvithavani[2]
[1]*M.E Computer Science and Engineering, Sri Shakthi Institute of Engineering and Technology, Coimbatore India*
[2]*Assistant Professor, Department of Computer Science and Engineering, Sri Shakthi Institute of Engineering and Technology, Coimbatore India*

Abstract: *Privacy preservation is important for machine learning and data mining, but measures designed to protect private information often result in a trade-off: reduced utility of the training samples. This introduces a privacy preserving approach that can be applied to decision tree learning, without concomitant loss of accuracy. It describes an approach to the preservation of the privacy of collected data samples in cases where information from the sample database has been partially lost. This approach converts the original sample data sets into a group of unreal data sets, from which the original samples cannot be reconstructed without the entire group of unreal data sets. Meanwhile, an accurate decision tree can be built directly from those unreal data sets. This novel approach can be applied directly to the data storage as soon as the first sample is collected. The approach is compatible with other privacy preserving approaches, such as cryptography, for extra protection.*

Keywords: *Classification, data mining, machine learning, security and privacy protection.*

I. Introduction

Data mining is widely used by researchers for science and business purposes. Data collected (referred to as "sample data sets" or "samples") from individuals (referred as "information providers") are important for decision making or pattern recognition. Therefore, privacy-preserving processes have been developed to sanitize private information from the samples while keeping their utility.

A large body of research has been devoted to the protection of sensitive information when samples are given to third parties for processing or computing [1], [2], [3], [4], [5]. It is in the interest of research to disseminate samples to a wide audience of researchers, without making strong assumptions about their trustworthiness.

Even if information collectors ensure that data are released only to third parties with non-malicious intent (or if a privacy preserving approach can be applied before the data are released, there is always the possibility that the information collectors may inadvertently disclose samples to malicious parties or that the samples are actively stolen from the collectors. Samples may be leaked or stolen anytime during the storing process [6], [7] or while residing in storage [8], [9]. This focuses on preventing such attacks on third parties for the whole lifetime of the samples.

Contemporary research in privacy preserving data mining mainly falls into one of two categories: 1) perturbation and randomization-based approaches, and 2) secure multiparty computation (SMC)-based approaches [10]. SMC approaches employ cryptographic tools for collaborative data mining computation by multiple parties. Samples are distributed among different parties and they take part in the information computation and communication process. SMC research focuses on protocol development [11] for protecting privacy among the involved parties [12] or computation efficiency [13]; however, centralized processing of samples and storage privacy is out of the scope of SMC.

We introduce a new perturbation and randomization-based approach that protects centralized sample data sets utilized for decision tree data mining. Privacy preservation is applied to sanitize the samples prior to their release to third parties in order to mitigate the threat of their inadvertent disclosure or theft. In contrast to other sanitization methods, our approach does not affect the accuracy of data mining results. The decision tree can be built directly from the sanitized data sets, such that the originals do not need to be reconstructed. Moreover, this approach can be applied at any time during the data collection process so that privacy protection can be in effect even while samples are still being collected.

The following assumptions are made for the scope of this paper: first, as is the norm in data collection processes, a sufficiently large number of sample data sets have been collected to achieve significant data mining results covering the whole research target. Second, the number of data sets leaked to potential attackers constitutes a small portion of the entire sample database. Third, identity attributes (e.g., social insurance number) are not considered for the data mining process because such attributes are not meaningful for decision making. Fourth, all data collected are dis-cretized; continuous values can be represented via ranged-value attributes for decision tree data mining.

II. Related Work

In Privacy Preserving Data Mining: Models and Algorithms [14], Aggarwal and Yu classify privacy preserving data mining techniques, including data modification and crypto-graphic, statistical, query auditing and perturbation-based strategies. Statistical, query auditing and most crypto-graphic techniques are subjects beyond the focus of this paper. In this section, we explore the privacy preservation techniques for storage privacy attacks.

Data modification techniques maintain privacy by modifying attribute values of the sample data sets. Essentially,

data sets are modified by eliminating or unifying uncommon elements among all data sets. These similar data sets act as masks for the others within the group because they cannot be distinguished from the others; every data set is loosely linked with a certain number of information providers. K-anonymity [15] is a data modification approach that aims to protect private information of the samples by generalizing attributes. K-anonymity trades privacy for utility. Further, this approach can be applied only after the entire data collection process has been completed.

Perturbation-based approaches attempt to achieve privacy protection by distorting information from the original data sets. The perturbed data sets still retain features of the originals so that they can be used to perform data mining directly or indirectly via data reconstruction. Random substitutions [16] is a perturbation approach that randomly substitutes the values of selected attributes to achieve privacy protection for those attributes, and then applies data reconstruction when these data sets are needed for data mining. Even though privacy of the selected attributes can be protected, the utility is not recoverable because the reconstructed data sets are random estimations of the originals.

Most cryptographic techniques are derived for secure multiparty computation, but only some of them are applicable to our scenario. To preserve private information, samples are encrypted by a function, f, (or a set of functions) with a key, k, (or a set of keys); meanwhile, original information can be reconstructed by applying a decryption function, f^{-1}, (or a set of functions) with the key, k, which raises the security issues of the decryption function(s) and the key(s). Building meaningful decision trees needs encrypted data to either be decrypted or interpreted in its encrypted form. The (anti)monotone framework [17] is designed to preserve both the privacy and the utility of the sample data sets used for decision tree data mining. This method applies a series of encrypting functions to sanitize the samples and decrypts them correspondingly for building the decision tree. However, this raises the security concerns about the encrypting and decrypting functions. In addition to protecting the input data of the data mining process, this approach also protects the output data, i.e., the generated decision tree. Still, this output data can normally be considered sanitized because it constitutes an aggregated result and does not belong to any individual information provider. In addition, this approach does not work well for discrete-valued attributes.

III. Dataset Complementation Approach

In Dataset Complementation approach, Unrealized training set algorithm is used. Traditionally, a training set, T_S, is constructed by inserting sample data sets into a data table. However, a data set complementation approach, requires an extra data table, T^P. T^P is a perturbing set that generates unreal data sets which are used for converting the sample data into an unrealized training set, $T^{'}$. The algorithm for unrealizing the training set, T_S, is shown as follows:

Algorithm Unrealize-Training-Set (T_S, T^U, T', T^P)
Input: T_S, a set of input sample data sets
T^U, a universal set
T', a set of output training data sets
T^P , a perturbing set
Output: <T', T^P >

1. if T_S is empty then return <T',T^P >
2. t ←a dataset in T_S
3. if T is not an element of T^P or T^P={t} then
4. $T^P \leftarrow T^P + T^U$
5. $T^P \leftarrow T^P - \{t\}$
6. t' ← the most frequent dataset in T^P
7. return Unrealize-Training-Set (T_S-{t}, T^U , T'+{t'} , T^P-{t'})

To unrealize the samples, T_S, we initialize both T' and T^P as empty sets, i.e., we invoke the above algorithm with Unrealize-Training-Set ($T_{S,\ TU}$,{},{}). The resulting unrealized training set contains some dummy data sets excepting the ones in T_S. The elements in the resulting data sets are unreal individually, but meaningful when they are used together to calculate the information required by a modified ID3 algorithm.

IV. Decision Tree Generation

The well-known ID3 algorithm [18] shown above builds a decision tree by calling algorithm *Choose-Attribute* recursively. This algorithm selects a test attribute (with the smallest entropy) according to the information content of the training set T_S. The information entropy functions are given as

$$H_{a_i}(T_S) = -\sum_{e \in K_i} \left(\frac{\left| T_{S_{(a_i=e)}} \right|}{|T_S|} \right) \log_2 \left(\frac{\left| T_{S_{(a_i=e)}} \right|}{|T_S|} \right)$$

and

$$H_{a_i}(T_S/a_j) = \sum_{f \in K_j} \left(\frac{\left|T_{S_{(a_j=f)}}\right|}{|T_S|} \right) H_{a_i}\left(T_{S_{(a_j=f)}}\right)$$

Where K_i and K_j are the sets of possible values for the decision attribute, a_i, and test attribute, a_j, in T_S, respectively, and the algorithm Majority-Value retrieves the most frequent value of the decision attribute of T_S.

Algorithm Generate-Tree*(T_S, attribs, default)*
Input: T_S, the set of training data sets
attribs, set of attributes
default, default value for the goal predicate
Output: tree, a decision tree
1. **if** T_S is empty **then return** default
2. default ←Majority- Value(T_S)
3. **if** $H_{a_i}(T_S) = 0$ **then return** default
4. **else if** *attribs* is empty **then return** default
5. **else**
6. best← Choose-Attribute(attribs; T_S)
7. tree← a new decision tree with root attribute best
8. **for** each value v_i of best **do**
9. T_{S_i} ←{datasets inT_S as best =K_i}
10. subtree ←Generate-Tree(T_{S_i}; attribs-best,default)
11. connect *tree* and *subtree* with a branch labelled K_i
12. return tree

Already, we discussed an algorithm that generates an unrealized training set, T', and a perturbing set, T^P, from the samples in T_S. In this section, we use data tables T' and T^P as a means to calculate the information content and information gain of TS, such that a decision tree of the original data sets can be generated based on T' and T^P.

4.1 Information Entropy Determination

From the algorithm Unrealize-Training-Set, it is obvious that the size of T_S is the same as the size of T'. Furthermore, all data sets in (T' + T^P) are based on the data sets in T^U, excepting the ones in T_S, i.e., T_S is the q-absolute complement of (T' + T^P) for some positive integer q. The size of qT^U can be computed from the sizes of T' and T^P , with qT^U = 2* |T'|+|T^P|. Therefore, entropies of the original data sets, T_S, with any decision attribute and any test attribute, can be determined by the unreal training set, T', and perturbing set, T^P.

4.2 Modified Decision Tree Generation Algorithm

As entropies of the original data sets, T_S, can be determined by the retrievable information—the contents of unrealized training set, T', and perturbing set, T^P—the decision tree of T_S can be generated by the following algorithm.

Algorithm. Generate-Tree' (size, T', T^P, attribs, default)
Input: *size*, size of qT^U
T', the set of unreal training data sets
T^P , the set of perturbing data sets
attribs, set of attributes
default, default value for the goal predicate
Output: *tree*, a decision tree
1. if (T', T^P) is empty **then return** default
2. *default* ←Minority_Value(T'+T^P)
3. if $H_{a_i}(q[T' + T^P]^c) = 0$ then return default
4. **else if** attribs is empty **then return** default
5. **else**
6.*best*←Choose-attribute'(attribs,Size,(T',T^P))
7.*tree*←a new decision tree with root attribute *best*
8. *size*← *size*=number of possible values k_i in best
9. **for** each value v_i of best **do**
10. T_i'= {data sets in T' as best= k_i}
11. T_i^P={data sets in T^P as best=k_i}
12. *subtree*← Generate-Tree(*size*, T_i', T_i^P, *attribs-best*, default)

13. connect *tree* and *subtree* with a branch labelled k_i
14. **return** *tree*

Similar to the traditional ID3 approach, algorithm Choose-Attribute' selects the test attribute using the ID3 criteria, based on the information entropies, i.e., selecting the attribute with the greatest information gain. Algorithm Minority-Value retrieves the least frequent value of the decision attribute of ($T' + T^P$), which performs the same function as algorithm Majority-Value of the tradition ID3 approach, that is, receiving the most frequent value of the decision attribute of T_S.

To generate the decision tree with T', T^P and $| qT^U |$ (which equals $2* |T'|+|T^P|$), a possible value, k_d, of the decision attribute, a_d, (which is an element of A—the set of attributes in T) should be arbitrarily chosen, i.e., we call the algorithm *Generate-Tree (*$2* |T'|+|T^P|$, T_S, T^U, A- a_d, k_d). The resulting decision tree of our new ID3 algorithm with unrealized sample inputs is the same as the tree generated by the traditional ID3 algorithm with the original samples

4.3 Data Set Reconstruction

Section B introduced a modified decision tree learning algorithm by using the unrealized training set, T', and the perturbing set, T^P. Alternatively, we could have reconstructed the original sample data sets, T_S, from T' and T^P, followed by an application of the conventional ID3 algorithm for generating the decision tree from T. The reconstruction process is dependent upon the full information of T' and T^P (whereas $q =2* |T'|+|T^P|/|T^U|$); reconstruction of parts of T_S based on parts T' and T^P is not possible.

4.4 Enhanced Protection with Dummy Values

Dummy values can be added for any attribute such that the domain of the perturbed sample data sets will be expanded while the addition of dummy values will have no impact on T_S. Dummy represents a dummy attribute value that plays no role in the data collection process. In this way we can keep the same resulting decision tree (because the entropy of T_S does not change) while arbitrarily expanding the size of T^U. Meanwhile, all data sets in T' and T^P , including the ones with a dummy attribute value, are needed for determining the entropies of $(q[T' + T^P]^c)$ during the decision tree generation process.

4.5 C5.0 algorithm

In the proposed algorithm, consider C5.0 Algorithm for data mining. The enhancement and the optimization of the C4.5 emerge as algorithm C5.0, which exhibits the better performance as compared to the other existing mining algorithms. C5.0 algorithm to build either a decision tree or a rule set. A C5.0 model works by splitting the sample based on the field that provides the maximum information gain. Each sub sample defined by the first split is then split again, usually based on a different field, and the process repeats until the sub samples cannot be split any further. Finally, the lowest-level splits are re-examined, and those that do not contribute significantly to the value of the model are removed or pruned. C5.0 can produce two kinds of models. A decision tree is a straightforward description of the splits found by the algorithm. Each terminal (or "leaf") node describes a particular subset of the training data, and each case in the training data belongs to exactly one terminal node in the tree.

In contrast, a rule set is a set of rules that tries to make predictions for individual records. Rule sets are derived from decision trees and, in a way, represent a simplified or distilled version of the information found in the decision tree. Rule sets can often retain most of the important information from a full decision tree but with a less complex model. Because of the way rule sets work, they do not have the same properties as decision trees. The most important difference is that with a rule set, more than one rule may apply for any particular record, or no rules at all may apply. If multiple rules apply, each rule gets a weighted "vote" based on the confidence associated with that rule, and the final prediction is decided by combining the weighted votes of all of the rules that apply to the record in question. If no rule applies, a default prediction is assigned to the record. It was introduced an alternative formalism consisting of a list of rules of the form "if A and B and C and ... then class X", where rules for each class are grouped together. A case is classified by finding the first rule whose conditions are satisfied by the case; if no rule is satisfied, the case is assigned to a default class. Each case belongs to one of a small number of mutually exclusive classes. Properties of every case that may be relevant to its class are provided, although some cases may have unknown or non-applicable values for some attributes. C5.0 can deal with any number of attributes. Rule sets are generally easier to understand than trees since each rule describes a specific context associated with a class. Furthermore, a rule set generated from a tree usually has fewer rules than the tree has leaves, another plus for comprehensibility. Another advantage of rule set classifiers is that they are often more accurate predictors than decision trees.

C5.0 decision tree is constructed using *GainRatio*. *GainRatio* is a measure incorporating entropy. Entropy (*E(S)*,) measures how unordered the data set is. It is denoted by the following equation when there are classes $C_1 \ldots C_N$ in data set *S* where $P(S_c)$ is the probability of class *C* occurring in the data set *S*:

$$E(S) = -\sum_{c=1}^{N} P(S_c) * \log_2 P(S_c)$$

Information Gain is a measure of the improvement in the amount of order.

$$Gain(S,V) = E(S) - \sum_{Values(V)} (S_v|S) * E(S_v)$$

Gain has a bias towards variables with many values that partition the data set into smaller ordered sets. In order to reduce this bias, the entropy of each variable over its *m* variable values is calculated as *SplitInfo: GainRatio* is calculated by dividing *Gain* by *SplitInfo* so that the bias towards variables with large value sets is dampened.

$$Gain(S,V) = \frac{Gain(S,V)}{SplitInfo(S,V)}$$

C5.0 builds a decision tree greedily by splitting the data on the variable that maximizes gain ratio. A final decision tree is changed to a set of rules by converting the paths into conjunctive rules and pruning them to improve classification accuracy.

V. Theoretical Evaluation

This section provides a concise theoretical evaluation of our approach. For full details on our evaluation process, we refer to [19].

5.1 Privacy Issues

Private information could potentially be disclosed by the leaking of some sanitized data sets, T_L (a subset of the entire collected data table, T_D), to an unauthorized party if

1. The attacker is able to reconstruct an original sample, t_S, from T_L, or
2. If T_L (a data set in T_L) matches t_S (a data set in T_S) by chance

In the scope of this paper, t_S is non reconstructable because $|T_L|$ is much smaller than $|T'+T^P|$. Hence, we are focusing on the privacy loss via matching. Without privacy preservation the collected data sets are the original samples. Samples with more even distribution (low variance) have less privacy loss, while data sets with high frequencies are at risk. The data set complementation approach solves the privacy issues of those uneven samples. This approach converts the original samples into some unrealized data sets[$T' + T^P$], such that the range of privacy loss is decreased. Data Set complementation is in favour of those samples with high variance distribution, especially when some data sets have zero counts. However, it does not provide significant improvement for the even cases.

Adding dummy attribute values effectively improves the effectiveness of the data set complementation approach; however, this technique requires the storage size of $cR|T^U| - |T_S|$, where c is the counts of the most frequent data set in T_S. The worst case storage requirement equals $(R|T^U|-1)*|T_S|$.

VI. Experiments

This section shows the experimental samples of data's from the data set complementation approach,

1. normally distributed samples and evenly distributed samples
2. extremely unevenly distributed samples
3. Six sets of randomly picked samples, where (i) was generated without creating any dummy attribute values and (ii) was generated by applying the dummy attribute technique to double the size of the sample domain.

For the artificial samples (Tests 1-3), we will study the output accuracy (the similarity between the decision tree generated by the regular method and by the new approach), the storage complexity (the space required to store the unrealized samples based on the size of the original samples) and the privacy risk (the maximum, minimum, and average privacy loss if one unrealized data set is leaked).

6.1 Output Accuracy

In all cases, the decision tree(s) generated from the unrealized samples (by algorithm Generate-Tree' described in Section 4.2) is the same as the decision tree(s), Tree T_S, generated from the original sample by the regular method. This result agrees with the theoretical discussion mentioned in Data Set Complementation approach

6.2 Storage Complexity

From the experiment, the storage requirement for the data set complementation approach increases from $|T_S|$ to $(2|T^U| -1)^*|T_S|$, while the required storage may be doubled if the dummy attribute values technique is applied to double the sample domain. The best case happens when the samples are evenly distributed, as the storage requirement is the same as for the originals. The worst case happens the samples are distributed extremely unevenly. Based on the randomly picked tests, the storage requirement for our approach is less than five times (without dummy values) and eight times (with dummy values, doubling the sample domain) that of the original samples.

6.3 Privacy Risk

Without the dummy attribute values technique, the average privacy loss per leaked unrealized data set is small, except for the even distribution case (in which the unrealized samples are the same as the originals). By doubling the sample domain, the average privacy loss for a single leaked data set is zero, as the unrealized samples are not linked to any information provider. The randomly picked tests show that the data set complementation approach eliminates the privacy risk for most cases and always improves privacy security significantly when dummy values are used.

VII. Conclusion

We introduced a new privacy preserving approach via data set complementation which confirms the utility of training data sets for decision tree learning. This approach converts the sample data sets, T_S, into some unreal data sets ($T'+ T^P$) such that any original data set is not reconstructable if an unauthorized party were to steal some portion of ($T'+ T^P$) .Meanwhile, there remains only a low probability of random matching of any original data set to the stolen data sets, T_L. The data set complementation approach ensures that the privacy loss via matching is ranged from 0 to $|T_L|*(|T_S|/|T^U|)$, where T^U is the set of possible sample data sets. By creating dummy attribute values and expanding the size of sample domain and the privacy loss via matching will be decreased.

Privacy preservation via data set complementation fails if all training data sets are leaked because the data set reconstruction algorithm is generic. Therefore, further research is required to overcome this limitation. As it is very straightforward to apply a cryptographic privacy preserving approach, such as the (anti)monotone framework, along with data set complementation, this direction for future research could correct the above limitation. This covers the application of this new privacy preserving approach with the ID3 decision tree learning algorithm and discrete-valued attributes only. In proposed approach, we can develop the application with the help of algorithm, C5.0, and data mining methods with mixed discretely—and continuously valued attributes. The storage size of the unrealized samples, the processing time when generating a decision tree from those samples and privacy can be increased using C5.0 algorithm for both continuous and discrete data sets. When compared with the existing Modified ID3 algorithm, proposed method provide the better results.

REFERENCES

[1] S. Ajmani, R. Morris, and B. Liskov, "A Trusted Third-Party Computation Service," Technical Report MIT-LCS-TR-847, MIT, 2001.
[2] S.L. Wang and A. Jafari, "Hiding Sensitive Predictive Association Rules," Proc. IEEE Int'l Conf. Systems, Man and Cybernetics, pp. 164-169, 2005.
[3] R. Agrawal and R. Srikant, "Privacy Preserving Data Mining,"Proc. ACM SIGMOD Conf. Management of Data (SIGMOD '00),pp. 439-450, May 2000.
[4] Q. Ma and P. Deng, "Secure Multi-Party Protocols for Privacy Preserving Data Mining," Proc. Third Int'l Conf. Wireless Algorithms, Systems, and Applications (WASA '08), pp. 526-537, 2008.
[5] J. Gitanjali, J. Indumathi, N.C. Iyengar, and N. Sriman, "A Pristine Clean Cabalistic Fortuity Strategize Based Approach for Incremental Data Stream Privacy Preserving Data Mining," Proc. IEEE Second Int'l Advance Computing Conf. (IACC), pp. 410-415, 2010.
[6] N. Lomas, "Data on 84,000 United Kingdom Prisoners is Lost," Retrieved Sept. 12, 2008, http://news.cnet.com/8301-1009_3-10024550-83.html, Aug. 2008.
[7] BBC News Brown Apologises for Records Loss. Retrieved Sept.12, 2008, http://news.bbc.co.uk/2/hi/uk_news/politics/7104945.stm, Nov. 2007.
[8] D. Kaplan, Hackers Steal 22,000 Social Security Numbers from Univ.of Missouri Database, Retrieved Sept. 2008, http://www.scmagazineus.com/Hackers-steal-22000-Social-Security-numbers-from-Univ.-of-Missouri-database/article/34964/, May 2007.
[9] D. Goodin, "Hackers Infiltrate TD Ameritrade client Database," Retrieved Sept. 2008, http://www.channelregister.co.uk/2007/09/15/ameritrade_database_burgled/, Sept. 2007.
[10] L. Liu, M. Kantarcioglu, and B. Thuraisingham, "Privacy Preserving Decision Tree Mining from Perturbed Data," Proc. 42nd Hawaii Int'l Conf. System Sciences (HICSS '09), 2009.
[11] Y. Zhu, L. Huang, W. Yang, D. Li, Y. Luo, and F. Dong, "Three New Approaches to Privacy-Preserving Add to Multiply Protocol and Its Application," Proc. Second Int'l Workshop Knowledge Discovery and Data Mining, (WKDD '09), pp. 554-558, 2009.
[12] J. Vaidya and C. Clifton, "Privacy Preserving Association Rule Mining in Vertically Partitioned Data," Proc Eighth ACM SIGKDD Int'l Conf. Knowledge Discovery and Data Mining (KDD '02), pp. 23-26, July 2002.
[13] M. Shaneck and Y. Kim, "Efficient Cryptographic Primitives for Private Data Mining," Proc. 43rd Hawaii Int'l Conf. System Sciences (HICSS), pp. 1-9, 2010. [14] C. Aggarwal and P. Yu, Privacy-Preserving Data Mining:, Models and Algorithms. Springer, 2008.
[15] L. Sweeney, "k-Anonymity: A Model for Protecting Privacy," Int'l J. Uncertainty, Fuzziness and Knowledge-based Systems, vol. 10, pp. 557-570, May 2002.
[16] J. Dowd, S. Xu, and W. Zhang, "Privacy-Preserving Decision Tree Mining Based on Random Substitutions," Proc. Int'l Conf. Emerging Trends in Information and Comm. Security (ETRICS '06), pp. 145-159, 2006.
[17] S. Bu, L. Lakshmanan, R. Ng, and G. Ramesh, "Preservation of Patterns and Input-Output Privacy," Proc. IEEE 23rd Int'l Conf.Data Eng., pp. 696-705, Apr. 2007.

[18] S. Russell and N. Peter, Artificial Intelligence. A Modern Approach 2/E. Prentice-Hall, 2002.
[19] P.K. Fong, "Privacy Preservation for Training Data Sets in Database: Application to Decision Tree Learning," master's thesis, Dept. of Computer Science, Univ. of Victoria, 2008.

AUTHOR BIOGRAPHY

Ms.Sathya Rangasamy received B.E degree in CSE from Avinashilingam University, Coimbatore and currently pursuing M.E degree in Computer Science and Engineering in Sri Shakthi Institute of Engineering and Technology, under Anna University, Chennai. Her research interest includes Computer Networks and Data Mining.

Mrs.Suvithavani.P received M.Sc (Integrated-5Yrs) degree in IT from Government College of Technology, Coimbatore and received her M.E degree from Computer Science and Engineering in Sun College of Engineering and Technology, Nagercoil. She is currently working as Assistant Professor in Department of CSE in Sri Shakthi Institute of Engineering and Technology, Coimbatore. Her main research interest is Data Mining.

International Journal of Modern Engineering Research (IJMER)
www.ijmer.com Vol.3, Issue.2, March-April. 2013 pp-816-820 ISSN: 2249-6645

Night Vision Techniques and Their Applications

Rupesh P.Raghatate, [1] Swapnil S.Rajurkar, [2] Manisha P.Waghmare, [3]
Pooja V. Ambatkar[4]
[1]*M-tech SEM-I BDCOE, WARDHA,*
[2]*M-tech SEM-I APGCET, NAGPUR,*
[3]*M-tech SEM-I SDCOE, WARDHA,*
[4]*Lecturer AVBIT, WARDHA*

Abstract: *This paper describes the various Night vision techniques."Night Vision" is referenced as technology that provides us with the miracle of vision in total darkness and the improvement of vision in low light environments. This technology is an amalgam of several different methods each having its own advantages and disadvantages. The most common methods described here are Low-Light Imaging, Thermal Imaging and Illumination's. This paper also give brief idea about various night vision device (NVD) that allows images to be produced in levels of light approaching total darkness,it also explains various applications where night vision technology is used to solve various problems due to low light conditions .*

Keywords: *Image intensification, Active illumination, Thermal imaging, night vision technology, NVD*

I. INTRODUCTION

Night vision signifies the ability to see in dark (night). This capability is normally possessed by owls and cats, but with the development of science and technology devices has been develop which enables human being to see in dark as well an in adverse atmospheric conditions such as fog ,rain, dust etc.The muscles in the human eye have the ability to stretch or contract automatically, depending upon the intensity of light falling on the eye. When we go out in bright sunlight, the pupil gets contracted. Alternatively, when we enter a shaded or dark room at that time the muscles of eye relax and make the aperture of the eye lens big enough to allow sufficient amount of light to pass through,therefore the objects in the room appear blurred. Because of this human eye have limitations. The muscles of eye cannot increase the aperture indefinitely. Therefore, in poor light we are unable to see the objects because the image cannot be formed on the retina clearly. The capability to detect and identify targets at night and under poor visibility conditions has been an essential military requirement. The modern army's need to operate at night and under conditions of extremely poor visibility , Since the soldiers have to often fight in the dark at night, they have to face a severe stress as far as the location of target is concerned. Also various wild life observer have to to face problems of low light because many wild animals are more active during night time than day ,therefore to observe there lifestyle and study it night vision is important . Therefore to make human being unable to see in dark by technological means, night vision technology has been developed. This paper describes various techniques and different devices developed to enable viewing in dark.

Night vision technologies can be broadly divided into three main categories:
1: Image intensification
2: Active illumination
3: Thermal imaging

1.1. Image Intensification System

Image intensification systems support direct observations by amplifying low levels of available light. They do not 'turn night into day' Nor do they overcomes the problems that affect vision in low light environments. The image intensifier is a vacuum-tube based device that converts invisible light from an image to visible light so that a objects in the dark can be viewed by a camera or the naked eye. When light strikes a charged photocathode plate, electrons are emitted through a vacuum tube that strike the micro channel plate that cause the image screen to illuminate with a picture in the same pattern as the light that strikes the photocathode, This is much like a CRT television, but instead of color guns the photocathode does the emitting. The intensified image is, typically, viewed on a phosphor screen that creates a monochrome, video-like image, on the user's eyepieces.

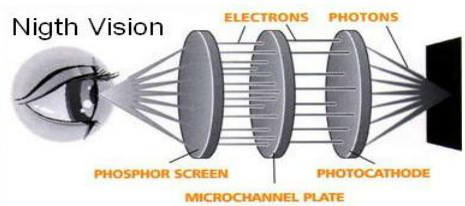

Fig 1: Image intensification systems

Advantages

- Excellent low-light level sensitivity.
- Enhanced visible imaging yields the best possible. recognition and identification performance.
- High resolution.
- Low power and cost.
- Ability to identify people.

Disadvantages:

- Because they are based on amplification methods, some light is required. This method is not useful when there is essentially no light.
- Inferior daytime performance when compared to daylight-only methods.
- Possibility of blooming and damage when observing bright sources under low-light conditions.

1.2. Active Illumination

Active illumination technologies work on the principle of coupling imaging intensification with an active source of illumination in the near infrared (NIR) band. Infrared is used in night vision technology when there is insufficient visible light to see, active illumination involves conversion of ambient light photons into electrons which are then amplified by a chemical and electrical process and then converted back into visible light. Active infrared night vision combines infrared illumination in spectral range 0.7–1 μm. Due to which The scene, which appears dark to a human observer now appears as a monochrome image on a normal display device. Since active infrared night vision systems can incorporate illuminators that produce high levels of infrared light, the resulting images are typically higher resolution than other night vision technologies.

The use of infrared light and night vision devices should not be confused with thermal imaging which creates images based on differences in surface temperature by detecting infrared radiation (heat) that emanates from objects and their surrounding environment

1.3. Thermal Imaging

In order to understand thermal imaging, it is important to understand something about light. The amount of energy in a light wave is related to its wavelength: Shorter wavelengths have higher energy. Of visible light, violet has the most energy, and red has the least. Just next to the visible light spectrum is the infrared spectrum.

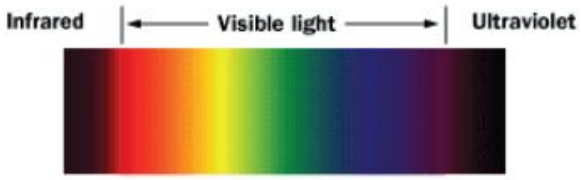

Fig 2: spectrum of light

Infrared light can be split into three categories:

1. Near-infrared (near-IR) - Closest to visible light, near-IR has wavelengths that range from 0.7 to 1.3 microns, or 700 billionths to 1,300 billionths of a meter.
2. Mid-infrared (mid-IR) - Mid-IR has wavelengths ranging from 1.3 to 3 microns. Both near-IR and mid-IR are used by a variety of electronic devices, including remote controls.
3. Thermal-infrared (thermal-IR) - Occupying the largest part of the infrared spectrum, thermal-IR has wavelength ranging from 3 microns to over 30 microns.

1.3.1. Working Of Thermal Imaging

A special lens focuses the infrared light emitted by all of the objects in view. The focused light is scanned by a phased array of infrared-detector elements. The detector elements create a very detailed temperature pattern called a thermogram. It only takes about one-thirtieth of a second for the detector array to obtain the temperature information to make the thermogram. This information is obtained from several thousand points in the field of view of the detector array. The thermo gram created by the detector elements are translated into electric impulses.

The impulses are sent to a signal-processing unit, a circuit board with a dedicated chip that translates the information from the elements into data for the display. The signal-processing unit sends the information to the display, where it appears as various colors depending on the intensity of the infrared emission. The combination of all the impulses from all of the elements creates the image.

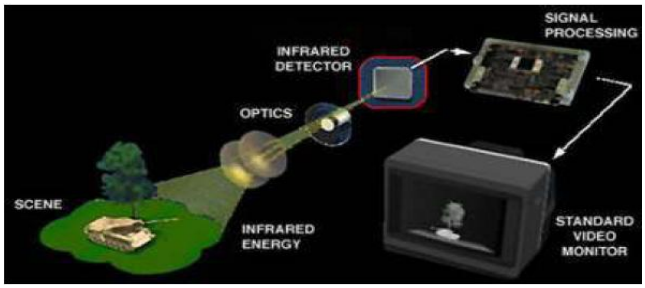

Fig 3: Thermal imaging system

There are two common types of thermal-imaging devices:

i) **Un-cooled** - This is the most common type of thermal-imaging device. The infrared detector Elements are contained in a unit that operates at room temperature. This type of system is completely quiet, activates immediately and has the battery built right in.

ii) **Cryogenically cooled** - More expensive and more susceptible to damage from rugged use, these systems have the elements sealed inside a container that cools them to below 32 F (zero C). The advantage of such a system is the incredible resolution and sensitivity that result from cooling the elements. Cryogenically-cooled systems can "see" a difference as small as 0.2 F (0.1 C) from more than 1,000 ft (300 m) away, which is enough to tell if a person is holding a gun at that distance.


Fig 4: captured image by thermal imaging system

II. GENERATIONS OF NIGHT VISION TECHNIQUES

Table 1: Generations of night vision techniques

S. No.	Generations	Specifications
1	Generation 0	In 1950's,
		Based on Image Conversion, Require source of Invisible Infrared to illuminate the target.
2	Generation 1	In 1960's,
		Based on image intensifier, Larger and heavier systems.
3	Generation 2	In 1970's,
		Micro Channel Plate (MCP) electron multiplier, Development of hand held and helmet mounted goggles.
4	Generation 3	In early 1980's,
		Gallium Arsenide photocathode and ion-barrier film on MCP,
5	Generation 4	In 2000's

III. APPLICATIONS OF NIGHT-VISION

The main purpose for the development of this technology was for the military use, to locate enemies at night. Not only is it used extensively for military purposes, but also for navigation, surveillance and targeting.

Thermal imaging and Image enhancement technologies are used for surveillance purpose by the police and security departments. It is also used for the maneuverability of the hunters and nature enthusiasts through the woods at night. Following are some other applications of the night-vision:

- Law-Enforcement
- Wildlife Observation
- Security
- Hidden Object detection
- Entertainment

1.4. Law-Enforcement

To support law enforcement during the hours of darkness and low light situations and help them detect, deter and prevent the disruption of a enemy. When an event is designated, the Secret Service assumes the role as the lead agency for the design and implementation of the operational security plan. The challenge around events is security on all fronts. During daylight hours and within areas of full light, the playing field is fairly level; however, remove the element of light and someone has the advantage. During events, The challenge is to eliminate low light situations as a potential threat. Prevention, readiness and diligence are the key factors in securing an event from a terrorist threat. Night vision surveillance is a crucial means of protecting an area and its assets before, after and during an event. Night vision techniques give law enforcement the advantage of monitoring activity in darkness and areas of low light. The most effective way to prepare for and provide effective security for an event is to ensure that law enforcement officials have the equipment and training they need long before an event takes place. Therefore with the help of night vision techniques best surveillances can be done in low light conditions.

Fig 5: various night vision devices

1.5. Wildlife Observation

Keen-eyed observer can see much wildlife during the day .but many animals, including most large mammals, are more active at night or twilight. Night-vision binoculars give the option of continuing our observations after the sun has set and the chance to see elusive creatures that are less active during the day. Once a good pair of night-vision binoculars is acquired we can find the best spots to spot critters.

Fig 6: Observed wildlife using night vision technique

1.6. Security

There are lots of challenges in performing video surveillance at night. The optimal solution for a particular application will depend on the requirements for the specific application. For example, is daytime operation required? Does the system need to be covert what is the size and shape of the area to be monitored? Is the goal of the surveillance to detect, recognize or identify subjects in the field of view? The night vision camera provide best surveillance during night or low light condition and thus prevents the chances of theft, terriost attack etc

Fig 7: night vision camera

IV. CONCLUSION

In this paper we have described various night vision technologies which are available and also its working in order to avoid various low light problem, this paper shows that how efficiently a soldiers can work efficiently during night also wild life observer can work during dark and also shown how surveillance can be kept in low light condition .this paper summarize a various generations of night vision technology.

REFERENCES

Journal Papers:

[1] Tsz-Ho Yu,Yiu-sang Moon, An Intelligent Night Vision System For Automobiles, MVA 2009 IAPR Conference On Machine Vision Application ,May 20-22,2009,Yokohama ,Japan

[2] A. ROGALSKI*1 and K. CHRZANOWSKI, Infrared Devices and techniques, OPTO-ELECTRONICS REVIEW 10(2), 111–136 (2002)

[3] Chris Johnson, The Role of Night Vision Equipment in Military Incidents and Accidents, Dept. of Computing Science, University of Glasgow, Glasgow, G12 9QQ

[4] www.morovision.com/how_thermal_imaging_works.htm

[5] http://night-vision-technology.com/technologies.

International Journal of Modern Engineering Research (IJMER)
www.ijmer.com Vol.3, Issue.2, March-April. 2013 pp-821-831 ISSN: 2249-6645

A Study of Reverse Engineering Program Based on Obtaining Point Clouds from Object Images

Gürcan Samtaş
Faculty of Engg., Department of Mechatronics Engg., Düzce University, Düzce,-Türkiye

Abstract: *This study focuses on developing a program which obtains 3D point clouds by interpreting images taken with a digital camera, using image processing. In the developed program, images taken with a digital camera without using a specific shooting condition are evaluated pixel by pixel. These evaluations are made with reference points marked on the image in the designed area by user. The 3D point clouds of the objects in the marked area can be obtained in a short time interpreting pixel values of the limited area. In the study, a different approach is presented, in which image processing and Reverse Engineering (RE) techniques are used, in the process of 3D design and manufacturing. Furthermore, the developed program has the advantages of keeping a relatively short processing, and because of using reference area, images and point clouds used can express objects in image. In this study, in addition, algorithms used while processing images in developed program are explained on a sample image in detail, and sample images which obtained point clouds and their solid models are given.*

Keywords: *reverse engineering; CAD; image processing; point cloud*

I. INTRODUCTION

Engineering is a process conducting activities related to design, analysis, manufacturing and maintenance of the system and presenting analytical solutions to problems by modeling, physical events, and situations mathematically. Forward engineering and reverse engineering are two types of engineering. Forward engineering is the traditional process of moving from high-level abstractions and logical designs to the physical implementation of a system. In some situations, there may be a physical part/product without any technical details, such as drawings, bills-of-material, or without engineering data. The process of duplicating an existing part, subassembly, or product, without drawings, documentation, or a computer model is known as reverse engineering [1]. In other words, reverse engineering can also be defined as the process of digitizing existing parts and acquiring a Computer Aided Design (CAD) model with three dimensional (3D) point clouds. Reverse engineering, which is defined as a process of digital capturing of one element's physical existence, can be defined in different ways according to special business areas by researchers [2].

The development of image processing applications has proven to be a highly complex and time consuming activity. This prevents the penetration of image processing into industry, whereas the demand for concrete applications is growing in all domains: medicine, biotechnology, remote sensing, astronomy, ecology, security, forensics, chemistry, surveillance, quality control, etc. As a result, it is becoming indispensable to develop systems that can help end-users build customized applications. The challenge is to allow end-users to program software at the image feature level rather than at the computer code level [3]. In image processing main goals are to obtain useful information about the scene and to observe the image in a good way by defining the image. Here, machine or human is the observer. If raw material is not clear enough, it should be treated for the desired purpose. When transactions are often done by people in an electronic environment, optical and electronic devices are needed to obtain the image. When digital image processing is applied in accordance with the purpose, it has many advantages such as speed, low cost and achieving the desired result. There are also architectural applications in the RE area. A different approach has developed for image based architectural modeling, which processes images, by using library support of 3D objects. With the presented model, the images which are 1024x768, 24 bit and BMP extension are used. In the system, a model library is used to generate realistic 3D models [4].

Primitive recognition methods are used in image processing area which uses model mapping comment rate in computer aided design and photometry measurement systems, and this study consists of review angle, graphic angle and model matching [5]. Three dimensional models of urban areas are generated with the help of such devices as 2D laser beam scanner, density cameras. There are several approaches to obtain 3D models of cities, for instance the objects in images obtained by satellite or antenna are determined by stereo vision or synthetic aperture radar stereo. In this approach, although the objects are generated quickly, the resolution and accuracy of generated models are also very low [6, 7]. On the other hand, 3D camera tracking systems are used occasionally in industrial augmented reality applications. Bleser et al. [8] presented real time 3D camera tracking systems, and with this presented solution, there is no need for forecasting, posing, monitoring systems and pointers used in other similar applications. Augmented reality offers new approaches such areas as machine repair, design, medicine and cultural heritage [9-11]. Song and Wang [12] have developed a new grid matching method for 3D reconstruction. Three dimensional automatic building of surfaces has been the subject of research of digital photometry for many years. Today, photometry is applied in the fields of both computer vision and computer graphics such as industrial inspection and reverse engineering [13, 14]. The reconstruction of 3D models includes four main steps such as data capture, recording, surface integration and texture map. Partially generated 3D shapes and texture information are obtained from a different point of views [15]. Computer vision and image understanding are areas of research related to incremental number of images, image quality, object perception in the image and its applications [16, 17]. Barbero and Ureta

[18] compared five digitization techniques in the field of Reverse Engineering for the quality of the distribution of points and triangular meshes: 1. An ordered point cloud obtained with a laser incorporated in a Coordinate Measurement Machine (CMM); 2. A disordered point cloud obtained with a manual laser, the position of which is determined with a Krypton Camera; 3. An EXA scan manual laser with targets; 4. An ordered point cloud obtained by high accuracy computerized tomography; 5. An atos fringe projection scanner with targets. Bosche [19] presented a new approach for automated recognition of project 3D Computer-Aided Design (CAD) model objects in large laser scans. Test results were given with data obtained from the construction of an industrial building's steel structure. Yang et al. [20], in their study, presented a fast and precise 3D laser scanner to recover point cloud data and then import the data into Rapid Form XOR2, an application used in reverse engineering, to process point cloud data and construct 3D models. Their study results were converted from 3D models into 2D pictures by parameterization software Pro/ENGINEER to provide designers precise and realistic dimensional data, which efficiently reduced time in cartography and increased historic building dimension precision during digitization.

In this study, it is aimed to develop a RE application which processes color images obtained by a digital camera, achieves 3D point clouds from these images without using a specific shooting environment. In the developed program, *.NET* programming sub-structure and *PHP* scripting language have been used, and 3D point clouds are obtained by processing color images belonging to sample engineering models. Three dimensional point clouds obtained from the program are converted into solid models in the *CATIA* design program to obtain reconstruction of 3D objects.

II. EXPERIMENTAL WORKS AND IMAGE ANALYSIS

Experimental work is done to testing of the program and developing of the image processing algorithms. The obtained samples images with the prepared testing apparatus are used in developing program (fig.1). Sample models are expressed in two views. Images are obtained from a general environment without the need for a specific shooting condition. In developed program, jpg and bmp formatted images taken from a digital camera can be used. To obtain pixel values in the images, RGB (red, green, blue) color system is used. In RGB color value, each color has maximum 256 color value. Combination of three colors (256x256x256) consists of a total of 16,777,216 colors. These colors are expressed as real colors. For example, a pixel having (178, 229, 41) colors is expressed as (10110010, 11100101, 00101001) in the binary system. These values are defined for each pixel. Pixels on the processed images in the system are scanned according to color values. During this scanning, pixels of the object are detected according to the color values and translated into the language of binary encoding and stored temporarily side by side as 0 and 1 without distinction. When colors are scanned pixel by pixel, each color values up to +12 or -12 is considered the same fig. (2).

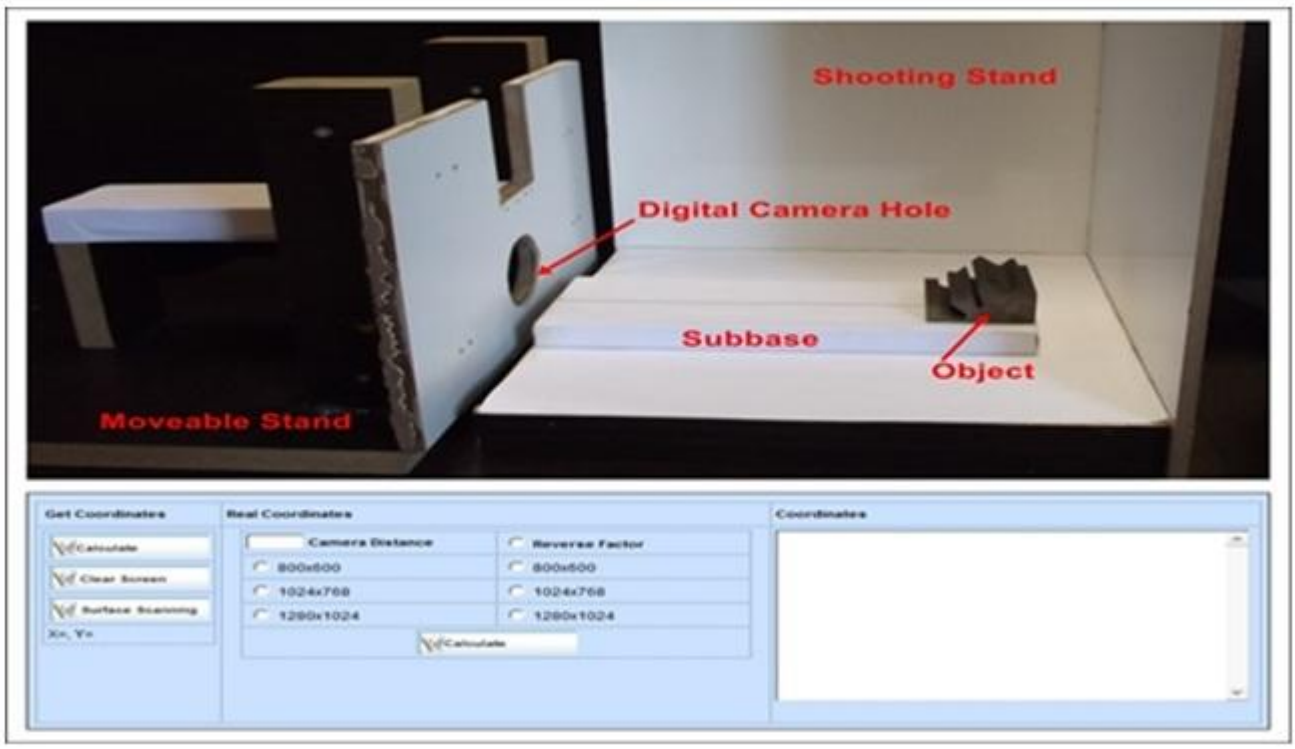

Figure1: Testing apparatus and developed system interface

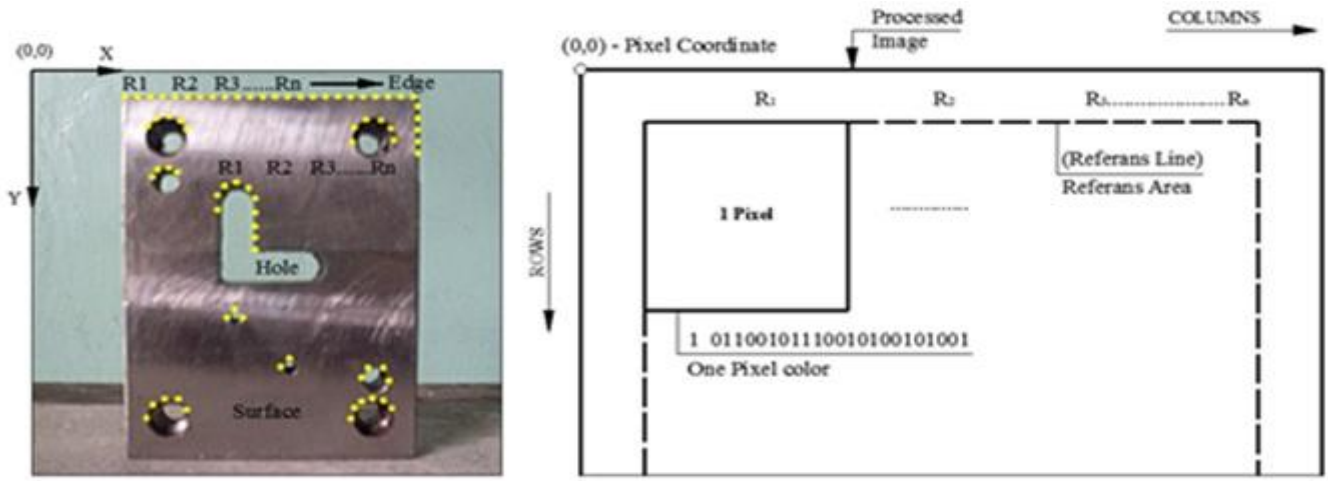

Figure 2: Color analysis applied to an image

Where R1 R2 R3 … Rn are reference points, and they marked by user. Images are processed according to color values, evaluating the whole image requires long processing time. Therefore, as shown fig. (2), because of reference points are given to target object in the image, the processing time is shortened. This process will also help to identify the edges of the object, and system scans from left to the right in the reference area, starting from the first marked reference point.

III. OBTAINING POINT CLOUDS

Reference points are marked from right to the edges of the target object in the image randomly (fig. 2). As a result of the analysis, the scanning for obtaining point clouds is superficial, and slopes on the surface are determined according to perpendicular orientations. These perpendicular orientations are horizontal or vertical orientations, which are according to X and Y planes, on the front view of the part. Therefore, circular edges of processed piece can be processed as superficial. In the system, to interpret the images, edge-hole model and surface-area model have been developed in two different algorithms.

Edge-Hole Model

Edge-hole model algorithm is based on marking surface and hole-edges of the processed piece. It is a model which is created for edge and hole of the processed piece. In general, there are edges of each object, but holes may not be available in all of them. In this model, holes are processed as edges. After making the reference point, and the color analysis is applied to the area within the marked points. If there is an area which will be processed as a hole in the outer surface area, this time program scans the area which is between these two markings and applies color analysis to two different areas (fig. 3).

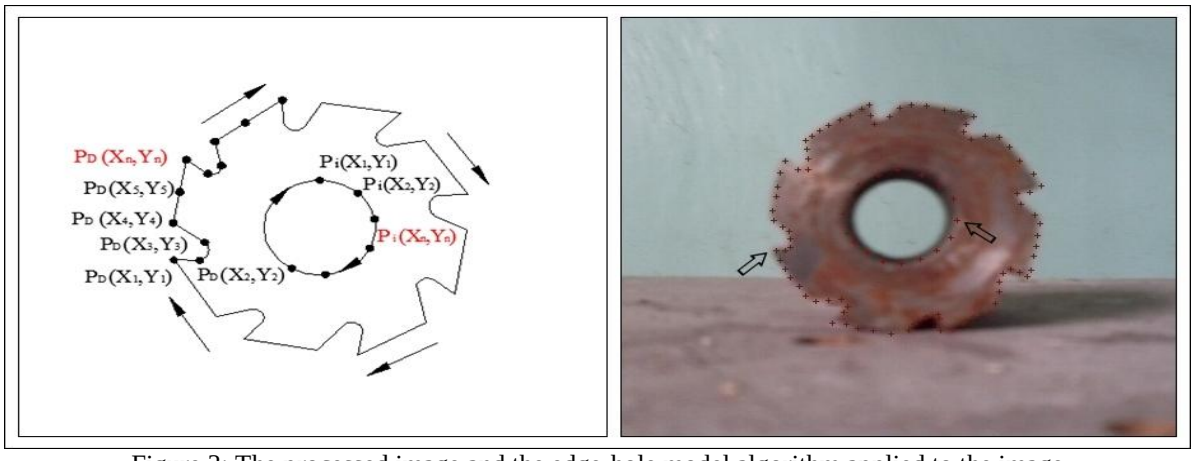

Figure 3: The processed image and the edge-hole model algorithm applied to the image

The processed sample image and edge-hole model algorithm applied by the system and the marked reference points to this image are shown in fig. (3). Reference points are marked randomly to the edges and holes of the target object in the image by the user. The system combines the P_D $(X_1, Y1)$ starting point marked for outer surface with the ending point P_D (X_n,Y_n) and scans the space which is the result of this combination.. If there is a hole in the object to be processed, as in the outer edge of the object, a P_i (X_1,Y_1) starting point and an ending point P_i (X_n,Y_n) are marked and a scanning in itself is carried out. The system scans the area between edge-hole and inner hole area for outer surface for this type pieces. In edge-hole model, a process applied to the images to detect the points is shown in fig. (4).

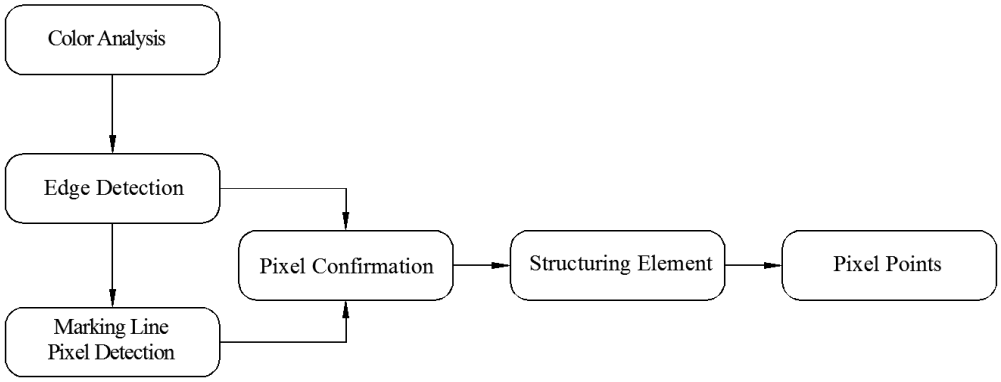

Figure 4: Processes applied to the images in the edge-hole model

In fig. (4), the processes applied to the image for edge-hole model are shown respectively. Processes applied to the image consist of 6 stages as follows: (1) providing borders with making color analysis in the inner region of the marked area; (2) determination of the edges in these provided borders with edge detection; (3) pixels detection of the line which is from the beginning to the ending of the marking according to the colors; (4) confirmation of the pixels obtained by edge detection and color analysis (5) applying structural elements to the detected edge pixels; (6) point detection from the remaining pixels. The pixels which are in the marked space are detected by the color analysis and approximate edge border is determined. With the edge detection carried out in the determined area, pixel sequence of first order derivative edge border of processed object is determined. There are several algorithms used for edge detection. Two fundamental methods are used for first order derivative edge detection from these algorithms [21]. In this study, orthogonal gradient generation method for first order derivative edge detection is used (Eq.1).

$$\theta(x,y) = \tan^{-1}\left\{\frac{I_C(x,y)}{I_R(x,y)}\right\} \quad (1)$$

$$I_C(x,y) = P(x,y) - P(x+1,y) \quad (2)$$

$$I_R(x,y) = P(x,y) - P(x,y-1) \quad (3)$$

In Eq. 1, each column elements taken from the image and slope angle (θ) obtained from the row element is shown. In Eq. 2, column matrix obtained from pixel values in columns is shown. Each value of column matrix (IC) is defined as the difference between the pixel value in the scanning (P) and the value of the next pixel. In Eq. 3, row matrix (IR) is defined as the difference between the pixel value in the scanning and the previous pixel value [21]. The pixel matrixes obtained after the edge detection are shown as PKTd and PKTi matrices.

$$P_{KTd} = \begin{bmatrix} P_{Kd}(X_1,Y_1) \\ P_{Kd}(X_2,Y_2) \\ \cdots \\ \cdots \end{bmatrix} \quad , \quad P_{KTi} = \begin{bmatrix} P_{Ki}(X_1,Y_1) \\ P_{Ki}(X_2,Y_2) \\ \cdots \\ \cdots \end{bmatrix}$$

The size of *nx1* edge matrix (P_{KTd}) obtained from edge detection and the size of *nx1* hole matrix (P_{KTi}) done for edge-hole are shown in Eq. 4. Where, P_{Kd} represents the pixel points obtained by edge detection for the outer edge and P_{ki} represents the pixel points obtained by inner edge detection. Edge pixels, which are obtained by edge detection from the outer and inner edges, are stored in the system to compare with the pixel values which will be obtained along with the line of reference point. Other groups of pixel are obtained along with the line beginning and the end of the reference points. This line is applied for the inner and outer edges as in the edge detection. The application is done the way that each marked point follows the next point along with the observed line and obtained pixel values are stored in the matrix (P_{KHd}, P_{KHi}).

$$P_{KHd} = \begin{bmatrix} P_{Hd}(x_1,y_1) \\ P_{Hd}(x_2,y_2) \\ \cdots \\ \cdots \end{bmatrix} \quad , \quad P_{KHi} = \begin{bmatrix} P_{Hi}(x_1,y_1) \\ P_{Hi}(x_2,y_2) \\ \cdots \\ \cdots \end{bmatrix}$$

Where, P_{Hi} is expressed as inner edge pixel point marked on the inner hole line. The pixels, which are obtained through reference points marked from the outer and inner edges, are stored in the system temporarily as in the edge detection. Other pixels, which are not detected by edge detection, are covered with line detection and the pixels, which are on the slope of edge aren't detected by line detection, are detected by edge detection. The pixels detected for outer and inner edges by edge detection are compared with the pixels detected for outer and inner edges along the line. When this comparison is done with each other line by line, pixel verification is finished. Missing pixels are covered with this verification. As a result of this integration, the starting point and end point, two types of pixel appear along with the line as inner and outer as shown in the following matrices.

$$P_d = \begin{bmatrix} P_d(x_1, y_1) \\ P_d(x_2, y_2) \\ \dots \\ \dots \end{bmatrix} \quad , \quad P_i = \begin{bmatrix} P_i(x_1, y_1) \\ P_i(x_2, y_2) \\ \dots \\ \dots \end{bmatrix}$$

Where, P_d is expressed as the combination of the pixel obtained from the edges along with the edge detection and edge line, P_i is expressed as the combination of the pixels obtained from the inner edges along with the edge detection and edge line. New pixel points, which are attained by combining the pixels obtained by edge detection and line detection, contains unwanted pixel points due to their brightness differences arising from color and light in the image. The parts containing pixel points which are unwanted and which have gone out of the line cause disturbances on the surface of the work piece in part modeling. To prevent this kind of deformation is necessary to eliminate such pixels, and unwanted pixel points are removed with implementation of structural element (fig. 4). This structural element is panned from the marked starting point to the last reference point of the detected line. Panning process is applied separately to the pixels obtained from the outer edge and the pixels obtained from the inner edge in their own group. During panning process, pixels which are on the structural element's parts specified with '0' are removed and the pixels which are on the '1' are left (fig.5).

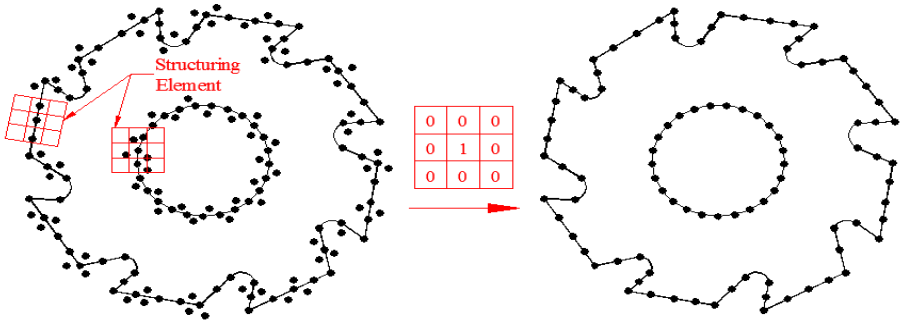

Figure 5: Implementation of the structural element

In fig (5), implementation of the structural element to the combination of the outer and inner pixels obtained by edge detection along with the reference line. With the implementation of the structural element, the last pixel line is obtained. In this way, irregularity formed by the pixels along the line is eliminated. With the elimination of the unnecessary pixels on the outer (P_d) and inner (P_i) pixel matrixes, inner pixel matrix (P_i) is added the way that it will continue under the last line element of the outer pixel matrix (P_d). With the addition of two matrixes to each other, general pixel points are obtained for edge-hole model ($P_{(X,Y)}$).

$$P_{(X,Y)} = \begin{bmatrix} P(X_1, Y_1) \\ P(X_2, Y_2) \\ \dots \\ P(X_n, Y_n) \end{bmatrix}$$

In Eq.7, pixel points obtained by applying structural element are shown in the matrix. $P_{(X,Y)}$ is the expression of combination of outer and inner pixel matrixes as one under the other. In Eq.10, X and Y values of the pixel points having X and Y values expressed lastly are obtained and coordinate matrices are created separately ($X_{(coor)}$ and $Y_{(coor)}$).

$$X_{(coor)} = \begin{bmatrix} X_1 \\ X_2 \\ \dots \\ X_n \end{bmatrix} \quad , \quad Y_{(coor)} = \begin{bmatrix} Y_1 \\ Y_2 \\ \dots \\ Y_n \end{bmatrix}$$

These obtained $X_{(coor)}$ and $Y_{(coor)}$ matrices are stored in the system temporarily to be combined with *Z* coordinates which will be obtained from the side view of the object. Two reference points obtained from the side view determine the quality of the pixel detection (fig. 6).

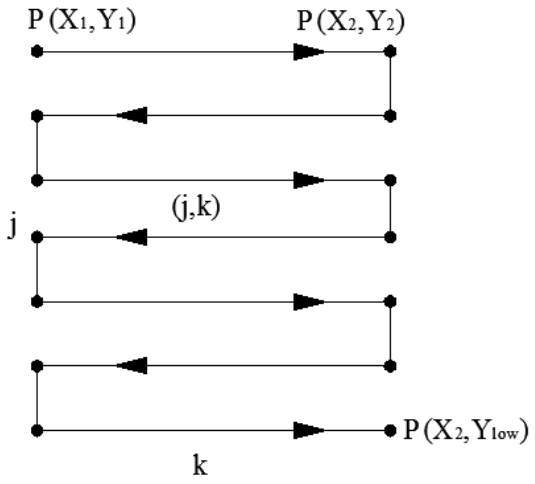

Figure. 6: Pixel detection in side view for edge and hole model

Applied pixel detection in side view for edge and hole model is shown in fig. (6). As in the front view, color analysis is performed to provide information about the edge of the part in side view. This color analysis starts from the first marked $P(X_1, Y_1)$ point, continues within the borders of the second $P(X_2,Y_2)$ point and continues to the sub-reference point of $P(X_2,Y_{Low})$ in side view. Y_{Low} is the bottom *Y* value of reference point detected in the front view. The pixel points which are obtained from the *(jxk)* sized analysis area which is determined with the marked two points and pixel points from view as reference is shown in the bellowing matrix.

$$P_{(Z)} = \begin{bmatrix} (X_1,Y_1) & . & . & (X_2,Y_2) \\ . & . & . & . \\ . & . & . & . \\ . & . & . & (X_2,Y_{Low}) \end{bmatrix} \Rightarrow \; Y_1 = Y_2$$

The area which is between two reference points marked in the side view for edge-hole model, and the *Z* value of the pixels, which are detected between this area's edges detected by color analysis and represented with '*P*', are determined. As in the previous pixel detections, the pixel points acquired from these processes are expressed in the form of matrix. While the scanning in horizontal is done for each X value, the scanning in the vertical is the each projection distance of the points in vertical obtained in the front view. In this way pixel points, which are acquired in vertical, have consistent and homogeneous distribution with the pixel points in the front view. Each pixel points obtained in the side view are represented with *X* and *Y* values. Each *X* value detected from these values is taken as *Z* value. In other words, each *X* pixel point obtained in the side view is actually *Z* pixel point as shown in the following matrix;

$$Z_{(coor)} = \begin{bmatrix} Z_{(j,k)} & . & . & . \\ . & . & . & . \\ . & . & . & . \\ . & . & . & . \end{bmatrix} \Rightarrow \begin{matrix} j_{first} = Y_1, \quad j_{end} = Y_{lower} \\ k_{first} = X_1, \quad k_{end} = X_2 \end{matrix}$$

This obtained *Z* value is combined with *X* and *Y* coordinates value obtained in the side view and converted to a single matrix form (*X, Y, Z*).

$$X,Y,Z = \begin{bmatrix} X_{(n,1)} & Y_{(n,2)} & Z_{(j,k)} \\ . & . & . \\ . & . & . \\ . & . & . \\ (n,1) & (n,2) & (n,3) \end{bmatrix}$$

X, *Y* and *Z* coordinate values obtained for edge-hole models are shown in the form of matrix. The points obtained in the front view as 'n', and each *Y* value of these points indicate the number of rows of *Z* coordinate values. In the system, for each element of *X*, *Y* and *Z* coordinates combined in a matrix form, .txt file is written separated by commas. With the writing process, coordinates are transferred to the file. Processing of images and obtaining points are based on the algorithms of edge-hole model. If the processed area is between edge and hole of sample pieces which have edge and hole elements, program uses the surface-area model algorithm.

Surface-Area Model

Surface-area model is an algorithm which processes surface area of front view of pieces and which is used to obtain point cloud from this area. It is completely based on a superficial structure and obtains surface points from the front and back view of the processed piece. In surface area processing, edge detection is not done, and marking line is done randomly between the points marked with pixel detection. The pixels, which are obtained by color analysis done during the processes in the edge-hole model, are used in this model (fig.7).

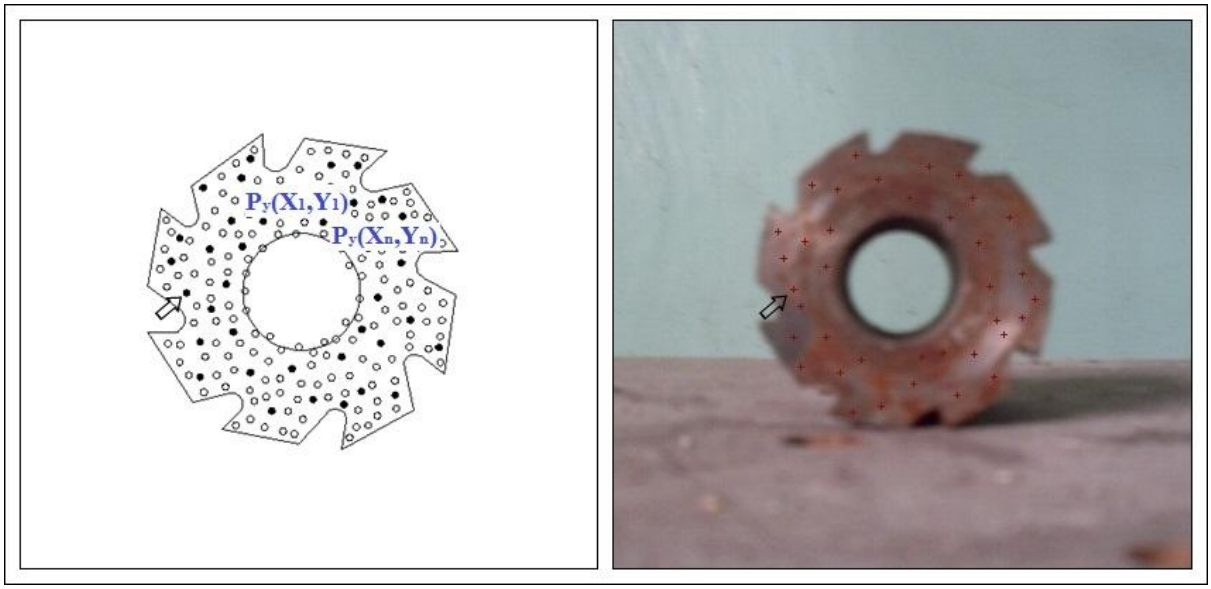

Figure 7: Pixel distribution in the processed image and surface area models

In fig. (7), the marked reference points for surface-area model are shown together with the distribution of pixels. P_y (X_1, Y_1) reference points are shown where filled point are marked as much as the number of P_y (X_n,Y_n) to represent the object the best. The other hollow points are the pixel points detected by color analysis. As in the objects having inner elements as hole, pixel detection is made in the hole. The area, where point detection is made, is the area between inner hole edges (fig.7). For this reason, reference points marked for surface area should be able to indicate and express the analysis area. Reference points identify the area which will be examined. The system acquiring reference points puts these points to the neighboring pixels, which are detected by color analysis the closest to these reference points. In this way, the pixel points acquired from reference points, and color analysis are determined in the following matrix.

$$P_y(X,Y) = \begin{bmatrix} P_y(X_1,Y_1) \\ P_y(X_2,Y_2) \\ \cdots \\ P_y(X_n,Y_n) \end{bmatrix}$$

In Eq.12, reference points marked on the surface area and the pixel points which are taken as neighbor to these reference points are shown. Neighbor pixels taken with these reference points can be included within the borders of hole in the pieces where internal elements such as hole are available (fig.7). The point cloud taken in such cases, cannot define the object exactly because of the possible pixel overflows and hence modeling is corrupted. Therefore, structural element is applied to the obtained pixel points as in edge-hole model. With this applied structural element, unwanted pixels are eliminated (fig.8).

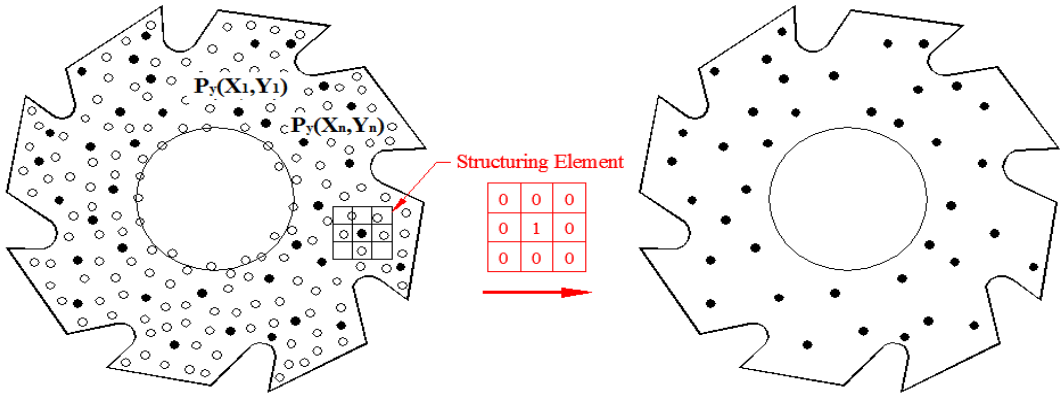

Figure. 8: Applying structural element to the obtained surface pixels

In fig. (8), reference points and pixel distribution before and after the structural element applied to the neighbor pixel of reference points are shown. Panning structural element on the curved and different formed objects is difficult. Therefore, cleaning unnecessary surface pixels from these different edge structured objects is performed by panning marked reference points of structural element. This panning process is done for each reference point. In this way, unnecessary pixels are removed from the image and pixel points from the first stage are simplified. Coordinate values are obtained by taking each *X* and *Y* points from the simplified pixel point matrices ($X_{y(coor)}$, $Y_{y(coor)}$).

$$X_{y(coor)} = \begin{bmatrix} X_{y1} \\ X_{y2} \\ \dots \\ X_{yn} \end{bmatrix} \quad , \quad Y_{y(coor)} = \begin{bmatrix} Y_{y1} \\ Y_{y2} \\ \dots \\ Y_{yn} \end{bmatrix}$$

X and *Y* coordinate values of pixel points obtained from surface-area model are shown in the matrix. With the removed pixels, *X* and *Y* values of simplified pixel point matrix are defined as 'n' in the different matrixes. Surface-area model uses the two reference points taken from side view for *Z* coordinate value (fig. 9).

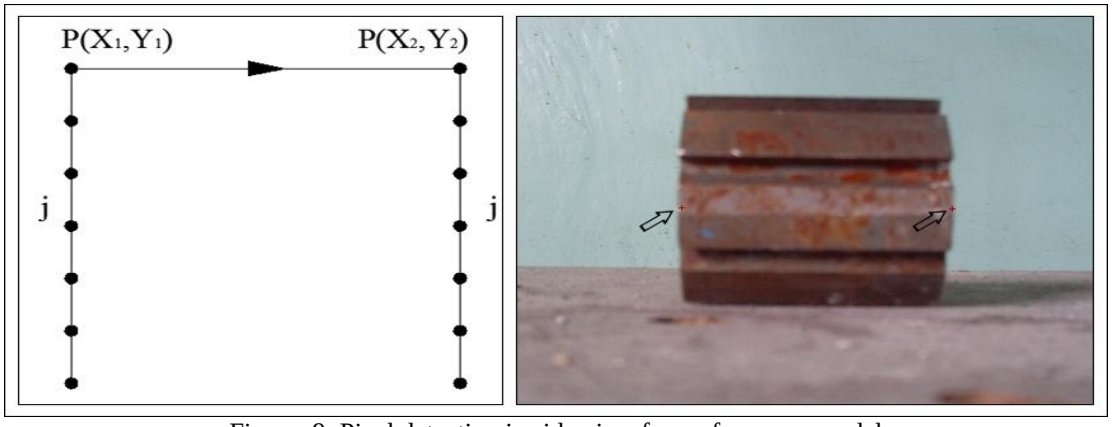

Figure. 9: Pixel detection in side view for surface-area model

In fig. (9), pixel detection for side view in surface-area model is shown after the reference point marked on the image. For side view, two types of *Z* value are determined. The first *Z* value is as X_1 and this X_1 value is also coordinate value of front view of the piece and is accepted as 0. Regardless of the pixels between two reference points marked for side view in the second *Z* value, the distance from X_1 to X_2 are taken. In this way, the pixels belonging to surface area detected in the front view of the piece are determined for the back side at the same time. These obtained Z values are added to X and Y values obtained from the front view, so point matrix is obtained as X_y, Y_y, Z_y matrix form.

$$X_y, Y_y, Z_y = \begin{bmatrix} X_{y(n,1)} & Y_{(n,2)} & a \\ . & . & . \\ . & . & . \end{bmatrix} \Rightarrow a = X_2 - X_1$$

In the Eq. 14, coordinate values, which are obtained from surface areas, are shown. '*a'* is the difference between two *X* values marked in the side view. The first *Z* value is as 0, and the second *Z* value is as '*a*'. The first *Z* is added to each *X* and *Y* coordinate values and obtained point number is written down one under the other in the matrix. Again, the same *X* and *Y* values are expressed with the second *Z* value, and it is added under the first written values, and matrix is maintained. *X* and *Y* coordinate values obtained from the front view; these binary values (X_2-X_1) are used and these values are taken in a matrix by combining one under the other and so *X*,*Y* and *Z* coordinate values are obtained. These points obtained by the surface-area model are combined with the points acquired from the edge-hole model and point cloud of processed object is achieved (fig.10).

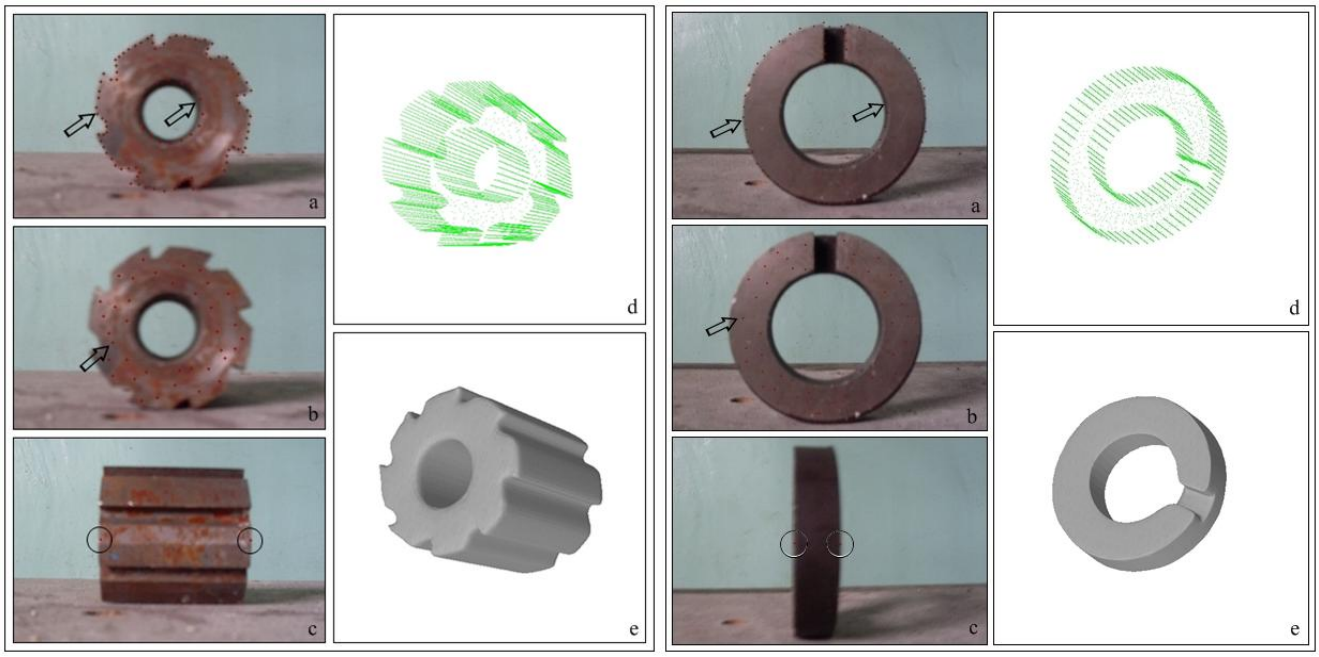

Figure 10: Obtaining point cloud and solid model; a. Front view edge-hole model, b. Front view surface-area model, c. General reference points for side view, d. Point cloud, e. Solid model

In fig. (10), reference points marked by the user on the image are specified, after processing the image acquired point clouds are shown with their solid models. Solid models are generated through a computer aided design program by using obtained point clouds.

IV. RESULTS AND DISCUSSION

In the developed image processing system, images taken with a digital camera in an ordinary environment without the need for calibration are evaluated easily. With the algorithms developed for evaluating the image, point clouds of many pieces, which are expressed in two appearances from simple to complex, are can be obtained. The number of marked reference points may vary depending on the marked images. This case is proportional with the number of edge and hole of the processed target object. If the number of marked reference point is too much, this shortens the time process of the system. After reference points are marked, the elapsed time to obtain 3D point clouds is not more than 4 seconds.

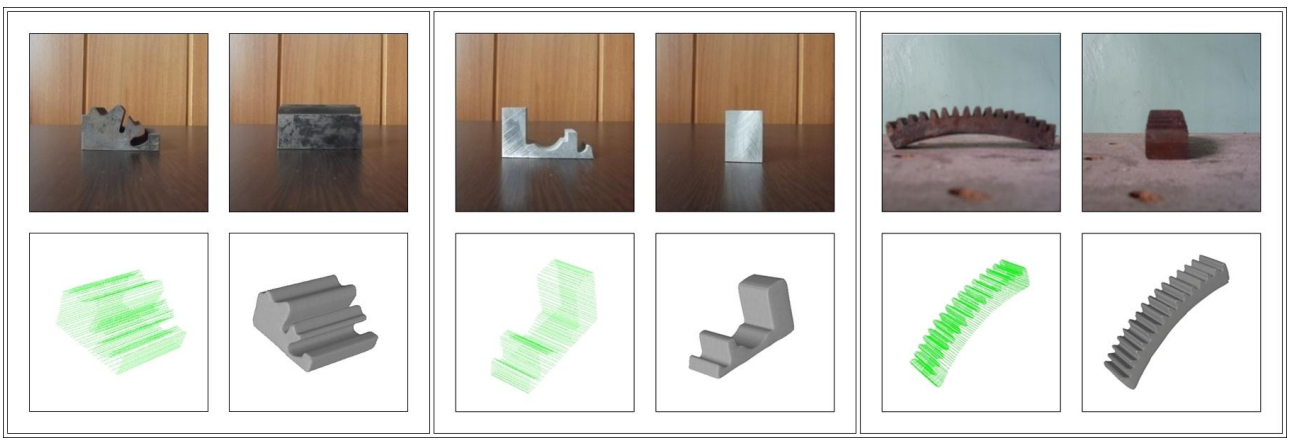

Figure11: Point clouds obtained from the images not containing element of hole and their solid models

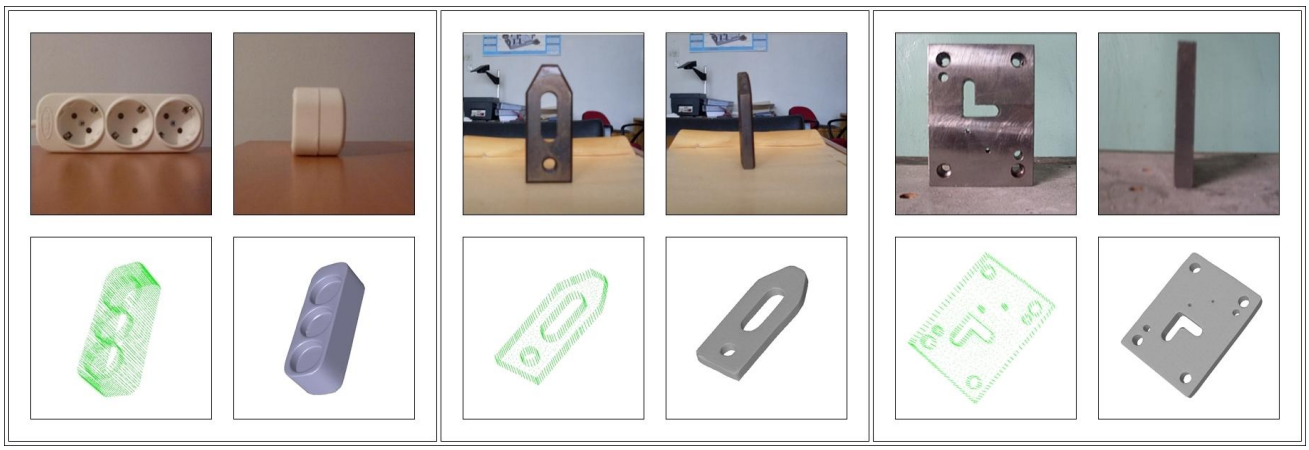

Figure 12: Point clouds obtained from the images containing element of hole and their solid model

The processed sample images and obtained point clouds are shown with their solid models in fig. (11) and fig. (12). The elapsed time to remove the point clouds is between 2-4 seconds. Sample images were taken in natural light environment and were taken by placing on a flat surface. The system can detect the elements of the area which will be processed as on and off, and it evaluates the images by using reference points, color analysis and developed algorithms. In many studies where image processing and interpreting digital images are available, special shooting environment and calibration for the camera are used [22]. Camera calibrations are made by using such techniques as grid projection, markers placed on the target objects [23]. At the same time, markers are one of the helper tools used in non-contact systems which is a Reverse Engineering application. In other studies, object libraries are formed for the target object so that the objects in the images can be identified. In evaluating and comparing similar form of objects, object libraries are frequently used [4]. In addition, edge detection algorithms are used to determine the target object as 2D [24]. In this study, to obtain 3D point cloud of objects, such engineering environment as calibration, taking pose, monitoring systems and positional markers are not required.

V. CONCLUSION AND FURTHER WORK

In developed program, effective use of elapsed time, which is for design and manufacturing, reduces costs in an effective way. One of the main reasons for the use of reverse engineering applications, it shortens the design process. The studies intended to shorten the time spent on the design stages of products will affect manufacturing process in an efficient way. The advantages provided by the developed system are as follows:

- In the program, point clouds can be achieved from the simple, and complex structured pieces
- The pieces, which will be designed in the computer environment or manufacturing operation, will be applied, are transmitted more quickly into the design environment with developed system. If desired computer-aided static, dynamic analysis procedures and manufacturing processes can be performed. In addition, obtained model can be loaded to rapid prototyping machines and prototype of the object can be obtained.
- Images with different resolution are used in the program and obtained point clouds express the target object in the image fully.
- In developed program, with the use of reference point method, image interpreting area is limited and only by processing the target area, undesirable point clouds, which are formed by the elements of background of the image, are removed. This reduces the processing time to 2-4 seconds, and at the same time, it enables the images taken to be processed in the program faster.

The new modules can be added to the program and with the developed new algorithms, processing the images expressed in more appearances and having more complex geometry can be achieved. The image processing technique, in which developed algorithms and color analysis are used, will be beneficial for the future studies in this field. The images processed in the program do not have resolution limit, so it will allow to processing the high-resolution images in parallel with technology. Next study target is to obtain 3D point clouds from completely cylindrical and curvilinear structured and more complex object images by adding a new module to the developed software.

References

[1] V. Raja, Introduction to reverse engineering, in V. Raja and K.J. Fernandes (Eds.), Reverse engineering an industrial perspective, (London: Springer, 2008) 1-9.
[2] S. Motavalli and R. Shamsaasef, Object-oriented modeling of a feature based reverse engineering system. Int J Comp Integ Manufac, 9(5), 1996, 354–368.
[3] R. Clouard, A. Renouf and M. Revenu, Human-computer interaction for the generation of image processing applications, Int J Human-Comp Studies, 69, 2011, 201-219.
[4] L. Hua and W. Weiyu, A new approach to image-based realistic architecture modeling with featured solid library. Auto in Const 13, 2004, 555-564.
[5] G. Zhou, Primitive recognition using aspect-interpretation model matching in both CAD and LP based measurement systems, ISPRS J of Photog and Rem Sensing 52, 1997, 74-84.

[6] D. Frere, J. Vandekerckhove, T. Moons and L. Van Gool, Automatic modeling and 3D reconstruction of urban buildings from aerial imagery, IEEE Int Geoscience and Rem Sensing Symp Proc, Seattle, 1998, 2593-2596.
[7] A. Huertas, R. Nevita and D. Landgrebe, Use of hyperspectral data with intensity images for automatic building modeling, Proc of the Sec Int Conf on Inf Fusion, Sunnyvale, 1999, 680-687.
[8] G. Bleser, Y. Pastarmov and D. Stricker, Real-time 3D camera tracking for industrial augmented reality applications, J of Winter Sch of Compt Graphics, 2005, 47–54.
[9] R. Azuma, A survey of augmented reality, Computer Graphics SIGGRAPH Proc, 1995, 1-38.
[10] U. Bockholt, A. Bisler, M. Becker, W.K. Müller-Wittig and G. Voss, Augmented reality for enhancement of endoscopic interventions, Proc IEEE Virtual Reality Conf , Los Angeles, 2003, 97-101.
[11] S. Wesarg, E. Firle, B. Schwald, H. Seibert, P. Zogal and S. Roeddiger, (2004) Accuracy of needle implantation in Brachtherapy using a medical AR system-a phantom study, SPIE Medical Imaging Symp, USA, 2004, 341-352.
[12] L. Song and and D. Wang, A novel grating matching method for 3D reconstruction, NDT & E Int, 39, 2006, 282-288.
[13] Z. Xie , J. Wang and Q. Zhang , Complete 3D measurement in reverse engineering using a multi-probe system, Int J of Mach Tools Manuf , 45, 2005, 1474-1486.
[14] L. Song , X. Qu, K. Xu and L. Lv, (2005) Novel SFS-NDT in the field of defect detection, NDT&E Int., 2005, 38:5 381-386.
[15] L. Song , X. Qu, Y. Yang, C. Yong and S. Ye, (2005) Application of structured lighting sensor for online measurement, Opt and Laser in Eng, 43,10, 2005, 1118-1126.
[16] A.P. Witkin, Scale-space filtering. Proc of 8th Int Joint Conf Art Intel Karlsruhe, Germany, 1983, 1019–1022.
[17] T. Lindeberg, Scale-space for discrete signals, IEEE Trans Patt Recog Mach Intel 12, 1990, 234–254.
[18] B.R. Barbero and E.S. Ureta, Comparative study of different digitization techniques and their accuracy, Computer Aided Design, 43, 2011, 188-206.
[19] F. Bosche, Automated recognition of 3D CAD model objects in laser scans and calculation, Adv. Eng. Informatics, 24, 2010, 107-118.
[20] W-B. Yang, M-B. Chen and Y-N Yen, An application of digital point cloud to historic architecture in digital archives, Advn in Eng Soft, 42, 2011, 690-699.
[21] W.K. Pratt, Digital image processing, A Willey-InterScience, New York, 1991, 490-530.
[22] K. Lee, K. Wong , S.Y. Fung, (2001) 3D face modeling from perspective-views and contour based generic model, Real-Time I, 7, 2001, 173-182.
[23] L. Song and D. Wang, A novel grating matching method for 3D reconstruction. NDT & E Int., 39, 2006, 282-288.
[24] D. Tubic, P. Hébert , D. Laurendeau , 3D surface modeling from curves, Img and Vis Comp 22, 2004, 719-734.

International Journal of Modern Engineering Research (IJMER)
www.ijmer.com Vol.3, Issue.2, March-April. 2013 pp-832-838 ISSN: 2249-6645

Experimental Investigation of Performance Parameters of Single Cylinder IC Engine Using Mustard Oil

Gaurav Sharma, [1] DevendraDandotiya, [2] S. K. Agrawal[3]
[1]*M.Tech Student (Thermal System & Design), SRCEM, Banmore*
[23]*Asst.Prof Mechanical Engineering, SRCEM, Banmore*

***Abstract*:** *The conversion of biomass to energy (also called bio energy) encompasses a wide range of different types and sources of biomass, conversion options, end user applicationsand infrastructure requirements. Mustard oil biodiesel performed very well in vehicles. Fuel consumption increased compared to fossil diesel because biodiesel has slightly less energy per gallon than diesel fuel. The fuel filter had to be changed more often compared to what would normally be experienced with petroleum diesel. This may have been because the fuel filter material did not hold up well with biodiesel. This is due to the combined effects of the fuel density, viscosity and lower heating value of blends. It is observed that dual biodiesel blends BB 10 and BB 20 shows closer BSFC values with diesel than other dual biodiesel blends.*

Keywords: *Biodiesel, IC Engine, Methanol, Mustard Oil*

I. Introduction

India ranks sixth in the world in the term of energy demand accounting for 3.5 % of world commercial energy demand. It is expected to grow at 4.8%. The growth in energy demand in all forms is expected to continue unabated owing to increasing urbanization ,standard of living and expanding population with stabilization not before mid of the current century .

The demand of diesel (HSD) is projected to grow from 52.33 millions of tons in 2006-07 to 61.55 millions of tons in 2009-10. Our crude oil production as per the tenth plan working group is estimated around 33-34 million metric tons per annum. The import bills are rising to $ 15.7 billion or so which is a huge amount for a country like ours. Consumption of diesel can be minimized by implementing biodiesel program expeditiously. [1]

The potential of bio-diesel production from mustard oil have been found to be a promising fuel for diesel engine in a number of studies [2].Mustard (Brassica juncea) is a widely growing seed in Rajasthan, Madhya Pradesh Uttar Pradesh, Haryana, Punjab in India. Many countries consider mustard oil as unsuitable for human consumption as it has a high content of a substance known as Uric Acid which is harmful to the body. Mustard plant is characterized by yellowish green leaves and round stems with long inter-nodes. The grayish brown seeds are tiny and round in shape and on reacting with water emit a strong smell. It is generally used in cooking.[4]

II. Biodiesel

Bio-diesel consists of mono alkyl esters produced from vegetable oils, animal or old cooking fats. Bio-diesel contains no petroleum diesel, but it can be blended with petroleum diesel**.** Mono-alkyl esters of long chain fatty acids (biodiesel) is a promising substitute of petro diesel fuel that can be produced from natural, renewable resources such as wide variety of vegetable oils and animal fats. These resources are biodegradable and nontoxic. The term, biodiesel, was first introduced in the United States during 1992 by the National Soy development Board (presently National Biodiesel Board), which has pioneered the commercialization of biodiesel in the USA [3].

- Bio-diesel is a clean burning fuel
- Bio-diesel does not have any toxic emissions like mineral diesel
- Bio-diesel is made from any vegetable oil such as Soya, Canola, Palm, Coconut, mustard, peanut or from any animal fat like Lard or Tallow.
- Bio-diesel is a complete substitute of Mineral diesel.

III. Organic Chemistry

The major components of vegetable oils are triglycerides. Triglycerides are esters of glycerol with long-chain acids (fatty acids). The composition of vegetable oils varies with the plant source. The fatty acid profile describes the specific nature of fatty acids occurring in fats and oils. The chemical and physical properties of fats and oils and the esters derived from them vary with the fatty acid profile. Trans-esterificationis the process where an alcohol and an ester react to form a different alcohol and a different ester. For bio-diesel, an ethyl ester reacts with methanol to form a methyl ester and ethanol. These ethyl esters react with methanol to form bio-diesel and glycerol. As mentioned above, the purpose of transesterification is to reduce the viscosity of the oil. [5]

The Vegetable oils are extracted from crude oil. Therecrude oil usually contains free fatty acids (FFA), water, sterols, phospholipids, odorants and impurities. Its cancause numerous problems in diesel engines. It alsoincreased viscosity, low volatility and poor cold flowproperties. They lead to severe engine deposits, injectorcoking, piston ring sticking etc. Bio-diesel may beproduced by following four ways: Pyrolysis, Microemulsification, Dilution and Transesterification.[6]

In the present work Transesterification process is used toprepare bio-diesel from mustard oil. It is the process ofusing an alcohol (e.g. methanol, ethanol or butanol), inthe presence of a catalyst, such as sodium hydroxide orpotassium hydroxide, to break the molecule of the rawrenewable oil chemically into methyl or ethyl esters of therenewable oil, with glycerol as a byproduct. Transesterificationreaction for vegetable oil

.

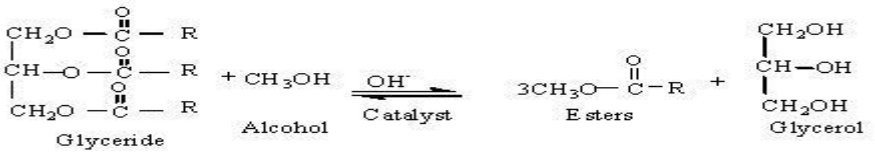

IV. Cost Estimation Of Bio-Diesel

- NaoH 150ml 0.20 (Sodium Hydroxide)
- Methanol 250ml 25 Rs.
- Mustard oil 1 lit. 85 Rs.
- Electric heater 1
- Jar 1
- Thermometer 1

V. Preparation Of Bio-Diesel From Mustard Oil

For the transesterification of mustard oil, Dr. Peeper's style has been followed in our work [7, 8]. First 250 ml (90% pure) methanol was mixed with 150 ml (1 N) NaOH. This mixture was swirled in a glass container until NaOH is fully dissolved in methanol. As this is an exothermic reaction, so the mixture would get hot. This solution is known as meth oxide, which is a powerful corrosive base and is harmful for human skin. So, safety precautions should be taken to avoid skin contamination during meth- oxide producing [9-14].

Next, meth oxide was added with 1 liter of mustard oil, which was preheated about 55 degrees Celsius. Then the mixture was jerked for 5 minutes in a glass container. After that, the mixture was left for 24 hours (the longer is better) (Figures 1) for the separation of glycerol and ester. This mixture then gradually settles down in two distinctive layers. The upper more transparent layer is 100% bio-diesel and the lower concentrated layer is glycerol. The heavier layer is then removed either by gravity separation or with a centrifuge. In some cases if the mustard oil contains impurities, then a thin white layer is formed in between the two layers. This thin layer composes soap and other impurities.Bio-diesel produced in the above process contains moisture (vaporization temperature 100 degree Celsius) and methanol (vaporization temperature 60 degree Celsius) and usually some soap. If the soap level is low enough (300 ppm - 500 ppm), the methanol can be removed by vaporization and the methanol will usually be dry enough to directly recycle back to the reaction. Methanol tends to act as a co-solvent for soap in biodiesel; so at higher soap levels the soap will precipitate as a viscous sludge when the methanol is removed. Anyway, heating the biodiesel at temperature above 100 degree Celsius would cause the removal of both the moisture and methanol as well. In our study, food grade quality mustard oil was used, other than raw mustard oil to ensure that the vegetable oil contains lesser impurities.

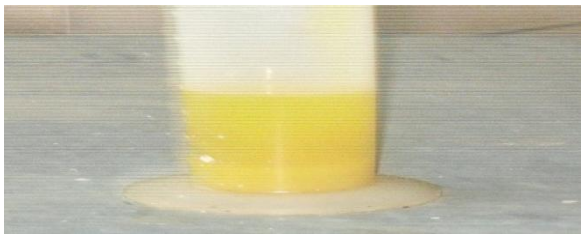

FIG: 1

Table: 1. PROPERTIES OF BIO-FUEL BLENDS, MUSTARD OIL AND BIO- DIESEL

Properties and Standards	Unit	B10	B20	B30	B40	B50	B100	Diesel
Density 35°C (ASTM D4052-11)	kg/m^3	832.2	838.2	840.9	851.6	860.1	880.2	826.2
Specific Gravity (ASTM D5453-09)		0.872	0.899	0.906	0.912	0.918	0.941	0.901
Kinematic Viscosity (ASTM D2161-79)@35°C	mm^2	4.534	5.5918	11.528	11.891	11.982	24.982	3.87
Dynamic Viscosity (ASTM D7042-11a)@35°C	cP	4.056	4.685	9.678	9.857	10.347	22.264	3.34
Calorific Value (ASTM 2382)	MJ/kg	43.12	42.68	42.15	42.09	41.94	39.45	44
Flash Point (ASTM D93-85)	°C	74	78	83	98	111	296	72
Fire Point (ASTM D92-11)	°C	82	95	106	115	130	345	211

VI. Description Of Experimental Setup

FIG: 2

The experimental setup (**Figure 2**) consisted of engine test bed with fuel supply system and different metering and measuring devices with the engine. A water brake dynamometer was coupled with the engine. Load was varied by means of flow control of the dynamometer. Fuel was supplied from an external source. Preheating of fuel was done manually by gas burner. B40 blend was pre- heated at 55°C and B50 blend was preheated at 60°C. However B100 was not possible to use directly in the engine as it causes excessive vibration. Engine speed was measured by digital tachometer. Lube oil temperature and exhaust gas temperature was measured by platinum-type thermocouple. Operating condition of the engine is given in **Table 2.**

TABLE: 2 TECHNICAL SPECIFICATION OF THE ENGINE

Sr. no.	Items	Specifications
1	Model	KIRLOSKAR, AV1
2	Compression ratio	19:1
3	Method of starting	Hand starting
4	Type, no. of cylinders	Vertical – 4 stroke, 1 cylinder
5	Bore x stroke(mm)	87.5x110
6	Cubic capacity	624
7	Maximum power	5 Hp
8	Nominal speed	1500 rpm
9	Cooling system	Water-cooled
10	Fuel filter	Present
11	Lube oil filter	Present

TABLE 3.ENGINE OPERATING CONDITIONS.

Engine Speed	1500
Engine load	1 kg to 7 kg
Fuel Tested	100% diesel, B10, B20, B30, B40 and B50
Lube oil used	SAE 40

VII. Equipments Used For the Experiment

- Single - cylinder four stroke diesel engine,
- Tachometer
- Stop watch
- Bio-diesel
- Diesel
- Plastic Jar
- Nob

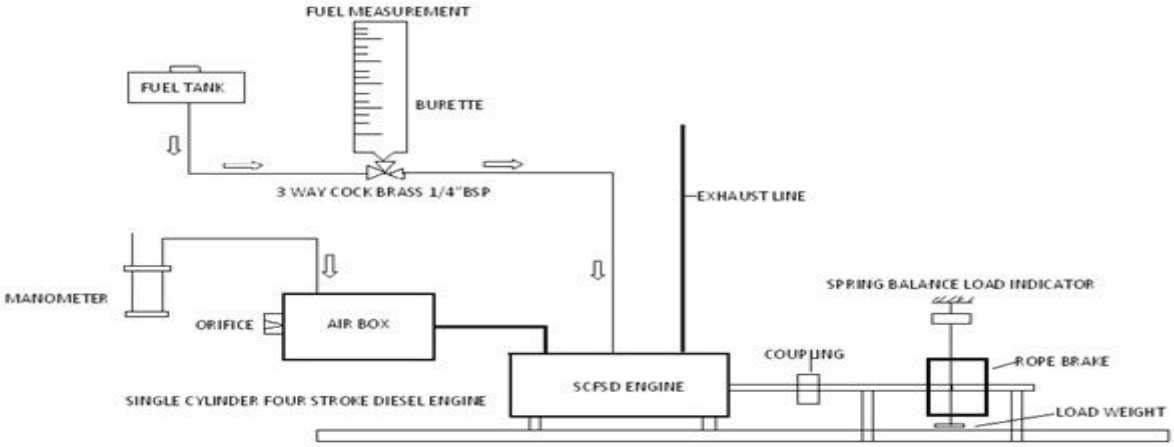

FIG: 3 BLOCK DIAGRAM OF SINGLE CYLINDER FOUR STROKE DIESEL ENGINES

VIII. Results & Discussion

The experiments were conducted using each fuel sample thrice and performance of the engine was evaluated using several parameters such as thermal efficiency, brake specific fuel consumption, exhaust gas temperature, nitrogen oxides and smoke opacity. Brake specific fuel consumption (BSFC) is a measure of volumetric fuel consumption for any particular fuel. Fig. 2 shows the BSFC for dual blended bio fuels and its blends. The engine BSFC decreased with the increase of engine loads. This is due to the combined effects of the fuel density, viscosity and lower heating value of blends. The BSFC of BB 10, BB 20, BB 30, BB 40, BB 50, are 0.765 kg/kWh, 0.325 kg/kWh, 0.338 kg/kWh, 0.341 kg/kWh, respectively whereas the diesel is 0.301 kg/kWh at the maximum load. It is observed that dual biodiesel blends BB 10 and BB 20 shows closer BSFC values with diesel than other dual biodiesel blends.

TABLE: 4 VARIATION OF BSFC WITH BP FOR DIFFERENT FUELS

0 B		10 B		20 B		30 B		40 B		50 B	
BSFC (kg/k W-hr)	BP (kW)	BSFC (kg/k W-hr)	BP (kW)	BSFC (kg/k W-hr)	BP (kW)	BSFC (kg/k W-hr)	BP (kW)	BSFC (kg/k W-hr)	BP (kW)	BSFC (kg/k W-hr)	BP (kW)
3.350	0.242	2.293	0.244	2.719	0.242	2.725	0.244	2.625	0.245	2.508	0.244
1.227	0.724	0.975	0.731	1.218	0.727	1.192	0.729	1.142	0.727	0.962	0.730
0.863	1.231	0.712	1.241	0.936	1.234	0.82	1.237	0.666	1.236	0.795	1.239
0.765	1.729	0.598	1.747	0.831	1.729	0.834	1.737	0.822	1.734	0.701	1.744

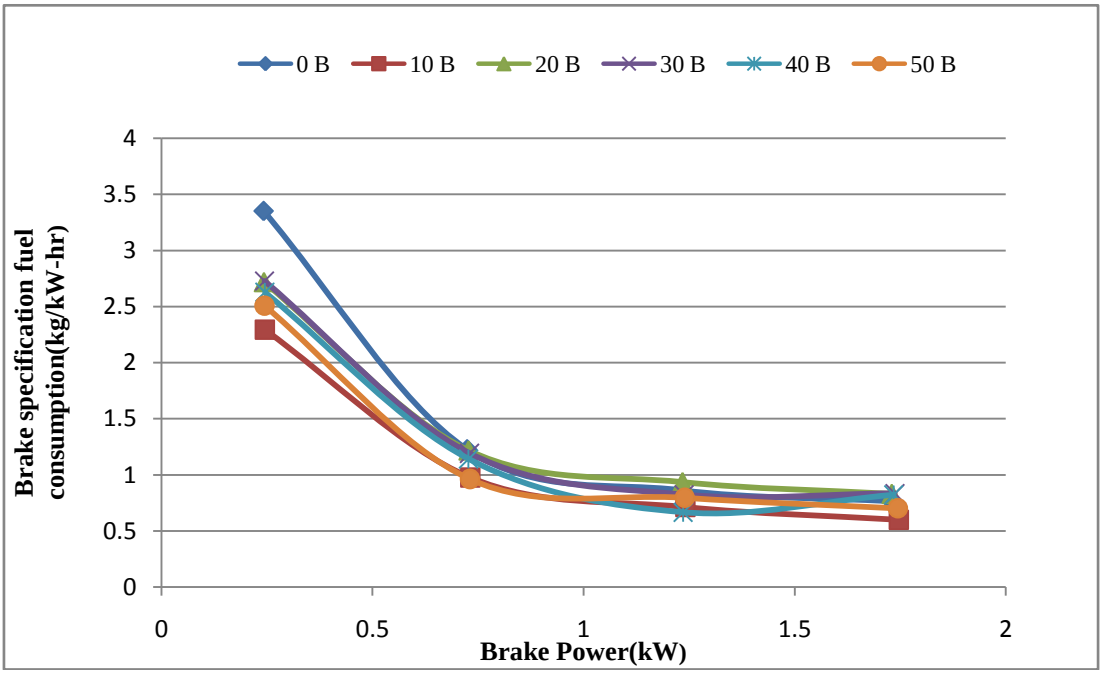

FIG: 4

FIGURES: 4. shows the variation of BSFC with BP for the different fuels. The curve shows that, Bsfc for biodiesel blends is higher at low % load. And it decreases with the increase in % load. it is also observed from the curve that, specific fuel consumption increase with the increase in biodiesel blend. This is mainly due to the relationship among volumetric fuel injection system, fuel specific gravity, viscosity and heating value. As a result more biodiesel blend is needed to produce the same amount of energy due to its higher density and lower heating value in comparison to conventional diesel fuel. Again as biodiesel blends have different viscosity than diesel fuel, so biodiesel causes poor atomization and mixture formation and thus increases the fuel consumption rate to maintain the power.

TABLE: 5 VARIATION OF THERMAL EFFICIENCY WITH BP FOR DIFFERENT FUELS

0 B		10 B		20 B		30 B		40 B		50 B	
BTE	BP(kW)	BTE	BP(kW)	BTE	BP(kW)	BTE	BP(kW)	BTE	BP(kW)	BTE	BP(kW)
2.441	0.242	3.641	0.244	3.101	0.242	3.134	0.244	3.257	0.245	3.421	0.244
6.665	0.724	8.560	0.731	6.921	0.727	7.164	0.729	7.676	0.727	8.918	0.731
9.470	1.231	11.719	1.241	9.008	1.234	9.373	1.237	10.717	1.236	10.785	1.239
10.685	1.729	13.938	1.747	10.144	1.729	10.236	1.737	12.122	1.735	12.237	1.744

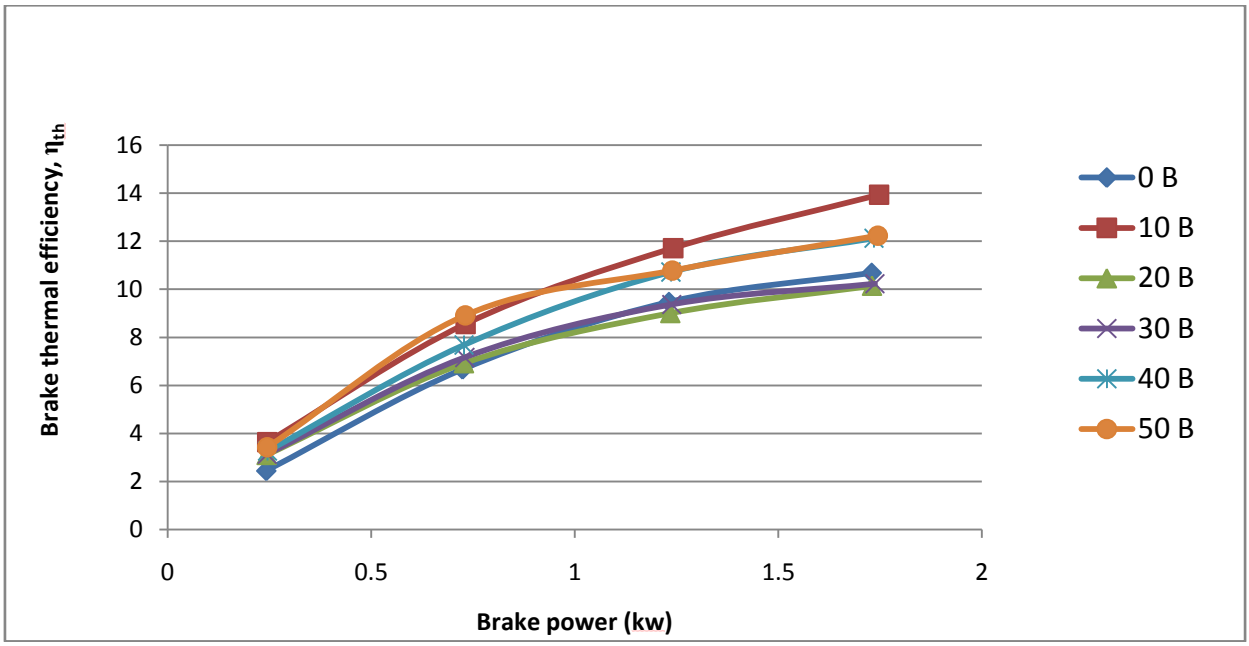

FIG: 5

Figure: 5. shows the relation in between BP and brake thermal efficiency ηb for different fuels. Bsfc is a measure of overall efficiency of the engine. Bsfc is inversely related with efficiency. So lower the value of Bsfc, higher is the overall efficiency of the engine .however, for different fuels with different heating values, the Bsfc values are misleading and hence brake thermal efficiency is employed when the engines are fueled with different type of fuels. From the figure, it is evident that Bsfc for biodiesel blends is always higher and ηb is always lower than that of diesel fuel. This is because biodiesel has lower heating value than conventional diesel fuel. One other cause for lower ηb for biodiesel blends is the poor atomization which is attributed to higher density and kinematic viscosity of biodiesel blends.

TABLE: 6 VARIATION OF EXHAUST GAS TEMPERATURE WITH BREAK POWER FOR DIFFERENT FUELS

0 B		10 B		20 B		30 B		40 B		50 B	
Temperature (°C)	BP(kW)	Temperature (°C)	BP(kW)	Temperature (°C)	BP(kW)	Temperature (°C)	BP(kW)	Temperature (°C)	BP(kW)	Temperature (°C)	BP(kW)
95	0.242	100	0.244	105	0.243	108	0.244	100	0.245	104	0.244
145	0.724	115	0.732	145	0.727	128	0.729	117	0.727	126	0.730
187	1.231	165	1.241	190	1.234	162	1.238	170	1.236	152	1.239
254	1.729	192	1.747	231	1.729	206	1.737	208	1.734	191	1.744

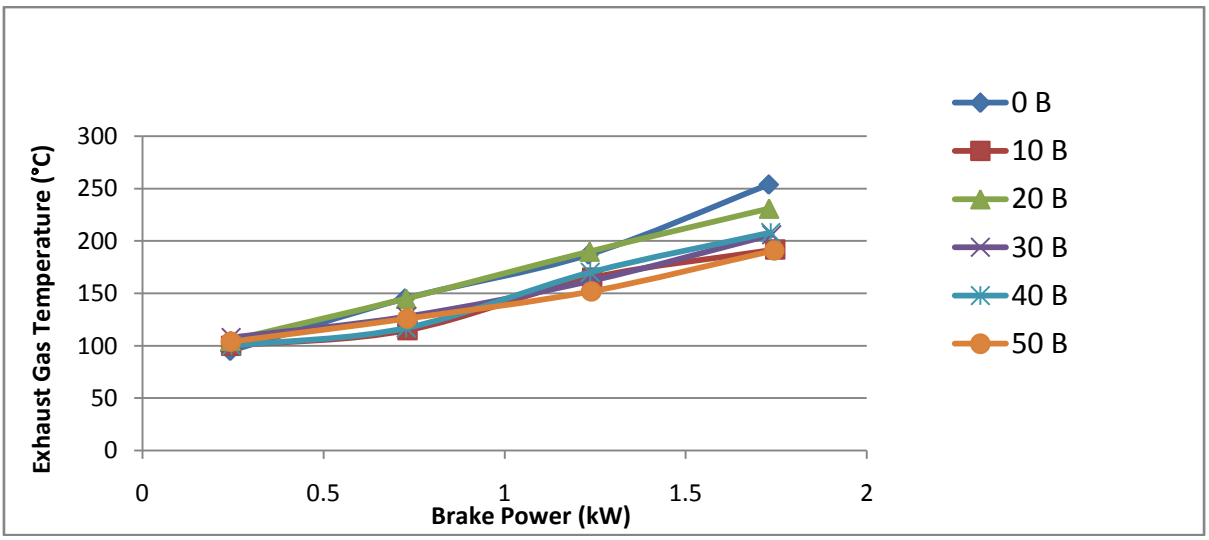

FIG: 6

FIGURE: 6. Depicts about variation in exhaust gas temperature with BP for different fuels. From the curve it is observed that except B30, all other biodiesel blends have higher exhaust gas temperature than diesel fuel. At starting condition, higher exhaust gas temperature but low power output for biodiesel blends indicate late burning to the high proportion of biodiesel. This would increase the heat loss, making the combustion a less efficient. At higher load condition, B30 and B40 have lower exhaust temperature as compared to diesel fuel.

IX. Cost of Running Engines With Different Fuels

Fuel	Cost (tk/lr)
Diesel	54
B10	57.10
B20	60.20
B30	63.30
B40	66.40
B50	69.50

The present costing for a diesel engine for bio-diesel obtained from bio-diesel are given above. It is clear from cost that diesel engine running with biodiesel is more costly as comapred to pure diesel fuel.
The present costing of running a diesel engine with bio- diesel blends derived from mustard oil are given in **Table 4.**

From **Table 4** it is clear that, running diesel engine with biodiesel blends is costly as compared to diesel fuel. However, cost can be drastically reduced, if methanol can be recycled after the Trans esterification reaction. Moreover, in our experiment we have used food grade mustard oil. And using raw or unprocessed oil would also cause to decrease the biodiesel production cost.

In India, government grants a huge subsidy on diesel fuel, which causes the lower price for diesel fuel. So a thorough study is required for the feasibility analysis of biodiesel by comparing it production cost with international market price of diesel.

X. Conclusion

- It is possible to run diesel engine with bio-diesel blends.
- In the beginning for smaller values of Brake Power and Load blended biodiesel consumption is higher than the neat diesel consumption which narrows down with higher values of brake power and load.
- BSFC values for smaller load is higher for blended bio-diesel and this gap reduces later for higher value of load.
- Brake power for neat diesel have higher values than blended bio-diesel at all loads and difference of brake power between neat diesel.
- Brake thermal efficiency is higher for neat diesel at all loads and lowers for blends of bio-diesel and difference of brake thermal efficiency between neat diesel and blended bio-diesel decreases as load increases.
- Fuel consumption is nearly same for neat diesel and blended diesel at all BMEP and have lower value at all BMEP for neat diesel.
- Bio-diesel can be produced from mustard oil using trans-esterification reaction.
- BSFC for bio-diesel increases for higher blending of bio-diesel, because of the lower heating value of bio-diesel as compared to diesel fuel.

Refrences

[1] Ministry of Petroleum and Natural gas Gazette Dated Sept 12th 2003, part 1.page 230.
[2] A. Forhad, A. R. Rowshan, M. A. Habib and M. A. Islam, "Production and Performance of Biodiesel as an Alternative to Diesel," International Conference on Mechanical Engineering, London, 1-3 July 2009.
[3] Ramadhas A. S., Jayraj S. and Muraleedharan C., Use of vegetable oils as I. C. engine fuels – A Review, Renewable Energy (2004), (29), 727-742
[4] Hasib Z. M., Hossain J., Biswas S., Islam A., 2011, "Bio-Diesel from Mustard Oil: A Renewable Alternative Fuel for Small Diesel Engine," Modern Mechanical Engineering, 1,77-83.
[5] J. Otera, "Transesterification," Chemical Reviews, Vol. 93, No. 4, 1993, pp. 1449-1470.
[6] Azad K. A. , Uddin A. M. S. , and Alam M. M., 2012, "Mustard oil, an alternative Fuel: An Experimental Investigation of Bio-diesel properties with & without trans-esterification reaction," Global Advanced Research Journal of Engineering, Technology and Innovation Vol. 1(3) pp. 075-084.
[7] R. Da Tech, "Single Stage Base Recipes", 2010. http://www.make-biodiesel.org/index.php?option=com_ctent&view=article&id=74:single-stage-base-recipes&catid=51:recipes&Itemid=96
[8] Z. M. Hasib, K. A. Rahman and S. Alam, "Prospect of Bio Diesel Production from Mustard Oil," Bachelor of Science in Engineering Project and Thesis, Bangladesh University of Engineering and Technology, Dhaka, 2010
[9] J. Van Gerpen, "Cetane Number Testing of Biodiesel," Liquid Fuels and Industrial Products from Renewable Resources—Proceedings of the Third Liquid Fuels Con- ference, Nashville, 15-17 September 1996, pp. 166-176.
[10] M. Stumborg, A. Wong and E. Hogan, "Hydro processed Vegetable Oils for Diesel Fuel Improvement," Biore- source Technology, Vol. 56, 1996, pp. 13-18. Doi: 10.1016/0960-8524(95)00181-6
[11] M. Stumborg, D. Soveran and W. Craig, "Conversion of Vegetable Oils to Renewable Diesel Additives," Presented at the 1991 International Winter Meeting of the ASAE Paper No. 911567, Chicago, 17-20 December 1991.
[12] N. M. Strete, "Evaluation of Detergency Effects of Bio-diesel Using Cummins L10 Injector Depositing Test— Cell 19," Final report from ETS to NBB, 30 September 1996.
[13] L. L. Stavinoha and S. Howell, "Potential Analytical Methods for Stability Testing of Biodiesel and Biodiesel Blends," Society of Automotive Engineering (Special Edition), USA Paper No. 1999-01-3520, 1999, pp. 73-79.
[14] H. Stage, "Principle of the New ATT-Process for Converting Vegetable Oils to Diesel Fuels," ZeitschriftfürWissenschaft und Technologie der Fette, Öle und Wachse, Vol. 90, No. 1, 1988, pp. 28-32.
[15] Rattan R., Kumar M., 2012, "Biodiesel production from mustard oil and its performance on domestic small diesel engine," International Referred Research Journal, February,2012.ISSN-0975-3486,RNI-RAJBIL 2009/30097;VoL.III, Issue-29.
[16] Datta A., Mandal K. B., 2012, "Biodiesel productions & its Emissions & Performance: A Review", International Journal of Scientific & Engineering Research Volume 3, Issue 6.
[17] Prasad L., Agarwal A. , 2012,"Experimental Investigation of Performance of Diesel Engine Working on Diesel & Neem oil Blends ", IOSRJMCE.
[18] Xue J , Grift E. T., Hansen C. A., 2010 , "Renewable & Sustainable Energy Reviews", ELSEVIER.

Experimental Performance Analysis of Air-Cooled Condenser for Low Pressure Steam Condensation

Manish Baweja, [1] Dr.V.N Bartaria[2]
[1]*M.E, Scholar HPT LNCT Bhopal, MP, India*
[2]*Professor & HOD, Mechanical Engg LNCT Bhopal, MP, India*

Abstract: *An experimental set up is made for an air-cooled condenser and observations are obtained at different air velocities. The comparisons are done between various quantities like pressure of steam, mass flow rate, velocity of air , and temperature difference of inlet steam and Outlet steam. It is found that mass flow rate of condensed steam decreases with decrease in pressure of Steam. It also decreases with decrease in Temperature difference. So the capacity of Air cooled condenser is sometimes limited by ambient conditions, but due to other problems concerned with reduced availability of water as the cooling medium for the condensation of exhaust steam, combined with an increased emphasis on environmental considerations. it is still a better alternative than traditional steam surface condenser.*

Keywords**:** *Heat transfer, Condenser, Air cooled condenser, Performance analysis, Low pressure condensation.*

I. Introduction

A condenser is a heat transfer device or unit used to condense a substance from its gaseous to its liquid state, typically by cooling it. In doing so, the latent heat is given up by the substance, and will transfer to the condenser coolant. Condensers are typically heat exchangers which have various designs and come in many sizes ranging from rather small (hand-held) to very large industrial-scale units used in plant processes. For example, a refrigerator uses a Condenser to get rid of heat extracted from the interior of the unit to the outside air. Condensers are used in air conditioning, industrial chemical processes .Such as distillation, steam power plants and other heat-exchange systems. Use of cooling water or surrounding air as the coolant is common in many condensers. The main use of a condenser is to receive exhausted steam from a steam engine or turbine and condense the steam. The benefit being that the energy which would be exhausted to the atmosphere is utilized .A steam condenser generally condenses the steam to a pressure significantly below atmospheric. This allows the turbine or engine to do more work. The condenser also converts the discharge steam back to feed water which is returned to the steam generator or boiler. In the condenser the latent heat of condensation is conducted to the cooling medium flowing through the cooling tubes.

II. Condensers Used In Power plant

1. **Water Cooled Condenser or Steam Condenser**
2. **Air Cooled Condenser**

2.1 Water Cooled Condenser (Steam Condenser)

It is a device or an appliance in which steam condenses and heat released by steam is absorbed by water. A steam condenser is a device which condenses the steam at the exhaust of turbine. It serves two important functions. Firstly, it creates a very low pressure at the exhaust of turbine, thus permitting expansion of the steam in the prime mover to very low pressure. This helps converting heat energy of steam into mechanical energy in the prime mover. Secondly, the condensed steam can be used as feed water to the boiler.

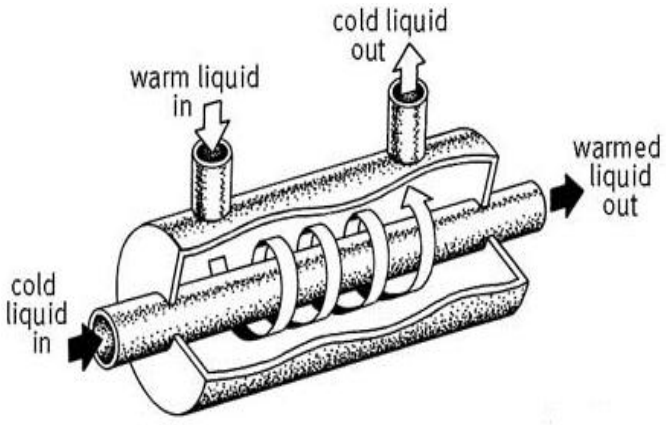

Fig 1.Water Cooled Condenser

There are two principal types of Steam Condensers
a). Jet condensers
b). Surface condenser

a) Jet condensers: In a jet condenser, cooling water and exhausted steam are together. Therefore, the temperature of cooling water and condensate is the same when leaving the condenser. Advantages of this type of condenser are low initial cost, less flow area required, less cooling water required and low maintenance charges. However its disadvantage is condensate is wasted and high power is required for pumping water.

b) Surface condenser: In a surface condenser, there is no direct contact between cooling water and exhausted steam. It consists of a bank of horizontal tubes enclosed in a cast iron shell. The cooling water flows through the tubes and exhausted steam over the surface of the tubes. The steam gives up its heat to water and is itself condensed. Advantage of this type of condenser are : condensate can be used as feed water, less pumping power required and creation of better vacuum at the turbine exhaust. However, disadvantage of this type of condenser are high initial cost, requires large floor area and high maintenance charges. The surface condenser is used for the majority of steam engine & steam turbine applications.

2.2 Air Cooled Condenser

Air Cooled condensers are largely in use today due to growing attention being paid to environmental safety. Also, growing demand for water for both domestic and industrial use has brought an increased interest in use of Air Cooled condensers.

An Air cooled condenser, is simply a pressure vessel which cools a circulating fluid within finned tubes by forcing ambient air over the exterior of the tubes. A common example of an Air cooled condenser is car radiator Air cooled heat exchangers are used for two primary reasons.

i. They increase plant efficiency
ii. They are a good solution as compared to cooling towers and shell and tube heat exchangers because they do not require an auxiliary water supply (water lost due to drift and evaporation, plus no water treatment chemicals are required).

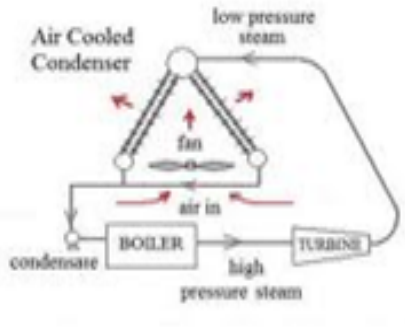

Fig 2.Basic Air Cooled Condenser cycle

An air-cooled heat exchanger can be as small as your car radiator or large enough to cover several acres of land, as is the case on air coolers for large power plants the air-cooled heat exchangers are mostly used when the plant location and the ambient Conditions do not allow an easy and economic use of other cooling systems

The most evident advantages of air-cooled Condensers are:

a) No problem arising from thermal and chemical pollution of cooling fluids
b) Flexibility for any plant location and plot plan arrangement because equipment requiring cooling need not be near a supply of cooling water.
c) Reduction of maintenance costs
d) Easy installation
e) Lower environmental impact than water cooled condenser due to the elimination of an auxiliary water supply resulting in water saving
f) No use of water treatment chemicals and no need for fire protection system.

Air-cooled finned-tube condensers are widely used in refrigeration and air-conditioning applications. For the same amount of heat transfer, the operation of air cooled condensers is more economic as compared with water cooled condensers typically air-cooled condensers are of the round tube and fin type. To improve the performance of air-cooled condensers multiple techniques can be achieved such as enhancements on inner pipe surface, changing the tube geometry from round to flat shape and external fins.

III. Literature Survey

[1] A Study was performed on Performance Characteristics of an Air-Cooled Condenser under Ambient Conditions in December 2011. In this study effects of air flow pattern as well as ambient conditions were studied. Unfortunately ACC becomes less effective under high ambient temperature and windy conditions. Fin cleaning plays a vital role in heat rejection. External cleaning improves air side heat transfer coefficient. Ambient conditions affect the steam temperature and heat rejection rate. It is observed that rise in wind velocity decreases thermal effectiveness of ACC up to considerable level. Ambient temperature not only affects performance of ACC at the same time turbine back pressure also increases with rise in ambient temperature. Skirts are effective solution to reduce the effect of wind on volumetric effectiveness. Hot air recirculation increases with wind velocity. Now a day's wind walls are used to reduce this effect. Second option is to increase fan speed. It counter affects on electrical power consumption.

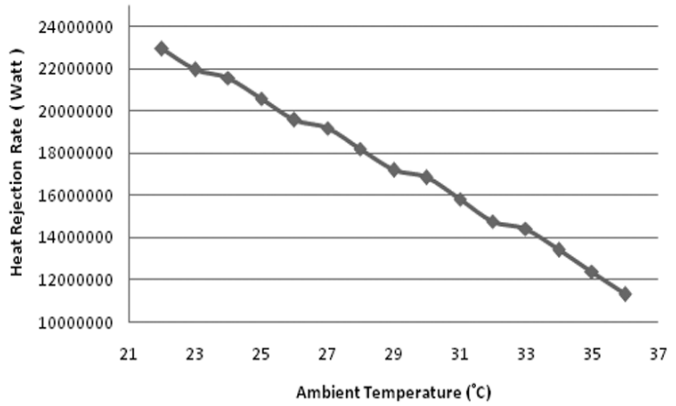

Fig. 3 Heat Rejection for various Ambient Temperatures (Courtesy:Nirma Institute of technology - NUiCONE – 2011)

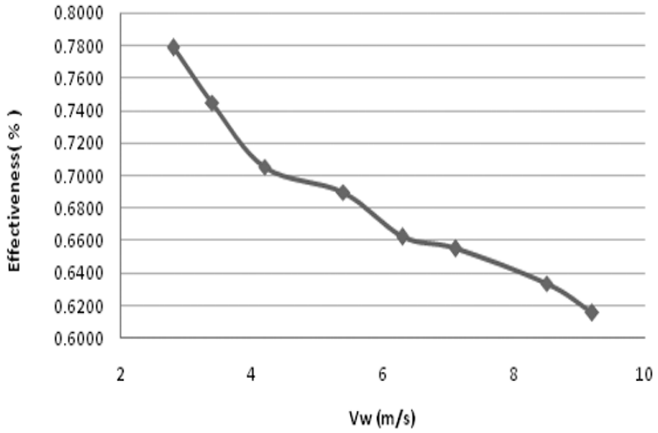

Fig4. Effectiveness at different Wind Velocities (Courtesy: Nirma Institute Of technology - NUiCONE – 2011)

[2] A study was performed to evaluate the performance characteristics of a power plant incorporating a steam turbine and a direct air-cooled dry/wet condenser operating at different ambient temperatures. The proposed cooling system uses existing A-frame air-cooled condenser (ACC) technology and through the introduction of a hybrid (dry/wet) dephlegmator achieves measurable enhancement in cooling performance when ambient temperatures are high. [3] In this study they found that air-conditioning system with air cooled condensers, the condensing unit has to be kept in open for easy access to outdoor air in order to efficiently dissipate heat, During Daytime the solar radiation falling on the surface of the condenser and high ambient temperature can be detrimental for the energy performance. They studied the effectiveness of shading the condensing unit to mitigate the adverse effect of high ambient temperatures due to solar radiation .and analyzed that the theoretical increase in COP due to shading is found to be within 2.5%. [4] Heat transfer by convection in air cooled condensers is studied and improved in this work. In order to enhance the performance of air cooled condensers, it is important to take into consideration both of condensation inside condenser tubes and convection outside, where the enhancement in convection side is the dominant one. Aluminum extruded micro-channel flat tubes improve the performance of condensation more than conventional circular tubes but still has potential for air side improving. So the enhancement of convective heat transfer in air side is achieved in this study by inclination of the flat tubes by a certain angle with respect to horizontal in two cases.

IV. Experimental Analysis

Fig. 5. Experimental set up

4.1 Experimental Setup

Experimental set up consist of –

4.1.1 Fan- Fan is used to provide ambient air to the steam flowing through the finned tube this air cools the steam and thus condenses it.

4.1.2 Steam Generator – Steam Generator is used to produce the steam required for Experimental purpose. A ISI marked pressure cooker is used for this purpose .A funnel & a valve is brazed at the Top of Pressure Cooker to start and stop the supply of water in it.also in another opening pipe is brazed to take out the steam to condenser.

4.1.3 Heater-A Heater is placed below the pressure cooker to heat the water and generate the steam required for experimental purpose.

4.1.4 Pressure Gauge- A Low-Pressure gauge is used to measure the pressure of generated steam in kg/cm2.

4.1.5 Ammeter – Ammeter is used to measure current in amperes.

4.1.6 Voltmeter –Voltmeter is used to measure current in amperes.

4.1.7 Dimmer Switch- A Dimmer Switch is used to regulate voltage and current

4.1.8 Thermocouple- A thermocouple consists of two conductors of different materials (usually metal alloys) that produce a voltage in the vicinity of the point where the two conductors are in contact. The voltage produced is dependent on, but not necessarily proportional to, the difference of temperature of the junction to other parts of those conductors. Thermocouples are a widely used type of temperature sensor for measurement and control and can also be used to convert a temperature gradient into electricity. They are inexpensive, interchangeable, are supplied with standard connectors, and can measure a wide range of temperatures. In contrast to most other methods of temperature measurement, thermocouples are self powered and require no external form of excitation. The main limitation with thermocouples is accuracy; system errors of less than one degree Celsius (C) can be difficult to achieve.

4.1.9 Temperature Indicator- Temperature indicator is a device used to indicate the temperature measured by the thermocouple wire.

4.1.10 Anemometer:-It is a device for measuring wind speed, and is a common weather station instrument. The term is derived from the Greek word anemos, meaning wind, and is used to describe any airspeed measurement instrument used in meteorology or aerodynamics. The first known description of an anemometer was given by Leon Battista Alberti around 1450.

4.1.11 Crimped Fin Tube- Crimped fin made of copper or aluminum. It is brazed over the tube to increase the rate of heat transfer.

The components that are available on the external surface of the bare tube to increase its surface area are called fins. Finned Tubes help better transfer of heat between the outside and inside of tube. With the usage of these tubes having surface area almost eight times of the outer tube, the length of the tube required to heat the viscous oil can be reduced by one sixth. Our Spiral Finned Tubes are popular because of their following advantages:

- High efficiency
- Excellent quality
- Smooth

4.1.12 Experimental Procedure- First of all water is poured in the pressure cooker through funnel brazed above it. The valve for entering water is then closed. Then the heater is switched on and water is allowed to heat. Steam is generated in the pressure cooker which is taken out by opening the valve on other side of cooker .steam is taken out through pipes and its pressure is noted with the help of pressure gauge. This steam enters into finned tube fixed inside the duct and cooled by running the fan at various air-velocities .various temperature readings are taken with the help of thermocouple. The condensed steam coming out of condenser is taken out in a wicker for certain time and mass flow rate is noted.

V. Results

The various quantities like velocities of air, pressure of steam, various temperatures including temperature of inlet steam to condenser and outlet steam from condenser, mass flow rate of condensed steam etc are noted and comparisons between various quantities are plotted.

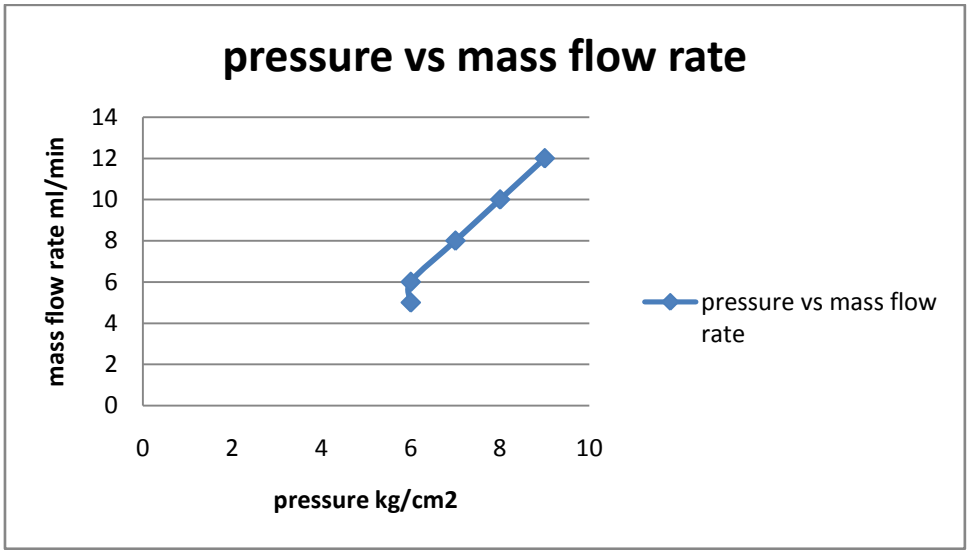

Fig-6 Pressure v/s mass flow rate

This comparison shows that mass flow rate of condensed steam decreases with decrease in pressure of inlet steam

5.1.2 Comparison between Temp Difference and Mass Flow Rate.

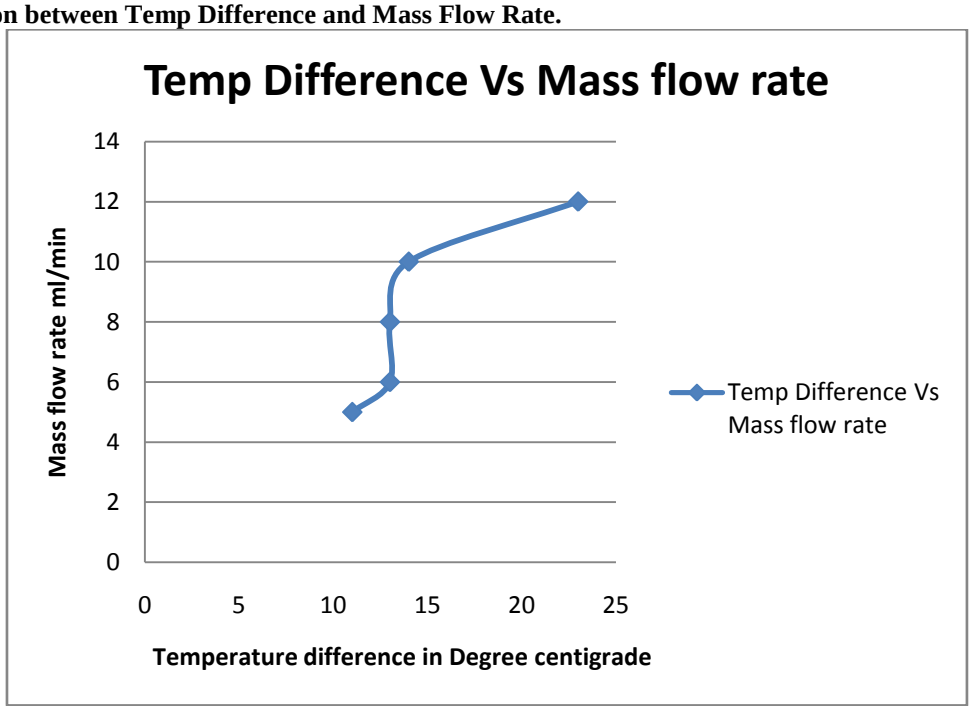

Fig-7 Temp. Difference v/s mass flow rate

This comparison shows that mass flow rate of condensed steam decreases with decrease in Temp. Difference of inlet & outlet steam

5.1.3 Comparison between Velocity and Temperature Difference

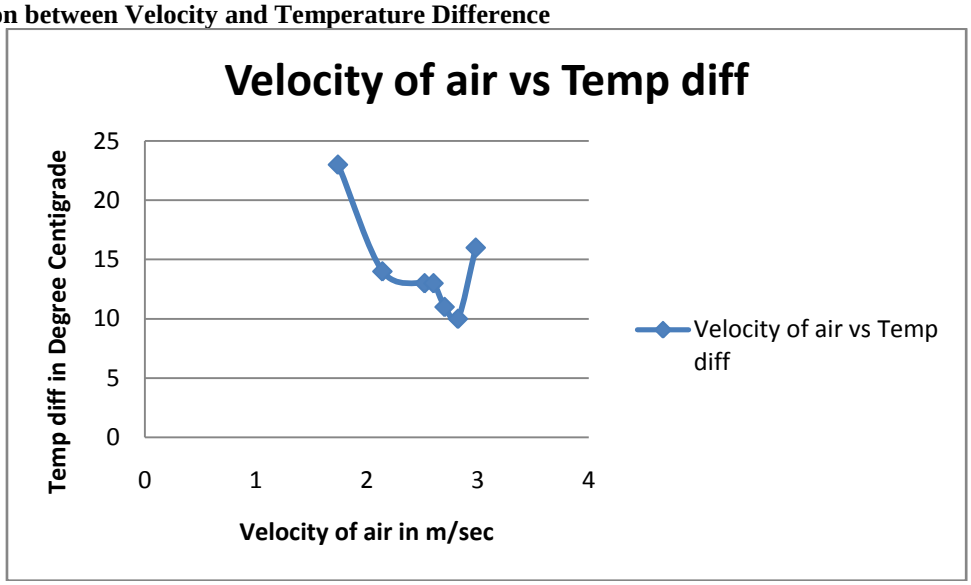

Fig-8 Velocity of air v/sTemp. Difference

5.1.4 Comparison between Pressure and Temperature Difference.

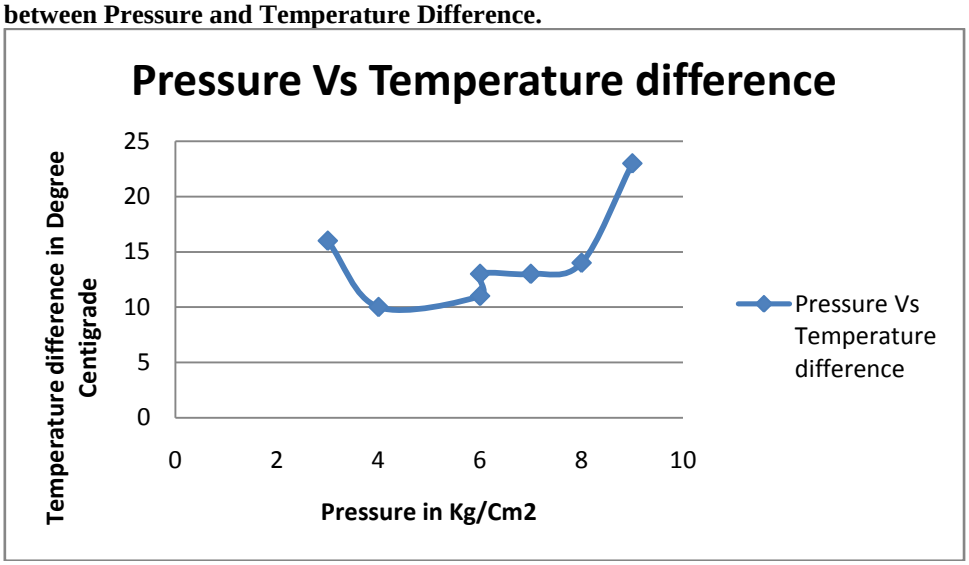

Fig- 9 Pressure V/s Temperature .Difference

VI. Conclusion

It is found that mass flow rate of condensed steam decreases with decrease in pressure of Steam. It also decreases with decrease in Temperature difference of inlet steam and outlet steam of condenser. Although the capacity of Air cooled condenser is sometimes limited by ambient conditions, their selection can avoid a number of other problems concerned with reduced availability of water as the cooling medium for the condensation of exhaust steam, combined with an increased emphasis on environmental considerations. This often makes the selection of an air-cooled condenser a viable alternative to the traditional steam surface condenser.

References

[1] A. Rupeshkumar V. Ramani, B. Amitesh Paul, D. Anjana D. Saparia Nirma University Ahmedabad (December 2011) Performance Characteristics of an Air-Cooled Condenser under Ambient Conditions NUiCONE 2011

[2] Johan Adam Heynes and D.G Kroger University of stellenbosh (December 2008) enhancement in cooling performance using a Dry/Wet Dephlegmator when ambient temperatures are high.

[3] EA.I.ElSherbini and G. P. Maheshwari Building and Energy Technologies Department Kuwait Institute for Scientific Research (October-2010). ESL-IC-10-10-52 Effectiveness of Shading Air-Cooled Condensers of Air-Conditioning Systems.

[4] M.M.Awad, H.M.Mostafa, G. I. Sultan, A.Elbooz, A.M.K.El-ghonemyFaculty of Engineering, Mansoura University, Egypt (2007).Alexandria Engineering Journal, Vol42, No-4, july2003 Enhancement in heat transfer by changing tube geometry

International Journal of Modern Engineering Research (IJMER)
www.ijmer.com Vol.3, Issue.2, March-April. 2013 pp-845-848 ISSN: 2249-6645

Enhanced Energy Aware Geographic Routing Protocol in MANET: A Review

Gaurav Sachan, [1] D. K. Sharma, [2] Karishma Tyagi, [3] Abhimanyu Prasad[4]
[1234]*Department of Computer Science & Engineering, Vishveshwarya Group of Institutions, Dadri, G.B.Nagar-273010, U. P., INDIA*

Abstract: *Mobile ad hoc networks (MANET) are characterized by multi-hop wireless links and resource constrained nodes. One of the major challenges in mobile ad hoc networks (MANETs) is link failures due to mobility. Because nodes in a MANET act as routers for any ongoing packet communication and have limited transmission ranges, the communication links are broken, and packet losses occur. To improve network lifetime, energy balance is an important concern in such networks. Geographic routing has been widely regarded as efficient and scalable. However, it cannot guarantee packet delivery in some cases, such as faulty location services. The matter gets even worse when the nodes on the boundaries of routing holes suffer from excessive energy consumption, since geographic routing tends to deliver data packets along the boundaries by perimeter routing. This paper will be a basis for study in the domain of geographic routing for the new researcher point of view.*

Keywords: *MANET, geographic routing, energy efficient, location information.*

I. Introduction

An ad-hoc network, as the name suggests, is a network formed by nodes connected arbitrarily for some temporary time. They provide a powerful paradigm for modeling open self configuring wireless networks and seem so appropriate to use in the fourth generation of mobile networks. Obviously, a convergence of all these technologies with 3G/4G [18] mobile networks will probably lead to various integrated solutions.

A Mobile Ad-hoc network (MANET) is consists of mobile routers connected wirelessly to each other where each node is free to move. This results in a continuously changing topology. Some examples of the possible uses of ad hoc networking include business associates sharing information during a meeting, soldiers relaying information for situational awareness on the battlefield and emergency disaster relief personnel coordinating efforts after a hurricane or earthquake.

In recent years, geographic routing algorithms have been extensively studied due to the popularity and availability of positioning services such as the global positioning system (GPS). Geographic routing is a promising candidate for large-scale wireless ad hoc networks due to its simplicity and scalability and takes advantage of the location information of the nodes are the very valuable for wireless networks. Since geographic routing does not require a route management process, it carries a low overhead compared to other routing schemes, such as proactive, reactive, and hybrid topology based routing protocols. Geographic routing protocols work on the assumption that every node is aware of its own position in the network; via mechanisms like GPS or distributed localization schemes and that the physical topology of the network is a good approximation of the network connectivity. In other words, these routing protocols assume that if two nodes are physically close to each other, they would have radio connectivity between them, which is true in most cases. Hence the protocols use node location information to route packets from source to destination. One big advantage of geographic routing schemes is the fact that there is no need to send out route requests or periodic connectivity updates. This can save a lot of protocol overhead and consequently, energy of the nodes. The most significant difference between MANETs and traditional networks is the energy constraint. Some applications such as environment monitoring need MANETs to run for a long time. Therefore, extending the lifetime of MANETs is important for every MANET routing protocol. However, most geographic routing algorithms take the shortest local path, depleting the energy of nodes on that path easily. The nodes located on the boundaries of holes may suffer from excessive energy consumption since the geographic routing tends to deliver data packets along the whole boundaries by perimeter routing if it needs to bypass the hole.

There should be a mechanism at node for robust communication of high priority messages. This can be achieved by keeping nodes all the time powered up which makes nodes out of energy and degrades network life time. Also, there can be a link or node failure that leads to reconfiguration of the network and re-computation of the routing paths, route selection in each communication pattern results in either message delay by choosing long routes or degrades network lifetime by choosing short routes resulting in depleted batteries. Therefore the solutions for such environments should have a mechanism to provide low latency, reliable and fault tolerant communication, quick reconfiguration and minimum consumption of energy. Routing protocols have a critical role in most of these activities. To measure the suitability and performance of any given protocol, some metrics are required. On the basis of these metrics any protocol can be assessed against its performance [3].

The remaining part of this survey paper is organized as follows:-In section II, we will discuss the taxonomy related to Geographic routing. In section III literature review in the field of geographic routing mechanism and in section IV we describe research challenges for geographic routing in MANET, the comparative study of previous protocols given in section V and in section VI; we will conclude the paper and give the future scope of this paper.

II. Literature Review

A number of research has been conducted on the geographic routing in MANET but still current result are not appropriated for MANET and geographic routing for MANET is still an open problem for research work. In this section, we briefly present routing protocols in MANETs. Then, we focus particularly on energy aware geographic routing since it is the Early research of geographic routing includes DREAM [1] and LAR [2] that proposed constrained flooding. The expected zone is defined by predicting the boundary of the destination node's movement. In both protocols, prediction is made based on the time difference between sending data and the location information's update, as well as the destination node's speed. We adopt this approach in our routing protocol and describe it in the third section. In the LAR protocol, before the transmission of a data packet, the source node finds a route by flooding routing packets in its *request zone*. In the DREAM protocol, however, according to the location information, the data packet is flooded in a restricted directional range without sending a routing packet. Although this kind of forwarding effectively guarantees delivery, its energy use is notably high, especially in large-scale networks. Recently, *Local maxima* in geographic routing have received much attention. Many routing protocols for planar network graphs are presented for solving this problem, such as GFG [3], GPSR [4], GOAFR+ [5] and CLDP [6].

In the following, we review the shared characteristics of these geographic routing algorithms. Geographic routing schemes use greedy routing where possible. In greedy routing, packets are stamped with the position of their destination; and a node forwards a packet to a neighbor that is geographically closer to the destination. Local maximum may exist where no neighbor is closer to the destination. In such cases, greedy forwarding fails, and making progress toward the destination requires another strategy. In particular, the packet needs only to find its way to a node closer to the destination than the local maximum; at that point, greedy routing may once again make progress.

Note that if the graph is not planar, face routing may fail. Wireless networks connectivity graphs typically contain many crossing edges. A method for obtaining a planar sub graph of a wireless network graph is thus needed. Greedy routing operates on the full network graph, but to work correctly, face routing must operate on a planar sub graph of the full network graph. Geographic routing algorithms planarize graphs using two planar graph constructs that meet that requirement: the Relative Neighborhood Graph (RNG) and the Gabriel Graph (GG). The RNG and GG give rules for how to connect vertices placed in a plane with edges based purely on the positions of each vertex's single-hop neighbors. Up to the present, literature, such as GOAFR+, CLDP and LCR [15], has focused on methods of deleting these crossing links.

However, there are several drawbacks to pure geographic routing. In certain circumstances, one cannot guarantee delivery by greedy routing, for example, when there is the rapid movement of nodes. Because of this, the location information of a destination node is rather inaccurate. Secondly, greedy routing is a single-path transmission process which means once the process drops a data packet the whole routing fails. Thirdly, there have been several schemes to overcome the *Local maxima*.

All the schemes can be classified into two categories: perimeter routing [5, 6] and the back pressure rule [7, 8].

Mobile networks use a power-aware routing protocol in [17]. However, to save energy as much as possible, its iterative relay process will result in unacceptable end-to-end delay. Due to the non-linear attenuation of wireless signals, it is possible that one hop consumes more energy than multiple hops. Yet it can be impractical to change from one hop to several, following the mechanism in [17]. The end-to-end delay may increase significantly, especially in a high-density network.

III. Challenges in Manet

The major challenges [1] faced by this architecture can be broadly classified as:

1) Dynamic topologies: Nodes are free to move arbitrarily; thus, the network topology--which is typically multi hop, may change randomly and rapidly at unpredictable times, and may consist of both bidirectional and unidirectional links.

2) Device discovery- Identifying relevant newly moved in nodes and informing about their existence need dynamic update to facilitate automatic optimal route selection.

3) Bandwidth-constrained-variable capacity links: Wireless links will continue to have significantly lower capacity than their hardwired counterparts.

4) Energy-constrained operation: Some or all of the nodes in a MANET may rely on batteries or other exhaustible means for their energy. For these nodes, the most important system design criteria for optimization may be energy conservation.

5) IP-Layer Mobile Routing-An improved mobile routing capability at the IP layer can provide a benefit similar to the intention of the original Internet, viz. "an interoperable internetworking capability over a heterogeneous networking infrastructure".

6) Limited physical security: Mobile wireless networks are generally more prone to physical security threats than are fixed-cable nets. The increased possibility of eavesdropping, spoofing, and denial-of-service attacks should be carefully considered.

7) Diffusion hole problem: The nodes located on boundaries of holes may suffer from excessive energy consumption since the geographic routing tends to delivers data packets along the hole boundaries by perimeter routing if it needs to bypass the hole. This can enlarge the hole because of excessive energy consumption of the node boundaries nodes.

IV. Comparative Study

As per literature survey we have done yet there are many parameter in the geographic routing based techniques which we can compare and put them in such a graph which will be helpful for the future researchers. There are various

protocols are available in this area. So we are doing a comparative study of main geographic routing protocols, listed in tables based on characteristics and advantages and disadvantages-

Geographic routing technique	Major characteristics	Route Discovery
Zone Based Routing	• Use a fixed zone-based partition scheme to partition the network. • Usage of source based routing. • ZBR has a good scalability.	• Source based route request.
Global Positioning System	• GPS-free has been developed that provides knowledge of the geometric location of nodes in a MANET	• It uses optimization technique for Route Discovery.
Location Aided Routing	• Region stability is based on the expected zone as well as request zone.	• Interregional route discovery. • Intraregional route discovery
DREAM Protocol	• The data packet is flooded in a restricted directional range without sending a routing packet.	• It use discount factor for RREQ.
Energy aware geographic routing protocol	• It is based on the expected zone and forwarding area. It uses greedy approach and when it fails it switch to the perimeter routing.	• Source node multicast RREQ packet.

LINK STABILITY TECHNIQUES	ADVANTAGES	DISADVANTAGES
Zone Based Routing	• lower overhead, • lower probability of link breakage • higher throughput	• Being a Proactive protocol it consumes high bandwidth.
Location Aided Routing	• It has minimized the size of the route discovery process by defining the range of the destination node.	• Control complexity is higher then GPSR.
DREAM Routing Protocol	• This kind of forwarding effectively guarantees delivery. • Its energy use is notably high, especially in large-scale networks.	• Packet loss ratio is higher then GPSR.
GPSR Protocol	• Data forwarding overhead is low. • Local maxima are easily found.	• It induces great traffic. • Group Leader is Single Point of Failure. • Its packet delivery ratio is less than EGR.
Energy Aware Geographic Routing Protocol	• It has higher packet delivery ratio when compared with GPSR.	• It suffers from diffusion hole problem.

V. Conclusion and Future Scope

We have started this work by a simple thing keeping in mind to detect the parameter which affects the geographic routing in a network. This paper described basic concepts and functionalities of the energy constrained geographic routing based routing techniques and reviewed the work carried out in the areas of MANET. The detailed paper review major geographic based techniques and also put the comparative study of few of them and also tabulate on the basis of their main characteristics. In future there is a need to develop more enhanced energy efficient geographic routing protocols which will also good in terms of high packet delivery ratio, increased network lifetime and delay time in packet delivery should be minimized.

References

[1] Gang Wang and Guodong Wang, An Energy Aware Geographic Routing Protocol for Mobile Ad Hoc Networks, Int J Software informatics, Vol. 4, No. 2, June 2010, pp. 183-196.
[2] Adel Gaafar A. Elrahim and et al., An Energy Aware WSN Geographic Routing Protocol, Universal Journal of Computer Science and Engineering Technology, 1(2), 105-111, Nov. 2010.
[3] S.Corson and J. Macker, "Routing Protocol Performance Issues and Evaluation Considerations," Naval Research Laboratory, Jan.1999.
[4] B. Karp and H. Kung, "GPSR: Greedy perimeter stateless routing for wireless networks," in the Proceedings of the 6th Annual ACM/IEEE International Conference on Mobile Computing and Networking (MOBICOM), pp.243-254, Boston, August 2000.
[5] Ko Y, aidya NHV. Location-aided routing (LAR) in mobile ad hoc networks. Proc. The ACM/IEEE International Conference on Mobile Computing and Networking, 1998. 66{75}.
[6] Ma XL, Sun MT, Zhao G, et al. An efficient path pruning algorithm for geographical routing in wireless networks. IEEE Trans. Vehicuar Technology, 2008, 57(4): 2474{2488}.
[7] Kim Y J, Govindan R, Karp B, et al. Geographic routing made practical. Proc. the 2nd Symposium on Networked Systems Design and Implementation, 2005. 217{230}.
[8] Watanabe M, Higaki H. No-Beacon GEDIR: Location-Based Ad-Hoc Routing with Less Communication Overhead. Proc. the International Conference on Information Technology, 2007.
[9] Singh S, Woo M, Raghavendra CS. Power-Aware routing in mobile ad hoc networks. Proc. the ACM/IEEE International Conference on Mobile Computing and Networking, Oct. 1998.
[10] Basagni S, Chlamtac I, Syrotiuk VR. A distance routing e®ect algorithm for mobility (DREAM). Proc. the ACM/IEEE International Conference on Mobile Computing and Networking, 1998.
[11] Kuhn F, Wattenhofer R, Zhang Y, et al. Geometric ad-hoc routing: Of theory and practice Proc. the 22nd ACM Symposium on Principles of Distributed Computing, 2003. 63-72.
[12] Zeng K, Ren K, Lou W, et al. Energy Aware Geographic Routing in Lossy Wireless Sensor Networks with Environmental Energy Supply. Proc. the 3rd International Conference on Quality of Service in Heterogeneous Wired/Wireless Networks, Waterloo, Canada, Aug. 2006.
[13] Stojmenovic I. A scalable quorum based location update scheme for routing in ad hoc wireless networks. Technical Report TR-99-09, SITE, University of Ottawa, Sep. 1999.
[14] Stojmenovic I. Home agent based location update and destination search schemes in ad hoc wireless networks. Technical Report TR-99-10, SITE, University of Ottawa, Sep. 1999.
[15] Li J, Jannotti J, Douglas S J De Couto, et al. A scalable location service for geographic ad hoc routing. Proc. the 6th Annual International Conference on Mobile Computing and Networking, Aug. 2000. 120-130.
[16] Kuruvila J, Nayak A, Stojmenovic I. Progress and location based localized power aware routing for ad hoc and sensor wireless networks. International Journal of Distributed Sensor Networks, 2006, 2(2): 147-159.
[17] Kim YJ, Govindan R, Karp B, et al. Lazy Cross-Link Removal for Geographic Routing. Proc. the ACM Conference on Embedded Networked Sensor Systems, Nov. 2006. 112-124.
[18] Y. -C. Tseng, S. -L. Wu, W. -H. Liao and C. -M. Chao, "Location Awareness in Ad Hoc Wireless Mobile Networks,"IEEE Computer, Vol. 34, No. 6, June 2001, pp. 46-52

International Journal of Modern Engineering Research (IJMER)
www.ijmer.com Vol.3, Issue.2, March-April. 2013 pp-849-856 ISSN: 2249-6645

Application and Manufacturing of Microfluidic Devices: Review

R.M.Chanmanwar, [1]R.Balasubramaniam, [2] L.N.Wankhade[3]
[1,3]*Production Engg. Dept., SGGS, Nanded, India*
[2]*Precision Engg. Division, BARC, Mumbai, India*

Abstract:*Micro fluidic devices are gaining increasingly popularity owing to their many advantages. Microfluidics varies in terms of forces operating from other domains as well as from macro-scale fluidic devices. Effects which can be omitted on a macro scale are dominant when fluid dynamic faces the issue of scale. With the recent achievement in the biotechnology, microfluidic devices promise to be a big commercial success. To have a better understanding of the various types of microfluidic devices, their application areas, basic design and manufacturing issues, a brief review is carried out and reported in this paper. Few devices and their applications are discussed.*

Keywords: *Microfluidics, Design, Micro-Machining, Bonding, Interfacing.*

I. Introduction

Microfluidics deals with the behavior, precise control and manipulation of fluids that are geometrically constrained to a small, typically sub-millimeter scale. Typically, micro means one of the following features,

- small volumes (nL, pL, fF)
- small size
- low energy consumption

The behavior of fluids at the microscale can differ from 'macrofluidic' behavior in many aspects such as surface tension, energy dissipation and fluidic resistance dominating the system. Microfluidics studies how these behaviors change and how they can be worked around or exploited for new uses. In particular, the Reynolds number (which compares the effect of momentum of a fluid to the effect of viscosity) can become very low. A key consequence of this is that fluids, when side-by-side, do not necessarily mix in the traditional sense; molecular transport between them must often be through diffusion. High specificity of chemical and physical properties (concentration, pH, temperature, shear force, etc.) can also be ensured resulting in more uniform reaction conditions and higher grade products in single and multi-step reactions. [1, 2,3, 9] Micro domain varies not only from the macro domain but also from each other in basic characteristics. The microfluidic domain differs from other domains in terms of area, which is indicated by difference in the whole design process, as well as in design support and manufacturing. Effects which can be omitted on a macro scale are dominant when fluid dynamic faces the issue of scale. Lack of proper understanding of this area creates difficulties and causes error prone designs. In comparison to the macro-domain, where precision in many cases is required and tolerances can be tight, in the micro-scale, dimensions are in the scale of macro-scale tolerances. Due to this, the majority of manufacturing methods start to be costly and the selection of materials for new devices is constrained. Fig.1. shows the macro and micro scales and devices for some application areas. Since, the application of microfluidic devices are continuously increasing, to have a better insight about this area, a brief review about the application areas and applicable manufacturing process and various issues is carried-out and presented in this paper.[6,7,8]

With the recent achievement in the biotechnology, microfluidic devices promise to be a big commercial success. Microfluidic devices are tools that enable novel applications unrealizable with conventional equipment. The apparent interest and participation of the industry in microfluidic research and development show the commercial values of microfluidic devices for practical applications. [10,11]

In response to the commercial potential and better funding environments, microfluidics quickly attracted the interest of the scientific community. Peoples from almost all traditional engineering and science disciplines have begun pursuing microfluidic research, making it a truly multidisciplinary field representative of the new economy of the twenty-first century. The classification of microfluidic devices based on the application areas such as pharmaceutical, biotechnology, chemical energy, cosmetics etc., is shown in Table.1 [12, 13, 17, 22]

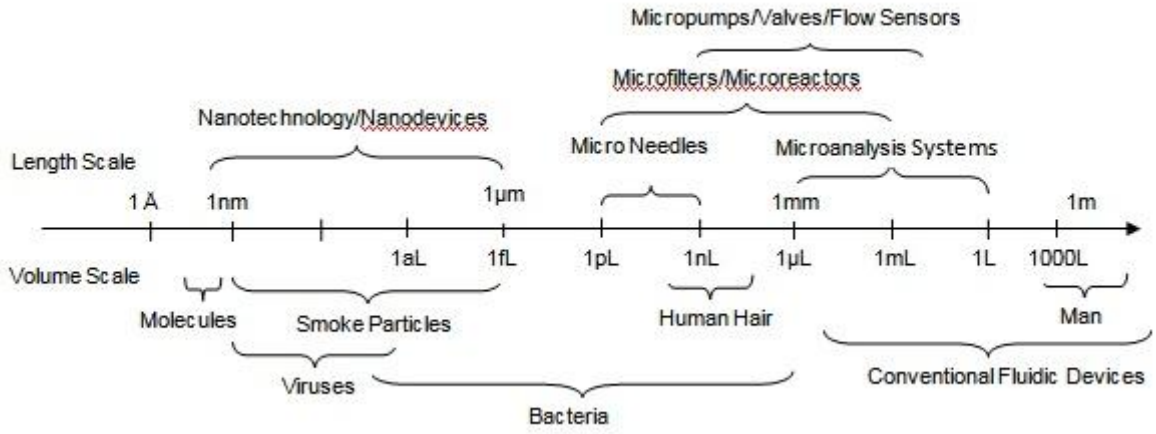

Fig.1 Macro and Micro Domain and Application Areas[11]

Table.1 Application Areas of Microfluidic Devices [10, 17, 18, 20]

Application Area	Benefits	Application
Pharmaceutical	High shear particle size reduction, uniform particle size distribution, Reliable scaleup	Vaccines, Cancer, Antibiotics, Injectables, Inhalables, Steroids
Biotechnology	High shear particle size reduction, Uniform shear rates, Rapid cell rupturing, Ease of use	Quantification of E. coli, Yeast, Algae, Bacteria, Plant, Insect, Fungi
Chemical Energy	Reduces particle size to a submicron level to create stable nanoemulsions and suspensions	Inkjet inks, conductive inks, toners, Carbon nanotubes, Resins
Cosmetics	Precisely controlling particle size reduction to the optimal level with a uniform distribution	Sunscreens, makeup's and mascaras, waxes and lipsticks
Nutraceuticals	Utilize chemistry to deliver benefits and nutrients from plants, fish oils and other natural sources	Vitamins, weight loss powders, oral vitamin sprays and functional foods
Energy	Reduce reliance on fossil fuels, never degrade, and emit minimal greenhouse gases.	Fuel cells, batteries, photovoltaics, biodiesel

II. Applications

Microfluidics has large number of applications. In the following sections, some of the extensively used devices are discussed here.

1.1. Rapid Quantification of Bacterial Cells (Cytometer)

A simplified microfluidic device for quantification of bacteria in potable water by the microfluidic system and by epifluorescence microscopy is shown in Fig.2. [1] Bacteria in natural mineral water and in purified household tap water were accurately enumerated by using this system within 15 min after fluorescent staining.The dimensions are the channels with Long & short lengths, width & depth of the channels are 28.5mm & 14mm and 60µm & 25µm, respectively. Samples are injected at inlet A, and sheath fluid at inlets B and C. sample flow: 0.5µl/min; sheath flow: 2.5µl/min. The Critical features of the systems are biocompatibility of material, surface finish, length, width and depth of channels.[1,2]

1.2. Particle Size Reduction (Microfluidizer)

There are several ways to reduce large particles into smaller ones - but Microfluidizer high shear fluid processors stand alone in their ability to achieve uniform target particle sizes on the nano-scale. Some of the reliable features are small particle sizes, narrowest particle size distribution, repeatable and consistent results and improved processing efficiencies. As depicted in Fig.3, product is input into a reservoir which supports high solid content. A high pressure pump generates forces up to 40,000 psi (2578 bar) in order to force the product stream intoprecisely engineered microchannels within the unique interaction chamber. Inside the chamber, product is exposed to consistent and intense impact and shears forces and then is immediately cooled. This repeatable process results in tiny particles with a uniform distribution. The critical features of the systems are pressure and cross section of channels.[5,23]

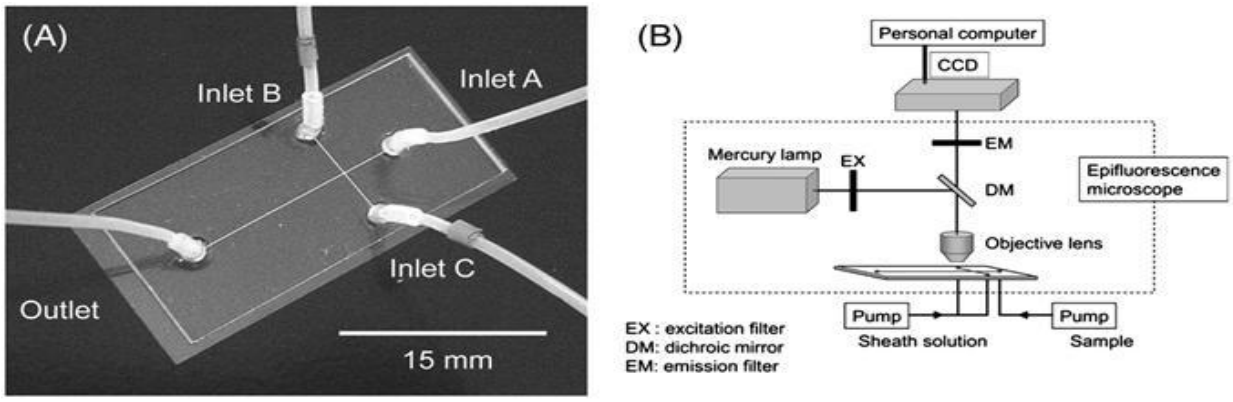

Fig.2. Design of the on-chip flow cytometer. (A) Microfluidic device with simple cross microchannels. (B) Schematic representation of the on-chip flow cytometer

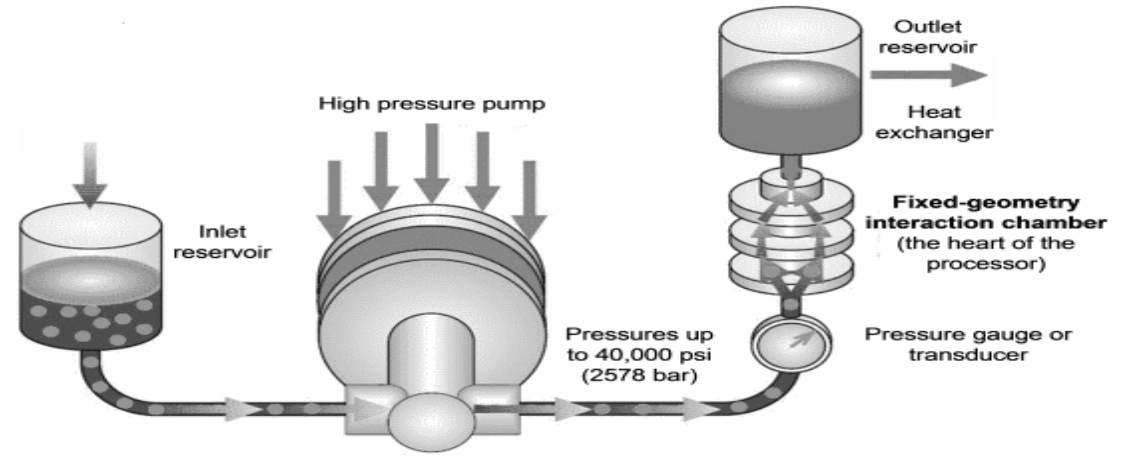

Fig: 3 Schematic of particle size reduction

1.3. Fuel Cells

The operation of a fuel cell involves the chemical interaction between hydrogen and oxygen to produce water, heat and electrical energy. Typically, a fuel cell consists of a pair of electrodes (the 'anode' and the 'cathode') separated by a membrane that allows protons (hydrogen ions) to pass through the membrane but does not allow an electric current to pass. A main objective of current research is the application of micro scale fuel cells to portable electronic devices such as cell phones and computers. The main problem with applying fuel cell concepts to mobile devices is that the power source (battery or fuel cell) must be able to deliver around 300mA of current at 3.6V. [4, 25, 26] The critical features of the fuel cell are compact size, operating temperature and electrolyte substance.

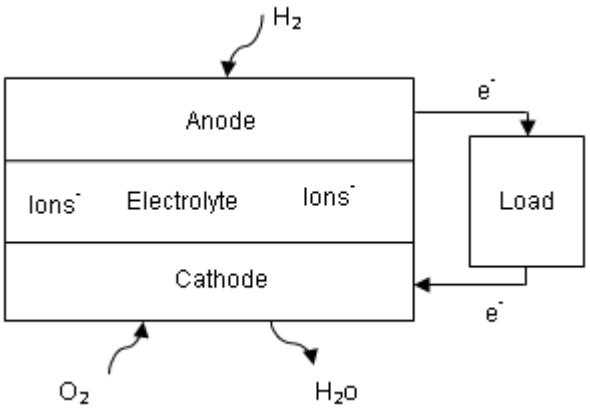

Fig: 4 Block Diagram of Fuel Cell

III. Design of Microfluidic Devices

The obvious discerning characteristics of micro-reactors are compact size, light weight, and lower material and energy consumption. Secondly, smaller linear dimensions lead to increased species gradients which are particularly important for chemical reactor processing. This results in rapid heat and mass transport, and short diffusion lengths. Faster

system response gives better process control and high product yields. Besides these, the attractive feature of micro-reactors is their high surface to volume ratio compared to conventional chemical reactors. Because of smaller passage size, flow through micro-reactors usually remains laminar. Thus, the heat/mass transfer coefficients become inversely proportional to the channel hydraulic diameter; however there is an increase in pressure drop. [11, 13, 29, 30]

The higher heat and mass transfer characteristics of micro heat exchangers are an added advantage for utilizing the full potential of catalysts used, especially during endothermic/exothermic reactions. Thus, local hot-spot formations are avoided because of high heat removal capacity. Additionally, because of higher reaction temperature, catalysis can be utilized effectively, thus requiring a smaller volume. Finally, because of smaller reactants and products inventories, high level of safety is achieved. In the following sections, the importances of the critical design features are discussed with two types of microfluidic devices.[27, 28]

1.4. Micromixer

In micromixers, diffusion or mixing time depends upon square of the mixing path. Because of their small size, micromixer decreases the diffusion time significantly. In general, fast mixing can be achieved with small mixing path and large surface area. Design considerations of micromixers are fast mixing time, small device area, integration ability in a more complex system. Mixing time is proportional to the square of the channel width and the velocity is inversely proportional to the channel width. The residence time is determined by flow velocity and channel length as given in Eq. (1). [20, 31,32,33]

$$\boldsymbol{L = \frac{(\mathrm{Qw} + \mathrm{QE}) * w}{2 * A * D}} \ldots\ldots\ldots\ldots\ldots\ldots\ldots \boldsymbol{equation1}$$

Where, Q=flow rate, A=cross sectional area, D=diffusion coefficient, w=width of channel. Hence, the smallest cross-section and longest channel length are desired. Fig.6 shows typical geometry of micromixer in which width of micro-channel is 300µm, depth is 90µm and length is 3m.

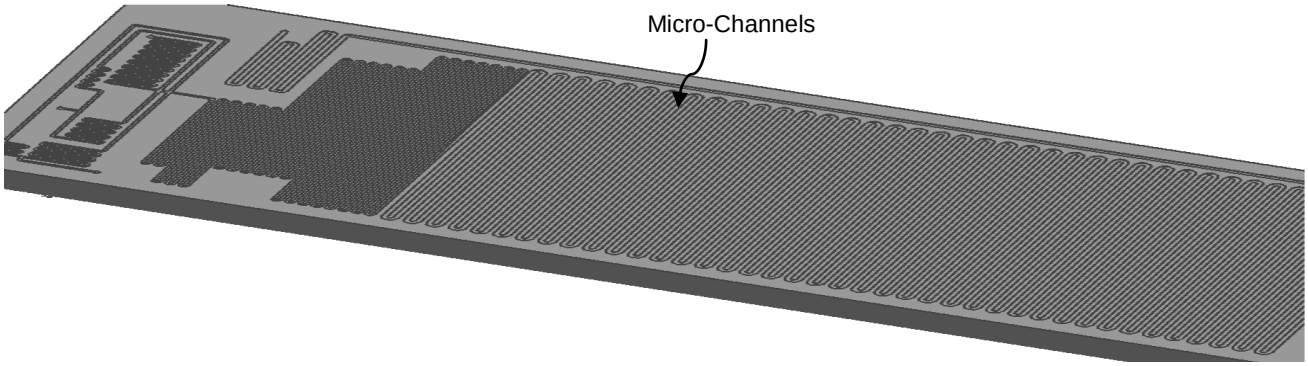

Fig.6 Typical geometry of micromixer (90^{x} 30^{x} 5mm)

1.5. Heat Exchangers

The heat exchanger are of two types 1) The high temperature heat exchanger takes high temperature gas and uses that gas to boil and superheat working fluid. 2) The second type of heat exchanger uses ambient air to cool down and condense the working fluid. The parasitic pump power required to flow the air through the heat exchangers is taken directly from the power turbine and is proportional to the product of the air volumetric flow rate and the pressure drop across the heat exchanger. [19, 34]

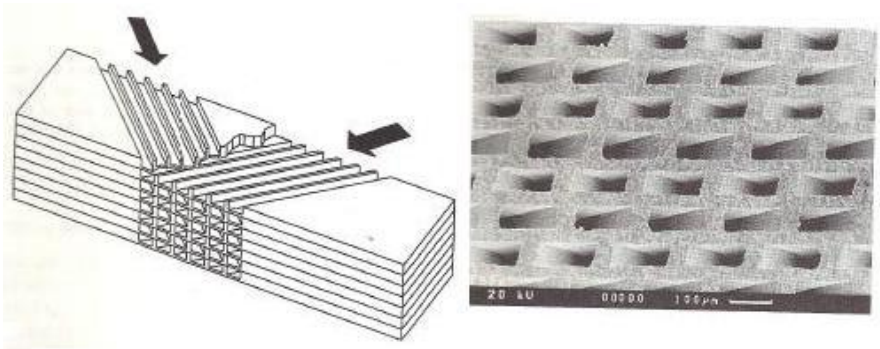

Fig.5 Multi-stack heat exchanger

There are eight sets of parameters that must be determined to establish the design of a specific heat exchanger, air inlet and outlet conditions namely pressure, temperature and mass flow, the working fluid inlet and outlet conditions, heat exchanger channel width, channel depth, channel length, total number of channels, heat exchanger fin thickness, number of stacks. [19, 43, 46] The most critical futures are smallest cross-section and longest possible length.

IV. Manufacturing

1.6. Manufacturing Methods

The manufacturing capability of device depends upon material selection.Following materials are generally used for manufacturing of microfluidic devices. Table.2 shows the different manufacturing processes and material capabilities. [7, 11, 13]

Table.2. Microfluidic Channel Manufacturing Methods

Manufacturing Methods	Principle	Materials	Features
Wet silicon etching	Chemically removal of layer	Silicon,Silicon Dioxide, Silicon Nitride	Low cost, High surface area, low aspect ratio
Dry silicon etching	Plasma assisted etching	Silicon, Silicon Dioxide, Silicon Nitride	High surface area, minimum feature size, High aspect ratio
Lithography	Series of Chemical Reactions	Aluminium , Steel, Glass	Minimum feature size, Maximum surface area, Choice of geometry
Laser Ablation	Bond-Breakage by Pulsed UV Source	Copper, Steel	High aspect ratio, Choice of geometry, Minimum feature size
LIGA	Uses X-ray or UV Light	Silicon wafer, PMMA, SU-8	Minimum feature size, High aspect ratio, Choice of geometry
Micromachining	Cutting of materials with tool	Steel, Copper, Aluminium	Maximum lifetime, Choice of geometry, maximum surface area
µ-EDM	Melting and evaporation of material	Aluminium, Copper	Maximum life time High aspect ratio

1.7. Materials

Commonly used materials for the microfluidic chip manufacturing are Low fluorescence Schott Borofloat glass, Corning 0211 borosilicate glass Fused silica, Quartz Silicon, PMMA, SU-8, PDMS, Steel, Aluminum, copper, etc. [7, 14, 35, 36]

1.8. Effect of Surface Roughness

Pressure drop during internal flow is one of the most important considerations in designing a fluid flow system. Surface roughness was identified as an important parameter in fluid flow as early as in the nineteenth century by Darcy,[21,37,38,39] who carefully conducted experiments with pipes of varying roughness. The Darcy friction factor for laminar flow (Reynolds number less than 2000) is given by the following Eq. (2).

$$f = \frac{64}{R_e} \dots\dots\dots\dots\dots equation\ 2$$

Where, 'f' is the Darcy friction factor and 'R_e' is the Reynolds number. [21]

Wall roughness can be increased to promote mixing of the fluid, or reduced to eliminate flow disturbances. Recently, the effects of surface roughness became of interest from the point of view of passive/active flow control strategies, where one is interested in determining the smallest possible surface modification that may induce the largest possible changes in flow field.[40,41,49,50]

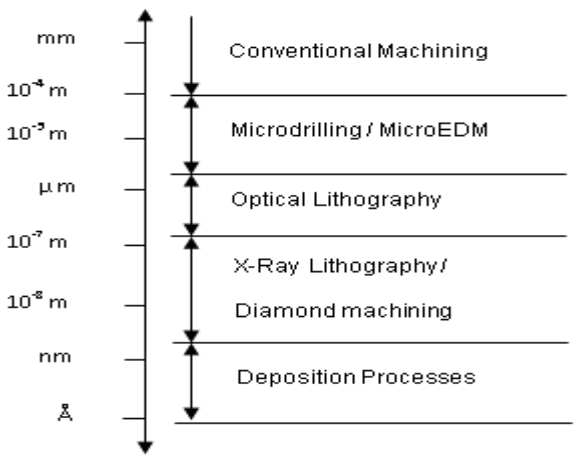

Fig:6 Comparison of surface roughness of different micro-manufacturing processes

V. Bonding Techniques

Bonding methods can be divided into mainly two categories: direct wafer bonding or bonding with intermediate layers. As shown in table.3 [8,15,16] "Wafer bonding" refers to the phenomenon that mirror polished, flat, and clean wafers of almost any material, when brought into contact at room temperature, are locally attracted to each other by van der walls forces and adhere or "bonds" to each Other. [15, 16] ''Wafer bonding'' refers to the phenomenon that mirror polished, flat, and clean wafers of almost any material, when brought into contact at room temperature, are locally attracted to each other by van der Waals forces and adhere or ''bond'' to each other. [41,42,44]

Table.3 Bonding Techniques

Direct Wafer Bonding (Without Intermediate layer)	**Fusion Bonding (same materials)**	• Surfaces must be flat and clean • Substrate washed with piranha solution and immersed in ammonium hydroxide (500C, For 30 min) • Two wafers pressed together for few hours
	Anodic Bonding (Different Materials)	• Use of electric field • surface topologies greater than about 500 Å • 300 to 450 °C and high DC voltage (500-1000V)
Indirect Wafer Bonding(With intermediate layer)	**PDMS Bonding**	• irreversible PDMS bond with an O2 plasma treatment before bonding • siloxane bond created between two wafers
	SU-8 Bonding	• Substrate is cleaned using piranha solution. • Layer of SU-8 photoresist is spun onto the substrate • The cross-linked SU-8 structures are sealed by a second cleaned substrate.

Above bonding techniques used for silicon, glasses, polymers, ceramics, and metals. Ceramic green taps and metal sheets structured by serial techniques can be directly bonded together at high pressure and high temperatures. Ceramic green types are typically bonded at 138 bars, 70^0C for 10 minutes. Stainless steel sheets are typically bonded at 276 bars, 920^0C for 4 hours.[45]

"Diffusion soldering" bonding process is an advanced type of solder bond that can form high- quality hermetic seals at lower temperatures than other bonding technologies. This technique uses one thin metal layer (typically 1-10µm thick) which during a thermal process inter-diffuses with its bonding partner forming an inter-metallic compound layer with re-melting temperature higher than the bonding temperature.[47,48]

In thermo-compression bonding process the two surfaces adhere to each other due to a metal bond established between two metal surfaces pressed together under heating. The bonding mechanism is enhanced by the deformation of the two surfaces in contact in order to disrupt any intervening surface films and enable metal-to-metal contact. By heating the two metal surfaces the contact force applied for the bond process can be minimized due to metal softening. High force uniformity across the bonding area enables high bonding yield. Several metals are used for metal thermo-compression wafer bonding, as Au-Au, Cu-Cu or Al-Al. [24,51,52,53]

The important issues in bonding are, maintaining surface finish & flatness of bonding surface and bonding of metal surfaces for which bonding techniques are not well developed.[59,60,61]

VI. Interfacing with Micro-Systems

Fig.6.illustrates the use of the PDMS connector chips The connector chip self adheres to the micro fluidic component. Aligning is easy due to matching surface relief. The single lithography mask needed for mold fabrication is almost identicalto the one that defines the inlet holes on the microfluidicchip. The only difference is that additional cutting marks forseparation of individual chips have been added. Misalignmentof microfluidic chip and PDMS connector causes airbubbles to remain at the interface, but because PDMS istransparent they can be seen and realignment is easy.Whenalignment is satisfactory, the capillary tube are gently pushed tothe holes in the connector chip. Depending on pressure toleranceneeded, an additional jig can be used to compressesthe connector chip against the microfluidic chip. [17, 54, 55, 56]

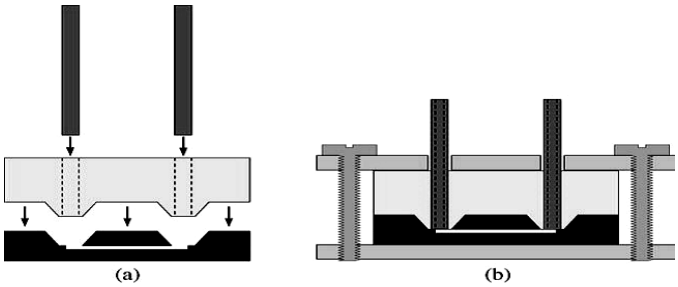

Fig.6 Connector chip usage. (a) Connector chip is aligned to matching surface relief of the microfluidic chip and capillary tubes are pushed to the holes. (b) If higher operating pressures are required, additional mechanical jig provides required tightness.

The design of connector chip mechanism include easy of assembly, reliability, chemical compatibility, minimal dead weight, minimal pressure drop.[57,58]

VII. Conclusion

Micro fluidic devices play important role in the pharmaceutical, biotechnology and chemical energy sectors. There are several issues in design & manufacturing of microfluidic devices and hence selection of material & manufacturing process are important. The material should not participate in the reaction process and hence, they should be chemically inert on the fluid flow passage. Since most of the devices undergo larger pressure, the selected material should withstand such pressures. Most of the microfluidic devices are small cross-sections and long length of channels; similarly extremely flat and high level of surface finish is required on bonding surfaces.

VIII. Acknowledgement

I would like to thanks Mr.Shinoy, Mr.Dandekar, Mr.K.K.Singh, Chemical Engineering Division, BARC, Mumbai for their kind and continuous support.

References

Journal Papers:

[1] Chieko Sakamoto, Nobuyasu Yamaguchi, Masumi Yamada, Rapid quantification of bacterial cells in potable water, Journal of Microbiological Methods 68 (2007) 643–647
[2] J. Tan, J.H. Xu, S.W. Li, G.S. Luo, Drop dispersion in cross junction microfluidic devices, Chemical Engineering Journal 136 (2008) 306–311
[3] Holger Becker, Laurie E. Locascio, Polymer microfluidic devices, Talanta 56 (2002) 267–287
[4] Erik Kjeanga, Ned Djilali, David Sintona, "Microfluidic fuel cells: A review" Journal of Power Sources 186 (2009) 353–369
[5] Agustin Gonz´alezCrevill´en, Miriam Herv´as, Miguel Angel L´opez, "Real sample analysis on *microfluidic* devices" Talanta 74 (2007) 342–357
[6] Mark Bown, Jordan Macinnes and Alexander Vikhanshy, "Reynolds and Peclet Number effects in folding flow mixers", Chemical process engineering 78 (2011) 110-119
[7] A.A.G. Bruzzone, H.L. Costa, P.M. Lonardo, D.A. Lucca, "Advances in engineered surfaces for functional performance" CIRP Annals - Manufacturing Technology 57 (2008) 750–769
[8] Susana Aura and TiinaSikanen, "Novel hybrid material for microfluidic devices", Sensors and Actuators 132 (2008) 397-403
[9] Erik Kjeang, Ned Djilali and David Sinton, "Microfluidic fuel cells: A review", J. Power Sources 186 (2009) 353-369
[10] Chieko Sakamoto and Nobuyasu, "Rapid Quantification of Bacterial Cells in portable Water using a simplified microfluidic devices", J. Microbiological Methods 68 (2007) 643-647
[11] Agustin Gonzalez and Miriam Hervas, "Real sample analysis on microfluidic devices", Talanta 74 (2007) 342-357
[12] Sang Youl Yoon and Sung Yang, "Microfluidic device for refractive index measurement of fluidic sample", Procedia Engineering 5 (2010) 1340-1343
[13] Erica D.Pratt, Chao Huang and Benjamin G. Hawkins, "Rare cell capture in microfluidic devices", J. Chemical engineering science 66 (2011) 1508-1522
[14] Birgit Ungerbock and Gunter Mistlberger, "Oxygen imaging in microfluidic devices with optical sensors applying color cameras", Procedia Engineering 5 (2010) 456-459
[15] Manoj Kumar Moharana, NageswaraRaoPeela, Sameer Khandekar, "Distributed hydrogen production from ethanol in a microfuel processor" Renewable and Sustainable Energy Reviews 15 (2011) 524–533
[16] Chunsun Zhang, Da Xing and Yuyung Li, "Micropumps, microvalves and Micromixers for Microfluidic Chip: Advances and Trends", J. Biotechnology Advances 25 (2007) 483-514
[17] Holger Becker and Laurie E. Locascio, "Polymer Microfluidic Devices", Talanta 56 (2002) 267-287
[18] H. A. Stone, S. Kim, "Microfluidics: Basic Issues, Applications, and Challenges" IEEE 14 (2007)
[19] Sang youlyoon, sung yang, "refractive index measurement" Procedia Engineering 5 (2010) 1340–1343
[20] EugenAxinte, "Glasses as engineering materials: A review" Materials and Design 32 (2011) 1717–1732
[21] Lingxin Chen, GuoanLuo, Kehui Liu, Jiping Ma, Bo Yao, " Bonding of glass based microfluidic chip at low or room temperature" J. Sensors and Actuators B 119 (2006) 335–344
[22] Chung-Xia Zhao and Anton P.J.Middelberg, "Two-phase microfluidic flows", Chemical Engineering Science 66 (2011) 1394-1411
[23] Mario Castan˜o-A´ lvarez a, Diego F. PozoAyuso b, Miguel Garc´ıaGranda b, "Critical points in the fabrication of microfluidic devices on glass substrates" Sensors and Actuators B 130 (2008) 436–448
[24] A.A.G. Bruzzone, H.L. Costa, P.M. Lonardo, D.A. Lucca, "Advances in engineered surfaces for functional performance" CIRP Annals - Manufacturing Technology 57 (2008) 750–769
[25] T.Rogers, J.Kowal, " Selection of glass, anodic bonding conditions and material compatibility" Sensors and Actuators B 130 (2008) 436–448
[26] M.M.R. Howlader, Satoru Suehara, TadatomoSuga, "Room temperature glass/glass wafer bonding"
[27] Tamer Sinmazçelik, EgemenAvcu, Mustafa Özgür Bora, OnurÇoban, "fiber metal laminates and bonding techniques" Materials and Design 32 (2011) 3671–3685
[28] A.S.Rawool and SushantaK.Mitra, "Numerical Simulation of flow through microchannels with roughness", microfluidic nanofluidics 10 (2005) 1007-1040
[29] Osamu Tonomura, masaru Noda and manabu Kano, "Optimal Design Approch for Microreactors with Uniform Residence Time Distribution", APCChE, 4B-07 (2004) 17-21
[30] Yu Chang Kim, JooH.Kang and Sang-Jin Park, "Microfluidics biomechanical devices for compression of cell stimulation and lysis", Sensors and Actuators 128 (2007) 108-116

[31] Gerardo Perozziello, FrederikBundgaard, Oliver Geschke, "Fluidic interconnections for microfluidic systems" Sensors and Actuators B 130 (2008) 947–953
[32] Manoj Kumar Moharana, NageswaraRaoPeela, Sameer Khandekar, "Distributed hydrogen production from ethanol in a microfuelprocessor" Renewable and Sustainable Energy Reviews 15 (2011) 524–533
[33] Pádraig Mac Suibhne,aToshkoZhelev,aErzengXue, RegMannb,"Micro reactor design for Distributed Fuel generation"
[34] E. Vásquez-Alvarez, F. T. Degasperi, L. G. Morita," Develpoment of Micro-Heat Exchangers With Stacked Plates"
[35] Viorel DR¸AGOI1, Erkan CAKMAK2, Eric PABO2," Metal Wafer Bonding for MEMS Devices, Volume 13, Number 1, 2010, 65{72}
[36] Ackermann KR, Henkel T, Popp J, Quantitative onlinedetection of low concentrated drugs via a SERS microfluidic system. ChemPhysChem 8:2665–2670 (2007)
[37] Agrawal A, Zhang C, Byassee T, Tripp RA, Nie S, Counting single native biomolecules and intact viruses with color-coded nanoparticles. Anal Chem 78:1061–1070 (2006)
[38] Albrecht MG, Creighton JA, Anomalously intense Raman spectra of pyridine at a silver electrode. J Am ChemSoc 99:5215–5219 (1977)
[39] Alivisatos P, The use of nanocrystals in biological detection. Nat Biotechnol 22:47–52 (2004)
[40] Aubin KL, Huang J, Park SM, Yang Y, Kondratovich M, Craighead HG, Ilic BR Microfluidic encapsulated nanoelectromechanical resonators. J VacSciTechnol B 25:1171–1174 (2007)
[41] Bailey RC, Kwong GA, Radu CG, Witte ON, Heath JR DNA-encoded antibody libraries: a unified platform for multiplexed cell sorting and detection of genes and proteins. J Am ChemSoc 129:1959–1967 (2007)
[42] Banholzer MJ, Millstone JE, Qin L, MirkinCA Rationally designed nanostructures for surface-enhanced Raman spectroscopy. ChemSoc Rev 37:885–897 (2008)
[43] Bell SEJ, SirimuthuNMS Surface-enhanced Raman spectroscopy (SERS) for submicromolar detection of DNA/RNA mononucleotides. J Am ChemSoc 128:15580–15581 (2006)
[44] Benchaib A, Delorme R, Pluvinage M, Bryon PA, Souchier C Evaluation of five green fluorescence-emitting streptavidin-conjugated fluorochromes for use in immunofluorescence microscopy. Histochem Cell Biol 106:253–256 (1996)
[45] Biswal SL, Raorane D, Chaiken A, Birecki H, Majumdar A, Nanomechanical detection of DNA melting on microcantilever surfaces. Anal Chem 78:7104–7109 (2006)
[46] Bizzarri AR, Cannistraro S (2007) SERS detection of thrombin by protein recognition using functionalized gold nanoparticles. NanomedNanotechnolBiol Med 3:306–310
[47] Bonham AJ, Braun G, Pavel I, Moskovits M, Reich NO, Detection of sequence-specific protein-DNA interactions via surface enhanced resonance Raman scattering. J Am ChemSoc 129:14572–14573 (2007)
[48] Braun G, Lee SJ, Dante M, Nguyen TQ, Moskovits M, Reich N Surface-enhanced Raman spectroscopy for DNA detection by nanoparticle assembly onto smooth metal films. J Am ChemSoc 129:6378–6379 (2007)
[49] Briggs MS, Burns DD, Cooper ME, Gregory SJ A pH sensitive fluorescent cyanine dye for biological applications. ChemCommun 23:2323–2324 (2000)
[50] Bruchez M, Moronne M, Gin P, Weiss S, Alivisatos AP Semiconductor nanocrystals as fluorescent biological labels. Science 281:2013–2016 (1998)
[51] Bunimovich YL, Shin YS, Yeo WS, Amori M, Kwong G, Heath JR Quantitative real-time measurements of DNA hybridization with alkylated nonoxidized silicon nanowires in electrolyte solution. J Am ChemSoc 128:16323–16331 (2006)
[52] Burg TP, Godin M, Knudsen SM, Shen W, Carlson G, Foster JS, Babcock K,Manalis SR Weighing of biomolecules, single cells and single nanoparticles in fluid. Nature 446:1066–1069 (2007)
[53] Cai H, Wang Y, He P, Fang Y Electrochemical detection of DNA hybridization based on silver-enhanced gold nanoparticle label. Anal ChimActa 469:165–172 (2002)
[54] Chan WCW, Nie SM Quantum dot bioconjugates for ultrasensitive nonisotopic detection. Science 281:2016–2018 (1998)
[55] Chan WCW, Maxwell DJ, Gao X, Bailey RE, Han M, NieS Luminescent quantum dots for multiplexed biological detection and imaging. CurrOpinBiotechnol 13:40–46 (2002)
[56] Chang-yen DA, Myszka D, Gale BK A novel PDMS Microfluidic spotter for fabrication of protein chips and micro-arrays. J MicroelectromechSyst 5:1145–1151 (2006)
[57] Chen L, ChooJ,Recent advances in surface-enhanced Raman scattering detection technology for microfluidic chips. Electro-phoresis 29:1815–1828 (2008)
[58] Cheng MM-C, Cuda G, Bunimovich YL, Gaspari M, Heath JR, Hill HD, Mirkin CA, Nijdam AJ, Terracciano R, Thundat T, Ferrari M Nanotechnologies for biomolecular detection and medical diagnostics. CurrOpinChemBiol 10:11–19 (2006)
[59] Cheong KH, Yi DK, Lee JG, Park JM, Kim MJ, Edel JB, Ko C Gold nanoparticles for one step DNA extraction and real-time PCR of pathogens in a single chamber. Lab Chip 8:810–813 (2008)
[60] Chinowsky TM, Soelberg SD, Baker P, Swanson NR, Kauffman P, Mactutis A, Grow MS, Atmar R, Yee SS, Furlong CE Portable 24-analyte surface plasmon resonance instruments for rapid, versatile biodetection. BiosensBioelectron 22:2268–2275 (2007)
[61] Cross SE, Jin YS, Rao J, Gimzewski JK, Nanomechanical analysis of cells from cancer patients. Nat Nanotechnol 2:780–783 (2007)

International Journal of Modern Engineering Research (IJMER)
www.ijmer.com Vol.3, Issue.2, March-April. 2013 pp-857-863 ISSN: 2249-6645

On wgr □-Continuous Functions in Topological Spaces

A.Jayalakshmi, [1] C.Janaki[2]
[1]*Department of Mathematics, Sree Narayana Guru College, Coimbatore, TN, India*
[2]*Department of Mathematics, L.R.G.Govt.Arts.College for Women, Tirupur, TN, India*

Abstract: *In this paper, we introduce new type of continuous functions called strongly wgrα-continuous and perfectly wgrα-continuous and study some of its properties. Also we introduce the concept of wgrα-compact spaces and wgrα-connected spaces and some their properties are analyzed.*

Subject Classification: *54C05, 54C10.*

Keywords: *perfectly wgrα-continuous, strongly wgrα-continuous, wgrα-compact spaces and wgrα-connected spaces.*

I. Introduction

Balachandran et al in [9, 10] introduced the concept of generalized continuous maps of a topological space. A property of gpr continuous functions was discussed by Y.Gnanambal and Balachandran K [5]. Strong forms of continuity and generalization of perfect functions were introduced and discussed by T.Noiri [11, 12]. Regular α-open set is introduced by A.Vadivel and K. Vairamanickam [14]. Rg-compact spaces and rg-connected spaces, τ^*-generalized compact spaces and τ^*-generalized connected spaces, gb-compactness and gb-connectedness introduced by A.M.Al.Shibani [1], S.Eswaran and A.Pushpalatha [4], S.S.Benchalli and Priyanka M.Bansali [2] respectively. In this paper we establish the relationship between perfectly wgrα-continuous and strongly wgrα-continuous. Also we introduce the concept of wgrα-compact spaces and wgrα-connected spaces and study their properties using wgrα-continuous functions.

II. Preliminary Definitions

Definition: 2.1
A subset A of a topological space (X, τ) is called α-closed [10] if a ⊂ int (cl (int (A)).
Definition:2.2
A subset A of a topological space (X, τ) is called gα-closed [9] if αcl (A) ⊂ U,when ever A ⊂ U and U is α-open in X.
Definition: 2.3
A subset A of a topological space (X, τ) is called rwg-closed [14] if cl (int (A)) ⊂ U, whenever A ⊂ U and U is regular-open in X.
Definition: 2.4
A map f: X→Y is said to be continuous [3] if $f^{-1}(V)$ is closed in X for every closed set V in Y.
Definition: 2.5
A map f: X→Y is said to be wgrα- continuous [6] if $f^{-1}(V)$ is wgrα-closed in X for every closed set V in Y.
Definition: 2.6
A map f: X→Y is said to be perfectly-continuous [12] if $f^{-1}(V)$ is clopen in X for every open set V in Y.
Definition: 2.7
A map f: X→Y is said to be strongly-continuous [8] if $f^{-1}(V)$ is clopen in X for every subset V in Y.
Definition: 2.8
A function f: X →Y is called wgrα- irresolute [6] if every $f^{-1}(V)$ is wgrα-closed in X for every wgrα-closed set V of Y.
Definition: 2.9
A function f: X → Y is said to be wgrα-open [7] if f(V) is wgrα-open in Y for every open set V of X.
Definition: 2.10
A function f: X → Y is said to be pre wgrα-open [7] if f(V) is wgrα-open in Y for every wgrα-open set V of X.
Definition: 2.11
A space (X,τ) is called wgrα-$T_{1\backslash 2}$ space[7] if every wgrα-closed set is α-closed.
Definition: 2.12
A space (X,τ) is called $T_{wgr\alpha}$-space[7] if every wgrα-closed set is closed.
The complement of the above mentioned closed sets are their respective open sets.

III. Strongly Wgr □-Continuous and Perfectly Wgr □-Continuous Functions

Definition: 3.1
A function f :(X,τ) → (Y,σ) is called strongly wgrα-continuous if $f^{-1}(V)$ is open in (X,τ) for every wgrα-open set V of (Y,σ).
Definition: 3.2
A function f :(X,τ) → (Y,σ) is called perfectly wgrα-continuous if $f^{-1}(V)$ is clopen in (X,τ) for every wgrα-open set V of (Y,σ).
Definition: 3.3

A function f :$(X,\tau) \to (Y,\sigma)$ is called strongly wgrα- irresolute if $f^{-1}(V)$ is open in (X,τ) for every wgrα-open set V of (Y,σ).

Definition: 3.4

A function f :$(X,\tau) \to (Y,\sigma)$ is called strongly rwg-continuous if $f^{-1}(V)$ is open in (X,τ) for every rwg-open set V of (Y,σ).

Definition: 3.5

A function f :$(X,\tau) \to (Y,\sigma)$ is called perfectly rwg-continuous if $f^{-1}(V)$ is clopen in (X,τ) for every rwg-open set V of (Y,σ).

Theorem: 3.6

If a function f :$(X,\tau) \to (Y,\sigma)$ is perfectly wgrα-continuous, then f is perfectly continuous.

Proof

Let F be any open set of (Y,σ).Since every open set is wgrα-open.We get that F is wgrα-open in (Y,σ).By assumption , we get that $f^{-1}(F)$ is clopen in (X,τ). Hence f is perfectly continuous.

Theorem: 3.7

If f: $(X,\tau) \to (Y,\sigma)$ is strongly wgrα-continuous, then it is continuous.

Proof

Let U be any open set in (Y,σ).Since every open set is wgrα-open, U is wgrα-open in (Y,σ).Then $f^{-1}(U)$ is open in (X,τ). Hence f is continuous.

Remark: 3.8

Converse of the above theorem need not be true as seen in the following example.

Example: 3.9

Let $X=\{a,b,c,d\},\tau=\{\phi,X,\{a\},\{c,d\},\{a,c,d\}\}$ and $\sigma=\{\phi,Y,\{a\},\{b,c\},\{a,b,c\}\}$. Define $f:X \to Y$ by f(a)=a, f(b)=d, f(c)=c, f(d)=b. Here f is continuous, but it is not strongly wgrα-continuous.

Theorem: 3.10

Let (X,τ) be any topological space and (Y,σ) be a $T_{wgr\alpha}$-space and f: $(X,\tau) \to (Y,\sigma)$ be a map. Then the following are equivalent:

(i) f is strongly wgrα-continuous.

(ii) f is continuous.

Proof

(i) $\Rightarrow$(ii) Let U be any open set in (Y,σ).Since every open set is wgrα-open,U is wgrα-open in (Y,σ).Then $f^{-1}(U)$ is open in (X,τ). Hence f is continuous.

(ii)$\Rightarrow$(i) Let U be any wgrα-open set in (Y,σ).Since (Y,σ) is a $T_{wgr\alpha}$-space,U is open in (Y,σ).Since f is continuous. Then $f^{-1}(U)$ is open in (X,τ). Hence f is strongly wgrα-continuous.

Theorem: 3.11

If f: $(X,\tau) \to (Y,\sigma)$ is strongly rwg -continuous, then it is strongly wgrα- continuous.

Proof

Let U be any wgrα-open set in (Y,σ).By hypothesis,$f^{-1}(U)$ is open and closed in (X,τ). Hence f is strongly wgrα-continuous.

Remark: 3.12

Converse of the above theorem need not be true as seen in the following example.

Example: 3.13

Let $X=\{a,b,c\},\tau=\sigma=\{\phi,X,\{a\},\{b\},\{a,b\}\}$.Define map $f:X \to Y$ is an identity map. Here f is strongly wgrα-continuous, but it is not strongly rwg-continuous.

Theorem: 3.14

Let f: $(X,\tau) \to (Y,\sigma)$ be a map.Both (X,τ) and (Y,σ) are $T_{wgr\alpha}$-space . Then the following are equivalent:

(i)f is wgrα-irresolute.

(ii)f is strongly wgrα-continuous.

(iii) f is continuous.

(iv) f is wgrα-continuous.

Proof

Straight forward.

Theorem: 3.15

If f :$(X,\tau) \to (Y,\sigma)$ is strongly wgrα-continuous and A is open subset of X, then the restriction f |A:$A \to Y$ is strongly wgrα-continuous.

Proof

Let V be any wgrα-closed set of Y. Since f is strongly wgrα-continuous,then $f^{-1}(V)$ is open in (X,τ).Since A is open in X,$(f|A)^{-1}(V)=A \cap f^{-1}(V)$ is open in A. Hence f|A is strongly wgrα-continuous.

Theorem: 3.16

If a function f :$(X,\tau) \to (Y,\sigma)$ is perfectly wgrα-continuous, then f is strongly wgrα-continuous.

Proof

Let F be any wgrα-open set of (Y,σ).By assumption, we get that $f^{-1}(F)$ is clopen in(X,τ),which implies that $f^{-1}(F)$ is closed and open in (X,τ).Hence f is strongly wgrα-continuous.

Remark: 3.17

Converse of the above theorem need not be true as seen in the following example.

Example: 3.18

Let X={a,b,c},τ={ϕ,X,{a},{c},{a,c}}= σ. Define f:X → Y by f(a)=a, f(b)=b, f(c)=c. Here f is strongly wgrα-continuous, but it is not perfectly wgrα-continuous.

Theorem: 3.19

If f: (X,τ) → (Y,σ) is perfectly rwg-continuous, then it is perfectly wgrα-continuous.

Proof

As f is strongly continuous,f^{-1}(U) is both open and closed in (X,τ) for every wgrα-open set U in (Y,σ). Hence f is perfectly wgrα-continuous.

Remark: 3.20

The above discussions are summarized in the following diagram.

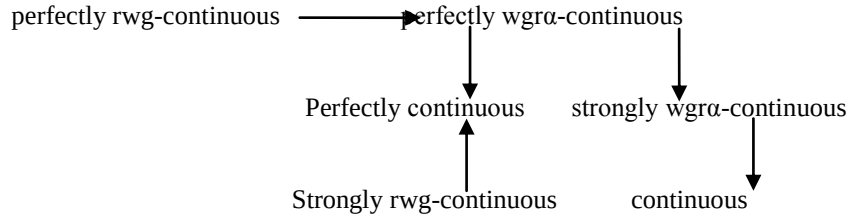

Theorem: 3.21

Let (X,τ) be a discrete topological space and (Y,σ) be any topological space .Let f: (X,τ) → (Y,σ) be a map. Then the following statements are equivalent:

(i) f is strongly wgrα-continuous.

(ii) f is perfectly wgrα-continuous.

Proof

(i) ⟹ (ii) Let U be any wgrα-open set in (Y,σ).By hypothesis f^{-1}(U) is open in (X,τ).Since(X,τ) is a discrete space,f^{-1}(U) is also closed in (X,τ). f^{-1}(U) is both open and closed in (X,τ). Hence f is perfectly wgrα- continuous.

(ii) ⟹ (i) Let U be any wgrα-open set in (Y,σ).Then f^{-1}(U) is both open and closed in (X,τ). Hence f is strongly wgrα-continuous.

Theorem:3.22

If f:(X,τ) → (Y,σ) and g:(Y,σ) → (Z,μ) are perfectly wgrα-continuous ,then their composition g ∘ f:(X,τ) → (Z,μ) is also perfectly wgrα-continuous.

Proof

Let U be a wgrα-open set in (Z,μ).Since g is perfectly wgrα-continuous, we get that g^{-1}(U) is open and closed in (Y,σ).As any open set is wgrα-open in (X,τ) and f is also strongly wgrα-continuous, $f^{-1}(g^{-1}(U))= (g \circ f)^{-1}$(U) is both open and closed in (X,τ). Hence g ∘ f is perfectly wgrα-continuous.

Theorem:3.23

If f:(X,τ) → (Y,σ) and g:(Y,σ) → (Z,μ) be any two maps. Then their composition g ∘ f: (X,τ) → (Z,μ) is

(i) wgrα-irresolute if g is strongly wgrα-continuous and f is wgrα-continuous.

(ii) Strongly wgrα-continuous if g is perfectly wgrα-continuous and f is continuous.

(iii) Perfectly wgrα-continuous if g is strongly wgrα-continuous and f is perfectly wgrα-continuous.

Proof

(i)Let U be a wgrα-open set in (Z,μ). Then g^{-1}(U) is open in (Y,σ).Since f is wgrα-continuous, $f^{-1}(g^{-1}(U))=(g \circ f)^{-1}$(U) is wgrα-open in (X,τ). Hence g ∘ f is wgrα-irresolute.

(ii)Let U be any wgrα-open set in (Z,μ).Then g^{-1}(U) is both open and closed in (Y,σ) and therefore $f^{-1}(g^{-1}(U))= (g \circ f)^{-1}$(U) is both open and closed in (X,τ). Hence g ∘ f is strongly wgrα-continuous.

(iii) Let U be any wgrα-open set in (Z,μ).Then g^{-1}(U) is open and closed in (Y,σ).By hypothesis, $f^{-1}(g^{-1}(U))$ is both open and closed in (X,τ).Hence g ∘ f is perfectly wgrα-continuous.

Theorem: 3.24

If f:(X,τ) → (Y,σ) and g:(Y,σ) → (Z,μ) are strongly wgrα-continuous ,then their composition g ∘ f:(X,τ) → (Z,μ) is also strongly wgrα-continuous.

Proof

Let U be a wgrα-open set in (Z,μ).Since g is strongly wgrα-continuous, we get that g^{-1}(U) is open in (Y,σ).It is wgrα-open in (Y,σ) As f is also strongly wgrα-continuous,$f^{-1}(g^{-1}(U))= (g \circ f)^{-1}$(U) is open in (X,τ). Hence g ∘ f is continuous.

Theorem:3.25

If f:(X,τ) → (Y,σ) and g:(Y,σ) → (Z,μ) be any two maps. Then their composition g ∘ f :(X,τ) → (Z,μ) is (i) strongly wgrα-continuous if g is strongly wgrα-continuous and f is continuous.

(ii) wgrα-irresolute if g is strongly wgrα-continuous and f is wgrα-continuous.

(iii) Continuous if g is wgrα-continuous and f is strongly wgrα-continuous.

Proof

(i) Let U be a wgrα-open set in (Z,μ).Since g is strongly wgrα-continuous, g^{-1}(U) is open in (Y,σ).Since f is continuous, $f^{-1}(g^{-1}(U))= (g \circ f)^{-1}$(U) is open in (X,τ). Hence g ∘ f is strongly wgrα-continuous.

(ii) Let U be a wgrα-open set in (Z,μ).Since g is strongly wgrα-continuous, $g^{-1}(U)$ is open in (Y,σ).As f is wgrα-continuous, $f^{-1}(g^{-1}(U))= (g \circ f)^{-1}(U)$ is wgrα-open in (X,τ). Hence g ∘ f is wgrα-irresolute.
(iii)Let U be any open set in (Z,μ).Since g is wgrα-continuous, $g^{-1}(U)$ is wgrα-open in (Y,σ).As f is strongly wgrα-continuous, $f^{-1}(g^{-1}(U))= (g \circ f)^{-1}(U)$ is open in (X,τ). Hence g ∘ f is continuous.

Theorem: 3.26

Let f: $(X,\tau) \to (Y,\sigma)$ and g: $(Y,\tau) \to (Z,\eta)$ be two mappings and let $g \circ f : (X,\tau) \to (Z,\eta)$ be wgrα-closed.If g is strongly wgrα-irresolute and bijective, then f is closed.

Proof

Let A be closed in (X,τ),then $(g \circ f)(A)$ is wgrα-closed in (Z,η).Since g is strongly wgrα-irresolute,$g^{-1}(g \circ f)(A)=f(A)$ is closed in (Y,σ).Hence f(A) is closed.

Theorem: 3.27

If $f : (X,\tau) \to (Y,\sigma)$ is perfectly wgrα-continuous and A is any subset of X, then the restriction $f|A : A \to Y$ is also perfectly wgrα-continuous.

Proof

Let V be any wgrα-closed set in(Y,σ). Since f is perfectly wgrα-continuous, $f^{-1}(V)$ is both open and closed in (X,τ).$(f|A)^{-1}(V)=A \cap f^{-1}(V)$ is both open and closed in A. Hence f|A is perfectly wgrα-continuous.

IV. Wgr □-Compact Spaces

Definition: 4.1

A collection $\{A_\alpha : \alpha \in \nabla\}$ of wgrα-open sets in a topological space X is called wgrα-open cover of a subset B of X if $B \subset \cup \{A_\alpha : \alpha \in \nabla\}$ holds.

Definition: 4.2

A topological space (X,τ) is wgrα-compact if every wgrα-open cover of X has a finite subcover.

Definition: 4.3

A subset B of X is called wgrα-compact relative of X if for every collection $\{A_\alpha : \alpha \in \nabla\}$ of wgrα-open subsets of X such that $B \subset \{A_\alpha : \alpha \in \nabla\}$,there exists a finite subset $\nabla_\circ$ of ∇ such that $B \subset \cup \{A_\alpha : \alpha \in \nabla_\circ\}$.

Definition: 4.4

A subset B of X is said to be wgrα-compact if B is wgrα-compact subspace of X.

Theorem: 4.5

Every wgrα-closed subset of a wgrα-compact space is wgrα-compact space relative to X.

Proof

Let A be wgrα-closed subset of X, then A^c is wgrα-open. Let $O=\{G_\alpha : \alpha \in \nabla\}$ be a cover of A by wgrα-open subsets of X.Then $W=O \cup A^C$ is an wgrα-open cover of X. That is $X=(\cup \{G_\alpha : \alpha \in \nabla\}) \cup A^C$ .By hypothesis, X is wgrα-compact. Hence W has a finite subcover of X say $(G_1 \cup G_2 \cup G_3 \cup \cdots \cup G_n) \cup A^C$. But A and A^C are disjoint, hence $A \subset G_1 \cup G_2 \cup \cdots \cup G_n$. So O contains a finite subcover for A, therefore A is wgrα-compact relative to X.

Theorem: 4.6

Let f: $X \to Y$ be a map:
(i) If X is wgrα-compact and f is wgrα-continuous bijective, then Y is compact.
(ii)If f is wgrα-irresolute and B is wgrα-compact relative to X, then f(B) is wgrα-compact relative to Y.

Proof

(i)Let f: $X \to Y$ be an wgrα-continuous bijective map and X be an wgrα-compact space. Let $\{A_\alpha : \alpha \in \nabla\}$ be an open cover for Y.Then $\{f^{-1}(A_\alpha) : \alpha \in \nabla\}$ is an wgrα-open cover of X. Since X is wgrα-compact, it has finite subcover say $\{f^{-1}(A_1), f^{-1}(A_2), \ldots, f^{-1}(A_n)\}$,but f is surjective,so $\{A_1,A_2,\ldots,A_n\}$ is a finite subcover of Y.
Therefore Y is compact.

(ii) Let $B \subset X$ be wgrα-compact relative to X,$\{A_\alpha : \alpha \in \nabla\}$ be any collection of wgrα-open subsets of Y such that $f(B) \subset \cup \{A_\alpha : \alpha \in \nabla\}$.Then $B \subset \cup \{f^{-1}(A_\alpha) : \alpha \in \nabla\}$. By hypothesis, there exists a finite subset $\nabla_\circ$ of ∇ such that $f(B) \subset \cup \{A_\alpha : \alpha \in \nabla\}$.Then $B \subset \cup \{ f^{-1}(A_\alpha) : \alpha \in \nabla\}$.By hypothesis, there exists a finite subset $\nabla_\circ$ of ∇ such that $B \subset \cup \{f^{-1}(A_\alpha) : \alpha \in \nabla_\circ\}$.Therefore, we have $f(B) \subset \cup \{A_\alpha : \alpha \in \nabla_\circ\}$ which shows that f(B) is wgrα-compact relative to Y.

Theorem: 4.7

If f: $X \to Y$ is prewgrα-open bijection and Y is wgrα-compact space, then X is a wgrα-compact space.

Proof

Let $\{U_\alpha : \alpha \in \nabla\}$ be a wgrα-open cover of X.So $X=\bigcup_{\alpha\in\nabla} U_\alpha$ and then $Y=f(X)=f(\bigcup_{\alpha\in\nabla} U_\alpha)=\bigcup_{\alpha\in\nabla} f(U_\alpha)$ .Since f is prewgrα-open, for each $\alpha \in \nabla$,$f(U_\alpha)$ is wgrα-open set. By hypothesis, there exists a finite subset $\nabla_\circ$ of ∇ such that $Y=\bigcup_{\alpha\in\nabla_\circ} f(U_\alpha)$

Therefore, $X=f^{-1}(Y)=f^{-1}(\bigcup_{\alpha\in\nabla_\circ} f(U_\alpha))=\bigcup_{\alpha\in\nabla_\circ} U_\alpha$ This shows that X is wgrα-compact.

Theorem: 4.8

If $f:X \to Y$ is wgrα-irresolute bijection and X is wgrα-compact space, then Y is a wgrα-compact space.

Proof

Let $\{U_\alpha : \alpha \in \nabla\}$ be a wgrα-open cover of Y. So $Y=\bigcup_{\alpha\in\nabla} U_\alpha$ and then $X=f^{-1}(Y)=f^{-1}(\bigcup_{\alpha\in\nabla} U_\alpha)=\bigcup_{\alpha\in\nabla} f^{-1}(U_\alpha)$ .Since f is wgrα-irresolute, it follows that for each $\alpha \in \nabla$, $f^{-1}(U_\alpha)$ is wgrα-open set. By wgrα-compactness of X, there exists a finite subset $\nabla_\circ$ of ∇ such that $X=\bigcup_{\alpha\in\nabla_\circ} f^{-1}(U_\alpha)$. Therefore, $Y=f(X)=f(\bigcup_{\alpha\in\nabla_\circ} f^{-1}(U_\alpha))=\bigcup_{\alpha\in\nabla_\circ} U_\alpha$ .This shows that Y is wgrα-compact.

Theorem: 4.9

A wgrα-continuous image of a wgrα-compact space is compact.

Proof

Let $f: X \to Y$ be a wgrα-continuous map from a wgrα-compact space X onto a topological space Y. let $\{A_i : i \in \nabla\}$ be an open cover of Y.Then $\{f^{-1}(A_i) : i \in \nabla\}$ is wgrα-open cover of X. Since X is wgrα-compact,it has finite subcover,say$\{f^{-1}(A_1),f^{-1}(A_2),\ldots,f^{-1}(A_n)\}$.Since f is onto,$\{A_1,A_2,\ldots,A_n\}$ and so Y is compact.

Theorem: 4.10

A space X is wgrα-compact if and only if each family of wgrα-closed subsets of X with the finite intersection property has a non-empty intersection.

Proof

X is wgrα-compact and A is any collection of wgrα-closed sets with F.I.P. Let $A=\{F_\alpha : \alpha \in \nabla\}$ be an arbitrary collection of wgrα-closed subsets of X with F.I.P, so that $\bigcap\{F_{\alpha_i} : i \in \nabla_o\} \neq \phi \to (1)$**,**we have to prove that the collection A has non-empty intersection ,that is, $\bigcap\{F_\alpha : \alpha \in \nabla\} \neq \phi \to (2)$.Let us assume that the above condition does not hold and hence $\bigcap\{F_\alpha : \alpha \in \nabla\} = \phi$.Taking complements of both sides,we get $\bigcup\{F_\alpha^C : \alpha \in \nabla\} = X \to (3)$.But each F_α being wgrα-closed,which implies that F_α^C is wgrα-open and hence from (3),we conclude that $C=\{F_\alpha^C : \alpha \in \nabla\}$ is an wgrα open cover of X. Since X is wgrα-compact, this cover C has a finite subcover. $C=\{F_{\alpha_i} : i \in \nabla_o\}$ is also an open subcover. Therefore $X=\bigcup\{F_{\alpha_i}^C : i \in \nabla_o\}$.Taking complement , we get $\phi=\bigcap\{F_{\alpha_i} : i \in \nabla_o\}$which is a contradiction of (1).Hence $\bigcap\{F_\alpha : \alpha \in \nabla\} \neq \phi$. Conversely, suppose any collection of wgrα-closed sets with F.I.P has a empty intersection.Let $C=\{G_\alpha : \alpha \in \nabla\}$,where G_α is a wgrα-open cover of X and hence $X=\bigcup\{G_\alpha : \alpha \in \nabla\}$**.**Taking complements, we have $\phi=\bigcap\{G_\alpha^C : \alpha \in \nabla\}$**.**But G_α^C is wgrα-closed. Therefore the class A of wgrα-closed subsets with empty intersection.So that it does not have F.I.P. Hence there there exists a finite number of wgrα-closed sets $G_{\alpha_i}^C$ such that $i \in \nabla_o$ with empty intersection. That is,$\{G_{\alpha_i} : i \in \nabla_o\} = \phi$.Taking complement, we have $\{G_{\alpha_i}^C : i \in \nabla_o\} = X$ **.**Therefore C of X has an open subcover $C^*=\{G_{\alpha_i} : i \in \nabla_o\}$.Hence (X,τ) is compact.

Theorem :4.11

If f: $(X,\tau) \to (Y,\sigma)$ is a strongly wgrα-continuous onto map, where (X,τ) is a compact space, then (Y,σ) is wgrα-compact.

Proof

Let $\{A_i : i \in \nabla\}$ be a wgrα-open cover of (Y,σ).Since f is strongly wgrα-continuous,$\{f^{-1}(A_i) : i \in \nabla\}$ is an open cover (X,τ).As (X,τ) is compact, it has a finite subcover say,$\{f^{-1}(A_1),f^{-1}(A_2),\ldots, f^{-1}(A_n)\}$ and since f is onto, $\{A_1,A_2,\ldots,A_n\}$ is a finite subcover of (Y,σ) and therefore (Y,σ) is wgrα-compact.

Theorem :4.12

If a map f: $(X,\tau) \to (Y,\sigma)$ is a perfectly wgrα-continuous onto map, where (X,τ) is compact, then (Y,σ) is wgrα-compact.

Proof

Since every perfectly wgrα-continuous function is strongly wgrα-continuous. Therefore by theorem 4.11, (Y,σ) is wgrα-compact .

V. Wgr □-Connected Spaces

Definition: 5.1

A Space X is said to be wgrα-connected if it cannot be written as a disjoint union of two non-empty wgrα-open sets.

Definition: 5.2
A subset of X is said to be wgrα-connected if it is wgrα-connected as a subspace of X.
Definition: 5.3
A function f: $(X,\tau) \to (Y,\sigma)$ is called contra wgrα-continuous if $f^{-1}(V)$ is wgrα-closed in (X,τ) for each open set V in (Y,σ).
Theorem: 5.4
For a space X, the following statements are equivalent
(i)X is wgrα-connected.
(ii)X and φ are the only subsets of X which are both wgrα-open and wgrα-closed.
(iii)Each wgrα-continuous map of X into some discrete space Y with atleast two points is a constant map.
Proof
(i) $\Rightarrow$(ii) Let X be wgrα-connected. Let A be wgrα-open and wgrα-closed subset of X. Since X is the disjoint union of the wgrα-open sets A and A^C, one of these
sets must be empty. That is, A =φ or A=X.
(ii) $\Rightarrow$(i) Let X be not wgrα-connected, which implies $X=A \cup B$,where A and B are disjoint non-empty wgrα-open subsets of X. Then A is both wgrα-open and wgrα-closed. By assumption A=φ or A=X, therefore X is wgrα-connected.
(ii)$\Rightarrow$(iii) Let $f:X \to Y$ be wgrα –continuous map from X into discrete space Y with atleast two points, then$\{ f^{-1}(y):y\in Y\}$ is a cover of X by wgrα-open and wgrα-closed sets. By assumption, $f^{-1}(y)=\varphi$ or X for each y$\in$ Y. If $f^{-1}(y)=\varphi$ for all y$\in$ Y, then f is not a map. So there exists a exactly one point y$\in$ Y such that $f^{-1}(y)\neq \varphi$ and hence $f^{-1}(y)$
=X. This shows that f is a constant map.
(iii)$\Rightarrow$(ii) Let O≠φ be both an wgrα-open and wgrα-closed subset of X.Let $f:X \to Y$ be wgrα-continuous map defined by $f(O)=\{y\}$ and $f(O^C)=\{\omega\}$ for some distinct
points y and ω in Y. By assumption f is constant, therefore O=X.
Theorem: 5.5
Let f: $X \to Y$ be a map:
(i) If X is wgrα-connected and f is wgrα-continuous surjective, then Y is connected.
(ii) If X is wgrα-connected and f is wgrα-irresolute surjective, then Y is wgrα-connected.
Proof
(i) If Y is not connected, then $Y= A \cup B$, where A and B are disjoint non-empty open subsets of Y. Since f is wgrα-continuous surjective, therefore $X=f^{-1}(A) \cup f^{-1}(B)$, where $f^{-1}(A)$ and $f^{-1}(B)$ are disjoint non-empty wgrα-open subsets of X. This contradicts the fact that X is wgrα-connected. Hence, Y is connected.
(ii)Suppose that Y is not wgrα-connected, then $Y=A \cup B$, where A and B are disjoint non-empty wgrα-open subsets of Y. Since f is wgrα-irresolute surjective, therefore $X=f^{-1}(A) \cup f^{-1}(B)$,where $f^{-1}(A),f^{-1}(B)$ are disjoint non-empty wgrα-open subsets of X. So X is not wgrα-connected, a contradiction.
Theorem: 5.6
A contra wgrα-continuous image of a wgrα-connected space is connected.
Proof
Let f: $(X,\tau) \to (Y,\sigma)$ be a contra wgrα-continuous from a wgrα-connected space X onto a space Y. Assume Y is not connected. Then $Y=A \cup B$, where A and B are non-empty closed sets in Y with $A \cap B=\varphi$. Since f is contra wgrα-continuous,we have that $f^{-1}(A)$ and $f^{-1}(B)$ are non-empty wgrα-open sets in X with $f^{-1}(A) \cup f^{-1}(B)= f^{-1}(A \cup B)$
$=f^{-1}(Y)=X$ and $f^{-1}(A) \cap f^{-1}(B)=f^{-1}(A \cap B)= f^{-1}(\varphi)$.This means that X is not wgrα-connected, which is a contradiction. This proves the theorem.
Theorem: 5.7
Every wgrα-connected space is connected.
Proof
Let X be an wgrα-connected space. Suppose X is not connected. Then there exists a proper non-empty subset B of X which is both open and closed in X. Since every closed set is wgrα-closed,B is a proper non-empty subsets of X which is both wgrα-open and wgrα-closed in X. Therefore X is not wgrα-connected. This proves the theorem.
Remark: 5.8
Converse of the above theorem need not be true as seen in the following example.
Example: 5.9
Let $X=\{a,b,c\}$,$\tau=\{\varphi,\{a,b\},X\}$.$\{X,\tau\}$ is connected. But {a} and {b} are both wgrα-closed and wgrα-open, X is not wgrα-connected.
Theorem: 5.10
Let X be a $T_{wgr\alpha}$-space. Then X is wgrα-connected if X is connected.
Proof
Suppose X is not wgrα-connected. Then there exists a proper non-empty subset B of X which is both wgrα-open and wgrα-closed in X. Since X is $T_{wgr\alpha}$-space, B is both open and closed in X and hence X is not connected.
Theorem: 5.11
Suppose X is wgrα-$T_{1\backslash 2}$ space. Then X is wgrα-connected if and only if X is gα-connected
Proof
Suppose X is wgrα-connected. X is gα-connected.

Conversely, we assume that X is gα-connected. Suppose X is not wgrα-connected. Then there exists a proper non-empty subset B of X which is both wgrα-open and wgrα-closed in X .Since X is wgrα-$T_{1\backslash 2}$ -space is both α-open and α-closed in X. Since α-closed set is gα-closed in X, B is not gα-connected in X, which is a contradiction. Therefore X is wgrα-connected.

Theorem: 5.12

In a topological space (X,τ) with at least two points , if $\alpha O(X,\tau)=\alpha C(X,\tau)$,then X is not wgrα-connected.

Proof

By hypothesis, we have $\alpha O(X,\tau)=\alpha C(X,\tau)$ and by the result,we have every α-closed set is wgrα-closed, there exists some non-empty proper subset of X which is both wgrα-open and wgrα-closed in X . So by theorem 5.4, we have X is not wgrα-connected.

References

[1] A.M. Al-Shibani, rg-compact spaces and rg-connected spaces, Mathematica Pannonica17/1 (2006), 61-68.
[2] S.S Benchalli, Priyanka M. Bansali, gb-Compactness and gb-connectedness Topological Spaces, Int.J. Contemp. Math. Sciences, vol. 6, 2011, no.10, 465- 475.
[3] R. Devi, K. Balachandran and H.Maki, On Generalized α-Continuous maps, Far. East J. Math., 16(1995), 35-48.
[4] S. Eswaran, A. Pushpalatha, τ*-Generalized Compact Spaces and τ*- Generalized Connected Spaces in Topological Spaces, International Journal of Engineering Science and Technology, Vol. 2(5), 2010, 2466-2469.
[5] Y.Gnanambal and K.Balachandran, On gpr-Continuous Functions in Topological spaces, Indian J.Pure appl.Math, 30(6), 581-593, June 1999.
[6] A. Jayalakshmi and C. Janaki, wgrα- closed sets in Topological spaces, Int.Journal of Math. Archieve, 3(6), 2386- 2392.
[7] A. Jayalakshmi and C. Janaki, wgrα-Closed and wgrα-Open Maps in Topological Spaces (submitted).
[8] Levine.N, Strong Continuity in Topological Spaces, Am Math. Monthly 1960; 67:267.
[9] H. Maki, R. Devi and K.Balachandran, Generalized α-Closed sets in Topology, Bull. Fukuoka Univ. Ed. Part -III, 42(1993), 13-21.
[10] H.Maki, R.Devi and K.Balachandran, Associated Topologies of Generalized α-Closed Sets and α-Generalized Closed Sets Mem.Fac. Sci. Kochi.Univ. Ser.A. Math.15 (1994), 51-63.
[11] T.Noiri, A Generalization of Perfect Functions, J.London Math.Soc., 17(2)(1978) 540-544.
[12] Noiri .T,On δ-Continuous Functions, J.Korean Math.Soc 1980;16:161-166.
[13] T.Noiri,Super Continuity and Strong Forms of Continuity,Indian J.Pure Appl.Math.15 (1984),no.3,241-250.
[14] A.Vadivel and K. Vairamanickam, rgα-Closed Sets and rgα-Open Sets in Topological Spaces, Int. Journal of Math. Analysis, Vol. 3, 2009, no.37, 1803-1819.

International Journal of Modern Engineering Research (IJMER)
www.ijmer.com Vol.3, Issue.2, March-April. 2013 pp-864-868 ISSN: 2249-6645

Development of Multinozzle Pesticides Sprayer Pump

Sandeep H. Poratkar, [1] Dhanraj R. Raut[2]
[1]*Mechanical Engineeringt, Tulsiramji Gaikwad Patil College of Engg & Technology, India*
[2]*Department of Mechanical Engineering, Uumrer Polytechnic, Umrer*

Abstract: *India is a land of agriculture which comprises of small, marginal, medium and rich farmers. Small scale farmers are very interested in manually lever operated knapsack sprayer because of its versatility, cost and design. But this sprayer has certain limitations like it cannot maintain required pressure; it lead to problem of back pain. However this equipment can also lead to misapplication of chemicals and ineffective control of target pest which leads to loss of pesticides due to dribbling or drift during application. This phenomenon not only adds to cost of production but also cause environmental pollution and imbalance in natural echo system. This paper suggests a model of manually operated multi nozzle pesticides sprayer pump which will perform spraying at maximum rate in minimum time. Constant flow valves can be applied at nozzle to have uniform nozzle pressure.*

Keywords: *Back pain, constant flow valves, drift, multinozzle pesticides sprayer pump, small; marginal; medium farmer.*

I. INTRODUCTION

Agriculture plays a vital role in Indian economy. Around 65% of population in the state is depending on agriculture. Although its contribution to GDP is now around one sixth, it provides 56% of Indian work force [10]. Table 1 shows that share of marginal and small farmer is around 81% and land operated is 44 % in 1960-61. As far as Indian scenario is concerned, more than 75 percent farmers are belonging to small and marginal land carrying and cotton is alone which provide about 80 % employment to Indian workforce. So any improvement in the productivity related task help to increase Indian farmer's status and economy. The current backpack sprayer has lot of limitation and it required more energy to operate. The percentage distribution of farm holding land for marginal farmers is 39.1 percentage, for small farmers 22.6 percentage, for small and marginal farmers 61.7 percentage, for semi-medium farmers 19.8 percentage, for medium farmers 14 percentage and for large farmers 4.5 percentage in year 1960-61.Table 1 clearly explain that the maximum percentage of farm distribution belonged to small and marginal category.

Table I: Percentage distribution of farm holding and operated area for various farmers

	Percentage distribution of farm holding				Percentage distribution of Operated Area			
Land Class	1960-61	1981-82	1991-92	2002-03	1960-61	1981-82	1991-92	2002-03
Marginal	39.1	45.8	56	62.8	6.9	11.5	15.6	22.6
Small	22.6	22.4	19.3	17.8	12.3	16.6	18.7	20.9
Small & Marginal	61.7	68.2	75.3	80.6	19.2	28.1	34.3	43.5
Semi-medium	19.8	17.7	14.2	12	20.7	23.6	24.1	22.5
Medium	14	11.1	8.6	6.1	31.2	30.1	26.4	22.2
Large	4.5	3.1	1.9	1.3	29	18.2	15.2	11.8
Total	100	100	100	100	100	100	100	100

Fig I Percentage-wise Land distribution from 1960 to 2003

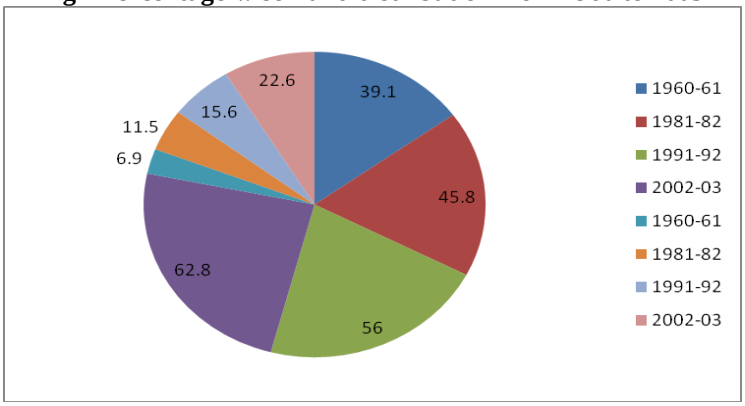

Fig I shows that percentage of the marginal, small and semi medium farmers is about 92.15 %, which states that growth of these farmers require advanced equipment which will work faster than existing one.

II. DESIGN REQUIREMENT

2.1 Drawbacks in Existing Sprayer Pumps:

The Indian farmers (small, marginal, small and marginal, semi-medium) are currently using lever operated backpack sprayer. A backpack sprayer consists of tank 10 -20 liter capacity carried by two adjustable straps. Constant pumping is required to operate this which result in muscular disorder[1].Also, the backpack sprayer cant maintain pressure, results in drifts/dribbling[9].Developing adequate pressure is laborious and time consuming.[13].Pumping to operating pressure is also time consuming[6]. Moreover, very small area is covered while spraying. So, more time are required to spray the entire land. Back pain problems may arise during middle age due to carrying of 10-20 liter tank on back.

2.2 Uneconomical Existing High cost Pumps for Indian Marginal and Small Farmers

Presently farmers are using knap-sack sprayer for spraying pesticides on crops in their farms which costs for Rs 1800-4500/-.Pesticides are diverse and omnipresent[5].This sprayer has a wide limitations and thus farmers can use the other sprayer also like bullock driven sprayer pump and tractor mounted sprayer. Cost of bullock driven is about Rs 28000/-[7]. But though this these sprayer has high advantages but are not affordable by farmers of developing nation .So, it's a need to find out a golden mean among these. The height factor also play a key role in spraying .For cotton, about 5 to 6 times spraying of pesticides is done. Cotton is one of the important commercial crops grown extensively in India. Over 4 million farmers in India grow cotton as their main source and income & livelihood. The textile sector, which is primarily based on cotton fibre, is the largest employer & income provider in India, second only to agriculture. It employs close to 82 million people – 35 million in textile & 47 million in allied sector Table III flashes the light on No. of crops on which spraying is done and their horizontal, vertical distances and maximum height

Table II:-Existing high features high cost sprayer

S.N.	Type of sprayer pump	No. of workers required for spraying	Area for which sprayer is used generally	Time required for spraying	Cost
1	Bullock Driven	2	More than manually operated	Less than manually operated	More than manually operated Rs 28000/-
25	Tractor Operated	1	More than other two	Less than above two	More than other two Rs 6.00 lacks to 7.00 lacks

2.3 Distances (horizontal & Vertical) and height of crop:

Table III:-No. of crops on which spraying is done and their horizontal, vertical distances and maximum height

Sr. no.	Name of crop	Distance between plants (horizontal/vertical)	Height of crop
1.	Sorghum	15 inch /3-4 inch	5.5-7 feet
2.	Pearl millet	15 inch /3-4 inch	5.5-7 feet
3.	Sugarcane	15 inch /3-4 inch	5.5-7 feet
4.	Soybean	15 inch / 2 inch	5.5-7 feet
5.	Corn	15 inch /3 inch	5-7 feet
6.	Groundnut	15 inch / 3 inch	1.5 feet
7.	Cotton	24-36 inch /24-36 inch	2-5 feet
8.	Pigeon Pea	15 inches / 6 inches	3-4 feet

III. Development of Model

Fig II CAD model of manually operated multi-nozzle pesticides sprayer pump

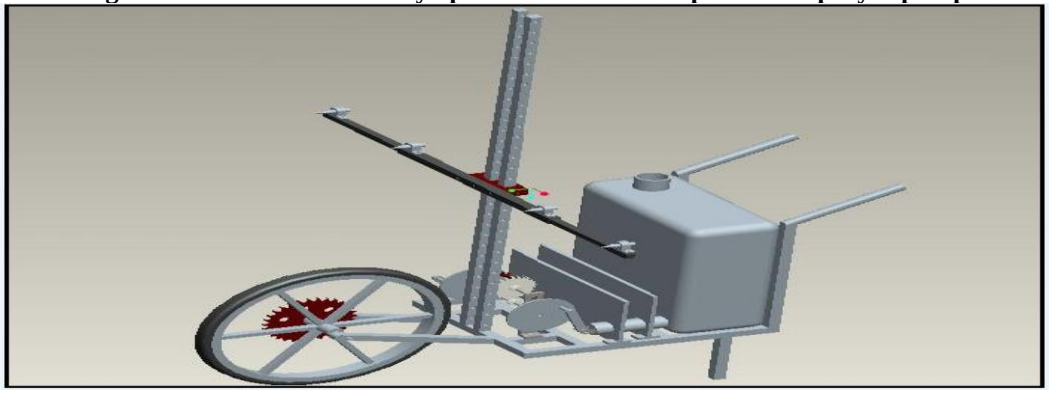

Fig III Side View of Manually operated multi-nozzle pesticides sprayer pump.

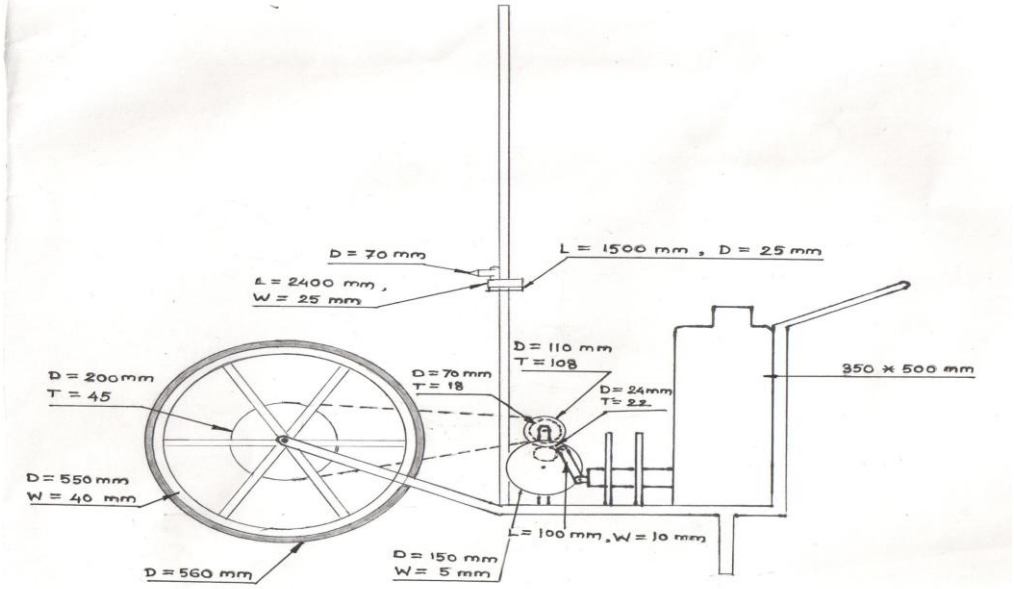

IV. Working

The working of this manually operated multi nozzle pesticides sprayer pump is based on the principles of motion transmission due to chain and sprocket arrangement and plunger cylinder arrangement. The operator first stand behind the trolley. He will grab the handle and lift it and push the trolley forward. As trolley move forward, the wheel rotates in counterclockwise direction. As sprocket is mounted on same shaft of wheel, it also rotates in counter clockwise direction. This motion is transferred to freewheel via chain drive arrangement. The freewheel, thus, also starts rotating in counterclockwise direction. As freewheel and big spur gear are mounted on same shaft, it also start rotating in anticlockwise direction. This will rotate small spur gear in clockwise direction as it is externally meshed with it. Due to this, the disc start rotating which give motion to link as it is fixed on the disc. The plunger is attached to disc via link. The plunger got motion due to this which stimulates pesticides to come outside via six nozzles.

Table IV Selection of components with their material specifications

Sr. No	Name of component	Dimensions	Material used	Material specification
1.	Frame	350*900 mm.	M.S.	Cheap, durable, good strenght
2.	Tank	350*500 mm.	plastic	Light in weight , dureble
3.	Nozzle	D = 70 mm.	Plastic	For P upto 3 bar from traditional sprayer..... wrtlr
4.	Nozzle bar	L = 2400 mm., W = 25 mm.	Steel	Dureble , light in weight
5.	Adjuster bar	L = 1500 mm., D = 25 mm.	Steel	Dureble , light in weight
6.	Link	L= 100 mm., W=10 mm.	M.S.	Cheap, durable,good strenght
7.	Disc	D = 150 mm.,w =5 mm.	M.S.	Cheap, durable,good strenght
8.	Wheel	D =550 mm., W=40 mm.	Steel	Cheap, durable,good strenght
9.	Tyre	D=560 mm.	Rubber	For friction purpose
10.	Sprocket	D=200 mm.,T = 45, m= 4.45	Steel	Adopted from Hero Cycles Specification for transmittinf force upto 50 N, chip, durable,
11.	Free wheel	D=70 mm.T= 18, m= 3.88	Steel	
12.	Spur gear big	D=110 mm., T=108, m=1.01	Nylon	For parallel shaft power transmission and have high velocity ration
13.	Spur gear small	D=24 mm.,T=22, m=1.09	M.S with hardened upto 60 BHN	
14.	Shaft	L=200 mm.,D=18 mm.	M.S. bright bar	Shaft is taken with respect to inner diameter of freewheel of Hero cycle
15.	Shaft	L=230 mm.	M.S. bright bar	

V. Design Calculations

Sprocket: No. of Teeth = T1=45, Diameter = D1= 200 mm, Pitch = 12.5 mm
Freewheel: No. of Teeth = T2=18, Diameter = D2= 70 mm, Pitch = 12.5 mm
Spur gear big:No. of Teeth = T3=45, Diameter = D3= 110 mm
Spur gear small: No. of Teeth = T4=22, Diameter = D4= 24 mm

5.1Chain and sprocket

Gross weight of system = 25 kg=25*9.81=245.25 i.e. 246 N
Radius of rear wheel = r_w=350 mm
Designed acceleration = t_a=10 sec
Coefficient of rolling resistance = Crr=0.017
Gradient= 0^0
Total tractive force= sum of Rolling resistance, Gradient resistance and Accelerating force
Rolling resistance=weight* Crr =246*.017=4.17 N
Gradient Resistance=Weight * sin θ = 246*0=0
Accelerating force= (weight*V)/(g*t_a)=(246*2)/(9.81*10) = 5N
Total Tractive Force = 4.17+0+5=9.17 N
Thus,
Force required to drive a system = 9.17 N
Now,
Pulling force transferred to handle = F_R = (($F*R_C$* R2) / (R_W* R1))
Where,
F=Force transmitted to wheel=9.17N
Rc=Distance between Pulling Centre to sprocket centre=520mm
R2=Radius of Rear Sprocket=200/2=100mm
R1=Radius of freewheel=70/2=35 mm
Therefore,
F_R= ((9.17*350*100) / (520*35)) = = 17.63 N is a Pulling Force
Thus,
Torque = F_R* distance =17.63*.2=3.526 N-m
Thus,
Power, P_R= (2 * Pi* N *T)/60= (2*3.142*2*3.526)/60=0.7384 watts.
Design Power=P_d= P_R*K_l=0.7384*1.2=0.88603 watts K_l=1.2 from pn 150 TN XIV1 s.n.1
(D1* N1 / 60) = (D2*N2 / 60)
(200/70)= (N2/2) i.e. N2=5.82=6 rpm
Torque Available at freewheel is (T1/T2) = (D1/D2) i.e.T2=T1/(D1/D2)=1.2341 N-m
F_R = (($F*R_C$* R2) / (R_W* R1))
Power available at freewheel, P2= (P1*90%) = 0.7384*0.9=0.66456 watts
As Freewheel and Sprocket Mounted on Same shaft
T2=T3=1.2341 N-m and P2=P3=0.6656 Watts; N2=N3=6 rpm
As Gear 3 and Gear 4 are externally meshed,
(D4/D3) = (N3/N4) i.e. (24/110)/(6/N4) i.e. N4=28rpm

5.2 Calculation of Spur gear/Design of Spur gear

Tg = T3 = 108
Tp=T4=22
N2=N3=6 rpm
Np=N4=28 rpm

1. Pitch line velocity = Vp = (Pi*Dp*Np)/60000 =(Pi*264*28)/60000=0.387 m/s where, Dp=No. of teeth * module=22*12=264
2. Design Power= Pd=Pr*Kl =(0.7384*1.25)=0.88603watts where, Kl=1.25 by Table no. XVI-2/P.N.166 of DDB
3. Velocity factor= Cv=0.885 T.N.XVI-3/pn166
4. Basic Stress for gears=So=175 Mpa T.N.XVI10
5. Modified Lewis Form Factor= Y=0.39- (2.16/Tp) = 0.39-(2.16/22)=0.291 TN XVI5
6. Bending Strength= F_B=So*Cv*b*Y*m = 175*0.885*264*0.2918*12=1431.6 N
7. Dynamic load F_d=Ft+((21 Vp(c*e*b+Ft)) / (21 Vp(c*e*b+Ft)$^{1/2}$))) C=12300 TNXVI4

E=0.097mm for m=12 mm,
B=8m=8*12=96
Vp =0.387
Thus, Fd=2688 N

8. Limiting Wear Strength Fw= Dp*b*K*Q TN XIV1

Dp=364
b=8*12=96,
K=302 i.e.load stress factor pnXVI-6
Q = Size factor = 2 tg/(tg+tp) for externally meshing gear..
= (2*108)/(108+22)
=1.6615

Thus, Fw=12717.1 N
Check Fw Limiting Wear Strength > Dynamic loadF_d,
As (Fw=) 12717.1 N > (Fd=) 2688 N Thus Design is safe

VI. Conclusion

1. The suggested model has removed the problem of back pain, since there is no need to carry the tank (pesticides tank) on the back.
2. As suggested model has more number of nozzles which will cover maximum area of spraying in minimum time & at maximum rate.
3. The c.f. valves can also be applied which help in reducing the change of pressure fluctuation and c.f. Valves helps to maintain pressure.
4. Proper adjustment facility in the model with respect to crop helps to avoid excessive use of pesticides which result into less pollution.
5. Imported hollow cone nozzles should be used in the field for better performance.
6. Muscular problems are removed an there is no need to operate the lever.
7. This alone pump can used for multiple crops

References

[1] Application technology: Problems and opportunities with Knapsack sprayer, Including the cf valves or Constant Flow Valves.- David McAuliffe and Vanessa P. Gray
[2] Journal of arboriculture weed control in landscape plantings1 by J.F. ahrens april 1981 vol. 7, no. 4.
[3] Backpack Sprayer-Modified for small farm Crop Protection-Rutgers Snyder Research & Extension Farm Staff–Edited by John Grande and Jack Rabin.
[4] To Spray or Not to Spray: Pesticides, Banana Exports, and Food Safety John S. Wilsona Tsunehiro Otsuki*,b a b Development Research Group (DECRG), World Bank, 1818 H Street NW, Washington, D.C. 20433, USA March 2002.
[5] Farmers understanding of pesticides safety labels and field spraying practices. By Oluyede Clifford Ajayi and Festus K. Akinnifesi_Scentific Research and Essay Vol (2), pp.204-210, June 2007 ISSN 1992-2248@2007 Academic Journals
[6] Wilcoz. M. 1969. A sprayer for application of small amounts of herbicides to flats. Weed Sci. 17:263-264
[7] Performance evaluation of bullock drawn sprayers for cotton crop-m. Veerangouda, k. V. Prakash, jag jiwan ram and g. Neelakantayya
[8] Designing, construction and evaluation of tractor-back sprayer with Variable Rate Technology (VRT) by using aerial maps information Mehrdad Fouj Lali1, Parviz Ahmadi Moghadam2 1 msc in Mechanics of Agricultural Machinery, Urmia University, Iran 2 Assistant Professor in Mechanics of Agricultural Machinery, Urmia University, Iran.
[9] Effect of the Constant Flow Valves on Performance of Pesticide Sprayer by A. R. Tahir, F .H .Khan, A. A. Khan 1560-8530/2003/05-1-49-52 International Journals of Agriculture and Biology
[10] Maharashtra Progressive Agriculture – A new Horizon –Confederation of Indian Industry
[11] Modification of a knapsack sprayer for more efficient use j. Founk
[12] Small farmers in India-Challenges and opportunities- S.Mahendra Dev-
[13] Modification of a Knapsack Sprayer for more efficient use- J.Founk Research Station, Agriculture Canada, Harrow, Ontario NOR.

International Journal of Modern Engineering Research (IJMER)
www.ijmer.com Vol.3, Issue.2, March-April. 2013 pp-869-883 ISSN: 2249-6645

Invention of the plane geometrical formulae-Part I

Mr. Satish M. Kaple
Asst. Teacher Mahatma Phule High School, Kherda Jalgaon (Jamod) - 443402 Dist- Buldana, Maharashtra (India)

Abstract: *In this paper, I have invented the formulae of the height of the triangle. My findings are based on pythagoras theorem.*

I. Introduction

A mathematician called Heron invented the formula for finding the area of a triangle, when all the three sides are known. From the three sides of a triangle, I have also invented the two new formulae of the height of the triangle by using Pythagoras Theorem. Similarly, I have developed these new formulae for finding the area of a triangle.

When all the three sides are known, only we can find out the area of a triangle by using Heron's formula.By my invention, it became not only possible to find the height of a triangle but also possible for finding the area of a triangle.

I used Pythagoras theorem with geometrical figures and algebric equations for the invention of the two new formulae of the height of the triangle. I proved it by using geometrical formulae & figures, 50 and more examples, 50 verifications (proofs).

Here myself is giving you the summary of the research of the plane geometrical formulae- Part I

II. Method

First taking a scalene triangle PQR

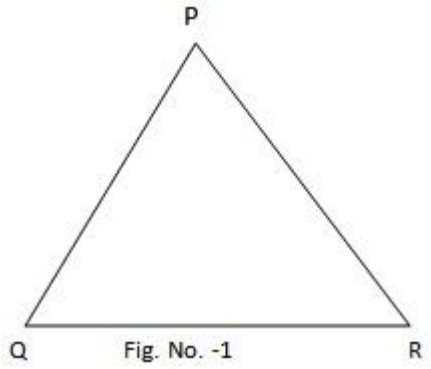

Fig. No. -1

Now taking a, b & c for the lengths of three sides of △ PQR.

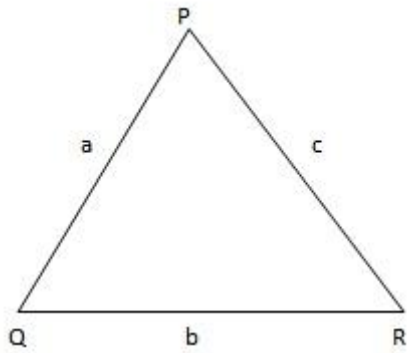

Fig. No. – 2

Draw perpendicular PM on QR.

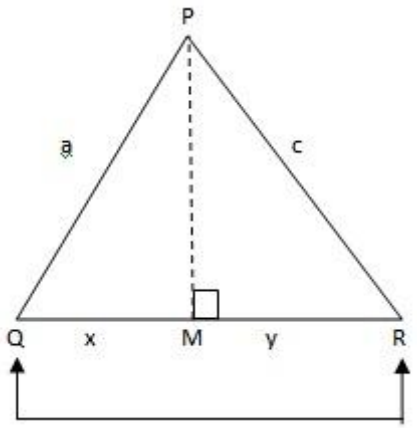

Fig. No. - 3

In PQR given above,

 PQR is a scalene triangle and is also an acute angled triangle. PM is perpendicular to QR. Two another right angled triangles are formed by taking the height PM, on the side QR from the vertex P. These two right angled triangles are PMQ and PMR. Due to theperpendicular drawn on the side QR, Side QR is divided into two another segment, namely, Seg MQ and Seg MR. QR is the base and PM is the height.

Here, a,b and c are the lengths of three sides of PQR. Similarly, x and y are thelengths of Seg MQ and Seg MR.

Taking from the above figure,

PQ = a, QR = b, PR = c

and height, PM = h

But QR is the base, QR = b

MQ = x and MR = y

QR = MQ + MR

Putting the value in above eqn

Hence, QR = x + y

b = x + y

x+y = b ---------- (1)

Step (1) Taking first right angled PMQ,

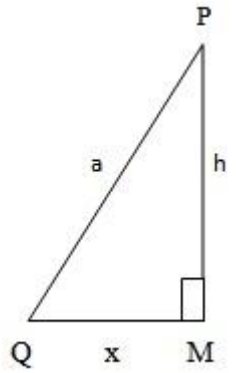

Fig. No.- 4

In PMQ,

Seg PM and Seg MQ are sides forming the right angle. Seg PQ is the hypotenuse and

$\angle PMQ = 90^0$

Let,

PQ = a, MQ =x and

height , PM = h

According to Pythagoras theorem,

$(\text{Hypotenuse})^2 = (\text{One side forming the right angle})^2 +$

$(\text{Second side forming the right angle})^2$

In short,

$(\text{Hypotenuse})^2 = (\text{One side})^2 + (\text{Second side})^2$

$PQ^2 = PM^2 + MQ^2$

$a^2 = h^2 + x^2$

$h^2 + x^2 = a^2$

$h^2 = a^2 - x^2$ ---------- (2)

Step (2) Similarly,
Let us now a right angled triangle □PMR

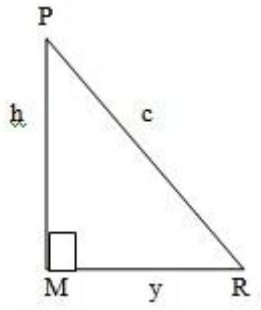

Fig. No. - 5

In □ PMR,
Seg PM and Seg MR are sides forming the right angle. Seg PR is the hypotenuse.
Let, PR = c , MR = y and
height, PM = h and m ∠PMR = 90^0
According to Pythagoras theorem,
$(\text{Hypotenuse})^2 = (\text{One side})^2 + (\text{Second side})^2$

$PR^2 = PM^2 + MR^2$

$c^2 = h^2 + y^2$

$h^2 + y^2 = c^2$

$h^2 = c^2 - y^2$ ---------- (3)

From the equations (2) and (3)

$a^2 - x^2 = c^2 - y^2$

$a^2 - c^2 = x^2 - y^2$

$x^2 - y^2 = a^2 - c^2$

By using the formula for factorization, $a^2 - b^2 = (a+ b)(a - b)$

$(x + y)(x – y) = a^2 - c^2$

But, $x + y = b$ from eqn. (1)

$b \times (x - y) = a^2 - c^2$

Dividing both sides by b,

$$\frac{b \times (x-y)}{b} = \frac{a^2 - c^2}{b}$$

$$(x - y) = \frac{a^2 - c^2}{b} \quad \ldots\ldots\ldots\ldots\ldots\ldots (4)$$

Now , adding the equations (1) and (4)

$x + y = b$

$+ \quad x – y = \frac{a^2 - c^2}{b}$

$$2x + 0 = b + \frac{a^2 - c^2}{b}$$

$$2x = b + \frac{a^2 - c^2}{b}$$

Solving R.H.S. by using cross multiplication

$$2x = \frac{b}{1} + \frac{a^2 - c^2}{b}$$

$$2x = \frac{b \times b + (a^2 - c^2) \times 1}{1 \times b}$$

$$2x = \frac{b^2 + a^2 - c^2}{b}$$

$$x = \frac{a^2 + b^2 - c^2}{b} \times \frac{1}{2}$$

$$x = \frac{a^2 + b^2 - c^2}{2b}$$

Substituting the value of x in equation (1)

$x+y = b$

$$\left(\frac{a^2 + b^2 - c^2}{2b} \right) + y = b$$

$$y = b - \left(\frac{a^2 + b^2 - c^2}{2b} \right)$$

$$y = \frac{b}{1} - \left(\frac{a^2 + b^2 - c^2}{2b} \right)$$

Solving R.H.S. by using cross multiplication

$$y = \frac{b \times 2b - (a^2 + b^2 - c^2) \times 1}{1 \times 2b}$$

$$y = \frac{2b^2 - (a^2 + b^2 - c^2)}{2b}$$

$$y = \frac{2b^2 - a^2 - b^2 + c^2}{2b}$$

$$y = \frac{-a^2 + b^2 + c^2}{}$$

2b

The obtained values of x and y are as follow.

$$x = \frac{a^2 + b^2 - c^2}{2b} \quad \text{and}$$

$$y = -\frac{a^2 + b^2 + c^2}{2b}$$

Substituting the value of x in equation (2) .

$$h^2 = a^2 - x^2$$

$$h^2 = a^2 - \left(\frac{a^2 + b^2 - c^2}{2b}\right)^2$$

Taking the square root on both sides,

$$\sqrt{h^2} = \sqrt{a^2 - \left(\frac{a^2 + b^2 - c^2}{2b}\right)^2}$$

$$\text{Height, } h = \sqrt{a^2 - \left(\frac{a^2 + b^2 - c^2}{2b}\right)^2} \quad \ldots\ldots\ldots\ldots\ldots\ldots\ldots\ldots\ldots(5)$$

Similarly,

Substituting the value of y in equation (3)

$$h^2 = c^2 - y^2$$

$$h^2 = c^2 - \left(\frac{-a^2 + b^2 + c^2}{2b}\right)^2$$

Taking the square root on both sides

$$\sqrt{h^2} = \sqrt{c^2 - \left(\frac{-a^2 + b^2 + c^2}{2b}\right)^2}$$

$$\sqrt{h^2} = \sqrt{c^2 - \left(\frac{-a^2 + b^2 + c^2}{2b}\right)^2}$$

$$\text{Height,} h = \sqrt{c^2 - \left(\frac{-a^2 + b^2 + c^2}{2b}\right)^2} \quad \ldots\ldots\ldots\ldots\ldots\ldots\ldots\ldots\ldots..(6)$$

These above two new formulae of the height of a triangle are obtained.

By using the above two new formulae of the height of the triangle, new formulae of the area of a triangle are developed. These formulae of the area of a triangle are as follows:-

∴ Area of □ PQR = A (□ PQR) --------- (A stands for area)

$= \frac{1}{2} \times \text{Base} \times \text{Height}$

$= \frac{1}{2} \times QR \times PM$

$= \frac{1}{2} \times b \times h$ ---------- (b for base and h for height)

From equation (5), we get

$$\therefore \text{Area of } \square PQR = \frac{1}{2} \times b \times \sqrt{a^2 - \left(\frac{a^2+b^2-c^2}{2b}\right)^2}$$

OR

∴ Area of □ PQR = A (□ PQR)

$= \frac{1}{2} \times \text{Base} \times \text{Height}$

$= \frac{1}{2} \times QR \times PM$

$= \frac{1}{2} \times b \times h$

From equation (6), we get

$$\therefore \text{Area of } \square PQR = A(\square PQR) = \frac{1}{2} \times b \times \sqrt{c^2 - \left(\frac{-a^2+b^2+c^2}{2b}\right)^2}$$

From above formulae, we can find out the area of any type of triangle. Out of two formulae, anyone formula can use to find the area of triangle.

For example:-

Now consider the following examples:-
Ex. (1) If the sides of a triangle are 17 m. 25 m and 26 m, find its area.

Here,

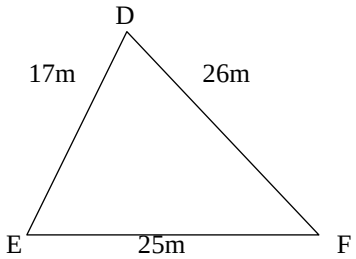

Fig.No.6

□ DEF is a scalene triangle

l (DE) = a = 17 m

l (EF) = Base , b = 25 m

l (DF) = c = 26 m

By using The New Formula No (1)

$$\text{Height,h} = \sqrt{a^2 - \left(\frac{a^2+ b^2- c^2}{2b}\right)^2}$$

Area of □ DEF = A (□ DEF)

$$= \frac{1}{2} \times \text{Base} \times \text{Height}$$

$$= \frac{1}{2} \times b \times h$$

$$= \frac{1}{2} \times b \times \sqrt{a^2 - \left(\frac{a^2+ b^2- c^2}{2b}\right)^2}$$

$$= \frac{1}{2} \times 25 \times \sqrt{17^2 - \left(\frac{17^2+ 25^2- (26)^2}{2 \times 25}\right)^2}$$

$$= \frac{25}{2} \times \sqrt{17^2 - \left(\frac{289+ 625- 676}{50}\right)^2}$$

$$= \frac{25}{2} \times \sqrt{17^2 - \left(\frac{238}{50}\right)^2}$$

The simplest form of $\frac{238}{50}$ is $\frac{119}{25}$

By using the formula for factorization,

$a^2 - b^2 = (a - b)(a + b)$

$$= \frac{25}{2} \times \sqrt{\left(17 - \frac{119}{25}\right)\left(17 + \frac{119}{25}\right)}$$

$$= \frac{25}{2} \times \sqrt{\left(\frac{425 - 119}{25}\right)\left(\frac{425 + 119}{25}\right)}$$

$$= \frac{25}{2} \times \sqrt{\left(\frac{306}{25}\right) \times \left(\frac{544}{25}\right)}$$

$$= \frac{25}{2} \times \sqrt{\frac{306 \times 544}{25 \times 25}}$$

$$= \frac{25}{2} \times \sqrt{\frac{166464}{625}}$$

The square root of $\frac{166464}{625}$ is $\frac{408}{25}$

$$= \frac{25}{2} \times \frac{408}{25}$$

$$= \frac{408}{2}$$

The simplest form of $\frac{408}{2}$ is 204

= 204 sq. m

∴ Area of □ DEF = 204 sq .m.

By using the new formula No (2)

$$\text{Height,h} = \sqrt{c^2 - \left(\frac{-a^2 + b^2 + c^2}{2b}\right)^2}$$

Area of □ DEF= A (□ DEF)

$$= \frac{1}{2} \times \text{Base} \times \text{Height} = \frac{1}{2} \times b \times h$$

$$= \frac{1}{2} \times b \times \sqrt{c^2 - \left(\frac{-a^2 + b^2 + c^2}{2b}\right)^2}$$

$$= \frac{1}{2} \times 25 \times \sqrt{(26)^2 - \left(\frac{-(17)^2 + 25^2 + 26^2}{2 \times 25}\right)^2}$$

$$= \frac{25}{2} \times \sqrt{(26)^2 - \left(\frac{-289 + 625 + 676}{50}\right)^2}$$

$$= \frac{25}{2} \times \sqrt{(26)^2 - \left(\frac{1012}{50}\right)^2}$$

The simplest form of $\frac{1012}{25}$ is $\frac{506}{25}$

$$= \frac{25}{2} \times \sqrt{(26)^2 - \left(\frac{506}{25}\right)^2}$$

By using the formula for factorization,

$a^2 - b^2 = (a - b)(a + b)$

$$= \frac{25}{2} \times \sqrt{\left(26 - \frac{506}{25}\right)\left(26 + \frac{506}{25}\right)}$$

$$= \frac{25}{2} \times \sqrt{\left(\frac{650 - 506}{25}\right)\left(\frac{650 + 506}{25}\right)}$$

$$= \frac{25}{2} \times \sqrt{\left(\frac{144}{25}\right) \times \left(\frac{1156}{25}\right)}$$

$$= \frac{25}{2} \times \sqrt{\frac{144 \times 1156}{25 \times 25}}$$

$$= \frac{25}{2} \times \sqrt{\frac{166464}{625}}$$

The square root of $\frac{166464}{625}$ is $\frac{408}{25}$

$$= \frac{25}{2} \times \frac{408}{25}$$

$$= \frac{408}{2}$$

The simplest form of $\frac{408}{2}$ is 204

= 204 sq. m

∴. Area of □ DEF = 204 sq .m.

Verification:-
Here , l (DE) = a = 17 m
l (EF) = b = 25 m
l (DF) = c = 26 m
By using the formula of Heron's
Perimeter of □ DEF = a+ b + c
= 17+25+26
= 68 m
Semiperimeter of □ DEF,

$$S = \frac{a + b + c}{2}$$

$$S = \frac{68}{2} = 34 \text{ m.}$$

Area of □ DEF = A (□ DEF)

$$= \sqrt{s (s – a) (s – b) (s – c)}$$

$$= \sqrt{34 \times (34 – 17) (34 – 25) (34 – 26)}$$

$$= \sqrt{34 \times 17 \times 9 \times 8}$$

$$= \sqrt{2 \times 17 \times 17 \times 9 \times 8}$$

$$= \sqrt{(17 \times 17) \times 9 \times (2 \times 8)}$$

$= \sqrt{289 \times 9 \times 16}$

$= \sqrt{289} \times \sqrt{9} \times \sqrt{16}$

The square root of 289 is 17,
The square root of 9 is 3 and
The square root of 16 is 4 respectively
$= 17 \times 3 \times 4$

$= 204.$

∴. Area of □ DEF = 204 sq .m.

Ex. (2) In □ ABC , l (AB) = 11 cm,

l (BC) = 4 cm and l (AC) = 7 cm
Find the area of □ ABC.
☞□ ABC is a scalene triangle

Here,

l (AB) = a = 11 cm

l (BC) = Base , b = 6 cm

l (AC) = c = 7 cm

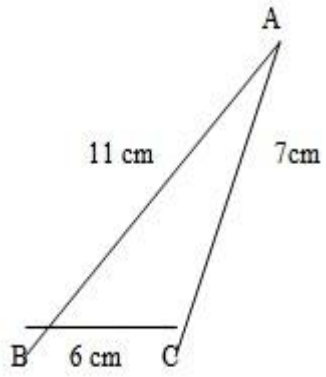

Fig.No.7

By using The New Formula No. (1)
Area of □ ABC = A (□ ABC)

$= \frac{1}{2} \times \text{Base} \times \text{Height}$

$= \frac{1}{2} \times b \times h$

$= \frac{1}{2} \times b \times \sqrt{a^2 - \left[\frac{a^2 + b^2 - c^2}{2b}\right]^2}$

$$= \frac{1}{2} \times 6 \times \sqrt{11^2 - \left(\frac{11^2 + 6^2 - (7)^2}{2 \times 6} \right)^2}$$

$$= \frac{6}{2} \times \sqrt{121 - \left(\frac{121 + 36 - 49}{12} \right)^2}$$

$$= 3 \times \sqrt{121 - \left(\frac{108}{12} \right)^2}$$

The simplest form of $\frac{108}{12}$ is 9

$$= 3 \times \sqrt{121 - (9)^2}$$

$$= 3 \times \sqrt{121 - 81}$$

$$= 3 \times \sqrt{40}$$

$$= 3 \times \sqrt{4 \times 10}$$

$$= 3 \times \sqrt{4} \times \sqrt{10}$$

The square root of 4 is 2

$$= 3 \times 2 \times \sqrt{10}$$

$$= 6\sqrt{10} \text{ sq.cm}$$

∴ Area of □ ABC = $6\sqrt{10}$ sq.cm

By using The New Formula No. (2)

Area of □ ABC = A(□ ABC)

$$= \frac{1}{2} \times \text{Base} \times \text{Height}$$

$$= \frac{1}{2} \times b \times h$$

$$= \frac{1}{2} \times b \times \sqrt{c^2 - \left(\frac{-a^2+b^2+c^2}{2b}\right)^2}$$

$$= \frac{1}{2} \times 6 \times \sqrt{7^2 - \left(\frac{-(11)^2+6^2+7^2}{2 \times 6}\right)^2}$$

$$= \frac{6}{2} \times \sqrt{49 - \left(\frac{-121+36+49}{12}\right)^2}$$

$$= 3 \times \sqrt{49 - \left(\frac{-36}{12}\right)^2}$$

The simplest form of $\frac{-36}{12}$ is (-3)

$$= 3 \times \sqrt{49 - (-3)^2}$$

The square of (-3) is 9

$$= 3 \times \sqrt{49 - 9}$$

$$= 3 \times \sqrt{40}$$

$$= 3 \times \sqrt{4 \times 10} \qquad = 3 \times \left(\sqrt{4} \times \sqrt{10}\right)$$

The square root of 4 is 2.

$$= 3 \times 2 \times \sqrt{10}$$

$= 6\sqrt{10}$ sq.cm

Area of $\triangle ABC = 6\sqrt{10}$ sq. cm

Verification : -

EX (2) In $\triangle ABC$, $l(AB) = 11$ cm,
$l(BC) = 6$ cm and $l(AC) = 7$ cm

Find the area of $\triangle ABC$.

☞ Here, l (AB) = a = 11 cm

l (BC) = b = 6 cm

l (AC) = c = 7 cm

By using the formula of Heron's

Perimeter of □ ABC = a+ b + c

Semiperimeter of □ ABC,

$$S = \frac{a + b + c}{2}$$

$$S = \frac{11 + 6 + 7}{2}$$

$$S = \frac{24}{2} = 12 \text{ cm.}$$

Area of □ ABC = A (□ABC)

$$= \sqrt{s (s – a) (s – b) (s – c)}$$

$$= \sqrt{12 \times (12 – 11) (12 – 6) (12 – 7)}$$

$$= \sqrt{12 \times 1 \times 6 \times 5}$$

$$= \sqrt{6 \times 2 \times 6 \times 5}$$

$$= \sqrt{(6 \times 6) \times (2 \times 5)}$$

$$= \sqrt{36 \times 10}$$

$$= \sqrt{36} \times \sqrt{10}$$ (The square root of 36 is 6.)

$$= 6 \times \sqrt{10}$$

∴ Area of □ ABC = $6\sqrt{10}$ sq.cm

III. Explanation

We observe the above solved examples and their verifications, it is seen that the values of solved examples and the values of their verifications are equal.

Hence, The New Formulae No. (1) And (2) are proved.

IV. Conclusions

$$\text{Height},h = \sqrt{a^2 - \left(\frac{a^2+ b^2- c^2}{2b}\right)^2}$$

$\therefore$ Area of triangle $= \frac{1}{2} \times \text{Base} \times \text{Height}$

$$= \frac{1}{2} \times b \times h$$

$$\text{Area of triangle} = \frac{1}{2} \times b \times \sqrt{a^2 - \left(\frac{a^2+ b^2- c^2}{2b}\right)^2}$$

OR

$$\text{Height},h = \sqrt{c^2 - \left(\frac{- a^2+ b^2 + c^2}{2b}\right)^2}$$

$\therefore$ Area of triangle $= \frac{1}{2} \times \text{Base} \times \text{Height}$

$$= \frac{1}{2} \times b \times h$$

$$\text{Area of triangle} = \frac{1}{2} \times b \times \sqrt{c^2 - \left(\frac{- a^2+ b^2 + c^2}{2b}\right)^2}$$

From above two new formulae, we can find out the height & area of any types of triangles.

These new formulae are useful in educational curriculum, building and bridge construction and department of land records.

These two new formulae are also useful to find the area of a triangular plot of lands, fields, farms, forests etc. by drawing their maps.

References

[1] Geometry concepts & pythagoras theorem

International Journal of Modern Engineering Research (IJMER)
www.ijmer.com Vol.3, Issue.2, March-April. 2013 pp-884-887 ISSN: 2249-6645

Study the Effect of Aluminum Variation on Hardness &Aluminum Loss in Zn-Al Alloy

Mr. D. R. Raut, [1] Mr. S. H. Poratkar[2]
[12]*Yeshwantrao Chavan College of Engineering, Nagpur-441110*

Abstract: *The objective of this research is to study the hardness &aluminiumloss with percentage variation in Aluminium content added to zinc. As there is a method for coating known as Galfan is available, in which combination of 95%zinc and 5% Aluminium is used for protecting steel from corrosion.As there are not much details available about why this composition is used Zinc-5%Al, we are interested in study of effects of different composition of Aluminum with Zinc, so we study the effect by adding different composition 2.5%,4.5%,6.5%,8.5% & 11.5% Aluminum in Zinc, for this study we are using hot dip galvanizing process for studying this coating. Hot-dip galvanizing is widely used to improve the corrosion resistance of steel. To obtain high-quality coatings, some alloy elements are added to the zinc bath. Aluminum is one of the most important elements in galvanizing.Fe-Al phase diagram indicated thatα Fe is obtained between 1 to 11% of AluminiumGalfan alloy consist of 95% Zn and 5% Al. It was decided to study the effect of variation in Al content in Zinc-Aluminium alloy .Also during melting of this alloy we wanted to observed loss of Al due to oxidation hence the above compositions were decided.*

Keywords: *Galfan, mildsteel*

I. INTRODUCTION

In the zinc bath various elements are added in order to improve the melting characteristics of zinc and / or of the layer deposited on the steel support.

Aluminiumis added to the zinc-plating bath in a continuous flow of the steel strips/plates at a rate of 0.1-0.3% (optimal 0.14-0.17% [1]. Aluminium is added primarily to act as a brake to the reaction between zinc and steel support. Reducing the iron-zinc reactions results a decrease in the brittle intermetallic compound layer which has a negative impact the layer adhesion and plasticity. Because, compared with zinc, it has a higher affinity to iron; the aluminium present in the zinc bath will quickly form the Fe2Al5-XZnX compound on the steel surface. This ternary compound arranged in a thin layer onto the steel support will limit the diffusion processes leading to the formation of Fe-Zn intermetallic compounds [2]. The aluminum content in the layer will be much higher than that in the zinc bath. At 0.14% Al in the bath, the entire zinc coating (Including the ternary alloy layer) contains about 0.20% Al [2].

We know that hot dip galvanized coating has excellent electrochemical protection (also known as the expense of protection), when the coating damages, the coating of electrochemical protection can effectively protect the substrate and prevents corrosion, galvanized coating layer also has welding protection. Thermal aluminum coating has excellent atmospheric corrosion resistance and heat resistance, but at the expense of welding and poor protection. The new material (Galfan) is integrated zinc and aluminum possessing coating advantages of both [3]. Galfan is a 5% Al + 95% Zn coating with a small amount of mischmetal (Cerium, Lanthanum Neodybium) [4]. Mischmetal addition, containing lanthanum and cerium additions upto about 0.5%[5]. As per ASTM B750 the specification covers GALFAN, zinc- aluminium – mischmetal (Zn-5Al-MM) alloy is used in the production of hot dip coating on the steel. Cathodic protection provided by Galfan is more or less the same as that for galvanizing, while general resistance to corrosion is up to twice than pure Zn [6].

Galfan is a trademark for hot dip galvanized steel sheet or wire covered with zinc 5% aluminium alloy coating,the composition of which is near the eutectic point in the Zn-Al equilibrium phase diagram[7,8]. Two compositions based on additions to the eutectic composition have been reported: small composition metal additions containing lanthanum and cerium up to about 0.5%[9,10],and addition of 0.5% magnesium[11].

Shih reported that the nucleation and growth of Fe-Al intermetallics deplete the melt adjacent to the steel surface in Al. If the dipping time is longer and the depletion continues, the usual Fe-Zn phases can be developing [12]. According to Fe-Al-Zn ternary phase diagram at 4500c, [13, 14], the delta phase will be in thermodynamic equilibrium with the alpha iron, as well an Fe2Al5 phase layer. According to Urednicek and Kirkaldy[15] and Perrot et al[14], the delta phase could dissolve up to 8 wt%Al, therefore if the delta phase has been nucleated on the steel surface it would be in equilibrium with the Galfan bath.

The present study is intended to evaluate experimentally the influence on the hardness and aluminium losses in Zn-Al alloy due to variation in Aluminium content in alloy.

II. EXPERIMENTAL PROCEDURE

In order to study the effects of aluminium variation in Zn-Al alloy on hardness & loss of aluminium, the following parameters were taken into consideration. The sizes of mild steel samples taken are 25mm*20mm with thickness of 5mm.After that polishing was carried out on all sides of samples with different grades of emery papers. Grades of emery papers used are as follows 1/0, 2/0,3/0..Polished mild steel samples were immersed in CH3OH for 5 to 10 minutes. Then samples were washed in distilled water. Samples were dried in in air for 5 to 10 minutes. These dried samples were ready for

hot dip galvanizing. Graphite crucible was used for melting pure zinc and aluminium in the muffle furnace at 460 to 470 0c with mixture of Zncl2 +Nicl2.Polished sample one at a time was dipped into molten zinc-aluminium in the crucible for 5 to 10 minutes (Batch type dipping) After dipping Mild steel sample in molten zinc-Al in crucible, the crucible with dipped sample was kept in the furnace for maintaining the temperature of molten zinc-Al. Then samples wesre removed and cooled in air. The remaining molten zn-al alloy was poured in square pipe. The specimens for examination were carefully cut from these samples so that section across the thickness is revealed. The specimens were then prepared for microstructural examination by abrading on series of emery papers. These samples then polished on velvet cloth adding 70 micron alumina powder suspension in water. An inverted stage metallurgical microscope was used for this purpose. Zinc-Aluminium coating was done on different surface roughness which showed in the table.

III. RESULTS AND DISCUSSIONS

Microstructures of Zinc-Aluminium alloy at 500x magnification is presented in figures

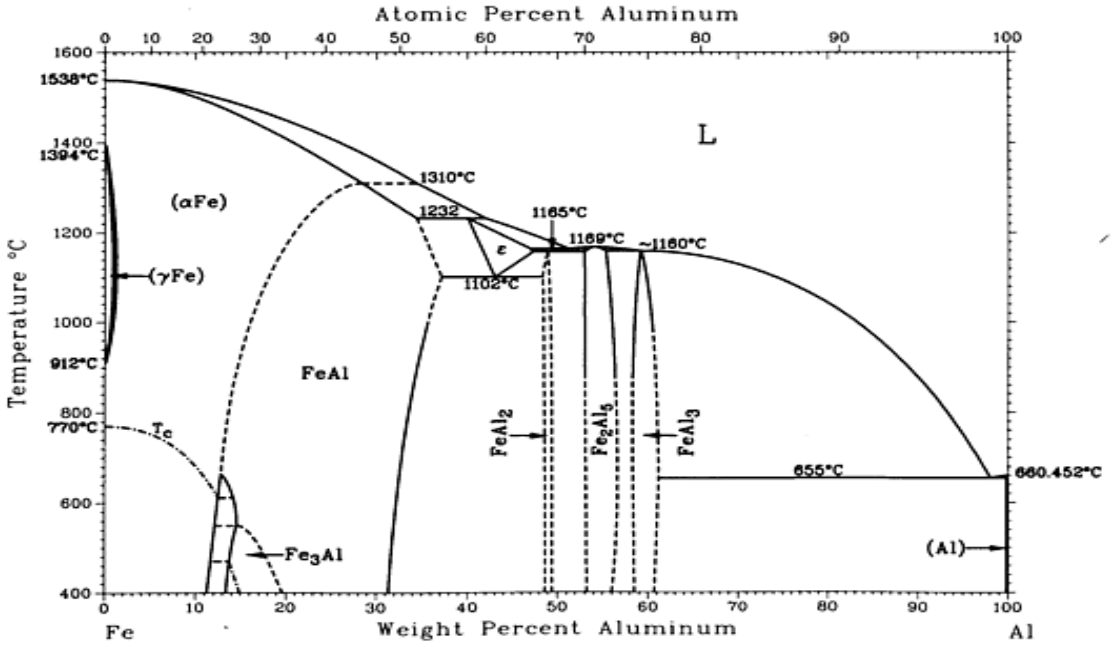

Fe-Al phase diagram

Microstructure of Zn+2.5%Al

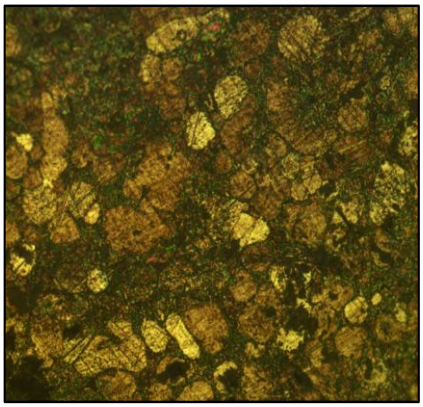

Microstructure of Zn+4.5%Al alloy

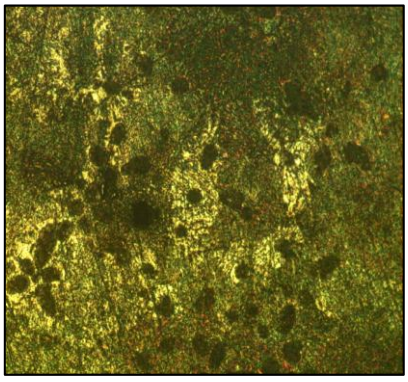

Microstructure of Zn-6.5% Al alloys

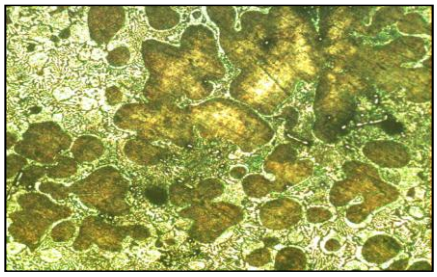

Microstructure of Zn+8.5%Al

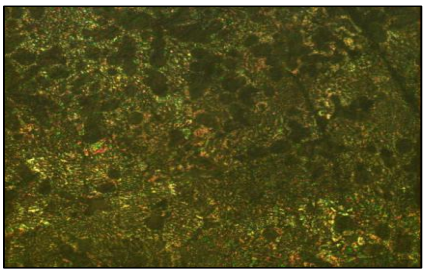

Microstructure of Zn+8.5%Al

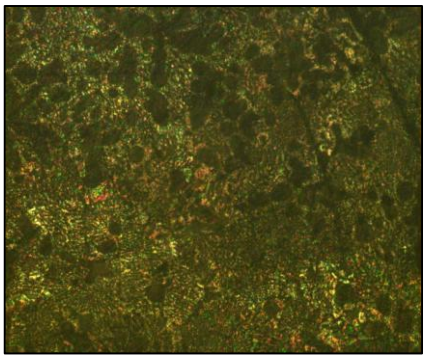

Microstructure of Zn+11.5%Al

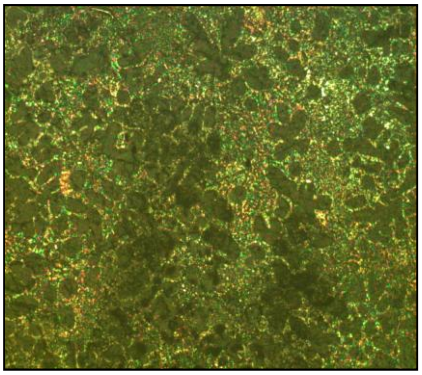

Microstructures of Zn-Al alloys with variations in Al as2.5%Al, 4.5%Al, 6.5%Al, 8.5%Al and 11.5%Al showing eutectic structure of Zn-Al alloy with eutectic lamellar structures and Zn- Al dendrites in the eutectic structure

MICRO HARDNESS VALUES OF EUTECTIC STRUCTURE IN VPN

Sr. No.	Composition	Hardness in VPN
1.	Zn-2.5% Al	78.5 to 81.3
2.	Zn-4.5% Al	82.3 to 85.1
3.	Zn-6.5% Al	85.4 to 87.2
4.	Zn-8.5% Al	87.1 to 88.1
5.	Zn-11.5% Al	90.0 to 91.2

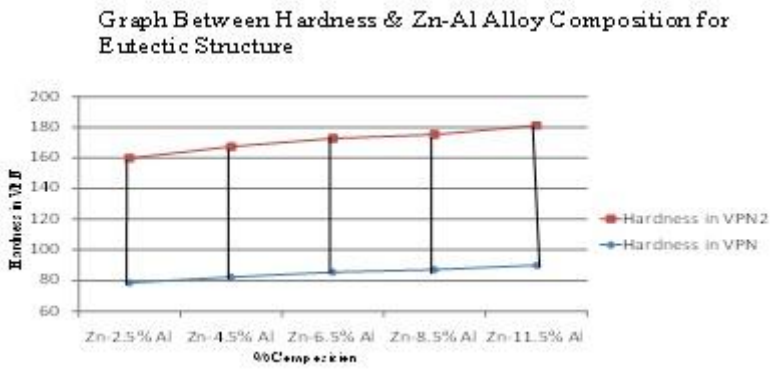

MICRO HARDNESS VALUES OF DENDRITIC STRUCTURE IN VPN

Sr. No.	Composition	Hardness in VPN
1.	Zn-2.5% Al	68.2 to 70.1
2.	Zn-4.5% Al	75.1 to 76.2
3.	Zn-6.5% Al	77.2 to 78.5
4.	Zn-8.5% Al	78.0 to 79.4
5.	Zn-11.5% Al	83.1 to 85.3

Graph Between Hardness and Zn-Al Alloy Composition for Dendritic Structure

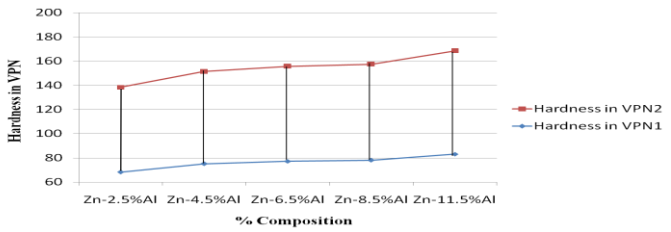

Result of loss of Aluminum (due to oxidation)

Sr. No.	Initial Al % in Zn	Al % After Coating	Loss of Al %
1.	2.5	2.48	0.02
2.	4.5	4.28	0.22
3.	6.5	6.23	0.27
4.	8.5	7.48	1.02
5.	11.5	8.44	3.06

IV. OBSERVATION

- Hardness of eutectic lamellar structure with Al variation in Zn shows increasing order.
- Hardness of dendrites also shows increasing order with increasing Al content in Zn.
- Microstructures of Zn-Al alloys with variation in Al as 2.5%Al, 4.5%Al, 6.5%Al, 8.5%Al, & 11.5%Al showing eutectic structure of Zn-Al alloy with eutectic lamellar structures and Zn-Al dendrites in the eutectic structure.
- Loss of Al increases with increase in percentage of Al in Zn-Al alloy.

V. CONCLUSION

From the present study it can be concluded that

- Zinc-Aluminium alloys with variation in Al such as 2.5%, 4.5%, 6.5%,8.5%and 11.5%showing the formation of Zn-Al dendritic structure inside the eutectic lamellar structure Dendrides formation is directly proportion to the Al content .
- The loss of aluminium increases with increase in aluminium percentage in Zn-Al alloy
- Hardness at eutectic lamellar structure & at dendritic structure is increasing in order with Al content in Zn.

REFERENCE

[1] The Role of Aluminium in Continuous Hot-Dip Galvanizing, GalvInfoNote1.9, Rev 1.0 mar. 2009.
[2] Zinc Bath Management on Continuous Hot-Dip Galvanizing GalvInfoNote 2.4.1 Rev 1.0 Aug-09.
[3] Manxiu Zhao, Fucheng Yin, Zhi li, Yongxiong Liu, Zhahui Long, and Xuping Su. "PhaseEquilibria of the Al-Co-Zn system at 450°
[4] Gilles et al."Preparation of steel surfaces for single dip Aluminium rich Zinc galvanizing" by United States patent application publication.Pub. No.:US2005/0069653. Pub.Date:March 31, 2005
[5] Frank E.Goodwin,Roger N. Wright "The process Metallurgy of Zinc-Coated steel wire and Galfan Bath Management".
[6] Wen-Ben Chena, Peter Chen[b.] , H.Y. Chenc, Jack Wuc, Wen-Ta Tsaia "Devlopment of Aluminium-containing Zinc-rich for corrosion resistance"Applied surface science 187 (2002) accepted on 5 November, 2001
[7] J.L. Murray,Al-Zn binary alloy phase diagram. In:Massalski T. B., ed., 1986.Binary alloy phase diagram. Metals Park, OH 44073, ASM1, 1983,185.
[8] R.Branders, A.Stacey, Zinc-aluminium coating: Management of Galfan lines, Wire Journal International, 41,11,2008, 74-77.
[9] D.C. Herrscaft, S.F. Radke., D.Coutsouradis, J.Pelerin, Galfan-A New Zinc-Alloy Coated Steel for Automotive Body Use. Warrendale, PA: SAE, 1983, SAE Paper No.
[10] S.F. Radtke, D.C.Herrschaft, Role of mischmetal in galvanizing with a Zn-5%Al alloy.J.Less Common Met 93, 1983, 253.
[11] G.J. Harvey and P.N.Richards, Zinc-based coatings for corrosion protection of steel sheet and strip. Metals forum 6, 4, 1984, 235-247
[12] H.C.Shih, J.W.Hsu, C.N.Sun and S.C.Chung, The lifetime assessment of hot-dip 5% Al-Zn coatings in chloride environments. Surface and Coatings Technology, 150, 1, 2002, 70-75.
[13] Z.W.Chen, R.M.Sharp, J.T.Gregory, Fe-Al-Zn ternary phase diagram at 450^0c. Mater. Sci. Technol.6, 1990, 1173.
[14] P. Perrot, J.C.Tissier, J.Y.Dauphin, Stable and metastable equilibria in the Fe-Zn –Al system at 450^0c. Z Metallkde 83,1992,11
[15] Urednicek and Kirkaldy, investigation of the phase constitution of iron-zinc-aluminium at 450^0c .Z Metallkde/Materials Research and Advanced Techniques, 64, 6, 1973, 419-427.

Development of a new device system for the determination of Leg-defective or/and Pelvis-defective position

Thomas Lekscha,[1] Xuan Vinh Pham,[2] Stephan Bartelmei[3]
[1]*Faculty of Engineering Science, Department of Medical Technology, Jade University, Germany, Mail: thomas.lekscha@jade-hs.de*
[2]*Institute of Innovations-Transfer, Field Mechatronics, Jade University, Germany*
[3]*Faculty of Engineering Science, Department of Medical Technology, Jade University, Germany*

Abstract: *The aim of this development was to produce an innovative examination and measuring device for the analysis and evaluation of the physical statics of patients. The new measuring system should be able to determine and evaluate any dysbalance of the leg length, pelvic obliquity and possible misalignment of the feet. In future, the system should be implemented as a semi-automatic measuring device within the scope of medical diagnosis.*

Keywords: *Device system, Video-Footprint, Leg-Pelvis defective position, Measurement, Medical technology*

I. INTRODUCTION

A wide variety of processes and measuring methods are currently used to determine leg or pelvic misalignment of patients. These include purely manual palpating or tapping the body, measurement with tape measures and angle measures or even image processing such as computer tomography and magnetic resonance tomography [1]. All these methods attempt to determine misalignment of the body by analyzing length or angular measurements. The newly developed semi-automatic measuring system (Fig. 1) could be used to compile the following parameters:

- Body size
- Shoulder height
- Leg length difference
- Pelvic obliquity
- Footprint analysis
- Gravimetric analysis.

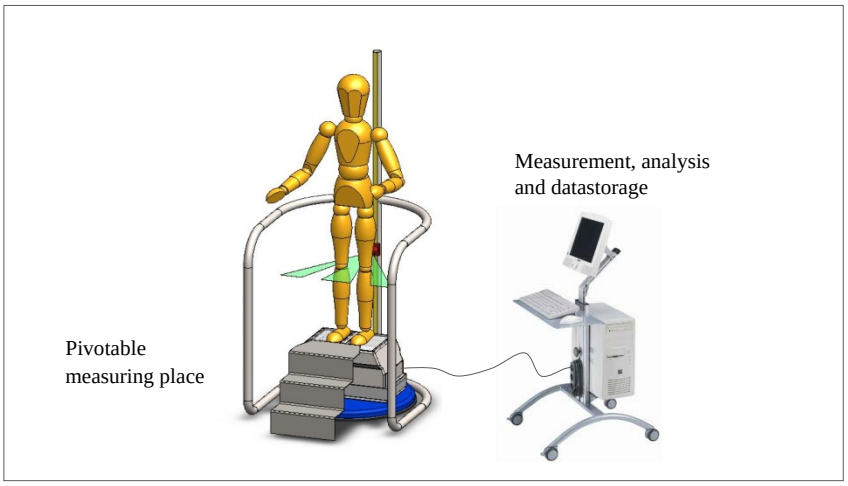

Fig. 1 Measuring system to determine leg and pelvic misalignment with measuring place and data storage

II. PROCEDURAL METHOD

In order to compile the above mentioned parameters, a semi-automatic measuring system was developed which can produce and compensate for dysbalances using motorically adjustable footsteps, determine body sizes and differences using laser-assisted length and difference measurements and compile, archive and analyse all the data by implementing a specially develop software. The following sections describe the individual devices and/or measuring modules.

III. MEASUREMENT OF LENGTHS

The length measuring device concerns a laser-assisted, magnetic absolute length measuring system. With this type of measurement, a sensor is guided over a magnetically coded metallic band. Due to the different lengths of three magnetic tracks, phase shifts are produced which, together with the signals from the sensor, produce absolute length values [2]. The measuring system used can realistically achieve accuracies up to 1 mm. The measured values established are transferred via an RS232 interface to a PC where they are processed or evaluated by project-specific software. Prior to each measurement, marker points are adhered to patients in relevant body areas. The laser beam is then focussed on these relevant measuring points and the distance between them measured. The laser used is assigned to Laser Class 2M [3] with a wavelength of 650 nm and output power of 5 mW. The length measurements can be taken with the patient standing and in three different positions (Fig. 2). Each measurement involves measuring the right and left halves of the patient as well as a rear view, following which the measurements are analysed.

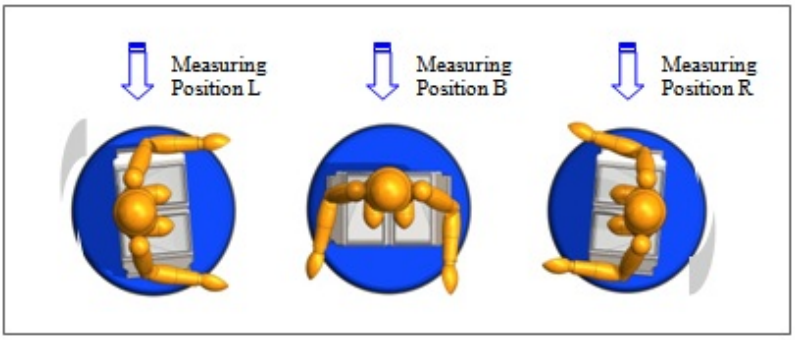

Fig. 2 Illustration of the various measuring positions (Positions L, B, R) as a plan view

IV. FOOT POSITIONING KINEMATICS

In order to be able to compensate or simulate the differences in leg length or pelvic misalignment, foot positioning devices have been developed which enable each leg (foot) to be raised, lowered and/or tilted independent of the opposite side of the body. These devices (Fig. 3) can compensate for dysbalances in the human body. While the patient is standing on the two (right and left) motorically adjustable moving units, an external operating panel can be used to move the right and/or left leg (foot) up and down or tilt them to the side. Following compensation of any misalignment, the length measurement of the body size can be completed again.

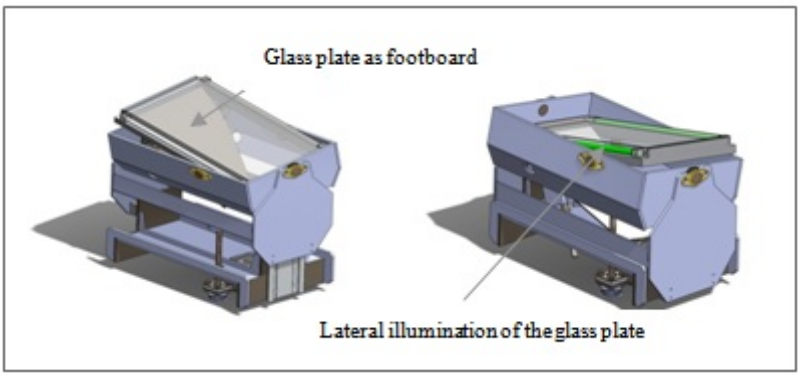

Fig. 3 Foot positioning devices, right and left, with illustration of the extreme positions in lateral, dorsal and up/down

V. FOOTPRINT ANALYTICS

A further special feature of our newly developed system is the capability to take photographs of the soles of the feed when a load is applied and when the load applied is changed. To do this, green light is derived laterally from the cold light cathodesin two glass plates (left and right foot positions). The light is reflected to the top surfaces of the glass through total reflection and, therefore, cannot escape from the glass plates. However, as a result of the pressure applied by a foot, the light can escape from the glass plates at the pressure points exerted by the feet [4], and these point are particularly well highlighted visually (Fig. 4). A visual foot sole analysis or pressure diagnosis can be completed. The pressure images of the feet are recorded in real time by a video camera and stored as individual frames. The images of the feet can be produced before and after compensation of a dysbalance. A comparison of the footprint images can also be used as evidence of successful compensation of a dysbalance.

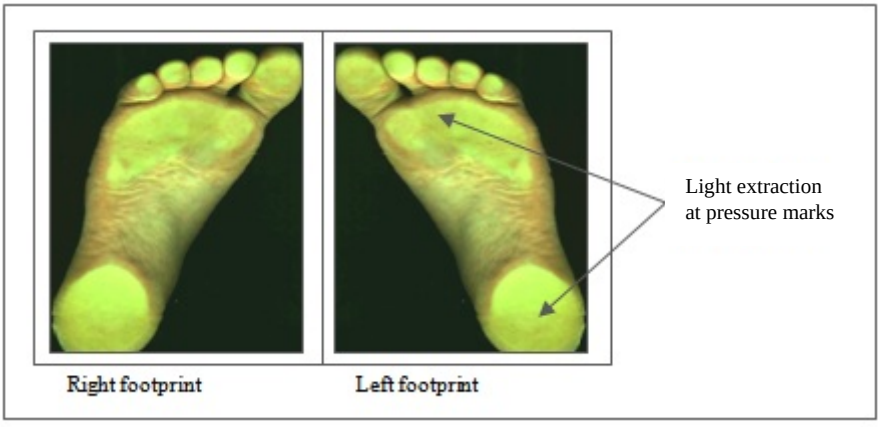

Fig. 4 Illustration of two video-footprints with highlighted pressure points through decoupling light

VI. CONCLUSION

During the development of this innovative system of devices for measuring leg and pelvic misalignment, a prototype was produced which is currently in the practical trial phase. The prototype is being tested with regard to its everyday practicality in a large, North German orthopaedic practice by medical students. The results of the practical tests should serve as a basis for optimising the system. An application for a patent has been registered at the Deutschen Patent- und Markenamt (German Patent and Trademark Office) for the above measuring system. The patent is registered under Patent Number: DE 10 2010 047 460 A1 [5]. Following the practical tests and optimisation phase in 2013 and 2014, it is planned to put the new measuring system into series production.

VII. ACKNOWLEDGEMENTS

For the support by realization of this project, we would like to thank the Faculty of Engineering Science and the Institute of Innovations-Transfer, both at the Jade University in Wilhelmshaven, Germany. We would also like to thank Brigitte Bohlen from ESBO Schuhtechnik, domiciled in Oldenburg, Germany. Some further thanks go at the Lower Saxony Country, Germany, and onto the European Union, for the partial financing of the development.

REFERENCES

[1] Zerres, S.: Vermessungen in der Orthopädie. Ortho Press, Edition 1/2013, Page 34-35, Version 19 North, Deutscher Patientenverlag, D-51065 Köln, Germany
[2] ELGO Electric: EMAX und FEMAX, Magnetische Absolut-Längenmesssysteme.EMAX_FEMAX_D_06-03, ELGO ElectricGmbH2003, D-78239 Rielasingen, Germany
[3] German Institute forStandardization: Sicherheit von Lasereinrichtungen, Klassifizierung von Anlagen und Anforderungen. DIN EN 60825-1, VDE 0837-1 (2012-11-00), Beuth Verlag, D-10787 Berlin, Germany
[4] Ott, P.: Lichttechnik. Chapter: Lichtleiter für Beleuchtungsanwendungen. E-Learning University Heilbronn, http://ilias.hs-heilbronn.de/goto.php?target=lm_151982&client_id=hshn, current access 28.01.2013
[5] German Patent and Trade Mark Office: Verfahren und Vorrichtung zur Erfassung der Körperstatik. DE 10 2010 047 460 A1 2012.04.12, D-80331 München, Germany

AUTORS

Dr. Thomas Lekscha received his Ing. From the Faculty of Engineering Science, Jade University in Wilhelmshaven, Germany. He received his M.Sc. and also his Ph.D. from the Faculty of Electrical Engineering and Information Technology, STU University of Technology in Pressburg. His research activities are in the field of medical technologies and electronics. Today, he is a member of a research staff for medical technologies and Assistant Professor at the Department of Medical Technology, Jade University, Germany.

XuanVinh Pham (Final Year Student) received his Bc.Eng. From the Faculty of Engineering Science, Jade University in Wilhelmshaven, Germany. He is still working at his M.Sc. at the RWTH Aachen University, Germany.

Prof. Dr. Stephan Bartelmei received his Ing. From the TUHH Technical University Hamburg Harburg, Germany. He received his Dr. from the University Hannover, Germany. His research activities are in the field of hydraulic systems and manufacturing systems engineering. Today, he is Professor for Mechanical Engineering at the Faculty of Engineering Science and also the Head of the Institute of Innovations-Transfer at the Jade University in Wilhelmshaven, Germany.

International Journal of Modern Engineering Research (IJMER)
www.ijmer.com Vol.3, Issue.2, March-April. 2013 pp-891-897 ISSN: 2249-6645

Indoor Air Quality Monitoring For Human Health

Prajakta P. Shrimandilkar
Department of Electronics Engineering Amrutvahini College of Engineering, Sangamner Guide Name: R. B. Sonawane Sangamner, India

Abstract: The assessment of indoor air quality (IAQ) risks to building occupants has become a complex and challenging issue for building owners and facility managers. Recent research has defined causal links between construction practices and infection rates in health care building and renovation projects. Attention to IAQ management during building construction is being elevated because of its potential role in fungal, mold, related problems in buildings. Advanced environmental control techniques and are now being developed to better manage IAQ in health care facilities, including improved particulate control, air disinfection systems, moisture control, and pressurization strategies. Each of these creates additional sequencing and process requirements during construction with related implications for construction cost and schedules. As a result, the role of the contractor in managing and implementing indoor air quality in health care construction and renovation is becoming increasingly complex. This paper presents an analysis the relationships emerging between IAQ technologies and construction practices, with an emphasis on heath care facility construction. A case study of IAQ management during construction is presented to illustrate the lack of current formal processes, and the implications of state-of-the art infection control strategies on construction projects. Recommendations are made for improved assessment, control, and monitoring of moisture in buildings during construction as an example of how to improve current practice. Future directions for research in this critical area of the construction industry are also provided.

Keywords: Indoor Air Quality, ealth care Construction, Mold, Allergen, IAQ Risk

I. Introduction

Air-conditioning systems have been used in many parts of the world. The purpose of most systems is to provide thermal Comfort and an acceptable indoor air quality (IAQ) for Occupants. With the improvement of standard of living, occupants require more and more comfortable and healthful Indoor environment. People spend 80_90% of their time indoors, and indoor environment has important effects on human health and work efficiency. The factors affecting indoor environment mainly include temperature, humidity, air exchange rate, air movement, ventilation, particle pollutants, biological pollutants, and gaseous pollutants (Graudenzet al., 2005). By analyzing recent studies, Seppanen and Fisk (2002) found that there was an increase in prevalence of sick building syndrome (SBS) between 30% and 200% in the buildings with air-conditioning systems when compared with natural ventilation systems. Death caused by Legionnaires' disease even occurred in air conditioned buildings. In addition, SARSoccurred in 2003. All of these events are a warning for indoor environment problems related to AC systems. It is fair to say that indoor environment problems still exist in many air-conditioned and mechanically ventilated buildings, even though existing standards may be met. One of the consequences of the worldwide energy crisis in 1970s is the public recognition of the importance of energy saving. The buildings built since then are more airtight and use a great deal of insulation materials to minimize the loss of energy through the building envelope. Fresh air is reduced in air-conditioning systems in order to reduce the energy consumption. Meanwhile, synthetic materials and chemical products (e.g., building materials and decorating materials) have widely been used indoors. The combination of low ventilation rates and the presence of numerous synthetic chemicals results in elevated concentrations of indoor particle pollutants and volatile organic compounds (VOCs) (e.g. benzene, toluene, and formaldehyde). This is deemed to be a major contributing factor to compound hypersensitiveness (Wang et al., 2004a). However, it is exciting that some comfortable and healthy air- conditioning systems were proposed in the past few years.

In order to control the concentration level of indoor pollutants and to improve IAQ, many researchers have investigated the control methods of IAQ. In this paper, recent research will be reviewed on air-conditioning systems and indoor air quality control for human health.2. Indoor air environment indoor air environments must meet the requirement of thermal comfort and IAQ. Thermal comfort is affected by many factors, which mainly include air temperature, air humidity, air velocity, mean radiant temperature, human clothing, and activity levels. The wide use of air conditioning helps to improve thermal comfort, but health problems associated with poor IAQ appear more frequently (e.g., SBS) (Niu, 2004).Many experts believe that IAQ may be the most important and relatively overlooked environmental issue of our time (Gao, 2002). It is indoor pollutants that lead to poor IAQ. Indoor pollutants include particle pollutants and gaseous pollutants.

II. Particle Pollutants

The sources of indoor particle pollutants can be divided into Indoor pollution sources and outdoor pollution sources, and the concentrations and composition of indoor particle pollutants are different with different pollution sources. In residential buildings, particles released by indoor pollution sources (e.g., cooking, smoking) were mostly fine particles and ultra-fine particles which were about 80% of the particles in terms of particle counts (See and Bala subramanian, 2006).

And PM2.5 concentrations could be up to 3and 30 times higher than the ordinary levels during smoking and cooking, respectively (He et al., 2004). The sources such as sweeping and vacuum cleaner tended to elevate concentrations in the coarse fraction (Howard-Reed et al., 2003). Outdoor particles penetrate into indoor environment through the aperture of doors and windows, and the fresh air of air-conditioning systems. In an urban environment the most abundant particulate matter in terms of number was in the ultra-fine size, smaller than 0.1 mm. There was only a very small share of particles (less than 10%) with diameters larger than 0.1 mm (Thomas and Morawska, 2002; Gramotnev and Ristovski, 2004; Morawska et al., 2004).Chemical characteristic of indoor particles is another research topic. Sawant et al. (2004) and Cao et al. (2005) investigated the chemical characteristics of PM2.5. The main composition of PM2.5 and mass percentage inside the residences are organic carbon (40–60%), nitrate (13–14%), trace elements (11–12%), ammonium (8%), elemental carbon (6%), and sulfate (4%). The main composition of PM2.5 and mass percentage at the schoolroom sites are organic carbon (26–50%), nitrate (20%), trace elements (22%), elemental carbon (6–7%), and sulfate (6–7%). From the results above, it can be found that organic carbon is the largest contributor toPM2.5, and has largest impact on the characteristics of PM2.5.PM2.5 containing much organic carbon not only contribute to the propagation of bacteria, but help bacterial spread. PM2.5endanger occupants' health directly or indirectly. Furthermore, the dust accumulating on hot surfaces (e.g. heaters and light fixtures) is likely to emit chemicals when heated. Pedersen et al. (2001, 2003) compared the emission characteristics of VOCs during heating of different dust samples relevant to the indoor environment. Emissions of VOCs from heated dust from different sources were surprisingly similar. For most of the samples studied, the emissions were considerable already at 150 _C. Inorganic gases such as CO, CO2, NOX and NH3 have been identified among the emissions from indoor dust heated at 150–600 _C. Particle pollutants endanger human body through three approaches, namely respiration canal, skin, and alimentary canal. It is the most dangerous approach that particle pollutants enter human body through respiration canal (Kavourasand Stephanou, 2002). The harm degree of particle pollutants to human body is related to the chemical characteristic, diameter magnitude, and quantity. The chemical characteristic of particle pollutants is the main factor because the chemical characteristic determines the degree and speed of biochemistry processes which particle pollutants participate in and disturb in human body. Most of the particle pollutants in air are quite small. They have difficulty in settling and being captured. Conversely, it is easy for them to enter respiration canal deeply together with inhaled air. Moreover, the surface of particle pollutants can adsorb harmful gases, liquid and microbe, which increases the harm to human body (Tham and Zuraimi, 2005;Morawska, 2006).Most of indoor particle pollutants are ultra-fine particles (smaller than 100 nm, nanoscale particles called by toxicologist)in terms of particle counts. Ultra-fine particles possess new physical, chemical and biologic characteristics (Kagonet al., 2005). Therefore future research could explore the behavior of indoor ultra-fine particles, distribution and effects on indoor environment, and the aggradations of ultra- fine particles in human body, movement and effects on health.

2.1. Gaseous pollutants

2.1.1. Primary gaseous pollutants

Primary gaseous pollutants mainly include CO, CO2, SO2, NOX, O3, radon and VOCs. Chemical materials have widely been used indoors recently. The chemical materials can release many kinds of chemical pollutants at room temperature, and VOCs are the main composition of these chemical pollutants.VOCs can cause many symptoms, such as headache; eye, nose, and throat irritations; dry cough; dizziness and nausea; tiredness. VOCs also have bad effects on respiration systems, blood vessel systems, and nerve systems. Moreover, VOCs may be carcinogenic (Huang and Highlight, 2002). The physical and chemical characteristics of VOCs attract many researchers, and become a research topic. Indoor pollution sources of VOCs mainly include building materials, decorating materials, and articles used indoors. Among them building materials and decorating materials are the main pollution sources of VOCs (Cox et al., 2002).They mainly include carpet, man-made board, fine board, agglutination board, composite floor, cork, paint, adiabatic layer, and heat pipeline. Many numerical models have been developed for simulating the surface emission of VOCs from building materials and decorating materials, and VOC absorption (Won et al., 2001; Yang et al., 2001; Hodgson et al., 2002; Highlight and Huang, 2003; Huang and Haghighat,2003; Murakami et al., 2003; Zhang and Xu, 2003; Wilke et al.,2004; Xu and Zhang, 2004; Zhang and Niu, 2004; Kim and Kim, 2005; Lee et al., 2005; Li and Niu, 2005). Some experiments have also been performed to investigate VOCs diffusion inside the materials (Meininghaus and Uhde, 2002; Onwandee et al., 2005; Huang et al., 2006; Zhang et al., 2007).

The main Conclusions are as follows:

_the dimensionless emission rate of VOCs is only a function of the ratio of mass transfer Biot number to the partition coefficient and of mass transfer Fourier number.

_For the multi-layer materials, the top layer materials Strongly delay VOCs emission from the bottom layer Materials. The multi-layer materials have a much longer VOCs emission time and a slower VOCs decay rate than the single-layer materials.

_Polar VOCs are more easily adsorbed and quickly desorbed from building materials and decorating materials, which can reduce VOCs concentrations in the room air initially and elevate them as the time progresses .Plenty of paint is usually used to protect or beautify decorating materials and furniture, but VOCs emitted by paint affect IAQ more seriously. Many experimental and numerical investigations on the emission of VOCs from paint have been conducted (Chang et al., 2002; Fja¨ llstro¨m et al., 2003; Zhang and Niu, 2003a, b; Li et al., 2006).

The main conclusions are as follows:

_23 individual VOCs were detected and the 7 major VOCs Were1-ethyl-3-methylbenzene, 1, 2, 4-trimethylbenzene, nhexane, 1, 3, 5-trimethylbenzene, propylbenzene, o-xylene, and toluene. The sum of the amount of these 7 VOCs was 85% of that of the total VOCs detected.

_ about 65.2% of the VOCs were emitted within the first 4 h, and the emission then slows down and persists for a long period. After 10 days, about 99% of the VOCs were released to indoor air.

_the substrates with high adsorption capacity act as a secondary source for VOCs emission, and such effects may prolong the decay of VOCs. Although the emission and sorption of many VOCs pollution sources have been investigated experimentally and numerically, the following need to be researched further.

_Some hypothesizes have been adopted in the numerical Models, such as one-dimensional mass transfer, constant Physical properties and uniform materials. Many materials actually do not meet these hypothesizes.

_ Excessive VOCs do damage human health, but the damage of individual VOCs in pathology is lack of research. Moreover, it is not clear that the effect mechanism of VOCs to human body and the influences of exposure concentrations and exposure time on human health are uncertain.

2.2.2. Secondary gaseous pollutants

The mix of pollutants in indoor environments can be transformed as a consequence of chemical reaction. Reaction Between ozone and some unsaturated hydrocarbons is an important source of indoor secondary pollutants which mainly include free radicals, aldehydes, ketones, alcohols, carboxylic acids, and fine particulate matter (Sarwar et al., 2003). Secondary pollutants may be more irritating than the original reactants (Wainman et al., 2002; Rohr et al., 2003).During the past few years, many investigations were conducted on indoor secondary pollution due to ozone reacting with limonene (Clausen et al., 2001; Schell et al., 2001;Knudsen et al., 2002; Nøjgaard et al., 2005; Sirakarn et al.,2005; Tama´s et al., 2006; Sarwar and Corsi, 2007), terpene(Knudsen et al., 2002; Weschler and Shields, 2003; Kleno and Wolkoff, 2004; Sarwar et al., 2004; Fiedler et al., 2005; Nøjgaardet al., 2005), a-pinene (Fick et al., 2003; Pommer, 2003; Pommeret al., 2004), VOCs (Fan et al., 2003; Liu et al., 2004), organism deposited on a dirty filter (Beko¨ et al., 2003; Hyttinen et al.,2003), and airborne particulate (Mølhave et al., 2004, 2005).Much significant research has occurred in three subtopics:

_confirming the importance of hydroxyl radical in indoor transformations. Hydroxyln radical is a product of ozone/terpene reactions and goes on to react with other products. Hydroxyl radical is responsible for a large fraction of oxidized products, including certain products that cannot be made by ozone pathways alone.

_Chemical reactions that occur on indoor surfaces. Such reactions may have larger impact on IAQ than those that occur in the gas phase because of the large indoor surface to-volume ratio.

_the impact of secondary pollutants on occupants. A major Limitation in evaluating the impact of secondary pollutants is the inability to measure many of the reaction products .Sensory measurements are useful in detecting changes derived from indoor chemistry and changes missed by the Analytical methods routinely used to evaluate indoor air. Indoor secondary pollutants have significant impact on comfort and human health, but the degree of impact and the frequency of occurrence are uncertain at present. In addition, many secondary pollutants cannot be measured because of the complexity of composition and it is necessary to improve the measure level.

III. Air-conditioning systems

3.1. Air-conditioning systems

Many kinds of AC systems are used to improve indoor thermal comfort and IAQ. Recent research is focused on dedicated outdoor air system (DOAS), independent control of temperature and humidity system (ICTHS), and cooling ceiling and displacement ventilation systems (CC/DV).

3.1.1. Dedicated outdoor air system (DOAS)

With the occurrence of SARS, avian flu and anthracnose in some countries, the safety of AC systems becomes more important .DOAS, an effective measure to realize ‘‘immune building’’, has gradually been appreciated by international AC industry (Mumma, 2001). The reason why DOAS is called

‘‘new concept’’ AC system is that the techniques used in DOAS have widely been applied but are subtly combined to Show its broad prospect.DOAS results in a significant revolution in air-conditioning industry Typical DOAS, shown in Fig. 1, consists of the following several parts (Yin and Mumma, 2003):

_Cold source: As the outlet air temperature of the outdoor air Producer is required to be no more than 7 _C, its inlet water temperature should be no more than4

_C.Though the conventional chiller could be used as the cold source of DOAS, the outlet water temperature of the chiller should be no more than5 _C. So the chiller should be redesigned. The optimal cold source will be the ice-storage system.

_Outdoor air processor: To ensure that indoor terminal devices run in dry condition, outdoor air heat load, total latent heat load and partial sensible heat load are removed by Fig. 1

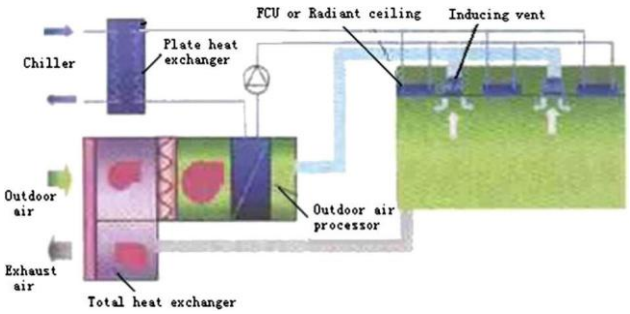

Fig.1–: Schematic diagram of typical DOAS.

Outdoor air processor whose outlet air temperature should be no more than 7_C

_Sensible heat removing terminal device (SHRTD): The residual sensible heat load is removed by SHRTD which includes cooling ceiling (CC), fan coil unit (FCU), and unitary air conditioner. Among them CC is the best one. DOAS using CC as SHRTD can save the primary energy by 18%, compared with DOAS using FCU as SHRTD (Li and Zhang, 2007).

Total heat exchanger: Outdoor air is dehumidified by solid Dehumidizer in desiccant wheel, and then exchanges total heat or sensible heat with exhaust air in heat recovery wheel to recover the energy of exhaust air. Automatic control system: Automatic control system is necessary for DOAS. The controlled parameters mainly include the outlet water temperature and the cold water flux of outdoor air processor, cold water flux and inlet water temperature of SHRTD, indoor dry-bulb temperature and dew-point temperature. The inlet water temperature of SHRTD is controlled based on indoor dew-point temperature, and the total latent heat load is removed by outdoor air processor. Therefore, SHRTD runs in dry condition completely and there is no need to worry about the condensing water. Moreover, DOAS is an all air system without return air, and it eliminates intercrossing infection existing in all air system with return air. DOAS also exhibits better effect of energy saving. When the effectiveness of total heat exchanger is 65%, DOAS using CC as SHRTD can save the electric energy by 42%, compared with conventional VAV systems (Jeong et al., 2003). As the energy consumption of DOAS highly depends on the efficiency of total heat recovery devices, it would be important to develop the heat recovery devices with high efficiency. In addition, to ensure that DOAS runs effectively and safely, further work needs to be done to improve automatic control system and to enhance the Compatibility among different parts of DOAS.

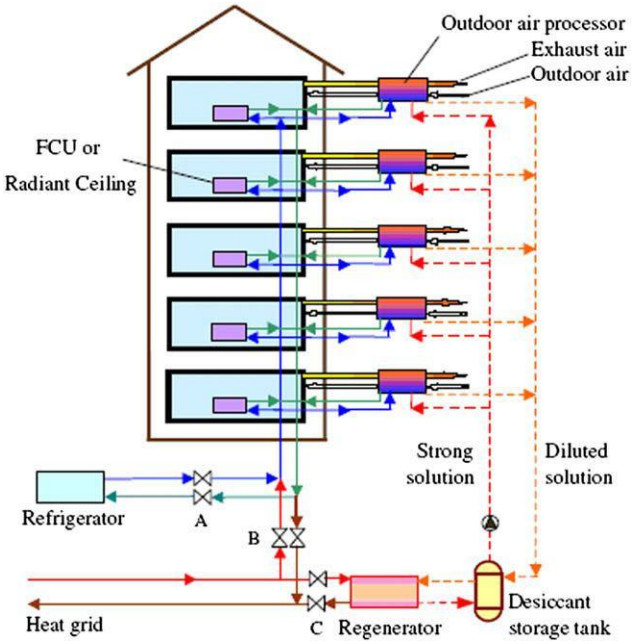

Fig. 2 -: Schematic diagram of ICTHS.

3.1.2. Independent control of temperature and humidity system (ICTHS) Conventional AC systems firstly cool air below the dew-point temperature in order to condense moisture out, and then heat it to the supply comfortable temperature before delivering it to the occupied spaces. This leads to low evaporating temperature, a poor COP value for the chiller, and higher energy consumption. Moreover, the FCU may become the hotbed of many kinds of mildew due to the existence of condensing water, which will deteriorate IAQ. The reason for all these problems is that the cooling process and the dehumidifying process are in the same unit and at the same time, but there is an essential difference between the two processes (Chenet al., 2004). ICTHS can realize the independent control of temperature and humidity, and resolve the problems above .An ICTHS is shown in Fig. 2 (Liu et al., 2006). The ICTHS consists of a liquid desiccant system and a cooling/heating grid system. The liquid desiccant system is composed of outdoor air processors (serving as dehumidifier in summer and humidifier in winter), a regenerator, and a desiccant storage tank. LiBr solution is used as liquid desiccant in

the system and the regeneration temperature is about 60 _C. The cooling/ heating grid system is composed of the power driven refrigerator, the heat grid, and the FCU or radiant ceiling. In summer operations, valves A and C are turned on and valve B is turned off, and the ICTHS performs dehumidification and cooling of the air. Chilled water with temperature of 15–18 _C flows from the refrigerator into the outdoor air processors and the indoor terminal devices. The outdoor air processors remove the total latent load and a portion of sensible load of the occupied space, while the indoor terminal Devices deal with the remained sensible load. IAQ is greatly Improved because of the following two main reasons: (i) indoor terminal devices operate in dry condition, and no condensing water will be produced on the surfaces of the AC system; (ii) the liquid desiccant can remove a number of pollutants from the air stream. In winter operations, valves A and C are turned off and valve B is turned on, and the ICTHS Performs humidification and heating of the air. Hot water from the heat grid flows into the outdoor air processors and indoor terminal devices. The operating principle of the outdoor air processor is shown in Fig. 3. The outdoor air processor consists of two parts. The left of the broken line is a three stage total heat recovery device using liquid desiccant, and the right of the broken line is a single-stage spray unit(Li et al., 2003).The ICTHS can not only improve IAQ but reduce energy consumption and operation cost. In summer, when the latent load of the building covers from 10% to 50%, the primary energy consumption of the ICTHS is 76–80% and the operation cost is about 75% of that of the conventional AC systems. In winter, when latent load of the building are 5%, 10% and 15%, the primary energy consumption of the ICTHS is 77%, 62% and 45%, respectively, and the operation cost is 75%, 57% and 42%, respectively, compared with that of a conventional AC systems (Liu et al., 2006). If solar energy or waste Fig. 2 – Schematic diagram of ICTHS. Heat is used to regenerate desiccant, and ground water is used to cool indoor air, more energy and operation cost would be saved. However, the FCU in ICTHS is only used to cool indoor air and is different from the FCU in conventional AC systems. So the FCU in ICTHS needs to be redesigned

IV. Control of IAQ

In order to provide a comfortable and healthy indoor air Environment, measures must be adopted to control the concentration level of indoor pollutants and improve IAQ. The current methods mainly include control of pollution sources, ventilation and indoor air purification. The recent research on ventilation has been described .Control of pollution source sIt is a most economical and effective approach in improving IAQ to eliminate or reduce indoor pollution sources (Guo et al., 2003). The best ways of controlling indoor air pollution are to use pollution-free or low-pollution materials and to adopt the design and maintenance measures that avoid producing indoor pollutants. They are outlined in detail in

The following (Li et al., 2004; Zhang et al., 2005a; Zhang et al., 2006b):

_Filtrating the outdoor air to prevent outdoor pollutants from entering the room.

_Isolating the sites that may form pollution sources (e.g, copycat rooms, printer rooms, kitchen and toilet) in order to avoid intercrossing infection, and using the enforced ventilation when necessary.

_making full use of pollution-free or low-pollution building Materials and decorating materials Preventing building products with high pollution from entering market by government Legislating and setting up industry standard. For the products in markets, government can label them with different grade. The building materials and decorating materials with high pollution can be eliminated by market mechanism.

_Dust and liquid drops are the important medium for bacteria to spread. It is necessary to trebly clean the components that are easy to be infected in air-conditioning systems (e.g., filter, heat exchanger and muffler) and to replace them in time in order to avoid the aggradations of pollutants. Moreover, the condensing water should be eliminated in time or ICTHS is employed in air-conditioning systems to prevent bacteria from propagating. In addition, occupants' behavior is also an important origin for indoor pollutants, so we should form better customs such as no high strength activities in room, keeping better individual sanitation, no smoking in room, and avoiding using pressurized spray and cosmetic. Researchers should keep on investigating chemical pollutants' releasing characteristics of materials used indoors and exploiting new types of materials without release of pollutants.

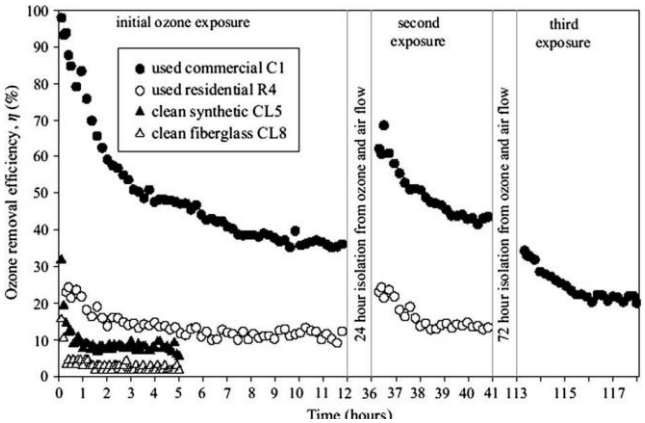

Fig. 3 – Zone removal efficiency

4.2. Indoor air purification

Indoor air purification is an important method of removing indoor pollutants and improving IAQ under the circumstances that the ventilation and the control of pollution sources are impossible. The major methods of indoor air purification include filtration, adsorption, photo catalytic oxidation (PCO), Negative air ions (NAIs) and non-thermal plasma (NTP).

4.2.1. Filtration

Filtration is a quite economical and efficient method of improving IAQ. Filters are important components in all AC systems. It has been found that AC filters can remove ozone significantly at steady state (Hyttinen et al., 2003, 2006; Beko¨ et al., 2005, 2006). Zhao et al. (2007) measured the ozone removal efficiencies of clean filters and field-loaded residential and commercial filters in a controlled laboratory (air temperature 22–26_C, 45–60% RH). The steady-state ozone removal efficiency varied from 0% to 9% for clean filters. The mean steady-state ozone removal efficiencies for loaded residential and commercial filters were 10% and 41%, respectively. From the results above it can be seen that the particles deposited on the filters can increase the ozone removal efficiencies.

Zhao et al. (2007) also observed a partial regeneration of ozone removal efficiency after filters were isolated from ozone and treated with clean air, nitrogen, and/or heat (Fig. 3). The ozone removal efficiency of AC filters appeared to decay with time (Hyttinen et al., 2006; Beko¨ et al., 2005, 2006). Beko¨etal. (2006) found that the initial ozone removal efficiency was 35–50%, only 5–10% after an hour. The removal of ozone from indoor environments is generally desirable. However, the ozone removal on AC filters is mainly due to the chemical reactions between ozone and the particles deposited on the filters, which can lead to oxidation products such as formaldehyde, carbonyls, formic acid, and ultra-fine particles (Beko¨ et al., 2005; Hyttinen et al., 2006). Processes involved in the removal of ozone on HVAC filters include: (i) ozone advection through the filter, (ii) ozone diffusion into the boundary layer near particles, (iii) ozone diffusion into particles, (iv) diffusion of reactive organic compounds out of particles, and (v) ozone reactions with reactive organic compounds. Based on time scales analysis, it appeared that the diffusion processes of ozone and reactive organic compounds were the limiting factors for ozone removal in filters. The speed of the two processes depended largely on the composition of deposited particles (Zhao et al., 2007). Further research is needed to identify and quantify time-dependent emissions of oxidized products and their potential significance with respect to IAQ. Despite the fact that air filtration systems represent a good solution for the improvement of IAQ, they could become a source of contamination from micro-organisms harmful to human health. The organic/inorganic matter deposited on the filter contributes to microbial growth, which inevitably leads to a loss of filter efficiency and filter deterioration. Anti-microbial treatments of filters may be a solution to these problems (Verdenelli et al., 2003). It is possible to prevent the accumulation and dispersion of microorganisms by adding anti-microbial agents on the surfaces of filter, which contributes to the improvement of air quality. The filter sections stereomicroscope analysis on untreated and treated filter media showed that the anti- microbial treatments can reduce microbial colonization significantly (Cecchini et al., 2004). The active component of the anti-microbial agent is cis-1-(3-chloroallyl)-3, 5, 7-triaza-1- azoniaadamantane chloride. The incubation experiments indicated that untreated filter medium released microorganisms after 27 days, while release from the treated filter medium was delayed, after 67 days. The experimental results of Verdenelli et al. (2003) also showed that compared with untreated filters, the anti-microbial treatments could delay the deterioration of filter and result in a lower release of metabolic products. Verdenelli et al. (2003) experimentally investigated the pressure loss of the untreated.

4.2. Indoor air purification

Indoor air purification is an important method of removing indoor pollutants and improving IAQ under the circumstances that the ventilation and the control of pollution sources are impossible. The major methods of indoor air purification include filtration, adsorption, photo catalytic oxidation (PCO), Negative air ions (NAIs), and non-thermal plasma (NTP).

V. Conclusion

A comfortable and healthy indoor air environment is favorable to occupants. In recent years, indoor thermal comfort has been improved greatly due to the development of air-conditioning systems. However, health problems related to poor IAQ appear more frequently, and it is the indoor pollutants that lead to poor IAQ. Many researchers have widely investigated the composition of indoor pollutants, sources, physical and chemical characteristics, and effects on human health. However, a given symptom usually has different causes, and a given pollutant may result in (or trigger) many different symptoms. The biological effects of different pollutants may differ by orders of magnitude. Moreover, the composition of indoor pollutants is quite complex and their concentrations are greatly different. The chemical reactions among indoor pollutants may occur, which can produce more irritating secondary pollutants .Many secondary pollutants even cannot be measured for the moment. It is not clear that the effect mechanism of these pollutants to human body with exposure under low concentrations and short time levels. It is also uncertain that the impact of exposure amount and exposure time on human health. Only if these problems are resolved can indoor air environment be controlled accurately and reasonably.

REFERENCES

[1] Boyd N, Mindorff C, Bruce D et al. Infection prevention during construction/renovation in hospitals: sample policies and bibliography. Sarnia, Ontario: St. Joseph's Health Centre, 1995.
[2] Cheple M., Construction and Renovation Impact on Indoor Air Quality-Control Strategies, University of Minnesota, Vol. 1, Issue 2, August 1998.
[3] James C.A., Article on Air Pollution in Healthcare Facilities, Indoor Air Quality Problems in Healthcare Facilities, 2003.
[4] Keiser R., Planning Is Easier Said than Done, 2002, http://www.facilitiesnet.com/BOM/Sep02/Sep02constructio na.shtmlKuehn, T. Construction/renovation influence on indoor air quality. ASHRAE Journal, 1996.
[5] Martone WJ, Jarvis WR, Incidence and nature of endemic and epidemic nosocomial infections (p.577-596).MS Hospital Consulting, 2001 (http://www.mshospitalconsulting.com/page20.htm)
[6] Streifel J., C. Henrickson, Assessment of Health Risks Related to Construction, Minimizing the threat of infection from construction-induced air pollution in health-care facilities, Minneapolis, Minn., HPAC Engineering, 2002
[7] Sandrick K., Health Facilities Management, Using environmentally friendly construction, 2003

International Journal of Modern Engineering Research (IJMER)
www.ijmer.com Vol.3, Issue.2, March-April. 2013 pp-898-902 ISSN: 2249-6645

Mobile Operated Landrover Using Dtmf Decoder

K.Aruna, [1] A.Sri Ramsagar, [2] G.Venkateswarlu[3]
Department of Electronics and Communication Engineering, Bapatla Engineering College, Bapatla,

Abstract: *In this project, the robot is controlled by a mobile phone that makes a call to the mobile phone attached to the robot. In the course of a call, if any button is pressed, a tone corresponding to the button pressed is heard at the other end of the call. This tone is called 'dual-tone multiple-frequency' (DTMF) tone. The robot perceives this DTMF tone with the help of the phone stacked in the robot.*

Key words: *DTMF*

I. Introduction

In this project, the robot is controlled by a mobile phone that makes a call to the mobile phone attached to the robot. In the course of a call, if any button is pressed, a tone corresponding to the button pressed is heard at the other end of the call. This tone is called 'dual-tone multiple-frequency' (DTMF) tone. The robot perceives this DTMF tone with the help of the phone stacked in the robot

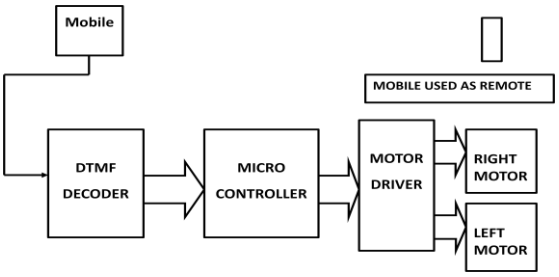

Fig 1: Block Diagram of Cell phone –Operated Land Rover

The received tone is processed by the ATmega32 microcontroller with the help of DTMF decoder MT8870 .The decoder decodes the DTMF tone into its equivalent binary digit and this binary number is sent to the microcontroller. The microcontroller is pre programmed to take a decision for any given input and outputs its decision to motor drivers in order to drive the motors for forward or backward motion or a turn.

The mobile that makes a call to the mobile phone stacked in the robot acts as a remote. So this simple robotic project does not require the construction of receiver and transmitter units.

DTMF signaling is used for telephone signaling over the line in the voice- frequency band to the call switching centre. The version of DTMF used for telephone tone dialing is known as 'Touch-Tone'. DTMF assigns a specific frequency (consisting of two separate tones) to each key so that it can easily be identified by the electronic circuit. The signal generated by the DTMF encoder is a direct algebraic summation, in real time, of the amplitudes of two sine (cosine) waves of different frequencies, i.e., pressing '5' will send a tone made by adding 1336 Hz and 770 Hz to the other end of the line.

The tones and assignments in a DTMF system are shown in Table I.

Frequencies	1209 Hz	1336 Hz	1477 Hz	1633 Hz
697 Hz	1	2	3	A
770Hz	4	5	6	B
852Hz	7	8	9	C
941Hz	*	0	#	D

Table 1: Tones and Assignment in DTMF system

The important components of this mobile operated land rover are

1. DTMF Decoder
2. ATMEGA32 Microcontroller
3. Motor Driver
4. Voltage regulator
5. Regulated power supply

Let us briefly explain about the components

II. Dtmf Decoder

DTMF is a generic communication term for touch tone (a Registered Trademark of AT&T). The tones produced when dialing on the keypad on the phone could be used to represent the digits, and a separate tone is used for each digit. However, there is always a chance that a random sound will be on the same frequency which will trip up the system. It was suggested that if two tones were used to represent a digit, the likelihood of a false signal occurring is ruled out.

This is the basis of using dual tone in DTMF communication. sDTMF dialing uses a keypad with 12/16 buttons. Each key pressed on the phone generates two tones of specific frequencies, so a voice or a random signal cannot imitate the tones. One tone is generated from a high frequency group of tones and the other from low frequency group. The frequencies generated on pressing different phone.

i. FEATURES:

• Complete DTMF Receiver
• Low power consumption
• Internal gain setting amplifier
• Adjustable guard time
• Central office quality

ii. APPLICATIONS:

• Receiver system for British Telecom (BT) or CEPT Spec (MT8870D-1)
• Paging systems
• Repeater systems/mobile radio
• Credit card systems
• Remote control
• Personal computers
• Telephone answering machine

iii. DESCRIPTION:

An MT8870 series DTMF decoder is used here. The MT8870D/MT8870D-1 is a complete DTMF receiver integrating both the band split filter and digital decoder functions. The filter section uses switched capacitor techniques for high and low group filters, the decoder uses digital counting techniques to detect and decode all 16 DTMF tone-pairs into a 4-bit code. All types of the MT8870 series use digital counting techniques to detect and decode all the 16 DTMF tone pairs into a 4-bit code output.

Table ii
DTMF data output

Low group(hz)	High group(hz)	digit	OE	D3	D2	D1	D0
697	1209	1	H	L	L	L	H
697	1366	2	H	L	L	H	L
697	1477	3	H	L	L	H	H
770	1209	4	H	L	H	L	L
770	1336	5	H	L	H	L	H
770	1477	6	H	L	H	H	L
852	1209	7	H	L	H	H	H
852	1336	8	H	H	L	L	L
852	1477	9	H	H	L	L	H
941	1336	0	H	H	L	H	L
941	1209	*	H	H	L	H	H
941	1477	#	H	H	H	L	L
697	1633	A	H	H	H	L	H
770	1633	B	H	H	H	H	L
852	1633	C	H	H	H	H	H
941	1633	D	H	L	L	L	L
-	-	ANY	L	Z	Z	Z	Z

III. Atmega32 Microcontroller

The Atmel AVR ATmega32 is a low-power CMOS 8-bit microcontroller based on the AVR enhanced RISC architecture. By executing powerful instructions in a single clock cycle, the ATmega32 achieves throughputs approaching 1 MIPS per MHz allowing the system designer to optimize power consumption versus processing speed.

i. **FEATURES:**

• High-performance, Low-power Atmel AVR 8-bit Microcontroller
• Advanced RISC Architecture
• High Endurance Non-volatile Memory segments
• JTAG (IEEE std. 1149.1 Compliant) Interface
• Peripheral Features
• Special Microcontroller Features
• I/O and Packages

• Operating Voltages
• Speed Grades
• Power Consumption at 1MHz, 3V, 25°C

The Atmel AVR core combines a rich instruction set with 32 general purpose working registers. All the 32 registers are directly connected to the Arithmetic Logic Unit (ALU), allowing two independent registers to be accessed in one single instruction executed in one clock cycle. The resulting architecture is more code efficient while achieving throughputs up to ten times faster than conventional CISC microcontrollers.

The ATmega32 provides the following features: 32Kbytes of In-System Programmable Flash Program memory with Read-While-Write capabilities, 1024bytes EEPROM, 2Kbyte SRAM, 32 general purpose I/O lines, 32 general purpose working registers, a JTAG interface for Boundary scan, On-chip Debugging support and programming, three flexible Timer/Counters with compare modes, Internal and External Interrupts, a serial programmable USART, a byte oriented Two-wire Serial Interface, an 8-channel, 10-bit ADC with optional differential input

IV. L293 Motor Driver

The L293 is an integrated circuit motor driver that can be used for simultaneous, bi-directional control of two small motors. The L293 is limited to 600 mA, but in reality can only handle much small currents unless you have done some serious heat sinking to keep the case temperature down. Unsure about whether the L293 will work with your motor? Hook up the circuit and run your motor while keeping your finger on the chip. If it gets too hot to touch, you can't use it with your motor.

The L293 comes in a standard 16-pin, dual-in line integrated circuit package. There is an L293 and an L293D part number. Pick the "D" version because it has built in fly back diodes to minimize inductive voltage spikes. The L293D can be purchased for somewhere between $2 and $3 (quantity one) from http://www.mouser.com/ (PN 511-L293D) or http://www.digikey.com/ (PN 296-9518-5-ND). For complete information, consult the Unit rode L293 data sheet (PDF file, 626Kb).

V. Lm7805 (Voltage Regulator)

I. FEATURE:

- 3-Terminal Regulators
- Output Current up to 1.5 A
- Internal Thermal-Overload Protection
- High Power-Dissipation Capability
- Internal Short-Circuit Current Limiting
- Output Transistor Safe-Area Compensation

VI. Serial Communication

Connection between the microcontroller and peripheral devices established through I/O ports is an ideal solution for shorter distances- up to several meters. But, when it is needed to enable communication between two devices on longer distances or when for any other reason it is not possible to use "parallel" connection (for example remote control of the aircraft) it is obvious that something so simple cannot be taken into account. In such and similar situations, communication through pulses, called serial communication is the most appropriate to use.

The circuit diagram of mobile operated land rover is as follows

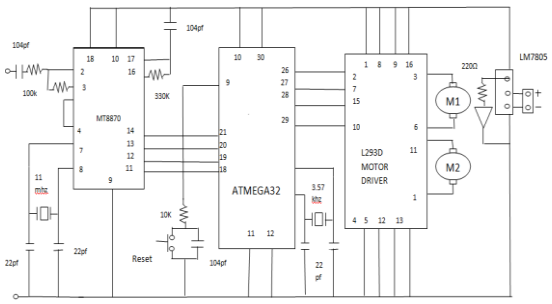

Fig2: circuit diagram of mobile operated land rover

VII. Power Supply

A variable regulated power supply, also called a variable bench power supply, is one where you can continuously adjust the output voltage to your requirements. Varying the output of the power supply is the recommended way to test a project after having double checked parts placement against circuit drawings and the parts placement guide.

VIII. Construction

When constructing any robot, one major mechanical constraint is the number of motors being used. Either a two-wheel drive or a four-wheel drive can be used. Though four-wheel drive is more complex than two-wheel drive, it provides more torque and good control. Two-wheel drive, on the other hand, is very easy to construct. The chassis used in this model is a 10×18cm2 sheet made up of par ax. Motors are fixed to the bottom of this sheet and the circuit is affixed firmly on top of the sheet. A cell phone is also mounted on the sheet as shown in the picture. In the four-wheel drive system, the two motors on a side are controlled in parallel. So a single L293D driver IC can drive the rover. For this robot, beads affixed with glue act as support wheels.

IX. Working

In order to control the robot, make a call to the cell phone attached to the robot (through head phone) from any phone, which sends DTMF tunes on pressing the numeric buttons. The cell phone in the robot is kept in 'auto answer' mode. (If the mobile does not have the auto answering facility, receive the call by 'OK' key on the rover-connected mobile and then made it in hands-free mode.) So after a ring, the cell phone accepts the call. press any button on your mobile to perform actions as listed in Table III. The DTMF tones thus produced are received by the cell phone in the robot. These tones are fed to the circuit by the headset of the cell phone. The MT8870 decodes the received tone and sends the equivalent binary number to the microcontroller. According to the program in the microcontroller, the robot starts moving.

When you press key '2' (binary equivalent 00000010) on your mobile phone, the microcontroller outputs '10001001' binary equivalent. Port pins PD0, PD3 and PD7 are high. The high output at PD7 of the microcontroller drives the motor driver (L293D). Port pins PD0 and PD3 drive motors M1 and M2 in forward direction (as per Table III). Similarly, motors M1 and M2 move for left turn, right turn, backward motion and stop condition

TABLE III
DTMF DATA OUTPUT

Number pressed by user	Output of DTMF	Input to the micro controller	Output from micro	Actions performed
2	0X20	0X20	0XAA	Forward motion
4	0X40	0X40	0X22	Left turn
6	0X60	0X60	OX88	Right
8	0X80	0X80	OX55	Backward motion
5	0X50	0X50	0X00	stop

X. Software Description

The software is written in 'C' language and compiled using Code Vision AVR 'C' compiler. The source program is converted into hex code by the compiler. Burn this hex code into Atmega32 AVR microcontroller.

i.AVR STUDIO:

AVR Studio, with its Integrated Development Environment (IDE), is the ideal software for all AVR development. It has an editor, an assembler and a debugger and is front-end for all AVR emulators. And needs the GCC compiler i.e. WIN-AVR tool.

Two Software's are needs to install

1. AVR Studio
2. AVR GCC Compiler

ii. AVR COMPILER (WINAVR):

WinAVR is a suite of executable, open source software development tools for the Atmel AVR series of RISC microprocessors and AVR32 series of microprocessors hosted on the Windows platform. It includes the GNU GCC compiler for C and C++.

WinAVR is a collection of executable software development tools for the Atmel AVR processor hosted on Windows.

These software development tools include:

- Compilers
- Assembler
- Linker
- Librarian
- File converter
- C Library

- Programmer software
- Debugger
- In-Circuit Emulator software
- Editor / IDE

XI. Applications

- Cell phone controlled robot can be used in the borders for displaying hidden Land mines
- The robot can used for reconnaissance or surveillance
- The robot can be used anywhere there is the service provider tower of the connection provided that is mounted on robot.
- Robot is small in size so can be used for spying

XII. Conclusion

The primary purpose of the mobile phone operated land rover with DTMF decoder is to know the information in the places where we cannot move. The robot perceives the DTMF tone with the help of the phone stacked in the robot. It provides the advantage of robust control, working range as large as coverage area of service provider.

References

[1] "The 8051 Microcontroller and Embedded Systems" By Muhammad Ali Mazidi and Janice Gillispie Mazidi. Pearson Education.
[2] S. Chemishkian, "Building smart services for smart home", Proceedings of IEEE 4thInternational Workshop on Networked Appliances, 2011 pp: 2 15 -224.s
[3] R. Sharma, K. Kumar, and S. Viq, "DTMF Based Remote Control System," IEEE International Conference ICIT 2006, pp. 2380-2383, December 2006.
[4] R.C. Luo, T.M. Chen, and C.C. Yih, "Intelligent autonomous mobile robot control through the Internet,"IEEE International Symposium ISIE 2000, vol. 1, pp. 6-11, December 2000
[5] G. Arangurenss, L. Nozal, A. Blazquez, and J. Arias, "Remote control of sensors and actuators by GSM", IEEE 2002 28th Annual Conference of the Industrial Electronics Society IECON 02, vol. , 5-8 Nov. 2002,pp.2306 – 2310
[6] Robotics and automation proceedings,1997 IEEE international conference on robotics & control systems .
[7] Intelligent control 1989 proceedings IEEE international symposium on robotics & control systems.
[8] Emerging trends in robotics and communication technologies, 2010 International conference on Robotics & control systems.

International Journal of Modern Engineering Research (IJMER)
www.ijmer.com Vol.3, Issue.2, March-April. 2013 pp-903-907 ISSN: 2249-6645

Topologies in Unstructured Peer To Peer Networks

B. Supraja, [1] N. Krishna Kumar, [2] U. Penchala Prasad, [3] Sk. Mohiddin[4]
[1]*M. Tech (CSE), PBRVITS, Nellore.*
[234] *Associate Professor, CSE, PBRVITS, Nellore*

Abstract: *The Peer-to-Peer (P2P) architectures that are most prevalent in today's Internet are decentralized and unstructured. As the peers participating in unstructured networks interconnect randomly, they rely on flooding query messages to discover objects of interest and thus introduce remarkable network traffic. Empirical measurement studies indicate that the peers in P2P networks have similar preferences, and have recently proposed unstructured P2P networks that organize participating peers by exploiting their similarity. The resultant networks may not perform searches efficiently and effectively because existing overlay topology construction algorithms often create unstructured P2P networks without performance guarantees. Thus, we propose a novel overlay formation algorithm for unstructured P2P networks. Based on the file sharing pattern exhibiting the power-law property, our proposal is unique in that it poses accurate performance guarantees. Based on the simulation results, our proposal clearly outperforms the competing algorithms in terms of 1) the hop count of routing a query message, 2) the successful ratio of resolving a query, 3) the number of messages required for resolving a query, and 4) the message overhead for maintaining and formatting the overlay.*

Index Terms: *Peer-to-peer systems file sharing, unstructured overlay networks, search.*

I. Introduction

Peer-To-Peer (P2P) networks (overlay networks) have been widely deployed in the Internet, and they provide various services such as file sharing, information retrieval, media streaming, and telephony. P2P applications are popular because they primarily provide low entry barriers and self-scaling. Prior studies reveal that P2P applications may dominate up to around 20 percent of Internet traffic.

Gnutella is a popular P2P search protocol in the mass market. Specifically, because Gnutella networks are unstructured, and the peers participating in networks connect to one another randomly, peers search objects in the networks through message flooding. To flood a message, an inquiry peer broadcasts the message to its neighbors. (by the neighbors of peer i, we mean those peers that have end-to-end connections with i). The broadcast message is associated with a positive integer time-to-live (TTL) value. Upon receiving a message, the peer (say, j) decreases the TTL value associated with the message by 1 and then relays the message with the updated TTL value to its neighbors, except the one sending the message to j, if the TTL value remains positive. Aside from forwarding the message to the neighbors, j searches its local store to see if it can provide the objects requested by peer i. Conceptually, if j has the requested objects and is willing to supply them, then j either directly sends i the objects or returns the objects to the overlay path where the query message traverses from i to j.

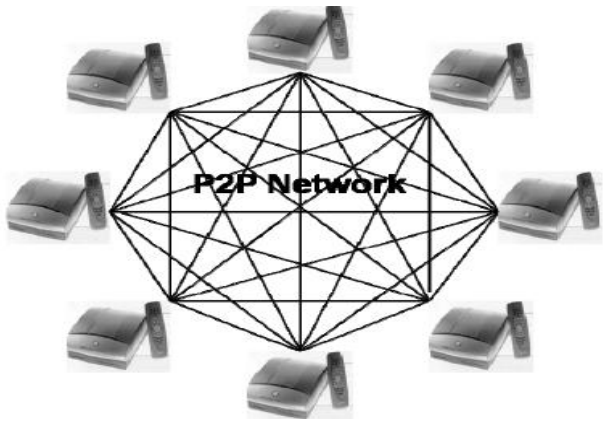

Fig: 1. Peer to Peer Overlay Network

In this paper, we first observe that existing P2P file sharing networks exhibit the power-law file sharing pattern. Based on such sharing pattern, we present a novel overlay construction algorithm to enhance the efficiency and effectiveness of searches in unstructured P2P networks. Compared with previous proposals our proposal has the following unique features:

- In a constant probability, the search hop count between any two nodes is $O(\ln^{c_1} N)$, where $1 < c1 < 2$ is a small constant, and N is the number of active peers participating in the network.
- In a constant probability of approximately 100 percent, the peers on the search path from the querying peer to the destination peer progressively and effectively exploit their similarity.

- Whereas some prior solutions require centralized servers to help organize the system, our proposal needs no centralized servers to participate in. Unlike most decentralized overlay construction algorithms for enhancing searches in unstructured P2P networks, our solution is mathematically provable and provides performance guarantees.

Moreover, we suggest a search protocol to take advantage of the peer similarity exhibited by our proposed overlay network.

II. Related Work

PSearch and SSW are content-based P2P networks providing semantic search. Similar to most P2P networks based on distributed hash tables in pSearch and SSW, each published object, which is represented by a latent semantic vector, needs to be indexed first into the network where the participating peers are formatted in a well-structured manner and host a disjoint key subspace. Therefore, the participating peers need to maintain foreign indices, that is, the indices of objects stored in remote peers. To locate an object, a requesting peer routes a message toward the peer responsible for the key subspace where the object is indexed.

Flooding and RW are two typical examples of blind search algorithms by which query messages are sent to neighbors without any knowledge about the possible locations of the queried resources or any preference for the directions to send. Some of search algorithms include modified BFS (MBFS), directed BFS, expanding ring and random periodical flooding (RPF). These algorithms try to modify the operation of flooding to improve the efficiency. However, they still generate a large amount of query messages. We propose a Light Flood algorithm, which is a combination of the initial pure flooding and subsequent tree-based flooding. DS and Light Flood operate analogously, but DS avoids the extra cost to construct and maintain the treelike sub overlay. Knowledge-based search algorithms take advantage of the knowledge learned from previous search results and route query messages with different weights based on the knowledge. Thus, each node could relay query messages more intelligently. Some examples are adaptive probabilistic search (APS) , biased RW, routing index (RI) , local indices , and intelligent search. APS builds the knowledge with respect to each file based on the past experiences. RI classifies each document into some thematic categories and forwards query messages more intelligently based on the categories. The operation of local indices is similar to that of super peer networks. Each node collects the file indices of peers within its predefined radius. If a search request is out of a node's knowledge, this node would perform a flooding search. The intelligent search uses a function to compute the similarity between a search query and recently answered requests. Nodes relay query messages based on the similarity. There are some other research works that focus on replicating a reference pointer to queried resources in order to improve the search time.

III. Our Proposal

Consider any given unstructured P2P network G = (V, E), where V is the set of participating peers, and E is the set of overlay connections linking the peers in V. The peers in G may be interconnected randomly. Our goal is to restructure G to satisfy the following properties:

C1. (High clustering) - Each peer u connects max_u peers in V, and these neighbors, selected among the peers in V, are the top- max_u nodes most similar to v.
C2. (Low diameter) - Consider any two distinct peers u and v in V. There should exists at least one overlay path P connecting u and v, and the hop count of P should be as small as possible, enabling a query message to be rapidly propagated from u to v. Here, the hop count of an overlay path P means the number of overlay links in P.
C3. (Progressive) - Let s be the peer that issues a query, and d be the peer that can resolve the query. There should exist an overlay path P connecting s and d such that for any two neighboring peers u and v on P, upon receiving a query message, u forward the message to v that is more similar to d than u.

3.1. Peer Similarity Graphs

Let V be the set of peers participating in a P2P network.

Definition 1:

The peer similarity function measures the degree of similarity between any two peer's u ∈ V and v ∈ V in the system.

$$\mathbf{F: V \times V \rightarrow R_0^+}$$

Definition 2:

A peer similarity graph G =(V, E) is a graph where V denotes the set of participating peers, and E is the set of edges. Each edge (u, v) ∈ E indicates that peers u and v are similar to some extent.

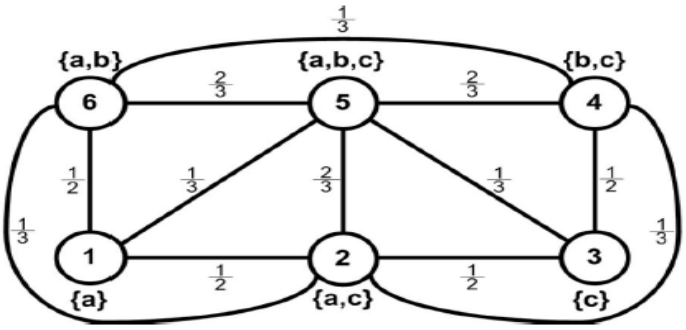

Fig. 1. An example of a peer similarity graph $\mathcal{G} = (V, \mathcal{E})$. Here, $V = \{1, 2, 3, 4, 5, 6\}$. Peers 1, 2, 3, 4, 5, and 6, respectively, host sets of objects $\mathcal{O}_1 = \{a\}$, $\mathcal{O}_2 = \{a, c\}$, $\mathcal{O}_3 = \{c\}$, $\mathcal{O}_4 = \{b, c\}$, $\mathcal{O}_5 = \{a, b, c\}$, and $\mathcal{O}_6 = \{a, b\}$. Any two peers u and v have an edge in $\mathcal{E}$ if both peers share at least one common object. That is, $\mathcal{F}(u, v) = \frac{|\mathcal{O}_u \cap \mathcal{O}_v|}{|\mathcal{O}_u \cup \mathcal{O}_v|}, \forall u \neq v \in V$, and if $\mathcal{F}(u, v) > 0$, then $(u, v) \in \mathcal{E}$. The value nearby an edge (u, v) indicates $\mathcal{F}(u, v)$.

3.2. Overlay Formation

3.2.1 Exploiting Similar Peers

As previously mentioned, each peer u will connect to the peers selected among all peers in V _ {u} that are most similar to u; that is, u intends to satisfy Property C1. Let I_u be the set of neighbors that u currently maintains in the network G = (V, E). Define $A_{current}$ as representing the averaged peer similarity value of u and u's neighbors in I_u.

$$\mathcal{A}_{\text{current}} = \frac{\sum_{v \in \mathcal{I}_u} \mathcal{F}(u, v)}{|\mathcal{I}_u|},$$

By exploiting the peers most similar to u, u seeks a peer w ∈ V – I_u – {u} and invites w as its neighbor such that

$$\mathcal{A}_{\text{update}} \geq \mathcal{A}_{\text{current}},$$

Where

$$\begin{cases} \mathcal{A}_{\text{update}} = \dfrac{\sum_{v \in \mathcal{I}_u \cup \{w\}} \mathcal{F}(u, v)}{|\mathcal{I}_u \cup \{w\}|}, & \text{if } |\mathcal{I}_u| < \max_u; \\ \mathcal{A}_{\text{update}} = \dfrac{\sum_{v \in \mathcal{I}_u \cup \{w\} - \{q\}} \mathcal{F}(u, v)}{|\mathcal{I}_u \cup \{w\} - \{q\}|}, & \text{otherwise;} \end{cases}$$

Algorithm 1 details our proposal

input : $\mathcal{I}_u$ and $\mathcal{I}_u^2$
output: $\mathcal{I}_u$

$q \leftarrow \arg\min_{v \in \mathcal{I}_u} \mathcal{F}(u, v)$;
if there is a $w \in \mathcal{I}_u^2$ satisfying Eq. (3) and w is willing to link to u **then**
  if $|\mathcal{I}_u| < \max_u$ **then**
    $\mathcal{I}_u \leftarrow \mathcal{I}_u \cup \{w\}$;
  else
    $\mathcal{I}_u \leftarrow \mathcal{I}_u \cup \{w\}$;
    $\mathcal{I}_u \leftarrow \mathcal{I}_u - \{q\}$;
else
  u randomly picks a $w \in \mathcal{I}_u^2$;
  if w is willing to link to u **then**
    if $|\mathcal{I}_u| < \max_u$ **then**
      u performs $\mathcal{I}_u \leftarrow \mathcal{I}_u \cup \{w\}$ with a probability of Eq. (6);
    else
      u performs $\begin{cases} \mathcal{I}_u \leftarrow \mathcal{I}_u \cup \{w\} \\ \mathcal{I}_u \leftarrow \mathcal{I}_u - \{q\} \end{cases}$ with a probability of Eq. (6);
return $\mathcal{I}_u$;

3.2.2 Minimizing Semantic Overlay Diameter

To minimize the overlay diameter in our proposal, each peer u ∈ V will create a number of extra overlay links. Denote such extra connections for u by Φ_u. Each t ∈ Φ_u is selected in a probability of Pr(u, t), where Pr(u, t) depends on the peer similarity distance between u and t, that is, D(u, t).

Algorithm 2: Peer t forwards a query message Q.

input : $\mathcal{I}_t$, Φ_t, and a query message Q

1 **if** t receives Q for the first time and $Q.TTL \leq$ MAXTTL **then**
2 **foreach** $t' \in \mathcal{I}_t \cup \Phi_t$ **do**
3 **if** $\mathcal{F}(t', Q) > \mathcal{F}(t, Q)$ **then**
4 $Q.TTL \leftarrow Q.TTL + 1$;
5 t forwards Q to t';

IV. Performance Evalution

Comparing with Guided Search, Routing protocol, filtering with routing updating table provides optimum results for the search performance. Initially when the queries are minimum guided search performance was good. When the queries are getting increased, filtering mechanism with routing updating table is the suitable one which gives the best results up to 90%.Hence it improve the searching performance of the peer. Routing updating table protocol contains the past successful search results and it is used for future references. Updating process can be taken place in each and every second.

V. Simulations

We have developed an event-driven simulator to evaluate the performance of our proposal. The input trace to our simulator is the eDonkey data set. The data set maintains the files shared by peers participating in the eDonkey file sharing network. Specifically, the files shared by each peer are recorded in the data set.

As the eDonkey data set lacks the details for describing each shared file (e.g., the keyword metadata), we measure the similarity level between any two peers u and v in the trace as the similarity function $\mathcal{F}(u, v) = \frac{|\mathcal{O}_u \cap \mathcal{O}_v|}{|\mathcal{O}_u \cup \mathcal{O}_v|}$ Where O_u and O_v represent the files shared by peers u and v, respectively.

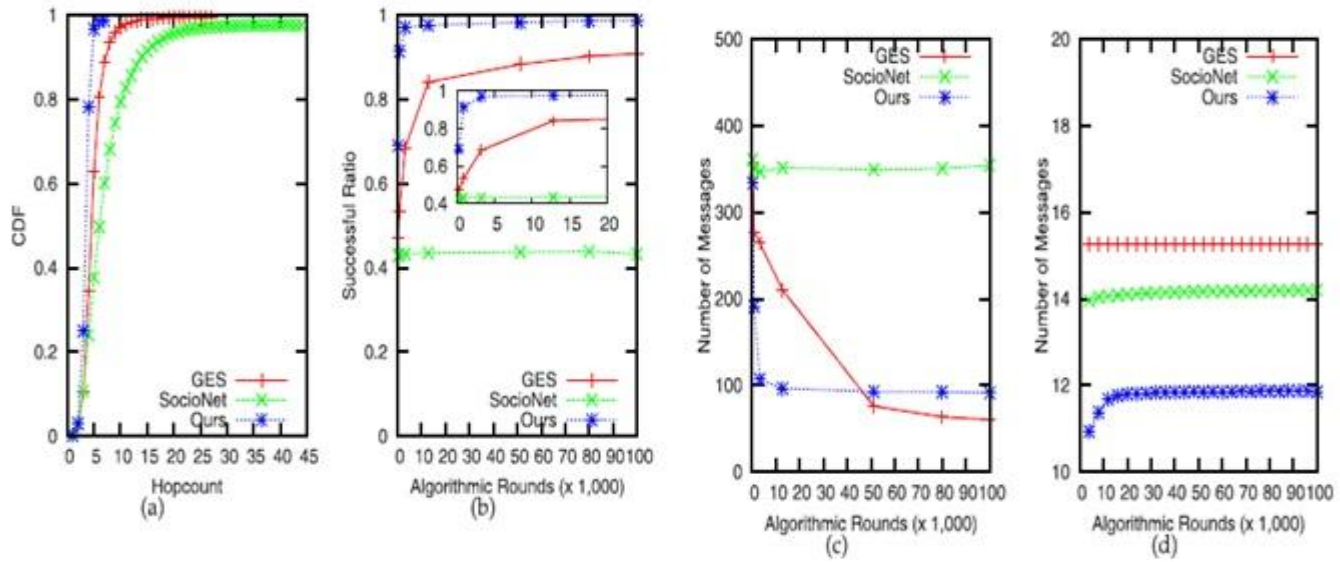

Fig: (a) The query hop count, (b) the successful query ratio. (c) The overhead for resolving a query, (d) The overhead of rewiring and maintaining the network.

VI. Summary and Future Work

We have presented an unstructured P2P network with rigorous performance guarantees to enhance search efficiency and effectiveness. In a constant probability, a querying peer takes $O(\ln^c \mathcal{N})$ hops (where c is a small constant) to reach the destination node capable of resolving the query, whereas the query messages can progressively and effectively exploit the similarity of the peers.

We validate our proposal with simulations. The simulation results reveal that whereas GES and SocioNet, that is, the two representative distributed algorithms among, introduce fair traffic overhead to maintain and rewire their overlay topologies, ours clearly outperforms GES and SocioNet in terms of

1. The query message hop count,
2. The successful ratio of resolving a query,
3. The query traffic overhead, and
4. The overlay maintenance overhead.

Moreover, we find that together with a similarity-aware overlay topology, the search protocol we have suggested in this paper, which takes advantage of the similarity of peers exploited by our overlay network, can considerably reduce the search traffic. Peers participating in a P2P network are often heterogeneous in terms of their network bandwidth, storage space, and/or computational capability. It would be interesting for our future work to investigate how the heterogeneity affects our proposal. Moreover, the overlay formation algorithm presented in this paper is oblivious to the physical network topology, and this may introduce considerable wide-area network traffic.

References

[1] S. Sen and J. Wang, "Analyzing Peer-to-Peer Traffic across Large Networks," IEEE/ACM Trans. Networking, vol. 12, no. 2, pp. 219- 232, Apr. 2004.
[2] Gnutella, http://rfc-gnutella.sourceforge.net/,
[3] E. Cohen and S. Shenker, "Replication Strategies in Unstructured Peer-to-Peer Networks," Proc. ACM SIGCOMM '02, pp 177-190, Aug. 2002.
[4] Q. Lv, P. Cao, E. Cohen, K. Li, and S. Shenker, "Search and Replication in Unstructured Peer- to-Peer Networks," Proc. ACM Int'l Conf. Supercomputing (ICS '02), pp. 84-95, June 2002.
[5] Y. Liu, L. Xiao, X. Liu, L.M. Ni, and X. Zhang, "Location Awareness in Unstructured Peer-to-Peer Systems," IEEE Trans. Parallel and Distributed Systems, vol. 12, no. 2, pp. 163- 174, Feb.2005.
[6] L. Xiao, Y. Liu, and L.M. Ni, "Improving Unstructured Peer-to-Peer Systems by Adaptive Connection Establishment," IEEE Trans. Computers, vol. 54, no. 9, pp. 1091-1103, Sept. 2005.

International Journal of Modern Engineering Research (IJMER)
www.ijmer.com Vol.3, Issue.2, March-April. 2013 pp-908-914 ISSN: 2249-6645

Breast Cancer Detection Using Histogram Based Decomposition

Ms. Jayashree R. Parate, [1] Prof.R.K.Krishna[2]
[1]Department of Computer science, Rajiv Gandhi college of Eng. and research, chandrapur, R.T.M.N.U, Nagpur
[2]Department of ETC, Rajiv Gandhi college of Eng. and research, chandrapur, R.T.M.N.U, Nagpur

Abstract: *Breast disease are continues to be a common health problem in the world for womens. The mammographic diagnostic method is very famous method for detecting breast cancer. But sometimes in some cases, it is not so easy for the radiologist for detecting the typical diagnostic symptoms, such as masses and micro calcifications on the mammograms. Compact region in digital mammographic images are usually contain noisy and have very low contras and the infected regions are very difficult to recognize by radiologist. In this paper, we develop a Histogram base adaptive thresholding to detect suspicious cancerous location in mammograms. The algorithm consumes the combination of adaptive histogram thresholding segmentation and adaptive wavelet based thresholding segmentation on a multiresolution representation of the original mammogram. At last it shows adaptive wavelet techniques to produce the best denoised mammographic image using efficient thresholding algorithm. The algorithm has been checked with different types of around 100 mammograms in the Mammographic Image Analysis Society. Mini Mammographic database the experimental results show that the detection method has a Shows 94% correct result with exact micro calcified area.*

Keywords: *Breast, CAD, Speculated masses, Thresholding, Segmentation, Cancer detection.*

I. INTRODUCTION

A journey of Cancer begins with cells, after those building blocks that create tissues starts. Normal cells grow and divide to form new cells as the body needs them.in case of normal body, regular cells grow old or get damaged, after that they expire, and new cells take their place. Sometimes the process not working properly because of some reason New cells continue their production when the body doesn't need them, and old cells don't die as they are still in working situation. The continually formation of extra cells often forms a mass of tissue called a tumor. Cancer that forms in the tissues of breast, usually in the pectoral and in the duct is the breast cancer. Breast cancer is the famous and common disease in women and the second major cause of death [1]. For minimizing morbidity and mortality, it forcefully need an early detection of breast cancer. Breast cancer is one of the most affected disease in the female specially in India. The average affected rate varies from 22-28 per 1, 00,000 women per year in highly developed area settings to 6 per 100,000 women per year in rural areas. Due to rapid changing in lifestyles, The previous study proves that the early detection can reduces the chances of death as well as detect it n very early stages will help women to taking proper care of breast so that the chances reduced effectively also if someone is affected by it can easily curable. Mammography is now a days the best technique for reliable detection of early non curable breast cancer [3]. But the symptoms of breast cancer is very unstable in their early stages which is not easily understand by any radiologist or doctors and therefore, doctors can miss the abnormality very easily if they only diagnose by experience. Manual diagnosis is required laborious work because it need number of attempt to check the output of one image. Mammography is the most usefull modality for the detection of breast cancer. Because mammograms are projection images, they suffer from the superimposition of tissues, which may produce false alarms or hide lesions. The computer aided detection technology can help doctors to getting a more exact and effective result, since it checks the mammograms as the "second reader," thus giving to doctors and radiologists a favorable advice. Usually, a detection algorithm consists of two main steps:

- The first step is to detect suspicious lesions with segmentation.
- Second is detecting through fine segmentation.

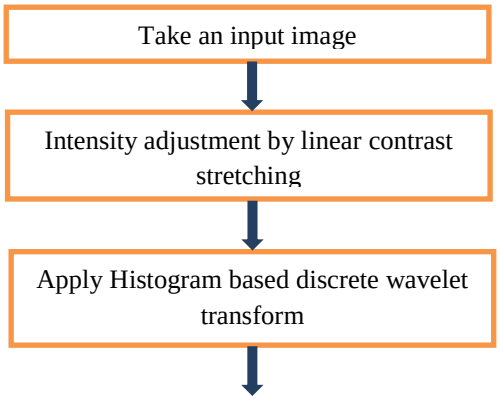

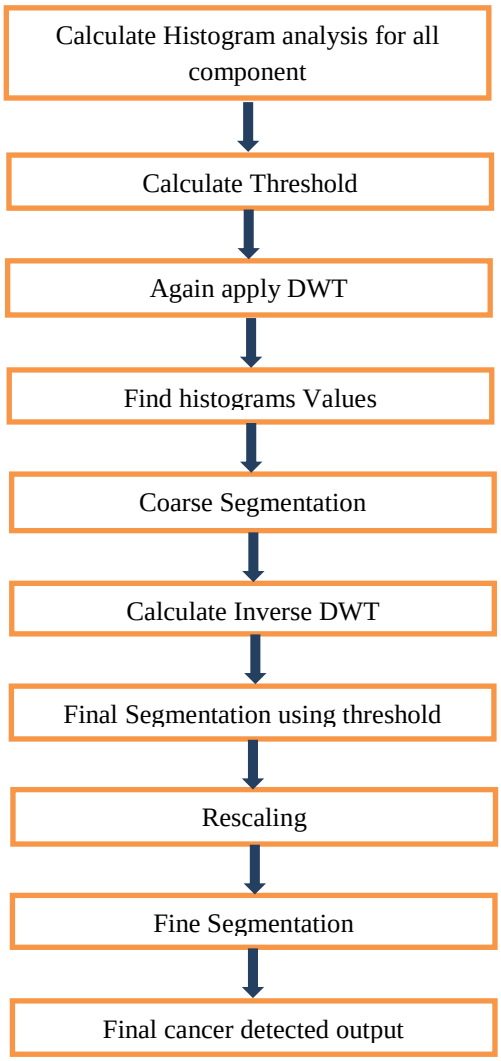

Fig-1 Flow chart for the proposed technique

Different kinds of methods was proposed for detecting Lesion in digital mammograms such as morphological approach[6],neural network analysis[7],wavelet based techniques[5],fuzzy logic based analysis[8],except the fact, all these techniques are usefull but still not detecting cancer easily. Different kinds of lesions are introduced habing different properties like star shape, oblique shape some of them are shown in fig 2. But still technology is not acceptable particularly for premenopausal women with dense breast tissue. it still required extra efforts to improve detection accuracy and reduce false positive rate. In the last surveyed works it is noticed that the thresholding based segmentation has outstanding advantages for detection of micro calcification. Mammograms contain structures with a wide range of sizes and contrasts. For example, a mammograms may contain masses, as well as micro-calcifications.

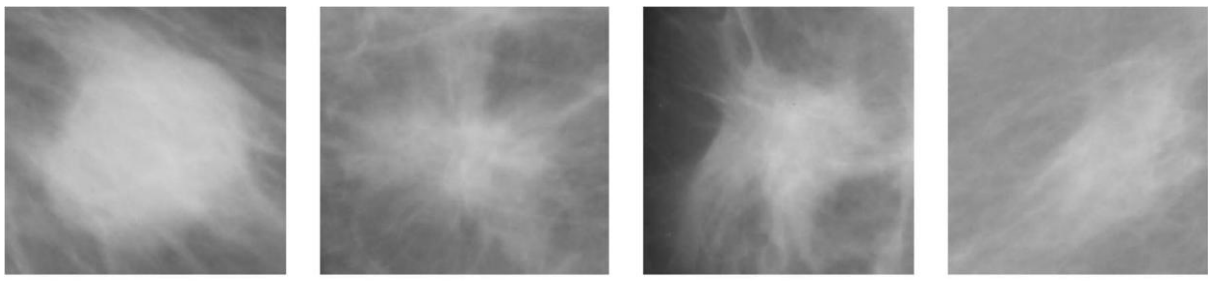

Fig.2 Typical example of different types of LESION A) CIRC, B)SPIC, C)ARCH , D)MISC.

These suspicious regions are surrounded by normal dense tissue that may make the radiologists' identification very difficult; multi threshold analysis is needed to distinguish these different structures. Wavelet based adaptive thresholding is an ideal tool for analyzing images with such a combinational patterns; it can decompose mammograms into different scale components. This property is quite helpful for micro-calcifications detection. this paper is organized as follows: section 2

describes the theories and methods used section 3, the mammogram images used through result together with the tests carried out in order to assess the performance of the methods; finally, conclusions are drawn in section 4.

II. WORKING

histogram based tumour detection can be achieved by using wavelet based adaptive thresholding value in which multiple threshold are taken to calculate calcified location in breast. Flow chart for the proposed technique is given in Fig.1.The following are the main stairs of computation used to segment the tumours in digital mammograms:

1.1 Intensity adjustment:

Intensity adjustment is used to improve the quality of image data by suppressing the un-useful distortions or enhances some image features necessary for next processing and analyse different task. In this paper, linear contrast stretching is used as intensity adjustment step. This is the simplest contrast stretch algorithm. The gray values in the input image and the modified image continuing to use linear relation in this algorithm. A value in the low range of the original histogram is assigned to extremely black and a value at the high end is assigned to extremely white. Block diagram or preprocessing using CAD system is shown in Fig-3. Image pre-processing techniques are necessary; in order to find the representation of the mammogram, to remove noise and to modified the quality of the image. before any image-processing algorithm can be applied on mammogram, pre -processing steps are very important in order to minimize the search for affected without removing influence from background of the mammilla .digital mammograms are medical images that are difficult to be calculated, thus a preparation stage is needed in order to maximize the image quality and make the segmentation results more accurate. The main objective of this process is to improve the quality of the image to make it ready for further processing by removing the unrelated and unwanted parts in the back ground of the mammogram.

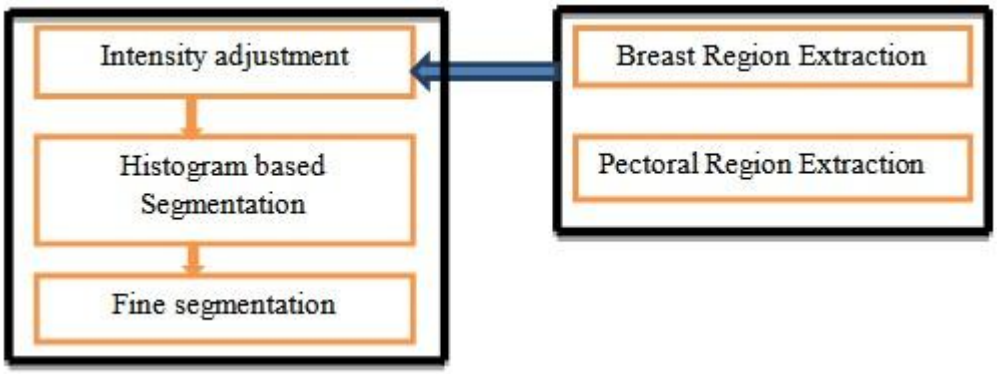

Fig.3 Block diagram of preprocessing using CAD system

There are methods of linear contrast enhancement ie Minimum-Maximum Linear Contrast Stretch.when applying this technique, the original minimum and maximum values of the data are assigned to a newly specified set of values that utilize the full range of available brightness values. The original minimum and maximum values of the data are assigned to a newly specified set of values that utilize the full range of available brightness values. Consider an picture with a minimum brightness value of 45 and a maximum value of 205. When such an image is digitised without enhancements, the values of 0 to 44 and 206 to 255 are not focussed. Important spectral differences can be detetected by stretching the minimum value of 45 to 0 and the maximum value of 120 to 255. As shown in fig4

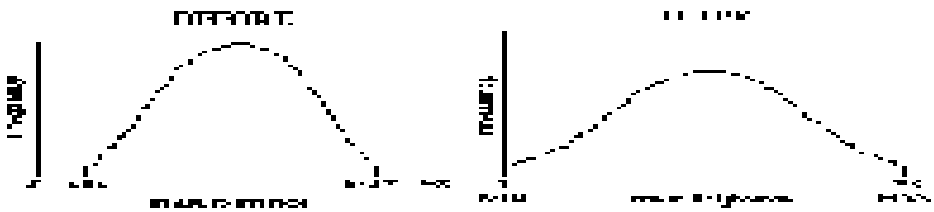

Fig 4: Minimum–Maximum Linear Contrast Stretch.

An algorithim can be used that relates the old minimum value to the modified minimum value, and the old maximum value to the modified maximum value. All the old intermediate values are placed exactly between the new minimum and maximum values. Many digital image processing systems have built-in capabilities that automatically expand the minimum and maximum values to optimize the full range of available brightness values. This is the simplest contrast stretch algorithm. The gray values in the original picture and the modified image follow a linear relation in this algorithm. A value in the low range of the original histogram is assigned to extremely black and a value at the high end is assigned to extremely white. noise may be of various type and according to the intensity value the noise can be removed.

1.2 Histogram based segmentation:

Segmentation subdivides an image into its same size but in number of regions or objects that have similar features according to a set of given criteria. In this paper, the random segmentation is done by using wavelet based histogram thresholding where, the thereshold value is selected by performing 1-D wavelet based analysis of PDFs of wavelet transformed images at different channels.

- **Introduction of different types of Wavelet transform**

The Discrete Wavelet Transform (DWT) of image signals produces a non-redundant image representation, which provides better global and spectral region of image creation. The DWT can be taken as signal dividation in a set of independent, spatially oriented frequency path. The signal is passed through two complementary filters and emerges as two signals, approximation and details. This is called decomposition. Fig.2. shows the bank of filters iterated for the 2DDWT standard. The components can be assembledback into the original signal without loss of information. This process is called reconstruction.The components can be gain back into the original signal without loss of information. This process is called reproduction of signals.

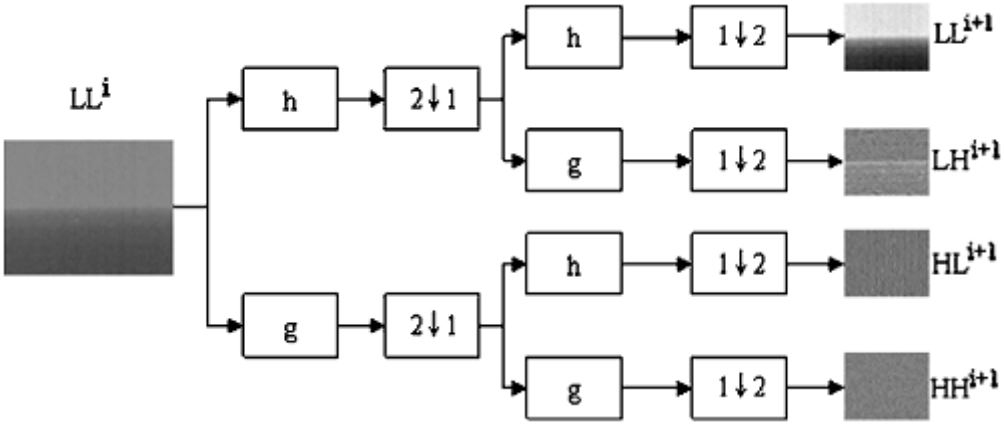

Fig.5 bank of filters iterated for DWT standard

The mathematical calculation, which implies analysis and synthesis, is called discrete wavelet transform and inverse discrete wavelet transform. An image can be divided into a sequence of different spatial resolution images using DWT. In case of a 2D image, an N level decomposition can be performed resulting in 3N+1 different frequency bands. The second level of wavelet transform is applied to the low level frequency sub band image LL only. The 2D-DWT with 3-level decomposition is shown in figure 6. The Gaussian noise almost averaged out in low frequency wavelet coefficients and hence only the wavelet coefficients in the high level frequency need to be thresholded In this paper, the concepts of Daubechies 6 wavelet transform are discussed. The Daubechies wavelets are a family of orthogonal wavelets defining a discrete wavelet transform and characterized by a max number of removing moments for some given support .With each wavelet type of this class, there is a scaling function which generates an eight sided multi resolution analysis. Daubechies wavelets are widely used in solving a big range of problems, e.g. self-similarity properties of a signal or fractal problems, signal discontinuities, etc.

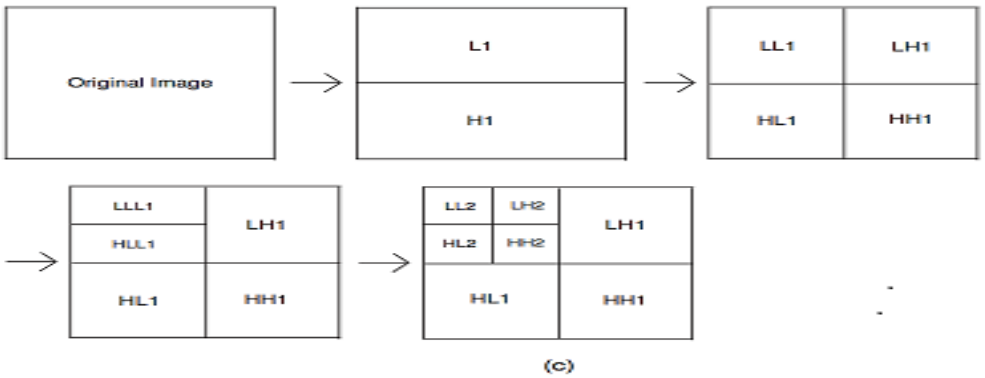

1, 2, 3 --- Decomposition levels
H --- High Frequency Bands,L --- Low Frequency Bands
Fig.6. 2D-DWT with 3-level decomposition

The decomposition of the image into different resolution levels which are sensitive to different frequency bands. By choosing an appropriate wavelet with a right resolution level, tumours can be detected effectively in digital mammogram. Experimental results show that the Daubechies wavelet achieves the best detecting result.

- **Wavelet based histogram Thresholding**

With the fulfilment of preprocessing, the daubechies wavelet transform is applied to a preprocessed image. Proper scaling channel is selected using prior information of appropriate size of the destination. After applying wavelet transform, find the histogram. Then perform 5 scale (on given LL, HL, LH, HH) 1-D db-6 wavelet transform. Calculate the local minimum of the 1-D wavelet transformed pdf at the selected scale .then threshold value t is calculated that retains bright pixels in the image. Pixels with values greater than **t** are set to white (1) and values less than **t** are set to black (0).related characteristic component labeling is applied to the binary image using eight pixel connectivity to indicate each discrete region in the binary segmented image. These discrete regions are subjected to following criteria given below which select the most important candidate regions that strongly resemble a suspicious mass in terms of their area and their statistical characteristics such as their pixel's intensity, higher order moments, etc.

(a) **Requirent 1:** From the data given in the database, it is noticed that area of the mass ranges between 900 to 5000 pixels. So the region whose area lies between 900 pixels and 5000 pixels is considered to be suspicious. This rule is applied to each segmented region and this reduces the number of the candidate regions to Ri , i = 1, ..,M. Regions that don't meet this requirement are rejected.

(b) **Requirement 2:** Each remaining region is considered a suspi-cious region if its third order moment (skewness) is negative in nature otherwise they are rejected.

(c) **Requirement 3:** Each remaining region is still considered suspicious if its mean intensity is greater than a threshold value Tm. The regions that do not satisfy this criterion are cancelled. the threshold value is selected accordingly the character of the behind breast tissue is given in table 1. These threshold values were chosen after experimenting with the images in the database.

This selected threshold value is used to calculate local minima value. Then segmentation is done by using threshold value to obtain the coarse segmented areas. This course segmented result is then send to fine segmentation processing to get super fine output. Coarse segmentation gives good output on given database available.

Background	**Threshold Value Tm**
Fatty	160 < Tm< 170
Glandular	171 < Tm< 180
Dense	Tm> 181

Table 1: Threshold values for different types of back-ground tissue

2.3 Fine-Segmentation:

In fine segmentation first of all small window is selected which are use to calculate suspicious area in given mammograms and then large window is selected for calculating main highlighted area on breast. The procedures contain two phases:

- **Small Window Selection**

A small window is the first step in fine segmentation. Here the entire image is partitioned into a fixed number of large regions where R1, R2,……, Rm.Then this window is taken inside the next window Ri and which are use to calculate threshold for each window.normally the smaller the window size will better the result. However, when the window size becomes too small, it may produce the problem of same properties windows, i.e., windows contain only background or object pixels,Therefore, there is a strong need to develop a correct window size in order to get the optimal result. Final segmentation depends on the proper selection of initial window size.

- **Window based histogram Thresholding**

Fig.1 shows the flowchart of the proposed method for tumor detection. Histogram based segmentation is considered For each pixel P (i, j), a decision is fixed to detect the potential suspicious lesion pixel or a normal pixel by the following rule. If the neighborhood P [i,j] is having smaller value than T threshold ,Then convert pixel to background i.e. '0' Otherwise declare the pixel as suspicious. In this rule, T (i, j) is an adaptive Threshold value calculated by histogram based segmentation output. Each step is described further below.

1. Set threshold in middle of window sum.[11*11].
2. Check the neighbourhood pixels position
3. If the neighbourhood addition is not greater than threshold value, change pixel to '0' Otherwise define it as '1' which makes it suspicious region.

   If

   P [I, j] <T

   Then

   Change pixel to '0'.

   Else

   Define it as suspicious area.
4. Repeat steps (2)-(3) till the whole image is checked.

III. OUTPUT

The data used in given experiments are taken from the mini- MIAS database of mammograms [4]. The same collection of database has also been used by other researcher for their studies in different fields, such as automatic mammogram classification, mass segmentation, and micro calcification detection. All images are covered at the resolution of 1024 ×1024 pixels and 8-bit accuracy (for gray level). The proposed algorithm was implemented in a MATLAB environment on acomputer (Intel Pentium IV, 3.0-GHz CPU, and 512-MB (RAM). It has been licenced with 170 mammograms in the mini-MIAS database. The testing images include some normal images and out of this some are real space-occupying lesion images, with 100 lesions in total. To calculate the accurate output throught computer-aided diagnosis, we adopted the following criteria given in [10], a computer aided system searching considered as a correct result if its area is covered by at least 50% of a true defects. The detection results are evaluated by terms of sensitivity and the number of false positives per image (FP/I).The original image is shown as Fig.7 (a). The intensity adjustment is done by linear contrast stretching which is shown in Fig.7 (b). Daubechies 6-point wavelet is selected to process the image.

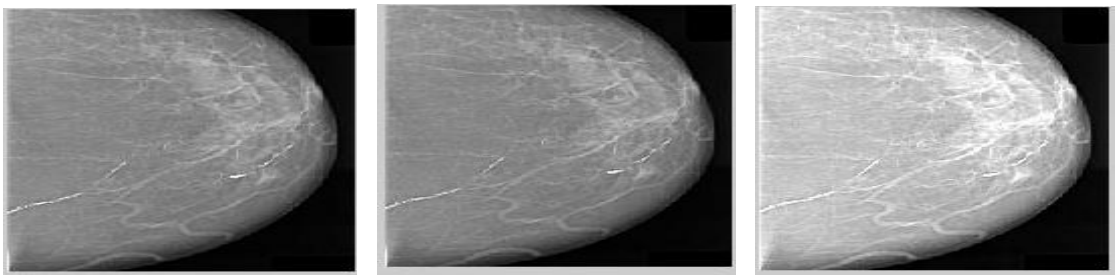

a)original image b)grey scale image c)intensity adjust image

Fig.7 original image and preprocessed image

Then wavelet transforms applied on the input image from scales 1 to 4. Then histogram is taken for transformed images.Next, 5-scale wavelet transforms applied for the histogram of the image in scale 2. By selecting the local minima at adaptively selected scale, four local minima are calculated using the top most local minimum as the threshold value, the histogram segmented areas are obtained. there are some example images which are collected from minimias databases for locating good result for segmentation this output shows how this histogram based hresholding is superior then other thresholding(ex.local or global thresholding)

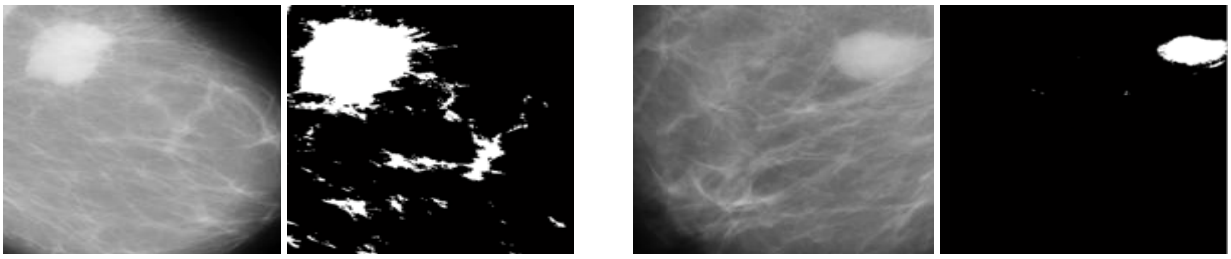

(a) Original image (b) Segmented image (a) Original image (b) Segmented image

Fig 8. Example of segmentation results by the histogram based decomposition

Fig.9 (a) shows the original mammilla picture, then Fig.9 (b) shows the intensity adjusted image output. Fig.9(c) shows the histogram based segmented result. Fig.9 (d) shows the fine segmented result. The exact result can be obtained with small window size as 15*15 and large window size as 128*128 which is shown in Fig.9 (d). hence the given histogram based decomposition algorithm obtained a good detection result.

Image mdb115

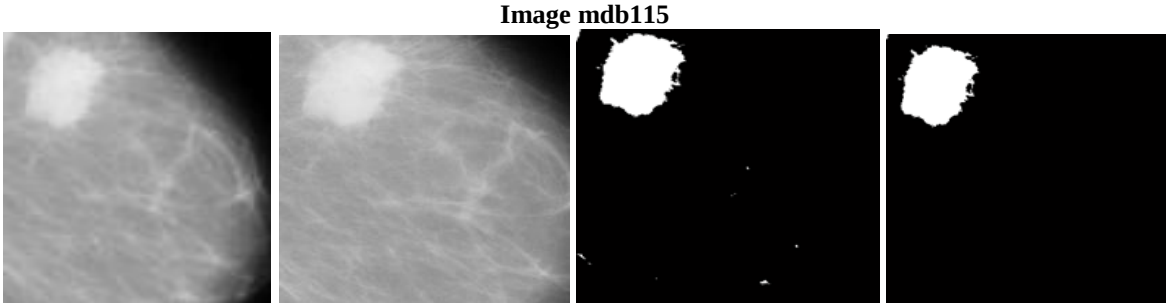

(a) Original image (b) Preprocessed image c) histogram based segmented result (d) Fine segmented result

Image mdb184

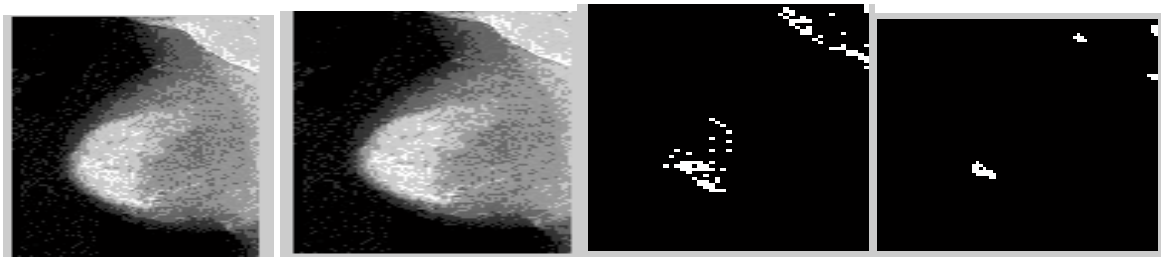

(a) Original image (b) Preprocessed image c) histogram based segmented result (d) Fine segmented result

Image mdb94

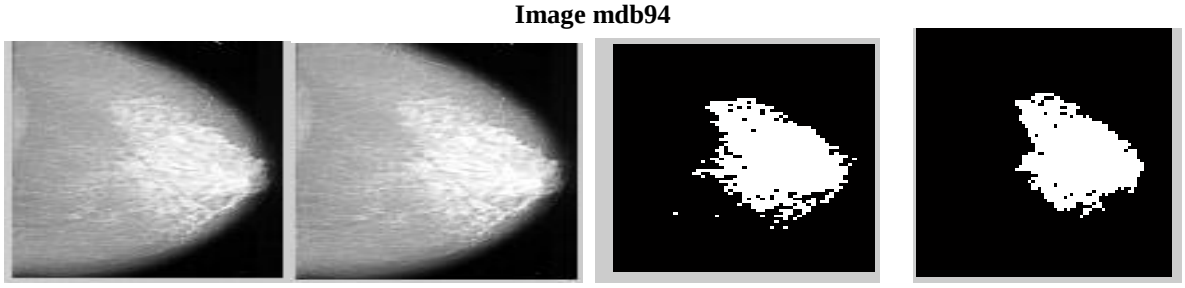

(a) Original image (b) Preprocessed image c) histogram based segmented result (d) Fine segmented result

Fig 9. Example of segmentation results by the wavelet based adaptive windowing method of thresholding

IV. CONCLUSION

Hence at the end we, conclude that a new algorithm based on the histogram based wavelet decomposition method is used for the segmentation of bright targets in an image. Histogram based segmentation is proposed by using wavelet based histogram thresholding in which thereshold value is chosen by performing 1-D DWT analysis of Power Density Functions of wavelet transformed images at different channels. Final segmented result is found by choosing threshold by using windowing method. The main feature of this method, with respect to the other techniques proposed is its adaptability and convenience to the different nature of solve a problem relevant to the nature in the image under analysis, allowing the use of the same basic algorithm for both micro-calcifications and mass detection. Many computerized results prove the suitability and availability of this approach to maximize both i.e. micro calcifications, and very low-contrast structures, such as masses. The improving quality of the processed images has been considered by radiologists as a true significant aid for the early detection of breast cancer.

REFERENCES

[1] S. Liu, C. F. Babbs, and E. J. Delp, "Multiresolution detection of spiculated lesions in digital mammograms," IEEE Trans. Image Process.,vol. 10, no. 6, pp. 874–884, Jun. 2001.
[2] K. Bovis and S. Singh, "Detection of masses in mammograms using texture features," in Proc. 15th Int. Conf. Pattern Recog., 2000, vol. 2, pp. 267–270.
[3] G. Cardenosa, "Mammography: An overview," in Proc. 3rd Int. Workshop Digital Mammography, Chicago, IL, Jun. 9–12, 1996, pp. 3–10.
[4] J. Suckling, S. Astley, D. Betal, N. Cerneaz, D. R. Dance,S.-L. Kok, J. Parker, I. Ricketts, J. Savage, E. Stamatakis, andP. Taylor, Mammographic Image Analysis Society MiniMammographic Database, 2005. [Online]. Available: http://peipa.essex.ac.uk/ipa/pix/mias/
[5] Kai-yang Li, Zheng Dong, "A Novel Method of Detecting Calcifications from Mammogram Images Based on Wavelet and Sobel Detector," ICMA. June 2006.
[6] Diyana, W.M., Besar, R., "Methods for clustered microcalcifications detection in digital mammograms," ISSPIT, Dec.2004.
[7] Songyang Yu, Ling Guan, "A CAD system for the automatic detection of clustered microcalcifications in digitized mammogram films" IEEE Transactions on Medical Imaging, Vol 19, Issue 2, pp. 115 - 126, Feb. 2000
[8] Auephanwiriyakul, S., Attrapadung, S., Thovutikul, S., Theera- Umpon N., "Breast Abnormality Detection in Mammograms Using Fuzzy Inference System," Fuzzy Systems, May. 2005, pp. 155-160 conclusion might elaborate on the importance of the work or suggest applications and extensions.

International Journal of Modern Engineering Research (IJMER)
www.ijmer.com Vol.3, Issue.2, March-April. 2013 pp-915-919 ISSN: 2249-6645

Replica Allocation In Mobile Adhoc Network For Improving Data Accessibility Using SCF-Tree

K.P.Shanmuga Priya[1] V.Seethalakshmi [2]
Sri Shakthi Institute of Engineering and Technology, Coimbatore, Tamilnadu

Abstract: *In a mobile ad hoc network, the mobility and resource constraints of mobile nodes may lead to network partitioning or performance degradation. Several data replication techniques have been proposed to minimize performance degradation. Most of them assume that all mobile nodes collaborate fully in terms of sharing their memory space. In reality, however, some nodes may selfishly decide only to cooperate partially, or not at all, with other nodes. These selfish nodes could then reduce the overall data accessibility in the network. In this paper, the impact of selfish nodes in a mobile ad hoc network from the perspective of replica allocation is examined. A selfish node detection algorithm was developed that considers partial selfishness and novel replica allocation techniques to properly cope with selfish replica allocation. The conducted simulations demonstrate the proposed approach outperforms traditional cooperative replica allocation techniques in terms of data accessibility, communication cost and average query delay.*

Keywords: *Manet, Selfish nodes, data accessibility, communication cost and query delay.*

I. Introduction

Mobile ad hoc networks (MANETs) have attracted a lot of attention due to the popularity of mobile devices and the advances in wireless communication technologies. A MANET is a peer-to-peer multihop mobile wireless network that has neither a fixed infrastructure nor a central server. Each node in a MANET acts as a router, and communicates with each other. A large variety of MANET applications have been developed. For example, a MANET can be used in special situations, where installing infrastructure may be difficult, or even infeasible, such as battlefield or a disaster area. A mobile peer-to-peer file sharing system is another interesting MANET application [4].

Network partitions can occur frequently, since nodes move freely in a MANET, causing some data to be often inaccessible to some of the nodes. Hence data accessibility is often an important performance metric in a MANET. Data are usually replicated at nodes, other than the original owners, to increase data network partitions. A considerable amount of research has recently been proposed for replica allocation in a MANET [6][7].

In general replication can simultaneously improve data accessibility and reduce query delay, i.e., query Response time, if the mobile nodes in a MANET together have sufficient memory space to hold both all the replicas and the original data. For example, the response time of a query can be substantially reduced, if the query accesses a data item that has a locally stored replica. However, there is often a trade-off between data accessibility and query delay, since most nodes in a MANET have only limited memory space. For example, a node may hold a part of the frequently accessed data items locally to reduce its own query delay. However, if there is only limited memory space and many of the nodes hold the same replica locally, then some data items would be replaced and missing. Thus, the overall data accessibility would be decreased. Hence, to maximize data accessibility, a node should not hold the same replica that is also held by many other nodes. However, this will increase its own query delay. The nodes can be divided into three types. They are, Type-1 node: The nodes are non-selfish nodes. The nodes hold replicas allocated by other nodes within the limits of their memory space.

- Type-2 node: The nodes are fully selfish nodes. The nodes do not hold replicas allocated by other nodes, but allocate replicas to other nodes for their accessibility.
- Type-3 node: The nodes are partially selfish nodes. The nodes use their memory space partially for allocated replicas by other nodes. Their memory space may be divided logically into two parts: selfish and public area. These nodes allocate replicas to other nodes for their accessibility.

II. Overview of Existing Methods

This section deals with the replica allocation methods in MANET environment having selfish nodes which influence the performance of data accessibility.

2.1 Static Access Frequency (SAF) Method

In SAF method, the nodes allocate replica of data items according to the access frequencies of that data items. Mobile nodes with the same access frequencies to data items allocate the same replica. A mobile node can access data items held by other connected mobile hosts, and it is more possible to share different kinds of replica among them. The SAF method causes low data accessibility when many mobile hosts have the similar access characteristics hence some of the data items to be duplicated in many nodes.

2.2 Dynamic Connectivity Based Grouping Method (DCG)

The DCG method shares replicas in larger groups of mobile hosts than DAFN. At every relocation period, each mobile host broadcasts its host identifier. After all mobile hosts complete the broadcasts; every host knows the connected mobile hosts and the network topology from the received host identifiers. In each set of mobile hosts connected to each other, the mobile host with the lowest host identifier suffix executes an algorithm to find bi-connected components with the network topology known by received messages. Even if a mobile host belongs to more than one bi-connected component, it can only belong to one group in which the corresponding bi-connected component was found first. By grouping mobile hosts as bi-connected components, the group is not divided even if one mobile host disappears from the network or one link is disconnected in the groups. Thus, it is assumed that the group has high stability affected, unless they were in sleep mode and also if the selected routes are via specific host, the battery of this host will be exhausted quickly.

2.3 Dynamic Connectivity-Based Grouping with Detection (DCG +)

The technique combines DCG with our detection method. Initially, groups of nodes are created according to the DCG methodology. Subsequently, in each group, selfish nodes are detected based on our detection method. For the detection, each node in a group sends its nCR scores to the coordinator with the lowest suffix of node identifier in the group. The coordinator excludes selfish node(s) from the group for replica allocation. As a result, only non-selfish nodes form a group again. The replica allocation is only performed within the final group without any selfish nodes. After replica allocation, the coordinator shares the information of replica allocation with group members for the subsequent selfishness detection. In particular, selfish nodes are determined to be selfish only when all other nodes in the group agree with the node's selfishness. The other approaches to determine selfishness, including the agreement of 1) at least one and 2) the majority of nodes.

2.4 Dynamic Access Frequency and Neighbourhood (DAFN)

The algorithm of this method is as follows:

1) At a relocation period, each mobile host broadcasts its host identifier and information on access frequencies to data items. After all mobile hosts complete the broadcasts, from the received host identifiers, every host shall know its connected mobile hosts.
2) Each mobile host preliminary determines the allocation of replicas based on the SAF method.
3) In each set of mobile hosts which are connected to each other, the following procedure is repeated in the order of the breadth first search from the mobile host with the lowest suffix (i) of host identifier (Mi). When there is duplication of a data item (original/replica) between two neighbouring mobile hosts, and if one of them is the original, the host which holds the replica changes it to another replica. If both of them are replicas, the host whose access frequency value to the data item is lower than the other one changes the replica to another replica. When changing the replica, among data items whose replicas are not allocated at either of the two hosts, a new data item replicated is selected where the access frequency value to this item is the highest among the possible items. This eliminates replica duplication among neighboring hosts. The above procedure is executed every relocation period. Overhead and traffic is much higher than SAF.

III. Problem Definition

The problem of selfishness in the context of replica allocation in a MANET, i.e., a selfish node may not share its own memory space to store replica for the benefit of other nodes. A node may act selfishly, i.e., using its limited resource only for its own benefit, since each node in a MANET has resource constraints, such as battery and storage limitations. A node would like to enjoy the benefits provided by the resources of other nodes, but it may not make its own resource available to help others. Such selfish behavior can potentially lead to a wide range of problems for a MANET. Existing research on selfish behaviors in a MANET mostly focus on network issues. For example, selfish nodes may not transmit data to others to conserve their own batteries. Although network issues are important in a MANET, replica allocation is also crucial, since the ultimate goal of using a MANET is to provide data services to users [10].

IV. Proposed Method (SCF-Tree)

Novel replica allocation techniques for selfish node detection and elimination were devised. They are based on the concept of a self-centered friendship tree (SCF-tree) and its variation to achieve high data accessibility with low communication cost in the presence of selfish nodes. The SCF-tree is inspired by our human friendship management in the real world. Main aim is to reduce the communication cost, while still achieving good data accessibility. The technical contributions of this paper can be summarized as follows

i) **Recognizing the selfish replica allocation problem:** selfish nodes in a MANET from the perspective of data replication are viewed, and recognize that selfish replica allocation can lead to degraded data accessibility in MANET.
ii) **Detecting the fully or the partially selfish nodes effectively:** A selfish node detection method is devised to measure the degree of selfishness.
iii) **Allocating replica effectively:** Set of replica allocation techniques are proposed, that use the self-centered friendship tree to reduce communication cost, while achieving good data accessibility.
iv) **Verifying the proposed strategy:** The simulation results verify the efficacy of the proposed strategy.

4.1 Proposed Strategy

The paper consists of three parts: 1) detecting selfish nodes, 2) building the SCF- Tree, and 3) allocating replica. At a specific period, or relocation period, each node executes the following procedures:

- Each node detects the selfish nodes based on credit risk scores.
- Each node makes its own topology graph and builds its own SCF-tree by excluding selfish nodes.
- Based on SCF-tree, each node allocates replica in a fully distributed manner.

4.1.1 Detecting Selfish Node

The notion of credit risk can be described by the following equation:

Credit Risk =expected risk / expected value

Each node calculates a CR score for each of the nodes to which it is connected. Each node shall estimate the "degree of selfishness" for all of its connected nodes based on the score. First, selfish features may lead to the selfish replica allocation problem were both expected value and expected risk are determined.

4.1.2 Building SCF-Tree

The SCF-tree based replica allocation techniques are inspired by human friendship management in the real world, where each person makes his/her own friends forming a web and manages friendship by himself/herself. He/she does not have to discuss these with others to maintain the friendship. The decision is solely at his/her discretion. The main objective of our novel replica allocation techniques is to reduce traffic overhead, while achieving high data accessibility. If the novel replica allocation techniques can allocate replica without discussion with other nodes, as in a human friendship management, traffic overhead will decrease.

4.1.3 Allocating Replica

After building the SCF-tree, a node allocates replica at every relocation period. Each node asks non-selfish nodes within its SCF-tree to hold replica when it cannot hold replica in its local memory space. Since the SCF-tree based replica allocation is performed in a fully distributed manner, each node determines replica allocation individually without any communication with other nodes. Since every node has its own SCF-tree, it can perform replica allocation at its discretion. Replica can be allocated at each node in descending order of its own access frequency. This is quite different from existing group-based replica allocation techniques (e.g., DCG) where replicas are allocated based on the access frequency of group members. Each node N_i executes this algorithm at every relocation period after building its own SCF-tree. At first, a node determines the priority for allocating replicas. The priority is based on Breadth First Search (BFS) order of the SCF-tree.

V. Results and Discussion

In the simulation, the number of mobile nodes is set to 40. Each node has its local memory space and moves with a velocity from 0~1 (m/s) over 50(m) 50 (m) flatland. The movement pattern of nodes follows the random waypoint model, where each node remains stationary for a pause time and then it selects a random destination and moves to the destination. After reaching the destination, it again stops for a pause time and repeats this behaviour. The radio communication range of each node is a circle with a radius of 1~ 19 (m). We suppose that there are 40 individual pieces of data, each of the same size. In the network, node Ni ($1 \leq i \leq 40$) holds data D_i as the original. The data access frequency is assumed to follow *Zipf* distribution. The default relocation period is set to 256 units of simulation time which we vary from 64 to 8,192 units of simulation time. Table 1 describes the simulation parameters.

5.1 Simulation Parameters

Table 1: Simulation Environment

Parameter (unit)	Value (default)
Number of nodes	40
Number of data items	40
Radius of communication range (m)	1~19 (7)
Size of the network (m)	50*50
Size of memory space (data items)	2~40(10)
Percentage of selfish nodes	0~100(70)
Maximum velocity of a nodes	1
Relocation period	64~8192 (256)

5.2 Metrics used for Evaluation

Overall selfishness alarm: This is the ratio of the overall selfishness alarm of all nodes to all queries that should be served by the expected node in the entire system.

Communication cost: This is the total hop count of data transmission for selfish node detection and replica allocation/relocation, and their involved information sharing.

Average query delay: This is the number of hops from a requester node to the nearest node with the requested data item. If the requested data item is in the local memory of a requester, the query delay is 0. We only consider successful queries, i.e., it is the total delay of successful requests divided by the total number of successful requests.

Data accessibility: This is the ratio of the number of successful data requests to the total number of data requests.

5.3 Simulation Results

The Communication cost (fig 5.1) of a network using SCF-tree is minimum compared to normal replica (DCG). Where as Data Accessibility, Overall Selfishness, Average Query delay of a network is maximum (fig 5.2, 5.3, 5.4)

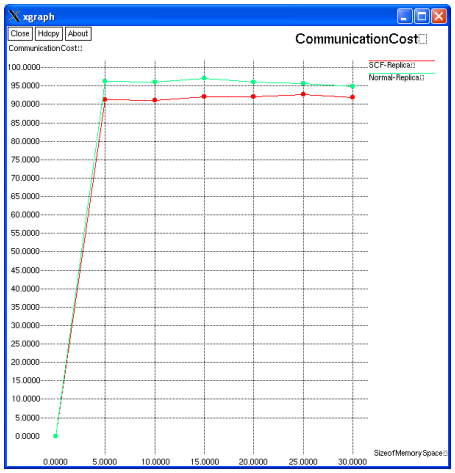

Fig 5.1 Comparison of Communication cost Vs Size of memory space using 40 nodes

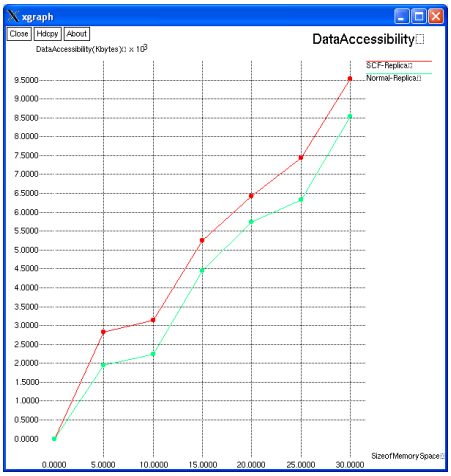

Fig 5.2 Comparison of Data Accessibility Vs Size of memory space using 40 nodes

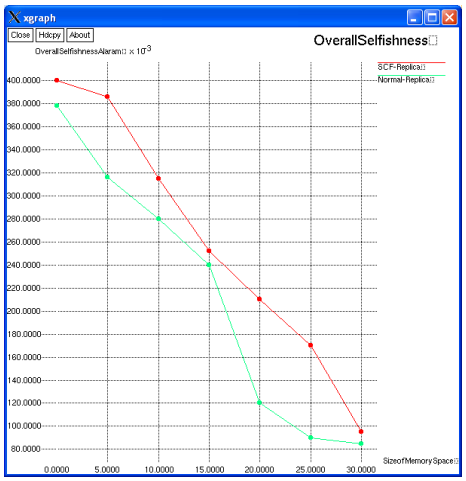

Fig 5.3 Comparison of Overall Selfishness Vs Size of memory space using 40 nodes

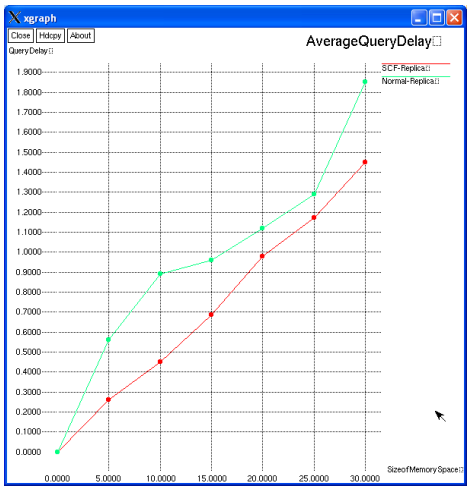

Fig 5.4 Comparison of Average Query delay Vs Size of memory space using 40 nodes

VI. Conclusion

In contrast to the network viewpoint, the problem of selfish nodes from the replica allocation perspective is addressed. This problem is known as selfish replica allocation. The work was motivated by the fact that a selfish replica allocation could lead to overall poor data accessibility in a MANET. A selfish node detection method and novel replica allocation techniques to handle the selfish replica allocation appropriately have been proposed. The proposed strategies are inspired by the real-world observations in economics in terms of credit risk and in human friendship management in terms of choosing one's friends completely at one's own discretion. The notion of credit risk from economics to detect selfish nodes is applied. Every node in a MANET calculates credit risk information on other connected nodes individually to measure the degree of selfishness. Since traditional replica allocation techniques failed to consider selfish nodes, novel replica allocation techniques also proposed. Extensive simulation shows that the proposed strategies outperform existing representative cooperative replica allocation techniques in terms of data accessibility, communication cost, and query delay.

VII. Future work

This paper proposes further research into more replica allocation technique that can improve the performance of MANETs. Currently working on the impact of different mobility patterns, and plan to identify and handle false alarms in selfish replica allocation.

References

[1] K. Balakrishnan, J. Deng, and P.K. Varshney, "TWOACK: Preventing Selfishness in Mobile Ad Hoc Networks," Proc. IEEE Wireless Comm. and Networking, pp. 2137-2142, 2005.
[2] G. Cao, L. Yin, and C.R. Das, "Cooperative Cache-Based Data Access in Ad Hoc Networks," Computer, vol.37, no. 2, pp. 32-39, Feb. 2004
[3] B.-G. Chun, K. Chaudhuri, H. Wee, M. Barreno, C.H. Papadimitriou, and J. Kubiatowicz, "Selfish Caching in Distributed Systems: A Game-Theoretic Analysis," Proc. ACM Symp. Principles of Distributed Computing, pp. 21-30, 2004
[4] G. Ding and B. Bhargava, "Peer-to-Peer File-Sharing over Mobile Ad Hoc Networks," Proc. IEEE Ann Conf. Pervasive Computing and Comm. Workshops, pp. 104-108, 2004
[5] M. Feldman and J. Chuang, "Overcoming Free-Riding Behavior in Peer-to-Peer Systems," SIGecom Exchanges, vol. 5, no. 4, pp. 41-50, 2005.
[6] T. Hara and S.K. Madria, "Data Replication for Improving Data Accessibility in Ad Hoc Networks," IEEE Trans. Mobile Computing, vol. 5, no. 11, pp. 1515-1532, Nov. 2006.
[7] T. Hara and S.K. Madria, "Consistency Management Strategies for Data Replication in Mobile Ad Hoc Networks," IEEE Trans. Mobile Computing, vol. 8, no. 7, pp. 950-967, July 2009.
[8] S.U. Khan and I. Ahmad, "A Pure Nash Equilibrium-Based Game Theoretical Method for Data Replication across Multiple Servers," IEEE Trans. Knowledge and Data Eng., vol. 21, no. 4, pp. 537-553, Apr. 2009.
[9] M.J. Osborne, An Introduction to Game Theory. Oxford Univ., 2003.
[10] D. Hales, "From Selfish Nodes to Cooperative Networks-Emergent Link-Based Incentives in Peer-to-Peer networks," Proc. IEEE Int'l Conf. Peer-to-Peer Computing, pp. 151-158, 2004

International Journal of Modern Engineering Research (IJMER)
www.ijmer.com Vol.3, Issue.2, March-April. 2013 pp-920-923 ISSN: 2249-6645

A Production of biodiesel from rice bran oil and experimenting on small capacity diesel engine

Subhan Kumar Mohanty
Department of mechanical engineering, G.I.E.T, Bhubaneswar, INDIA

Abstract: *Increased environmental awareness and depletion of resources are driving industry to develop viable alternative fuels from renewable resources that are environmentally more acceptable. Vegetable oil is a potential alternative fuel. The most detrimental properties of vegetable oils are its high viscosity and low volatility, and these cause several problems during their long duration usage in compression ignition (CI) engines. The most commonly used method to make vegetable oil suitable for use in CI engines is to convert it into biodiesel, i.e. vegetable oil esters using process of transesterification.*

Rice bran oil is an underutilized non-edible vegetable oil, which is available in large quantities in rice cultivating countries, and very little research has been done to utilize this oil as a replacement for mineral Diesel. In the present work, the transesterification process for production of rice bran oil methyl ester has been investigated. The various process variables like temperature, catalyst concentration, amount of methanol and reaction time were optimized with the objective of producing high quality rice bran oil biodiesel with maximum yield. The optimum conditions for transesterification of rice bran oil with methanol and NaOH as catalyst were found to be 55 °C reaction temperature, 1 h reaction time, 9:1 molar ratio of rice bran oil to methanol and 0.75% catalyst (w/w). Rice bran oil methyl ester thus produced was characterized to find its suitability to be used as a fuel in engines. Results showed that biodiesel obtained under the optimum conditions has comparable properties to substitute mineral Diesel, hence, rice bran oil methyl ester biodiesel could be recommended as a mineral Diesel fuel substitute for compression ignition (CI) engines in transportation as well as in the agriculture sector.

Keywords: *Biodiesel, Rice bran oil, Transesterification*

I. Introduction

Due to global depletion of world petroleum reserves and the impact of environmental pollution of increasing exhaust emission there is an urgent need for suitable alternative fuel. The various alternative fuel options researched for diesel are mainly biogas producer gas, methanol, ethanol and vegetable oil. Out of this which rice bran oil is one of the promising alternate fuel for diesel engine. Rice bran oil is a non conventional, in expensive and low–grade vegetable oil. Crude rice bran oil is also source of high value added by-products are derived from the crude rice bran oil and the resultant oil is used as a feed stock for bio diesel, the resultant bio diesel could be quite economical and affordable. Rice bran oil is the oil extracted from the germ and inn er husk of rice. It is the notable for its very high smoke point of 490° F (254° C) and its mild flavour, making it suitable for high temperature cooking method such as stir frying and deep frying. It is popular as cooking oil in several asian countries including japan and china. Rice bran oil contains a range of fats, with 47% of its fats monounsaturated, 33% polyunsaturated, and 20% saturated. The fatty acid composition of rice bran oil is palmitic 15.0%, Stearic acid 1.9%, Oleic acid 42.5%, Linoleic acid 39.1%, Linolenic acid 1.1%, Arachidic 0.5%, Behenic 0.2%.

II. Transesterification

Due to very high free fatty acid, rice bran oil was converted into methyl ester by the two stage process.IN the first stage rice bran oil was reacted with CH3OH in presence of an acid catalyst (H2SO4) to convert free fatty acid inyo fatty ester. A specified ammount 1000g of rice bran oil was taken in a round bottom flask and heated up to 60-65°C. In a separate flas CH3OH (950 g) and H2SO4 (22 g) were taken and properly mixed and then stirred for 4 h and maintained at 60°C.It was allowed to cool overnight without stirring. When acid number of the mixture reaches to less than 1,the second stage was started .During this stage mixture 1000g obtained from the first stage was taken in around bottom flask and heated upto 60°C methanol(200ml) and KOH 4.5g were properly mixed in other flask and then introduced into the round bottom flask containing the mixture from first stage. The mixture stirred vigorously for 2h and then allowed to cool overnight. Glycerol was seperated by adding wram water at 60°C to the mixture. Glycerol and soap formed during the process settled down the bottom. Top layer containing rice bran oil methyl ester 91% was removed with the help of a separating funnel and wasted two times with water and dried.

III. Engine Test

A diesel engine with single cylinder, direct injection it is widely used in agriculture and industrial purpose. It is a single cylinder, four stoke, vertical, air cooled engine having bore X Stroke (mm) 78X62 respectively. At rated speed 3000rpm,it develops power of 4.4kw with diesel engine. It hasa provision of loading electrically since it is coupled with a single-phase motor through flexible coupling .The engine can be kick started using decompression lever and is provided with centrifugal speed governer. The inlet valve opens at before top dead centre (BTDC) and closes at 35.5□ After bottom dead centre(ABDC).The exhaust valve opens at35.5□ before Bottom dead centre(BBDC)and closes at 4.5□ After Top dead

centre(ATDC).The 220v ac alternator coupled with engie has sufficient capacity to absorb the maximum power produced by the engine. Fuel injection pressure was maintained at 200bar throughout the experiment. The engine was tested with 20, 40, 60, 80% and full rated output and full rated speed of 3000rpm only. The engine ran smoothly throughout the study and no major problem was reported. The engine produced and 10% excess power without any difficulty

Comparative analysis of rice bran oil biodiesel and diesel

Fuel properties	Rice bran oil biodiesel	DIESEL
Density(gm/cc)	0.872	0.831
Viscosity(cSt)	4.81	3.21
Flash point(C)	157	76
Cetane number	51.6	47.2
Calorific value(KJ/KG)	41382	44585

IV. Result & Discussion

The power developed by engine at varying load for diesel and biodiesel suggests that maximum power is higher in case of diesel (3.911kw) than biodiesel (3.757kw).This is primarily because of less heating value of biodiesel as compared to diesel variation of fuel consumption rate for diesel and biodiesel of rice bran oil suggests that fuelfl ow rate is marginally higher in case RBOME than diesel. Higher density of biodiesel leads to more discharge of fuel injection pump thereby increasing fuel consumoption rate. Brake specific fuel consumption (BSFC) (FIG-1) is higher for RBOME as compard to diesel at the entire brake load, because of less heating value and more consumption of RBOME as compared to diesel engine .BSFC for RBOME and diesel are as follows minimum load 0.848, 0.687 and am load 0.450, 0.367 kg/Kwh.

FIGURE 1 :

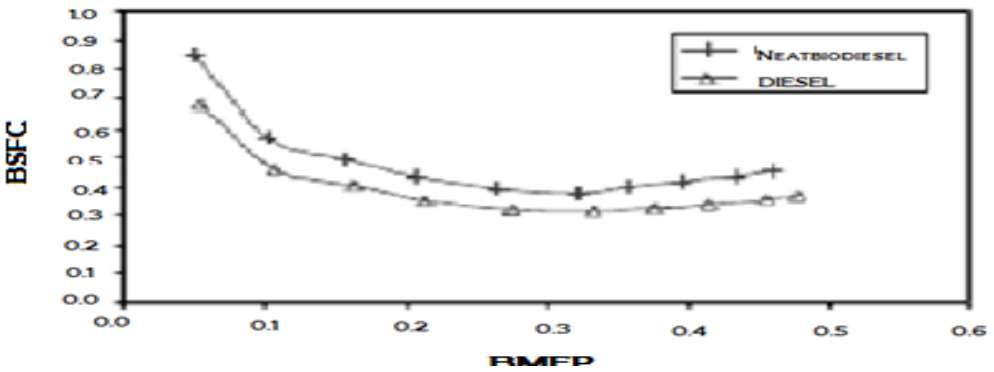

Since both the fuels have different calorific values, viscosity and density, BSFC is not a reliable tool to compare the fuel consumption per unit power developed. A better approach is to compare the two fuel on the basis of energy required to develop unit power outpur, kown as brake specific energy cosumption (BSEC).The BSEC (Fig 2) corresponding to maximum load for diesel was 16.311kJ/Kwh where for biodiesel it was 18.603kj/Kwh, which sugest that energy required by bio diesel to develop unit output is more in comparison to diesel.

FIGURE 2 :

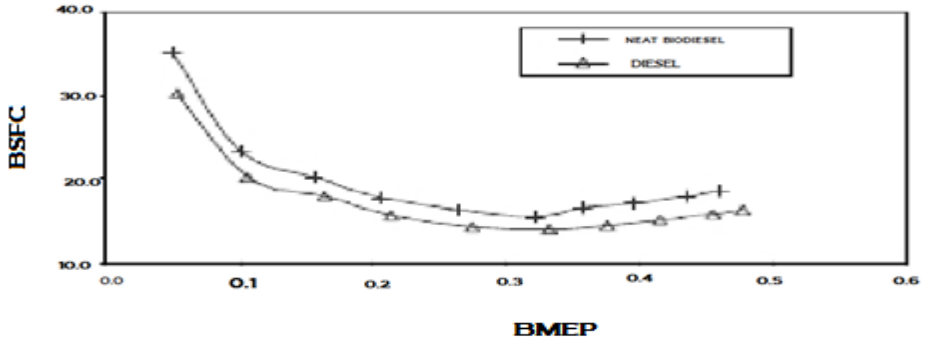

BSFC vs BMEP

Brake thermal efficiency (BTE) (Fig 3) for RBOME and diesel are as follows:

FIGURE 3 :

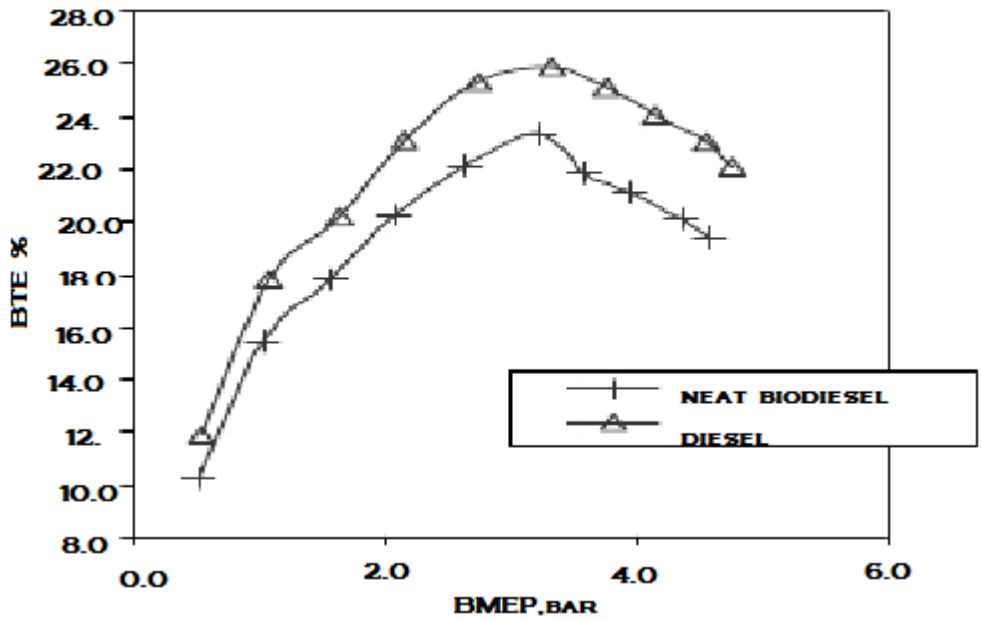

Brake thermal efficiency (BTE) vs BMEP

At minimum load -10.53%, 11.88%
At maximum load-19.35%, 22.07%

Here efficiency is observed higher in case of diesel than the biodiesel at all values of load this could be attributed to inbuilt 10% oxygen content in biodiesel, which helps in better combustion and higher cetane rating of the fuel. Smoke capacity (Fig 4) has been observed higher in case diesel then the methyl ester at all value of value of loads. This is probably because of inbuilt oxygen content and lower sulfur content in biodiesel.

FIGURE 4 :

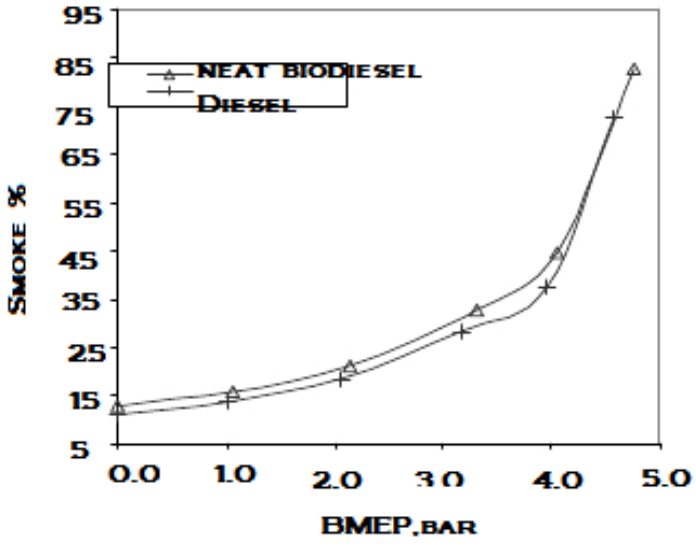

Smoke capacity vs BMEP

V. Conclusion

Biodiesel made from high free fatty acid rice bran oil using two stage formulation process had viscosity and density similar to diesel. Calorific value of biodiesel was around 7% lower that of diesel. Flash point of biodiesel is quite high as compared to diesel making is safer to safer to store and transport. Sulfur in biodiesel is very low as compared to diesel and is an important feature interm of reduction of sulphur-oxide from the exhaust emission. The HFFR test suggests that lubricity of biodiesel in comparison to diesel. Biodiesel was used as a fuel in an unmodified, small capacity diesel engine. The power developed from the engine with biodiesel as a fuel was 4% lower as compared to diesel, because of lower heating value of biodiesel. BSFC and brake specific energy consumption were also higher due to some reason.BTE was higher in diesel as compared to biodiesel. Smoke capacity was lesser of biodiesel than diesel making it more environmental friendly fuel. The study suggests that it is possible to convert high FFA RBO into biodiesel which has similar properties to diesel and can be used to fuel an existing unmodified diesel engine without any difficulty.

Refrences

[1] Nwafor O M I, Effect of choice of pilot fuel on the performance of natural gas in diesel engines, Renewable Energy , 21 (2000) 495-504.
[2] Selim M Y E, Radwan M S & Elfeky S M S, Combustion of jojoba methyl ester in an indirect injection diesel engine, Renewable Energy, 28 (2003) 1401-1420.
[3] Ajav E A, Singh B & Bhattacharya T K, Experimental study of some performance parameters of a constant speed stationary diesel engine using ethanol-diesel blends as fuel, Biomass & Bio-energy, 17 (1999) 357-365.
[4] Srivastava A & Prasad R, Triglycerides-based diesel fuels, Renewable & Sustainable Energy Rev, 4 (2000) 111-133
[5] www.ricebranoil.info/index.html
[6] Lai Chao-Chin, Zullaikah Siti, Vali Shaik Ramjan & Ju Yi- Hsu, Lipase-catalyzed production of biodiesel from rice bran oil, J Chem Technol Biotechnol, 80 (2005) 331-337.
[7] Mattil K F, Norris F A, Stirton A J & Swern D, Baileys Industrial Oils and Fats Products (Inter Science Publisher, New York) 1964, 215-216.

International Journal of Modern Engineering Research (IJMER)
www.ijmer.com Vol.3, Issue.2, March-April. 2013 pp-924-927 ISSN: 2249-6645

XML Based Reverse Engineering System

Soon-kak Kwon[1], Hyungchul Park[2]
[12]*Department of Computer Software Engineering, Dongeui University, Korea*

Abstract: *Reverse engineering that gets data such as an original document or design technique by tracing reversely from certain software system is required in the sides of maintenance and reuse. This paper describes how to implement a system which can get class from one source file, member variable and method within class, and association of between different classes by using reverse engineering, and then can display to XML document and save the document. Also, it analyzes the number of declared variables and functions used in reverse engineered project and displays it as GUI form to give convenience to user.*

Keywords: *Reverse Engineering, Package, xml, Class*

I. INTRODUCTION

Reverse engineering [1, 2] is one field of software engineering. It means the process that gets data such as a document or design technique by reversely tracing an already made software system. It must be essential in software maintenance process that understands the system and changes it appropriately, and has significant meaning of reuse from expansion through the analysis of the implementation of the system.

Software programmers as well as consumers who buy the software has tendency to ignore inner structure and attach importance to result of the project. So, as many team members make one software project, individual of team members makes one by using own method, and assemble them. As a result, unused resources waste resources, and independent modules are not implemented optimally, also association among modules may not be correctly defined.

Therefore, if we use reverse engineering, we can extract information such as class, member variable and method within class, and association of between different classes from one source file, and save them in a specific document. Through it, we can extract the number of declared variables and functions used in target project for reverse engineering to be useful for maintenance, and draw class diagram in detail which is drawn on basic tool.

This paper describes how to implement a system which can do reverse engineering from source file made by JAVA, and save the result as an XML document.

II. XML BASED REVERSE ENGINEERING

The flowchart of proposed reverse engineering is shown in Fig. 1.

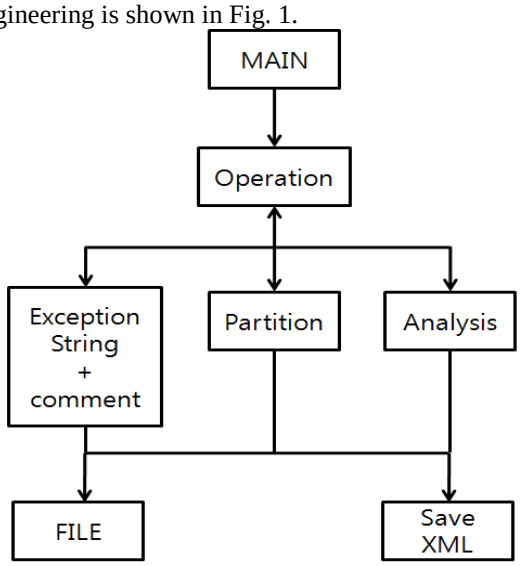

Fig. 1. Flowchart of proposed reverse engineering system

If the square is one class, the main class starts program and the operation class maintains classes by dividing three classes of string+comment exception, partition, and analysis.

The string+comment exception class removes comments and string variable values. The partition class makes a file separately and saves it when many classes are declared in one class file.

In the analysis class, information are saved in sense of class types (class, interface), variable types(data variable, instance variable), and function types(general method, abstract method). Also, information of relationship whether it is inherited or built through interface are extracted and saved.

The file class, used as API, has functions of file open, close, write, save, find, etc.

Then, the usage count class makes a report by extracting usage count of declared functions and variables, and draws a class diagram to see relation between classes easily.

A class is analyzed by five steps of removing risks, partition, sentence analysis, saving XML document, extracting association.

1) Removing risks

For example, when 'String str = "class";' is declared, it may be risky because 'class' word partitions the class. So, we need to remove risky elements when a sentence is analyzed.

Also, because we need not to analyze a single line comment (//~~~\n) and a multiple comment (/* ~~~ */) when a project is analyzed, the comments are first removed.

2) Partition

Class division divides

Many classes can be declared by inner classes in one JAVA file or many classes within one class. The partition divides into individual classes. Partitioned classes are saved to temporary files and they are used into sentence analysis.

3) *Sentence analysis*

Fig. 2 shows algorithm which explains flow of sentence analysis. In Fig, 'public class A{' sentence is presented as an example, it reads each one character, then if there is a non-character like a blank or special character, it recognizes one word to before non-character.

Recognized words are analyzed by finding out meaning of each word through a file that defines reserved words and keywords. And the analyzed words are saved to matched values, then the sentence analysis catches properties about the line, that is, class, interface, method, abstract method, data variable, instance variable, or association as existence of special characters((), {}, ;). Then, analyzing current line is complete.

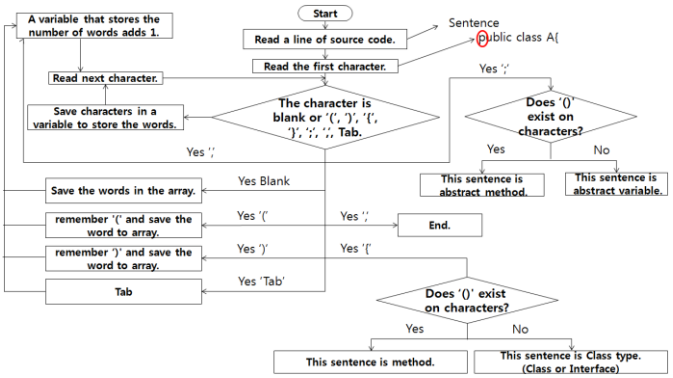

Fig. 2. Algorithm of sentence analysis

4) Saving XML document

The values which get through sentence analysis are saved in order as XML structure. The values which are saved through node's name and sentence analysis are constructed into four depths by condition statements.

```
<Package>
  <Package Name>
  </Package Name>
  <Class Type>
    <Class Type Data>
    </Class Type Data>
    <Method>
      <Method Data>
        <Parameter Data>
        </Parameter Data>
      </Method Data>
    </Method>
    <Variable>
      <Variable Data>
      </Variable Data>
    </Variable>
    <Relation>
      <Relation Data>
      </Relation Data>
    </Relation>
  </Class Type>
</Package>
```

Fig. 3. XML structure

Xml document is saved as structure following depth.
Depth 1 is package.
Depth 2 is package name, and class type (class, interface).
Depth 3 is class type information (extends, implement, visibility, static, final, etc.), method, and variable.
Depth 4 is method information, variable information, and relation information.
Depth 5 is parameter information (visibility, return type, static, final, etc.)

5) Extracting association

The information whether the value saved in XML is function built to override abstract method through interface, or whether it is function or variable inherited from parents class are extracted from class name built by 'implements' and class name inherited through 'extends', and then saved.

III. IMPLEMENTATION

It is easy to extract and find particular information, but it is hard to see information easily when saved as XML.

So, the XML based GUI is implemented. A method which is implemented to input directly path is more comfortable and accurate. Fig. 4 shows the classes saved as tree form after analysis.

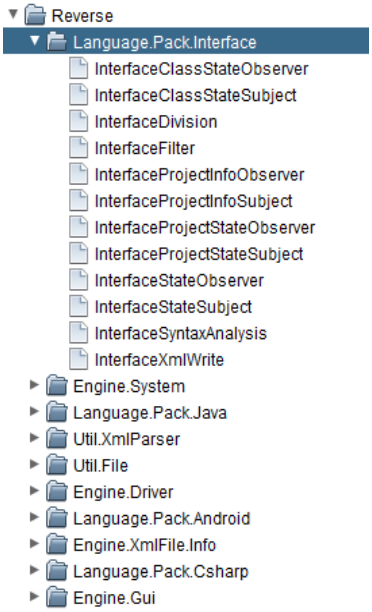

Fig. 4. Classes categorized by tree form

It looks more easy because it is classified package specifically, and when we click on the package we can see classes of package shown in Fig. 6.because it is stored in the tree form.
When we click certain class in Fig. 4, the analyzed contents are displayed as variables and methods shown in Fig. 5.

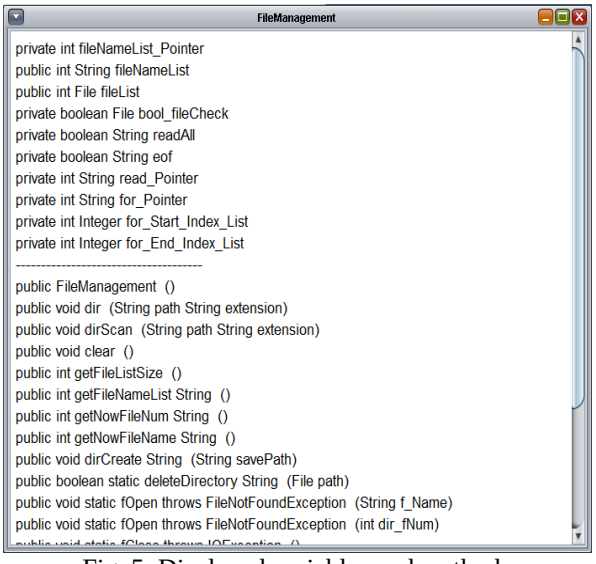

Fig. 5. Displayed variables and methods

Fig. 6 shows the saved XML values. Fig. 7 shows the GUI type of proposed reverse engineering system.

```
- <attribute>
    <visibility>private</visibility>
    <instance>String</instance>
    <name>readAll</name>
  </attribute>
- <method>
    <visibility>public</visibility>
    <returnType>void</returnType>
    <name>dir</name>
  - <parameter>
      <instance>String</instance>
      <name>path</name>
      <instance>String</instance>
      <name>extension</name>
    </parameter>
  </method>
- <relation>
    <name>br</name>
    <new>new</new>
    <instance>BufferedReader</instance>
    <RelationShip>dependency</RelationShip>
  </relation>
</relationLevel>
- <class>
    <visibility>public</visibility>
    <class>class</class>
    <name>FileManagement</name>
  </class>
</classLevel>
<package>package</package>
<package_name>Util.File</package_name>
<import>import</import>
<import_name>java.io.*</import_name>
<import>import</import>
<import_name>java.util.*</import_name>
</packageLevel>
```

Fig. 5. Values saved as XML

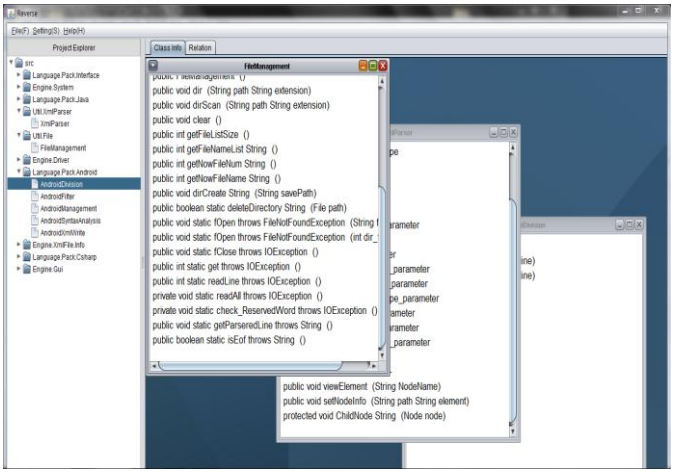

Fig. 6. GUI type

IV. CONCLUSION

Reverse Engineering has an object to facilitate maintenance and increase reuse of software by extracting maximum of information necessary to source code through tracking reversely system. Also, it can decrease unnecessary waste of resource that consumers who buy a program and developers who develop the program. Reverse Engineering system which is proposed in this paper is composed of some parts, removing comments and strings to facilitate distinguishing reversed words, dividing up inner class and many of classes declared within one class into independent classes, analyzing a received line through hash map, saving value made by the analyzing part as XML document, and saving association through extracting saved XML. In addition, it can display such as GUI form.

V. ACKNOWLEDGEMENTS

The authors would like to thank uBASIC, Ltd for developing this system. Corresponding author: Soon-kak Kwon (skkwon@deu.ac.kr).

REFERENCES

[1] T. Panas, J. Lundberg, W. Lowe, “Reuse in Reverse Engineering,” International Workshop on Program Comprehension, pp. 52-61, June 2004.
[2] M. Garg, M. K. Jindal, “Reverse Engineering – Roadmap to Effective Software Design,” International Journal of Recent Trends in Engineering, Vol 1, No. 2, pp. 186-188, May 2009.

International Journal of Modern Engineering Research (IJMER)
www.ijmer.com Vol.3, Issue.2, March-April. 2013 pp-928-938 ISSN: 2249-6645

Effect of Fuel and Air Injection Pattern on Combustion Dynamics in Confined and Free Diffusion Flame

M. A. Abdel-Al, [1] M. A. Yehia, [2] M. R. Taha, [3] T. W. Abou-Arab[4]
[1]*Mechanical Power Engineering, Faculty of Engineering, Cairo University, Egypt*
[234]*Prof. of Mechanical Power Engineering, Faculty of Engineering, Cairo University, Egypt*

Abstract: *A new burner is developed and its performance is experimentally studied. The principle of this new burner, circumferential alternative air and fuel burner (CAFB) is to admit fuel and air circumferentially alternative patterns. This burner also allow for swirling both fuel and air jets injecting from different circumferential holes. The outlet angle of air and fuel jet is changed between 0, 15, 30, 45 and 60 injection angles. A new definition and number for swirl is defined, this is called the Injection Swirl Number (ISN) and found to be accurate to describe the flame characteristics.*

Complete test rig was developed to facilitate characterization of the new burner. A new micro controller traverse mechanism was programmed and fabricated to control the sensitively moving of the thermocouple and gas analyzer sampling probe in all directions. Measurements of gas temperature at different positions, and the oxygen concentrations at the flame centerline were made. The thermal and chemical flame heights were obtained from the maximum temperature and oxygen concentration at the flame centerline. The visible flame height was obtained from direct photography and Infrared (IR) radiometry. The vortex breakdown creation period as a results of a high intensity swirling flow were been captured by the infrared radiation camera.

Comparisons of the new CAFB with other flames have also been performed. Experiments showed that the flame height decreases with the increase of the injection jet angles which improves the mixing between air and fuel generating an intense combustion zone and, hence, shortens the flame length. A new injection swirl ratio has been introduced for the new CAFB burner namely the injection swirl number (ISN), ISN = tan θ, where θ is the injection angle. The injection swirl number (ISN) used is 0, 0.26, 0.58, 1 and 1.75 which corresponding to the injection angles 0, 15, 30, 45 and 60 degree respectively. An empirical correlation has been derived for the new CAFB burner flame length as a function of the new derived (ISN).

Keywords: *Burner–Swirl–confined/free diffusion flame–flame length–Combustion efficiency–Injection angle*

I. Introduction

Combustion is the oldest technology of mankind and has furnished man with a major source of energy for more than one million years and at present, about 90% of our worldwide energy support (e.g., in traffic, electrical power generation, heating) is provided by combustion.

Multiple co- or counter- rotating swirlers with distributed fuel injection system characterize modern gas turbine combustion systems. Swirling flows are commonly used to improve and control the mixing process between fuel and oxidant streams to achieve flame stabilization and enhance heat release rate. The organization of swirling flow field governs the main flow structure; its match-up with fuel distribution is the key for achieving homogeneity of fuel/air mixture and consequently low NOx emission.

The most commonly used parameter for characterizing swirling flows is the swirl number SN, which is defined as the ratio of axial flux of the angular momentum Gφ to the axial momentum Gx [1]

$$S_N = \frac{G_\varphi}{G_x R} \qquad \textbf{(1-1)}$$

$$G_\varphi = \int_0^R (Wr)\rho U 2\pi r dr \qquad \textbf{(1-2)}$$

$$G_x = \int_0^R U\rho U 2\pi r dr \qquad \textbf{(1-3)}$$

Where U, W are the axial and tangential components of the velocity; R is the radius of the cross section plane; r is the radial coordinate. This swirl number characterizes the strength of swirling flow. It is commonly agreed that a vortex breakdown will occur in swirling flow if the swirl number exceeds certain limit, e.g. 0.6 for swirling flow without expansion cone.

Combustion will affect the shape of recirculation zone and the turbulence intensity of swirling flow. Experimental results based on pitot tube [1] showed that combustion induce comparatively small changes in aerodynamics of swirling flow fields; the boundary of recirculation zone and reversed mass flow rate are only slightly reduced compared with isothermal

cases. LDV measurement for swirling flow of reacting and nonreacting cases revealed that: compared with the isothermal case, the turbulence kinetic energy and velocity fluctuation substantially increased due to combustion, and the axial velocity increased for the combustion case because of gas expansion caused by heat release.

Rotating direction of each swirler component in multiple swirler configurations have significant effects on flow structures, temperature fields and exhaust gas concentrations. Due to the complexity of this problem, experimental results show different aspects of the physics and people made controversial observations. Counter-rotating swirl generated a large recirculation zone and large turbulent velocity fluctuation in the inter region of jet shear layer, consequently with observation of low oxides of nitrogen (NOx), high carbon monoxide (CO), and lower temperature field [2]. Recently, experimental data show that a consequence of the counter-rotating swirl brings up larger area of near-stoichiometric mixture of fuel and air, resulting in higher temperature field distribution within the stabilization zone compared with the co-rotating swirl case. To clarify the influence of rotating direction of swirl on combustion, it is necessary to correlate information of flow structures to combustion dynamics and emissions based on state-of-art laser diagnostics, optical sensing technology and emission analyzer.

Makel and Kenndy [3] measured the carbon atoms concentrations in diffusion of Sidebotham and Glassman [4]. Takagi et al [5], have carried out their investigation on two types of double concentric jet burner nozzles with different air and fuel locations, as one with the central air surrounded by fuel stream and the second is the opposite.

Wentzell [6] investigated new pattern for fuel and air admission. This pattern consisting of a central air jet surrounded by fuel stream in unconfined condition. He measured the flame temperature and flame length at different fuel and air jet diameters and at different fuel and air Reynolds numbers. Lee et al [16] applied an ethylene central air diffusion flame for the synthesis of carbon nano-tubes on a catalytic metal substrate. In a trial to investigate the effect of burner geometry on flame shape.

As a combination of premixed and diffusion flames, circumferential alternative air and fuel burner CAFB is capable of exploiting the advantages of both premixed flames and diffusion flames, in regards to operational safety, pollutant emission, and flame stability. Specifically, circumferential alternative air and fuel burner CAFB have no flash-back, a wide range of operational conditions and flexibility in flame length adjustment, coupled with potential NOx-reburning capability. These advantages of circumferential alternative air and fuel burner CAFB and their potential industrial and domestic applications have motivated this research work.

In this paper, a new burner is developed and its performance is experimentally studied. The principle of this new burner CAFB is to admit fuel and air circumferentially alternative patterns. This burner also allow for swirling both fuel and air jets injecting from different circumferential holes. The outlet angle of air and fuel jet is changed between 0, 15, 30, 45 and 60 injection angles. A new definition and number for swirl is defined, this is called the Injection Swirl Number (ISN) and found to be accurate to describe the flame characteristics.

II. Experimental Setup

The test rig shown in figure (1) consists of a main burner, oxidizer supply system, fuel supply system, flow controllers and measuring devices which hold in the Cairo university laboratory. The burner under investigation was fixed on a vertical position and a new transverse mechanism could be moved in the x, y, and z- directions. A new software programming is designed to move in a step control using the micro control technique to ensuring the high accuracy measurements. The traversing mechanism which carries thermocouple and gas sampling probe, supports by PIC microcontroller chips16F877 type as shown in figure (4.2). It offers all microcontroller I/O pins to external connectors for direct port accessing , while provides the most common primary devices and circuits , such as 2 X 16 LCD, Multiplexed 7SEG, Matrix KEYPAD, variable analog voltage, and RS232 serial interface. Thus, it saves most of the wasted time and efforts in hardware design and test,

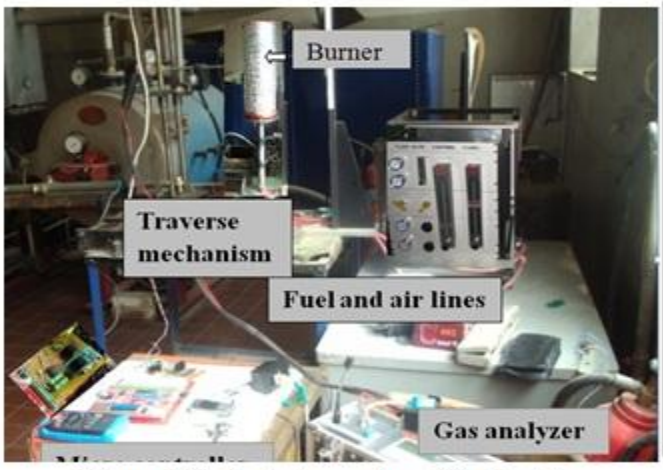

Figure (1): A photograph of the test rig

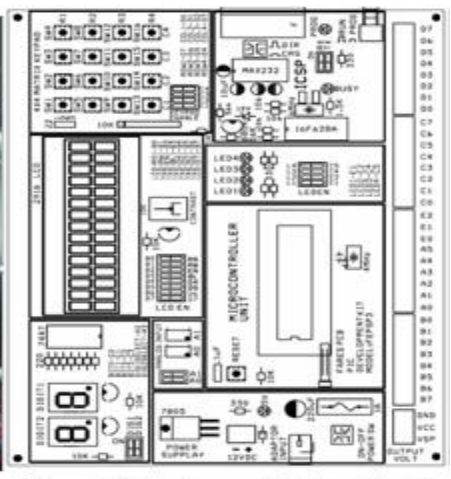

Figure (2): microcontroller circuit diagram

2.1 Air and fuel supply

The fuel used in this work is a bottled liquefied petroleum gas LPG (50% Propane, 50% Butane). A pressure regulator is mounted directly at the exit of the gas bottle to control the exit pressure of the fuel. The supplying of fuel is controlled by two needle valves which used to switch the fuel line between two rotameters (Dwyer Instruments Inc) with different ranges,

The primary air is supplied continuously from a reciprocating compressor equipped with a large storage tank (2 m^3) and delivers a pressurized air up to 10 bars. The air is regulated and delivered to the rotameter (Dwyer Instruments Inc). Pressure gauges are used to measure the pressure of the air and fuel before delivering to the test section, the flow-rate readings taken were corrected according to the calibration equations supplied by the manufacturer for the flow pressure.

2.2 Burner

Establishing the circumferentially alternated ports burner, (CAAB) diffusion flame, requires separate fuel/air supply systems enabling alternative distribute and supply of oxygen and fuel through burner holes. The reacting system is composed of three parts, namely, the burner tube, burner disc and the combustion chamber (combustor). The air and fuel jets are annular alternated to each others at the circumferential of the circular burner disc with sixteen equally distributed ports, each of 2.4 mm in diameter. The sixteen (eight to the each) ports are arranged alternatively in a circular array with an angular distance of 22.5º and the central distance is 11.5 mm to the head center line. The thickness of the burner head is 5 mm. The even air jets are directly connected to the air supply which passes through the burner tube. The odd fuel jets accumulate in the fuel chamber to equalize the flow from the fuel supply by placing layers of grids in the chamber. The grid layers are to ensure that the flow from each of the fuel and air ports is equal as shown in Figure (3).

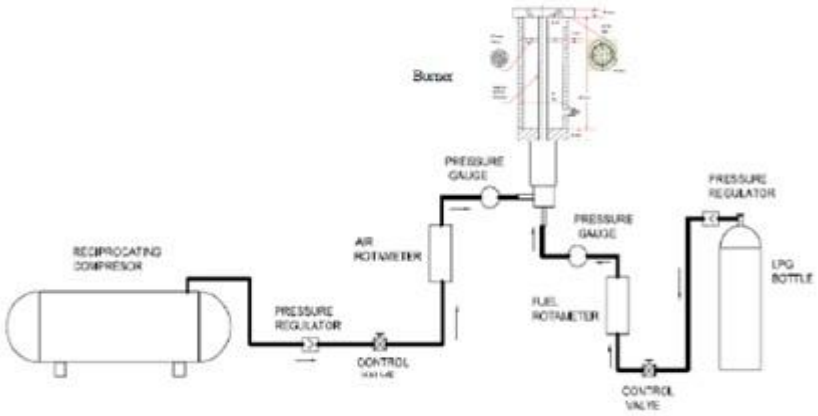

Figure (3): Flow diagram of the fuel and oxidizer

The main reason of the improvement of fuel/air interaction is in the smart design in the CAFB burner nozzle, in which each fuel stream is embedded between two air streams, and vice versa such that each air stream is localized between two main fuel streams, and finally the two air and fuel streams are rotated with each others. It means a higher volume to surface ratio for the fuel and the oxidizer, which increases the shear layers acting as a rapid mixing mechanism. The burner outwards flow rotates in a tangential injection bore angles. For parametric study and optimization, these angles varied to covering the entire available tangential span. The burner holes injection angles exhibits at 0, 15, 30, 45 and 60 degree Stability occurs mainly due to the IRZ by the recirculation flow process. A schematic of the design of the CAFB diffusion flame burner is shown in figure (4).

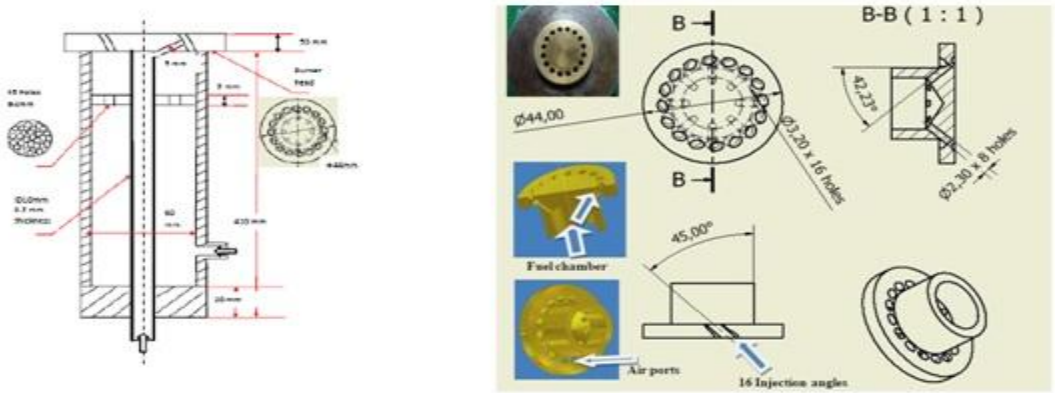

Figure (4) Schematic of the circumferentially alternated ports (CAAB) burner

2.3 Combustor

The combustor as shown in Figure 5 is an iron cylinder with 300mm diameter and 600mm length; there are 60 holes along the surface of confinement at successive distance of 5mm in the axial direction. These holes are used for inserting thermocouple or gas analyzer probe. A rectangular sight glass (200mm x 500mm) is mounted on the outer surface of the confinement and sealed to prevent leakage; this sight glass is used to facilitate capturing photos for flames. The exhaust section was ended by a cone with 40mm exit diameter to eliminate air entrainment.

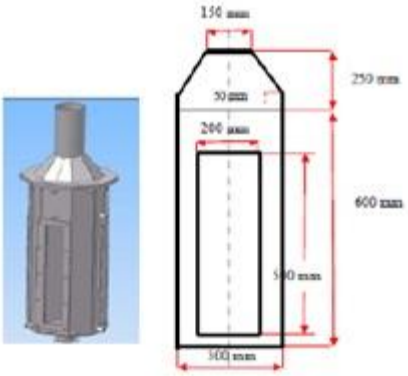

Figure (5): Schematic of the combustor

2.4 Measuring Techniques

A Nikon COOLPIX 990 digital camera is used to take the flame photographs. The camera has 3.1 million effective pixels. The major adjustable parameters of the camera are the exposure time and the aperture stop. In this study, an aperture of 3.6 is used for each photograph. The exposure time used for these photographs is 1/4th of a second to obtain global information on the average flame image. In this investigation the camera is mounted on a tripod (model Manfrotto 3021PRO) to ensure stable camera positioning. The height of the tripod was fixed at 125 cm from the floor of the lab. The distance from the test section was set with the legs fully spread and the front leg touching the base of the burner stand. The distance between the camera and the fuel nozzle exit is approximately 75 cm. The lens is positioned in line with the top of the burner exit plane injector. Black painted aluminum sheets are placed behind the flame and on top of the test section bottom plate. This is done to eliminate reflections of the flame in the photographic image.

A thermal imager used is a ThermaCAM SC 3000 & TI45 with cooled quantum well infrared photodetector (QWIP) manufactured by FLIR. The detector is 320 x 240 pixels that detect an infrared signal in the 8-9 micrometer range. It is stirling cooled down to 70K and has a cooling down time of less than 6 minutes. The basic operation of the camera is to detect the electromagnetic energy radiated in the IR spectral band from the flames. It then converts the radiated energy into an electronic video signal. The IR energy is first radiated through a medium (typically the atmosphere). It then enters the sensing system, passing through a lens, a filter, and finally incidents on a single IR detector or a focal plane array (FPA) sensor, which transforms the radiation into an electrical signal. The radiance captured by an infrared camera depends mainly on the object temperature, background temperature and emissivity of the source object.

The temperature is measured by a bare wire thermocouple. The measuring temperature has been corrected to eliminate the effect of radiation and conduction errors initiated when measuring the temperature by the bare wire thermocouple inside the flame. The type of thermocouple used is a type-B thermocouple (Platinum-6% Rhodium vs. Platinum-30% Rhodium) with a diameter of 200 μm, and length of 20 cm, manufactured by OMEGA Engineering Inc., the wire of the thermocouple is inserted in a fine ceramic tube of 1.5 mm diameter to insulate them.

The data acquisition system used consists of a data acquisition card (type NI6024M series, maximum sampling rate 200 kHz, ± 10 v input). The data acquisition card was installed in a personal computer and programmed via Labview. The program function is to record the differential voltage coming from the thermocouple with a rate of 500 Hz/s and a sampling time of 20 s, then calculate the mean of every 10 sample before calculating the total mean of reading to illuminate the effect of fluctuation and noise generating due to measurements. An I/O Connector Block with 4 Signal Conditioning slots for use in integrating thermocouple is used between the connection of thermocouple and data acquisition card to isolate voltage input into the measurement system. The type of I/O Connector Block is SCC-68 which is also a product of national instrument company.

The emission concentrations were measured using IMR-2800A gas analyzer. Gas samples are withdrawn from the flame by a water-cooled sampling probe. Three concentric stainless steel tubes of 1.5 mm and 4 mm and 6 mm outside diameter with length of 20 cm are used as a cooled probe.

III. Results and Discussions

3.1 Flame stability & different burner designs

The burner introduces the flow pattern into the combustion chamber with the recirculation induced flow by collection of the two ways of stabilization mechanisms namely swirl and bluff body nozzle concepts. The burner outwards flow rotates in a tangential injection bore angles. For parametric study and optimization, these angles varied to covering the

entire available tangential span. The burner holes injection angles exhibits at 0, 15, 30, 45 and 60 degree. The corresponding swirl number is 0, 0.3, 0.6,1 and 1.75 respectively. A comparative study with the traditional designated swirlers is utilized in this study. The new burner is a circumferential air and fuel burner denoted as (CAFB), in which the eight fuel ports are alternatively circumferentially arranged with the eight air ports. Stability occurs mainly due to the IRZ by the recirculation flow process. The IRZ, being storage of heat and chain carriers, carries heat and active chemical species towards the root of the flame, and ignites the fresh mixture of fuel and air. Therefore, between the forward going reactants and the reverse flow of the combustion products is the flame front which is associated with intensive mixing and combustion.

Figure (6) shows a flame stability map of the new burner (CAFB) at different injection angles. The conclusion drawn from this Figure is that the optimum injection angle. Therefore the experimental work and parametric study are carried out at this optimum injection angle 30˚. The improved stability of this burner is due to the diffusion process, i.e. the fuel diffuses into the air and causes simultaneous mixing and combustion, thus the rate of combustion depends on the rate of mixing between the fuel and air rather than the much faster chemical reaction rate. Figure (6-a) also shows that the optimum injection angle is at 30 degree, in which the stability zone as increased and the extinction zone is decreased.

The optimum injection angle of 30˚exhibits in confined condition with a higher stability limits than the other injection angles as shown in Figure (6-b).

It is noticed that the stability limit increases as the injection angle increase up to 30o injection angle (ISN =0.6). At higher injection swirl number (ISN), an abrupt change in the structure of the core of a swirling flow which namely, vortex breakdown as a result of instability. This phenomenon agreed with the results and studies given in Escdier and Keller believing [18], and Syred Beer [19]. They proposed that when the flow reaches a certain swirl number, instability develops and the central forced region of flow starts to precess about the axis of symmetry. This precession forms the so-called precessing vortex core (PVC).

Using the infrared radiation technique for the flame visualization, we found that the incubation period for the precessing vortex core (PVC) based on the concept of the recirculation, core has a highly temperature zone at the flame basement. Therefore it can be seen microscopically in the infrared band width. Figure (7), shows the formation cycle of the PVC in free in Figure (7- a), and confined conditions in Figure (7 -b) respectively.

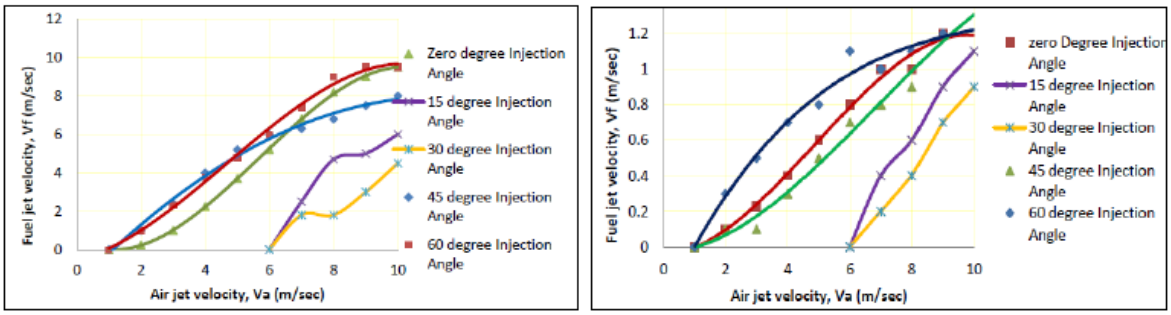

Figure (6): Flame stability limit at different injection swirl numbers (ISN),
(a) Free and (b) confined

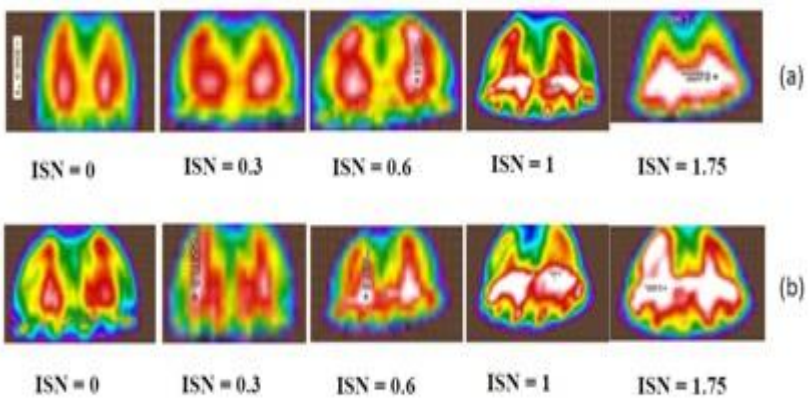

Figure (7): Formation cycle of PVC at different injection swirl numbers (ISN), (a) free and (b) confined conditions

It is shown clearly in the formation cycle mechanism that the PVC increases as the injection swirl number increase. When injection swirl number (ISN) exceeds 0.6, eddy shedding occurs as shown in Figure (7).

3.2 Combustion Efficiency

As basically known and as mentioned before, mixing improvement results in combustion efficiency increases due to the complete molecular diffusion level that speeds up between the fuel and oxidizer which enhances the combustion process. Combustion efficiency (ηc) is defined as:

(heat released in combustion)/(heat available in fuel)

$$\eta_c = 100\% - (m.g\ Cp_g(T_{exh.} - T_{amb}))/(m_f\ C_{pf}) \quad \textbf{(1-4)}$$

Where m_g……. the gas mass flow rate and equal to (mf + ma) from mass balance
T_{Exh}…. the average exhaust gas temperature at chimney accumulator
T_{amb}…...the ambient temperature (30˚C)
C_{pf}…….the lower calorific value of fuel

3.2.1 Effect of equivalence ratio on combustion efficiency

Figure (8) represents the effect of equivalence ratio on the combustion performance (efficiency). It shows that, when the equivalent ratio increases the combustion efficiency increase simultaneously, due to increasing of the fuel to air interaction in the new CAFB burner. Comparison between current experimental results and others shows an agreement and difference is attributed to same geometrical differences between current burner and others geometry for air and fuel admission.

The main reason of the improvement of fuel/air interaction is in the smart design in the CAFB burner nozzle, in which each fuel stream is embedded between two air streams, and vice versa such that each air stream is localized between two main fuel streams, and finally the two air and fuel streams are rotated with each others. It means a higher volume to surface ratio for the fuel and the oxidizer, which increases the shear layers acting as a rapid mixing mechanism.

Figure (8) shows higher combustion efficiency with the new CAAB burner as a result of complete combustion process due to the higher mixing efficiency as a result of increasing injection swirl number (ISN).

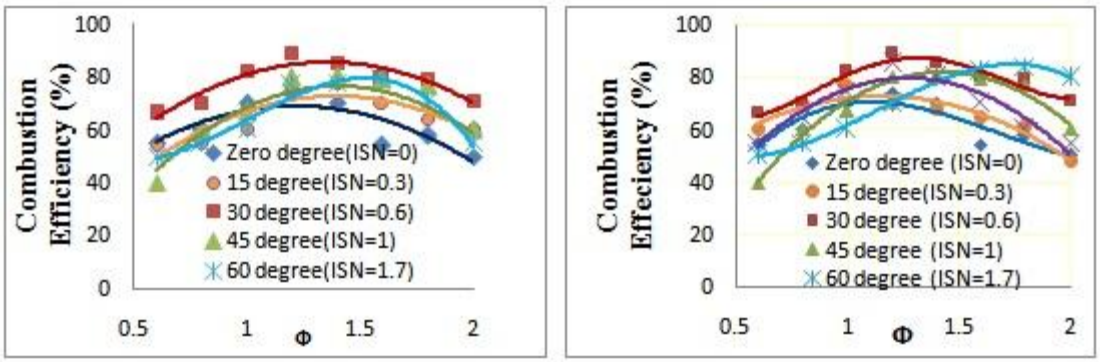

Figure (8): Combustion efficiency at different equivalence ratio and different (ISN),
(a) Free and (b) confined

3.2.2 Effect of ISN on combustion efficiency

The maximum combustion efficiency obtained at optimum injection swirl number (ISN) which corresponding to the burner stability curves was found to be about 90 % in the new burner (CAFB) compared to the others. For single swirled burner the combustion efficiency was (65%) Tomas et al [7], and for the circumferential fuel ports surrounding by a single central air jet (CAP) introduced by Sze [8] this combustion efficiency was (75%) in a free jet cases. In confined conditions as shown in Figure (9-b), the combustion efficiency reaches (85%) with the new CAFB burner and was the highest compared to four previous designs of burners of Brakely [9], Oymar Chiu [10], K.D. Kenshof [11] and Tomas et al [7] for the same heat release rates. The combustion efficiency in lower in confined than in free jets which may be due to the walls effects, and due to the entrainments effect in free jets.

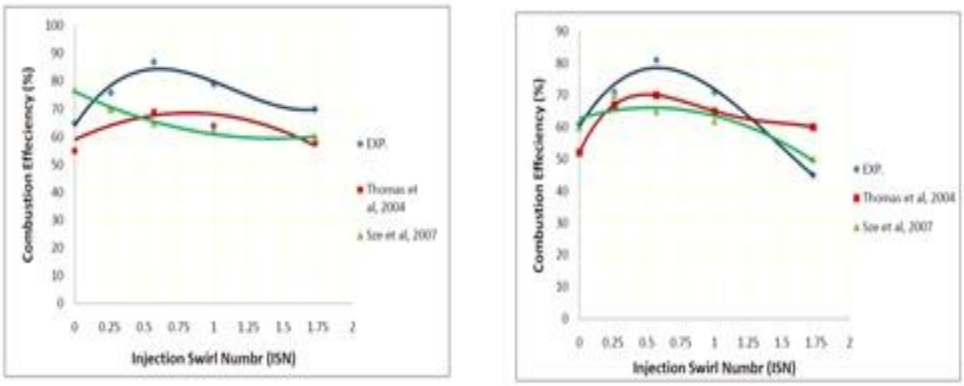

Figure (9): Effect of ISN on Combustion efficiency, ηc (%), (a) free and (b) confined

3.3 Flame Length

The visible flame length is an important parameter to determine the flame characteristics. As mentioned in the literature review, the flame length defines the high temperature zone for diffusion flame (temperature based flame length) and the global residence time available for pollutant formation within the flame (pollutant based flame length).
Generally in normal diffusion flame, combustion is controlled by diffusion of air molecule into the fuel stream. The effects of air flow rate and fuelling rate on flame length have been investigated in free and confined conditions, and the results are shown in the following sections. Photographic images of the average visual appearance of the new burner (CAFB) were obtained using a high resolution camera of 10 Mega pixels (CANON A 1000 SI). All Camera shots were taken in the night vision mode with shutter speed of 1/60 s to express the average flame shape. The visual flame length was measured by comparing the flame length in the photo by a reference length scale. For the real flame length evaluations, the thermal Infrared has been used to investigate the flame length which is related to the radiated photons from the flame in the infrared spectroscopy band.

3.3.1 Effect of air jet velocity and fuel jet velocity on flame length

Firstly, experiments were conducted to investigate the effects of air jet and fuel jet velocities on flame length. Fuel jet velocities of (1 to 10 m/sec) were used for the experiments while air jet velocities were varied from (1 to 10 m/sec). Secondly, experiments were carried out at a fixed air jet velocity of 6 m/sec while the fuel jet velocity was varied from 1 to 10 m/sec. The results are shown in Figure (10) in both free (a) and confined conditions (b). Figure (10) shows a decrease in the flame length when the air jet Reynolds number is increased from 2000 to 10000. It is observed that the flame is shorter in the new circumferential alternative fuel and air burner (CAFB) compared to the same air and fuel flow rates in single jet with central air and annular fuel jet in free diffusion flame studied by Valdiesh, [12] and F. D. Koalidof [13]. This is because of more intensive mixing with CAFB and hence more complete combustion occurs in the IRZ of the new burner. The flame length is longer in confined than in free flame at the same air and fuel flow rates and shorter than the non- swirled confined burner used by John K. et al [14] as shown clearly in Figure (10-b). Numerical simulation shows results nearly of same values of the experimental results in both of free and confined conditions.

The Reynolds number (Re) is increased progressively from zero to the maximum value for a stable flame to establish, and meanwhile the overall equivalence ratio (Φ) is kept at 1.5. This means increasing the volumetric flow rates of both fuel and air and simultaneously keeping their ratio unchanged. The resultant flame images are shown in Figure (10). To understand the effect of fuel flow rates on the flame length, the fuel jet velocities increased from 1 to 10 m/sec, while the air jet velocity remains constant at 6 m/s. basically, when the fuel jet velocity is increased, the fueling rate as well as the overall equivalence ratio is increased. Figure (11) shows an increase in the flame length when the fuel jet velocity is increased from 1 to 10 m/sec in both free (a) and confined condition (b). This is attributed to the increase of fuel jet momentum and therefore axial penetration in the flow field.

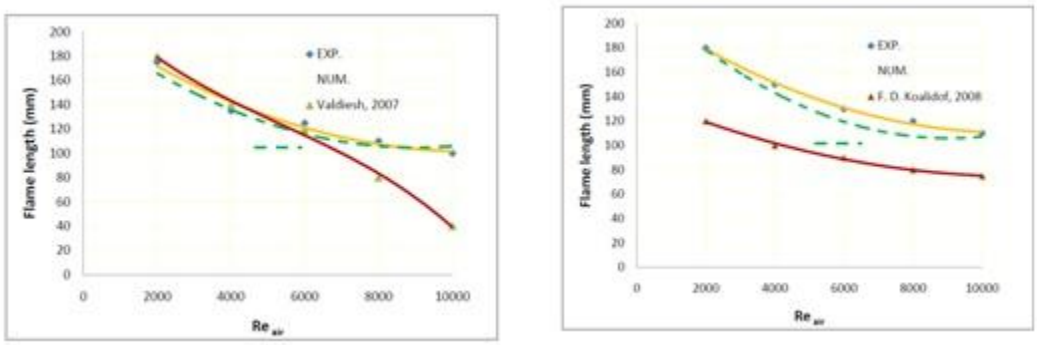

Figure (10): (a) Effect of Re on flame length, H (mm),(a) free (b) confined

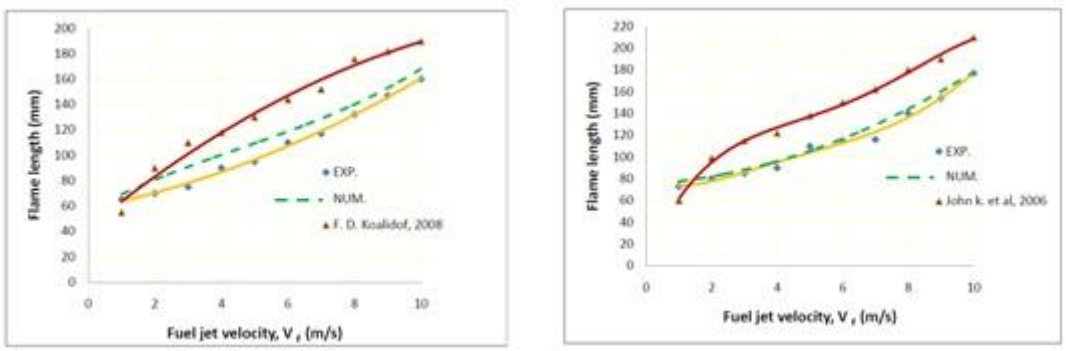

Figure (11): Effect of fuel jet velocity on flame length, H (mm), (a) free (b) confined

The camera or thermal imager used is a ThermaCam SC 3000, and TI 45 with cooled quantum well infrared photo detector (QWIP) manufactured by FLIR.

The infrared radiation comes from the flame has been observed by the ThermaCam shown in Figure (12), which presents the thermal flame length. The thermal flame length is agreed with the observed flame length from the digital camera, but the infrared image explains more details about the inner constructions of the flame length. An internal recirculation zone (IRZ) is formed in the centre of the flame, specifically in the centre of the flame root. The yellow color makes the IRZ easily recognizable to the naked eyes. The IRZ is observed to occupy a large proportion of the main flow field (flame root) due to a large portion of the initial flow being recirculated, and two vortexes reside symmetrically to the burner nozzle axis due to the rotational motion of the fluid. As the value of Re increases, the flame root augments in size and the flame tail diminishes in both size and length. Free condition in Figure (12) shows the long flame tail totally disappears and an entirely blue flame is formed, which is mainly premixed in nature because of more intensive mixing of the supplied fuel and air and hence more complete combustion. The blue colour makes the IRZ invisible to the eyes so that a flow visualization technique is of necessity for the purpose of visually observing the flame.

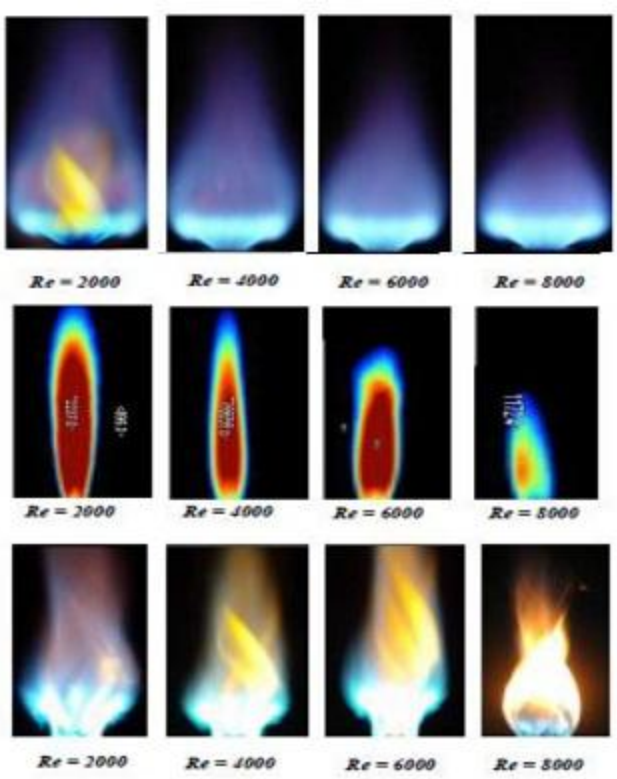

Figure (12): Flame images at different Re at fixed Φ = 1.5, free (upper), thermal and confined (lower) conditions

3.3.2. Effect of Air/Fuel ratio on flame length

Generally an increase in Φ corresponds to an increase in the amount of supplied fuel. The effect of equivalence ratio Φ on the flame length at fixed Re = 6000 is shown in Figure (13).

Figure (13) shows an increase in the flame length for both the swirling and the non-swirling flames, while the non-swirling flames are much longer than the swirling flames. The non-swirling flames are observed to consist of a premixed bluish flame overlapped by a diffusion flame, with a growth in the downstream diffusion flame as Φ increases from 1.0 to 2.0. However, the new burner CAFB remains fairly premixed in nature with the post-combustion zone, which is weakly diffusional in nature, becoming more and more observable with increasing Φ. A typical case at Re = 8000 with Φ increasing from 1.0 to 2.0 is shown in Figure(13). The increasing of equivalent ratio Φ means an increase in the amount of supplied fuel, thus the flame becomes more diffusional in nature and the flame length increases accordingly. It is clear from previous Figures that the flame length of the new burner CAFB is dependent on both Re and Φ, just as that in premixed flames Kwok et al. [15]. At fixed Re, for both swirling and non-swirling the CAFB burner lengthens the flame with increasing Φ due to increased fuel supply. Furthermore, the IRZ was found to play an important role in flame length shortening. The flame length variation with equivalence ratio is shown in Figure (13). The current experimental and numerical results are in partial agreement with the data of Sze et al 2007, but in full agreement with the trend.

As a result of the increasing amount of supplied fuel and due to the fact that Zone 3 or the post-combustion zone becomes more and more diffusional and thus as Φ increases from 1.0 to 2.0, the flame length increases monotonically.

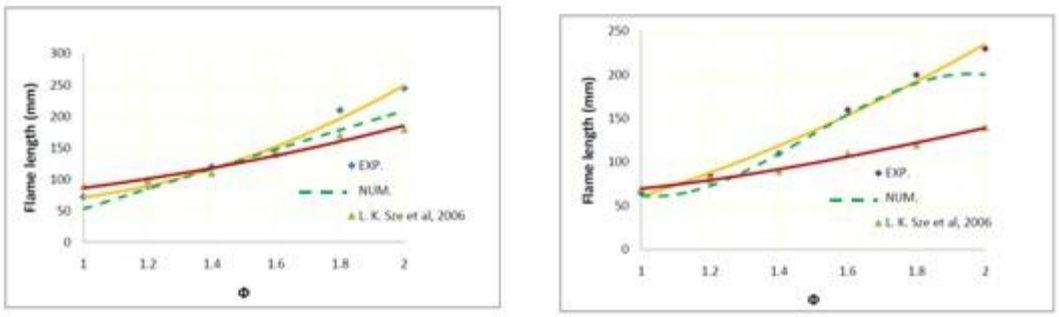

Figure (13): Effect of (Φ) on the flame length, (a) free (b) confined

3.3.3. Effect of Injection Swirl Number (ISN) on flame length

In theory, the IRZ is noticed when the actual swirl number is higher than 0.6. Below that, the weak adverse axial pressure gradient is not strong enough to induce a reverse flow. We found that, for the new circumferential air and fuel burner (CAFB), the flow injected at different injection angles of 0, 15, 30, 45 and 60 degrees rotated at different swirling intensities in so called a swirl number.

As mentioned in the literature review, there are several relations that can define the swirl number, however here we concluded a new number, namely, injection swirl number (ISN) which describes this circumferential air and fuel burner (CAFB).

The new formula accepted mathematically with the traditional Swirl Number formula.

The swirl number is defined by [1]:

$$S = \frac{G_{ang}}{R_b G'_x} = \frac{\int_0^{\infty} \rho U W r^2 dr}{R_b \int_0^{\infty} \rho (U^2 - \frac{1}{2} W^2) r dr} \qquad \textbf{(1-5)}$$

Where Gang is the angular momentum in the swirled section and G'x is the liniear momentum flux through the unswirled center core and the swirled annulus. This terms can be calculated by integrating the mean axial, U, and the mean swirl, W, velocity components across the burner exit. With the assumption that the distribution of the axial flow remains flat, and U and W at the burner exit are kinematically related to the blade angle as tan α = U/W , the axial flux of angular momentum in the annular section is then written as follows:

$$G_{ang} = 2\pi\rho \int_{R_c}^{R_b} U_a (U_a \tan\alpha) r^2 dr = 2\pi\rho U_a^2 \tan\alpha \left(\frac{R_b^3 - R_c^3}{3} \right) \qquad \textbf{(1-6)}$$

Here, Ua is a mean axial velocity supplied through the swirl annulus. By assuming flat axial velocity distribution, the linear momentum flux from the two regions of the burner is then calculated as follows:

$$G_x = 2\pi\rho \int_{R_c}^{R_b} U_a^2 r dr + 2\pi\rho \int_0^{R_c} U_c^2 r dr = \pi [\rho U_a^2 (R_b^2 - R_c^2) + \rho U_c^2 R_c^2] \qquad \textbf{(1-7)}$$

Where Uc is a mean axial velocity through the center core. With Equation (1) as defined, the geometric swirl number for the vane swirl burner is then:

$$S = \frac{\frac{2}{3}\tan\alpha(1 - R^3)}{1 - R^2 + \frac{U_c^2}{U_a^2} R^2} = \frac{2}{3}\tan\alpha \frac{1 - R^3}{1 - R^2 + [m^2 (1/R^2 - 1)^2] R^2} \qquad \textbf{(1-8)}$$

Where: α…..the injection angle

R….ratio of the center channel radius (Rc) to injector radius (Ri)

m….mass flux ratio (between mass flux through center channel (mc) and mass flux through swirl annulus (ms))

For the new burner (CAFB):

a- Channel radius is the injection radius (R≡1), let R=0.9 for simplicity.

b- Channel in annulus, so the center channel is the swirl annulus. i.e m=1.

Substitute in Equation (1-8) we got the new formula for the injection swirl number for the new burner (CAFB)..

S = 2/3 tanα (3/2)

i.e. **ISN = Tan** □ **(1-9)**

Where θ is the injection angle tangent to the burner surface, and ISN is the new correlation for injection swirl number for the multi fuel jet in this case (CAFB).

Figure (14) show the effect of injection swirl number on the flame length, it shows that the flame length decreases as the injection swirl number increase. Figure (14) shows the flame length for CAFB burner is lower than the central air surrounded by the fuel ports described by Sander bad et al 2004 in free condition. In confined condition, the flame length decrease steeply as ISN increase. Figure (15-b) shows lower heights in CAFB burner with respect to the traditional burners compared to Sanderbad et al [33] in the similar confined conditions. On the other side and for further justifications and validation of present data, the numerical simulation gives a good agreement with the experimental results as shown in Figure (15-a and b)

It can be easily concluded that swirl greatly enhances the mixing of air and fuel streams causing the shorter flame length to both jet and swirl mixing parameters. A new semi-empirical correlation could be developed between flame lengths as a function of ISN.

$$\text{Flame length (mm)} = 58.69\,(\text{ISN})^3 + 72.00\,(\text{ISN})^2 - 543.9\,(\text{ISN}) + 467.4 \qquad \textbf{(1-10)}$$

The calculated flame length is consistent with the measured flame length in free jet only as shown in Figure (16). Figure (16) shows the flame height is about 0.51 m at ISN = 0, which is near to the result obtained photographically before. Figure (17) shows the flame height correlation in confined conditions with a dissatisfactory result with the experimental data. The main reason of the un-consistent in confined conditions is the flame disturbance due to the flame shedding and the flame wall interaction which disturb the flame where we cannot introduce an exact correlation.

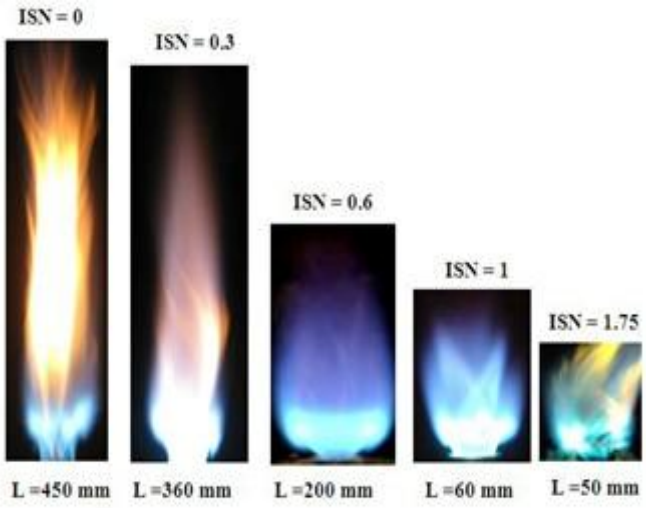

Figure (14): Photo images showing the effect of ISN on the flame

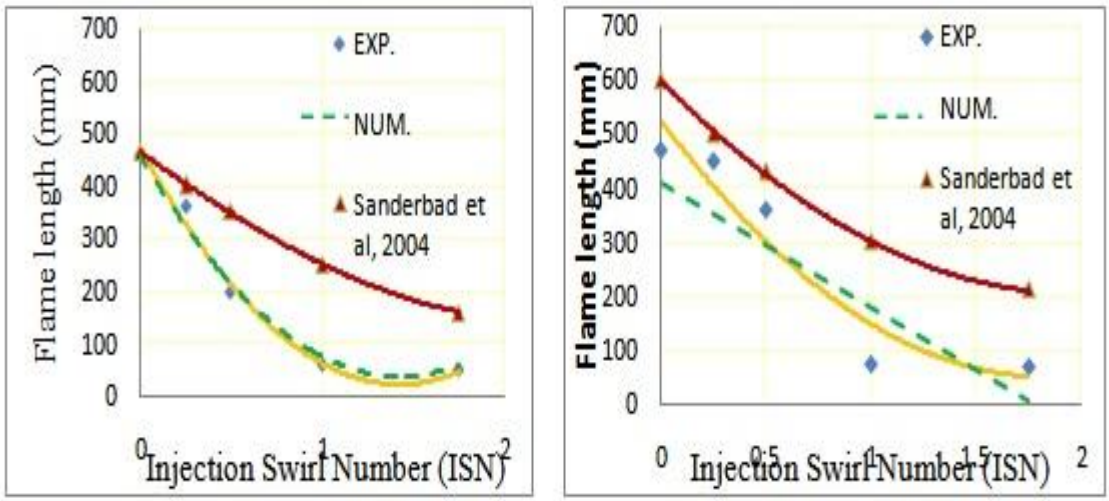

Figure (15): Effect of ISN on flame lengths, H (mm), (a) free (b) confined

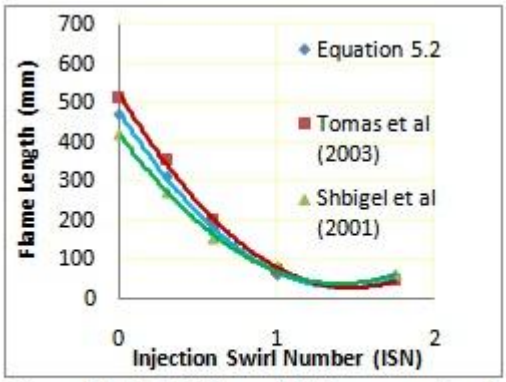

Figure (16a): Effect of ISN on correlated flame length (equation 1-10), free

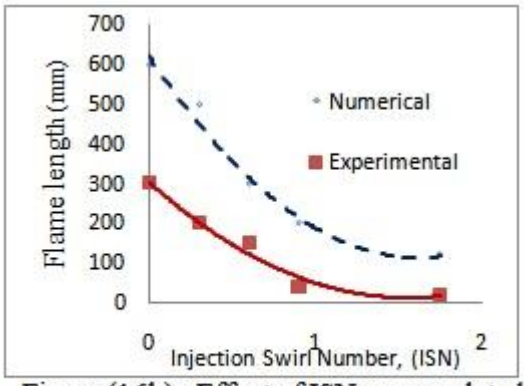

Figure (16b): Effect of ISN on correlated confined length (equation 1-10), confined

IV. Conclusions and recommendation

Experimental investigations have been conducted on the **characteristics** of the new burner including flame appearance, flame structure, flame temperature. Comparisons of the new CAFB with other flames have also been performed. The main conclusions can by summarized as:

- The optimum injection angle of 30˚exhibits in free/confined condition with a higher stability limits than the other injection angles.
- When the equivalent ratio increases the combustion efficiency increase simultaneously, due to increasing of the fuel to air interaction in the new CAFB burner. The maximum combustion efficiency obtained at optimum injection swirl number (ISN)which corresponding to the burner stability curves was found to be about 90 % in the new burner (CAFB) compared to the others
- The flame height decreases with the increase of the injection jet angles which improves the mixing between air and fuel generating an intense combustion zone and, hence, shortens the flame length.
- A new injection swirl ratio has been introduced for the new CAFB burner namely the injection swirl number (ISN), ISN = tan θ, where θ is the injection angle. The injection swirl number (ISN) used is 0, 0.26, 0.58, 1 and 1.75 which corresponding to the injection angles 0, 15, 30, 45 and 60 degree respectively.
- An empirical correlation has been derived for the new CAFB burner flame length as a function of the new derived (ISN).

References

[1] Beer, J.M, Chigier, N.A. Flame stabilization in recirculation zones of jets with swirl, Proceedings of the seventeenth International Symposium on Combustion, The Combustion Institute, 1971, 563.
[2] Syred, N. and Beer, J.M. Combustion in swirling flows: a review. Combustion and Flame, 1974, 23, 143-201.
[3] Makel, D.B. and Kennedy, I.M. Soot formation in laminar inverse diffusion flame. Combustion Science and Technology, 1993, 81, 207.
[4] Sidebotham, G..W. and Glassman, I. Flame temperature, fuel structure, and fuel concentration effects on soot formation in inverse diffusion flames. Combustion and Flame, 1992, 90, 269-283.
[5] Takagi, T., Xu, Z. and Komiyama, M. Preferential diffusion effects on the temperature in usual and inverse diffusion flames. Combustion and Flame, 1996, 106, 252-260.
[6] Wentzell J.C. The Characteristics and Structure of Inverse Flames of Natural Gas MSc Thesis, the Queen's University 1998.
[7] Tomas, G.B. and Jawurek, H.H. The ''hood method'' of measuring emissions of rural cooking devices. Biomass Bioenergy, 1999, 16, 341–345.
[8] Sze, L.K., Cheung, C.S. and Leung, C.W. Appearance, temperature and NOx emission of two inverse diffusion flames with different port design. Combustion and Flame, 2006, 144, 237-248.
[9] Brakely, S.P. and Schumann, T.E. Diffusion flames Industrial & Engineering Chemistry, 1988, 20, 988-1004.
[10] Oymer, B.L., Cziesla, T., Mitra, N.K. and Biswas, G. Numerical investigation of heat transfer in impinging axial and radial jets with superimposed swirl. International Journal of Heat and Mass Transfer, 1997, 40, 141-147.
[11] K. D. Ken Shaf and Gore, J.P. Flow structure in lean premixed swirling combustion. Proceedings of the Combustion Institute, 2002, 861-867.
[12] Valdiesh, L. Turbulent combustion modeling. Progress in Energy and Combustion Science, 2002, 28, 193-266.
[13] F. D. Koalidof. Experimental and Numerical Investigation of the Novel Low Nitrogen Oxide CGRI Burner PhD Thesis, the Queen's University, 1998
[14] John, k.G. The prediction of laminar jet diffusion flame size: Part I, Theoretical model. Combustion and Flame, 1977, 29, 219-226.
[15] Kwok, L.C., Leung, C.W. and Cheung, C.S. Heat transfer characteristics of an array of impinging pre-mixed slot flame jets. International Journal of Heat and Mass Transfer, 2005, 48, 1727-1738.

International Journal of Modern Engineering Research (IJMER)
www.ijmer.com Vol.3, Issue.2, March-April. 2013 pp-939-943 ISSN: 2249-6645

On Contra-#Rg–Continuous Functions

S. Syed Ali Fathima, [1] M. Mariasingam[2]
[1]*Department of Mathematics, Sadakathullah Appa College, Tirunelveli- 627 011, Tamil Nadu, India*
[2]*Post Graduate and Research Department of Mathematics, V.O. Chidambaram College, Thoothukudi-628 008 (T.N.), India*

Abstract: *In this paper we introduce and investigate some classes of generalized functions called contra-#rg- continuous functions. We get several characterizations and some of their properties. Also we investigate its relationship with other types of functions.*

Mathematics subject classification: *54C08, 54C10*

Keywords*: #rg- closed, #rg- continuous, #rg- irresolute.*

I. Introduction

In 1996, Dontchev [1] presented a new notion of continuous function called contra – continuity. This notion is a stronger form of LC – continuity. The purpose of this present paper is to define a new class of generalized continuous functions called contra #rg-continuous functions and almost contra #rg-continuous and investigate their relationships to other functions.

II. Preliminaries

Throughout the paper X and Y denote the topological spaces (X, τ) and (Y, σ) respectively and on which no separation axioms are assumed unless otherwise explicitly stated. For any subset A of a space (X,τ), the closure of A, interior of A and the complement of A are denoted by cl (A), int (A) and A^c or X\A respectively. (X, τ) will be replaced by X if there is no chance of confusion. Let us recall the following definitions as pre requesters.

Definition 2.1. A subset A of a space X is called
1) a preopen set [2] if $A \subseteq$ intcl (A) and a preclosed set if clint (A)$\subseteq$ A.
2) a semi open set [3] if $A \subseteq$ clint (A) and a semi closed set if intcl (A) $\subseteq$A.
3) a regular open set [4] if A = intcl (A) and a regular closed set if A = clint (A).
4) a regular semi open [5] if there is a regular open U such U $\subseteq$A$\subseteq$cl(U).

Definition 2.2. A subset A of (X,τ) is called
1) generalized closed set (briefly, g-closed)[6] if cl (A)$\subseteq$ U whenever A$\subseteq$U and U is open in X.
2) regular generalized closed set (briefly, rg-closed)[7] if cl (A)$\subseteq$U whenever A$\subseteq$U and U is regular open in X.
3) generalized preregular closed set (briefly, gpr-closed)[8] if pcl (A)$\subseteq$U whenever A $\subseteq$ U and U is regular open in X.
4) regular weakly generalized closed set (briefly, rwg-closed)[9] if clint(A)$\subseteq$U whenever A $\subseteq$U and U is regular open in X.
5) rw-closed [10] if cl(A)$\subseteq$U whenever A$\subseteq$U and U is regular semi open.

The complements of the above mentioned closed sets are their respective open sets.

Definition 2.3. A subset A of a space X is called #rg-closed[11] if cl(A)$\subseteq$U whenever A$\subseteq$U and U is rw-open. The complement of #rg-closed set is #rg-open set. The family of #rg-closed sets and #rg-open sets are denoted by #RGC(X) and #RGO(X).

Definition 2.4. A map f :(X,τ) $\rightarrow$(Y,σ) is said to be
(i) #rg-continuous [12] if f^{-1}(V) is #rg-closed in (X,τ) for every closed set V in (Y,σ).
(ii) #rg-irresolute [12] if f^{-1} (V) is #rg-closed in (X,τ) for each #rg-closed set V of (Y,σ).
(iii) #rg-closed [12] if f(F) is #rg-closed in (Y,σ) for every #rg-closed set F of (X,τ).
(iv) #rg-open[12] if f(F) is #rg-open in (Y,σ) for every #rg-open set F of (X,τ).
(v) #rg-homeomorphism [13] if f is bijection and f and f^{-1} are #rg-continuous.

Definition 2.5. A map f:$(X,\tau)\rightarrow(Y,\sigma)$ is said to be contra- continuous [1] if f^{-1}(V) is closed in (X,τ) for every open set V in (Y,σ).

Definition 2.6. A space X is called a $T_{\#rg}$-space [11] if every #rg-closed set in it is closed.

III. Contra #rg–Continuous Function

In this section, we introduce the notions of contra #rg- continuous, contra #rg-irresolute and almost contra #rg-continuous functions in topological spaces and study some of their properties.

Definition 3.1
A function $f:(X,\tau) \to (Y,\sigma)$ is called contra #rg- continuous if $f^{-1}(V)$ is #rg-closed set in X for each open set V in Y.

Example 3.2
Let X = Y = { a,b,c } with topologies τ = { X, ϕ, {a} } and σ = { Y , ϕ, {b , c} }.Define f:(X,τ)$\to$(Y,σ) by an identity function. Clearly f is contra #rg – continuous.

Example 3.3
Let X = Y = {a,b,c} with τ = { X,ϕ,{a} ,{b},{a,b} } and σ = { Y,ϕ,{a,b} }. Define f:X$\to$Y by f(a) = c, f(b) = b and f(c) = a. Clearly f is contra #rg – continuous.

Remark 3.4.
The family of all #rg-open sets of X is denoted by #RGO(X). The set #RGO(X,x)={V$\in$#RGO(X) / x$\in$V }for x $\in$ X.

Theorem 3.5
Every contra – continuous function is contra #rg-continuous.
Proof: It follows from the fact that every closed set is #rg-closed set.
The converse of the above theorem is not true as seen from the following example.

Example 3.6
Let X = Y = {a,b,c,d } with τ = { X,ϕ,{a},{b},{a,b},{a,b,c}} and σ = { Y,ϕ, {a,b}}. Define f: X$\to$Y by f(a) = a, f(b) = d, f(c)=c and f(d)=b. Here f is contra #rg-continuous but not contra continuous since f^{-1} ({a, b}) = {a, d} which is not closed in X.

Theorem 3.7
If a function f: X $\to$Y is contra #rg-continuous and X is $T_{\#rg}$- Space. Then f is contra continuous.
Proof: Let V be an open set in Y. Since f is contra #rg-continuous, $f^{-1}(V)$ is closed in X. Hence f is contra –continuous.

Remarks 3.8
The concept of #rg – continuity and contra #rg continuity are independent as shown in the following examples.

Example 3.9
Let X = Y = {a, b, c, d }. τ = {X,ϕ,{a},{b},{a,b},{a,b,c}}and σ= {Y,ϕ,{a},{b},{a,b}}. Define f: X$\to$Y by identity mapping then clearly f is #rg – continuous. Since f^{-1}({a}) = {a} is not #rg-closed in X where {a} is open in X.

Example 3.10
Let X = Y = {a,b,c,d } , τ = {x,ϕ,{a},{b},{a,b},{a,b,c} }and σ={Y,ϕ,{a,b}}. Define f: X$\to$Y by f (a)=a, f (b) = d, f (c)=c and f(d) = b. Here f is contra #rg-continuous, but not #rg-continuous, because f^{-1}({c,d}) = {b,c} is not #rg-closed in X, where {a,d} is closed in Y.

Theorem 3.11
Every contra - #rg- continuous function is contra g – continuous.
Proof. Since every #rg – closed set is g- closed, the proof follows.
The converse of the theorem is need not be true as shown in the following example.

Example 3.12
Let X = Y = { a,b,c,d },τ = {X,ϕ,{a},{b},{a,b } } and σ= {Y,ϕ,{a},{b}, {a,b,c} }. A function f: X$\to$Y defined by f(a)=c, f(b)=d, f(c)=a and f(d)=b. Clearly f is contra g – continuous but not contra #rg –continuous since f^{-1}\{c} = {c} is not #rg-closed.

Remark 3.13
1. Every contra #rg-continuous is contra *g –continuous
2. Every contra #rg –continuous is contra rg – continuous
3. Every contra #rg –continuous is contra –gpr – continuous
4. Every contra #rg – continuous is contra – rwg-continuous.

Remark 3.14
The composition of two contra - #rg-continuous functions need not be contra #rg –continuous as seen from the following example.

Example 3.15
Let X = Y = Z = { a,b,c}, τ = { X,ϕ,{a},{b},{a,b} }, σ= {Y,ϕ,{a,b}} and η={Z,ϕ,{a}}. Let f:X $\to$ Y defined by f(a)=c, f(b)=b, f(c)=a and g:Y$\to$Z is defined by g(a)=b, g(b)=c and g(c)=a. Then clearly f and g are contra #rg – continuous. But gof:X$\to$Z is not contra #rg continuous, since $(gof)^{-1}$ {a} = $f^{-1}(g^{-1}\{a\})=f^{-1}(\{c\})=\{a\}$ which is not #rg – closed in X.

Theorem 3.16
If f: $(X,\tau) \to (Y,\sigma)$ is contra #rg–continuous and g: Y $\to$ Z is a continuous function, then gof: X$\to$Z is contra #rg-continuous.
Proof: Let V be open in Z. Since g is continuous, $g^{-1}(V)$ is open in Y. Then $f^{-1}(g^{-1}(V))$ is #rg- closed in X, since f is contra #rg – continuous. Thus $(gof)^{-1}$ (V) is #rg – closed in X. Hence gof is contra #rg – continuous.

Corollary 3.17
If f : X $\to$ Y is #rg – irresolute and g : Y $\to$ Z is contra – continuous function then gof:X$\to$Z is contra #rg – continuous.
Proof. Using the fact that every contra – continuous is contra #rg – continuous

Theorem 3.18
Let f: X $\to$Y be surjective, #rg – Irresolute and #rg – open and g: Y $\to$Z be any function then gof is contra #rg – continuous iff g is contra #rg – continuous.
Proof. Suppose gof is contra #rg continuous. Let F be an open set in Z. Then $(gof)^{-1}(F) = f^{-1}(g^{-1}(F))$ is #rg – open in X. Since f is #rg – open and surjective $f(f^{-1}(g^{-1}(V))$ is #rg –open in Y. (i.e.) $g^{-1}(V)$ is #rg –open in Y. Hence g is contra #rg – continuous. Conversely, suppose that g is contra #rg – continuous. Let V be closed in Z. Then $g^{-1}(V)$ is #rg –open in .Since f is #rg – irresolute, $f^{-1}(g^{-1}(V))$ is #rg – open. (i.e.) $(gof)^{-1}$ (V) is #rg – open in X. Hence gof is contra #rg – continuous.

Theorem 3.19
Let f : X $\to$ Y be a map. Then the following are equivalent.
(i) f is contra #rg – continuous.
(ii) The inverse image of each closed set in Y is #rg – open in X.
Proof : (i) $\Rightarrow$(ii) & (ii) $\Rightarrow$ (i) are obvious.

Theorem 3.20
If f : X $\to$ Y is contra #rg- continuous then for every x $\in$ X, each F $\in$ C(Y,f(x)), there exists U $\in$ #RGO (X,x), such that f(U)$\subset$F (i.e.) For each x$\in$X, each closed subset F of Y with f(x) $\in$ F, there exists a #rg- open set U of X such that x $\in$U and f(U)$\in$F.
Proof . Let f: X $\to$ Y be contra #rg – continuous. Let F be any closed set of Y and f(x) $\in$ F where x $\in$ X. Then f^{-1} (F) is #rg – open in X, also x$\in f^{-1}$(F). Take U = f^{-1}(F). Then U is a #rg-open set containing x and f(U) $\subseteq$ F.

Theorem 3.21
If a function f: X $\to$Y is contra #rg –continuous and X is $T_{\#rg}$ – space then f is contra continuous.
Proof. Let V be an open set in Y. Since f is contra #rg- continuous, f^{-1}(V) is #rg- closed in X .Then f^{-1}(V) is closed in X , since X is $T_{\#rg}$- space . Hence f is contra – continuous.

Corollary 3.22
If X is a $T_{\#rg}$-Space then for a function f:X$\to$Y the following are equivalent.
(i) f is contra continuous
(ii) f is contra #rg-continuous.
Proof: It is obvious.

Theorem 3.23
Let (X,τ) be a #rg-connected space and (Y,σ) be any topological space. If f: X$\to$Y is surjective and contra #rg-continuous, then Y is not a discrete space.
Proof. Suppose Y is discrete space. Let A be any proper non empty subset of Y. Then A is both open and closed in Y. Since f is contra #rg-continuous f^{-1} (A) is both #rg open and #rg-closed in X. Since X is #rg- connected, the only subsets of X which are both #rg-open and #rg-closed are X and ϕ. Hence $f^{-1}(A)$ = X, then it contradicts to the fact that f: X $\to$ Y is surjective. Hence Y is not a discrete space.

Definition 3.24
A function f: X $\to$Y is called almost contra #rg-continuous if f^{-1}(V) is #rg-closed set in X for every regular open set V in Y.

Theorem 3.25
Every contra #rg-continuous function is almost contra #rg-continuous but not conversely.
Proof: Since every regular open set is open, the proof follows.

Definition 3.26
A function f: X → Y is called contra #rg-irresolute if $f^{-1}(V)$ is #rg-closed in X for each #rg-open set V in Y.

Definition 3.27
A function f: X → Y is called perfectly contra #rg-irresolute if $f^{-1}(V)$ is #rg-closed and #rg-open in X for each #rg-open set V in Y.

Theorem 3.28
A function f: X→Y is perfectly contra #rg-irresolute if and only if f is contra #rg-irresolute and #rg-irresolute.
Proof: It directly follows from the definitions.

Remark 3.29
The following example shows that the concepts of #rg irresolute and contra #rg – irresolute are independent of each other.

Example 3.30
Let X = Y = { a,b,c,d }, τ={X,ϕ,{c},{a,b},{a,b,c } } and σ= {Y,ϕ,{a},{b}, {a,b,} }. A function f: X→Y defined by f(a)= f(b)=a, f(c)=d and f(d)=b. Clearly f is contra #rg–irresolute but not #rg –irresolute, since $f^{-1}(\{b\}) = \{d\}$ which is not #rg-open in X.

Example 3.31
Let X = Y = {a,b,c,d}, τ={X,ϕ,{c},{a,b},{a,b,c}} and σ= {Y,ϕ,{a},{b}, {a,b,}}. Define f: X→Y by an identity function. Clearly f is #rg–irresolute but not contra #rg –irresolute, since $f^{-1}(\{b\}) = \{b\}$ which is not #rg-closed in X.

Remark 3.32
Every contra #rg-irresolute function is contra #rg-continuous. But the converse need not be true as seen from the following example.

Example 3.33
Let X = Y = {a,b,c,d } with τ = { X,ϕ,{a},{b},{a,b},{a,b,c}} and σ = { Y,ϕ, {a,b}}. Define f:X→Y by f(a) = a, f(b) = d, f(c)=c and f(d)=b. Here f is contra #rg-continuous but not contra #rg- irresolute.

Theorem 3.34
Let f:X→Y and g:Y→Z be a function then
(i) if g is #rg-irresolute and f is contra #rg-irresolute then gof is contra #rg-irresolute.
(ii) If g is contra #rg-irresolute and f is #rg- irresolute then gof is contra #rg-irresolute.
Proof.(i) Let U be a #rg-open in Z. Since g is #rg-irresolute, $g^{-1}(U)$ is #rg-open in Y. Thus $f^{-1}(g^{-1}(U))$ is #rg-closed in X, since f is contra #rg-irresolute. (i.e.) $(gof)^{-1}(U)$ is #rg-closed in X. This implies that gof is contra #rg-irresolute.
(ii) Let U be a #rg-open in Z. Since g is contra #rg-irresolute, $g^{-1}(U)$ is #rg-closed in Y. Thus $f^{-}(g^{-1}(U))$ is #rg-closed in X, since f is #rg-irresolute. (i.e.) $(gof)^{-1}(U)$ is #rg-closed in X. This implies that gof is contra #rg-irresolute.

Theorem 3.35
If f: X→Y is contra #rg-irresolute and g:Y→Z is #rg-continuous then gof is contra #rg-continuous.
Proof. Let U be an open set in Z. Since g is #rg- continuous, $g^{-1}(U)$ is #rg-open in Y. Thus $f^{-1}(g^{-1}(U))$ is #rg-closed in X, since f is contra #rg-irresolute. (i.e.) $(gof)^{-1}(U)$ is #rg-closed in X. This implies that gof is contra #rg-irresolute.

Remark 3.36
Every perfectly contra #rg-irresolute function is contra #rg-irresolute and #rg-irresolute. The following two examples shows that a contra #rg-irresolute function may not be perfectly contra #rg-irresolute and a #rg-irresolute function may not be perfectly contra #rg-irresolute.
In example.3.30, f is contra #rg-irresolute but not perfectly contra #rg-irresolute.
In example 3.31, f is #rg-irresolute but not perfectly contra #rg-irresolute.

Theorem 3.37.
A function is perfectly contra #rg-irresolute iff f is contra #rg-irresolute and #rg-irresolute.
Proof. It directly follows from the definitions.

Remark 3.37 From the above results we have the following diagram where A→B represent A implies B but not conversely.

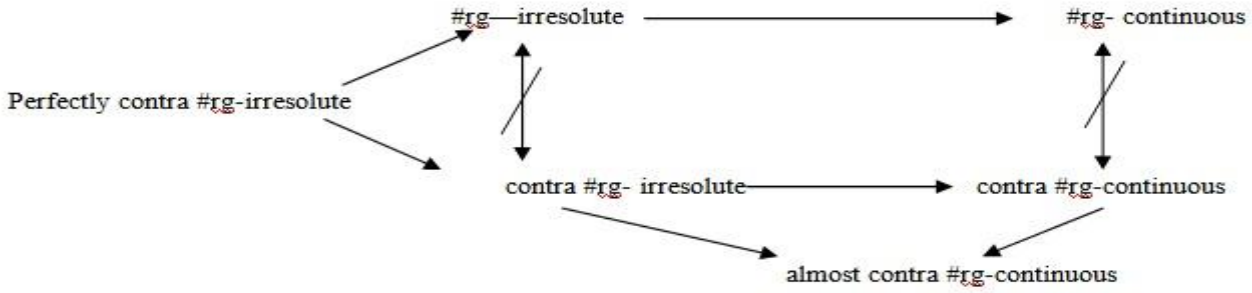

References

[1] Dontchev. J, "Contra-continuous functions and strongly S closed spaces", Internat.J.Math. & Math.Sci.19 (1996), 303-310.
[2] Mashhour. A.S., Abd. El-Monsef. M. E. and El-Deeb S.N.," On pre continuous mappings and weak pre-continuous mappings", Proc Math, Phys. Soc. Egypt 53(1982), 47–53.
[3] Levine. N, "Semi-open sets and semi-continuity in topological spaces", Amer. Math. Monthly, 70, 1963, 36–41,963.
[4] Stone. M, "Application of the theory of Boolean rings to general topology", Trans. Amer. Math. Soc. 41, 1937, 374–481.
[5] Cameron. D.E., "Properties of S-closed spaces", Proc. Amer Math. Soc. 72, 1978, 581–586.
[6] Levine. N., "Generalized closed sets in topology", Rend. Circ. Mat. Palermo 19, 1970, 89–96
[7] Palaniappan. N. and Rao. K. C, "Regular generalized closed sets" , Kyungpook Math. J. 33,, 1993,211–219.
[8] Gnanambal. Y, "On generalized preregular closed sets in topological spaces", Indian J. Pure App. Math. 28, 1997, 351–360.
[9] Nagaveni. N., "Studies on Generalizations of Homeomorphisms in Topological Spaces", Ph.D. Thesis,, 1999, Bharathiar University, Coimbatore.
[10] Benchalli. S.S.,and Wali. R.S., "On RW-Closed sets in topological spaces", Bull. Malays. Math. Sci. Soc(2) 30(2),2007, 99 – 110.
[11] Syed Ali Fathima. S and Mariasingam. M, "On #regular generalized closed sets in topological spaces", International journal of mathematical archive-2(11), 2011, 2497 – 2502
[12] Syed Ali Fathima. S and Mariasingam. M, "On #RG-Continuous and #RG-irresolute functions",Journal of Advanced Studies in Topology, 3(4),2012, 28-33
[13] Syed Ali Fathima. S and Mariasingam. M, "#RG- Homeomorphisms in topological spaces", International Journal of Engineering Research and Technology, 1(5) 2012..

International Journal of Modern Engineering Research (IJMER)
www.ijmer.com Vol.3, Issue.2, March-April. 2013 pp-599-603 ISSN: 2249-6645

Water Susceptible Properties of Silt Loam Soil in Sub grades in South West Pennsylvania

Robert M. Brooks, [1] Mehmet Cetin[2]
[1]*Corresponding Author, Associate Professor, Department of Civil and Environmental Engineering, Temple University, USA,*
[2]*Ph.D. Student, Department of Civil and Environmental Engineering, Temple University, USA,*

Abstract: *Water susceptible properties of subgrade soils play important role in the structural design of highways. In this research study laboratory investigations were conducted on subgrade soil samples for determining the influence of water susceptible properties on Natural moisture content, Optimum moisture content, Compaction, California Bearing Ratio (CBR)-soaked and unsoaked, and Unconfined Compression Strength (UCS). All tests were done using appropriate ASTM standards. Relationships were developed using regression equations for predicting the performance of seven engineering variables.*

Key Words: *Water Absorption characteristics, Engineering Properties, Optimum Moisture Content, CBR, UCS.*

I. INTRODUCTION

Water is an enemy of road materials [1, 2, 3]. This is because water plays an important role in causing cumulative damage of road structure over time [4, 5, 6]. Because of highwater absorption property silt loam poses performance problems especially under heavy loads over longer periods of time [7, 8, 9]. The problem is aggravated during rainy season because of significant loss of bearing capacity and shear strength of the subgrade material [10, 11, 12]. These losses in the subgrade material will translate into the loss of structural performance of the road itself. Silt loam soils are found on and around the river beds in Southwest Pennsylvania. In these regions many rural roads are usually constructed on compacted silt loam soils. Therefore, there is need to study in detail the influence of water susceptibility on various engineering properties of this material as applicable to Southwest Pennsylvania. This research study attempts to determine relationship between the degree of water absorption of loam soils at subgrade level and essential engineering properties.

II. MATERIALS AND METHODS

Twenty samples were collected at 3 feet depth of the subgrade soil of US 19 near Pittsburg.

The following laboratory tests were conducted on the soil according to the ASTM standards.

1. Grain size distribution (wet/dry sieving),
2. Soil classification, ASTM D2487 – 11
3. Natural moisture content, ASTM D2216 – 10
4. Optimum moisture content ASTM D558 – 11
5. Compaction test, ASTM D 698, D 1557
6. California Bearing Ratio (CBR) – soaked and unsoaked, ASTM D1883 - 07e2 and
7. Unconfined Compression Strength (UCS). ASTM D2166 – 06

The following statistical tests were conducted to establish the mean values and associated variances of the parameters. The variances were determined for inter and intra-groups of samples at a statistical significance of $\alpha = 0.05$.

1. One-way Analysis of Variance (ANOVA)
2. Two-way ANOVA

Seven regression equations were establishedshowing the influence of independent variable on the dependent variable. For each regression equation correlation coefficient was determined. The correlation coefficient was significant at $\alpha = 0.05$ level for the following correlated quantities: Swell and UCS, Swell and CBR (soaked), Void Ratio and MDD, Shrinkage limit and liquid limit, Clay content and NMC.

The correlation coefficient was significant at $\alpha = 0.01$ level for the following correlated quantities: Swell and CBR (unsoaked), Plasticity index, and Shrinkage limit. All the significance tests were done at 2 tailed tests.

III. Results and Discussions

3.1 Soil Classification

As per the ASTM D 2487 standard the Unified Soil Classification System was used in classifying the soils. 57% of the samples were classified as inorganic sandy clays of low to medium plasticity (CL). Others were classified as elastic silt (MH).

3.2 Comparison of Sections

Comparison of the mean values of many of the geotechnical properties of soils beneath the stable and unstable sections of roads in the region revealed that there was significant differences shown in the results of California Bearing Ratio (CBR) and Maximum Dry Density (MDD), swell and UCS.The high values for these propertieswere due to the presence of high clay content (though statistically insignificant in difference)and low degree of compaction of the subgrade.

3.3 Natural Moisture and Clay Contents

The minimum and maximum natural moisture contents were 10% and 24% respectively as shown in Table I. The mean moisture content was 17%. The minimum and maximum clay contents were18 and 54% respectively. The mean clay content was 38%. Alinear correlation with R = 0.98 was established between the clay content and the natural moisture content as shown in Table II and Fig. 1. The correlations between shrinkage limit and liquidlimit; and shrinkage limit and plasticity index were R = 0.78 and R = 0.89 [13,14,15] respectively as shown in Fig. 2 and Fig.3.The correlation established in this study indicates that the clay content has a strong positive influence on water content. Other researchers established that there is strong attraction between the water and the clay particles. This is because the high ratio of particles surface to particle mass for clay soils attracts large amount of water [16].

3.4 Void Ratio and MDD

The minimum and maximum void ratio were0.44 and 0.65 respectively as shown in Table I. The mean void ratio was 0.52. The minimum and maximum MDD were 1594 kg/m^3 and 1884 kg/m^{3}respectively. The mean MDD was 1788 kg/m^3. A linear correlation with R = 0.81 was established between the void ratio and MDD as shown in Table II and Fig.4.

The void ratio has a linear relationship with the Maximum Dry Density (MDD). The coreThe soil void increased rather than decrease as shown by the laboratory compaction tests ASTM D 698 and D 1557 as shown in Fig. 4. The results indicate that adequate field compaction was not obtained.

3.5 Swell, CBR and UCS

The minimum and maximum Swell were 0.02 and 0.267 respectively as shown in Table I. The mean Swell was 0.14. The minimum and maximum CBR unsoaked were 3% and 6% respectively. The mean CBR unsoaked was 4%. A linear correlation with R = 0.88 was established between Swell and CBR unsoaked as sown inTable II and Fig. 5. The minimum and maximum CBR soaked were 1% and 3% respectively. The mean CBR soaked was 2%. A linear correlation with R = 0.93 was established between Swell and CBR soaked as shown in Fig. 6.

The minimum and maximum UCS were 16 KN/m^2 and 63 KN/m^2 respectively. The mean Swell was 28 KN/m^2. A linear correlation with R = 0.21 was established between Swell and UCS as shown in Fig. 7.

It is important to note that swell has a negative influence on the CBR unsoaked and CBR soaked. This means that a swell % increased both CBR unsoaked and CBR soaked decreased indicating strength loss. Similarly swell has negative influence on the UCS indicating strength loss while swell % increased.

Table I: Comparison of ranges and mean values of various geotechnical properties of subgrade soils.

Properties	Stable Location Range	Unstable Location Range	Differences	Mean Value
Clay content (%)	18-48	22-54	Insignificant	38
Natural Moisture Cont. (%)	10-19	12-24	Insignificant	17
OMC (%)	10-18	13-20	Insignificant	18
Shrinkage limit	2-9	2-9	Insignificant	6
Plastic Limit (%)	13-21	16-25	Insignificant	21
Liquid Limit (%)	36-48	38-52	Insignificant	44
Absorption Limit (%)	17-39	21-42	Insignificant	32
Max. Dry Density (kg/m^3)	1742-1884	1594-1676	Significant	1788
CBR (%)-unsoaked	4-6	3-4	Significant	4
CBR (%)-soaked	2-3	1-2	Significant	2
Void Ratio	0.44-0.58	0.56-0.65	Significant	0.52
UCS (KN/m^2)	20-63	16-43	Significant	28
Swell	0.02-0.18	0.10-0.267	Significant	0.14

Table II: Correlation and regression equations among the variables

Correlated Quantities	Correlation Coefficient	Significance	Regression Equation
Swell and CBR (soaked)	0.93	0.018, α = 0.05	Y=-8.2873x+3.1375
Void Ratio and MDD	0.81	0.018, α = 0.05	Y=1069.9x+1215.4
Swell and CBR (unsoaked)	0.88	0.007, α = 0.01	Y=-8.2026x+6.2326
Swell and UCS	0.21	0.112, α = 0.05	Y=-60.703x+36.433
Shrinkage limit and liquid limit	0.78	0.038, α = 0.05	Y=2.4165x+30.073
Clay content and NMC	0.98	0.016, α = 0.05	Y=0.3404x+4.865
Shrinkage limit and Plasticity index	0.89	0.004, α = 0.01	Y=1.7463x+10.887

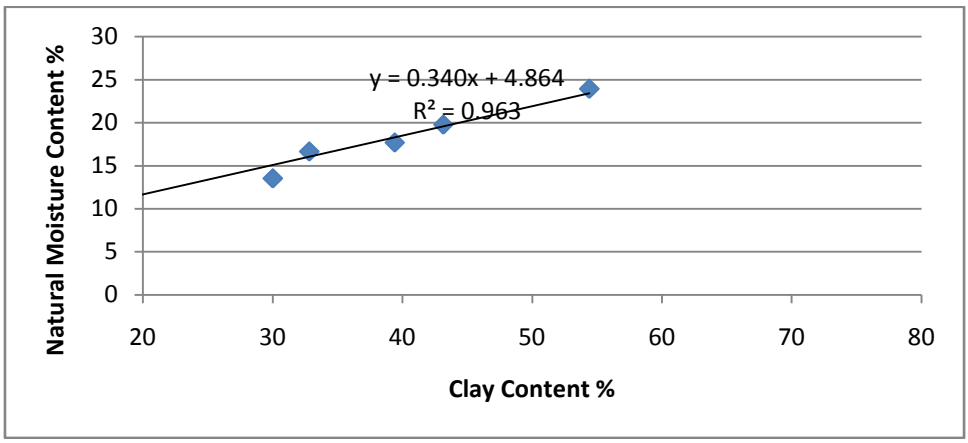

Figure 1: Influence of clay content on natural moisture content.

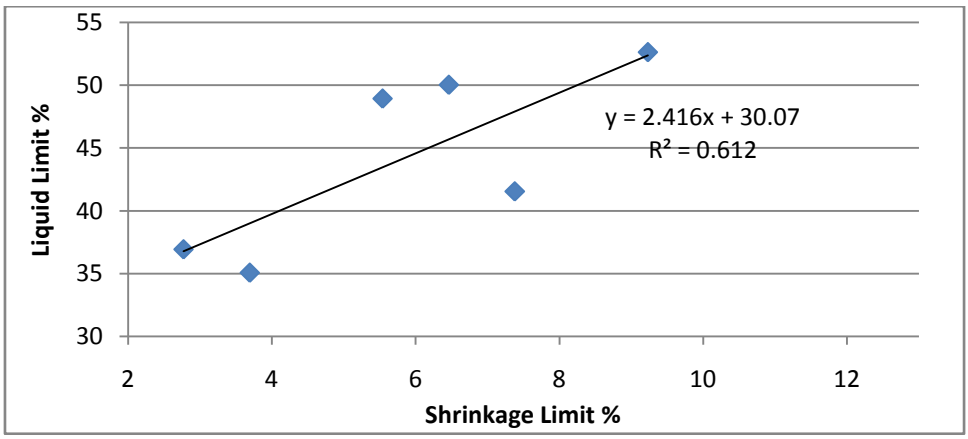

Figure 2: Influence of shrinkage limit on liquid limit.

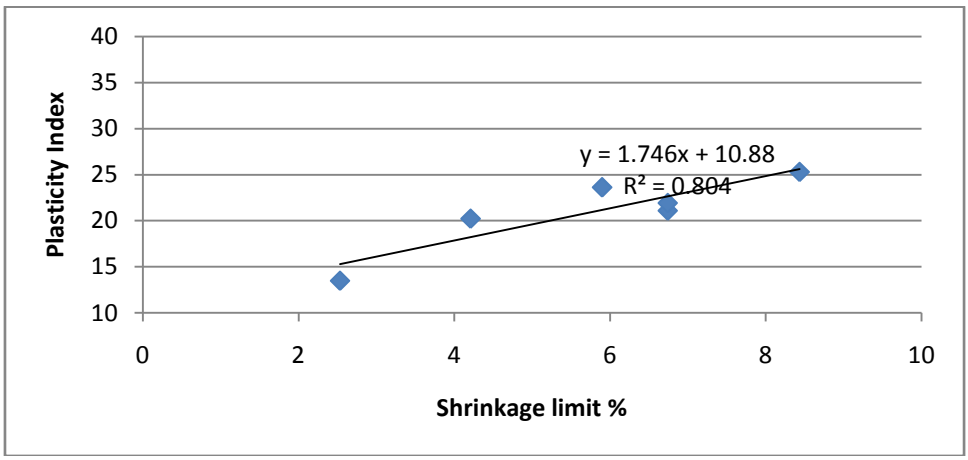

Figure 3: Influence of shrinkage limit on plasticity index.

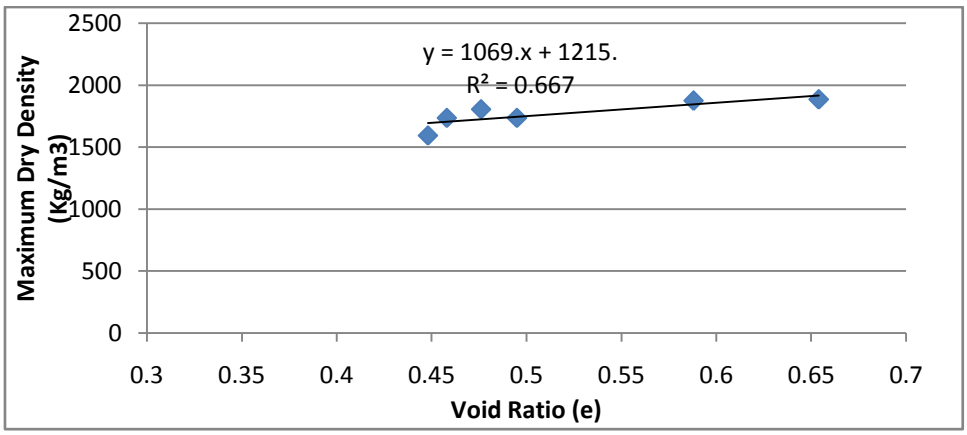

Figure 4: Influence of void ratio on maximum dry density.

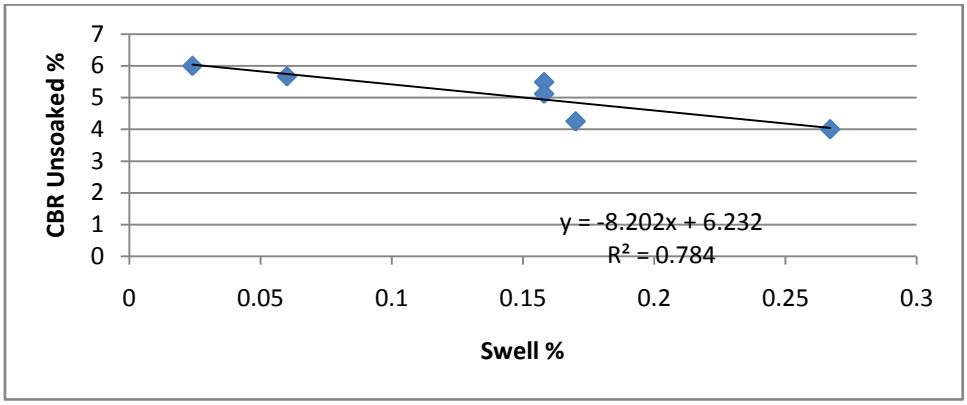

Figure 5: Influence of swell on CBR unsoaked.

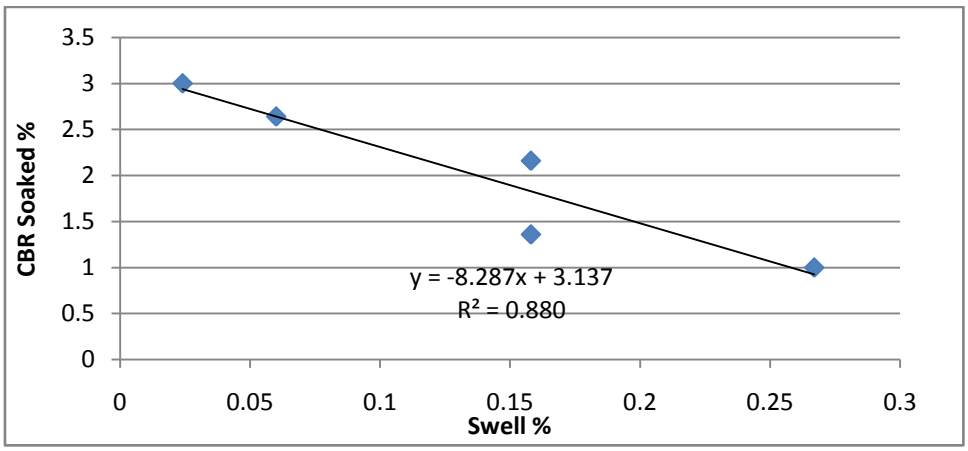

Figure 6: Influence of swell on CBR soaked.

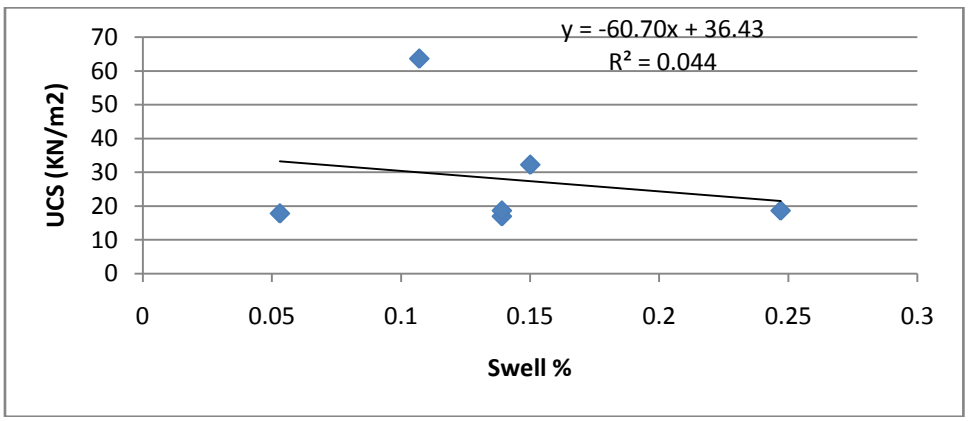

Figure 7: Influence of swell on UCS.

Similar results were found by Alayaki F. M. (2012) [17].

When an engineer is encountered with subgrade soils with high water absorption properties it is important for him or her to consider improving the drainage condition of the pavement. Additionally, the engineer should also consider improving the soil performance by adding admixtures such as lime, fly ash, cement.

IV. CONCLUSIONS

The following seven regression relationships were found with statistically significant correlation coefficients for predicting the performance of several engineering variables.

1. Clay is content is directly proportional to the moisture content of the soil with a linear correlation with R = 0.98.
2. Shrinkage Limit is directly proportional to the Liquid Limit of the soil with a linear correlation with R = 0.78.
3. Shrinkage Limit is directly proportional to the Plasticity Index of the soil with a linear correlation with R = 0.89.
4. Void Ratio is directly proportional to the Maximum Dry Density of the soil with a linear correlation with R = 0.81.
5. Swell percentage is inversely proportional to the Unsoaked California Bearing Ratio of the soil with a negative linear correlation with R = 0.88.
6. Swell percentage is inversely proportional to the Soaked California Bearing Ratio of the soil with a negative linear correlation with R = 0.93.
7. Swell percentage is inversely proportional to the Unconfined Compressive Strength of the soil with a negative linear correlation with R = 0.21.

V. ACKNOWLEDGMENTS

The Republic Of Turkey, Ministry Of National Education Scholarships is duly acknowledged for providing scholarship.

REFERENCES

[1] Brooks, R., Udoeyo, F., and Takkalapelli, K. Geotechnical Properties of Problem Soils Stabilized with Fly Ash and Limestone Dust in Philadelphia. J. Mater. Civ. Eng., American Society of Civil Engineers, 23(5), 711–716, 2011.

[2] Brooks R. M. (Corresponding author), Udoeyo F., and Takkalapelli K. V., Compaction Delay Characteristics of Clay with Cement Kiln Dust, UK Institute of Civil Engineers, Geotechnical Engineering Volume 162, issue 5, ISSN: 1353-2618, pp 283-286, Oct 2009.

[3] Brooks R. M. (AKA James M. Matthews), Crause J., and Monismith C. L., Investigation of Laboratory Fatigue Test Procedures for Asphalt Aggregate Mixtures. Transportation Engineering Journal of American Society of Civil Engineering, Vol. 119, No.4, Washington D.C., pp 634-654, Aug. 1993.

[4] Brooks R. M. (AKA James M. Matthews), and Monismith C. L., The Effect of Aggregate Gradation on the Creep Response of Asphalt Mixtures and Pavement Rutting Estimates, Effects of Aggregates and Mineral Fillers on Asphalt Mixture Performance, ASTM, STP 1147, Richard C. Meininger, Ed., American Society for Testing and Materials, Philadelphia, pp 329-347, 1992.

[5] Brooks R. M. (AKA James M. Matthews), and Pandey B. B., Performance of Flexible Pavements.Transportation Research Record, No. 1307, Transportation Research Board, National Research Council, Washington D.C., pp 51-62, 1990.

[6] Brooks R. M. (AKA James M. Matthews), and Monismith C. L., Direct Tension and Simple Stiffness Tests-Tools for the Fatigue Design of Asphalt Concrete Layers Transportation Research Record, No. 1388. Transportation Research Board, National Research Council, Washington D. C., pp 182-199, 1993.

[7] Brooks, R., Soil Stabilization with Lime and RHA, International Journal of Applied Engineering, Volume 5, Number 7. pp. 1077-1086, 2010.

[8] Brooks, R. M. Soil Stabilization with RHA and Flyash, International Journal of Research and Reviews in Applied Sciences Volume 1, Issue 3, pp.209-217, 2009.

[9] Donaldson K., Brooks R. M.(Corresponding author), Udoeyo F. F., and Takkalapelli K. V., Effects of Fly Ash on Engineering Properties of Clays. International Journal of Applied Engineering Research.Volume 6, Number 1, pp. 43-52, 2011.

[10] Brooks R. M. (Corresponding Author), and Cetin M., Application of Construction Demolition Waste for Improving Performance of Subgrade and Subbase Layers, International Journal of Research and Reviews in Applied Sciences, ISSN: 2076-734X, Vol. 12, Issue 3, pp. 375-381, September 2012.

[11] Cetin M., Brooks R. M.(Corresponding Author), and Udo-Inyang P., An Innovative Design Methodology Of Pavement Design By Limiting Surface Deflection. International Journal of Research and Reviews in Applied Sciences, ISSN: 2076-734X, Volume 13, Issue 2, Pages 607-610, November, 2012.

[12] Cetin M., Brooks R. M. (Corresponding Author), and Udo-Inyang P., A Comparative Study Between The Results Of An Innovative Design Methodology By Limiting Surface Deflection And AASHTO Design Method, International Journal of Research and Reviews in Applied Sciences, ISSN: 2076-734X, Volume 13, Issue 2, Pages 611-616, November, 2012.

[13] Moore D. S., McCabe G. P., and Craig, B. A., Introduction to the practice of statistics (W H Freeman & Co (Sd),7th Edition, New York., 2005).

[14] Devore J. L., and FarnumN. R., Applied statistics for engineers and scientists (Duxbury Press. ISBN 05435601X, 1stedition., 2004).

[15] Montgomery, D. C., Design and analysis of experiments (John Wiley & Sons Inc. 7thedition., 2008).

[16] McCarthy, D. F., Essential of soil mechanics and foundations (Basic Geotechnics. Pearson Prentice Hall. New Jersey. 2007).

[17] Alayaki F. M., Water absorption properties of laterite soil in road pavement: a case study If-Ilesha Highway, South Western Nigeria, International Journal of Emerging Technology and advanced Engineering. Volume 2, issue 11, November, 2012.

International Journal of Modern Engineering Research (IJMER)
www.ijmer.com Vol.3, Issue.2, March-April. 2013 pp-949-954 ISSN: 2249-6645

Economic efficiency calculation and Scenarios for the installation and direction of solar thermal systems at the example of a reference

Sejdo Ferati
Department of Engineering, University of Applied Sciences Brandenburg, Germany

Abstract: *The article examines different possibilities of the installation and the azimuth of solar thermal systems on a rooftop at the example of a reference building. The outcome of a different azimuth and installation are different costs of solar energy, savings of wood pellets and different degrees of system efficiency. In this way the economic efficiency of a solar thermal installation can be influenced strongly.*

Keywords: *Solar Thermal Installation, installation and direction of the solar thermal installation, economic efficiency of the solar thermal installation, costs of solar energy, savings of wood pellets and degrees of system efficiency*

I. INTRODUCTION

Environment-friendly solar thermal energy which is gained from the solar irradiation onto the own roof becomes increasingly more attractive. The sun is an inexhaustible source of energy. Thermally gained energy can be produced increasingly more favorably by most modern technique through a solar thermal system. The quality of the systems is safeguarded and controlled by norms of the European Union. In this way the independence on fossil fuel and of their prices increases. CO_2-emissions resulting from the combustion of fossil energy carriers are reduced. The installation of solar thermal systems can partly be supported by state measures. The living comfort increases and last but not least new jobs can be created in the domestic economy.

The figure shows a model of a complete pellet boiler plant with solar support for the hot water generation and for the heating support (Company August Brötje GmbH) [2].

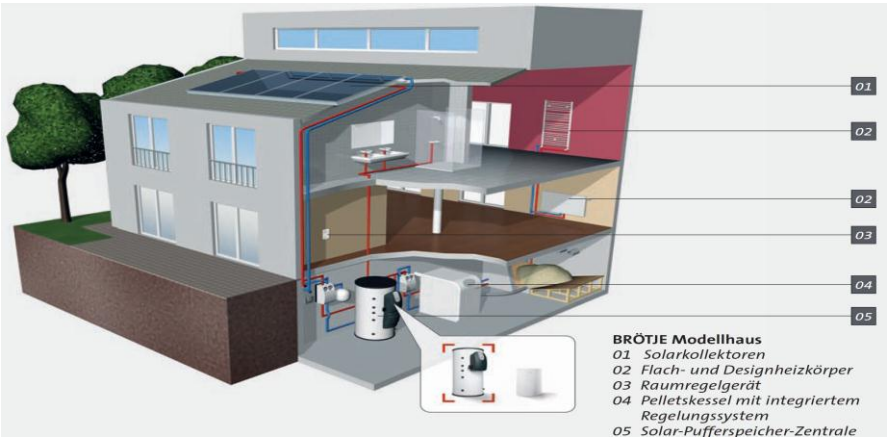

Figure 1: Pellet boiler with solar support to hot water generation and heating support [2]

Basics of the simulation of the system

With the help of Dr. Valentin energy software a simulation of the system is carried out [12].

By increasing improvement of the thermal insulation at buildings a reduced energy demand for the heating can be achieved. In this way the energy demand for the hot water generation gets more importance. This demand in part can be produced by thermal solar systems which convert the solar irradiation with the help of collectors into heat. At present these systems can produce an annual energy yield of 350-500 kilowatt-hours per m^2 collector surface area. This leads to a decrease of the CO_2-emissions of up to 150 kg [12].

Thermal solar systems convert solar energy with the help of collectors into heat. Then the produced heat is transported over pipelines into a so-called buffer storage. The energy losses occurring from the production up to the storage should be held as small as possible. The losses, resulting from the relation between the usable energy and the irradiated energy can be assessed with the help of degree of efficiency of the system. A solar system is established according to its mode of operation:

With a collector the solar irradiation is absorbed and converted into heat. The so won energy is transported over a net of pipelines and heat exchangers to a storage tank. The storage tank has the task of balancing the temporal variations of energy offer and energy demand. For a maximum utilization of the solar irradiation a control system is useful, that turns on a circulating pump as soon as a temperature difference arises between collector and storage tank. Thus the heat transportation to the storage tank is guaranteed.

Description of the reference building

The single-family house completely with basement is constructed in massive design on strip foundation. The walls consist of burned stones (Cellar: Lime sandstone). The floors consist of reinforced concrete, the grounds are made of floating floor and tiled (Attic: fitted carpeting). The stairs consist of reinforced concrete with timber sheeting. The attic is fully developed and is to be reached over the staircase. The cellar can also be reached over the staircase. Additionally there are stairs outside the house which lead to the cellar. The external walls have got brick facing. The building has a gable roof with clay bricks. The chimneys consist of burned stones.

Degree of efficiency and solar fraction

The degree of efficiency results from the relation between energy put out to the irradiated energy.

The degree of efficiency of the collector circuit results from the relation between the energy output of the collector circuit over the heat exchanger to the irradiated energy (irradiated onto the collector surface).

The degree of efficiency of the system results from the relation between the energy output of the solar system to the rradiated energy (irradiated onto the collector surface).

The energy output gained from the solar system is that energy which is passed on from the solar storage tank to the standby storage tank.

The solar fraction results from the relation between the energy provided by the stand by storage tank of the solar system to the sum of all energies provided to the standby system (Solar system and upstream with conventional systems).

The energy delivery for the heating of the drinking water is the energy which is necessary to get the temperature of the cold water to the temperature of the tapped drinking water. Losses are not considered here.

The used combustible is the combustible which is necessary to heat the standby storage tank to the nominal temperature. The heat losses of the storage tank and the degree of efficiency of the kettle are considered here.

Calculation of Economic Efficiency according to the cash value method (with T*SOL) [12]

- Investment Costs = Installation Costs – Subsidy
- yearly Operating Costs = Pump Performance*Operating Time*Electricity Costs

The cash value (CV) of a price-dynamic payment sequence Z, Z · r, Z · r^2... over T years (Lifespan) is calculated as follows (according to VDI 2067 [14]):

Cash value CV = Z · b(T,q,r)

Cash value factor b (T, q, r)= $\begin{cases} \frac{1-(r/q)^T}{q-r} & for\ r <> q \\ \frac{T}{q} & for\ r = q \end{cases}$

q: Simple interest factor on capital (e.g. 1,08 at 8 % of simple interest on capital)

r: Price change factor (e.g. 1,1 at 10 % of price change)

Capital value of the total investment (C):

C = sum of the cashl value of the price-dynamic payment sequence over the lifespan
+ promotions
- Investments

The pay-back time is the period the system must operate for the investment in order to yield a cash value of zero. Pay-back times of more than 40 years are not included here [12].

In order to calculate the heating price, the cash value of the costs must be calculated:

CV of the costs = Investments + Cash value of the Operating and Maintenance Costs.

If the Cash value of the costs is converted into a constant payment sequence (r=1) over the lifespan, then Z turns out for this consequence:

Z = CV of the costs / b(T, q, r).

According to VDI 2067 is valid:

For r =1 be comes 1/b(T, q, r) for the annuity factor a(q, T) = q^T · (q-1) / (q^T-1).

The heating price then represents itself as follows:

Heating price = $\frac{\text{yearly Costs Z}}{\text{yearly Energy Yield}}$

In the following the components of the system - as indicated in the figure - are described:

-Collector: Manufacturer August Brötje, Type: Solar Plus HP 20, denomination: Tube collector Parameter: Gross face 2,84 m^2, reference area 2,16 m^2, specific heat capacity 4300 Ws/(m^2K), collector field volume flow: 40 (l/h)/m^2, medium: Water Glycol, resulting specific heat capacity: 3588 Ws/(kg K) [2]

-tank: Pellets-Central heating boiler, Manufacturer Vaillant [13], Type: renerVIT VKP 202, capacity: 20 kilowatts

-Hot water tank: Standard, volume: 300 l

-Buffer storage: Standard, volume: 800 l
-Hot Water need: average day consumption: 200 l, nominal temperature hot water: 50 °C, interpretation for single-family home (morning top).

Simulation results of the reference building [12]:

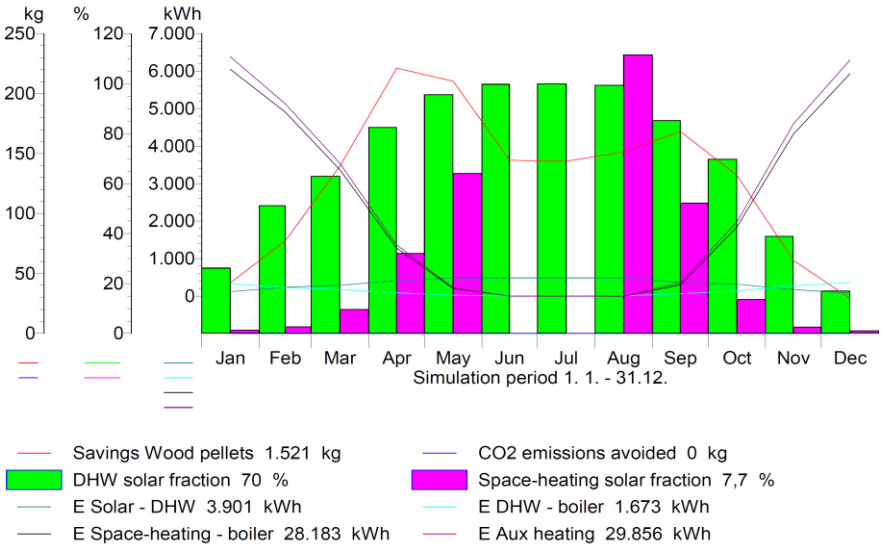

Figure 2: Fraction heating, hot water, total & saving natural gas [12]

Solar energy consumption as percentage of total consumption

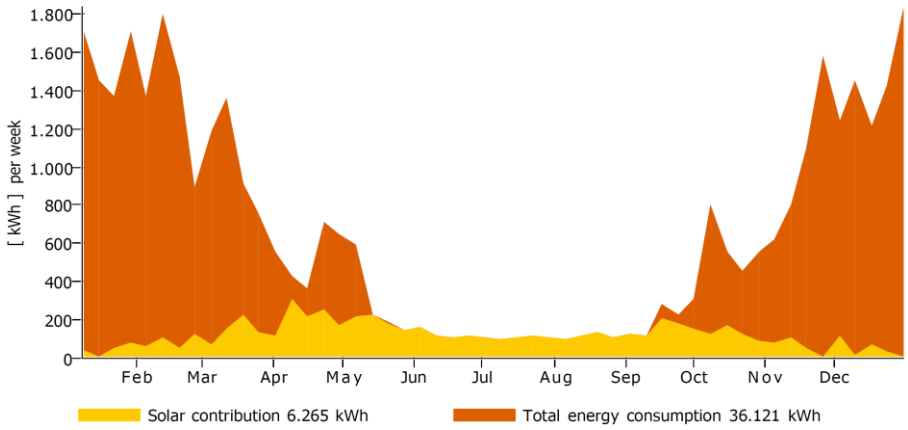

Figure 3: Solar energy consumption as percentage of total consumption [12]

Energy balance schematic

Legend

1	Irradiation on to collector surface (active)	20 MWh
1.1	Optical collector losses	5 MWh
1.2	Thermal collector losses	6 MWh
2	Energy from collector array	9 MWh
2.1	Solar energy to storage tank	4 MWh
2.3	Solar energy to buffer tank	3 MWh
2.5	Internal piping losses	1.396 kWh
2.6	External piping losses	228 kWh
3.1	Tank losses	851 kWh
3.2	Circulation losses	1.264 kWh
5.1	Buffer tank losses	1.005 kWh
5.2	Buffer tank to heating	2.364 kWh
6	Final energy	33 MWh
6.1	Supplementary energy to tank	1.673 kWh
6.4	Supplementary energy to space-heating	28 MWh
6.5	Electric element	0 kWh
9	DHW energy from tank	3 MWh
10.1	Heat to HT heating	6 MWh
10.2	Heat to LT heating	24 MWh

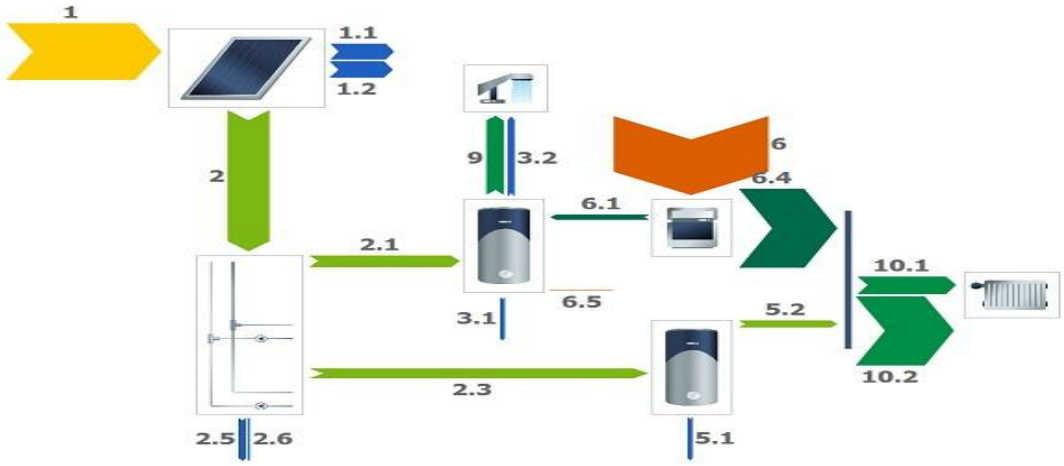

Figure 4**:** Energy balance schematic [12]

Financial analysis:

System		
System yield	6, 26	MWh
Active surface area	22, 74	m2
Yearly electricity consumption for additional energy	610, 40	kWh/a
Annual fuel savings	1.520,40	kg
Financial analysis parameters		
Lifespan	20	Years
Interest on capital	2, 5	%
Energy cost escalation rate	3, 0	%
Running cost escalation rate	1, 5	%
Costs (Cash value)		
Investments	-52.000, 00	€
Subsidy	3.750,00	€
Savings	3.108,00	€
Running costs	-15.410, 00	€
Net present value	**-60.552, 00€**	
Amortization period	**No amortization**	
Cost of solar energy	**0, 65 €/kWh**	

Provisional Result

The variant does not show any amortization for a period of 20 years so that this variant is uneconomical.

II. SCENARIO „ A", TILT ANGLE 35° (DEGREE) = CONST., AZIMUTH = VARIABLE

The tilt angle of the solar thermal collectors on the roof (roof parallel system) is 35 °. That is the existence of the reference building. The Scenario A shows the dependence of the costs of solar energy, the saving of wood pellets and the system efficiency of the solar thermal system on the azimuth of the reference building into the respective cardinal point.

Table 1: Dependence of the costs of solar energy, the saving of wood pellets and the system efficiency of the solar thermal system on the azimuth of the reference building

Azimuth ° (Degree)	Cost of solar energy 0,01 x €/kWh	Wood pellets savings 0,1 x t (Ton)	System efficiency %
135 °	71	14,064	30,3
175 °	65	15,226	31,2
180 °	65	15,277	31,3
225 °	70	14,398	30,7

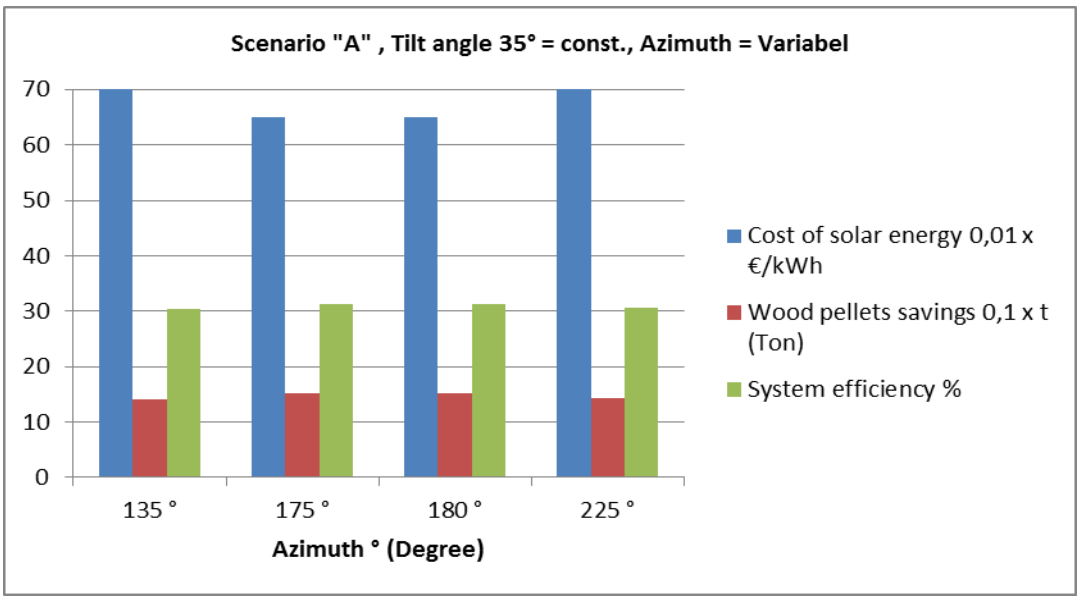

Diagram 1: Dependence of the costs of solar energy, the saving of wood pellets and the system efficiency of the solar thermal system on the azimuth of the reference building

Provisional Result

The optimal results for the costs of solar energy, the saving of wood pellets and the system efficiency are achieved at an azimuth of 180° of the reference building (to south).

III. SCENARIO „B", TILT ANGLE = VARIABLE, AZIMUTH 175° (DEGREE) = CONST.

The azimuth of the solar thermal collectors on the roof (roof parallel system) is 175 °. That is the existence of the reference building. The Scenario B shows the dependence of the costs of solar energy, the saving of wood pellets and the system efficiency of the solar thermal system on the tilt angle of the solar thermal system on the roof.

Table 2: Dependence of the costs of solar energy, the saving of wood pellets and the system efficiency of the solar thermal system on the tilt angle

Azimuth	Cost of solar energy	Wood pellets savings	System efficiency
° (Degree)	0,01 x €/kWh	0,1 x t (Ton)	%
25 °	69	14,579	30,1
30 °	67	14,921	30,6
35 °	65	15,209	31,2
40 °	64	15,421	31,8
45 °	65	15,209	31,2
50 °	63	15,636	32,9

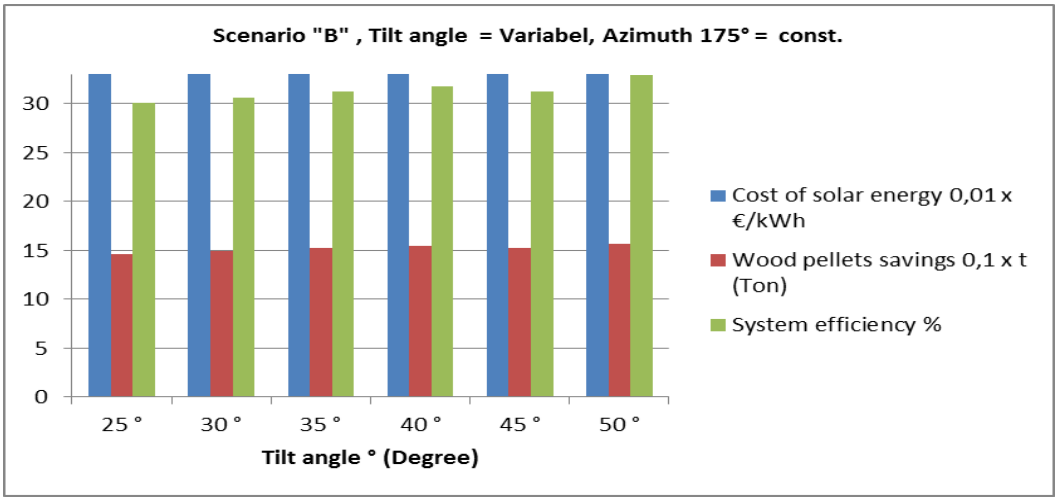

Diagram 2: Dependence of the costs of solar energy, the saving of wood pellets and the system efficiency of the solar thermal system on the tilt angle

Provisional Result

The optimal results for costs of solar energy, the saving of wood pellets and the system efficiency are achieved with a tilt angle of the solar thermal system on the roof of approx. 50 °.

IV. Conclusion

Solar power is good for the human being and for the environment. With a solar thermal system on the own roof a secure and clean kind of heat supply is guaranteed for water heating and heating support. With the correct azimuth of the house to south and the correct tilt angle of the solar thermal system on the roof the costs of solar energy, saving of wood pellets and the system efficiency can be optimized.

REFERENCES

[1] Abele, E. u.a.: EcoDesign. Berlin: Springer-Verlag, 2008
[2] August Brötje GmbH, August-Brötje-Straße 17, 26180 Rastede August Brötje GmbH – offizielle Seite: www.broetje.de
[3] DIN 4710 (01/2003): Statistiken meteorologischer Daten zur Berechnung des Energiebedarfs von heiz- und raumlufttechnischen Anlagen in Deutschland
[4] Döring, S.: Pellets als Energieträger. Berlin: Springer-Verlag, 2010
[5] Dratwa, F., u.a.: Energiewirtschaft in Europa. Berlin: Springer-Verlag, 2010
[6] EEG (10/2008): Erneuerbare-Energien-Gesetz , Gesetz für den Vorrang Erneuerbarer Energien
[7] EnEv 2009: Energieeinsparungsverordnung
[8] Kaltschmitt, M., Streicher, W., Wiese, A. (Hrsg.): Erneuerbare Energien. 4. Auflage (Berlin: Springer-Verlag, 2006)
[9] Oberzig, K.: Solarwärme, Heizen mit Sonne. Stiftung Warentest Berlin: Verlagsherstellung: Rita Brosius, 2012
[10] Pelte, D.: Die Zukunft unserer Energieversorgung. 1. Auflage (Wiesbaden: Vieweg + Teubner | GWV Fachverlage GmbH, 2010)
[11] Quaschning, V.: Regenerative Energiesysteme. 6. Neu bearb. u. erw. Auflage (München: Hanser Verlag, 2009)
[12] Simulationssoftware, Dr. Valentin Energiesoftware GmbH, Stralauer Platz 34, 10243 Berlin, Studentenversion (inkl. Benutzerhandbücher): T*SOL Pro 5.0
[13] Vaillant Deutschland GmbH & Co. KG, Berghauser Str. 40, 42859 Remscheid Vaillant Deutschland GmbH & Co. KG – offizielle Seite: www.vaillant.de
[14] VDI 2067 – Blatt 1 Entwurf (09-2010): Wirtschaftlichkeit gebäudetechnischer Anlagen, Grundlagen und Kostenberechnung
[15] VDI 2067 – Blatt 10 Entwurf (10-2011): Wirtschaftlichkeit gebäudetechnischer Anlagen, Energiebedarf von Gebäuden für Heizen, Kühlen, Be- und Entfeuchten
[16] VDI 2067 – Blatt 12 (06-2000): Wirtschaftlichkeit gebäudetechnischer Anlagen, Nutzenergiebedarf für die Trink wassererwärmung
[17] VDI 2067 – Blatt 20 (08-2000): Wirtschaftlichkeit gebäudetechnischer Anlagen, Energieaufwand der Nutzenübergabe bei Warmwasserheizungen
[18] VDI 2067 – Blatt 22 (02-2011): Wirtschaftlichkeit gebäudetechnischer Anlagen, Energieaufwand der Nutzenübergabe bei Anlagen zur Trinkwassererwärmung
[19] VDI 2067 – Blatt 40 Entwurf (01-2012): Wirtschaftlichkeit gebäudetechnischer Anlagen, Energieaufwand der Erzeugung
[20] VDI 2078 – Entwurf (03/2012) Berechnung von Kühllast und Raumtemperaturen von Räumen und Gebäuden
[21] VDI 6020 – Blatt 1 (05/2001): Anforderungen an Rechenverfahren zur Gebäude- und Anlagensimulation
[22] VDI 6025 (11/1996): Betriebswirtschaftliche Berechnungen für Investitionsgüter und Anlagen

AUTHOR

Sejdo Ferati received his M.Sc. from the Faculty of Technical Sciences in Novi Sad, Serbia,
his M.Eng. from the Beuth Hochschule für Technik (University of Applied Sciences) in Berlin, Germany and
his Dr. degree from the Comenius University in Bratislava, Slovakia.
He is honorary professor at the Fachhochschule Brandenburg (University of Applied Sciences) in Brandenburg an der Havel, Germany.
He is Member of The Association of German Engineers (VDI)

International Journal of Modern Engineering Research (IJMER)
www.ijmer.com Vol.3, Issue.2, March-April. 2013 pp-955-961 ISSN: 2249-6645

Coverage Analysis of Various Wireless Sensor Network Deployment Strategies

Utkarsh Aeron, [1] Hemant Kumar[2]
[1]*Dehradun Institute of Technology, Dehradun, India*
[2]*Galgotia's College of Engineering and Technology, Greater Noida, India*

Abstract: *Recent years have seen a developing interest in deploying large number of sensor nodes that coordinate in a distributed fashion on data gathering and analysing. These nodes can be deployed over a Wireless Sensor Network in random or deterministic fashion. While the random node deployment is preferred in many applications, if possible, other deployments should be investigated since an inappropriate node deployment can increase the complexity of other problems in Wireless Sensor Networks(WSNs) such as excessive energy consumption. Thus, we examine three competitors of node deployment for a sensor network: a regular hexagon based, a octagon-square based and a tri-beehive based tiling. We have taken a major performance evaluation measure namely coverage analysis for all the three sensor node deployment strategies*

Keywords: *Sensor Nodes, Deployment, Coverage Analysis, K-coverage, Sensing Radius*

I. INTRODUCTION

Many of us talks about our common sense but do we know what the technology has got for itself, it's the Wireless Sense. A Wireless Sensor Network consist of distributed sensor nodes to monitor physical or environmental conditions such as temperature, moisture, heat etc and to coordinately pass the recorded information for further processing. Each sensor node has several organs namely a radio transceiver with an internal antenna or connected with external antenna, a microcontroller for interfacing between sensor and energy source and energy source i.e. battery. Now days modern Wireless Sensor Networks (WSN) are bidirectional, also enabling control of sensor activity. The nodes communicate wirelessly and often self-organize after being deployed in an ad hoc fashion. Such systems can revolutionize the way we live and work.

The Wireless Sensor Networks (WSN)'s applications can be generally classified into target tracking and area monitoring. In the target tracking scenarios, we concern if we can trace the moving object accurately or not. The number of sensors and the position of sensors affect the performance and accuracy of tracking. In the area monitoring scenarios, we need to have enough sensors to avoid blind angle. Thus, it might seem as a solution that a denser infrastructure cause a more effective WSNs. However, if not deployed well, a denser network will lead to a larger number of packet collisions and traffic congestions. So, the efficiency and effectiveness of the Wireless Sensor Network (WSN) depends on the fact that how its sensor nodes have been deployed in the field. Some of the factors to explain the importance of the good deployment strategy for Wireless Sensor Networks (WSN) are discussed below:

- **Limited Energy:** A well-known characteristic is that wireless sensor nodes have limited energy and have difficult in recharging. According to the energy consumption model, the longer the transmitting range is, the more energy the wireless sensor nodes will consume. For energy saving, proper distance among sensors nodes is important for Wireless Sensor Network (WSNs). Transmitting by multiple hops path is usually better than by directly. The topology of WSNs affects the network lifetime considerably.

- **Transmission Jobs:** To extend the lifetime of WSNs, we usually regularly schedule sleep intervals for sensor nodes. Usually, multiple sensor nodes sensing similar data will need to aggregate them towards the source. Transmission jobs will cost a lot, if the WSN's don't have uniform sensing coverage.

- **Unprotected Areas:** The monitoring area is not usually protected, especially for military applications and other security related tasks. To prevent being invaded, deployment information is a good option to key management schema for WSNs, that is, deployment strategy affects the key schema for encoding and decoding the confidential information.

Thus, we have taken three different deterministic deployment patterns for Wireless Sensor Network (WSNs) namely a regular hexagon based, a octagon-square based and a tri-beehive pattern for sensor nodes deployment and analysed each of them on the basis of their average coverage provided in the application field.

II. REGULAR HEXAGON PATTERN

A grid-based deployment is considered as a good deployment in WSNs, especially for the coverage performance. There are several grid based designs like as unit square, equilateral triangle, regular hexagon etc. We have chosen the regular hexagon grid deployment pattern for the evaluation purpose.

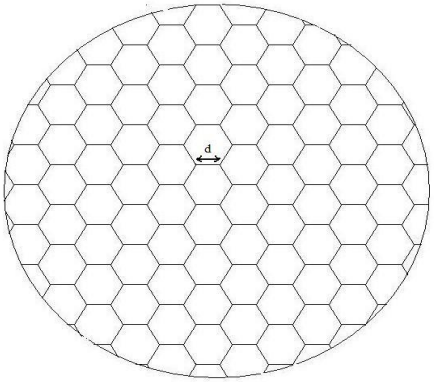

Fig (1) A regular hexagon based deployment pattern

A regular hexagon based node deployment pattern is depicted above in fig (1). Each of the sensor nodes are deployed on the intersection points of the grid in a considered circular field with radius, say R. The pattern within a circular field with radius R is assumed to be symmetric tessellations i.e. all the unit cells within the circular field have equal edge length d and thus equal area within each unit hexagon cell.

1.1. Sensing Range For Regular Hexagon Deployment Pattern

The Sensing Range, R_{sense} of the sensor nodes can be defined as the maximum distance up to which the nodes are capable to sense the or monitor the objects. The Sensing Range, R_{sense} varies in its values for various deployment patterns. The sensing range R_{sense} is assumed to be equal to the edge length say 'd' of the unit hexagon cell of the circular field shaped Regular Hexagon based deployment pattern. In fig (1), a grid deployment of n sensor nodes in a circular field is shown, where each of the n grid points hosts a sensor mote. The approximate length of a unit hexagon, d, can be calculated in the following way:

First, the approximate area of a unit hexagon with length d can be computed by dividing the whole area of a given field having radius R, with the number of cells, k.

Area of unit square cell = Whole Area of circular field / Number of cells in field (1)

For regular hexagon based deployment pattern, the approximate value of k is (n/3 – 1). So, from the relation (1), we derive relation (2) for R_{sense}, the sensing radius or the sensing range for the regular hexagon based deployment pattern.

$$R_{sense} = \pi R^2 / (3\sqrt{3}/2)(n/3 - 1)$$
$$R_{sense} = \sqrt{(6\pi R^2 / 3\sqrt{3}n)} \quad (2)$$

III. OCTAGON-SQUARE PATTERN

Octagon-Square based deployment pattern for Wireless Sensor Network (WSN) is based on tiling also considered as tessellations. In octagon-square based tessellations we have regular octagons with their vertex surrounded with the squares. Both have same edge length say d'. The basic structure of octagon-square based deployment pattern is shown in fig(2).

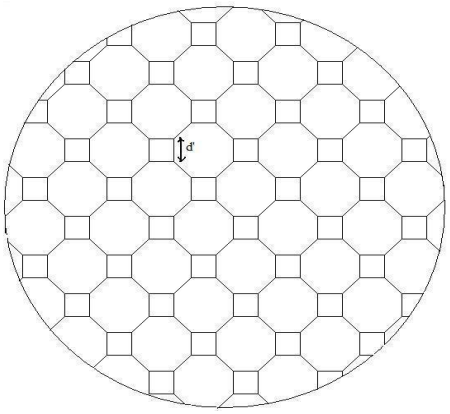

Fig(2) Octagon-Square based deployment pattern

3.1 Sensing Range for Octagon-Square Deployment Pattern

In the similar way, like as we have used to find out the sensing radius, R_{sense} for the regular hexagon based pattern, the sensing radius for octagon-square based deployment pattern can also be calculated by dividing the whole area of the considered circular field with radius R with the number of unit octagon-square cells. The approximate number of cells, k for octagon-square based pattern is $(\sqrt{n}/2 - 1)^2$.

Thus, the sensing range R_{sense} calculated for Octagon-Square node deployment pattern is,

$$R_{sense} = \pi R^2 / (3+\sqrt{2})(\sqrt{n}/2 - 1)^2$$

$$R_{sense} = \sqrt{(2\pi R^2 / (3+\sqrt{2})n)} \quad (3)$$

IV. Tri-Beehive Pattern

Tri-Beehive deployment pattern for Wireless Sensor Network (WSN) uses triangle and hexagon in the two dimensional plane. The edge length for tri-beehive deployment pattern say d'' is considered to be symmetrical throughout the coverage field with radius R.

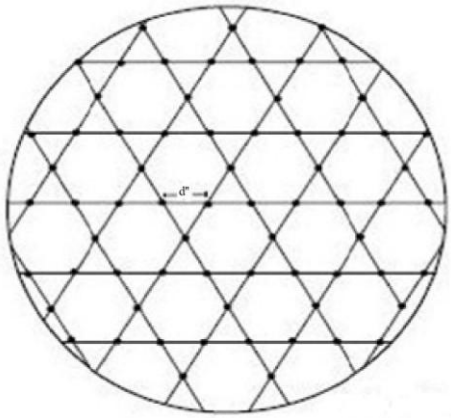

Fig (3) Tri-Beehive based deployment pattern

4.1 Sensing Range for Tri-Beehive Deployment Pattern

In the similar way, like as we have used to find out the sensing radius, R_{sense} above, the sensing range calculated for Tri-Beehive node deployment pattern is,

$$R_{sense} = \sqrt{(4\pi R^2 / 3\sqrt{3}n)} \quad (4)$$

V. COVERAGE

The term coverage in the respect for the Wireless Sensor Network(WSN) can be considered as the maximum range or area up to which the network is able to send or receive the data and also able to track the objects for monitoring them. In Wireless Sensor Network (WSN), the simple reason for checking coverage is to provide the high quality of information in the region of application. To fulfil the desired coverage of a region, adjusting the sensing range has its limitations due to the expensive energy consumption and restricted sensor node capabilities. Therefore, node deployment becomes very important. We have studied the K-coverage map for resolving the coverage issue which is the usual way of specifying conditions on coverage.

5.1 K-Coverage

A network is said to have k-coverage if every point in it is covered by at least k sensor nodes. If a particular point in the area which is being monitored by the Wireless Sensor Network (WSN) nodes is monitored by two sensor nodes, then that particular point of area is said to have 2-coverage.

A k-coverage map is drawn for the area to be analysed and the area is divided into different sectors based on the value of K for various points in the area of inspection.

5.2 Assumptions for K-Coverage

The K- coverage map, which is used to check all possible coverage areas and to analyze the relative frequency of exactly K-covered points Using the idea of the K- coverage map we measure the quality of coverage performance of all the three considered node deployment strategies.

There are certain assumptions which need to be made before proceeding further for the K- coverage maps for the Regular Hexagon deployment pattern, Octagon-Square deployment pattern and the Tri-Beehive node deployment pattern. Following are those assumptions:

- A disc-based sensing model is used for homogeneous nodes where each sensor has a maximum sensing range of the Sensing Radius, R_{sense}.
- The Sensing Radius, R_{sense}, is the same as the length of a unit cell namely d, d' and d''. Therefore R_{sense} is different for the regular hexagon node deployment, octagon-square node deployment and the tri-beehive node deployment pattern.
- A point is covered by a sensor node if it lies either within a disc of Sensing Radius, R_{sense}, or falls exactly at circumference of a disc shaped circular field undertaken.
- No boundary conditions are considered for the three of the patterns which seems reasonable for large-scale Wireless Sensor Network (WSN) conditions.

5.3 Average Coverage and Standard Deviation

The Average K- coverage or the weighted coverage can be computed to be provide the coverage capacity of all of the three deployment strategies. The average coverage is computed through following equation,

K- coverage * exactly K- covered points (%) / 100

For finding out the Standard Deviation in the coverage of each of the three strategies, it is necessary firstly to compute the sample variance through following method:

$$\sigma^2_{\text{weighted}} = \frac{\sum_{i=1}^{N} w_i \left(x_i - \mu^*\right)^2}{V_1} \tag{5}$$

$$\text{where} \quad V_1 = \sum_{i=1}^{n} w_i \tag{6}$$

Where

μ^* = is the weighted average or the average coverage
w_i = exactly K- covered points(%)
x_i = K- coverage (value of K)

Then, the Standard Deviation for the coverage will be the square root of the sample variance calculated in equation (5).

$$\text{Standard Deviation} = \sqrt{\sigma^2_{\text{weighted}}} \tag{7}$$

5.4 K-Coverage for Regular Hexagon Pattern Unit Cell

Fig (4) shows the unit hexagon cell for Regular Hexagon deployment pattern. In the regular hexagon cell, sensor nodes are placed at the vertices of the hexagon and their sensing range forms the intersected regions within the cell giving the k-coverage. As it is assumed that the sensing range, R_{sense} is equal to the edge length of a cell, a regular hexagon grid cell has exact 2-coverage, 3-coverage and 6-coverage regions.

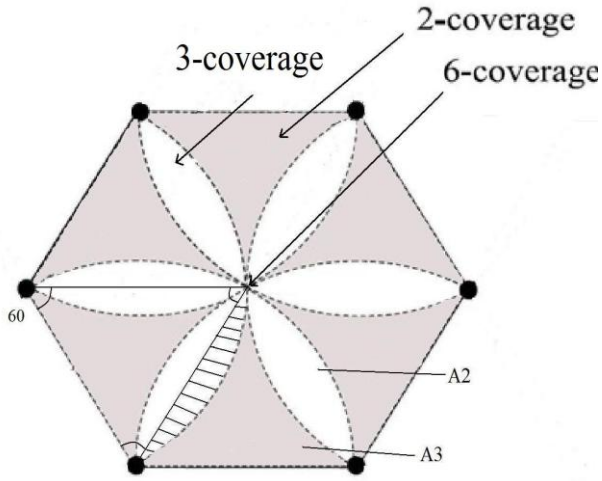

Fig (4) Regular Hexagon Cell K-coverage map

To compute the total area of exact k-coverage of a Regular Hexagon grid cell, we firstly need to find out the individual areas A2 and A3 shown in the fig (4).

Starting with the intersection area between two circles if the circumference of one circle passes through the origin of the other circle and vice versa,

$$A1 = [\ (4\pi - 3\sqrt{3}) / 6\ ] * (\ R_{sense}\ )^2 \tag{8}$$

Now, we know that internal angles in an equilateral triangle is of 60^0 , so area of sector with 60^0 angle is,

$$S = (60/360)\pi(R_{sense})^2 \tag{9}$$

Also, area of an equilateral triangle is,

$$T = \sqrt{3}/4*(R_{sense})^2 \tag{10}$$

Thus, the 3-coverage area i.e. A2 will be,

$$A2 = 2* (S - T) \tag{11}$$

Also, the 2-coverage area i.e. A3 will be,

$$A3 = (0.5*A1 - 2*A2) \quad (12)$$

The total 3-coverage will be six times of A2 and total 2-coverage will be six times of A3. The exact 6-coverage area, in which a single point is available for each regular hexagon cell is assumed to be zero (0) in a perfect Regular Hexagon deployment pattern.

5.5 K-Coverage for Octagon-Square Pattern Unit Cell

The octagon-square cell is illustrated in fig (5) which is a combination of a octagon and four squares. In a octagon-square unit cell, sensor nodes are placed on the vertices of the cell with symmetrical edge length corresponding to the sensing radius R_{sense}.

Inside an octagon, there are four possible coverage: 0-, 1-,2-,3-coverage and in each square there are 2-,3- and 4-coverage. Total areas of exact k-coverage for a Octagon-Square cell can be calculated by individually considering the 0-, 1-, 2-, 3- and 4-coverage areas.

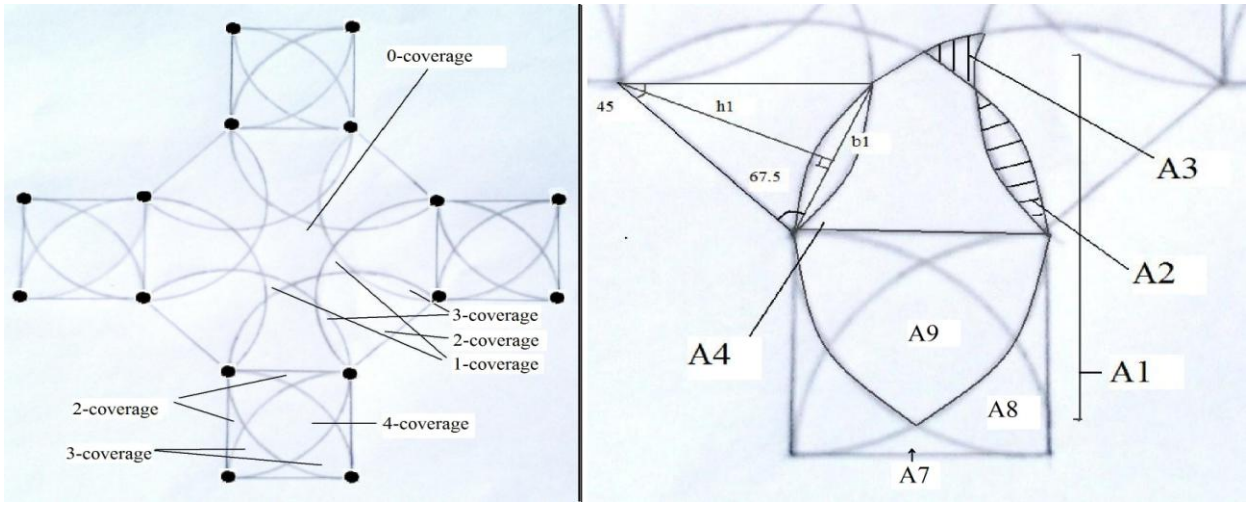

Fig (5) Octagon-Square cell k-coverage map

$$Oct = 2* (1+\sqrt{2})*(R_{sense})^2 \quad (13)$$

$$A1 = [(4\pi - 3\sqrt{3}) / 6] * (R_{sense})^2 \quad (14)$$

Equation (13) gives the area of a regular octagon and equation (14) gives the intersection area between two circles if the circumference of one circle passes through the origin of the other circle and vice versa.

According to fig (5), the area of sector with angle of 45^o and the area of triangular region within it will be as follows,

$$S = (45/360)\pi*(R_{sense})^2 \quad (15)$$

$$T = (R_{sense} * h1) / 2 \quad (16)$$

Where 'h1' is the height of the triangular region based on base length of triangle say 'b1' which can derived through equation (17) and (18).

$$h1 = \sqrt{(b1)^2 - (R_{sense}^2 / 4)} \quad (17)$$

$$b1 = 2* (\cos(67.5)*R_{sense}) \quad (18)$$

So, the 3-coverage and the 2-coverage i.e. A2 and A4 can be derived with equation (19) and (20) respectively.

$$A2 = 2 * (S - T) \quad (19)$$

$$A4 = (0.5*A1 - 2*A2) \quad (20)$$

The internal angle of a regular octagon is 135^o which gives the area of a sector of circle with angle of 135^o.

$$S1 = (135/360)\ \pi\ (R_{sense})^2 \quad (21)$$

Thus, the 1-coverage area A3 will be using equation (14),(19) and (21),

$$A3 = S1 - A1 + A2 \quad (22)$$

For the square part of the cell, the area between two circles, $x^2 + (y - r)^2 = r^2$ and $(x - r)^2 + y^2 = r^2$ is calculated.

$$A5 = (\pi - 2) / 2*(R_{sense})^2 \quad (23)$$

Now, we compute the area of the combination of 2- and 3-coverage, which is the difference of a quarter circle area and a half of area A1.

$$A6 = [(\pi R_{sense}^2 / 4) - 0.5A1] \quad (24)$$

Next the equation (25) is used to calculate the 2-coverage area near the border line of the square part of the cell.

$$A7 = [R_{sense}^2 - (\pi\ R_{sense}^2 / 4)] - A6 \quad (25)$$

Knowing A6 and A7 from equation (24) and (25), we calculate A8, which is one of the exact 3-coverage areas in equation (26).

$$A8 = A6 - A7 \quad (26)$$

The exact 4-coverage area is computed by using Equations (23) and (26) by the difference of A5 and two times A8.

$$A9 = A5 - 2*A8 \quad (27)$$

Thus, the total 0-,1-, 2-, 3- and 4-coverage in the Octagon-Square unit cell can be viewed from equation (28) to (32) using above equations respectively.

$$0\text{-coverage} = Oct - 8*(A2+A3+A4) \quad (28)$$
$$1\text{-coverage} = 8*A3 \quad (29)$$
$$2\text{-coverage} = (16*A7+8*A4) \quad (30)$$
$$3\text{-coverage} = (16*A8+8*A2) \quad (31)$$
$$4\text{-coverage} = 4*A9 \quad (32)$$

5.5 K-Coverage for Tri-Beehive Pattern Unit Cell

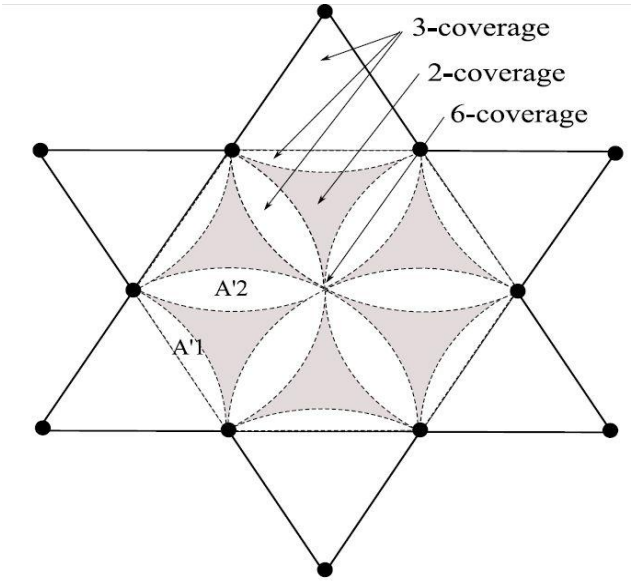

Fig (6) Tri-Beehive cell k-coverage map

The Tri-Beehive deployment cell is illustrated in fig (6), which is the combination of six equilateral triangles and one regular hexagon. Total areas of exact k-coverage for a Tri-Beehive cell can be calculated by individually considering the 2-, 3- and 6 coverage areas.

For the K-coverage, we have the areas of the regular hexagon and an equilateral triangle with edge length R_{sense} in equation (33) and (34).

$$A_h = [(3\sqrt{3} / 2) * R_{sense}^2] \quad (33)$$
$$A_t = [(\sqrt{3} / 4) * R_{sense}^2] \quad (34)$$

Now, we need to compute the difference between one-sixth area of a circle having the radius R_{sense} and A_t , which occupies the exact 3-coverage from the corner nodes of the equilateral triangle in fig (6).

$$A1' = [(\pi Rsense^2 / 6) - A_t] \quad (35)$$

Therefore, one of the exact 3-coverage area within a regular hexagon from fig (6) has the area twice of the value of A1'.

Thus,

$$A2' = [2 * A1'] \quad (36)$$

Now, the total area of the exact 3-coverage and 2-coverage within the Tri-Beehive symmetric tessellation cell will be,

3-coverage: $A3' = [9 * A2'] + 6 * A_t$ (37)

2-coverage: $A4' = [A_h - (A' + €)]$ (38)

The term '€' in equation (38) refers towards the exact 6-coverage area point for each regular hexagon (€ = zero(0) in a perfect Tri-Beehive pattern).

VI. RESULTS

In all of the three deployment patterns undertaken, a single unit cell is sufficient for the whole network coverage analysis since three of them are symmetrical in nature according to our basic assumptions. For evaluating the deployment strategies on the basis of their coverage capacity, we have assumed to have number of sensor nodes 'n' = 500 and 'R' = 150 as the radius of the circular field.

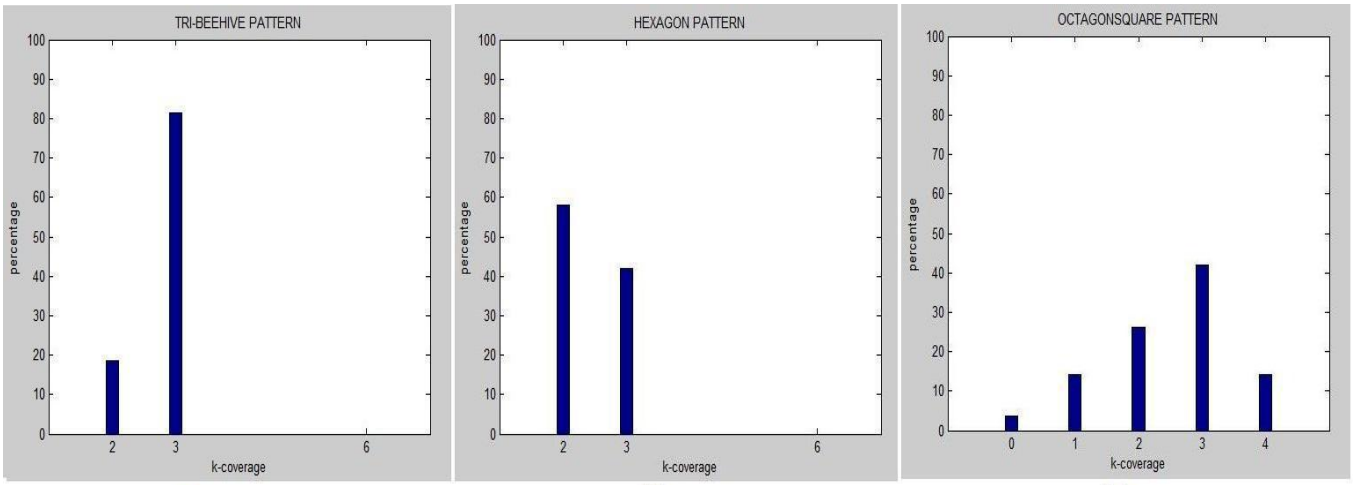

Fig (7) The K-coverage of :(a) Tri-beehive (b) Regular Hexagon (c) Octagon-Square deployments

The frequency bar graph of the exactly k-covered points of a Tri-Beehive deployment unit cell is shown in fig (7)(a) between the percentage of the coverage achieved and the value of k in k-coverage. The sensing radius , R_{sense} used for Tri-Beehive unit cell is 10 m on the basis of the equations described in 4.1. Almost two-third of the network are covered by 3-coverage whereas the rest is the exactly 2- coverage points. A negligibly small percentage of the network is 6-covered.The Tri-Beehive node deployment pattern has an average 2.81- coverage with standard deviation of 0.38.

Next is the frequency bar graph drawn for the Regular Hexagon node deployment pattern unit cell in fig (7)(b). The sensing radius, R_{sense} for regular hexagon unit cell as derived from equations formed in section 2.1 is 13m. About 60% percent of the area is within 2- coverage. The Regular Hexagon node deployment pattern has an average 2.42- coverage with standard deviation of 0.49.

The frequency bar graph between k-coverage and percentage for the Octagon-Square node deployment pattern unit cell is shown in fig (7) (c).The sensing radius, R_{sense} for octagon-square unit cell is 8m based on section 3.1. Most of the area comes under the 3- coverage. With a variation of different k-coverage, octagon-Square node deployment pattern has an average 2.49- coverage and a standard deviation of 1.02.

VII. CONCLUSION

A Wireless Sensor Network (WSN) can be composed of homogeneous or heterogeneous sensor nodes also termed as motes, which adapts the same or different coordination, sensing and computation abilities, respectively. The conclusion of this work points towards the Tri-Beehive node deployment pattern as a better option for Wireless Sensor Networks (WSN) in the sense of coverage performance evaluation, as its average coverage is better than the other two strategies.

REFERENCES

[1] http://en.wikipedia.org/wiki/Wireless_Sensor_network.
[2] http://www.google.co.in/url?q=http://classes.soe.ucsc.edu/cmpe080u/Winter08/sensonetwork.pdf
[3] Wint Yi Poe, Jens B. Schmitt, 'Node Deployment in Large Wireless Sensor Networks: Coverage, Energy Consumption, and Worst-Case Delay' AINTEC'09, November 18–20, 2009.
[4] Kumar, S., Lai, T. H., and Balogh, J. On k-Coverage in a Mostly Sleeping Sensor Network. In Proceedings of the 10th Annual International Conference on Mobile Computing and Networking (MobiCom04) (New York, NY, USA, 2004), ACM, pp. 144–158.
[5] K. Akkaya and M. Younis, "A Survey of Routing Protocols in Wireless Sensor Networks," in the Elsevier Ad Hoc Network Journal, Vol. 3/3 pp. 325-349, 2005.
[6] Hairong Qi, Yingyue Xu, Xiaoling Wang, "Mobile-Agent-Based Collaborative Signal and Information Processing in Sensor Networks," in Proceeding of the IEEE, Vol. 91, NO. 8, pp.1172-1183, Aug. 2003
[7] Karl, H., and Wittig, A. Protocols and Architectures for Wireless Sensor Networks. Wiley, 2005.
[8] http://my.safaribooksonline.com/book/electrical engineering/communications engineering/9781615207015/ Introduction-and-general-issues/ch002

International Journal of Modern Engineering Research (IJMER)
www.ijmer.com Vol.3, Issue.2, March-April. 2013 pp-962-969 ISSN: 2249-6645

A Solar Desalination System Using Humidification-Dehumidification Process- A Review of Recent Research

Y.B.Karhe, [1] Dr. P.V.Walke[2]
[1]*Student IV Semester, M. Tech. Heat Power Engineering, G.H.Raisoni College of Engineering, Nagpur, India*
[2]*Professor, Mechanical Engineering Departments, G.H.Raisoni College of Engineering, Nagpur, India*

Abstract: *Desalination involves any process in which dissolved minerals are removed from saline or brackish water. The paper evaluates the characteristics for several layouts for the humidification dehumidification desalination process. It gives bird-eye view to Humidification-Dehumidification (HDH) process by comparing various authors' works. Necessary schematic figures, graphs between affecting operational and environmental parameters and tables are reviewed. Particular attention was given to all vital components in the system. It is concluded that HDH technology has great promise for decentralized small-scale water production applications, although additional research and development is needed for improving system efficiency and reducing capital cost.*

Keywords: *Humidification-Dehumidification (HDH), Desalination, Double Glazing, Heat Exchanger, Closed Water Open Air System (CWOA), Conventional desalination system, solar air heater.*

I. Introduction

There are two main challenges for the world in the future, shortage of energy and shortage of fresh water, both play a crucial role in the overall economic development of any country [19].Conventional desalination technologies are usually large-scale, technology intensive systems is most suitable for the energy rich and economically advanced regions of the world. They also cause environmental hazards because they are fossil-fuel driven and also because of the problem of brine disposal. In the following sections these conventional desalination technologies are introduced and their drawbacks are discussed .These heaters can amount to over 40% of the total cost of a humidification-dehumidification system and so the development of a cost effective and efficient solar collector is essential to the system's overall feasibility [1].

II. Conventional Desalination Technologies

Desalination processes.
Phase-change processes
1. Multi-stage flash (MSF)
2. Multiple effect distillation (MED)
3. Vapor compression (VC)
Membrane processes
1. Reverse osmosis (RO)
2. Electrodialysis (ED)

Multi Stage Flash (MSF):

Pressurized seawater [2, 8] flows through closed pipes where it exchanges heat, with vapour condensing in the upper sections of the flash chambers. Water is then heated to a certain initial high temperature, using burnt fuel or external steam, and this allows flashing along the lower part of the chambers, from chamber to chamber under reduced pressure conditions. Vapour generated is allowed to flow through a mist eliminator to meet the condensing tubes, where heat is transferred to the heating feed seawater. The condensate drips into collectors and is pumped out as the plant product. Exhausted brine, concentrated in salt, is pumped out and rejected to the sea. Part of the brine is recirculating with the feed in order to increase water recovery.

Multi-effect Distillation (MED):

Basically, the method [2, 17] can use low temperature, low-pressure steam as the main energy source. Steam from burnt coal or fuel can be used, as well as spent steam emerging at the outlet of a steam-operated power station. The primary steam is used to evaporate heated seawater and to generate more steam at a lower pressure, while the primary steam condensate is taken back to the generation chamber, or to the steam generator of the power station. The secondary steam generated goes into a second stage to condense while transferring the latent heat to low temperature seawater, flowing in falling film. The process is repeated as many times as the design permits, between the upper possible temperature and the lower possible cooling temperature, which depends on seawater temperature. The condensate is accumulated stage wise as the product water. A vacuum pump takes the remaining vapour after the last condensation stage, to maintain the gradual pressure gradient inside the vessel.

Vapour Compression (VC):

VC [2] operates mainly at a small scale, on small locations. The main mechanism is similar to MED except that it is based on compression of the vapour generated by evaporating water to a higher pressure, which allows reuse of the vapour for supplying heat for the evaporating process. Compression of the vapour may be carried out by using a mechanical compressor (the most common way), or by mixing with small amounts of high-pressure steam (Thermal Compression). Feed water is preheated against brine and the product leaving the system. Heat transfer usually takes place in the form of a double falling film, which is an effective heat transfer mechanism. The latent heat of the condensing vapour is used to make more vapours on the other side of the heat transfer surface, basically a "heat pump" process, so that the main need for energy is for elevating the pressure to provide the driving force by temperature difference. The process takes place usually from one to three stages, thus the operating temperature may be chosen for the best optimization of the process. No external heat is needed for the mechanical compressor, so basically the technique relies on the electric power supply. Part of the water circulates to increase the water recovery.

Reverse Osmosis (RO):

Osmosis [17] is the movement of a solvent through a semi-permeable membrane into a solution of higher solute concentration. This action tends to equalize the concentrations of solute on the two sides of the membrane. The reverse osmosis process uses pressure as the driving force to overcome the osmotic pressure of the salt solution. A reverse osmosis plant consists of four major systems: Pre-treatment system, High-pressure pumps, Membrane systems and Post-treatment.

Mechanism: Pre-treatment is very important because membrane surfaces need to remain clean. All suspended solids must be removed, microbial bacterial must be removed, and processes include coagulation/flocculation/sedimentation. High-pressure pumps supply pressure from about 150 psi for brackish water to 800-1,000psi for seawater. Membrane materials consist of cellulose acetate or of other composite polymers. Pressure applied to feed water causes clean water to permeate across membrane into central colleting tube. Salts are rejected from the membrane and separation is complete. Post-treatment consists of stabilizing the water by adjusting the pH and disinfection.

Benefits: Continuously operating process, 24 hours a day. New membranes have high rate of water flow per unit area (flux). It is having high overall water recovery rates, salt removal, up to 99.8% low power consumption. Development of energy recovery devices (turbines)is possible. Minimal cleaning is required, longer service.

Limitations: Pesticides, herbicides, and chlorine are molecularly smaller than water and can pass through membrane if not pre-treated correctly. There will be chances of removal of healthy, naturally occurring minerals in water. Wastes a portion of the water that runs through its system. Slower process than other water treatment alternatives.

Electrodialysis:

A voltage is used to move salts through a membrane, leaving fresh water behind. Electro dialysis depends on some general principles; most salts dissolved in water are ionic, meaning they contain a positive (cat-ion) or negative (anion) charge. These ions are attracted to electrodes with an opposite electric charge. Semi-permeable membranes allow selective passage of either an anion or a cat-ion but not both.

Mechanism: Electrodes connected to battery are placed in container of saline water. As electrical current is applied through the solution, the ions (Na^+, Cl^-, Ca^{2+}, Carbonate $^{2-}$) migrate to the electrode of opposite charge. Anions (Cl^-, Carbonate $^{2-}$) travel opposite of current and pass through an anion semi-permeable membrane. Once through this their path is blocked by a cat-ion semi-permeable membrane and is trapped. The same event happens to the cat-ions, (Na^+, Ca^{2+}) which pass through a cat-ion semi-permeable membrane and are trapped by an anion semi-permeable membrane. The result is two flows of fresh water and three flows of concentrated brine are formed.

Benefits: Automatic operation of the plant, requiring very little maintenance and supervision, except for membrane replacement. It is very effective process for removing and purifying salt concentrate. Applications in many commercial industries, tartaric wine stabilization, de-acidification of fruit juices etc.

Limitations: Pre-treatment is required to prevent materials, which could harm or clog membranes. Works most efficient in low-salinity applications brackish water desalination. Distillation plants produce water that ranges from 1.0 to 50 ppm total dissolved solids (TDS), while reverse osmosis plants produce water that ranges from 10 to 500 ppm TDS. Household RO units typically deliver small amounts (2 to 10 gallons per day) of treated water and waste 3 to 20 times the amount of water treated. RO units use a lot of water. They recover only 5 to 15 % of the water entering the system. The remainder is discharged as wastewater.

Conclusions of Conventional Desalination System:

All configurations i.e. cooling, compression, condensation, or any other form of air drying will result in processing of the large air stream together with the water vapour product. As a result, the process efficiency is drastically reduced. Also, the required size of a condenser or other drying units will be large. Further evaluation of these configurations is necessary to optimize the unit product cost and to minimize the equipment. This would require detailed design of some special equipment such as the desiccant heat exchanger, the absorber, and regeneration units.

III. Review of Humidification-Dehumidification (HDH) Systems

Humidification-dehumidification desalination is a thermal desalination cycle that operates similar to the natural water cycle, where water is evaporated from the oceans by the sun and condenses into fresh water precipitation, which returns to earth and can be used for drinking. This basic principle is behind the operation of a solar still, where the sun evaporates seawater and the vapor condenses on the cooler glazing of the still where it can be recovered for drinking. However, in the process of condensation all the latent heat of evaporation of the water is lost to the environment, leading to poor thermal performance. The HDH cycle improves on this principle by separating the evaporation and condensation processes into different devices thereby recovering the latent heat of evaporation and using it to heat the seawater.

HDH systems are classified under three broad categories. One is based on the form of energy used such as solar, thermal, geothermal, or hybrid systems. This classification brings out the most promising merit of the HDH concept: the promise of water production by use of low-grade energy, especially from renewable resources. The second classification of HDH processes is based on the cycle configuration (Fig. 1). As the name suggests, a closed-water open air (CWOA) cycle is one in which the air is heated, humidified and partially dehumidified and let out in an open cycle as opposed to a closed-air cycle wherein the air is circulated in a closed loop between the humidifier and the dehumidifier. The air in these systems can be circulated by either natural convection or mechanical blowers. The third classification of the HDH systems is based on the type of heating used: water- or air-heating systems. The performance of the system depends greatly on whether the air or water is heated.

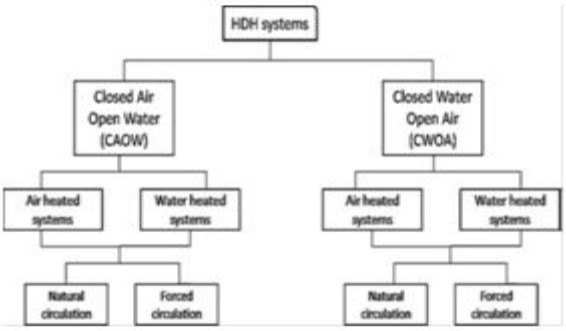

Figure.1 Classification of typical HDH processes (based on cycle configuration).

Y.J. Dai et al [3] has performed on water heated closed water open air (CWOA) system havingunit features like honeycomb wall humidifier, forced air circulation; the condenser is a fin-tube type. Main observations are large pressure losses can be avoided, condensation heat is recovered efficiently, other low-grade heat resources such as waste heat, gas/oil/coal burning, etc, can also be efficiently utilized. Guofeng Yuan et.al [4] work on water heated CWOA system having unit features of honeycomb paper used in humidifier, forced convention for the air circulation, condenser is fin tube type. Main observations are performance strongly dependent on temperature of inlet salt water to the humidifier, the mass flow rate of salt water, and the mass flow rate of the process air, the authors report that there is an optimal air velocity for a given top temperature of water. CemilYamali et al. [5] has performed on water heated CWOA having a single stage double-pass flat-plate solar collector heats the water, a pad humidifier is used and the dehumidifier used is a finned tube heat exchanger also a tubular solar water heater was used for some cases. It was observed that the plant produced 4 kg/day maximum, increase in air flow rate had no effect on performance, and an increase in mass flow rate of water increased the productivity. nil Kr Tiwari [6] was worked by using double-pass flat plate solar air heater with two glass covers, mathematical modeling & observed that the productivity of the proposed system increases up to 10% & air mass flow rate should have optimum value. Orfi et al [7] used combined air heated (open or closed one) and water heated solar heater, evaporator, the condenser contains two rows of long cylinders made of copper in which the feed water flows. Longitudinal fins are soldered to outer cylinder. Both theoretical & experimental study was made on the system. The theoretical results show that there exists an optimum mass flow rate corresponding to a maximum fresh water product.

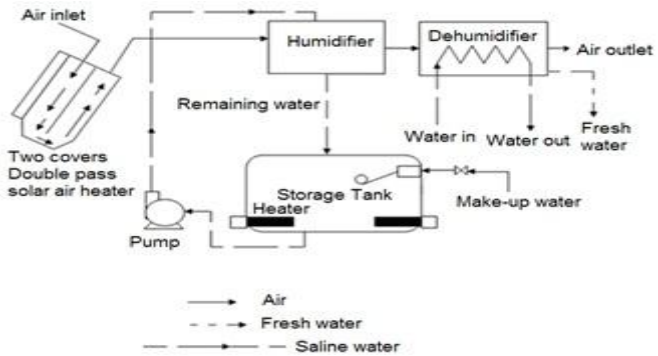

Figure.2 Schematic of humidification-dehumidification desalination process

Procedure starting from air intake into solar air heater to final product fresh water is described by schematic of desalination system as shown in Figure 2. It essentially consists of a tilted, two-pass solar air heater with two glass covers, a humidifier, a dehumidifier and a storage tank. In this system, air alone is heated in a solar air heater. The system is composed of three main fluid-circulation lines identified in Fig. 2 as saline water, air/vapor, and freshwater. The saline water which is circulated in the humidifier is in contact with a continuous flow of ambient air already heated in a solar collector. Then, air is cooled and humidified as it passes upward through the falling saline water in the humidifier. The humidified air is passed through a dehumidifier where it is cooled using cooling water stream in the condenser. The partially dehumidified air leaves the unit, while the distillate (condensate) is collected as fresh water. The saline water leaving the humidifier is collected in a storage tank and recirculates to the humidifier. In this study, air is heated by using a tilted two-pass solar air heater whereas water is only heated by bringing it to contact with air in the humidifier and a inside the storage tank so that a constant temperature in the storage tank is accordingly maintained. The effect of the air temperature on the system productivity is examined at different values of air mass flow rates.Nafey et al. [9] uses system which is unique in that it uses a dual heating scheme with separate heaters for both air and water. Humidifier is a packed bed type with canvas as the packing material. Air cooled dehumidifier is used and hence there is no latent heat recovery in this system. The authors reported a maximum production of 1.2 L/h and about 9 L/day. Higher air mass flow gave less productivity because increasing air flow reduced the inlet temperature to humidifier.Chafik et al [12] work with solar collectors (four-fold-web-plate, or FFWP, design) of 2.08 m^2area heat air to 50^0 –80^0C, multi-stage system, pad humidifier with corrugated cellulose material, 3 separate heat recovery stages & forced circulation of air. The solar air heaters constitute 40% of the total cost. Also he observed that the system can be further improved by minimizing the pressure drop through the evaporator and the dehumidifiers.

IV. Review of Solar Air Heater

Various types of solar air heaters according to construction & there features are discussed one by one. Air flow over the absorber plate where the absorber decreases losses from the top of the absorber plate and eliminates conduction resistance through the plate. Roughened absorber plate used to improves convection heat transfer into the air. A rough configuration also increases pressure drop, but only marginally as compared with a smooth plate. Multiple passes of air through the collector improves heat gain by increasing contact with the absorber and makes the absorber run cooler, decreasing lose. Multiple glazing layers, it reduces heat loss by infrared radiation and trap an insulating air layer between the glazing. Glass and metal construction, it provides better heat transfer characteristics and better durability. All the best performing collectors used glass and metal construction, as polymer alternatives, especially for glazing's, suffer from low durability, although initially providing optical properties comparable to glass. Packing materials in the air stream improve heat transfer by mixing the air and providing more surface area to absorb radiation. Packing also provides sensible heat storage but comes at the cost of high pressure drop.

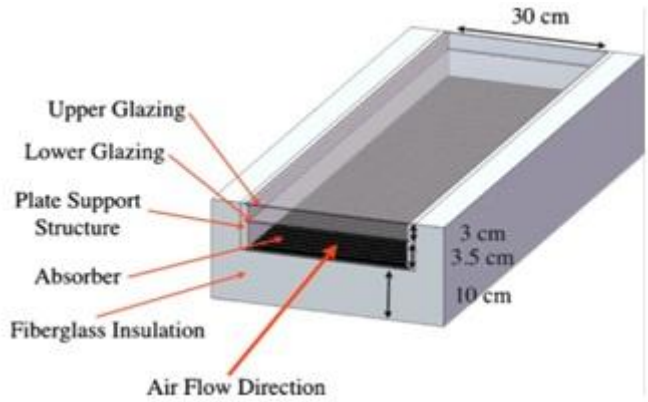

Figure.3 Double pass solar air heater

Guofeng Yuan [4] works on the72 pieces of solar air heaters with a total surface area of approximately 100 m^2. These collectors use evacuated tubes with inner pipes, which could provide higher air temperature than panel solar collectors. 72 pieces is divided into 2 subgroups containing 36 pieces/group & they are connected in parallel. Then each group is divided again into 3 sub-groups (12 pieces/sub-group), with pieces in every single sub-group connected in parallel, and sub-groups connected in parallel as to each other in order to ensure the uniformity of air distribution and reduce air flow rate in the air Trunk. Author [5, 6&11] used double-pass flat plate solar air heater (100*50*10 cm^3) as shown in Fig. 3. It consists of two glass covers having a thickness of 3 mm matt black painted 1 mm thick copper absorber plate. The container of the solar air heater that was made of iron sheets of 2 mm thickness was fabricated by welding. The solar air heater was positioned at a tilt angle of 30° facing south Productivity increases about 15% by double-pass solar air heater. A tubeless flat plate solar collector with a single glass cover is used for air heating. The Heater effective area is 0.5 m*1 m, and the absorber plate is made of copper with a thickness of 0.5 mm. The air gap between the absorber and the glass cover is 0.01 m [7-10] which could provide higher air temperature than panel solar collectors. Heat gain by air is denoted by process 3-1 in psychometric chart (Fig .8).

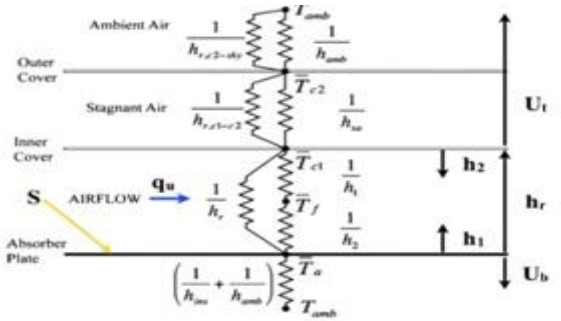

Figure.4 Heat transfer resistances with lumped parameters

When considering the design of a solar air heater Edwerd K. Summers [1] suggest two design parameters that vary based on collector design. One is the overall heat loss coefficient, U_L, which is related to the heat-transfer coefficients in the collector, and which needs to be minimized. This is given by Eq. (1) for a flat-plate air heater with air flowing over the absorber.

$U_L = [(U_t + U_b)(h_1h_2 + h_1h_r + h_2h_r) + U_bU_t(h_1 + h_2)]/ [h_1h_r + h_2U_t + h_2h_r + h_1h_2]$ Eq. 1

The second parameter is F_0, which is the useful heat gain coefficient or the ratio of actual energy gain to the energy gain that would result if the absorber plate was at the local fluid temperature. This ratio needs to be maximized to enhance efficiency. Eq. (2) gives $F_0$for the same flat-plate air heater.

$F_0 = [h_rh_1 + h_2U_t + h_2h_r + h_1h_2] / [(U_t + h_r + h_1)(U_b + h_r + h_2) – h_r^2]$ Eq. 2

To see how each parameter fits into the overall useful heat gain Eq. (3), or the overall collector governing equation, is also given. $q_u = (S – U_L(T_f – T_a))$ Eq. 3

S is the total energy that is absorbed by the absorber. U_b and U_t are the overall heat-transfer coefficients from the top and bottom of the air stream to the outside, respectively, h1 is the heat-transfer coefficient from the glazing plate to the air stream, h_2 is the heat transfer coefficient from the absorber to the air stream, and h_r is the linearised radiation heat-transfer coefficient from the absorber to the glazing.

Gained-Output-Ratio (GOR): the ratio of the latent heat of evaporation of the distillate produced to the total heat input absorbed by the solar collector(s). This parameter is, essentially, the efficiency of water production and an index of the amount of the heat recovery effected in the system. This parameter does not account for the solar collector efficiency as it just takes into account the heat obtained in the solar collector. For the HDH systems to have thermal performance comparable to MSF or MED, a GOR of at least 8 (corresponding to energy consumption rates of 300 kJ/kg) should be achieved.

Solar air heater efficiency: It is defined by $\eta = m\, c_p\, (T_{out} - T_{in})/ I_T$, Eq. 4

Where m is mass flow rate of air through the collector in kg/s; C_p is specific heat capacity of air at constant pressure in J/kg K; T_{out} outlet temperature of air, K; T_{in}-inlet temperature of air, K; I_T solar irradiation, W/m^2.Efficiency of different type of solar collector is provided in figure5.

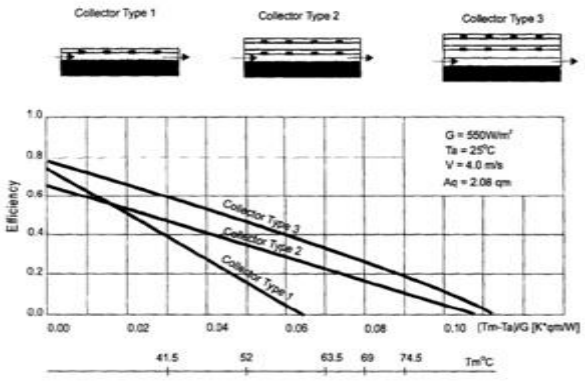

Figure.5 Efficiency of different collector types [12]. Tm, mean temperature of air in the collector, ‘C; Ta, ambient temperature, “C; G solar irradiation, W/m2; Aq, collector area, m^2; C: air velocity, m/s.

V. Review of Humidifier

Kreith [24] used spray tower which is cylindrical vessel in construction water is sprayed at the top of the vessel and air stream flowing upward (Fig.6). The diameter-to-length ratio is a very important parameter in spray tower design. Design of spray towers requires knowledge of heat and mass transfer coefficients as well as the contact surface area of the water droplets. Minimal pressure drop on the gas side considerable pressure drop on the water side due to the spray nozzles High capacity but low efficiency, the low efficiency is as a result of the low water hold-up due to the loose packing flow. Many empirical correlations and design procedures are used by various authors.

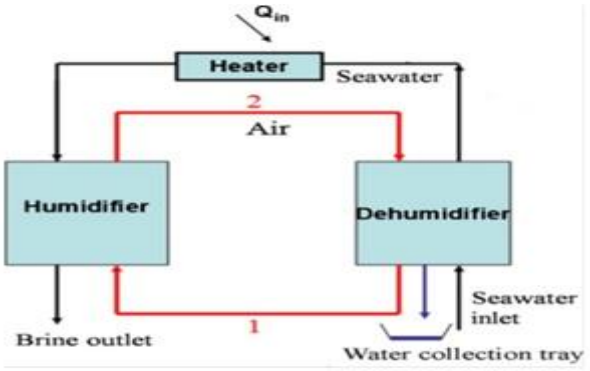

Figure.6 A typical water-heated CAOW HDH process

The most common way to express performance of the humidifier is its efficiency given by eq.5 [5] $\eta = (\omega_{out} - \omega_{in})/(\omega_{out,sat} - \omega_{in})$, where ω_{out} is outlet humidity ratio; ω_{in} is inlet humidity ratio; and $\omega_{out,sat}$ is outlet humidity ratio at saturation. During humidification specific humidity increases with small drop in temperature as given by process 1-2 in a psychometric chart (Fig. 8). El-Agouz and Abugderah [25] studied the single Bubble column exactly opposite in principle to the spray tower is the bubble column. A vessel is filled with water and air bubbles are ejected from several orifices located at the bottom of the vessel. The diffusion of water into the air bubbles depends on many parameters such as bubble diameter, bubble velocity, gas hold-up (the ratio of air bubbles-to-water volume), water and air temperatures as well as the heat and mass transfer coefficients geometrical factors such as the orifice diameter, number of orifices, water head height and column diameter influence the performance. Muller-Holst et al. [26] was worked with Wetted-wall towers in which Pipes are arranged in vertical manner water is loaded into the top of the tower. A weir distributes the flow of water around the inner perimeter of the tube that wets the inner surface of the tube down its length. Such devices have been used for theoretical studies of mass transfer. A thin film of water is formed running downward inside a vertical pipe, with air flowing either co-currently or counter currently. J. Orfi [7] in his experiment use evaporators to increase saturation point of incoming hot air. Evaporators is horizontal and has a rectangular cross section is constructed with wood. The fiber glass is used for insulation. Five parallel plates made with wood and covered with textile (cotton) are fixed in the evaporator. Tubes are placed on the vertical plates. The feed water and the air are counter current. Evaporators provide better heat and mass exchange. The horizontal surface of the evaporator is covered by the hot water. The vertical plates are wetted by capillarity and finally the water is sprayed by means of tubes with small holes set in them.

Table I: Packing material used in packed bed towers for humidification in HDH systems.

Author	Packing material
Al-Hallaj et al. [20]	Wooden surface
Nafey et al. [9]	Canvas
Yamali et al. [5]	Plastic packing
EfatChafik [12]	Corrugated cellulose material
Dai and Zhang [3,4]	Honeycomb paper

VI. Review of Dehumidifier

Dehumidifiers is heat exchanger in which heat exchange is takes places between two fluids i.e. hot and cold that are at different temperatures. The heat exchange in the heat exchanger may be in the form of latent heat or sensible heat or combination of both. Solid wall may or may not separate two fluids.
There are various types of heat exchangers (dehumidifier) which may be classified on the basis of the following

Nature of heat exchange process:

Direct contact (open): Heat exchange takes place through direct mixing of hot and cold fluids. Examples are cooling towers, jet condensers and direct contact feed heaters.

Indirect contact (surface): Regenerators- In this hot and cold fluids are flow alternately through same space alternately with no or little mixing between the streams. Examples are the regenerators are used in most of the gas to gas heat exchangers such as internal combustion engine and gas turbines. Other applications include open hearth and glass melting furnaces and air heaters of blast furnaces. Recuperators- This is the most common type of heat exchanger in which two fluids are separated by surface between them. Examples are oil coolers, intercoolers, economiser, super heaters, condensers, radiators and evaporator.

Relative Directions of Fluid Motions:

Parallel flow-In this hot and cold fluids flow in the same directions. Examples are water heaters, oil coolers etc.
Counter flow-This is the most favourable device in which hot and cold fluid flows in opposite directions.
Cross flow-Two fluids are flow in normal to each other for example automobile radiators.

Design and Construction Features:
It includes concentric tube**,** shell and tubes; multipleshellsand tube passes and compact heat exchanger.

Physical State of the Fluids:
In this category Condensers and Evaporators are present according to state of fluid.

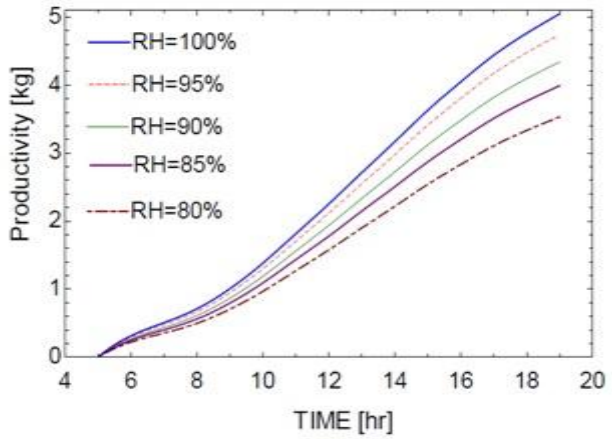

Figure.7 The effect of the relative humidity on the system productivity

The process air passes through the condenser cooled by cold seawater where water vapor condenses and turns into fresh water.The condenser of a fin-tube type one of cross sectional area 1.5*1.5 m was used by Y.J. Dia [3]. Cold seawater flows in the tube channel and fresh water is produced on condensation surface in the condenser at the same time. The effect of the relative humidity on the system productivity is given in Fig. 7. In similar study G. Yuan [4] is used two parallel fin tube heat exchanger one above other to strengthen the cooling capacity. Special feature is that humidifier and dehumidifier is composed as single equipment having no physical isolation between them. J. Orfi [7] used. The condenser consists of a chamber with a rectangular cross section. It contains two rows of long cylinders made of copper in which the feed water flows. On outer surface of it saturated water vapour flow along length, during the process (process 2-3 in Fig. 8) fresh water is recovered and thereby drop in temperature and specific humidity of air. Longitudinal fins were soldered to the outer surface of the cylinders. The condenser is characterized by an exchange surface, 1.5 m ^{2}and 28 m total length. K. Bouroni [8] used horizontal tube bundle through which the brine coolant passes in counter-current flow to the fresh water stream surrounding the tube bundle is the most used configuration. Cemil Yamali [5] worked with three-air cooler heat exchangers manufactured with copper tubes and corrugated aluminum fins were used as a dehumidifier. They were connected to each other with copper tubes in series (exit of one cooler was connected to the inlet of the other cooler). The surface area of each condenser is 3.5 m^2 (i.e., the total surface area of the dehumidifier is 10.5 m^2). In order to prevent air leakage and heat gain, dehumidifier heat exchanger was placed on an insulated metal box. It was constructed of 2 mm thick galvanized steel by welding. Its dimensions are 40 cm × 47 cm × 34 cm.

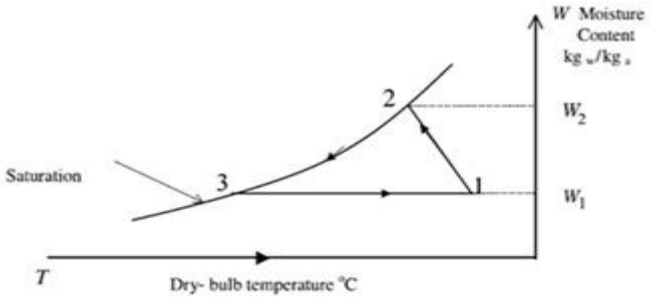

Figure.8 A typical air-heated HDH cycle on psychometric chart

Chafik [12] used seawater as a coolant wherein the water is heated by the humid air before it is pumped to the humidifiers. Three heat exchangers were used in three different condensation stages. A additional heat exchanger is added at the intake of sea water (low temperature level) for further dehumidification of air. The heat exchangers (dehumidifiers) are finned-tube type air coolers. They developed a theoretical model. The standard method as developed by McQuiston [14] considers finned-tube multi-row multi-column compact heat exchangers and predicts heat and mass transfer rates using Colburn j-factors along with flow rate, dry- and wet-bulb temperatures, fin spacing and other dimensions. The air side heat-transfer coefficient is based on log-mean temperature difference for the dry surface whereas under the condensing conditions, the moist air enthalpy difference is used as a driving potential.

VII. Conclusions

The Humidification-Dehumidification (HDH) process presents a very interesting solution for small units (hotels, rural regions, light industry, etc.), especially when new materials are used. The process is very convenient in cases where heat is available at low temperature at an attractive cost (cogeneration, solar energy, geothermal energy, etc.)[8]. From the present review it is found that among all HDH systems, the multi-effect CAOW water-heated system is the most energy efficient[14]. A collector with a double glazing, a highly roughened absorber, and a carbon black coated absorber, results in a collector efficiency of 58% at a normalized gain of 0.06 K m^2 /W [1]. It is necessary to obtain the best design and operating conditions that give the minimum product cost.

References

[1] Edward K. Summers, John H. Lienhard, Syed M. Zubair, "Air-Heating Solar Collectors for Humidification-Dehumidification Desalination Systems", DOI: 10.1115/1.4003295.
[2] HishamEttouney, "Design & Analysis of humidification dehumidification desalination process" Desalination 183(2005)341-352 received 7 feb 2005; accepted 15 march 2005.
[3] Y.J. Dai, R.Z. Wang, H.F. Zhangb "Parametric analysis to improve the performance of a solar desalination unit with humidification and dehumidification" Desalination 142 (2002) 107-l 18, Received 26 April 200 1; accepted 28 May 2001.
[4] Guofeng Yuan, Zhifeng Wang, Hongyong Li , Xing Li, "Experimental study of a solar desalination system based on humidification–dehumidification process" ,Desalination 277 (2011) 92–98.
[5] CemilYamale, Ismail Solmusf "A solar desalination system using humidification–dehumidification process: experimental study and comparison with the theoretical results" Desalination 220 (2008) 538–551, Received 14 December 2006; accepted 3 January 2007.
[6] Anil Kr Tiwari, TaranjeetSachdev, " Conceptual Analysis of Desalination System working on Humidify and Dehumidify technique using Solar Air Heater", International Conference on Mechanical and Robotics Engineering (ICMRE'2012) May 26-27, 2012 Phuket.
[7] J. Orfi, M. Laplante, H. Marmouch, N. Galanis, B. Benhamou, S. Ben Nasrallah, C.T. Nguyen, "Experimental and theoretical study of a humidification dehumidification water desalination system using solar energy", Desalination 168 (2004) 151-159, Received 16 February 2004; accepted 25 February 2004.
[8] Bourounia, M.T. Chaibib, L. Tadrist, "Water desalination by humidification and dehumidification of air: state of the art", Desalination1 37 (2001) 167-176, Received 3 November 2000; accepted 17 November 2000.
[9] A.S. Nafey , H.E.S. Fath , S.O. El-Helaby, A.M. Soliman, " Solar desalination using humidification dehumidification processes Part I. A numerical investigation", Energy Conversion and Management 45 (2004) 1243–1261, Received 20 May 2002; received in revised form 28 December 2002; accepted 2 June 2003.
[10] A.S. Nafey , H.E.S. Fath , S.O. El-Helaby, A.M. Soliman, " Solar desalination using humidification dehumidification processes Part II. An experimental investigation", Energy Conversion and Management 45 (2004) 1243–1261, Received 20 May 2002; received in revised form 28 December 2002; accepted 2 June 2003.
[11] A. A. Shabaneh, P. Gandhidasan, M. A. Antar and H. Baig "SIMULATION OF HDH DESALINATION SYSTEM USING TILTED, TWO-PASS SOLAR AIR HEATER" Fifteenth International Water Technology Conference, IWTC 15 2011, Alexandria, Egypt
[12] EfatChafik, "A new seawater desalination process using solar energy", Desalination 153 (2002) 25-37, Received 15 April 2002; accepted 30 April 2002.
[13] Adel M. Abdel Dayem, "Pioneer Solar Water Desalination System: Experimental Testing and Numerical Simulation", ENERGY SCIENCE AND TECHNOLOGY Vol. 1, No. 1, 2011 PP. 33-48, ISSN 1923-8460 [PRINT], ISSN 1923-8479 [ONLINE].
[14] G. Prakash Narayan, Mostafa H. Sharqawy, Edward K. Summers, John H. Lienhard, Syed M. Zubair, M.A. Antar, "The potential of solar-driven humidification–dehumidification desalination for small-scale decentralized water production", Renewable and Sustainable Energy Reviews 14 (2010) 1187–1201.
[15] Mohammad Zamen, Seyyed Mehdi Soufar, MajidAmidpour, "Improvement of Solar Humidification-Dehumidification Desalination Using Multi-Stage Process"
[16] M. Zamena, M. Amidpourb, S.M. Soufaria, "Cost optimization of a solar humidification–dehumidification desalination unit using mathematical programming", Desalination 239 (2009) 92–99, Received 30 July 2007; Accepted 10 March 2008.
[17] Hassan E.S. Fath, Ahmad Ghazy, " Solar desalination using humidification dehumidification technology", Desalination 142 (2002) 119-133, Received 2 March 2001; accepted 28 August 2001.
[18] A.M.I. Mohamed, N.A. El-Minshawy, "Theoretical investigation of solar humidification–dehumidification desalination system using parabolic trough concentrators", Received 8 June 2010 Accepted 24 April 2011 Available online 1 June 2011.
[19] United Nations, Water for People, Water for Life — UN World Water Development Report, Unesco Publishing, Paris, 2003.
[20] Said Al-Hallaj, Sandeep Parekh, M.M. Farid, J.R. Selman, "Solar desalination with humidification–dehumidification cycle: review of economics", Desalination 195 (2006) 169–186.
[21] M. Vlachogiannis, V. Bontozoglou, C. GeorgalasandG.Litinas, "Desalinationbymechanical compression of humid air". Desalination, 122 (1999) 35–42.
[22] H.T. El-Desscutey and H.M.Ettovney, "Fundamentals of Salt Water Desalination", Elsevier, ISBN: 0–444–50810–4, February 2002.
[23] Khedr M. Techno-"Economic Investigation of an Air humidification–dehumidification DesalinationProcess." Chemical Engineering Technology 1993; 16: 270–4
[24] Kreith F, Bohem RF. Direct-contact heat transfer. Washington: Hemisphere Pub. Corp.; 1988.
[25] El-Agouz SA, Abugderah M. Experimental analysis of humidification process by air passing through seawater. Energy Conversion and Management 2008; 49(12):3698–703.
[26] Mu¨ ller-Holst H. Solar thermal desalination using the multiple effect humidification (MEH) method. In: Book chapter, solar desalination for the 21st century; 2007. pp. 215–25. Measurement 45 (2012) 1807–1813.

International Journal of Modern Engineering Research (IJMER)
www.ijmer.com Vol.3, Issue.2, March-April. 2013 pp-970-979 ISSN: 2249-6645

Hybrid Polymer Matrix Composites for Biomedical Applications

Dr. Mohammed Haneef, [1] Dr. J. Fazlur Rahman, [2] Dr. Mohammed Yunus, [3]
Mr. Syed Zameer, [4] Mr. Shanawaz patil, [5] Prof.Tajuddin Yezdani[6]

[1]*Principal, Department of Mechanical Engineering Ghousia College Engineering, Ramanagara, Karnataka State, India*
[2]*Professor Emeritus, Department of Mechanical Engineering, H.K.B.K. C.E., Bangalore, Karnataka State, India*
[3]*Professor Lecturer Department of Mechanical Engineering H.K.B.K.C.E., Bangalore, Karnataka State, India*
[4]*Assistant Professor Department of Mechanical Engineering Ghousia College Engineering, Ramanagara, Karnataka State, India*

***Abstract*:** *Bones and joints in human body made of a natural composite material are fractured due to excessive loads and impact stress. The various types of bone fractures which occur in human body depend upon crack size orientation, morphology and its location. In general, the mean load on the hip joint is expected up to three to five times of the body weight during jumping, jogging etc. .These loads are fluctuating depending on the activities such as standing, sitting, jogging, climbing the staircase etc. The material of prosthesis and the durability of alternate bone material is of critical importance, because it largely determines how load is transferred through the stem. In the geometry and design of the material, the young's modulus of a material is critical design variable.*

The polymeric biocomposites reasons, why they are becoming most common composites, include their low cost, high strength and simple in manufacturing principles by molding process. But they suffer from poor mechanical properties like higher wear rate, lower hardness and Young's modulus.

An attempt has been made to develop hybrid bio polymer matrix composites using high density poly ethylene as the matrix material with Titanium Oxide (TiO_2) particles and Alumina (Al_2O_3) particles as the reinforcement material with varying parcentage using extrudal injection moulding machine. The different testing namely, tensile, hardness, flexural strength, density, fractography, corrosion and wear test were conducted on the standard samples prepared. It is found an appreciable improvements in the mechanical and tribological properties of the hybrid polymer matrix composite, which can be used for variety of applications in thehuman body bone replacement. In this case, their application in orthopaedic as implantable material in the bone surgery has been considered and studied. These composite materials have found wide use in orthopaedic applications, particularly in bone fixation plates, hip joint replacement, bone cement and bone graft.

Keywords: *A Polymer Matrix Composite, polyeuthylene+ Titanium Oxide (TiO_2) particles + Alumina (Al_2O_3), Orthopaedic applications.*

I. INTRODUCTION

Bone, which is a natural composite material, consists mainly of collagen fibers and an inorganic bone mineral matrix in the form of small crystal called apatite. Collagen is the main fibrous protein, the composite of mineral component in the body. Cartiligen is a collagen based tissue which contains large protein saccharit molecules that form a gel in which collagen fibrous are bonded [1]. Articular cartillery forms the baring surfaces of the moveable joints of the body which behaves linear visco elastic. It has also very low coefficient of friction (μ) largely attributed to the presence of senovial fluid that can be squeezed upon compressive loading [5].

Bone replacement materials are required for variety of reasons [11]. They may require when section of bone is missing and the gap needs to be filled. There are several options for the types of bone replacement.

1) Allograft: means material from another patient.
2) Autograft: It means using material of a person from different site.

Synthetic materials are gradually becoming more popular. Hydroxy apatite is prepared easily, but it is ceramic, which is too brittle to be used on its own for large scale applications. Copmosites of a hydroxy apatite with degradable polymers can also be used which allows bone to regrow and fill the same. Bio materials both natural and synthetic materials are used to replace part of a living system. This group of materials include metals (such as stainless steel, titanium alloy) and ceramics (such as alumina and toughened Zirconia) known for high strength, ductility and resistance to wear, but metals exhibit low bio compatibility, corrosion and high stiffnees compared to tissues and also metal ions which cause allergic reactions. Ceramics are known for their good bio compatibilty, corrosion resistance but main drawback is brittleness, low fracture strength, difficult to fabricate and low mechanical properties and high density. But polymer composite bio-materials provide better alternative choice for replacing because of bio-compatibility, corrosion resistant and easy to fabricate etc. Composite materials are having the advantages of high specific modulus and strength to weight ratio besides, they have superior toughness to prevent crack propagation.

Metal matrix and Fiber reinforced composite materials have been used these days due to their durability, less weight and better compatibility. The basic requirements for human joints include mechanical property (yield stress, plasticity, Young's Modulus, Fatigue strength), Physical properties (density, magnetic properties etc.), chemical properties (resistance

to different forms of corrosion and wear degradation), biological property (bio –compatibility) and lesser cost [1]. The following polymer composite bio- materials are used for various bio medical applications.

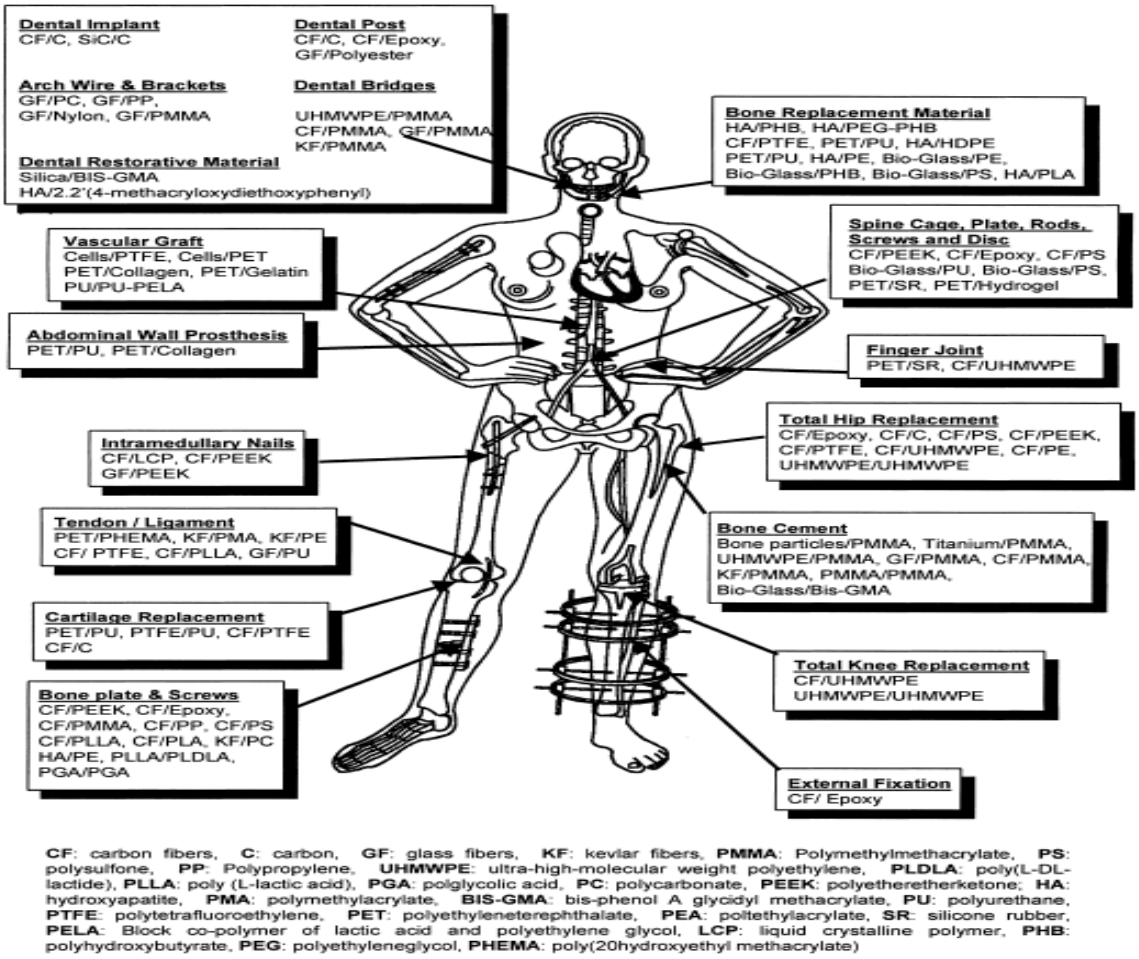

Fig.1. Application of different composites in different parts of body

1) Total knee replacement: polyethylene, carbon fibers and ultra molecular weight polyethylene.
2) Total hip replacement: carbon fibres-Epoxy carbon fiber- Polysulphone, polyeyhylene carbon fibers etc.
3) Finger joint: ultra high molecular weight polyethylene, poly sulphone etc.,
4) Bone cement: Titanium, carbon fibers- ultra high molecular weight polyethylene, Kevlar fibers/ poly tetra fluoroethylene (PTFE) etc.,
5) Dental implant: Carbon fibers/ carbon, Silicon carbide (SiC)/ Carbon.
6) Bone plates and screws: Polyethylene/ hydroxy apatite, carbon fiber/ epoxy, Kevlar fiber/ poly carbonate etc.
7) Cartilage replacement: Carbon fibers/ PTFE, Polyeurethane.

At present steel, titanium and titanium based alloys are being widely used for the bone replacement of materials and also different ceramic materials like hydroxyl apatite, Alumina, Zirconia are widely researched materials for implant applications and they are commercially produced despite of their high cost. Different bio-compatible polyethylene (PE) and poly ehterther ketone (PEEK) based materials are being used as low loading bearing application for bone and other bio medical applications for having good bio-compatibility.

From the literature survey, it is found that, most of the research was carried out with respect to bio-compatible materials using stainless steel 316L, Ti-6AL-4V alloy, Co-Cr alloy, hydroxyl apatite (HAP), ultra high molecular weight polyethylene (UHMWPE), Alumina (Al_2O_3), Titanium oxide (TiO_2), Silicon carbide (Sic) etc. as the replacement material for various types of bone fractures like knee joint, hip joint, ankle joint and also for dental applications[18].

II. METHODOLOGY

This paper highlights about the study of basic properties required to replace bone materials for various types of bones and joints fractured by the synthesis of bio-compatible, hybrid polymer matrix composites.

Polymer matrix composite is the material consisting of polymer (resin) as matrix combined with a fibrous reinforcing dispersed phase. Polymers make ideal matrix material, they can be processed i.e. fabricated more easily, with light weight and offer desirable mechanical properties. The reasons for the selection of these composites are low cost, high strength and simple manufacturing principles.

The various mechanical properties of typical polymeric bio-materials are shown in the table.1.

Table1. Material Properties

Material	Modulus (GPa)	Tensile Strength (MPa)
Metal alloys		
Stainless steel	190	586
Co-Cr alloy	210	1085
Ti alloy	116	965
Amalgam	30	58

The some of the commonly used areas of these biomaterials are joint replacements, total hip replacements, bone plate and bone cement, dental implants for tooth fixation, heart valves, contact lenses, vascular grafts, dialysis membrane, catherters, pace makers, leads, blood vessel prosthesis and opthalmagic devices. Although an organic material bone can often be considered in the same way as manmade engineering materials due to the nature of its synthesis, it is likely to show more variations in measured properties than with typical engineering materials, which are due to the following factors.

1) Age
2) Gender
3) Location in the body
4) Mineral content
5) Amount of water present
6) Diseases

With the increase in the age of human beings, the bones becomes less dense and the strength of these bone also decreases, thereby more susceptible to fracture. The various mechanical properties of bio materials studied are 1) Tensile strength 2) Young's modulus 3) Hardness 4) Fracture strength 5) Bending flexural strength and 6) Factography.

Based on geometry, design and material of prosthesis the young's modulus of material becomes a critical design variable as it largely determines how load is transformed through the stem. In order to study the durability of alternate material which is of critical importance, an attempt has been made to develop a hybrid bio polymer matrix composites using HDPE as the matrix, with titanium oxide particles and Al_2O_3 Particles as the reinforcement material with varying percentage. Using rule of mixture of composites, namely, with 10% weight titanium oxide and 5%, 10%, 15% and 20% of Al_2O_3 and the reinforcing HDPE as matrix material, hybrid biopolymer composites were fabricated using injection molding machine.

Using extruder injection type molding, all the samples prepared as per ASTM Standard D3039. They were subjected to various tests, mechanical and tribological properties to investigate and study the various properties like Tensile strength, young's modulus, flexural strength, hardness tests.

Factography test using SEM and salt sprayed corrosion test were also conducted to study wear behavior of bio polymer composites. This is being done to assess the suitability of bio polymer composites (i.e. HDPE + Titanium oxide+ Aluminium oxide) in bio medical applications.

The schematic work plan of this research work is shown below.

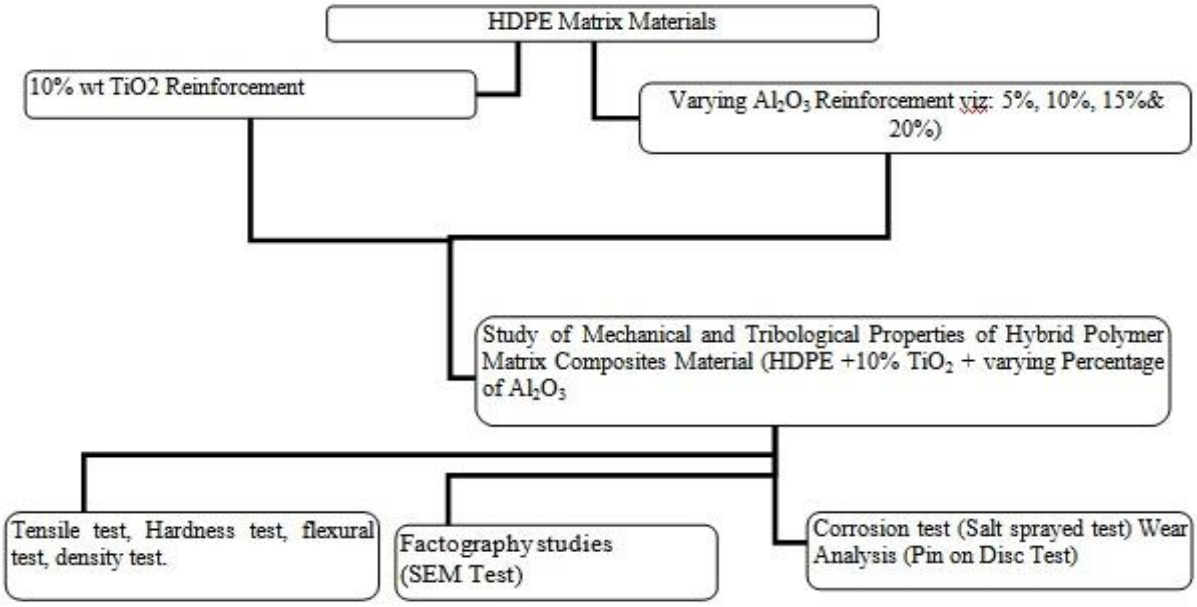

Fig.2. Organization Chart

List of samples prepared with different composition are shown in Table 1.

Table1.

SAMPLE	HDPE	TiO_2	Al_2O_3
1	85 wt %	10 wt %	05 wt %
2	80 wt %	10 wt %	10 wt %
3	75 wt %	10 wt %	15 wt %
4	70 wt %	10 wt %	20 wt %

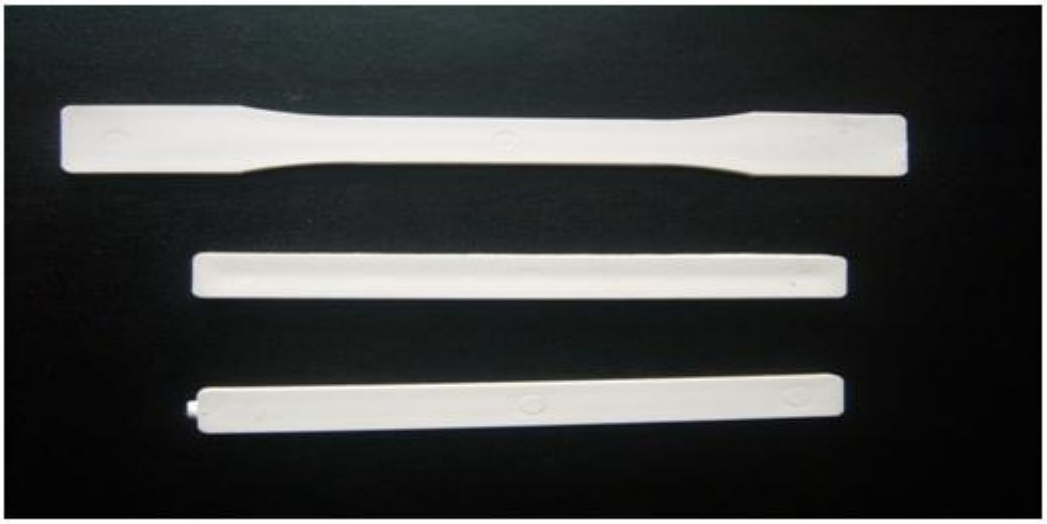

Fig.3. Photographs of specimens of HDPE matrix +TiO_2/Al_2O_3 as varying reinforcement

III. RESULTS AND DISCUSSIONS

1) T It is inferred from the test results that, the tensile strength of composite material increases with increasing percentage of filler contents namely, 5%, 10%, 15% and 20% of Al_2O_3 keeping 10% of Titanium Oxide constant. This results in the increase of the load carrying capacity of composite material. The maximum peak tensile stress achieved is 16.1 MPa and young's modulus of 500 MPa (for HDPE +10% TiO_2 + 20% Al_2O_3 of the composite specimens) as shown in figure 4 and figure 5.

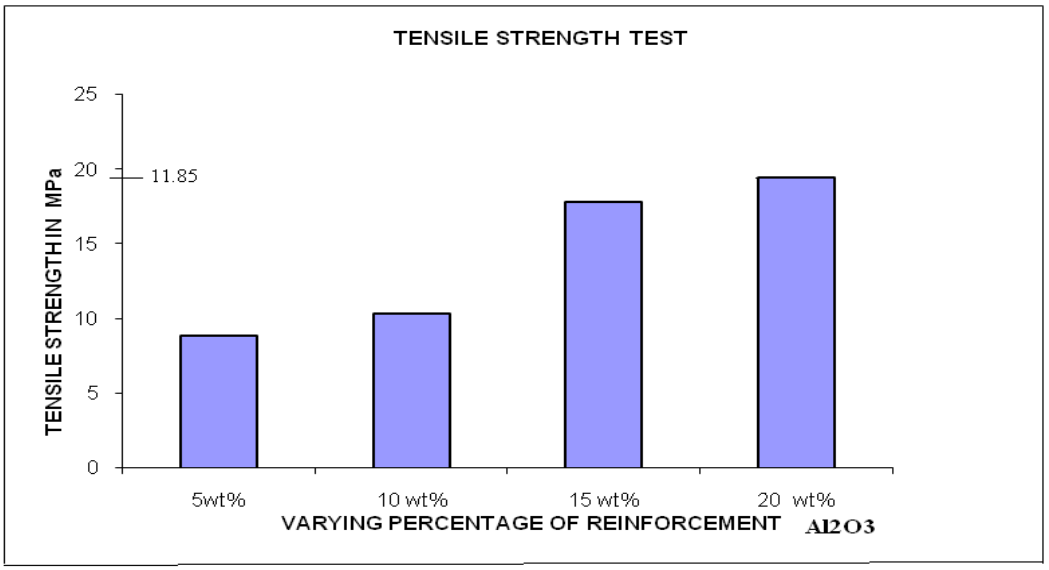

Fig.4. Variation of Tensile Strength for varying percentage of Reinforcement

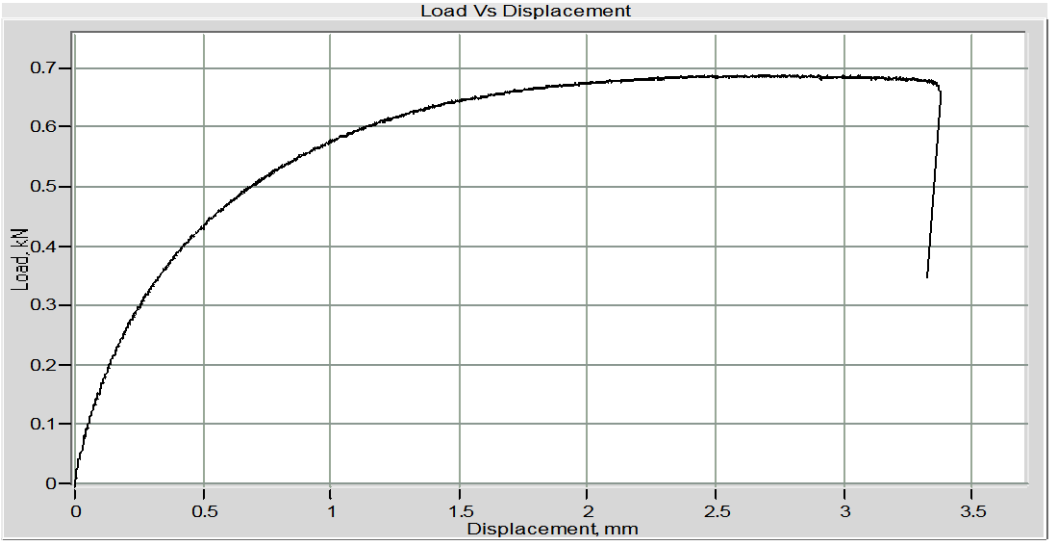

Fig.5. Load Vs Displacement curve for HDPE/10wt% TiO_2 -20wt% Al_2O_3

2) Flexural strength: The figure 6 shows the variation in the flexural strength of composite specimen with varying percentage of reinforcement material Al_2O_3. Flexural strength of composite material increases with increasing percentage of filler contents (from 5% to 20% of Al_2O_3). The maximum Flexural strength achieved is 11.85 MPa for HDPE+10% TiO2 + 20% Al2O3 of the composite specimen shown in figure 6.

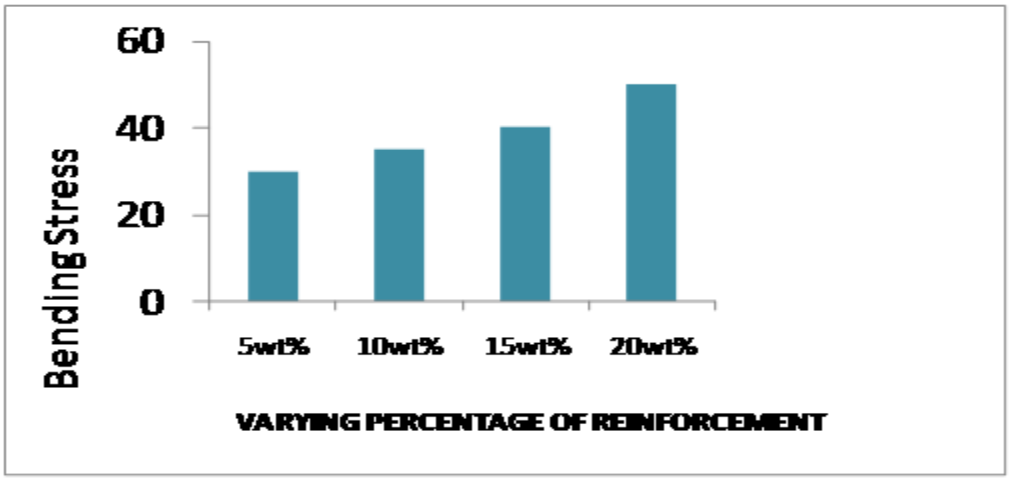

Fig.6. Variation of Bending Stress for varying percentage of Reinforcement

3) Hardness: Figure 7 shows the variation in the hardness of specimen with varying percentage of reinforcement. The maximum hardness shore D hardness number is found to be 55.

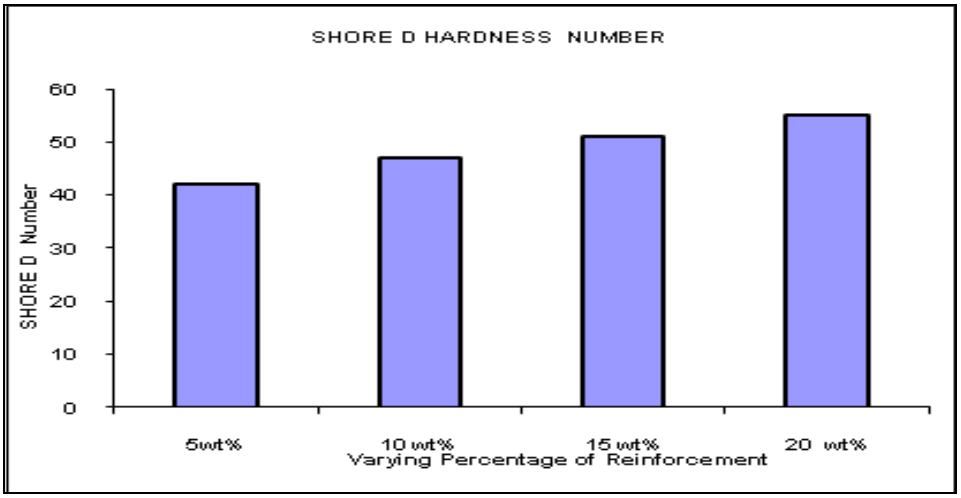

Fig.7. Variation of Hardness for HDPE/10wt% TiO_2 -5 wt% to 20wt% Al_2O_3

4) Density Test: figure 8 shows the variation of density with percentage of reinforcement. The increased density of composites are attributed to good bonding between the matrix and reinforcement.

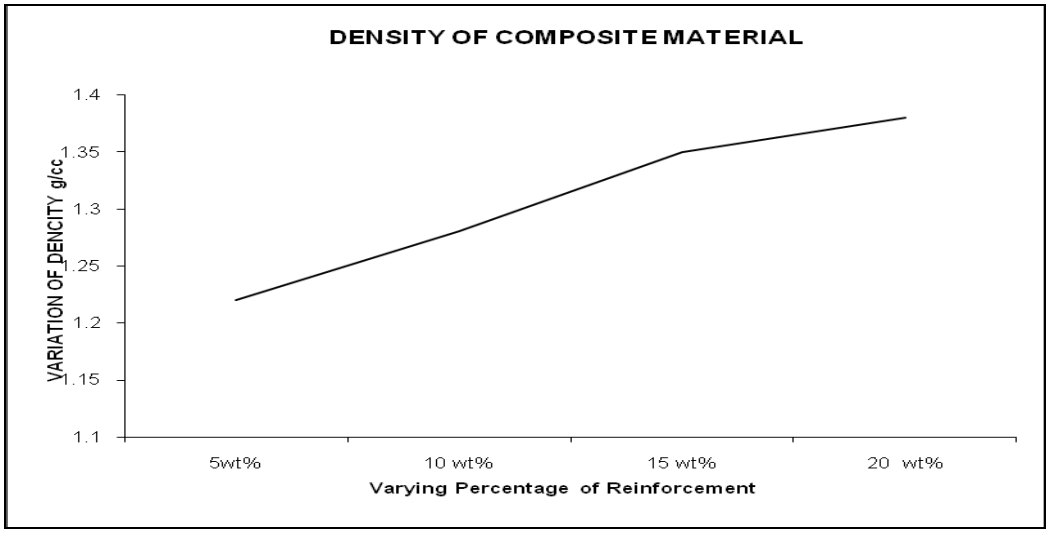

Fig.8. Variation of Density with Persentage of Reinforcement

5) Factography study: the fractured surface of +10% TiO_2 + (5%, 10%, 15% and 20%) Al_2O_3 indicates homogeneous mixing of HDPE+TiO_2 + Al_2O_3 particles with no casting defects resulting in enhancing the mechanical properties of composite material.

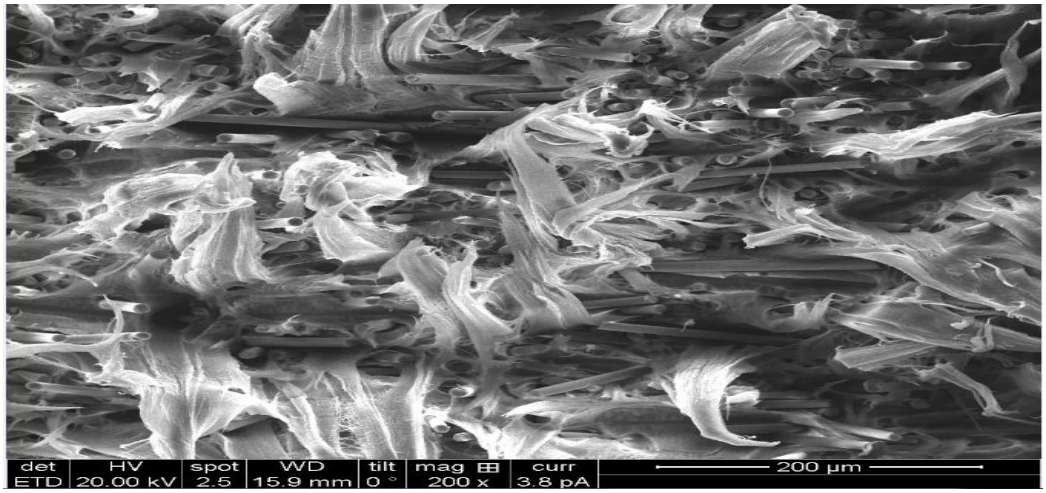

Fig.9. Fractured surface after tensile strength test for HDPE+ 10% TiO_2 +15% OF Al_2O_3

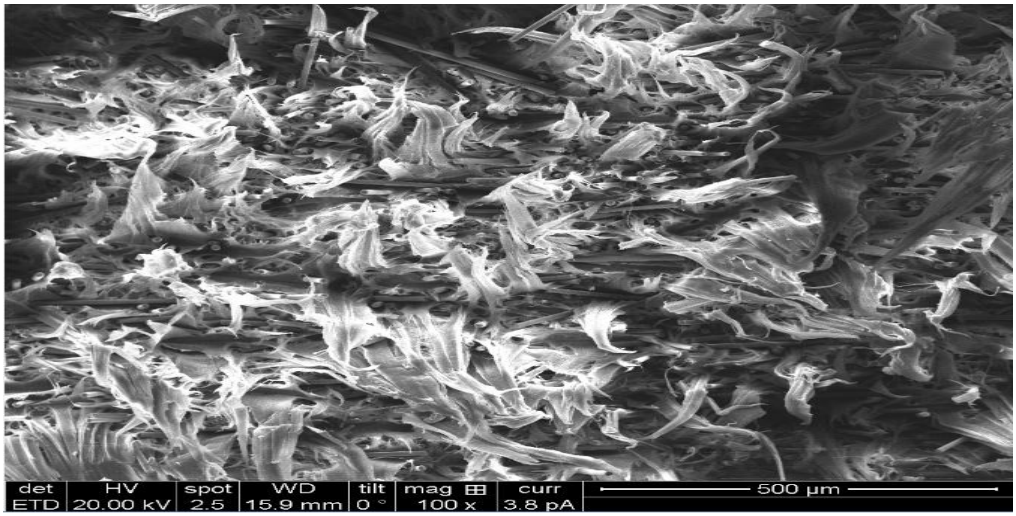

Fig.10. Fractured surface after tensile strength test for HDPE+ 10% TiO_2 +20% of Al_2O_3

6) Corrosion test / Salt sprayed test: It has been observed for a given time period of 24 hours, no corrosion was found on all the specimens of hybrid polymer matrix composites.

Table 2. Corrosion Test for 5% of Al_2O_3 & 10% of Al_2O_3

Methodology for corrosion test	
After Test	Cleaned with running Water
Test Solution	5% NaCl (AR Grade) Solution in distilled water
Test Temperature	35°+/-2°C
Volume of Solution Collected/Hr/80Cm^2 Area	1.41 ml
pH of test Solution	7.08
Required Exposure Period	Not Specified
Type of protection Used	Nil

Observation:

PH value	**Time in Hours**	**Observation**
7	24	No Corrosion was observed

7) Wear analysis- Pin on disc wear test: The wear data i.e. wear loss in grams for different loads namely, 10 N, 20N and 30 N at constant speed of 500 rpm for different samples are shown in table 2. The following observations were made in the wear analysis test.

a. With increase in the load on the specimen, the wear loss of composite increases. Whereas, wear loss decreases with increase in the percentage of reinforcement of composite.

b. It is also noticed with increase in sliding time, wear of the component also increases.

c. The coefficient of friction as well as frictional force of composite decreases with increase in percentage of reinforcement as shown in figures.

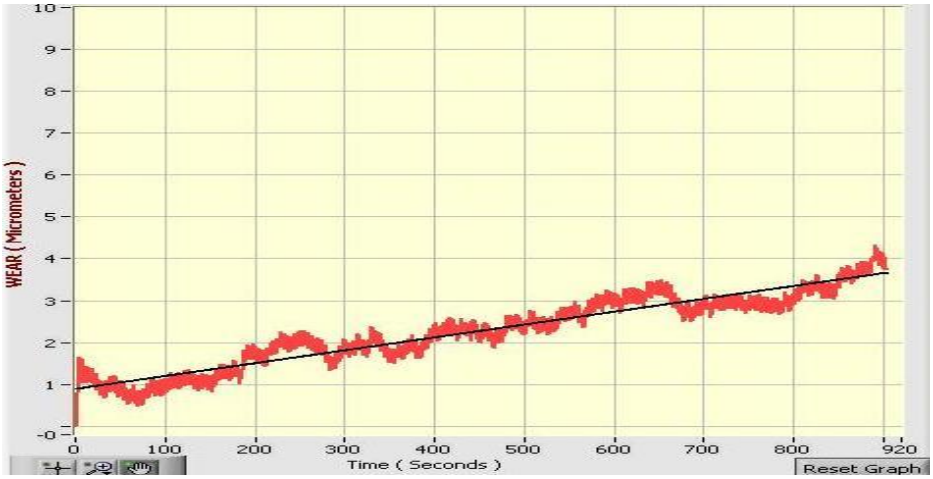

Fig.11. Wear (Micrometers) V/s Time (Seconds) at load 10N for 20wt% Al_2O_3

Fig.12. Coefficient of Friction V/s Time (Seconds) at loads 10N for 20wt% Al_2O_3

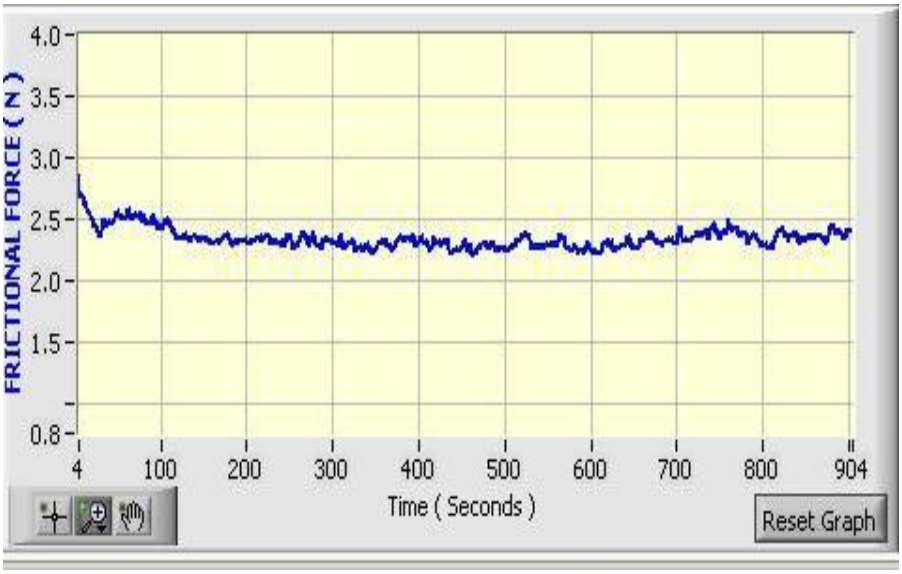

Fig.13. Frictional Force (N) V/s Time (Seconds) at load 10N for 20wt% Al_2O_3

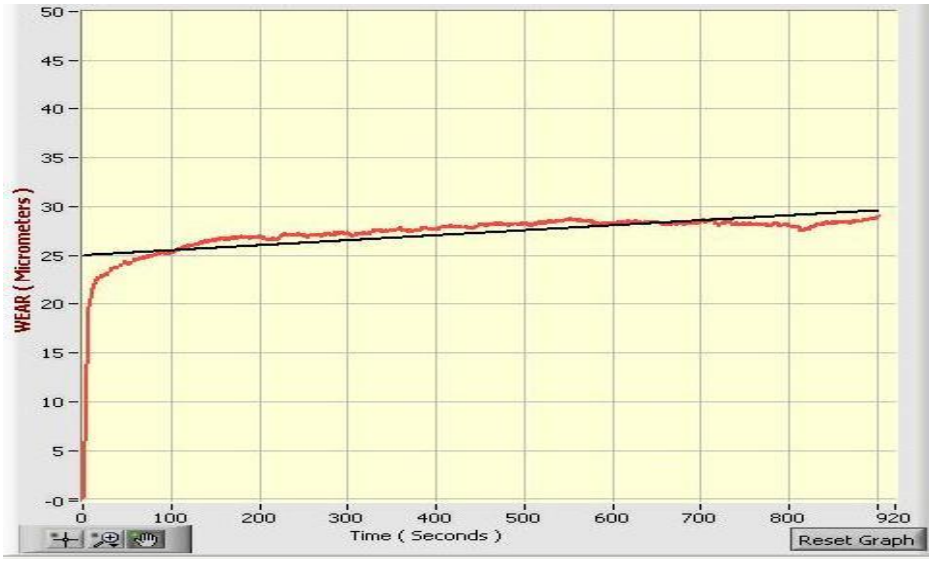

Fig.14. Wear (Micrometers) V/s Time (Seconds) at load 20N for 20wt% Al_2O_3

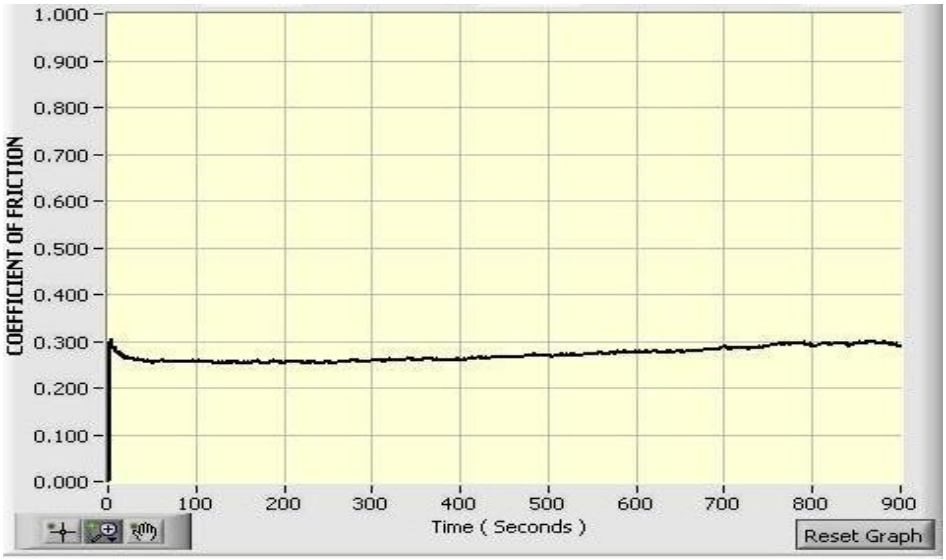

Fig.15. Coefficient of Friction V/s Time (Seconds) at load 20N for 20wt% Al_2O_3

Fig.16. Frictional Force (N) V/s Time (Seconds) at load 20N for 20wt% Al_2O_3

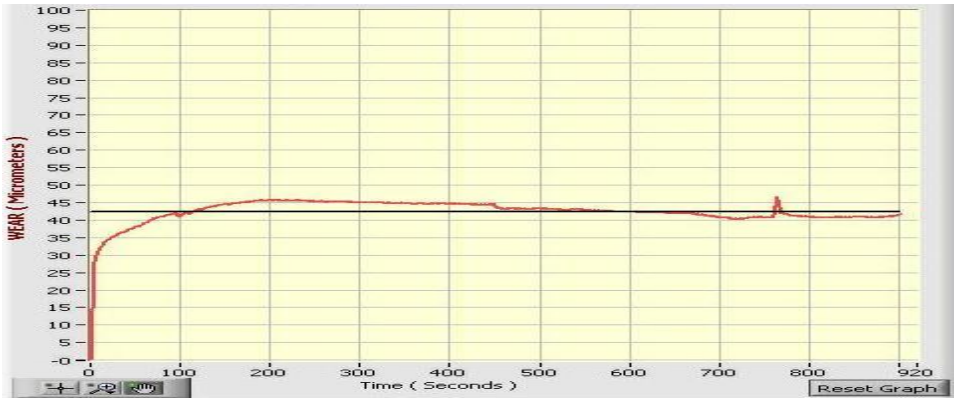

Fig.17. Wear (Micrometers) V/s Time (Seconds) at loads 30N for 20wt% Al_2O_3

Fig.18. Coefficient of Friction V/s Time (Seconds) at load 30N for 20wt% Al_2O_3

Fig.19. Frictional Force (N) V/s Time (Seconds) at load 30N for 20wt% Al_2O_3

IV. CONCLUSION

Based on the investigations carried out on hybrid polymer matrix composites, the following conclusions were made

1. It is observed that, the tensile strength, hardness and bending strength and density of this hybrid polymer composite increases with the increase in percentage of reinforcement.
2. Maximum tensile strength of 16.7 MPa, Maximum hardness of 55 shore D number and Maximum Bending strength of 12MPa was achieved with HDPE + 10% TiO_2 and 20% Al_2O_3 reinforcement.
3. Factography of specimens indicates absence of casting defects and proper bonding behaviour matrix material and reinforcement.
4. No corrosion was observed on the specimens after the corrosion test was conducted for a time duration of 24 hours at PH value of 7.
5. Based on the observations of results of various tests, it is suggested that, HDPE+10% TiO_2 + 20% Al_2O_3 reinforcements could be used as a suitable for bone materials, in orthopedic applications.
6. This polymer matrix composite (HDPE+10% TiO_2 + 20% Al_2O_3) have variety of applications in the human body and they can be applied on hard and soft tissues of implantable materials.
7. Composite materials are extensively used in orthopaedic applications particularly in bone fixation plates, hip joint replacement, bone cement and bone graft. The investigations of all possible factors which may affect the life time, together with response of human body, body parts, tissues and muscles changing itself with increasing age, may be performed by special procedures with sophisticated approach.
8. A prototype of bone specimens made of the above composite materials needs to be analyzed in a host body conditions for compatibility of human body.

REFERENCES

[1] M S.Ramakrishna, J. Mayer, E. Wintermantel, Kam W. Leong, paper entitled "Biomedical application of polymer-composite materials: a review", Composites science and technology journal, 61 (2001), pp (1189-1224), ELSEVIER.
[2] Soo Whon Lee, Carlos Morillo, Joaquin Lira-Olivares, Seung Ho Kim, Tohru Sekino, Koichi Niihara, Bernard J. Hockey, paper entitled "Tribological and microstructural analysis of Al_2O_3/TiO_2 Nan composites to use in the femoral head of hip replacement", WEAR journal, Science direct, wear 255 (2003), PP (1040-1044), ELSEVIER.
[3] C.X. Dong, S.J. Zhu, Mineo Mizuno and Masami Hashimoto, paper entitled "Fatigue behavior of HDPE composite reinforced with silane modified TiO_2", Journal Material Science Technology (JMST), Science direct, 2011 27(7), pp (659-667), ELSEVIER.
[4] S. Mazurkiewicz et al, paper entitled "The Methods of evaluating mechanical properties of polymer matrix composites", Archives of foundry engineering journal ISSN (1897-3310), Volume 10, Special Issue 3/2010, pp (209 – 212).
[5] K. Van de velde and P. Kiekens paper entitled "Biopolymers: overview of several properties and consequences on their applications", POLYMER TESTING Journal 21 (2002), pp (433-422), ELSEVIER.
[6] Santiago Visbal, Joaquin Lira-Olivares, Tohru Sekino, Koichi Niihara, Byung Kyu Moon, Soo Whon Lee, paper entitled "Mechanical properties of Al_2O_3 - TiO_2- Sic Nan composites for femoral Head of Hip Joint Replacement", Material Science forum Journal, June (2005), Volumes (486-487), pp (197-200), Material Science forum.
[7] Mirigul Altan and Huseyin Yildirim, paper entitled "Mechanical and morphological properties of polypropylene and high density polyethylene matrix composites reinforced with surface modified nano sized TiO2 particles", World Academy of Science, Engineering and technology Journal, 70, 2010.
[8] W.Pompe, H. Worch, M. Epple, W. Friess, M. Gelinsky, P. Greil, U. Hempel, D. Scharnweber, K. Schulte, paper entitled "Functionally graded materials for biomedical applications" Materials Science and Engineering journal, A362, (2003), pp (40–60), ELSEVIER.
[9] R M Hall et al, paper entitled "The friction of explanted hip prosthesis", British Journal of Rheumatology, 1997, 36: pp (20-26).
[10] T.Kameyama et al, paper entitled "Hybrid bioceramics with metals and polymers for better Biomaterials" T KAMEYAMA.Vol no 22, no 3.1999 Indian academy of science.
[11] C. M. Manjunatha, S. Sprenger, A. C. Taylor,A. J. Kinloch, paper entitled "The Tensile Fatigue Behavior of a GFRP Composite with Rubber Particle Modified Epoxy Matrix", Journal of Reinforced Plastics and Composites 2010, 29: pp 2170.
[12] Subhadip Bodhak, Shekar Nath and Bikramjit Basu, paper entitled "Friction and Wear Properties of Novel HDPE-Hap-Al_2O_3 Biocomposites against Alumina counter face", Laboratory for Advanced Ceramics, Department of Materials and Metallurgical Engineering. Indian Institute of Technology IIT-Kanpur, 208016, India.
[13] E.J.Giordani et al, paper entitled "Effect of precipitates on the corrosion-fatigue crack initiation of ISO58329 stainless steel biomaterial", International journal of Fatigue 26 (2004), pp (1129-1136), ELSEVIER.
[14] Ravikumar et al, paper entitled "Compliance calibration for fatigue crack propagation testing of ultra high molecular weight polyethylene", Journal of Biomaterials 27 (2006) pp (4693-4697), ELSEVIER.
[15] XiSHi WanG et al, paper entitled "The hip stress level analysis for human routine activities", Journal of Biomedical engineering-Applications, basis and communications, June (2005), 17: pp (153-158).
[16] Santavirta S, Bohler M, Harris WH, Konttinen YT, Lappalainen R, Muratoglu O. Rieker C, Sazler M, paper entitled "Alternative Materials to improve total hip replacement tribology", Department of Mechanical Engineering, University of Leeds, UK.
[17] Shekar Nath and Bikramjit Basu, Paper entitled "Development of designed Biocomposites for Orthopedic Applications" Department of Materials and Metallurgical Engineering. Indian Institute of Technology IIT-Kanpur, India.
[18] Amogh Tathe, Mangesh Ghodke, Anna Pratima Nikalje Paper entitled "Brief review on biomaterials and their applications", International Journal of Pharmacy and Pharmaceutical Sciences ISSN-(0975-1491) Volume 2, Suppl 4 (2010), pp (19-23).
[19] Black J, Hasting GW. Handbook of biomaterials Properties. London, UK: Chapman Hall, 1998.
[20] A text book of "Manufacturing Engineering and Technology" Serope kalpakjian and Steven R. Schmid, Pearson Education, ISBN 81-7808-157-1, 2001.Ozaki, Y. Adachi, Y. Iwahori, and N. Ishii, Application of fuzzy theory to writer recognition of Chinese characters, International Journal of Modeling and Simulation, 18(2), 1998, 112-116.

Improved Accuracy of Automatic Speech Recognition System using Software and Hardware Co design

P Jayaseelan[1], B Padmasri [2], K Ganeshkumar[3]
[1]*Department.of Electronics and communication Engg, PRIST University, Trichy, Tamildau, India*
[2]&[3]*Dept. of ECE, PRIST University, Trichy.*

Abstract: *We Present Automatic Speech Recognition System For Human Machine Interaction By Using Hardware and Software Co design, The Entire Speech Signal Is Segmented Into a sequence Shorter Signal Is done By Future Extraction, This System Improves the Timing Performance by using Hardware Accelerator GMM (Gaussian mixture model), This hardware accelerator is performed by emission probability Calculation, In order to avoid large memory requirement and this accelerator adopts a double buffering scheme for accessing the acoustic parameters, The weighted finite state transducer (WFST) in Viterbi search model gives Word Sequence from Emission probability calculation. The word accuracy rate is preserved at 93.33%, as a part of recognizer is very suitable for Embedded Real time Application By Using New Adaptive Beam Pruning algorithm. Which is about four times faster than pure Software based system.*

Key words: *Automatic Speech Recognition system (ASR), Hardware software co design, Feature Extraction, Gaussian Mixture model (GMM), real time embedded application, Adaptive beam pruning algorithm.*

I. Introduction

RECENTLY, automatic speech recognition (ASR) on embedded platforms has been gaining its popularity. ASR has been widely used in human-machine interaction [1], [2]; Speech recognition applications are becoming more useful nowadays. Various interactive speech applications are available in the market. With growth in the needs for embedded computing and the demand for emerging embedded platforms, it is required that the Automatic speech recognition systems (ASR) are available on them too. A hardware–software codesign approach seems to be attractive and typically hardware–software co processing system consists of a general purpose processor and hardware accelerator unit operation is to achieve required timing performance. Computationally intensive parts of the algorithm can be handled by the hardware accelerator(s) [4], while sequential and control-oriented parts can be run by the processor core.

The additional advantages of the hardware–software approach include the following.

1) Rapid prototyping of applications. Developers can build their applications in software without knowing every detail of the underlying hardware architecture.
2) Flexibility in design modification. The parts of the algorithm which require future modification can be implemented initially in software.
3) Universality in system architecture. The use of the general purpose processor core enables developers to integrate ASR easily with other applications.

The system includes an optimized hardware accelerator that deals with the critical part of the ASR algorithm. The final system achieves real-time Performance with a combination of software- and hardware implemented functionality and can be easily integrated into applications with voice (speech) control [1]-[4]

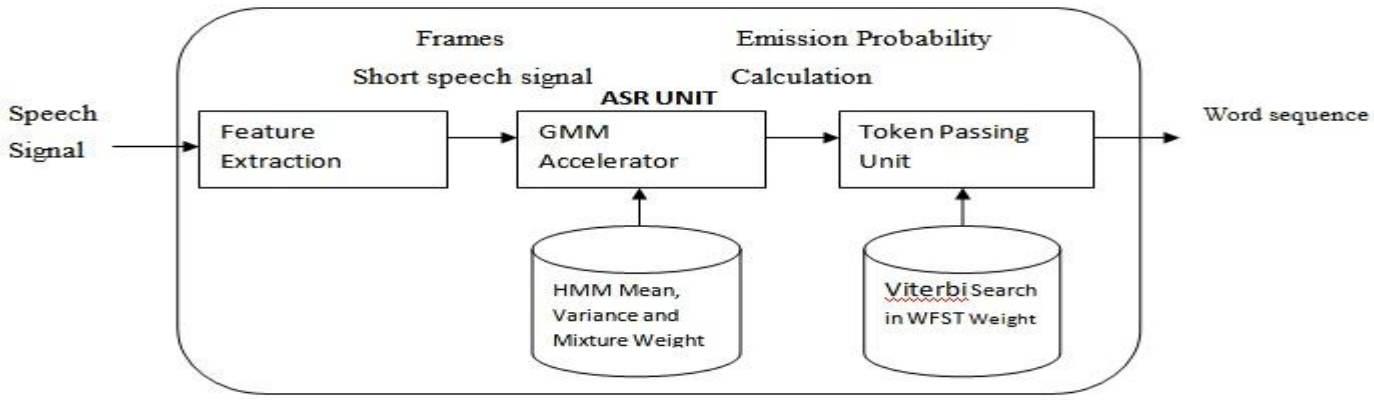

Fig. 1 Data flow diagram of ASR System

II. Automatic Speech Recognition System

In a typical hidden Markov model (HMM)-based ASR system [5], three main stages are involved. Fig. 1 shows the data flow within the ASR algorithm. The first stage is feature extraction. Its main purpose is to convert a speech signal into a sequence of acoustic feature vectors,

oT1 = *{***o**1, **o**2, . . . , **o***T }*, Where *T* is the number of feature vectors in the sequence. The entire speech signal is segmented into a sequence of shorter speech signals known as frames. The time duration of each frame is typically 25 ms with 15 ms of overlapping between two consecutive frames. Each frame is characterized by an acoustic feature vector consisting of *D* coefficients. One of the widely used acoustic features is called Mel frequency cepstral coefficient (MFCC) [3]. Feature extraction continues until the end of the speech signal is reached. The next stage is the calculation of the emission probability which is the likelihood of observing an acoustic feature vector. The emission probability densities are often modeled by Gaussian mixture models (GMMs) [7]. The last stage is Viterbi search which involves searching for the most probable word transcription based on the emission probabilities and the search space. The use of weighted finite state transducers (WFSTs) offers a tractable way for representing the search space. The advantage is that the search space represented by a WFST is compact and optimal .a WFST is a finite state machine with a number of states and transitions. Each WFST transition has an input symbol, an output symbol, and a weight.

In ASR, a word is considered as a sequence of sub word units called phones. Two or three phones are concatenated to form biphones or triphones. Each triphone or biphone label is modeled by an HMM. In other words, each WFST transition is substituted by an HMM. The entire WFST is essentially a network of HMM states.

III. Feature Extraction

The MFCC (Mel-frequency Cepstrum Coefficient) computation employed for the feature of our recognition system consists of 512- point FFT. Filter bank analysis, log operation and IDCT so that it requires intensive arithmetic computations. However, the overhead of the feature extraction is not changed with varying vocabulary size of the recognition task because it only depends on the input speech sample. All the arithmetic operations of the feature extraction are implemented in fixed-point operations to reduce the additional overhead of handling the floating-point operations. The Micro Blaze needs more processing power to achieve the same level of performance with the conventional ARM7 based implementation. The most computation intensive part for MFCC is the 512-point FFT which requires many add and multiply operations. Because the base Micro Blaze processor is not equipped with hardware multiplier, the data path is not adequate to perform FFT. The log arithmetic is implemented by table lookups, and the cache can reduce the overhead of accessing the log table in the external DRAM. Because the Micro Blaze is a soft core that can easily adopt these features in its data path, we adopted the hardware multiplier and the data cache. Figure 2 shows the execution cycles for the feature extraction with various data path configurations. We can see that the performance of Micro Blaze is similar to that of ARM7 architecture by configuring data path. Note that the ARM7 is operating at 60MHz whereas Micro Blaze is at 100MHz.

IV. GMM Accelerator

Feature extraction continues until the end of the speech signal is reached. The next stage is the calculation of the emission probability which is the likelihood of observing an acoustic feature vector. The emission probability densities are often modeled by Gaussian mixture models (GMMs).

$$\Psi(t, sj)=\max\{\Psi(t-1,si)+\log(aij)\}+ \log(b(Ot ; sj)) \quad (1)$$

aij indicates the transition probability from state si to sj and b(Ot; sj) represents the emission probability. For the word-level transcription which will be the output of the speech recognition system, we have to keep the best predecessor word for each word hypothesis.

$$H(w,t)=\max\{\log(p(w/v))+\Psi(t,Sw)\} \quad (2)$$

P (w/v) shows the bigram probability from word v to word w and S,,, indicates the last states of the word w. Since exhaustive search in Viterbi search is prohibited, pruning is employed at both the state level and the language model level. Therefore the paths which have low accumulated likelihood are pruned at the early stage to reduce the search space size .For the DP recursion shown in Eq. 1, the output probability of the current observation for each HMM state should be computed. The log likelihood for the Gaussian mixture m of HMM state s is computed. Eq 2 is a pre-computed Gaussian constant that is independent of the observation Ot = {X1X2 X39}. p and a indicate the mean and the variance of the Gaussian mixture respectively. Because all the model parameters are stored in 16 bit format, if we assume the worst case of loading all the mixture model from memory to compute the emission probability, it requires up to 64MB/s memory bandwidth. In real time implementation, however, we do not compute the mixture models which are decided to be excluded in the Viterbi beam search by beam pruning. The memory bandwidth for the emission probability required is thus reduced to about 7MB/s as shown in Fig. 3

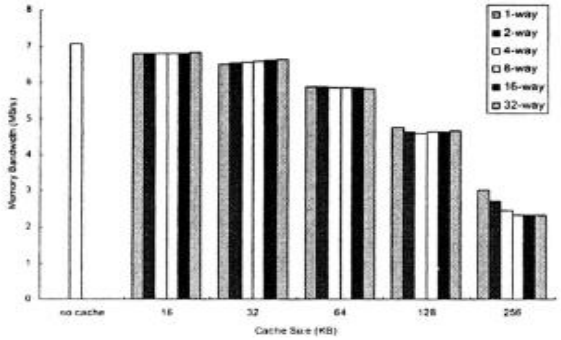

Fig 2. Memory bandwidth of various caches

4.1 Architecture Design

Figure 3 shows the architecture of hardware accelerator for the emission probability. The feature vector which is computed in the Micro Blaze processor is stored in the dedicated feature storage so that the feature vector can be reused for the single frame. The model data to be filled in the internal memory of the hardware accelerator is transferred via FSL. The cache is also employed in the micro blaze

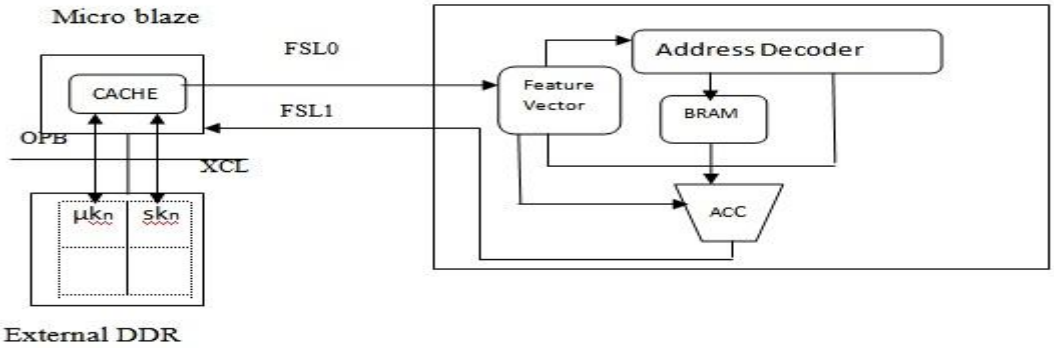

Fig 3. Hardware Accelerator for Emission Propability Calculation

To accommodate the faster bus XCL. As we can see from the architecture, the memory bandwidth is the main factor that decides the total execution time. It requires only 5 cycles to generate the output after loading the model parameter. A naive solution for the extreme memory access is storing all the acoustic model data into the internal memory which can be implemented using BRAM blocks. The result showed about 20 times reduction in the execution cycle for the emission probability. However, this approach is not adequate for a large vocabulary speech recognition system simply because it requires an excessively large BRAM size and the solution is no longer feasible.

4.2 Cache Analysis

The second option is adopting cache in the accelerator. Figure 3 shows the memory bandwidth requirement with various cache configurations. In this experiment, the cache hit ratio looks relatively high considering that the system loads large amount of data. The reason is that the Gaussian computation for one mixture loads 80 consecutive 16 bit data generating only 5 cache misses assuming the 32 bytes line size. Thus we employed memory bandwidth as the performance measure. Figure 3 shows that relatively small size of cache from 16KB to 32KB does not improve the performance much. The Gaussian mixture model should be reused as many times as possible to reduce the memory bandwidth between cache inside the hardware accelerator and memory. However, the large size of the mixture models makes the data easily flushed out of the cache. Even 32KB dedicated cache can hold up to only 200 mixtures at once whereas the number of mixtures that are accessed in one frame can reach over 1000 in usual cases. Note that caching actually start to take place when the memory size is increased to 256KB. Cache configurations below 256KB would produce only capacity misses therefore cache associatively would not yield any effect.

4.3 Data Partition

The behavior of speech recognizer varies with the input speech, especially when we adopted adaptive techniques such as beam pruning to achieve high performance. However, the underlying language model of the system also plays an important role in the recognizer. The mixture model to be computed is decided by the active states in the Viterbi beam search network.[3] .There are two components that are responsible for making the decision on which states are to remain active. The first one is the accumulated likelihood of the state. The beam pruning compares the accumulated likelihood of a state to the best accumulated likelihood so that the states with low values are pruned. The other is the language model. Figure 1 shows the back off bigram language model which is usually employed for a large vocabulary speech recognition system.

In this model, all the words in the vocabulary are composed of the word-loop grammar and the corresponding bigram suppresses the unlikely paths. The next state of an active state within a word should be active in the next iteration. The first state of a word which comes from the active final state of a word should also be active. The former is mostly dependent on the input speech where there is a little room for us' to exploit. However, the latter is highly dependent on the language model so that we can use the feature regardless of the input speech. Developing a speech recognition system requires very sensitive tuning because the performance heavily depends on the configuration parameters such as acoustic beam pruning threshold, language model scale factor, word insertion penalty, etc [1]. The parameter setting is done based on the test set that is independent of the training set. Similarly, we extracted the feature of the language model exploiting the training set. Access pattern of the emission probability computation for all the speech in the test set is recorded and the N most probable states are chosen. The memory bandwidth can be reduced by placing these states in the internal memory of the hardware accelerator. Figure 5 shows the required memory bandwidth when the internal memory is employed. The experiment of placing random states in the internal memory is also performed to emphasize the importance of efficient selection of the states. The experiment where we store the states which are known to be the most probable by profiling showed about 15% to 27% performance improvement as total internal memory size varies from 32KB to 256KB. The experiment where the random states are stored shows the performance worse than when the cache is adopted. This result shows that the carefully partitioned internal BRAM [6-8] can outperform when the same size of the cache is employed. However, if we randomly partition the model data, the performance is worse than that of the cache. Note that the profiling is performed by 300 various test speeches with all of them having different speakers and transcriptions and only one of them is matched to the speech used in this experiment. This means that the profiling results contain language model information rather than acoustic model information.

V. Adaptive Pruning Algorithm

The hardware–software co processing system demonstrates a significant improvement on the decoding speed. Out of the 1200 utterances in the RM1 corpus, about 94% of them have a real-time factor of less than one. In this section, we aim at further increasing this percentage. One method for lowering the number of active tokens is to adopt a tighter pruning beam width. However, it will introduce search errors which often decrease the recognition accuracy. Our goal is to reduce the decoding time of those utterances which have a relatively greater real-time factor, while keeping the recognition accuracy of the other utterances. In order to fulfill this goal, an adaptive pruning scheme is proposed, where the pruning beam width is adaptive according to the number of active tokens.

5.1. Importance of Algorithm

The proposed pruning scheme is more flexible than the narrow and fixed pruning scheme. The number of active tokens is often time varying in the duration of an utterance. The fixed pruning scheme applies a tight beam width throughout the entire utterance regardless of the number of active tokens. On the other hand, the adaptive scheme allows relaxation of the beam width in parts of the utterance where the workload is less heavy.

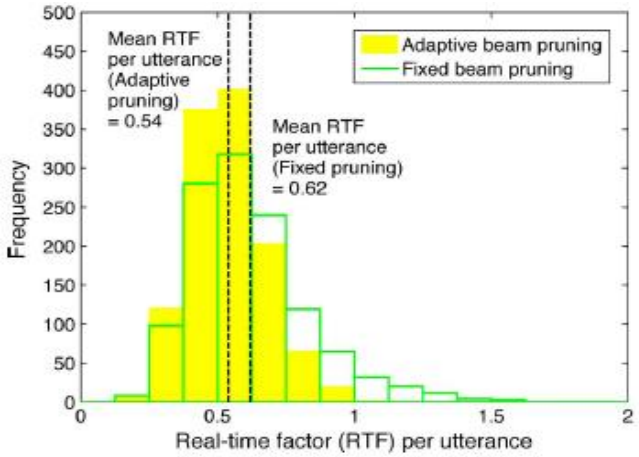

Fig 4. Real time factor utterance in HW-SW co design system, Adaptive beam pruning versus fixed beam pruning algorithm

VI. Token Passing Unit

The last stage is Viterbi search which involves searching for the most probable word transcription based on the emission probabilities and the search space. The use of weighted finite state transducers (WFSTs) offers a tractable way for representing the search space [7]. The advantage is that the search space represented by a WFST is compact and optimal [8], Fig. 1 shows an example of a search space. Each WFST transition has an input symbol, an output symbol, and a weight. The input symbols are the triphone or biphone labels. The output symbols are the word labels. In ASR, a word is considered as a sequence of sub word units called phones. Two or three phones are concatenated to form biphones or triphones. Each triphone or biphone label is modeled by an HMM. In other words, each WFST transition in Fig. 3 is substituted by an HMM. The entire WFST is essentially a network of HMM states. The WFST weights are the language model probabilities which

model the probabilistic relationship among the words in a word sequence. Usually, a word is grouped with its preceding (n − 1) words. The n-word sequence called n-gram is considered as a probabilistic event. The WFST weights estimate the probabilities of such events. Typical n-grams used in ASR are unigram (one word), bigram (two word, also known as word pair grammar), and trigram (three word). For implementation purposes, each HMM state has a bookkeeping entity called *token* which records the probability (*score*) of the best HMM state sequence ended at that state. Each token is propagated to its succeeding HMM states according to the topology of the search space.

VII. Conclusion

The proposed ASR system shows much better real-time factors than the other approaches without decreasing the word accuracy rate. Other advantages of the proposed approach include rapid prototyping, flexibility in design modifications, and ease of integrating ASR with other applications. These advantages, both quantitative and qualitative, suggest that the proposed co processing architecture is an attractive approach for embedded ASR. The proposed GMM accelerator shows three major improvements in comparison with another co processing system [5], [6]. First, the proposed accelerator is about four times faster by further exploiting parallelism. Second, the proposed accelerator uses a double-buffering scheme with a smaller memory footprint, thus being more suitable for larger vocabulary tasks. Third, no assumption is made on the access pattern of the acoustic parameters, whereas the accelerator in [6] and [7] has a predetermined set of parameters. Finally, we have presented a novel adaptive pruning algorithm which further improves the real-time factor. Compared with other conventional pruning techniques, the proposed algorithm is more flexible to deal with the time-varying number of active tokens in an utterance. The performance of the proposed system is sufficient for a wide range of speech-controlled applications. For more complex applications which involve multiple tasks working with ASR, further improvement of timing performance, for example, by accelerating the Viterbi search algorithm, might be required. The proposed co processing architecture can easily accommodate additional hardware accelerators. Aside from better word accuracy and timing performance, power consumption is also another important issue for embedded applications. The proposed architecture is not tied to any specific target technology. One of the future development paths is to transfer the current implementation from FPGA to very large scale integration which consumes less power. Our future work includes some further refinements of the speech recognition algorithm, exploration of design space to look for improvements of the hardware–software co processing system, and encapsulation of the speech recognizer into an intellectual property block that can be easily used in other applications.

References

[1] A.Green and K.Eklundh.”Designing for learn ability in human-robot communication,” IEEE trans, ind.Electron, vol.50, no.4.pp.644-650, Aug, 2003.
[2] M.Imai.T. Ono. And H.ishiguro.”Physical relation and expression: joint attention for human-robot nitration.”IEEE Trans.Ind.Electron. vol.50, no.4, pp.636-643, Aug.2003.
[3] N.Hataoka, Y.Obuchi, T.Mitamura, and E.Nyberg.”Robust Speech dialog interface for car elematics service,” in proc.IEEE consumer commun, netw.conf. 2004, pp.331-335.
[4] K.Saeed and M.nammous,” A Speech and Speaker identification, and classification of Speech- signal image,” IEEE Trans.Ind.Electron. vol.54, no.2, pp.887-897, Apr.2007
[5] K.You, H.Lim, and w. Sung, “Architectural design and implementation of an FPGA softcore based speech recognition system.” In Proc, 6th int. Workshop syst. Chip real time appl,.2006.pp.50-55.
[6] L.Raniner.”A tutorial on hidden markov models and selected applications in speech recognition,” Proc.IEEE, vol 77, no. 2, pp257-286.
[7] H.Ney , D.Mergel , A,Noll, and A. Paeselar,” A data-driven organition of the dynamic programming beam search for continous speech recognition,” in Proc, ICASSP.1987, pp.833-836.
[8] H.Ney. R.Haeb-Umbach, B.Tran, and M.Oerder,”Improvements in beam search for 10000-word Continous speech recognition,” in Proc ICASP. 1992. DD.9-12

Authors

P.Jayaseelan, Received B.E. in Electronics and communication Engg (with first-class honors) and Doing M.Tech Embedded systems in PRIST University, Trichy, India. He is Currently Working Lecturer in Ponnaiyah Ramajaym Polytechnic College, kumbakonam. His Research interests include embedded system, Speech recognition and machine learning.

B .Padmasri, received her Master of Technology in Communication systems from PRIST University, India. She is currently working as Assistant professor in PRIST University, India. Her Research Interest in Real time embedded application.

K.Ganeshkumar, doing M.tech in PRIST University, He currently working in ponnaiyah ramajayam polytechnic College, His research interest in Real time embedded security system.

International Journal of Modern Engineering Research (IJMER)
www.ijmer.com Vol.3, Issue.2, March-April. 2013 pp-985-989 ISSN: 2249-6645

Ontology Extraction from Heterogeneous Documents

Kirankumar Kataraki, [1] Sumana M[2]
[1]*IV sem M.Tech/ Department of Information Science & Engg / M S Ramaiah Institute of Technology, Bangalore-54*
[2]*Assistant Professor/Department of Information Science & Engg/ M S Ramaiah Institute of Technology, Bangalore-54*

Abstract: *Ontology Extraction play an important role in the Semantic Web as well as in knowledge management. The emergence of Semantic Web and the related technologies promise to make the Web a meaningful experience. Conversely, success of Semantic Web and its applications depends largely on utilization and interoperability of well-formulated ontology bases in an automated heterogeneous environment. Ontology is what exists in a domain and how they relate with each other. The advantage of an ontology is that it represents real world information in a manner that is machine understandable. This leads to a variety of interesting applications for the benefit of the target user groups. An ontology defines the terms used to describe and represent an area of knowledge. Ontologies are critical for applications that need to search across or merge information from diverse communities. In this paper, we present our approach to extract relevant ontology concepts and their relationships from a knowledge base of heterogeneous text documents.*

Keywords: *heterogeneous, knowledge, machine understandable, Ontology Extraction, Semantic Web*

I. Introduction

The Semantic Web is a major research initiative of the World Wide Web Consortium (W3C) [1] to create a metadata-rich Web of resources that can describe themselves not only by how they should be displayed (HTML) or syntactically (XML), but also by the meaning of the metadata. We consider Semantic Web as next generation Web that provides great benefits in Web Services, Internet Commerce, and other promising application areas. However, Semantic Web is still in its primary stage means not fully implemented. and has lots of unsolved problems. One of the major problem is to extract data from heterogeneous documents in such way that it has to understand by machine, which we call ontology extraction.

A basic approach for ontology extraction is by manual. Most of the current research focuses on exploiting various methods to generate ontology automatically or semi-automatically. Manual ontology building is a time consuming activity that requires a lot of efforts for knowledge domain acquisition and knowledge domain modeling. In order to overcome these problems many methods have been developed, including systems and tools that automatically or semi-automatically, using text mining and machine learning techniques, allows to generate ontologies. The research field which study this issues is usually called "ontology generation" or "ontology extraction" or "ontology learning". However, most approaches have "only" considered one step in the overall ontology engineering process [2], for example, generating concepts & relationships[3] or extracting concepts & relationship whereas one must consider the overall process when building real-world applications. In this paper, we describe our approach for ontology extraction from an existing knowledge base of heterogeneous documents. We required Information Extraction from heterogeneous text because it gives direct access to knowledge when in textual format, only relevant information is accessed by people Knowledge Sharing.

A. Background and Related Works

Two main approaches have been developed in ontology extraction. The first one facilitates manual ontology engineering by providing natural language processing languages, and ontology import tools. The second approach is based on machine learning and automated language processing techniques to extract concepts and ontological relations from structured and unstructured data such as databases and texts. A number of systems have been proposed for ontology extraction from text. We describe some of them in the following.

ASIUM [4] extracts verb frames and taxonomic knowledge, based on statistical analysis of syntactic parsing of texts.
Text-To-Onto [5] is an Open source ontology management infrastructure, with a tool suite for building ontologies from an initial core ontology. It combines knowledge acquisition and machine learning techniques to discover conceptual structures.

Information Retrieval[6] is a domain independent that creates clusters of the words appearing in the text. The scope of this is to build a hierarchy of concepts. Its learning method is based on distributional approach: nouns playing the same syntactic role in sentences with the same verb are grouped together in the same class.
Effective ontology management in virtual learning environments[7] is a semi-automatic data driven topic ontology which integrates machine learning and text mining algorithms. Main features are represented by automatic keyword extraction from documents given as an input to the system (the extracted keywords are "candidate concepts" of the ontology) and by the concepts suggestions generation.

II. Approach For Ontology Extraction

Ontology is a basic building block for semantic web[8]. An active line of research in semantic web is focused on how to build and evolve ontologies using the information from different ontological sources such as txt, doc, ppt, pdf etc inherent in the domain. A large part of the IT industry uses software engineering methodologies to build software solutions that solve real-world problems. Ontology Building process consists of following phases.

A. Clustering

We have implemented statistical[9] and data mining algorithm[10] in order to identify the concepts and their relationship in the resulting ontology. This method aims to build ontologies using a data mining approach called cluster mining from domain repositories written in XML.

Algorithm: Generating Concepts and relations.
Input: Folder containing heterogeneous file
Output: Dynamically created XML data by parsing the contents of files from ontology testing folder.

❖ **Begin**
Step1: Read all the file names from input folder.
Step2: Create a string buffer variable to collect all the file names.
Step3: Create a temporary string buffer to read content of each file.
Step4: Process each data of file based on end of sentence.
Step5: Using temporary string buffer which will list the number of possibilities of meaningless words in sentence, Cluster the data by filtering it from meaningless string content.
Step6: Mark first word of sentence as parent and next beginning word will be marked as child.
Step7: Continue to read all the sentences from the folder.
❖ Stop

B. Harmonization

This is an optional step that is needed when the user wants to "harmonize" the extracted ontology with the available knowledge bases.

With the term ontology harmonization, we want to refer to the ability of harmonizing two or more ontologies in a unique ontology in order to improve the available knowledge base. It is strictly related to two main issues: ontology matching[11] for the recognition of correspondences between ontologies and ontology merging[12] for the actual fusion of those ontologies.Main aim of harmonization is Extracting concepts and relations means for input string it has to display list of all the match able relations from the input string.

Algorithm: Extracting concepts and relations
Input: Testing string query
Output: Displaying list of all the match able relations from the input string.

❖ **Begin**
Step1: Read the Input text.
Step2: Compare input test string with concept from ontology data.
Step3: Search input text with set of relations from ontology data.
Step4: Read the number of term frequency of the input string appearing in the ontology data.
Step5: Display the number of strings appearing both as concept and relation.
❖ **Stop**

III. Results

This chapter presents the results obtained from the developed system , mainly it shows extracted ontology data, constructed "concept & relationship" data created using the ontology data & verified ontology data process.

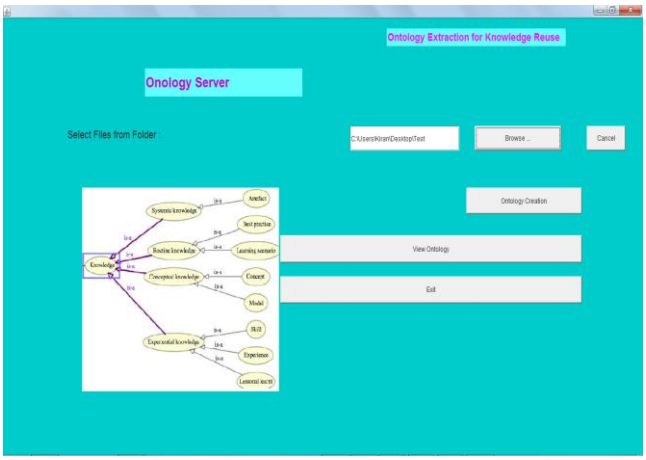

Fig1: ontology server containing various options.

In fig1 we can see ontology server containing various options. Here the first process you have to browse the folder which contains various heterogeneous documents. In the above figure we are browsing the folder from "c:\Users\Kiran\Desktop\Test" location.

Our experimentation has been made considering the TXT, DOC and PDF formats so our Test folder contains three different format files. The fig2 indicates that.

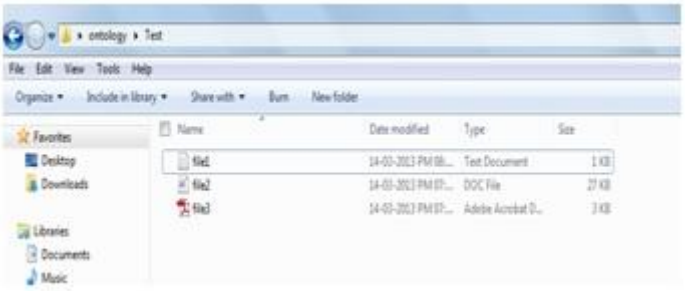

Fig2: Test folder which contains three different formatfiles.

File1 is of text format, Which contains the following text. "Hypertext Markup Language, the languages of the World Wide Web, allows users to produces Web pages that include text, graphics and pointer to other Web pages.HTML provides tags to make the document look attractive"

File2 is of doc format, Which contains the following text. "A HTML document is small and hence easy to send over the net. It is small because it does not include formatted information."

File3 is of pdf format, Which contains the following text. "HTML is platform independent. HTML tags are not case-sensitive."

We want to analyze our input data so in all files we taken small amount of text. Our system works fine with huge amount of data also. After browsing the input folder, to construct the ontology data we have to click ontology creation tab. As soon as you click the ontology creation tab within few seconds our system will generate ontology data. After generating ontology data it shows "ontology creation has been successfully completed." which is shown in fig3.

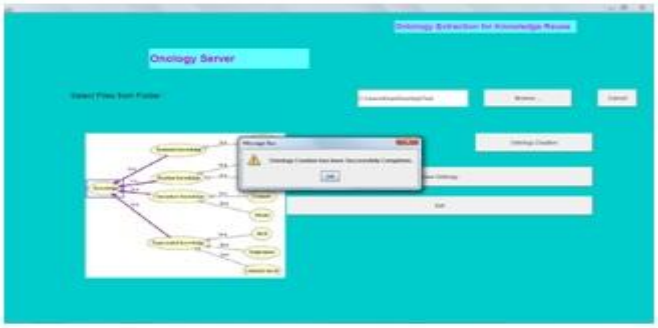

Fig3: Ontology sever displaying message after creating ontology data.

Once the ontology creation successfully completed you can see ontology data by clicking view ontology tab. When you click view ontology tab it displays two xml files. In our system ontology data is stored in xml format. First xml file contains ontology data.

Fig4: Contents of first xml file

The fig4 shows content of first xml file. Here you can observe that our system concatenated all contents of different files. Then content breaks by sentence.

For example by considering content of file1, I will explain the working of our system. First sentence of file1 is stored like below.

"Hypertext Markup Language, the languages of the World Wide Web, allows users to produces Web pages that include text, graphics and pointer to other Web pages."

Second sentence of file1 is stored like below.

"HTML provides tags to make the document look attractive"

Finally our system removes stopwords(unrelated words) from each sentence. Unrelated words means in first sentence the, of, allows, to, that & other words are having no importance when creating ontology data. So those words have been trimmed from the sentence. So trimmed content with respect to first sentence of file 1 is

"Hypertext Markup Language, languages World Wide Web, users produces web pages include text, graphics pointer Web pages"

Trimmed content with respect to second sentence of file 1 is

"HTML tags make document attractive"

Similar process applied to whole content & stopwords have removed from each sentence(refer fig4 for output).

Next the each sentence of ontology data is stored in "Concept-Relationship" manner which is useful when extracting ontology data. In each sentence first word is stored as concept & next words will be stored as relations.

Fig5: second xml file storing ontology data in concept-relationship manner.

Once the ontology data is created next optional step is to check match able relations from sentence for input string. In our system it is working fine. Suppose for example your sarching html as input string then it will display mach able relations. Math able relations for html are tags, make, document, attractive, small, easy, send, net, platform, independent, casesensitive. It also shows in which file the particular sentence is found. so you can easily find the exact information.

In fig5 each sentence first word is stored as concept & next words will be stored as relations. It does not mean that you have to search only concept. You can search any word means the particular input string is treated as concept related words are treated as relations.

Suppose if you given input that is not present in documents then it will display the message "search not found, try with another concept."

IV. Conclusion

In this paper, we have presented an ontology information extraction system to extract ontologies from a knowledge base of heterogeneous text documents. We have proposed our approach to build the Concept and Relationship from heterogeneous documents which gives dynamically created XML data by parsing the contents of files. In our project harmonization is an optional step but it is needed to check whether builded ontology is efficient or not, so we even proposed our approach to extracting concepts and relations. Means when you given input as string query our system gives output as list of all the match able relations from the input string. Our work mainly explains the ontology extraction process is general and is not domain dependent. Thus ontology has been served as a most effective technique to solve semantic issues irrespective of any domain.

References

[1] M. Dean and G. Schreiber, "OWL Web ontology language reference," W3C Recommendation, Feb. 2004.
[2] J. Euzenat and P. Shvaiko, Ontology Matching. Heidelberg, Germany: Springer-Verlag, 2007.
[3] R. Farkas, V. Vincze, I. Nagy, R. Ormándi, G. Szarvas, and A. Almási, "Web-based lemmatisation of named entities," in Proc. TSD, vol. 5246, Lecture Notes in Computer Science, P. Sojka, A. Horák, I. Kopeček, and K. Pala, Eds. Berlin, Germany: Springer-Verlag, 2008, pp. 53–60.
[4] D. Faure and T. Poibeau, "First experiences of using semantic knowl- edge learned by ASIUM for information extraction task using INTEX," in Proc. ECAI Workshop Ontology Learning, vol. 31, CEUR Work- shop Proceedings, S. Staab, A. Maedche, C. Nédellec, and P. Wiemer- Hastings, Eds., 2000.
[5] A. Maedche and S. Staab, "The Text-To-Onto ontology learning environ- ment," in Proc. 8th Int. Conf. Conceptual Struct., Darmstadt, Germany,2000, pp. 14-18.
[6] W. B. Frakes and R. A. Baeza-Yates, Eds., Information Retrieval: Data Structures & Algorithms. Englewood Cliffs, NJ: Prentice-Hall,1992.
[7] M. Gaeta, F. Orciuoli, S. Paolozzi, and P. Ritrovato, "Effective ontology management in virtual learning environments," Int. J. Internet Enterprise Manage., vol. 6, no. 2, pp. 96–123, 2009.
[8] A. D. Maedche, Ontology Learning for the Semantic Web. Norwell, MA: Kluwer, 2002.
[9] C. D. Manning and H. Schtze, Foundations of Statistical Natural Language Processing. Cambridge, MA: MIT Press, Jun. 1999.
[10] D. L. McGuinness, R. Fikes, J. Rice, and S. Wilder, "The Chimaera ontology environment," in Proc. AAAI/IAAI, 2000, pp. 1123–1124.
[11] R. Navigli and P. Velardi, "Semantic interpretation of terminological strings," in Proc. 6th Int. Conf. TKE, 2002, pp. 95–100.
[12] R. Navigli, P. Velardi, and A. Gangemi, "Ontology learning and its application to automated terminology translation," IEEE Intell. Syst., vol. 18, no. 1, pp. 22–31, Jan. 2003.

International Journal of Modern Engineering Research (IJMER)
www.ijmer.com Vol.3, Issue.2, March-April. 2013 pp-990-995 ISSN: 2249-6645

Implementation of Metamorphic Testing on Spreadsheet Applications

Balinder Singh

Abstract: *End-user programmers do not have broad knowledge about software testing methodologies. Errors are persistent in program due to lack of testing approaches take up by end-user programmers. It is not easy to employ oracle for end-users programs. Metamorphic testing is very effective approach for end-users which also address the oracle problem. In this paper, a metamorphic testing approach for spreadsheet application is used effectively. Metamorphic testing is automated testing approach, which uses expected properties of the objective function to test program without human contribution. This approach defines a set of expected properties called Metamorphic Relations to detect errors in spreadsheet.*

Keywords: *Metamorphic Testing, Oracle, Spreadsheet, Metamorphic Relations.*

I. Introduction

These days, it has become very usual for the end-users to write the program code themselves [4]. End-user programmers are not properly skilled in programming, but they write program to achieve their main goals, such as accounting, office work, scientific work, designing web application etc. Softwares like spreadsheets, databases, web application, simulations etc are being created by end-users. Unluckily, errors are persistent in end-user programs, because End-user programmers do not develop the program according to the software engineering principles as software developed by professional developers. Manuscripts must be in English. These guidelines include complete descriptions of the fonts, spacing, and related information for producing your proceedings manuscripts.

Evidence has pointed out that errors are persistent in Software developed by end-users and may be the reason of losing millions of US dollars [3]. End-user programmers do not have sufficient training for testing, debugging, code inspection etc as like by professional programmers. A variety of software testing methodologies are not easily understood by end-users. So it is required to introduce effective and simple software testing techniques for end- user programmers [6], [11].

Spreadsheet systems have become usual end-user programming environment which is used in different enterprises [5], [12], [18]. Spreadsheets are used for a variety of important tasks such as accounting, scientific computations, data analysis, office work, graphical representation of data.

The Metamorphic Testing (MT) technique that is practical and appropriate where test oracle is very difficult to apply. In software testing, an *oracle* is a procedure that helps the tester to decide whether the output of a program is correct [19]. According to *oracle assumption* [19], Let $foo(x)$ be a function such that $\{foo(x): x \in X\}$ and $pro(x)$ be a program, implementation of $foo(x)$. Let a set of test cases: $T = \{t_1, t_2, ..., t_n\} \subset X$, where $n \geq 1$ generated according to some test case selection strategy. Executing the *pro* on these test cases, the tester checks the outputs $pro(t_1)$, $pro(t_2)$,...., $pro(t_n)$ against the expected results $foo(t_1)$, $foo(t_2)$,...., $foo(t_n)$ respectively. If $pro(t_i) = foo(t_i)$, for some i, where $1 \leq i \leq n$, then t_i is known a *successful* test case, otherwise t_i is a *failure-causing* test case. The method by which the tester can decide whether $pro(t_i) = foo(t_i)$ is known as an *oracle* [19]. For example, let $foo(x) = x^2$, the test case t_i will be $\{x = 2.6\}$, the $pro(t_i)$ is = 6.76. The output can be verified by the tester either manually evaluating the multiplication of 2.6 * 2.6 or by using the inverse function to verify whether 6.76 / 2.6 = 2.6. The inverse can be made either using a correct inverse program or manually.

In the literature of software testing, it has to take assumption for the availability of the oracle. In many circumstances, the oracle is not too simple to apply. This is called as the *oracle problem* [19]. For instance, the output of complicated computations program, such as solving partial differential equations; when compilers are tested, it is very difficult to test the equivalence between source code and the generated object code; conducting testing for a program that compute combinatorial problems, testing program which performs simulations, drawing the complicated graphics to the monitor etc. Indeed, when the oracle is available and if it is not automated, then human tester performs comparison and predication on the test result manually, that means it becomes too expensive, time consuming and prone to error [2], [21]. As a matter of fact, in software testing, the oracle problem has been one of the most difficult tasks [2].

A Metamorphic Testing method [19] was introduced by *Chen et al.* to use successful test cases and to address the oracle problem. The idea behind this method is to generate follow-up test cases based on the existing successful test cases. The output of the follow-up test cases can be checked by using relation (called metamorphic relations (MR)), these are the relations between multiple executions of the target program. Follow-up test cases can be automatically generated, executed, and the verification of program *pro* does not require an oracle.

In this paper, we present the implementation of metamorphic testing for spreadsheet applications. We develop six metamorphic relations to find out errors in spreadsheet application. The rest of the paper is organized as follows. Section II introduces Background details of Metamorphic testing and Spreadsheet. Problem Analysis has been done in section III, in section IV Proposed Work and Conclusion has been done in section V.

II. Background Details

2.1. Metamorphic Testing

Metamorphic testing (MT) technique is a simple and cost-effective approach to find out the important information from the existing successful test cases (test cases those display no failure) to generate the follow-up test cases [7]. MT can be applied with the combination of other test case selection strategies which generate the initial test cases. Let $foo(x)$ be a function such that $\{foo(x): x \in X\}$ and $pro(x)$ be a program, implementation of $foo(x)$. To test program *pro*, the tester has adopted *Ss* as the test case selection strategy, such as branch coverage testing, data flow testing or random testing [1]. Let a test set $T = \{t_1, t_2, ..., t_n\} \subset X$, where $n \geq 1$, generated according to *Ss*. Execute the *pro* on *T* produces the output results $pro(t_1)$, $pro(t_2)$,...., $pro(t_n)$. If the output results $pro(t_1)$, $pro(t_2)$,...., $pro(t_n)$ notice any failure, testing is stopped and the program is started to be debugged; otherwise *T* is known as a set of *successful* test cases.

MT can be performed to make use of *T*, where in other testing methods, successful test cases have been ignored and considered useless [9]. Based on the successful test set *T*, follow-up test cases $T'=\{t'_1, t'_2, ..., t'_n\} \subset X$ can be automatically generated by MT. Further, program *pro* is executed against some necessary expected properties (called metamorphic relations) of the target function *foo*. MR contains multiple executions of the target program. As an example, If $foo(x) = \beta^y$, where β is rational number excluding zero, y is an integer, then a program *pro* implemented on function $foo(x)$ which calculates the result of target function. The property $\beta^y * \beta^{-y} = 1$ is considered as a metamorphic relation. Metamorphic testing checks the program against some necessary excepted properties called Metamorphic Relations. Therefore, Metamorphic testing executes the implemented program twice, firstly, for a successful test case, i.e. $t_i = \{\beta = -3.68, y = -6\}$, secondly, for follow-up test case generated by MT, i.e. t'_i: $\{\beta = -3.68, y = 6\}$. Finally, the computed results of both executions are checked against the expected property $pro(t_i) * pro(t'_i) = 1$. If this property is not true, then a fault is detected. If the given property is true, then MT does not specify that program's output may be correct or not. In other words, it is necessary for MT to check the properties of target function, which may not be sufficient for correctness of implemented program. Limitation of this type is found in all software testing methods.

The successfully use of MT in many areas such as numerical, spreadsheet and database, graph theory, computer graphics, compilers, interactive software were described in [13], [14]. Guidelines for selecting good metamorphic relations in metamorphic testing have been proposed in [10], [16]. To alleviate the oracle problem, fault based testing has been described in [8].

2.2. Spreadsheet Basis

A spreadsheet is a computing application that displays a rectangular table (or grid) of information, consisting of text and numbers, where values sit in cells. Spreadsheets allow defining the type of data for each cell (usually limited to texts and numbers) and defining how different cells depend on each other ([15]). Formulas describe relationships between cells. As earlier mentioned spreadsheet is end-users application and are very errors-prone. Estimates point out that half of all the spreadsheets which are created contain errors, this number may be more than as 90% [20].

In [17], a hierarchical classification of spreadsheet errors has been developed which is based on the nature as well as characteristics of the error and development life cycle of spreadsheet. In [12], three categories of spreadsheet errors namely, mechanical, logic and omission errors are described. *Mechanical* errors happen due to mistyping or pointing to a wrong cell. *Logic* errors occur due to selecting the wrong algorithm for a particular formula cell or incorrectly use of formula, resulting incorrect output. *Omission* errors occur when a spreadsheet developer does not have complete knowledge of the problem and resulting, an incomplete spreadsheet model of the problem. In experiment, 1.8% of spreadsheet cells contain mechanical errors and logic errors of 4.1% [3].

In [13], concepts, procedures and applications are defined for Metamorphic Testing but not sufficient gain for spreadsheet Applications. In [14], Metamorphic testing framework is introduced for finding error in spreadsheet using circular shift columns. If more than one column involved in formula have same value in their cells, then circular shifting column is not sufficient to detect errors. We have developed MRs that can detect errors for this problem also.

III. Problem Analysys

1.1. Problem

A spreadsheet may have many rows and columns. It is not easy to check huge amount of rows and columns manually as it is very time consuming. Test oracle [19] is too difficult for spreadsheet, if it is available and cannot be automated, resulting too expensive as verification of spreadsheet having huge amount to data is very time consuming. Therefore, to check spreadsheet application, an effective testing approach is required (generated**)** that should be simple to implement and less time consuming. Following assumptions are made:

3.1.1 It is very difficult to create test oracle on the huge amount of data in spreadsheet. Metamorphic testing is carried out to remove this problem. Many Metamorphic relations are generated that are based on the properties of target spreadsheet. Metamorphic testing does not guarantee that *program under test* produces correct output. It guarantees only to check the properties of target function.

3.1.2. A typical spreadsheet may have hundreds of rows and columns. Checking the huge amount of rows and columns manually is very time consuming, although, Metamorphic testing method [14] is applied to check errors in huge amount of data for spreadsheet quickly. As an illustrative instance, lets us take a simplified **Excel** spreadsheet shown below in Fig.1.

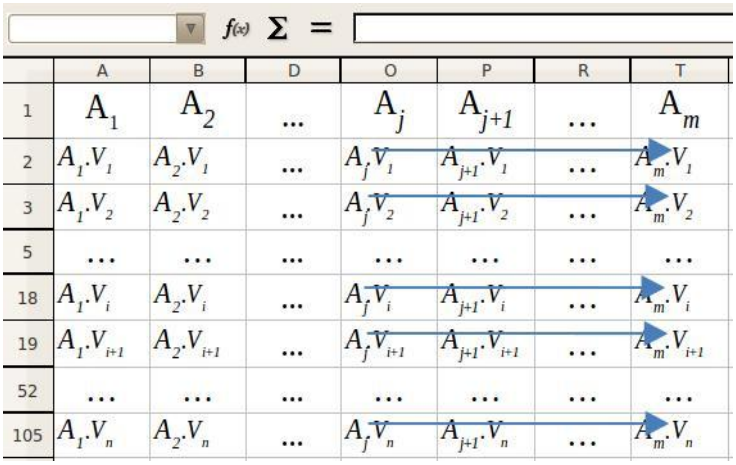

Fig.1: Spreadsheet

In Fig.1, A_j denotes the attribute, where $1 \leq j \leq m$ and $A_j.V_i$ denotes the value of that attribute, where $1 \leq i \leq n$. Values of attributes may be numeric and character type. Horizontal arrows in Fig.1, indicate the columns (A_j , $A_j + 1$,..., A_{m-1}) are involving in formula, which is laying in column A_m. Formula may be of finding sum, average, percentage, calculating discount or tax etc. on the attributes values which are involved in formula. The spreadsheet representation of this type can be used for many real life applications such as calculating total price of sold/purchased items, calculating the discount or tax on items, finding average marks or aggregate marks of different class tests in a teaching institutes etc. There may be error in any cells which contain formula [14]. Error of this type can occur when someone tries to enter the formula manually without copying formula from adjacent cells. The error cannot be noticed due to huge amount of data in spreadsheet.

This may be very harmful, if the cell containing wrong formula is dragged to copy the formula for cells below it. Formula errors are very difficult to detect as mentioned in [3]. On the other hand, by using MT, problems of this type can be easily handled. Take the example of spreadsheet mentioned above to apply MT approach. Suppose Fig.2 describes a spreadsheet as *Real Spreadsheet*, which contains few records so that MT approach can be shown easily.

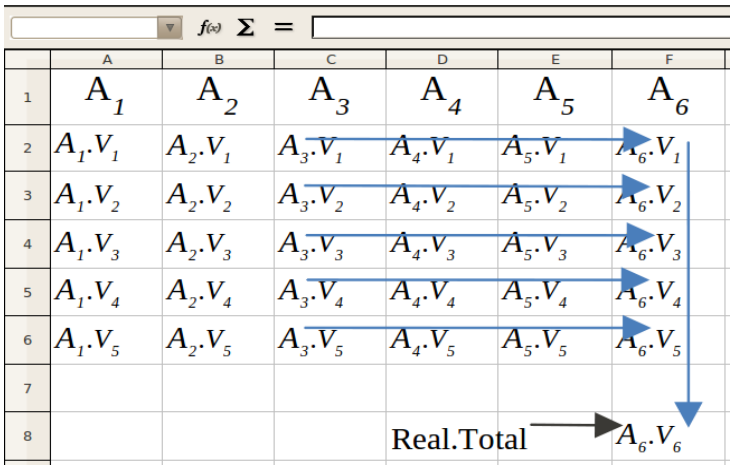

Fig.2: Real spreadsheet

In Fig.2, A_6 contains a formula, which may be according to the user requirement. For example, calculating the discount on attributes, therefore, the formula is "$A_6 = A_3 - (A_3 * 40\%) + A_4 - (A_4 * 50\%) + A_5 - (A_5 * 60\%)$". Cell F_8 describes the *Total* of all the values of A_6, calculated from the formula. Suppose the formula in the cell F_5 has been mistakenly entered as "$A_6 = A_3 - (A_3 * 60\%) + A_4 - (A_4 * 50\%) + A_5 - (A_5 * 40\%)$". Error of this type cannot be identified easily, if the $A_3.V_4 = A_5.V_4$, then $A_6.V_4$ is correct according to real formula, although, the formula in cell F_5 is really wrong. Errors of this type can be easily tackled by identifying suitable metamorphic relations corresponding to the nature of spreadsheet.

1.2. Metamorphic Testing

For the problem described above, oracle is not effective to apply because (1) spreadsheet contain huge amount of data, (2) spreadsheet allows performing complicated function on numeric values. In this situation, if oracle is not automated then it is too time consuming, expensive and prone to error. For this problem, Metamorphic Testing is effective and less time consuming, resulting not too expensive. Other advantage of MT is that it only requires the domain knowledge of spreadsheet to generate the metamorphic relations. On the other hand, spreadsheet is generally used by end-users and end-users contain great knowledge about their application domain. But they have no knowledge about software testing approach;

therefore, metamorphic testing for spreadsheet applications can be very efficient for end-users where test oracle is not available. A spreadsheet has many features like copy, paste, sorting (ascending, descending) etc and many functions. i.e. sum, average, count, etc which can be used to generate the metamorphic relations. All Metamorphic relations are generated manually using spreadsheet features and functions.

IV. Our Approach

4.1. Metamorphic Relation generation

For each and every Metamorphic Relation, we have to use *Real Spreadsheet* to create a new spreadsheet by *copy* and *paste*. The operations used in Metamorphic Relations are easily applied by "copy and paste" on the attributes which are involved in formula. We have generated six Metamorphic Relations as follow:

1.2.1. Metamorphic Relation1

First, create a new spreadsheet as MR1spreadsheet as shown in Fig.3 by copying the *Real Spreadsheet*. Apply an operation (on MR1spreadsheet) i.e. "circular shift up" [14] on the values of attributes. The *operation* which shift the values of a single attribute circularly one place up at a time Then compare the *Total* of all the values of A_6, calculated by the formula, from *Real Spreadsheet* and MR1spreadsheet i.e. *Real. Total = MR1.Total* as shown in Fig.2 and Fig.3 in cells F_8. If both *Totals* are not equal, it means *Real Spreadsheet* has an error; otherwise perform operation "circular shift up" again on same attribute and then check the equivalence between *Totals*. This process is repeated *n*-1 time on single attribute, where *n* is number of values of that attribute. This process is carried on until error is detected or all attributes (involved in formula) are not passed out by this process.

	A	B	C	D	E	F
1	A_1	A_2	A_3	A_4	A_5	A_6
2	$A_1.V_1$	$A_2.V_1$	$A_3.V_2$	$A_4.V_1$	$A_5.V_1$	$A_6.V_1$
3	$A_1.V_2$	$A_2.V_2$	$A_3.V_3$	$A_4.V_2$	$A_5.V_2$	$A_6.V_2$
4	$A_1.V_3$	$A_2.V_3$	$A_3.V_4$	$A_4.V_3$	$A_5.V_3$	$A_6.V_3$
5	$A_1.V_4$	$A_2.V_4$	$A_3.V_5$	$A_4.V_4$	$A_5.V_4$	$A_6.V_4$
6	$A_1.V_5$	$A_2.V_5$	$A_3.V_1$	$A_4.V_5$	$A_5.V_5$	$A_6.V_5$
7						
8				MR1.Total	→	$A_6.V_6$

Fig.3: MR1spreadsheet

Shifting is easily done manually by using *copy* and *paste* the values of attribute. Fig.3 shows the *operation* on *A*3 only one time.

1.2.2. Metamorphic Relation2

Like Metamorphic Relation1, take copy of *Real Spreadsheet* and paste to make a new spreadsheet as MR2spreadsheet, shown in Fig.4.

	A	B	C	D	E	F
1	A_1	A_2	A_3	A_4	A_5	A_6
2	$A_1.V_1$	$A_2.V_1$	$A_3.V_4$	$A_4.V_1$	$A_5.V_1$	$A_6.V_1$
3	$A_1.V_2$	$A_2.V_2$	$A_3.V_5$	$A_4.V_2$	$A_5.V_2$	$A_6.V_2$
4	$A_1.V_3$	$A_2.V_3$	$A_3.V_1$	$A_4.V_3$	$A_5.V_3$	$A_6.V_3$
5	$A_1.V_4$	$A_2.V_4$	$A_3.V_2$	$A_4.V_4$	$A_5.V_4$	$A_6.V_4$
6	$A_1.V_5$	$A_2.V_5$	$A_3.V_3$	$A_4.V_5$	$A_5.V_5$	$A_6.V_5$
7						
8			MR2.Total	→		$A_6.V_6$

Fig.4: MR2spreadsheet

In MR2spreadhsheet, apply an operation "circular shift down" [14] which performs shifting the values of an attribute circularly only one place down at a time. Similar to MR1, compare the *Total* of *Real Spreadsheet* and MR2spreadsheet. If both *Totals* (*Real. Total = MR2.Total*) are not equal, it means *Real Spreadsheet* has an error; otherwise perform operation "circular shift down" again on same attribute and then check the equivalence. This process is repeated *n*-1 time on single attribute, where *n* is declared earlier. We apply this operation until error is detected or all the attributes

involved in formula are not passed out by this process. *Operation* is performed manually by *copy* and *paste*. In Fig.4, this *operation* is performed only two times on A_3, manually by "copy and paste".

1.2.3. Metamorphic Relation3

Sorting is one of the main features of spreadsheet. Create a new spreadsheet as MR3spreadsheet by copying *Real Spreadsheet*. MR3spreadsheet is used to perform an operation "ascending sort" which sort the values of an attribute in ascending order. Then, compare the *Total* of both the spreadsheets i.e. *Real Spreadsheet* and MR3spreadsheet. If there is no equivalence between both *Totals*, it means error in *Real Spreadsheet*; otherwise perform the *operation* on the second attribute and check the equivalence between *Totals* and so on until error is detected or this procedure is not carried on for all the attributes involved in formula.

1.2.4. Metamorphic Relation4

Like Metamorphic Relation3, first, form a new spreadsheet as MR4spreadsheet by copying the *Real Spreadsheet*. In MR4spreadsheet, apply "descending sort" as an operation on the values of an attribute. The operation produces result sorting the values in descending order. Then compare the *Total* of both spreadsheets i.e. *Real Spreadsheet* and MR4spreadsheet. If there is no equivalence between both *Totals*, it means, there is an error in *Real Spreadsheet*; otherwise perform the *operation* on second attribute and check the equivalence between *Totals* and so on until error is detected or this process is not applied for all the attributes involved in formula.

1.2.5. Metamorphic Relation5

If in *Real Spreadsheet*, more than one attribute involved in formula contain same values i.e. $A_j.V_i = \alpha$, Then Metamorphic Relation5 can be very effective to detect error. First, create a new spreadsheet as *Additive Increase* (as shown in Fig.5) by copying the *Real Spreadsheet*. In *Additive Increase*, add consecutive integer with value α, for all the attributes which have same values and also involved in formula. Suppose, A_3 and A_5 have same values in *Real Spreadsheet*, then addition of consecutive integer has been also shown in *Additive Increase* in Fig.5.

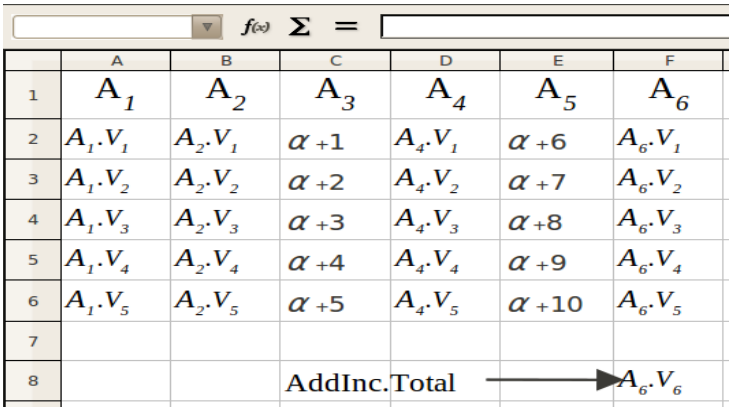

Fig.5: Additive Increase

Finally, *Additive Increase* is copied and paste to make a new spreadsheet as MR5spreadsheet. Then apply any one of Metamorphic Relations like (Metamorphic Relation1, Metamorphic Relation2, Metamorphic Relation3, and Metamorphic Relation4) on the MR5spreadsheet. Finally, compare the *Totals* (*AddInc. Total* = *MR5.Total*) of *Additive Increase* and MR5spreadsheet to check the error.

1.2.6. Metamorphic Relation6

Create a new spreadsheet as MR6spreadsheet by copying the *Additive Increase*.

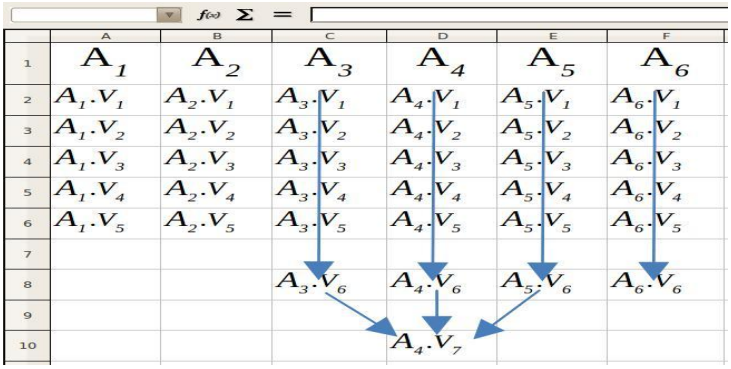

Fig.6: MR6spreadsheet

In MR6spreadsheet as shown in Fig.6, calculate the total of all the values of A_3, A_4, and A_5 which are involved in formula, in the cells C8, D8 and E8 respectively. Apply *real* formula on the values of the cells C8, D8 and E8. Calculate the result in cell D10. If the $A_4.V_7 \neq A_6.V_6$, then *Real Spreadsheet* has error; otherwise it has no error.

V. Conclusion

In this paper, metamorphic testing is employed for spreadsheet due to lack of test oracle. Test oracle for spreadsheet is very difficult to use, as a spreadsheet contains huge amount of data. Apply oracle for spreadsheet containing large range of data is very time consuming, this may result of being costly. Therefore, we use MT for spreadsheet, which is very simple and easy to implement. It also addresses the oracle problem by generating the metamorphic relations according to the expected properties of the target function. MT is very effective for end-users because end-user have domain knowledge of spreadsheet that helps to generate good metamorphic relations. Finally, we concluded that MT can be used to check the spreadsheet effectively and quickly.

References

[1] B. Beizer. Software Testing Techniques. Van Nostrand Reinhold, New York, 1990.
[2] Manolache, L. I. and Kourie, D. G. Software testing using model programs, Software: Practice and Experience, 31 (13), 2001, pp. 1211-1236.
[3] R. Panko. Finding spreadsheet errors. InformationWeek, Issue 529, page 100, May 1995.
[4] B. Boehm, C. Abts, A. Brown, S. Chulani, B. Clark, E. Horowitz, R. Madachy, D. Reifer, and B. Steece. Software Cost Estimation with Cocomo II. Prentice Hall PTR, Upper Saddle River, NJ, 2000.
[5] Ballinger, D., Biddle, R., and Noble, J. Spreadsheet Structure Inspection Using Low Level Access and Visualization. In Proceedings of the Fourth Australasian Conference on User Interfaces (Darlinghurst, Australia, 2003), Australian Computer Society, Inc., pp. 91-94.
[6] G. Rothermel, M. Burnett, L. Li, C. Dupuis, and A. Sheretov. A methodology for testing spreadsheets. ACM Transactions on Software Engineering and Methodology, 10(1):110-147, 2001.
[7] T.Y. Chen, S.C. Cheung, and S.M. Yiu. Metamorphic testing: a new approach for generating next test cases. Technical Report HKUST-CS98-01, University of Science and Technology, Hong Kong, 1998.
[8] Chen, T. Y., Tse, T. H., Zhou, Z. Q.: Fault-based testing without the need of oracles. Information and Software Technology 45 (2003), pp. 1-9.
[9] G. J. Myers. The Art of Software Testing. Wiley, New York, 1979.
[10] J. Mayer, and R. Guderlei, "An empirical study on the selection of good metamorphic relations", In Proc. of the 30th Annual International Computer Software and Applications Conference (COMPSAC), 2006, pp. 475-484.
[11] M. Burnett, C. Cook, and G. Rothermel. End-user software engineering. Communications of the ACM, 47(9), 2004, pp. 53-58.
[12] Panko, R. R. Spreadsheet Errors: What We Know. What We Think We Can Do. In Proceedings of the European Spreadsheet Risk Interest Group Symposium (2000).
[13] Z. Q. Zhou, D. H. Huang, T. H. Tse, Z. Yang, H. Huang, and T. Y. Chen. Metamorphic testing and its applications. In Proceedings of the 8th International Symposium on Future Soft- ware Technology (ISFST 2004), Xian, China, October 20-22 2004.
[14] Chen TY, Kuo FC, Zhou ZQ. An Effective Testing Method for End-User Programmer. In Proceedings of the First Workshop on End-User Software Engineering. 2005. pp. 1-5.
[15] Obrenović, Gašević, D., "End-User Service Computing: Spreadsheets as a Service Coordination Interface," IEEE Transactions on Services Computing, Vol. 1, No. 4, 2008, pp. 229-242.
[16] T. Y. Chen, D. H. Huang, T. H. Tse, and Z. Q. Zhou. Case studies on the selection of useful relations in metamorphic testing. In Proceedings of the 4th Ibero-American Symposium on Software Engineering and Knowledge Engineering (JIISIC 2004), Polytechnic University of Madrid, Madrid, Spain, 2004, pp. 569-583.
[17] Rajalingham, K., Chadwick. D., and Knight, B. (2000). "Classification of Spreadsheet Errors." Proceedings of the European Spreadsheet Risks Interest Group Annual Conference, Greenwich, UK. pp. 23-34.
[18] Wilson, A., Burnett, M., Beckwith, L., Granatir, O., Casburn, L., Cook, C., Durham, M., and Rothermel, G. Harnessing Curiosity to Increase Correctness in End-User Programming. In Proceedings of the SIGCHI Conference on Human Factors in Computing Systems (New York, NY, USA, 2003), ACM, pp. 305-312.
[19] E.J. Weyuker. On testing non-testable programs. The Computer Journal, 25(4), 1982, pp. 465-470.
[20] "What we know about spreadsheet errors, Human Error Website, Honolulu, HI: University of Hawai'i", Retrieved May 15, 2005 http site, "http://panko.cba.hawaii.edu/ HumanErr/"
[21] Hamlet, D. Predicting dependability by testing, In Proceedings of the ACM SIGSOFT International Symposium on Software Testing and Analysis (ISSTA 1996), ACM Press, New York, 1996, pp. 84-91.

International Journal of Modern Engineering Research (IJMER)
www.ijmer.com Vol.3, Issue.2, March-April. 2013 pp-996-999 ISSN: 2249-6645

Multicasting in Wireless Ad Hoc Networks Using ODMRP

Jayaprakash.S, [1] Ilamathi.V, [2] Nithyakalyani.K[3]
[123]*Asst.Professor, Department of MCA, Srinivasan Engineering College, Perambalur, Tamilnadu, (India)*

Abstract: *Wireless mesh networks are self-organized and usually without centralization control. Protocols in such networks are also required to be distributed for robustness and scalable. In this project localized mechanisms are adopted to support multicasting in wireless ad hoc networks without throttling unicast flows. The proposed scheme combines the layered multicast concept with the routing-based congestion avoidance idea to reduce the aggregated rate of multicast flows when they use excessive bandwidth on a wireless link. Our analysis and sweeping simulations show that the fully localized scheme proposed in this paper is effective in ensuring the fairness of bandwidth sharing between multicast and unicast flows in wireless ad hoc networks.*

Keyword: *wireless self configuring infrastructure less network, Mesh Topology, localized scheme, ODMRP.*

I. Introduction

Wireless ad hoc networks such as mobile ad hoc networks and wireless mesh networks are self-organized and usually without centralised control. Protocols in such networks are also required to be distributed for robustness and scalable. If a distributed protocol only relies on local information and local actions for fulfilling its functional, then the protocol is also localised. In the sense of using only local resources, a localised protocol is usually efficient and scalablized, which are the basic characteristics required for protocols in wireless ad hoc networks. In this project localized mechanisms are adopted to support multicasting in wireless ad hoc networks without throttling unicast flows.

Multicasting has emerged as one of the most focused areas in the field of networking. As the technologies and popularity of the Internet have grown, applications that require multicasting (e.g., video conferencing) are becoming more wides. Another interesting recent development has been the emergence of dynamically reconfigurable wireless ad hoc networks to interconnect mobile users for applications ranging from disaster recovery to distributed collaborative computing. Multicast plays a key role in ad hoc networks because of the notion of teams and the need to show data/images to hold conferences among them. Protocols used in static networks (e.g., DVMRP, MOSPF, CBT, and PIM), however, do not perform well in a dynamically changing ad hoc network environment. Multicast tree structures are fragile and must be readjusted continuously as connection to be changed. Furthermore, typical multicast trees usually require a global routing substructure such as link state or distance vector. The frequently exchange of routing vectors or link state tables, triggered by continuous topologies changed, yields excessive channel and processing overhead. Limited bandwidth, constrained power, and mobility of network hosts make the multicast protocol design particularly challenging. Multicast congestion control is source-based rate control, in which a multicast source regulates its transmission rate in response to loss indications (e.g. NAKs) from receivers. A number of specific source-based rate control schemes have been proposed, these represent im-portant first solutions in a very large solution space. However, a number of basic issues remain open and have to be addressed by any source-based approach towards multicast congestion control.

II. Problem Statement and Challenges

The scalability issue is essential to all multicast based protocols. A multicast congestion control protocol not only needs to scale to a large number of receivers but also needs to scale in a more heterogeneous environment with different link capacities and delays. Two resulting problems need to be addressed: feedback implosion and rate drop-to-zero. The implosion problem has been well explained in the literature on multicast error control, and various feedback suppression mechanisms have been introduced. However, all these mechanisms come with the cost of introducing extra delay in feedback. Feedback delay directly contributes to the responsiveness of congestion control schemes, the longer the delay the less the responsiveness. Additionally, in contrast to error control in which feedback is only triggered by packet losses discovered at receivers; in congestion control, the source needs constant feedback from the receivers to discover not only congestion but re-availability of resources as well. This continuous feedback should be well managed to avoid implosion and to a scalable can be achieve, yet they should also be delivered in a timely manner for sender to react to network congestion. The drop-to-zero problem is also known as loss multiplicity problem. The problem arises when receivers use packet losses as congestion signals and the source uses these signals to regulate its transmission rate without accumulated properly. When packets are lost multiple paths independent, receivers downstream of these paths will all send congestion signals to the source resulting in multiple rate drops at the source. In the current IP multicast model, the data source does not know the receiver topologies, hence cannot aggregate the congestion signals over receiver locations. Typically, when there are multiple bottleneck paths, the source has to adapt to the sum of the congestion signals generated on these paths and its rate will be quickly throttled as the number of congested paths increases.

III. Related Work

ODMRP applies on-demand routing techniques to avoid channel overhead and improve scalability. It uses the concept at forwarding group, a set of nodes response for forwarding multicast data on shortest paths between any member pairs, to build a forwarding mesh topology for each multicast group. By maintaining and using a mesh topology related to the tree, the drawbacks of multicasting trees in mobile wireless networks (e.g. traffic concentration, frequent tree reconfigure, non-shortest path in a share the tree, etc.) are avoided. A soft-state approach is taken in ODMRP to maintain multicast group members. No explicitly control message is required to leave the groups. We believe the reduction of storage overhead and the relaxed connectivity make ODMRP more scalable for large networks and more stable for mobile wireless networks. Instead of relying on end-to-end congestion control schemes, this project proposes a fully localized scheme in the network layer to support multicasting in wireless ad hoc networks while maintaining fairness with uncast flows. This integrates layered multicast with routing-based congestion avoidance to achieve its rate control over multicasting flow. The proposed scheme is fully localised. Each node acts based on local collected information and no additional interaction between nodes is required for the rate-control operations over multicast flows, except those required for standard multicast service. With the proposed scheme, a multicasting source encodes its signal into several layers of different priorities. The source then sends each layer to a separate multicast grouping. Receivers of the multicast source subscribe to these multicast groups and packets for all or some of these groups flow into the receivers can receives. At the same time, each intermediate node in the wireless ad hoc network monitoring its wireless links. When the link starts becoming congested, the node cuts the aggregate rate of multicast flows if the multicast flows are using excessive bandwidth on the links. The local rate-cut on multicasting flows is possible because each multicast flow has multiple layers, and layer priorities information is embedded in the multicast addresses of these layers. Our analysis and detailed frequently results show that the proposed scheme enables multicasting in wireless ad hoc networks and provides uncast flows their fair share of bandwidth.

IV. Functional Design and Analysis

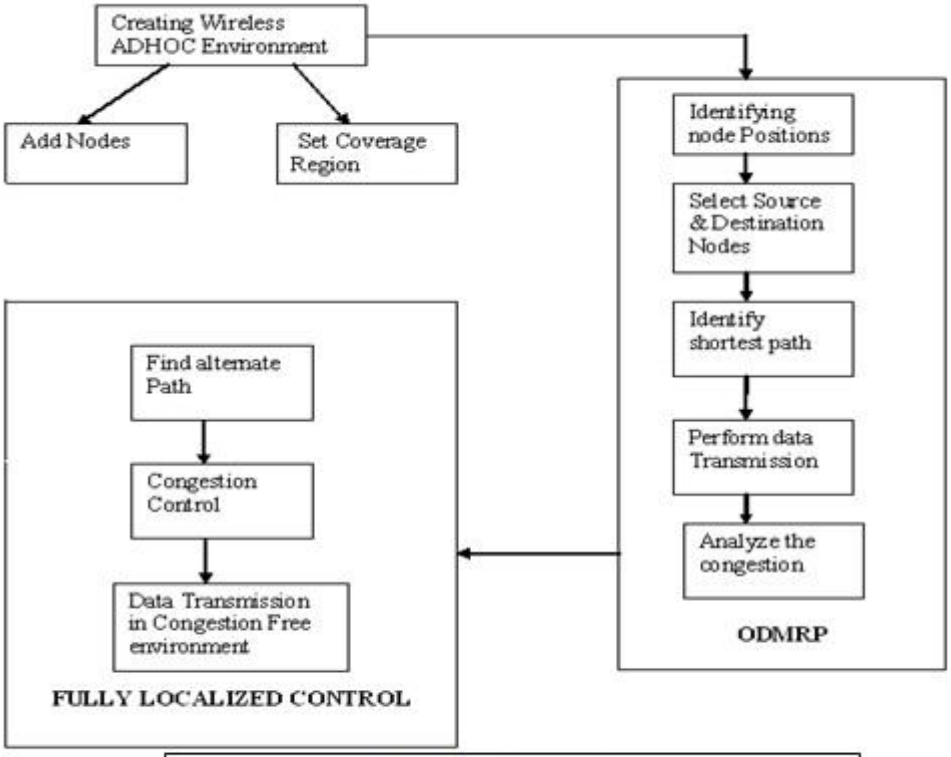

Fig-1: Overview architecture

Three set of functional steps needed as follows:

1. Creating wireless Adhoc Environment
2. On-Demand Multicast Routing Protocol (ODMRP)
3. Fully Localized Scheme

1. Creating Wirless Adhoc Environment

Wireless adhoc networks are self-organized and usually without centralized control. In this module we are going to create simulation of wireless adhoc environments.

The steps involved in this module are, measuring the number of nodes in every region. Fix the coverage region for each node. Design the adhoc environment that consists of nodes. Identify every node positions by getting the X and Y value

positions of every node. The node can transmit data only up to the coverage region. If positions of the node exceed coverage regions the popup window displays the nodes are not in coverage distance

***2.* Odmrp**

In this group membership and multicast routes are established and updated by the source on demand. In ODMRP, Identify the source node from where multicasting is going to be performed. Identify the destination nodes or group members that are going to receive the multicast data.

Design the routing table that consist of

i. Source node
ii. Destination node
iii. Shortest path

Source node Destination node shortest path Transmit the data according to the path present in the routing table. In this module heavy congestion will occur due to data transmission over same path at same time. Due to congestion in the network path the data may lose, this can be avoided by identifying the alternate path for every multicast data passing in the networks.

3. Fully Localized Scheme

There is no direct control over any uncast flows and assume that each uncast flow is controlled by the protocol without any queue management. Each node act based on locally collected information. Each node collects flow information about traffic traversing and congestion about the path. The fully localized control scheme identified the following Node positions Number of passing's per node

In this module we are going to implement layer priority information, lower layers have high priority and higher layers have less priority.

The alternate route can be identified by the following methods. Based on the number of passings through the nodes the alternate flow is identified. If the routes are become more congested, we identify the alternate path based on the shortest distance to transmit data via other nodes. Finally the data transmission takes place between source to multiple destinations can be performed without any congestion

V. Experimental Result

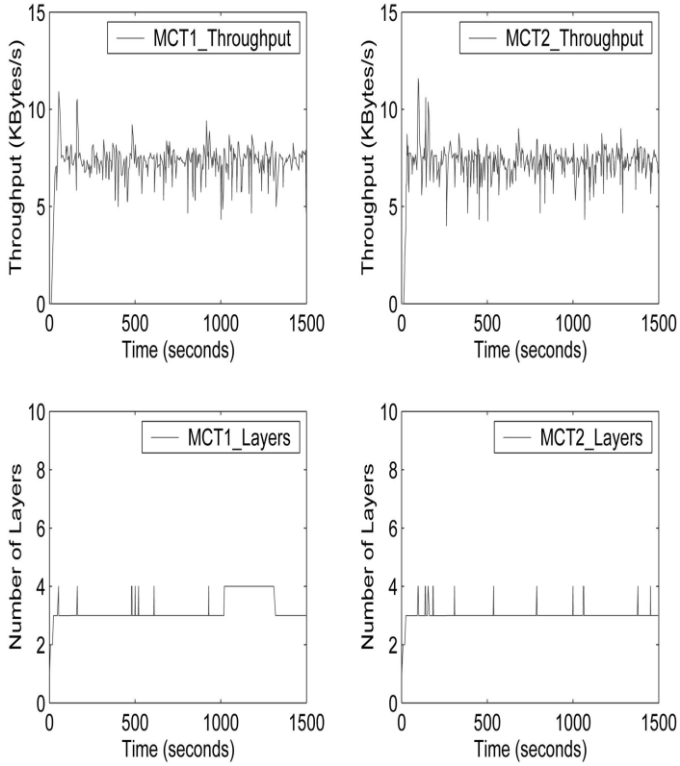

Fig-2: Individual multicast throughput and number of layers (RLM case)

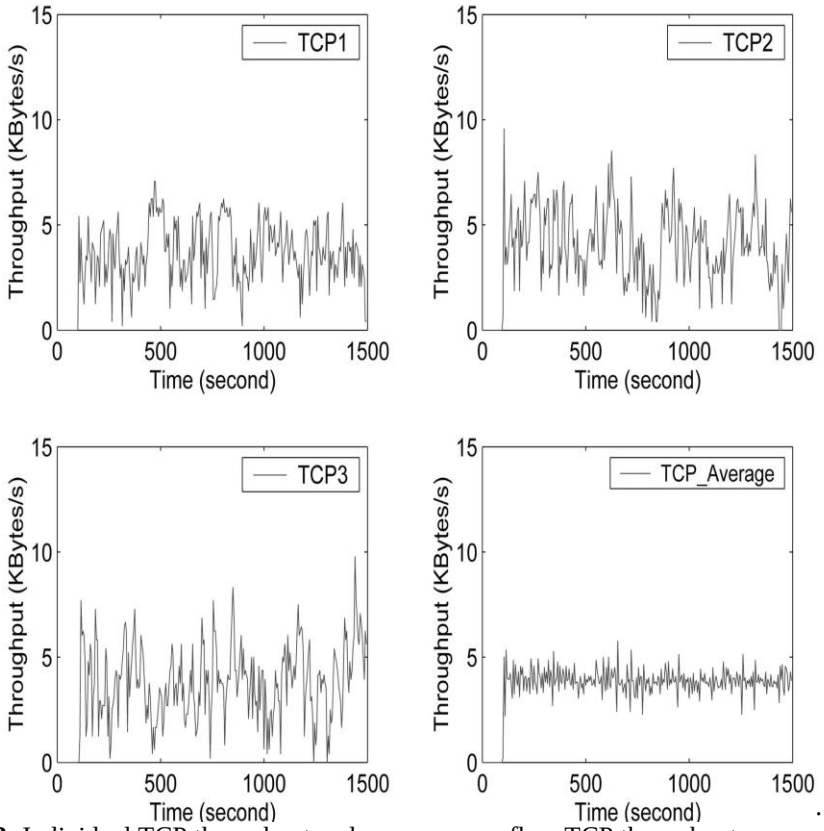

Fig-3: Individual TCP throughput and average per-flow TCP throughput

VI. Conclusion

Win runner is a automated functional GUI testing tool , as it allows us to record and playback the user actions from a vast variety of user applications as if a real user had manually executed those actions. It implements a automated Test Script Language (TSL) that allows customization and parameterization of user input. The test script is in the form of C language syntax, the user can edit script by adding some extra condition, to verify its functionality.

VII. Acknowledgments

This work was presented in part at the IEEE International Conferences on Communications (ICC), 2009. This work was can be taken in part of in our institution and support all staff members.

References

[1] Bhattacharya's, Towsley.D, and Kurose.J,(1999), "The Loss Path Multiplicity Problem in Multicast Congestion Control," Proc. IEEEINFOCOM 99, pp. 856-863.
[2] Byers.J, Luby.M, Mitzenmacher.M, and Rege.A (1998),"A Digital Fountain Approach to Reliable Distribution of Bulk Data," Proc. ACM SIGCOMM 98, pp. 56-67.
[3] Byers.J, Luby. M and Mitzenmacher. M (2001) "Fine-Grained Layer Multicasting," Proc. IEEE INFOCOM 01, Apr. 2001.
[4] Gopalakrishnan.R, Griffioen.J, Hjalmtysson.G, Sreenan. C, & Wen.S, " (2000), A Simple LoDifferentiation Approach to Layer Multicasting," Proc. IEEE INFOCOM 00.
[5] Kwon.G and Byers.J, (2000) "Smooth Multi-rate Multicasting Congestion Controls," Proc. IEEE INFOCOM '03.
[6] Lee.S.-J, Gerla.M, and Chiang.C.-C,(1999), "On-Demand Multicast Routing Protocol," Proc. IEEE Wireless Comm. and Networking Conf. (WCNC '99), pp. 1298-1304.
[7] McCanne.S, Jacobson.V, and Vetterli.M, (1996) "Receiver-Driven Layered Multicast," Proc. ACM SIGCOMM '96, pp. 117-130
[8] Rhee.I, Balaguru.N, and Rouskas.G,(1999), "MTCP: Scalable TCPLike Congestion Control for Reliable Multicast," Proc. IEEE INFOCOM '99, pp. 1265-1273.
[9] Rizzo.L, (2000)" PGMCC: A TCP-Friendly Single-Rate Multicast Congestion Control Scheme" Proc. ACM SIGCOMM '00.
[10] Royer .E.M and Perkins. C.E, (Aug 1999), "Multicast Operation of the Ad Hoc On-Demand Distance Vector Routing Protocol," Proc. ACM MobiCom '99, pp. 207-218

.

International Journal of Modern Engineering Research (IJMER)
www.ijmer.com Vol.3, Issue.2, March-April. 2013 pp-1000-1005 ISSN: 2249-6645

Total Harmonic Distortion Analysis and Comparison of Diode Clamped Multilevel Z-Source Inverter

P.Vanaja [1], R.Arun Prasaath [2], P.Ganesh[3]
[1]*PG scholar (PED), Dept of EEE, Karpagam University, Coimbatore, India*
[2]*Assistant Professor, Dept of EEE, Karpagam University, Coimbatore, India*
[3]*PG scholar (PED), Dept of EEE, SSCET, Anna University, Palani, India*

Abstract: *A desired AC voltage is achieved from several levels of DC voltages is done by multilevel inverters. These inverters are applied to high voltage and high power applications due to better harmonic spectrum and faithful output. In recent years a single X-shaped LC network is important development in multilevel inverters. The power quality improvement is obtained by reducing the harmonics present at the output voltage of the inverter. This paper presents the comparative THD analysis of several multicarrier PWM control techniques which is effectively used for harmonic mitigation in the proposed diode clamped multilevel Z-source inverter and this work is compared with conventional three level inverter by using MATLAB/SIMULINK.*

Keywords: *DCMLI, Multi-Carrier PWM control, Multilevel Inverter, Total Harmonic Distortion (THD), Z-Source Inverter.*

I. Introduction

In the recent years, the revolution of multilevel inverters has many attractive features. In particular, high voltage capability, reduced common mode voltages near sinusoidal outputs, lower value of dv/dt, smaller or even number output filters make multilevel inverter is a suitable topology for variable frequency induction motor drives and have recently been explored for low-voltage renewable grid interfacing applications [1]. Despite of their generally favourable output performance , NPC inverters are constrained by their ability to perform only voltage-buck operation if no additional dc–dc boost stages are added to their front-ends. To overcome this limitation, a buck–boost Z-source NPC inverter is proposed with reduced passive elements in [2]. Higher and lower carrier cells alternative phase opposition PWM technique was discussed for hybrid-clamped multilevel inverters [3]. Phase shift and phase opposition disposition PWM techniques were produces a same harmonic distortion in five level diode – clamped multilevel inverter, five level cascaded and hybrid inverters [4]. A zero harmonic distortion of the output wave can be obtained by an infinite number of levels. To synthesize multi level output ac voltage using different levels of dc inputs, semiconductors devices must be switched ON and OFF in such a way that desired fundamental is obtained with minimum harmonic distortion. There are different types of approaches for the selection of switching techniques for the multilevel inverters. The multilevel inverters are mainly controlled with sinusoidal PWM technique and the proposed inverter can reduce the harmonic contents by using multicarrier PWM technique arrangements [5]. Several types of PWM control techniques for various multilevel inverters are discussed [6], [7]. An additional X-shaped impedance networks are added between two isolated dc sources and a neutral clamped circuitry. The unique structure of the multilevel Z-source inverters allows them to reach high voltage with low harmonics without the use of transformers [8]. The various levels of NPC or DC inverters with space vector modulation are discussed in the references [9] - [11].

In proposed paper, various multicarrier PWM techniques like Phase disposition (PD), Phase opposition disposition (POD), Alternative phase opposition disposition (APOD), phase shifted (PS) are proposed for three phase five level diode clamped multilevel Z-Source inverter and the total harmonic distortion (THD) analysis is done for different modulation schemes. The proposed inverter can reduce the harmonic contents in the output phase voltages significantly. The total harmonic distortion (THD) reduction performance of three phases five level neutral clamped multilevel Z-Source inverter by using multicarrier PWM techniques are presented and the proposed work is compared with conventional three level diode clamped multilevel inverter.

II. Design And Operation of Diode Clamped Multilevel Inverter

The diode clamped inverter also known as neutral clamped inverter. The diode clamped inverter delivers the staircase output voltage using several levels of DC voltages developed by DC capacitors. If m is the number of level, then the number of capacitors required on the DC bus are (m-1), the number of power electronic switches per phase are 2(m-1) and the number of diodes per phase are 2(m-2). This design formula is most common for all the diode clamped multilevel inverters. The DC bus voltage is split into three levels using two capacitors C_1 and C_2, for five levels using four capacitors C_1, C_2, C_3 and C_4 are shown in Fig .1 and Fig .2. The voltage across each capacitor is $V_{dc}/4$ and the voltage stress across each switch is limited to one capacitor voltage through clamping diodes. The switching sequences of three phase 3-level and 5-level diode clamped multilevel inverter are shown in table. I and II. As the number of levels increase the harmonic distortion decreases and efficiency of the inverter increases because of the reduced switching losses. The number of levels in multilevel inverters is limited because of the large number of clamping diodes required. The reverse recovery of these diodes is especially with multicarrier PWM techniques in a high voltage application is a major design challenge.

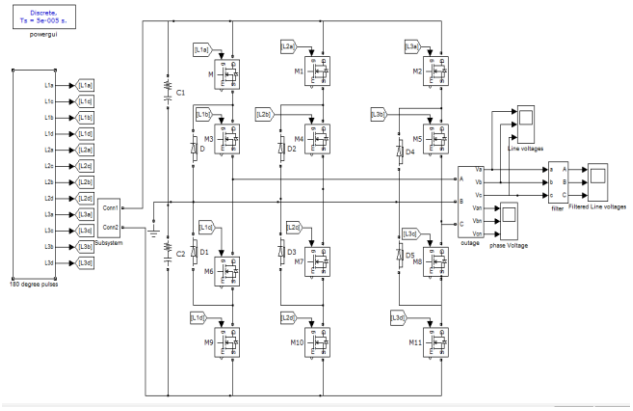

Fig.1.Three level diode clamped multilevel inverter

TABLE I
Three-level switching sequences

Terminal voltages	Switching sequences			
	S_{a1}	S_{a2}	S_{a3}	S_{a4}
$+v_{dc}$	On	On	Off	Off
0	Off	On	On	Off
$-v_{dc}$	Off	Off	On	On

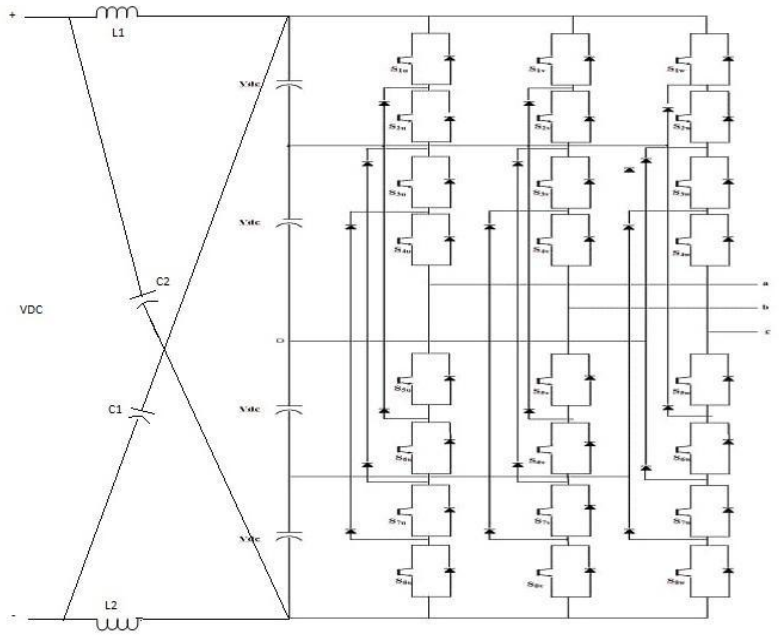

Fig.2. Five level diode clamped multilevel inverter.

TABLE II
Five-level switching sequences

Terminal voltages	Switching sequences							
	S_{a1}	S_{a2}	S_{a3}	S_{a4}	S_{a5}	S_{a6}	S_{a7}	S_{a8}
$+2v_{dc}$	On	On	On	On	Off	Off	Off	Off
$+v_{dc}$	Off	On	On	On	On	Off	Off	Off
0	Off	Off	On	On	On	On	Off	Off
$-v_{dc}$	Off	Off	Off	On	On	On	On	Off
$-2v_{dc}$	Off	Off	Off	Off	On	On	On	On

III. Control Techniques of Multilevel Inverter

Multicarrier PWM techniques involves the natural sampling of single modulating reference waveform typically being sinusoidal, through several carrier signals typically being triangular waveforms This modulation method is the logical extension of sine-triangle PWM for multilevel inverters, in which (m-1) carriers are needed for m-level inverter. They are

arranged in vertical shifts in continuous bands defined by the levels of the inverter. Each carrier has the same frequency and amplitude. A single voltage reference is compared to the carrier arrangement and the generated pulses are associated to each switching devices.

3.1Phase Disposition (PD)

This technique involves a number of carriers (m-l) which are all in phase accordingly. In 5 -level inverter all the four carrier waves are in phase with each other and compared with reference signal. According to that, the gate pulses are generated and are associated to each switching devices. The phase disposition PWM technique is illustrated in Fig. 3

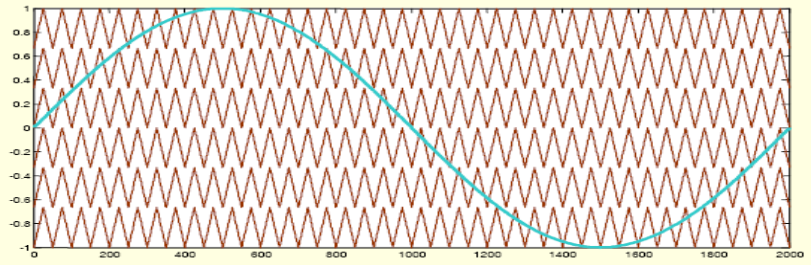

Fig.3. Phase disposition PWM technique

3.2. Phase Opposition Disposition (POD)

This technique employs a number of carriers (m-1) which are all in phase above and below the zero reference. In 5-level converters all the four carrier waves are phase shifted by 180 degrees between the ones above and below zero reference. The reference signal is compared with all four carrier waves there by gate pulses are generated and are associated to each switching devices. The phase opposition disposition PWM technique is illustrated in Fig.4.

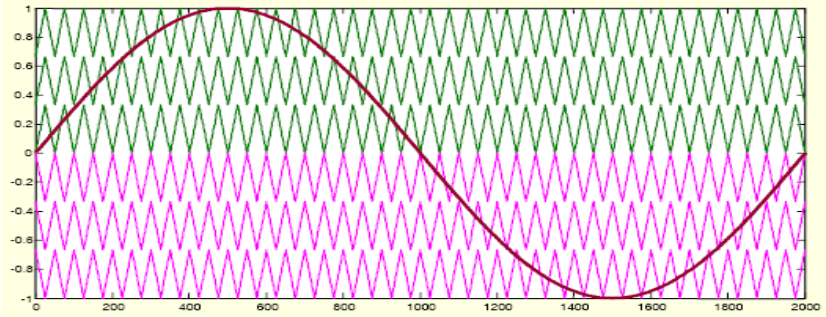

Fig.4. Phase opposition disposition PWM technique

3.3. Alternative Phase opposition Disposition (APOD)

This technique requires number of carriers (m-1) which are all phase displaced from each other by 180 degrees alternatively. The alternative phase opposition disposition PWM technique is illustrated in Fig. 5.

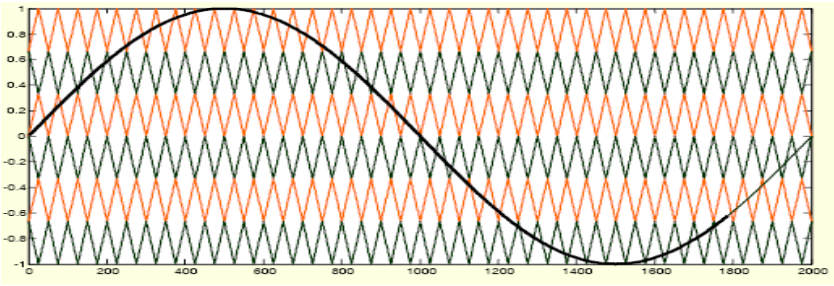

Fig.5. Alternative phase opposition disposition.

3.4. Phase Shift (PS)

This technique employs a number of carriers (m-l) phase shifted by 90 degree accordingly. In 5 -level converter all the four carrier waves are phase shifted by 90 degree. The phase shifted PWM technique is illustrated in Fig. 6.

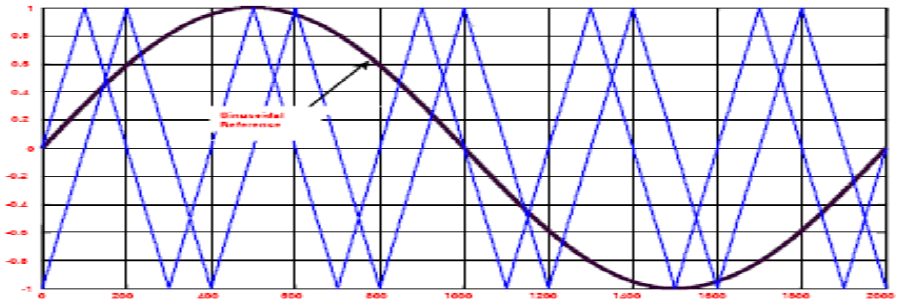

Fig.6. Phase shifted PWM technique.

IV. Simulation Results

Three level diode clamped multilevel inverter consist of 12 MOSET switches 6 clamping diodes and 2 DC link capacitor are connected with single DC source. Five level diode clamped multilevel Z-source inverter consist of 24 MOSET switches 12 clamping diodes and 4 DC link capacitor are connected with single DC source. The figure 7 and 9 shows the output voltages of 3-level and 5-Level respectively. THD values of 3-level neutral clamped multilevel inverter with PWM technique as illustrated in Fig.8. THD values of different multicarrier PWM techniques are shown in figure 10 to 13.

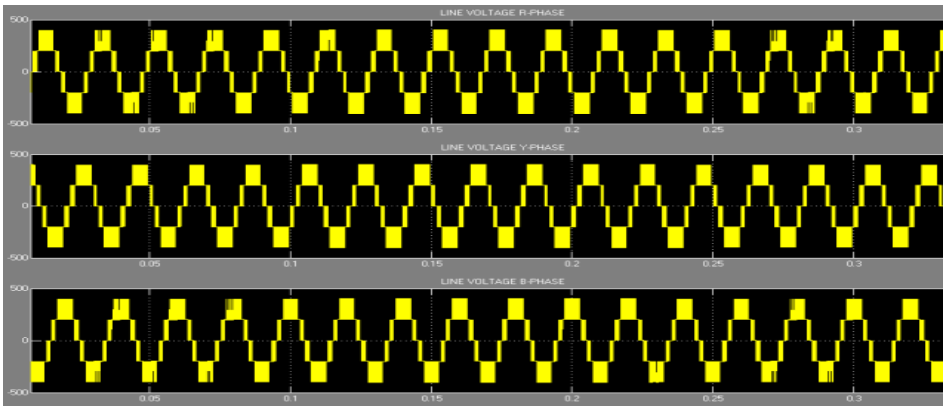

Fig.7. Line voltages of three level diode clamped multilevel inverter.

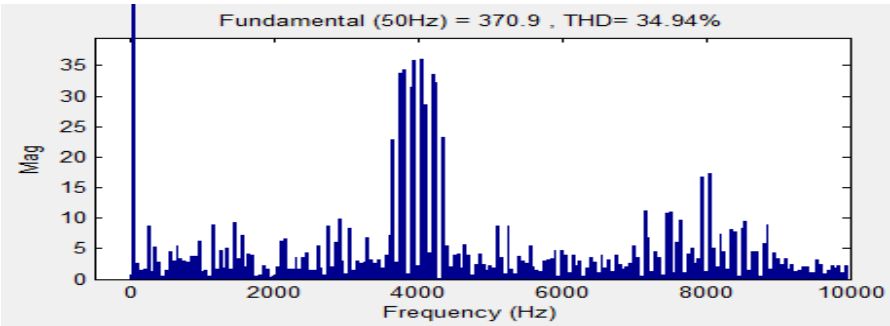

Fig.8. THD values of three level diode clamped multilevel Inverter with PWM technique.

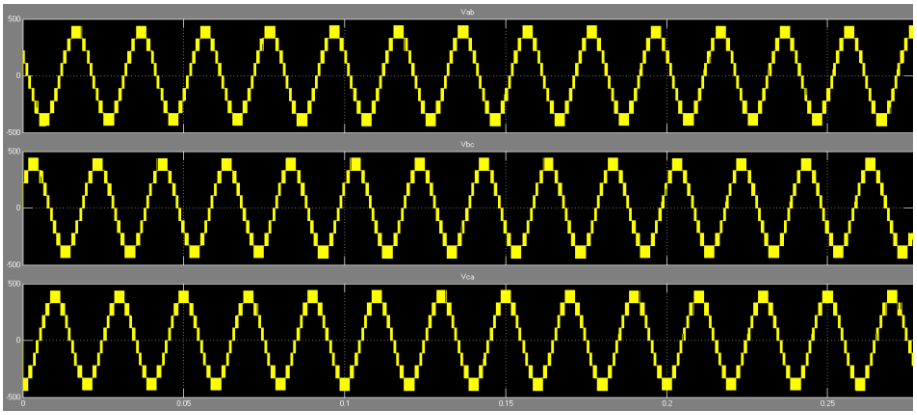

Fig.9. Line voltages of five level diode clamped multilevel z-source inverter.

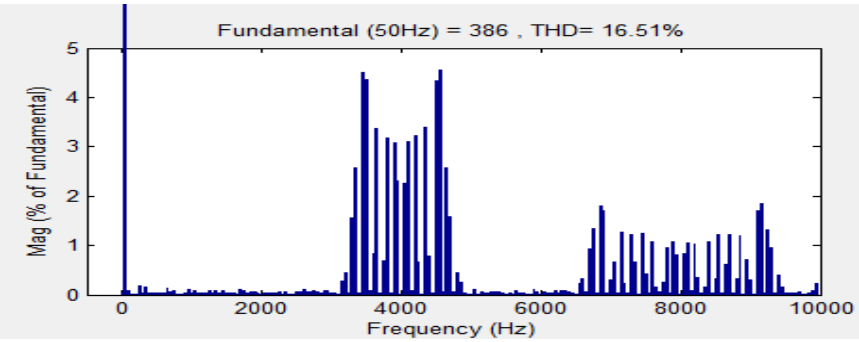

Fig .10.THD values of phase disposition PWM technique

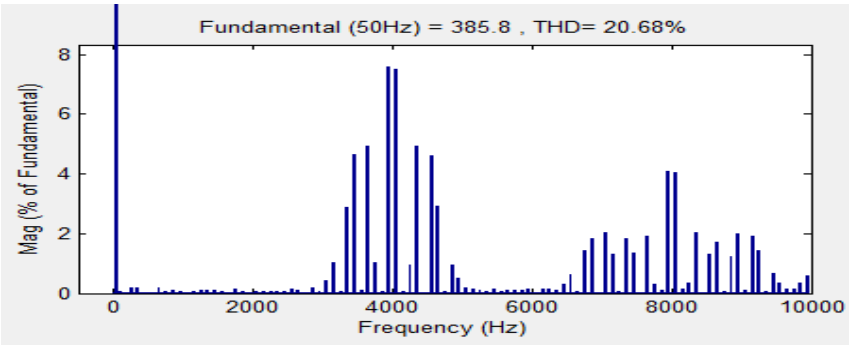

Fig.11. THD values of phase opposition disposition PWM technique.

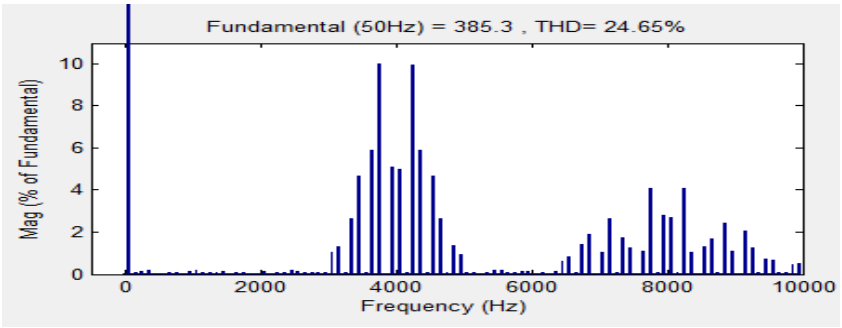

Fig.12. THD values of alternative phase opposition disposition PWM technique.

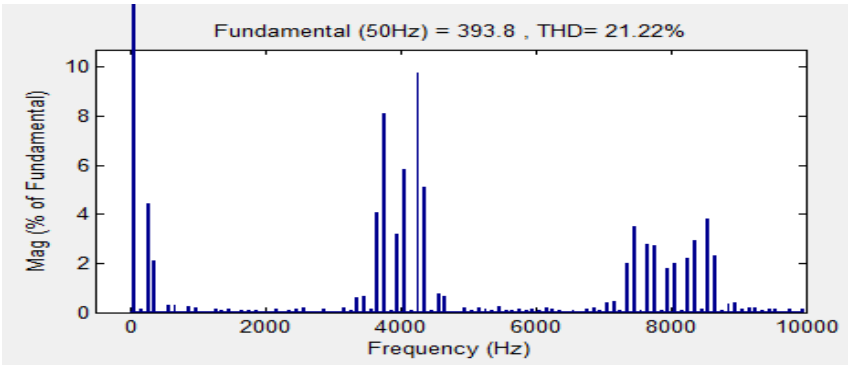

Fig.13. THD values of phase shifted PWM technique.

TABLE III
% OF THD VALUES

PWM TECHNIQUES	Three level DCMLI (%THD)	Five level DCMLI (%THD)
PD	34.94%	16.51%
POD	31.50%	20.68%
APOD	31.50%	24.65%
PS	57.12%	21.22%

V. Conclusion

The comparative THD analysis of a three phase five level diode clamped multilevel Z-source inverter is performed using various multicarrier PWM techniques. In proposed converter, Phase Disposition (PD), Phase Opposition Disposition (POD), Alternative Phase Opposition Disposition (APOD) and Phase Shifted (PS) PWM techniques are applied**.** The THD values of the output voltages of above mentioned techniques are compared with each other. From the above analysis, it is absorbed that the phase shifted PWM technique has less harmonic content in the output phase voltage compared with other multicarrier PWM control techniques and the proposed work has compared to the conventional three level inverter with PWM techniques by using MATLAB/SIMULINK.

References

[1] Poh Chiang Log, Feng Gao, Frede Blaabjerg and Sokweilim, ”Operational analysis and modulation control of three-level Z-source inverter with enhanced output wave form quality,”IEEE Transaction on power electronics,vol.24, no.7,july 2009.
[2] Poh Chiang Log, Feng Gao, Pee-Chain Tan, and Frede Blaabjerg,”three-level AC-DC-AC Z-source converter using reduced Passive component count,” IEEE Transaction on power electronics,vol.24, no.7,july 2009.
[3] Jing Zhao, Xiangning he and Rongxiang Zhao, “A Novel PWM Control method for Hybrid-clamped multilevel inverter,”IEEE Transaction on industrial electronics, vol.57, no.7, July 2010
[4] Brendan Peter Mcgrath and Donald Grahame Holmes,”Multicarrier PWM strategies for multilevel inverter,”IEEE Transaction on industrial electronics, vol.49, no.4, August 2002
[5] Samir Kouro, Pablo Lezana, Mauricio Angulo and Jose Rodriguez, “multicarrier PWM with Dc-Link ripple feed forward compensation for multilevel inverter, “IEEE Transaction on power electronics, vol.23, no.1, January 2008
[6] Leon M.Tolbert, Fang Zheng Peng and Thomas G.Habetler, “multilevel PWM methods at low modulation indices, “IEEE Transaction on power electronics, vol.15, no.4, July 2000.
[7] M.A.Saqib and S.A.R.Kashif, “Artificial neural network Based Space vector PWM for a five-level diode-clamped inverter,” AUPEC, 2010.
[8] Sreenivasarao D, Pramod agarwal and B.das, “a carrier-transposed modulation technique for multilevel inverters,” PEDES, 2010.
[9] S.Ebaneza Pravin and R.Narciss Starbell,”Induction motor drive using seven level multilevel inverter for energy saving in variable torque load application,” ICCCET March 2011
[10] P.T.Josh, Jovitha Jerome and Arul Wilson, The Comparative Analysis of Multicarrier Control Techniques for SPWM Controlled cascaded H-bridge multilevel inverter,” Proceedings of ICETCT 2011.
[11] G.Durgasukumar and M.K.Pathak, “THD reduction performance of multi-level inverter fed induction motor drive,” IICPC, 2011.

International Journal of Modern Engineering Research (IJMER)
www.ijmer.com Vol.3, Issue.2, March-April. 2013 pp-1006-1014 ISSN: 2249-6645

Improvement Of Airborne Antennas' Noise Immunity With The Usage Of Periodic Structures

Jean-François D. Essiben[1], Eric R. Hedin[2], Yong S. Joe[2]
[1]*Department of Electrical Engineering, Advanced Teachers' Training College for Technical Education, University Of Douala, Cameroon*
[2]*Center for Computational Nanoscience, Department of Physics and Astronomy Ball State University, Muncie IN 47306, USA*

Abstract: *This article presents a review of different methods of reducing coupling in radio systems. Specifically, we consider the problem of coupling between aperture antennas located on a common impedance surface, and analyze structures which are typically used to solve this form of problem, i.e., periodic structures. We also note that for better design of the structure, there is a need to develop the techniques of synthesis of these structures and, for the future, to develop new electrodynamics and mathematical models, and for research on new electromagnetic bandgap materials.*

Keywords: *Electromagnetic compatibility, electromagnetic bandgap materials, impedance surface, periodic structure, coupling.*

I. Introduction

An analysis of the applications of radio electronic devices shows that, specifically, the number of active radio engineering systems is constantly growing. The total of mobile radio stations doubles every 4~5 years [1]. The number of radar installments is increasing even more rapidly. Many radio engineering systems operate in the immediate proximity of each other. This especially concerns airborne systems located onboard ships, aircraft and satellites. In addition, a growing number of radio electronic systems have a greater radiating power. There are, for example, klystrons with an average power of 1 megawatt (MW) and a pulse power of up to 100 MW; and magnetrons with an average power of 1 kilowatt and a pulse power of up to 10 MW. The imperfection of radio transmitting devices along with generation of the main frequency causes the presence of harmonics and sub harmonics in the spectrum of the generated power, which have a level of 50~90 decibels (dB) and can reach hundreds of watts. The sensitivity of modern receivers is several levels higher and reaches (-130 ~ -160 dB/watt). In this process, the problem of electromagnetic compatibility (EMC) of the receiving and the transmitting radio engineering systems modules becomes acute. This problem is connected with their mutual influence on each other.
The problem of EMC for different radio electronic systems consists in effecting the operation of these systems with no undesirable electromagnetic coupling between antennas, which destroys functioning with the required quality of these and other electronic systems. In other words, the problem of EMC is the problem of interference immunity, i.e., protection from the effects of natural interference of different types, and it has much in common with the problem of protection from interference of the desired signal [2].

The main purpose of this paper is the analysis of the problem of EMC of radio engineering systems and the presentation of the methods of providing EMC by using antenna design techniques. In particular, we review a solution to the problem of reducing coupling between antennas located on the same surface using periodic structures. In addition, we notice the importance of the level of the cross-polarization components on the reduction of coupling between antennas, and present methods to help reduce the influence of aberrations of mirror antennas on EMC parameters. Finally, we suggest some prospects for further research.

The paper is organized as follows: In Section II, we present the main methods of spatial reduction of antenna coupling, and principles of ensuring antenna decoupling using corrugated periodic structures are presented in Section III. The influence of polarization characteristics on decoupling between antennas is presented in section IV. Section V presents the influence of aberration of the mirror antennas on EMC parameters. Finally, Section VI is devoted to the conclusion.

II. Main Methods for Spatial Reduction Of Antennas Coupling

II.1. General Questions

One of the most important problems in radio electronic device development is the provision of EMC of different radio systems, i.e., the provision of their simultaneous and normal functioning under the conditions of real collocation. Accomplishing EMC is most desirable through the use of the strict methods of electrodynamics, without interference into the equipment and without temporal regulation, which destroys normal functioning, i.e., only due to reduction of coupling (increase of decoupling) between antennas. The quantitative estimation of decoupling of antennas is characterized [3], by the coefficient of antenna coupling:

$$K_c = \frac{P_{rec}}{P_{tr}}, \qquad (1)$$

where P_{rec} and P_{tr} are the powers of the signals (the received signal at the exit of the receiving antenna and the transmitted signal at the entrance of the transmitting antenna). The inverse value of K_c, called the decoupling coefficient *K*, is defined as $K = -10\log(K_c)$.

For antennas in the free space, decoupling is defined by directivity diagram levels (in fractions of increasing coefficient) in the direction of the coupling line (taking into account the polarization and spatial spreading). In the case of airborne placement, the electromagnetic field (EMF) of an antenna depends on the configuration of the object. In addition, coupling is provided along spatial and geodesic lines on the object surface. The problem of EMC includes many aspects, from which it is possible to single out the following: the problem of sources of unintended interference, primarily those of radio transmitting devices; reasons and mechanisms giving rise to the interference; ways to control them and to mitigate the interference; the problem of unintended interference receptors, and those of radio receiver devices; mechanism of the interference passage through the receiver; ways to measure interference and reduce it, and methods of EMC calculation and evaluation.

Among the existing methods of providing EMC of radio electronic systems, we can single out technical and organizational methods. Technical methods in their turn can be subdivided into infra-apparatus and extra-apparatus methods. Intra-apparatus methods include the use of frequency selective spatial filters and those methods of EMC provision which are based on reducing interference by means of improved antenna system parameters. At the initial stage of radio engineering development, EMC was provided in one of two ways: frequency distribution or schematic and structural improvements of separate units by each radio engineering systems developer. However, the technical possibilities of both of these methods are practically exhausted. That is why a new direction has appeared in radio electronics which focuses on design, development and exploitation of radio engineering systems subject to the conditions of the existing limitations.

II.2. Methods of reduction of antenna coupling

Investigations into solving EMC problems, conducted at present in many countries of the world, include the development of enhanced interference-protected radio electronic systems, as well as the issues of optimum design from the viewpoint of reduction of the generated interference. Significant attention in these investigations is paid to antennas, because 12 out of almost 30 basic parameters which influence EMC in radio electronic equipment are defined by the antenna system [4]. Spatial and frequency discrimination of interference accomplished by antenna systems allows for significant improvement of EMC. In the process of development and design of new antennas, primary attention is paid not only to their internal parameters, such as amplification, conformity, bandwidth, etc., but also to EMC problems between the antennas [5, 6].

In most cases, when solving the question of EMC of radio engineering complexes, we are working with ready-made radio electronic complexes and antenna systems. Therefore, methods related to the growth of noise immunity of antennas have a great practical application, since the main features of the antennas' construction cannot be changed [4]. If we have the possibility of choosing the point of location of the receiving antennas, then in order to provide decoupling between the receiving and transmitting antennas located in proximity to each other on the same plane, we can use the following methods:

[1] Choice of the point of antennas location

(A) Two transmitting antennas with a phase shift between their currents, along with a receiving antenna [7]. The disadvantages of such a system are complexity of actual construction, immense size and small bandwidth.

(B) The receiving antenna is located in the space where the currents of the transmitting antennas are minimal and are directed in such a way that they do not stimulate the receiving antenna [7]. However, this method also has some disadvantages. In particular, it requires a specific mutual orientation of the antennas, which limits the range of the antennas` spatial directivity diagrams and their polarization characteristics.

[2] Utilization of metallic screen

In this case, metallic longitudinal and transverse diffraction screens which significantly rise above the plane of the antennas are placed between the transmitting and the receiving antennas [7]. From the data of reference [8], with the use of a screen of height λ it is possible to obtain weakening of about 20 dB in the frequency band with an overlapping of 1.5:1. In Ref. [9], the authors propose weakening the electromagnetic coupling between antennas by the use of longitudinal conducting plates placed between the antennas along the line of communication in E-plane. The possibility of weakening the lateral radiation of the aperture antennas in this case is connected with the wave's interference from the edges of the antenna and the borders of the plates. Varying the amplitude-phase correlations, we can obtain in some directions a decrease of radiation of 10~15 dB. The possibility of reducing the mutual coupling of antennas located on the edge of a semi-plane conductor with the help of longitudinal (in the case when the vector E is parallel to the semi-plane) and transverse (the vector H is parallel to the semi-plane) diffraction screens is shown by Yumashev [10]. There are other papers in which the question of reducing coupling between antennas by the use of diffraction screens is considered [8, 11].

[3] Utilization of a radio-frequency absorbing layer and corrugated structures

For this case, on a metallic plane between the antennas there is a radio-frequency absorbing layer (for example, graphite) with a constant thickness, or a corrugated structure [12]. Using an absorbing layer, the field weakening can be calculated by the formula of Shuleikin-Van-der-Paul. According to this formula, if distances are small, the weakening is proportional to the distance; for larger distances, the weakening is proportional to the distance squared. As experiments show, when measuring decoupling between two slot antennas, the best weakening is obtained when the distance between antennas is

equal to λ, which gives 30~35 dB of decoupling. This corresponds to additional decoupling in comparison with the case of a metallic plane, which gives 10~15 dB. A disadvantage of radio-frequency absorptive coverings is their large size, which reduces the aerodynamic properties of an object, because it is required that it cover all of the object or its significant parts. Another disadvantage of coverings is the dependence of the reflection coefficient on the frequency and on the incident angle of the electromagnetic waves.

III. Principles of Ensuring Antenna Decoupling Using Corrugated Periodic Structures

The easiest way to study the operation of decoupling devices based on a corrugated structure is by using the impedance approach. For this purpose, the notion of a transverse surface impedance Z is introduced. Z Equals the ratio of mutually perpendicular electric and the magnetic field components which are tangential to the surface:

$$\vec{\mathbf{n}} \times \vec{\mathbf{E}} = -\mathbf{Z}\vec{\mathbf{n}} \times (\vec{\mathbf{n}} \times \vec{\mathbf{H}}), \qquad (2)$$

where $\vec{\mathbf{n}}$ is the unit normal, Z is the surface impedance, $\vec{\mathbf{E}}$ is the $\mathrm{E}-$field, and $\vec{\mathbf{H}}$ is the $\mathrm{H}-$field.
For this case a wave can exist which, for a flat surface with a constant impedance distribution, has the following form [3]:

$$A\exp[-\alpha y - i\gamma z],$$

where z and y are the longitudinal and transverse Cartesian coordinates on the impedance plane, respectively. $\frac{\gamma}{k} = \sqrt{1-(Z/Z_0)^2}$, $\frac{\alpha}{k} = -i\frac{Z}{Z_0}$, ($k = 2\pi/\lambda$ is the wave number, λ is the wavelength), i is the imaginary operator and $Z_0 = \sqrt{\mu_0/\varepsilon_0}$ is the impedance of free space. Here, γ and α are decay constants.

If Z has an inductive imaginary part, with losses in the underlying surface, the amplitude of the field will proportionally diminish with y, as well as along the z direction. If the impedance has a purely reactive (capacitive) character, the amplitude of the field will increase with the distance along the normal to the y direction, i.e., the wave, remaining slow, will be a pseudo-surface wave. The increase in decoupling of near-surface antennas by this process will be accompanied by a decrease in the level of the communication signal. For the inductive case, the signal diminishes by means of ohmic losses, and in the capacitive case, by the reduction of the near-surface field. Real decoupling between the antennas is defined not only by the decoupling structure, but also by the influence of the whole field excited by the transmitting antenna, and this field will contain surface, pseudo-surface, and spatial waves [3].

The main methods of research on periodic structures can be subdivided into two categories: the first category seeks to solve the problem of flat wave scattering by a periodic structure. The results allow the definition of an equivalent impedance, $Z(0)$, of the periodic structure. This impedance conforms with normal incidence of the plane wave on an infinite flat structure and is equal to:

$$Z(0) = Z_0(1-R(0))/(1+R(0)), \qquad (3)$$

where $R(0)$ is the coefficient of reflection for normal incidence. The essense of the impedance method is that for arbitrary angles of incidence, $Z = Z(0)$ is assumed, and the periodicity of the structure is not taken into account. This supposition is certainly true only for periodic structures with high frequency for which the following condition is fulfilled: $0.05 < b/\lambda < 0.3$ (where b is the length of the corrugation). Conclusions obtained on the basis of the impedance approach are limited, since the method and the concept of impedance depend on initial values, which are approximate. As for the second category, more exact results can be obtained only with the use of strict electrodynamic methods, such as the method of integral equations through the results of numerical research.

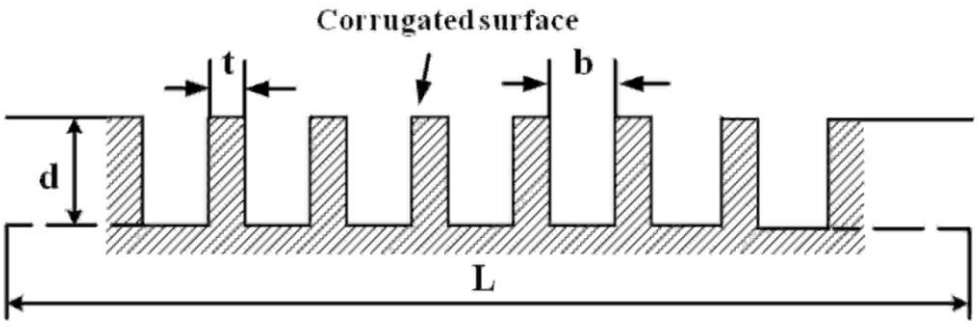

Figure 1. The corrugated metal surface with constant depths of corrugation, where L is the length, d is the depth of the corrugation, b is the width of the corrugation, and t is the thickness of the edges between them

The most common type of periodic structure is a metallic structure with a rectangular cut of corrugations. For example, in Figure 1 we present a sample of a corrugated metal surface usually used to solve the problem of coupling between antennas. The corrugated metal surface shown in Figure 1 is a metal slab into which a series of vertical slots have been cut. The slots are narrow, so that many of them fit within one wavelength across the slab. Each slot can be regarded as a parallel plate transmission line, running down into the slab and shorted at the bottom. If the slots are one quarter-wavelength deep, then the short circuit is at the top end. Thus, the impedance at the top end is very high. In this situation, the surface impedance is capacitive and transverse magnetic (TM) surface waves are forbidden. Furthermore, a plane wave polarized with the electric field perpendicular to the ridges will appear to be reflected with no phase reversal [13]. In fact, such a class of corrugated metal surfaces has been rigorously analyzed and published in numerous papers since the mid-20th century [14]. For instance, the propagation of surface waves along a uniform planar corrugated structure, under TM mode operation, was investigated in the 1950s by Rotman [15], Elliott [16], Hurd [17] and Vainshtein [18]. Additionally, we can also use other corrugation shapes which have been investigated, as shown in Figures 2-6, to solve the problem of reducing coupling between antennas located on different surfaces (see Figures 7 and 8).

Figure 2. Cavity-loaded corrugations Such corrugations have been applied in horn-antenna design, but they are very expensive to machine. The relative bandwidth is about 2.4 [39].

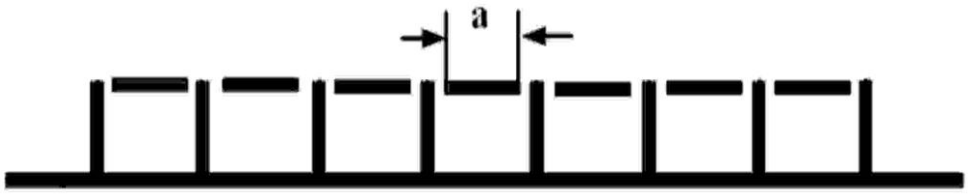

Figure 3. Strip-loaded corrugations This loading is inexpensive to fabricate and is equivalent to the cavity loading even though there is no metal contact between the strips and the corrugations. The relative bandwidth is about 2.1 [39]. *a* is the strip width.

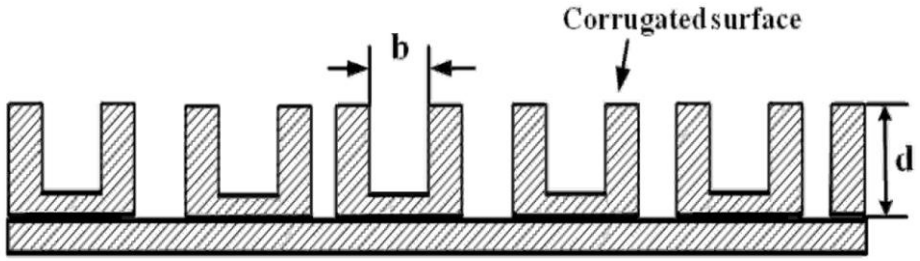

Figure 4. The dual-depth corrugations are used to realize dual-band application. The analysis shows that the soft surface occurs in two narrow bands. In between the two bands there are always surface waves occurring. Also, the two bands must be widely separated; otherwise the performance in the lower band is destroyed by surfaces waves in the shallower corrugations designed for the upper band [39].

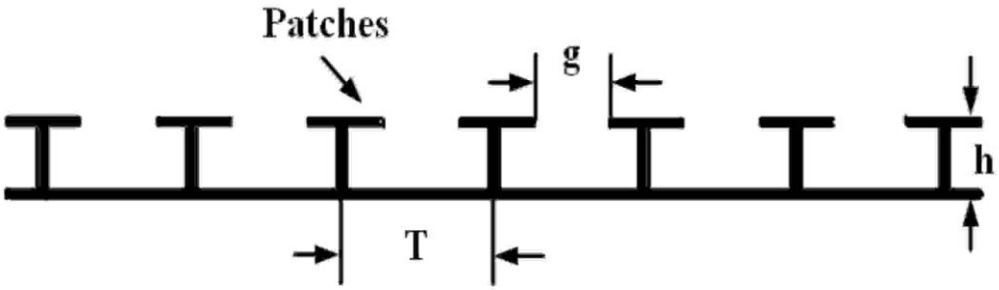

Figure 5. The cross section of a high impedance surface, fabricated as a printed circuit board. The geometrical parameters of the structure are: h the height, **g** the gap between the patches, **T** the periodicity of the high impedance surface. The periodic structure is composed of infinitely many identical cavities, each with an opening to the air half-space. Each cavity may be viewed as a parallel-plate waveguide that is completely short-circuited at one end and partially short-circuited at the other end. Such a structure had been modeled as an impedance surface to explain Wood's anomaly in the scattering of light [14].

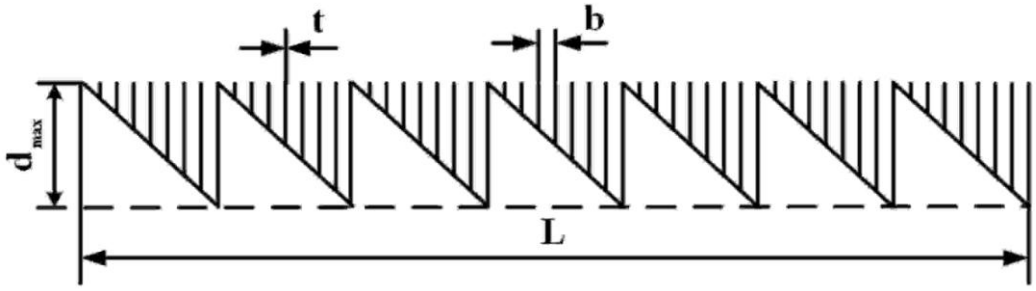

Figure 6. The corrugated metal surface with variable depths of corrugation, where L is the length, $d_{\max}$ is the depth of the corrugation, b is the width of the corrugations and t is the width of the thickness of the edges between them.

It seems that the efficiency of a decoupling structure is 10~15 dB higher when it is located in direct proximity to a source or radiating receiver, as compared with the case when the structure is placed midway between the antennas. This is explained by the fact that the "take-off" and "landing" grounds near the antennas produce a greater influence on the propagation across a plane surface [19]. Often, in quality airborne antenna systems, we use antennas located directly on a surface of complex shape as shown in Figures 7 and 8. Such antennas allow the realization of a considerably wider directional spectrum, in comparison with plane aperture antennas. When a corrugated structure is located on a convex surface, the absolute value of the increase in decoupling with a fixed antenna location is weaker in comparison with the planar case because of shading due to the convex surface. The presence of the corrugated structure therefore has a smaller impact on the form of the directional diagram of the antennas.

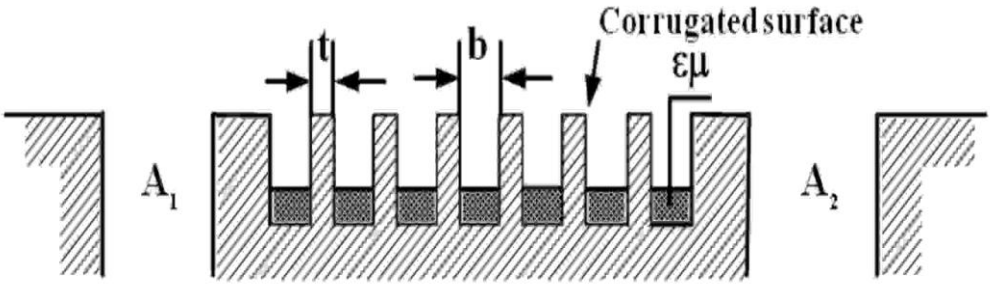

Figure 7. A corrugated metal surface (with a dielectric material of relative permittivity ε and a relative permeability μ) located on the plane with the view of defining the degree of decoupling of the two microwave antennas (transmitting (A_1) and receiving (A_2)).

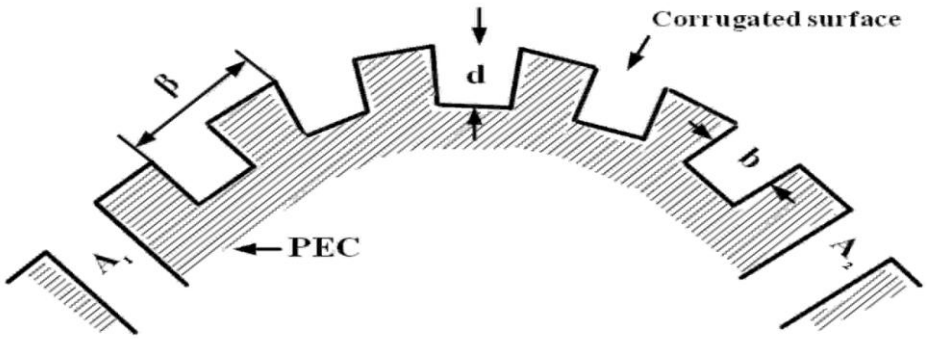

Figure 8. A corrugated metal surface located on a circular cylinder for defining the degree of decoupling between two microwave antennas (transmitting (A_1) and receiving (A_2)). β Is the period.

The broadband properties of the structure can be increased by using trapeze-shaped corrugations and by adding subsidiary resonant elements, for example, a layer of magneto-dielectric. If the equivalent depth of the corrugations is increased, the structure with filled corrugations is excited less effectively, and the dependence of the value of decoupling on geometrical parameters becomes more gradual. With the help of decoupling corrugated structures, it is possible to obtain decoupling of nearly 30 dB in 20% of the frequency band when the length of the structure is on the order of λ. Increasing the bandwidth property of decoupling features can be obtained by the combined use of decoupling structures based on reflection from separate heterostructures by means of radiation losses [11].

The engineering solutions for reducing interference and EMC problems are of increasing importance, particularly for airborne systems located onboard ships, aircraft and satellites. One of the simplest, but most effective ways to reduce the radiating interference is to introduce an electromagnetic bandgap (EBG) by means of periodic structures [7, 12−28, 30−37], such as a corrugated metal surface between the two coupled systems. The EBG materials are periodic structures that exhibit wide band pass and band rejection properties at microwave frequencies [13]. Due to their unique properties, EBG materials find potential applications in antennas, waveguides, amplifiers, filters, power combining, phased arrays, EMC measurements and in many microwave devices. The EBG property emerges by virtue of periodic reactive loading of the guiding structure. Adopting a circuit model, loads can generally be inductive (L), capacitive (C) or resonant (both L and C) [20].

A corrugated structure solution of the EMC problem was first investigated by Tereshin and Chaplin [7]. The application of periodic structures causes the suppression of surface waves. It is well known that a corrugated surface supports surface waves when the depth of the corrugations, *d*, provides an inductive surface impedance, i.e., when $0 < d/\lambda < 1/4$. When the depth of the corrugations is greater than one quarter wavelength, i.e., $1/4 < d/\lambda < 1/2$, the surface wave vanishes, and the surface impedance becomes infinite and provides the soft boundary condition for the field. Consequently, the performance of active and passive microwave components and devices is enhanced. Using a corrugated structure with an inductive impedance of a constant length for the purpose of decoupling, it is impossible to obtain large decoupling, because the surface waves are spread across the impedance surface. However, if a corrugated structure with a capacitive impedance is used, the far-field weakens inversely to the 3/2 power of the distance. The corrugated surfaces have also been classified and named as soft and hard surfaces [21], and different applications have been found, e.g., to control the radiation, scattering, and propagation characteristics of the waves [22−25], to reduce coupling through slots [26], and to improve the performance of element antennas on ground planes [27]. The soft surfaces have been used in corrugated horns to improve their radiation characteristics [28]. The soft and hard surfaces have also been realized by loading a dielectric coating with metal strips [29].
The concept of suppressing surface waves on metals is not new. It has been done before using several geometries, such as a corrugated metal slab [30]. It is well known that the excitation of surface waves may degrade the performance of microwave or millimeter wave circuits and antennas, due to the mutual coupling between antenna elements, resulting in the alteration of the radiation pattern and the reduction of radiation efficiency of antennas. Several methods have been developed for surface-wave suppression, such as the concept of artificial soft and hard surfaces, which has been introduced to generally characterize the interaction between the load surface and surface waves. In particular, various soft surfaces were proposed by Kidal to suppress the lateral lobe in monopole antennas [21, 22, 39].

Recently, a planar periodic structure fabricated by printed-circuit technology had been developed for application as a high impedance surface that suppresses surface waves with a complete stopband [14]. In Ref [8, 12, 31, 32], authors considered two-dimensional problems relating to coupling between waveguide antenna grates with corrugated impedance structures located between them. The results of these studies showed that the value of decoupling generally depends on the electrical and geometrical parameters of the periodic structures. The geometrical sizes of the corrugated surface can be chosen through analysis of infinite periodic structures. However, to solve the problem of the optimum placement of the decoupling devices using such an approach is impossible, since the change in the coupling value is noticeably influenced by surface

properties of areas located near the antennas. It has been shown that the weakening of coupling between antennas over a wide band of frequencies can be obtained to a greater extent on convex surfaces than on flat ones [32]. In Ref [8], authors considered obtaining decoupling between antennas located above a corrugated plane with purely reactive surface impedance. It has been shown that the degree of decoupling which can be obtained with the use of a decoupling surface is defined by the practical maximum rate of change of the surface impedance, and by the length of the decoupling structure, i.e., the difference between the impedance at the beginning and at the end of the structure.

Different variations of decoupling structures, namely metal and strip have been examined; as a rule, they are located on the communication line as a plane (a geodesic line) or as a ring covering the reception and transmitting antennas [32]. The main calculation methods used for the study of periodic structures properties (the impedance method and the method of integral equations) are listed. It has been shown that the decoupling properties of the structure are defined only by the structure's length and in fact do not depend on the period of the structure. Moreover, the most effective means of obtaining the required spatial decoupling of antennas, which should be taken into account in their design, is the correct choice of the mutual placement and orientation of the antennas**.** Besides this, a structure considerably influences the directivity diagram of an antenna which it is located close to (being more dependent on the depth of corrugation in corrugated structures). It has been also noted that the presence of losses in the structure makes the decoupling properties worse. It is shown that application of rapid alternating impedance in a decoupling structure allows a greater decrease of the field with distance [3]. Decoupling cannot be increased without limit by making the decoupling structure bigger or by placing the antennas farther apart. The main reason is because of the fact that on the edges of a finite structure, diffraction effects appear and the field is scattered. Analogous effects are also caused by inaccuracy in the production of the structure. This has a noticeable influence during the use of resonance elements in the structure. It has been shown that to reach the required levels of decoupling between antennas, it is necessary to use structures with a complicated reactive impedance corrugation on the flange of the antennas [36, 37]. For this purpose, it is necessary to set up and solve the problem of synthesis of such structures. Lastly, independent of the conditions of the antenna placement, an increase in decoupling over 130~140 dB is limited as a consequence of the scattering of the radiation field on inhomogeneous elements in the atmosphere.

One of the most important characteristics of a periodic structure is the bandwidth of frequencies over which it can be used. In particular, the frequency band can be limited by the maximum required decoupling which is determined by fixed size of the structure. This limitation is typical for low frequencies. For example, for corrugated structures with period b and rectangular corrugations with width a and depth d, the impedance Z is [3]:

$$Z/Z_0 = i(a/b)tg(k_g d), \qquad (4)$$

where $k_g = k\sqrt{\varepsilon\mu/(\varepsilon_0\mu_0)}$ is the propagation coefficient in the corrugations, taking into account their dielectric filling; the impedance is capacitive when $1/4 < d/\lambda < 1/2$. $Z_0 = \sqrt{\mu_0/\varepsilon_0}$, ε and μ are the parameters of the filling of the corrugations. Such structures in principle can be used only in the band of frequencies with an overlap less than 2:1.

There are on the whole, approximate rather than precise methods of investigation of periodic corrugated structures. In general, decoupling structures are placed on the communication line or in the form of a ring enveloping the receiving and transmitting antennas. Specifically, however, there is a selected direction, along which the properties of the decoupling structures are determined. Therefore, it is appropriate to set corresponding boundary problems for cylindrical structures, the form of which are perpendicular to the selected direction. Since in practice the widths of decoupling structures are comparable to the wavelength, the results of optimization calculations of geometrical parameters of the structure (providing maximum decoupling or broadband response of the system) amount to the same thing as for real three dimensional structures.

During the development of the periodic structure, it should be taken into account that radio electronic systems, such as components of radio engineering complexes, function as a rule in different frequencies ranges, i.e., the operating frequency of the transmitter often does not belong to the range of operating frequencies of the antenna of the receiver. For this reason, during EMC analysis one must consider the defining characteristics of the antenna radiation not only over the operating frequency range, but also over its harmonic components. Hence, the level of harmonics in terminal amplifying cascades is not more than -10 ~ -20 dB, but characteristics of antennas at their harmonic frequencies can sufficiently differ from characteristics at their operating frequency. In addition, the level of backscattering can be significant from the viewpoint of EMC. Moreover, for the analysis of antennas, EMC characteristics are required to create the models which adequately describe the operation of the antenna at the main frequency, as well as over the harmonics, which is only possible with the use of strict electrodynamic methods.

IV. Influence of Polarization Characteristics On The Reduction Of Coupling Between Antennas

The level of cross-polarization radiation of an antenna well describes its noise immunity. In a working frequency band, the polarization of radiated antenna fields corresponds to the calculated direction (for example: vertical, horizontal, and circular). In the limit of the main lobe at a level of 3 dB, the cross-polarization component, as a rule, does not exceed -25 ~ -40 dB. For a level of -10 dB, it increases to -25 ~ -15 dB. For an axially symmetric antenna, the lowest values of the cross-polarization components are orientated in the directions of the primary planes of □ and □. Concurrently, in diagonal planes situated at 45^o with respect to the planes of □ and □, a sharp growth of those components are registered. In the lateral and back lobe regions, values of cross components can exceed the level of the main polarization, but averaging the com-

ponents shows that the main component always prevails with the level around 10 dB [38]. For deep mirror antennas, part of the cross-polarization field increases in the back half-space, and it can exceed 20% of the main polarization.

Improvement of polarization characteristics and growth of the polarization frequency can be obtained with appropriate construction of the antenna itself. Examples of this type are circular horn antennas and feeds with corrugated or smooth walls, but using a dielectric hub. In mirror antennas working in the band 3.4 ~ 7 GHz, with the help of corrugated horn feeds, we can decrease the relative maximum level of cross-polarization components more than 30 dB [38]. To decrease the cross-polarization components, wire netting can be used, covering all of the radiation area or its parts. The conductors of such a netting must be oriented perpendicularly to the main polarization. This allows a decrease in the level of these cross components by 10~13 dB. A technical solution of this sort is applied on the re-transmitter of satellite communication systems, where repeating the use of the working frequency band causes decoupling between the orthogonal polarized components to reach 32 dB in the range of 4~6 GHz. The use of polarization decoupling to solve the problems of EMC is effective only when the antenna is coupled to the main and nearby side lobes; in the distant lobes, it is difficult to manage the polarization.

V. Influence of Aberration of Mirror Antennas on EMC Parameters

When the directivity of the antennas is higher (in the centimeter and decimeter wave range), the violation of EMC conditions can be affected by the presence of different types of aberration. Such violations can arise, for example, in satellite communication systems. In quality, the methods of correcting aberrations include different electronics, mechanical methods, construction, or other measures and methods. For instance, with lattice antennas, such adjustments can be realized with the help of the location or energizing of particular antennas elements. The aberration of mirror antennas can be eliminated with the help of the choice of the necessary forms of the feeds and mirrors themselves. In particular, to accomplish this, the so-called "reactive mirror" can be used to constitute segments of the waveguide, one of the ends of which is shunted. Characteristically, for such artificial reflecting surfaces which satisfy the condition of sinusoidal aberration, the angle of reflection doesn't equal the angle of incidence. Such a reactive reflector provides inadequate adjustment from the viewpoint of EMC aberration.

VI. Conclusion

We conclude that conducting further research on the design of decoupling structures based on the synthesis of impedance boundary conditions is necessary. In this connection, it is natural to increase the efficiency of existing methods and to develop new ways of reducing coupling of antennas. Beyond this, the prospects of further research are expressed in the following points:

- Development of electrodynamic and mathematical models describing the process of electromagnetic wave distribution in radiating and distributing devices (those found in practice and in prospective ones), and evaluation of the possibility of their experimental realization
- Research and development of anisotropic periodic structures
- Research and development of new EBG periodic structural materials, such as nanomaterials, taking into consideration the fundamental limits of antennas.

Reference

[1] K. G. Klimachev, Fundamentals of Forecasting and Provision of Electromagnetic Compatibility of Radio Engineering Systems and Devices, Moscow: Moscow Aviation Institute, 1994.
[2] D. I. Voskresenskiy, Problems of Antennas Theory and Engineering, Antennas, vol. 1, No. 40, 1998.
[3] L. D. Bakhrakh and E. G. Zelkin, Reference Book on Antenna Engineering, vol.1, Moscow: 1997.
[4] V. G. Yampolskiy and O. P. Frolov, Antennas and Electromagnetic Compatibility, Moscow: Radio and Communication Press, 1983.
[5] V. G. Yampolskiy and O. P. Frolov, Optimization of Antenna Systems on Connection Lines, Moscow: Radio and Communication Press, 1999.
[6] L. D. Bakhrakh, Modern Issues of Antenna Engineering, Moscow: Radio and Communication Press, 1989.
[7] O. N. Tereshin, V. M. Sedov, and A. F. Chaplin, Synthesis of Antennas on Decelerating Structures, Moscow: Communication Press, 1980.
[8] A. G. Kurkchan, "Coupling between Antennas in the presence of Corrugated Structures," Radiotechnics and Electronics, vol. 22, No. 7, pp. 1362–1373, 1977.
[9] Yu. L. Lomukhin, S. D. Badmayev, and N. B. Chimindorzhiev, "Decoupling of Antennas by the edge of conducting semi-plane", Radiotechnics, No. 8, pp. 47–50, 1985.
[10] M. M. Yumashev, "Decoupling of the Receiving and Transmitting Waveguide-and-Slot Antenna Grates", Collection of Scientific Works, Moscow: Moscow Energetic Institute, No. 159, pp. 81–86, 1998.
[11] U. L. Lomukhin and N. B. Chimitdorzhiev, "Increase of Decoupling of Antennas Located on a Convex Object", Radiotechnics and Electronics, vol. 24, No. 10, pp. 1989–1995, 1979.
[12] O. N. Tereshin, "Decoupling of Two Aperture Antennas by Using a Corrugated Structure Located in the Plane of the Apertures," Radiotechnics and Electronics, No. 12, vol. 5, pp. 1944–1950, I960.
[13] N. C. Karmakar and M. N. Mollah, "Potential Applications of PBG Engineered Structures in Microwave Engineering: Part I," Microwave Journal, vol**.** 47, No. 7, pp. 22–44, 2004.
[14] R. B. Hwang, and S. T. Peng, "Surface-Wave Suppression of Resonance-Type Periodic Structures," IEEE Transactions on Antennas and Propagation, vol. 51, No. 6, pp. 1221–1229, June 2003.

[15] A. Harvey, "Periodic and Guiding Structures at Microwave Frequencies," IRE Transactions on Microwave Theory and Techniques, vol. 8, pp. 30–61, June 1959.
[16] W. Rotman, "A Study of Single-Surface Corrugated Guides," Proc. IRE, vol. 39, pp. 952–959, Aug. 1951.
[17] R. Elliot, "On the Theory of Corrugated Plane Surfaces," IRE Trans. Antennas Propagation, vol. 2, pp. 71-81, Apr. 1954.
[18] R. A. Hurd, "The propagation of an electromagnetic wave along an infinite corrugated surface," Can. J. Phys., vol. 32, pp. 727–734, 1954.
[19] A. G. Kurkchan, and M. Kh. Zimnov, "Coupling between Antennas on a Cylinder in the Presence of Corrugated Structures," Radiotechnics and Electronics, vol. 12, No. 9, pp. 2308–2316, 1985
[20] G. Goussetis, A. P. Feresidis, and P. Kosmas, "Efficient Analysis, Design, and Filter Applications of EBG Waveguide with Periodic Resonant Loads," IEEE Transactions on Microwave Theory and Techniques, vol. 54, No. 11, pp. 3885–3892, November 2006.
[21] P. S. Kildal, "Artificially Soft and Hard Surfaces in Electromagnetics," IEEE Transactions on Antennas and Propagation, vol. 38, No. 10, pp. 1537–1544, October 1990.
[22] P. S. Kildal, A. A. Kishk, and A. Tengs, "Reduction of Forward Scattering from Cylindrical Objects Using Hard Surfaces," IEEE Transactions on Antennas and Propagation, vol. 44, No. 11, pp. 1509–1520, November 1996.
[23] R. E. Lawrie, "The Control of Echo Area of Ogives by Cutoff Corrugated Surfaces," IEEE Transactions on Antennas and Propagation, vol. 17, No. 3, 1966.
[24] I. Short and K. M. Chen, "Backscattering from an Impedance Loaded Slotted Cylinder," IEEE Transactions on Antennas and Propagation, vol. 14, No. 6, 1969.
[25] D. D. Gabrieliyan, M. Yu Zvezdina, and P. I. Kostenko, "Reduction of side and back radiation antenna level based on the use of impedance structures," Radio electronics, vol. 46, pp. 38–43, 2003.
[26] J. Carlsson and P. S. Kildal, "Transmission through Corrugated Slots," IEEE Transactions on Electromagnetic Compatibility, vol. 37, pp. 114–121, Feb. 1995.
[27] Z. Ying and P. S. Kildal, "Improvements of dipole, helix, spiral, Microstrip patch and aperture antennas with ground planes by using corrugated soft surfaces," IEE Proc. Microwaves, Antennas, Propagation, vol. 143, No. 3, pp. 244–248, June 1996.
[28] A. D. Olivier, P. J. B. Clarriocoats, A. A. Kishk, and L. Shafai, Microwave Horns and Feeds, New-York: IEEE Press, 1994.
[29] A. A. Kishk and P. S. Kildal, "Asymptotic boundary conditions for strip-loaded scatterers applied to circular dielectric cylinders under oblique incidence," IEEE Transactions on Antennas and Propagation, vol. 45, No. 10, pp. 551–557, January 1997.
[30] D. Sievenpiper, L. Zhang, R. F. J. Broas, N. G. Alexopolous, and E. Yablonovitch, "High-Impedance Electromagnetic Surfaces with a Forbidden Frequency Band," IEEE Transactions on Microwave Theory and Techniques, vol. 47, No. 11, pp. 2059–2074, November 1999.
[31] A. G. Kurkchan and M. Kh. Zimnov, "Coupling between Antennas on a Cylinder in the Presence of Corrugated Structures," Radiotechnics and Electronics, vol. 12, No. 9, pp. 2308–2316, 1985
[32] S. Benenson and A. I. Kurkchan, "Decoupling of Antennas by Means of Periodic Structures," Radiotechnics and Electronics, vol. 12, pp. 77–89, 1995
[33] G. I. Markov and D. M. Sazonov, Antennas, Moscow: Publishing House ENERGY, 1975.
[34] A. Freni, C. Mias, and R. L. Ferrari, "Hybrid Finite-Element Analysis of Electromagnetic Plane Wave Scattering from Axially Periodic Cylindrical Structures," IEEE Transactions on Antennas and Propagation, vol. 46, No. 12, pp. 1859–1866, December 1998
[35] V. V. Martsafey and I. G. Shvayko, "Influence of Corrugated Structures on Interaction of Near-Omnidirectional Antennas," Transactions of Higher Education Institutions, Series Radio Electronics, vol. 24, No. 5, pp. 18–22, 1981.
[36] Y. S. Joe, J-F. D. Essiben, and E. M. Cooney, "Radiation characteristics of waveguide antennas located on the same impedance plane", Journal of Physics D.: Applied Physics, vol. 41, No. 12, May 2008.
[37] J-F. D. Essiben, E. R. Hedin, and Y. S. Joe, "Radiation Characteristics of Antennas on the Reactive Impedance Surface of a Circular Cylinder Providing Reduced Coupling," Journal of Electromagnetic Analysis and Applications, vol. 2, No. 4, pp.195-204, April 2010.
[38] Yu. A. Kravsov, Z. I. Feizoulin, and A. G. Vinogradov, Passage of Radio Waves across Atmosphere Earth, Moscow: Radio and Communication, 1983.
[39] Z. Ying, P. S. Kildal, and A. A**.** Kishk, "Study of Different Realizations and Calculation Models for Soft Surfaces by Using a Vertical Monopole on a Soft Disk as a Test Bed," IEEE Transactions on Antennas and Propagation, vol. 44, No. 11, pp. 1474–1481, 1996.

International Journal of Modern Engineering Research (IJMER)
www.ijmer.com Vol.3, Issue.2, March-April. 2013 pp-1015-1018 ISSN: 2249-6645

A Survey of Positioned Based Routing Protocol in VANET

Mrs.D.M.Nikumbh, [1] Mr.A.D.Bhoi[2]
[1]*E &Tc, G.H.R.C.O.E.Chas Ahmednagar, Pune University, India,*
[2]*E & Tc, G.H.R.C.O.E. Nagpur, India,*

ABSTRACT: *Vehicular ad-hoc network mainly involves vehicle to vehicle (v2v) and vehicle to infrastructure (v2i) communication. This communication facilitates in reducing number of accidents, avoiding traffic congestion, enhancing the transport facility with the aid of infotainment and entertainment application. One of the major challenges of VANET application is in routing the packet in efficient and effective manner since the network topology is dynamic. In this paper we studied the different position based routing protocols. The position based routing protocols are used to find the position of destination node.*

Key Words: *VANET, MANET, DBR, Protocols*

I. INTRODUCTION

The arrival of ad hoc wireless networking point is one of the most significant developments in wireless networking and telecommunications. Basically it was introduce for military combat operations in hostile territories. But from last few years automobile industry used Ad Hoc networks in Vehicles. It is called as Vehicular Ad hoc Network (VANET).

A Vehicular Ad-Hoc Network or VANET is a technology that uses moving vehicles as nodes in a network to create a mobile network. VANET turns every participating vehicle into a wireless router or node, allowing vehicles approximately 100 to 300 meters of each other to connect and, in turn, create a network with a wide range. As vehicles fall out of the signal range and drop out of the network, other vehicles can join in, connecting vehicles to one another so that a mobile Internet is created.VANET is a subgroup of MANET where the nodes refer to vehicles. Since the movements of Vehicles are restricted by roads, traffic regulations we can deploy fixed infrastructure at critical locations.

The primary goal of VANET is to provide road safety measures where information about vehicle's current speed, location coordinates are passed with or without the deployment of Infrastructure. Apart from safety measures, VANET also provides value added services like email, audio/video sharing etc,

The VANET has two types 1) V2V (Vehicle to Vehicle) 2) V2I (Vehicle to Infrastructure) communication. Basically automobile industries are uses V2V communication than V2I. Vehicle to Vehicle communication approach is most suited for short range vehicular networks. It is Fast and Reliable and provides real time safety It does not need any roadside Infrastructure.V2V does not have the problem of Vehicle Shadowing in which a smaller vehicle is shadowed by a larger vehicle preventing it to communicate with the Roadside infrastructure In V2V the connectivity between the vehicles may not be there all the time since the vehicles are moving at different velocities due to which there might be quick network topology changes. The anonymity problem: The addresses of vehicles on highways are unknown to each other. Periodic broadcasts from each vehicle may inform direct neighbors about its address, but the address-position map will inevitably change frequently due to relative movements among vehicles.

It is the receiver's responsibility to decide the relevance of emergency messages and decide on appropriate actions. Location based broadcast and multicast are the proper communication methods for collision avoidance in V2V Communication. Without any roadside infrastructure, multihop forwarding must be enabled to propagate the messages or signals Hence, V2V communication is not very useful in case of sparsely connected or low density vehicular networks.

In terms of V2V communications, the use of both radio (VHF, micro and millimeter waves) and infrared waves have been used. While infrared and millimetre waves can support only line-of-sight communications, VHF and microwaves can support broadcast communications But drawback of VHF is, It can provide long links but at low speed and for this reason the mainstream mode of communications is to use microwaves.

In V2I Stringent delay requirement i.e. A rear-end collision occurs when the Available Maneuvering Time (AMT) is less than the Needed Maneuvering Time (NMT). NMT is dominated by the driver's perception response time, which is determined by many factors, and therefore difficult to change. To prevent a rear-end collision, a vehicle must receive the Message or Signal sufficiently prior to the lead vehicle's initiation of deceleration to provide more AMT.

In VANETs, the Wi-Fi limitations in coverage and capacity of the channel, the high mobility of the nodes, and the presence of obstacles generate packet loss, frequent topology changes, and network fragmentation. Thus, a great deal of effort is dedicated to offer new medium access control access strategies and to design efficient routing protocols. In turn, in such kind of networks, routing is a challenging task since there is no central entity in charge of finding the routing paths among the nodes.

Different routing strategies have been defined based on prior ad hoc network architectures by targeting the specific VANET needs of scenarios and applications. These protocols can be grouped into topology based it reactive, position based, cluster based and broadcasting.

Most of the VANET applications critically rely on routing protocols. Thus, an optimal routing strategy that makes better use of resources is crucial to deploy efficient VANETs that actually work in volatile networks. Finding well-suited

parameter configurations of existing mobile ad hoc network (MANET) protocols is a way of improving their performance, even making the difference between a network that does work or does not, e.g., networks with high routing load suffer from congestion and cannot ensure timely and reliable delivery of messages. The major challenges associated with VANET are lack of infrastructure and shorter communication session due to rapid change in the network topology.
Therefore routing protocols play asignificant role in achieving successful intervehicular communication.

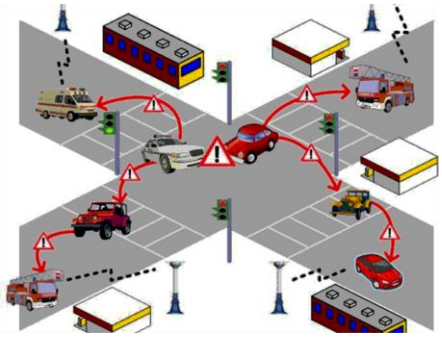

Figure 1

Ii. Different Types Of Routing Protocols Used In Manet And Vanet

"Global Frontrunner Routing Algorithm (GFRA) for V2V Communication in VANETs byA. Robertsingh, SuganyaA [1], has given four kinds of routing protocols in MANET.

2.1 Proactive routing

In the proactive protocols, each node sends periodical information of its routing tables. The routingtables ,eventually , tend to have the information of surrounding nodes and knowledge of more than just theone-hop neighbours. This kind of protocols have asignificant overhead due to the periodic alin formation transfer and the propagationo frouting messages to destination nodes that might probably carry out datesination formation, since the environment is highly mobile.

2.2Reactive routing

Reactive protocols only find the path to a destination when a node needs to start a session with that destination and there is no route available. Despite the type of strategy used to build the routing tables and select the paths, reactive routing protocols have two main problems that make them inadequate for VANET. First, there is a significant delay until the communication process is established due to the reactive nature of the protocol. Second, the packet delivery ratio is low when both nodes are far away, because the probability of a broken route increases due to the high mobility of the VANET.

2.3 Topology based routing

In Topology based routing protocol IP address is used to find node and setup route.For setup the route it uses the information of links that exists in network to find the best path for data forwarding.Topology based protocol may be reactive or proactive.

2.4 Positioned Based Routing Protocol

In position based routing protocol geographical position of node is used to select the best path.Hence in position based routing protocol each node determine location of itself as well as destination node.

2.5 Broadcast based routing protocol

Broadcast routing protocol is used to transimit data packet to all nodes in network.It uses the concept of flooding.It is mostly used when node is beyond range.

2.6 Geocast routing protocol

Geocasting routing protocol distributes the data packet bu flooding.Vechical rebroadcast the data packet if it is in the same geographic area of packet.

III. Different Positioned Based Routing Protocols

The functionality of a position based routing protocol may be split in three differentaspects:path selection, forwardingand and recovery.
For path selection
The different position based routing protocols are

3.1 OLSR:Optical link state routing protocol

T. H. Clausen and P. Jacquet. "Optimized Link State Routing (OLSR)", Optical link state routing protocol (OLSR) [2] unusual is a class of routing protocols for VANETs. OLSR protocols controls real-time vehicular traffic information to

create stable road-based paths consisting of successions of road intersections that have, with high probability, network connectivity among them. OLSR protocols working in conjunction with geographical forwarding show.

The vehicular networks in several useful applications, both safety and non-safety related, such as automatic road traffic alerts dissemination, dynamic route planning, service queries (e.g., parking availability), audio and video file sharing between moving vehicles, and context-aware advertisement.

3.2 Life time based protocol

In the paper "Global Frontrunner Routing Algorithm(GFRA) for V2V Communication In VANETs by A. Robertsingh, Suganya A[1],explained the life time based protocol , route expire time (RET) represents the stability of the route and helps the forwarding node to transmit the message towards the destination. The vehicles moving with same velocity will have same RET. IN an infrastructure based technique that address the problems of route maintenance by calculating the stability of route, based on which the route is selected for further communication. The mobility prediction model RB-MP divides the neighbours into several sets according to the direction of movement. Further it utilizes the position and velocity to predict the time required to maintain the information of all neighbours. Based on this, several rebroadcasting nodes are selected. The route discovery face is required to establish the routing table. A next hop selection technique is a position based routing method where the node uses a table to store the information about the position of neighbouring nodes.

The expected progress distance (EPD) is calculated from the table and it is used in selecting the next hop. The direction of the vehicle is not considered while forwarding the node. The location based routing algorithm significantly reduces the probability of dropping packet and the network traffic when compared to flooding based routing protocols. This routing can be implemented only in city model. Furthermore short falls of position based routing and reactive routing protocol are addressed in SNESA. This routing technique uses the relative position of the neighbouring vehicle calculated using speed and direction and thus reduces the frequent broadcast of position information. The SNESA uses destination of the vehicle due to which the efficiency of this protocol decreases when destination is unknown.

3.3 GSR (Geographic source routing)

This routing protocol is proposed by Lochert et al., it is basically position-based routing with topological knowledge [3]. In this routing scheme a shortest path is selected before greedy routing is applied. As compared to AODV and DSR, GSR performance is very good because packet delivery ratio is high and latency is low with the use of realistic traffic in city environment. Problem with GSR is that along a preselected path it is difficult to find end to end connection when the traffic density is low.

3.4 A-STAR (Anchor-based Street and traffic aware routing)

A-STAR is position based routing scheme proposed by Seet et al. whose basic purpose is to support routing in the city environment [4]. This routing scheme ensures end to end connection even in the case of low traffic density. It uses the information from city bus routes to find an anchor path for higher connectivity so that more and more packets can be delivered to the destination. This routing protocol is also very efficient in route recovery strategy and also proposed a new recovery strategy when the packets are routed to local optimum, which consists of the computation of new anchor path from local maximum.

3.5 GPCR (Greedy perimeter coordinator routing)

To deal with the city environment tasks Lochert et al [3], designed GPCR, which applies restricted greedy forwarding approach along a preselected path. In this routing when choosing next hop, a coordinator node (the node on the junction) is chosen even it is not the closest node to the destination. GPCR suffers the same problem as with GSR i.e. ignore the case whenever the traffic density is low.

3.6 Gytar (Greedy Traffic Aware Routing)

Improved Greedy Traffic Aware Routing protocol GyTAR [5], [6] is intersection-based routing protocol which dynamically selects junction to find robust routes within the city. It uses digital map to find the position of neighboring junctions and selects junction dynamically on the basis of traffic density and curve metric distance to the destination. A score is given to each neighboring junction and the junction with the highest score is selected as a next junction. The selected junction is the one which is closest to the destination International Journal of Computer and Communication Engineering, Vol. 2, No. 1, January 2013 21 and also has the highest traffic density. The improved greedy routing strategy is used to forward the packet between two involved Junctions. GyTAR uses carry and forward approach in order to recover from the local maximum. This mechanism of junction selection has maximum connectivity and thus increases the packet delivery ratio and at the same time decreases the end-to-end delay.

3.7 DBR

Ramakrishna M, "DBR: Distance Based Routing Protocol" ,International Journal of Information and Electronics Engineering, Vol. 2, No 2[7] , DBR is capable of handling a highly form of mobile network. It is also evident that DBR is not affected by the GPS error, because of the use of relative speed and position of the vehicle. The proposed protocol locates the neighboring in digital map using the velocity information even though an error occurs in position information obtained

by GPS. It also avoids periodic broadcast of hello message unless there is change in velocity and direction of the vehicle, thus reducing the network overhead. Therefore DBR deals with challenges of both rural and urban road environment.

3.8 DBR-LS

Ramakrishna M," DBR-LS: Distance Based Routing protocol using Location Service for VANETs" , Dept. of Information and Communication Technology Manipal Institute Technology, Manipal, 576104 INDIA[8], DBR_LS routing protocol uses both position based and map based technique along with Location service. It is also evident that DBR-LS is not affected by the GPS error, because of the DBR in which algorithm uses relative speed and position of the vehicle. The proposed protocol locates the neighboring in digital map using information obtained from Location Servers. It also avoids broadcasting of data packet.

IV. CONCLUSION

In VANET the major challenge is finding the accurate position of node because it is very dynamic in nature. Hence in this paper we studied different positioned based routing protocols. In DBR the distance between vehicles can be calculated using relative speed and position of vehicle. Therefore DBR deals with challenges of both rural and urban road environment.

References

[1] A. Robertsingh, Suganya A, "Global Frontrunner Routing Alogorithm (GFRA) for V2V Communication in VANETs
[2] .T. H. Clausen and P. Jacquet. "Optimized Link State Routing (OLSR)", RFC 3626, 2003.
[3] C. Lochert, M. Mauve, H. Fler, and H. Hartenstein, "Geographic routing in city scenarios," (poster), MobiCom 2004, ACM SIGMOBILE Mobile Computing and Communications Review (MC2R) vol. 9, no. 1, pp. 69–72, 2005.
[4] M. Jerbi, S.-M.Senouci, R. Meraihi, and G.-D.Yacine, "An improved vehicular Ad hoc routing protocol for city environments," Reviewed at the Direction of IEEE International Conference on Communications, pp. 3972 – 3979, 24-28 June 2007.
[5] M. Jerbi, R. Meraihi, and S. Senouci, "An improved vehicular Ad hoc routing protocol for city environments," IEEE 2007.
[6] J. Li, J. Jannotti, D. De Couto, D. Karger, and R. Morris, "A scalable location service for geographic ad hoc routing," ACM/IEEEMOBICOM'2000, pp. 120.130, 2000.
[7] Ramakrishna M, "DBR: Distance Based Routing Protocol", International Journal of Information and Electronics Engineering, Vol. 2, No 2
[8] Ramakrishna M," DBR-LS: Distance Based Routing protocol using Location Service for VANETs", Dept. of Information and Communication Technology Manipal Institute Technology, Manipal, 576104 INDIA

.

International Journal of Modern Engineering Research (IJMER)
www.ijmer.com Vol.3, Issue.2, March-April. 2013 pp-1019-1021 ISSN: 2249-6645

Runtime Solution for Minimizing Drive-By-Download Attacks

Pratik Upadhya, [1] Farhan Meer, [2] Acquin Dmello, [3] Nikita Dmello[4]
[123]*Department of Computer Engineering, St. Francis Institute of Technology, Mumbai, India*
[4]*Department of Computer Engineering, Fr. Conceicao Rodrigues College of Engineering, Mumbai, India*

Abstract: *The ever growing use of internet has given rise to a lot of security vulnerabilities to web application users. One of the most dangerous among these threats is drive-by-download attacks which target those victims with some vulnerability in their browser or browser plug-ins. Drive-by-download attack allows the attacker to download a code on the victim's host and execute it on victim's host without any prior knowledge to the victim. Due to this, the attacker may get full control of the victim's host. We present a runtime; Behavior based solution, to protect a Browser against Drive-by-download attacks. This paper extends the concept of Behavior based solution to the domain of Internet Browsers, which protects a browser against drive-by-download attacks. Our approach will enhance the security of a browser, thereby avoiding attackers to penetrate a victim's host.*

Keywords: *behavior-based solution, browser, intrusion detection, security.*

I. INTRODUCTION

Web developers recognize the importance of Cyber security for safe browsing on internet. Through this paper, we propose a Runtime, behavior-based solution which is called Browser Guard, against drive-by-download attacks which is one of the most dangerous threat for browsers these days. Malicious web content has become the primary instrument used by miscreants to perform their attacks on the Internet. In particular, attacks that target web clients, as opposed to infrastructure components, have become pervasive [2]. It is observed that, around 45% of the internet users use an outdated browser [3]. Recently, several approaches to protect browsers from drive-by-download attacks have been proposed [1, 4, 5, 6] which addresses protection for browsers against drive-by-download attacks. However many of them take the trouble by false positive, false negative or performance overhead and some are limited to detection of drive-by-attacks of JavaScript [4]. This seriously impacts the usability of web applications.

This paper proposes a runtime, Browser-based solution called as Browser Gaurd, which prevents the drive-by-download attack. Browser Gaurd is the tool being used to monitor the download scenario of all the files that are loaded into the host through a browser. After the inspection of the download scenario, Browser Gaurd restricts the execution of any file that is automatically downloaded into the host without any prior knowledge of the user. As this approach depends on the Behavior-based detection, Browser Gaurd does not need to analyze the source code file of any web application or the run-time states of any script code. Browser Gaurd also does not need to maintain any exploit code samples to compare with malicious web pages and does not need to query the reputation value of any website.

In summary, the contribution of this paper is a runtime, browser-based solution for detecting, analyzing and mitigating drive-by-download attacks.

II. RELATED WORK

A number of approaches and tools have been proposed in recent years to identify and analyze malicious code on the web. We will now briefly present the most relevant ones and compare them with our approach.

Patch Exe: Many drive-by-download attacks are triggered by vulnerable ActiveX controls. Microsoft uses Kill-Bit [7] to mitigate this problem. However, Kill-Bit does not patch any executable. Instead, it just blocks the use of certain known vulnerable ActiveX Controls. If a particular ActiveX Control is marked as unsafe through Kill-Bit, the ActiveX Control will never be invoked by any application. However, attackers can utilize non- ActiveX Control vulnerabilities to launch a drive-by-download attack and not all vulnerabilities of all ActiveX controls are unveiled.

NOP sleds and Shell code: Nozzle [8] detects heap spray attacks based on the observation that shell code used in a heap spray attack is usually prepended with a long NOP sled. Experimental results showed that Nozzle has small number of false positives and false negatives. However, if an attacker writes NOP sleds and shell code into a heap string after Nozzle finishes its examination, Nozzle is not able to detect the attack.

Performance issues to non-browser processes: Blade adopt similar philosophy of blocking the execution of suspicious executable files as Browser Guard does. By sandboxing all downloaded objects in a secure zone, their work, Blade, prohibits supervised process from operating unauthorized files in the secure zone. Blade captures user behaviors, such as clicking a mouse button on a download related popup window, to mark user-consent downloaded files as authorized. Blade has zero error rate. However, it may pose performance issues to non-browser processes due to the special secure zone design that once a user tries to manipulate a file, OS should check whether this file is in the secure zone.

Non-trivial False positives of Browser Reputation System: In this system, before displaying a web page on a browser, the browser automatically connects to a remote database to check the reputation of the web page first. Only web pages with good reputation can display on the browser. Various antivirus vendors adopted this approach to deal with drive-by-download attacks. However, the browser reputation system has no guarantee that all websites are under their monitor. Besides, they have non-trivial false positives and it takes a while to update out-of-date or wrong data in the database or to add new data to the database.

Inter-Module Communications: IMC monitoring [5] detects drive-by download attacks by matching the inter-module communication events with predefined vulnerability signatures. However, its signature-based property makes it difficult to detect zero-day attacks.

III. LIMITATIONS

A behavior based solution is not acceptable in case of shadow attacks [10]. Specifically, shadow attacks create shadow process communication (SPC) channels between the rewritten malware and its shadow processes to achieve the original malicious functionalities. As of writing of this Paper, most behavior-based malware detectors are designed based on malicious specifications in terms of system call sequences/graphs of individual single-process program (or these with simple inheritance/fork relationships). It is worth noting that the practically used system call sequence/graph behaviors are rarely just a single system call because that will have high false positive rates as likely many normal programs could use the same single system call with similar parameters as a malware does. Therefore, these behavior-based malware detectors could hardly detect shadow processes because they only contain small segments (e.g., just one system call) of the malicious behavior of malware.

Most existing scanners use file or network flow as scanning granularity [5]. However, to help web application developers, most browsers have the ability to let scripts include other scripts. By leveraging this feature, attackers can split one exploit script into several files without affecting the correct functionality. As a result, scanners without a mature reassemble mechanism will be bypassed. By using behavior-based detection mechanism, the unpacking and reassembling problem stated above could be avoided. But the situation for existing behavior-based protection systems is no better. Firewalls can block illegal traffic, yet from the perspective of firewall, since drive-by download attack is almost the same as legitimate visiting web pages, it has no reason to block this kind of traffic. Even though black lists (e.g. Google Safe Browsing API [11]) can be used to prevent visiting malicious servers, these lists trend to be incomplete and sometimes outdated.

IV. IMPLEMENTATION

This section of the paper specifies the implementation details, design goal and design principle of BrowserGaurd. There are three components involved in the file download operation and the file execution operation in IE [1,7]. There are file download component, file execution component, and event component. According to the file download steps of a browser, Browser Guard sets several *check points* on a browser and the Windows kernel to detect secret download and blocks the execution of downloaded malware at runtime. The structure of Browser Gaurd is not sophisticated. It consists of a Browser Guard Browser Helper Objet in every IE process, a Browser Guard Kernel in the kernel space, and a *list server process*. Each host has only one list server process. But the host may have several browsers executing simultaneously; hence, there may exist multiple Browser Guard-Browser Helper Objects in a host at the same time. A Browser Guard Browser Helper Objet communicates with the list server process through a named pipe. Multiple Browser Guard-Browser Helper Objects can communicate with the list server process simultaneously. The list server process contains two lists, a white-list and a blacklist. The white-list records the URLs of trusted files and the hash vales of trusted executable files. The blacklist records the hash values of detected malicious files.

Browser Guard-Kernel is a kernel component of Browser-Guard. Browser Guard-Kernel enforces the following two tasks to prevent the execution of malware and illegal modifications of a white-list and blacklist. First, Browser Guard-Kernel ensures that the execution of a program is issued by an internal system command which has been hooked by Browser Guard. Second, Browser Guard-Kernel denies a request to modify a white-list, if the request is not issued through the code in functions of Browser Guard.

4.1 Browser Guard Workflow

Browser Guard provides its protection to a host through a two-phase mechanism and a kernel component. In the first phase, namely the filtration phase, Browser Guard distinguishes malicious files from trusted ones based on the situations under which the files are downloaded to a local host. In the second phase, namely the prohibition phase, Browser Guard denies the request to execute malicious files. The kernel component blocks attempts to bypass Browser Guard.

4.1.1Filtration Phase

To be able to distinguish malicious files from trusted ones, Browser Guard needs to know the situation under which a file is downloaded to a local host. With the information, Browser Guard can deduce whether a downloaded file is a trusted one or malicious one. In order to collect the required information, Browser Guard installs several check points to monitor the behavior of a browser.

While a user is surfing the WWW, a browser needs to download various files. All these files are placed in a directory called Temporary Internet Files and they cannot be directly executed without the permission of the browser user. On a Browser

Guard protected browser, normal file download triggers the execution of download functions. These functions connect to the list server process of a host to record URLs in the white-list of the process. The URLs are the URLs of the files that are going to be downloaded to the host. Then other functions checks whether the URL of the file that this function is asked to download is within the white-list. If the URL is within the white-list, the file is downloaded as usual; but if the URL is not within the white-list, Browser Guard calculates the hash value of the file and adds the hash value to the black list.

Instead of using file extensions to find executable files, Browser Gaurd uses hash value to find executable files. This can prevent an attacker from naming an executable file with a non-executable filename extension first and then changing its filename extension back to an executable filename extension before executing the file. The hash value is calculated based on the first 512 bytes of a file. Hence, instead of comparing all the bits of a file to check if it's malicious, Browser Gaurd just compares the first 512 bytes of a file.

4.1.2 Prohibition phase

A system function resides in IE browser to execute executable file on the disk. Browser Guard hooks this API to ensure that the API will not execute malware. Browser Guard calculates the hash value of the executable file first. Then Browser Guard checks whether the white-list and blacklist contain the same hash value. If the blacklist does not contain the hash value but the white-list contains the hash value, Browser Gaurd runs the executable file. Otherwise, it blocks the execution of the file.

4.1.3Avoiding Checkpoint-Bypassing

Various checkpoints installed by Browser Guard are the critical instructions used to detect downloaded malware and prevent the execution of the downloaded malware. If an attacker can bypass these checkpoints, she/he can successfully accomplish a drive-by-download attack on a Browser Guard protected browser. Browser Guard utilizes various approaches to ensure that, if the download and execution of a program do not follow the normal path and does not pass the predefined checkpoints, Browser Guard can detect it and block the execution.

V. CONCLUSION AND FUTURE WORK

As the web browser advances to an integral component in every day computing, it becomes an attractive target for attackers. Outdated browsers and plug-ins allow attackers to infect computer systems via drive-by attacks that download and install malicious software upon the mere visit of a web page containing malicious content. As drive-by attacks target the browser and its components directly, we propose to have defensive mechanisms built into the browser itself to mitigate the threats that arise from drive-by download attacks. Therefore, the paper proposes and elaborates a runtime browser-based strategy that bares the potential to protect users from these threats. Implementing countermeasures in the browser, to some extent, also allows for the protection of otherwise vulnerable components. Therefore, users would benefit directly and immediately from the security enhancements that browser built-in protection mechanisms would provide. In this paper, we present Browser Guard, a runtime, behavior-based solution to drive-by-download attacks. Browser Guard analyzes the download scenario of every downloaded object. Based on the download scenario, Browser Guard blocks the execution of any executable file that is downloaded to the host machine without the consent of a user.

In future, we try to work on the limitations and to make it compatible to more number of browsers across multiple platforms and also improve the usability of our technique.

References

[1] Fu-Hau Hsu, Chang-Kuo Tso, Yi-Chun Yeh, Wei-Jen Wang, and Li-Han Chen, Browser Guard: A Behavior-Based Solution to Drive-by-Download Attacks, IEEE JOURNAL ON SELECTED AREAS IN COMMUNICATIONS, VOL. 29, NO. 7, AUGUST 2011.

[2] N. Provos, P. Mavrommatis, M. Rajab, and F. Monrose, All Your iFRAMEs Point to Us, In Proceedings of the USENIX Security Symposium, 2008.

[3] S. Frei, T. Dübendorfer, G. Ollman, and M. May, Understanding the Web browser threat: Examination of vulnerable online Web browser populations and the "insecurity iceberg", In Proceedings of DefCon 16, 2008.

[4] Marco Cova, Christopher Kruegel, and Giovanni Vigna, Detection and Analysis of Drive-by-Download Attacks and Malicious JavaScript Code, International World Wide Web Conference Committee (IW3C2), April 26–30, 2010.

[5] Chengyu Song, Jianwei Zhuge, Xinhui Han, Zhiyuan Ye, Preventing Drive-by Download via Inter-Module Communication Monitoring, ASIACCS'10 April 13–16, 2010.

[6] Konrad Rieck, Tammo Krueger, Andreas Dewald , Cujo: Efficient Detection and Prevention of Drive-by-Download Attacks, ACSAC '10 Dec. 6-10, 2010.

[7] Microsoft Security Research & Defense, [Online], Available: http://blogs.technet.com/srd/archive/2008/02/06/The-Kill 2D00 Bit-FAQ 3A00 -Part-1-of-3.aspx

[8] P. Ratanaworabhan, B. Livshits, and B. Zorn, NOZZLE: a defense against heap-spraying code injection attacks, USENIX Association, 2009, pp. 169–186.

[9] L. Lu, V. Yegneswaran, P. Porras, and W. Lee, BLADE: an attack agnostic approach for preventing drive-by malware infections, 17th ACM conference on Computer and communications security, ser. CCS '10. ACM, 2010, pp. 440–450.

[10] Weiqin Ma, Pu Duan, Sanmin Liu, Guofei Gu and Jyh-Charn Liu, Shadow Attacks: Automatically Evading System-Call-Behavior Based Malware Detection, Department of Computer Science and Engineering, Texas A&M University College Station, TX, USA 77843-3112

[11] G. Inc. Google safe browsing api. http://code.google.com/apis/safebrowsing/.

International Journal of Modern Engineering Research (IJMER)
www.ijmer.com Vol.3, Issue.2, March-April. 2013 pp-1022-1025 ISSN: 2249-6645

Thermal Performance on Single Basin Solar Still with Evacuated Tubes Solar Collector-A review

Syed Firozuddin, [1] Dr. P. V. Walke[2]
[1]*Student IV Semester, M. Tech. Heat Power Engineering, G.H.Raisoni College of Engineering, Nagpur*
[2]*Professor, Mechanical Engineering Departments, G.H.Raisoni College of Engineering, Nagpur-440016, India*

Abstract: *Various aspects of single basin solar still with evacuated tubes solar collector have been discussed in this paper with a focus on the use of evacuated tubes to increase the daily productivity of solar still with less heat losses. The pure water can be obtained by distillation in the simplest solar still. Various active methods have been adopted to increase the temperature of the basin so as to improve the productivity of solar still.*

Keywords: *Augmentation, distillation, evacuated tubes, Solar still.*

I. Introduction

Water is a precious natural gift and is being polluted by human activities, urbanization and industrialization. The ground water is often over exploited to meet the increasing demand of the people. Less than 1% of earth's water is available for human consumption and more than 1.2 billion people still have no access to safe drinking water. Over 50% of the world population is estimated to be residing in urban areas, and almost 50% of mega cities having population over 10 million are heavily dependent on ground water, especially in the developing countries like India .

Most of the rural people still live in absolute poverty and often lack access to clean drinking water. Nearly half of the population is illiterate, not at all aware of the waterborne diseases affecting their health. Nearly 70% of the infectious diseases in India are waterborne. Indian villages are posed with problem of overexploitation of ground water due to increasing dependence on it as other fresh water resources are dwindling fast. Various desalination techniques are used to purify the water. Solar distillation is an easy and cost effective method to provide pure drinking water in rural areas without affecting the nature. Solar distillation process is carried out both in passive and active modes. [13]

Passive Method: Passive solar still operates in low temperature and the daily productivity is comparatively low.

Active method: To increase the evaporation rate in an active mode the extra thermal energy is fed into the basin. To increase the productivity of solar still, the various active methods are being carried out by many researchers. Most of the works were based on the flat plate collector and concentrating collector.
Following are the various active methods to increase the productivity of solar still.

Basin type solar still: Such solar stills have been operated for farm and community use in several countries. It consists of a blackened basin containing saline water at a shallow depth, over which is a transparent air tight cover that encloses completely the space above the basin. It has a roof-like shape. The cover which is usually glass, may be of plastic is sloped towards a collection trough. Solar radiation passes through the cover and is absorbed and converted into heat in the black surface. Impure water in the basin or tray is heated and the vapor produced is condensed to purified water on the cooler interior of the roof. The transparent roof material, (mainly glass) transmits nearly all radiation falling on it and absorbs very little; hence it remains cool enough to condense the water vapor. The condensed water flows down the sloping roof and is collected in troughs at the bottom. [1], [2], [3]

Vertical solar stills with a flat plate solar collector: The distillation unit consists of 'n' parallel vertical plates. The first plate is insulated on its front side and the last plate is exposed to ambient. Each plate in the enclosure is covered with wetted cloth on one side. The cloth is extended into a feed through along the upper edge of each plate. Feed water in the through is then drawn onto the plate surface by capillary. Excess water moves down the plate and is conducted out of the still. The last plate is cooled by air or water. The authors found that, the distillation output increases slightly when the plate number is over 5, and it increased by about 34% and 15% when the evaporating plate numbers are 1 and 6, respectively. [4], [5].

Solar still integrated with mini solar pond: Solar pond is an artificially constructed pond in which significant temperature rises are caused to occur in the lower regions by preventing convection. Solar ponds are used for collection and storage of solar energy and it is used for various thermal applications like green house heating, process heat in dairy plants, power production and desalination.

The results show that, average increase in productivity, when a pond is integrated with a still is 27.6% and when pond and sponge are integrated with a still is 57.8%. Industrial effluent was used as feed for fin type single basin solar still and stepped solar still. A mini solar pond connected to the stills to enhance the productivity and tested individually. The results show that, maximum productivity of 100% was obtained when the fin type solar still was integrated with pebble and sponge. The productivity increases with increase in solar intensity and water glass temperature difference and decreases with

increase in wind velocity. Pebbles, baffle plates, fins and sponges are used in the stepped solar still for productivity augmentation. Their finding shows that, maximum productivity of 78% occurred when fins and sponges were used in the stepped solar still and also found that the productivity during night also improved when pebbles were used in the solar stills. [10], [11], [12].

There are three main types of solar stills: the box solar still, the cone solar still and the pit solar still

II. Box Solar Stills

The box shaped solar still is fairly complex compared to the other solar stills made for obtaining pure emergency drinking water. This type of still is usually created with a box that has a slanted glass or plastic top with an insulated bottom. A set of tubes allow in impure water and let out over flow and pure distilled water. Maintaining a tight seal on a box shaped solar still is essential. Clearly, this is more of a home project for a green minded person, but having a solid understanding of how all solar stills work might come in handy when trying to construct one from scratch for emergency drinking water.

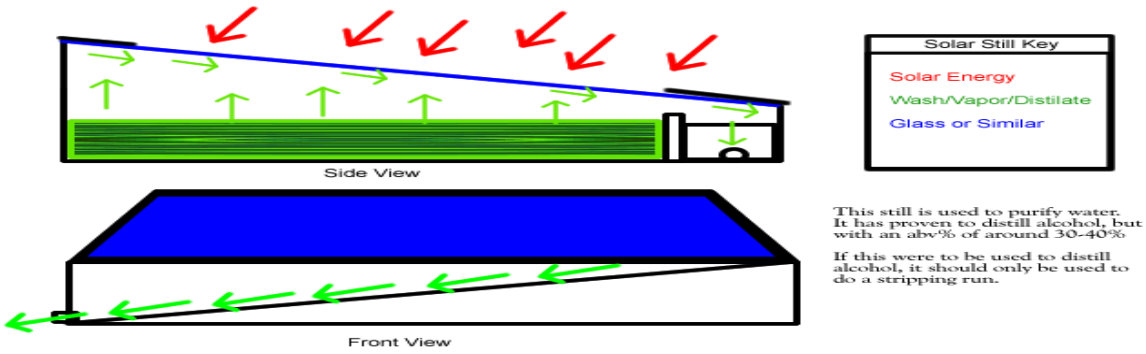

Figure 1: Box type solar still

III. Cone Solar Still

A cone shaped solar still is a method of treating impure emergency drinking water rather than gathering it from the atmosphere. A cone is constructed out of plastic designed so that impure water in the bottom evaporates and is captured in a makeshift reservoir as it runs down the side, relieved of impurities. The Water cone is commercial solar still that allows you to distill water naturally at home or on the go with having to construct a solar still of your own. Designed as a water purification system that can generate potable water out of even brackish sea water, the Water cone is also a candidate for providing clean drinking water in developing and failed nations.

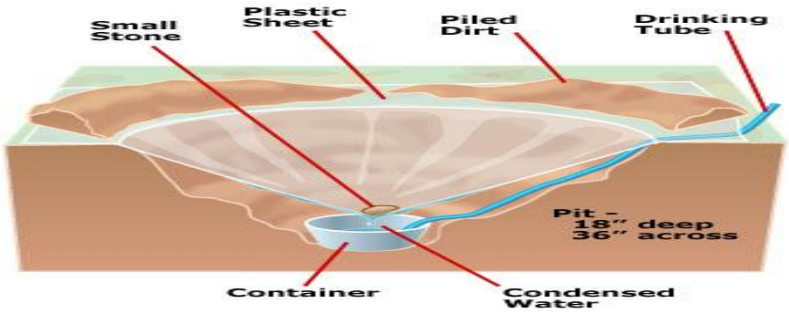

Figure 2: Cone type solar still

IV. Pit Solar Still

Pit shaped solar stills are the simplest solar still to make and require little equipment or technical know-how. Simply dig a pit in the earth approximately two feet deep and place a Number 10 sized can at the bottom. If available, set a drinking tube in the bottom of the can leading out of the hole. Then secure a sheet of plastic over the hole a place a stone in the sheet so that it indents the sheet to just above the can's lid. So long as this solar still receives plenty of sun, it will provide a pint or more of emergency drinking water. [15]

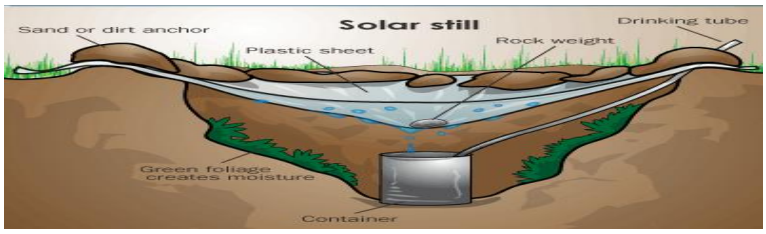

Figure 3: Pit type solar still

V. Literature Survey

Solar Still alone:

- An experimental study is conducted by Bhanu Pratab Singh [1] in a single slope solar still integrated with solar water heater. It has been found that still productivity increases up to 120% when combined with solar water heater. Also, the ambient conditions are found to have direct effect on the productivity of the still. The production in night in the absence of solar radiation contributes up to 14% of the daily output due to availability of hot water as basin water with the integration of solar water heater.
- The work carried out by Ahmed Z. AL-Garni. [2] To enhance the productivity of a double slope solar still by using an immersion type water heater. The effect of using an external fan to cool the glass surface is also examined. Experiments were carried out for winter season in Saudi Arabian climatic conditions at solar still is more for low water depths, the water level in the base tank was maintained at 1cm. The experimental results showed that the productivity increased by a significant 370% when two water heaters each having 500 W capacities was used. When external cooling fan was used the productivity was found to decrease by 4% and 8% for wind speeds of 7 m/s and 9 m/s, respectively.
- V. Velmurugan, et al. [3] performed productivity enhancement of stepped solar still. For comparison purpose, the ordinary stepped solar still is tested without any modification and the average water productivity is found to be 1.01 litres per 8 hour. To improve the productivity, theoretical and experimental analyses were made for fin type, sponge type, and combination of fin and sponge type stepped solar still. When the fin and sponge type stepped solar is used, the productivity is 1.98 litres per 8 hours which is 96% more compared to the productivity of ordinary stepped solar still. The average daily water production has been found to be 80% higher than ordinary single basin solar still.

Solar still coupled with flat plate collector:

- Badran and Al-Tahainesh [4] presented the effect of coupling a flat plate collector on the solar still productivity. It has been found that coupling of a solar collector with a still has increased by 36%. The results showed that, the output of the still is maximum for the least water depth in the basin (2 cm). Also, the increase in water depth has decreased the productivity, while the still productivity is found to be proportional to the solar radiation intensity.
- A work is carried out by A.M. Rajesh, et al. [5] on single basin solar still integrated with a flat plate collector [FPC]. A single stage basin type solar still and a conventional flat plate collector were connected together in order to study the effect of augmentation on the still under local conditions. The still inlet was connected to a locally made fin tube collector. The unit as operated with and without coupling flat plate collector. Measurements of various parameters, temperatures, solar intensities and distilled water production were noted between 8 AM to 5 PM sunlight day.25 to 40% enhancement in the yield is observed with this system.

Solar still coupled with parabolic concentrator:

- Zeinab and Ashraf [6] conducted experimental and theoretical study of a solar desalination system coupled with solar parabolic through with a focal pipe and simple heat exchanger. The results show that, as time goes on, all the temperatures increase and begin to decrease after 4.00 pm with respect to the solar radiation, although the temperature values of the modified system are still higher than the conventional one. In case of the modified design, the fresh water productivity increased an average by 18%.
- Garcia Rodriguez and Gomez Camacho [7] experimentally studied the multi effect distillation system coupled to a parabolic through collector (PTC) for sea water desalination and suggested the following, (i) the annual energy production is about 23% grater for a north–south collector than for an east west one. (ii) The optimum axis height for a single collector is 298 and it is 12% higher production than a horizontal collector for an inlet/outlet thermal oil temperature of 225 ^{o}C /300 ^{o}C. (iii) The maximum yearly average of the daily operation time is only about 12 h/day in coastal areas in southern Spain.
- T. Arunkumar , R.Jayaprakash[8] performed Desalination Process Of Single Slope Solar Still Coupled In CPC With Crescent Absorber using two modes of operation: (1) Single slope solar still top surface open condition operating with crescent absorber, (2) Single slope solar still top surface closed condition which is operating with crescent absorber for a period of 9:00 hours to 16:00 hours. In the first modes of the operation the productivity the still 2.1 litres per day and 1.03 litres/ day for second mode of the operation. The efficiency of the first mode of study is calculated as 23.19% and 13.01% is the second mode of the still performance.
- T. Arunkumar et. al. [9] conducted experimental study on a compound parabolic concentrator tubular solar still tied with pyramid solar still. These type of behaviour is studied by using of a pyramid solar still directly coupled with compound parabolic concentrator – tubular solar still in this work. These results showed that the maximum output extracted from the proposed system as 6928 ml/m^2/day for with cooling. The overall efficiency of the system is calculated as 17.01% for without cooling and 21.14% for with cooling.

Solar Still Integrated to Solar Pond:

- Performance analysis of vapour adsorption solar still integrated with mini-solar pond for effluent treatment is done by Dr. K. Srithar [10]. To enhance the productivity, the single basin solar still was modified with activated carbon, methanol with sponge, pebbles and sand were used. The overall productivity of the still is increased by 32.32 %.

- The experimentation was carried out by V. Velmurugan; et al. [11] on solar stills integrated with a mini solar pond and found that the productivity is maximum. Optimum salinity of 80gm/kg of water was used in solar pond. Productivity of still alone was found to be 2.77 L/m^2 /day. And when sponge cubes is used in solar still production rate is increases by about 33%, i.e. 3.3 L/m^2 /day. When a mini solar pond was integrated with solar still productivity is increased by about 58%. I.e. 3.4 L/m^2 /day. But maximum productivity is obtained when the sponged solar still is integrated with the mini solar pond, i.e. 4.4 L/m^2 /day.
- Velmurugan et al. [12] experimentally investigated the possibility of enhancing the productivity of the solar stills by connecting a mini solar pond, stepped solar still and a single basin solar still in series. Pebbles, baffle plates, fins and sponges are used in the stepped solar still for productivity augmentation. Their finding shows that, maximum productivity of 78% occurred when fins and sponges were used in the stepped solar still and also found that the productivity during night also improved when pebbles were used in the solar stills.

Solar still coupled with evacuated tube:

- The solar still coupled with evacuated tubes were carried out by K. Sampathkumar, et al. [13] to enhance the productivity of the solar still. These experiments were conducted using tap water as feed. It was found that, after augmentation of the evacuated tubes, the daily production rate has increased by 49.7 % and it increased by 59.48% with black stones.
- Ahmed et al. [14] designed, fabricated and tested the multistage evacuated solar still system that consists of three stages stacked on the top of each other. The results show that, the maximum production of the solar still was found in the first stage and is 6 kg/m^2/day, 4.3 kg/ m^2/day in second stage and 2 kg/m^2/day in first stage at a vacuum pressure of 0.5 bars. Indeed, the total productivity of the solar still is affected very much by changing the internal pressure. The productivity decreased as the pressure increased due to the lower evaporation rates at the higher pressure values.

VI. Conclusion

The forgone discussion on the use of solar still system suggests that there is a need for developing a reliable and higher productivity solar still. The review is focused on the still coupled with solar collectors, Solar still coupled with flat plate collector, solar still coupled with parabolic concentrator, Solar still integrated to Solar Pond and solar still coupled with evacuated tube are discussed and their effectiveness are compared. The review is mainly focused on production of distilled water from Single Basin Solar Still with Evacuated Tubes Solar Collector.

References

[1]. Bhanu Pratap Singh., "Performance Evaluation of a Integrated Single Slope Solar Still With Solar Water Heater", MIT International Journal of Mechanical Engineering Vol. 1, No. 1, Jan 2011, pp 68-71 ISSN No, 2230-7699.
[2]. Ahmed Z. Al-Garni, "Productivity Enhancement of Solar Still Using Water Heater and Cooling Fan", Solar Energy Division of ASME for publication in the JOURNAL OF SOLAR ENERGY ENGINEERING, AUGUST 2012, Vol. 134.
[3]. V. Velmurugan, S. Senthil Kumaran, V. Niranjan Prabhu, and K. Srithar, "Productivity Enhancement of Stepped Solar Still–Performance Analysis", Desalination 2009; 249 s (3):902–9.
[4]. Badran OO, Al-Tahaineh HA., "The effect of coupling a flat plate collector on the solar still productivity". Desalination 2005; 183:137 –42.
[5]. Rajesh. A.M, Bharath. K.N, Babu Kumar B R, "Design and Performance of Hybrid Solar Still", International Conference on Control, Automation, Communication and Energy Conservation-2009, 4th-6th June 2009.
[6]. Zeinab S Abdel Rehim, Ashraf Lasheen., "Experimental and theoretical study of a solar desalination system located in Cairo", Egypt. Desalination 2007; 217:52–64.
[7]. Garcia Rodriguez L, Gomez Camacho C., "Design parameter selection for a distillation system coupled to a solar parabolic through collector", Desalination 1999; 122:195–204.
[8]. T. Arunkumar , R. Jayaprakash, K. Perumal and Sanjay Kumar, "Desalination Process Of Single Slope Solar Still Coupled In CPC With Crescent Absorber", Journal of Environmental Research And Development ,Vol. 5 No. 1, July-September 2010.
[9]. T. Arunkumar, K. Vinothkumar, Amimul Ahsan,R. Jayaprakash and Sanjay Kumar, " Experimental Study on a Compound Parabolic Concentrator Tubular Solar Still Tied with Pyramid Solar Still", Advancing Desalination, Chapter 9,ppg 183-194.
[10]. Dr. K. Srithar," Performance Analysis of Vapour Adsorption Solar Still Integrated with Mini- Solar Pond for Effluent Treatment", International Journal of Chemical Engineering and Applications, Vol. 1, No. 4, December 2010 ISSN: 2010-0221, pp. 336-341.
[11]. V. Velmurugan, K. Mugundhan, K. Srithar, "Experimental Studies On Solar Stills Integrated With A Mini Solar Pond", Proceedings of the 3rd BSME-ASME International Conference on Thermal Engineering 20-22 December, 2006, Dhaka, Bangladesh.
[12]. Velmurugan V, Pandiarajan S, Guruparan P, Harihara Subramanian, David Prabaharan C, Srithar K., "Integrated performance of stepped and single basin solar stills with mini solar pond", Desalination 2009;249(3):902–9.
[13]. K.Sampathkumar, K.Mayilsamy, S.Shanmugam and P. Senthilkumar, "A Experimental Study on Single Basin Solar Still Augmented With Evacuated Tube".
[14]. Ahmed MI, Hrairi M, Ismail A., "On the characteristics of multistage evacuated solar distillation", Renewable Energy 2009; 34:1471–8.
[15]. G. D. Rai, "Non-Conventional Energy Sources". 5.8: Solar Distillation. 5th Edition: 2011, April. Page no 195-196.

International Journal of Modern Engineering Research (IJMER)
www.ijmer.com Vol.3, Issue.2, March-April. 2013 pp-1026-1031 ISSN: 2249-6645

Environmental Impact of Thermal Power Plant in India and Its Mitigation Measure

Sahithi Avirneni, [1] Dharmateja Bandlamudi[2]
[12]*Electrical and Electronics Engineering, Koneru Lakshmaiah University, India*

Abstract: *This research paper discusses the impacts of the coal combustion in thermal power plant, emphasized the problems associated with fly ash, collection using Electro Static Precipitator, mitigation measures for fly ash has also been highlighted such as development of bricks, use of fly ash for manufacturing of cement, development of ceramics, fertilizer, development of distemper and use of fly ash in road construction and road embankment. This article gives the direction for the beneficial use of fly ash generated during coal combustion in power plants*

Keywords: *Coal, fly ash, thermal power plant, Electro Static Precipitator, combustion.*

I. Introduction

Coal is the only natural resource and fossil fuel available in abundance in India. Consequently, it is used widely as a thermal energy source and also as fuel for thermal power plants producing electricity [1]. Power generation in India has increased manifold in the recent decades to meet the demand of the increasing population [2]. Generating capacity has grown many times from 1362MW in 1947 to 147,403MW (as on December 2008). India has about 90,000 MW installed capacity for electricity generation, of which more than 70% is produced by coal- based thermal power plants. The only fossil fuel available in abundance is coal, and hence its usage will keep growing for another 2–3 decades at least till nuclear power makes a significant contribution. The coal available in India is of poor quality, with very high ash content and low calorific value, and most of the coal mines are located in the eastern part of the country. Whatever good quality coal available is used by the metallurgical industry, like steel plants. The coal supplied to power plants is of the worst quality. Some of the coal mines are owned by private companies, and they do not wish to invest on quality improvement [1]. Combustion process converts coal into useful heat energy, but it is also a part of the process that produce greatest environmental and health concerns. Combustion of coal at thermal power plants emits mainly carbon dioxide (CO_2), sulphur oxides (SOx), nitrogen oxides (NOx); CFCs other trace gases and air borne inorganic particulates, such as fly ash and suspended particulate matter (SPM). CO_2, NOx and CFCs are greenhouse gases (GHGs) High ash content in Indian coal and inefficient combustion technologies contribute to India's emission of air particulate matter and other trace gases, including gases that are responsible for the greenhouse effect. And mercury which is a dangerous metal released by this coal combustion.

II. Fly Ash

The present coal consumption in thermal power station in India results in adding ash estimated 12.21 million tons fly ash in to the environment a year of which nearly a third goes in to air and the rest is dumped on land or Water in spite of various research results a consistent utilization is not evident, and it expected that stocks piles Of fly ash will continue to grow with the increasing number of super thermal power station in India. As reliance upon coal as a fuel source increases, this large quantities of this material will be increasingly brought into contact with the water and soil environment [3].

2.1 Problems associated of increasing fly ash

India has about 211 billion tons of coal reserves, which is known to be the largest resource of energy and presently 240MT of coal is being used annually to meet the Nation's electricity demand. In terms of energy, India stands at world sixth position accounting 3.5% of the world commercial energy demand in 2001, but the electricity generation yet not completely fulfilled the present requirement. Environmental pollution by the coal based thermal power plants all over the world is cited to be one of the major sources of pollution affecting the general aesthetics of environment in terms of land use, health hazards and air, soil and water in particular and thus leads to environmental dangers[4]. Fly ash water also affects the scale structure because it is a directly in contact with water. Heavy metals can also adversely affect the growth rate in major carps[5]. Coal combustion residues (CCRs) are a collective term referring to the residues produced during the combustion of coal regardless of ultimate utilization or disposal. It includes fly ash, bottom ash, boiler slag, and fluidized bed combustion ash and other solid fine particles [6]. In India, presently coal based thermal power plants are releasing 105MT of CCRs which possess major environmental problems [7]. Presently from all these thermal power plants, dry fly ash has been collected through Electrostatic Precipitator (ESP) in dry condition as well as pond ash from ash ponds in semi-wet condition. In India most of the thermal power plants do not have the facility for automatic dry ash collection system. Commonly both fly ash and bottom ash together are discharged as slurry to the ash pond/lagoon these effect on environment, economy, and social factor.

Table-I
Composition of Indian coal and fly ash in ppm

Elements	Coal	Fly ash	Coal	Fly ash
Na	1500	6700	289	1299
K	10,000	15,000	2075	18,275
La	22.2	94	47.6	238
Ce	42	212	30.2	145
Hg	0.6	9	11	48
Te	NA	NA	1.83	8.87
Th	5.1	6.6	5.34	25
Cr	55	210	62.8	404
Hf	1.8	7	7.1	32.6
Sc	8.9	64	22.9	106
Zn	170	3100	539	2027
Fe	11,000	51,000	20,088	1,06,665
Ta	NA	NA	153	5.05
Co	13.9	520	33.4	128
Eu	0.8	8.6	0.95	5.6
Sm	NA	NA	0.65	1.99
Am	0.4	0.2	0.136	0.69

NA –Not Available

Table-II
Chemical Composition of Fly Ash

Name	Formula	Percentage
Silica	SiO_2	62
Iron oxide	Fe_2O_3	63
Aluminium	Al_2O_3	26
Titanium oxide	TiO_2	1.8
Potassium oxide	K_2O	1.28
Calcium oxide	CaO	1.13
Magnesium oxide	MgO	0.49
Phosphorus pent oxide	P2O5	0.40
Sulphate	SO_4	0.36
Disodium oxide	Na_2O	0.28

2.2 Problems associated with radionuclide increase in atmosphere coal combustion: Coal, like most materials found in nature, contains radionuclides. The levels of natural radionuclides in a geological formation depend on its composition and geological history. In the production of electric power, coal is burned in a furnace operating at temperatures of up to 1700°C [8]. In the combustion process, volatile radionuclide's such as Pb^{210} and Po^{210} are partly released in the flue gases and escape to the atmosphere. A significant fraction of the radioactivity is also retained in the bottom ash or slag .The greatest part of the radioactivity in coal remains with the ash but some of the fly ash from coal-fired power plants escapes into the atmosphere [9]. Air pollution in the vicinity of a coal fired thermal power station affects soil, water, vegetation, the whole ecosystem and human health [10]."Environmental impact of coal utilization in thermal power plant" notes that "Radon is a colourless, odourless but noble gas, which is radioactive and ubiquitously present. It poses grate health hazards not only to uranium miners but also people living in normal houses and buildings and at work place like coal mines, cement industry, thermal power plants etc. Coal, a naturally occurring fossil fuel is burnt in conventional power plants to meet out about 72% of the electricity needs in our country [11]. It was lesser known hitherto until recently that the fly ash which is a by-product of burnt coal is a potential radioactive air pollutant and it modifies radiation exposure.

III. Collection of Fly Ash

After the combustion of the coal in the boiler, 20% of the ash is collected at the bottom of the boiler called bottom ash and 80% is carried along with flue gases called fly ash. Bottom ash is mixed with water and made into sludge form and sent through pumps into the ash ponds. The Electro Static Precipitator is used to collect the ash particles in the flue gases. The era after the introduction of the Electro Static Precipitator has partly protected the environment from harmful gases and hazardous chemicals. Generally dust is collected from the waste in two processes that is mechanically and electrically.

Mechanically is by using filters and electrically is by using Electro Static Precipitators. The ESP is efficient in precipitation of particles from sub microns to large sizes of particles and hence they are preferred to mechanical precipitators. The efficiency of modern ESP's is of the order 99.9%.The Electro Static Precipitators have high collecting efficiency, low sensitivity to high temperatures, low pressure drop, limited process controls and an easy and reduced maintenance make the electro static precipitators one of the most reliable and appreciated units available at the moment in the market.

Electrostatic precipitators can be used for collecting virtually all kinds of dust coming from coal and oil fired power stations, blast furnaces and industrial furnaces, iron and steel processes, cement factories, municipal solid wastes incinerators , paper mills, wood factories, textile industries, food and pharmaceuticals industries.

3.1 Principle of Electro Static Precipitator

The electro static precipitator utilizes electrostatic forces to separate dust particles from the gas to be cleaned. The flue gas is ionized in the electro static field and large quantities of positive and negative ions are formed. The positive ions are immediately attracted towards the negative wires by the strength of the field. The negative ions however attracts towards the positive diode.

IV. Fly Ash Mitigation Measure

Fly ash is fine glass powder, the particles of which are generally spherical in shape and range from 0.5 to 100 micron in size. The fine particles of fly ash reach the pulmonary region of the lungs and remain there for long periods of time; they behave like cumulative poisons. The submicron particles enter deeper into the lungs and are deposited on the alveolar walls where the metals could be transferred to the blood plasma across the cell membrane fly ash can be disposed-off in a dry or wet state. Studies show that wet disposal of this waste does not protect the environment from migration of metal into the soil. Heavy metals cannot be degraded biologically into harmless products like other organic waste. Studies also show that coal ash satisfies the criteria for landfill disposal, according to the Environmental Agency of Japan. According to the hazardous waste management and handling rule of 1989, fly ash is considered as non-hazardous. With the present practice of fly-ash disposal in ash ponds (generally in the form of slurry), the total land required for ash disposal would be about 82,200 ha by the year 2020 at an estimated 0.6 ha per MW. Fly ash can be treated as a by-product rather than waste [12].

4.1 Fly ash bricks: The Central Fuel Research Institute, Dhanbad has developed a technology for the utilization of fly ash for the manufacture of building bricks. Fly ash bricks have a number of advantages over the conventional burnt clay bricks. Unglazed tiles for use on footpaths can also be made from it (Figure 1). Awareness among the public is required and the Government has to provide special incentives for this purpose [12]. Six mechanized fly ash brick manufacturing units at Korba are producing about 60000 bricks per day. In addition to this, two mechanized fly ash brick manufacturing units have been set up by private entrepreneurs also at Korba [13], the total production being about 30000 bricks/day. Apart from this about 23 entrepreneurs have registered in DTIC proposals for establishing ash brick units. To give impetus to ash brick manufacturing [13]

Orissa Government in India has banned the use of soil for the manufacture of bricks up to 20 km. of a thermal power station. In the case of fly ash-clay fired bricks, a mixture of clay and fly ash is fired. The unburnt carbon of the fly ash serves as fuel for burning. Approximately 20-30% energy can be reduced by adding25-40% fly ash [14].

Figure-1

Fly ash using for making bricks

4.2 Fly ash in manufacture of cement: In the presence of moisture, fly ash reacts chemically with calcium hydroxide and CO_2 present in the environment attack the free lime causing deterioration of the concrete. A cement technologist observed that the reactive elements present in fly ash convert the problematic free lime into durable concrete [15]. Fly ash can substitute up to 66% of cement in the construction of dams. Fly ash in R.C.C. is used not only for saving cement cost but also for enhancing strength and durability. Fly ash can also be used in Portland cement concrete to enhance the performance

of the concrete. Portland cement is manufactured with Calcium oxide, some of which is released in a free state during hydration. Studies show that one ton of Portland cement production discharges 0.87 tonnes of carbon dioxide in the environment. Another Japanese study indicates that every year barren land approximately 1.5 times of the Indian Territory need to be afforested to compensate for the total global accumulation of carbon dioxide discharged into the atmosphere because of total global cement production. Utilization of fly ash in cement concrete minimizes the carbon dioxide emission problem to the extent of its proportion in cement.

4.3 Fly ash-based ceramics: Ceramic products with up to 50 wt% of mullite and 16 wt% of feldspars were obtained from binary mixtures of fly ash from the Teruel power station (NE Spain) and plastic clays from the Teruel coal mining district [16]. The firing behaviour of fly ash and the ceramic mixtures was investigated by determining their changes in mineralogy and basic ceramic properties such as colour, bulk density, water absorption and firing shrinkage. To determine the changes on heating suffered by both the fly ash and the ceramic bodies, firing tests were carried out at temperatures between 900 and 1200°C in short firing cycles [17]. The resulting ceramic bodies exhibit features that suggest possibilities for use in paving stoneware manufacture, for tiling and for conventional brick making (fig-2). The National Metallurgical Laboratory; Jamshedpur has developed a process to produce ceramics from fly ash having superior resistance to abrasion [12].

(a)

(b)

Figure-2

a) Mosaic tile b) Interlocking paver

4.4 Fly ash as fertilizer: Fly ash provides the uptake of vital nutrients/minerals (Ca, Mg, Fe, Zn, Mo, S and Se) by crops and vegetation, and can be considered as a potential growth improver [18]. Because it can be a soil modifier and enhance its moisture retaining capacity and fertility the improvement in yield has been recorded with fly ash doses varying from 20 tone / hectare to 100 tone / hectare (Figure 3). On an average 20-30% yield increase has been observed. Out of 150 million hectare of land under cultivation, 10 million hectares of land can safely be taken up for application of fly ash per year. The fly ash treated fields would give additional yield of 5 million tone food grains per year valued at Rs.3000 per year.

(a)

(b)

Figure-3

a) Cabbage at Dobhar, fly ash amended soils
b) Reclamation of saline soils using fly ash
(75% saving in gypsum)

4.4 Fly ash based polymer products: Fly ashes are also being used as wood substitutes. They have been developed by using fly ash as the matrix and jute cloth as the reinforcement. The Jute cloth is laminated by passing through a polymer fly ash matrix and then cured. The number of Laminates is increased to get the desired thickness. The product can be used in many applications like door shutters, partition panels, flooring tiles, wall panelling and ceiling. The developed material is stronger more durable, resistant to corrosion and cost effective as compared to wood. This technology has been developed by the Regional Research Laboratory, Bhopal in collaboration with Building Materials and Technology Promotion Council (B.M.T.P.C) and TIFAC [19]. One commercial plant has been set up based on this technology near Chennai, India. The Government of India has withdrawn an 8% excise duty imposed earlier on fly ash products.

4.5 Fly ash in road construction: The use of fly ash in large quantities making the road base and surfacing can result in low value–high volume utilization technology demonstration projects at New Delhi, Dadri (U.P.) and Raichur (Karnataka) have been successfully completed for use of fly ash in road / flyover embankments (figure-4). Guidelines have been prepared and approved by Indian Roads Congress (IRC) as national standard. More than 10 multiplier effects have taken place across the country.

In the recent past CRRI offered advise/ consultancy services in the following road/embankment projects in which fly ash was utilized:

1. Construction of plant roads at Budge-Budge thermal power plant using fly ash based pavement specifications (Collaboration with CESC Ltd, Kolkata),
2. Construction of one km long rural road near Raichur in Karnataka with fly ash based flexible/semi-rigid pavement composition (Collaboration with Karnataka PWD and Raichur thermal power station -executed as Fly Ash Mission demonstration project)
3. Construction of plant road and two rural roads using fly ash (collaboration with National Capital Power Station, NTPC, Dadri, U.P) [20].

Figure 4
Nizamuddin Bridge approach road embankment at New Delhi (in flood zone of river Yamuna)

4.6 Roads and Embankments: Another area that holds potential for utilization of large volumes of fly ash is road and flyover embankments. Fly ash embankments at Okhla, Hanuman Setu, Second Nizamuddin bridge in Delhi and roads at Raichur, Calcutta, Dadri etc. have established that on an average Rs. 50 to 75 per MT of earth work cost can be saved by using fly ash (in lieu of soil) in such works, primarily due to reduction in excavation & transportation costs[18].

In the recent past CRRI offered advise/ consultancy services in the following road/embankment projects in which fly ash was utilized:

1. Fly ash embankment construction for Okhla flyover at Delhi adopting 'Reinforced Embankment Technique' (Collaboration with Delhi PWD – executed as Fly Ash Mission demonstration project),
2. Fly ash embankment construction for Hanuman Setu flyover at Delhi adopting 'Reinforced Embankment Technique' (Collaboration with Delhi PWD and Badarpur Thermal Power Station, Delhi).
3. Construction of reinforced approach embankment using fly ash at SaritaVihar flyover in Delhi (Collaboration with Delhi Development Authority and Badarpur Thermal Power Station, Delhi).
4. Construction of embankment for Noida-Greater Noida Expressway project (Collaboration with IRCON International and Badarpur Thermal Power Station, Delhi)[19]

V. Environmental Impact of Fly Ash Usage

Utilization of fly ash will not only minimize the disposal problem but will also help in utilizing precious land in a better way. Construction of road embankments using fly ash, involves encapsulation of fly ash in earthen-core or with RCC facing panels. Since there is no seepage of rain water into the fly ash core, leaching of heavy metals is also prevented. When fly ash is used in concrete, it chemically reacts with cement and reduces any leaching effect. Even when it is used in stabilization work, a similar chemical reaction takes place which binds fly ash particles. Hence chances of pollution due to use of fly ash in road works are negligible [21].

VI. Energy Saving and Environmental Benifits

Most of the developing countries face energy scarcity and huge housing and other infrastructure shortage. Ideally in these countries materials for habitat and other construction activities should be energy efficient (having low energy demand). The following table shows some examples of energy savings achieved through the use of Fly Ash in the manufacture of conventional building materials [22].

VII. Conclusion

Coal is used widely as a thermal energy source in thermal power plant for production of electricity but available coal in India is of poor quality, with very high ash content and low calorific value. Utilization of huge amount of coal in thermal power plant has created several adverse effects on environment leading to global climate change and fly ash management problem. Coal based thermal power plants all over the world is cited to be one of the major sources of pollution affecting the general aesthetics of environment in terms of land use, health hazards and air, soil and water in particular and thus leads to environmental dangers. So, the disposable management of fly ash from thermal power plant is necessary to protect our environment. It is advisable to explore all possible application for fly ash utilization. Several efforts are needed to utilize fly ash for making bricks, in manufacture of cement, ceramics etc. Various governmental and nongovernmental bodies working in the field of utilization of fly ash for construction of road/road embankment The utilization of fly ash gives good result in almost every aspects including good strength, economically feasible and environmental friendly.

References

[1] Mishra U.C., Environmental impact of coal industry and thermal power plants in India, J Environ Radio act, 72(1-2), 35-40 (2004)
[2] Jamil S., Abhilash P.C., Singh A., Singh N. and BhelHari M., Fly ash trapping and metal accumulation capacity of plant, implication of for green belt around thermal power plant, J. Land Esc. And Urban Plan, 92, 136-147 (2009)
[3] Fulekar M.H. and Dave J.M., Release and behavior of Cr, Mn, Ni and Pb in a fly-ash/soil/water environment: column experiment, IntJ. Of Environmental Studies, 4, 281-296 (1991)
[4] Ashoka D., Saxena M. and Asholekar S.R., Coal Combustion Residue-Environmental Implication and Recycling Potential, Resource Conservation and Recycling, 3, 1342-1355 (2005)
[5] Shrivastava Shikha and Dwivedi Sushma, Effect of fly Ash Pollution on Fish Scales, Re. J. of Che. Sci, 1(9), 24-28 (2011)
[6] Keefer R.F., Coal ashes-industrial wastes or beneficial by-products. In: Keefer R.F., Sajwan K., editors, Trace Element in Coal and Coal Combustion Residues. Advances in Trace Substances Research, Florida: Lewis Publishers, CRC Press, 3–9 (1993)
[7] Kumar Vimal and Mathur Mukesh, Clean environment through fly as utilization Cleaner (2003)
[8] Critical Review in Environmental Control, CRC Press, 3, (1989)
[9] Pvrecek, Lbendik, Pb^{210} and Po^{210} in fossil fuel at the sostanj thermal power plant (Slovenia), Czechoslovak j of phy, 53 a, 51-a (2003)
[10] F˙IL˙IZ G ¨ UR and G ¨ UNSEL˙I YAPRAK, Natural radionuclide emission from coal-fired power plants in the southwestern of Turkey and the population exposure to external radiation in their vicinity, J. of Environ. Sci. and Health Part a, 45, 1900–1908 (2010)
[11] Kant K., Chakarvarti S.K Environmental impact of coal utilization in thermal power plant, J. of Punjab Acad. of For. Med. &Toxi, 3, 15-18 (2003)
[12] Senapati Manas Ranjan, Fly ash from thermal power plants–waste management and overview current science, 100, 1791-1794 (2011)
[13] korba.gov.in/kwflyash.htm (2012)
[14] www.wealthywaste.com/fly-ash-utilization-in-india (2012)
[15] Cement Manufacturing Association, (1999)
[16] IgnasiQuerlt,XavierQuerol ,Angel Lopez-Solar ,Felicano Plana ,Use of coal fly ash for ceramics ;a case study for large Spanish power station, fuel,8 , 787-791, (1997)
[17] SaikatMaitra, Cremic product from fly ash global prospective. In preceding of the national seminar on fly ash utilization, February 26-27 NLM Jamshedpur India (1999)
[18] Kumar Vimal and MathurMukesh, Clean environment through fly as utilization. Cleaner Technology, Impacts/12/2003-2004, MOEF-CPCB, Govt. of India, 235-255, (2003)
[19] Fly Ash Mission', (TIFAC), Department of Science and Technology, Ministry of Science and Technology, Government of India, Technology (1994)
[20] www.crridom.gov.in/techniques-facilities/10.pdf (2012)
[21] M.Ahmaruzzaman, A review of utilization of fly ash In Energy and Combustion. Sci.30, 327-363 (2010)
[22] Jha C. N. & Prasad J. K. Fly ash: a resource materifsinceal for innovative building material - Indian perspective substitute and paint from coal ash" 2nd international conference on "fly ash disposal &utilization", New Delhi, India, (2000).

International Journal of Modern Engineering Research (IJMER)
www.ijmer.com Vol.3, Issue.2, March-April. 2013 pp-1032-1037 ISSN: 2249-6645

Statistical Performance Analysis Routing Algorithms for Wimax - Wi-Fi Integrated Heterogeneous Network

Poulomi Das, [1] Arindam Banerjee, [2] Prof. Siladitya Sen[3]
[123]*Department of Electronics and Communication Engineering, Heritage Institute of Technology, West Bengal, India*

***Abstact*:** *To provide uninterrupted service to every subscribe in a wireless network, there is a need to incorporate a low cost, flexible heterogeneous network which can able to couple any kind of network for efficient spectrum utilization, hence improve system capacity. For data communication Wi-Fi/ Wi-MAX integrated network seems to be an ideal solution as it is able to provide easy deployment, high speed data rate and wide range coverage with high throughput, low end to end delay, flat and low jitter. As Wi-Fi (IEEE 802.11n) & WiMAX (IEEE 802.16m) network support mobility so from real time service providing to surveillance activities for mobile users can be supported by this integrated network. The selection of appropriate routing protocol for high speed uninterrupted applications is an important parameter while designing of scalable, flexible and efficient integrated network. The routing protocol should take into account the mobility factor in the network and the topology being used. So, in this paper we have first designed an integrated Wi-Fi/WiMAX network and then statistically analyze the performance of the network for various routing algorithms. This analysis will help to forecast the best suitable algorithm.*

Keywords: *Integrated network, Network performance, Routing algorithm, Wi-Fi (IEEE 802.11n), Wi-MAX (IEEE 802.16e)*

I. Introduction

Recent surveys enlighten the fact that there will be an exponential growth for mobile data demand due to massive development in mobile devices like smart phones, laptop, tabs etc. It is also forecasted that demand of mobile data will be doubled from 2013 where the growth rate is 66 times in between 2008 to 2013. Chronologically the high speed internet access from cable, Digital Subscriber Line (DSL), and other fixed broad-band connections are going to replace by wireless hotspots, Wi-Fi & WiMAX services. Due to advent of portable, low cost & user friendly devices users are attracted towards wireless services. As time & users demands for uninterrupted services so the last mile winner WiMAX can be able to cover large areas in metropolitan, suburban, rural or terrine with high speed mobile broadband internet access called wide area networks (WANs). Where Wi-Fi can provide high data rate in short range communication. Providing proper network services to every user, from time of registration to time to leave is the function of a network. As both networks support mobility so integration of both networks can be a best solution to maintain proper QoS. It is important that the apparent similarity between Wi-Fi and WiMAX, But complementary natures between them are key designing aspects of this integrated network. While Wi-Fi has a short coverage range of about 100 meters, WiMAX offers a significantly greater coverage in a range of 500 meters and beyond; while Wi-Fi offers high raw data (up to 500 Mb/s is envisaged) capacity due to the use of unlicensed frequency bands with poor traffic control capabilities, WiMAX is capable of highly sophisticated traffic management and QoS control [1] with low data rates, due to the use of licensed frequency bands. These integrated networks have become more efficient with the introduction of mobility concept of nodes. One of the challenging aspects in these integrated networks is to find and develop routing protocols that can efficiently find routes between any two nodes (may be static or mobile). The routing protocol should take into account the mobility factor in these networks and the topology being used. For this reason, performance evaluation of various protocols has been carried out by different researchers. Routing is a function in the Network layer which determines the path from source to destination for the traffic flow. Router in the network needs to be able to look at a packet's destination address and then determines which of the output port is the best choice to get the packet to that address. In this paper, first we have designed Wi-Fi/ WiMAX integrated network and proposed a survey on routing algorithms used in this integrated networks for both uplink and downlink traffic using QualNet 5.0.2 simulator. Also this paper will enlighten best suitable routing algorithm for an integrated heterogeneous network to maintain proper QoS all applications.

II. Theoritical Overview of Wi-Fi (IEEE 802.11n) and Wimax (IEEE 802.16e) Technologies

2.1. Wi-Fi (IEEE 802.11n) Technology:

In 1997, the Institute of Electrical and Electronics Engineers (IEEE) created the first WLAN standard. They called it 802.11 after the name of the group formed to oversee its development. Unfortunately, 802.11 only supported a maximum network bandwidth of 2 Mbps - too slow for most applications. For this reason, ordinary 802.11 wireless products are no longer manufactured. The new generation of IEEE 802.11n-based Wi-Fi technology is expected to pick up significant market momentum in 2008. The currently available draft 802.11n technology can comfortably cover a typical house with sufficient bandwidth to support video, gaming, data and voice applications. In the enterprise environment, 802.11n is expected to support mission-critical applications with the throughput, QoS and security capabilities comparable to Ethernet. The developing IEEE 802.11n standard is based on MIMO (multiple-input multiple-output) air interface technology. MIMO is a significant innovation and a technology that is being adapted for use by several non-802.11 wireless data communications standards, including 4G cellular. 802.11n is an amendment which improves upon the previous 802.11 standards by adding

multiple-input multiple-output antennas (MIMO). 802.11n operates on both the 2.4 GHz and the lesser used 5 GHz bands. It operates at a maximum net data rate from 54 Mbits/s to 600 Mbits/s. The IEEE has approved the amendment and it was published in October 2009

Table 1: Features of Advance Wi-Fi Protocols

	IEEE 802.11n	IEEE802.11ac
Frequency Band	2.4GHz & 5GHz	5GHz only
Channel Widths	20,40MHz	20, 40, 80MHz & optional 160MHz
Spatial Streams	1 to 4	1 to 8 total up to 4 per client
Multi User MIMO	No	Yes
Signal Stream [1x1] Multi Client Data Rate	150Mbps	450Mbps
Three Stream [3x3] Multi Client Data Rate	450Mbps	1.3Gbps

2.2. WiMAX (IEEE 802.16e) Technology:

The IEEE 802.16 Standard, first published in 2001, defines a means for wireless broadband access as a replacement for current cable and DSL "last mile" services to home and business. The adoption of this standard is currently in progress through the use of WiMAX Forum certified networking equipment and wide & spread adoption should appear over the next few years. This paper provides an overview of the 802.16 standard in regards to frequency bands, the physical layer specification, security sub-layer, MAC common part sub-layer, and service specific convergence sub-layer. The IEEE 802.16e air interface standard extends its fixed wireless access predecessor, IEEE 802.16–2004, to support mobile broadband wireless access systems [2, 3]. In addition to enhancing several advanced orthogonal frequency division multiple access (OFDMA) technology features, IEEE 802.16e incorporates the functionality needed to support user mobility. In particular, technologies such as hybrid automatic repeat request (HARQ), space time coding (STC), advanced antenna systems (AAS), multiple input multiple output (MIMO), and space division multiple access (SDMA) have been enhanced to support mobile environments and to improve the broadband access speed. some of these enhancements are similar in concept to those incorporated in third generation cellular standards such as CDMA2000 high rate packet data (HRPD) or the high speed downlink packet access (HSDPA) feature within the Universal Mobile Telecommunications System (UMTS) standard [4], they have been specifically tailored to an OFDMA air interface. Additional sub-channelization options have been added in IEEE 802.16e to improve recourse management flexibility and achieve better system performance under a wide range of operating conditions. IEEE 802.16e also adds new medium access control (MAC) procedures related to handover support. Multiple carrier bandwidths and associated fast Fourier transform (FFT) sizes are included to allow bandwidth scalability. Furthermore, time division duplexing (TDD) and frequency division duplexing (FDD) support are available in each of these cases to allow operation in unpaired or paired spectrum allocations respectively.

III. Routing Algoritms

Routing algorithms are required to build the routing tables and hence forwarding tables. The basic problem of routing is to find the lowest-cost path between any two nodes, where the cost of a path equals the sum of the costs of all the edges that make up the path. Routing is achieved in most practical networks by running routing protocols among the nodes. The protocols provide a distributed, dynamic way to solve the problem of finding the lowest-cost path in the presence of link and node failures and changing edge costs.

3.1. Bellman- Ford Routing Algorithm:

Bellman- Ford routing algorithm is the shortest path routing algorithm. In a network how a packet reached to destination using available shortest path is described by this algorithm. It is popular algorithm in networking. The algorithm is usually named after two of its developers, Richard Bellman and Lester Ford, Jr., who published it in 1958 and 1962.

3.2. AODV (Ad-hoc On Demand Distance Vector Routing Protocol):

This protocol is based on source-initiated on-demand routing. This type of routing creates routes only when desired by the source node. Route discovery process starts on demand by the source. This process is completed once a route is found or all possible routes have been explored. It provides unicast, broadcast, and multicast communication in ad hoc mobile networks [5]. Routes are maintained as long as they are needed by the source node. AODV nodes maintain a route table in which next hop routing information for destination nodes is stored. When a source node desires to send a data to a destination node and no route information is available, a path exploration process to find the destination node takes place. It broadcasts a route request (RREQ) packet to adjacent nodes, which in turn, forward the request to their adjacent nodes, and so on, until the destination node is found. Each node maintains a sequence number and a broadcast ID. The broadcast ID is incremented for each generated RREQ. The RREQ packet consists of the node sequence number, broadcast ID and the most recent sequence number it has for the destination node. Only those nodes reply to the RREQ which have their sequence numbers greater than or equal to that contained in the RREQ.

3.3. DYMO (DYnamic MANET On demand Routing Protocol)

It is one such protocol that is intended for the use by mobile nodes in wireless multihop networks. It can adapt to the changing network topology and determine unicast routes between nodes within the network. In On-demand protocols [6], nodes compute the routes and maintain routing information only when it is needed, thereby establishing routes as and when required by the source. This algorithm has two basic operations- route discovery and route management [7]. In route discovery operation, initiating node sends a route request to all the nodes in the network to find the target node then the target node sends the reply, in this way proper route is discovered. In order to respond to the changes in network topology, nodes maintain their routes and monitor the links over which the network traffic flows. DYMO can be typically utilized in a large mobile network consisting of large number of nodes where only a part of the nodes communicate with each other.

3.4. OLSRv2 NIIGATA (Optimized Link State Routing, version 2 Routing Protocol)

OLSRv2[8] retains the same basic algorithms as its predecessor (OLSR), however offers various improvements, e.g. a modular and flexible architecture allowing extensions, such as for security, to be developed as add-ons to the basic protocol. OLSRv2 contains three basic processes: Neighborhood Discovery, MPR Flooding and Link State Advertisements. In Neighborhood Discovery process, each router discovers the routers which are in direct communication range of itself (1-hop neighbors), and detects with which of these it can establish bi-directional communication. In MPR Flooding process each router is able to, efficiently, conduct network-wide broadcasts. Each router designates, from among its bi-directional neighbors, a subset (MPR set) such that a message transmitted by the router and relayed by the MPR set is received by all its 2-hop neighbors. In Link State Advertisement process routers are determining which link state information to advertise through the network. Each router must advertise links between itself and its MPR-selector-set, in order to allow all routers to calculate shortest paths.

3.5. RIP (Routing Information Protocol)

The Routing Information Protocol (RIP) is a distance-vector protocol that uses hop count as it's metric. RIP is widely used for routing traffic in the global Internet and is an *interior gateway protocol* (IGP), which means that it performs routing within a single autonomous system. RIP routers maintain only the best route (the route with the lowest metric value) to a destination. Routers running RIP send their advertisements regularly (e.g., every 30 seconds). A router also sends an update message whenever a triggered update from another router causes it to change its routing table.

3.6. OSPFv2

OSPFv2 is an IETF link-state protocol for IPv4 networks. An OSPFv2 router sends a special message, called a hello packet, out each OSPF-enabled interface to discover other OSPFv2 neighbor routers. Once a neighbor is discovered, the two routers compare information in the Hello packet to determine if the routers have compatible configurations. The neighbor routers try to establish adjacency, which means that the routers synchronize their link-state databases to ensure that they have identical OSPFv2 routing information. Adjacent routers share link-state advertisements (LSAs) that include information about the operational state of each link, the cost of the link, and any other neighbor information. The routers then flood these received LSAs out every OSPF-enabled interface so that all OSPFv2 routers eventually have identical link-state databases. When all OSPFv2 routers have identical link-state databases, the network is converged. Each router then uses Dijkstra's Shortest Path First (SPF) algorithm to build its route table.

IV. Statistical Analysis

Wi-Fi & WiMAX systems are using OFDM system of a block of N complex symbols are formed with each symbol modulation one of N subcarrier with frequency for the N chosen as orthogonal set. The complex envelope of the transmitted OFDM signal is represented by

$$x(t) = \frac{1}{N}\sum_{n=0}^{N-1} S_n e^{j2\pi f_n t} \quad \text{..... (1)}$$

S_n = Data Symbol, N= Number of Sub-Carrier, f_n =Represent frequency, n= bit subcarrier

Let $\Delta D_i \geq 0$ denote the expected decreases in distortion if the ith packet decoded. The overall distortion can be written as follows,

$$D(I) = D_0 - \sum_{i=1}^{l} P_i \Delta D_i \quad \text{..... (2)}$$

Where D_0 is the expected distortion when the rate is zero P_i is the probability that the ith packets are received correctly & l is the number of source packet that transmitted choose to send. The P_i can be written form,

$$P_i = \prod_{j=1}^{i} Q_j(r_j) \quad \ldots\ldots\ldots (3)$$

Where $Q_j(r_j)$ is the probability that the j^{th} of packet is received correctly when sending in a rate of $r_{f.}$ If packets are transmitted in AWGN channel then packet loss probability will be $S(p) = 1-\{1-p\}^m$ where m is the number of bits in data a packet. This relation helps to calculate throughput of the network.

Average Throughput (τ_{t_1})**:** The amount of data selected for transmission by a user per unit time. The value is expressed in Kbps and calculated using an exponential moving average as follows

$$\tau_{t_1} = \alpha^*(\tau_t) + (1-\alpha)\tau_{t-1} \ldots. (4)$$

Packet Loss (ρ)**:** The percentage of packets dropped from the queue out of all the packets that arrived in the queue. The metric indicates the percentage of packets that missed their deadlines and is calculated as follows:

$$\rho = \frac{\sum_{i=1}^{m} \omega_i}{\sum_{j=1}^{n} Kj} \ldots. (5)$$

Where, $\sum_{i=1}^{m} \omega_i$ is the sum of packets dropped, $\sum_{j=1}^{n} Kj$ is the sum of packets arrived in the queue.

Both average delay and packet loss will allow us to determine how effectively a scheduling algorithm satisfies the QoS requirements of real-time SSs.

Frame Utilization: The number of symbols utilized for data out all the symbols in the uplink sub-frame. The metric reported as a percentage is calculated as follows

$$F_{util} = \frac{\sum_{i=1}^{n} \omega_i}{C} \times 100\% \quad \ldots. (6)$$

Average Queuing delay (d)**:** The time between the arrival of a packet in the queue to the departure of the packet from the queue. The value is reported in milliseconds (ms) and is calculated for each SS as follows

$$d = \frac{\sum_{i=1}^{N} (f_i - a_i)}{N} \quad \ldots. (7)$$

V. System Model

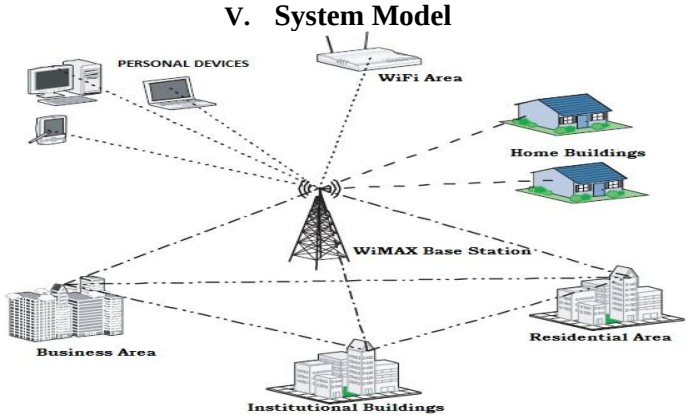

Figure 1: An Integrated WiMAX & Wi-Fi Network

As shown in above figure1, WiMAX service providers providing connectivity to Wi-Fi networks situated in office business area, residential area. The devices which are not in apartment can directly connect with WiMAX network [4].

The Wi-Fi network uses 802.11a physical layer. The auto rate fallback is turned off. The data rate is always 54Mbps. The number of APs is 16. We vary the number of original Wi-Fi users. The service area is a 1500x1500 m^2 square. APs are regularly placed in the service area. That is, they form a 4x4 grid. Since 802.11a has 12 orthogonal channels, we carefully assign the channels among neighboring APs such that any AP will have different channel from its neighbors. By doing this, we eliminate possible inter-cell interference among neighboring cells. In order to eliminate the interference from hidden-node collision, we use the following strategy. Each user randomly selects one AP to associate with. But once the association is determined, it will be placed very close to that AP. This ensures a random distribution of users, while at the same time guarantees that users belong to the same cell can hear each other. WiMAX BS is placed at the center of the service area (i.e., (750, 750)). The adaptive modulation is on by default. But the transmission power is large enough so that each WiMAX user can obtain roughly the same QoS over a long period of time. The traffic source is CBR. Payload size is 1000 bytes. The rate is 16Mbps in the application layer. All traffic is uplink. That is, from users to APs or BS. Roughly speaking, 2 users can saturate a Wi-Fi network, and 6 users can saturate the WiMAX.

VI. Simulation Results

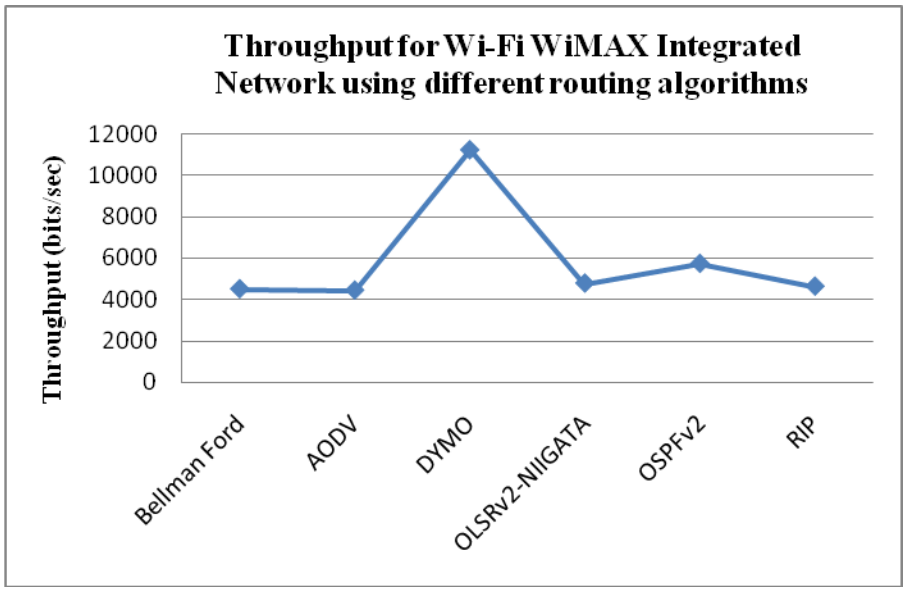

Figure 2: Throughput for Different Routing Algorithm for the network

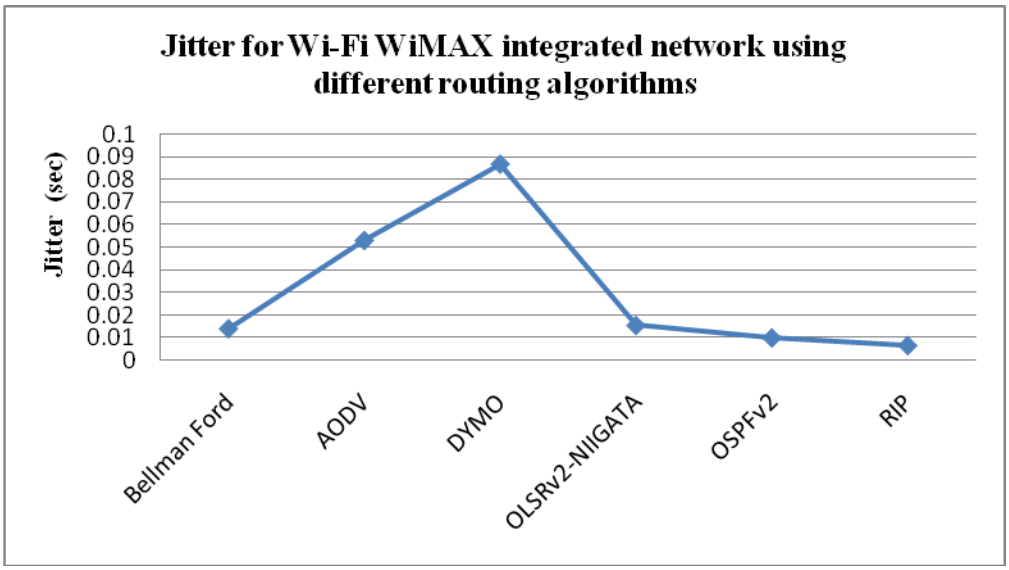

Figure 3: Average Jitter for for Different Routing Algorithm for the network

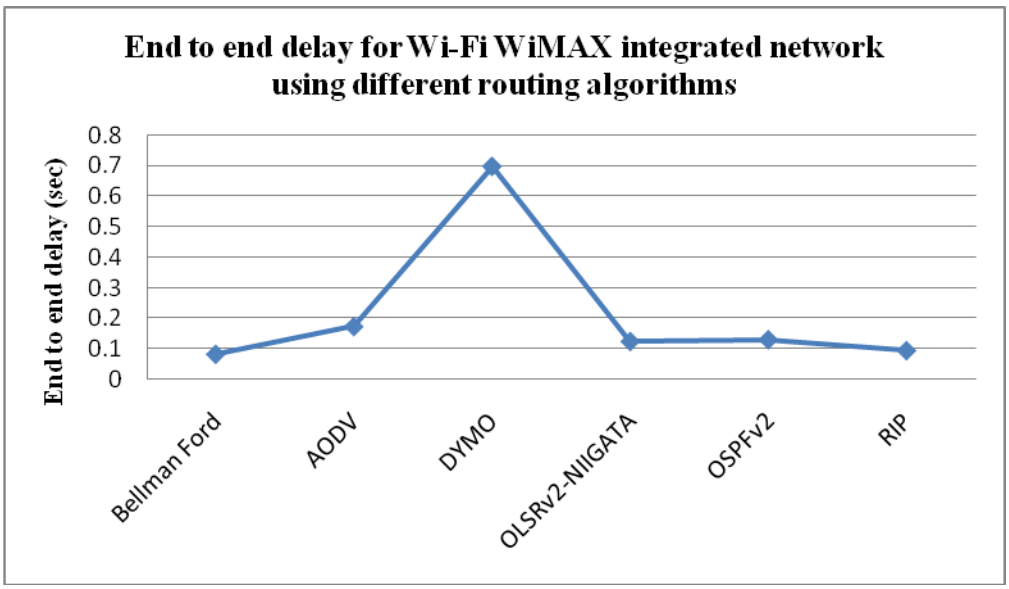

Figure 4: Average End to End Delay for Different Routing Algorithm for the network

VII. Conclusion

For this heterogeneous integrated network OSPF v2 shows better performance among all routing algorithms in terms of low jitter, End to End delay & High throughput. Such performance are helpful for implementing such networks for real time application & for better QoS for high speed mobile users.

References

[1] IEEE 802.16e-2005: "IEEE Standard for Local and Metropolitan Area Networks – Part 16: Air Interface for Fixed and Mobile Broadband Wireless Access Systems".

[2] Institute of Electrical and Electronics Engineers, ―IEEE Standard for Local and Metropolitan Area Networks—Part 16: Air Interface for Fixed Broadband Wireless Access Systems,‖ IEEE 802.16–2004, Jun. 2004.

[3] Institute of Electrical and Electronics Engineers, ―IEEE Standard for Local and Metropolitan Area Networks—Part 16: Air Interface for Fixed and Mobile Broadband Wireless Systems— Amendment 2: Physical and Medium Access Control Layers for Combined Fixed and Mobile Operation in Licensed Bands, and Corrigendum 1,‖ IEEE 802.16e-2005 and 802.16/ COR1, Feb. 2006.

[4] "Integration of Wimax and Wi-Fi services: Bandwidth sharing and channel collaboration" by Yung-Ming Li, Jhih-Hua Jhang-Li. www.pacis-net.org/file/2010/S15-04.pdf

[5] Elizabeth M. Royer and Charles E. Perkins, "An Implementation Study of the AODV Routing Protocol," in Proc. IEEE Wireless Communications and Networking Conference (WCNC 2000), Chicago, IL, September 2000.

[6] Elizabeth Belding-Royer, Ian Chakeres, David Johnson, and Charlie Perkins. DYMO – dynamic MANET on-demand routing protocol. In Rebecca Bunch, editor, Proceedings of the Sixty First Internet Engineering Task Force, Washington, DC, USA, November 2004. IETF

[7] Ian D. Chakeres and Charles E. Perkins. Dynamic MANET on demand (DYMO) routing protocol. Internet-Draft Version 06, IETF, October 2006

[8] T. Clausen, C. Dearlove, P. Jaquet, "I-D: The Optimized Link State Routing Protocol version 2 (OLSRv2)", Work in progress, http://tools.ietf.org/id/draft-ietf-manet-olsrv2

International Journal of Modern Engineering Research (IJMER)
www.ijmer.com Vol.3, Issue.2, March-April. 2013 pp-1038-1040 ISSN: 2249-6645

Autonomously-Reconfigurable Wireless Mesh Networks

Sanjay Pawar, [1] Vinod Kimbahune[2]
[12]*Smt. Kashibai Nawale college of Engineering pune/pune University, India*

Abstract: *Multi-hop wireless mesh network experience link-failure due to channel interference, dynamic obstacles etc. which causes performance degradation of the network in Wireless Mesh Networks. The paper proposes "Autonomously Reconfigurable Wireless Mesh Networks system based upon IEEE 802.11" for mr-WMN to recover autonomously in case the network failure occurs, to improve the network performance. The paper presents an autonomously network reconfiguration system (ARS) that allows a multiradio WMN to self-recover from local link failure to maintain network performance. By using channels and radio variability in WMNs, ARS generates needful changes in local radio and channel assignments in order to recover from failures. Next, based on the generated configuration changes, in which the system cooperatively reconfigures network setting among local mesh routers.*

Keywords: *IEEE 802.11, multi-radio wireless mesh networks (mr-WMNs), Autonomous-Reconfigurable Network, Wireless Link Failures.*

I. INTRODUCTION

A wireless mesh networks: (WMN) is a communications network made up of radio nodes organized in a mesh topology. Wireless mesh networks consist of mesh clients, Gateways and mesh routers. The mesh clients like laptops, cell phones and other wireless devices also mesh clients can work as router. The mesh routers send network traffic and the gateways which may connect to the Internet [1]. It supports larger applications and also it provides some benefits to users such as no cabling cost, automatic connection to all nodes, network flexibility, ease of installation and it also discovers new routes automatically.

Wireless mesh networks are not stand alone they are connected with other wireless networks through mesh routers. It provides greater range of data transfer rates in the networks. Wireless mesh networks in which protocols are used for communication at small cost. So that here is more chances of packet losses and link failures. Information transmission are generally started from the source node to their specified destination node [3].

The transmission strategies can be similar for different kinds of networks. In wireless mesh networks in which link failures occurs because of increase the application bandwidth demand, channel interference and dynamic obstacles. Even though various solution for WMNs to recover from wireless link failures have been proposed such as resource-allocation algorithm, greedy channel assignment algorithm and fault-tolerant routing protocols [2].

First is resource-allocation algorithm it allocates the resources initially, also can used only theoretical guidelines for initial network planning. The disadvantages is that they provide optimal solution they require the global configuration changes, which is not suitable for the frequently link failures occurs. Next, a greedy channel assignment algorithm can change the settings of only the faulty link(s the drawback is that we need to consider configurations of neighbor nodes in mesh along with the faulty link(s). Third, fault-tolerant routing protocols, it can be used for avoiding the faulty links in routing protocol for local rerouting, multipath routing This fault-tolerant routing protocol depends on repetition transmission, used for more amounts of network resources than the reconfiguration in link-level network [2][5].

This paper presents an autonomous network reconfiguration system (ARS) to overcome the above mentioned limitations that allows multiradio WMN (mr-WMN) autonomously reconfigure local network settings. To maintain the healthy networks using autonomous network reconfiguration system (ARS). ARS consists of reconfiguration planning algorithm that will find the configuration changes in local network for recovery, thus reducing the changes in healthy network. It means ARS initially search for local reconfiguration changes that are available faulty area.

Autonomously reconfiguration system also supervising the protocol that enables a WMN to perform real-time recovery form failures It also prevents the ripple effects. The protocol run in each mesh node and simultaneously measure wireless link conditions. For measuring the information of ARS calculate the failure of link and generates the reconfiguration plan. The rest of this is arrange as follows, Section II related work Section III describe ARS Architecture, IV Concludes the paper.

II. RELATED WORK

A considerable amount of work has been done for solving the problem in WMNs and maintains the healthy networks. And Networks reconfiguration used a planning algorithm that keeps necessary network changes (to recover from link failures) as local as possible as opposed to change in entire network settings. Scheduling algorithms and existing channel assignment provide guidelines such as throughput bounds and schedule ability for channel assignment during a network deployment stage. The paper by A. Brzezinski, G. Zussman, and E. Modiano, [2] provides brief study to develop practical algorithms to solve problems of wireless mesh networks also they have discussed various theories to solve these problems.

A survey paper by IAN F. Akyildiz, Georgia [3] gives a brief survey of wireless mesh networks. The authors of this paper give emphasis on architectural design of WMNs, layered communication in network and security.

New Autonomous System for WMN [4] the author have suggested a new Autonomous System for WMNs. He proposes this as for WMN to reduce manual configuration of network which solve failure recovery problems. He also fulfills the Quality of service (QoS) requirement of network.

As discussed above there are some problems in WMNs, a research by Kyu-Han kim and Kang G. shin [5] suggested a self- reconfigurable WMNs. The authors claim to solve the above discussed problems. We are extending our work from this paper.

2.1. ARS ARCHITECTURE

2.1.1 ARCHITECTURE.

The fig 1 Shows architecture of ARS. ARS is used for collect and sends the packets related to ARS similar to the group formation information. For this module in which it include algorithm and related protocols of ARS [4][5].

Link status information provides the information related to links in wireless mesh networks and network controller resides in device driver and interacts with failure finder in the algorithm [6].

1. Failure Finder, which is interact frequently with network monitor with device driver and maintain information about updated link state table.
2. Group organizer, designed for formation of local groups within mesh networks.
3. Planner Gateway- It is used for generating the network reconfiguration plan only for gateway nodes. The planner gateway includes plan producer, QoS filter and Benefit filter to generate plan.
4. NIC setting administrator receives new plan from group organizer and uses this new plan for further communication in the wireless mesh networks.

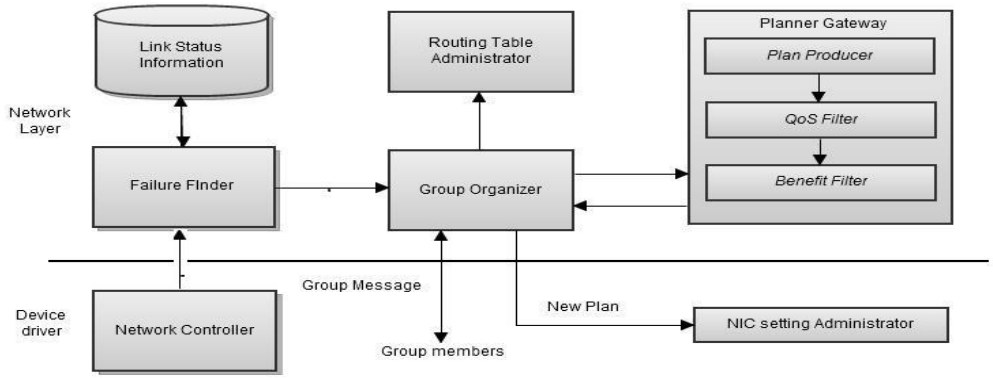

Fig 1. ARS Architecture

2.1.2. Ars Algorithm

1. Network controller time (*tc*)

1: For every link *l* do
2: calculate link quality (*lq*) using passive monitoring
3: end for
4: Send controlling result to a gateway *g*;

2. Failure Finder and group organization time (*to*)

5: if link *l* disconnect link requirement *r* then
6: request group organization on channel *c* of link *l*;
7: end if
8: start a leader election if it is receiver a request

3. Planning time (*C,tp*)

9: if node x is elected as leader then
10: send planning request message (*m,C*) to gateway
11: generate a reconfiguration plan (*p*) to *Cx*;
12: send a reconfig plan (*p*) to a leader of Cx;
13: end if

4. Reconfiguration Time (*p, tr*)

14: if p has changes of node *x* then
15: apply changes to link at *t*;
16: end if
17: relay p to neighboring members, if any

First, ARS in every mesh node checks the outgoing links quality and sends result to a gateway by sending message. Second, if it detects a link failure, ARS in the detector node trigger the group formation within local mesh routers and one group member becomes leader using election algorithm for coordinating reconfiguration. Third, leader sends a planning request message to a gateway then the gateway generate reconfiguration plan for the request. Forth, the gateway sends reconfiguration plan to leader node and the group members and Finally all nodes in group execute the new plan, if any, and resolve the group[5][7].

III. CONCLUSION

This paper presents Autonomous Reconfiguration System (ARS) that helps a WMN to reconfigure autonomously from link failure. Also ARS help in generating reconfiguration plan. ARS implements the reconfiguration plan that satisfies QoS constraint. User interface for application deployment.

REFERENCES

[1]. I. Akyildiz, X. Wang, and W. Wang, "Wireless mesh networks: Survey," Comput. Netw, vol. 47, no. 4, pp. 445–487, Mar. 2005.
[2]. A. Brzezinski, G. Zussman, and E. Modiano, "Enabling distributed throughput maximization in wireless mesh networks: A partitioning approach," in Proc. ACM MobiCom, Los Angeles, CA, Sep. 2006, pp.
[3]. F. AKYILDIZ, GEORGIA INSTITUTE OF TECHNOLOGYXUDONG WANG, KIYON, INC.A "Survey on Wireless Mesh Networks"
[4]. P. S. Khanagoudar "A New Autonomous System (AS) for Wireless Mesh Network", IJEIT Vol 2, Issue 1, july 2012.
[5]. kyu-Han kim, Member, IEEE and Kang G. Shin " Self-Reconfigurable Wireless Mesh Network", IEEE ACM TRANSACTION ON NETWORKING, VOL 19.NO.2, April 2011.
[6]. Jensilin Mary A, "Autonomously Reconfiguring Failure in Wireless Mesh Network", Journal of Computer Application ISSN, Vol-5, EICA 2012 Feb 10
[7]. R. Draves, J. Padhye, and B. Zill, "Routing in multi-radio, multi-hop wireless mesh networks," in Proc. ACM MobiCom, Philadelphia, PA, Sep. 2004, pp. 114–128.
[8]. A. Raniwala and T. Chiueh, "Architecture and algorithms for an IEEE 802.11-based multi- channel wireless mesh network," in Proc. IEEE IN-FOCOM, Miami, FL, Mar. 2005, vol. 3
[9]. Xiao Shu, Xining Li, "Link Failure Rate and Speed of Nodes in Wireless Network", Computingand Info. SCi. University Canada, 2008 IEEE.
[10]. L.Qiu, P.Bahl,A. Rao, and L. Zhou, "Troubleshooting multi-hop wire- less networks," in Proc. ACM SIGMETRICS, Jun. 2005, pp. 380–381.
[11]. P. Kyasanur and N. Vaidya, "Capacity of multi-channel wireless net-works: Impact of number of channels and interfaces," in Proc. ACM Mobi Com, Cologne, Germany, Aug. 2005, pp. 43–57.

International Journal of Modern Engineering Research (IJMER)
www.ijmer.com Vol.3, Issue.2, March-April. 2013 pp-1041-1055 ISSN: 2249-6645

Reduction of Noise Effect in Land-Buried Target Shape Recognition through Polari Metric GPR Images

Khalid M. Ibrahim, [1]Khalid F. A. Hussein, [2]Abd-El-Hadi A. Ammar[3]
[1]*Assoc. ResearchersMicrowave Engineering Dept., Electronics Research Inst., Cairo, Egypt*
[2]*Assoc.Prof. Microwave Engineering Dept., Electronics Research Inst., Cairo, Egypt*
[3]*Prof. Electronics and Electrical Communications Dept., Faculty of engineering, El-AZHAR University, Cairo, Egypt*

Abstract:*A new treatment of the buried object shape retrieval and target recognition from noisy polarimetric GPR images is introduced. The construction of GPR system proposed for obtaining high resolution polarimetrictwo-dimensional cross-range images of objects buried under the surface of a ground soil is described. A granular noise filter (GNF) is introduced to get an image with increased signal-to-noise ratio (SNR). An algorithm to extract a two-dimensional shape of the buried object is introduced. A shape smoothing filter (SSF) is then applied for further elimination of the errors resulting due to granular noise effect on the two-dimensional shape retrieval process. A shape recognition algorithm is applied to compare the retrieved shape for the buried object to a reference target shape to take a match or mismatch decision. The proposed GPR antenna system and the suggested algorithms for noise reduction, shape extraction and target recognition are examined through FDTD simulation. The numerically obtained results show that proposed noise reduction technique with the proposed GPR system and the suggested algorithms for shape extraction and target shape recognition are efficient and successful in all the examined cases.*

I. INTRODUCTION

The imaging of the ground subsurface is becoming more important for land mine detection and archaeological investigations. It is important to obtain an image of the subsurface to find out the position of buried objects and the composition of the subsurface. This information is preferably obtained without disrupting the subsurface, and the technique dedicated to this task is called a non-destructive technique, to which category the imaging GPR belongs. Many GPR imaging systems have been proposed in the literature [1–9]. Although good depth resolution can usually be realized in GPR images using frequency diversity, good resolution in the cross-range dimensions is much harder to achieve [10].The present work introduces a new polarimetric GPR imaging system to obtain two-dimensional image for the buried objects causing in homogeneity in the ground soil. This imaging GPR system was partially described in [11].

The noise added at the receiver of a GPR system results in distortion of the GPR image that may disturb the process of image construction and hence may lead to an erroneous decision during the process of buried target recognition and, thereby, leading to false alarms or missed target detections. To make the GPR data more reliable for retrieving the correct information for the ground subsurface, a number of filtering techniques have been proposed to enhance the SNR of the data [1].

The present work introduces a new technique to reduce the effect of white Gaussian noise in a polarimetric GPR system that uses four polarization channels to obtain four high resolutiontwo-dimensional images in the cross-range for the objects buried in the ground soil. Two of the obtained images represent the complex scattering parameters from co-polarization channels (*xx* and *yy*) whereas the other images represent the complex scattering parameters from cross-polarization channels (*xy* and *yx*). A Granular Noise Filter (GNF) and a Smoothed Shape Filter (SSF) are applied to enhance the SNR of the GPR image and hence leading to a more reliable target recognition process.

The paper introduces mathematical and numerical algorithms for extracting the buried object shape and recognizing the shape of a reference target and to show the effect of the SNR on the target shape recognition process. Numerical results are presented to demonstrate the efficiency of the proposed noise reduction techniques and the imaging GPR system together with the developed mathematical and numerical techniques.

II. CONSTRUCTION AND PRINCIPLE OF OPERATION OF THE IMAGING GPR SYSTEM

The antenna system of the GPR is constructed as a clustered two-dimensional planar array of coplanar crossed-dipole antennas. This array can be viewed as two-dimensional array of $K \times K$ rectangular clusters; each cluster can be considered as a sub-array of $M \times N$ crossed-dipole elements. A cluster composed of 7×7 elements is shown in Figure 1a. The element of a cluster, or sub-array, is composed of an *x*-oriented dipole crossed with another *y*-oriented dipole. All the elements of a cluster act as receiving antennas except for the central one which is housed in a conducting reflector and acts as a transmitter for illuminating the rectangular area just below the corresponding cluster of the antenna array. As shown in Figure1b, the conducting housing over the transmitting crossed-dipole is a partial cover made to prevent direct coupling between the transmitting antenna and all the receiving antennas.

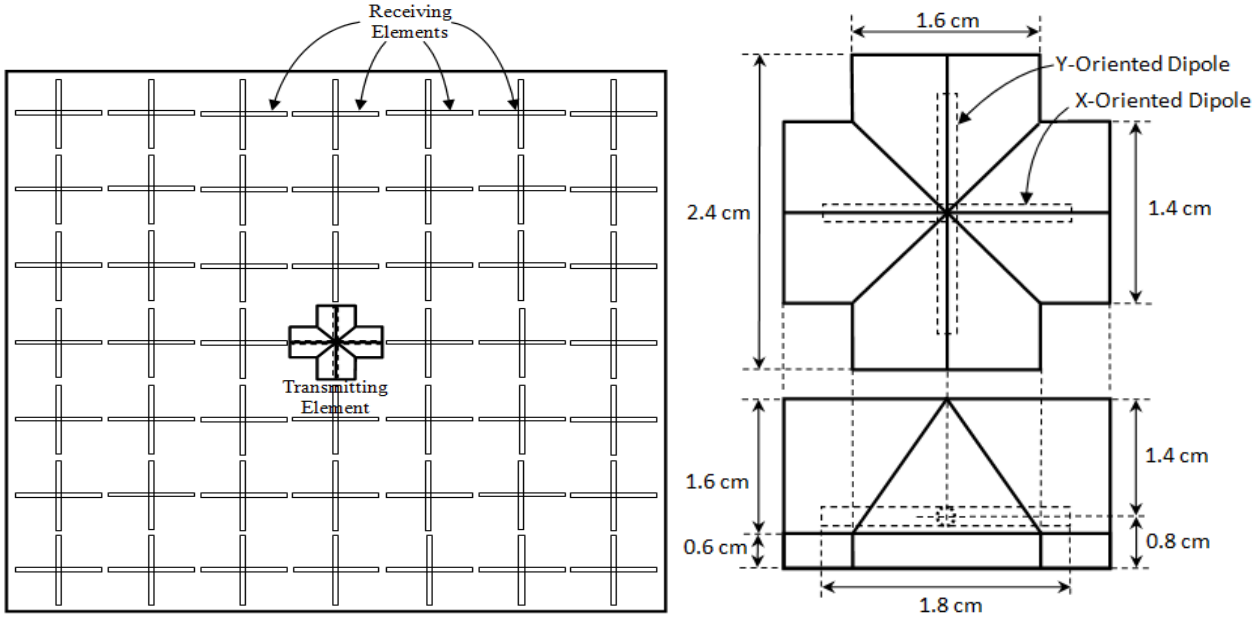

(a) GPR antenna system (b) Transmitting antenna

Figure 1: GPR antenna system composed of 7×7 antenna elements; the central element is a transmitting crossed-dipole partially enclosed inside a metallic reflector and the remaining elements are receiving crossed dipole antennas.

Let the GPR antenna system consist of a reflector housed horizontal (parallel to the ground surface) dipole antenna for illuminating the soil. Let an array of similar receiving dipole antenna elements be arranged in rows and columns so as to get two dimensional images for inhomogeneous bodies underlying the ground surface. The transmitting dipole antenna is housed in metallic reflector to prevent direct coupling between the transmitting antenna and all receiving antennas. When the sensor is placed over empty ground, the coupling between the transmitting antenna '1' and a receiving antenna '2', $|S_{21}|$, is very small. As the sensor is placed over a soil with an object buried near enough to the ground surface, the inhomogeneity occurring due to the difference between the electromagnetic properties of the soil and that of the buried object leads to scatter a portion of the signal radiated by the transmitting antenna to the receiving antenna and, thereby, increasing the coupling between the transmitting and receiving antennas. Thus, the increase in the electromagnetic coupling can be used to indicate the presence of an in homogeneity just below the receiving dipole. If an enough number of closely spaced receiving elements which are regularly arranged in the plane just above the ground surface, a two dimensional image can be constructed from the scattering parameter data between transmitting and receiving antenna elements. This can be explained in view of the FDTD simulation results presented in Figure2. The electric field distribution in an empty soil due to the radiation from the *x*-oriented transmitting dipole is presented in Figure2a. The electric field at the ground surface is very weak and hence the signal arriving at an *x*-oriented receiving antenna element is almost zero. When a metallic block is buried in the soil near the ground surface, the electric field launched into the soil by the transmitting dipole is guided between the upper face of the metallic block and the ground surface, as shown in Figure2b and, thereby, arriving at the receiving dipoles. Thus the existence of the metallic block leads to increase the coupling between the transmitting dipole and those receiving dipoles lying just above the buried block. Similarly, the coupling between a *y*-oriented transmitting dipole and *y*-oriented receiving dipoles is considerably increased due the existence of a buried metallic block. This can be shown by comparing between Figures 2c and 2d.

For the soil types that result in changing the polarization of the propagating wave due the rotation of the electric field vector about the direction of propagation, the data obtained from the four polarimetric channels are required to get the complete GPR image. For the other types of the soils the data obtained from the co-polarization channels (*xx* and *yy*) are enough to get the complete two-dimensional image for the ground subsurface.

The complete GPR operation including polarimetric imaging, granular noise filter, buried object shape retrieval, and target shape recognition is described by the block diagram presented in Figure 3. The detailed explanations of the processes involved in this block diagram are provided by the following sections.

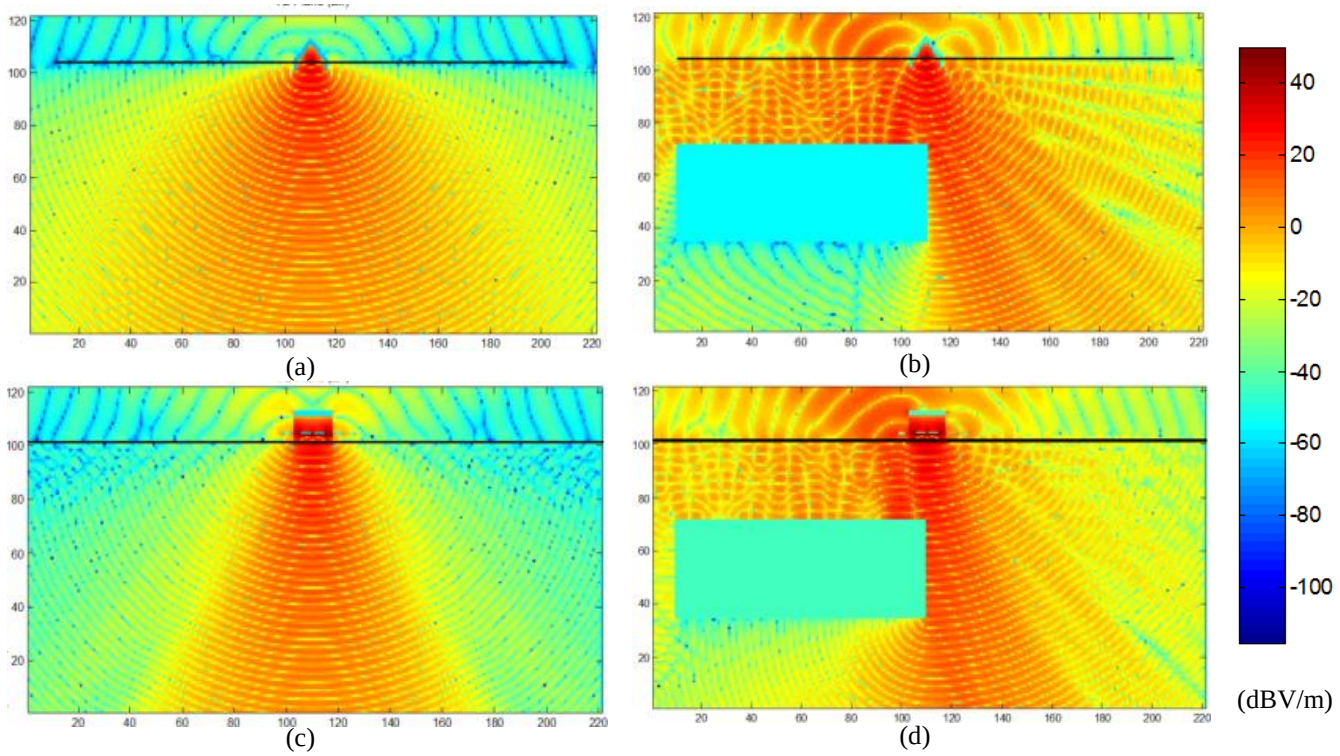

Figure2: Distribution of the electric field in the longitudinal section (*yz*-plane) of the soil when:(a) the soil is empty and the transmitting *x*-oriented dipole is activated, (b) a rectangular box-shaped block is buried at a depth of 10 cm below the ground surface and the transmitting *x*-directed dipole is activated, (c) the soil is empty and the transmitting *y*-oriented dipole is activated, and (d) a rectangular box-shaped block is buried at a depth of 10 cm below the ground surface and the transmitting *y*-directed dipole is activated

III. TWO-DIMENSIONAL IMAGE CONSTRUCTION

AGPR image for the inhomogeneous bodies buried below the ground surface is constructed through four polarimetric channels. For explaining the imaging method, we can take the *xy*-channel as an example. The scattering parameters from the *xy*-channel are obtained by activating only the *y*-oriented transmitting dipole elements at the center of each cluster without activating the *x*-oriented transmitting elements. Under this situation, the received signals at the *x*-oriented dipole elements of a specific sub-array are divided by the signal applied to the central *y*-oriented transmitting dipole for each cluster of the GPR array to obtain the corresponding scattering parameters. Thus, the resulting *xy*-channel images are actually the complex scattering parameters representing the electromagnetic coupling between each of the *x*-oriented receiving dipoles and the *y*-oriented transmitting dipole at the center of the same cluster of the receiving dipoles. By gathering the data obtained from each cluster of the GPR array, the complete *xy*-channel image is obtained.

The four-channel two-dimensional complex polarimetric images for the buried object can be constructed by the following four matrices obtained from each cluster of the antenna array:

$$S_{k,l}^{xx} = \left[S_{k,l,m,n}^{xx}\right], k = 1,2,..,K; l = 1,2,..,K; m = 1,2,..,M;\ n = 1,2,..,N \quad (1)$$

$$S_{k,l}^{xy} = \left[S_{k,l,m,n}^{xy}\right], k = 1,2,..,K; l = 1,2,..,K; m = 1,2,..,M;\ n = 1,2,..,N \quad (2)$$

$$S_{k,l}^{yx} = \left[S_{k,l,m,n}^{yx}\right], k = 1,2,..,K; l = 1,2,..,K; m = 1,2,..,M; n = 1,2,..,N \quad (3)$$

$$S_{k,l}^{yy} = \left[S_{k,l,m,n}^{yy}\right], k = 1,2,..,K; l = 1,2,..,K; m = 1,2,..,M;\ n = 1,2,..,N \quad (4)$$

Where$K$is the number of clusters, constituting the GPR antenna array; M and N are the numbers of rows and columns, respectively, of the receiving antenna elements in each cluster.

For each of the four polarimetric channels, the complete image is constructed from the $K \times K$ clusters; for example to the complete *xx*-channel image is constructed as follows

$$S^{xx} = \begin{bmatrix} \left[S_{1,1,m,n}^{xx}\right]\left[S_{1,2,m,n}^{xx}\right] & \cdots & \left[S_{1,K,m,n}^{xx}\right] \\ \left[S_{2,1,m,n}^{xx}\right]\left[S_{2,2,m,n}^{xx}\right] & & \left[S_{2,K,m,n}^{xx}\right] \\ \vdots & \ddots & \vdots \\ \left[S_{K,1,m,n}^{xx}\right]\left[S_{K,2,m,n}^{xx}\right] & \cdots & \left[S_{K,K,m,n}^{xx}\right] \end{bmatrix}, m = 1,2,..,M;\ n = 1,2,..,N \quad (5)$$

The other three images for the other three polarization channels are similarly constructed. In this way, eight real visualized images can be constructed from the polarimetric GPR data using a proper numerically scaled color maps for displaying the following eight sets of two-dimensional data:$\mathrm{Re}(S^{xx}), \mathrm{Im}(S^{xx}), \mathrm{Re}(S^{xy}), \mathrm{Im}(S^{xy}), \mathrm{Re}(S^{yy}), \mathrm{Im}(S^{yy}), \mathrm{Re}(S^{yx}), \mathrm{Im}(S^{yx})$.

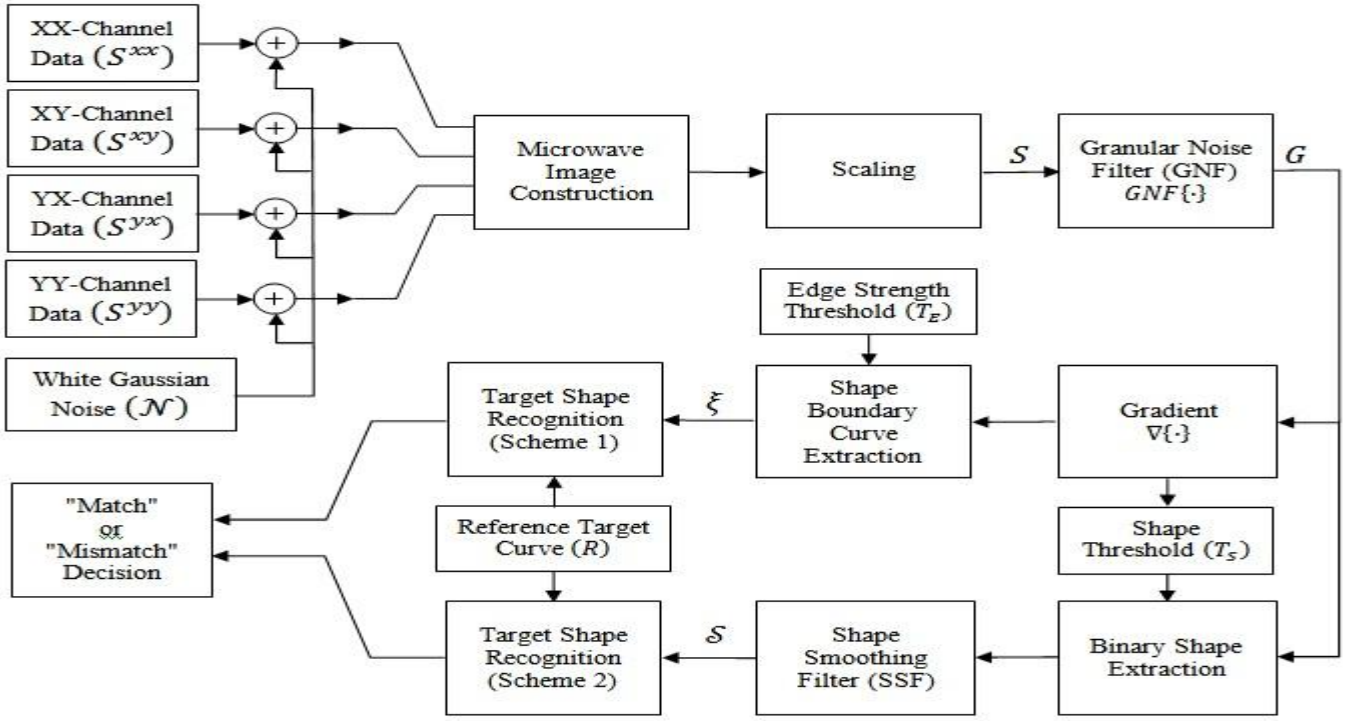

Figure 3: Block diagram showing GPR imaging and target shape recognition scheme

IV. EXTRACTION OF BURIED OBJECT SHAPE (BOS)

The value assigned to a given pixel(x, y) of the GPR image is compared to a predefined global threshold value T_S (the determination of which depends on the comparison with the images obtained for the same soil when there no target is present). If the value of a specific pixel exceeds the threshold value,T_S, it is considered that the pixel belongs to a buried object; otherwise it will be considered that the pixel belongs to the soil. In spite of being based on the above idea, it will be shown, in the following description, that the detection algorithm is cluster-based rather than pixel-based.

4.1. Application of Smoothing Shape Filter (SSF)

For avoiding false-alarm or erroneous target-missing while detecting a target of an arbitrary shape, the following cluster-based shape retrieving procedure is applied. Let a square window of size $W_S \times W_S$pixels be made in the GPR image and be centered at the pixel(x, y). Let the number of pixels belonging to this window and satisfying the condition $L > T_S$ be $n_b(x, y)$ and that the number of pixels satisfying the condition $L \leq T_S$be $n_s(x, y)$.

To scan the GPR image, the square window will slide over this image starting so that the upper-left corner of the window coincides with the upper-left pixel of the image and then moving towards right (i.e. on the image rows) pixel by pixel. When the upper-right corner of the sliding window reaches the right most pixel on the present row of the GPR image the window jumps to a new location so that its upper-left corner coincides with the left most pixel on the next row of the GPR image and then moving towards right again. This will be repeated until the GPR image is completely scanned and the decision is taken for all the image pixels. Following the above sliding window algorithm, a new image described by $n_b(x, y)$ is constructed; where x and y are the pixel coordinates in the new image (corresponding to the same coordinates in the original GPR image).

To get a two-dimensional drawing for the shape of the detected buried object, the following procedure is applied. For a window centered at the pixel(x, y): if $n_b(x, y) > n_s(x, y)$ a decision that the central pixel$(x, y)$of this widow belongs to a buried object should be taken; otherwise the decision will be that this pixel belongs to the soil. To construct a binary image showing the shape of the detected buried object one defines:

$$\mathcal{S}(x, y) = \begin{cases} 1, & n_b(x, y) > n_s(x, y) \\ 0, & n_b(x, y) \leq n_s(x, y) \end{cases} \tag{6}$$

An edge detection algorithm is then applied to the shape image, $\mathcal{S}(x, y)$, to get the shape boundary curve$\xi(x, y)$. This is described in detail in the next section.

V. EXTRACTION OF SHAPE BOUNDARY CURVE(SBC)

The Gradient Method is applied to the image$G(x,y)$ at the output of the GNF. A simplified one-dimensional method for edge detection is presented in Figure 4. The gradient of $G(x,y)$is a vector that can be calculated as follows:

$$\nabla G(x,y) = \begin{Bmatrix} Q_x \\ Q_y \end{Bmatrix} \tag{7}$$

Where,

$$Q_x = \frac{\partial G}{\partial x}, Q_y = \frac{\partial G}{\partial y} \tag{8}$$

The strength of the edge can be determined by the magnitude of the gradient

$$|\nabla G| = \sqrt{Q_x^2 + Q_y^2} \tag{9}$$

The direction of the gradient can be determined by the angle of the gradient

$$\angle \nabla G = \tan^{-1}\left(\frac{Q_y}{Q_x}\right) \tag{10}$$

The gradient can be approximated by finite differences as

$$Q_x = \frac{\partial G}{\partial x} = \frac{G(x+\Delta x, y) - G(x,y)}{\Delta x} \tag{11}$$

$$Q_y = \frac{\partial G}{\partial y} = \frac{G(x, y+\Delta y) - G(x,y)}{\Delta y} \tag{12}$$

Using pixel coordinate notaiton and setting $\Delta x = 1$ and $\Delta y = 1$ (*i.e.* one pixel)

$$Q_m \equiv Q_x = G(m+1, n) - G(m,n) \tag{13}$$

$$Q_n \equiv Q_y = G(m, n+1) - G(m,n) \tag{14}$$

The strength of the edge is expressed as

$$|\nabla G|_{m,n} = \sqrt{Q_m^2 + Q_n^2} \tag{15}$$

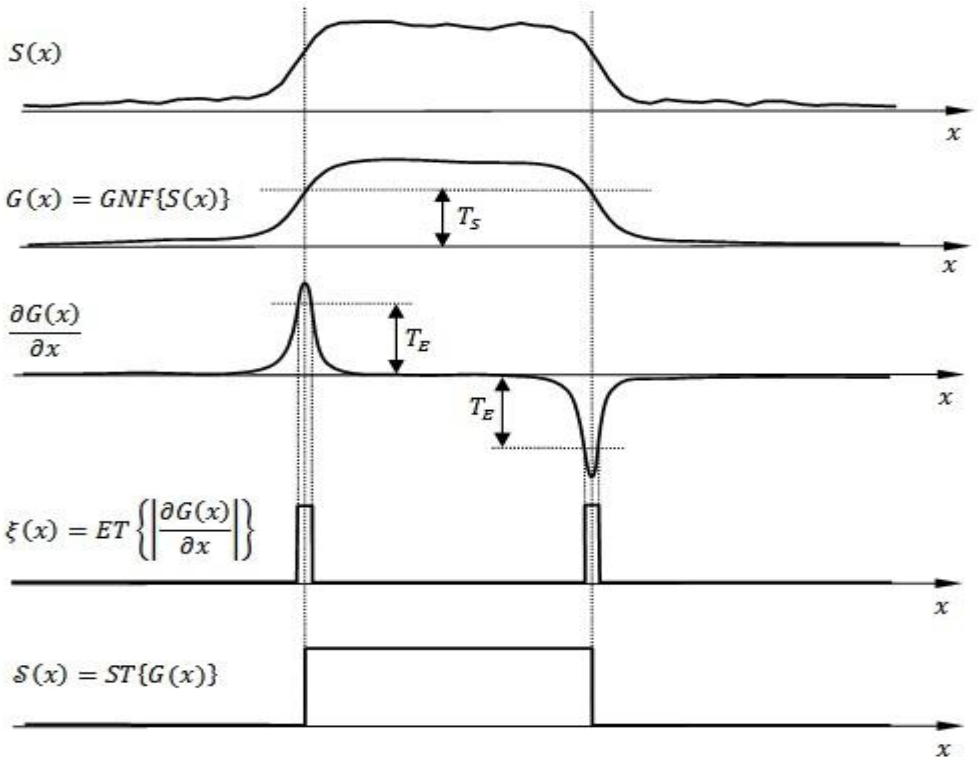

Figure 4: Simplified one-dimensional explanation of the edge detection technique used for extracting of the boundary curve of the buried object shape.

An edge strength threshold T_E is set to decide whether or not a pixel(m,n) belongs to an edge. If $|\nabla G|_{m,n} \geq T_E$ then the pixel(m,n) belongs to an edge otherwise it does not belong to any edge.

VI. TARGET SHAPE RECOGNITION

Given the retrieved SBC,$\xi(x,y)$, and the reference target boundary$R(x,y)$, a least-squared error method is applied to take the match or mismatch decision with a specific reference target shape. This method is described in thefollowing. Let $\xi(x,y)$ be designated as shape curve ξ and $R(x,y)$ be designated as the reference shape curve R. The shape curve ξ is translated so as to get its centroid coincident with the centroid of the reference shape curve R. The match or mismatch decision is taken based of the relative error defined as the ratio between the dashed area shown in Figure 5and the area enclosed by the boundary of the original target shape curve R.

$$\hat{e} = \frac{e}{A} \tag{16}$$

Where$e$ is the area subtended between the reference and retrieved curves (shown as dashed area in Fig. 5) and A is the area of enclosed by the reference curve.

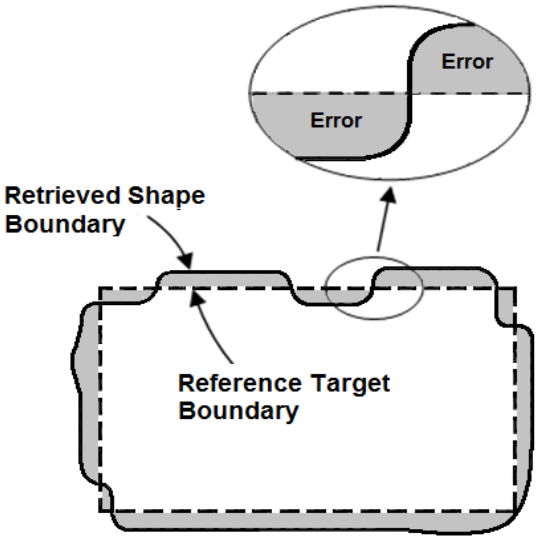

Figure5: Target shape recognition is achieved by comparing the retrieved shape to the original shape by subtracting the curvesξ and R for each corresponding pixel and summing the squared errors.

The polar coordinate system is used to allocate the corresponding points on both curves. The shape recognition process is applied by comparing the corresponding points on both curves. Referring to Figure 6, the differential area subtended between the differential element of the curve representing the retrieved shape and that of the curve representing the original target shape can be expressed as

$$\delta = \Delta_S \, d\varphi \tag{17}$$

Where,

$$\Delta_S = \frac{1}{2}[(r^S)^2 - (r^R)^2] \tag{18}$$

The absolute mismatch error can be expressed as

$$e = \int_0^{2\pi} |\Delta_S| d\varphi = \frac{1}{2}\int_0^{2\pi} |(r^S)^2 - (r^R)^2| d\varphi \tag{19}$$

The area of the original shape can be expressed as

$$A = \frac{1}{2}\int_0^{2\pi} (r^R)^2 \, d\varphi \tag{20}$$

By the aid of Figure 6, this squared error can be calculated numerical as follows.

$$e = \frac{\pi}{N}\sum_{n=1}^{N}[(r_n^S)^2 - (r_n^R)^2]^2 \tag{21}$$

Where$N$ is the number of angular segments to which the complete angle, 2π is divided as shown in Figure 7. The area enclosed by the reference (target) curve can be obtained as

$$A = \frac{\pi}{N}\sum_{n=1}^{N}(r_n^R)^2 \tag{22}$$

The relative error or shape mismatch can be expressed as

$$\hat{e} = \frac{e}{A} = \frac{\sum_{n=1}^{N}[(r_n^S)^2 - (r_n^R)^2]^2}{\sum_{n=1}^{N}(r_n^R)^2} \tag{23}$$

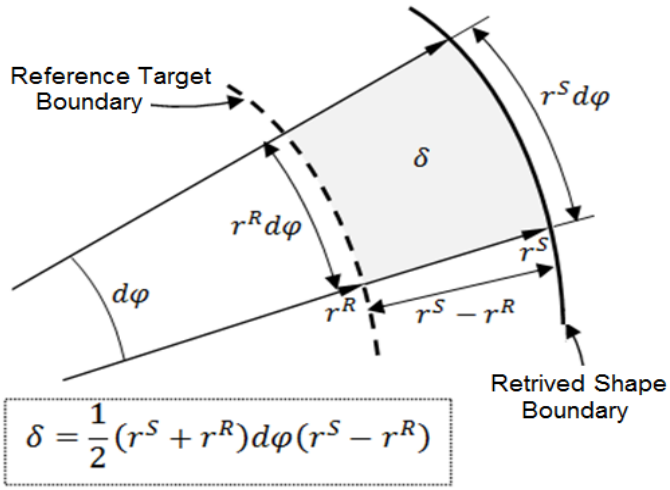

Figure6: Differential area subtended between the differential elements of the original and retrieved shape curves

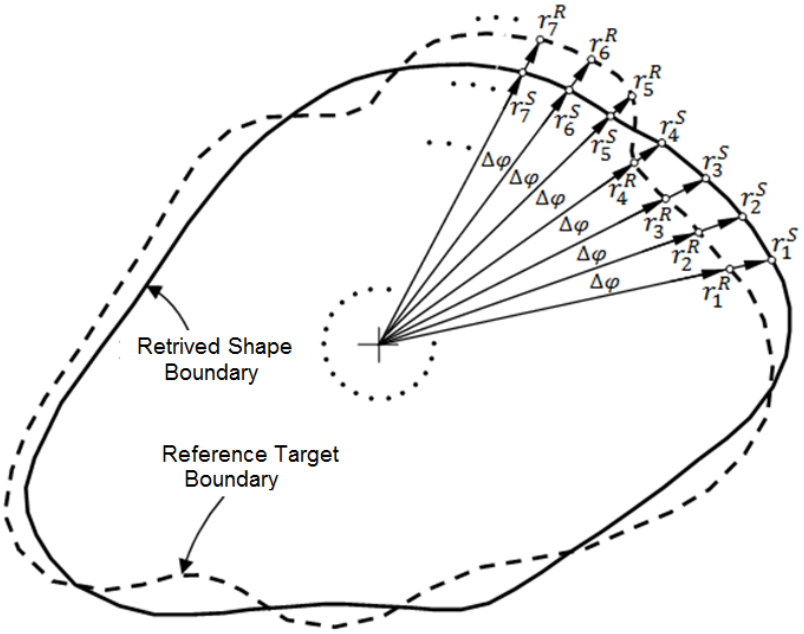

Figure 7: Target shape recognition is achieved by comparing the retrieved shape to the original shape by subtracting the curves S and R for each corresponding pixel and summing the squared errors.

VII. Noise Effect On The Shape Recognition Process

Considering a two-dimensional GPR image constructed according to the method described above, the value of the pixel$(m,n)$is determined by the coupling coefficient$S(m,n)$between the transmitting antenna and the receiving antenna on the m^{th} row and n^{th} column of the GPR antenna array.

$$S(m,n) = \frac{V_r(m,n)}{V_t} \tag{24}$$

Where$V_r(m,n)$is the complex voltage received by the antenna on the m^{th} row and n^{th} column of the GPR antenna array and$V_t$is the amplitude of transmitted sinusoidal voltage signal. Additive Gaussian noise causes the coupling coefficient to be modified as follows.

$$\acute{S}(m,n) = \frac{V_r(m,n) + \mathcal{N}(m,n)}{V_t} \tag{25}$$

Where$\mathcal{N}(m,n)$ is the value of the signal representing the noise picked by the same antenna. This noise is additive white Gaussian and causes a granular effect when viewing the GPR image as its value is randomly evaluated for each pixel.

$$\acute{S}(m,n) = S(m,n) + \frac{\mathcal{N}(m,n)}{V_t} \tag{26}$$

Equation (26) can be rewritten as

$$\acute{S}(m,n) = S(m,n) + \widehat{\mathcal{N}}(m,n) \tag{27}$$

Where$\widehat{\mathcal{N}}(m,n)$ is the value of the noise at the pixel(m,n)normalized to the amplitude of the transmitted voltage signal?

Equation (26) can be rewritten as

$$\acute{S}(m,n) = S(m,n)\left[1 + \left(\frac{V_r(m,n)}{\mathcal{N}(m,n)}\right)^{-1}\right] \tag{28}$$

The SNR at each pixel is defined as the ratio between the received signal power and the noise power at this pixel.

$$SNR(m,n) = \left|\frac{V_r(m,n)}{\mathcal{N}(m,n)}\right|^2 \tag{29}$$

Thus, the magnitude of the quantity $\left(\frac{V_r(m,n)}{\mathcal{N}(m,n)}\right)^{-1}$ appearing in (28) is inversely proportional to the square root of $SNR(m,n)$. It is clear from (28) that the lower the SNR, the more the deviation of $\acute{S}(m,n)$from$S(m,n)$, which means more distortion of the resulting GPR image.

VIII. GRANULAR NOISE FILTER (GNF)

For removing the granular noise effect appearing in the GPR image as described in section 7, the following filtering process to remove or reduce the noise "granules" from the GPR image is applied. Let a square window of size $W \times W$ pixels be made in the GPR image $\acute{S}(x,y)$and be centered at the pixel(x,y).

To scan the GPR image, the square window will slide over this image starting so that the upper-left corner of the window coincides with the upper-left pixel of the image and then moving towards right (i.e. on the image rows) pixel by pixel. When the upper-right corner of the sliding window reaches the right most pixel on the present row of the GPR image the window jumps to a new location so that its upper-left corner coincides with the left most pixel on the next row of the GPR image and then moving towards right again. This will be repeated until the GPR image is completely scanned pixel by pixel. At each position of the sliding window, the central pixel of the window is reassigned a new value calculated according to a weighted average as follows

$$p(x,y) = \frac{\sum_{i=1}^{W}\sum_{j=1}^{W} a_{i,j}\, p_0\left(x - \frac{W-1}{2} + i - 1, y - \frac{W-1}{2} + j - 1\right)}{\sum_{i=1}^{W}\sum_{j=1}^{W} a_{i,j}} \tag{30}$$

Where$p_0(x,y)$ is the original value of the pixel at the center of the sliding window and $p(x,y)$ is the newly calculated one; $a_{i,j}$ is the weights of the surrounding pixel values in the averaging process.

Following the above sliding window algorithm, a new image described by $G(x,y)$ is constructed; where x and y are the pixel coordinates in the new image corresponding to the same coordinates in the original GPR image, $\acute{S}(x,y)$.

IX. Results andDiscussion

In the following presentation and discussions, the two-dimensional complex polarimetric images are constructed from FDTD simulation where the operating frequency is 8 GHz. The cell size is 2×2×2 mm^3.Seven-cell PML is used to satisfy absorbing boundary condition. A GPR antenna array with one cluster and 54×54 crossed-dipole antenna elements is used. The dimensions of the antenna array are42.4cm×42.4cm and the length of the single dipole element is 6mm.The soil model represents red clay soil with 9.6% water content; which has the following electrical properties:$\varepsilon_r = 8.1, \mu_r = 1.0$, and $\sigma = 0.038$ S/m.

It should be noted that the soil type considered in the following investigations is polarization conservative and hence, the GPR data obtained from the co-polarization channels (*xx* and *yy*) are used for image construction, buried object shape extraction and target shape recognition.

9.1. Target Recognition under the Condition of High SNR

The GPR images areobtained for a metallic block of dimensions 14×14×7.2 cm buried at a depth of about 10 cm

below the ground surface using the polarimetric data given by equations (1)–(4). For visualizing the two-dimensional GPR data, the absolute value of the scattering parameters are shown in Figure8a for the *xx*-channel and Figure 8b for the *yy*-channel. Due to the high level of the SNR (30 dB), the granular effect is not clear in both figures. The image shown in Figure 8c is constructed from the *xx*-channel and *yy*-channel databy averaging the values corresponding to the each pixel in the two co-polarization channels. The image shown in Figure 8d is obtained by applying the GNF to the image shown in Figure 8c.

The procedure described in section 4 for BOS extraction is applied without using the SSF and the binary image described by equation (6) is then obtained and presented in Figure 8e. The SSF described in section 4is then applied to get the smoothed shape of the buried object shown in Figure 8f.

The procedure described in section 5 is applied to extract the SBC, which is presented in Figure 8g. For target shape recognition, the reference target shape and the retrieved SBC are compared with their centroids coincident with each other. The relative mismatch error between the two boundary-curves is then calculated using the expression given by (23). In this case the percentage mismatch error is 4.5%. Such small value of the relative mismatch error (less than 10%) means that the target is recognized.

9.2. Target Recognition under the Condition of Low SNR

The GPR images areobtained for the same block buried at the same depth. For visualizing the two-dimensional GPR data, the absolute value of the scattering parameters are shown in Figure 9a for the *xx*-channel and Figure 9b for the *yy*-channel. Due to the low level of the SNR (5 dB), the granular effect is clear in both figures. The image shown in Figure 9c is constructed from the *xx*-channel and *yy*-channel data by averaging the values corresponding to the each pixel in the two co-polarization channels. The image shown in Figure 9d is obtained by applying the GNF to the image shown in Figure 9c. It is clear, by comparing Figures 9c and 9d, that the granular noise is considerably reduced due to the application of the GNF.

The procedure described for BOS extraction is then applied without the SSF and the binary image is then obtained and presented in Figure 9e. The SSF is then applied to get the smoothed shape of the buried object shown in Figure 9f.

The procedure described in section 5 is applied to extract the SBC presented in Figure9g. For target shape recognition, the reference target shape and the retrieved SBC are compared with their centroids coincident with each other. The relative mismatch error between the two boundary-curves calculated in this case is 9.5%. The error is increased in comparison with the last case due to the increased noise level. However, the value of the relative mismatch error is still less than 10%, which means that the target is recognized. This reflects the efficiency of the applied technique which leads to successful recovery of the buried object shape even in the case of low SNR.

9.3. Effect of the SNR on the Buried Target Shape Recognition Process

The GPR images and the retrieved SBC obtained for a metallic block of dimensions 14×14×7.2 cm buried at a depth of about 10 cm below the ground surface are shown in Figure 10 for different values of the SNR ranging from 30 dB to 0 dB.The relative mismatch error resulting from the comparison between the reference target shape and the retrieved SBC for each value of the SNR is shown on the right-most column of Figure 10.It is clear that, with reducing the SNR, the relative mismatch error increases leading to erroneous missed-target decision for SNR≤3 dB for this target.

The GPR imagesand the retrieved SBC obtained for a metallic cylinder of 7 cm radius and 7.2 cm height buried at a depth of about 10 cm below the ground surface are shown in Figure 11 for different values of the SNR ranging from 30 dB to 0 dB. The relative mismatch error resulting from the comparison between the reference target shape and the retrieved SBC for each value of the SNR is shown on the right-most column of Figure 11. It is clear that, with reducing the SNR, the relative mismatch error increases leading to erroneous missed-target decision for SNR≤4 dB for this target.

9.4. Reduction of the Noise Effect due to the Application of the GNF

The application of the GNF on the GPR image constructed from the four polarimetricchannels data has the effect of considerable reduction of the relative mismatch error especially at the low values of SNR.

For a metallic block of dimensions 14×14×7.2 cm buried at a depth of about 10 cm below the ground surfacea plot for the relative mismatch error against the SNR is shown in Figure 12. It is shown that the application of the GNF results in the possibility of correct decision for target shape recognition even at SNR of 3 dB.

For a metallic cylinder of 7 cm radius and 7.2 cm height buried at a depth of about 10 cm below the ground surface a plot for the relative mismatch error against the SNR is shown in Figure 13. It is shown that the application of the GNF results in the possibility of correct decision for target shape recognition even at SNR of 4 dB.

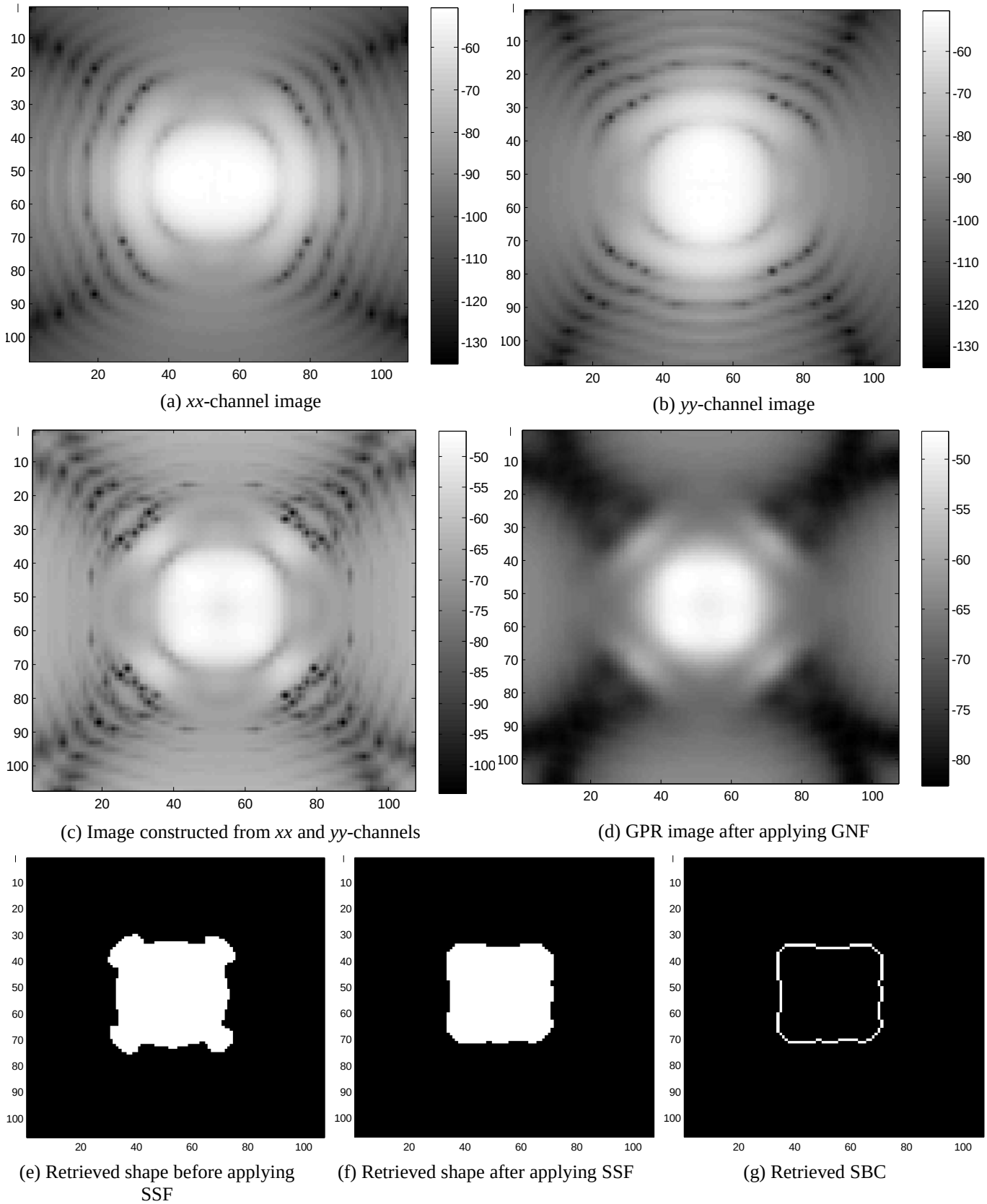

(a) *xx*-channel image

(b) *yy*-channel image

(c) Image constructed from *xx* and *yy*-channels

(d) GPR image after applying GNF

(e) Retrieved shape before applying SSF

(f) Retrieved shape after applying SSF

(g) Retrieved SBC

Figure 8:The process of retrieving boundary curve for the buried object under high SNR for a metallic box of dimensions 14×14×7.2 cm buried at a depth of about 10 cm below the ground surface using the proposed GPR system(SNR=30dB) (Mismatch error = 4.5%)

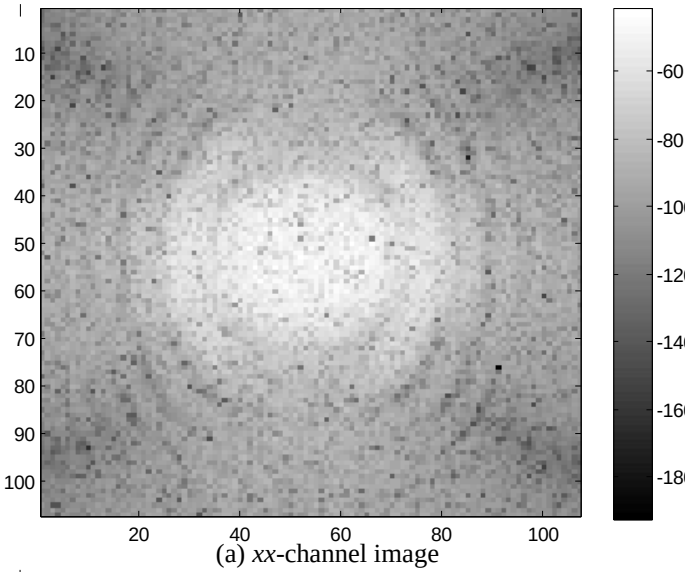

(a) *xx*-channel image

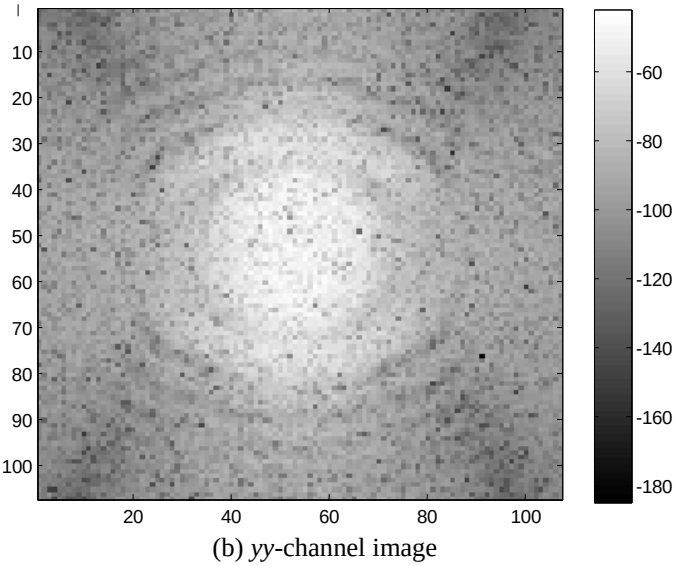

(b) *yy*-channel image

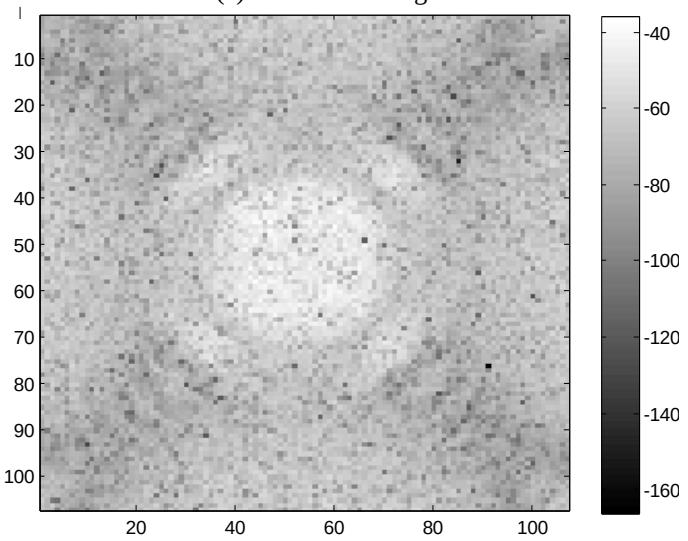

(c) Image Constructed from *xx* and *yy*-channels

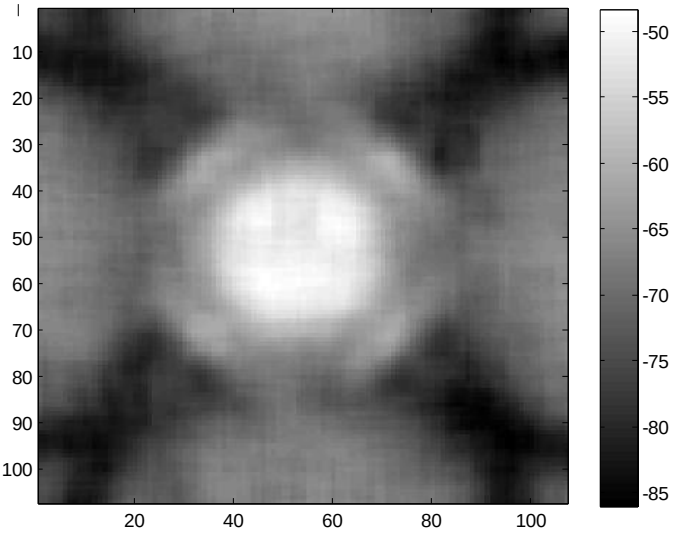

(d) GPR image after applying GNF

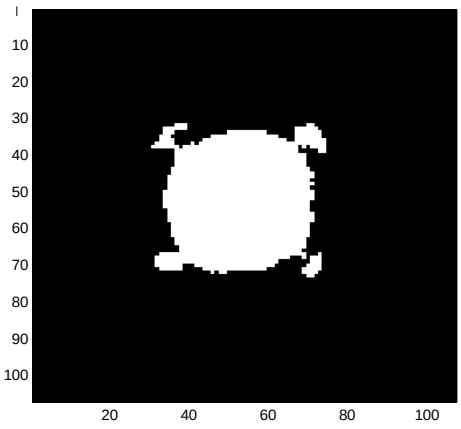

(e) Retrieved shape before applying SSF

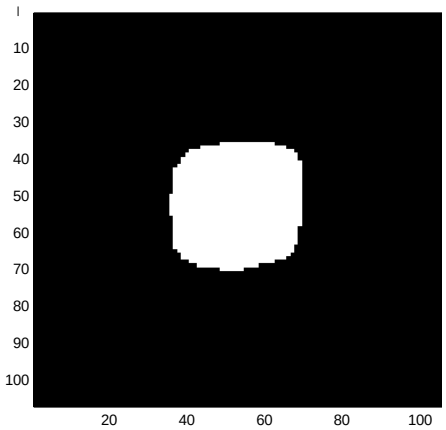

(f) Retrieved shape after applying SSF

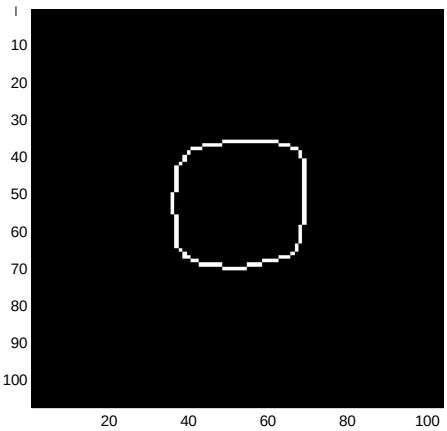

(g) Retrieved SBC

Figure 9: The process of retrieving boundary curve for the buried object under low SNR for a metallic box of dimensions 14×14×7.2 cm buried at a depth of about 10 cm below the ground surface using the proposed GPR system (SNR=5dB) (Mismatch error = 9.5%)

SNR (dB)	GPR Image	GNF Image	Extracted SBC	%Error
30	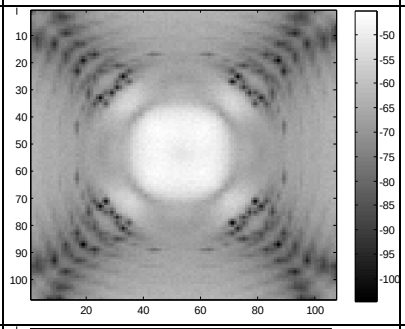	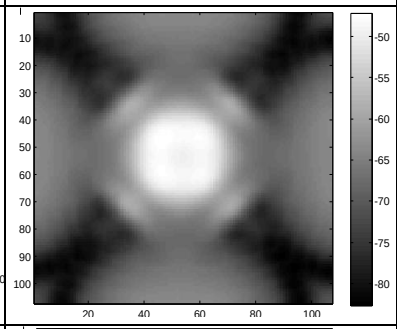	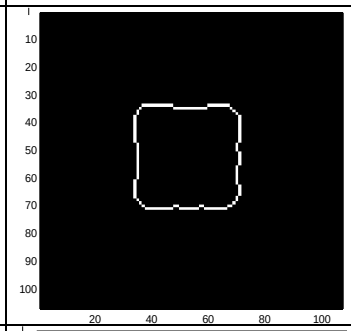	7%
15	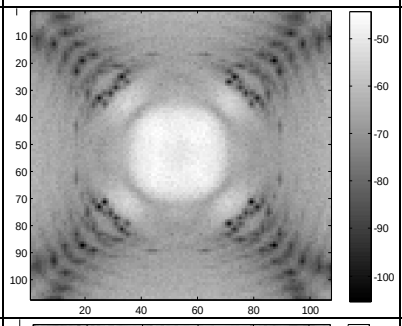	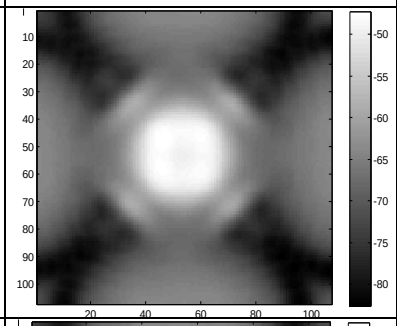	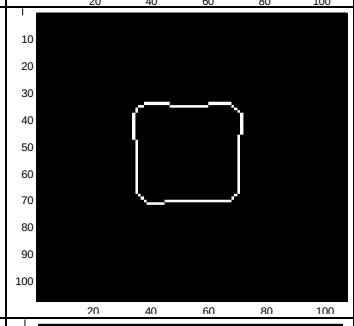	8%
10	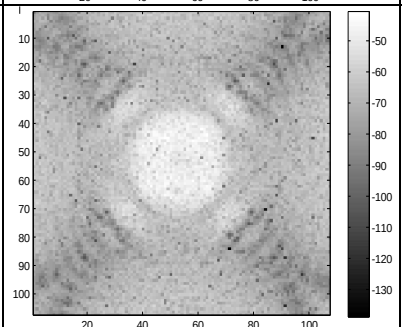	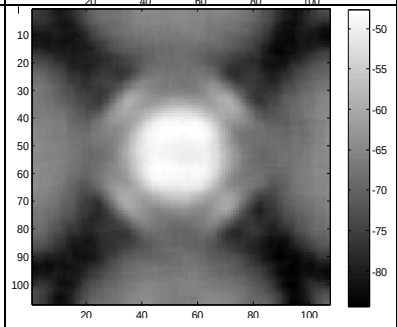	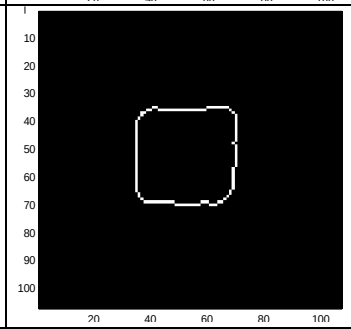	9%
1	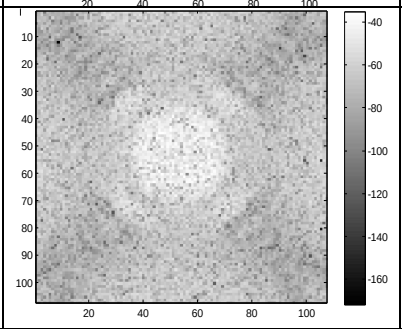	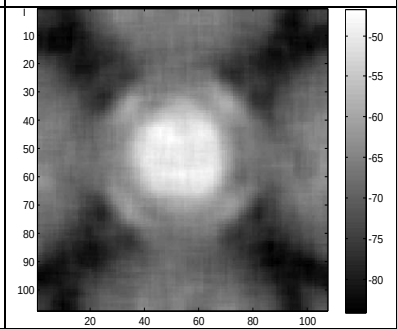	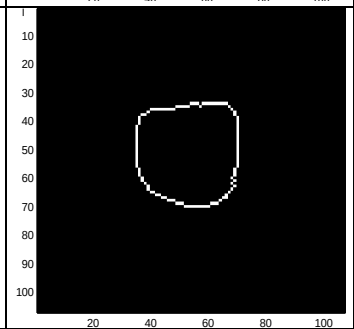	19%
0	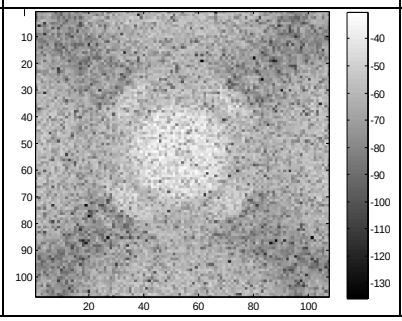	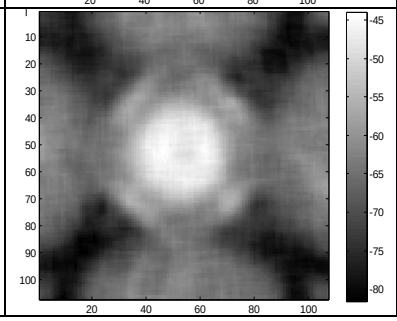	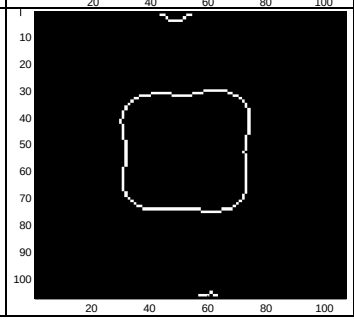	34%

Figure 10: Effect of the SNR ratio on the GPR image and the resulting mismatch error between the retrieved SBC and the reference target shapefor a metallic box of dimensions 14×14×7.2 cm buried at a depth of about 10 cm below the ground surface using the proposed GPR system

SNR (dB)	GPR Image	GNF Image	Extracted SBC	%Error
30	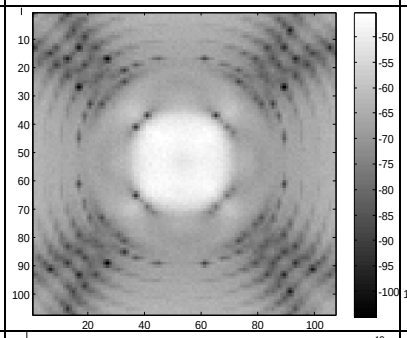	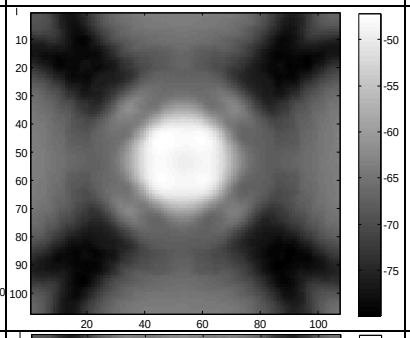	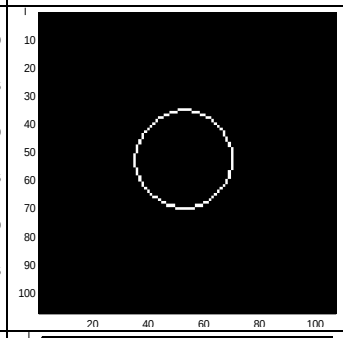	3%
15	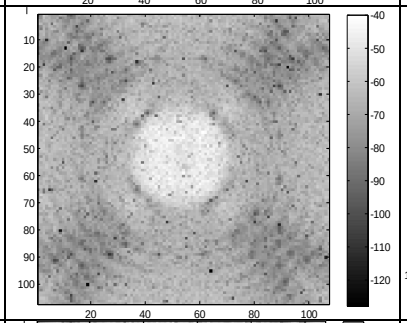	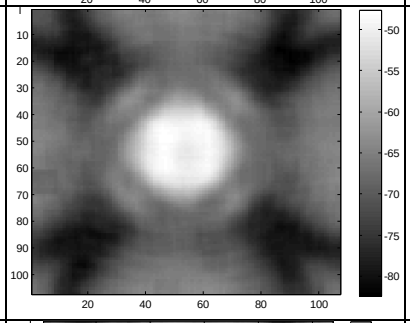	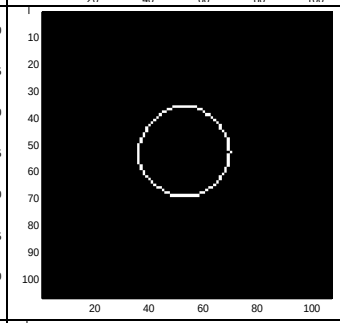	4%
10	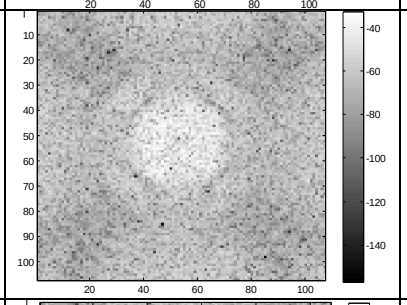	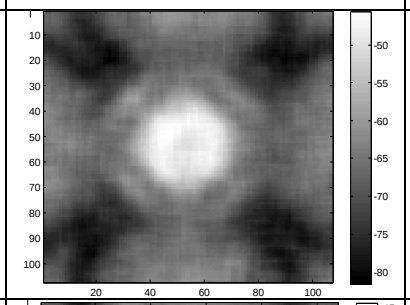	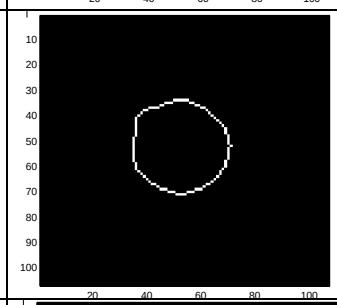	4.5%
3	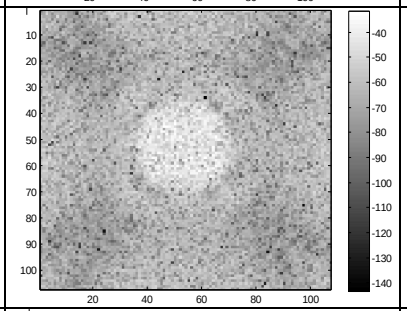	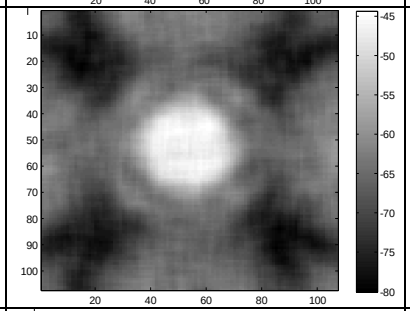	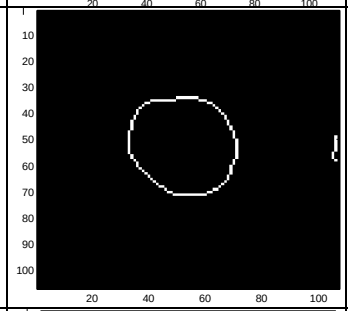	12%
0	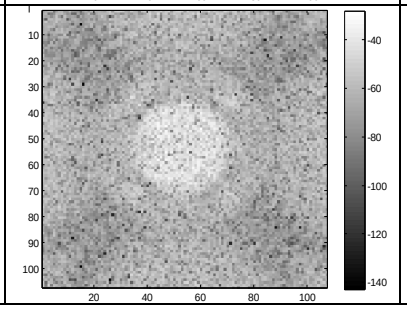	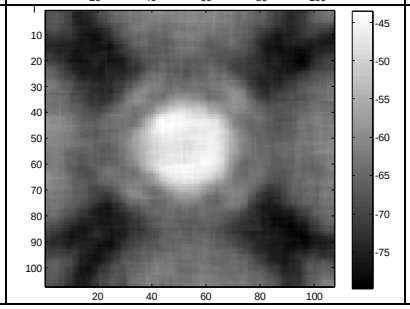	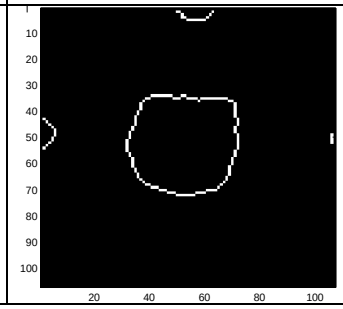	35%

Figure 11: Effect of the SNR ratio on the GPR image and the resulting mismatch error between the retrieved SBC and the reference target shape for a metallic cylinder of 7 cm radius and 7.2 cm height buried at a depth of about 10 cm below the ground surface using the proposed GPR system

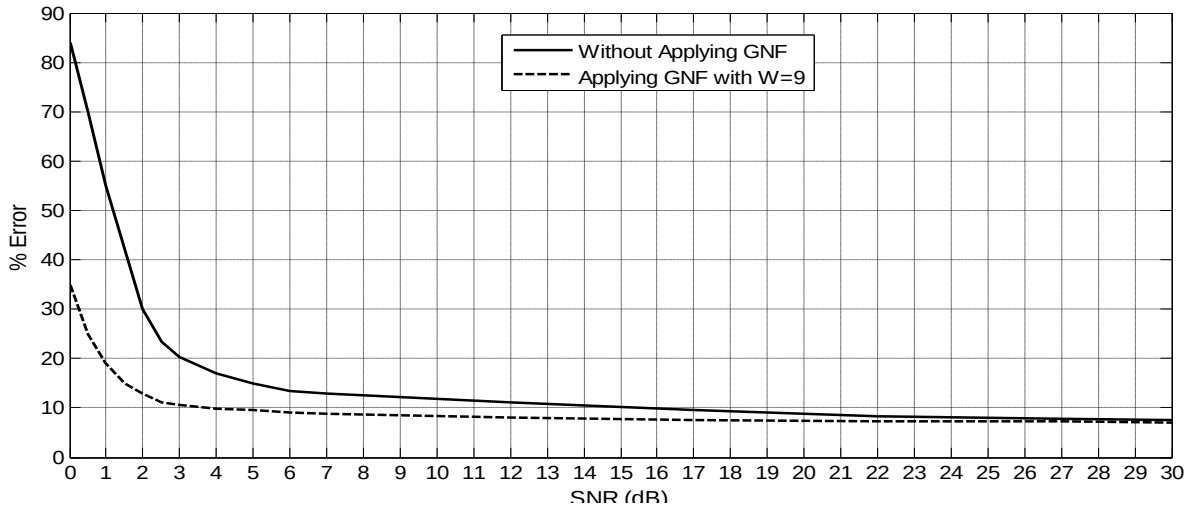

Figure 12: Reduction of the resulting error in target shape recognition algorithm due to the application of granular noise filter for a metallic box of dimensions 14×14×7.2 cm buried at a depth of about 10 cm below the ground surface using the proposed GPR system.

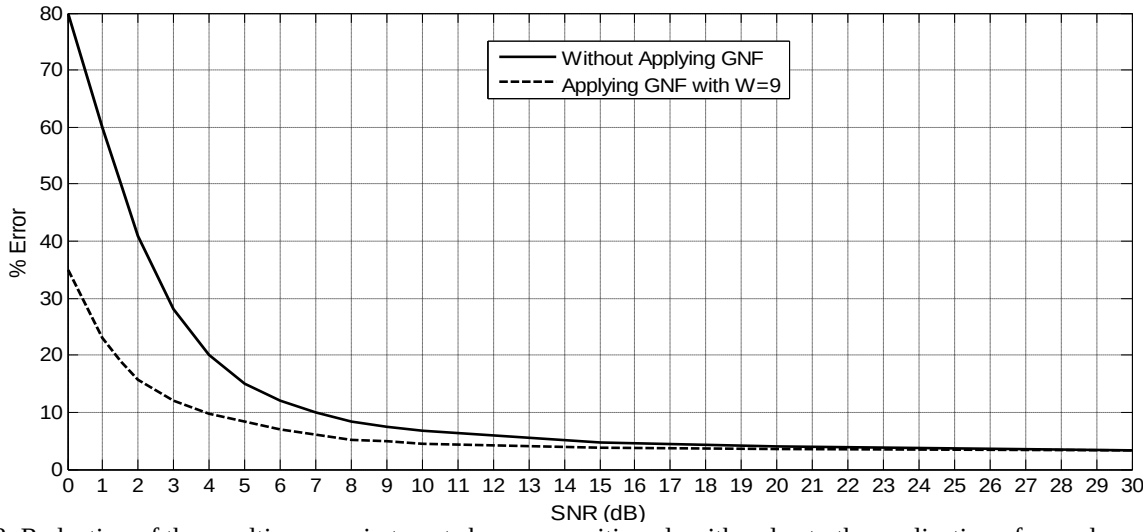

Figure 13: Reduction of the resulting error in target shape recognition algorithm due to the application of granular noise filter for a metallic cylinder of 7 cm radius and 7.2 cm height buried at a depth of about 10 cm below the ground surface using the proposed GPR system

X. CONCLUSION

An efficient technique for the treatment of buried object shape recognition from noisy polarimetric GPR images is introduced. The GPR system used for obtaining high resolution polarimetric images for objects buried under the surface of a ground soil together with the object shape retrieval and target recognition are completely described. A GNF is introduced to get an image with increased SNR. An algorithm to extract a two-dimensional shape of the buried object is introduced. An SSF is then applied for further elimination of the errors resulting due to granular noise effect on the two-dimensional shape retrieval process.A shape recognition algorithm is applied to compare the retrieved shape for the buried object to a reference target shapeto take a match or mismatch decision. The proposed GPR antenna system and the suggested algorithms for noise reduction, shape extraction and target recognition are examined through FDTD simulation running on different buried target shapes. The numerically obtained results show that proposed noise reduction technique with the proposed GPR system and the suggested algorithms for shape extraction and target shape recognition are efficient and successful in all the examined cases.

REFERENCES

[1] Y. Jeng, Y. Li, C. Chen, H. Chien, "Adaptive filtering of random noise in near-surface seismic and ground-penetrating radar data", Journal of Applied Geophysics No. 68, pp. 36–46, 2009.

[2] L. Crocco and F. Soldovieri, "Bistatic tomographic GPR imaging for incipient pipeline leakage evaluation", Progress In Electromagnetics Research, PIER 101, pp. 307-321, 2010.

[3] R. Roberts, D. Cist, and A. Kathage, "Full-resolution GPR imaging applied to utility surveying: insights from multi-polarization data obtained over a test pit", IWAGPR 2009, 5th International Workshop on GPR, Granada, Spain, May 27-29, 2009.

[4] J. Groenenboom and A. Yarovoy, " Data Processing and Imaging in GPR System Dedicated for Landmine Detection", Subsurface Sensing Technologies and Applications, Vol. 3, No. 4, pp 387-402, Oct. 2002.

[5] L. Morrow and P.Genderen, "2D polarimetricbackpropagation algorithm for ground-penetrating radar applications", Microwave and Optical Technology Letters, Vol. 28, pp. 1–4, 2001

[6] K. Dongen, P. Berg, and J.Fokkema, "Adirectional borehole radar for three-dimensional imaging", Proceedings of the 9thInternationalConf. GPR I,pp. 25–30, 2002.

[7] I. Catapano, F. Soldovieri, and L. Crocco, "On the feasibility of the linear sampling method for 3D GPR surveys," Progress In Electromagnetics Research, Vol. 118, 185-203, 2011.

[8] Y. Huang, Y. Liu, Q. H. Liu, and J. Zhang, "Improved 3-d GPR detection by NUFFT combined with MPD method," Progress In Electromagnetics Research, Vol. 103, 185-199, 2010.

[9] G. E. Atteia and K. F. A. Hussein, "Realistic model of dispersive soils using PLRC-FDTD with applications to GPR systems," Progress In Electromagnetics Research B, Vol. 26, 335-359, 2010.

[10] C.Ozdemir, S. Lim and H. Ling, "A synthetic aperture algorithm for ground-penetrating-radar imaging", Microwave and Optical Technology Letters, Vol. 42, pp. 412-414, 2004.

[11] K. M. Ibrahim, K. F. A. Hussein and A. A.Ammar, " Two-dimensional imaging and shape recognition of land buried objects through polarimetric ground penetrating radar", The 2nd Middle East Conference on Antennas and Propagation“ MECAP” 2012 in Cairo, Egypt, December 2012.

International Journal of Modern Engineering Research (IJMER)
www.ijmer.com Vol.3, Issue.2, March-April. 2013 pp-1056-1060 ISSN: 2249-6645

Thinking of Programmed Instructional Design: Need of Today's Learner

Shaik Fathima
Department of Education, Malla Reddy college/osmania university, India

***Abstract*:** *This article stresses on adopting appropriate instructional design for providing learner, experiences and organizing teacher pupil activities which is crucial for effective use of curricular content and achievement of curricular objectives. In India programmed instruction is still in its infancy, as regards its classroom use is almost nil. While designing with curricular organization, the curriculum designer should treat teaching learning strategies as an essential component of curricular cycle and while transacting the curriculum, the curriculum practitioner should be consistently conscious about careful selection of appropriate programmed instructional design. It would be imperative that, in spite of the mastery over the content on the part of the teacher, he/she should be appropriately oriented with regard to the importance and various types of instructional design and the principles that should govern their selection and administration. Programmed instruction is a systematic, step by step, self instructional programme aimed to ensure the learning of the stated behavior. It is thought as the way of "growing" or improving instruction. It places the learner at the centre where he himself constructs knowledge rather than passively absorbing it. An individual's knowledge is a function of ones prior experiences, mental structures, and beliefs that are used to interpret objects and events. In some classrooms, the predominant training model is direct instruction which is called instructivism or objectivism(based on information processing theory).The trainers central role is to transmit knowledge to learners and learners role is to absorb information(reception and compliances).the learning experiences in programmed instruction is self corrective. This instruction is an application of the principles of behavior sciences and technology in the field of education. The National Council of Educational Research and Training has done some work, yet the application of Programmed instruction has not shown appreciable impact on our classroom teaching.*

Key Words: *Branched programme, frames, linear programme, mathematics programme, programmed instruction.*

I. Introduction

However, in today's real- world context, the work environment is becoming a learning Environment (learning organization).Learners will not make use of concepts and ideas unless they use them through some type of process, that is, learners master only those activities they actually practice. Both constructivism and instructivism are required as learners need to be able to solve complex problems and be able to understand the reasons or methods they use to reach their conclusions. As a field, instructional design is historically and traditionally rooted in cognitive and behavioral psychology, though recently constructivism (learning theory) has influenced thinking in the field. Behaviorists place "an emphasis on producing observable and measurable outcomes in students" (Ertmer & Newby, 1993). They believe that learning occurs when learners show the correct response to a certain stimulus (Smith & Ragan, 1999). The current instructional design application of behavioral objectives is reminiscent of these behaviorist views. However, most current instructional designers writing objectives based on action do not share the behaviorists' disinterest in the cognitive processes that also take place. Rather, they write objectives with an attempt to extract "best evidence" of the cognitive processes that cannot be directly observed. Programmed instruction owes its origin to the psychology of learning .The psychologist bearing direct relevance to programming is E.L.Thorndike(1874-1949).Other important psychologist who made significant contribution in the field are: Sidney.L .Pressy, Robert .M. Gagne, Robert Mager and B.F.Skinner. "GITA" is the first example of programmed learning.

II. Teaching Instruction and Programme Instruction

Teaching is a broad term and instruction is a purposeful, orderly, controlled sequencing of experience to reach a specified goal. Programmed instruction is a sub-head under instruction and represents a more rigorous attempt to develop a mastery over specialized goals to secure "insured learning".

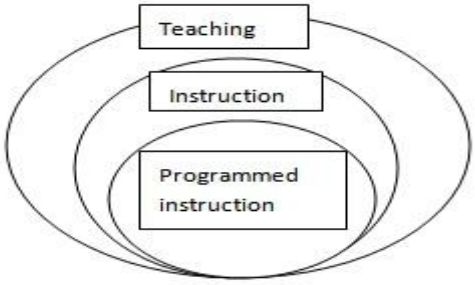

Fig. Teaching, Instruction and Programmed Instruction

III. Programmed Instruction

Programmed instruction or programmed learning is one of the important innovations in the teaching learning process. It is carefully specified, systematically planned, empirically established, skillfully arranged and effectively controlled self instructional technique for providing individualized instruction or learning experiences to the learner. The subject matter or learning experiences is sequenced into small segments. In order to help the learner to give assistance primes and prompts are provided in the introductory frames. Prompts are classified into two types: formal prompt and thematic prompt.

Formal prompt-one of the optical phenomena which can be studied by using rays of light is reflection. Rays of light bounce on certain surfaces

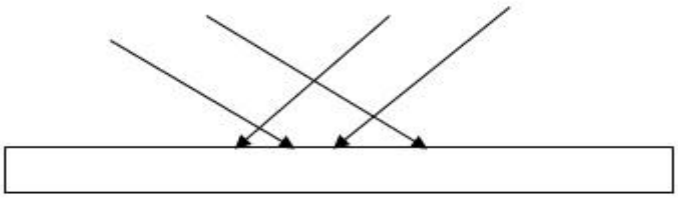

The phenomenon that you see in the figure is called re----------.

Response: reflection.

Thematic prompt -depends on the general properties of the prompting stimulus. It provides a hint.

> The ray that is incident on a reflecting surface is called incident ray. The ray which is reflected by the mirror is called----------ray.
>
> Response: reflected

As a result of experimental studies and research there are different types of programmed instructions-

- Linear, Branched and Mathetics Programming- Represents actual basic formats in teaching.
- Ruleg system of Programming-deductive and inductive approach in teaching. Here a perfect rule works as a stimulus for evoking the responses. This system is just the extension of linear or branched programming.
- Computer assisted instruction and learner controlled instruction-ways and means of providing instruction.

The idea of Programmed instruction is "if a miracle of mechanical ingenuity, a book can be so arranged that only to him who had done what was directed on page one and page two would become visible and so on, that requires personal instruction then the miracle later on becomes reality." It has exercised a revolutionary impact on teaching learning process. It is the innovative step in direction towards automation and individualized instruction. It may be treated as "software approach" for instructional technology.

3.1 Linear/Extrinsic Programming

B.F.Skinner is the originator, Single track or straight line programme, content is broken into sequence of steps which remain unchanged and presented in a series of small steps (frames), learner respond actively to each frame and immediate reinforcement is given, the programmer sitting at a distant place controls externally the learner's responses and the learner constructs the response, simple linear machine design, 5% rate of error and helpful in the modification of the behavior of the learner. It depends on the principle of- small steps, active responding, minimum errors, self pacing and knowledge of results.

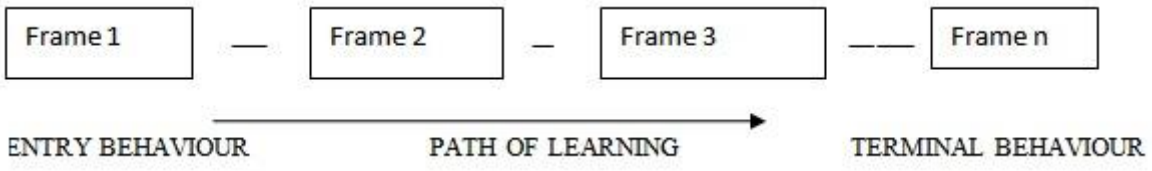

Example of linear programming: The angle having 90 degree is called---------- angle. (Acute, obtuse, right, straight angle) Response: right angle

3.2 Branching/Intrinsic Programming

Norman.A.Crowder is the originator, Frame is relatively bigger in size compared to linear programming, it contains two or three related ideas or related sequences, learner has to arrive at the answer by setting the relationship between one idea and the other and by filling up the gaps not fully covered in the frame, it contains multiple choice items where the learner selects the response, ,it is applicable where the information of broader concepts is to be given and remedial solution

to the difficulties of the learner and rate of error varies according to the programme which is usually 20%,it employs three principles: principles of exposition, diagnosis and remediation , student's learn better if the whole content is exposed, student's errors help in diagnosis and doesn't necessarily hinder learning, student's learn better if the remediation is provided side by side. Frame package is large, may be paragraph or page in frame. Frame structure consists of three aspects-exposition, diagnosis and remediation.

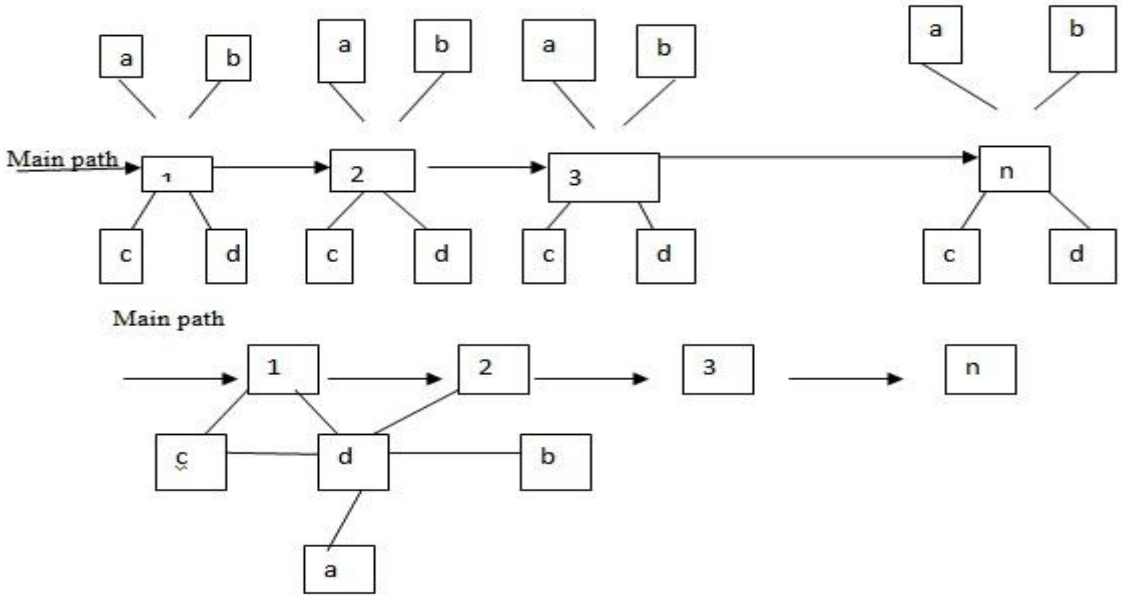

Xample: Branched program me in Simple Arithmetic

PAGE1
In a multiplication the two numbers that are multiplied together may be called the "factors" and the result is called the product. Thus in 2x3=6, the numbers 2 and 3 are called factors and the number 6 is called the product.
Below you will find a question. Pick what you think as the right answer to the question and go to the page number given against the answer.

The question is: what is the result (product) if 3 is used as a factor twice in a multiplication?
Answer: 6-turn to page 3
Answer: 9-turn to page 5
If you do not understand turn to page 7

PAGE 5
Your answer on page 1 was 9.You are correct. If we use as a factor twice, in a multiplication, we get 3x3=9 as a result.
Now, what result would we get if we used the number 2 as a factor three times?
Answer 6-turn to page 4
Answer 8-turn to page 10

PAGE 3
Your answer on page 1 was 6.you seem to have merely used 2 &3 factors in a multiplication. The problem was to use the number 3 as a factor twice. In other words, we want the result of the multiplication 3x3-? Now return to page 1 and try again.

PAGE 7
Your answer to page 1 was "I don't understand." We are asking you what product you get from a multiplication in which you use the number 3 as a factor twice: in other words what is the result of the multiplication in which the numbers that are multiplied together are both 3's? i.e., what is the product of 3x3?
Now return to page 1 and choose the right answer, and so on.

Continued

3.3 Mathetics Programming

Thomas.P.Gilbert is the originator; it is the systematic application of reinforcement theory to the analysis and construction of complex behavior repertories usually known as subject-matter mastery, knowledge and skills. Mathetics if applied diligently produces material that exceeds the efficiency of lessons produced by any known method. It involves task

analysis which may be stated as---description of the task which the learner has to learn, isolation of the required behavior, identification of the conditions under which the behavior occurs and determination and generalization of a criterion of acceptable performance. It involves three principles: Principle of chain, discrimination and generalizations. The prescription helps in learning, mastery steps can be placed anywhere in chain of learning. Reverse-contiguity is helpful for the mastery of the content and completion of task provides motivation to the students. Learning packages are developed in small steps. It provides three types of frames.

Example: Programme- To find the square of 26

Demonstration frame 1.Multiply the first digit 2 by the next higher consecutive number.
2. Write 76 to the right of the result
3. The square of 26 is 676.

Programme - To find the square of 21

Teaching frame 1.multiply 2 by 2.
2. Write 41 to the right of 4.
3. The square of 21 is 441.

Testing frame Programme- what is the square of 25? --------

IV. Specific Skills Needed For the Construction of Programme

4.1 Skills needed for the planning stage: skill in writing behavioral objectives, skill in defining entry behavior, skill in content analysis, skill in preparing a criterion test.

4.2 Skills needed at writing stage: skill in differentiating the functional and structural ingredients of frames, skill of using primes and prompts skill in ordering and arranging frames in a proper sequence.

4.3 Skills needed at revision, editing and testing: linguistic skill, editing skill, skill in individual testing which requires establishing a rapport, skill in obtaining evidence about the worthiness of the programme.

Illustrative Programme: Silent features of the Constitution of India.

In this programme you will find paragraphs which are called frames. Study each frame carefully and write down what is required. Answers are given at the end, after stating the answers, check them, if your answer is wrong or you don't understand anything, you can again go back to the frame. This is not a test but instead it is called as a self- study programme.

Frame 1-The Constituent Assembly of India was set up under the provisions of the Cabinet Mission Plan to frame the Constitution of India which was formally adopted on 26th November,1949 and came into force on 26th January 1950.It took nearly three years to complete the work.

- What was the work assigned to Constituent Assembly?
- Under whose provision was it formed?
- When did our Constitution come into force?
- When was it adopted?
- How much time did Constituent Assembly take to complete its work?

Frame 2- The Preamble of the Constitution has a great significance but is not a part of the Constitution. The Constitution was framed by the people of India through their representatives. It stresses the fact that the reign of the land lies with the people of India.

- Is the preamble a part of the constitution?
- By who was the constitution framed?
- In whose hands does the reign of law of India lie?

Frame 3- The Preamble of our Constitution is as under: We the people of India having solemnly resolved to constitute India into a Sovereign Socialistic Secular Democratic Republic and to secure to all citizens: Justice, Social, economic and political; Liberty of thought, expression, belief, faith and worship; Equality of status and of opportunity; and to promote them all; Fraternity assuring the dignity of the individual and the unity and integrity of the Nation.

- Who has given the Constitution of India?
- What kind of justice has been ensured by the Preamble?
- What type of Republic is to be constituted?
- What kind of equality has been given to its citizen?

FRAME 4- People themselves adopted and enacted the Constitution. Thus, the representatives of the people frame the laws of the country and they have the power to change or amend the Constitution.

- Who frame the laws of the country?
- Who has the power to amend the constitution?

Answers:
Frame1- To frame the Constitution of India Provision of the Cabinet Mission Plan, 26th January 1950, 26th November 1949, Nearly 3 years.
Frame 2- No, People of India through their Representatives, People of India.
Frame 3-people of India, Social Economic and Political, Sovereign Socialism Secular Democratic, Equality of status.
Frame4- Representatives of the people, Representatives of the people.

V. Impact of Programmed Learning

Tutorial experiences are provided for individual learners on large scale, control on homework and study enable the learner to catch up the loss of absence from school, technological solution to the problem of individual difference, eliminates the teacher variable in the research, immediate scoring promotes the learning process, classroom efficiency may increase about 30%, difficulties of the students can easily be diagnosed and there can be great increase in interest and improvement in learning.

VI. Conclusion

I especially favor the idea of using an objective approach to provide the learner with an "anchor" before they set sail on the open seas of knowledge. A basic understanding of the material in question provides the learner with a guiding compass for further travel. Another consideration is the distinction between "training" and "education". In today's competitive world, Programmed instruction may be required to establish and meet the objectives. On the other hand, the designer may be challenged to provide material that fosters an individual to find divergent approaches to problem solving. Whichever situation the instructional design finds themselves in, they will require a thorough understanding of learning theories to enable them to provide the appropriate learning environment.

Finally, the idea of individualized self instructional prompted by programmed instruction approach has reached its climax by the introduction of computer assisted instruction. The technique of programmed instruction is becoming more and more technical and empirical by using the systematic and objective principles of mathematics, applied sciences and engineering. Basically originating from the psychology of learning and instruction, it has now been developed as one of the important aspects of instructional technology. Programmed instruction may prove a big helping hand in all the tasks and aspects of education. With intelligent application of learning theory strategies and technology, the modern designer will find solutions to the learning requirements of the 21st century.

References

[1] Aggrawal, J.C. (2003).Educational technology and management.New Delhi: vinod Pustak Mandir.
[2] Bandura, A. (1997). Social learning theory. Englewood cliffs, NJ: Prentice Hall.
[3] Collins, A., Brown, J.S., &Holum, A. (1991). Cognitive apprenticeship: Making thinking visible. American Educator, 6-46.
[4] Ely, D.P., T. (1996).Classical writing on instructional technology. Englewood, CO: Libraries unlimited.vol.2.
[5] Gagne, R. (1985).The Conditions of Learning and the Theory of Instruction, (4th Ed.). New York: Holt Rinehart, Winston.
[6] Good, T., Brophy, J. (1990).Educational psychology: A realistic approach. New York: Holt Rinehart, Winston.
[7] Merrill, M.D. (1983).Instructional Design Theories and Models: An Overview of their Current States. Hillsdale, NJ; Lawrence Erlbaum.
[8] Reigeluth, C.M. (1979).In search of a better way to organize instruction: The elaboration theory. Journal of instructional development, 2(3), 8-15.
[9] Shukla , C.(2008). Essentials of educational technology and management New Delhi: Dhanpatrai Publications.

International Journal of Modern Engineering Research (IJMER)
www.ijmer.com Vol.3, Issue.2, March-April. 2013 pp-1061-1065 ISSN: 2249-6645

Dynamic Model Of Anthropomorphic Robotics Finger Mechanisms

Abdul Haseeb Zaidy,[1] Mohd. Rehan,[2] Abdul Quadir,[3] Mohd. Parvez[4]
[1234]*Mechanical Engg. Department,AFSET Dhauj Faridabad, India*

Abstract: *Research on Dynamic Model of Anthropomorphic Robotics Finger Mechanisms (ARFM) is being carried out to accommodate a variety of tasks such as grasping and manipulation of objects in the field of industrial applications, service robots, and rehabilitation robots. The first step after kinematic modeling in realizing a fully functional of anthropomorphic robotics Finger mechanisms is dynamic modeling. In this paper, a dynamic Model of Anthropomorphic robotics Finger mechanism is proposed based on the biological equivalent of human hand where each links interconnect at the metacarpophalangeal (MCP), proximal interphalangeal (PIP) and distal interphalangeal (DIP) joints respectively. The Lagrangian method was used to derive the dynamics for the proposed of Mathematical Model of Anthropomorphic robotics Finger mechanisms.*

Keywords: *Anthropomorphic robot Finger, Modeling, Robotics, Simulation.*

I. Introduction

Among the vast applications of robotics, robotic assistance in human daily life and has been the major factor that contributes to its development. The focus on the anthropomorphism robotic limbs is currently undergoing a very rapid development. The creation of a multifingered anthropomorphic robotic hand is a challenge that demands innovative integration of mechanical, electronics, control and embedded software designs.

II. Literature Review

The normal human hand has a set of hand which includes palm and fingers. There are five fingers in each hand, where each finger has three different phalanxes: Proximal, Middle and Distal Phalanxes. These three phalanxes are separated by two joints, called the Interphalangeal joints (IP joints). The IP joints function like hinges for bending and straightening the fingers and the thumb. The IP joint closest to the palm is called the Metacarpals joint (MCP). Next to the MCP joint is the Proximal IP joint (PIP) which is in between the Proximal and Middle Phalanx of a finger. The joint at the end of the finger is called the Distal IP joint (DIP). Both PIP and DIP joints have one Degree of Freedom (DOF) owing to rotational movement [1]. The thumb is a complex physical structure among the fingers and only has one IP joint between the two thumb phalanxes. Except for the thumb, the other four fingers (index, middle, ring and pinky) have similar structures in terms of kinematics and dynamics features. Average range of motion among the four fingers for flexion-extension movement is 650 at the DIP joint, 1000 at the PIP joint and 800 at the MCP joint while the abduction-adduction angles for the index finger has been measured as 200 at the MCP joint[1,2]. Figure 1 illustrates the structure of a human finger.

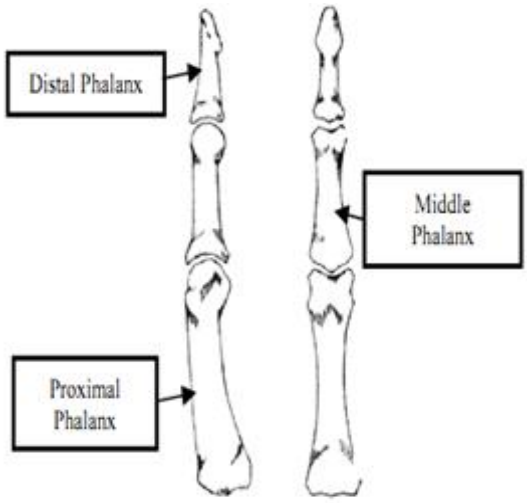

Fig.1: Structure of Human Finger

III. Dynamic Model Of Finger Mechanism

Based on the Fig. 2, the Lagrangian method was used to derive the dynamics. In dynamic part, the equations have been derived to find out the torque of ARFM. Referring to the derived forward kinematics,

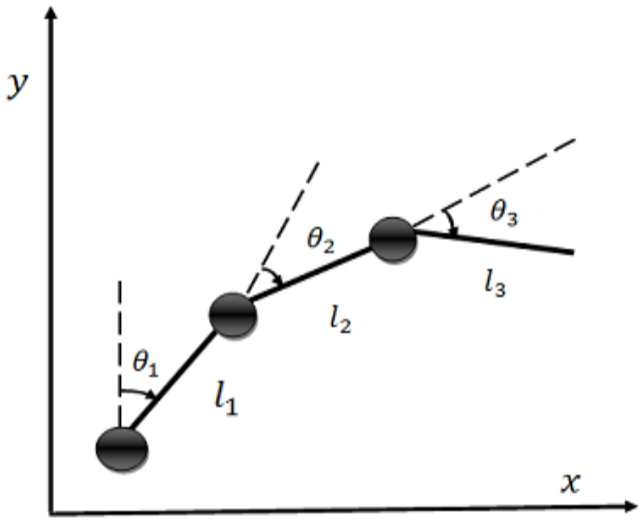

Fig. 2. Flexion of angles of one finger

$$x = l_1 \cos\theta_1 + l_2 \cos(\theta_1 + \theta_2) + l_3 \cos(\theta_1 + \theta_2 + \theta_3)$$
$$y = l_1 \sin\theta_1 + l_2 \sin(\theta_1 + \theta_2) + l_3 \sin(\theta_1 + \theta_2 + \theta_3)$$

Referring equation forward kinematic above, the angular velocity is computed using Euler langrange formula [3]

$$\omega_i = \frac{d\theta_i}{dt}$$

The angular velocity

$$\omega_1 = \dot{\theta}_1$$
$$\omega_2 = \dot{\theta}_1 + \dot{\theta}_2$$
$$\omega_3 = \dot{\theta}_1 + \dot{\theta}_2 + \dot{\theta}_3$$

Then, the linear velocity of mass centre each link of the finger was found using Euler langrage formula [3].

$$\dot{x}_1 = -\frac{1}{2} l_1 S_1 \dot{\theta}_1$$
$$\dot{y}_1 = \frac{1}{2} l_1 C_1 \dot{\theta}_1$$
$$\dot{x}_2 = -l_1 S_1 \dot{\theta}_1 - \frac{1}{2} l_2 S_{12} (\dot{\theta}_1 + \dot{\theta}_2)$$
$$\dot{y}_2 = l_1 C_1 \dot{\theta}_1 + \frac{1}{2} l_2 C_{12} (\dot{\theta}_1 + \dot{\theta}_2)$$
$$\dot{x}_3 = -l_1 S_1 \dot{\theta}_1 - l_2 S_{12} (\dot{\theta}_1 + \dot{\theta}_2) - \frac{1}{2} l_3 S_{123} (\dot{\theta}_1 + \dot{\theta}_2 + \dot{\theta}_3)$$
$$\dot{y}_3 = -l_1 C_1 \dot{\theta}_1 - l_2 C_{12} (\dot{\theta}_1 + \dot{\theta}_2) - \frac{1}{2} l_3 C_{123} (\dot{\theta}_1 + \dot{\theta}_2 + \dot{\theta}_3)$$

The equation of the velocity linear above should be square and sum of the equations to find V1 , V2 and V3,

$$v_1 = \dot{x}_1^{\,2} + \dot{y}_1^{\,2}$$

$$= (-\frac{1}{2} l_1 S_1 \dot{\theta}_1)^2 + (\frac{1}{2} l_1 C_1 \dot{\theta}_1)^2$$
$$= \frac{1}{4} l_1^2 \dot{\theta}_1^2$$

$$v_2 = \dot{x}_2^{\,2} + \dot{y}_2^{\,2}$$
$$= \left(-l_1 S_1 \dot{\theta}_1 - \frac{1}{2} l_2 S_{12} (\dot{\theta}_1 + \dot{\theta}_2) \right)^2 + \left(l_1 C_1 - \frac{1}{2} l_2 C_{12} (\dot{\theta}_1 + \dot{\theta}_2) \right)^2$$
$$= l_1^2 \dot{\theta}_1^2 + \frac{1}{4} (\dot{\theta}_1 + \dot{\theta}_2)^2 + l_1 l_2 C_2 \dot{\theta}_1 (\dot{\theta}_1 + \dot{\theta}_2)$$
$$= l_1^2 \dot{\theta}_1^2 + \frac{1}{4} (\dot{\theta}_1^2 + 2\dot{\theta}_1 \dot{\theta}_2 + \dot{\theta}_2^2) + l_1 l_2 C_2 (\dot{\theta}_1^2 + \dot{\theta}_1 \dot{\theta}_2)$$

$$v_3 = \dot{x}_3^{\,2} + \dot{y}_3^{\,2}$$
$$= (-l_1 S_1 \dot{\theta}_1 + l_2 S_{12} (\dot{\theta}_1 + \dot{\theta}_2) + l_3 S_{123} (\dot{\theta}_1 + \dot{\theta}_2 + \dot{\theta}_3))^2$$
$$+ ((l_1 C_1 \dot{\theta}_1 + l_2 C_{12} (\dot{\theta}_1 + \dot{\theta}_2) + l_3 C_{123} (\dot{\theta}_1 + \dot{\theta}_2 + \dot{\theta}_3))^2$$

$$= l_1^2 \dot{\theta}_1^2 + l_2^2 (\dot{\theta}_1 + \dot{\theta}_2)^2 + \frac{1}{4} l_3^2 (\dot{\theta}_1 + \dot{\theta}_2 + \dot{\theta}_3)^2$$
$$+ 2 l_1 l_2 C_2 \dot{\theta}_1 (\dot{\theta}_1 + \dot{\theta}_2) + l_1 l_3 C_{23} (\dot{\theta}_1 + \dot{\theta}_2 + \dot{\theta}_3)^2$$
$$+ l_2 l_3 C_3 (\dot{\theta}_1 + \dot{\theta}_2)(\dot{\theta}_1 + \dot{\theta}_2 + \dot{\theta}_3) + l_1 \dot{\theta}_1^2$$
$$+ l_2 (\dot{\theta}_1 + \dot{\theta}_2)^2 + l_3 (\dot{\theta}_1 + \dot{\theta}_2 + \dot{\theta}_3)^2$$

And the link kinetic energy ,

$$(K) = K_i = \frac{1}{2} \sum_1^3 (m_i v + l_i \omega_i^2)$$
$$K = \frac{1}{2} m_1 (v_1) + \frac{1}{2} m_2 (v_2) + \frac{1}{2} m_3 (v_3) + \frac{1}{2} l_1 \omega_1^2$$
$$+ \frac{1}{2} l_2 \omega_2^2 + \frac{1}{2} l_3 \omega_2^2$$
$$= \frac{1}{2} m_1 \left(\frac{1}{4} l_1^2 \dot{\theta}_1^2 \right) + \frac{1}{2} m_2 (l_1^2 \dot{\theta}_1^2 + \frac{1}{4} l_2^2 (\dot{\theta}_1 + \dot{\theta}_2)^2 + l_1 l_2 C_2 (\dot{\theta}_1 + \dot{\theta}_2)$$
$$+ \frac{1}{2} m_3 [l_1^2 \dot{\theta}_1^2 + l_2^2 (\dot{\theta}_1 + \dot{\theta}_2)^2 + \frac{1}{4} l_3^2 (\dot{\theta}_1 + \dot{\theta}_2 + \dot{\theta}_3)^2$$
$$+ 2 l_1 l_2 C_2 \theta_1 (\dot{\theta}_1 + \dot{\theta}_2) + l_1 l_3 C_{23} (\dot{\theta}_1 + \dot{\theta}_2 + \dot{\theta}_3)^2$$
$$+ l_3 l_3 C_3 (\dot{\theta}_1 + \dot{\theta}_2)(\dot{\theta}_1 + \dot{\theta}_2 + \dot{\theta}_3)^2 + \frac{1}{2} l_1 \dot{\theta}_1^2 + \frac{1}{2} l_2 (\dot{\theta}_1 + \dot{\theta}_2)^2$$
$$+ \frac{1}{2} l_3 (\dot{\theta}_1 + \dot{\theta}_2 + \dot{\theta}_3)^2 + \frac{1}{2} l_1 \dot{\theta}_1^2 + \frac{1}{2} l_2 (\dot{\theta}_1 + \dot{\theta}_2)^2$$
$$+ \frac{1}{2} l_3 (\dot{\theta}_1 + \dot{\theta}_2 + \dot{\theta}_3)^2 + l_1 \dot{\theta}_1^2 + l_2 (\dot{\theta}_1 + \dot{\theta}_2)^2$$
$$+ l_3 (\dot{\theta}_1 + \dot{\theta}_2 + \dot{\theta}_3)^2]$$

The kinetic energy in matrix form is referring this formula [24] Below:

$$K = \frac{1}{2}\left(\dot{\theta}_1 \dot{\theta}_2 \dot{\theta}_3\right)\begin{bmatrix} A_{11} & A_{12} & A_{13} \\ A_{21} & A_{22} & A_{23} \\ A_{31} & A_{32} & A_{33} \end{bmatrix}\begin{bmatrix} \dot{\theta}_1 \\ \dot{\theta}_2 \\ \dot{\theta}_3 \end{bmatrix}$$

$$A_{11} = \frac{1}{4}m_1 l_1^2 + m_2\left(l_1^2 + \frac{1}{4}l_2^2 + l_1 l_2 C_2\right) + m_3\left(l_1^2 + l_2^2 + \frac{1}{4}l_3^2 + 2l_1 l_2 C_2 + l_1 l_3 C_{23} + l_2 l_3 C_3\right) + l_1 + l_2 + l_3$$

$$A_{12} = \frac{1}{2}\left[m_2\left(\frac{1}{2}l_2^2 + l_1 l_2 C_2\right) + m_3\left(2l_2^2 + \frac{1}{2}l_3^2 + 2l_1 l_2 C_2 + l_1 l_3 C_{23} + l_2 l_3 C_3\right) + l_2 + l_3\right]$$

$$A_{13} = \frac{1}{2}m_3\left(\frac{1}{2}l_3^2 + l_1 l_3 C_{23} + l_2 l_3 C_3\right) + l_3$$

$$A_{21} = A_{12}$$

$$A_{22} = \frac{1}{4}l_2^2 m_2 + m_3\left(l_1^2 + \frac{1}{2}l_3^2 + l_2 l_3 C_3\right) + l_2 + l_3$$

$$A_{23} = \frac{1}{2}m_3\left(\frac{1}{2}l_3^2 + l_2 l_3 C_3\right) + l_3$$

$$A_{31} = A_{13}$$

$$A_{32} = A_{23}$$

$$A_{33} = \frac{1}{4}m_3 l_3^2 + l_3$$

The kinematic energy

$$K = \frac{1}{2}\left(A_{11}\dot{\theta}_1^2 + 2A_{12}\dot{\theta}_1\dot{\theta}_2 + 2A_{13}\dot{\theta}_1\dot{\theta}_3 + A_{22}\dot{\theta}_2^2 + 2A_{13}\dot{\theta}_2\dot{\theta}_3 + A_{33}\dot{\theta}_3^2\right)$$

$$K = 0.5\left(A_{11}\dot{\theta}_1^2 + 2A_{12}\dot{\theta}_1\dot{\theta}_2 + 2A_{13}\dot{\theta}_1\dot{\theta}_3 + A_{22}\dot{\theta}_2^2 + 2A_{13}\dot{\theta}_2\dot{\theta}_3 + A_{33}\dot{\theta}_3^2\right)$$

The potential energy is

$$(\mathrm{p}) = p_i = \frac{1}{2}\sum_{1}^{3}(m_i g y_i)$$

$$p_1 = \frac{1}{2}m_1 g l_1 S_1$$

$$p_2 = m_2 g\left(l_1 S_1 + \frac{1}{2}l_2 S_{12}\right)$$

$$p_3 = m_3 g(l_1 S_1 + l_2 S_{12} + \frac{1}{2} l_3 S_{123})$$

$$p = p_1 + p_2 + p_3$$

$$p = \frac{1}{2} m_1 g l_1 S_1 + m_2 g(l_1 S_1 + \frac{1}{2} l_2 S_{12}) + m_3 g(l_1 S_1 + l_2 S_{12} + \frac{1}{2} l_3 S_{123})$$

The Langrangian is computed as:

$$L = K - P$$

By using the Lagrange-Euler Formulation, The equation of motion for three degree of freedom finger can be written as:

$$\frac{d}{dt}\left(\delta / \delta \dot{\theta}_i\right) - \delta / \delta \theta_i = \tau_i \quad (i = 1-3)$$

Thus, this completes the Dynamic modeling of Anthropomorphic Robotics Finger Mechanisms (ARFM). These equations are used in the simulation of the design of Anthropomorphic Robotics Finger Mechanisms (ARFM). The results of the simulation shall be communicated in the next publication.

IV. Conclusion

The Dynamic Modeling plays an important role in simulation of Anthropomorphic Robot Finger Mechanisms (ARFM). In this paper, the complete derivation of the dynamic modeling of Anthropomorphic Robot Finger Mechanisms (ARFM) was carried out to enable subsequent simulation work. The results will be published in future. Other work such as development of control algorithm and development of Anthropomorphic Robot Finger Mechanisms (ARFM) will be addressed in the next phase of study.

References

Journal Papers:

[1] Neil A. Davidoff, Andris Freivalds (August4, 1993). "A graphic model of the human hand using CATIA". Department of Industrial and Management Systems Engineering, Pennsylvania State University, University Park, PA 16802, USA

[2] Jung Won Kang, Hyun Seok Hong, Bong Sung Kim , Myung Jin Chung, "Work Assistive Mobile Robots Assisting the Disabled in a Real Manufacturing Environment", International Journal of Assistive Robotics and Mechtronics, Volume 8 Number 3, September 2007.

[3] J. K. Salisbury M.T. Mason: "Robot Hands and the Mechanics of Manipulation", MIT Press, Cambrige, MA, 1985.

International Journal of Modern Engineering Research (IJMER)
www.ijmer.com Vol.3, Issue.2, March-April. 2013 pp-1066-1070 ISSN: 2249-6645

A mechanistic study of the initial stage of the sintering of sol-gel derived silica nanoparticles

A. Pramanik, [1] K. Bhattacharjee, [2] M.K. Mitra, [3] G.C Das, [4]
B. Duari[5]

[1234] *Dept. of Metallurgical and Material Engineering, Jadavpur University, Kolkata 700032, India*
[5]*NACE Corrosion Specialist, Kolkata, India*

Abstract: *Dried silica gel powders were prepared by acid catalyzed controlled hydrolysis followed by polycondensation of tetraethyl orthosilicate (TEOS) in 1:1 by volume water-alcohol solution. The dried powders were pressed and isothermally heat treated over the temperature range of 200-600 ^oC. The mechanism of sintering of silica-gel particles during the initial stage of heating has been delineated and related to the formation of –Si-O-Si- siloxane bonds among the silica particles. This is experimentally substantiated by detailed diffusion reflectance infrared Fourier transformed spectroscopy (DRIFT) and thermo gravimetric/differential thermal (TG/DSC) analyses.*

Keywords: *Sol-gel, mechanism, sintering, DRIFT spectroscopy*

I. Introduction

Sol-gel derived silica glasses are branded for their wide applications in optics, electronic and other field of technology [1, 2]. Most of the cases in gel condition, especially for lakeside-derived silica gel, a water-alcohol solution remains in the space of the silica gel-network leaving high porosity upon drying. Preparation of monolithic gel is often very difficult because during drying a tremendously high stress is generated due to the presence of extremely fine capillary and the pressure gradient due to the differential shrinkage of the xerogel, frequently cause its cracking. This often leads to the formation of small granules of dried silica. Therefore to get the bulk sample one has to go through the sintering process of the powder sample at high temperatures. Sintering at high temperatures and the subsequent development of highly dense material is then the most important prerequisites of silica gel in achieving the desired applicability in this respect. A significant contribution has been made over a decade in understanding the physical background of the sintering process of the silica gel [3], particularly at a high temperature. However, there still remains plenty of space for research work. There is hardly any work reported in the literature on the structural changes that occur at the interface of the fine silica gel granules during the early period of heating. Thus the objective of this paper is to elucidate the bonding at the molecular level of the dried silica gel at the initial stage of heating, as it is extremely necessary in order to find ways to improving the quality of the prepared materials [4].

Fourier transformed Infrared spectroscopy (FTIR) is probably one of the best methods to investigate the structure of amorphous silica derived from sol-gel process [5-9] down to the molecular level. Among the various modes of techniques, associated with IR spectroscopy e.g., IR absorption (KBr technique), IR emission, IR reflectance (including both specular and diffuse reflectance), attenuated total reflection (ATR), photo acoustic Fourier transform infrared (PAS-FTIR) spectroscopy, the diffuse reflectance infrared Fourier transform spectroscopy (DRIFT) is one of the most promising techniques for the qualitative analysis of the rough surface [10-12]. The positions of different O-H stretching vibrational bands are important in this respect: 3745 cm^{-1} for O-H stretching vibrations of the isolated (or terminal) hydroxyl group that are not hydrogen bonded, 3660-3550 cm^{-1} for O-H stretching vibration of H-bonded bridged hydroxyl groups that are in a chain, 3400-3300 cm^{-1} for O-H stretching vibration of H-bonded water molecule, 960 cm^{-1} for Si-OH stretching vibration of surface Si-OH group. In this paper we systematically make use of the DRIFT spectroscopy to better understand the mechanism of sintering of the silica gel during the early stage of heating. Thermo gravimetric (TG) and differential scanning calorimetric analysis (DSC) of silica gel further substantiate the observation delineated by the DRIFT spectroscopy.

II. Experimental

The silica gels were prepared through the hydrolysis followed by poly-condensation of tetraethyl-orthosilicate (TEOS) in water/ethanol solution under acidic condition. In a typical process a homogeneous solution of 10 ml of absolute alcohol and 10 ml of double distilled water is added in drops to a solution of 10 ml of TEOS and 10 ml of absolute alcohol under constant stirring followed by the addition of a few drops of 8 (N) HCl as a catalyst to the solution. The solution is stirred for 15 min and left for gelling for 8–9 days at room temperature. The gel was air-dried at room temperature (310 K) for an extended period of time. To investigate the mechanism of the initial stage of the sintering, the air-dried gel was pressed uniaxially into a cylindrical disc of diameter 15.0 mm. The pellets of dried gels were isothermally heated over the temperature range of 200 ^oC to 600 ^oC in a horizontal tube furnace for 2 h. The heating rate employed to reach the desired temperature is 6 ^oC/min

Thermal analysis: Thermo gravimetric/Differential scanning calorimetry analysis (TG/DSC) of the gel was carried out from room temperature to 800 ^{o}C, using a Pyris diamond (PerkinElmer) thermal analyzer under nitrogen atmosphere with a flow rate of 150 ml/min.

Diffuse reflectance Infrared Fourier Transform spectroscopy (DRIFT): DRIFT spectra of the silica samples sintered at different temperature were collected using IR-prestige FTIR spectrometer equipped with a baseline diffuse reflectance kit over the wave number region of 400-4000 cm^{-1}.

III. 3. Result & Discussion

3.1. TG-DSC analysis: Figure 1 shows the thermal behavior of the silica gel sample prepared by sol-gel method. A two-step loss of the weight was found for the air dried-gel sample, of which, the first sharp drop of around 12% centered at ~ 90 ^{o}C in association with the endothermic trough at the same temperature is attributed to the removal of water and alcohol present in the pores of the gel [13]. The second slow weight loss of around 6% at 200 ^{o}C onwards upto 600 ^{o}C, is due to the elimination of water molecule generated from the condensation of silanol (-Si-OH) groups. Condensation predominately occurs at the surface of the silica particles and thus helps for the aggregation of the particles close to each other. The appearance of a broad exothermic hump in the same temperature range (200 ^{o}C-600 ^{o}C) is the signature of this densification process which results in the formation of new siloxane (-Si-O-Si-) bond at the interface by the condensation of the surface silanol groups [14]. Due to the formation of –Si-O-Si- bonds the product become more ordered which makes ΔS negative This makes the enthalpy change ($\Delta H = T\Delta S$) negative. Hence the exothermic peak appears in the DSC curve.

3.2. DRIFT-spectroscopy analysis:

Fingerprint region of water and hydroxyl group: In order to unambiguously interpret the change in O-H vibration upon heat treatment, one thus necessarily needs to know the temperature limit within which dehydration and/or dehydroxylation has occur. Thus the TG and DSC analysis of the air dried gel was carried out in the present case to monitor the above fact and from the study (detail shown previously), the elimination of the adsorbed (or, molecularly associated) water molecule was found to occur in the temperature range of 100 ^{o}C to 200 ^{o}C. Figure 2 demonstrates the IR-spectra of all the silica samples for different OH stretching frequencies. It was observed that for initial heating conditions bands appeared at (1) 3260 cm^{-1} and (2) 3635 cm^{-1} which are due to the stretching modes of hydrogen-bonded bridged O-H group and for the stretching modes of hydrogen-bonded water molecule respectively [15]. While at relatively higher temperature, two bands appeared at (3) 3722 cm^{-1} and (1) 3372 cm^{-1} which are due to the free hydroxyl group and some H-bonded water molecule respectively [15]. Molecular arrangements of the different hydroxyl species are shown on the below of the figure 2. This means the removal of adsorbed water molecules followed by the removal of bridged hydroxyl groups leads to the formation of the free hydroxyl spices. The appearance of the broad absorption in 3400-3300 cm-1 for the 600 ^{o}C heated sample is also may be due to the progressive evolution and adsorption of the water molecule as the by-product of the condensation reaction at the surface.

Ideally, when silica samples are sintered, surface hydroxyl moiety (depending on the relative position, i.e. isolated, neighboring, external, internal, etc.) can be eliminated in the form of water molecule and new siloxane (-Si-O-Si-) linkages are formed. As shown in the figure 2, a strong band appeared at ~950 cm^{-1} ascribed for the surface Si-OH stretching vibration [15], is present up to a temperature of 600 ^{o}C, but the sharpness of the appeared trough is progressively decreases. This is because there remain plenty of hydroxyl groups at the surface of the silica particles as the condensation does not eliminate all of them at the initial stages. However, the elimination of the surface bound –OH group at selective region of the silica surface can also be occur through the formation of the new –Si-O-Si- linkages between particles.

Skeletal bonding structure of silica: IR spectra of the dried and the heat treated silica samples were given in the figure 3. All the spectra exhibit three major absorption troughs for the fingerprints of silica, viz, at ~460, 785 and 1100 cm^{-1}. These are the characteristics vibrations of Si-O-Si bridges cross linking the silica network. The band ~ 460 cm^{-1} was attributed to the rocking (R) motion of the bridging oxygen (O) atom perpendicular to the Si-O-Si plane. The 785 cm^{-1} band is due to the symmetric stretching (SS) of O atom along the bisector of the Si-O-Si bridge angle, and the high frequency band peaking at 1100 cm^{-1} ascribed to the asymmetric stretching (AS) mode of O atom back and forth parallel to the Si-Si line [15]. However, in the present case the AS is accompanied by the presence of an intense shoulder at the high frequency site, whose nature will be discussed in the next section.

Asymmetric stretching of silica: While dealing with the IR-spectra of the silica samples, one important observation is the longitudinal-optic (LO) and transverse-optic (TO) splitting of the vibrational mode. This splitting, which was first observed by Galeener and Lucovsky [16] and later theoretically supported by other authors [17,18], was attributed to long range coupling of Columbic interactions arising due to the partial iconicity in the material. Though all the characteristic vibrational modes of silica shows the LO-TO splitting to different extents, the occurrence is more pronounced in the asymmetric stretching region of Si-O-Si bond constituting the SiO_4 tetrahedral and is shown in the figure 4. The LO component for this part was found to appear typically at 1225 cm^{-1}, while the TO component appear at 1065 cm^{-1}. The deconvolution of the AS band (1300-1000 cm^{-1}) into two Gaussian curves gives the exact position of the respective LO and TO components. A typical deconvolution of the AS band in the absorption mode was shown in the figure 5 for the air dried gel and the detail information extracted from the deconvolution is listed in the table 1. From the table (as well as from the spectra Fig 3), it can

be observed that the frequency of LO mode appeared at higher wave number than that of the TO mode and the difference between the two modes (ν_{LO}-ν_{TO}) increases with the increase in the heat treatment temperature. As pointed out by Kittel [19], for a given normal vibration the LO frequency, $\boldsymbol{\nu}_{LO}$, is greater than the TO frequency, $\boldsymbol{\nu}_{TO}$, because the local electric field causes polarization of the surrounding atoms in the opposite direction for the LO mode but in the same direction for the TO mode. Since the (LO-TO) splitting is originated from the long range Coulombic interaction, higher the splitting higher will be the long range Coulombic force. Kamitsos et al. [20] reported the increase in AS-(LO-TO) splitting width with annealing temperature, is associated with the formation of siloxane network. Thus the increase in the LO-TO splitting width from 200 ^{o}C to higher temperature as pointed in the table-1, is due to the increase in Si-O-Si crosslinkings which predominately occur at the surface of the silica particles during the heating of the sample. Thus the above IR spectroscopic data clearly establish that the increased cross linking of Si–O–Si bond at the surface with the elimination of the water molecule may allow the aggregation of the fine grained silica particles and be responsible for initial stage of the sintering process. This mechanism of initial sintering has been schematically shown in figure 6 starting with the initial air dried gel.

IV. Conclusion

From the details of DRIFT study of the sample in association with TG-DSC analysis it can be inferred that, dehydration followed by the condensation of surface OH groups of silica particles forms the siloxane bonds, which are responsible for initial sintering.

V. Acknowledgement

One of us (K. Bhattacharjee) wishes to thank the University Grants Commission (UGC), the Government of India for financial assistance under the University with the 'potential for excellence' programme.

References

[1] S.H. Wang, C. Campbell, and L.L. Hench, in Ultra structure Processing of Advanced Ceramics, edited by J. D. Mackenzie and D. R. Ulrich (Wiley, New York, 1988), p. 145.
[2] Sol-Gel Science: The Physics and Chemistry of Sol-Gel Processing, C. Jeffrey Brinker, George W. Scherer, Academic Press, Inc. (London).
[3] R.K. Iler, the Chemistry of Silica (1979) John Wiley & Sons
[4] P.F. James, The gel to glass transition: Chemical and microstructural evolution, Journal of Non-Crystalline Solids 100, (1988) 93-114.
[5] C.J. Brinker and G.W. Scherer, Sol-Gel Science (Academic Press, NY, 1990), Chap. 11.
[6] H. Yoshino, K. Kamiya, and H. Nasu, IR study on the structural evolution of sol-gel derived SiO_2 gels in the early stage of conversion to glasses, Journal of Non-Crystalline Solids 126 (1990) 68-78.
[7] R.M. Almeida and C.G. Pantano, Structural investigation of silica gel films by infrared spectroscopy, Journal of Applied Physics 68 (1990) 4225-4233.
[8] C.T. Kirk, Quantitative analysis of the effect of disorder-induced mode coupling on infrared absorption in silica Physics Review B 38 (1988) 1255-1273.
[9] P.G. Pai, S.S. Chao, Y. Takagi, and G. Lucovsky, Infrared spectroscopic study of SiO_x films produced by plasma enhanced chemical vapor deposition, Journal Vaccum Science and Technology A 4 (1986) 689-695.
[10] M.P. Fuller, and P.R.Griffiths, Diffuse reflectance measurements by infrared Fourier transform spectrometry, Analytical Chemistry 50(13) (1978) 1906-1910.
[11] D.M. Krol and J.G. Lierop, The densification of monolithic gels, Journal of Non-Crystallization Solids 63 (1984) 131-144.
[12] L.L. Hench, Science of Ceramic Chemical Processing, edited by L. L. Hench and D. R. Ulrich (Wiley, New York, 1986), p. 52.
[13] K. Kamija, S. Sakka and Y. Ymanaka, Proceedings of the 10th International Congress On Glass, Vol. 13 (1974) p. 44.
[14] C.J. Brinker and S.P. Mukherjee, Conversion of monolithic gels to glasses in a multicomponent silicate glass system, Journal of Materials Science 16 (1981) 1980-1988.
[15] V.D.V. Pascal, G-D'Hamers lwan and E.F. Vansant, Estimation of the Distribution of Surface Hydroxyl Groups on Silica Gel using Chemical Modification with Trichlorosilane, Journal of the Chemical Socity, Faraday Transaction 86(22) (1990) 3751-3755.
[16] F.L. Galeener, G. Lucovsky, Longitudinal Optical Vibrations in Glasses: GeO_2 and SiO_2 Physics Review Letter 37 (1976) 1474-1478.
[17] M.C. Payne, J.C. Inkson, Longitudinal-optic-transverse-optic vibrational mode splittings in tetrahedral network glasses, Journal Non-Crystalline Solids 68 (1984) 351-360.
[18] S.W. de Leeuw, M.F. Thorpe, Coulomb splittings in glasses, Physics Review Letter 55 (1985) 2879-2882.
[19] Kittel, C. Introduction to Solid State Physics, 4th ed. Wiley: New York, 1971.
[20] E.I. Kamitsos, A.P. Patsis, G. Kordas, Infrared-reflectance spectra of heat-treated sol-gel-derived silica, Physics Review B 48 (1993) 12499–12505.

Figure caption:

Figure 1: TG-DSC plot of the air dried silica gel

Figure 2: DRIFT spectra at the selective region for the stretching vibration of O-H goup present in the air dried gel (a), and the silica gels heat treated at 200 ^{o}C (b), 400 ^{o}C (c), 600 ^{o}C (d).

Figure 3: DRIFT spectra at the fingerprint region of the silica for the air dried gel (a), and the silica gels heat treated 200 ^{o}C (b), 400 ^{o}C (c), 600 ^{o}C (d).

Figure 4: Asymmetric stretching vibration of the Si-O-Si bond for the air dried gel (a), and the silica gels heat treated 200 ^{o}C (b), 400 ^{o}C (c), 600 ^{o}C (d).

Figure 5: Typical deconvolution of the asymmetric stretching vibration of Si-O-Si bond for the air dried gel.
Figure 6: Pictorial reprentation of initial stage of sintering of sol-gel silica particle. Open circle and circular arcs represents the silica particles. (a) primary particles, (b) enhanced crosslinking at intermediate temperature, (c) agglomaration of silica particles.

Table caption:
Table 1: Analysis of the DRIFT spectra of the air dried and the heat treated silica samples

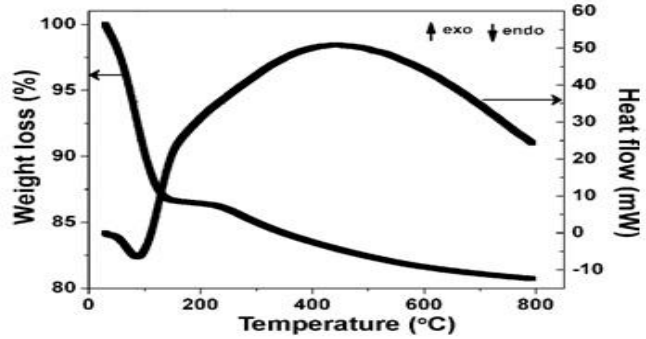

Figure 1: Pramanik et al.

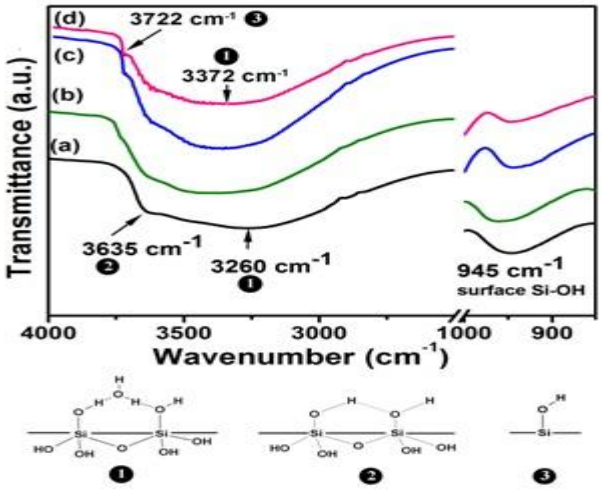

Figure 2: Pramanik et al.

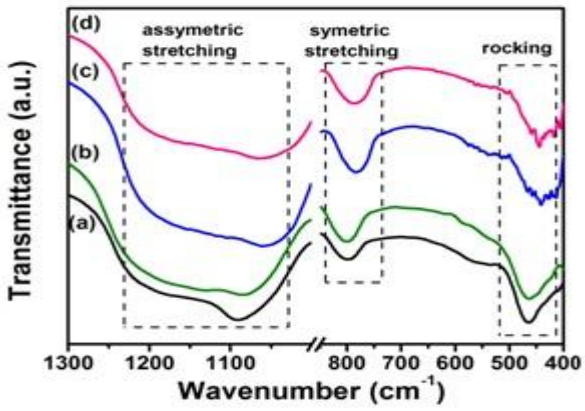

Figure 3: Pramanik et al.

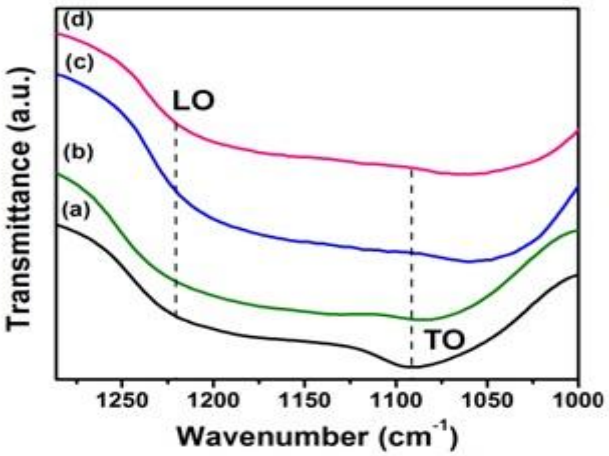

Figure 4: Pramanik et al.

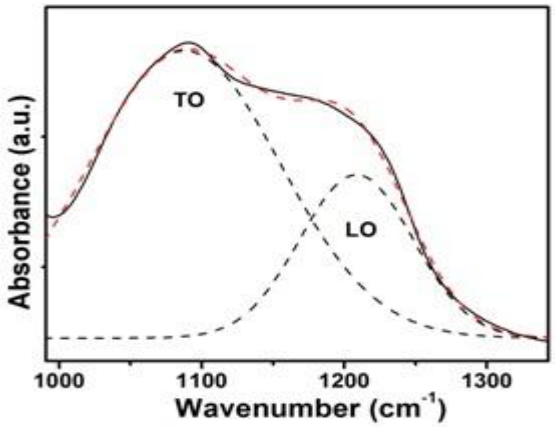

Figure 5: Pramanik et al.

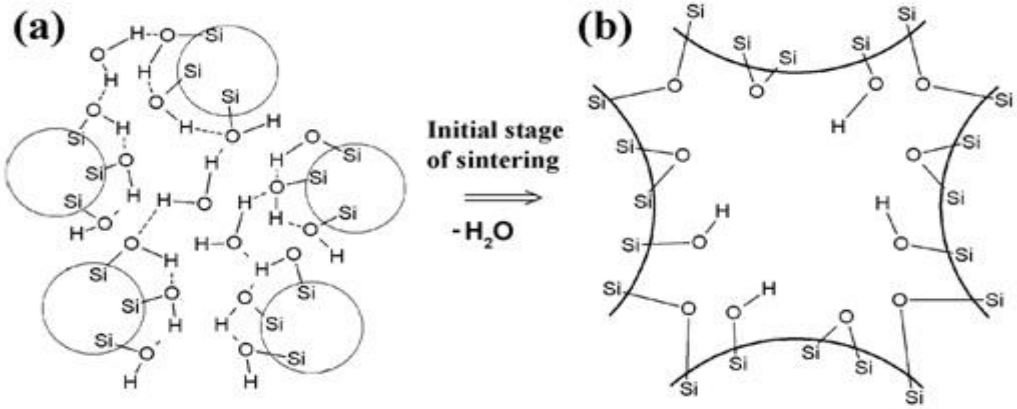

Figure 6: Pramanik et al.

Table 1: Pramanik et al.

Sample name	R (cm^{-1})	SS (cm^{-1})	AS-TO (cm^{-1})	AS-LO (cm^{-1})	LO-TO (cm^{-1})
Air dried gel	463	794	1085	1206	121
200 ^{o}C	463	800	1086	1211	125
400 ^{o}C	441	787	1052	1183	131
600 ^{o}C	443	781	1057	1192	135

International Journal of Modern Engineering Research (IJMER)
www.ijmer.com Vol.3, Issue.2, March-April. 2013 pp-1071-1074 ISSN: 2249-6645

Integration of Wired and Wireless Networks through a Personal Communication network (PCN)

Dr Jagannath Ghatuary
Department of Computer Science and Engg, Wollega University, Nekemte, Ethiopia

Abstract: *The Personal Communication Network (PCN) is known as the personal communication services (PCS) and is the result of the evolution of a mobile phone system. The PCN aims to support the services provided by the second generation mobile systems and also provides services which were not previously implemented. Thus the PCN is visioned as a system that will integrate all the wired and wireless networks. As we know that all the wired and wireless networks are widespread while others are emerging. Thus we need to study how these networks are being interconnected to each other to form a communication infrastructure.*

I. Theory

The Personal Communication Network(PCN) is known as the Personal Communication Services (PCS) in North America [57] and is the result of the evolution of a mobile phone system whose first deployments can be traced back to tile early 1980s. In order to understand why tile PCN is now emerging it is worth going through the different stages of its evolution.

First-generation mobile phone systems

The first-generation of mobile wireless phone systems were analogue and invented by Bell Laboratories about 1982. They were deployed in several countries: in the USA AMPS (Advanced Mobile Phone Systems) standardized was widely used; in England TACS (Total Access Communication System) was deployed; while in Japan the NTT (Nippon Telephone and Telegraph). The only service provided by these system was voice communication transmitted using frequency modulation techniques using two bands of frequencies; one for base station to mobile phone and another for mobile phone to base station transmission.

Second generation mobile phone systems

The second-generation of mobile phone systems is characterized by the use of digital technology. They have been in use in several countries since the early 1980s. Currently there are three inter- national standards
GSM: The Global System for Mobile Communication used in European countries.
IS-54: The North American Electronic Industry Association system used in the USA, Canada and Mexico. In contrast with the GSM and Japanese Personal Digital Cellular (PDC) systems which are fully digital, this system is digital-analogue, i.e. it enhances rather than replaces the old AMPS analogue system.
PDC: The Personal Digital Cellular System used in Japan.
Second-generation systems offer advanced transmission techniques like speech coding, error correcting channel codes, and bandwidth modulation techniques

Third generation mobile phone systems

As second-generation mobile phone networks are still being deployed a third generation is emerging. This system is a digital one and expected to integrate existing and future wire and wireless phone systems and called the PCN (Personal Communication Network) in Europe and PCS (Personal Communication Systems) in North America. Briefly, the PCN can be described as a system with enhanced capabilities for worldwide ubiquitous multimedia communication.

II. The PCN

Tile PCN is aimed not only at supporting the existing services provided by existing second generation mobile systems but also to provide

• **ubiquitous communication**: based on personal and terminal mobility the PCS will provide facilities for communication between two parties anywhere at any time i.e. regardless of the terminal they use two parties will be able to communicate at any time independently of their geographical location even when one of the or both are on tile move.

• **single universal phone number**: Users will 11ave a mobile handset which will respond to the same number regardless of where in the world the user is located; naturally, users will get a single bill.

• **Customized set of services**: independent of location a user will have the services she is used to.

• **high-functionality handset**: Tile mobile user handset is expected to evolve towards a mobile device with multimedia data communication and computation capabilities; among those capabilities are: voice telephony, voice e-mail, fax, video

telephony, teleconferences, database access, navigation, location, etc.

III. Mobile Data Networks

Mobile cellular phone networks like the European GPS, the North American IS-54, -and the Japanese PDC were designed mainly for voice communication. Although they can also transmit data messages at 9.6 Kbps, they have to compete against mobile data networks in this field. Mobile data networks have been designed specifically to provide data services in urban regions and offer data rates of 8 to 19.2 kbps. They offer wireless data transmission upon which several applications can be built; among the most important are: Internet access, e-mail, remote database and file access, wireless bank card verification, and real time vehicle (taxis, trucks) location. Currently MOBITEX (developed by Ericsson), ARDIS (developed and run by Motorola), and CDPD (the Cellular Digital Packet Network introduced by IBM) dominate the market.

IV. Satellite Networks

Thanks to their high location (thousands of kilometres up in the sky) and their wireless communication medium satellites can offer unique features that can certainly complement both wire and wireless terrestrial communications.

Wide coverage A single geostationary satellite can cover 1/3 of the earth's surface. In other words, a constellation (a group of satellites working for the same purpose) of three of them can cover the whole surface of the earth (the polar regions excluded Needless to ay, communication takes place regardless of-the distance and obstacles between the communicating points.

Wide mobility support Worldwide communication is guaranteed for everyone located under the satellite communication umbrella, even for users on the move walking, driving, sailing and flying.

Independence of geographical impediments A satellite communication infrastructure is a suit- able solution for hostile terrains (archipelagos for example).

Flexibility Having the satellite in orbit it is relatively easy and quick to deploy a communication network over a wide geographical area and to reconfigure it according to changes in user location and traffic requirements; this facility could be the answer to the problem of casual concentrations of mobile users for short periods of time (at football stadiums for example); moreover, in cases of terrestrial catastrophes when terrestrial networks are normally damaged a satellite link might be of great use.

Broadcast capability a satellite beam is inherently a broadcast medium; for applications of broadcast nature like remote conferences satellite communications might offer advantages over terrestrial ones.

V. Related Work

Projects aimed at the integration of these networks are currently under way. The International Telecommunication Union (lTU) is supporting the so-called Future Public Mobile Land Telecommunication System (FPLMTS) project that will provide a world-wide Personal Communication Network (PCN). In Europe The RACE programme was launched in 1987 and include projects to identify the enabling techniques for what would be the Universal Mobile Telecommunication System (UMTS); it concluded its activities in 1995; more exactly its activities were continued by the R&D into Advanced Communications Technologies and Services (ACTS) programme. In the USA the Defence Advanced Research Agency (DARPA) initiated the Global Mobile Information System (GloMo) programme in 1994. The GloMo aims to conduct research on new opportunities for advancing the state of the art in mobile, wireless, multimedia system technologies.

Integration of wired and wireless networks

In most industrialized countries people are familiar with services provided by the communication networks we have studied. In the future the number of these communication networks and their services is expected to be even larger. If this is true, we are on the way to ending up with a mess of incompatible networks offering similar services unless some work is conducted toward their integration. The purpose of this integration is to ensure that a user, be he indoors or on the move, is provided with the communication services he demands, no matter what terminal he is using or what computers or networks his information travels through on its way to its final destination.

For this to be possible it is necessary to integrate all the individual networks together into what we foresee as a global ubiquitous communication network (we will call it a global communication network for short) i.e. a network made up of multiple interconnected local and wide area networks with the already well established wired telephone and Internet networks serving as backbones. The essential goals of FPLMTS, UMTS, and GloMo] are the same. The system everybody has in mind is in fact the global worldwide universal ubiquitous communication network expected to be at least partially operational in 2000. In order that this goal be met the following must be achieved:

- Integration of existing wired and wireless networks. The PSTN, ISDN, B-ISDN, Internet and cellular telephone network to mention some of them,
- Deployment of services for delivering voice, video, and data communication between ubiquitous communicating counterparts, be they people or computers. Among these services are:

- dialogue (eg., speech, video telephony)

- messaging (email, fax, paging voice)
- Information retrieval (eg. multimedia WWW documents, voice, music, video on demand, newspapers)
- Access to electronic libraries
- When applicable the quality of wireless services should match that of wired networks.
- Support of unlimited mobility for both computers and users.
- Development of new computing techniques supporting mobile computing.

A picture of how the global ubiquitous communication network will probably look in the near future in presented in figure 1.1. In this figure a computer equipped with a wireless antenna and called a mobile support station plays the role of a bridge between the wireless PDA and the wired world. This will be explained below.

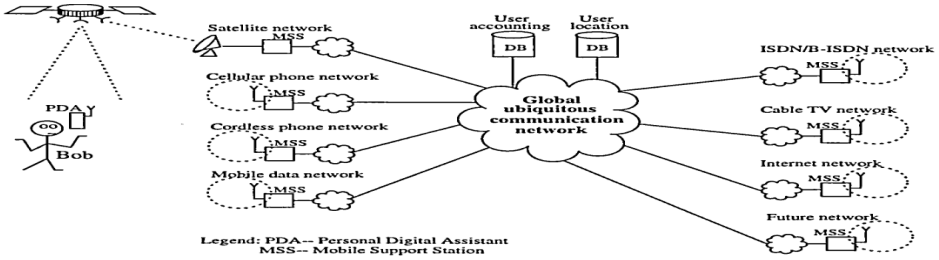

FIGURE 1.1 Global Communication Network

As illustrated in figure 1.2 there are many existing and potential services that make our predictions appealing to both ordinary individuals and business oriented people, an individual will use this global ubiquitous communication network to access several facilities:

- To exchange information (e-mailing) with his wife who is home and with his son who is on his way to the cinema.
- To retrieve information from his office, from a central database for example.
- To access publicly available databases; for example, databases of job vacancies, tourist attractions, etc.
- To access remote available services like bank transactions, Internet shopping, train booking, weather forecasts, financial news, and so on.

VI. WAP Protocol

An essential component of the global ubiquitous communication network is the mobile computer represented in figures1.1 and 1.2 by Bob's PDA. Although in the figure is called a PDA, it can be any electronic dev ice equipped with a wireless antenna to send and receive messages and, in most

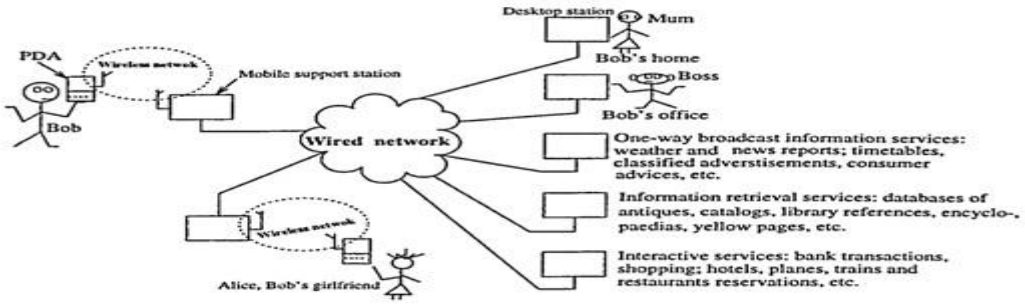

FIGURE 1.2: Services of a Communication Network

Cases, with computational power to process information Good examples of SUCll electronic device are: PDAs, mobile telephones, pagers, and other handheld communicators.

As its name and the name of its promoters imply, the WAP protocol is an industrial standard for integrating mobile communicators and the Internet. It primarily aims at providing access to Web information and services to mobile telephone users. Consequently, it is designed to run on top of already deployed wireless transports (called bearers) like GSM, IS-54, PDC, CDPD, MOBITEX, DECT, etc.}. The WAP designers decided to include IP as a separate bearer to leave room for integrating wireless devices with any IP-based network, for example a wireless LAN.\

Rather than inventing new technology, the designer of the WAP protocol made intensive Use of already proven technology, in particular, they based their design on the Web technologies and philosophies. To gain access to the large amount of information stored on Web pages from a devices with power, energy, communication bandwidth, and screen-size limitations they proposed a proxy architecture shown in figure 1.3.

The WAE User Agent that runs on the wireless client on top of its WAP protocol stack is a micro browser specially designed to run on a small screen and manipulated by a mobile telephone notepad. The Gateway is a proxy server that translates requests from the WAP protocol stack to the WWW protocol stack. To reduce the size of data over the network and the size of the data received from a Web server (Origin Server in WAP terminology) Encoders and Decoders are

used in the gateway. The latest news about the WAP protocol and complete specification of each layer of its protocol stack can be found in the Web page Forum [88].

Based on the latest tendencies in wireless communications we are positive that tile WAP protocol will be well established in the market in about three to five years time.

If our prognosis about the WAP success and the massive proliferation of PDAs in the future is correct, PDAs and similar devices will serve as the most popular outdoor interface to gain access to the global ubiquitous communication network. For this to be possible, MSS have to be widely geographically available and handy.

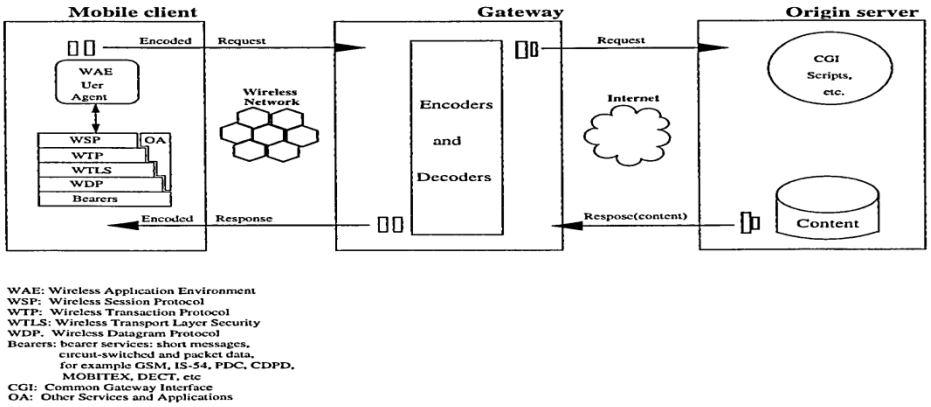

FIGURE 1.3: WAP Architecture

Based on the latest tendencies in wireless communications we are positive that tile WAP protocol will be well established in the market in about three to five years time.

If our prognosis about the WAP success and the massive proliferation of PDAs in the future is correct, PDAs and similar devices will serve as the most popular outdoor interface to gain access to the global ubiquitous communication network. For this to be possible, MSS have to be widely geographically available and handy.

- We assume that in the near future the earth will be crowded by thousands of MSS; some of them will belong to private LANs and be located indoors; others will belong to communication providers (WAP bearers for example) and be located outdoors.
- A private MSS will be run by a private company and provide access solely to PDAs belonging to its company.
- A public MSS will be run by a public communication provider and serve any PDA user willing to pay for the communication service.
- Optionally, a private MSS may serve visitors.

VII. Conclusion

Based on the latest tendencies in wireless communications we are positive that the WAP Protocol will be well established in the market in about 3 to 5 years time. If our prognosis about the WAP success and the massive proliferation of PDAs in the future is correct, PDAs and similar devices will serve as the most popular outdoor interface to gain access to the global ubiquitous communication network. If the above assumptions provides to be true in the future, a PDA user located inside a building will gain access to network services through his WLAN mobile support stations, if he decides to leave the building than his connection will switch to a public mobile support station, then if he drives his car to an area of sparse population where no public MSSs are available, his mobile terminal should be able to switch to a satellite network and remain connected to the world.

References

[1] George Lawton. The Internet's challenge to privacy Computer, 31(6), June 1998
[2] Lorrie Faith Cranor, Roger Clarke, Josef Dietl, Daniel Jaye, and Yves Le Roux. Laws, self-regulation, and p3p: Will w3c's privacy platform help make the web safe for privacy. Computer Networks and ISDN Systems, 30(1-7):751-753, April 1998. Proceedings of the Seventh International World Wide Web Conference 14-18 April 1998, Brisbane Australia
[3] Lincoln D. Stein. The World Wide Web security FAQ http://www .w3.org/Security /Faq/www-security-faq.lltm, April 1998
[4] Chris Pounder Security and the new data protection law. Computers & Security, 17(2), 1998.
[5] UK Parliament. Data protection act 1998. http.j' /www.hmso.gov.uk/acts/acts1998/19980029.1ltm, July 1998
[6] Charles P. Pfleeger and Deborah M. Cooper Security and privacy: Promising advances. IEEE Software, sep-oct 1997.
[7] World Wide Web Journal, 2(3), Summer 1997.
[8] Simson Garfinkel and Gene Spafford Practical Unix and Internet Security O'Reilly & Associates, Inc, second edition, 1996

International Journal of Modern Engineering Research (IJMER)
www.ijmer.com Vol.3, Issue.2, March-April. 2013 pp-1075-1081 ISSN: 2249-6645

IPv6, an Internet Protocol for efficient expansion capacity in addressing and routing

Bikki Lakshmi Manasa, [1] Guttikonda Chaitra Bharti, [2] Mikkili Ramya Teja, [3] Akkela Rama Krishna[4]
[1234]*Dept. of Electronics and Communication Engineering, K L University, India*

Abstract: *On February 3, 2011 the current version of the Internet IPv4 was depleted of addresses. Since the Internet today uses IPv4 for 99% of the traffic, it will be a slow migration to IPv6.1.The shortage of addresses has led to the introduction of IPv6 which has 128-bit (16-byte) source and destination IP addresses. Many organizations do not see a reason to convert to IPv6, and believe they are not running IPv6.2 whether an organization knows it or not, any laptop/PC running Vista or Windows 7 is a vulnerability from which attacks can come that will be invisible to IPv4 networks. Three transition strategies are being employed: header translation, dual stack and tunneling of IPv6 inside IPv4.4 Tunneling is the most precarious method for today's IPv4 networks. The IPv6 packet is included inside the message field of an IPv4 packet. The contents of the IPv6 packet will not be noticed by an IPv4 firewall or intrusion detection system. Hidden IPv6 traffic running across an organization's network can wreak havoc, allow malware to enter the network, and be the basis for a denial of service attack. The only defense against such attacks is deep packet inspection (DPI). The widespread use of DPI is inevitable. The first serious security breach caused by tunneled IPv6 inside an IPv4 packet is certain to come in the near future. This event will be a motivation to organizations to defend against such attacks.*

Keywords**:** IPv4, IPv6, deep packet inspection, cyber terrorism, security

I. Introduction

Under the Action Plan Europe 2005, it was recognized by the Commission that "IPv6 is essential on the road leading to network-based technologies, products and services that will contribute to an "everywhere", user-centric Information Society".

This gave rise to the European Commission's Communication to the Council and the European Parliament (COM/2002/96) – "Next Generation Internet – priorities for action in migrating to the new Internet protocol IPv6", which creates a context for the EU Members to take action in focusing on broadband availability and the development of IPv6.

These developments require a concerted action aiming at the structuring, consolidation and integration of European efforts on IPv6, notably through:

1. Increased support towards IPv6 in public networks and services;
2. The establishment and launch of educational programmers on IPv6;
3. The adoption of IPv6 through awareness raising campaigns;
4. The continued stimulation of the Internet take-up across the European Union;
5. Increased support to IPv6 activities in the Framework's Programme;
6. The strengthening of the support towards the IPv6 enabling of national and European Research Networks;
7. An active contribution towards the promotion of IPv6 standards work;
8. The integration of IPv6 in all strategic plans concerning the use of new Internet services.

In order to take some of the proposed actions, various European Countries have created an IPv6 Task Force group open to the different market players, including manufactures, operators, providers, applications developers, academic institutions, etc.

Following the European Commission's Communication, the present document explains the different aspects involved in IPv6 implementation that could lead to guidelines on the priorities for implementing and adopting IPv6 in public networks and services. The consequences for the market parties, including the users are also discussed.

II. Ipv6 – The Next Generation of Ip

"In the general sense, an internet is a computer network that connects several networks. The Internet is a publicly available internationally interconnected system of computers plus the information and services provided to their users using a TCP/IP suite of packet switching communications protocols[1]".

To interconnect two or more computer networks it is necessary to have a routing device to exchange traffic, and steer traffic via several different nodes on the path across a network to its destination. The devices used to interconnect different networks are routers. Others devices with specific functions like gateways or bridge are also used. All network elements such as routers, switches, gateways, bridges, LAN cards, need to have at least one IP address.

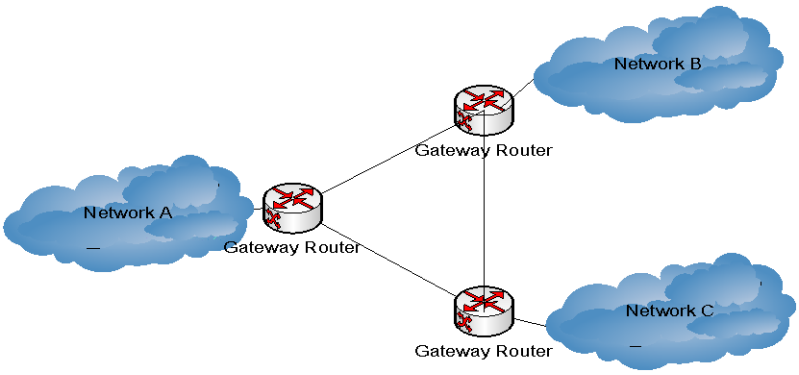

Figure 1: Use of routers

Different IP packet networks are normally interconnected by Routers that have added functionality to permit accounting between the interconnected networks. In other configurations they act also as interworking devices between different protocols.

2.1 Major benefits of the IPv6 – Why change?

The new version of IPv6 was conceived to replace the previous IPv4 standard that was adopted two decades ago as a robust, easily implemented standard.

However IPv4 is being used successfully to support the communications systems in the emerging information society and has been updated to extend its useful life (e.g. NAT mechanism, IPsec protocol), MPLS, Tunneling). However its capabilities are somewhat limited in the following areas:

- Exhaustion of the IPv4 address space;
- Growth of the Internet and the maintenance of routing tables
- Auto-configuration
- Mobility
- Security
- Quality of service

And the purpose of developing IPv6 is to overcome these limitations.
The areas where IPv6 offers improvement are:

- **Expansion capacity for addressing and routing** – the IP address space is expanded from 32 bits to 128 bits, enabling a greatly increased number of address combinations, levels of hierarchical address organization and auto-configuration of addresses;
- **Simplified header format** – the IPv6 basic header is only 40 bytes long in spite of the greatly increased address allocation;
- **Enhanced options support** – several different, separate "extension headers" are defined, which enable flexible support for options without all of the header structure having to be interpreted and manipulated at every router point along the way;
- **Quality of service** – the Flow Label and the Priority fields in the IPv6 header are used by a host to identify packets that need special handling by IPv6 routers, such as non-default quality of service or "real-time" service. This capability is important in that it needs to support applications that require some degree of consistent throughput, delay, and jitter;
- **Auto-configuration** – adds the concept of dynamic assignment of part of the address space, based on geographic and topographic features of a given physical connection
- **Elimination of the need for NATs (network address translators)** – since the IP address space supports approximately 3.4×10^{38} possible combinations, the need for private addressing schemes behind NATs is unnecessary on grounds of address conservation;
- **Improved security with mandatory IPsec implementation** – IPv6 provides for integral support for authentication, privacy and data integrity measures, by requiring all implementations to support these features;
- **Mobility** - mobile computers are assigned with at least two IPv6 addresses whenever they are roaming away from their home network. One (the home address) is permanent; the other (the IPv6 link-local address) is used temporarily. In addition, the mobile node will typically auto-configure a globally-routable address at each new point of attachment. Every IPv6 router supports encapsulation, so every router is capable of serving as a home agent on the network(s) to which it is attached.

2.2IP addressing architecture

An IP address is a binary number, which identifies any user's computer directly connected to the Internet. An IPv4 address consists of 32 bits, but it is usually represented by a group of four numbers (8 bits hexadecimal), from 0 to 255 ranges and separated by full stops. An example of this representation is showed below

124.32.43.4

Several domain names can also be linked to the same IP address, in effect similar to having more than one name for the same person.

The most recognized change from IPv4 to IPv6 is the length of network addresses. The IPv6 addresses have 128 bits length. The 128 bits provide approximately $3.4x10^{38}$ separate values. An IPv6 address consists of eight numbers in the hexadecimal format, from 0 to 65535 (decimal) ranges and separated by a colon ":". An example of this new representation is showed following:

FECA: 0000:234A:0043:AB45: FFFF: 9A3E:000B

In order to compare with the IPv4 header next figure 3 shows the IPv6 header format:

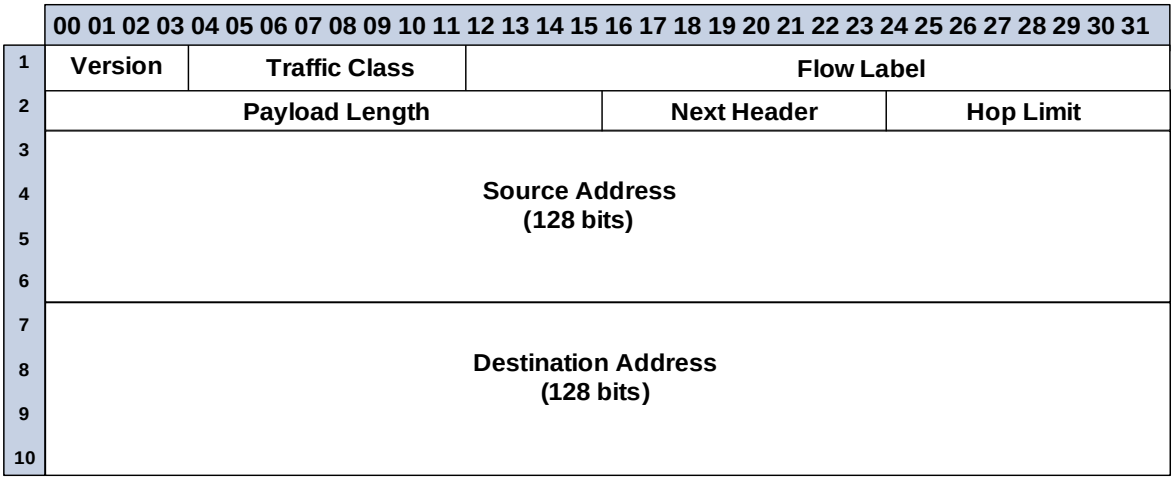

Figure 3: IPv6 Structure

III. Services and Equipments

The "converging" new generation communication networks are using and planning to use an IP based network infrastructure with multi-functional end-devices, always on, always reachable peer-to-peer, with mobility, quality of service and end-to-end security. Even non telecom industries such as music, radio and television will be supported in the IP environment. There are applications that need or will benefit from IPv6 such as:

- Mobile broadband IP;
- Mobile IP broadcast;
- Peer to peer VoIP;
- Digital radio;
- iTV and IPTV;
- Grids;
- P2P multiplayer games;
- RFID;
- Control networks;
- Remote manufacturing systems;
- Sensor networks;
- Microsoft (native support of IPv6 in the next version of Windows – Longhorn).

There are also a few technologies that will support the migration to IPv6 like:

- Power line Communication;
- Wi-Fi;
- Wi-Max;
- ZigBee;
- Unlicensed Mobile Access (UMA).
-

IV. Migration

The current IP-based network will gradually migrate from IPv4 to IPv6. Signaling interworking will need to be supported between the IPv6 network and the existing IPv4 network. Mapping of signaling between IPv6 and IPv4 is required. From the deployment point of view, there are three stages of evolution scenarios:

- First stage (stage 1): IPv4 ocean and IPv6 island;
- Second stage (stage 2): IPv6 ocean and IPv4 island;
- Third stage (stage 3): IPv6 Ocean and IPv6 Island.

There are several migration mechanisms from the IPv4 protocol to IPv6 protocol. The most discussed techniques are:

- Dual stack – to allow IPv4 and IPv6 to coexist in the same devices and networks;
- Tunneling – to avoid order dependencies when upgrading hosts, routers or regions;
- Translation – to allow IPv6 only devices to communicate with IPv4 only devices.

Most of these techniques can be combined in a migration scenario to permit a smooth transition from IPv4 to IPv6. In the following sub-sections, these three techniques are described briefly.

4.1 Dual Stack Technique

In this method it is proposed to implement two protocols stacks in the same device. The protocol stack used for each link depends on the device used at the other end of the link. Figure 4 shows this arrangement.

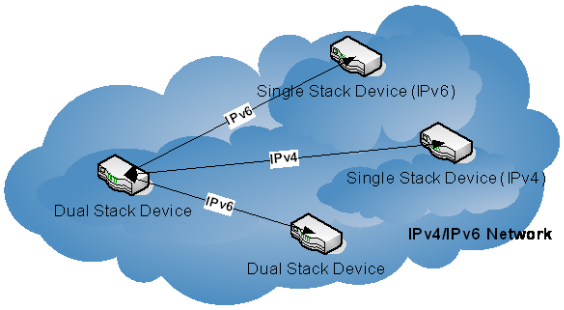

Figure 4: Dual stack operation

4.2 Tunnelling Techniques

Tunneling techniques are used in two phases in the migration to a fully IPv6 network. In the first phase the core of the network uses the IPv4 protocol and there are only small islands IPv6. Figure 5 shows this phase. The IPv6 protocol is encapsulated in IPv4 tunnels.

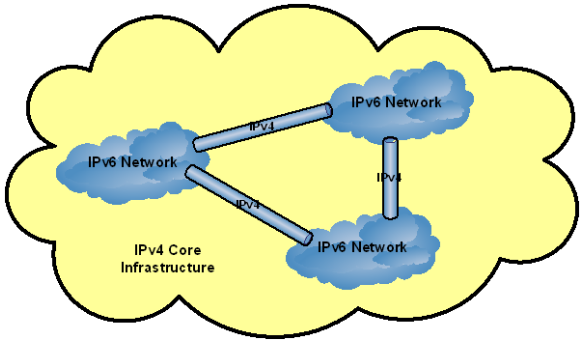

Figure 5: IPv4 Tunneling with islands of IPv6 in and IPv4 core network (phase 1)

In a second phase, when many nodes in the core of the network have already changed to IPv6, the situation is reversed and IPv4 is encapsulated in IPv6 tunnels. The following figure shows this second phase.

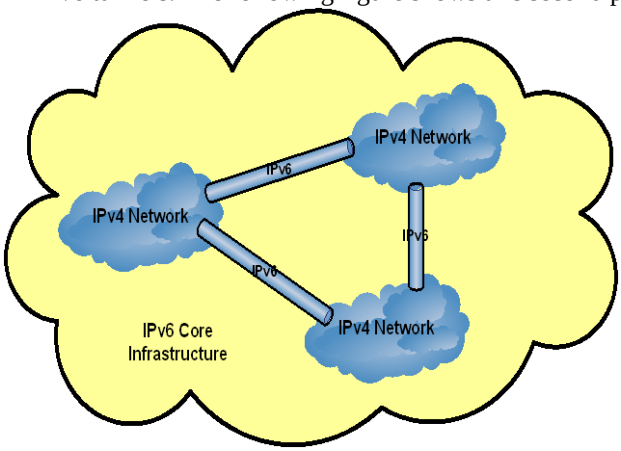

Figure 6: IPv6 Tunneling with islands of IPv4 in and IPv6 core network (phase 2)

4.3 Translation Techniques

This technique uses a device, the NATPT (Network Address Translation – Protocol Translation) that translates in both directions between IPv4 and IPv6 at the boundary between an IPv4 network and an IPv6 network. Figure 7 shows this arrangement.

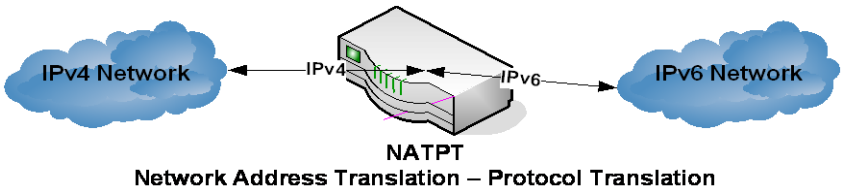

Figure 7: the arrangement with Network Address Translation – Protocol Translation

4.4 Some Proposals

As it was stated before that the solution for the migration from IPv4 to IPv6 will be a combination of the techniques described above.

The most preferable solution on the backbone of the IP Network is the use of the dual stack technique by ISPs and Network operators. This solution is already possible, because almost all hardware providers have already updated the software to support this technique.

In the access network, considering that there are many routers at the user's premises and these routers do not support IPv6 at present, the best solution is the use of the translation technique by access devices. In a further phase is possible to switch to the dual stack technique.

V. Security

"Security is the most common concern with regard to the Internet and to financial transactions via the Internet in particular. Security issues such as authenticating users, controlling access to resources, encrypting communications, and generally ensuring the privacy of transactions all need to be addressed" (European Commission).

The IPv6 is considered to have "Native Security" included by adding different extensions headers in the protocol. This security has the following characteristics:

- It works end-to-end – it is possible to have IPsec services between a pair of hosts; the authentication is separate from the encryption;
- It has an Authentication Header (AH) – this header refers to the entire packet; providing data integrity and authentication and mitigating the replay;
- It has an Encapsulating Security Payload (ESP) Header - encapsulated payload packet (tunnel); providing data integrity and authentication and/or confidentiality; mitigating the replay and limits sniffing when confidentiality is enabled.

Network Address Translation (NAT) appears to add little value in the IPv6 environment. With the increased capacity of addressing, there is no need to continue to use NATs to conserve addresses.

The Firewalls have following functions:

- They enforce uniform policy at perimeter;
- They stop outsiders from performing dangerous operations;
- They provide a check point and scalable, centralized control.

In an IPv6 network end-to-end connectivity, tunneling and encryptions can conflict with this policy. To avoid these limitations, in an IPv6 network it is necessary to combine the firewall functions and the router functions in the same equipment and to locate it in the edge of the private network. See figure 8 below:

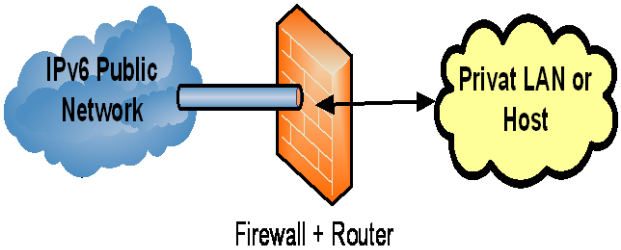

Figure 8: Combined firewall and router

VI. Ipv6 and the Ngn

The current IP network is in a process of transition from IPv4 to IPv6. Mobile access networks are one of the major potential application areas for IPv6. This is mainly due to the large address space of IPv6. Besides, a large percentile of packets in such networks will carry real time traffic such as voice or video. These applications are expected to be important for IPv6, as they may depend heavily on the QoS mechanism in IPv6 networks. Nevertheless 3GPP is considering using IPv4 addresses initially instead of IPv6 addresses.

From the signaling point of view, the IPv6 protocol has many features related to QoS and other capabilities. By utilizing IPv6 features, such as ease of defining explicit route, flow labeling capability and improved support for extensions and options like hop-by-hop option header or destination option header, it is possible to improve the efficiency of IPv6 networks without modifying the existing signaling protocols.

VII. Standards and Tests

The IETF (Internet Engineering Task Force) created a working group to develop the IPv6 protocol. The "IPv6 Working Group" is responsible for the specification and standardization of the Internet Protocol version 6 (IPv6). IETF produced several specifications and protocols; these can be found at the following URL:

http://playground.sun.com/pub/ipng/html/specs/specifications.htm

The core IPv6 standards are widely implemented and are starting to see global deployment.

A European IPv6 Task Force has also been created. Delegates of the different national Task Forces take part. The link for the documents prepared for this TF is showed:

http://www.ec.ipv6tf.org/in/i-documentos.php

Another organization founded to promote de IPv6 protocol and implementation was the IPv6 Forum. IPv6 Forum is a world-wide consortium of leading Internet vendors, Research & Education Networks, with a clear mission to promote IPv6 by dramatically improving the market and user awareness of IPv6, creating a quality and secure Next Generation Internet and allowing world-wide equitable access to knowledge and technology.

To achieve these proposals the IPv6 FORUM will:

- Establish an open, international FORUM of IPv6 expertise;
- Share IPv6 knowledge and experience among members;
- Promote new IPv6-based applications and global solutions;
- Promote interoperable implementations of IPv6 standards;
- Co-operate to achieve end-to-end quality of service;
- Resolve issues that create barriers to IPv6 deployment.

The web site from this forum can be found in:

http://www.ipv6forum.com

The European Commission has been instrumental in providing necessary funding for the research and development of IPv6 related issues. In particular, and in response to the conclusions of the Stockholm Summit, the Commission stepped up its R&D efforts. A large number of IPv6 projects are currently operational, including two large-scale IPv6 trials, namely 6NET and Euro6IX.

These trials are fully complementary to the efforts deployed at national level and at European level in the context of initiatives such as GEANT.

VIII. Possible Actions

In order to complete some of the actions proposed by the Commission and the European Task Force, guidelines should be developed to help the operators and the users gradually take the necessary steps to start the migration to IPv6 and in a near future to adopt the new version of IP protocol (IPv6).

Technical guidance is a valuable way to promote the adoption of IPv6 in public networks and services.

IX. Conclusion

The deployment of IPv6 is important to the future health of the Internet. An average of 4Tbps of traffic per day is seen for a one-year measurement period. This provides a best available estimate of overall IPv6 traffic on the Internet. The dwindling supply of available IPv4 addresses has been broadly documented, as have the challenges faced by those wishing to migrate to IPv6.

In terms of hard data, however, industry and academia have had little visibility into the rate of IPv6 deployment in the Internet.

Providing support for IPv6 in the world is still predominantly IPv4 based. Also, it seems interesting that there is no significant migration of users from IPv4 to IPv6 as per the data. However, the significant growth of IPv4 traffic implies that the usage of IPv6 is also increasing, but at a comparatively slower pace.

References

[1] C. Caicedo, J. Joshi, and S. Tuladhar, "IPv6 Security Challenges", Computer, IEEE Computer Society, February 2009
[2] Bihrouzan A. Forouzan, "TCP/IP Protocol Suite", 4th Edition, McGraw Hill, ISBN: 978- 0-07-337604-2, 2010
[3] C. Balanis, Antenna Theory, Analysis and Design, 3rd edition, New York: Wiley, 2005.
[4] S. Bradner and A. Mankin, "The Recommendation for the Next Generation IP Protocol", RFC 1752, Jan. 1995
[5] Christian Huitema, "IPv6: The New Internet Protocol (2nd Edition)", Jan. 1998.
[6] Andrew S. Tanenbaum,David J. Wetherall,"Computer Networks (5th edition)",Oct. 2010.

Bikki Lakshmi Manasa was born in Guntur District ,Andhra Pradesh, India on 1st August 1992, is currently pursuing B.TECH (4th year) in Electronics and Communication Engineering(ECE) in K.L.University. Areas of interest are Digital Communications, Computer Networks, Antennas and Wave Propagation, VLSI and Digital Signal Processing.

Guttikonda Chaitra Bharti was born in Warangal District ,Andhra Pradesh, India on 23rd February 1992, is currently pursuing B.TECH (4th year) in Electronics and Communication Engineering(ECE) in K L University. Areas of interest are Digital Communications, Computer Networks, Antennas and Wave Propagation, VLSI and Digital Signal Processing.

Mikkili Ramya Teja was born in Guntur District, Andhra Pradesh, India, on 30th may 1992, and is currently pursuing B.TECH (4th year) in Electronics and Communication Engineering (ECE) in K L University. Areas of interest are Digital Communications, Computer networks, Antennas and Wave Propagation and Digital Signal Processing.

Akkela Rama Krishna is working as an Asst. Professor in the department of Electronics and Computers Engineering at K L University. Areas of interest are Artificial Intelligence, Digital Communications and Computer Networks.

International Journal of Modern Engineering Research (IJMER)
www.ijmer.com Vol.3, Issue.2, March-April. 2013 pp-1082-1087 ISSN: 2249-6645

Optimum Relay Selection for Energy-Efficient Cooperative Ad Hoc Networks

Krishna K. Pandey, [1] Nitesh Baghel, [2] Sitesh K. Sinha[3]
[123]*C.S.E. Dept., AISECT University, India*

Abstract: *The Cooperative Communication (CC) is a technology that allows multiple nodes to simultaneously transmit the same data. It can save power and extend transmission coverage. However, prior research work on topology control considers CC only in the aspect of energy saving, not that of coverage extension. We identify the challenges in the development of a centralized topology control scheme, named Cooperative Bridges, which reduces transmission power of nodes as well as increases network connectivity. Prior research on topology control with CC only focuses on maintaining the network connectivity, minimizing the transmission power of each node, whereas ignores the energy efficiency of paths in constructed topologies. This may cause inefficient routes and hurt the overall network performance in cooperative ad hoc networks. In this paper, to address this problem, we studied topology control problem for energy-efficient topology control problem with cooperative communication. We proposed optimum relay nodes selection for CC network to reduce overall power consumption of network.*

Keywords: *Cooperative communication, topology control, power efficient, greedy algorithm, Optimum relay.*

I. INTRODUCTION

Increasing demand for high-speed wireless networks has motivated the development of wireless ad-hoc networks. In order to fully exploit the technological development in radio hardware and integrated circuits, which allow for implementation of more complicated communication schemes, the fundamental performance limits of wireless networks should be reevaluated. In this context, the distinct characteristics of wireless networks compared to their wired counterpart lead to more sophisticated design of protocols and algorithms. Some of the most important inherent properties of the Physical Layer (PHY) that make the design more complicated include the attenuation of radio signals over long range communications called path loss, and the fading effect caused by multipath propagation. In order to mitigate these effects, the user has to increase its transmission power or use more sophisticated reception algorithms. Another important limitation of wireless performance caused mainly as a result of communication over a limited bandwidth is the interference from other users, communicating over the same frequency spectrum.

Wireless ad hoc networks are multi-hop structures, which consist of communications among wireless nodes without infrastructure. Therefore, they usually have unplanned network topologies. Wireless ad hoc networks have various civilian and military applications which have drawn considerable attentions in recent years. One of the major concerns in designing wireless ad hoc networks is to reduce the energy consumption as the wireless nodes are often powered by batteries only. Wireless nodes need to save their power as well as sustain links with other nodes, since they are battery powered. Topology control deals with determining the transmission power of each node so as to maintain network connectivity and consume the minimum transmission power. Using topology control, each node is able to maintain its connection with multiple nodes by one hop or multi-hop, even though it does not use its maximum transmission power. Consequently, topology control helps power saving and decreases interferences between wireless links by reducing the number of links. Topology control [1-4] is one of the key energy saving techniques which have been widely studied and applied in wireless ad hoc networks. Topology control lets each wireless node to select certain subset of neighbors or adjust its transmission power in order to conserve energy meanwhile maintain network connectivity.

Topology control have been widely studied and applied in wireless ad hoc networks as one of the key energy saving techniques. In order to save energy and extend lifetime of networks topology control lets each wireless node to select certain subset of neighbors or adjust its transmission power meanwhile maintain network connectivity. Recently, a new class of communication techniques, cooperative communication (CC) [37], [38], has been introduced to allow single antenna devices to take the advantage of the multiple-input-multiple-output (MIMO) systems. This cooperative communication explores the broadcast nature of the wireless medium and allows nodes that have received the transmitted signal to cooperatively help relaying data for other nodes. Recent study has shown significant performance gain of cooperative communication in various wireless network applications: energy efficient routing [39]–[41] and connectivity improvement [42].

In this paper, we study the energy efficient topology control problem with CC model by taking the energy efficiency of routes into consideration. Taking advantage of physical layer design that allows combining partial signals containing the same information to obtain the complete data, we formally define cooperative energy spanner in which the least energy path between any two nodes is guaranteed to be energy efficient compared with the optimal one in the original cooperative communication graph. We then introduce the energy-efficient topology control problem with CC (ETCC), which aims to obtain a cooperative energy spanner with minimum total energy consumption,

The cooperative communication techniques can also be used in topology control. In [35], Cardei et al. first studied the topology control problem under cooperative model (denote by TCC) which aims to obtain a strongly-connected topology with minimum total energy consumption. They proposed two algorithms that start from a connected topology assumed to be

the output of a traditional (without using CC) topology control algorithm and reduce the energy consumption using CC model. The first algorithm (DTCC) uses 2-hop neighborhood information of each node to reduce the overall energy consumption within its 2-hop neighborhood without hurting the connectivity under CC model. The second algorithm (ITCC) starts from a minimum transmission power, and iteratively increases its power until all nodes within its 1-hop neighborhood are connected under CC model. Observing that the CC technique can also extend the transmission range and thus link disconnected components. In [36], Yu et al. applied CC model in topology control to improve the network connectivity as well as reduce transmission power. Their algorithm first constructs all candidates of bidirectional links using CC model (called cooperative bridges) which can connect different disconnected components in the communication graph with maximum transmission power. Then they apply a 2-layer MST structure (one MST over the CC links to connect the components, the other is inside each component) to further reduce the energy consumption.

II. RELATED WORK

Topology control has drawn a significant amount of research interests in wireless ad hoc networks [6-12]. Primary topology control algorithms aim to maintain network connectivity and conserve energy by selecting certain subset of neighbors and adjusting the transmission power of wireless nodes. Comprehensive surveys of topology control can be found in [1-4].

Cooperative communication (CC) exploits space diversity through allowing multiple nodes cooperatively relay signals to the receiver so that the combined signal at the receiver can be correctly decoded. Since CC can reduce the transmission power and extend the transmission coverage, it has been considered in topology control protocols. However, prior research on topology control with CC only focuses on maintaining the network connectivity, minimizing the transmission power of each node, whereas ignores the energy efficiency of paths in constructed topologies. This may cause inefficient routes and hurt the overall network performance in cooperative ad hoc networks. Paper [43] address this problem, author introduce a new topology control problem: energy-efficient topology control problem with cooperative communication, and propose two topology control algorithms to build cooperative energy spanners in which the energy efficiency of individual paths are guaranteed. Both proposed algorithms can be performed in distributed and localized fashion while maintaining the globally efficient paths.

Cooperative communication (CC) allows multiple nodes to simultaneously transmit the same packet to the receiver so that the combined signal at the receiver can be correctly decoded. Since CC can reduce the transmission power and extend the transmission coverage, it has been considered in topology control protocol. However, prior research on topology control with CC only focuses on maintaining the network connectivity, minimizing the transmission power of each node, whereas ignores the energy-efficiency of paths in constructed topologies. This may cause inefficient routes and hurt the overall network performance. Paper [44] introduces a new topology control problem: energy-efficient topology control problem with cooperative communication, and propose two topology control algorithms to build cooperative energy spanners in which the energy efficiency of individual paths are guaranteed.

Chen and Huang [5] first studied the strongly connected topology control problem, which aims to find a connected topology such that the total energy consumption is minimized. They proved such problem is NP-complete. Several following works [8-12] have focused on finding the minimum power assignment so that the induced communication graph has some "good" properties in terms of network tasks such as disjoint paths, connectivity or fault-tolerance. On the other hand, several localized geometrical structures [13-18] have been proposed to be used as underlying topologies for wireless ad hoc networks. These geometrical structures are usually kept as few links as possible from the original communication graph and can be easily constructed using location information.

Recently, a new class of communication techniques, cooperative communication (CC) [19], [20], has been introduced to allow single antenna devices to take the advantage of the multiple-input-multiple-output (MIMO) systems. This cooperative communication explores the broadcast nature of the wireless medium and allows nodes that have received the transmitted signal to cooperatively help relaying data for other nodes. Recent study has shown significant performance gain of cooperative communication in various wireless network applications: energy efficient routing [21-24], broadcasting [25-27], multicasting [28], connectivity/coverage improvement [29], [30], and relay selection for throughput maximization or energy conservation [31-34].

III. COOPERATIVE COMMUNICATION

Wireless communication technique with a wireless network, of the cellular or ad hoc selection, where the wireless users, may increase their valuable quality of service via cooperation a cooperative communication system, each wireless user is assumed to transmit data as well as act as a cooperative agent for an additional user (Fig. 1).

For example, in figure 1, node S is unable to communicate with node D, since D is out of its maximum transmission range of S. On the other hand, S can send a cooperation request message and data to adjacent connected nodes R as relay node and then the three nodes all together pass on the data to D. Therefore, D can receive it due to the extended transmission range of nodes S, R, and R.

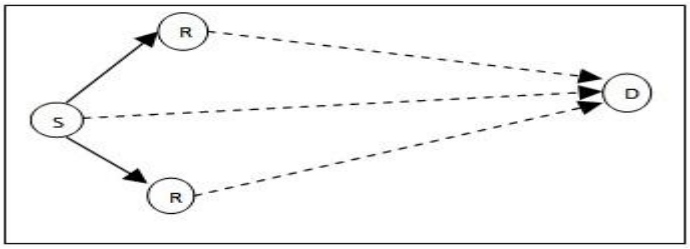

Figure 1: Coverage Extension using CC

Cooperative communication means in any system users share and cooperative their resources to enhance their performance jointly with help of each other. This method is very useful for enhance transmission range of a node in mobile adhoc network as diverse channel quality and limited energy and limited bandwidth limitations wireless environment. Due to cooperation, users that know-how a deep weaken in their connection towards the target can utilize quality channels provided by their partners to achieve the preferred quality of service (QoS). This is also identified like the spatial diversity gain, which is in the same way achieved in multiple-input-multiple-output (MIMO) wireless systems.

Cooperation has an interesting trade-off between code rates and transmit power. In the case of power, extra power is needed because to every user, when system is in cooperative mode, is transmitting for both users. But transmits power for both users will be reduced because of diversity. Due to this trade-off, one hopes for a net reduction of transmit power, given every-thing else being constant.

In cooperative communication every user sends both his/her personal bits as well as a few data for his/her neighbor; one may believe this causes loss of rate in the system. However, the spectral efficiency of each user improves because; due to cooperation diversity the channel code rates are able to be improved. Hence one more trade-off is occurred. So whether cooperation is worth the incurred cost, has been studied positively by numerous research studies.

IV. COOPERATIVE MODEL

Here, we explain a cooperative communication model and a network representation for topology control system. In addition, we define two problems: Topology Control considering Extended Links caused by CC and Energy-Efficient Extended Link with CC.

4.1 Cooperative Communication Model

In Cooperative Communication Model PMAX represents every node's maximum transmission power limit. Pi is the transmission power of node i. α is the path loss exponent and τ is the minimum average SNR for decoding received data. dij is the distance between node i and node j. For a source node i to communicate with node j directly (figure 1), they must satisfy

$$Pi\ (dij)\ -H \geq \tau\ (Pi \leq PMAX).$$

H denotes the set of a source node and helper nodes. If nodes in H transmit simultaneously, i.e., use cooperative communication, the following formula must be satisfied for correct decoding at destination node j.

$$i \in H\ Pi(dij) - H \geq \tau\ (Pi \leq PMAX)$$

CC leads to extended transmission coverage. For example, in figure 1, node S cannot communicate with node D, since D is out of the maximum transmission range of S. Node S can send a cooperation request message and data to nodes R and R, and then the three nodes simultaneously transmit the data to D. Therefore, D can receive it due to the extended transmission range of nodes R, R, and S. The physical layer issues including synchronization for implementing the CC technique can be found in [8]. In figure 1, if node R applies CC with partner S in sort to communicate with D, which is already accessible to R by straight links, the network can decrease the sum of node transmission power. Cardei et al. [26] focus their problem formulation on saving power with CC, not extended CC links.

4.2 Network Model

The wireless network topology is form as a 2-dimensional graph is collection of vertices V and edges E, graph G = (V, E). V = (v1, ..., vn) is a set of random nodes and E is a set of pairs of nodes as link between them (vi, vj), with vi, vj $\in$ V. The notations V (G) and E (G) are used for the vertex- and edge-set of G. The weight of a directional link from u to v is denoted as w (u $\rightarrow$ v). Edge (u, v) has weight, w (u, v), which indicates the average power utilization for maintaining a bi-directional link (u, v). N (v) is the set of neighbor nodes within the maximum transmission range of node v. All elements in N (v) are the candidate nodes, which are eligible as helper nodes for v. Node v is capable to communicate directly with its neighbors within 1 hop. R(u) is the set of nodes which are accessible to node u by 1-hop or multi-hop, i.e., have a path to a node u.

4.3 Problem Formulation

Major difficulty in given a wireless multi-hop network G=(V,E) which is restricted under CC connection model, it that assign transmission power Pi for every node vi such that make topology G' from this power assignment is a cooperative

energy t-spanner of G and the sum of transmission power of all nodes, ∑viεVPi , is minimized. Key point is that the spanner property also guarantees that the induced topology G' is strongly connected under CC model.

Paper [43] presents an Energy-Efficient Topology Control in Cooperative Ad Hoc Networks, but if neighbor nodes are more for any node so they all will help to source node for transmitting data to destination whether only some nodes of them as capable to transmit data till destination so power of other nodes are unnecessarily used during this transmission as given in figure 2.

V. PROPOSED WORK

This paper proposed efficient in two phase first phase is to Energy-efficient topology control with cooperative communication and then optimum relay node selection. First phase propose two topology control algorithms which build energy-efficient cooperative energy spanners. To keep the proposed algorithms simple and efficient, we only consider its one-hop neighbors as possible helper nodes for each node when CC is used [43]. Thus, the original cooperative communication graph G contains all direct links and CC links with one hop helpers, instead of all possible direct links and CC-links. In addition, for each pair of nodes vi and vj, we only maintain one link with least weight if there are multiple links connecting them. Here, all links are directional links. Both proposed algorithms are greedy algorithms. The major difference between them is the processing order of links. The first algorithm deletes links from the original graph G greedily, while the second algorithm adds links into G'' greedily. Here, G00 is a basic connected sub graph of G. Both algorithms can guarantee the cooperative energy spanner property of the constructed graph G'.

5.1 Phase One

5.1.1 Greedy method for Deleting Links from network graph

Step 1: Construction of G. Initially, G is an empty graph. First, add every direct links vivj into G, if node VI can reach node VJ when it operates with PMAX. Then, for every pair of nodes vi and vj, we select a set of helper nodes Hij for node vi from its one-hop neighbors N (vi), such that the link weigh w (vi,vj) of the constructed CC-link is minimized. Notice that this helper node decision problem is challenging even under our assumption that the transmission powers of VI and its helper node set to maintain CC-link are the same. If we try all combinations of the helper sets to find the optimal helper set which minimizes the total energy consumption of vi and its helpers, the computational complexity is exponential to the size of the one-hop neighborhood N (vi). It is impractical to do so in case of a large number of neighbors. Therefore, we directly use the greedy heuristic algorithm Greedy Helper Set Selection (vi, N (vi), vj), to select the helper set Hij. Then, we compare w (vivj) with p (PG(vi,vj)) which is the current shortest path from node vi to node vj in G. If w (vivj) ≤ p (PG (vi,vj)) and

$$\frac{\tau}{\sum_{v_k \in v_i \cup H_{ij}} (d_{kj})^{-\alpha}} \leq P_{MAX},$$

Add this CC-linkg vivj into G. If there already exists a direct link vivj, delete it after the new CC-link g vivj is added (since it costs more energy than the CC-link). Notice that if

$$\frac{\tau}{\sum_{v_k \in v_i \cup H_{ii}} (d_{kj})^{-\alpha}} \leq P_{MAX},$$

Node vi cannot communicate with node vj within one-hop even in CC model.

Step 2: Construction of G'. Copy all links in G to G', and sort them in the descending order of their weights. Start to process all links one by one and delete the link vi vj from G' if G-vivj is still a cooperative energy t-spanner of G.

Hereafter, we use G- e or G+e to denote the graph generated by removing link e from G or adding link e into G, respectively. In addition, when a CC-link g vivj is kept in G', all its helper links must be kept in G' too.

Step 3: Power Assignment from G'. For each node vi, its transmission power is decided by the following equation:

Here $P_i^d(j) = \frac{\tau}{d_{ij}^{-\alpha}}$ and $P_i^{cc}(j) = \frac{\tau}{\sum_{v_k \in v_i \cup H_{ij}} (d_{kj})^{-\alpha}}$ are the energy consumption at vi for a direct link vivj and a CC-link vivj , respectively.

5.1.2 Greedy method for adding Links

The second topology control algorithm starts with a sparse topology G'' which is strongly connected under CC model. We can use the output of the algorithm in [36] as the initial topology. Then, we gradually add the most energy-efficient link into G''. Here, the energy-efficiency of a link is defined as the gain on reducing energy stretch factors by adding this link. Our algorithm will terminate until the constructed graph G' satisfies the energy stretch factor requirement. The detail steps are summarized as follows:

Step 1: Construction of G and G''. The step of constructing G is the same as the one in Algorithm 1. Then, we call the algorithm in [36] to generate G'', a connected sparse sub graph of G.

Step 2: Construction of G'. Initialize G'=G'', for every link vivjεG but not G', compute its stretch-factor-gain g G'G (vivj) as follows:

$$g_G^{G'}(v_i v_j) = \sum_{v_p, v_q \in V} \left(\rho_G^{G'}(v_p, v_q) - \rho_G^{G'+v_i v_j}(v_p, v_q)\right)$$

In other words, the total gain of a link vivj is the summation of the improvement of stretch factors of every pair of nodes in G' after adding this link In each step, we greedily add the link with the largest stretch-factor-gain into G'. If there is

a tie, we use the link weight to break it by adding the link with the least weight. We repeat this procedure until G' meets the stretch factor requirement t.

Step 3: Power Assignment from G'. For every node VI, assign its power level Pi using equation for Pi.

5.2 Phase Two

5.2.1 Optimum relay nodes selection

Once communication topology has been created optimum nodes can be selected from this topology for efficient transmission. As problem definition mention in example in figure 2(a) according to CC model if S sends packets to D which is not in transmission range of S because of power saving fixed transmission range but it can be increase its transmission range with help of its relay nodes and transmit packets. In this example node S uses its all 1-hop neighbors where as other hand only few nodes are enough for sending data till D. hence power of other nodes are useless for this communication if ∑viεVPi for selected neighbors of node S.

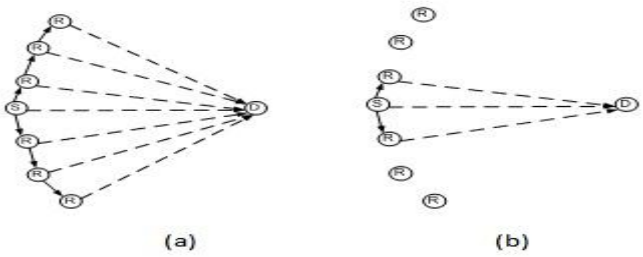

Figure 2: Demonstration to reduce energy consumption in CC ad-hoc network

We propose two topology control algorithms which build energy-efficient cooperative energy spanners. To keep the proposed algorithms simple and efficient, we only consider its one-hop neighbors as possible helper nodes for each node whenCCis used. Thus, the original cooperative communication graph G contains all direct links and CClinks with one hop helpers, instead of all possible direct links and CC-links. In addition, for each pair of nodes vi and vj, we only maintain one link with least weight if there are multiple links connecting them.

VI. CONCLUSION

In this paper, we deliberate a topology control problem in detailed, energy-efficient topology control problem with cooperative communication, which aims to keep the energy-efficient paths in the constructed topology. Also key point has been discussed as in wireless ad-hoc network for effective energy transmission. In this paper, we introduced a new topology control problem: optimum relay selection topology control problem with cooperative communication, which aims to keep the energy efficient paths in the constructed topology and reduce power consumption in network. In future this scheme is implemented and tested in real simulation for result gathering.

This paper proposes novel algorithm for optimum relay selection rather selecting all nodes only those nodes will be selected which are capable for large enough to make transmission range within destination node to save power of other nodes hence overall network power consumption is minimize. Every node also store power level of every neighbor node in routing table with routing information. For transmit data packets relay selection is based on highest power level nodes. The nodes having maximum power level in direct neighbor selected for relay transmission. As given in figure 2(b) proposed algorithm can be given as follow. This will helpful for saving battery power for other nodes in to reduce overall network power consumption.

REFERENCES

[1] R. Rajaraman, "Topology Control and Routing in Ad Hoc Networks: A Survey," SIGACT News, vol. 33, pp. 60-73, 2002.
[2] X.-Y. Li, "Topology Control in Wireless Ad Hoc Networks," Ad Hoc Networking, S. Basagni, M. Conti, S. Giordano, and I. Stojmenovic, eds., IEEE Press, 2003.
[3] C.-C. Shen and Z. Huang, "Topology Control for Ad Hoc Networks: Present Solutions and Open Issues," Handbook of Theoretical and Algorithmic Aspects of Sensor, Ad Hoc Wireless and Peer-to-Peer Networks, J. Wu, ed., CRC Press, 2005.
[4] A.E. Clementi, G. Huiban, P. Penna, G. Rossi, and Y.C. Verhoeven, "Some Recent Theoretical Advances and Open Questions on Energy Consumption in Ad-Hoc Wireless Networks," Proc. Workshop Approximation and Randomization Algorithms in Comm. Networks, 2002.
[5] W.-T. Chen and N.-F. Huang, "The Strongly Connecting Problem on Multihop Packet Radio Networks," IEEE Trans. Comm., vol. 37, no. 3, pp. 293-295, Mar. 1989.
[6] L.M. Kirousis, E. Kranakis, D. Krizanc, and A. Pelc, "Power Consumption in Packet Radio Networks," Theoretical Computer Science, vol. 243, nos. 1/2, pp. 289-305, 2000.
[7] A.E.F. Clementi, P. Penna, and R. Silvestri, "On the Power Assignment Problem in Radio Networks," Proc. Electronic Colloquium on Computational Complexity (ECCC), 2000.
[8] D. Blough, M. Leoncini, G. Resta, and P. Santi, "On the Symmetric Range Assignment Problem in Wireless Ad Hoc Networks," Proc. Second IFIP Int'l Conf. Theoretical Computer Science, 2002.
[9] E. Althaus, G. Caˆlinescu, I. Mandoiu, S. Prasad, N. Tchervenski, and A. Zelikovsly, "Power Efficient Range Assignment in Ad-Hoc Wireless Networks," Proc. IEEE Wireless Comm. and Networking (WCNC), 2003.

[10] R. Ramanathan and R. Hain, "Topology Control of Multihop Wireless Networks Using Transmit Power Adjustment," Proc. IEEE INFOCOM, 2000.
[11] M. Hajiaghayi, N. Immorlica, and V.S. Mirrokni, "Power Optimization in Fault-Tolerant Topology Control Algorithms for Wireless Multi-Hop Networks," Proc. ACM Mobicom, 2003.
[12] J. Cheriyan, S. Vempala, and A. Vetta, "Approximation Algorithms for Minimum-Cost K-Vertex Connected Subgraphs," Proc. Ann. ACM Symp. Theory of Computing (STOC), 2002.
[13] P. Bose, P. Morin, I. Stojmenovic, and J. Urrutia, "Routing with Guaranteed Delivery in Ad Hoc Wireless Networks," Proc. Int'l Workshop Discrete Algorithms and Methods for Mobile Computing and Comm., 1999.
[14] X.-Y. Li, Y. Wang, and W.Z. Song, "Applications of K-local MST for Topology Control and Broadcasting in Wireless Ad Hoc Networks," IEEE Trans. Parallel and Distributed Systems, vol. 15, no. 12, pp. 1057-1069, Dec. 2004.
[15] X.-Y. Li, P.-J. Wan, and Y. Wang, "Power Efficient and Sparse Spanner for Wireless Ad Hoc Networks," Proc. 10th Int'l Conf. Computer Comm. and Networks (ICCCN), 2001.
[16] R. Wattenhofer, L. Li, P. Bahl, and Y.-M. Wang, "Distributed Topology Control for Wireless Multihop Ad-Hoc Networks," Proc. IEEE INFOCOM, 2001.
[17] N. Li, J.C. Hou, and L. Sha, "Design and Analysis of a MST-Based Topology Control Algorithm," Proc. IEEE INFOCOM, 2003.
[18] Y. Wang and X.-Y. Li, "Localized Construction of Bounded Degree and Planar Spanner for Wireless Ad Hoc Networks," Mobile Networks and Applications, vol. 11, no. 2, pp. 161-175, 2006.
[19] N. Laneman, D. Tse, and G. Wornell, "Cooperative Diversity in Wireless Networks: Efficient Protocols and Outage Behavior," IEEE Trans. Information Theory, vol. 50, no. 12, pp. 3062-3080, Dec. 2004.
[20] Nosratinia, T.E. Hunter, and A. Hedayat, "Cooperative Communication in Wireless Networks," IEEE Comm. Magazine, vol. 42, no. 10, pp. 74-80, Oct. 2004.
[21] G. Jakllari, S.V. Krishnamurthy,M. Faloutsos, P.V. Krishnamurthy, and O. Ercetin, "A Framework for Distributed Spatio-Temporal Communications in Mobile Ad Hoc Networks," Proc. IEEE Infocom, 2006.
[22] Khandani, J. Abounadi, E. Modiano, and L. Zheng, "Cooperative Routing in Static Wireless Networks," IEEE Trans. Comm., vol. 55, no. 11, pp. 2185-2192, Nov. 2007.
[23] J. Zhang and Q. Zhang, "Cooperative Routing in Multi-Source Multi-Destination Multi-Hop Wireless Networks," Proc. IEEE INFOCOM, 2008.
[24] Ibrahim, Z. Han, and K. Liu, "Distributed Energy-efficient Cooperative Routing in Wireless Networks," IEEE Trans. Wireless Comm., vol. 7, no. 10, pp. 3930-3941, Oct. 2008.
[25] M. Agarwal, J. Cho, L. Gao, and J. Wu, "Energy Efficient Broadcast in Wireles Ad Hoc Networks with Hitch-hiking," Proc. IEEE INFOCOM, 2004.
[26] J. Wu, M. Cardei, F. Dai, and S. Yang, "Extended Dominating Set and Its Applications in Ad Hoc Networks Using Cooperative Communication," IEEE Trans. Parallel and Distributed Systems, vol. 17, no. 8, pp. 851-864, Aug. 2006.
[27] G. Jakllari, S. Krishnamurthy, M. Faloutsos, and P. Krishnamurthy, "On Broadcasting with Cooperative Diversity in Multi-Hop Wireless Networks," IEEE J. Selected Area in Comm., vol. 25, no. 2, pp. 484-496, Feb. 2007.
[28] F. Hou, L.X. Cai, P.H. Ho, X. Shen, and J. Zhang, "A Cooperative Multicast Scheduling Scheme for Multimedia Services in IEEE 802.16 Networks," IEEE Trans. Wireless Comm., vol. 8, no. 3, pp. 1508-1519, Mar. 2009.
[29] L. Wang, B. Liu, D. Goeckel, D. Towsley, and C. Westphal, "Connectivity in Cooperative Wireless Ad Hoc Networks," Proc. ACM Mobihoc, 2008.
[30] A.K. Sadek, Z. Han, and K.J.R. Liu, "Distributed Relay-Assignment Protocols for Coverage Expansion in Cooperative Wireless Networks," IEEE Trans. Mobile Computing, vol. 9, no. 4, pp. 505-515, Apr. 2010.
[31] Y. Shi, S. Sharma, and Y. Hou, "Optimal Relay Assignment for Cooperative Communications," Proc. ACM Mobihoc, 2008.
[32] Q. Zhang, J. Jia, and J. Zhang, "Cooperative Relay to Improve Diversity in Cognitive Radio Networks," IEEE Comm. Magazine, vol. 47, no. 2, pp. 111-117, Feb. 2009.
[33] Wang, Z. Han, and K.J.R. Liu, "Distributed Relay Selection and Power Control for Multiuser Cooperative Communication Networks Using Stackelberg Game," IEEE Trans. Mobile Computing, vol. 8, no. 7, pp. 975-990, July 2009.
[34] M. Veluppillai, L. Cai, J.W. Mark, and X. Shen, "Maximizing Cooperative Diversity Energy Gain for Wireless Networks," IEEE Trans. Wireless Comm., vol. 6, no. 7, pp. 2530-2539, July 2007.
[35] M. Cardei, J. Wu, and S. Yang, "Topology control in ad hoc wireless networks using cooperative communication," IEEE Trans. on Mobile Computing, 5(6):711-724, 2006.
[36] J. Yu, H. Roh, W. Lee, S. Pack, and D.-Z. Du, "Cooperative bridges: topology control in cooperative wireless ad hoc networks," in IEEE InfoCom, 2010.
[37] N. Laneman, D. Tse, and G. Wornell, "Cooperative diversity in wireless networks: efficient protocols and outage behavior," IEEE Trans.Information Theory, 50(12):3062-3080, 2004.
[38] Nosratinia, T.E. Hunter, and A. Hedayat, "Cooperative communication in wireless networks," IEEE Comm. Magazine, 42(10):74-80, 2004.
[39] Khandani J. Abounadi E. Modiano and L. Zheng, "Cooperative routing in static wireless networks," IEEE Trans. on Communications, 55(11):2185-2192, 2007.
[40] Ibrahim, Z. Han and K. Liu, "Distributed energy-efficient cooperative routing in wireless networks," IEEE Trans. on Wireless Communications, 7(10):3930-3941, 2008.
[41] M. Agarwal, J. Cho, L. Gao, and J. Wu, "Energy efficient broadcast in wireles ad hoc networks with hitch-hiking," in IEEE InfoCom, 2004.
[42] L. Wang, B. Liu, D. Goeckel, D. Towsley, and C. Westphal, "Connectivity in cooperative wireless ad hoc networks," in ACM Mobihoc, 2008.
[43] Ying Zhu, Minsu Huang, Siyuan Chen, and Yu Wang, "Energy-Efficient Topology Control in Cooperative Ad Hoc Networks", IEEE TRANSACTIONS ON PARALLEL AND DISTRIBUTED SYSTEMS, VOL. 23, NO. 8, page 1480-1491, IEEE, 2012
[44] Ying Zhu Minsu Huang Siyuan Chen Yu Wang, "Cooperative Energy Spanners: Energy-Efficient Topology Control in Cooperative Ad Hoc Networks", IEEE, 2010.

International Journal of Modern Engineering Research (IJMER)
www.ijmer.com Vol.3, Issue.2, March-April. 2013 pp-1088-1096 ISSN: 2249-6645

Real-Time Implementation of Multi-Channel Audio Crosstalk Cancellation Using Mixed Single Frequency Delay Line Filtering Algorithm

Chunduri SreenivasaRao, [1] Dhulipalla VenkataRao[2]
[1]*ECE Department, KL University, India*
[2]*Principal, Narsaraopet Institute of Technology, JNT University, India*

Abstract : *To reproduce high fidelity audio sound and spatial reverberation characteristics, it is desired to use the long filter coefficients in audio surround systems. To implement these long filters, the existing frequency domain based techniques such as overlap save method, multi-rate running convolution suffer from more computational complexity. Apart from computational complexity, algorithm delay is another important factor that needs to be reduced in the real time implementation of these systems. In this paper, mixed single frequency delay line filtering technique was proposed to optimize these factors in multichannel audio crosstalk cancellation and showed analytically how the computations are reduced for different multichannel cases. The ability of proposed method is that it provides less computational complexity even at the impulse response lengths of more than 100msec duration. Unlike in existing methods, algorithm delay depends only on processing frame size instead of filter length so that it provides short processing delay. The proposed technique was implemented on 32-bit floating point DSP processor and efficient design is provided to achieve processor level optimization and less implementation complexity. The computational comparison of this method with conventional methods shows that the proposed technique is very efficient for long filters*

Keywords: *Crosstalk Cancellation, FFT, Frequency Delay Line, Mixed Filtering, Overlap Save method.*

I. INTRODUCTION

The objective of 3D audio system is the ability to reproduce high fidelity audio sound at the desired locations by preserving the reverberation characteristics and spatial sound pattern of original audio signal in the reproduced sound. This technology has many spatial audio applications such as home theatre entertainment, gaming, teleconference and remote control. In 1983, Blauert discovered Head Related Transfer Function (HRTF) Technology, which is the measurement of free field sound pressure transformation from a specific location to the ears of the listener. The Headphones use HRTF functions to convolve the input signal in order to reproduce spatial audio pattern [1]. Even though they have excellent channel separation and equalization, they are little bit cumbersome and inconvenient to use when more number of users are enjoying the audio. An alternative to HRTF is the binaural or multichannel based loudspeaker technology that assumes the centered listener at some distance from the loudspeakers. The transmission path equalization is obtained by filtering the input signals with acoustic inversion matrix (AIF), obtained by inverting the acoustic transfer matrix (ATF) that contains the impulse responses of intended and unintended sound paths. To make sure that the unintended sounds are cancelled, the product of AIF and ATF should be unit matrix. This approach is generally applicable to two input sources and is called binaural audio crosstalk cancellation (CTC). When multi-channels (or) sources are involved, this becomes multi-channel audio CTC, where the outputs become the linear combination of filtering with the respective source signal [2][3][4][5][6].

For N audio sources, the outputs are derived as

$$y_L(n) = h_{L1}(n) * x_1(n) + h_{L2}(n) * x_2(n) + \ldots + h_{LS}(n) * x_S(n) = \sum_{i=1}^{S} h_{Li}(n) * x_i(n) \quad (1)$$

$$y_R(n) = h_{R1}(n) * x_1(n) + h_{R2}(n) * x_2(n) + \ldots + h_{RS}(n) * x_S(n) = \sum_{i=1}^{S} h_{Ri}(n) * x_i(n) \quad (2)$$

To obtain such transmission path equalization, the impulse responses of AIF matrix may last for several hundreds of milliseconds, which leads to the requirement of thousands of FIR filter coefficients [5]. This demands more computational power to implement these long filters on real-time DSP processors. To overcome the complexity issues, it is essential to develop new implementation techniques without compromising for performance. The aim of this paper is to investigate the optimized algorithms in order to reduce the computational complexity as well as algorithmic delay.

The general scenario of real-time filtering implementation is that the frame length, L can be chosen as very less than filter length, M. The standard and original approach for the filtering is the time domain convolution, which has the major drawback of more computations and because of this, single DSP processor may not sufficient to support the multi-channel audio CTC for long filtering. On the other hand, frequency domain approaches based on overlap save and overlap add methods that provide less computational complexity. This has the disadvantage of algorithm delay that arises due to the addition of zeros in the impulse responses to make the FFT length as a power of 2.

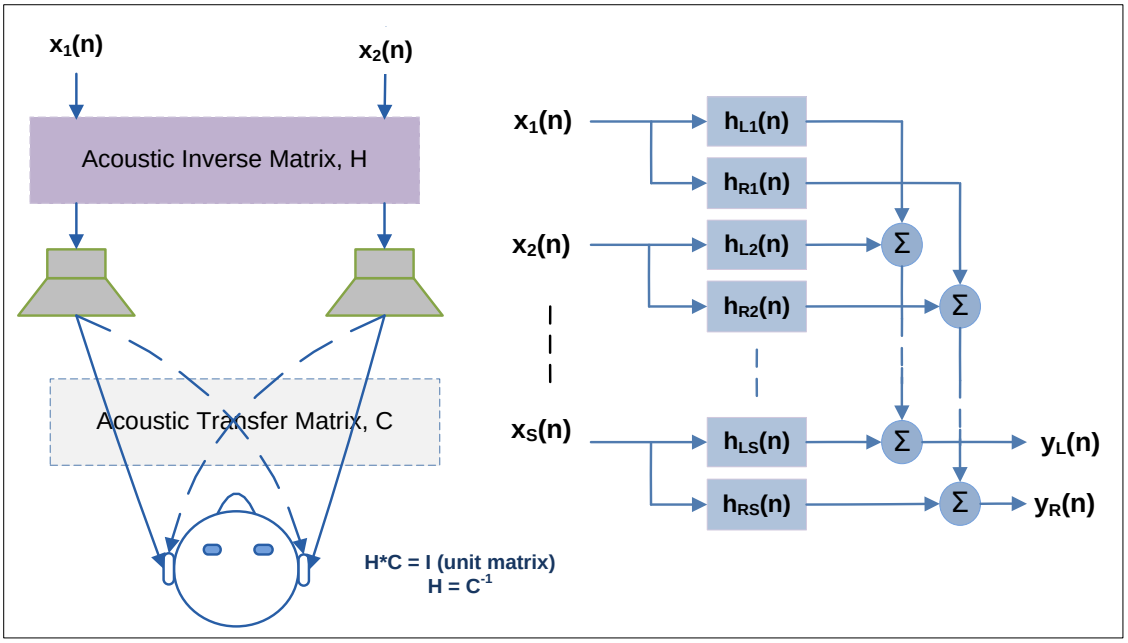

Fig.1.The binaural audio CTC system model (left) describing the perception of filtered audio signals at the listeners' ears (meant for two audio sources). The audio CTC technology with multi-channel sources (right) for real-time implementation point of view

For instance, if the processing frame length is 256 and filter has 1024 coefficients, FFT length becomes 1024 + 256 -1 = 1279. As FFT requires length to be power of 2, the length should be chosen as 2048, which means 1024 zeros are appended to the impulse response and hence the delay of 1024 samples at the output. Hence the sample delay of at least filter length will be introduced at the output [7] [8].

Martin Vetterli proposed multi-rate running convolution algorithm to reduce the delay but no major computational savings can be achieved in this method and also, this technique requires more buffering of data[9][10].

Single frequency Delay Line Filtering (SFDL) efficiently reduces the delay by partitioning the filter length into equal sizes, applying overlap save method to each partition and combining the results of all partitions. This is also called Uniform partitioned convolution as all partitions are of the same size [11][12][13][14]. A brief review of this technique is explained in next Section. If this technique is applied individually to each filter of Fig.1, the implementation complexity is huge and internal DSP memory may not hold all required buffers, particularly for long filters. To avoid such problems, SFDL is combined with mixed filtering [15] in this paper and presented as a new proposed algorithm to reduce computational complexity as well as processing delay. With efficient memory management and the properties of FFT, the proposed technique is very good choice for audio CTC of long filters.

This paper is organized as follows. Section 2 provides the review of mixed filtering and Single Frequency Delay Line Filtering methods. The combination of these two techniques is explained as proposed method in section 3. It also contains theoretical computational complexity, efficient design to avoid more buffer copying routines and better processor level optimization techniques. Section 4 details about the experimental details and results. The computational complexity of proposed method is compared with that of overlap save method. Finally chapter 5 provides the conclusion and future scope to update the proposed method.

II. REVIEW OF EXISTING WORK

In this section, the background details of mixed filtering and single Frequency Delay Line filtering are explained.

II.1 MIXED FILTERING

The word 'Mixed filtering' means all the filtering operations of CTC can be performed in single equation. To understand this, let us form a complex sequence with real-time outputs $y_L(n)$ and $y_R(n)$.

$$y(n) = y_L(n) + jy_R(n) = \sum_{i=1}^{S} [h_{Li}(n) + jh_{Ri}(n)] * x_i(n) \quad (3)$$

The frequency domain representation of above equation is obtained as

$$Y(k) = \sum_{i=1}^{S} H_i(k) X_i(k) \quad (4)$$

$$k = 0,1,...N-1 \quad \& \quad N = L + M - 1$$

where the following assumption made in above equation.

$$H_i(k) = F[h_{Li}(n) + j\,h_{Ri}(n)] \quad \& \quad h_i(n) = h_{Li}(n) + j\,h_{Ri}(n)$$

The implementation procedure is simple. The FFTs of two consecutive source signals are obtained by applying single FFT with decomposition [9] [10]. If the system model has S sources, this step requires 0.25*S*O(N) complex multiplications and 0.5*S*(O(N)+2N) complex additions. The 2nd step is implementation of equation (4) i.e. complex frequency multiplication and addition, which requires S*N complex multiplications and (S-1)*N complex additions. Finally 3rd step requires single IFFT computations i.e. 0.5*O(N) complex multiplications and O(N) complex additions. The real and imaginary components of IFFT output yield $y_L(n)$ and $y_R(n)$ respectively. This complexity is applicable for even number of sources. For odd sources, FFT decomposition is not needed as imaginary term will be zero. In Reference [15], mixed filtering was explained for two channel sources. Here, this technique is adapted for multichannel source case.

II.2 SINGLE FREQUENCY DELAY LINE FILTERING

In overlap save method, the FFT size is chosen as N = L+M-1 in order to represent the samples of the spectrum uniquely at discrete set of frequencies. Also, N must be a power of 2. Due to this, overlap save method provides output samples delay of at least filter length, M. If filter length is M = 8192 and the system is operating at 48 kHz sampling frequency, this method provides a delay of 170.67msec (8192/48000), which is not acceptable in real time audio applications. Also, as FFT length increases, this method suffers from computational complexity. These issues are efficiently solved in single frequency delay line filtering. This method relies on partitioning the filter impulse response into equal sizes so that the overlap save method can be applied on each partition and finally the outputs of each partition will be summed to yield the filter output. This method can be understood with the following explanation [11][12][13][14].

Let us assume that x (n), h (n) and y (n) be the input, impulse response and outputs of an LTI system respectively. The lengths of input frame and filter are L and M. The impulse response is partitioned into number of parts m = M/L so that each partition has L samples.

In z-domain, the impulse response is expressed as

$$\begin{aligned} H(z) &= \sum_{n=0}^{N-1} h(n)z^{-n} = \sum_{n=0}^{L-1} h(n)z^{-n} + \sum_{n=L}^{2L-1} h(n)z^{-n} + \ldots + \sum_{n=M-L}^{M-1} h(n)z^{-n} \\ &= \sum_{n=0}^{L-1} h(n)z^{-n} + z^{-L}\sum_{n=0}^{L-1} h(n+L)z^{-n} + \ldots + z^{-(M-L)}\sum_{n=0}^{L-1} h\left(n+\overline{M-L}\right)z^{-n} \\ &= \sum_{n=0}^{L-1}\left[h_0(n) + z^{-L}h_1(n) + \ldots + z^{-(M-L)}h_{m-1}(n)\right]z^{-n} \end{aligned} \quad (5)$$

Where

$$\left.\begin{aligned} h_0(n) &= h(n), \\ h_1(n) &= h(n+L), \\ &\ldots \\ h_{m-1}(n) &= h(n+M-L), \end{aligned}\right\} \quad n = 0,1,..L-1 \quad \& \quad m = M/L \quad (6)$$

These are called partitioned impulse responses of equal length, L. The total partitions are M/L.
The output in z-domain is expressed as

$$\begin{aligned} Y(z) = H(z)X(z) &= \sum_{n=0}^{L-1}\left[h(n) + z^{-L}h(n+L) + \ldots + z^{-(M-L)}h\left(n+\overline{M-L}\right)\right]X(z)z^{-n} \\ &= X(z)\sum_{n=0}^{L-1} h_0(n)z^{-n} + z^{-L}X(z)\sum_{n=0}^{L-1} h_1(n)z^{-n} + \ldots + z^{-(M-L)}X(z)\sum_{n=0}^{L-1} h_{m-1}(n)z^{-n} \\ &= X(z)H_0(z) + \underline{z^{-L}X(z)}H_1(z) + \ldots + \underline{z^{-(M-L)}X(z)}H_{m-1}(z) \end{aligned} \quad (7)$$

From the above equation, output, Y (z) is expressed as sum of all partitioned outputs. For 1st frame, the FFT is calculated for x (n). When 2nd frame arrives, FFT of x (n) is delayed by L samples and become the input to 2nd partitioned filter. During 3rd frame, FFT of 2nd frame becomes the input to 2nd partitioned filter and FFT of 1st frame becomes the input to 3rd partitioned filter. In this way, only frequency samples of input frames will be delayed and they are summed after complex frequency multiplication with the respective FFTs of partitioned filters before acting as input to IFFT. As FFT values of input samples are delayed and all delays are equal in size, this technique is single frequency delay line filtering. A

block diagram of this method is shown in Fig.2. As overlap save method is applied to each partitioned filter, the FFT size of each filter is derived as L + L -1 = 2L as length of each partitioned filter now becomes L. So, it is required to append zeros of length, L, results in output sample delay of L. Hence the delay is reduced from M to L. For our example, the output sample delay becomes 5.33msec (256/48000) for a frame length of 256 samples.

For each frame, one FFT and one IFFT of size 2L are required. The frequency multiplier length is 2L. Such frequency multipliers are m = M/L and hence complex multiplications of *2L*.M/L = 2M are needed. All frequency multipliers have to be added before providing as input to IFFT and hence 2L (m-1) = 2(M - L) complex additions are required.

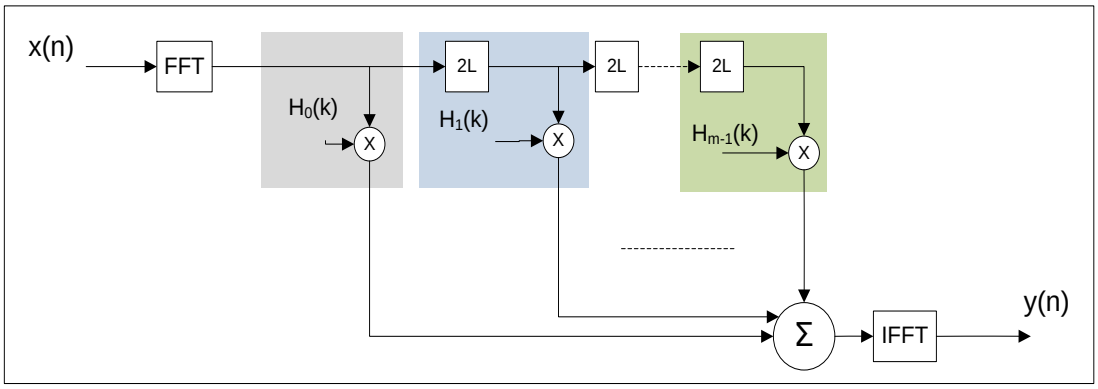

Fig.2. Interpretation of SFDL using block diagram representation. A delay of L samples become 2L samples in FFT domain due to the FFT length N= L+L-1≈2L.

III. MIXED SINGLE FREQUENCY DELAY LINE FILTERING ALGORITHM

The proposed algorithm is the combination of mixed filtering and SFDL applied to multi-channel audio CTC structure of Fig1. The mathematical model of this is derived as follows. Note that the mathematical model was provided in z-domain and the computational complexity is provided in FFT domain for easy understanding and clarity.

Let us assume that the CTC model has S number of sources with each source is filtered by complex impulse response of length, M. The complex impulse response and its frequency response are represented as

$$h_i(n) = h_{Li}(n) + j\,h_{Ri}(n), \qquad i = 1,2,...S \tag{8}$$

and

$$H_i(z) = \sum_{n=0}^{M-1} h_i(n) z^{-n}, \quad i = 1,2,...S \tag{9}$$

Now each impulse response is partitioned into m=M/L parts of equal length, say, L. The partitioned impulse responses are represented by

$$h_i(n) = \{h_{i,0}(n), h_{i,1}(n), .. h_{i,m}(n)\}, \qquad i = 1,2,...S \tag{10}$$

And their frequency responses are given by

$$H_{i,j}(z) = \sum_{n=0}^{L-1} h_{i,j}(n) z^{-n}, \qquad i = 1,2,...S \quad \& \quad j = 0,1,...m-1 \tag{11}$$

The output complex frequency response is obtained by placing equation (11) in equation (7)

$$\begin{aligned} Y(z) &= \sum_{i=1}^{S} H_i(z) X_i(z) \\ &= \sum_{i=1}^{S} X_i(z) H_{i,0}(z) + \underline{z^{-L} X_i(z)} H_{i,1}(z) + \ldots + \underline{z^{-(M-L)} X_i(z)} H_{i,m-1}(z) \\ &= \sum_{i=1}^{S} \sum_{j=0}^{M/L-1} \left[z^{-jL} X_i(z) \right] H_{i,j}(z) \end{aligned} \tag{12}$$

For the case of stereo channel inputs, S=2. For this case, equation (12) becomes

$$Y(z) = \sum_{j=0}^{M/L-1} \left[z^{-jL} X_1(z) \right] H_{1,j}(z) + \sum_{j=0}^{M/L-1} \left[z^{-jL} X_2(z) \right] H_{2,j}(z) \qquad (13)$$

The implementation model can be represented in block diagram as shown in Fig. 3. The SFDL filtering algorithm can be applied to each input and the associated complex impulse response. After addition of complex frequency multiplier outputs of each partitioned filter, a single IFFT is sufficient to provide the filtered outputs yL(n) and yR(n) in real and imaginary parts of output y(n).

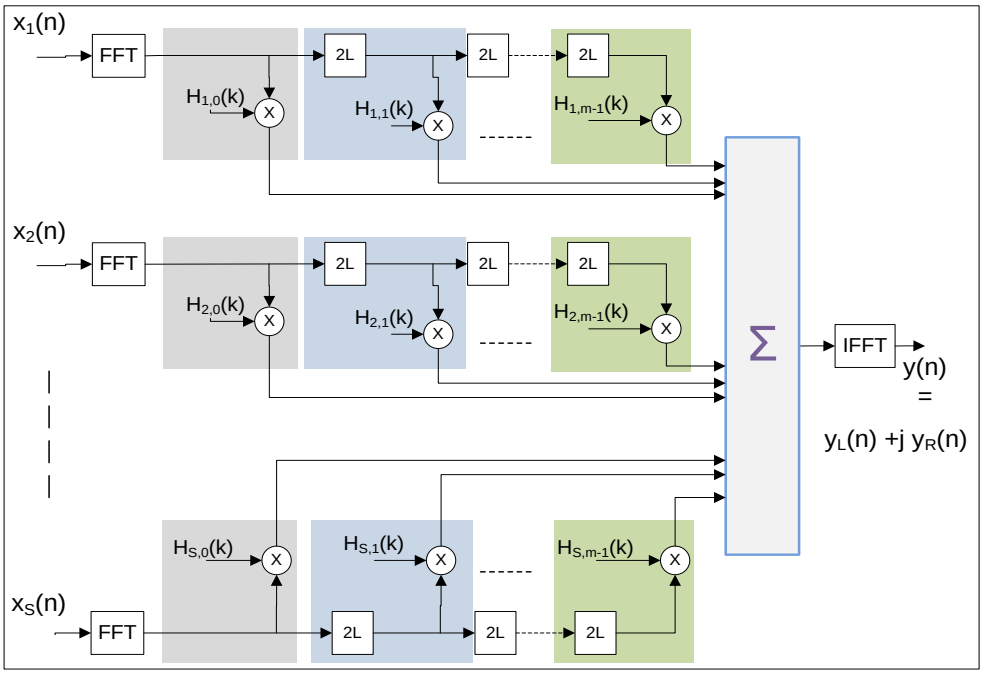

Fig.3. Block diagram of Mixed SFDL filtering algorithm

III.1 THEORETICAL COMPUTATIONAL COMPLEXITY

The following table provides the details of computations required for proposed algorithm. Note that $O(N)=N.\log_2 N$. Initially the computations are shown for a pair of input sources and the associated complex impulse responses. In Remarks column, this is generalized for S number of sources.

Table 1**:** Computational complexity of MSFDL algorithm

To calculate	Computational complexity		Remarks
	Complex multiplications	Complex additions	
$X_i(k)$ & $X_{i+1}(k)$	0.5 O(2L)	O(2L) + 4L	FFTs of two consecutive sources can be found using single FFT with decomposition [7]. When S is even, complex multiplications = 0.25*S*O(2L) complex additions = 0.5*S*(O(2L) + 4L). When S is odd, decomposition is not required for the last source when calculating its FFT as imaginary term of input becomes zero. complex multiplications = 0.25*(S-1)*O(2L)+0.5*O(2L) complex additions = 0.5*(S-1)*(O(2L) + 4L) +O(2L).
$X_i(k)H_i(k)$	2L * M/L = 2M	2(M-L)	This computation is needed for one input source with the associated filters. Each Partitioned frequency multiplication requires 2L multiplications. Such partitions are M/L and hence 2M complex multiplications are needed. All partitioned multiplier outputs are to be added, which requires 2(M-L) complex additions. For S sources, complex multiplications = 2*S*M complex additions = 2*S*(M-L).
Y(k)	-	(S-1)*2L	This is required due to the addition of individual FFT outputs. Equation (12) can be taken as reference for this calculation.
y(n)	0.5*O(2L)	O(2L)	This computation is required for IFFT calculation.

For even Sources,

Complex multiplications = 0.25*S*O (2L) + 2*S*M + 0.5*O (2L)
Complex additions = 0.5*S*(O (2L) + 4L) + 2*S*(M-L) + (S-1) *2L + O (2L)

For odd Sources,

Complex multiplications = 0.25*(S-1)* O (2L) + O (2L) + 2*S*M
Complex additions = 0.5*(S-1)*(O (2L) + 4L) + 2*O (2L) + 2*S*(M-L) + (S-1) *2L

IV. EFFICIENT MEMORY MANAGEMENT OF MSFDL FILTERING ALGORITHM

From the algorithm described so far, a lot of memory is required for storing FFT values of filter coefficients corresponding to all channels and for frequency delay buffers. If the filter length is 2048 and all the coefficients are stored in 32-bit floating point format, 32864 bytes of memory is needed for real and imaginary buffers, 16384 bytes for each. Also same size of memory is required for frequency delay buffers. This is needed for support of one input channel. Then we can imagine how much memory is required to support multi-channel cases. Most of the processors are available with less internal RAM memory and more memory with external RAM such as SDRAM, SRAM, etc. Because of less internal RAM, it is not possible to store these buffers in internal DSP memory. The major implementation complexity is involved in complex frequency multiplication as shown in Fig. 3. When implementing this method on real-time DSP processors, memory buffers should be managed efficiently without an increase in computational complexity. From here on, the word 'complex buffer' is used to represent the combination of real and imaginary buffers in the explanation.

Any DSP processor has a dedicated memory bus for DMA process. Using DMA, it is possible to copy the external memory contents into internal RAM based on processing needs. In this paper, the design was explained based on the architecture of SHARC DSP processor. SHARC 214xx series DSP has 5MB of internal memory and 64MB SDRAM. It is almost similar for any floating point processor.

In implementation of complex frequency multiplication for each partition, two complex buffers of size (one buffer of delayed frequency buffer and another one is FFT of filter coefficients), 2L are required in the proposed algorithm. Assume that the FFT values of all complex filters are stored in external RAM. For each partition, real and imaginary buffers are arranged in sequential order i.e. 2L size real buffer followed with 2L imaginary buffer of 1st partition and the same order of buffers for 2nd partition and so on. In the same way, the frequency delay buffers are also arranged in independent memory section of external RAM.

For processing needs, assume that two dedicated memory sections are reserved for real and imaginary buffers as shown in Fig. 4. Initially, the complex buffers of (m-1)th partition and that of 1st input frame are copied into one set of internal dedicated memory sections using DMA process. After this copying is completed, DMA process is enabled for copying the complex buffers of (m-2)th partition and 1st delayed complex input frame buffers into 2nd set of dedicated memory sections. As both memory sections are independent in external RAM, two separate channels are allocated for DMA copying process, say channel 0 for complex buffers of filters and channel 1 for delayed complex input frame buffers. During DMA process, the DSP starts its complex frequency multiplication on its core. So, both operations are performed in parallel. The execution time here is equal to the maximum of DMA process and core process. Once core process is completed, DMA also has to be verified for its completion. After DMA is completed, again it is configured to copy the (m-3)th partitioned complex frequency buffers and 2nd delayed complex input frame buffers into first set of dedicated memory sections. When DSP starts its core process, DMA copying is going on separate memory bus. After copying is over, DMA is verified for completion. In this way, the dedicated memory sections are filled alternatively with external complex buffers. This will be continued till all partitions are completed and repeated for all channel contents.

The high level summary of the implementation steps are provided below.

During initialization,

Calculate the FFTs of all partitioned filters with FFT size of 2L each. Repeat the same process for all filter sets based on the input source. Store these FFT values in external memory in the sequence shown in Fig. 4.

For each frame,

1) Receive the 1st input frame of size L samples of channel 1 and 2. Calculate their FFTs using complex FFT with decomposition. Store these FFT values in the external memory buffers using DMA process
2) Fill output buffer with zero contents to store the real and imaginary outputs of complex frequency multiplication (CFM).
3) Copy the complex buffers of filters and that of input frames into internal dedicated memory sections using DMA process. Verify for DMA completion.
4) Now again enable DMA process to copy next partition's complex buffers and 1st delayed buffer contents into 2nd dedicated internal memory sections. Start the core process to compute CFM of 1st set dedicated memory buffer contents.
5) After core process is completed, verify for DMA completion.
6) Continue steps 3 and 4 till all partitions are completed with the alternative internal memory sections to be used for storing complex buffer contents. For each iteration, make sure to add the complex output of CFM with that of output.
7) Repeat steps 1 to 5 for all input sources
8) After CFM of all sources is completed, calculate the IFFT for the output and send the real and imaginary buffer contents of size L samples as filtered contents.

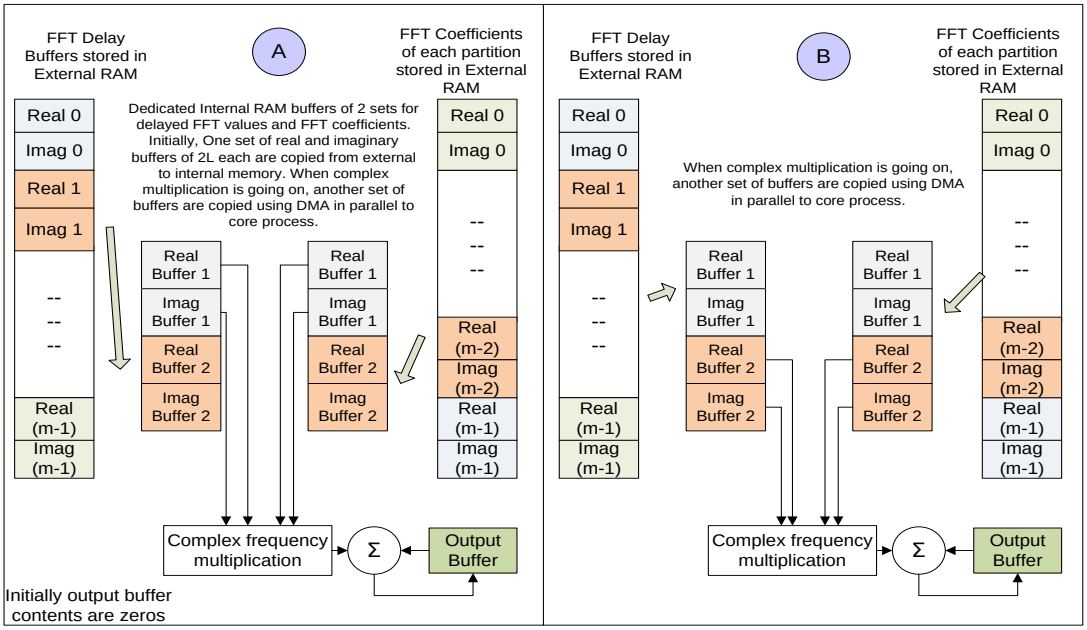

Fig.4. Block diagram showing the efficient Memory management for Mixed SFDL filtering on SHARC DSP processors using DMA processing. The diagram shows the processing for just initial two frames. The output buffer is initially filled with zeros before starting complex frequency multiplication. This is applicable for one input source with the associated complex buffers. The same is repeated for S number of sources in general.

V. EXPERIMENTAL RESULTS AND DISCUSSION

The proposed algorithm "Mixed Single Frequency Delay Line filtering" was implemented on ADSP SHARC 21469 Ez-Kit Lite board [16] as per the procedure stated in section IV. The frame length was taken as L = 256. The frequency multiplication was implemented efficiently with 4 parallel instructions inside the loop and making use of SIMD (Single Instruction Multiple Data). For FFT & IFFT, the built-in FFT software modules (available with installation package) were used.

During DMA process, it is required to make sure that the execution times of DMA and core process (i.e. complex frequency multiplication) are almost same. DMA execution is dependent on the buffer size to be copied (Here it is 4L in size i.e. for real and imaginary buffers) and the clock ratio of DSP and external RAM. The core process was optimized to make sure that its execution time should not exceed that of DMA process by making use of multiply add and SIMD (Single Instruction multiple data) instructions in SHARC architecture. The acoustic filter lengths from 1024 to 16384 with a step of 512 were considered as filter lengths. The computational complexity in terms of Mega Peak cycle count was recorded for different input channels. The Mega Peak cycle count at various filter lengths for different input channels was given in Table 2.

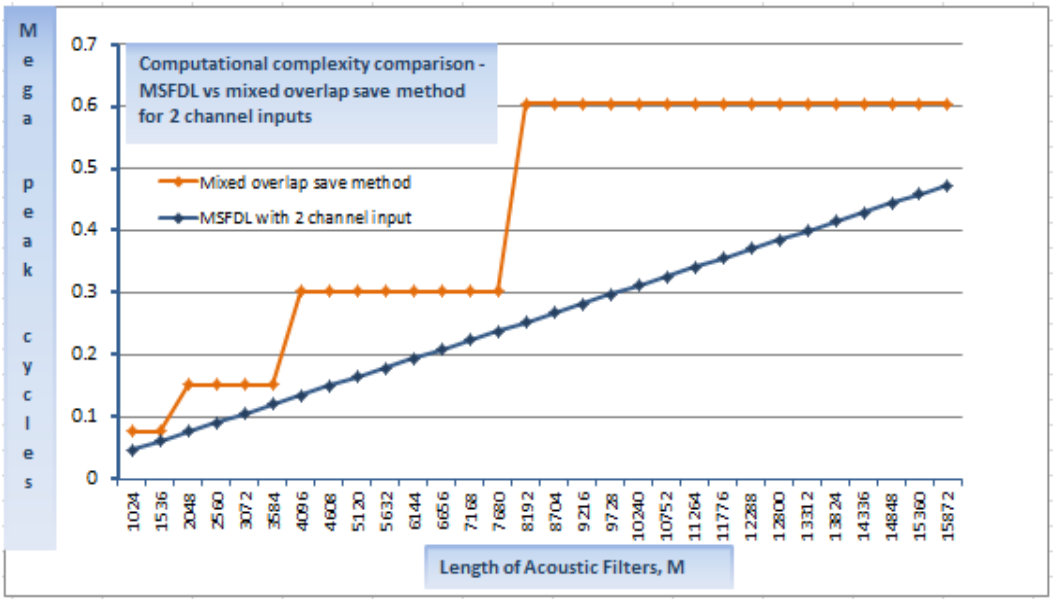

Fig.5. Graph showing the comparison of computational complexity between Mixed overlap save method and MSFDL algorithm for different filter lengths with stereo channel inputs. The frame length of the experiment is 256.

The same experiment was done with mixed overlap save method for stereo inputs. The comparison of computational complexity of this method and that of proposed method was shown in Fig. 5. From the graph, the mixed overlap save method obviously needs more computations than that of proposed method. Also, the curve resembles the staircase and sudden increase in computational complexity at power of 2 filter lengths and maintained the same complexity till next power of 2. This is expected because FFT/IFFT size is derived as N = L+M-1 in overlap save method. If N is not a power of 2, it will be chosen as next immediate power of 2.

Table 2**:** MSFDL algorithm - Mega Peak cycle count at different filter lengths with various input channels. The frame length was taken as 256.

Length of Acoustic filters, M	Mega Peak cycle count (rounded to 5 digits after decimal point)			
	2ch input	3ch input	4ch input	5ch input
1024	0.04594	0.06693	0.08393	0.10491
1536	0.06069	0.08905	0.11342	0.14178
2048	0.07543	0.11117	0.14291	0.17864
2560	0.09018	0.13329	0.17241	0.21550
3072	0.10492	0.15540	0.20189	0.25237
3584	0.11967	0.17752	0.23138	0.28923
4096	0.13442	0.19964	0.26087	0.32609
4608	0.14916	0.22176	0.29036	0.36296
5120	0.16391	0.24388	0.31986	0.39982
5632	0.17865	0.26605	0.34935	0.43669
6144	0.1934	0.28811	0.37884	0.47355
6656	0.20814	0.31023	0.40833	0.51042
7168	0.22289	0.33235	0.43782	0.54728
7680	0.23764	0.35447	0.46731	0.58414
8192	0.2524	0.37659	0.49680	0.62101

Length of Acoustic filters, M	Mega Peak cycle count (rounded to 5 digits after decimal point)			
	2ch input	3ch input	4ch input	5ch input
8704	0.26713	0.39870	0.52629	0.65787
9216	0.28187	0.42082	0.55579	0.69474
9728	0.29662	0.44294	0.58528	0.7316
10240	0.31136	0.46506	0.61477	0.76846
10752	0.32611	0.48718	0.64426	0.80533
11264	0.34085	0.5093	0.67375	0.84219
11776	0.3556	0.53141	0.70324	0.87906
12288	0.37035	0.55355	0.73273	0.91592
12800	0.38509	0.57565	0.76222	0.95278
13312	0.39984	0.59777	0.79171	0.98965
13824	0.41458	0.61989	0.82121	1.02651
14336	0.42933	0.64201	0.85069	1.06338
14848	0.44407	0.66412	0.88019	1.10024
15360	0.45882	0.68624	0.90968	1.13710
15872	0.47356	0.70836	0.93917	1.17397
16384	0.48831	0.73048	0.96866	1.21083

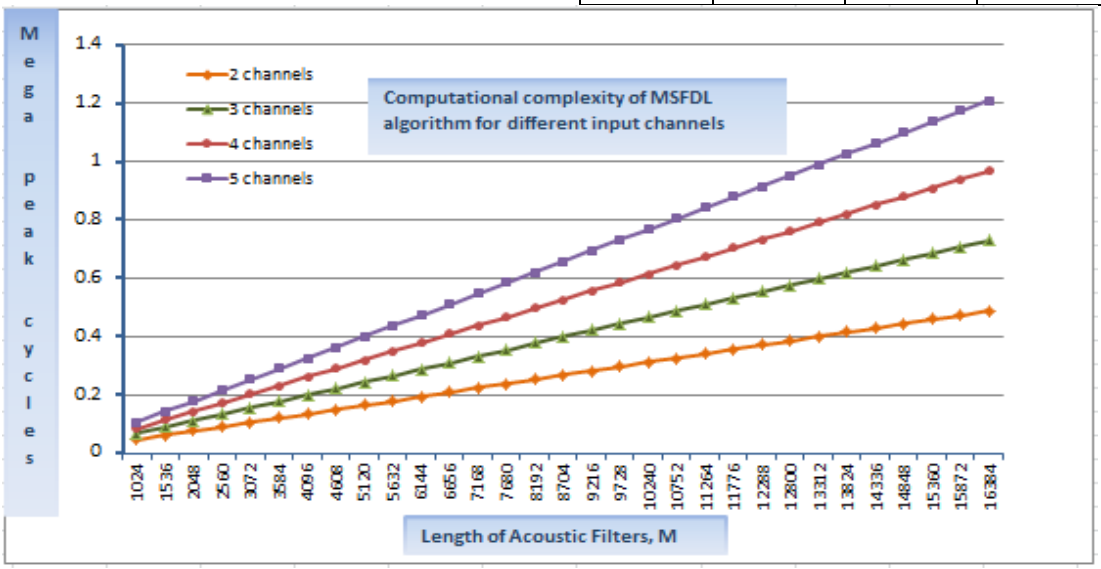

Fig.6. Graph showing the comparison of computational complexity of MSFDL algorithm for different filter lengths with various input sources. The frame length of the experiment is 256.

The variation of computational complexity for different input sources was provided in Fig.6. The graph shows linear relationship between the filter length and the computational complexity with increase in slope as number of sources is increased. This is expected because as number of sources is increased, the computations in complex frequency multiplication as well as number of FFTs will be increased.

The reason behind choosing floating point processor for implementation is because of the algorithm implementation complexity and computations. In high end applications such as audio surround systems, fixed point processors are not encouraged due to the lack of output quality.

VI. CONCLUSION

An efficient algorithm for the implementation of multichannel audio crosstalk cancellation was presented in this paper by combining the techniques of mixed and single frequency delay line filtering techniques as MSFDL algorithm. To reduce memory issues on DSP processors during implementation, efficient design was provided by utilizing the resources of DSP processor. The results were compared against mixed overlap save method for various filter lengths and these indicate that the proposed technique yields better results, particularly, at long filter lengths. Also the variation of computational complexity for different input sources were shown clearly.

The future scope of this work is mixed multiple frequency delay line filtering, in which the impulse response is partitioned non-uniformly and all non-uniform filters run in parallel. This requires multicore DSP for implementation point of view and suitable for filter lengths more than 16384. The main computations of the proposed algorithm are in complex frequency computation block. One can investigate on the methods related to this area to reduce computations. Also it is better to investigate on suitable frequency domain methods other than FFT based techniques. Not only algorithm optimization is enough but processor level optimization is also very important to achieve good computational complexity. For this, suitable DSP processor should be chosen to handle parallel instructions.

REFERENCES

[1] Blauert J., Spatial Hearing: The Psychophysics of Human Sound Localization, MIT Press, Cambridge, 1983.
[2] M. Otani and S. Ise, Fast calculation system specialized for head-related transfer function based on boundary element method, Journal of Acoustical Society of America, Vol. 119, 2006, No. 5, 2589-2598
[3] Kirkeby ole, Rubak Per, Nelson Philip A. and Farina Angelo, Design of Crosstalk cancellation Networks by using Fast deconvolution, Audio Engineering Society 15, May 1999, 9900 – 9905
[4] Lentz Tobias and Scmitz Oliver, Adaptive Cross-talk cancellation system for a moving listener, AES 21st International Conference Proc., June 2002. Paper No. 00134
[5] Linwang, Fuliang Yin and zhe Chen, A Stereo Crosstalk cancellation system based on common- acoustical pole/zero model, AES, August 2010
[6] William G. Gardner, 3-D Audio Using Loudspeakers, School of Architecture and Planning, Massachusetts Institute of Technology, September, 1997
[7] John G. Proakis and Dimitris G. Manolakis, Digital Signal Processing Principles, Algorithms and Applications, (New Jersey, Prentice Hall International, 3rd Edition, Page No. 430 to 476)
[8] Richard G Lyons, Understanding Digital Signal Processing, (New Jersey, Prentice Hall International, 3rd Edition, published on November 11, 2010).
[9] M.Vetterli, Running FIR and IIR Filters using Multi-rate Filter Banks, IEEE transactions on Acoustics, Speech and Signal Processing, Vol. 36, No.5, May 1988.
[10] Jason R. VandeKieft, Computational improvements to linear convolution with multi-rate filtering methods, April 30, 1998, http://mue.music.miami.edu/thesis/jvandekieft/jvtitle.htm.
[11] Garcia Guillermo, Optimal Filter Partition for efficient Convolution with short input/output Delay, AES 113th International Conference Proc., October 2002, pp. 2660.
[12] WG Gardiner, Efficient Convolution without input-output delay, Journal of AES, Vol. 43, No. 3, 1995, pp. 127-136.
[13] J. Hurchalla, A time distributed FFT for efficient low latency convolution, AES Convention 129, November 2010, Paper No.8257
[14] J. Hurchalla, Low latency convolution in one dimension via two dimensional convolutions-An intuitive approach, AES Convention 125, October 2008, Paper No. 7634
[15] SreenivasaRao. Ch, R. Udayalakshmi and Jeyasingh P., Fast implementation of audio crosstalk cancellation of audio crosstalk cancellation on DSP processors, AES 45 Conference Proc., March 1-4, 2012, Paper No. 2-2
[16] Analog Devices Inc., "ADSP-214xx SHARC Processor Hardware Reference Manual", Rev 0.3, Part Number 82-000469-01, July 27, 2010.

International Journal of Modern Engineering Research (IJMER)
www.ijmer.com Vol.3, Issue.2, March-April. 2013 pp-1097-1099 ISSN: 2249-6645

Analysis of Flywheel

Akshay P. Punde, [1] G.K.Gattani[2]
[1]*Student, M.E. [CAD/CAM] Department of Mechanical Engineering Babasaheb Naik college of Engineering, Pusad,*
[2]*Associate Professor Department of Mechanical Engineering BNCOE, Pusad (445215), S.G.B.A.U. Amravati (MS)*

Abstract: In present investigation, to counter the requirement of smoothing out the large oscillations in velocity during a cycle of a I.C. Engine, a flywheel is designed, and analyzed. By using Finite Element Analysis are used to calculate the stresses inside the flywheel, we can compare the Design and analysis result with existing flywheel

Keywords: *flywheel, stress analysis, FE analysis*

I. Introduction

A flywheel is an inertial energy-storage device. It absorbs mechanical energy and serves as a reservoir, storing energy during the period when the supply of energy is more than the requirement and releases it during the period when the requirement of energy is more than the supply A flywheel used in machines serves as a reservoir which stores energy during the period when the supply of energy is more than the requirement and releases it during the period when the requirement of energy is more than supply.

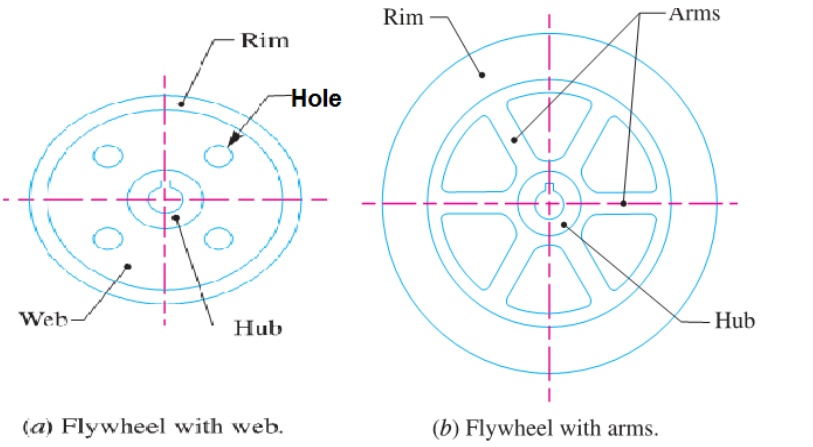

Fig-1 Types of flywheel

II. Literature Review

Literature review is an assignment of previous task done by some authors and collection of information or data from research papers published in journals to progress our task. It is a way through which we can find new ideas, concept. There are lot of literatures published before on the same task; some papers are taken into consideration from which idea of the project is taken.

In 2005 JohnA.Akpobi & ImafidonA.Lawani [1] have proposed, a computer-aided-designs of software for flywheels using object-oriented programming approach of Visual Basic. The various configurations of flywheels (rimmed or solid) formed the basis for the development of the software. The software's graphical features were used to give avisual interpretation of the solutions. The software's effectiveness was tested on a number of numerical examples, some of which are outlined in this work.

In 2012 Sushama G Bawane, A P Ninawe and S K Choudhary had proposed [2] flywheel design, and analysis the material selection process. The FEA model is described to achieve a better understanding of the mesh type, mesh size and boundary conditions applied to complete an effective FEA model.

Saeed Shojaei , Seyyed Mostafa Hossein Ali Pour Mehdi Tajdari Hamid Reza Chamani [3] have proposed algorithms based on dynamic analysis of crank shaft for designing flywheel for I.C.engine , torsional vibrasion analysis result by AVL\EXCITE is compared with the angular displacement of a desire free haed of crank shaft ,also consideration of fatigue for fatigue analysis of flywheel are given.

Sudipta Saha, Abhik Bose, G. SaiTejesh, S.P. Srikanth have propose [4] the importance of the flywheel geometry design selection and its contribution in the energy storage performance. This contribution is demonstrated on example cross-sections using computer aided analysis and optimization procedure. Proposed Computer aided analysis and optimization procedure results show that smart design of flywheel geometry could both have a significant effect on the Specific Energy performance and reduce the operational loads exerted on the shaft/bearings due to reduced mass at high rotational speeds.

Bedier B. EL-Naggar and Ismail A. Kholeif [5] had is suggested the disk-rim flywheel for light weight. The mass of the flywheel is minimized subject to constraints of required moment of inertia and admissible stresses. The theory of the rotating disks of uniform thickness and density is applied to each the disk and the rim independently with suitable matching condition at the junction. Suitable boundary conditions on the centrifugal stresses are applied and the dimensional ratios are obtained for minimum weight. It is proved that the required design is very close to the disk with uniform thickness.

III. Development Tools

3.1CATIA (Computer Aided Three-dimensional Interactive Application):

It is a multi-platform CAD/CAM/CAE commercial software suite developed by the French company Dassault Syste mes. Written in the C++ programming language, CATIA is the cornerstone of the Dassault Systemes Commonly referred to as a 3D Product Lifecycle Management software suite, CATIA supports multiple stages of product development from conce ptualization, design (CAD), manufacturing (CAM), and engineering (CAE). CATIA facilitates collaborative engineering acr oss disciplines, including surfacing & shape design, mechanical engineering, equipment and systems engineering.

CATIA can be applied to a wide variety of industries, from aerospace and defense, automotive, and industrial equipment, to high tech, shipbuilding, consumer goods, plant design, consumer packaged goods, life sciences, architecture and construction, process power and petroleum, and services.

3.2ANSYS

The ANSYS Workbench environment is an intuitive up-front finite element analysis tool that is used in conjunction with CAD systems and/or Design Modeler. ANSYS Workbench is a software environment for performing structural, thermal, and electromagnetic analyses. The class focuses on attaching existing geometry, setting up the finite element model, solving, and reviewing results. The class will describe how to use the code as well as basic finite element simulation concepts and results interpretation. The finite element method (FEM) is a method for dividing up a very complicated problem into small elements that can be solved in relation to each other. Its practical application is often known as finite element analysis (FEA)

IV. Modeling of Flywheel

There are generally two types of model used for analysis that are used in industry: 2-D modeling, and 3-D modeling. While 2-D modeling conserves simplicity and allows the analysis to be run on a relatively normal computer, it tends to yield less accurate results. 3-D modeling, however, produces more accurate results while sacrificing the ability to run on all but the fastest computers effectively .So the flywheel needs to be modeled into a 3-D solid.
Maruti 800 Flywheel was selected for Modeling

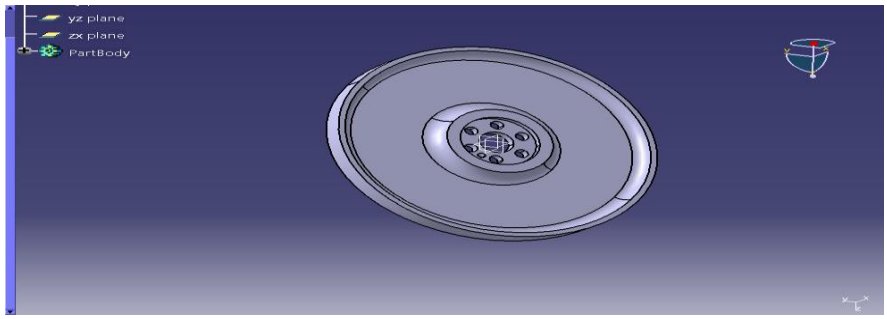

Figure 2: Model Of flywheel In CATIA

V. Analysis of flywheel with FEA

FEA (Finite Element Analysis) consists of a computer model of a material or design that is stressed and analyzed for specific results it is utilized to verify a proposed design will be able to perform to the client's specifications prior to manufacturing or construction. Modifying an existing product or structure is utilized to qualify the product or structure for a new service condition. In case of structural failure, FEA may be used to help determine the design modifications to meet the new condition.

To build the physical system into a finite element model easily, some assumptions are needed:
Assumption 1: A rigid installation is used to connect the flywheel and its drive-shaft, no key-ways are needed to fix/drive the flywheel and there exist no slide, built-in stress and deformations on the connection surface; therefore, displacement constraints can be simply applied on the shaft hole;
Assumption 2: The flywheel only works in the vertical plane (X-Y plane) so that the gravity can be simply applied;
Assumption 3: The material used are isotropic;
Assumption 4: The aerodynamically resistance can be neglected;
Assumption 5: There exists no vibration;
Assumption 6: The fillets/chamfers can be neglected unless dimensioned

5.1 Material Properties

Two materials that are used for Design of Flywheel & their properties are given below table.

Table 1: Material properties

Material	Ultimate stress(MPa)	Density	Poissons ratio
Gray Cast Iron	214	7510	0.23
S-glass-Epoxy	4800	2000	0.25

5.2 Element Type

Based on the consideration of rotational deformations in the flywheel, the element Soilid72, a 3D 4-node tetrahedral structural solid with rotations, is used to model meshes. The element is defined by 4

Figure 3: Normal Stress in (a) S-Glass-Epoxy Flywheel (b) cast Iron Flywheel

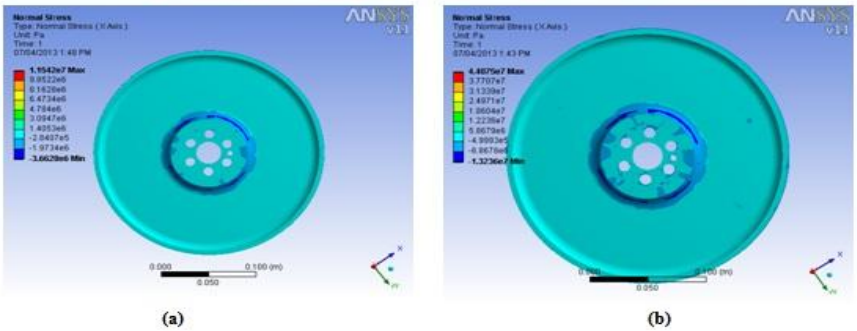

Nodes with 6 DOFs at each node and well suitable to create irregular meshes It also has stress stiffening capability.
But in ANSYS workbench Program control element are used.

5.3 Meshing method

Free mesh with smart element sizing is adopted to automatically and flexibly mesh the model. Compared to mapped mesh, which is restricted to only quadrilateral (area) or only hexahedron (volume) elements, free mesh has no restrictions in terms of element shapes. Smart sizing gives the user a greater opportunity to create reasonably shaped element during automatic element generation.

5.4 Boundary conditions and loads

Moment: MZ, applied on the nodes on the shaft-hole surface ANSYS 11 will be utilized for finite element analysis The ANSYS Workbench, together with the Workbench project and tabs, provides a unified working environment for developing and managing a variety of CAE information and makes it easier for you to set up and work with data at a high level.

VI. Results and Discussions

A structural analysis of was performed and normal stress are shown in fig 3. Flywheel was discredited into 19735 elements and 36539 nodes.
Table 2 shows that normal stress obtained for Gray cast iron is 44.07 Mpa and similarly for S glass Epoxy is 11.54 Mpa.

Table 2: Comparison result by ANSYS

Material	Normal stresses (Mpa)	Total Deformation (m)
Gray Cast Iron	44.07	$1.0484*10^{-3}$
S Glass Epoxy	11.54	$5.3399*10^{-4}$

VII. Conclusion

Based on the above work of flywheel and its optimization methods the following conclusion can be drawn.

It is clear that, cast iron flywheels are having higher Stress and deformation. S Glass Epoxy can be used in flywheels to store energy with less mass. It can be also used in high speed applications.

International Journal of Modern Engineering Research (IJMER)
www.ijmer.com Vol.3, Issue.2, March-April. 2013 pp-1100-1104 ISSN: 2249-6645

A Study on Dynamic and Static Clustering Based Routing Schemes for Wireless Sensor Networks

Prashant Krishan
Department of IT, Uttarakhand Technical University, Dehradun, INDIA

***Abstract*:** *A Wireless sensor network is an infrastructure comprised of sensing (measuring), computing, and communication elements that gives an administrator the ability to instrument, observe, and react to events and phenomena in a specified environment. The administrator typically is a civil, governmental, commercial, or industrial entity. The environment can be the physical world, a biological system, or an information technology (IT) framework. Routing is very difficult in wireless sensor network due to a large number of sensor nodes. In wireless sensor network, Routing can be divided into Flat Routing, Hierarchical Routing, Location - aware Routing. Hierarchical Routing can be further divided into two parts: Dynamic and Static Hierarchical Routing or Clustering-based Routing. Dynamic Clustering based protocols are those in which the clusters are formed and diminished dynamically. Static Clustering based Routing Protocols are those in which clusters once formed remain same throughout the network lifetime. In our paper, we discuss all Dynamic and Static Clustering based Routing Protocols and its pros and cons.*

***Keywords*:** *Wireless Sensor Networks, Network Lifetime Routing Protocols, Routing challenges, WSN applications.*

I. Introduction

A WSN is a specialized wireless network made up of a large number of sensors and at least one base station. The foremost difference between the WSN and the traditional wireless networks is that sensors are extremely sensitive to energy consumption. Energy saving is the crucial issue in designing the wireless sensor networks [1]. Since the radio transmission and reception consumes a lot of energy, one of the important issues in wireless sensor network is the inherent limited battery power within network sensor nodes. In order to maximize the lifetime of sensor nodes, it is preferable to distribute the energy dissipated throughout the wireless sensor network. So it is essential to design effective and energy aware protocols in order to enhance the network lifetime. A WSN can have network structure based or protocol operation based routing protocol .In this paper, a review on Dynamic and Static Clustering based Routing protocols which are the part of network structure protocol is carried out. Energy consumption and network life time has been considered as the major issues wireless sensor network (WSN) requires an enormous breadth of knowledge from an enormous variety of disciplines, so its study becomes challenging [1]. A wireless sensor network basically consists of small devices called sensor nodes having the capability of sensing the environment around them, computation the task, and performing wireless communications. Sensor networks may also consist of different type of sensors such as seismic, low sampling rate magnetic, thermal, visual, and infrared, radar and acoustic, which monitor a wide variety of ambient conditions that includes [2] habitat monitoring, temperature fluctuation, air pollution control, traffic control. In wireless sensor network, each node is connected to one or more sensors, because it is built of nodes from a few to several hundreds or even thousand .That sensor network node having several parts: a radio transceiver with an internal antenna, a microcontroller, an electronic circuit for interfacing with the sensors and an energy source, usually a battery. An important feature in wireless sensor networks is the battery lifetime of the node. Energy efficiency is a main challenge in wireless sensor networks and energy use is dominated by the energy required. In wireless sensor networks the size and cost of the sensor nodes may vary from micro to macro and from one to few hundred dollars respectively. Battery power decides whether the sensor nodes sense for long time or for short time even the battery cannot be recharged or replaced.

II. Routing Challenges

Routing in Wireless sensor Network is very challenging due to its wireless nature. There are many reasons: a) WSNs have a large number of sensor nodes, it is not possible to apply a global addressing scheme for the deployment of a large number of sensor nodes as the overhead will be high to maintain the Ids of the sensor Network. b) Sensor nodes are tightly constrained in terms of energy, processing, and storage capacity. So there must be some mechanism to manage the resources. There are many challenges and design issues that affect the routing process in Wireless sensor Network.

A. Node Deployment: Node deployment in WSNs is depend on the applications and can be either manual or randomized. In manual deployment, the sensors are manually placed and data is routed through predetermined paths. In random node deployment the sensor nodes are scattered randomly, creating an adhoc routing infrastructure. If the resultant distribution of nodes is not uniform, optimal clustering becomes necessary to allow connectivity and enable energy-efficient network operation. Inter sensor communication is normally within short transmission ranges due to energy and bandwidth limitations. Therefore, it is most likely that a route will consist of multiple wireless hops.

B. Fault Tolerance: Some sensor nodes may fail due to natural interferences, low battery power, any physical damage. One damaged sensor node can affect the overall performance of the sensor network. If many nodes fail, medium access control (MAC) and routing protocols must accommodate formation of new links and routes to the data collection BSs.

C. Quality of Service: In some applications, data should be delivered within a certain period of time from the moment it is sensed, or it will be useless. Therefore, bounded latency for data delivery is another condition for time-constrained applications.

D. Transmission Media: In a multihop sensor network, communicating nodes are linked by a wireless medium. The traditional problems associated with a wireless channel (e.g., fading, high error rate) may also affect the operation of the sensor network.

E. Connectivity: High node density in sensor networks precludes them from being completely isolated from each other. Therefore, sensor nodes are expected to be highly connected. This, however, may not prevent the network topology from being variable and the network size from shrinking due to sensor node failures.

F. Scalability: The number of sensor nodes deployed in the sensing area may be on the order of hundreds or thousands, or more. Any routing scheme must be able to work with this huge number of sensor nodes. In addition, sensor network routing protocols should be scalable enough to respond to events in the environment.

G. Heterogeneity: The existence of a heterogeneous set of sensors raises many technical issues related to data routing. For example, some applications might require a diverse mixture of sensors for monitoring temperature, pressure, and humidity of the surrounding environment, detecting motion via acoustic signatures, and capturing images or video tracking of moving objects.

III. Routing Protocols

In general, Routing in WSNs can be dividing into Flat-based Routing, hierarchical-based routing, and location-based routing depending on the network structure. In flat-based routing, all the nodes are typically assigned equal roles. In hierarchical-based routing nodes have different roles like low energy nodes sense the environment and high energy nodes used to transmit it. The figure (1) depicts the taxonomy of the routing protocols:

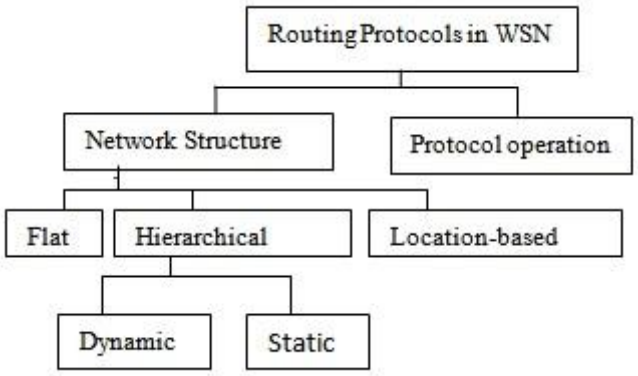

. Figure-1 Taxonomy of Routing Protocol

Hierarchical Routing: In hierarchical routing, higher energy nodes can be used to process and send the information, while low-energy nodes can be used to perform the sensing in the targeted area. The creation of cluster can help to achieve scalability, network lifetime, and energy efficiency. Hierarchical routing is two layer routing where one layer is used to select cluster heads and the other for routing. It can be further divided into two parts Dynamic and Static. In Dynamic, cluster are changed with the rounds but in Static, once the clusters are created remain same throughout network lifetime. Following is the explanation of some dynamic and static Hierarchical Routing.

LEACH: It is Dynamic Hierarchical Routing for sensor network, called Low Energy Adaptive Clustering Hierarchy (LEACH). A routing protocol is considered adaptive if certain system parameters can be controlled in order to adapt to current network conditions and available energy levels. LEACH randomly selects a few sensor nodes as cluster heads (CHs) and rotates this role to evenly distribute the energy load among the sensors in the network. In LEACH, the CH nodes compress data arriving from nodes that belong to the respective cluster, and send an aggregated packet to the BS in order to reduce the amount of information that must be transmitted to the BS. LEACH uses a TDMA/code-division multiple access (CDMA) MAC to reduce inter-cluster and intra-cluster collisions. However, data collection is centralized and performed periodically. Therefore, this protocol is most appropriate when there is a need for constant monitoring by the sensor network. A user may not need all the data immediately. Hence, periodic data transmissions are unnecessary, and may drain the limited energy of the sensor nodes. After a given interval of time, randomized rotation of the role of CH is conducted so that uniform energy dissipation in the sensor network is obtained. The operation of LEACH is separated into two phases, the setup phase and the steady state phase. In the setup phase, the clusters are organized and CHs are selected. In the steady state phase, the actual data transfer to the BS takes place. The duration of the steady state phase is longer than the duration of the setup phase in order to minimize overhead. During the setup phase, a predetermined fraction of nodes, *p*, elect themselves as CHs as

follows. A sensor node chooses a random number, r, between 0 and 1. If this random number is less than a Threshold value, T (n), the node becomes a CH for the current round. The threshold value is calculated based on an equation that incorporates the desired percentage to become a CH, the current round, and the set of nodes that have not been selected as a CH in the last (1/p) rounds denoted as G. it is given by

T (n) = (p/(1-p(mod(1/p)))) if n € G

Where *G* is the set of nodes that are involved in the CH election All elected CHs broadcast an advertisement message to the rest of the nodes in the network that they are the new CHs. All the non-CH nodes, after receiving this advertisement, decide on the cluster to which they want to belong. This decision is based on the signal strength of the advertisement. The non-CH nodes inform the appropriate CHs that they will be a member of the cluster. After receiving all the messages from the nodes that would like to be included in the cluster and based on the number of nodes in the cluster, the CH node creates a TDMA schedule and assigns each node a time slot when it can transmit. This schedule is broadcast to all the nodes in the cluster. During the steady state phase, the sensor nodes can begin sensing and transmitting data to the CHs. The CH node, after receiving all the data, aggregates it before sending it to the BS. After a certain time, which is determined a priori, the network goes back into the setup phase again and enters another round of selecting new CHs. Each cluster communicates using different CDMA codes to reduce interference from nodes belonging to other clusters.

Limitation: It is not applicable to networks deployed in large regions. It also assumes that nodes always have data to send, and nodes located close to each other have correlated data. It is not obvious how the number of predetermined CHs (*p*) is going to be uniformly distributed through the network.

B. EECS (Energy Efficient Clustering Scheme): EECS is a LEACH-like clustering scheme, where the network is partitioned into a set of clusters with one cluster head in each cluster. Communication between the cluster head and BS is direct (single-hop). In the *cluster formation* phase, we will use this distance to balance the load among cluster heads. In the *cluster head election* phase, well distributed cluster heads are elected with a little control overhead. And in the *cluster formation* phase, a novel weighted function is introduced to construct load balanced clusters. In the *cluster head election* phase, the cluster head is elected by localized competition which is unlike LEACH and with no iteration which differs from HEED. The optimal value of competition range produces a good distribution of cluster heads. Further in the *cluster formation* phase, plain nodes join clusters not only taking into account its intra-cluster communication cost, but also considering cluster heads' cost of communication to the BS. EECS is autonomous and more energy efficient, and simulation results show that it prolongs the network lifetime much more significantly than the other clustering protocols.

C. PEGASIS (Power-Efficient Gathering in Sensor Information Systems): The protocol, called Power-Efficient Gathering in Sensor Information Systems (PEGASIS), is a near optimal chain-based protocol. The basic idea of the protocol is that in order to extend network lifetime, nodes need only communicate with their closest neighbors, and they take turns in communicating with the BS. When the round of all nodes communicating with the BS ends, a new round starts, and so on. This reduces the power required to transmit data per round as the power draining is spread uniformly over all nodes. Hence, PEGASIS has two main objectives. First, increase the lifetime of each node by using collaborative techniques. Second, allow only local coordination between nodes that are close together so that the bandwidth consumed in communication is reduced. Unlike LEACH, PEGASIS avoids cluster formation and uses only one node in a chain to transmit to the BS instead of multiple nodes. To locate the closest neighbor node in PEGASIS, each node uses the signal strength to measure the distance to all neighboring nodes and then adjusts the signal strength so that only one node can be heard. The chain in PEGASIS will consist of those nodes that are closest to each other and form a path to the BS. The aggregated form of the data will be sent to the BS by any node in the chain, and the nodes in the chain will take turns sending to the BS. The chain construction is performed in a greedy fashion. Simulation results showed that PEGASIS is able to increase the lifetime of the network to twice that under the LEACH protocol. Such performance gain is achieved through the elimination of the overhead caused by dynamic cluster formation in LEACH, and decreasing the number of transmissions and reception by using data aggregation. Although the clustering overhead is avoided, PEGASIS still requires dynamic topology adjustment since a sensor node needs to know about the energy status of its neighbors in order to know where to route its data. Such topology adjustment can introduce significant overhead, especially for highly utilized networks. Moreover, PEGASIS assumes that each sensor node is able to communicate with the BS directly. In practical cases, sensor nodes use multihop communication to reach the BS. Also, PEGASIS assumes that all nodes maintain a complete database of the location of all other nodes in the network. The method by which the node locations are obtained is not outlined. In addition, PEGASIS assumes that all sensor nodes have the same level of energy and are likely to die at the same time. Note also that PEGASIS introduces excessive delay for distant nodes on the chain. In addition, the single leader can become a bottleneck. Finally, although in most scenarios sensors will be fixed or immobile as assumed in PEGASIS, some sensors may be allowed to move and hence affect the protocol functionality.

Static Hierarchical-based Routing Protocol: Static clustering based routing protocols are those in which once the cluster is created remain same throughout the network lifetime. We discuss some static clustering based routing protocol.

EEPSC (Energy Efficient Protocol with Static Clustering): EEPSC, partitions the network into static clusters, eliminates the overhead of dynamic clustering and utilizes temporary-cluster-heads to distribute the energy load among high power sensor nodes; thus extends network lifetime. The operation of EEPSC is broken up into rounds, where each round consists set-up phase, responsible node selection phase and steady-state phase.

Setup phase: cluster formation is performed only once at the beginning of network operation. For this aim, base station broadcasts *k-1* different messages with different transmission powers, which *k* is the desired number of clusters. By broadcasting the *k=1* message all the sensor nodes which hear this message (are in the radio range of this message) set their cluster ID to *k* and inform the base station that they are member of the cluster *k* via transmitting a join- request message (Join-REQ) back to the base station.

Responsible Node Selection Phase: After the clusters are established, network starts its normal operation and responsible nodes (temporary-CH and CH) selection phase begins. At the beginning of each round, every node sends its energy level to the temporary-CH in its time slot. Afterward, temporary-CH choose the sensor node with utmost energy level as CH for current round to collect the data of sensor nodes of that cluster, perform local data aggregation, and communicate with the base station; and the node with lowest energy level as temporary-CH for next round and sends a round-start packet including the new responsible sensor IDs for the current round. This packet also indicates the beginning of round to other sensor nodes. Since every sensor node has a pre-specified time slot, changing the CHs has no effect on the schedule of the cluster operation.

Steady State Phase: The steady-state phase is broken into frames where nodes send their data to the CH during pre-allocated time slots. These data contain node ID and the measure of sensed parameter. The duration of each slot in which a node transmits data is constant, so the time to send a frame of data depends on the number of nodes in the cluster. To reduce energy dissipation, the radio of each non-cluster head node is turned off until its allocated transmission time, but the CHs must be awake to receive all the data from nodes in the cluster.

Advantage:

- EEPSC benefits a new idea of using temporary-CHs and utilizes a new setup and responsible node selection phase.
- EEPSC utilizes static clustering scheme, therefore eliminates the overhead of dynamic clustering.

EEEPSC (Enhanced Energy Efficient Protocol with Static Clustering): Enhanced Energy-Efficient Protocol with Static Clustering (E3PSC) which is basically a modification of an existing routing scheme, Energy-Efficient Protocol with Static Clustering (EEPSC). In EEEPSC, cluster-head selection is performed by taking into account both the spatial distribution of sensors nodes in network and their residual energy with an objective to reduce the intra-cluster communication overhead among the nodes making the scheme more energy-efficient base station computes the mean positions of node-distribution (Pmeani) of every cluster where ***i*** is cluster id which help in reducing the inter-cluster communication.

IV. Conclusion

Routing in sensor networks is a new area of research, with a limited but rapidly growing set of research results. In this article we present a comprehensive survey of Dynamic and static Clustering based routing techniques in wireless sensor networks that have been presented in the literature. They have the common objective of trying to extend the lifetime of the sensor network while not compromising data delivery. Overall, the routing techniques are classified based on the network structure into three categories: flat, hierarchical, and location-based routing protocols. Furthermore, these protocols are classified into multipath-based, query-based, negotiation-based, and QoS-based routing techniques depending on protocol operation. Although many of these routing techniques look promising, there are still many challenges that need to be solved in sensor networks. We highlight those challenges and pinpoint future research directions in this regard.

References

[1] N. Bulusu, J. Heinemann, and D. Estrin, "GPS-less Low Cost Out Door Localization for Very Small Devices,"Tech. rep. 00729, Comp. Sci. Dept., USC, Apr. 2000.
[2] A. Savvides, C.-C. Han, and M. Srivastava, "Dynamic Fine-Grained Localization in Ad-Hoc Networks of Sensors," Proc. 7th ACM MobiCom, July 2001, pp. 166–79.
[3] I. Akyildiz et al., "A Survey on Sensor Networks," IEEE Commun. Mag., vol. 40, no. 8, Aug. 2002, pp. 102–14.
[4] S. Tilak, N. Abu-Ghazaleh, W. Heinzelman, "A Taxonomy of Wireless Micro-sensor Network Models," ACM SIGMOBILE Mobile Comp. Commun. Rev., vol. 6, no. 2, Apr. 2002, pp. 28–36.
[5] W. Heinzelman, A. Chandrakasan and H. Balakrishnan, "Energy-Efficient Communication Protocol for Wireless Microsensor Networks," Proc. 33rd Hawaii Int'l. Conf. Sys. Sci., Jan. 2000.
[6] F. Ye et al., "A Two-Tier Data Dissemination Model for Large-Scale Wireless Sensor Networks," Proc. ACM/IEEE MOBICOM, 2002.
[7] http://www.ieee802.org/15/
[8] F. Ye et al., "A Scalable Solution to Minimum Cost Forwarding in Large Sensor Networks," Proc. 10th Int'l. Conf. Comp. Commun. And Networks, 2001, pp. 304–09
[9] W. Heinzelman, J. Kulik, and H. Balakrishnan, "Adaptive Protocols for Information Dissemination in Wireless Sensor Networks," Proc. 5th ACM/IEEE Mobicom, Seattle, WA, Aug. 1999. pp. 174–85.

[10] J. Kulik, W. R. Heinzelman, and H. Balakrishnan, "Negotiation-Based Protocols for Disseminating Information in Wireless Sensor Networks," Wireless Networks, vol. 8, 2002, pp. 169–85.
[11] S. Hedetniemi and A. Liestman, "A Survey of Gossiping and brocadcasting in Communication Networks," IEEE Network, vol. 18, no. 4, 1988, pp. 319–49.
[12] C. Intanagonwiwat, R. Govindan, and D. Estrin, "Directed Diffusion: a Scalable and Robust Communication Paradigm for Sensor Networks," Proc. ACM Mobi- Com 2000, Boston, MA, 2000, pp. 56–67.
[13] D. Braginsky and D. Estrin, "Rumor Routing Algorithm for Sensor Networks," Proc. 1st Wksp. Sensor Networks and Apps., Atlanta, GA, Oct. 2002.
[14] C. Schurgers and M.B. Srivastava, "Energy Efficient Routing in Wireless Sensor Networks," MILCOM Proc. Commun. for Network-Centric Ops.: Creating the Info. Force, McLean, VA, 2001.
[15] M. Chu, H. Haussecker, and F. Zhao, "Scalable Information Driven Sensor Querying and Routing for Ad Hoc Heterogeneous Sensor Networks," Int'l. J. High Perf. Comp. Apps., vol. 16, no. 3, Aug. 2002.
[16] Y. Yao and J. Gehrke, "The Cougar Approach to Innetwork Query Processing in Sensor Networks," SIGMOD Record, Sept. 2002.
[17] N. Sadagopan et al., "The ACQUIRE Mechanism for Efficient Querying in Sensor Networks," Proc. 1st Int'l. Wksp. Sensor Network Protocol and Apps,. Anchorage, AK, May 2003.
[18] R. C. Shah and J. Rabaey, "Energy Aware Routing for Low Energy Ad Hoc Sensor Networks," IEEE WCNC, Orlando, FL, Mar. 17–21, 2002.
[19] S. Servetto and G. Barrenechea, "Constrained Random Walks on Random Graphs: Routing Algorithms for Large Scale Wireless Sensor Networks," Proc. 1st ACM Int'l. Wksp. Wireless Sensor Networks and Apps., Atlanta, GA, 2002.
[20] S. Lindsey and C. Raghavendra, "PEGASIS: Power-Efficient Gathering in Sensor Information Systems," IEEE Aerospace Conf. Proc., 2002, vol. 3, 9–16, pp. 1125–30.
[21] A. Manjeshwar and D. P. Agarwal, "TEEN: a Routing Protocol for Enhanced Efficiency in Wireless Sensor Networks," 1st Int'l. Wksp. on Parallel and Distrib. Comp. Issues in Wireless Networks and Mobile Comp., April 2001.
[22] A. Manjeshwar and D. P. Agarwal, "APTEEN: A Hybrid Protocol for Efficient Routing and Comprehensive Information Retrieval in Wireless Sensor Networks," Proc. Int'l. Parallel and Distrib. Proc. Symp., pp. 195–202. [24] L. Li, and J. Y. Halpern, "Minimum-Energy Mobile Wireless Networks Revisited," IEEE ICC 2001, vol. 1, pp. 278–83.
[23] L. Subramanian and R. H. Katz, "An Architecture for Building Self Configurable Systems," Proc. IEEE/ACM Wksp. Mobile Ad Hoc Net. and Comp., Boston, MA, Aug. 2000 Building Self Configurable Systems," Proc. IEEE/ACM Wksp. Mobile Ad Hoc Net. And Comp., Boston, MA, Aug. 2000.
[24] V. Rodoplu and T. H. Meng, "Minimum Energy Mobile Wireless Networks," IEEE JSAC, vol. 17, no. 8, Aug. 1999, pp. 1333–44.
[25] Q. Fang, F. Zhao, and L. Guibas, "Lightweight Sensing and Communication Protocols for Target Enumeration and Aggregation," Proc. 4th ACM MOBIHOC, 2003, pp. 165–76.
[26] J. N. Al-Karaki et al., "Data Aggregation in Wireless Sensor Networks — Exact and Approximate Algorithms," Proc. IEEE Wksp. High Perf. Switching and Routing 2004, Phoenix, AZ, Apr. 18–21, 2004.
[27] Y. Xu, J. Heidemann, and D. Estrin, "Geography informed Energy Conservation for Ad-hoc Routing," Proc. 7th Annual ACM/IEEE Int'l. Conf. Mobile Comp. and Net., 2001, pp. 70–84.
[28] J. N. Al-Karaki, and A. E. Kamal, "On the Correlated
Data Gathering Problem in Wireless Sensor Networks," to appear in the Proc. 9th IEEE Symp. Comp. and Commun., Alexandria, Egypt, July 2004.

International Journal of Modern Engineering Research (IJMER)
www.ijmer.com Vol.3, Issue.2, March-April. 2013 pp-1105-1114 ISSN: 2249-6645

Analysis and Design of an UWB Band pass Filter with Improved Upper Stop band Performances

Nadia Benabdallah, [1] Nasreddine Benahmed, [2] Fethi Tarik Bendimerad[3]
[1]*Department of Physics, Preparatory School of Sciences and Technology (EPST-Tlemcen), Tlemcen, Algeria*
[23]*Department of Telecommunications, University of Tlemcen, Algeria*

Abstract: *In this work, we are interesting in the analysis and the design of an ultra wideband (UWB) band pass filter with improved upper stop band performances, using microstrip lines.*
The design of the UWB band pass filter is based on the use of stepped-impedance low pass filter and high pass filter; whereas the simulation of its frequency response ([S]) is done using MATPAR software and it is based on the electromagnetic (EM) parameters for each section of line forming the band pass structure.
Our filter with bandwidth between 2.9-10.8 GHz, measures just 12.6×1.524×31.58 mm and was fabricated using RT/D 5880 substrate by means of stepped-impedance 5-pole microstrip low pass filter and high pass filter constructed from quasilumped elements. The simulated results of stop band performances are better than 15 dB for a frequency range up to 25 GHz.

Keywords**:** *Analysis design and simulation, EM-parameters, UWB band pass filter, stepped-impedance low pass filter, high pass filter with quasilumped elements, MATPAR software, S-parameters.*

I. INTRODUCTION

FILTERS play important roles in many RF/microwave applications. They are used to separate or combine different frequencies. The electromagnetic (EM) spectrum is limited and has to be shared; filters are used to select or confine the RF/microwave signals within assigned spectral limits. Emerging applications such as wireless communications continue to challenge RF/microwave filters with ever more stringent requirements-higher performance, smaller size, lighter weight, and lower cost. Depending on the requirements and specifications, RF/microwave filters may be designed as lumped element or distributed element circuits; they may be realized in various transmission line structures, such as waveguide, coaxial line [1-2], and microstrip [3-4].

The recent advance of novel materials and fabrication technologies, including monolithic microwave integrated circuit (MMIC), microelectromechanic system (MEMS), micromachining, high-temperature superconductor (HTS), and low-temperature cofired ceramics (LTCC), has stimulated the rapid development of new microstrip and other filters [5]. In the meantime, advances in computer-aided-engineering (CAE) tools such as full-wave electromagnetic (EM) simulators have revolutionized filter design. Many novel microstrip filters with advanced filtering characteristics have been demonstrated [5].

With the ready availability of accurate CAE tools, it is possible to apply some basic formulas for calculating the dimensions of these filters and simulating their frequency responses [5].

In this work, we are interesting in the analysis and the design of an ultra wideband (UWB) band pass filter with improved upper stop band performances, using microstrip lines. The design of the UWB band pass filter is based on the use of stepped-impedance low pass filter and high pass filter constructed from quasilumped elements. The cutoff frequencies of 3.1 and 10.6 GHz were selected respectively for each type of filter. Our filter has not only compact size but also a wider upper stop band resulting from low pass characteristics. The simulated results of stop band performances are better than 15 dB for a frequency range up to 25 GHz.

What follows are the analysis, the design and the simulation of this UWB band pass filter.

II. BASIC CONCEPTS

This section describes the basic concepts and theories necessary for the overall design of RF/microwave filters including microstrip lines structures.

The transfer function of a two-port filter network is a mathematical description of network response characteristics, namely, a mathematical expression of S_{21}. On many occasions, an amplitude-squared transfer function for a lossless passive filter network is defined as:

$$\left|S_{21}(j\omega)\right|^2 = \frac{1}{1+\varepsilon^2 F_n^2(\omega)} \qquad (1)$$

Where ε is a ripple constant, $F_n(\omega)$ represents a filtering or characteristic function, and ω is a frequency variable. For our discussion here, it is convenient to let ω represent a radian frequency variable of a low pass prototype filter that has a cutoff frequency at $\omega = \omega_c$ (rad/s).

For a given transfer function of equation (1), the insertion loss response of the filter can be computed by:

$$L_A(\omega) = 10 \log \frac{1}{|S_{21}(j\omega)|^2} \quad (dB) \qquad (2)$$

Since $|S_{11}|^2+|S_{21}|^2=1$ for a lossless, passive two-port network, the return loss response of the filter can be expressed by:

$$L_R(\omega) = 10 \log \left(1-|S_{21}(j\omega)|^2\right) \quad (dB) \qquad (3)$$

The transfer function is an essential feature of the filter. It is given by different mathematical laws called filtering function. The most ones used are: Butterworth and Chebyshev laws.

II.1 Butterworth (Maximally Flat) response

The amplitude-squared transfer function for Butterworth filters that have an insertion loss L_{Ar}=3.01 dB at the cutoff frequency ω_c is given by:

$$|S_{21}(j\omega)|^2 = \frac{1}{1+\left(\frac{\omega}{\omega_c}\right)^{2.n}} \qquad (4)$$

Where n is the degree or the order of filter, which corresponds to the number of reactive elements, required in the low pass prototype filter. This type of response is also referred to as maximally flat because its amplitude-squared transfer function defined in equation (4) has the maximum number of (2n-1) zero derivatives at ω=0. Figure 1 shows a typical maximally flat response.

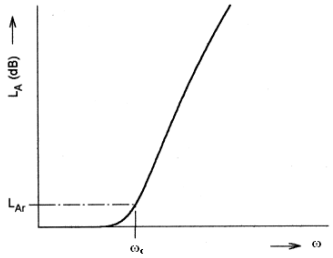

Fig. 1. Butterworth (maximally flat) low pass response.

II.2 Chebyshev response

The Chebyshev response that exhibits the equal-ripple pass band and maximally flat stop band is depicted in figure 2. The amplitude-squared transfer function that describes this type of response is:

$$|S_{21}(j\omega)|^2 = \frac{1}{1+\varepsilon^2 T_n^2(\omega)} \qquad (5)$$

Where:

The ripple constant ε is related to a given pass band ripple L_{Ar} in dB by:

$$\varepsilon = \sqrt{10^{\frac{L_{Ar}}{10}}-1} \qquad (6)$$

$T_n(\omega)$ is a Chebyshev function of the first kind of order n, which is defined as

$$T_n(\omega) = \begin{cases} \cos\left(n \cos^{-1}\left(\frac{\omega}{\omega_c}\right)\right) & for \quad \left|\frac{\omega}{\omega_c}\right| \le 1 \\ \cosh\left(n \cosh^{-1}\left(\frac{\omega}{\omega_c}\right)\right) & for \quad \left|\frac{\omega}{\omega_c}\right| \ge 1 \end{cases} \qquad (7)$$

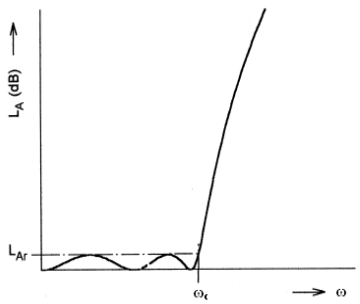

Fig. 2. Chebyshev low pass response.

II.3 Low pass prototype filter and elements

The main objective of this section is to present equations for obtaining element values of some commonly used low pass prototype filters. In addition, the determination of the degree of the prototype filter will be discussed.

In general, the design of microstrip low pass filters involves two main steps. The first one is to select an appropriate low pass prototype (figure 3). The choice of the type of response, including pass band ripple and the number of reactive elements, will depend on the required specifications. The couples [L_A; (ω/ω_c)] that we want to obtain at $\omega=\omega_a$ allows us to find the values of the order n of the filter while the L_k and C_k values are determined using the following g_k parameters.

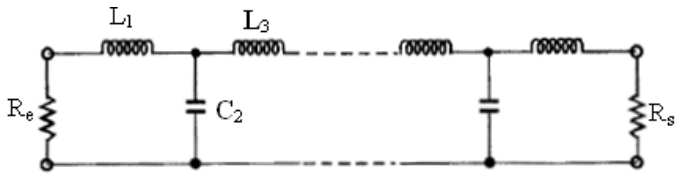

Fig. 3. Low pass prototype filter

For Butterworth or maximally flat low pass prototype filters having a transfer function given in (4), the g_k parameters may be computed using:

$$g_0 = 1$$

$$g_k = 2\sin\left(\frac{(2k-1)\pi}{2n}\right) \qquad k = 1 \; to \; n \qquad (8)$$

$$g_{n+1} = 1$$

For Chebyshev low pass prototype filters having a transfer function given in (5), the element values for the two-port networks may be computed using the following g_k parameters:

$$g_0 = 1$$

$$g_1 = \frac{2}{\gamma}\sin\left(\frac{\pi}{2n}\right)$$

$$g_k = \frac{1}{g_{k-1}} \frac{4\sin\left(\frac{(2k-1)\pi}{2n}\right)\sin\left(\frac{(2k-3)\pi}{2n}\right)}{\gamma^2 + \sin^2\left(\frac{(k-1)\pi}{n}\right)} \quad k = 2,\ldots,n \qquad (9)$$

$$g_{n+1} = \begin{cases} 1.0 & for\, n\, odd \\ \coth^2\left(\frac{\beta}{4}\right) & for\, n\, even \end{cases}$$

Where:

$$\gamma = \sinh\left(\frac{\beta}{2n}\right)$$

$$\beta = \ln\left[\coth\left(\frac{L_{Ar}}{17.37}\right)\right]$$

The input resistance R_e is given by the terms of reference since it is the characteristic impedance of the line on which the filter is inserted. Generally it is 50Ω.

The load resistance can be calculated by:

$$R_s = r.R_e \qquad (10)$$

Where: for Butterworth r = 1 and for Chebyshev response $r = \begin{cases} 1.0 & for\, n\, odd \\ tgh^2\left(\frac{\beta_r}{4}\right) & for\, n\, even \end{cases}$ with $\beta_r = In\left(\coth\left(\frac{L_{Ar}}{17.37}\right)\right)$

Finally the values of the elements L_k and C_k of low pass filter are computed using relations (11) and (12):

$$L_k = \frac{R_e}{\omega_c} g_k \qquad (11)$$

$$C_k = \frac{1}{R_e}\frac{1}{\omega_c} g_k \qquad (12)$$

II.4 High pass filter and elements

The following figure shows the structure of a high pass filter transformed from the low pass prototype and using L-C elements.

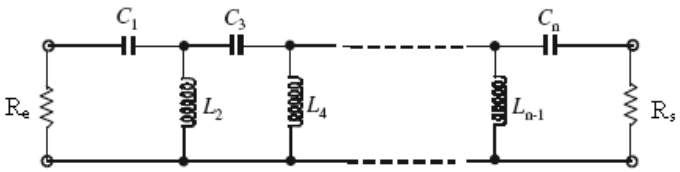

Fig. 4. High pass filter

This simple form of high pass filter consists of a series capacitor, which is often found in applications for direct current or dc block. For more selective high pass filters, more elements are required. This type of high pass filter can be easily designed based on a lumped-element low pass prototype such as one shown in figure 4 and on the following relations:

$$L_k = \frac{R_e}{\omega_c g_k} \qquad (13)$$

$$C_k = \frac{1}{R_e \omega_c g_k} \qquad (14)$$

II.5 Band pass filter and elements

Figure 5 shows the structure of a band pass filter using L-C elements.

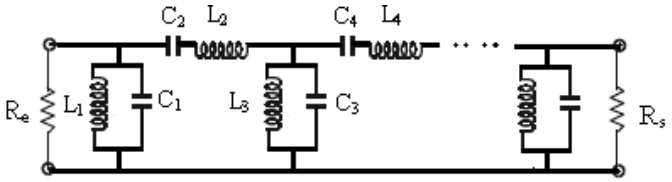

Fig. 5. Band pass filter

The Chebyshev response of this type of filter is represented in figure 6. The resonance frequency of the filter is indicated by ω_0 while the low and high pass frequencies are respectively ω_1 and ω_2.

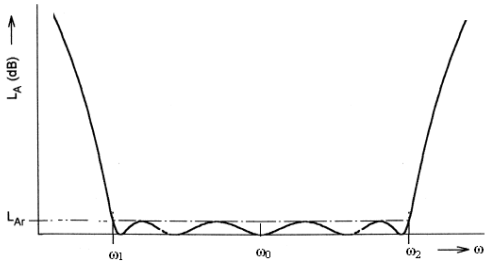

Fig. 6. Chebyshev band pass response.

This type of band pass filter can be easily designed based on a lumped-element low pass prototype and on the following expressions:

For the elements in series:

$$L_k = \frac{R_e g_k}{B\omega_0} \qquad (15)$$

$$C_k = \frac{B}{R_e g_k \omega_0} \qquad (16)$$

For the elements in parallel:

$$L_k = \frac{R_e B}{g_k \omega_0} \qquad (17)$$

$$C_k = \frac{g_k}{R_e B \omega_0} \qquad (18)$$

Where: $B = \frac{\omega_2 - \omega_1}{\omega_0}$

III. STEPPED-IMPEDANCE, L-C TYPE MICRO STRIP FILTERS

Having obtained a suitable lumped-element filter design, the next main step in the design of microstrip filters is to find an appropriate microstrip realization that approximates the lumped element filter. In this section, we concentrate on the second step.

Figure 7 shows a general structure of the stepped-impedance low pass microstrip filters, which uses a cascaded structure of alternating high- and low impedance transmission lines. The high-impedance lines act as series inductors and the low-impedance lines act as shunt capacitors. Therefore, this filter structure is directly realizing the L-C ladder type of low pass filters of figure 3.

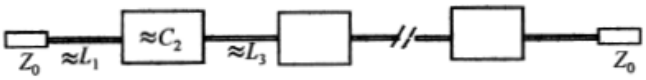

Fig. 7. General structure of the stepped-impedance low pass microstrip filters.

Figures 8 to 10 present three microstrip realizations of low pass, high pass and band pass filters.

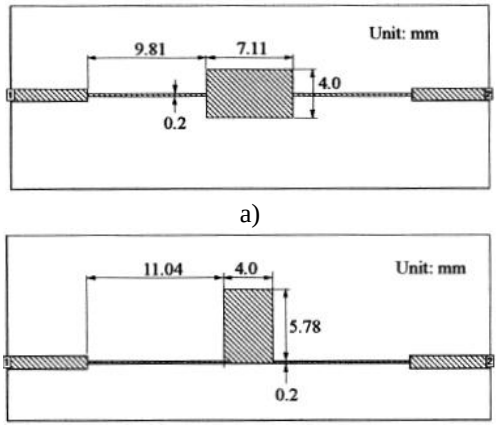

Fig. 8. Layout of a 3-pole microstrip low pass filter realized on a substrate with a relative dielectric constant of 10.8 and a thickness of 1.27 mm and using: stepped-impedance on a) and open-circuited stubs on b) [5].

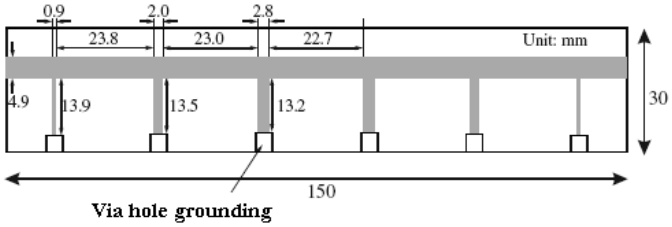

Fig. 9. A microstrip optimum high pass filter on a substrate with a relative dielectric constant of 2.2 and a thickness of 1.57 mm [5]

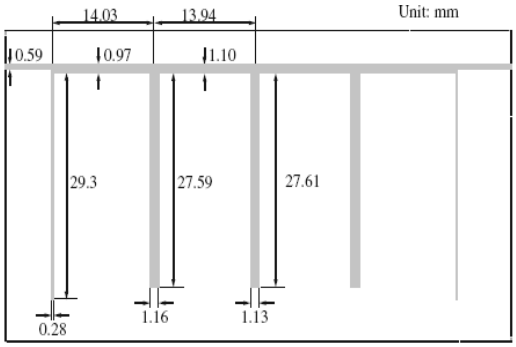

Fig. 10. Layout of a designed microstrip band pass filter with half-wavelength open-circuited stubs on a 0.635 mm thick substrate with a relative dielectric constant of 10.2 [5].

These structures have been studied and analyzed by various commercial EM simulation softwares. Their frequency responses are in good agreement with the requirements and specifications.

IV. EM ANALYSES AND DESIGN

Using the theory presented in this paper, we realized an accurate CAE tool which allows obtaining a suitable lumped-element filter design and finding an appropriate microstrip realization that approximates the lumped element filter. The frequency responses of our filters designs fabricated with microstrip lines can be obtained using MATPAR [6] or other software.

Our CAE tool suitable for low pass, high pass and band pass RF/microwave filters achieves a quick design according to Butterworth or Chebyshev responses and gives same results as those obtained with commercial electromagnetic (EM) simulation software. Here we applied it to the analysis and the design of an UWB band pass filter with improved upper stop band performances. The design of the UWB band pass filter is based on the use of stepped-impedance low pass filter and high pass filter constructed from quasilumped elements.

An example of design of a three-pole low pass filter is illustrated in figure 11. The specifications for the filter under consideration are: cutoff frequency f_c of 1 GHz, pass band ripple of 0.1 dB (or return loss < –16.42 dB) and source impedance of 50 Ω.

On a substrate with a relative dielectric constant of 10.8 and a thickness of 1.27 mm, figures 11-b and 11-c give two types of realizations that approximate the lumped element filter of figure 11-a. The first one uses stepped-impedance and the second one uses open-circuited stubs. Our obtained results are in good agreement with those shown in figure 8.

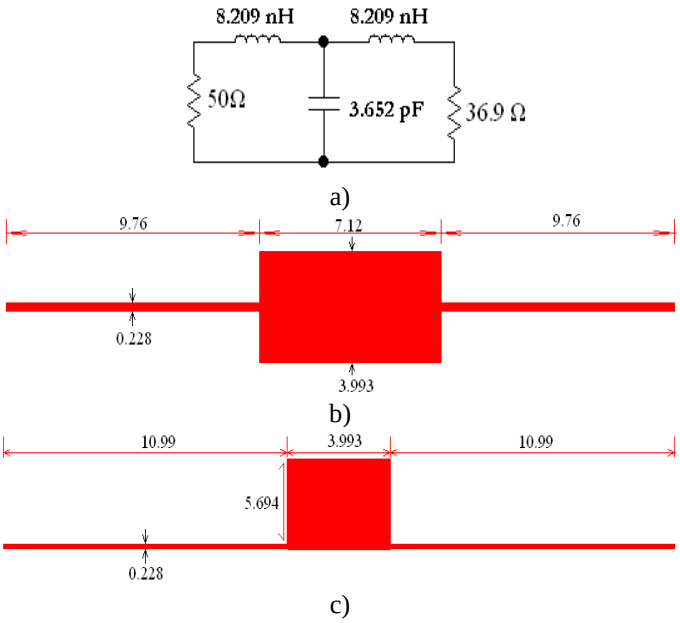

Fig. 11. Lumped-element filter design on a) and layouts: stepped impedance on b) and open-circuited on c) (Unit: mm).

High pass filters constructed from quasilumped elements may be desirable for many applications, provided that these elements can achieve good approximation of desired lumped elements over the entire operating frequency band. As part of this study on UWB microstrip lines band pass filters, we examined first the design of a high pass microstrip filter having a cutoff frequency f_c of 3.1 GHz, pass band ripple of 0.1 dB and source impedance of 50 Ω. Using design procedure we find the lumped elements of the following circuit.

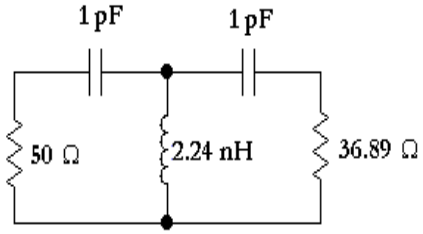

Fig. 12. Lumped-element highpass filter design.

A possible realization of such a high pass filter in microstrip, using quasilumped elements, is shown in figure 13. Here it is seen that the series capacitors are realized by two identical interdigital capacitors, and the shunt inductor is realized by a short-circuited stub. The microstrip high pass filter is designed on a commercial substrate (RT/D 5880) with a relative dielectric constant of 2.2 and a thickness of 1.524 mm.

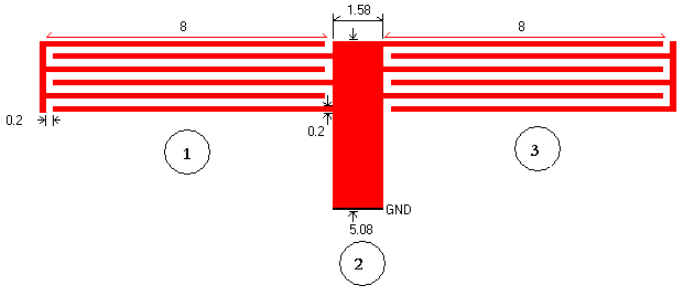

Fig. 13. A quasilumped highpass filter in microstrip on a substrate with a relative dielectric constant of 2.2 and a thickness of 1.524 mm (Unit: mm).

In order to facilitate the analysis of such structure under MATPAR environment, we divided it to three sections of lines (Figure 13). The obtained EM parameters of each section of lines using LINPAR software [7] are:
- For the interdigital capacitors (sections 1 and 3):

$$[L] = \begin{bmatrix} 772.0 & 41.38 & 28.57 & 21.24 & 16.43 & 13.10 \\ 41.38 & 763.3 & 40.97 & 28.34 & 21.12 & 16.43 \\ 28.57 & 40.97 & 761.4 & 40.89 & 28.34 & 21.24 \\ 21.24 & 28.34 & 40.89 & 761.4 & 40.97 & 28.57 \\ 16.43 & 21{,}12 & 28.34 & 40.97 & 763.3 & 41.38 \\ 13{,}10 & 16.43 & 21.24 & 28.57 & 41.38 & 771.9 \end{bmatrix} \left(\frac{nH}{m}\right)$$

$$[C] = \begin{bmatrix} 32.460 & -14.47 & -2.68 & -1.06 & -0.54 & -0.44 \\ -14.47 & 39.20 & -13.28 & -2.23 & -0.85 & -0.54 \\ -2.68 & -13.28 & 39.40 & -13.21 & -2.23 & -1.06 \\ -1.06 & -2.23 & -13.21 & 39.40 & -13.21 & -2.68 \\ -0.54 & -0.85 & -2.23 & -13.28 & 39.20 & -14.47 \\ -0.44 & -0.54 & -1.06 & -2.68 & -14.47 & 32.46 \end{bmatrix} \left(\frac{pF}{m}\right)$$

- For the shunt inductor (section 2): L = 218.0 nH/m; C = 96.8 pF/m; Z_c = 47.52 Ω and ε_{eff} = 1.4.

We applied the MATPAR software in the aim of checking the electrical performance of the designed high pass filter shown in figure 13. Figure 14 illustrates the simulated response (S_{21}) of the high pass filter constructed from quasilumped elements, in the frequency band [0.2-25] GHz. It can be seen that for S_{21}=-3 dB the cutoff frequency is 2.9 GHz.

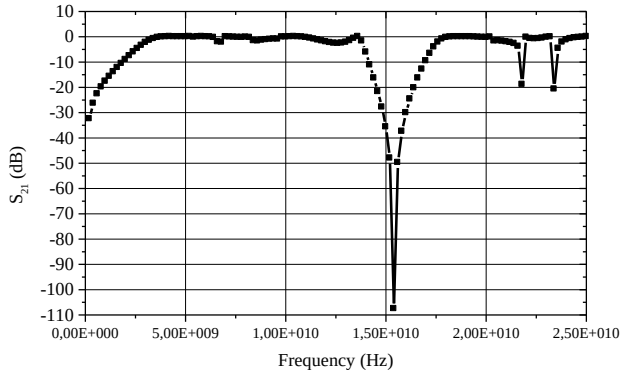

Fig. 14. EM simulated performance of the quasilumped high pass filter.

For the second part of our study on UWB microstrip lines band pass filters, we examined the design of a low pass microstrip filter having a cutoff frequency f_c of 10.6 GHz, pass band ripple of 0.1 dB and source impedance of 50 Ω. Using design procedure we find the lumped elements of the circuit shown in figure 15.

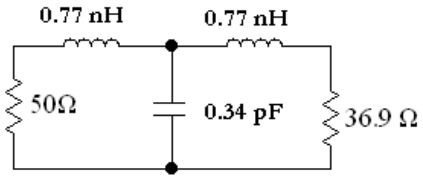

Fig. 15. Lumped-element low pass filter design.

A layout of this designed microstrip filter is illustrated in figure 16, and its performance obtained by MATPAR software is plotted in figure 17.

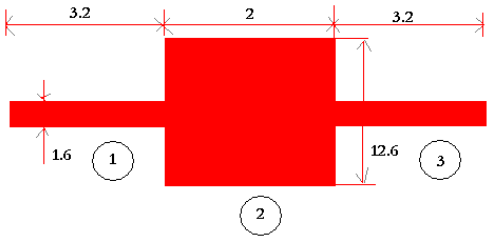

Fig. 16. Layout of the designed stepped-impedance low pass filter realized on a substrate with a relative dielectric constant of 2.2 and a thickness of 1.524 mm (Unit: mm).

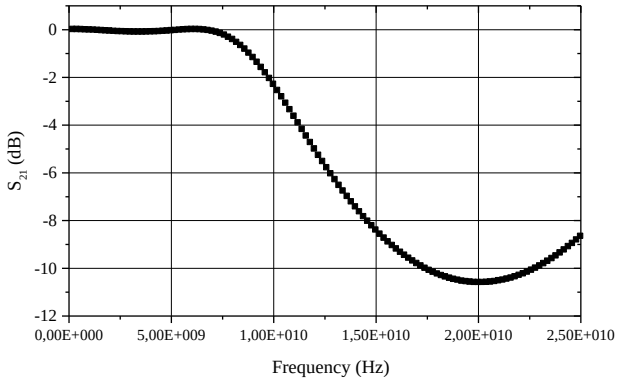

Fig. 17. EM simulated performance of the designed stepped-impedance low pass filter.

The frequency response of the stepped-impedance low pass filter was obtained for the EM parameters listed into table1 of each section of line forming the designed structure. From this response it can be seen that the cutoff frequency of the filter is 10.53 GHz obtained for S_{21}=-3 dB.

Table I. EM parameters of each section of line
of the stepped-impedance low pass filter

Section of line	**[L] (nH/m)**	**[C] (pF/m)**	**Z_c (□)**	**□$_{eff}$**
1	412.4	47.95	92.8	1.78
2	113.7	196.6	24.0	2.0
3	412.4	47.95	92.8	1.78

Finally the layout of the designed UWB band pass filter using a 3-pole microstrip low pass filter is illustrated in figure 18, and its performance obtained by MATPAR software is plotted in figure 19 in the frequency band [0.2-25] GHz. This response is in reasonable agreement with results of planar structures and it also meets the requirements for UWB applications per the FCC [8]. The simulated results of stop band performances are better than 5 dB for a frequency range up to 25 GHz.

In order to increase the stop band performances of our designed structure, figure 20 gives the layout of the final UWB band pass filter using a 5-pole microstrip low pass filter. In figure 21 we present the frequency response of our designed filter.

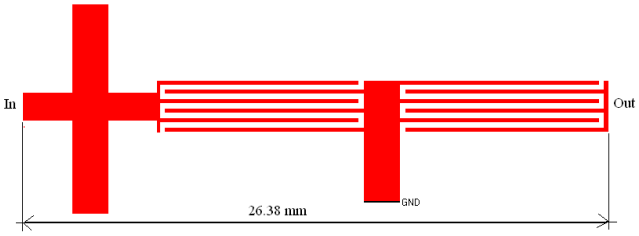

Fig. 18. Layout of the designed UWB band pass structure using a 3-pole micro strip low pass filter

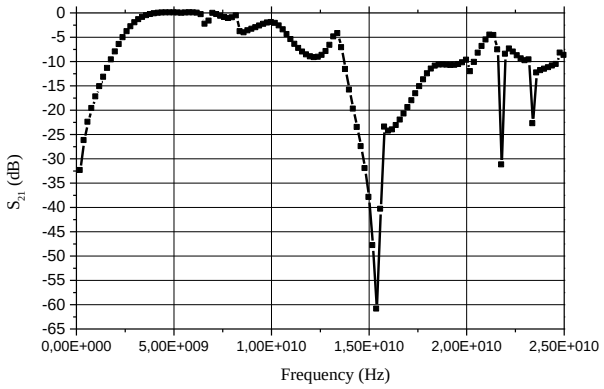

Fig. 19. EM simulated performance of the designed UWB band pass structure using a 3-pole micro strip low pass filter.

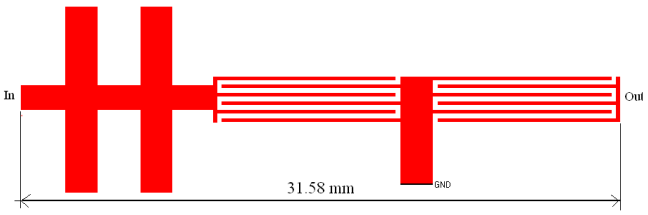

Fig. 20. Layout of the designed UWB band pass structure using a 5-pole microstrip low pass filter

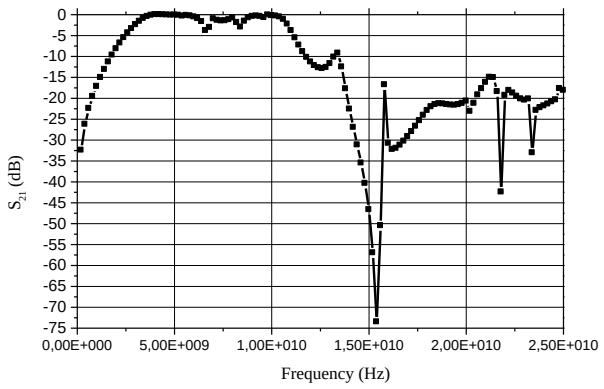

Fig. 21. EM simulated performance of the designed UWB band pass structure using a 5-pole micro strip low pass filter.

Our filter, which measures just 12.6×1.524×31.58 mm, was fabricated using RT/D 5880 substrate by means of stepped-impedance 5-pole microstrip low pass filter and high pass filter constructed from quasilumped elements. The simulated results of stop band performances are better than 15 dB for a frequency range up to 25 GHz.

V. CONCLUSION

In summary, this work presented the analysis, the design and the simulation of an ultra wideband band pass filter with improved upper stop band performances, using micro strip lines.

The filter which measures just $12.6 \times 1.524 \times 31.58$ mm, was fabricated using RT/D 5880 substrate by means of stepped-impedance 5-pole micro strip low pass filter and high pass filter constructed from quasilumped elements. The simulated results of stop band performances are better than 15 dB for a frequency range up to 25 GHz.

It was designed using our accurate CAE tools and with the aid of MATPAR software, although other commercial EM simulation software can also be used.

REFERENCES

[1] A. Benkaddour, N. Benahmed, N. Benabdallah and F.T. Bendimerad, Create UWB filters with coaxial cables, Microwaves & RF, 51(7), July 2012, 59-63.

[2] N. Benahmed, N. Benabdallah, S. Seghier, F.T. Bendimerad and B. Benyoucef, Analyzing an UWB band pass filter for high power applications using rectangular coaxial cables with square inner conductors, Circuits and Systems (CS), 2(3), July 2011, 121-126.

[3] N. Benahmed, N. Benabdallah, F.T. Bendimerad and B. Benyoucef, Analyse et conception d'un filtre stop-bande multicouche micro-usiné à coupleur micro ruban asymétrique, Lebanese Science Journal (LSJ), 12(1), 2011, 45-58.

[4] N. Benabdallah, N. Benahmed and F.T. Bendimerad, FEM Analysis, Design and Optimization of a Compact Bandpass Filter for Low-power UWB Communications Applications, International Journal of Microwaves Applications, 2(1), January-February 2013, 18-22.

[5] J. S. Hong and M. J. Lancaster, Microstrip Filters for RF/Microwave Applications (John Wiley & Sons, Inc., 2011).

[6] A.R. Djordjevic, M. Bazdar, G. Vitosevic, T. Sarkar, and R. F. Harrington, Scattering parameters of microwave networks with multiconductor transmission lines (Artech House, Norwood, MA, 1990).

[7] A.R. Djordjevic, M.B. Bazdar, T.K. Sarkan, LINPAR for windows: Matrix parameters of multiconductor transmission lines, Software and user's manual (Artech Housse, 1999).

[8] FCC, Revision of Part 15 of the Commission's Rules Regarding Ultra-Wideband Transmission System, Technical Report ET-Docket 98-153, 14 February 2002.

International Journal of Modern Engineering Research (IJMER)
www.ijmer.com Vol.3, Issue.2, March-April. 2013 pp-1115-1122 ISSN: 2249-6645

CFD Analysis of an Elliptical Pin Fin Heat Sink using Ansys Fluent v12.1

Vivek Kumar, [1] Dr. V. N. Bartaria[2]
[12]*M. Tech. Scholar, Mechanical Engineering Department, LNCT Bhopal (M.P)*

Abstract: *The present study carries out numerical physical insight into the flow and heat transfer characteristics. The governing equations are solved by adopting a control volume-based finite-difference method with a power-law scheme on an orthogonal non-uniform staggered grid. The coupling of the velocity and the pressure terms of momentum equations are solved by the computational fluid dynamics. The Elliptical Pin Fin Heat Sink is composed of a plate fin heat sink and some circular pins between plate fins. The purpose of this study is to examine the effects of the configurations of the pin-fins design. The results show that the Elliptical Pin Fin Heat Sink has better unnaturally performance than the plate fin heat sink. Computations of the Elliptical Pin Fin Heat Sink and provides.*

Key words: *Heat sink, Heat transfer, Thermal resistance, Elliptical Pin Fin Heat Sink (EPFHS)*

I. Introduction

With the increase in heat dissipation from microelectronics devices and the reduction in overall form factors, thermal management becomes a more a more important element of electronic product design [1]. Both the performance reliability and life expectancy of electronic equipment are inversely related to the component temperature of the equipment. The relationship between the reliability and the operating temperature of a typical silicon semi conductor device shows that a reduction in the temperature corresponds to an exponential increase in the reliability and life expectancy of the device. Therefore, long life and reliable performance of a component may be achieved by effectively controlling the device operating temperature within the limits set by the device design engineers.

The effective use of an electrical component is limited by its maximum operational junction temperature. To achieve a desired component temperature, excess heat dissipated by the device must be transferred to the environment [2]. The most common method for transferring heat from the component to the environment is to use a heat sink.To estimate a component's junction temperature, a required value is the heat sink's thermal resistance. The thermal resistance of heat sink can be determined analytically or experimentally.

In electronic systems, a heat sink is a passive component that cools a device by dissipating heat into the surrounding air. In computers, heat sinks are used to cool electronic components. Heat sinks are used with high-power semiconductor devices such as power transistors and optoelectronic devices such as lasers and light emitting diodes (LEDs), wherever the heat dissipation ability of the basic device package is insufficient to control its temperature.

II. Cfd Modeling

Computational Fluid Dynamics (CFD) is the science of determining numerical solution of governing equation for the fluid flow whilst advancing the solution through space or time to obtain a numerical description of the complete flow field of interest. The equation can represent steady or unsteady, Compressible or Incompressible, and in viscid or viscous flows, including non ideal and reacting fluid behavior. The particular form chosen depends on intended application. The state of the art is characterized by the complexity of the geometry, the flow physics, and the computing time required obtaining a solution [3].

The purpose of this research work is to simulate pressure Drop and heat transfer in a heat sink and validate the simulation with actual experimental result [4, 5, 6] using fluent software. Different solvers and turbulence models have been developed in CFD SOFTWARE for predicting Thermal Resistance, heat transfer coefficient, Nusselt number using Plate fin heat sink and Elliptical fin pin heat sink for various wind velocity.

Computational fluid dynamics (CFD) is a computer-based simulation method for analyzing fluid flow, heat transfer, and related phenomena such as chemical reactions. This dissertation uses CFD for analysis of flow and heat transfer. It will be advantageous to use CFD over traditional experimental-based analyses, since experiments have a cost directly proportional to the number of configurations desired for testing, unlike with CFD, where large amounts of results can be produced at practically no added expense. In this way, parametric studies to optimize equipment are very inexpensive with CFD when compared to experiments.

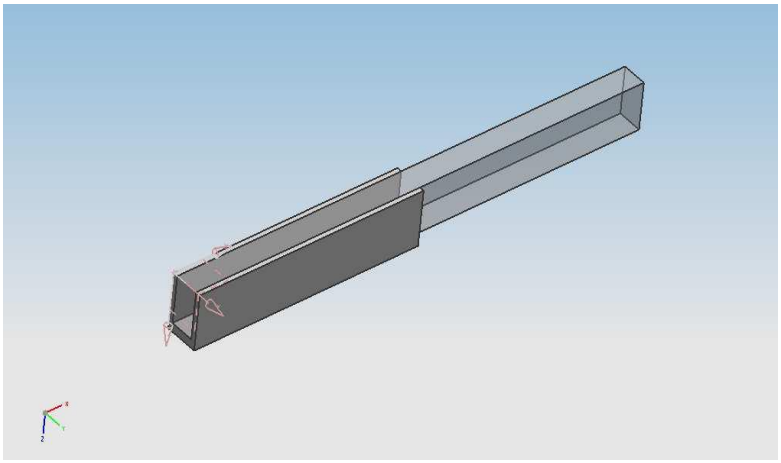

Fig.1 Model of Plate-fin Heat sink

The governing equations used in CFD for fluid flow and heat transfer are based upon the principles of conservation of mass, momentum, and energy [7]. These equations solve by the fluent software. The conservation laws of physics form the basis for fluid flow governing equation. The dimensions of the computational domain heat sink were based on the work by Yu et al [8].Geometry of Plate fin heat sink and elliptical pin-fin heat sink are shown in fig.1, 2, 3&4.

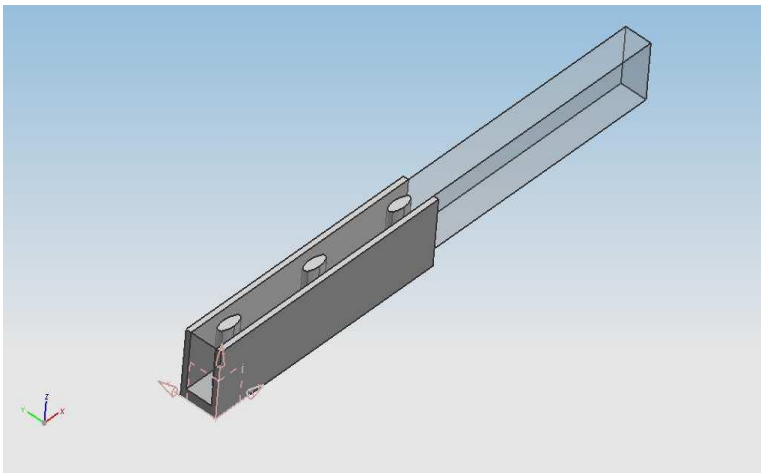

Fig.2 Model of1.5 Elliptical pin-fin Heat sink

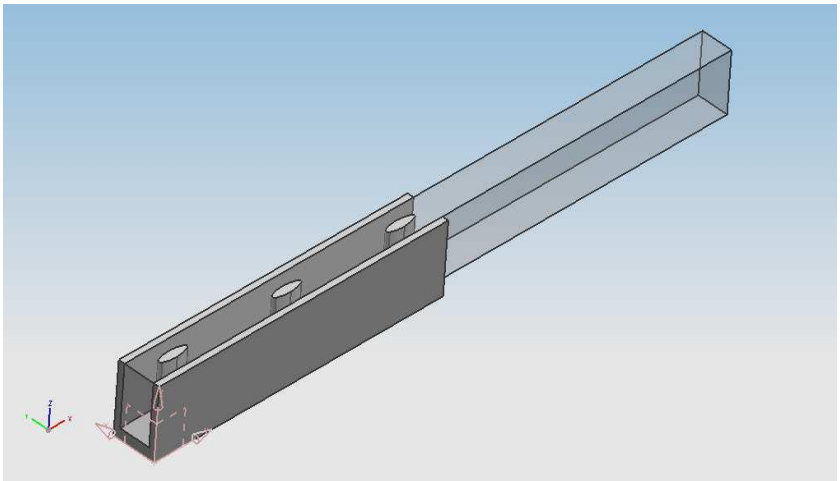

Fig.3 Model of2.0 Elliptical pin-fin Heat sink

In the analysis, the flow is assumed to 3-dimensional, turbulence, incompressible and steady flow. Buoyancy and radiation heat transfer are not consider in the crimped fin analysis. All the thermodynamics property i.e. (P-V-T) is assumed to constant. The K−ε turbulent model is used for describe the air flow characteristics. The continuity, momentum and energy equation are written below.

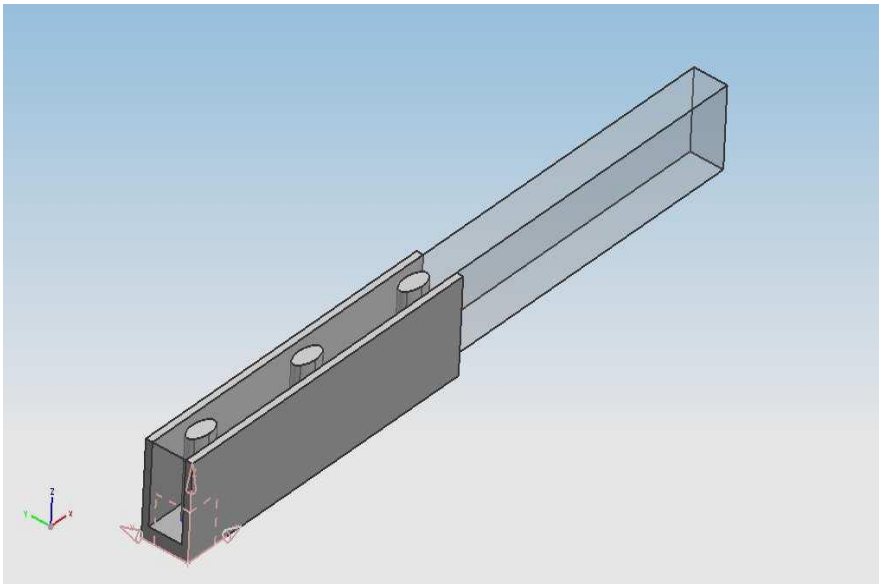

Fig.4 Model of 2.5 Elliptical pin-fin Heat sink

Geometrical Parameters are listed in table-1. In this new elliptical pin-fin heat sink model. There is periodic geometry is use. In which heat is transfer through the periodic wall and elliptical pins. Heat flow from inside i.e. base of the fin to the tip of the fin. The following Table 1 and 2 are showing the parameters of heat sink and elliptical pin fin.

Table 1 Geometric parameters of heat sink

Fin Length, L(mm)	Fin Height, H(mm)	Fin Number, N	Fin thickness, t(mm)	Fin-to-Fin distance, ξ(mm)
51	10	9	1.5	5

Table 2 Dimension of elliptical Pin fin heat sink

Model	Major Axis(mm)	Minor Axis(mm)
1.5Pin fin model	5	1.5
2Pin fin model	5	2.0
2.5Pin fin model	5	2.5

Momentum Equation (Navier-stokes Equation)

X- Momentum equation.

$$\frac{\partial}{\partial x_j}\left(\rho \bar{u}_j\right)=0 \tag{1}$$

$$\frac{\partial}{\partial x_j}\left(\rho \bar{u}_j \bar{u}_i\right)=-\frac{\partial \bar{p}}{\partial x_i}+\frac{\partial}{\partial x_j}\left(\mu \frac{\partial \bar{u}_i}{\partial x_j}+\tau_{ij}\right) \tag{2}$$

Where τ_{ij} is the Reynolds stress in term given by

$$\mu_{ij}=\mu_t\left(\frac{\partial \bar{u}_i}{\partial x_j}+\frac{\partial \bar{u}_j}{\partial \bar{x}_i}\right)-\frac{2}{3}\rho\delta_{ij}\kappa \tag{3}$$

Where μ_t is the turbulent viscosity and k=$\frac{1}{2}\left(\overline{u'^2}+\overline{v'^2}+\overline{w'^2}\right)$ is the turbulent kinetic energy. Eq. (3) introduces two unknowns (μ_t and k), which require two equations for closure. For high Reynolds number flows the turbulent viscosity can be represented as

$$\mu_t=\rho C_\mu \frac{k^2}{\varepsilon} \tag{4}$$

C_μ Is a constant and ε is the dissipation rate of energy.

The energy equation solved for the fluid flow is

$$\bar{u}_i \frac{\partial \bar{T}}{\partial x_i} = \frac{\partial}{\partial x_i}\left(\Gamma \frac{\partial \bar{T}}{\partial x_i} - \overline{T'u'}\right) \quad (5)$$

Where Γ is diffusion coefficient of air .The energy equation solving conduction heat transfer within the heat sink is

$$\frac{\partial}{\partial x_i}\left(\lambda_s \frac{\partial T_s}{\partial x_i}\right) + q = 0 \quad (6)$$

Where q is the heat generated per unit volume of the heat sink λ_s is the heat sink thermal conductivity andT_s is the temperature within the heat sink.

Given the periodic structure of the heat sinks, only one flow passage is investigated. The computational domain employed is shown in table 3. The material of the heat sink is aluminum. The bottom of the computational domain is heated at a constant heat transfer rateof 10W and different velocity (6.5, 9.5 and 12.5 m/s).The flow is assumed to be threedimensional, incompressible, steady, turbulent, and since the heating is low, constant air properties. Radiation effect is ignored.

Table3Boundary condition

Fin Profile	Fin type	Velocity(m/s)			Heating Power(Q)	Periodic boundary condition
	Plane pin	6.5	9.5	12.5	10	Translate in Y direction
Elliptical Pin	5mm major & 1.5mm minor	6.5	9.5	12.5	10	Translate in Y direction
	5mm major & 2.0mm minor	6.5	9.5	12.5	10	Translate in Y direction
	5mm major & 2.5mm minor	6.5	9.5	12.5	10	Translate in Y direction

III. Result And Discussion

A three-dimensional model is developed to investigate flow and conjugate heat transfer in the heat sink for electronic applications. A series of numerical calculations have been conducted by FLUENT and the results are presented in order to show the effects of temperature distribution, overall heat transfer coefficient, Thermal Resistance, Surface Nusselt number in the heat sinks. Both simulation results and Yue-Tzu Yang, Huan-SenPeng experiment results [7] for thermal resistances and pressure drops of the PFHS are plotted in Fig 3.1-a and 3.2-b respectively.

3.1 Experimental and Simulation Result-

The thermal resistance of the heat sink, Rth, can be defined by-

$$R_{th} = \frac{\Delta T}{Q} \quad (7)$$

ΔT Is taken as temperatures difference between highest temperature at the base of the fins and ambient temperatures and Q is heat dissipation power used in the base of the fins. Properties of the working fluid are the same as those of ambient air at 294 K, and the material of heat sinks is aluminum with thermal conductivity of 202 W/ (m-K). From the figure, shows that experimental data and simulation data for both thermal resistance and pressure drop changed.

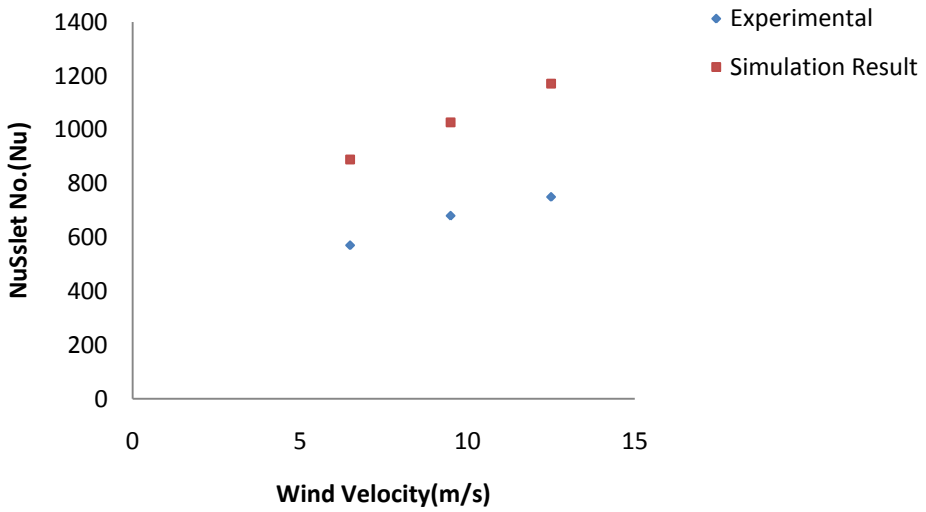

Fig.5Experimental and Simulation results for the PFHS: Nusselt Number vs. wind velocities.

The above fig.5 show experimental and simulation results of PFHS Nusselt number. This gives a slightly large deviation but in similar manner.

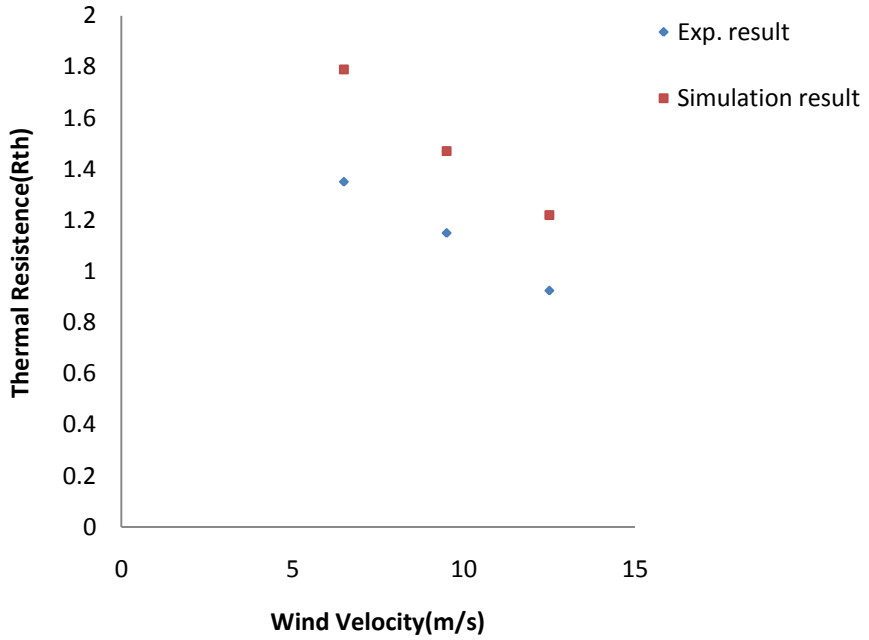

Fig.6 Experimental and Simulation results for the PFHS: Thermal resistance vs. wind velocities

The above fig.6 show thermal resistance for PFHS with experimental and simulation gives a constant deviation but in similar manner.

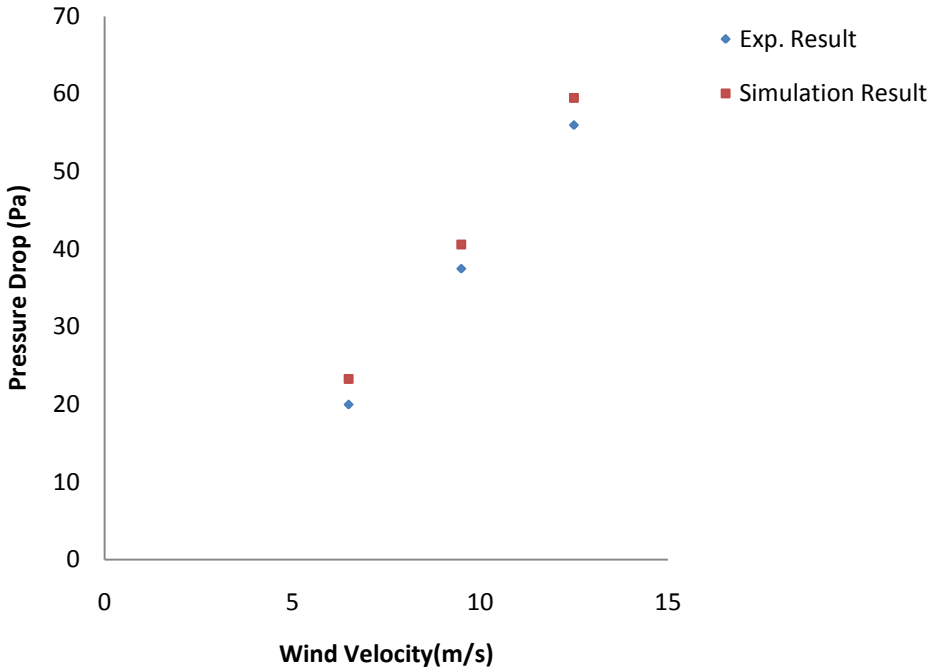

Fig.7 Experimental and Simulation results for the PFHS: Pressure drop vs. Wind velocities.

The above fig.7 show experimental and simulation results of PFHS pressure drop. The results are slightly above than experimental values, the deviation almost constant.

3.2. Compression on the Performance between PFHS and EPFHS

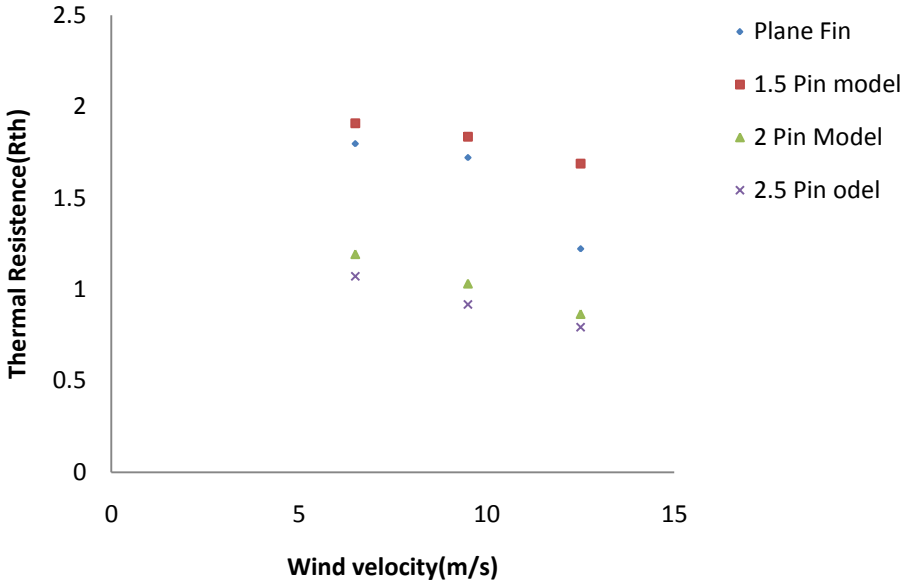

Fig.8 Thermal Resistance Variations for Different Fin Profile of Elliptical Pin

The above Fig.8shows the thermal resistance variations for different fin profile of elliptical pin with compare the experimental result(7) of PFHS and simulation result of various fin profile of elliptical pin gives a constant deviation but in similar manner. This fig. shows the decrease in the thermal resistance with increase the wind velocity (6.5, 9.5 & 12.5m/s).

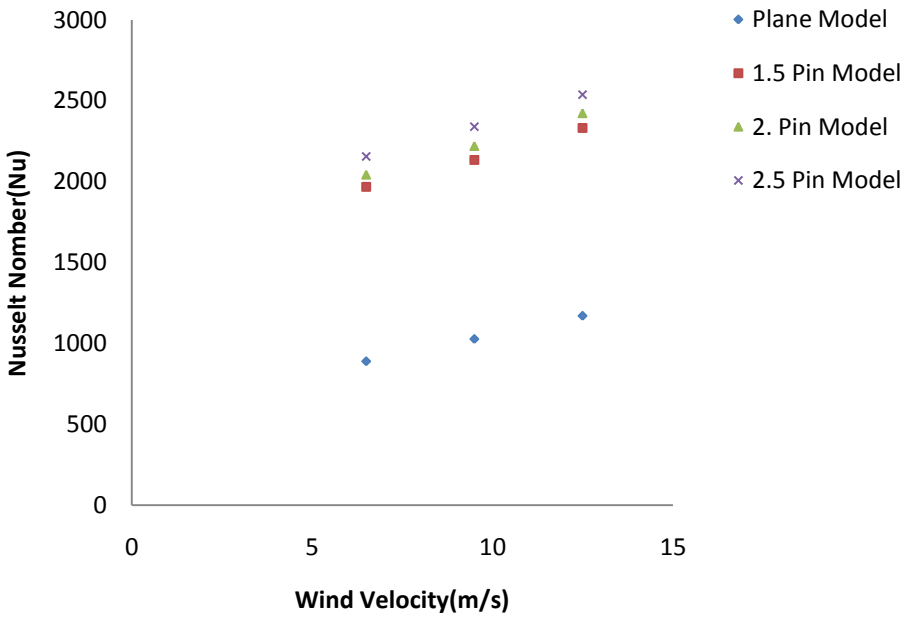

Fig.9Nusselt Number Variations for Different Fin Profile of Elliptical Pin.

The above Fig.9the Nusselt number variations for different fin profile of elliptical pin with compare the experimental result(7) of PFHS and simulation result of various fin profile of elliptical pin gives a constant deviation. This fig. shows the increase in the Nusselt number with increase the wind velocity (6.5, 9.5 & 12.5m/s).This is better result of experimental result.

Fig.10 Pressure Drop Variations for Different Fin Profile of Elliptical Pin.

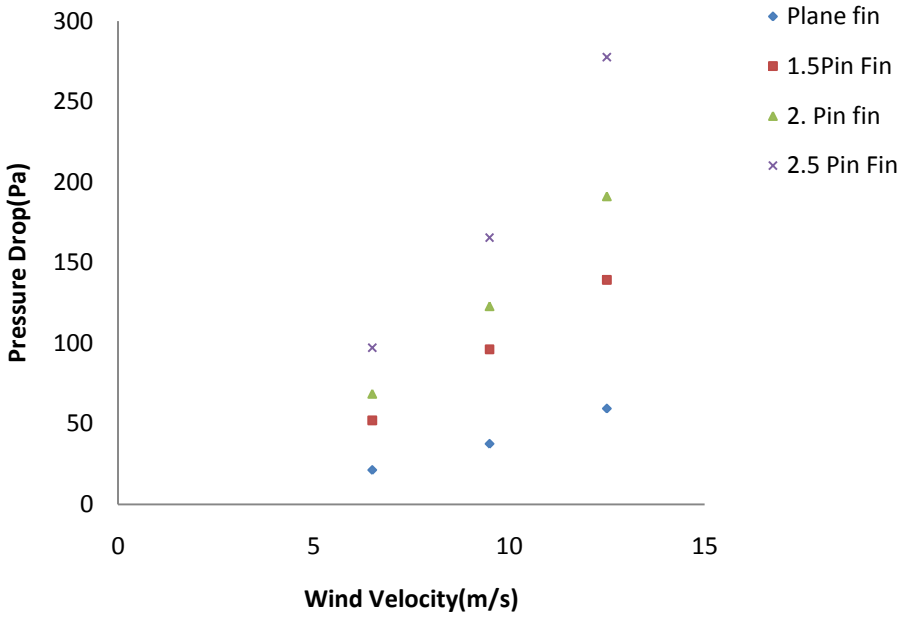

The above Fig.10the Pressure drop variations for different fin profile of elliptical pin with compare the plate fin result(7) of PFHS and simulation result of various fin profile of elliptical pin gives a constant deviation in elliptical fin pin heat sink but in similar manner of experimental results. This fig. shows the increase in the pressure drop with increase the wind velocity (6.5, 9.5 & 12.5m/s)

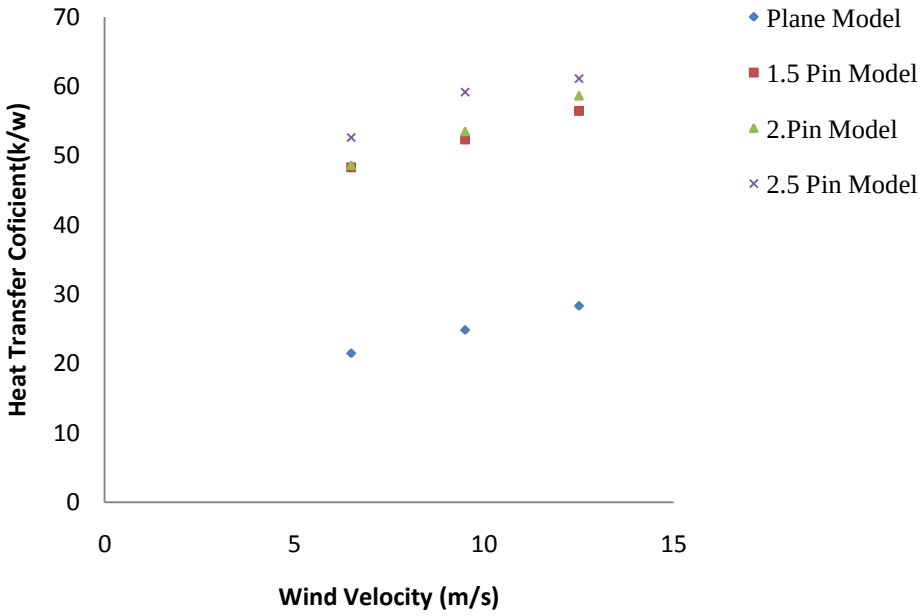

Fig.11Heat Transfer Coefficient Variations for Different Fin Profile of Elliptical Pin.

The above Fig.11as the wind velocity increases the heat transfer coefficient increases along the channel length because of growing boundary layer thickness.

3.3. Application:

Since heating power is uniform over the bottom of the fin base, thermal resistance of EPFHS always lower than PFHS. However heating of CPU is are always center of concentration on the fin base in real engineering application. Elliptical pin fin heat sink creates turbulence, so it can be use according to the cooling requirement.

IV. Conclusion

This paper proposes a special solution for improving heat transfer performance of elliptical pin fin by varying the major axis. Simulated the heat sink of elliptical pin fin having different minor axis (i.e. 1.5mm, 2.0mm & 2.5mm) and different velocities (i.e. 6.5, 9.5, & 12.5m/s) for constant heat input. From the above result we have least thermal resistance in elliptical pin fin with minor axis 2.5mm i.e. 0.7 K/W, after that 2mm minor axis i.e. 0.76K/W, subsequently with 1.5mm minor axis i.e. 1.7K/W. From the above result we have least pressure drop in elliptical pin fin with minor axis 1.5mm i.e. 145Pa, after that 2mm minor axis i.e. 180Pa, subsequently with 2.5mm minor axis i.e. 280Pa. So, from the above we can conclude that the 2mm minor axis elliptical pin fin at all velocity having better thermal resistance and pressure drop compared to 2.5mm and 1.5mm thermal resistance and pressure drop.

References

[1] S. Lee, Optimum Design and Selection of Heat Sinks, Proceedings of 11th IEEE Semi- Thermal Symposium, pp. 48-54, 1995.
[2] Sergent, J. and Krum, A., Thermal Management Handbook for Electronic Assemblies, First Edition, McGraw-Hill, 1998.
[3] Patankar SV. Numerical Heat Transfer and Fluid Flow. New York: McGraw-Hill; 1980.CFD-Wiki http://www.cfd-online.com/Wiki/Main Page
[4] Manay E., Sahin B., Yilmaz M., Gelis K, "Thermal Performance Analysis of Nanofluidsin Micro channel Heat Sinks", World Academy of Science, Engineering and Technology 67 2012.
[5] N. Nagarani, "Experimental Heat Transfer Analysis on Annular Elliptical Fins and Comparison with Circular Fins", European Journal of Scientific Research, ISSN 1450-216X Vol.73 No.2 (2012), pp. 143-156.
[6] Hung-Yi Li a, Go-Long Tsai et al, "Measurement of thermal and hydraulic performance of a plate-fin heat sink with a shield", Experimental Thermal and Fluid Science 42 (2012) 71–78.
[7] Yue-Tzu Yang, Huan-SenPeng, "Investigation of planted pin fins for heat transfer enhancement in plate fin heat sink", Microelectronics Reliability 49 (2009) 163–169.
[8] Xiaoling Yu , JianmeiFeng, "Development of a plate-pin fin heat sink and its performance comparisons with a plate fin heat sink", Applied Thermal Engineering 25 (2005) 173–182.

International Journal of Modern Engineering Research (IJMER)
www.ijmer.com Vol.3, Issue.2, March-April. 2013 pp-1123-1128 ISSN: 2249-6645

Genetic Algorithm based Fractal Image Compression

Mahesh G. Huddar
Lecturer, Dept. of CSE,Hirasugar Institute of Technology, Nidasoshi, India

Abstract:*Fractal Image Compression is a lossy compression technique that has been developed in the early 1990s. Fractal image compression explores the self-similarity property of a natural image and utilizes the partitioned iterated function system (PIFS) to encode it. The fractal image compression problem had three major requirements: speeding up the compression algorithm, improving image quality and increasing compression ratio. So far, several methods have been proposed in order to speed-up fractal image compression. The time is essentially spent on the search of the similar domain block. This paper aims to present a method that uses Genetic algorithms to speed up computation time in fractal image compression with acceptable image quality and high compression rate. These improvements are obtained by encoding all regions in the image with different size blocks.*

Keywords:*Fractal image compression; genetic algorithm.*

I. Introduction

Deterministic Fractals have the intrinsic property of having extremely high visual complexity while being very low in information content, as they can be described and generated by simple recursive deterministic algorithms. They are mathematical objects with a high degree of redundancy in the sense that they are recursively made of transformed copies of either themselves or parts of themselves.Fractal image compression (FIC) was introduced by Bernesly [1] and Jacquin [2]. Since then, many researches have improved the original approach in various ways [3]. The image compression problem puts forward three major requirements: speeding up the compression algorithm, improving image qualityafter compression/decompression or increasing compression ratio. The method based on the theory of partitioned Iterated Function Systems (PIFS) [3] has received a lot of attention in the last ten years. To encode an image according to the self-similarity property, each block must find the most similar domain block in a large domain pool.

In fractal image compression, the original image is partitioned into range blocks [8] and for each range block, a suitable domain block [2] D is searched, so it exists a transformation,

$$T: Dom(I) \rightarrow Ranges(I);$$
$$T \text{ must guaranty } \forall i, \exists j / T(D_j) \approx R_i$$

A transformation is associated to each R_i, it codes the D_j coordinates and parameters of the transformation.

The associated parameters for each R_i are: the isometric flip Rotation $\pi/2, \pi, 3\pi/2$, the horizontal flip, the vertical flip, the transposed of *Dom(I)*, the rotation π of the transposedof *Dom(I)*, the luminance and contrast.

A. General Structure of FIC Algorithm

A general structure for most proposed fractal compression algorithms, for both coding and decoding images can be given by:

Step 1: Encoding of an Image *I*

- Set t = some tolerance level
- Partitioning *I* into uncovered ranges R_i's.
- For each uncovered range $R_i$do
  - Search over all D_i's in the pool domains:
  - If ($\exists w_i$ such that$d(R_i, w_i(D_i)) < t$)
    - Report $w_i$and compress it using adaptivearithmeticCoding (or any other lossless compression scheme.)

    Else
  - Split R_i into sub-ranges and add them to the list of ranges to be covered.
- If the range can no longer be partitioned, return the minimum $d(R_i, wi(D_i))$.Remove R_i from the uncovered list.

Step 2: Decoding of a map $w = \cup w_i$

- Choose any image I_0, and then compute the image$w_n(I_0) = \cup w_{ni}(I_0)$. When n is big enough, $w_n(I0) \approx I_w \approx I$.

The major problem of this method is time consuming compared with others methods of image compression.In this paper, a new Genetic Algorithm forimage compression is proposed, that speed up this method when findinga LIFS [6] whose attractor is close to a given image.

II. Literature Survey

A fully automated fractal-based image compression technique of digital monochrome image was first proposed by Jacquin [2]. The encoding process consists of approximating the small image blocks, called range blocks, from the larger

blocks, called domain blocks, of the image, through some operations. In the encoding process, separate transformations for each range block are obtained. The scheme also uses the theory of vector quantization [4] to classify the blocks. The set consisting of these transformations, when iterated upon any initial image, will produce a fixed point (attractor) that approximates the target image. This scheme can be viewed as partitioned iterative function system (PIFS). One such scheme, using PIFS, to store fewer number of bits (or to increase the compression ratio) was proposed by Fisher et al. [7].

III. Fractal Image Compression Using Genetic Algorithm

There are many algorithms of optimization used for different domains. I have chosen Genetic Algorithm [7] [8] [9]to accelerate our fractal image compression algorithm.For each range domain R_i, the set of all possible domain blocks is genetically browsed until we find an appropriate solution. The genetic algorithm search space parameters are the domain block coordinates and the isometric flip.

A. Chromosome Attributes

A chromosome is constituted by 5 genes, from which only 3 genes are submitted to genetic modification, the two others are computed by the RMS equation.

- X_{dom},Y_{dom}, flip: which are optimised by genetic search?
- Contrast O, and scaling S: which are computed directly by RMS equation.

X_{dom}	Y_{dom}	Flip	O_{opt}	S_{opt}

Figure 1 Chromosome Representation

B. Genetic Operators

The crossover and mutation operators ensure the production of offspring. These genetic operators must be defined according to the chromosome specification. With these basic components, a Genetic Algorithm works as follows: The first procedure is to generate the first population represented with string codification (Chromosome) that represents possible solution to the problem. Each individual is evaluated, and according to its fitness, an associated probability to be selected for reproduction is assigned.

(1) Crossover Operator

The crossover operator combines two individuals in the current population, to produce two offspring individuals included in the new generation. The main role of this operator is to create good new solutions based on the characteristics of their parents. To perform this operation, individuals from current population are chosen randomly and proportionally to their fitness value. This operator with a probability value fixed as a parameter for the algorithm. Experimental results have shown that a value of 0.7 is good to ensure quick convergence of the algorithm. The result coordinates for the offspring individuals are obtained by a linear combination of the parents coordinates. A random number 'a' is generated in the interval [0, 1], then the new coordinates are calculated according to the following formula:

For the first offspring

$$X_{dom}=a* X_{dom1}+(1-a)* X_{dom2}$$
$$Y_{dom}=a* Y_{dom1}+(1-a)* Y_{dom2}$$

For the second offspring

$$X_{dom}=(1-a)* X_{dom1}+(1-a)* X_{dom2}$$
$$Y_{dom}=(1-a)* Y_{dom1}+(1-a)* Y_{dom2}$$

This crossover pattern is very efficient. It allows to explore all the image area if the two parents are in separated regions, and to explore the nearest neighbourhood if they are in the same region. Figure 2 illustrates the described crossover pattern.

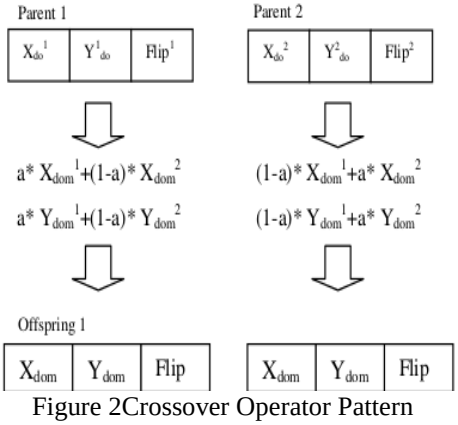

Figure 2Crossover Operator Pattern

(2) Mutation operator

Mutation operator is used in all implementations of genetic algorithms to introduce diversity in each population. Mutation is applied to individuals by changing pieces of their representations. These individuals are randomly selected according to their fitness value. At each position in the individual, we decide randomly, using a small mutation probability, whether the gene at this position is to be changed. This genetic operator allows the algorithm to explore new areas of the search space, and find new possible optimal solution. Here mutation operator is applied to some selected IFSs from the current population, one of the 3 genes X_{dom}, Y_{dom} and flip is selected randomly, and changed with a random generated value. Figure 3 shows the general pattern of the mutation operator in our algorithm.

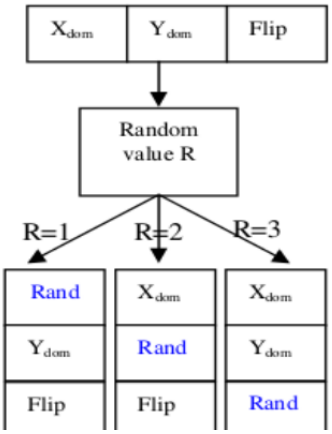

Fig. 3 Mutation Operator Pattern

C. Selection Process

To avoid the premature convergence effect, linear scaling is applied to each individual fitness then, the Roulette wheel method is used as a selection process.

D. Termination Criteria

Any genetic algorithm must find the optimal solution for a given problem in a finite number of steps. Two criteria can cause the termination of the algorithm when applied to a given range block:

- An acceptable value of fitness for the best in individual in the population is reached.
- A maximum predefined count of generations is reached.

This maximum count is a predefined parameter of the algorithm; it was determined experimentally and fixed to 20.

E. Parameters of the Algorithm

The set of parameters of genetic control is given by:

(1) Population size: specify the number of individuals in each generated population (constant during all steps);
(2) Crossover rate: specify the probability used to select individuals submitted to crossover operator;
(3) Mutation rate: specify the probability used to select individuals submitted to mutation operator;
(4) Maximum generations: specify the maximum number of generations to evaluate before assuming that a particular run has converged prematurely, and should be aborted.

F. The Fitness Function

In the case of IFS, the measure of quality for a given transformation is given by the RMS error between the coded range block, and the domain block determined by the transformation coordinates X_{dom} and Y_{dom}, and transformed with corresponding luminance and contrast values. This error is calculated using the root mean square equation. The fitness function is defined by the value of this error, which is inversely proportional to the efficiency of the corresponding individual.

G.The Genetic Fractal Image Compression Algorithm

Based on all these elements, the geneticcompression algorithm operate on an input image to the following general steps:

(Input I: NxNgrey scale image [Image would be square]
(Output W: Coded IFS);
(Region Size) = 16;
*(Fixed Error) = X * (Region Size)/4;*
Decompose the input image into (Region Size) blocks;
While Exist (Regions not coded)
-Scale the Domain Blocks;
-Generate a random population of chromosomes;
While Exist (Regions not coded) and (Last generation not reached)

-Compute fitness for all regions;
-When optimal domain block found write obtained transformation parameters to the output *W*;
-Generate new population {Apply Crossover and Mutation operators};

Wend
(RegionSize) = (RegionSize)/2;
*(FixedError) = X * (RegionSize)/4;*
If Regions size > 4
Decompose the rest region not coded into (Range Size) blocks;
Else
(FixedError) = (Fixed Error) +X;
Code all rest Regions;
IEnd
Wend

IV. Experimental Results

A. Std. Algorithm with Quad tree Partitioning

Image	RMS Limit	Execution Time	Quality (dB)	Compression Ratio
Lena	5.0	1:11:10	32.01	11.48 :1
Boat	5.0	1:27: 04	29.56	8.88:1
Peppers	5.0	1:05:17	33.07	24.56:1
Barb	5.0	1:22:15	33.07	10.85:1

Table 1. Result for different images with Quadtree blocks decomposition

B. Standard algorithm improved with Classification (Y. Fisher approach)

Image	RMS Limit	Execution Time	Quality (dB)	Compression Ratio
Lena	5.0	0:02:55	30.05	9.73 :1
Boat	5.0	0:03:22	25.86	7.9 :1
Peppers	5.0	0:02:45	29.36	10.16 :1
Barb	5.0	0:04:12	21.07	8.62:1

Table 2. Results for different images with Quad tree blocks decomposition using Fisher's classification

C. Genetic Algorithm

The genetic compression algorithm was used with Quad tree partitioning. Different parameters were used for each test, and the obtained results are given in both table forms and graphical forms. Examples of reconstructed images are also given to illustrate reconstruction quality.

The following table shows different performances with different value of RMS error limit using fixed value for other parameters: population size=100, mutation rate=0.1, crossover rate=0.7 and maximum generations count =20.

(1)Effect of parameters controlling fractal compression

We can see from the Graphs 1 and 2, that image quality is inversely proportionate to RMS error limit. And compression rate is proportionate to that value. The compromise value of this parameter is 5.0 and it gives very acceptable performances.

RMS Limit	Execution Time	Quality (dB)	Ratio	Ranges count
0.0	2 m 44 s	35.66	4.29:1	4096
2.0	1 m 56 s	35.03	6.35:1	2770
4.0	49 s	34.89	9.28:1	2023
5.0	43 s	34.80	9.82:1	1792
8.0	36 s	34.50	9.95:1	1768
10.0	33 s	30.50	10.05:1	1750
15.0	21 s	22.33	13.66:1	1288
20.0	14 s	19.36	19.34:1	910
25.0	13 s	19.01	26.25:1	670

Table 3. Different compression results of Lena image while applying different values ofRMS error limit

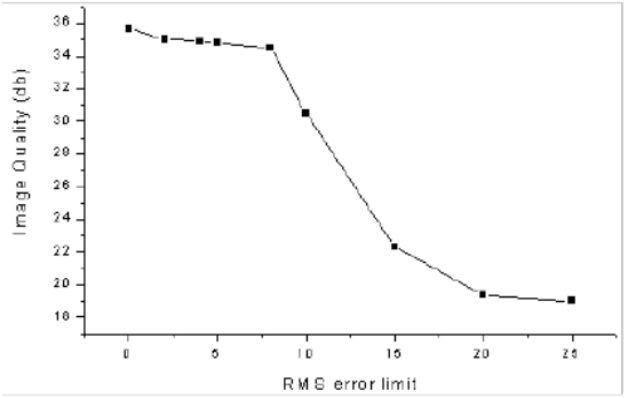

Graph 1 Lena image quality variation according to RMS limit values

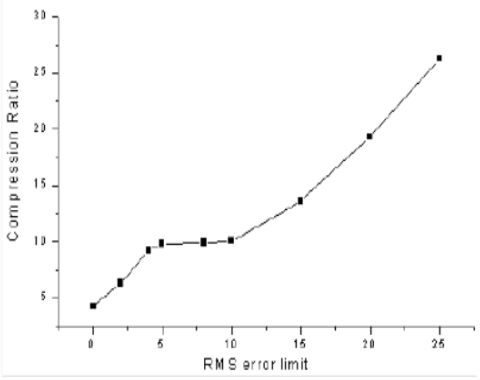

Graph 2 Lena image compression rate variation according to RMS limit values

(2) Effect of parameters controlling genetic evolution

Population Size	Execution Time	Quality (dB)	Ratio	Ranges count
5	9 s	29.62	8.30:1	2119
10	11 s	29.98	8.35:1	2107
20	14 s	30.21	8.72:1	2017
50	23 s	32.11	9.36:1	1879
100	44 s	32.23	9.83:1	1789
250	2 m 24 s	33.74	10.35:1	1699
500	7 m 4 s	34.56	10.83:1	1624
1000	23m 4 s	35.12	10.97:1	1603

Table 4 Different compression results of Lena image while applying different values of population size

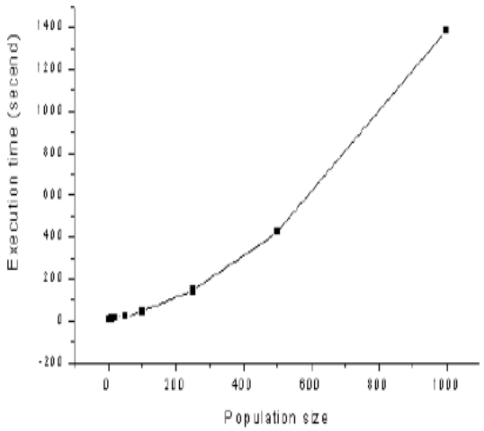

Graph3 Lena image compression time variation according to population size values

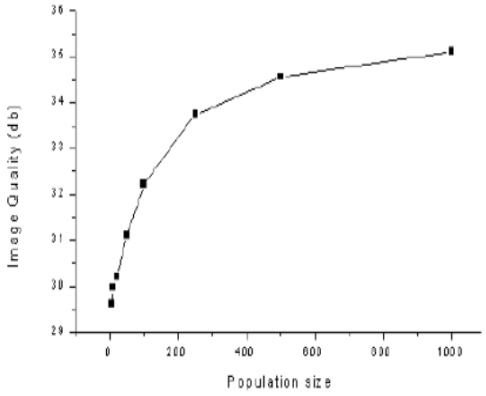

Graph 4 Lena image quality variation according to population size values

V. Conclusion

It is clear that the best image quality is always obtained using the standard schema, but its computation time makes it unpractical. So we must accept less quality in favour of quick compression. The main goal was to accelerate standard compression schema, without greatly decreasing both image quality and compression ratio. Furthermore this work demonstrates the genetic algorithms ability to solve complex problems.

References

[1] M. Barnsley and L. Hurt,"Fractal Image Compression", Peters, Wellesley, 1993
[2] A. E. Jaquin"Image coding based on a fractal theory of iterated contractive image transformations", IEEE Trans. on image Processing. 1, PP, 18-30, 1992.
[3] B.E. Wohlberg and G. de Jager,"A review of the fractal image coding literature", IEEE Trans. on image Processing. 8(12), PP, 1716-1729, 1999.
[4] VeenadeviS.V. And A.G.Ananth"Fractal Image Compression with Quadtrees", Signal & Image Processing: An International Journal (SIPIJ) Vol.3, No.2, April 2012.
[5] M.F. Barnsley and S. Demko. Iterated function systems and the global construction of fractals. In Proceedings of the Royal Society of London A399, pages 243 275, 1985.
[6] Arnaud E. Jacquin, "Fractal Image Coding: A Review", MEMBER, IEEE
[7] Y. Fisher, E. W. Jacbos, and R. D. Boss, "Fractal image compression using iterated transforms," in Image and Text Compression, J. A. Storer, Ed. Boston, MA: Kluwer, 1992, pp. 36–61.
[8] Y. Chakrapani and K. SoundaraRajan, "GENETIC Algorithm Applied To Fractal Image Compression", ARPN Journal of Engineering and Applied Sciences, VOL. 4, NO. 1, FEBRUARY 2009
[9] S. K. Pal, D. Bhandari, and M. K. Kundu, "Genetic algorithms for optimal image enhancement," Pattern Recognit. Lett, vol. 15, pp. 261–271, 1994.
[10] S. Forrest, Ed., Proc. 5th Int. Conf. Genetic Algorithms, San Mateo, CA, July 1993.

International Journal of Modern Engineering Research (IJMER)
www.ijmer.com Vol.3, Issue.2, March-April. 2013 pp-1129-1134 ISSN: 2249-6645

The Design and Implementation of an Android Game: Foxes and Chickens

Justin R. Martinez, [1] Wenbin Luo[2]
[12]*Engineering Department, St. Mary's University, San Antonio, United States*

Abstract: *In this paper, we present the design, implementation, and testing of an Android game, called Foxes and Chickens. It was developed for mobile devices with the Android mobile operating system. The Foxes and Chickens game itself has origins in South America, where it is very popular in some countries. However, to the best of our knowledge, no digital version of the game was available for mass consumption. Our research seeks to remedy this vacancy with the goal of adding values and enjoyment to users of the Android mobile devices. After going through strict software engineering processes of specification, design, coding, and testing, we successfully developed the game, as shown at the following link: http://www.youtube.com/watch?v=xeXYiR3Qwio. The game Foxes and Chickens is available for download from the Google play for anyone with an Android powered device. It has been tested for compatibility on the following mobile devices: T-Mobile's G1, HTC My Touch, and Verizon's Motorola Droid. It should run on other compatible Android handsets as well.*

Keywords: *Android development, foxes and chickens, Java, mobile games, software development*

I. INTRODUCTION

The Foxes and Chickens game is developed for mobile devices with an Android operating system, which was designed as an operating system for mobile devices by Google and the Open Handset Alliance based on the Linux kernel [1]. The Foxes and Chickens game is a turn-based strategy game that has similarities to Checkers and Chess (rules of the game can be found in Appendix). The game has two game modes (single player and two players) and three levels of difficulty (easy, intermediate, and hard). The object of the game is to move nine of the initial twenty chickens on the game board to safety, while the foxes attempt to prevent this by killing chickens within reach.

At the time of creation, game development on the Android platform was still in its early stage and few projects existed where the development process and sources were available for others to utilize. This research sought to remedy this vacancy by both documenting the creation and providing source code for others to learn from.

1.1 Product Features

A high level list of the major features of our developed game is as follows.

- Two operational modes: single player and two players.
- Three tiers of difficulty: easy, intermediate, and hard
- Invalid movements are not allowed.
- In-game rule-set, tutorial mode where invalid moves are explained.
- Non-Player Character (NPC) movement accomplished in fixed time.
- Intuitive and linear interface.
- Smooth animation system.
- Bright, vibrant colors.

These represent the major categories of the requirements and will be explained in more details in the remainder of this paper.

1.2 User Classes and Characteristics

There is one class of user for the game: the player class. The player can be either male or female, most likely technically savvy (due to the target platform), and can be classified as a casual gamer. Casual gamers tend to enjoy simple, yet dynamic games that are easy to understand, frequently reward the player, are short in duration (as opposed to games where characters must be developed and nurtured), and have high re-playability by not becoming boring or repetitive.

1.3 Online Help

A help screen will be provided to assist in understanding the rule-set for the game. No other documentation will be provided to the user. The linear and clean structure of the user interface makes additional help unnecessary. One of the help screens is shown in Fig. 4 of section III: user interfaces. Help screens are intended to give the player an overview of how the game is played.

II. SYSTEM ANALYSIS AND DESIGN

The system analysis of the proposed Foxes and Chickens game involved the formulation of use cases, sequence diagrams, and state diagrams of the game. To properly understand and explicate out the game's flow, we developed a number of use cases. All of these techniques allowed us to better articulate the requirements of the system in terms of objects, classes, attributes, relationships, scenarios, and actors. A sample use case is shown below.

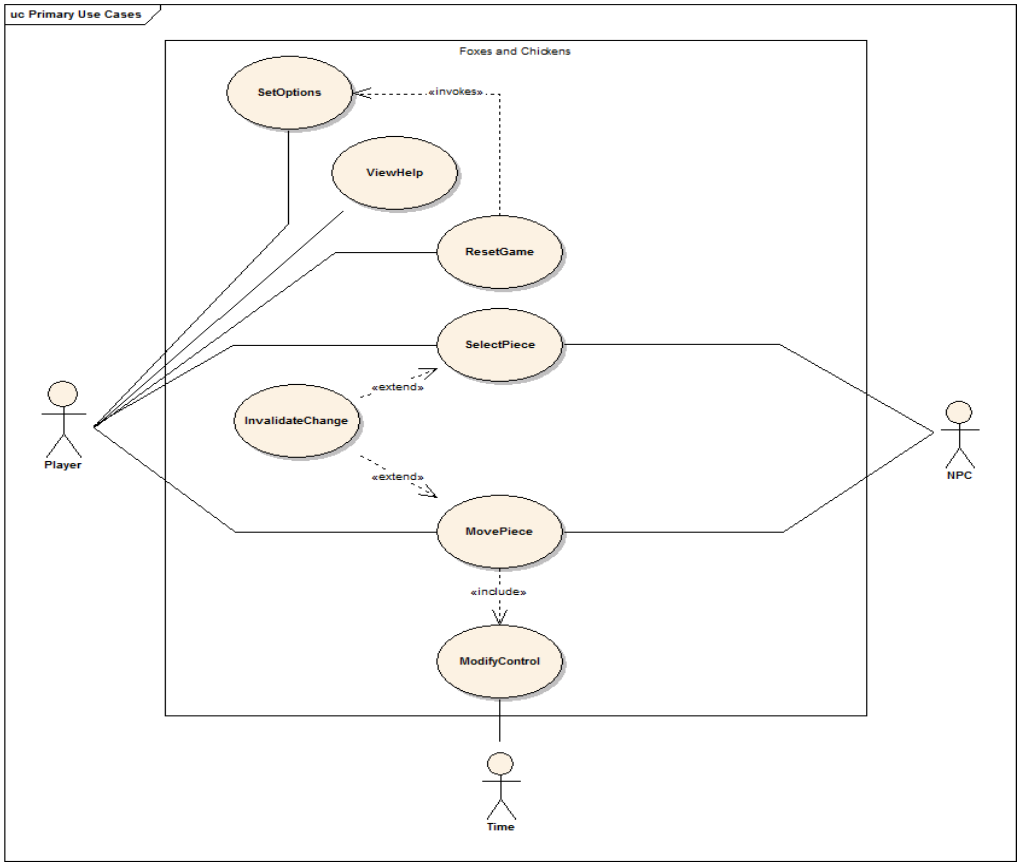

Figure 1. Use case

Sequence diagrams are the interaction diagrams that show how processes operate with one another and in what order. The aforementioned use case was captured in the following sequence diagram which we developed for the *Foxes and Chickens* game. In this use case, the player launches the game or has selected to reset the game while playing. If the player has launched a new game the default values are used for the selection available to them, while a reset game will use the setting from the previous play. After accepting the defaults or correcting them to the player's desire, the game is launched.

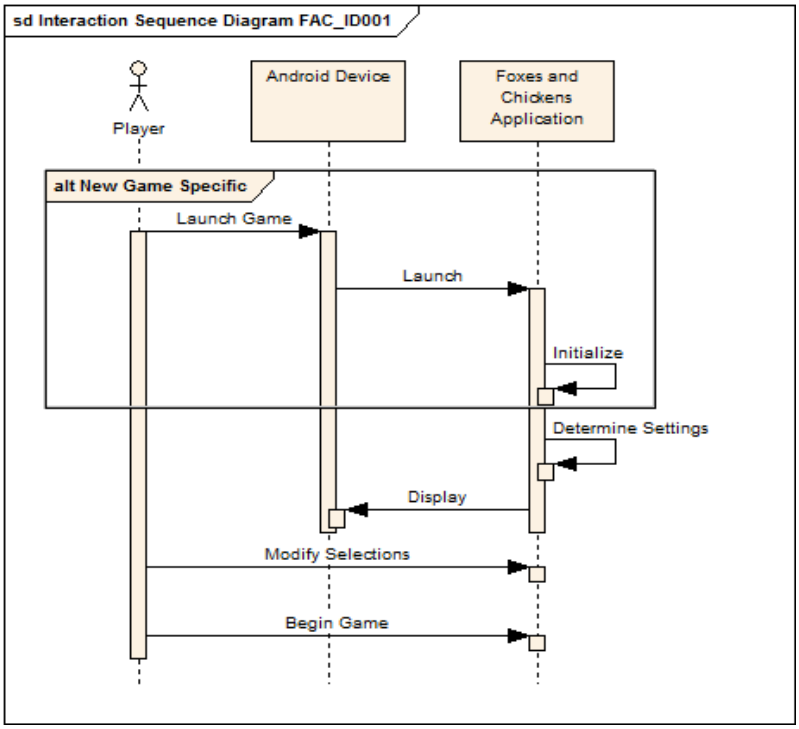

Figure 2. Sequence diagram

At its most basic, the game functions as a simple state machine. As the player interacts with the system, control flows between discreet points, each with separate logic. When the game is started, the user is prompted to select the number of players, dynamic help and whether to enable audio. If the number of players is "one", the user is then asked about the difficulty level. After that, the game begins. After the user selects a piece to move and selects a destination, the move is validated. In the case of the NPC mode, validation is skipped as it is an integral part of the artificial intelligent process in the system. The system then checks the game for a *game over* state. If the game is over, the user is prompted to reset. Otherwise, the active player is toggled and the process cycles.

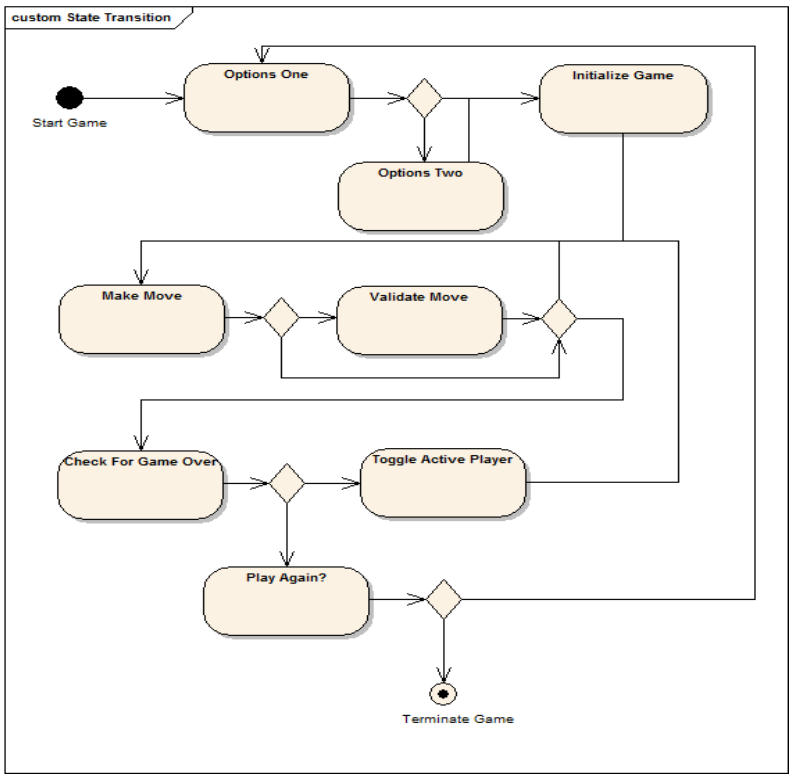

Figure 3. State map

III. USER INTERFACES

Usability and portability are the most important quality attributes applicable to this research project. Since the *Foxes and Chickens* game is targeted toward casual gamers, the interface and mechanics of game play are required to be simple and straight forward. This section provides several sample screen images representing the general "look and feel" of the interface and a visual representation of applicable system features and game states.

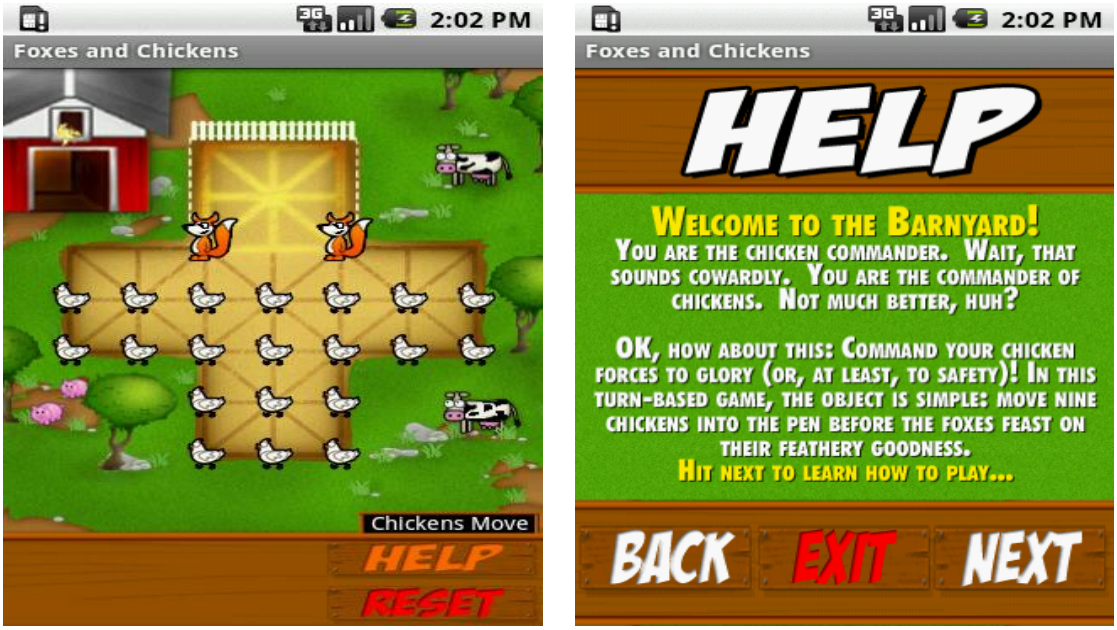

Figure 4. Sample screen images

Upon initial launch, the game enters *SelectPlayersState*, where the user notifies the system of the number of players. In the sample images presented, the user would have selected "One". This selection transitions to *Select Dificulty State* where the user notifies the system of the difficulty level at which he could like to play. After *Select Difficulty State*, the system has enough information to initialize the game and allow game play to begin. *Game play State* is not a single state but an aggregation of several states. Upon completion of game play, the system transitions to the *End Game State*, where the user is notified of his success or failure.

When the user options to be notified of invalid movements, he will see a text message appear in a notification area after an invalid move attempt.

IV. IMPLEMENTATION AND TESTING

The software development utilized the Eclipse Integrated Development Environment (IDE) with the Android Software Development Kit (SDK) that is cross platform among Windows, Linux, or Macintosh. In the case of this research project, the following configuration was used: Windows Vista SP2, Java 1.6, Eclipse 3.5, and Android SDK 1.5r3. Testing occurred on a T-Mobile G1 and HTC My Touch running the Android OS, versions 1.5 and 1.6 and on a Motorola Droid running the Android OS version 2.0.

The figure below shows the deployment model for the Foxes and Chickens game. As stated previously, required is a T-Mobile G1 Handset running the Android OS version 1.5. When packaged within Eclipse, the resultant file is of type *.apk, which is an encrypted and compressed java package. When the game is installed on a target device, the application icon is extracted and yet the application itself remains in the apk form.

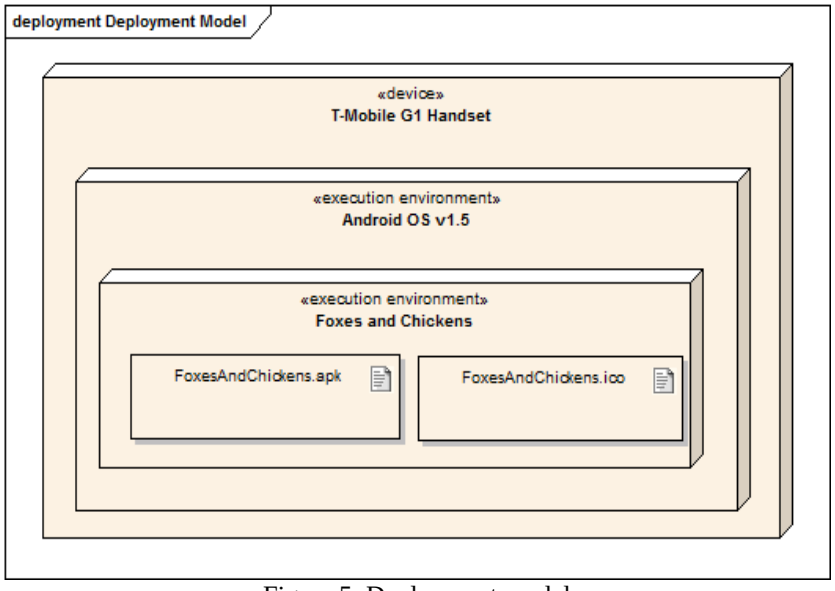

Figure 5. Deployment model

The final step, which is arguably one of the most important, is testing. It is of crucial importance to ascertain whether a software system does what it is supposed to do and fulfills the requirements set forth by the stakeholders of the system. Testing occurred throughout the development process and the findings helped shape development and game features. A few examples of the bugs found are listed below:

- Foxes, after completing a multi-jump, would land in invalid locations.
- Resetting the game would change the user selections from the previous launch.
- Several obscure issues that ended up being related to thread messaging.

At the time of this writing, there have been about 10,000~50,000 downloads of the *Foxes and Chickens* game from Google play (https://play.google.com/). The game is free to use and the source code will be made available to the public to help others learn about Android development. After we fixed issues found by users in the initial release of the game, users posted very positive comments on the game, such as 1) Very challenging, which is what makes it fun; 2) Challenging works flawlessly on Samsung Galaxy S; 3) Very smart game with cool graphics; 4) Fun game looks good; 5) Classic game - great when waiting for a flight or similar; works well.

V. CONCLUSION

In this paper, we presented an Android game named Foxes and Chickens that we have successfully designed and implemented for the Android mobile devices. Solid software engineering principles were utilized in the design and implementation of the Foxes and Chickens game. In addition, we performed extensive testing to validate different functionalities available in the game. Our testing and users' positive comments indicated that the Foxes and Chickens game met user expectations and is a fun game to play on Android mobile devices.

REFERENCES

[1] Open Handset Alliance, http://www.openhandsetalliance.com/
[2] Android Developers Web Portal, http://developer.android.com/index.html
[3] J. Arlow and I. Neustadt, UML 2 and the unified process (Addison-Wesley, MA: Boston, 2005).
[4] C. Fox, Introduction to software engineering design (Addison-Wesley, MA: Boston, 2006).
[5] R. Pressman, Software engineering (McGraw-Hill, NY: New York, 2005).

APPENDICES I: the Foxes and Chickens game rules

- Both players must move each turn. If a player is unable to move any pieces, that player loses. In the case of foxes, if a fox ever becomes trapped (i.e. cannot move), that fox is removed from the game.
- Foxes can move one unit in any direction, but in order to kill a chicken, the next unit beyond the chicken must be vacant. (This is akin to jumping in checkers).
- Foxes can perform multiple kills per turn provided that they do not violate any other rule (multi-jumps).
- Chickens can only move one unit in a forward or side direction. They may not move backwards. (Forward is defined as up, toward the chicken-pen).
- Movement is constrained to the directional paths as displayed on the game board.
- The chickens win by filling the pen with nine chickens. The foxes win by reducing the number of chickens on the board to a number less than nine.

APPENDICES II: Code snippet: scoring a move

```
//At intermediate difficulty, this method generates a score for the position passed in. For the Hard //setting, this is expanded to also take into account if a move will yield a future attack.
private int scoreMove(int curPos, int futPos, boolean hard) {
   int retVal = INVALID_MOVE;
   //foxes get a bonus for staying in the pen at hard difficulty
   int additive = futPos < (curPos-5) ? 1 : 0;
   if(fac.gameState[futPos] == 'x' || fac.gameState[futPos] == 'f')
      retVal = INVALID_MOVE;//impossible move
   else if (fac.gameState[futPos] == 's') {
      if(checkIndexForFutureKills(futPos)) {
         //movement which leads to a future kill (in one move)
         retVal = KILL_NEXT_ROUND;
         //if set to hard, give the applicable bonus
         retVal = hard ? (retVal + additive) : retVal;
      }
      else if(hard) {
         for(int i = 0; i < 8; i++) {
            int tempIdx = fac.movementMatrix[futPos][i];
            if(checkIndexForFutureKills(tempIdx))
               //movement which leads to a future kill (in two moves) is worth 2
```

```
                retVal = KILL_IN_2_ROUNDS;
            }
            //even if there are not future kill, this is still a valid move
            if(retVal == INVALID_MOVE)
                retVal = VALID_MOVE;
        }
        else
            retVal = VALID_MOVE;
    }
    else {//fac.gameState[futPos] == 'c' ... we need to check for a kill, or multiple kills
        if(checkIndexForKills(curPos, futPos) == false) {
            retVal = INVALID_MOVE;//no kill = invalid move
        }
        else {
            //by hitting this block we have a kill
            retVal = KILL_THIS_ROUND;
            //calculate the landing index
            int diff =  futPos - curPos;
            int landingIdx = futPos + diff;
            //check it for future kills
            if(checkIndexForFutureKills(landingIdx)) {
                retVal += KILL_NEXT_ROUND;//multiple kill
                if(hard) {
                    for(int i = 0; i < 8; i++) {
                        int tempIdx = fac.movementMatrix[landingIdx][i];
                        if(checkIndexForFutureKills(tempIdx))
                            retVal += KILL_IN_2_ROUNDS;
                    }
                }
            }
            retVal = hard ? (retVal + additive) : retVal;//if set to hard, give the applicable bonus
        }
    }
    return retVal;
}
```

International Journal of Modern Engineering Research (IJMER)
www.ijmer.com Vol.3, Issue.2, March-April. 2013 pp-1135-1138 ISSN: 2249-6645

A Review on Study of Analysis of Chassis

Monika S. Agrawal, [1] Md. Razik[2]
[1]*Pursuing M.E. Mechanical Engineering, Department, Babasaheb Naik college of Engineering, pusad, India*
[2]*Assistant Professor, Mechanical Engineering, Department, Babasaheb Naik college of Engineering, pusad, India*

Abstract: *In this paper an effort is made to review the investigations that have been made on the different analysis techniques of automobile frames. That analysis may be fatigue analysis, static analysis or dynamic analysis. A number of analytical and experimental techniques are available for the analysis of the automobile frames. Determination of the different analysis around different condition in an automobile frames has been reported in literature.*

Keywords: *Fatigue life prediction, Automotive Vehicles, static analysis, dynamic analysis*

I. Introduction

Truck chassis is a major component in a vehicle system. This work involves static and dynamics analysis to determine the key characteristics of a chassis. The static characteristics include identifying location of high stress area and determining the torsion stiffness of the chassis. The dynamic characteristics of chassis such as the natural frequency and mode shape were determined by using finite element (FE) method; Experimental modal analysis was carried out to validate the FE models. Modal updating of the chassis model was done by adjusting the selective properties such as mass density and Poisson's ratio. And other properties also the modification of the updated FE truck chassis model was proposed to reduce the vibration improve the strength and optimize the weight of the chassis. Chassis has a considerable affected to the performance of the vehicle. Also known as the "back bone" of the vehicle, it will be subjected to mechanical shocks, and vibrations and the result were the failures some component and resonant was the worst problem can be happened. Therefore, the prediction of the dynamic properties of the chassis is great significance to determine the natural frequencies of the structure to make sure working frequency are lower than natural frequency of the chassis to avoid resonant and determine the stress distribution on the chassis when receive the load. The finite element modeling issues regarding the experimental analysis of vehicle chassis is addressed for the natural frequency analysis (modal) by using different analysis software such as Ansys, Algor, Ls-Dyna

II. Fatigue, static & Dynamic Analysis

Fatigue damage concepts:

Stress-Life Diagram (S-N Diagram): The basis of the Stress-Life method is the Wohler S-N diagram, shown schematically for two materials in Figure 2.The S-N diagram plots nominal stress amplitude S versus cycles to

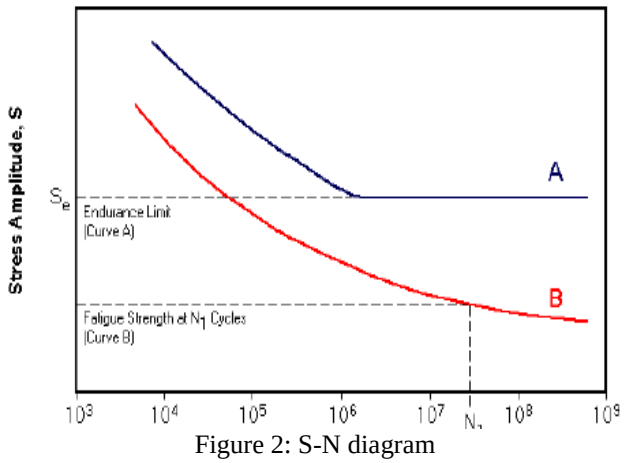

Figure 2: S-N diagram

Failure N. There are numerous testing procedures to generate the required data for a proper S-N diagram. S-N test data are usually displayed on a log-log plot, with the actual S-N line representing the mean of the data from several tests.

Roslan Abd Rahman, Mohd Nasir Tamin did the stress analysis of heavy duty truck chassis. The stress analysis is important in fatigue study and life prediction of components to determine the critical point which has the highes t stress which is shown in fig 4. The analysis was done for a truck model by utilizing a commercial finite element packaged Abaqus.

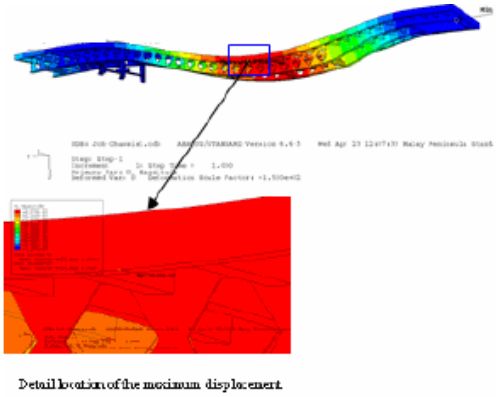

Fig 4: Displacement distribution of truck frame

Cicek Karao glu and N. Sefa Kuralay did the finite element analysis of a truck chassis. The analysis showed that increasing the side member thickness can reduce stresses on the joint areas, but it is important to realize that the overall weight of the chassis frame increases. Using local plates only in the joint area can also increase side member thickness. Therefore, excessive weight of the chassis frame is prevented.

In November 2008 Mohamad Tarmizi Bin Arbain Mechanical Engineering department Universiti Malaysia Pahang he use 3D model for finite element analysis issues regarding the experimental analysis of car chassis is addressed. The modeling approach is investigated extensively using both of computational and compared it to experimental modal analysis. A comparison of the modal parameters from both experiment and simulation shows the validity of the proposed approach. Then perform the computational stress analysis with linear material type analysis to find the stress concentration point in the car chassis.

Karaoglu and Kuralay investigated stress analysis of a truck chassis with riveted joints using Fem. Numerical results showed that stresses on the side member can be reduced by increasing the side member thickness locally. Fermer et al investigated the fatigue life of Volvo S80 Bi-Fuel using MSC/Fatigue Conle and Chu did research about fatigue analysis and the local stress –strain approach in complex vehicular structures. Structural optimization of automotive components applied to durability problems has been investigated by Ferreira et al

Filho Et. *al.* have investigated and optimized a chassis design for an off road vehicle with the appropriate dynamic and structural behavior.In1837, Wilhelm Albert publishes the first article on fatigue. He devised a test machine for conveyor chains used in

In July 2011 Kutay Yilmazçoban*, Yaşar Kahraman, Sakarya University, Mech. Eng. Dept., 54187 Serdivan-Sakarya, Turkey put some works on the chassis optimization by using the finite analysis, his main focus was on the redused the wight of the chassis for that he used three thickness 4 mm,5 mm & 6 mm and after analysis he conclude that the 4 mm thickness is better because the stress and the displacement in that is better than other two thickness.

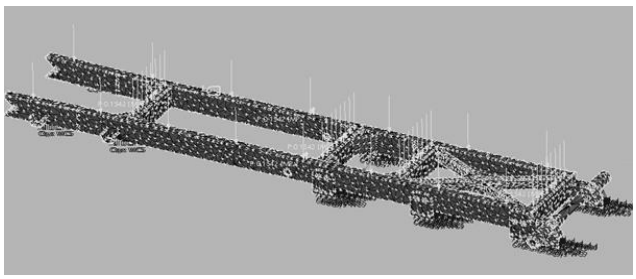

Figure: Truck chassis Finite Element Model

Teo Han Fui, Roslan Abd. Rahman, Faculty of Mechanical Engineering, Universiti Teknologi Malaysia, in December 2007, works on the Statics and Dynamics Structural Analysis of a 4.5 Ton Truck Chassis, he determined the dynamic characteristic, of the truck chassis, investigating the mounting locations of components on the truck chassis and observing the response of the truck chassis under static loading conditions. The local bending vibration occurs at the top hat cross member where the gearbox is mounted on it. And hence, the mounting location of the engine and transmission system is along the symmetrical axis of the chassis's first torsion mode where the effect of the first mode is less. However, the mounting of the suspension system on the truck chassis is slightly away from the nodal point of the first vertical bending mode. This might due to the configuration of the static loading on the truck chassis. For the linear static analysis, the stress distribution and deformation profile of the truck chassis subjected to two loading conditions: truck components loading and asymmetrical loading had been determined. Maximum stress occurred at the mounting brackets of the suspension system while the maximum translation occurred at the location where the symmetry and asymmetry load is acting. The maximum stress of the truck chassis is 490 MPa while the maximum translation is 33.6 mm. These values are acceptable as compared to the yield strength of the chassis material and the tolerance allowed for the chassis.

No.	Components	Weight (kg)	Load (N)	Position from origin (mm)
1	Cab	125	1226	4183
2	Engine	50	490	3875
3	Engine	100	981	3523
4	Cab	125	1226	3216
5	Gear box	50	490	2873
6	Pay load	417	4088	2873
7	Fuel tank	40	392	2433
8	Pay load	417	4088	2150
9	Chassis weight	200	1962	2150
10	Fuel tank	40	392	2023
11	Exhaust	20	196	1805
12	Pay load	417	4088	1710
13	Pay load	417	4088	1080
14	Pay load	417	4088	450
15	Pay load	417	4088	0

Table: Weights and forces of components and positions along the chassis

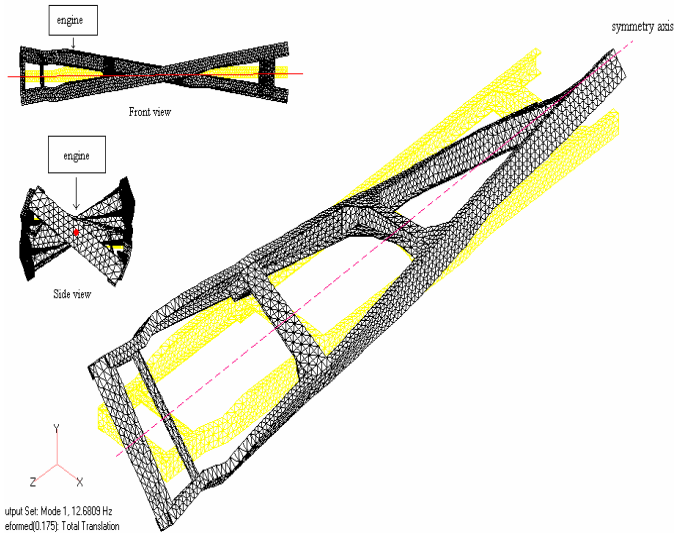

Figure: Mounting location of engine and transmission on the chassis

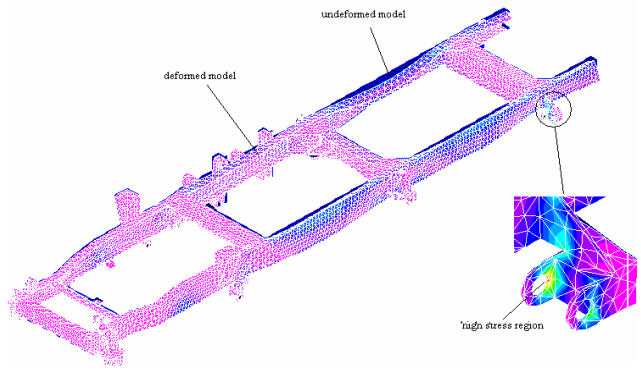

Figure: Stress contour and deformation pattern of the chassis under truck components loading.

O Kurdi, R Abd- Rahman, M N Tamin, Faculty of Mechanical Engineering Universiti Teknologi Malaysia 81310 Utm Skudai, Johor, works on the, Stress Analysis Of Heavy Duty Truck Chassis Using Finite Element Method, he mainly focus on the important steps in development of a new truck chassis is the prediction of fatigue life span and durability loading of the chassis frame. Fatigue study and life prediction on the chassis is necessary in order to verify the safety of this chassis during its operation. Stress analysis using Finite Element Method (FEM) can be used to locate the critical point which has the highest stress. This critical point is one of the factors that may cause the fatigue failure.

In June 2012 Haval Kamal Asker1, Thaker Salih Dawood1 and Arkan Fawzi, put some works on the Stress Analysis of Standard Truck Chassis during Ramping on Block Using Finite Element Method and he focused on the intensity and the strength of the frame play a big role in the truck's design. A frame of 6 wheels, standard dump truck has been studied and analyzed using Ansys package software. The static intensity of the frame has been analyzed when exposed to pure

bending and torsion stress, within two cases. First case is when the rear wheels zigzag gets over block (only one side of the chassis steps the block), and the second case is when both wheels gets over the block. The results show important differences between the two case studies, especially in the torsion and deformations results obtained from the chassis model. Also, vibration modes have been analyzed during the loading conditions. The more damping ratio Used, the more stabilizing of the stresses with respect to time

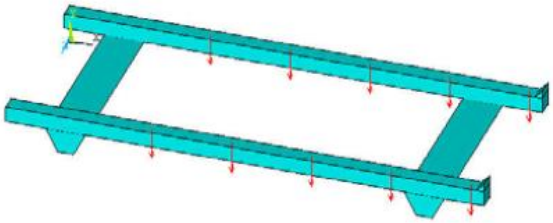

fig: model of chassis

III. Conclusion

In this paper an effort is made to review the investigations that have been made on the analysis of various automobile frames. An attempt has been made in the article to present an overview of various techniques developed for the analysis of automobile frames and results of that analysis due to which further study on the chassis will become easy An information of assessment of a suspension arm, vehicle suspension components, analysis of truck chassis, for the fatigue analysis of a truck chassis with riveted joints are considered.

References

[1] Stress Analysis Of Heavy Duty Truck Chassis As A Preliminary Data Using Fem, Roslan Abd Rahman, Mohd Nasir Tamin, Journal Mekanikal, December 2008, No.26, 76 – 85.
[2] Statics and Dynamics Structural Analysis Of A 4.5 Ton Truck Chassis, Teo Han Fui, Roslan Abd. Rahman*, Journal Mekanikal, December 2007, No. 24, 56 – 67
[3] Stress analysis of a truck chassis with riveted joints, Cicek Karaoglu, N. Sefa Kuralay, Journal of Finite Elements in Analysis and Design 38 (2002), Elsevier Science, page no- 1115–1130.
[4] Karaoglu, C. and Kuralay, N.S., 2000. Stress Analysis of a Truck Chassis with Riveted Joints, Elsevier Science Publishers B.V. Amsterdam, the Netherlands, Vol. 38, 1115-1130.
[5] Conle, F.A. and Chu, C.C., 1997. Fatigue Analysis and the Local Stress-strain Approach in Complex Vehicular Structures, International Journal of Fatigue.
[6] Filho, R.R.P., Rezende, J.C.C., Leal, M. de F., Borges, J.A.F., 2003. Automotive Frame Optimization, 12th International Mobility
[7] In July 2011 Kutay Yilmazçoban*, Yaşar Kahraman, Sakarya University, Mech. Eng. Dept., 54187 Serdivan-Sakarya, Turkey
[8] Teo Han Fui, Roslan Abd. Rahman, Faculty of Mechanical Engineering, University Teknologi Malaysia, December 2007, STATICS and Dynamics Structural Analysis of a 4.5 Ton Truck Chassis,
[9] O Kurdi, R Abd- Rahman, M N Tamin, Faculty of Mechanical Engineering University Teknologi Malaysia 81310 UTM Skudai, Johor, Stress Analysis Of Heavy Duty Truck Chassis Using Finite Element Method
[10] JUNE 2012 Haval Kamal Asker1, Thaker Salih Dawood1 And Arkan Fawzi Stress Analysis Of Standard Truck Chassis During Ramping On Block Using Finite Element Method

International Journal of Modern Engineering Research (IJMER)
www.ijmer.com Vol.3, Issue.2, March-April. 2013 pp-1139-1145 ISSN: 2249-6645

Virtual Reality: Opportunities and Challenges

Maryam Vafadar
Department of Electronic, Sama technical and vocational training college, Islamic Azad University, Islamshahr Branch, Islamshahr, Iran

Abstract: *Virtual Reality systems have drawn much attention by researchers and companies in the last few years. Virtual Reality is a term that applies to computer-simulated environments that can simulate physical presence in places in the real world, as well as in imaginary worlds. Interactivity and its captivating power, contribute to the feeling of being the part of the action on the virtual safe environment, without any real danger. So, Virtual Reality has been a promising technology applicable in various domains of application such as training simulators, medical and health care, education, scientific visualization, and entertainment industry. Virtual reality can lead to state of the art technologies like Second Life, too. Like many advantageous technologies, beside opportunities of Virtual Reality and Second Life, inevitable challenges appear, too. This paper is a technical brief on Virtual Reality technology and its opportunities and challenges in different areas.*

Keywords: *Virtual Reality, Virtual environment, training simulators, Second Life*

I. INTRODUCTION

Virtual Reality is described in various and sometimes inconsistent ways in some publications and conferences because this technology is new and writers attempt to define it based on different perspectives such as the tools it uses, its functions, etc [1]. If we consider the perspective based on functionality, Virtual reality (VR) is a term that applies to computer-simulated environments that can simulate physical presence in places in the real world, as well as in imaginary worlds. In other word, virtual Reality is a simulation in which computer graphics is used to create a realistic looking world. Moreover the synthesized world is dynamic and responds to user inputs such as gestures and verbal commands.

Virtual Reality is a real-time and interactive technology. It means that the computer is able to detect user inputs and modify the virtual world instantaneously. Interactivity and its captivating power contribute to the feeling of being the part of the action on the environment that the user experience. All human sensorial channels can be used to have a high level interaction. Most current virtual reality environments are primarily visual experiences, displayed either on a computer screen, but some simulations include additional sensory information, such as sound through speakers or headphones. Some advanced simulators, use haptic systems which include tactile information, generally known as force feedback. So, we can summarize the above ideas of Virtual Reality in one definition [1]: Virtual Reality is a high-end user interface that involves real time simulation and interaction through multiple sensorial channels like visual, auditory or tactile. Samples of Virtual Reality interaction are illustrated in Figure 1.

In1962, inspired by holographic movies, Morton Heilig patented the design called “sensorama”. The patent is the first video device of virtual reality by which a user can feel the vibration, sound, smell, and wind recorded in advance. The head-mounted video is similar to the head mounted display seen in the early 1990s. In1965, the founder of computer graphics, Sutherland [2] inherited and developed the design of Heilig. Sutherland presented the basic concept of a virtual reality system which had multi-senses, immersion, and interaction. In1966, funded by the navy scientic research office, American MIT Lincoln Laboratory developed the first head-mounted display (HMD) and applied the feedback devices which simulate the force and tactile in the system later. In1967, inspired by the conception of Sutherland’s system, the University of North Carolina launched the GROPE project which researched and developed force feedback devices that made users feel computer simulated force. In 1968, organized by Harvard University, Sutherland designed the helmet mounted display and later a virtual system which was considered as the first virtual reality system. In 1970, American MIT Lincoln Laboratory developed a full-fledged HMD system. In1973, Krurger [3] presented the term “artificial reality”, which was the early term of virtual reality.

In 1987, Foley [4] published a paper entitled “Interfaces for Advanced Computing” in the journal “Scientifc American”. Another paper [5] about data gloves was also published in this journal. These published papers about virtual reality attracted people greatly. In 1989, American Jarn Lanier formally presented the term “virtual reality”. In 1994, Burdea and Coiffet [6] published a book about virtual reality in which they summarized the basic characters of VR as 3I (imagination, interaction and immersion).

From 1995 up to now, by development of computer graphic science, “Virtual Reality” has become one of state of the art topics and researchers attempt to create more realistic environment and more active interfaces for high quality interaction in this field.

Figure. 1. Samples of Virtual Reality interaction

Virtual Reality technology has been a promising technology applicable in various domains of application such as training simulators [7], medical and health care, rehabilitation [8], education [9-10], engineering [11], scientific visualization [12], and entertainment industry. In addition, Virtual reality can lead to state of the art technologies like Second Life, too [13-14]. Like many advantageous technologies, beside opportunities of Virtual Reality and Second Life, inevitable challenges appear, too.

This paper is a technical brief on Virtual Reality technology and its opportunities and challenges in different areas. After this introduction, in section 2, virtual reality types and structural elements of a virtual reality system are described. Then sections 3 & 4 explain two main of these elements: Virtual Environment and Virtual Reality Interfaces, consequently. Section 5 presents applications of virtual reality that providing opportunities for humanity in various domains. Section 6 describes challenges of applying virtual reality technology and at last, conclusion appears in section 7.

II. VIRTUAL REALITY TYPES

We can categorize Virtual Reality systems into three groups depending on the degree of immersion and interactivity. These three groups are immersive systems, non-immersive systems and hybrid VR systems. Immersive systems replace our view of the real world with the computer-generated images that interact to the position and orientation of the user's head. A non-immersive system on the other hand, leaves the user visually aware of the real world but able to observe the virtual world through some display device such as graphics workstation. A hybrid VR system permits the user to view the real world with virtual images superimposed over this view. Such systems are also known as "Augmented Reality" systems. A practical example is found in the HMDs used by fighter pilot, which allow the pilot to view their outside world simultaneously with overlaid synthetic graphics. [15]

A generic immersive VR system consists of three system elements interacting with each other to make the whole functioning system. These three elements are the Virtual Environment, the computer environment and VR Interfaces. VE covers ideas such as model building, introducing dynamic features and physical constraints. The computer environment includes the processor configuration, the I/O channels the VE database and the real-time operating system and VR Interfaces encompass the hardware used for tracking head, recognizing hand gestures, detecting sound or haptic, 3D interfaces and multi-participant systems. The connectivity between the system elements is depicted in Figure 2 [15].

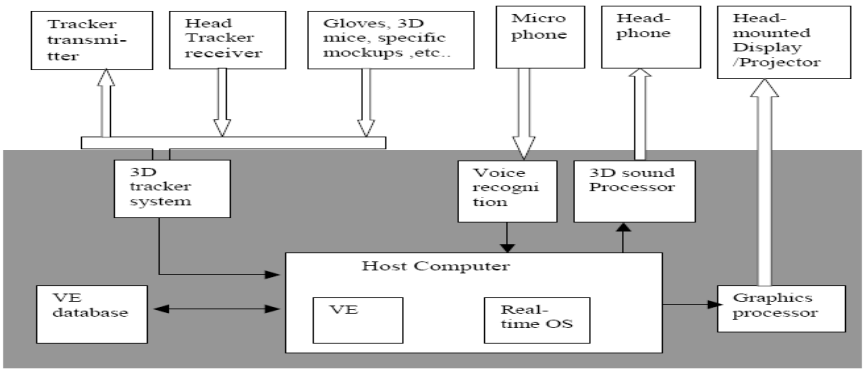

Figure. 2. Connectivity between elements of a Virtual Reality system

The core of our research in this paper is Virtual reality systems with realistic environment and active interfaces, so discussion about computer environment is out of this research framework. We describe virtual environment and VR interfaces in the following sections.

III. VIRTUAL ENVIRONMENT

Virtual Environment as its name implies is a virtual representation of an existing or non existing physical environment or an abstract information which offers end users real time interactivity and make them feel as if they are part of it. Due to the interactive and behaviors that occur in real, immersive nature of Virtual Environment have resemblance with behaviors that occur in real environments.

The VE can take many forms; for example it could be realistic representation of some physical environment such as the interior of a building, a kitchen or even an object such as a car. It could be that the VE does not have any physical basis at all. For instance, it might be a 3D database of a geographical, hierarchical network describing a multinational company or a multidimensional data set associated with stock transactions. Whatever the nature of the underlying data, a geometric model is required to represent atomic entities and their relationships with one another. Based on this geometric model a geometric database must be built to represent the environment and stored such that it can be retrieved and rendered in real time when required. The database storing VE includes 3D geometry, color and texture, dynamic characteristics, physical constraints and acoustic attributes [15].

HMD, BOOM, CAVE are common virtual environments now and virtual globe is an upcoming technology in virtual environments; in the follow sections, we describe about these VEs, separately.

a. HMD

Head mounted device was the first device to create, and provide its wearer with unseen world of virtual reality. In 1965, Evans and Sutherland first introduced head mounted display. But unfortunately, it was commercially available only after 20 years by the name "Eye phone" system. HMD device consist of two miniature display screens and an optical system. These two components channel the images from the screens to the eyes, presenting a stereoscopic imaging. Others use a single larger display to provide higher resolution, but without the stereoscopic vision. We can see HMD in Figure 3.

HMD provides virtual images by continuously tracking the position and orientation of the user`s head. This allows viewer to look around and walk through the surrounding virtual environment. However, HMDs have cables which restrict our movement.

Figure. 3. HMD (Head mounted device)

b. BOOM

The Binocular Omni-Orientation Monitor (BOOM) from fake space is a high-resolution stereoscopic viewing device. Screens and optical system are housed in a box that is attached to a multi-link arm. The user looks into the box through two holes, sees the virtual world, and can guide the box to any position within the operational volume of the device. Head tracking is accomplished via sensors in the links of the arm that holds the box. The main advantage of BOOM is that it has the ability to generate better images compared to HMD. When a user releases the BOOM, another person can view the same images from the same perspective, which is another advantage over HMDs. We can see BOOM in Figure 4.

Figure. 4. BOOM (Binocular Omni-Orientation Monitor)

c. CAVE

The Cave Automatic Virtual Environment (CAVE) is an immersive virtual reality facility designed for the exploration of and interaction with spatially engaging environments. Basically, the CAVE's comprises of four projection surfaces on which images are projected with uniquely immersive design. In addition, including projection on the ceiling gives a fuller sense of being enclosed in the virtual world. Furthermore, projection on all six surfaces of a room allows users to turn around and look in all directions. This allows user to interact with virtual environment in ways with better sense of full immersion. CAVE is shown in Figure 5.

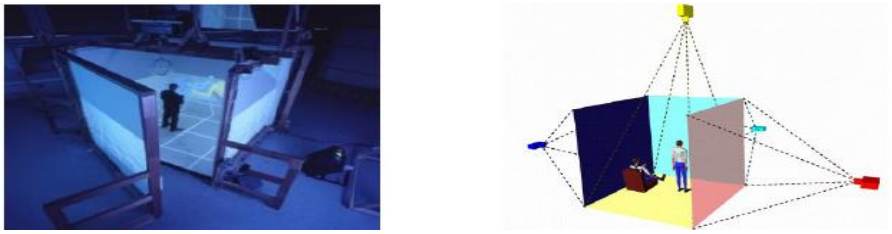

Figure. 5. CAVE(Cave Automatic Virtual Environment)

d. Virtual Globe

Virtual globe is a 3D software model or representation of the Earth or another world. Now, Virtual globes are rapidly becoming an easy and accessible way of finding, distributing and visualizing all sorts of data in a geographical context. In fact, a virtual globe provides the user with the ability to freely move around in the virtual environment by changing the viewing angle and position. So it may be used instead of the CAVE with up to six surfaces, in future and will provide full sense of immersion for users.

IV. VIRTUAL REALITY INTERFACES

One of the key features of Virtual Reality is interactivity. So HCI (Human-Computer Interaction) is one of domination factors in VR researches. In order to allow human-computer interaction it is necessary to use special tools designed both to allow input to the computer and to provide feedback to the users. Today's VR interfaces are varied in functionality and purpose as they address several human sensorial channels [1]. In this paper, we only describe those VR interfaces, which are popular and most used.

To generate the VE's images according to the movements of the user's body, it is fundamental to rapidly acquire data about the different body positions in the 3D space, and transmit them to the computer in order to elaborate the environment's modifications to be issued in response to the user's actions. This can be done by dedicated devices named 3D trackers. The technologies used predominantly in 3D tracking are four: mechanically based, optically based, magnetically based and acoustically based.

Mechanical tracking makes use of a mechanical armature with one side connected to the top of a helmet and the other end connected to an encoding device on the ceiling. As the user changes head position, the helmet moves the upper device like a mechanical arm, and data related on that movement is relayed to the computer. While mechanical position/orientation tracking is the most precise method of tracking, it has the disadvantage of being the most limiting.

Optical tracking can be implemented by sensor or by camera. Sensor-based tracking makes use of small markers - for example flashing infrared LED's- on the body. Sensors surround the subject and pick out the markers in their field. Software correlates the marker positions in the multiple viewpoints and calculates a 3D coordinate for each marker. Data glove is sensor-based tool in the optical trackers. Figure 6 shows a Data glove interfacing tool. Data glove reports position and pose information of the participant's hand to the VR system. They can also report pinching gestures (Fakespace Pinchglove), button presses (buttons built into the glove) and finger bends (Immersion CyberTouch). These glove actions are associated with virtual actions such as grasping, selecting, translation, and rotation. Data glove disadvantages include sizing problems (most are a one size fits all) and hygiene complications with multiple users. Gesture commands are limited by the number of finger positions that can be defined as unique, mutually exclusive, and comfortable. Gestures can require a degree of manual dexterity that many people do not have.

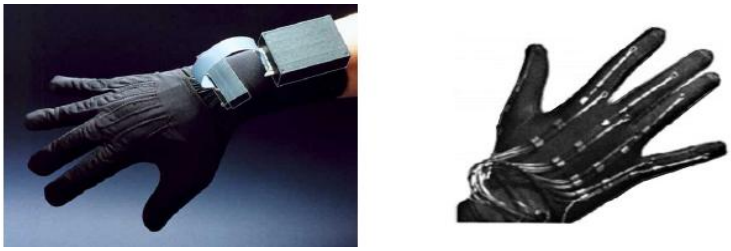

Figure. 6. Data glove

Generally, implementing sensor-based tracking often leads to three problems:

1. Sensor outputs need some filter stages to eliminate temperature, pressure and other noise effects.
2. Processing time needed to analyze several sensor information and determine each marker's 3D position slows down the system real-time interactions.
3. Using of sensors may be annoying the users.

Camera-based tracking makes use of several images captured from one or two cameras around the subject. Then by applying image processing and machine vision technologies on the camera's images, positions and movements can be tracked and gestures can be recognized for interaction of users with computer [16].

Magnetic tracking uses a source element radiating a magnetic field and a small sensor that reports its position and orientation with respect to the source. Magnetic systems do not rely on line-of-sight observation, as do optical and acoustic systems, but metallic objects in the environment will distort the magnetic field, giving erroneous readings.

Acoustic trackers use high-frequency sound to triangulate a source within the work area. Most systems like those from Logitech and the one used in the Mattel Pow pings from the source received by microphones in the environment [17].

Human vision is the most powerful sensorial channel and has an extremely large processing bandwidth. It is therefore not surprising that there is a multitude of Optical tracking tools. Human use their hands for many interaction tasks. So tracking and obtaining inputs from users hands images in camera-based technology are a natural evolution for VR interfaces, now [18-19].

V. VIRTUAL REALITY APPLICATIONS

The virtual domain offers reliability, speed, ease of access, compactness and security, and is easily transmitted to other virtual domains for example computers located in distant parts of the world [15]. Due to these facts, VR technology has been a promising technology applicable in various domains of application.

These most popular domains of application are training simulators, medical and health care, education, defense, engineering, ergonomics and human factors research, database and scientific visualization, and entertainment industry.

Training simulators are used for planes, submarines, power plants, surgery, endoscopes and air traffic control. Such simulation uses a replica of the real operational environment and real time computer to model its dynamics. Training through simulation provides significant benefits over other methods. Hazardous environment, such as a nuclear power station [20], or an aircraft landing in a fog can be accurately simulated without any danger to the trainee. Other benefit is the ability of computer software in providing flexibility to structure training programs and even monitor and measure the progress of a training session. Many simulators employ image processing and machine vision techniques to feel more real images in the virtual environments.

The key components of medical and health care where Virtual Environment can be applied are diagnosis, therapy, education and training and medical records. Diagnosis using virtual endoscopy is one of the areas that can achieve clinical efficiency in the earliest time frame. Virtual environments can be used in computer assisted surgery, image guided surgery, tele-surgery, and treatment of phobias and other psychological disorders. The VR system offers a sense of realism in a safe environment. By gradually exposing the person to their fear - for example, fear of flying -with a Virtual Environment the patient becomes accustomed to the trigger of their problem to an extent that it no longer becomes an issue. One of the advantages of this technology is that it allows healthcare professionals to learn new skills as well as refreshing existing ones in a safe environment. Plus it allows this without causing any danger to the patients and can record improvement stages of the patient. Thus Technology can therefore be used in innovative ways to provide support for those with mental health problems and nowadays Virtual Reality Therapy (VRT) is one of the newest treatment technologies.

Education is another area which has adopted virtual reality for teaching and learning situations. Virtual Environments can be used for learning of the kind expected to occur in schools, colleges and universities, that is, the acquisition of general problem solving skills, mastery of facts and concepts, and improvement of the learning progress itself. The advantage of this is that it enables large groups of students to interact with each other as well as within a three dimensional environment. It is able to present complex data in an accessible way to students which is both fun and easy to learn. Plus these students can interact with the objects in that environment in order to discover more about them.

VI. VIRTUAL RELITY CHALLENGES

Virtual reality can lead to state of the art technologies like second life [13-14]. In fact, virtual reality program Second Life poses new challenges to its more than millions of users that include economic interactions, methods of communication and documentation. In other words, Second Life is a MUVE, or Multi-user Virtual Environment. Growth rate of using Second Life in the world is illustrated in Figure 7.

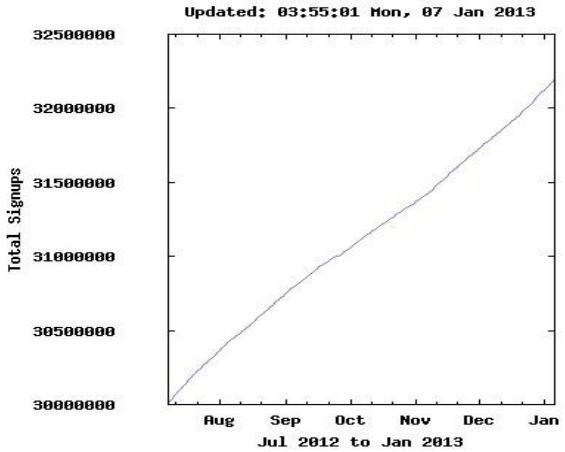

Figure. 7. Growth rate of using Second Life in the world [21]

Second Life is an online virtual world developed by an American company named Linden Lab. It was launched on June 23, 2003. A number of free client programs, or Viewers, enable Second Life users, called Residents, to interact with each other through avatars. Residents can explore the world (known as the grid), meet other residents, socialize, participate in individual and group activities, and create and trade virtual property and services with one another [22]. In the other hand, Second Life comprises the viewer (also known as the client) executing on the user's personal computer, and several thousand servers operated by Linden Lab. Second Life is intended for people aged 16 and over.

Now that worlds like Second Life have a stable and growing user base, various organizations and businesses are beginning to colonize, build and grow in these worlds [23]. Built into the software is a three-dimensional modeling tool based on simple geometric shapes that allows residents to build virtual objects. There is also a procedural scripting language, Linden Scripting Language, which can be used to add interactivity to objects. Sculpted prims (sculpties), mesh, textures for clothing or other objects, animations, and gestures can be created using external software and imported.

Like many advantageous technologies, beside opportunities of Virtual Reality and Second Life, unavoidable challenges appear, too. In fact, using Virtual Reality and Second Life offers both technical and cultural challenges. We can describe these challenges in two following sections.

a. TECHNICAL CHALLENGES

Second Life in Virtual Reality environments functions by streaming all data to the user live over the Internet with minimal local caching of frequently used data. The user is expected to have a minimum of 300kbit/s of Internet bandwidth for basic functionality, with 1Mbit/s providing better performance. Due to the proprietary communications protocols, it is not possible to use a network proxy/caching service to reduce network load when many people are all using the same location, such as when used for group activities in a school or business.

Due to Virtual Reality's and Second Life's rapid growth rate, it has suffered from difficulties related to system instability. These include increased system latency, and intermittent client crashes. However, some faults are caused by the system's use of an "asset server" cluster, on which the actual data governing objects is stored separately from the areas of the world and the avatars that use those objects. The communication between the main servers and the asset cluster appears to constitute a bottleneck which frequently causes problems [22]. Typically, when asset server downtime is announced, users are advised not to build, manipulate objects, or engage in business, leaving them with little to do but chat and generally reducing confidence in all businesses on the grid.

Cost is another issue. In addition to appropriate internet band width and virtual reality environment and interfaces charges, establishing Second Life in virtual environments offers several membership plans, too. For example for virtual learning, a premium account is required to purchase land, which is necessary to create a sustained and safe learning environment for students. However, increasingly powerful computer systems are becoming more affordable each year, but commercial VR systems that are sophisticated enough to offer complex models and diverse functionality are still expensive relative to personal computers.

b. CULTURAL CHALLENGES

Liability issues are still at question in virtual worlds. In Second Life private land can be pur-chased. Private land can be restricted to only authorized users. However, users in public areas may be subjected to violence or disruptive players (LaChapelle, 2007). There are many unresolved legal issues surrounding virtual violence, virtual assault, and sexual harassment that take place in Second Life and in other Virtual Reality worlds. And unfortunately no one is liable in these events, now [24]. So, It would seem the virtual world and second life is facing criminal problems of real-world.

Nowadays, the concept of "Virtual Reality" is new to law enforcement agencies around the world. Yet every day, millions of people connect in these worlds to socialize, shop and learn. Unfortunately, lawbreakers have also joined these virtual worlds and the full range of criminal activities is now also present. Common crimes are occurring every day in virtual worlds, including money-laundering, theft of intellectual property, exchange of child abuse images and even suspected terrorist activities. For these reasons, new virtual worlds and communities pose a unique set of challenges for the criminal justice system. Moreover, the near total lack of requisite jurisprudence means that criminals are often free to act with impunity [25].

A more disturbing fact, believed to be caused by the same issue, is "inventory loss" in which items in a user's inventory, including those which have been paid for, can disappear without warning or permanently enter a state where they will fail to appear in-world when requested (giving an "object missing from database" error). Linden Lab offers no compensation for items that are lost in this way, although a policy change instituted in 2008 allows accounts to file support tickets when inventory loss occurs. Many in-world businesses will attempt to compensate for this or restore items, but they are under no obligation to do so and not all are able to do so. Although "inventory loss" is much less from past years but it does still exists.

Second life and most virtual Reality worlds do not have appropriate tools for system management. For instance virtual worlds and Second Life were not created for educational purposes, inherently. Nonetheless, they are being adapted by educators for teaching and learning. Faculty can integrate text information in the form of note cards and use Web sites, content slides, video, and audio in addition to creating 3-D objects. However, many of the features educators take for granted in Learning Management Systems do not exist in Virtual Reality and Second Life. Additionally, Second Life is a random access environment thus giving instructors very little control over lesson sequencing. Nowadays some of the Learning

Management features that are lacking in virtual worlds are beginning to be addressed and efforts are underway to facilitate the use of these systems, in future.

VII. CONCLUSION

Nowadays, VR technology has been applied in various domains such as training simulators, medical and health care, education, scientific visualization, and entertainment industry. Virtual reality can lead to state of the art technologies like Second Life, too. Virtual Reality (VR) is a term that applies to computer-simulated environments that can simulate physical presence in places in the real world, as well as in imaginary worlds. Like many advantageous technologies, beside opportunities of Virtual Reality and Second Life, unavoidable challenges appear, too. In this paper, Virtual reality types and structural elements of a virtual reality system are described. Two main of these elements: Virtual Environment and Virtual Reality Interfaces are explained further. Then applications of virtual reality that providing us opportunities in various domains are described and at last, challenges of applying virtual reality technology are presented. Of course, efforts are underway to overcome the challenges in future to use the advantages of this technology as more as possible.

REFERENCES

[1] G. Burdea and P. Coiffet, "Virtual Reality Technology", John Wiley & Sons Inc, 1994.
[2] I. Sutherland."The Ultimate Display", In Proc. Of the IFIP Congress, pp.506–508,1965.
[3] M.W.Krueger, "Artifcial Reality", Addison-WesleyPress,1983.
[4] J.D.Foley, "Interfaces for Advanced Computing", Scientifc American, vol.257, no.4, pp.126–135,1987.
[5] J.Lanier, "TheDataGlove", Scientifc American, vol.257, no.4, cover,1987.
[6] G.Burdea and P.Coiffet, "Virtual Reality Technology", John Wiley and Son Inc., New York, USA, 1994
[7] L. Liu, "Virtual reality applications in simulated course for tour guides", IEEE Proc. Of 7th Int. Conf. on Computer Science & Education (ICCSE)**,** pp. 1672 – 1674, 2012.
[8] A. Rizzo, P. Requejo, C. J. Winstein, B. Lange, G. Ragusa, A. Merians, J. Patton, P. Banerjee and M. Aisen, "Virtual Reality Applications for Addressing the Needs of those Aging with Disability", Proc. of Workshop on Medicine Meets Virtual Reality(MMVR), pp. 510-516, 2011.
[9] A. G. Abulrub, A. N.Attridge and M. A. Williams, "Virtual Reality in Engineering Education", IEEE Global Engineering Education Conference (EDUCON), pp.751-757, 2011.
[10] V. Kovalcík, J. Chmelík, M. Bezdeka and J. Sochor, "Virtual Reality System as a Tool for Education", 20th International Conference on Computer Graphics, Visualization and Computer Vision, p. 15-18, 2012.
[11] V. Basso, M. Marello, C. Bar and M. Rabaioli, "Virtual Reality Applications as Design & Validation Support For A&R Exploration", Int. Sym. on Artificial Intelligence, Robotics and Automation in Space (i-SAIRAS), 2012.
[12] J. Allard, J. Lesage and B. Raffin, "Modularity for Large *Virtual Reality Applications*", Journal Presence: Teleoperators and Virtual Environments, Vol. 19 (2), pp. 142-161, April 2010.
[13] D. de Nood and J. Attema, "The Second Life of Virtual Reality", EPN - Electronic Highway Platform, December 2006.
[14] J. Helmer, "Second Life and Virtual Worlds", Learning Light Institute, October 2007.
[15] J. Vince, "Virtual Reality Systems", Wokingham Addison-Wesley, 1995.
[16] G. Derpanis, "A Review of Vision-Based Hand Gestures", York University, 2004.
[17] http://www.ehto.org/ht_projects/vrepar/sensing.htm
[18] M. Vafadar and A. Behrad, "Human Hand Gesture Recognition Using Motion Orientation Histogram for Interaction of Handicapped Persons with Computer", Proc. of Int. Conf. on Image and Signal Processing, ICISP2008, LNCS 5099, pp. 378-385, 2008.
[19] M. Vafadar and A. Behrad, "Human Hand Gesture Recognition Using Spatio-Temporal Volumes for Human-computer Interaction", IEEE Proc. Of Int. Symposium on Telecommunications, IST 2008, pp. 713-718, 2008.
[20] J. G. M. Gonçalves, T. Moltó-Caracena1 , V. Sequeira and E. Vendrell-Vidal, "Virtual Reality Baesd Systam For Nuclear Safeguards Applications", Int. Sym. On Safeguards-Preparing for Future Verification Challenges, December 2010.
[21] http://dwellonit.taterunino.net/sl-statistical-charts
[22] http://en.wikipedia.org/wiki/Second_Life
[23] K. Ferry, J. Gelfand, D. Peterman and H. Tomren, "Virtual Reality and Establishing a Presence in Second Life: New Forms of Grey Literature?", Proc. Of Int. Conf. on Grey Literature, pp. 113-118, 2008.
[24] S. Kluge and L. Riley, "Teaching in Virtual Worlds: Opportunities and Challenges", Issues in Informing Science and Information Technology, Vol. 5, pp. 127-135, 2008.
[25] J. P. Kennedy and B. Ticknor, "Studying Corporate Crime: Making the Case for Virtual Reality", Int. Journal of Criminal Justice Sciences (IJCJS), Vol. 7 (1), pp. 416–430, January– June 2012.

International Journal of Modern Engineering Research (IJMER)
www.ijmer.com Vol.3, Issue.2, March-April. 2013 pp-1146-1149 ISSN: 2249-6645

Torsional Behaviour of Asymmetrical Buildings

Sachin G. Maske, [1] Dr. P. S. Pajgade[2]
[1]*Department of civil Engineering Prof. Ram Meghe Institute of Technology and Research, Badnera, M.E. (Structural Engineering) Final Year*
[2]*Professor in Department of civil Engineering Prof. Ram Meghe institute of Technology and Research, Badnera*

Abstract: *Torsional behaviour of asymmetric building is one of the most frequent source of structural damage and failure during strong ground motions. In this work a study on the influence of the torsion effects on the behaviour of structure is done. In building two cases are considered, case one is without considering torsion and case two is considering torsion. The Indian standard code of practice IS-1893 (Part I: 2002) guidelines and methodology are used to analyzed and designed building. Results are compared in terms of % Ast in columns.*

Keywords: *Asymmetric plan, Earthquake, Eccentricity, Torsion.*

I. Introduction

Seismic damage surveys and analyses conducted on modes of failure of building structures during past severe earthquakes concluded that most vulnerable building structures are those, which are asymmetric in nature. Asymmetric-plan buildings, namely buildings with in-plan asymmetric mass and strength distributions, are systems characterized by a coupled torsional-translational seismic response. Asymmetric building structures are almost unavoidable in modern construction due to various types of functional and architectural requirements. Torsion in buildings during earthquake shaking may be caused from a variety of reasons, the most common of which are non-symmetric distributions of mass and stiffness. Modern codes deal with torsion by placing restrictions on the design of buildings with irregular layouts and also through the introduction of an accidental eccentricity that must be considered in design. The lateral-torsional coupling due to eccentricity between centre of mass (CM) and centre of rigidity (CR) in asymmetric building structures generates torsional vibration even under purely translational ground shaking. During seismic shaking of the structural systems, inertia force acts through the centre of mass while the resistive force acts through the centre of rigidity as shown in Fig. 1.

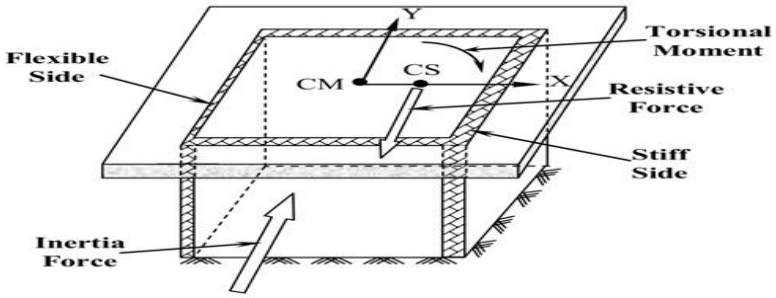

Fig1- Generation of torsional moment in asymmetric structures during seismic excitation.

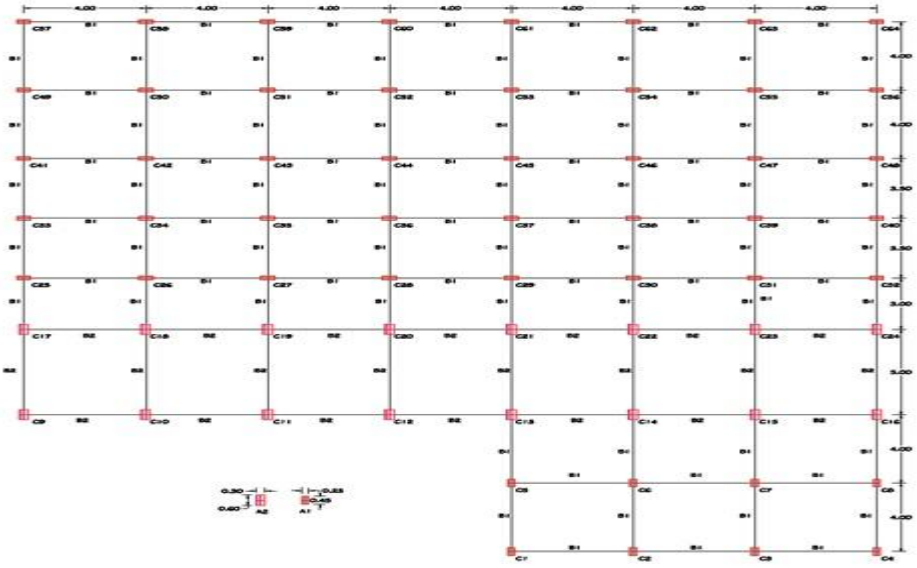

Fig 2- Building plan

II. Building Details

The structural analysis and design of four storey reinforced concrete asymmetrical frame building has been done with the help of Etab software. The building is assumed as commercial complex. Linear static analysis has been done. Regular grid plan of the structure is shown in fig 2. The structure is assumed to be located in seismic zone IV on a site with medium soil. Building contains different irregularity like plan irregularity and Re- Entrant corner irregularity. Building is studied for two cases as mentioned below:

Case 1: seismic analysis of building is done without considering design eccentricity.

Case 2: seismic analysis of building is done considering torsion. Centre of mass, Centre of rigidity, static eccentricity and design eccentricity is calculated for seismic forces at each floor level.

Structural data:

Table1: Structural data

No of storey	=	4
Ground storey height	=	3.5m
Intermediate storey height	=	3.2m
Total no of columns	=	64
Slab thickness	=	125mm
Outer wall	=	230mm
Inner wall	=	150mm
Parapet (1m height)	=	230mm
Beam size	=	B_1= 230 x 450 mm
	=	B_2= 300 x 600 mm
Column size	=	A_1 = 230 x 450 mm
	=	A_2= 300 x 600 mm
Grade of concrete	=	M_{20}
Grade of steel	=	Fe415
Density of concrete	=	25kN/m^3
Density of brick	=	20 kN /m^3
Live load	=	4 kN /m^2
Roof Live load	=	2 kN /m^2
Floor finish	=	1 kN /m^2
Earthquake data:		
Seismic Zone	=	IV
Importance factor	=	1.5
Response reduction factor	=	5 (SMRF)
Type of soil	=	TYPE II (Medium)
Damping	=	5%

III. Analysis And Design

The asymmetric building is analysed by modelling two models

Case 1- asymmetric building without considering design eccentricity (edi)

Case 2- asymmetric building considering design eccentricity (edi)

Case 1 building is modelled in Etab; a rigid diaphragm is assigned at different storey level. Supports are assigned as fixed supports neglecting soil structure interaction. A linear static analysis was performed for two earthquake cases, earthquake in X-direction (Eqx) and in Y-direction (Eqy) by defining auto seismic lateral loading in Etab. Case 1 is design for 13 load combinations.

Case 2 building is same as case1, from output data from Etab the design eccentricity is calculated as the difference between centre of mass and centre of rigidity.

Table 2- Design eccentricity in X- direction

Story	XCCM	XCR	esi=XCR - XCCM	0.05 x bi	edi=1.5(esi) + 0.05(bi)	edi=(esi) - 0.05(bi)
STORY5	15.014	15.549	0.535	1.4	2.2025	-0.865
STORY 4	15.036	15.49	0.454	1.4	2.081	-0.946
STORY3	15.036	15.438	0.402	1.4	2.003	-0.998
STORY2	15.035	15.313	0.278	1.4	1.817	-1.122

Table3 - Design eccentricity in Y- direction

Story	YCCM	YCR	esi=YCR - YCCM	0.05 x bi	edi=1.5(esi) + 0.05(bi)	edi=(esi) - 0.05(bi)
STORY5	17.225	18.634	1.409	1.55	3.6635	-0.141
STORY 4	17.329	18.671	1.342	1.55	3.563	-0.208
STORY3	17.349	18.738	1.389	1.55	3.6335	-0.161
STORY2	17.357	18.893	1.536	1.55	3.854	-0.014

XCCM = Centre of mass in X -direction
YCCM = Centre of mass in Y -direction
XCR = Centre of rigidity in X -direction
YCR = Centre of rigidity in Y -direction
edi = Design eccentricity at ith floor
esi = Static eccentricity at ith floor
bi = Floor plan dimension of floor i^{th} perpendicular to the direction of force.
The value of design eccentricity is calculated from table 2 and 3 is assigned to auto seismic lateral loading cases by overriding diaphragm eccentricity.
Earthquake cases
EXTP = Earthquake in X- direction torsion positive.
EXTN = Earthquake in X- direction torsion negative.
EYTP = Earthquake in Y- direction torsion positive.
EYTN = Earthquake in Y- direction torsion negative.
Case 2 building is design for 25 loading combination.

Results: Comparison of Ast for various columns.

- Graph 1- % Ast in columns on stiff side

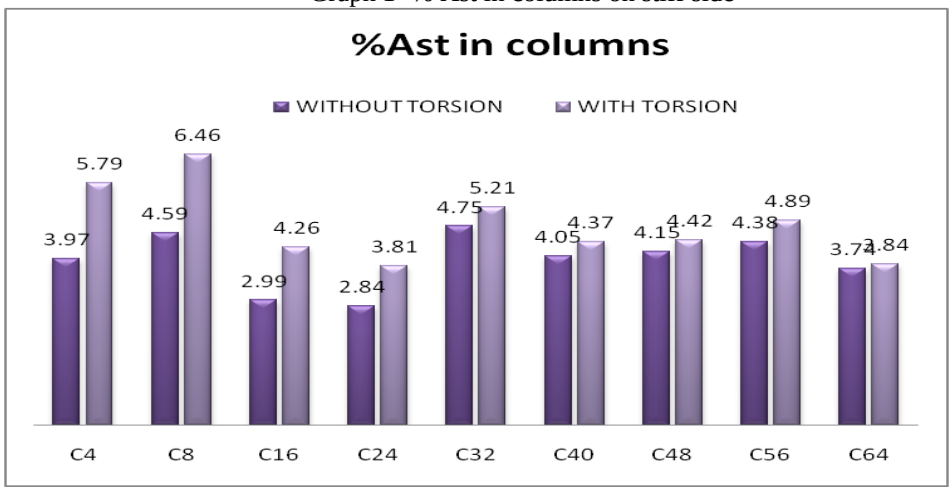

- Graph 2- % Ast in columns on flexible side

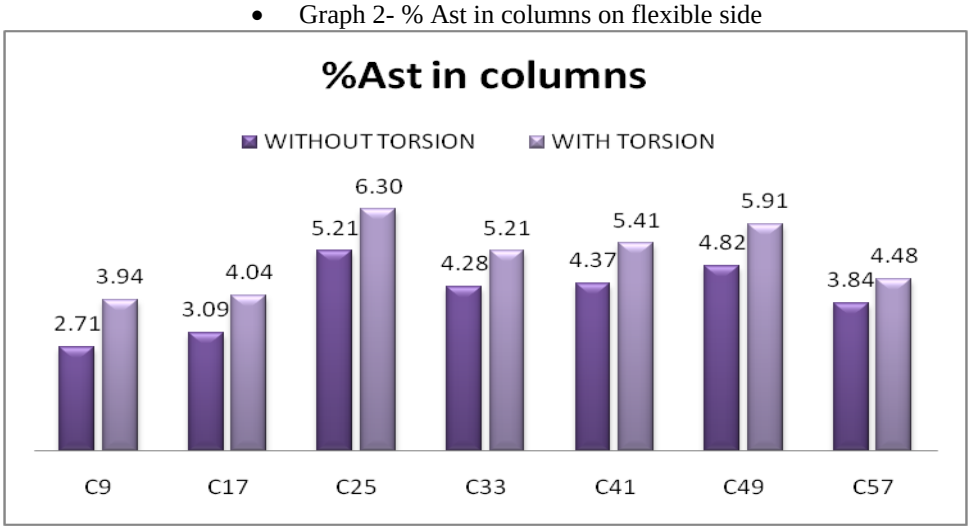

- Graph 3- % Ast in columns failed in torsion

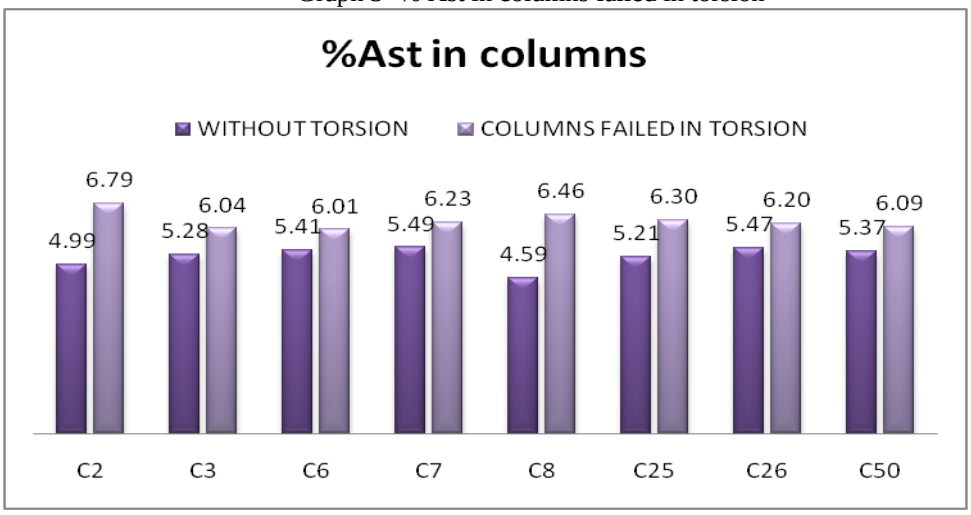

IV. Conclusion

In the asymmetric building case 2, it was observed that the forces in the columns located in the stiff side of the plan are much smaller than those obtained in the elements of the flexible side of the plan. There is no significant change in column forces around centre of rigidity.

It is observed that column no C2, C3, C6, C7 and C8 in case 2(columns which are farthest from centre of rigidity) while designing it considering design eccentricity are failed. Column no C25, C26 and C50 (columns on flexible side) are failed in case 2. (Reinforcement required exceeds maximum allowed).

Most of the designer adopts approximate methods for the torsional analysis of building. However this may be an inaccurate assessment. Several studies of structural damage during the past earthquake reveal that torsion is the most critical factor leading to major damage or complete collapse of building. It is, therefore, necessary that irregular buildings should be analyzed for torsion. A three dimensional analysis using Etab is able to calculate the center of rigidity; by getting these values we can perform torsional analysis.

References

[1] Bijily B, (2012) Critical evaluation of torsional provision in IS-1893: 2002.
[2] Dutta, S. C., (2001). Effect of Strength Deterioration on Inelastic Seismic Torsional Behaviour of Asymmetric RC Buildings, Building and Environment, 36(0), 1109-1118. 16.
[3] S. K. Dubey, (2011) Seismic behaviour of asymmetric R C buildings.
[4] H. J. Shah, S. K. Jain, Design example of six storey building.
[5] M.D. Bensalah, et. al., Assessments of the torsion effect in asymmetric buildings under seismic load.(15 WCEE).
[6] Rucha S. Banginwar, M. R. Vyawahare, (2012) Effects of plan configuration on the seismic behaviour of the structure by response spectrum method.
[7] Rudra Nevatia, Torsional Provisions In IS: 1893(2002)
[8] IS 1893 Part 1, (2002).Indian Standard Criteria for Earthquake Resistant Design of Structures.
[9] S K Jain et. al. Proposed Draft Provision and commentary on Indian seismic code IS 1893 (Part 1).

International Journal of Modern Engineering Research (IJMER)
www.ijmer.com Vol.3, Issue.2, March-April. 2013 pp-1150-1156 ISSN: 2249-6645

The Application of Ku-band VSAT Systems to Single Layer Hexagonal Micro strip Patch Antenna

Supriya Jana
ECE Department under West Bengal University of Technology, West Bengal, India

Abstract: *The application of Ku-band VSAT Systems to single layer hexagonal micro strip patch antenna is thoroughly simulated in this paper. The radiating elements in this antenna are composed of two triangular and one rectangular slots from the conventional micro strip patch antenna. These slots are engraved in the rectangular and triangular patch, joined together in two structures, and by single probe feed. The rectangular and triangular slots make the antenna to operate at multiband with relatively high gain. Therefore, this antenna can be used for wireless communication applications like WLAN, WiMax, radar system applications, satellite communication and VSAT systems. The initial design and optimization of the prototype operating in Ku-band has been performed in planar simulator Zeland IE3D software. The simulated antenna size has been reduced by 52.64% with an increased frequency ratio.*

Keywords: *Compact, Gain, Patch, Slot, Resonant frequency, Bandwidth.*

I. INTRODUCTION

Micro strip patch antennas have a huge number of advantageous features, their narrow bandwidths, however, has been one of the most noticeable limitations hindering their wider applications [1-8], such as mobile cellular telephones, cordless phones, pagers, WLAN and mobile radios. Because of their simplicity and compatibility with printed-circuit technology micro strip antennas are widely used in the microwave frequency spectrum. Simply a micro strip antenna is a rectangular or other shape, patch of metal on top of a grounded dielectric substrate. Micro strip patch antennas are attractive in antenna applications for many reasons. They are easy and cheap to manufacture, lightweight, and planar to list just a few advantages. Also they can be manufactured either as a stand-alone element or as part of an array. However, these advantages are offset by low efficiency and limited bandwidth. Throughout the years, authors have dedicated their investigations to creating new designs or variations to the original antenna that, to some extent, produce wider bandwidth and radiation efficiency of micro strip antennas.

The recent interest in broadband antennas as a micro strip patch antenna [10-13] was developed to meet the need for a cheap, low profile, broadband antenna. This antenna could be used in a wide range of applications such as in the communications [18-20] industry for cell phones or satellite communication. Our aim is to reduce the size of the antenna as well as increase the operating bandwidth. The proposed antenna (substrate with ε_r = 4.4) has a gain of 3.19 dBi and presents a size reduction of 52.64% when compared to a conventional micro strip patch antenna (10mm X 6mm). A logical approach, therefore, is to use a thick substrate or replacing the substrate by air or thick foam, dielectric constants are usually in the range of ($2.2 \leq \varepsilon_r \leq 12$)[9]. The X band and Ku-Band defined by an IEEE standard for radio waves and radar engineering with frequencies that ranges from 8.0 to 12.0 GHz and 12.0 to 18.0 GHz respectively.

Ku-Band [12-18GHz] is used for most VSAT systems on yachts and ships today. VSAT Vessels moving from region to region need to change satellite beams, sometimes with no coverage in between beams. VSAT Antenna sizes typically range from the standard 1 meter to 1.5. Some frequencies in this radio band are used for vehicle speed detection by law enforcement, especially in Europe.

Generally, VSAT technology can be applied in the following aspects. It can be applied for popularizing satellite television broadcast and satellite television [14-17], and transmitting signal of broadcast television and business television, financial system and securities system to dynamically track and manage market situation, which greatly shortens cash conversion cycle, water conservancy to manage and hydrological change in order to prevent and reduce natural disaster, meteorological satellite, maritime satellite, resource satellite and ground detection station ,military, emergency communication and communication in remote areas. VSAT is the most convenient emergency communication backup system for natural disaster or emergency incident.

II. ANTENNA DESIGN

The configuration of the conventional printed antenna is shown in Figure 1 with L=6 mm, W=10 mm, substrate (PTFE) thickness h = 1.6 mm, dielectric constant ε_r = 4.4. Coaxial probe-feed (radius=0.5mm) is located at W/2 and L/3. Assuming practical patch width W= 10 mm for efficient radiation and using the equation [6],

$$f_r = \frac{c}{2W} \times \sqrt{\frac{2}{(1+\varepsilon_r)}}$$

Where, c = velocity of light in free space. Using the following equation [9] we determined the practical length L (=6mm) & width W (=10mm).

$$L = L_{eff} - 2\Delta L$$

$$W = \frac{c}{2f\sqrt{(\varepsilon_r + 1)/2}}$$

Where, $\frac{\Delta L}{h} = \left[0.412 \times \frac{(\varepsilon_{reff} + 0.3) \times (W/h + 0.264)}{(\varepsilon_{reff} - 0.258) \times (W/h + 0.8)}\right]$

$$\varepsilon_{reff} = \left[\left(\frac{\varepsilon_r + 1}{2}\right) + \frac{\varepsilon_r - 1}{\left(2 \times \sqrt{\left(1 + 12 \times \frac{h}{W}\right)}\right)}\right]$$

and $$L_{eff} = \left[\frac{c}{2 \times f_r \times \sqrt{\epsilon_{eff}}}\right]$$

Where, L_{eff} = Effective length of the patch, $\Delta L/h$ =Normalized extension of the patch length, ε_{reff} = Effective dielectric constant.

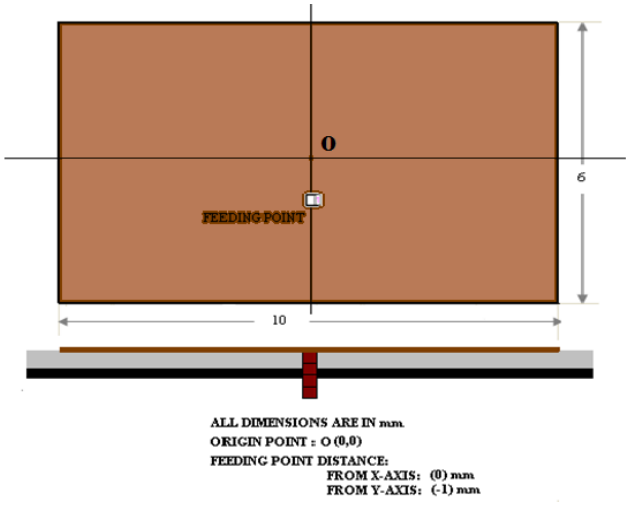

Figure 1: Conventional Antenna configuration

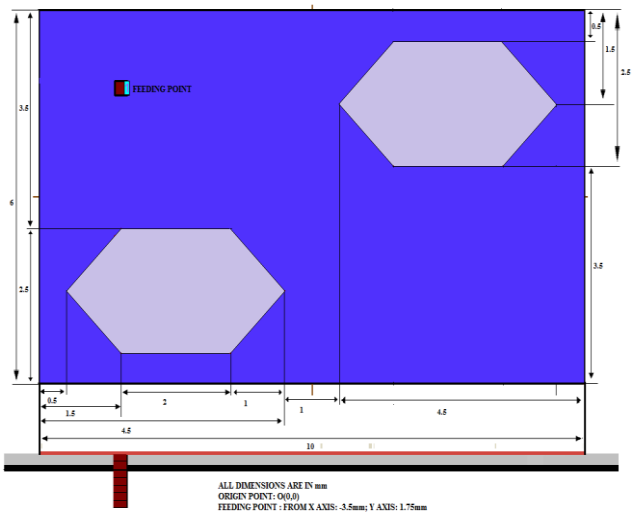

Figure 2: Simulated Antenna configuration

Figure 2 shows the configuration of simulated printed antenna designed with similar PTFE substrate. Two equal slots which are the combinations of two triangular and a rectangular slot at the upper right and lower left corner and the location of coaxial probe-feed (radius=0.5 mm) are shown in the figure 2.

III. Results And Discussion

Simulated (using IE3D [21]) results of return loss in conventional and simulated antenna structures are shown in Figure 3-4. A significant improvement of frequency reduction is achieved in simulated antenna with respect to the conventional antenna structure.

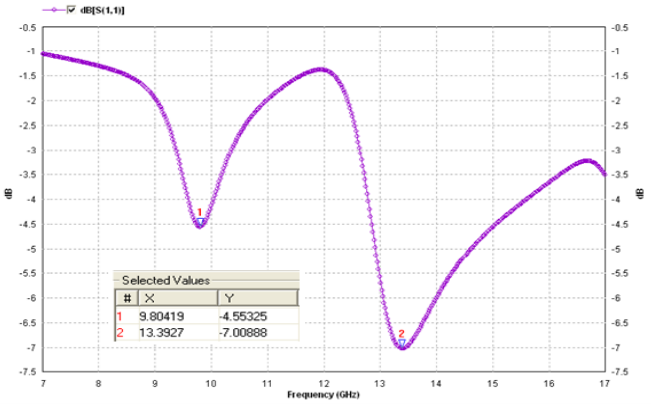

Figure 3: Return Loss vs. Frequency (Conventional Antenna)

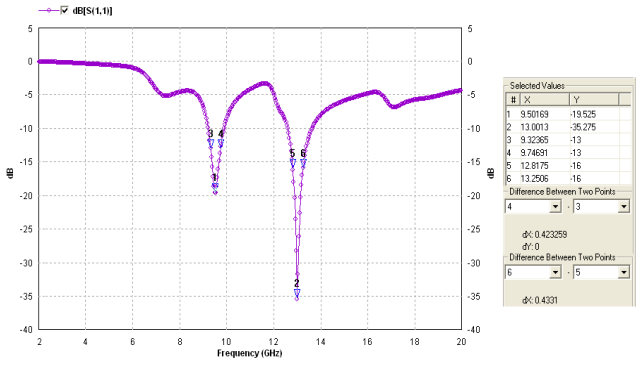

Figure 4: Return Loss vs. Frequency (Slotted Antenna)

In the conventional antenna return loss of about -7.01 dB is obtained at 13.39 GHz. Comparing fig.3 and fig.4 it may be observed that for the conventional antenna (fig.3), there is practically no resonant frequency at around 9.50 GHz with a return loss of around -6 dB. For the simulated antenna there is a resonant frequency at around 9.50169 GHz where the return loss is as high as -19.525 dB.

Due to the presence of slots in simulated antenna resonant frequency operation is obtained with large values of frequency ratio. The first and second resonant frequency is obtained at f_1= 9.50169 GHz with return loss of about -19.525 dB and at f_2 = 13.0013 GHz with return losses -35.275 dB respectively.

Corresponding 10dB band width obtained for Antenna 2 at f1, f2 are 423.259 MHz and 0.4331 GHz respectively. The simulated E plane and H-plane radiation patterns are shown in Figure 5-14. The simulated E plane radiation pattern of simulated antenna for 9.50169 GHz is shown in figure 5.

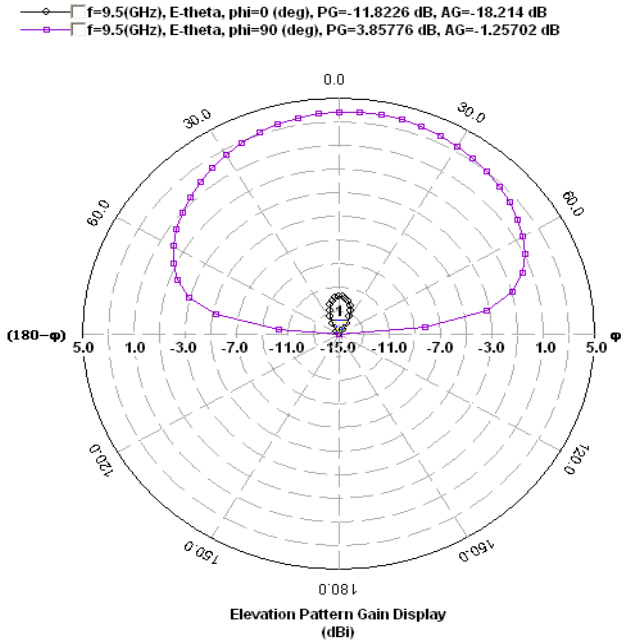

Figure 5: E-Plane Radiation Pattern for Slotted Antenna at 9.50 GHz

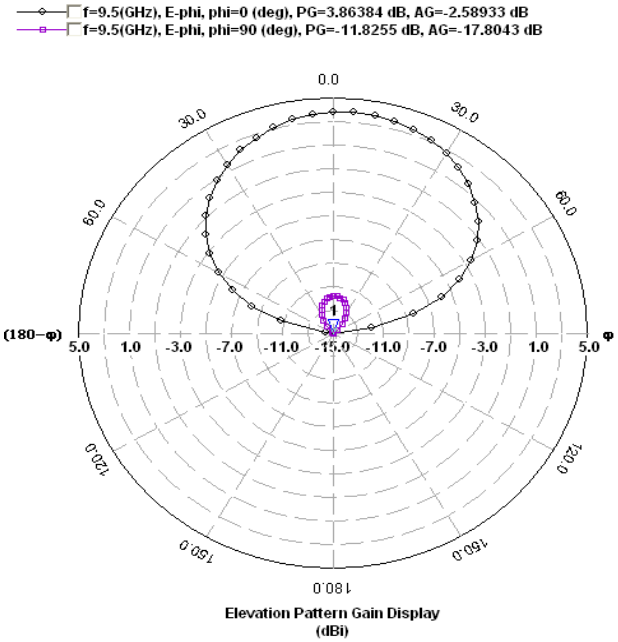

Figure 6: H-Plane Radiation Pattern for slotted Antenna at 9.50 GHz

The simulated H plane radiation pattern of simulated antenna for 9.50169 GHz is shown in figure 6.The simulated E plane radiation pattern of slotted antenna for 13.0013 GHz is shown in figure 7. The simulated H plane radiation pattern of slotted antenna for 13.0013 GHz is shown in figure 8.

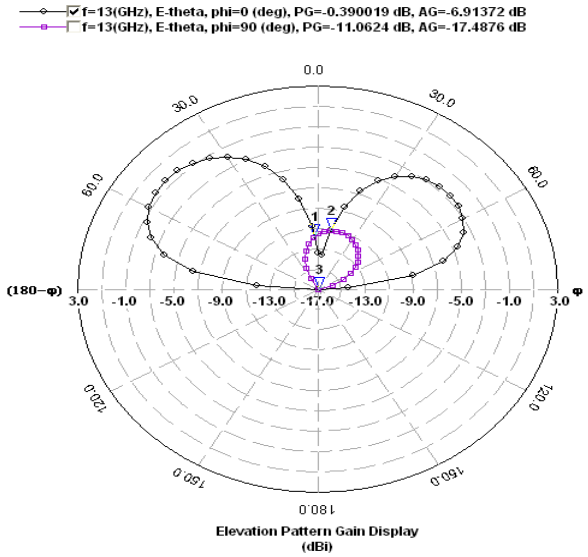

Figure7: E-Plane Radiation Pattern for slotted antenna at 13 GHz

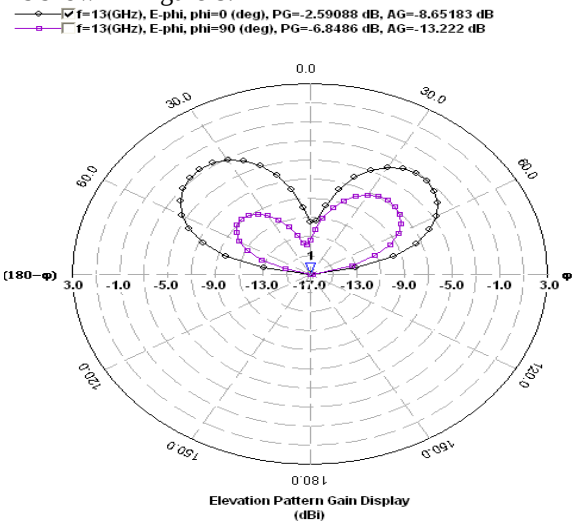

Figure 8: H-Plane Radiation Pattern for slotted antenna at 13 GHz

The simulated Cartesian E -plane & H-plane radiation pattern (2D) of simulated antenna for 9.50169 GHz is shown in figure 9 & figure 10.

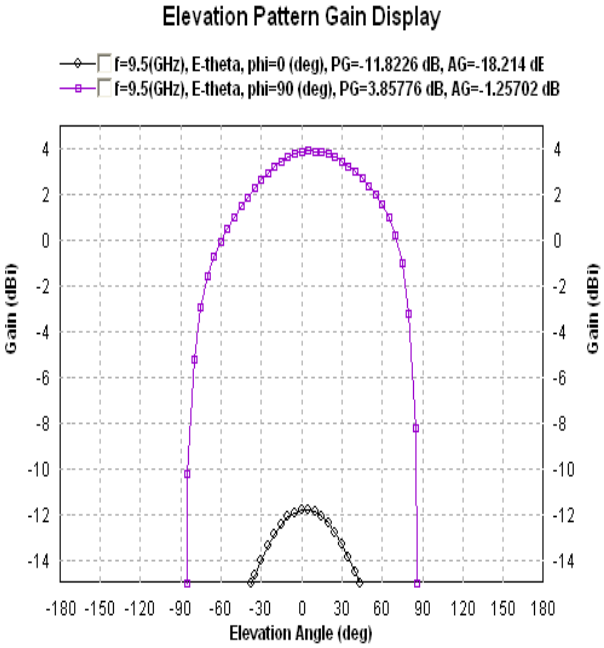

Figure 9: E-Plane Radiation Pattern (2D) for slotted antenna at 9.50 GHz

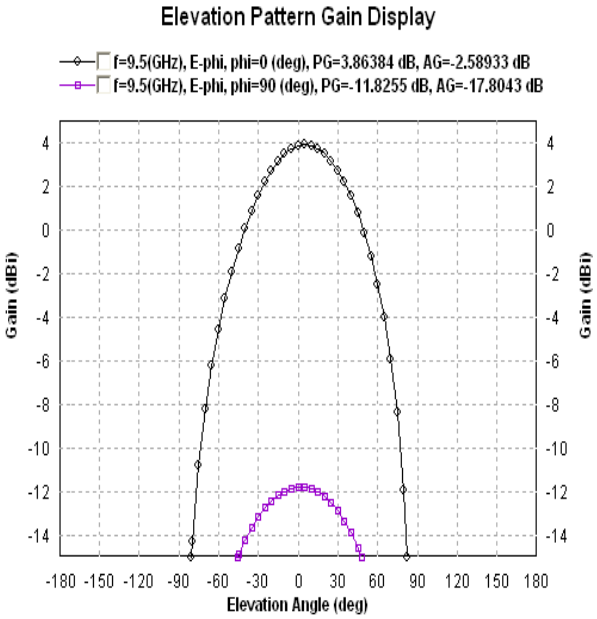

Figure 10: H-Plane Radiation Pattern (2D) for slotted antenna at 9.50 GHz

The simulated Cartesian E -plane & H-plane radiation pattern (2D) of simulated antenna for 13.0013 GHz is shown in figure 11 & figure 12.

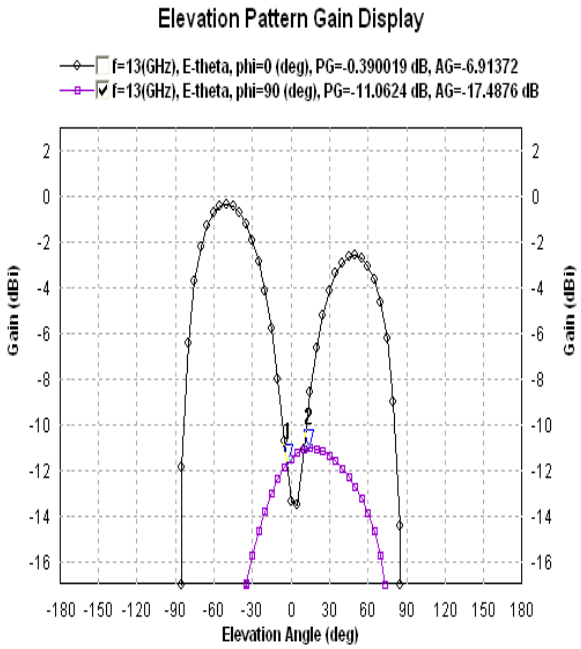

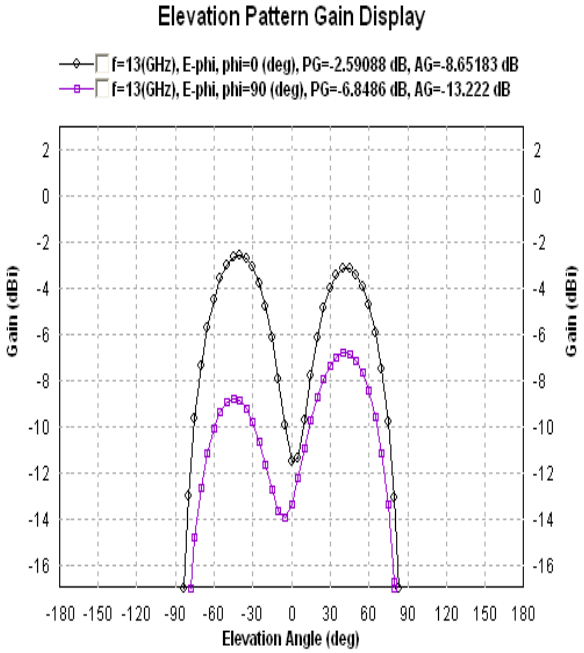

Figure 11: E-Plane Radiation Pattern (2D) for slotted antenna at 13 GHz
Figure 12: H-Plane Radiation Pattern (2D) for slotted antenna at 13 GHz

The simulated E plane & H-plane radiation pattern (3D) of simulated antenna for 9.50169 GHz is shown in figure 13 & figure 14.

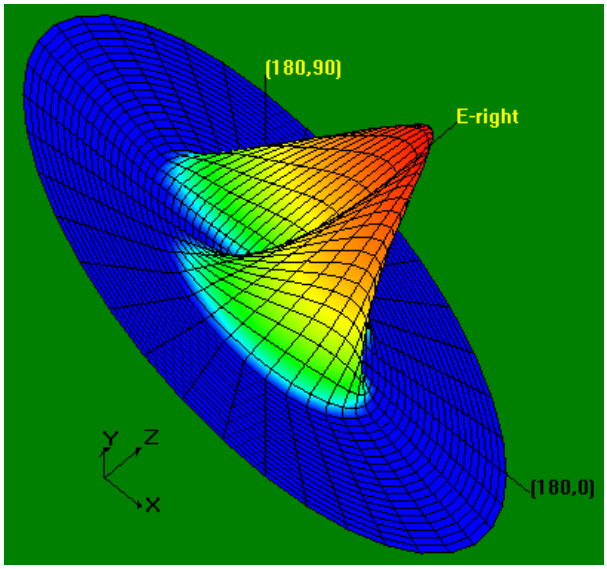

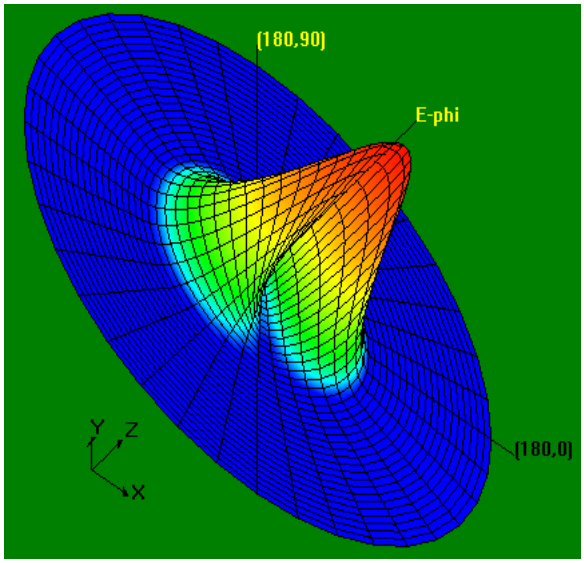

Figure 13: E-Plane Radiation Pattern (3D) for slotted antenna at 9.50 GHz
Figure 14: H-Plane Radiation Pattern (3D) for slotted antenna at 9.50 GHz

The simulated E plane & H-plane radiation pattern (3D) of simulated antenna for 13.0013 GHz is shown in figure 15 & figure 16.

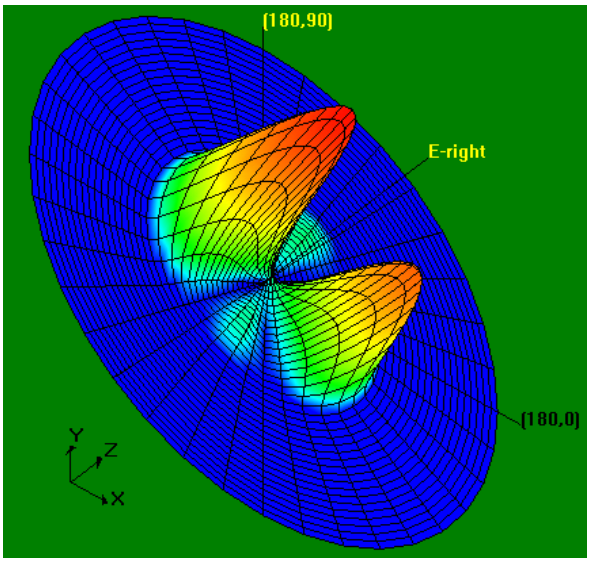

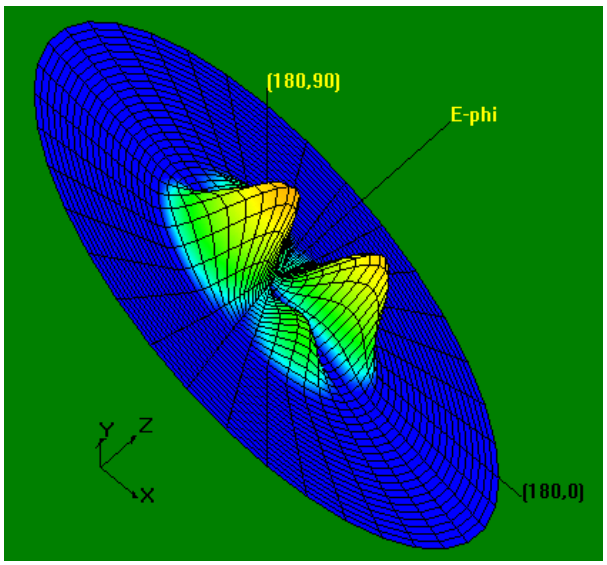

Figure 15: E-Plane Radiation Pattern (3D) for slotted antenna at 13 GHz
Figure 16: H-Plane Radiation Pattern (3D) for slotted antenna at 13 GHz

The simulated smith chart and VSWR of simulated antenna shown in figure 17 & figure 18.

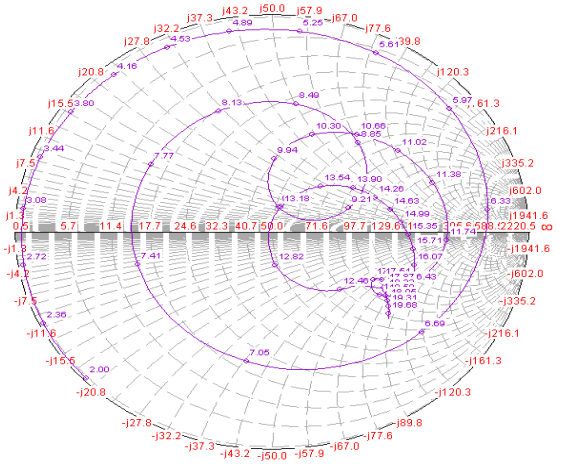

Figure17: Simulated Smith Chart for slotted antenna

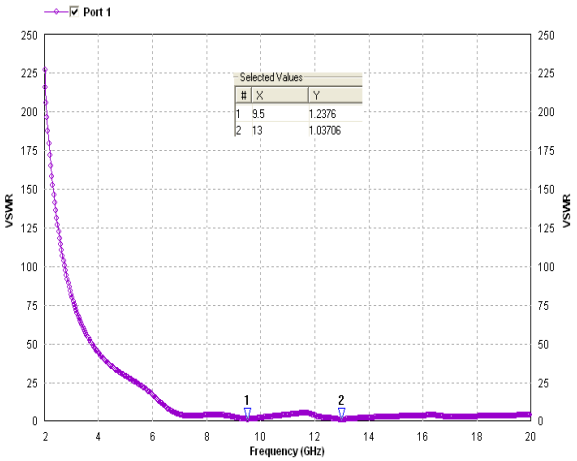

Figure 18: Simulated VSWR for slotted antenna

The simulation antenna showing the total current distribution and substrate in the following figure 19 & figure 20

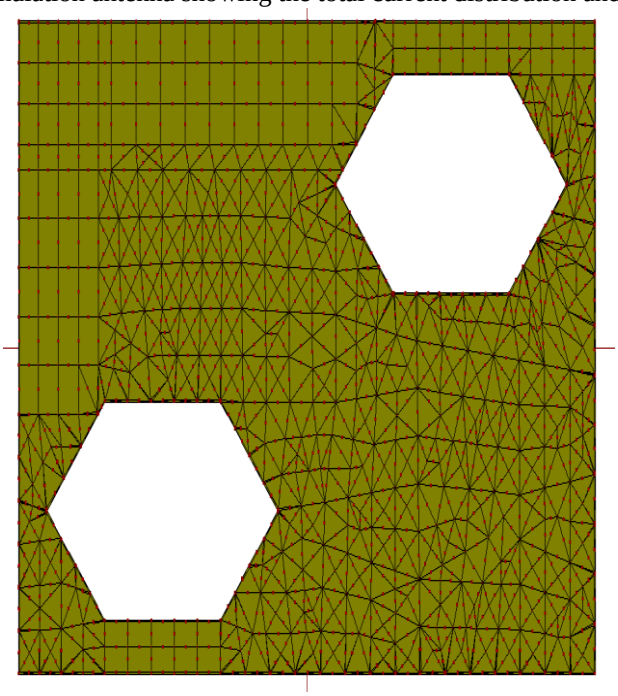

Figure 19: Total Current Distribution

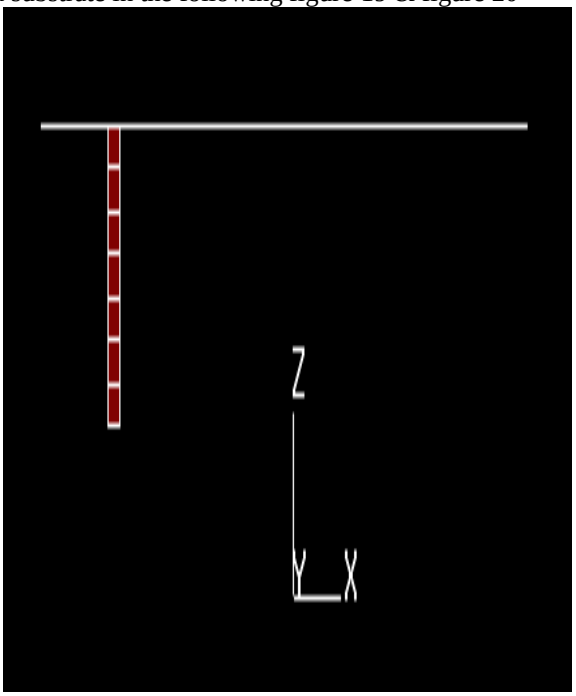

Figure 20: Substrate

All the simulated results are summarized in the following Table1 and Table2.

TABLE I: SIMULATED RESULTS FOR ANTENNA 1 AND 2 w.r.t RETURN LOSS

ANTENNA STRUCTURE	**RESONANT FREQUENCY (GHz)**	**RETURN LOSS (dB)**	**10 DB BANDWIDTH (GHz)**
Conventional	f_1= 9.80	-4.55	NA
	f_2= 13.39	-7.01	NA
Slotted	f_1= 9.50169	-19.525	0.423259
	f_2 = 13.0013	-35.275	0.4331

TABLE II: SIMULATED RESULTS FOR ANTENNA 1 AND 2 w.r.t RADIATION PATTERN

ANTENNA STRUCTURE	**RESONANT FREQUENCY (GHz)**	**3DB BEAMWIDTH (^{0})**	**ABSOLUTE GAIN *(dBi)***
Conventional	f_1= 9.80	NA	NA
	f_2= 13.39	NA	NA
Slotted	f_1= 9.50169	132.714	3.97715
	f_2 = 13.0013	152.585	1.50649
Frequency Ratio for Conventional Antenna			f_2 / f_1 = 1.366
Frequency Ratio for Slotted Antenna			f_2 / f_1 = 1.3683

IV. CONCLUSION

This paper focused on the simulated design on differentially-driven microstrip antennas. Simulation studies of a single layer hexagonal microstrip patch antenna have been carried out using Method of Moment based software IE3D [21]. Introducing slots at the edge of the patch size reduction of about 52.64% has been achieved. The 3dB beam-width of the radiation patterns are 132.714° (for f_1), 152.585° (for f_2) which is sufficiently broad beam for the applications for which it is intended. The resonant frequency of slotted antenna, presented in the paper, designed for a particular location of feed point (-3.5mm, 1.75mm) considering the centre as the origin. Alteration of the location of the feed point results in narrower 10dB bandwidth and less sharp resonances.

REFERENCES

[1] I.Sarkar, P.P.Sarkar, S.K.Chowdhury "A New Compact Printed Antenna for Mobile Communication", 2009 Loughborough Antennas& Propagation Conference, 16-17 November 2009, pp 109-112.

[2] S. Chatterjee, U. Chakraborty, I.Sarkar, S. K. Chowdhury, and P.P.Sarkar, "A Compact Microstrip Antenna for Mobile Communication", IEEE annual conference. Paper ID: 510

[3] J.-W. Wu, H.-M. Hsiao, J.-H. Lu and S.-H. Chang, "Dual broadband design of rectangular slot antenna for 2.4 and 5 GHz wireless communication", IEE Electron. Lett. Vol. 40 No. 23, 11th November 2004.
[4] U. Chakraborty, S. Chatterjee, S. K. Chowdhury, and P. P. Sarkar, "A comact microstrip patch antenna for wireless communication," Progress In Electromagnetics Research C, Vol. 18, 211-220, 2011 http://www.jpier.org/pierc/pier.php?paper=10101205
[5] Rohit K. Raj, Monoj Joseph, C.K. Anandan, K. Vasudevan, P. Mohanan, " A New Compact Microstrip-Fed Dual-Band Coplaner Antenna for WLAN Applications", IEEE Trans. Antennas Propag., Vol. 54, No. 12, December 2006, pp 3755-3762.
[6] Zhijun Zhang, Magdy F. Iskander, Jean-Christophe Langer, and Jim Mathews, "Dual-Band WLAN Dipole Antenna Using an Internal Matching Circuit", IEEE Trans. Antennas and Propag.,VOL. 53, NO. 5, May 2005, pp 1813-1818.
[7] James, J. R. and P. S. Hall, Handbook of Microstrip Antennas, Peter Peregrinus, London, 1989.
[8] Fujimoto, K. and J. R. James (eds.), Mobile Antenna Systems Handbook, Artech House, Norwood, MA, 1989.
[9] C. A. Balanis, "Advanced Engineering Electromagnetics", John Wiley & Sons., New York, 1989.
[10] J. -Y. Jan and L. -C. Tseng, " Small planar monopole Antenna with a shorted parasitic inverted-L wire for Wireless communications in the 2.4, 5.2 and 5.8 GHz. bands" , IEEE Trans. Antennas and Propag., VOL. 52, NO. 7, July 2004, pp -1903-1905.
[11] Samiran Chatterjee, Joydeep Paul, Kalyanbrata Ghosh, P. P. Sarkar and S. K. Chowdhury "A Printed Patch Antenna for Mobile Communication", Convergence of Optics and Electronics conference, 2011, Paper ID: 15, pp 102-107.
[12] Supriya Jana, Bipadtaran Sinhamahapatra, Sudeshna Dey "Single Layer Monopole Hexagonal Microstrip Patch Antenna for Fixed Service Satellite (FSS) System", 1st International e-Conference On Developments in Computer Sciences, Electronics and Communication Technologies(e-DCSECT-2013),March-2013; Organized by: Cosmic Journals; Under its : GREEN INITIATIVE PROGRAM; Published in: International Journal on Electronics & Communication Technology (IJECT), [ISSN:2230-7109(Online)] [,ISSN:2230-9543(Print)], Vol.4, Issue Spl-2 (January-March 2013),PP. 112-116; Global Impact Factor:0.306;Evaluation Score 2012: 12.31; Index Copernicus Evaluation Report 2011: 5.09.
[13] Supriya Jana , Bipadtaran Sinhamahapatra, Sudeshna Dey, Samiran Chatterjee, Arnab Das , Bipa Datta, Moumita Mukherjee, Santosh Kumar Chowdhury, "Single Layer Monopole Hexagonal Microstrip Patch Antenna for Microwave Communication", International Refereed Journal of Engineering and Science (IRJES),ISSN (Online) 2319-183X, (Print) 2319-1821 Volume 1, Issue 4(December 2012), PP.44-48.
[14] Supriya Jana, Bipadtaran Sinhamahapatra, Sudeshna Dey, Arnab Das, Bipa Datta, Moumita Mukherjee, Santosh Kumar Chowdhury, Samiran Chatterjee, "Single Layer Monopole Hexagonal Microstrip Patch Antenna for Satellite Television", International Journal of Soft Computing and Engineering (IJSCE), ISSN: 2231-2307, Volume-2, Issue-6, January 2013, PP.321-324.
[15] Supriya Jana, Bipadtaran Sinhamahapatra, Sudeshna Dey, Arnab Das, Bipa Datta, Moumita Mukherjee, Samiran Chatterjee, "Single Layer Monopole Hexagonal Microstrip Patch Antenna for Direct Broadcast Satellite (DBS) System", International Journal of Computational Engineering Research (ijceronline.com), ISSN: 2250-3005(online), Vol. 3 Issue. 1, January 2013, PP.110-115.
[16] Bipadtaran Sinhamahapatra, Supriya Jana , Sudeshna Dey, Arnab Das , Bipa Datta, Moumita Mukherjee, Samiran Chatterjee, "Dual-Band Size Deducted Un-Equal Arm Y-Shaped Printed Antenna for Satellite Communication" International Journal of Engineering Research and Development (IJERD), **e**-ISSN: 2278-067X, **p**-ISSN : 2278-800X , Volume 5, Issue 9 (January 2013), PP. 36-40.
[17] Supriya Jana, Bipadtaran Sinhamahapatra, Sudeshna Dey, Arnab Das, Bipa Datta, Moumita Mukherjee, Samiran Chatterjee, "Single Layer Monopole Hexagonal Microstrip Patch Antenna for Satellite Television", National Conference on Advancement of Computing in Engineering Research (ACER-13),Article No.-51,PP.19-20,March-2013;Co-sponsored by: IEEE Kolkata Section; Operational Research Society of India(ORSI) Kolkata Chapter; Rural Development Forum Institution of Engineers(India)[IEI]; Publication Partner: Academy & Industry Research Collaboration Center(AIRCC), (ISSN:2231-5403); (ISBN:978-1-921987-11-3); DOI:10.5121/csit.2013.3234; CS&IT-CSCP2013; vol.3,No.2,2013; PP.369-375,March 2013.
[18] Arnab Das, Bipa Datta, Samiran Chatterjee, Bipadtaran Sinhamahapatra, Supriya Jana, Moumita Mukherjee, Santosh Kumar Chowdhury, "Multi-Band Microstrip Slotted Patch Antenna for Application in Microwave Communication," International Journal of Science and Advanced Technology, (ISSN 2221-8386), Vol. 2, Issue-9, 91-95, September 2012.
[19] Bipa Datta, Arnab Das, Samiran Chatterjee, Bipadtaran Sinhamahapatra, Supriya Jana, Moumita Mukherjee, Santosh Kumar Chowdhury, "Design of Compact Patch Antenna for Multi-Band Microwave Communication", National Conference on Sustainable Development through Innovative Research in Science and Technology (Extended Abstracts), Paper ID: 115, pp 155, 2012.
[20] Arnab Das, Bipa Datta, Samiran Chatterjee, Bipadtaran Sinhamahapatra, Supriya Jana, Moumita Mukherjee, Santosh Kumar Chowdhury, "A Compact Multi-resonant Microstrip Antenna", 13th Biennial National Symposium on Antennas and Propagation 2012 (APSYM 2012), Paper ID: 13102, 2012.Co-sponsored by: IEEE Student Branch, Cochin; UGC;Indian National Science Academy;AICTE;Department of Atomic Energy(Govt. Of India); Department of Science & Technology (Govt. Of India); CSIR (Govt. Of India); KSCSTE (Govt. Of India). Published by The Directorate of Relations and Publications; ISBN: 978-43-80095-40-0; PP.99-102, December 2012.
[21] Zeland Software Inc. IE3D: MoM-Based EM Simulator. Web: http://www.zeland.com/

AUTHORS

Supriya Jana pursuing M.Tech degree in Electronics & Communication Engineering (Communication Specialization) under West Bengal University of Technology (WBUT) in 2011 to 2013 and received B.Tech degree in Electronics & Communication Engineering (E.C.E) under West Bengal University of Technology (WBUT) in 2007 to 2011.

International Journal of Modern Engineering Research (IJMER)
www.ijmer.com Vol.3, Issue.2, March-April. 2013 pp-1157-1160 ISSN: 2249-6645

A Route map for Detecting Sybil Attacks in Urban Vehicular Networks

V. Geetha Devi, [1] P.Shakeel Ahmed, [2] P.Babu, [3]
V. Hemanth Kumar Raju[4]
[1]*M. Tech (CSE), QCET, NELLORE*
[23]*Associate Professor, CSE, QCET, NELLORE*
[4]*Assistant Professor, CSE, NEC, GUDUR*

Abstract: *Security is important for many sensor network applications. A particularly harmful attack against sensor and ad hoc networks is known as the Sybil attack, where a node illegitimately claims multiple identities. In urban vehicular networks, the location privacy of anonymous vehicles is highly concerned and anonymous verification of vehicles is indispensable. Consequently, an attacker who succeeds in forging multiple hostile identifies can easily launch a Sybil attack, gaining excessively large influence. In Vehicular Ad Hoc Networks (VANETs), the vehicular scenario requires smart signaling, smart road maintenance and other services. A brand new security issue is that the semi-trusted Road Side Units (RSUs) may be compromised. The objective of our work is to propose a Threshold ElGamal system based key management scheme for safeguarding VANET from the compromised RSUs and their collusion with the malicious vehicles. By analyzing the packet loss tolerance for security performance demonstration, followed by a discussion on the threshold our method can promote security with low overhead in Emergency Braking Notification and does not increase overhead in and Decentralized Floating Car Data during security promotion.*

Index Terms: *Sybil attack, location privacy, urban vehicular networks, location-hidden trajectory, Signal Strength Distribution, Security*

I. Introduction

Over the past two decades, vehicular networks have been emerging as a cornerstone of the next-generation Intelligent Transportation Systems (ITSs), contributing to safer and more efficient roads by providing timely information to drivers and concerned authorities. In vehicular networks, moving vehicles are enabled to communicate with each other via inter vehicle communications as well as with road-side units (RSUs) in vicinity via roadside-to-vehicle communications.

In urban vehicular networks where the privacy, especially the location privacy of vehicles should be guaranteed vehicles need to be verified in an anonymous manner. A wide spectrum of applications in such a network relies on collaboration and information aggregation among participating vehicles. Without identities of participants, such applications are vulnerable to the Sybil attack where malicious vehicle masquerades as multiple identities, overwhelmingly influencing the result. The consequence of Sybil attack happening in vehicular networks can be vital. For example, in safety-related applications such as hazard warning, collision avoidance, and passing assistance, biased results caused by a Sybil attack can lead to severe car accidents. Therefore, it is of great importance to detect Sybil attacks from the very beginning of their happening. Detecting Sybil attacks in urban vehicular networks, however, is very challenging.

The First, vehicles are anonymous. There are no chains of trust linking claimed identities to real vehicles. Second, location privacy of vehicles is of great concern. Location information of vehicles can be very confidential. For example, it can be inferred that the driver of a vehicle may be sick from knowing the vehicle is parking at a hospital. It is inhibitive to enforce a one-to-one correspondence between claimed identities to real vehicles by verifying the physical presence of a vehicle at a particular place and time. Third, conversations between vehicles are very short. Due to high mobility of vehicles, a moving vehicle can have only several seconds to communicate with another occasionally encountered vehicle. It is difficult to establish certain trustworthiness among communicating vehicles in such a short time. This makes it easy for a malicious vehicle to generate a hostile identity but very hard for others to validate. Furthermore, short conversations among vehicles call for online Sybil attack detection. The detection scheme fails if a Sybil attack is detected after the attack has terminated.

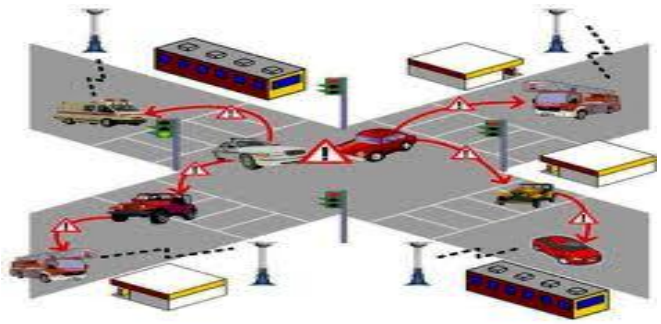

Fig. 1: Vehicular networks

II. Related Work

While it was first described and formalized by Douceur, the Sybil attack has been a severe and pervasive problem in many forms. In a Sybil attack, an attacker can launch a Sybil attack by forging multiple identifies, gaining a disproportionately large influence. In the literature, there have been many different approaches proposed to detect or mitigate the attack. Many studies have followed Douceur's approach, focusing on how to establish trust between participating entities based on trusted public key cryptographies or certificates in distributed systems, for example, P2P systems, sensor networks and mobile ad hoc networks. Although deploying trusted certificates is the only approach that has the potential to completely eliminate Sybil attacks, it also violates both anonymity and location has the problem of key revocation which is challenging, particularly in wireless mobile networks.

Another category of Sybil attack detection schemes is based on resource testing. The goal of resource testing is to determine if a number of identities possess fewer resources than would be expected if they were independent. The resources being tested can be computing ability, storage ability, and network bandwidth, as well as IP addresses. These schemes assume that entities have homogeneous hardware configurations. In vehicular networks, this assumption cannot hold since malicious vehicles can easily have more powerful resources than the normal vehicles.

Sybil Guard is an interesting scheme studying the social network among entities. In this scheme, human established real-world trust relationship among users is used for detecting Sybil attacks. Since even the attacker can generate as many as Sybil identities, building relationship between honest users and Sybil identities is much harder. Thus, there exists a small "cut" on the graph of trust relationship between the forged identities and the real ones. This is because vehicles are highly mobile. Communications often happen among temporarily met and unfamiliar vehicles. To exploit the fact that one single vehicle cannot present at multiple locations at the same time, Bouassida have proposed a detection mechanism utilizing localization technique based on Received Signal Strength Indication (RSSI). In this scheme, by successively measuring the RSSI variations, the relative locations among vehicles in vicinity can be estimated. Identities with the same estimated locations are considered as Sybil vehicles. In practice, the complicated outdoor environments can dramatically affect the wireless signal propagation so that RSSI measurements are highly time variant even measured at the same location. Xiao have proposed a Sybil attack detection scheme where the location of a particular vehicle can be determined by the RSSI measurements taken at other participating vehicles. In the scheme, the trust authority distributes a number of pseudonyms for each vehicle. Abused pseudonyms can be detected by RSUs. Since RSUs are heavily involved in the detection process, this scheme requires the full coverage of RSUs in the field. It is infeasible in practice due to the prohibitive cost. Furthermore, in such a scheme, vehicles should managed by a centralized trusted enter. Each time RSU detects suspicious pseudonyms, it should send all the pseudonyms to the trust center for further decision, which makes the trust center be the bottleneck of the detection.

The most relevant work to Footprint is the Sybil attack detection schemes proposed in. In these schemes, a number of location information reports about a vehicle are required for identification. RSU periodically broadcasts an authorized time stamp to vehicles in its vicinity as the proof of appearance at this location. Vehicles collect these authorized time stamps which can be used for future identity verification. Trajectories made up of consecutive time stamps and the corresponding public keys of RSUs are used for identification. However, these schemes did not take location privacy into consideration since RSUs use long term identities to generate signatures. As a result, the location information of a vehicle can be inferred from the RSU signatures it collects. In Footprint, authorized messages issued from RSUs are signer-ambiguous which means the information about the location where the authorized message was issued is concealed, and temporarily linkable which means using a single trajectory for long term identification of a vehicle is prohibited. Therefore, the privacy of location information and identity of vehicles are preserved in Footprint.

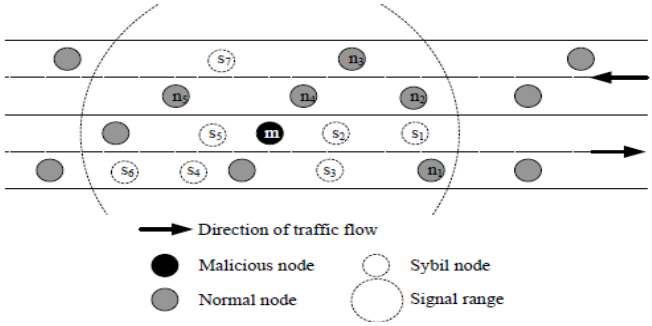

Fig 2: An example VANET under Sybil attacks

III. Models and Design Goals

3.1. System Model and Assumptions

In vehicular networks, a moving vehicle can communicate with other neighboring vehicles or RSUs via inter vehicle communications and roadside-to-vehicle communications. The architecture of the system model, which consists of three interactive components:

- RSU can be deployed at intersections or any area of interest. A typical RSU also functions as a wireless AP which provides wireless access to users within its coverage. RSUs are interconnected (e.g., by a dedicated network or through the Internet via cheap ADSL connections) forming a RSU backbone network.
- On board units (OBUs) are installed on vehicles. A typical OBU can equip with a cheap GPS receiver and a short-range wireless communication module. A vehicle equipped with an OBU can communicate with an RSU or with other vehicles in vicinity via wireless connections.
- Trust authority is responsible for the system initialization and RSU management. The TA is also connected to the RSU backbone network. Note that the TA does not serve vehicles for any certification purpose in Footprint. A vehicle can claim as many arbitrary identities as it needs.

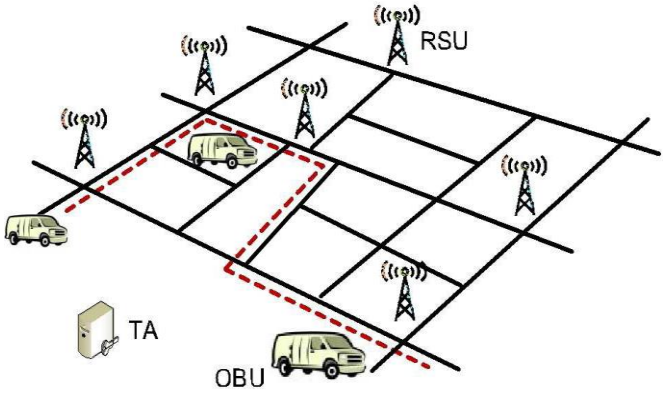

Fig 3: An Illustration of the System Model, Where the Dash Line Indicates the Travel Route of a Vehicle. as the Vehicle Traverses the Area, It Will Encounter Multiple RSUs, Typically Deployed at Intersections.

3.2. ATTACKS

In order to launch a Sybil attack, a malicious vehicle must try to present multiple distinct identities. This can be achieved by either generating legal identities or by impersonating other normal vehicles. With the following capabilities, an attacker may succeed to launch a Sybil attack in vehicular networks:

Heterogeneous configuration: malicious vehicles can have more communication and computation resources than honest vehicles. For example, a malicious vehicle can mount multiple wireless cards, physically representing different communication entities. Furthermore, having more powerful resources can also fail those resource testing schemes for detecting Sybil attacks.

Message manipulation: due to the nature of open wireless channels, the attacker can eavesdrop on nearby communications of other parties. Thus, it is possible that the attacker gets and interpolates critical information needed to impersonate others.

3.3. DESIGN GOALS

The design of a Sybil attack detection scheme in urban vehicular networks should achieve three goals:

1. Location privacy preservation— a particular vehicle would not like to expose its location information to other vehicles and RSUs as well since such information can be confidential. The detection scheme should prevent the location information of vehicles from being leaked.
2. Online detection— when a Sybil attack is launched, the detection scheme should react before the attack has terminated. Otherwise, the attacker could already achieve its purpose.
3. Independent detection— the essence of Sybil attacks happening is that the decision is made based on group negotiations. To eliminate the possibility that a Sybil attack is launched against the detection itself, the detection should be conducted independently by the verifier without collaboration with others.

IV. Generating Location-Hidden Trajectory

4.1 Location Hidden Authorized Message Generation

In order to be location hidden, authorized messages issued for vehicles from an RSU should possess two properties. The temporarily linkable property requires two authorized messages are recognizable if and only if they are generated by the same RSU within the same given period of time.

4.2. Sybil Attack Detection

During a conversation, upon request from the conversation holder, all participating vehicles provide their trajectory-embedded authorized messages issued within specified event for identification. With submitted messages, the conversation holder verifies each trajectory and refuses those vehicles that fail the message verification. After that, the conversation holder conducts online Sybil attack detection before further proceeding with the conversation.

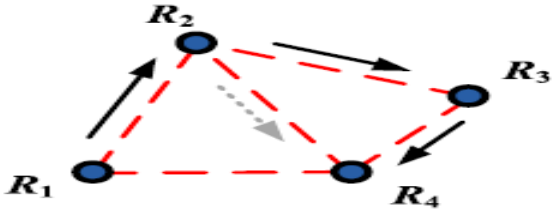

Fig. 4: RSU Neighboring Relationship and the Freedom of Trajectory Generation can Facilitate Sybil Trajectory Generation. In the Above Figure, Neighboring RSUs (Denoted by Dots) are connected with Dash Line. The Solid Arrows Indicate the Actual Sequence of RSUs a Malicious Meet and the Dash Arrow Presents a Possible Forged Trajectory.

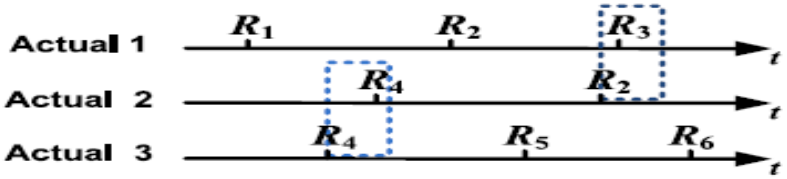

Fig 5: Checking for distinct trajectories by using a check window (denoted as the box of dotted line) and counting the total number of different RSUs contained in a pair of trajectories.

V. Proposed Work

Considering the scenario where a small fraction of RSUs are compromised and developing cost-efficient techniques to fast detect the corruption of an RSU. Here we delve into designing better linkable signer ambiguous signature schemes such that the computation overhead for signature verification and the communication overhead can be reduced. A brand new security issue is that the semi trusted Road Side Units (RSUs) may be compromised by providing a Threshold ElGamal system based key management scheme for safeguarding VANET from the compromised RSUs and their collusion with the malicious vehicles.

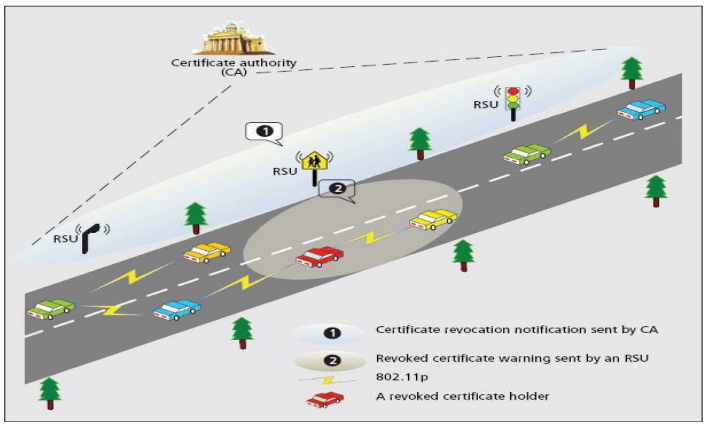

Fig 6: Security Architecture

VI. Conclusion

Secure routing in VANET have been emerging as a cornerstone of Intelligent Transportation Systems (ITSs), contributing to safer and more efficient roads by providing timely information to drivers and concerned authorities. Consecutive authorized messages obtained by an anonymous vehicle from RSUs form a trajectory to identify the corresponding vehicle. Location privacy of vehicles is preserved by realizing a location-hidden signature scheme. Utilizing social relationship among trajectories, Footprint can find and eliminate Sybil trajectories. The Footprint design can be incrementally implemented in a large city.

References

[1] Y. Sun, R. Lu, X. Lin, X. Shen, and J. Su, "An Efficient Pseudonymous Authentication Scheme with Strong Privacy Preservation for Vehicular Communications," IEEE Trans. Vehicular Technology, vol. 59, no. 7, pp. 3589-3603, Sept. 2010.
[2] R. Lu, X. Lin, H. Zhu, and X. Shen, "An Intelligent Secure and Privacy-Preserving Parking Scheme through Vehicular Communications," IEEE Trans. Vehicular Technology, vol. 59, no. 6, pp. 2772-2785, July 2010.
[3] J.R. Douceur, "The Sybil Attack," Proc. First Int'l Workshop Peer-to- Peer Systems (IPTPS '02), pp. 251-260, Mar. 2002.
[4] M. Castro, P. Druschel, A. Ganesh, A. Rowstron, and D.S.Wallach, "Secure Routing for Structured Peer-to-Peer Overlay Networks," Proc. Symp. Operating Systems Design and Implementation (OSDI '02), pp. 299-314, Dec. 2002.
[5] J. Newsome, E. Shi, D. Song, and A. Perrig, "The Sybil Attack in Sensor Networks: Analysis & Defenses," Proc. Int'l Symp. Information Processing in Sensor Networks (IPSN '04), pp. 259-268, Apr. 2004.

International Journal of Modern Engineering Research (IJMER)
www.ijmer.com Vol.3, Issue.2, March-April. 2013 pp-1161-1166 ISSN: 2249-6645

High Speed Trains

Shripad Shashikant Chopade[1], Dr. Pushpendra Kumar Sharma[2]
[1]*Shripad shashikant chopade, scholar student of Mechanical Department, Nri-ist Bhopal, India*
[2]*Dr. Pushpendra kumar sharma, Head & Guide of Mechanical Department, Nri-ist Bhopal, India*

Abstract: *When English inventor Richard Trevithick introduced the steam locomotive on 21 February 1804 in Wales, it achieved a speed of 8 km/h (5 mph). In 1815, Englishman George Stephenson built the world's first workable steam locomotive.*

Keywords: *Eurostar, Magnet train, TGV, Tilting tracks, tilting trains.*

I. Introduction

In 1825, he introduced the first passenger train, which steamed along at 25 km/h (16 mph). Today, trains can fly down the tracks at 500 km/h (311 mph). And fly they do, not touching the tracks.

There is no defined speed at which you can call a train a high speed train but trains running at and above150 km/h are called High Speed Trains.

A. The Decline of Rail as a Form of Passenger Transport

Since the automobile has become more widespread with the existence of motorways, cars may reach speeds of up to 75 mph (120 km/h) or thereabouts depending on local laws. Standard mainline railway trains running at 100 mph (160 km/h) have found it difficult to compete with the car, as once journey time to and from the station and waiting for the trains had been calculated, rail travel did no longer offer a significant journey time advantage over the car. In order to attract people to railways ticket prices had to be at the lowest possible, meaning minimal profits. No one would want to build a brand new railway line; the interest payments would crush any company. All this has meant that in the early-mid 20th century new railways were unheard of and some small lines were often closed down because they made a loss.

It seems quite exciting for rail that now today railways are making a come-back. Thousands of miles/km of new railways has been built in the last decade, and new lines are under construction all over the world. Since 1981, over 1000 km (600 miles) of new track has been laid for high speed trains in France.

B. Problems Running On Existing Railways

The primary problem with existing railways is that they can have tight curves. The centrifugal forces on an object going round a bend are the function of the square of velocity, i.e., double the speed, quadruple the centrifugal forces, triple the speed, centrifugal forces increase by nine-fold. Therefore even what might appear mild curves provide problems at speed.

Other key problems are that running on existing railway; the new fast trains have to be scheduled in around the conventional trains. This can be a tricky thing, especially on a busy network; fast trains can easily become stuck behind slow running ones, resulting in delays.

Safety is also a paramount consideration. Although since initial construction 100 years ago the track will have been replaced many times, the foundations of the railways are the same which means after heavy rains for example the track may sag slightly and lose some alignment, a real problem only at high speed. Level crossings also pose a problem.

1. High Speed Lines

To have a high speed rail system, making the high speed trains is really the tip of an iceberg. What really makes systems a success or failure is the railway that they run at. Railways like roads have speed restrictions, and like on roads, often the speed restrictions are below the top speed of the train. Building a fast train is easy, but its building tracks good enough to allow trains to safely and smoothly travel at 160-200 mph or 250-320 km/h, which are also long enough to allow the trains to accelerate up to these speeds (often many miles) and decelerate, is quite difficult.

1.1 Features of a High Speed Railway

i) No level crossings (grade crossings).
ii) Fenced off.
iii) Concrete foundations.
iv) Wide spacing between lines.
v) Curves of radius less than 5 km are avoided and are tilted.
vi) Gradients more than on conventional railway line.
vii) Through stations are constructed with 4 tracks.
viii) Tunnels avoided.

Level crossings are the most common reason for accidents on railways, where road vehicles break down or get stuck on the railway and the train crashes through them

All high speed lines are fenced off. Indeed in the UK all railway lines are fenced off anyway, however on continental Europe many railway lines are easy to get onto. High speed lines are fenced off for obvious reasons, to eliminate the risk of any animal or people wandering onto the railway line.
Foundations for high speed lines are much deeper than conventional railways. Usually a layer of concrete and tarmac is put down (like a road) and then the ballast is put on top. This is to try and stop movements in the ground from affecting the alignment of the railway.

The wide spacing between the lines is important because when two trains pass each other the speed difference can be as much as 600km/h or 370mph. If the two trains are too close together this causes at first a burst of air pressure when they first pass and then a drop in pressure during the coaches. Although this isn't enough to push the trains off the track, repeated stress on the windows may cause fatigue and they may break eventually. So for safety reasons two tracks in each direction are placed further apart than on normal lines.

Gentle curves are key in what high speed lines are about. Tight curves on TGV lines have a radius of about 3 miles or 5 km. Curves are also banked up a lot more than on conventional lines. This is because slow trains will not run on them and it is extremely rare for a TGV to come to a stop because of a signal. The degree of banking is calculated to exactly balance centrifugal forces at running speed.

Perhaps surprisingly greater gradients are allowed on high speed lines than conventional railways. There are two key reasons for this, first of all modern high speed trains are extremely powerful, TGVs generate as much as 12,000hp, steam engines were nowhere near as powerful (about 1,000hp) in the era when conventional railways were built. The second reason is that the faster a train travels the less it will slow down for the same rise in height. This is because as it is going fast it takes less time to climb the hill and so gravity has less time to act to slow the train down.

Generally speaking engineers try and avoid tunnels on high speed lines. This is because when a train enters a tunnel at speed it causes large pressure changes. This can be painful and harmful to passengers' ear drums. A solution was thought to pressure seal trains (as with the TGV). However with very high speed trains (300 km/h), the pressure changes can be so large it can shatter the windows, particularly when two trains pass in opposite directions in a tunnel with a closing speed of 600 km/h in a confined space. However German and Italian high speed lines include tunnels but they have subsequent speed restrictions. As a result the best average speeds along German (200 km/h) and Italian (165 km/h) lines are considerably lower than in France (254 km/h) and Japan (262 km/h), and even a British conventional railway outperforms the Italian high speed line in terms of speed with an average of 180 km/h between London and York.

1.2 Where High Speed Lines Run

It must be emphasized that high speed trains may run on conventional railway but are usually limited to 230 km/h-200 km/h. Most high speed railway services in Europe spend most of their journey on conventional lines, but come together for a fast run on a trunk line.

II. Tilting Trains

We all know that if you are driving in your car and you take a corner at speed you feel centrifugal forces. Well it is no different from trains, if a train takes a corner at speed then centrifugal forces come in. Often train operating companies face a decision for building a high speed railway transport system, i.e., they can either invest money in the train to make it tilt but use existing railway lines, or they invest money in a new railway but don't need to spend money on expensive tilting mechanisms. This is why TGV and bullet trains do not tilt, because they have their own dedicated high speed railway lines where curves are built with very high radii.

It is worth pointing out that the centrifugal force is a function of 'v^2/r' where 'v' is the velocity and 'r' is the radius. This means that if you double the velocity, you quadruple the centrifugal force. Similarly, if you want to triple the velocity but keep the centrifugal force the same, you must increase the radius by a factor of nine. This is why even apparently gentle curves can be much more of a problem with high speeds than one might think, because the force rises with the square of velocity.

2.1 Why Tilting Helps

When sitting on a corner going at speed there are two forces acting on you, gravitational force and the centrifugal force which is accelerating you into the corner. When two forces act, it causes a resultant force. The resultant force will push you into your seat and to the side. However if the train is tilting, then the normal contact force of you on your seat will be the same as the resultant force you are experiencing. This means as far as the passenger is concerned he or she is just being pulled into his or her seat, and he or she is used to that, so no discomfort is felt.

This is true also of aeroplanes, commercial planes tilt a large amount, up to 30 degrees when going around corners in some cases to cater for passenger comfort. As the tilting of the aero plane is to get rid of the problem of centrifugal forces,

or more accurately to disguise the centrifugal forces as a part of gravity as far as the passengers are concerned. The only way you know if the aeroplane is tilting is to look out of the window.

Trains that tilt can go up to 25% to 40% faster around curves than conventional trains without upsetting the passengers, and as mentioned before this can significantly increase average speeds and cut journey times.

2.2 Tilting Of Tracks

High speed lines in the UK are heavily banked up on corners, but going in a high speed train, you don't notice it at all. Occasionally when a high speed train comes to a stop because of a red signal or something on a curve you can really notice how much it's slanted. On a stop on a curve put a bottle on the floor and will slide across to the other side.

However there are limitations with tilting tracks. First of all, the banking has to be designed with a specific speed in mind. A banked up track meant for 125 mph trains is going to cause discomfort to passengers in a local 75 mph train, as when a slower train goes round a banked corner it will make passengers feel like they are falling to a side. Of course you could build dedicated high speed lines, but then you would engineer them without tight curves. This limits the extent to which tracks can be banked up. If the track is banked too much for really fast trains, then if any train comes to a stop on the curve due to a red signal the slant will cause discomfort to passengers. Also arranging for the overhead pantograph to make proper contact with the wire above a banked curve would be difficult.

Clearly trains themselves need to tilt. Then you get the double benefit of tilted track and tilting train, and the train can tilt to exactly suit the speed it is going at.

2.3 Tilting Of Trains

Carriages have tilting mechanisms. Obviously the bogies cannot tilt because they ride on the track and must follow the path of the track. So the coaches have to tilt on the bogies. The way they do this is simple, the bogie acts a fulcrum in the centre and it is free to tilt on either side. Then pistons control how much the coach tilts. The pistons are controlled by a small computer, which uses a spirit level. The spirit level is used to check the closeness to horizontal, remember, i.e. at right angles to the resultant force acting. Normally this force is gravity, but when going round a corner the resultant is a combination of gravity and centrifugal forces. This means the spirit level indicates it is no longer horizontal, so the computer adjusts the pistons until horizontal is read. Again this will not be horizontal to the ground, but as far as anyone on the train is concerned it will be horizontal, keeping the passengers happy.

In the early days it was tried to use inertial force to let the trains tilt. i.e., they would have no mechanism to make them tilt but the carriages would have a low centre of gravity so centrifugal forces on the carriage would cause them to tilt. This proved unsuccessful.

III. MAGLEV (MAGNETICALLY LEVITATED TRAINS)

The principle of a Magnet train is that it floats on a magnetic field and is propelled by a linear induction motor. They follow guidance tracks with magnets. These trains are often referred to as Magnetically Levitated trains which are abbreviated to Maglev. Although maglev don't use steel wheel on steel rail usually associated with trains, the dictionary definition of a train is a long line of vehicles traveling in the same direction - it is a train.

3.1 Working Principle

A maglev train floats about 10mm above the guide ways on a magnetic field. It is propelled by the guide way itself rather than an onboard engine by changing magnetic fields. Once the train is pulled into the next section the magnetism switches so that the train is pulled on again. The Electro-magnets run the length of the guide way.

3.2 Advantages of Maglev

Well it sounds high-tech, a floating train; they do offer certain benefits over conventional steel rail on steel wheel railways. The primary advantage is maintenance. Because the train floats along there is no contact with the ground and therefore no need for any moving parts. As a result there are no components that would wear out. This means in theory trains and track would need no maintenance at all. The second advantage is that because maglev trains float, there is no friction. Note that there will still be air resistance. A third advantage is less noise, because there are no wheels running along there is no wheel noise. However noise due to air disturbance still occurs. The final advantage is speed, as a result of the three previous listed it is more viable for maglev trains to travel extremely fast, i.e., 500 km/h or 300 mph. Although this is possible with conventional rail it is not economically viable. Another advantage is that the guide way can be made a lot thicker in places, e.g., after stations and going uphill, which would mean a maglev could get up to 300 km/h (186 mph) in only 5 km where currently takes 18 km. Also greater gradients would be applicable.

3.3 Disadvantages with Maglev

There are several disadvantages with maglev trains. Maglev guide paths are bound to be more costly than conventional steel railways. The other main disadvantage is incompatibility with existing infrastructure. For example if a high speed line between two cities is built, then high speed trains can serve both cities but more importantly they can serve other nearby cities by running on normal railways that branch off the high speed line. The high speed trains could go for a fast run on the high speed line, and then come off it for the rest of the journey. Maglev trains wouldn't be able to do that; they would be limited to where maglev lines run. This would mean it would be very difficult to make construction of maglev lines

commercially viable unless there were two very large destinations being connected. Of the 5000 km that TGV trains serve in France, only about 1200 km is high speed line, meaning 75% of TGV services run on existing track. The fact that a maglev train will not be able to continue beyond its track may seriously hinder its usefulness.

3.4 Effect on Environment

In terms of energy consumption maglev trains are slightly better off than conventional trains. This is because there is no wheel-on-rail friction. That said, the vast majority of resistive force at high speed is air resistance (often amounting to several tons), which means the energy efficiency of a maglev is only slightly better than a conventional train.

German engineers claim also that a maglev guide way takes up less room and because greater gradients are acceptable there is not so much cuttings and embankments meaning a new guide way would be less disruptive to the countryside than a new high speed conventional railway.

IV. Important High Speed Trains

4.1 The Pendonlini

Class	ETR 450	ETR 500
Introduced	1987	1996
Commercial Speed	250 km/h (155 mph)	300 km/h (186 mph)
Best Average Speed	164.5 km/h (102.4 mph)	N/A

Table 4.1: ITALIAN PENDOLINIS

4.2 The Advanced Passenger Train

Top Planned Commercial Speed	150 mph (240km/h)
Speed Records	APT_E 152 mph (244km/h) 1975 APT_P 162 mph (260km/h) 1979

Table 4.2: THE ADVANCED PASSENGER TRAIN

4.3 The Eurostar

Top Commercial Speed	186 mph, 300km/h
Top speed in England	100 mph 160km/h
Top speed in the Channel Tunnel	100 mph 160km/h

Table 4.3: EUROSTAR

The Eurostar was Europe's first international train, designed to take advantage of the Channel Tunnel, to provide a high speed rail service between London and the UK to destinations in Continental Europe.

4.4 Le Train À Grande Vitesse (TGV)

Name	TGV Paris Sud-Est	TGV At antique	AVE	TGV Reseau	Eurostar	TGV Thalys
Introduced	1981	1989	1991	1993	1994	1996
Top Average Speed	135mph	Unknown	132mph 209km/h	158mph (254.3km/h)	N/a	132mph
Operating Speed	168mph 270 km/h	186mph 300km/h	186mph 300km/h	186mph 300km/h	186mph 300km/h	186mph 300km/h
Design	168mph	186mph	186mph	200mph	200mph	200mph

Speed	270 km/h	300km/h	300km/h	320km/h	320km/h	320km/h
Speed Record	236mph 380 km/h	320mph 515km/h	N/A	N/A	N/A	N/A
Max speed on normal rails	138mph 220km/h	138mph 220km/h	No running	138mph 220km/h	100mph 160km/h	unknown

TABLE 4.4: DIFFERENT TYPES OF TGV

The name "Train à Grande Vitesse" translated into English means high speed train, not really very imaginative, but seeing as it is French it tends to get away with it. There is no single TGV as such; in fact there are many generations of TGV, each generation consisting many trains. The TGV project started in the 1960s where SNCF realized that if it was to compete against the ever growing automobile and air transport it had to offer seriously better speeds.

V. Advantages of High Speed Trains

a) Reduced CO2 Emission

The USA has the highest CO2 emission rates in the whole world. The rate of car ownership is slightly higher in the USA. People must use their cars very much more in the USA accounting for the extra emissions because, the USA has very little by the way of railways, both high speed and local. It would seem reasonable to conclude that the more trains you have, the lower your country's CO2 emissions.

b) Huge capacity

High speed railways have by far the highest capacity per unit land they use. A high speed rail needs just a double track railway, one rail for trains in each direction. These have a capacity for 16 trains per hour, each train with a capacity of 800 passengers. This means a high speed rail has a maximum capacity of 12,800 passengers per hour, which clearly is enough to satisfy the highest of demand; only one railway line is needed. This is unlike motorways which take up a very large amount of space and often cannot satisfy demand fully at peak times.

c) Reduced traffic

Imagine you have two cities about 500km or 312miles apart, by car, the journey time will be about 6 hours. The motorways will be jammed full. If you can provide a new rail service of 300km/h 186mph between two cities the journey time by rail will be about 2 hours. Provided the rail service is well priced, very few people are likely to drive any more between the cities, causing a massive decrease in traffic. Of course with a decrease in traffic, pollution decreases too.

d) Energy efficiency

The energy resources are limited. The train offers per passenger energy efficiency that no other form of transport can achieve. The reason is because of steel wheels on steel rails The hard smooth surfaces provide very little friction. Also because the wheels are held by steel ball bearings, friction is very low even at high speed. Air resistance of a train is not really a problem because it is thin and long. On the other hand aircraft must burn huge amounts of fuel even to move at all, and in flight the engines have to continue to burn just to keep the plane in the sky. Once a train is moving, even if the engines are switched off, the train doesn't even decelerate noticeably, even at very high speeds. Cars, as everyone knows, are by far the least efficient form of transport.

e) Reduced pollution

Because of their efficiency, the pollution that a train makes is very low, and if the electricity being used for the train is generated by a green source then there may well be no pollution at all as a result of running the train. Reduced traffic also reduces pollution, no more cars pumping out gases in huge amounts, and of course compared to aeroplanes which need to burn fuel at an astonishing rate just to get thrust. In fact, it has been calculated that a Eurostar train with a capacity of 800 causes pollution level through power stations about equivalent to 20 cars.

f) Speed

300 km/h is very fast. That is the speed at which these trains fly along. No time is wasted in getting people to their destinations. There is no worry about waiting in traffic, or having a long stressful drive. Also it means that flying can be avoided, which is particularly welcome for the more ecological people.

g) Convenience

While airports are often out of town and hard to access, railway stations are usually located in the heart of the city. Also with some services you can just buy a ticket and get straight on the train, with no advanced booking required. Aircraft have drawbacks such as long check-in times and constant moving around.

h) Safety

What is perhaps not known about is that high speed trains are in fact the safest form of transport. High speed trains are perhaps surprisingly safer than normal trains. Most use very advanced computer signaling systems meaning risk of collision is very low, and apart from that there is not a lot that can go wrong. France had a train going at 320 mph (512 km/h), which shows that dangerous, experimental speeds are a long way off commercial everyday speeds.

i) Comfort

With the possible exception of cruise ships trains are the most comfortable form of transport. Even at these very high speeds the train remains about as smooth as an aircraft, and of course very much quieter. Also there are no limitations, the seats are not cramped like in an aircraft, and unlike in a car you can get up, walk around, or buy a snack from the buffet car.

VI. Drawbacks of High Speed Rail

a) Social drawbacks (externalities)

The only real externality is the fact that in order to build high speed rail lines the country side has to be sacrificed. This particular externality applies to all forms of transport however (with the possible exception of water). Although high speed rail lines do not occupy a large amount of room, the fact that they have to be straight and level usually involves large amounts of embankments and cuttings causing considerable disruption to the countryside.

b) Economic drawbacks

The primary objection is always cost. High speed railways are very expensive. To build the high speed link in the UK between London and the Channel tunnel for 300km/h Eurostars it is costing the Government and private companies £3 billion (US $4.8 billion). This railway is just 68 miles long (108 km). This is perhaps an extreme example, high speed railways typically are not so expensive but difficult geography (rolling hills) and high population density of the area has pushed up the cost.

c) Cost-effectiveness on the basis of pollution control

High initial costs often mean public money has to be used because the private sector is usually unwilling to engage in such large projects. As a result many would argue that the money used to build such rail systems would be more effectively spent in other projects if the primary objectives were to reduce traffic congestion/pollution.

d) Limitations of high speed rail

High speed rail is only applicable to inter-city services in high density corridors (having said that connecting trains can deliver people door to door). This means that, in order to work effectively, high speed rail must be backed up by a decent urban/light rail transit system, as found in Europe and Japan. Such systems are rarer.

e) Limitations of geography

High speed railway lines need to be as straight and level as possible. Therefore often the railways are carried over dips and hills in the countryside by embankments, viaducts, cuttings and tunnels. (Tunnels are sometimes unsuitable due to wind turbulence problems.) However these greatly increase the cost of the railway and of course, if the landscape is mountainous then it becomes very difficult to build it straight and leveled. Naturally, railways cannot be built over water for long distances.

VII. Conclusion

Although there have been derailments, in the almost two decades of daily operation, there has been no casualties. While the very high speed trains like the TGV could be regarded as the Rolls Royce of trains, tilting trains could be thought of as the cheap and cheerful mini metro. The price differential is fairly similar too; it costs about 20 times more per unit distance to build a dedicated high speed line than it does to upgrade existing lines for tilting trains. This is what makes tilting trains extremely attractive. However there are disadvantages. 140 mph or 230 km/h is about as fast as trains go when not on dedicated lines. And then they have to be fitted in with slower moving traffic. With rail travel growing all over Europe, the problems of railways reaching saturation point has forced new lines to be build. This is why despite the success of the Italian Pendolini; a new high speed line with 300 km/h trains is being built, because existing lines are at saturation point. Most of the high speed train functions are controlled digitally, true to being the vehicle of the digital age.

VIII. Acknowledgment

The author wishes to acknowledge the Project Guide Dr. Pushpendra Kumar Sharma, Head of Department Nri-ist Bhopal, India, for their continual guidance.

References

[1] Science and Technology Review, June 1998.
[2] Hood, Christopher P, Shinkansen- From Bullet Train to Symbol of Modern Japan, Routledge, 2006.
[3] Moon, Francis C, Superconducting Levitation Applications to Bearings and Magnetic Transportation, Wiley-VCH, 1994.
[4] En.wikipedia.org
[5] www.o-keating.com

International Journal of Modern Engineering Research (IJMER)
www.ijmer.com Vol.3, Issue.2, March-April. 2013 pp-1167-1168 ISSN: 2249-6645

Approach to the prophylaxis of back and neck lesions at the office job through a universal mechanical chair add-on part

Thomas Lekscha, [1] Ulrich Dickel[2]
[1]*Faculty of Engineering Science, Department of Medical Technology, Jade University, Germany*
[2]*Institute of Innovations-Transfer,Field Mechatronics, Jade University, Germany*

Abstract:*The aim of this new development, this innovative proposal, was to develop a portable, mechanical add-on device for standard office chairs. The universally deployable add-on device should serve for the prevention of pain in the neck and back in office workplaces as well as aiding rehabilitation for those who already suffer such pain. The new development should provide the possibility of performing gymnastic impander and expander movements countering a preset, adjustable, mechanical resistance.*

Keywords:*Back pain, Neck pain, Office chair, Universaladd-on part, Active pain prevention, Medical technology*

I. INTRODUCTION

Sitting automatically represents the application of biomechanical stress to the spinal column and, as a result, to the muscle groups linked to it; particularly to the area of the pelvis, cervical/shoulder girdle and the entire spinal column. Problems with the back resulting from work completed in a sitting position are the most frequent causes of occupational illnesses. The ever-increasing amount of work performed on computer screens means that phases of relief and relaxation from the strain are essential with regard to both the biomechanical system as well as the cardiovascular system if serious health problems are to be avoided. Remaining in one position for longer periods while completing office work is damaging to health

Active, moving parts for the purpose of reconditioning are not provided on office chairs currently on the market. Complaints related to regions of the back, cervical spine and shoulder girdle are rising dramatically and resulting in increases in the inability to work. This aspect represents the focal point of our innovative concept. According to information from the Robert Koch Institute, 62% of the German population underwent medical treatment [1] for back problems in 2003. This information coincides with the results of a study completed by TNS Healthcare in 2008 whereby 70% of all women and 57% of all men in Germany suffered from back and neck pains [2]. The results of a questionnaire completed on people covered by the German AOK health insurance company in 2010 showed that “back pain” topped the rankings in respect of incapacity to work [3]. Back and neck pains top the list, being the main cause of employee absenteeism.

The new development with its innovative conceptual proposal (Fig. 1) fulfills the requirements demanded by the Berufsverbandes der deutschenRückenschulen (German Association of Back Therapy Training) and BerufsverbandesdeutscherÄrztefürOrthopädie (German Association of Orthopedic Surgeons) with regard to relief and relaxation phases when completing work while seated. The following explonation illustrate the realization of the concept.

Fig. 1 Illustration of the mechanical add-on device and its movement options

II. APPLICATION

The newly developed concept, or rather the prototype should be capable of being attached to as many common office chairs as possible. The mechanical device can be fixed either to the backrest via an adapter plate or to the chair frame via a clamping device. Both fixation methods have been tested and proven satisfactory. The figure on page 11077, (Fig. 2) illustrates the attachment of the mechanical device to the backrest of a standard office chair.

Fig. 2 Front, side and rear views of attachment to a standard office chair

III. STATIC LOAD TESTS

The first prototype was developed according to defined basic data. The basis for this was a person with a maximum weight of 120 kg. Assuming the application of an equal load to the levers (right/left), this produces a load of 60 kg on each. The degree of impander mobility was set to +/- 30° and expander mobility to +/- 45°. The force necessary to press the lever arms together or push them apart was set to a minimum of 35 N and maximum of 80 N. Both levers (right/left) have an angle of movement of 240°.

This data was defined and load tests were completed under laboratory conditions in order to simulate use by persons in practice. The continuous application of a load resulted in the necessity to optimize the system with regard to the adjustable mechanical resistance. Material weaknesses must be eliminated and the device operability improved.

IV. CONCLUSION

The newly developed prototype intended to support the prevention of back and neck pain resulting from office work represents the development of a mechanical, portable add-on device for chairs which can be attached to practically all standard office chairs. This mechanical add-on device enables the person using the chair to perform impander and expander movements during work breaks or at intervals during work.

As a result, users of the chair do not require any auxiliary equipment to exercise their back and neck muscles. Considering the data and facts compiled from the questionnaires regarding health problems related to the back and neck suffered by the German population outlined at the beginning of this report, there is an urgent need to develop a concept aimed at preventing the causes of such disorders. The prototype developed illustrates an option in the prevention.The prototype within the concept presented was developed based on the DE 44 04 282 C2 [4].

V. ACKNOWLEDGEMENTS

We would like to thank the following for their support in the realization of this project: Faculty of Engineering Science and Institute of Innovations-Transfer, both at the Jade University in Wilhelmshaven, Germany. We would also like to thank SanitätshausGebauer GmbH, Germany, Dr. Hermann Himmelmann and Dr. Bernd Wabbels for their cooperation throughout the project. Further thanks go at the State of Lower Saxony, Germany, and to the European Union for their partial financing of the development.

REFERENCES

[1] Kohler, M., Ziese, T.: Telefonischer Gesundheitssurvey. Ein Wort des Robert Koch-Instituts zu chronischen Krankheiten und ihren Bedingungen. 2004, RKI, Berlin
[2] TNS Healthcare: Spalt-Schmerz-Report. Art der Schmerzen, unter denen Männer und Frauen in Deutschland leiden. 2008, Whitehall-Much
[3] Wissenschaftliches Institut der AOK (WIdO): Die 10/20/50 Erkrankungen mit den längsten Arbeitsunfähigkeitszeiten in Tagen bei AOK-Pflichtmitgliedern ohne Rentner. 2011, WIdO, Berlin
[4] German Patent and Trade Mark Office: Sitzmöbel mit einer hohen Rückenlehne, vorzugsweise Arbeits- oder Bürostuhl. DE 44 04 282 C2. 1997.12.11, D-80331 München

AUTORS

Dr. Thomas Lekscha,received his Dipl.-Ing. from the Faculty of Engineering Science, Jade University in Wilhelmshaven, Germany. He received his M.Sc. and also his Ph.D. from the Faculty of Electrical Engineering and Information Technology, STU University of Technology in Pressburg. His research activities are in the field of Medical Technologies and Electronics. Today, he is a member of a research staff for medical technologies and Adjunct Professor at the Department of Medical Technology, Jade University, Germany.

Ulrich Dickel,received his Dipl.-Ing. from the Faculty of Engineering Science, Jade University in Wilhelmshaven, Germany. He is still working in the field of Mechanical Engineering and Mechatronics.

International Journal of Modern Engineering Research (IJMER)
www.ijmer.com Vol.3, Issue.2, March-April. 2013 pp-1169-1171 ISSN: 2249-6645

Smart Web Cam Motion Detection Surveillance System

Cynthia Tuscano, [1] Blossom Lopes, [2] Stephina Machado, [3]
Pradnya Rane[4]
[1234]*Department OF Computer Engineering, St. Francis Institute of Technology, Mumbai, India*

***Abstract**: The Basic Idea Behind "Smart Web Cam Motion Detection Surveillance System" Is To Stop The Intruder To Getting Into The Place Where A High End Security Is Required. This Paper Proposes A Method For Detecting The Motion Of A Particular Object Being Observed. The Motion Tracking Surveillance Has Gained A Lot Of Interests Over Past Few Years. This System Is Brought Into Effect Providing Relief To The Normal Video Surveillance System Which Offers Time-Consuming Reviewing Process. Through The Study And Evaluation Of Products, We Propose A Motion Tracking Surveillance System Consisting Of Its Method For Motion Detection And Its Own Graphic User Interface. Various Methods Are Used In Motion Detection Of A Particular Interest. Each Algorithm Is Found Efficient In One Way. But There Exits Some Limitation In Each Of Them. In Our Proposed System Those Disadvantages Are Omitted And Combining The Usage Of Best Method We Are Creating A New Motion Detection Algorithm For Our Proposed Motion Tracking Surveillance System. The Proposed System In This Paper Does Not Have Its Effect Usage In Office Alone. It Also Offers More Convenient, Effective And Efficient Usage Where High-End Security Comes Into Picture.*

***Keywords:** Intrusion, Motion Detector, Security, Surveillance, Web Camera.*

I. INTRODUCTION

The Theft Statistics Show That Out Of The Total Reported Thefts, The Breakage Can Be Shown :-Display Cases: 19%,Open Displays: 10%, Pictures: 04%,Other Displays: 02%,At Night: 06%,From Stores: 02%,Other: 03%.Although We Are Successful In Detecting And Gaining Evidence Against The Crimes, We Have To Find A Way Of Preventing Them Too. Stopping Thefts And Crimes While They Are In Progress Is The Main Motivation Of Our Paper. Motion Can Be Detected By Measuring Change In Speed And Vector Of An Object Or Objects In The Field Of View. This Can Be Achieved Either By Mechanical Devices That Physically Interact With The Field Or By Electronic Devices That Quantifies And Measures Changes In The Given Environment. Motion Detection Refers To The Capability Of The Surveillance System To Detect Motion And Capture The Events. Motion Detection Is Usually A Software-Based Monitoring Algorithm Which, When It Detects Motions Will Signal The Surveillance Camera To Begin Capturing The Event. This Paper Proposes That The Motion Detection System Which We Have Built Has Various Benefits In Terms Of Cost And Complexity. Our System Basically Consists Of The Webcam Which Is In-Built On The Computer System. The Webcam Thus Significantly Reduces The Cost Of The Overall System. On Detection Of Any Kind Of Malicious Activity The System Will Capture The Image Immediately And Send Notification To The Administrator In The Form Of Image (Mms) And E-Mail. Also At The Same Time The Alarm Will Be Set Off Signaling The Occurrence Of The Ongoing Illegal Activity, Which Can Also Have Benefit Of Causing Momentary Panic Among The Robbers And Alert The Concern Authorities Via Mms/E-Mail. The System Is Designed To Capture The Effects Of Light Sensitivity. In Case Of Sudden Changes In The Light The System Will Capture The Image And Set Off The Alarm. In Summary, The Contribution Of This Paper Is Tonot Only Detect The Ongoing Intrusion But Also To Stop It While It Is In Progress.

The Paper Is Organized As Follows. A Brief Introduction Followed By The Overall Study Of Existing Systems And Requirements Of The Surveillance Are Depicted In Section 2work Specification Of Motion Detection Is Presented In Section 3, Followed By The Work Implementation In Section 4.

II. RELATED WORK

A Number Of Approaches And Systems Have Been Proposed And Designed In Recent Years To Identify And Analyze Malicious Activity [6]. We Will Now Briefly Present The Most Relevant Ones And Compare Them With Our Approach.

VIDEO MOTION DETECTORS-OUTDOOR APPLICATIONS		LIST RICE USD
DS-16	A chassis which holds up to 16 channels of the dS-1S or dS-1SPL pCBS. The active backplane controls all Pcbs from front panel programming or rS-232.	1395.00
DS-16-MT	A chassis which holds up to 16 channels of the DS-1SPL Pcbs. The active backplane controls all Pcbs from front panel programming or RS-232	2096.00
DS-1	1channel motion detector, 262,144 detection points, day/night mode, video loss alarm and RS-232.	1595.00

VIDEO MOTION DETECTORS-INDOOR APPLICATIONS		List
VMD-2004	4-channels vMD-262,144 detection points, independent zone blocking, video loss, built-in alarming, bridging, looping switcher. 12VDC with included adapter.	1295.00
VMD-2008	8-channels VMD-262,144 detection points, independent zone blocking, video loss, built-in alarming, bridging, looping switcher. 12VDC with included adapter.	1995.00

LOW COST VIDEO MOTION DETECTOR		List
VMD-1001	1-channel Vmd, 62, 208 detection points, multi-zone areas, front panel push button operation, on screen menus, suitable for indoor and outdoor applications.	595.00
VMD-1001S	vmd-1001 pcb Only	590.00

Now the estimated cost of the existing systems will include the cost of various hardware equipment's that the system requires supporting it. Even the lowest cost motion detectors' which are currently available in the market are far more expensive then the system we have built.

III. WORK SPECIFICATION

In our project we have aimed to build such asurveillance system, which can not only detect motion, but will

A) Warn the User of the Intrusion by Setting on the Alarm,
B) Record the Footage from the Moment the Motion Was Detected,
C) Sends an E-Mail to the Logged In User And
D) Sends Mms On The Mobile Phone Of The User.

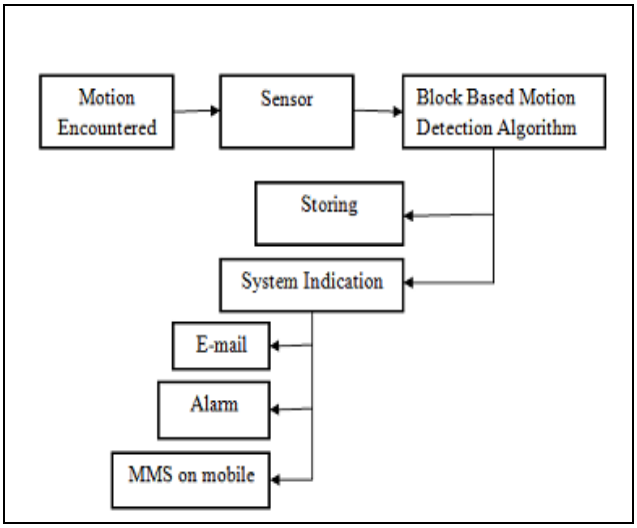

Figure 1: A Basic System Architecture of Our System

System Architecture Functioning

The system architecture is going to function in following way:

3.1capturing Phase

To detect Motion We First Have To Capture Live Images Of the Area to Be Monitored and Kept under Surveillance. This Is Done by Using a Web Cam which continuously provides A Sequence of Images in a Particular Speed of Fps (Frames per Second).

3.2comparing Phase

Comparing the Current Frames Captured with Previous Frames to Detect Motion: For Checking Whether Any motion Is Present in the Live Images, We Compare The live Images Being Provided By The Web Cam With each Other So That We Can Detect Changes In These Frames and Hence Predict The Occurrence Of Some Motion.

3.3storage Phase

Storing The Frames On The Memory If Motion Is Detected: If Motion Is Being Detected, We Would Require Storing such Motion So That The User Can View It In The Near Future. This Also Helps the User in Providing a Legal Proof of Some inappropriate Activity since a Video Coverage Can Be Used as A Proof in the Court Of Law.

3.4system Indication Phase

Indicating through an E-Mail, Alarm and Mms When the Motion Is Detected: The User May Want To Be Notified Immediately That There has Been Some Intrusion Detected By The Software, Hence an Alarm System Is Included In The Software. This Alarm system immediately activates a Wav File Format Audio alarm Signal If Any Kind Of Motion Is Detected Hence. This helps In Preventing Any Kind Of Breach of Security at That moment Of Time. As Soon As The Motion Is Detected An E-Mail Containing The Pictures Of The Intruder Are Sent To The Mail Account Of The User And Simultaneously An Mms Will Be Delivered On The User's Cell Phone.

IV. IMPLEMENTATION

4.1background AND Foreground Separation

The Discrimination between Background and foreground Is Based On Block-Based motion Estimation. In This Paper, The Modified Block-Based Estimator Is Used To Track Changes Of The Individual Block. Each Frame of The 320x240 Pixel Resolution Is Divided Into Non-Overlapping Of 32x24 Pixels. For The Block Motion Estimation, A 9x9 Window Region With The Maximum Standard Deviation Is Extracted Within Each Block [1].

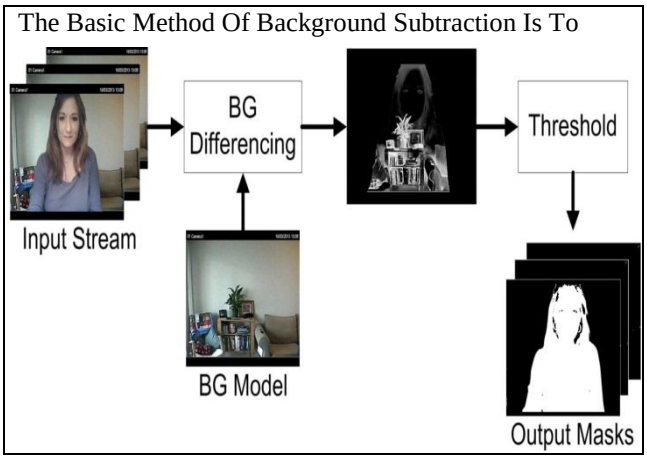

Figure 2: Background Separation

In the above figure, an input stream of images will be provided to the system which is then subject to background separation. Subtraction takes place based on the predefined threshold value and resultant is the foreground image which we obtain.

V. conclusion

The "smartweb cam motion detection surveillance system" is a Home/Office based security system which can be of great where security is a matter of concern. The Motion Detector patches up for the need of a cheap and small security system in day-to-day life. Computerized Home-based security can develop a lot with the coming future. Future is promising and easier with innovative technologies.

References

[1] Young-Kee Jung, Kyu-Won Lee, Dong-Min Woo, AND Yo-Sung Ho: "Automatic Video Object Tracking Using A Mosaic-Based Background", K. Aizawa, Y. Nakamura, And S. Satoh (Eds.): Pcm 2004, Lncs 3332, PP. 866–873, 2004. @Springer-Verlag Berlin Heidelberg 2004

[2] V. D. Ambeth Kumar, M. Ramakrishanv. D. Ambeth Kumar, M. Ramakrishna: "Web Cam Motion Detection Surveillance System Using Temporal Difference AND Optical Flow Detection WITH Multi Alerts".

[3] Jun Ke, Amit Ashok, Mark A. Neifelda: "Block-Wise Motion Detection Using Imaging System". Department OF Electrical Computer Engineering, University OF Arizona, Tucson, Az 85721-0104, Usa College OF Optical Sciences, University OF Arizona, Tucson, Az 85721-0104, Usa

[4] Microsoft Security Research & Defense, [Online], VAILABLE: http://Blogs.Technet.Com/Srd/Archive/2008/02 /06/The-Kill 2d00 Bit-Faq 3a00 -Part-1-OF-3.ASPX

[5] Eric Galloix, Janne Heikkila,¨ Olli Silvendepartment OF Electrical Engineering P.O. Box 4500, Fin-90014 University Of Oulu, Finland : "Motion Detection Against CHANGING ILLUMINATION: A Classifyingapproach".

[6] Http://Www.Videomotiondetectors.Com, Ave Thailand O., Ltd.147 Soi Onnut44, (Sampheenong Villa), Sukhumvit 77 Rd., Suanluang, Suanluang, Bangkok 10250 Thailand

International Journal of Modern Engineering Research (IJMER)
www.ijmer.com Vol.3, Issue.2, March-April. 2013 pp-1172-1175 ISSN: 2249-6645

QSAR Study for a Series of 31 Peptide-Mimetic Analogues with the Ability to Inhibit HIV-1 Protease Using Receptor Surface Analysis

Dr. T. Anthoney Swamy, [1] Dr. Gummadi Samuel Moses[2]
[1]*Department of Chemistry, University of Eastern Africa, Baraton, P O Box 2500-30100, Eldoret, Kenya*
[2]*P.G Dept. of Chemistry, Government College (NAAC 'A' Grade), Rajahmundry, Andhra Pradesh, India*

Abstract: *The quantitative structure–activity relationship analysis of a set of 31 peptide- mimetic analogues of HIV – 1 protease inhibitors was performed by receptor surface analysis. RSA is a useful tool in situations when the 3D structure of the receptor is unknown since one can build a hypothetical model of the receptor site. A receptor surface model embodies essential information about the hypothetical receptor site as a three-dimensional surface with associated properties such as hydrophobicity, partial charge, electrostatic (ELE) potential, van der Waals (VDW) potential, and hydrogen bonding propensity. The surface points that organize as triangle meshes in the construction of the RSA store these properties as associated scalar values. Receptor surface models provide compact, quantitative descriptors, which capture three-dimensional information of interaction energies in terms of steric and electrostatic fields at each surface point, which in other techniques are calculated using probe interactions at various grid points. These descriptors can be used for 3D QSAR studies.*

Key Words: *Receptor Surface Analysis, QSAR, HIV-1 Protease Inhibitors*

I. Introduction

Molecules with different substituents are generated electronically with their biological activities. All the molecules were coded with a prefix "Exa". The receptor surface model is normally generated from the most active compounds in the data set. The rationale is that the most active molecules tend to explore the best spatial and electronic interactions with the receptor, while the least active do not and tend to have unfavorable steric and electrostatic interactions. Receptor models generated using the five best active compounds Exa4, Exa6, Exa12, Exa18 and Exa33 in the training set. After the receptor surface model has been generated, all the structures in the training and test sets can be evaluated against the model. The model can be used to calculate the energy associated with the binding of a molecule in the model. It can also be used to minimize a molecule by adjusting the geometry of the structure into a "best-fit configuration" based on the constraints imposed by the receptor model. This method creates hypothetical models, called receptor surface models; those characterize the active site of macromolecule based on the construction of surfaces to represent spatial and electrostatic properties of a receptor's active site.

II. Result and Discussion

In Receptor Surface Analysis (RSA), the major steps were (1) generating conformers and energy minimization; (2) aligning molecules using the MCSG method; (3) generating the receptor model; (4) evaluating the compounds in the generated receptor model; and (5) generation of equations by the genetic function approximation method.

A receptor model was generated with the following:

- Activity data
- Soft receptor surface type
- Energies calculated using electrostatic charge complementarity

The option to minimizing molecules during evaluation was avoided. After the receptor model is generated, properties such as electrostatic potential and hydrophobicity were mapped on to the surface of the model. One property can be mapped at a time. Property maps were displayed as color regions on the receptor surface.

These properties reflect the anticipated characteristics of the receptor that is being modeled. The intensity of color reflects the magnitude of the mapped property at a particular location. Properties that can be mapped include the following:

a) **Electrostatic potential:** Each surface vertex is colored according to the potential value at the vertex position. Red areas have negative electrostatic potential, blue areas have positive potential and white areas have neutral potential.
b) **Charge:** when this property is mapped, the surface color is based on the average of the charges of the template atoms closest to the receptor surface. Red areas are positively charged, blue are negatively charged and white areas neutral.
c) **Hydrogen Bonding:** The color indicates the tendency for specific areas of the surface to act as hydrogen bond donors (green) or acceptors (blue). Areas of the model with no hydrogen bonding activity are colored cyan.
d) **Hydrophobicity**: The surface is colored brown to map the hydrophobic areas of the model. Areas that are not hydrophobic relative to the scale on the panel are white.

Figure 1.1a shows the best active compounds embedded into the receptor surface model mapped with electrostatic potential; the red color represents negative energy values as favorable interaction sites, while the blue-colored regions represent positive energy values that are favorable sites for binding of the molecule on the receptor surface. Intermediate colors indicate the intensity and gray indicates neutral. Figure 1.1b shows the best active compounds embedded into the receptor surface model mapped with charge; the red areas are positively charged, the blue areas are negatively charged, and the white areas are neutral. Similarly, Figure 1.1c shows the best active compounds embedded into the receptor surface model mapped with hydrogen bonding; the blue areas act as hydrogen bond donors, the green areas act as hydrogen bond acceptors, and the pale blue do not have hydrogen bonding activity. Figure 1.1d shows the receptor surface model mapped with hydrophobicity; the brown areas are hydrophobic.

This color coding of the ligand-receptor interactions can offer a qualitative way of examining compounds, by introducing them into the virtual receptor and visually inspecting the favorable/unfavorable interactions; substituents that increase or decrease the binding affinity can be easily recognized, and one can make easily simple but accurate structure-activity estimations. Though the outcome is with statistically acceptable results for the training set, the prediction results of the test set are not equally encouraging.

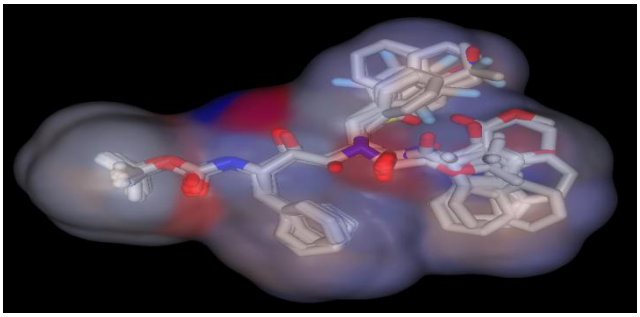

(Figure 1.1a: Electrostatic potential mapped on the receptor surface)

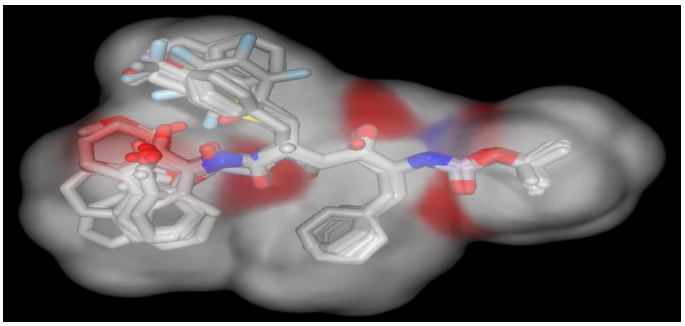

(Figure 1.1b: Charge mapped on the receptor surface)

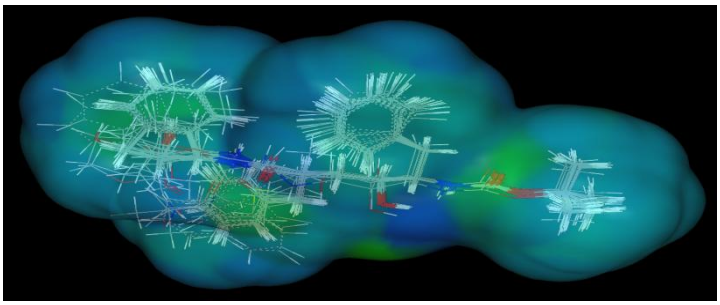

(Figure 1.1c: Hydrogen bonding mapped on the receptor surface)

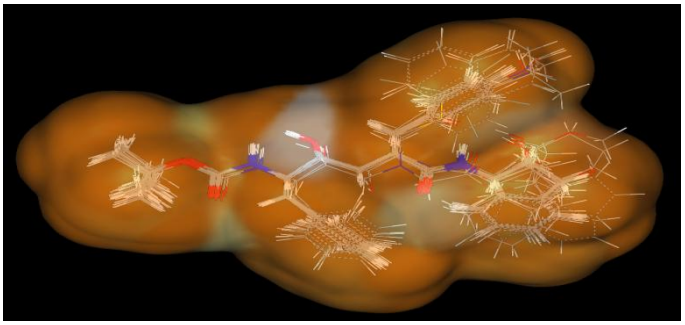

(Figure 1.1d: Hydrophobicity mapped on the receptor surface)

Four properties are independently mapped, generated and added them to study tables. Each study table was saved to do the QSAR model extraction. The relevant equations and their validation parameters are given here under.

Electrostatic mapping:
pIC50 = - 0.128124 - 1.33831 * "Inter VDW Energy" - 13.8893 * "VDW/693" - 27.1182 * ELE/3708"
Validation parameters are:
R−squared = 0.884
Cross validated R−squared = 0.799
PRESS = 11.89
Charge mapping:
pIC50 = 4.19565 - 11.1954 * "VDW/645" - 32.9953 * "ELE/3838" - 16.9802 * "VDW/692"
Validation parameters are:
R−squared = 0.883
Cross validated R−squared = 0.794
PRESS = 12.22
H-Bond mapping:
pIC50 = 3.76507 - 9.89141 * VDW/644" - 19.1306* "VDW/692" - 33.215 * "ELE/2131"
Validation parameters are:
R−squared = 0.874
Cross validated R−squared = 0.791
PRESS = 12.36
Hydrophobic mapping:
pIC50 = 3.75074 - 17.9708 * "VDW/692" - 12.0473 * VDW/1545" - 38.0359 * "ELE/3706"
Validation parameters are:
R−squared = 0.885
Cross validated R−squared = 0.814
PRESS = 11.03

The resultant models were of good statistical qualities having > 87 % explained variance and 79% predicted variance.

Table 1.4: Predicted activity values based on RSA

Code given	Experimental pIC50	Predicted pIC50 from RSA
Exa1	9.6	9.17
Exa3	8.11	9.25
Exa4	9.72	9.7
Exa5	9.59	9.67
Exa6	9.64	9.54
Exa7	9.22	9.64
Exa8	9.54	9.23
Exa9	9.51	9.48
Exa10	9.57	9.25
Exa11	5.53	6.34
Exa12	9.8	9.27
Exa13	7.56	6.73
Exa14	9.14	8.81
Exa15	8.27	8.89
Exa16	9.28	8.66
Exa17	9.6	9.75
Exa18	9.77	9.94
Exa19	6.94	6.75
Exa20	8.02	8.4
Exa21	7.47	8.07
Exa22	6.16	6.77
Exa23	6.79	6.57
Exa24	7.18	8.93
Exa25	6.67	9.19
Exa30	4.52	4.24
Exa31	6.89	6.45
Exa32	6.84	6.69
Exa33	10	10.22
Exa34	7.41	6.71
Exa49	5.33	5.4
Exa50	5.86	6.34

III. Conclusion

The descriptors VDW/693, ELE/3708, ELE/3838, VDW/692, VDW/644, VDW/692, ELE/2131, VDW/692, VDW/1545, ELE/3706, etc. are contributing at the grid point numbers in the space. The location and magnitude of a descriptor can be used as a guideline to improve the activity of molecules.

IV. Acknowledgement

I would sincerely thank Dr. M. Kishore Kumar, bio-Campus, Hyderabad for his guidance and invaluable technical assistance. My grateful acknowledgments are due to the management of bio-Campus, Hyderabad, for providing excellent working atmosphere with modern equipment in drug discovery and design during my stay at their campus.

References

[1] David E. Clark, David R. Westhead Journal of Computer-Aided Molecular Design 1996, 10 (4), 337-358-
[2] Hansch, C.; Leo, A.; Hoekman, D. (1995) Exploring QSAR. Hydrophobic, Electronic and Steric Constants; American Chemical Society: Washington, DC.
[3] Hahn, M. (1995) Receptor Surface Models. 1. Definition and Construction. J. Med. Chem., 38, 2080-2090.
[4] Franke, R. Theoretical Drug Design Methods; Elsevier: Amsterdam, 1984.
[5] Franke, R.; Gruska, A. (1995) In Chemo metric Methods in Molecular Design; van de Waterbeemd, H., Ed.; VCH: Weinheim, Vol. 2, pp 113-163.
[6] Kamal Azzaoui, Maria J. Diaz-Perez, Maria Zannis-Hadjoupoulos, Gerry B. Price, and Irving W. WainerJournal of Medicinal Chemistry **1998**, 41 (9), 1392-1398
[7] Sung-Sau So and Martin KarplusJournal of Medicinal Chemistry 1997, 40 (26), 4347-4359
[8] Rohrbaugh, R.H., Jurs, P.C., (1987) "Descriptions of Molecular Shape Applied in Studies of Structure/Activity and Structure/Property Relationships", Analytica Chimica Acta, 199, 99-109.
[9] Holloway, M. K., J. M. Wai, et al. (1995). "A priori prediction of activity for HIV-1 protease inhibitors employing energy minimization in the active site." J Med Chem 38(2): 305-17.
[10] Rogers, D.; Hopfinger, A. (1994) J. Application of genetic function approximation to quantitative structure-activity relationships and quantitative structure-property relationships. J. Chem. Inf. Comput. Sci., 34, 854-866.
[11] Chong Hak Chae, Sung-Eun Yoo, and Whanchul ShinJournal of Chemical Information and Computer Sciences 2004, 44 (5), 1774-1787
[12] Antonio Macchiarulo, Gabriele Costantino, Mirco Meniconi, Karin Pleban, Gerhard Ecker, Daniele Bellocchi, and Roberto PellicciariJournal of Chemical Information and Computer Sciences 2004, 44 (5), 1829-1839
[13] Jaroslaw Polanski, Rafal Gieleciak, Tomasz Magdziarz, and Andrzej BakJournal of Chemical Information and Computer Sciences 2004, 44 (4), 1423-1435
[14] http://www.ccdc.cam.ac.uk/products/csd/
[15] http://www.rcsb.org/pdb/home/home.do
[16] C. Pérez, M. Pastor, A.R. Ortiz, F. Gago, Comparative binding energy analysis of HIV-1 protease inhibitors: incorporation of solvent effects and validation as a powerful tool in receptor-based drug design, J. Med. Chem. 41 (1998) 836–852.
[17] A. Wlodawer, J. Vondrasek, Inhibitors of HIV-1 protease: a major success of structure-assisted drug design, Annu. Rev. Biophys.Biomol. Struct. 27 (1998) 249–284.
[18] A. Gavezzotti, Molecular packing and correlations between molecular and crystal properties, in: H.-B. Bürgi, J.D. Dunitz (Eds.), Structure Correlation, vol. 2, VCH, Weinheim, 1994, pp. 509–542.
[19] C. Flexner, HIV-1 protease inhibitors, New Engl. J. Med. 338 (1998) 1281–1292.
[20] K.R. Beebe, R.J. Pell, M.B. Seasholtz, Chemo metrics: A Practical Guide, Wiley, New York, 1998.
[21] Pirouette, Version 2.7., Infometrix Inc., Seattle, WA, 2000.
[22] M. Sakurai, S. Higashida, M. Sugano, H. Handa, T. Komai, R. Yagi, T. Nishigaku, Y. Yabe, Studies of human immunodeficiency virus type 1 (HIV-1) protease inhibitors. III. Structure–activity relationship of HIV-1 protease inhibitors containing cyclohexylalany lalanine hydroxyethane dipeptide isostere, Chem. Pharm. Bull. 42 (1994) 534–540.

International Journal of Modern Engineering Research (IJMER)
www.ijmer.com Vol.3, Issue.2, March-April. 2013 pp-1176-1179 ISSN: 2249-6645

DASH 7

Rahul.C, [1] Chinchu Krishna.S[2]
1M.E Computer and Communication, Department of Electronics and Communication, Erode Builders Educational Trust's Group of Institution EBET Knowledge Park, Kangayam, Tamil Nadu, India
2Assistant Professor, Department of Information Technology, Rajagiri School of Engineering and Technology, Cochin, Kerala, India

Abstract: *Dash7 is a new wireless networking scheme and appears to be gaining traction. The International Organization of Standardization first ratified the standard behind DASH7in 2004.The less power drawing feature make it especially appropriate for such things as radio-frequency tags, which may work for years without any external power source. If the system doesn't need high data rate can use Dash7. Dash7 tags are active, meaning that they make use of small batteries instead. It doesn't need to transmit high power levels and consequently can be manufactured inexpensively*

Keywords: *simple protocol, Low data rate, High efficiency, Long range applications, communication theory*

I. INTRODUCTION

DASH7 is a new wireless networking scheme and appears to be gaining traction. The International Organization of Standardization first ratified the standard behind DASH7 in 2004.The less power drawing feature make it especially appropriate for such things as radio-frequency tags, which may work for years without any external power source.DASH7 tags are active, meaning that they make use of small batteries instead. It doesn't need to transmit high power levels and consequently can be manufactured inexpensively.DASH7 operates at around 433megahertz.The corresponding wavelength is about 70 cms, which make it difficult to design efficient antennas that are conveniently compact. This wavelength enables it to penetrate such obstacles as concrete walls and work in environments with large amount of metallic clutter. The search for a market for DASH7 isn't new.Savi began developing this technology two decades ago. The US military embraced this radio tagging system and has been employing it increasingly.DASH7's general claim for less power use than Zigbee depends on the details of how the particular wireless network is setup. One uncontested attribute of DASH7 is that its name has a clear and sensible derivation.

II. LOW POWER RADIO FREQUENCY

2.1 Defining "Rf"

Solutions where the RF transceivers use a minimum of energy to communicate with each other, and where periods without communication are characterized by a minimal amount of energy spend idling. To quantify this statement for 2009, a low power RF technology worth its salt has no problem operating at an average current draw under 0.1mA and a max current draw under 50mA.

RF stands for "Radio Frequency". Low power radio frequency products need:

1. RF silicon parts, with as much integration as possible.
2. Power supplies, which are usually batteries. Low power RF devices absorb energy from its environment.
3. A microcontroller, which contains a small CPU and memory. For providing integration designers must expect RF silicon and the microcontroller in a single package.
4. Some kind of antenna for conveying the RF energy.
5. Optionally sensors, which are silicon parts, are also benefit from integration.

2.2 Rfid

RFID means Radio Frequency Identification. Passive RFID's requires a very high power transmitter, often called as interrogator, while the transponder must exhibit very low power characteristics. These systems do not require batteries in the transponders, which behaves similar to RADAR. But they cannot be considered to a low power RF system.

2.3 Blast

DASH7 is designed to use the BLAST concept. Bursty: Data transfer is abrupt and does not include content such as video, audio, or other isochronous forms of data. Light-data: In conventional applications, packet sizes are limited to 256 bytes. Transmission of multiple, consecutive packets may occur but is generally avoided if possible.

Asynchronous: DASH7's main method of communication is by command response, which by design requires no periodic network "handshaking" or synchronization between devices.
Transitive: A DASH7 system of devices is inherently mobile. It is upload centric, so devices do not have to be managed extensively by fixed infrastructure.

III. A SURVEY OF LOW POWER RF STANDARDS

3.1 Simple Protocol

Techniques for optimizing low-power RF systems always seek to maximize the amount of time spent in sleep mode, or, from another perspective, minimizing the amount of time spent in active modes. More-so than data-rate, the protocol is the means by which time spent in active modes can be determined. Good low-power RF solutions have protocols that do not specify extraneous features. In other words, these solutions are defined by considering not what features you could use but instead what features you could do without. Of the depicted solutions, the simplest protocols belong to ISO 18000-7 and low energy Bluetooth, although they operate very differently. The diagram below intends to show time spent in active modes vs. sleep for these two protocols, while also showing the amount of power consumed during each operational state. As we can see, low energy Bluetooth does not adhere to BLAST principles, but because it is just a wire-replacement technology it can succeed nonetheless. The other technologies, ZigBee and Wi-Fi, have protocols that are complicated enough that a diagram such as the ones below cannot come close to representing the many modes of operation. ZigBee cannot deliver low-latency (BLAST-like) behavior without expending a lot of power.

3.2. Symmetric protocol

A symmetric protocol is one where there is little or no difference between the way any sort of device communicates with any other sort of device. Symmetry does not necessarily make a standard low power optimized, but it does allow for more flexibility or innovation in the way that standard's technology is implemented and ultimately used. ISO 18000-7 uses a symmetric protocol, and certain modes of ZigBee are symmetric, as well. Low energy Bluetooth, WI-Fi, and other modes of ZigBee, on the other hand, are asymmetric as they are predicated on the existence of base station or coordinator-type devices.

IV. THE TECHNICAL MERITS OF UHF VS. MICROWAVE

4.1 The Friis Equation

It the form below, the Friis equation solves for free space communication range when receiver sensitivity (Pr), transmission power (Pt), receiver antenna gain (Gr), transmitter gain (Gt), and wavelength (λ). The range value derived here is highly optimistic for real world scenarios - at least because it doesn't account for bandwidth or modulation but more refined models of the Friis do exist and the ranges values these produce remain proportional to the basic form, nonetheless. The basic relationship is that as frequency goes up, range goes down.

Table shows how frequency relates to range and requisite antenna gain. The first three rows show that a 433MHz radio can have the same range as a similar 2.45GHz radio even if the 433 MHz antenna system is only 3% as efficient. This is important in real world applications where antennas are routinely de-tuned by

Solution	λ(cm)	Pt/Pr (dBm)	GtGr	Range(m)
Reference 433MHz	69	S	0.03A	R
Reference 900MHz	33	S	0.13A	R
Reference 2.45GHz	12	S	A	R
Typical DASH7	69	-100	.25	4500
Typical Bluetooth	12	-83	0.7	380
Typical WiFi	12	-100	0.7	1100
Typical Zigbee	12	-100	0.7	1100

Environmental factors, often quite severely. In the lower rows, typical book values are plugged-in to show the theoretical maximum range of each researched solution at 1 mW transmit power (0 dBm)

$$Range = \frac{1}{\frac{4\pi}{\lambda}\sqrt{\frac{P_r}{P_t G_t G_r}}}$$

4.2 Antennas

There is one major drawback to low frequency aside from reduced maximum data rate: the antenna. The classic antenna andone by which all others are judged is the half-wave dipole. It is similar in construction to the "rabbit ears"

TV antennas (the kind the next generation of engineers will never have as a mental reference).This antenna is excellent in most respects. The trouble is that below 1 GHz, the half-wave dipole is simply not an option for smaller products. At 433 MHz, for example, a half wave dipole is 35 cm long. Even when using slightly less efficient folded-dipoles, the antenna preferred by most 2.45 GHz radios, the size is too big for most use below 1 GHz.

Fortunately, there are quite a few designs for small antennas workable at lower frequencies. Some of them even come close to matching the folded dipole in performance. A common design is the small loop antenna, which depending on the design typically have efficiencies between 1/3and 1/8 of the half-wave dipole [3]. Small loops are popular because, in addition to being small and compact, they are easy to design, cheap, and easy to implement within a printed-circuit board. The "typical" DASH7 implementation from table 4.1 used a small loop system listed as 1/4th as efficient as the half-wave dipole system, even though more efficient antenna designs are available for use at 433MHz. One such well-known antenna design is the helical loop antenna. It is, as you might guess, a series of small loop antennas. Helical antennas require slightly more know-how to design than simple loops do, and they can cost more, but the cost difference is rarely noteworthy for applications at 433

Fig 4.2

MHz. Common characterization models for helical antenna designs show that a compact design, tuned at 433 MHz, is

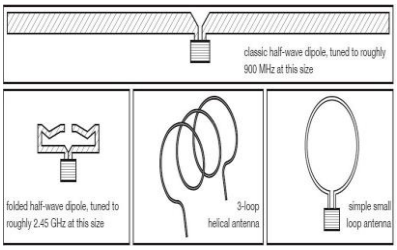

Roughly 2/3 as efficient as a half-wave dipole. Further performance improvements may be achieved by inserting a ferromagnetic core into the helix, particularly with smaller loop helixes.

4.3 COMMUNICATION THEORY

It has now been established that, from a purely scientific approach, lower frequency radio waves are more reliable than higher frequency waves are at delivering a signal over range, line-of-sight or otherwise. Communications theory is an engineering discipline focused on attaching rules (i.e. math) to phenomena involved in sending data via radio signals. When given a problem to solve, communications engineers go back to the rules to determine the best solution. There are always tradeoffs. Nonetheless, the primary solutions criteria depend on the following:

Allowable minimum data rate
Allowable signal to noise ratio
Allowable complexity of transmitter
Allowable complexity of receiver

4.3.1 Data Rate

In today's world, data rate is often confused with the term "bandwidth." The two are related, but they are not the same. Data rate is a digital phenomenon, expressing the amount of bits that a communication system can deliver in a given amount of time. Bandwidth is the frequency range between which a signal's energy can be realistically confined. Some modulation techniques are more efficient than others at cramming data into available bandwidth. Generally speaking, the more complex the modulation the more efficient it is at cramming raw data into a given amount of bandwidth, but sometimes further means are used to spread the band (i.e. spread spectrum technologies) in order to improve tolerance of noise. The latest exotic and complex methods manage to do both, although they are completely unsuitable for low power RF because the transmitters and receivers are too complex.

4.3.2 Signal to Noise Ratio

Maximizing signal to noise ratio (SNR) is a pursuit in which communications engineers put in a lot of time. Noise refers to any energy received [by the receiver] that does not come from the appropriate transmitter. Noise can be hard to predict, but there are some guidelines. A typical model for noise is additive gaussian white noise, as this is how "static" is modeled. It exists wherever there are charge carriers moving around randomly, for example in an antenna, and is often called thermal noise. The larger the bandwidth of the communication, the greater the received noise. There are other types of noise, too, and they all have one thing in common the larger the bandwidth, the greater the potential for noise ingress. We are interested, however, in signal to noise ratio, not just noise, and by increasing the bandwidth through modulation or encoding techniques it is possible to boost the signal energy in greater proportion than noise and interference. This is the basis for improving SNR and decreasing the effect of noise. By convention, DASH7 uses a marginally wideband FSK modulation (check appendix for more on modulations). It is set up to provide reasonably good resilience to noise and interference without expending too much energy doing so. Low energy Bluetooth's modulation is very similar. ZigBee, on the other hand, uses a more complex modulation

called QPSK that manages to be slightly more efficient at cramming data into bandwidth as well as better suited to delivering higher SNR. The added complexity, however, comes not without a price.

4.3.3 Simplicity vs. Complexity

Limits on targeted solution cost, development cost, and power requirements force communications engineers to be clever. Often we can evaluate two technologies, one simple and one sophisticated or complex, where the performance gap between the two can be closed by enhancing other areas of the total solution. One good area of study is the receiver. At the cost of higher power requirements, a more advanced modulation scheme may prove to have superior SNR than a simpler one, and a higher data rate may allow error correction coding to be part of the message. However, by changing the carrier frequency of the signal or by taking special attributes of the signal into account, the simpler solution may even outperform the more complicated offering. Without considering interference, ISO 18000-7 offers a greater SNR link budget than does the more complex, more sophisticated IEEE 802.15.4. When interference is in fact considered, the busy 2.45 GHz band has an increasingly negative impact on the performance of IEEE 802.15.4 vs. ISO 18000-7, and it actually becomes disastrous if newer 802.11n networks are in place. Performance enhancements like these that trickle-down from total system design can be relied upon when a technology is well defined to attack a focused set of problems. For example, in [9] we can see how design simplicity is maximized to solve problems of communication with small satellites. A clever solution (ISO 18000-7) can excel in BLAST type applications, one of which is even validated in [10]: RF performance of embedded devices in shipping containers.. In such cases where a focused design philosophy can be applied here simple, accessible technology can meet performance requirements - engineers can quickly develop products, testers can easily achieve interoperability, and marketers can immediately target users. It is the prisoners dilemma" for wireless standards: pursue the Holy Grail or pursue the strategy of most probable success. Simplicity and focus lend themselves to success.

V. MERITS

1. They use less power
2. Perfect to deliver long range
3. Highly reliable for delivering over long range and line of sight
4. High penetrating power
5. Multiyear battery life
6. Inter-operatability

VI. APPLICATIONS

1. DASH7 Tags from Savi are approved for use on all major common AIR carriers.
2. DASH7 can track a train moving @100 km per hr.
3. DASH7 can pinpoint location when s now is covers the yard.
4. DASH7 Motion & Temperature sensors can penetrate snow & ice
5. DASH7 can remotely monitor environmental conditions
6. Helps farmer for optimizing irrigation
7. DASH7 is used in TPMS
8. Used in moving advertisement
9. for mobile communication
10. Tags containing information about personal details

VII. CONCLUSION

If the system doesn't need high data rate can use DASH7. UHF systems operate better. UHF systems operate better in non-line-of sight conditions, they use less power, and they are so much more permissive that they can still offer superior range even when using suboptimal antennas. Thus UHF band is perfect choice to deliver the long range, highly reliable signal it needs, all the while preserving a tiny power budget.

REFERENCES

[1] BGR (Z-Wave), WLAN Interference to IEEE 802.15.4. Zensys, Inc, 2007.
[2] Constantine Balanis, Antenna Theory. Hoboken, NJ: John Wiley & Sons, 2005.
[3] G. Smith, Proximity Effect in Systems of Parallel Conductors. Cambridge, MA: Harvard University, 22 Nov 1971
[4] IEEE Computer Society, IEEE STD 802.15.4™-2003. New York, NY: IEEE, 2003.
[5] IHS News Service, WLAN Interference Raises Doubts about ZigBee, 802.15.4 Products.
[6] [http://electronics.ihs.com/news/zwave-zigbee-wlan.htm] 6 April 2007
[7] Mike McInnis, IEEE P802.15.4f Active RFID System Call for Applications. http://www.ieee802.org/15/pub/TG4f.html
[8] R. E. Ziemer, W. H. Tranter, Principles of Communications, 5th ed. Hoboken, NJ: John Wiley & Sons, 2002. IEEE Computer Society, Washington, DC, 2007.
[9] SY Shin, HS Park, S Choi, WH Kwon, Packet Error Rate Analysis of IEEE 802.15.4 under IEEE 802.11b Interference.
[10] Sofie Pollin et al, Distributed Cognitive Coexistence of 802.15.4 with 802.11. Belgium: Interuniversity Micro-Electronics Center (IMEC)

International Journal of Modern Engineering Research (IJMER)
www.ijmer.com Vol.3, Issue.2, March-April. 2013 pp-1180-11085 ISSN: 2249-6645

Suitability of Nigerian Agricultural By-Products as Cement Replacement for Concrete Making

L. O. Ettu, [1] N. N. Osadebe, [2] M. S. W. Mbajiorgu[3]
[1]*Department of Civil Engineering, Federal University of Technology, Owerri, Nigeria*
[2]*Department of Civil Engineering, University of Nigeria, Nsukka, Nigeria*
[3]*Department of Civil Engineering, Enugu State University of Science and Technology, Enugu, Nigeria*

Abstract: *This work investigated the strength characteristics of binary blended cement concrete made with Ordinary Portland Cement (OPC) and each of eight agricultural by-products in South Eastern Nigeria, namely Rice Husk Ash (RHA), Saw Dust Ash (SDA), Oil Palm Bunch Ash (OPBA), Cassava Waste Ash (CWA), Coconut Husk Ash (CHA), Corn Cob Ash (CCA), Plantain Leaf Ash (PLA), and Paw-Paw Leaf Ash (PPLA). 105 concrete cubes of 150mm x 150mm x 150mm were produced at percentage OPC replacement with each of the eight ashes of 5%, 10%, 15%, 20%, and 25%. Three concrete cubes for each percentage replacement of OPC with each ash and the control were tested for saturated surface dry bulk density and crushed to obtain their compressive strengths at 3, 7, 14, 21, 28, 50, and 90 days of curing. The compressive strengths of binary blended cement concrete increased with curing age and decreased with increase in percentage replacement of OPC with pozzolans. The 3-14 day compressive strength values were much lower than the control values for all percentage replacements of OPC with pozzolan. However, the 90-day strength at 5-10% replacement of OPC in binary blending with each of the eight pozzolans was higher than that of the control, ranging from 24.50N/mm^2 for 10% replacement of OPC with coconut husk ash (CHA) to 30.2N/mm^2 for 5% replacement of OPC with RHA compared with the control value of 23.8N/mm^2. Thus, all the eight agricultural by-products investigated in this work could be good for binary blending with OPC in making structural concrete. However, since blended cement concrete take a longer time to attain adequate strength than 100% OPC concrete, major structural elements constructed with blended cement concrete should be allowed a longer time before loading, say 28-50 days for 5-15% replacement of OPC with agricultural by-product pozzolans and 50-90 days for 15-25% replacement of OPC.*

Key Words: *Blended cement, binary, composites, compressive strength, concrete, curing method, mix ratio, pozzolan, sandcrete.*

I. Introduction

Gross inadequacy of accommodation for the densely populated areas ofSouth Eastern Nigeria and many other parts of Africa has constrained researchers to continue to seek ways of reducing the cost of building projects. Agricultural by-products regarded as wastes in technologically underdeveloped societiescould be used as partial replacement of Portland cement to achieve this purpose. Efforts have recently been focused on such substitute materials in making cement composites such as concrete and sandcrete (Olugbenga et al., 2007). Blended cements are currently used in many parts of the world (Bakar, Putrajaya, and Abdulaziz, 2010). Calcium hydroxide [Ca $(OH)_2$] is one of the hydration products of Portland cement and it greatly contributes toward the deterioration of cement composites. When a pozzolan is blended with Portland cement it reacts with the lime to produce additional calcium-silicate-hydrate (C-S-H), which is the main cementing compound. Thus the pozzolanic material reduces the quantity of lime and increases the quantity of C-S-H. Therefore, the cementing quality is enhanced if a pozzolan is blended in suitable quantity with Portland cement (Padney et al., 2003).

Agricultural by-product pozzolans have been used in the manufacture and application of blended cements (Malhotra and Mehta, 2004). Nimityongskul and Daladar (1995) highlighted the potentialities of coconut husk ash, corn cob ash, and peanut shell ash as good pozzolans. Elinwa and Awari (2001) successfully investigated the potentials of groundnut husk ash concrete by partially replacing Ordinary Portland Cement with groundnut husk ash. Adesanya (1996) investigated the properties of blended cement mortar, concrete, and stabilized earth made from OPC and corn cob ash and recommended that corn cob ash can serve as replacement for OPC in the production of cement composites. Dwivedia et al. (2006) successfully investigated the pozzolanicity of bamboo leaf ash.Martirena, Middendorf, and Budelman (1998) found that sugar industry solid wastes such as sugar cane straw ash has pozzolanic activity derived from its high content of amorphous silica. Some other researchers have also confirmed the possibility of using sugar industry wastes as pozzolans (Hernandez et al., 1998; Singh, Singh, and Rai, 2000; Middendorf et al., 2003). Many other researchers have confirmed rice husk ash a pozzolanic material that can be used to partially replace OPC in making cement composites (Cordeiro, Filho, and Fairbairn, 2009; Habeeb and Fayyadh, 2009; Rukzon, Chindaprasirt, and Mahachai, 2009). A number of researchers have also found good prospects in using blended cements made with sawdust ash (Mehta, 1997; Elinwa, Ejeh, and Mamuda, 2008; and Elinwa and Abdulkadir, 2011). Studies by Chandrasekar et al. (2003) suggest that soil, climatic, and geographical conditions could affect the physical and chemical properties and consequently the pozzolanicity of agricultural by-products.

The commitment to crop farmingby many Nigerian rural community dwellers have led to increased agricultural wastes, large quantities of which are generated in various rural communities all over South Eastern Nigeria. There is therefore a need to further investigate the suitability of using Nigerian agricultural by-products as possible cement replacement in concrete making. The successfulutilization of these products as pozzolanic materials would add commercial

value to the otherwise waste products and encourage massive cultivation of the crops for various uses. This work investigated the strength characteristics of binary blended cement concrete made with Ordinary Portland Cement (OPC) and each of eight agricultural by-products in South Eastern Nigeria, namely Rice Husk Ash (RHA), Saw Dust Ash (SDA), Oil Palm Bunch Ash (OPBA), Cassava Waste Ash (CWA), Coconut Husk Ash (CHA), Corn Cob Ash (CCA), Plantain Leaf Ash (PLA), and Paw-Paw Leaf Ash (PPLA).

II. Methodology

Rice husk was obtained from rice milling factories in Afikpo, Ebonyi State; Saw dust from wood mills in Owerri, Imo State; Oil palm bunch from palm oil mill in Ohaji-Egbema, Imo State; Cassava waste (the peel from cassava tubers) from Ihiagwa in Imo State; Coconut Husk from Orlu in Imo State; Corn cob from Aba district in Abia State; Plantain leaf from Ogbunike town in Anambra State; and Paw-paw leaf from Escobedo in Imo State, all in South Eastern Nigeria. These materials were air-dried; the bigger and harder ones such as corn cob and oil palm bunch were pulverized; and calcined into ashes in a locally fabricated furnace at temperatures generally below 650^{o}C. The resultant Rice Husk Ash (RHA), Saw Dust Ash (SDA), Oil Palm Bunch Ash (OPBA), Cassava Waste Ash (CWA), Coconut Husk Ash (CHA), Corn Cob Ash (CCA), Plantain Leaf Ash (PLA), and Paw-Paw Leaf Ash (PPLA) were sieved and large particles retained on the 600µm sieve were discarded while those passing the sieve were used for this work. No grinding or any special treatment to improve the quality of the ashesand enhance their pozzolanicity was applied because the researchers wanted to utilize simple processes that can be easily replicated by local community dwellers. Other materials used for the work are Ibeto brand of Ordinary Portland Cement (OPC), river sand free from debris and organic materials, crushed granite of 20 mm nominal size free from impurities, and water free from organic impurities.

Tests were carried out to determine the specific gravity, bulk density, and fineness modulus of each of the ashes and the aggregates. A simple form of pozzolanicity test was carried out for each of the ashes. It consists of mixing a given mass of the ash with a given volume of Calcium hydroxide solution [$Ca(OH)_2$] of known concentration and titrating samples of the mixture against H_2SO_4solution of known concentration at time intervals of 30, 60, 90, and 120 minutes using Methyl Orange as indicatorat normal temperature. For each of the ashes the titre value was observed to reduce with time, confirming the ash as a pozzolan that fixed more and more of the calcium hydroxide, thereby reducing the alkalinity of the mixture.

A common mix ratio of 1:2:4 (blended cement: sand: granite) was used for the concrete. Batching was by weight and a constant water/cement ratio of 0.6 was used. Mixing was done manually on a smooth concrete pavement. Rice husk ash (RHA) was first thoroughly blended with OPC at the required proportion and the homogenous blend was then mixed with the fine aggregate-coarse aggregate mix, also at the required proportions. Water was then added gradually and the entire concrete heap was mixed thoroughly to ensure homogeneity. The workability of the fresh concrete was measured by slump test, and the wet density was also determined. Each of the remaining seven ashes was also used to produce binary blended cement concrete using this same procedure. One hundred and five (105) concrete cubes of 150mm x 150mm x 150mm were produced at percentage OPC replacement with each of the eight ashes of 5%, 10%, 15%, 20%, and 25%. Twenty one concrete cubes with 100% OPC were also produced to serve as controls. This gives a total of 861 concrete cubes.All the cubes were cured by immersion. Three concrete cubes for each percentage replacement of OPC with each of the eight ashes and the control were tested for saturated surface dry bulk density and crushed to obtain their compressive strengths at 3, 7, 14, 21, 28, 50, and 90 days of curing. Average values of concrete compressive strengths and densities for the various curing ages and percentages of OPC replacement with each of the ashes were obtained and presented in tables and graphs.

III. Results and Discussion

A summary of the specific gravity, bulk density, and fineness modulus of each of the ashes and aggregates is shown in table 1.

Table 1. Summary of specific gravity, bulk density, and fineness modulus of ashes and aggregates

Material	Specific Gravity	Bulk Density (Kg/m^3)	Fineness Modulus
Granite	2.90	1500	3.62
Sand	2.68	1560	2.82
Laterite	2.40	1470	3.30
RHA	1.80	765	1.38
SDA	1.90	790	1.75
OPBA	2.00	800	1.95
CWA	1.85	810	1.80
CCA	1.80	795	1.90
CHA	1.78	760	1.55
PLA	1.75	755	1.36
PPLA	1.82	775	1.32
OPC	3.13	1650	NA

The particle size analysis showed that all the eight agricultural by-product ashes were much coarser than OPC, the reason being that they werenot ground to finer particles. The implication of this is that the compressive strength values obtained using each of theseashes can still be improved upon when the ash is ground to finer particles. It can also be seen from table 1 that the bulk density and specific gravity of each of the ashes were much lower than that of OPC. Thus, partially replacing the ashes with OPC would result in reduced weight of concrete members. The pozzolanicity test confirmed all the ashes aspozzolans since each of them fixed some quantities of lime over time, thereby reducing the alkalinity of the calcium hydroxide-ash mixture as reflected in the smaller titre value over time compared to the blank titre. The chemical compositions of the ashes showed that only RHA satisfied the ASTM requirement that the sum of SiO_2, Al_2O_3, and Fe_2O_3 should be not less than 70%. However, since the pozzolanicity tests were positive for all the eight materials, confirming them all as pozzolans, it couldbe reasoned that the ASTM requirement does not mean any material that falls short of it is not pozzolanic; it could rather be interpreted as criterion for high pozzolanicity of materials.

The compressive strengths of the binary blended cement concrete produced with OPC and each of the eight agricultural by-product pozzolans are shown in tables 2, 3, 4, 5, 6, 7, and 8 for 3, 7, 14, 21, 28, 50, and 90 days of curing respectively.

Table 2. Compressive strength of blended OPC-AgricPozzolan cement concrete at 3 days of curing

Age (days)	Compressive Strength (N/mm^2) for					
	0% Poz.	5% Poz.	10% Poz.	15% Poz.	20% Poz.	25% Poz.
RHA	8.00	5.40	4.90	4.40	3.70	3.50
SDA	8.00	5.10	4.40	4.20	3.80	3.40
OPBA	8.00	4.80	4.30	4.10	3.30	3.20
CWA	8.00	4.20	4.00	3.90	3.60	3.50
CCA	8.00	5.50	5.20	4.70	4.20	3.90
CHA	8.00	4.40	4.00	3.70	3.50	3.30
PLA	8.00	4.20	4.10	3.80	3.60	3.40
PPLA	8.00	4.10	3.90	3.60	3.40	3.20

Table 3. Compressive strength of blended OPC-AgricPozzolan cement concrete at 7 days of curing

Age (days)	Compressive Strength (N/mm^2) for					
	0% Poz.	5% Poz.	10% Poz.	15% Poz.	20% Poz.	25% Poz.
RHA	14.10	10.00	9.50	8.40	7.50	7.30
SDA	14.10	9.60	9.00	7.30	7.10	6.80
OPBA	14.10	9.30	8.30	4.50	4.30	4.00
CWA	14.10	7.00	6.40	5.60	5.10	4.60
CCA	14.10	9.70	9.40	8.30	7.40	6.60
CHA	14.10	8.30	8.10	7.30	6.80	6.40
PLA	14.10	7.80	7.70	7.50	7.20	6.70
PPLA	14.10	7.30	7.20	6.80	6.30	5.80

Table 4. Compressive strength of blended OPC-AgricPozzolan cement concrete at 14 days of curing

Age (days)	Compressive Strength (N/mm^2) for					
	0% Poz.	5% Poz.	10% Poz.	15% Poz.	20% Poz.	25% Poz.
RHA	21.60	18.30	18.00	15.80	12.00	11.30
SDA	21.60	17.40	16.60	15.20	13.10	11.80
OPBA	21.60	16.80	15.70	14.00	10.30	9.30
CWA	21.60	12.90	12.00	11.30	10.30	9.80
CCA	21.60	19.00	17.80	14.80	11.20	10.80
CHA	21.60	16.00	15.50	12.60	11.00	10.30
PLA	21.60	15.00	14.30	12.10	11.80	11.30
PPLA	21.60	13.40	12.90	11.30	11.10	10.30

Table 5. Compressive strength of blended OPC-AgricPozzolan cement concrete at 21 days of curing

Age (days)	Compressive Strength (N/mm^2) for					
	0% Poz.	5% Poz.	10% Poz.	15% Poz.	20% Poz.	25% Poz.
RHA	22.30	22.40	21.80	19.30	16.00	14.40
SDA	22.30	20.60	19.90	16.70	16.10	13.40
OPBA	22.30	20.00	17.50	15.50	13.40	11.40
CWA	22.30	18.60	14.40	14.30	12.40	11.40
CCA	22.30	21.60	18.90	16.40	13.40	11.40
CHA	22.30	19.20	17.50	16.40	14.00	12.90
PLA	22.30	18.70	18.30	17.60	13.80	12.40
PPLA	22.30	18.40	17.40	15.40	13.40	11.40

Table 6. Compressive strength of blended OPC-AgricPozzolan cement concrete at 28 days of curing

Age (days)	Compressive Strength (N/mm^2) for					
	0% Poz.	5% Poz.	10% Poz.	15% Poz.	20% Poz.	25% Poz.
RHA	23.20	25.70	22.90	21.20	18.30	16.40
SDA	23.20	22.60	20.40	19.40	18.20	16.20
OPBA	23.20	22.20	20.40	18.50	17.30	13.40
CWA	23.20	22.40	20.10	18.90	15.80	14.40
CCA	23.20	22.50	21.50	19.70	16.40	14.20
CHA	23.20	22.30	20.40	19.40	15.60	13.40
PLA	23.20	24.10	20.80	19.50	16.70	14.40
PPLA	23.20	23.40	20.90	18.90	17.40	15.40

Table 7. Compressive strength of blended OPC-AgricPozzolan cement concrete at 50 days of curing

Age (days)	Compressive Strength (N/mm^2) for					
	0% Poz.	5% Poz.	10% Poz.	15% Poz.	20% Poz.	25% Poz.
RHA	23.70	28.50	25.20	24.30	22.10	20.50
SDA	23.70	24.90	23.50	22.30	19.80	19.00
OPBA	23.70	23.90	23.40	20.60	19.00	17.50
CWA	23.70	25.80	23.60	22.10	18.50	17.70
CCA	23.70	24.60	23.60	21.50	19.60	18.50
CHA	23.70	23.90	22.20	20.50	18.50	17.00
PLA	23.70	24.80	22.60	21.90	19.90	18.50
PPLA	23.70	24.50	23.50	22.50	20.50	19.50

Table 8. Compressive strength of blended OPC-AgricPozzolan cement concrete at 90 days of curing

Age (days)	Compressive Strength (N/mm^2) for					
	0% Poz.	5% Poz.	10% Poz.	15% Poz.	20% Poz.	25% Poz.
RHA	23.80	30.20	27.30	26.40	23.60	22.50
SDA	23.80	27.10	25.50	24.20	22.50	22.00
OPBA	23.80	26.20	24.80	23.50	22.30	20.50
CWA	23.80	26.50	25.30	24.30	22.50	21.50
CCA	23.80	27.50	26.20	24.50	23.00	21.00
CHA	23.80	25.60	24.50	23.50	21.00	19.00
PLA	23.80	26.30	24.90	23.60	22.00	19.50
PPLA	23.80	26.50	25.00	23.50	23.00	21.70

It can be seen from tables2 to 8 that the compressive strength values of OPC-Agricultural by-product binary blended cement concrete consistently decrease with increase in percentage replacement of OPC with agricultural by-product ash. Tables 2 to 4 show that the 3-14 day compressive strength values are much lower than the control values for all

percentage replacements of OPC with each of the agricultural by-product ashes. Tables 5 and 6 show that the strength of the OPC-Agricultural by-product binary blended cement concrete begins to approach the control value at 21 to 28 days of curing, and tables 7 and 8 show that the binary blended cement concrete strengths for some of the ashes, notably RHA, exceeds the control value at 50 to 90 days of curing, especially for 5-15% replacement of OPC with agricultural by-product ash. The 3-14 day low strength values compared to the control can be attributed to the low rate of pozzolanic reaction at those ages. The silica from the pozzolans reacts with lime produced as by-product of hydration of OPC to form additional calcium-silicate-hydrate (C-S-H) that increases the binder efficiency and the corresponding strength values at later days of curing.The strength of 100% OPC concrete (the control) increases steeply with age until about 14 days. The strength still increases steadily but less steeply between 14 and 28 days, after which the strength increases much more slowly such that the strength at 90 days is not much greater than that at 50 days. Unlike the control, the binary blended cement concrete strength picks up more slowly up to 21 days, after which it begins to increase steadily until 90 days and beyond.

Comparatively speaking, it can be seen from tables 2 to 8 that OPC-RHA binary blended cement concrete consistently has higher strength than the other seven binary blends. Its value at 5% replacement of OPC becomes marginally greater than the control value at 21 days of curing and continues to increase more and more than the control value at later ages of hydration. Table 8 suggests that the good performance of rice husk ash (RHA) is followed in descending order by corn cob ash (CCA), saw dust ash (SDA), cassava waste ash (CWA), pawpaw leaf ash (PPLA), plantain leaf ash (PLA), oil palm bunch ash (OPBA), and coconut husk ash (CHA). It is interesting to note from table 8 that the 90-day strengths of the binary blended cement concrete made with each of these ashes is good enough for use in reinforced concrete works even at 25% replacement of OPC with any of the eight agricultural by-product ashes. The 90-day strength values at 5-10% replacement of OPC range from 24.50N/mm^2 for 10% replacement with CHA to 30.20N/mm^{2}for 5% replacement with RHA, compared to the control value of 23.80N/mm^2.

IV. Conclusions

All the eight Nigerian agricultural by-products investigated in this work, namely Rice Husk Ash (RHA), Saw Dust Ash (SDA), Oil Palm Bunch Ash (OPBA), Cassava Waste Ash (CWA), Coconut Husk Ash (CHA), Corn Cob Ash (CCA), Plantain Leaf Ash (PLA), and Paw-Paw Leaf Ash (PPLA) are reasonably pozzolanic since they fix some quantities of lime over time thereby reducing the alkalinity of their mixture with calcium hydroxide as reflected in the smaller titre values recorded over time compared to the blank titre. All the ashes were much coarser than OPC, the reason being that they were not ground to ultrafine particles. The implication of this is that the compressive strength values obtained using them can still be improved upon when they are ground to finer particles.

The compressive strength values of binary blended cement concrete consistently decrease with increase in percentage replacement of OPC with pozzolan and increase with increase in curing age. The 3-14 day compressive strength values are much lower than the control values for all percentage replacements of OPC with pozzolan. However, the 90-day strength at 5-10% replacement of OPC in binary blending with each of the eight pozzolans is higher than that of the control, ranging from 24.50N/mm^2 for 10% replacement of OPC with coconut husk ash (CHA) to 30.2N/mm^2 for 5% replacement of OPC with RHA compared with the control value of 23.8N/mm^2.

Thus, all the eight agricultural by-products investigated in this work could be good for binary blending with OPC in making structural concrete. However, since blended cement concrete take a longer time to attain adequate strength than 100% OPC concrete, structural elements constructed with blended cement concrete should be allowed a longer time before loading, say 28-50 days for 5-15% replacement of OPC with agricultural by-product pozzolans and 50-90 days for 15-25% replacement of OPC.

References

[1] Adesanya, D. A. (1996). Evaluation of blended cement mortar, concrete and stabilized earthmade from OPC and Corn Cob Ash. Construction and Building Materials, 10(6): 451-456.
[2] Bakar, B. H. A., Putrajaya, R. C., &Abdulaziz, H. (2010).Malaysian Saw dust ash–Improving the Durability and Corrosion Resistance of Concrete: Pre-review. Concrete Research Letters, 1 (1): 6-13, March 2010.
[3] Chandrasekhar, S., Pramada, S. K. G., &Raghavan, P. N. (2003). Review Processing, Properties And Applications of Reactive Silica From Rice Husk-An Overview. Journal Of Materials Science, 38: 3159-3168.
[4] Cordeiro, G. C., Filho, R. D. T., & Fairbairn, E. D. R. (2009). Use of ultrafine saw dust ash with high-carbon content as pozzolan in high performance concrete. Materials and Structures, 42: 983–992. DOI 10.1617/s11527-008-9437-z.
[5] Dwivedia, V. N., Singh, N. P., Das, S. S., & Singh, N. B. (2006). A new pozzolanic material for cement industry: Bamboo leaf ash. International Journal of Physical Sciences, 1 (3): 106-111.
[6] Elinwa, A. U., & Abdulkadir, S. (2011). Characterizing Sawdust-ash for Use as an Inhibitor for Reinforcement Corrosion. New Clues in Sciences, 1: 1-10.
[7] Elinwa, A. U., &Awari, A. (2001).Groundnut husk ash concrete. Nigerian Journal of Engineering Management, 2 (1), 8 - 15.
[8] Elinwa, A. U., Ejeh, S. P., &Mamuda, M. A. (2008). Assessing of the fresh concrete properties of self-compacting concrete containing sawdust ash. Construction and Building Materials Journal, 22: 1178 - 1182.
[9] Habeeb, G. A., &Fayyadh, M. M. (2009).Saw dust ash Concrete: the Effect of SDA Average Particle Size on Mechanical Properties and Drying Shrinkage. Australian Journal of Basic and Applied Sciences, 3(3): 1616-1622.
[10] Hernandez, J. F., Middendorf, B., Martirena, M. G., &Budelmaun, H. (1998). Use of wastes of the sugar industry as pozzolana in lime pozzolana binders: Study of the reaction. Cem.Concr. Res., 28 (11): 1528-1536.
[11] Malhotra, V. M., & Mehta, P. K. (2004).Pozzolanic and Cementitious Materials. London: Taylor & Francis.

[12] Martirena, J. F., Middendorf, B., & Budelman, H. (1998). Use of wastes of the sugar industry aspozzolan in lime-pozzolan binders: study of the reaction. Cem.Concr.Res., 28: 1525– 1536.
[13] Mehta, P. K. (1997). Properties of blended cements made with sawdust ash. ACI Journal Proceedings, 74:440-442.
[14] Middendorf, B., Mickley, J., Martirena, J. F., & Ray, R. L. (2003). Masonry wall materials prepared by using agriculture waste, lime and burnt clay. In: D. Throop, R.E. Klingner (Eds.), Masonry: Opportunities for the 21st Century. ASTM STP 1432: 274- 283.West Conshohocken, PA.
[15] Nimityongskul, P., &Daladar, T. U. (1995). Use of coconut husk ash, corn cob ash and peanut shell ash as cement replacement. Journal of Ferro cement, 25(1): 35-44.
[16] Olugbenga, A. (2007). Effects of Varying Curing Age and Water/Cement Ratio on the Elastic Properties of Laterized Concrete. Civil Engineering Dimension, 9 (2): 85 – 89.
[17] Padney, S. P., Singh, A. K., Sharma, R. L., &Tiwari, A. K. (2003). Studies on high-performance blended/multiblended cements and their durability characteristics. Cement and Concrete Research, 33: 1433-1436.
[18] Rukzon, S., Chindaprasirt, P., & Mahachai, R. (2009).Effect of grinding on chemical and physical properties of saw dust ash. International Journal of Minerals, Metallurgy and Materials, 16 (2): 242-247.
[19] Singh, N. B., Singh, V. D. &Rai., R. (2000). Hydration of bagasse ash-blended Portland cement. Cem.Concr. Res. 30: 1485-1488.

International Journal of Modern Engineering Research (IJMER)
www.ijmer.com Vol.3, Issue.2, March-April. 2013 pp-1186-1191 ISSN: 2249-6645

A Review on Enhancing the Linearity Characteristic of Different Types of Transducers-A Comparative Study

S.Murugan, [1] Dr.SP.Umayal[2]
[1]*Assistant Professor, Einstein College of Engineering, Department of Electrical and Electronics Engineering, Sir.C.V.Raman Nagar, Tirunelveli-12, India*
[2]*Professor, Sethu Institute of Technology, Department of Electrical and Electronics Engineering, Kariapatti, India*

Abstract: *Many types of sensors and transducers have a nonlinear response. Ideal transducers are designed to be linear. But since in practice there are several factors which introduce non-linearity in a system. Due to such nonlinearities, transducer's usable range gets restricted and also accuracy of measurement is severely affected. Similar effect is observed in different types of transducers. The nonlinearity present is usually time-varying and unpredictable as it depends on many uncertain factors. Nonlinearity also creeps in due to change in environmental conditions such as temperature and humidity. In addition ageing of the transducers also introduces nonlinearity. This particular paper concentrates a review on the compensation of difficulties faced due to the non-linear response characteristics of different types of sensors like resistive (thermocouple), capacitive (capacitive pressure sensor),inductive(LVDT) and humidity transducers. In this review, we identified many algorithms and ANN models like Functional Link Artificial Neural Network (FLANN), Radial Basis Function based ANN, Multi Layer Perceptron and Back Propagation Network to enhance the linearity performance of resistive, capacitive and inductive transducers. On comparison of different ANN models for non-linearity correction in different types of transducers, we identified FLANN model is used as a useful alternative to the MLP, BPN and the radial basis function (RBF)-based ANN. It has the advantage of lower computational complexity than the MLP, BPN and RBF structures and is, hence, easily implementable. Throughout the paper, we described the effects produced by each kind of nonlinearity, emphasizing their variations for different types of transducers with different ANN models.*

Keywords: *ANN, Thermocouple, Linear Variable Differential Transformer (LVDT), Capacitive Pressure Sensor (CPS), Humidity sensor*

I. Introduction

While still retaining the time independence assumption we can introduce non-linearity in the model of the sensor:
$Y'(x) = Ax + b_2x^2$+$b_3 x^3$+……. = A x+g (x)….. (1)

The function *g(x)* describes how much the sensor response deviates from its linearised description. There are several ways to describe linearity or nonlinearity, each one of them described by a different term. The terms linearity and nonlinearity are conjugate, are used interchangeably, and often a value of linearity is quoted as non-linearity, and vice-versa. Nonlinearity is usually measured in relative units, either as a percentage of the maximum full scale reading of the sensor or the instrument, or locally as a percentage of a reading. Ideally we wish the nonlinearity to vanish, so it must be proportional to $|g(x)|$.

II. Nonlinearity Correction

This Chapter.2 deals with the nonlinearity compensation and correction of various transducers like Thermocouple, LVDT, and Capacitive Pressure Sensor and Humidity sensor.

A.BPN based Thermocouple

The types, specifications, and structures of thermocouple variety, almost all have the serious problem of non-linear, and there is a non-linear relationship between its output and the measured temperature. In K-type thermocouple when the temperature ranges between 0 and 200°C,basing on the table of thermoelectric potential and temperature,we can fit the following E ~ t relationship by the least squares principle

$$E=c_0+c_1t+c_2t^2+\ldots\ldots\ldots\ldots\ldots\ldots\ldots\ldots \quad (2)$$

E is potential thermoelectric when the c_0= 0.0311*mv*, c_1 = 0.0415*mv / °C*, $c_{2\,=}$ - 3.5x10^{-6} *mv/ °C*^{2}. The equation (1) tells us that the *E-t* relationship is nonlinear. The temperature at the cold point of the thermocouple is zero [1].

The non-linear correction model structure established by BP neural network can be described by the weighted values and the threshold values, the threshold values and the weighted values are shown as follows:
The weighted values between the entering layer and the hidden layer:
*w*1 = [-30.473488 -38.820904 -1.644704 -2.235481 0.099258 95.799098]
The weighted values between the outputting layer and the hidden layer:
*w*2 = [-20.979834 31.472969 -6.901741 1.78862 1014.294648 -254.668243]
Hidden threshold values:

*b*1 = [-47.329741 -25.972066 12.099975 4.515939 -0.050021 86.879988]
The threshold of the outputting layer:
*b*2 = -234.662545
We can easily get an equality of t ' - *E*
The output of the entering layer: $O_i = E(t,0)$.
Hidden output: $Oj = f(Ij) = \frac{1}{1+e-I\lambda}$
The total input of the hidden layer j-node:

$$I_j = O_i * w_{1j} + b_j$$

The output of the outputting layer: $t' = I$,
While $I = \sum_{j-1}^{6} oj.w2j + b2$;

$$t' = \frac{w2}{1+e^{-(w1E(t,0)+b1)}} + b2$$

So any thermoelectric potential E can be passed on a *t'* corresponding temperature, which is the temperature after non-linear correction.
The testing samples with data on BP to build the network model were tested, and the testing results were shown in table 1.

Table 1.Theory Temperature and the Temperature Of Test Results

Theoretical values/°C	0.0	5.0	200.0
Test Results/°C	0.002668	4.973522	199.967966

The actual temperature curve and calculated curve based on BP networks are provided by figure 1.The largest fitting deviation is 0.8347°C.

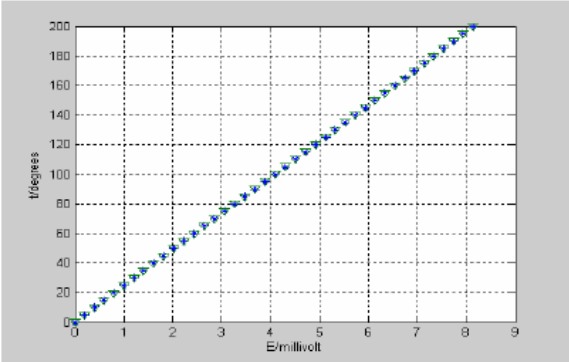

Figure 1 Comparisons between the actual temperature curve and calculated curve based on BP networks Before the neural network training, according to test sample data (E, t) can be obtained an equation by the linear least-squares fitting:

t = 24.4412 x E+0.2628

The largest fitting deviation can be obtained = 0.8347°C, then the linearity of K-type thermocouple:

$$\delta_L = \frac{\Delta Lm}{YFS} \text{ x } 100\% = 0.0421\%$$

Comparing specific linearity is shown in table 2

Table. 2 The Performance Comparison Before and After Nn Training

	The largest fitting deviation/°C	The Linearity
Before Training	0.8347	0.41%
After Training	0.0842	0.0421%

After the neural network training, the nonlinear of thermocouple has been significantly improved between temperatures of 0 and 200.

B.FLANN Based LVDT

The Functional Link Artificial Neural Network (FLANN) is a single layer network in which there are no hidden layers. The functional link acts as on an element of a pattern or on the entire pattern itself by generating a set of linearly independent functions and then evaluating these functions with the pattern as the argument. The differential voltage v at the output of the LVDT is fed to the FLANN model as the input. In this paper authors have used trigonometric expansion because it provides better nonlinearity compensation compared to other types of section.
Mathematical analysis of FLANN:

Let us consider the problem of learning with a flat net, which is a network with no hidden layers. Let V be the input vector of N elements. Let the net configuration have one output. Each element undergoes trigonometric nonlinear expansion

to form P elements such that the resultant matrix has the dimension of N×P. Since the nth input elements is v_n ,$1 \leq n \leq N$, the functional expansion is carried out as

$$s_i = \begin{cases} v_{n,} & i=1 \\ \sin(l\pi v_n), & i > 1, i \text{ is even} \\ \cos(l\pi v_n) & , i > 1, i \text{ is odd} \end{cases}$$

Let the weight vector is represented as W having Q elements. The output, y is given as

$$y = \sum_{i=1}^{Q} w_i s_i$$

In matrix notation, the output can be

$$Y = S.W^T$$

At the K^{th} iteration, the error signal e (k) can be computed as

$$e(k) = d(k) - y(k)$$

Where d (k) is the desired signal that is the same as the control signal given to the displacement actuator. Furthermore the above equation can be written as

$$\epsilon(k) = \frac{1}{2}\sum_{j \in P} e_j^2(k)$$

The weight vector can be updated by LMS algorithm as

$$w(k+1) = w(k) - \frac{\mu}{2}\hat{\nabla}(k)$$

Where $\hat{\nabla}(k)$ is an instantaneous estimate of the gradient of ϵ with respect to the weight vector w(k).

Now

$$\hat{\nabla}(k) = \frac{\partial \varepsilon}{\partial \omega} = -2e(k)\frac{\partial y(k)}{\partial \omega}$$
$$= -2e(k)\frac{\partial[\omega(k)s(k)]}{\partial w} \qquad = 2e(k)s(k).$$

By substituting the values of $\hat{\nabla}(k)$ in ( ), we get

$$\omega(k+1) = \omega(k) + \mu e(k)s(k)$$

Where μ denotes the step size ($0 \leq \mu \leq 1$), which controls the convergence of speed of LMS algorithm.

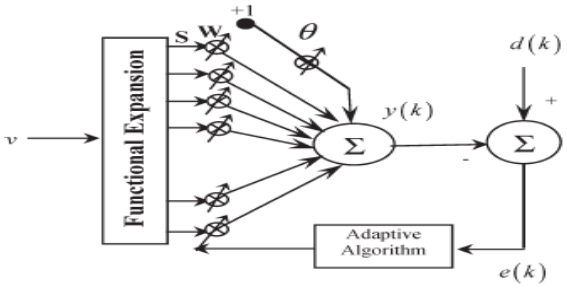

Figure 2. Structure of a FLANN

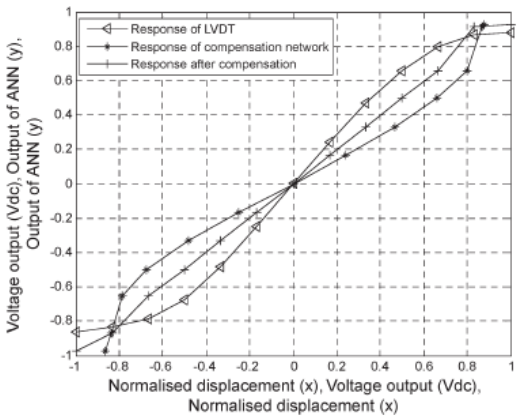

Figure 3. Compensation graph by FLANN

C.Mlp based Capacitive Pressure Sensor

A multilayer perceptron (MLP) is a feed forward artificial neural network model that maps sets of input data onto a set of appropriate output. An MLP consists of multiple layers of nodes in a directed graph, with each layer fully connected to the next one. Except for the input nodes, each node is a neuron (or processing element) with a nonlinear activation function. MLP utilizes a supervised learning technique called back propagation for training the network. MLP is a modification of the standard linear perceptron and can distinguish data that is not linearly separable

The problem of nonlinear response characteristics of a CPS further aggravates the situation when there is change in environmental conditions. This ANN model is capable of providing pressure readout with a maximum FS error of 2% over a wide variation of ambient temperature. Temperature range can be widened by training MLP with sufficient number of pattern sets covering the temperature range.

A CPS senses the applied pressure due to elastic deflection of its diaphragm. In the case of a simple structure, this deflection is proportional to the applied pressure P, and the sensor capacitance C (P) varies hyperbolically. Neglecting higher-order terms, C (P) may be approximated by

$$C(P) = C_o + \Delta C(P) = C_o(1+\gamma)$$

where C_o is the sensor capacitance when$P = 0; \Delta C(P)$ is the change in capacitance due to applied pressure;$\gamma = P_N(1-\alpha/(1\text{-}P_N)$ is the sensitivity parameter which depends upon the geometrical structure of the sensor; $P_N$is the normalized applied pressure given by $P_N = P/P_{max}$ and P_{max} is the maximum permissible input pressure.

In the 2-D problem discussed in this paper, the sensor capacitance is a function of the applied pressure and the ambient temperature. Assuming that the change in capacitance due to change in temperature is linear and independent of the applied pressure, the CPS model may be expressed as

$$C(P,T) = C_o f_1(T) + \Delta C(P,T_0) f_2(T)$$

Where $\Delta C(P,T_0)$represents the change in capacitance due to applied pressure at the reference temperature T_0 as given in (1).The functions $f_1(T)$ and$f_2(T)$ are given by

$$f_1(T) = 1 + \beta_1(T - T_0); \qquad f_2(T) = 1 + \beta_2(T - T_0)$$

Where the coefficients $\beta_1$and β_2 may have different values depending on the CPS chosen. The normalized capacitance of the CPS, $C_N$is obtained by dividing (2) by and may be expressed as

$$C_N = C(P,T)/C_0 = f_1(T) + \gamma f_2(T)$$

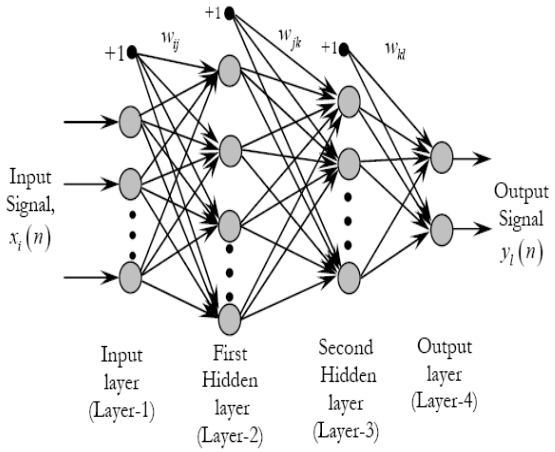

Figure.4. Structure of MLP Model

D.Rbf based Humidity Sensor

A radial basis function network is an artificial neural network that uses radial basis functions as activation functions. It is a linear combination of radial basis functions. They are used in function, time series prediction, and control.

The ANN employs radial basis function (RBF) network in the hidden layer, followed by an ADALINE network, for automatic adjustments of weights and biases to arrive within a desired maximum allowable error. This adaptive network, successfully trained, has been used as a neural linearizer for the sensor under consideration. The primary variable (humidity) values generated by the neural linearizer from the capacitance values of the sensor have been found to be in reasonably close agreement with those provided by the manufacturer.

A capacitive humidity sensor has a dielectric whose permittivity is dependent on humidity. Either one or both electrodes of the sensor are porous, which allow water molecules to pass into the dielectric. Thus the sensor capacitance depends on the humidity. For a typical capacitive humidity sensor, the relationship between capacitance C and relative humidity H_r can be approximated by:

$$C_s/C_{12} = 0.985 + 0.34(H_r/100)^{1.4}$$

Where C_{12} is the sensor capacitance at 12% relative humidity?

To make the artificial neural linearization most effective, input temperature range is equally divided into three segments (25^{o}C to 35^{o}C, 35^oC to 45^{o}C and 45^{0}C to55^0C) and for each of these temperature segment frequency range is divided into three segments (1 KHz to 10 KHz, l0KHz to l00KHz and 100 KHz to1MHz). Each segment covers the relative humidity range from 10% to 90%.

Radial basis function is a supervised learning algorithm that makes automatic adjustment of weights and biases to arrive within an expected maximum allowable sum squared error goal for the network. Then, using these trained sets of weights and biases, we can find output for any set of input values with reasonable accuracy. In RBFN, the hidden layer neurons actually simulate receptive fields which are locally tuned (bell shaped) and overlapping in nature. The activation level of receptive field unit is a function of exp [-$\|w1 - p\|^2$] where p is the RxQ matrix of Q input (column) vectors and wl is SlxR weight matrix. Where R = number of inputs, S1 = number of neurons in the hidden layer of RBF, Q = number of input (or output) column vectors i.e. number of sets of input-output combination data, S2 =number of neurons in the output ADALINE layer.

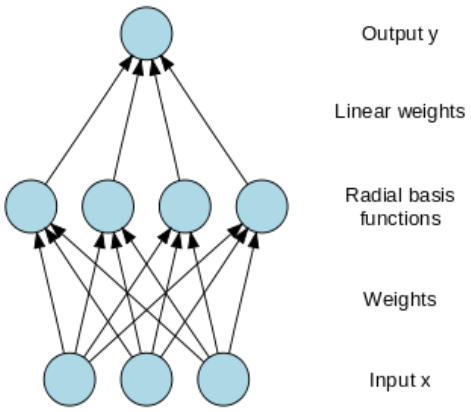

Figure 5. Structure of RBF Model

III. Comparative Analysis

Table.3.Comparative Analysis of Nn Techniques

Classification Technique	Resources/ Researcher	Notes
FLANN	[2]	Design and development of high linearity linear variable differential transformer based displacement sensing systems.
MLP	[7],[17] [9]	Extending the linear range of a negative temperature coefficient resistor sensor. The problem of nonlinear response characteristics of a CPS further aggravates the situation when there is change in environmental conditions. This ANN model is capable of providing pressure readout with a maximum FS error of 2% over a wide variation of ambient temperature.
RBF	[10]	Encountering the non linearity problems associated with the capacitive humidity sensor using ANN. Computations have been carried out with the manufacturers' data for an industrial capacitive humidity sensor.
BPN	[1],[7],[11]	The non linearity correction in input and output characteristics of thermocouple sensor.

IV. Conclusions

This review paper investigates on the nonlinearity issues relating to different types of transducers. The nonlinearity problem gives rise to the difficulties like Non accuracy in measurement; Limitation of dynamic range (linearity region).The nonlinearity problem also arises due to environmental changes such as change in temperature, humidity and atmospheric pressure, aging of transducers and constructional limitations. We reviewed different adaptive and intelligent methods for compensation of nonlinearities which have been applied to four typical sensors. The proposed review based on the structures like BPN, FLANN, MLP and RBFNN. The learning algorithms employed in this review are:LMS algorithm in FLANN,BP algorithm in MLP and RBF learning algorithm Exhaustive simulation studies of various methods show that RBFNN and FLANN structures provide improved non-linearity compensation performance but involves more computations and tedious to implement. Techniques used in Linearity enhancement of different transducers and classification has been briefly reviewed in this paper. Based on the review, FLANN is the most popular technique due to its accuracy.

References

[1] Jianwen Tang, Yong Zhang, Xiaojun Tang,Junhua Liu Nonlinearity correction of the thermocouple based on neural network, State Key Laboratory of Electrical Insulation and Power Equipment, Xi'an Jiao tong University, P.R.China, 710049, Global Congress on Intelligent Systems.
[2] S.K.Mishra, G.Panda and D.P.Das" A Novel Method of Extending the Linear range of linear variable differential transformer using artificial neural network" IEEE trans.instrum.meas., vol.59,no.4,pp.947 953,April.2010.
[3] A. Flammini, D. Marioli, E. Sisinni, and A. Taroni, "Least mean square method for LVDT signal processing," IEEE Trans. Instrum. Meas., vol. 56, no. 6, pp. 2294–2300, Dec. 2007.
[4] Liu Junhua, "The guidance of intelligent sensor System", 2007.
[5] S. K. Mishra, G. Panda, D. P. Das, S. K. Pattanaik, and M. R. Meher,"A novel method of designing LVDT using artificial neural network," in Proc. IEEE Conf. ICISIP, Jan. 2005, pp. 223–227.
[6] Qiu Xianbo," based on neural network thermistor temperature measurement system nonlinear correction" Chemical automation and Instrumentation 2005, 32 (2): 57~60.
[7] Nicolas J.Mernando-Marques and Bonifacio Martin-del-Brio, "Sensor Linearisation with Neural Networks," IEEE Transactions on Industrial Electronics', vol. 48 no. 6, pp. 1288-1290, Dec 2001.
[8] R.M. Ford, R. S.Weissbach, and D. R. Loker,"A novel DSP-based LVDT signal conditioner," IEEE Trans. Instrum. Meas., vol. 50, no. 3, pp. 768– 774, Jun. 2001.
[9] J. C. Patra, A. C. Cot, and G. Panda, "An intelligent pressure sensor using neural networks," IEEE Trans. Instrum. Meas., vol. 49, no. 4, pp. 829–834, Aug. 2000.
[10] A.Chatterjee, S.Munshi, M.Dutta"An Artificial neural linearizer for capacitive humidity sensor" IEEE Trans. Instrum. Meas., vol. 21, no. 8, pp. 313-316, April, 2000.
[11] Xing Xuejun,"The application of Neural Networks in platinum and rhodium 30–Platinum Lao6 thermocouple temperature" Wuhan University of Water Power (Yichang) Journal 1999, 21, 31~38.
[12] J. C. Patra, R. N. Pal, R. Baliarshing, and G. Panda, "Nonlinear channel equalization for QAM signal constellation using artificial neural network," IEEE Trans. Syst., Man, Cybern. vol. 29, no. 2, pp. 262–271, Apr. 1999.
[13] D. Crescini, A. Flammini, D. Marioli, and A. Taroni, "Application of an FFT-based algorithm to signal processing of LVDT position sensors,"IEEE Trans. Instrum. Meas., vol. 47, no. 5, pp. 1119–1123, Oct. 1998.
[14] G. Y. Tian, Z. X. Zhao, R. W. Baines, and N. Zhang, "Computational algorithms foe linear variable differential transformers (LVDTs)," Proc. Inst. Elect. Eng.—Sci. Meas. Technol., vol. 144, no. 4, pp. 189–192, Jul. 1997.
[15] J. C. Patra and R. N. Pal, "A functional link artificial neural network for adaptive channel equalization, "Signal Process., vol. 43, no. 2, pp. 181– 195, May 1995.
[16] Y. Kano, S. Hasebe, and H. Miyaji, "New linear variable differential transformer with square coils," IEEE Trans. Magn., vol. 26, no. 5, pp. 2020–2022, Sep. 1990.
[17] S. C. Saxena and S. B. L. Seksena, "A self-compensated smart LVDT transducer," IEEE Trans. Instrum. Meas., vol. 38, no. 3,pp. 748–753, Jun. 1989.
[18] J. C. Patra, G. Panda, and R. Baliarsingh,"Artificial neural network based nonlinearity estimation of pressure sensors," IEEE Trans.Instrum.Meas., vol. 43, pp. 874–881, Dec.1994.

International Journal of Modern Engineering Research (IJMER)
www.ijmer.com Vol.3, Issue.2, March-April. 2013 pp-1192-1211 ISSN: 2249-6645

Reincarnation–a Law of Nature

Subhendu Das
CCSI, West Hills, California, USA

Abstract: *This is a multidisciplinary paper. It is based on ideas taken from mathematics, physics, economics, engineering, and religion. (A) The paper justifies reincarnation by providing real life examples for three most important kinds of reincarnation. It also shows how some scientists and many ordinary people, of societies all over the world, and for all time have personally experienced, verified the phenomenon, and then accepted it as a law of nature and as an unique universal truth. The examples show that reincarnation is not based on faith, religion, or belief systems. (B) This research also investigates the consequences of reincarnation law and how it modifies all other existing physical laws of nature to give us a coherent and unified view of our life. (C) Reincarnation examples establish the eternal existence of our souls. These concepts have motivated people over centuries to search for truth and perform yoga meditation to understand, experience, and control our lives and nature. (D) In addition, the paper analyzes how the reincarnation law can cause damage to our existing social system. Money power is the most important power that controls every aspect of our activities. It is important that the truth hidden behind the money power must not be discovered for its own survival. This hidden force is preventing the discovery of all truths in all fields of science, religion, and in particular reincarnation.*

Keywords: *Reincarnation, yoga, meditation, religion, science, economics, laws of nature, money power, central bank*

I. Introduction

For thousands of years humanity has experienced reincarnations all over the world and in all cultures. The present days are no exceptions. However, most recognizable cases happen probably in one in a million births. Reincarnation is also detected, generally and naturally, in places where people are familiar about it, and the environment is susceptible to accept it. German philosopher Govinda [1, p. 205] says incarnations "happen as often in the West as in the East; the only difference is that the West does not pay any attention to them, because they do not fit into the mental attitude of the average Westerner whose religion teaches him that entirely new beings come into existence at birth...". Maybe this is why reincarnation, although a natural law, is considered as part of religion, belief, or faith system.

Here is one generalized overview of some real life reincarnation cases. (1) A baby is born with two gunshot wounds: G1 on the chest and G2 at the back. (2) Around age two, when he learns to speak, the boy says: in his past life his name was N, he lived in town T, and on date D he was killed by gunshot at chest. (3) Researchers go to the hospital of town T. They find that on date D a person named N indeed died there due to a gunshot. (4) They ask the hospital to show the autopsy photos of the dead body of N. (5) from the photos they verify that the wounds at chest and back are exactly like G1 and G2. Not only that, they are at same locations also.

In the above generalized example we see that physical marks from the previous body appeared on a newly born baby. This experience and observation cannot be denied by any means as a case of reincarnation. There are thousands of such well documented birth-defect type cases. This is as straightforward as – someone dropped a ball and it fell on the ground. It is not possible to deny such a trivial phenomenon.

In the video [2] the philosophy professor says we cannot discard reincarnation cases as statistically insignificant items. He says that it is irrational to disbelieve in reincarnation. The author of this paper proposes that in the case of reincarnation, we should specifically pursue these insignificant cases to find the real truth. The sample set of reincarnation cases are not the entire population. The sample set should be only those children who remember past life experiences. In Sanskrit language the word for such people is Jatismara. And this is a very small set of people. The objective of a philosopher should be to remain open minded, investigate thoroughly and carefully all such cases. Make no mistakes, every life is a reincarnation and it is a universal law of nature. We can detect it only when the child talks about his past life memories and identifies past life persons, objects, and events; that is, only by analyzing Jatismaras.

Reincarnation law can be used in many different ways in our societies. It helps us to understand many unexplained observations in our life. We all get same education but the results exhibit in different form in different people. One explanation of this phenomenon is reincarnation and past life experiences [3]. Reincarnation may also help to explain many social problems like gay, lesbian, transgender related confusions among people. Many childhood phobias can be explained and cured using reincarnation concepts [4]. Many hypnotherapists have also cured many patients using past life regression techniques [5]. It has been documented [1] that people who are expert in yogic meditation, called yogis, can heal any person from any disease. The idea of yoga meditation is a consequence of reincarnation law.

Reincarnation usually is demonstrated in three basic forms. (1) In the most Common Type - a child starts talking about her previous life. Parents listen, discuss, explore, and verify about the person in previous life. The information gets documented and becomes known to the community. (2) The Birthmark Type – This case has the same features of the common type, but in this case the child is born with severe physical birth marks or defects in the body. These cases provide the most convincing proof of reincarnation. Here physical body marks or defects get transported from the previous body to the present body. (3) The Scholastic Type - which is very rare but also gives a concrete proof of reincarnation. It has the

same characteristics of common type. In addition the child, from the very early age, demonstrates a power of super intelligence that is beyond comprehension.

We show that examples of reincarnation clearly indicate eternal existence of our soul. The book [6, p. 44] gives a very powerful logic to justify the existence of soul in our present life. His explanation says that there is something that tells us that we were alive when we were in our deep sleep. We know, when we are in deep sleep, that our mind and body both do not work and we are thus not physically active. Yet when we wake up we know that we were not dead. The object that gives us this knowledge, that we were not dead, is our soul. We all feel about the existence of our soul, in many occasions of our life, but we just cannot get hold of it in a test tube to examine it.

It is very surprising that such a fundamental law of nature, that directly impacts our life, has not been used by our modern society. The rest of the paper is organized in the following way. First we give some well known and well publicized examples of reincarnations. Then we discuss how reincarnation can help us to understand our lives. How yoga meditation, a direct consequence of reincarnation, can change our lives completely. Then in the next section we show how reincarnation law interacts with other natural laws, gives a better understanding of our society, and how it impacts our philosophy. Following that we discuss what major religions think about reincarnation. In the discussion section we show how our economic and scientific thoughts are deliberately trying to suppress the discovery of all truths including the reincarnation law and associated concepts.

II. Examples Of Reincarnation

We give some examples to describe three different types of reincarnation mentioned before. All three types have some common features and also some special features that distinguish them from other types. These cases, specifically birth mark and scholastic types, are very unique and cannot be made null and void by any kind of logic. The convincing proof of reincarnation however comes from the details of the large volume of well documented cases given by [7]. The best way to understand these cases is to select any one of them, and then analyze its details thoroughly.

It should be emphasized that all human beings are reincarnated. However, probably only one in a thousand remembers past life. Exceptional cases may happen only one in a million. Thus for research on reincarnations, the cases cannot be rejected using the concept of statistical insignificance. The universal sample set, for reincarnation, is not the total human population, it is all those who remember their past lives, who are called Jatismaras.

2.1 Common Type

In this category, a child between the ages of 2-6, starts talking about his previous life. He names the person of his previous life, identifies the city or town where he lived, recognizes people, photos, houses, and other objects that he used in his past life. The parents of the child explore the details; local people cooperate, and help to solve the mysteries. Researchers visit the place, explore the details systematically, document the discussions, take videos etc., and finally publish the results to authenticate the case.

The following example is taken from the TV news from the ABC channel of USA. The transcript [8] says that a six year old boy named James Leininger talked about his previous life as James Huston, who died at age 21 as a navy pilot, in a military plane accident, 60 years back, during World War II. Leininger's parents were an educated Christian family in USA. They never expected such things to happen to them. But over time, covering many incidents, and conversations with their child about extraordinary details of the pilot's life, they have become convinced that this is a case of reincarnation.

Here are some excerpts from the video [9]. From age two, Leininger used to get nightmares. Once he woke up from his dream and said "Airplane crash on fire, little man can't get out." Another time he said that the toy plane has a drop tank. The words "drop tank" were completely unknown to the family. Leininger gave many detailed accounts of the plane, that no one could have told him, or even could have known also. He said the plane used to get flat tires, which was verified later. The parents came to know about many such unusual and detailed information from their son. They investigated, many details that their son told about the air plane, pilot's friends who were still living, the name of the aircraft carrier, shooting down incident of the plane etc. Pilot's sister was still living and became convinced that the boy was her brother.

The proof of reincarnation does not come from only the few statements reported here and in the original references. Many of the above statements can be countered using standard logics. Professor Stevenson has discussed one by one all the powerful counter logics in his book [7]. But the totality of information covering the exact statements, the body languages, the circumstances, the trigger moments for each incidents, the objects that helped to trigger, many question and answer sessions with many people, and many such details, that spanned over 4-5 years in such cases of Jatismaras, cannot be disproved completely using any consistent logic. This is not just one case; there are hundreds of such different but unique cases that happen all over the world in every year. Most importantly there are no motive behind these cases; there are also not any financial gains, or fames, to be made by anyone involved. Reincarnation is the only single unified theory that can explain all of these cases.

2.2 Birthmark Type

This type is about Jatismaras, and transportation of one or more physical marks from one body in the past life to another new body in the present life, which has been verified from hospital or postmortem records. Real life examples include gunshot wounds, missing fingers in one hand, both legs missing below knees etc. The investigation and the documentation of this type of reincarnation give the most convincing proof of the reincarnation law for the modern scientific

community. It is not possible to counter these cases by any kind of logic or explanation other than reincarnation. It should be mentioned that these cases are rare, although well known.

Many such cases have been documented by Ian in [10]. Dr. Ian Stevenson (1918-2007) was the head of the Department of Psychiatric Medicine, at the University of Virginia, School of Medicine, at Charlottesville, Virginia, USA. He has investigated over 3000 cases, distributed all over the world, in 40 years period. His research was funded by one of the founders of Xerox Corporation. People say Stevenson will be considered as Galileo of next century.

The following case is taken from [11]. Here we see that birth defects extend deep inside the body. This is the case of an American boy named DG, who was born in 1997. When he learned to speak he mentioned to his mother that DG was her father LS. DG made a number of statements that indicated knowledge about his maternal grandfather's life that his mother thought he could not have obtained through normal means. DG's parents were Christian but his mother was open to reincarnation ideas. DG discussed the death of his grandfather. He said how LS died in an incident in a store where several people were shooting. He also described many aspects of the life of LS. He talked about the two cats LS had and even mentioned the nick name that LS had given to one of them.

DG had a narrowing of the pulmonary artery at the site of the valves. His mother reported no infections during her pregnancy that could cause such problems for her baby. There was no family history of congenital heart defects. DG's birth defect was very similar to the fatal wounds suffered by his grandfather in a shooting. The autopsy report of LS said something like the following: The gunshot wound went through the skin, soft tissue, and left ribs. Then it cut through the left lung, and main pulmonary artery. There was a 4 cm lacerated wound of the main pulmonary artery.

The paper says DG's birth defects had a pulmonary valve artesia with intact ventricular septum. This means narrowing of pulmonary artery. He had poor development of the right side of the heart. DG underwent a shunt, the first of several procedures, and has done quite well with no lifestyle restrictions. The narrowing of DG's pulmonary artery was a close match with the wound to LS's pulmonary artery.

In his many papers Stevenson has presented some photographs of birth marks and birth defects. In one of the photos he has discussed the case of a Turkish boy who had a malformed right ear and right side of the face. The boy remembers the life of a man who was shot by a gun at point blank range. The man died six days later of injuries to the brain by the shot that entered through the right side of the head. The case was verified from the hospital records. It is not just violent gunshot wounds and death cases that reappear on the new body; the normal medical surgery marks also appears. A Burmese child had a long vertical linear birth mark close to the mid line of her lower chest and upper abdomen, which corresponded to the surgical incision for the repair of the heart, of her deceased aunt which the child remembered.

These and many other examples found in the literature [12, p. 74] show that these birth marks are not medical malfunctions but the soul is reconstructing the baby in mother's womb in a very specific way and for some unknown reasons. It is then quite possible that the soul is doing many other things, and possibly everything, that we have not found out or may never be able to find out using normal research process. In one case a yogi predicted [13, pp. 13-16] to the parents, 18 months before birth that a boy will be born with a hole in the right year. This phenomenon has a profound impact in our social, physical, and medical problems that we encounter. Thus soul can decide if you will have the characteristics of your parents or not. An example is given in [1, pp. 210-216], where a person looks exactly like his past life photograph.

2.3 Scholastic Type

This type is same as common type with some additional features. In this type the child not only demonstrates and proves that he is a reincarnation of a previous life, but also demonstrates extraordinary human talent that one cannot attain by any means at that age. These talents are like exceptional musical talents or philosophical understanding of a subject, with an ability to express such knowledge like an adult.

Our first example is of a boy named Maung Tun Kyaing (MTK), from Burma during the British period, who preached Buddhism from very early age of 4 with profound understanding of the subject. The case has been authenticated by Lama Govinda, and also by the then British governor Sir Henry Butler of Burma. Both of them personally talked to the boy. Govinda has interviewed the boy, boy's father, and investigated many details related to MTK [1, pp. 190-197]. Lama Anagarika Govinda (1898-1985) was a German man, later became a Buddhist. Robert Thurman, a Columbia University professor describes him as the greatest philosopher of the west, although little known. Note the middle name "Anagarika", it is a Sanskrit word and it means a person with no nationality.

MTK was born in a very poor and illiterate mat-weavers family. Suddenly at age four he started preaching Buddhism, better than any religious teacher could have done. He visited a Buddhist Monastery in the local village, where he lived in his previous life, as an abbot named U Pandesia. He recognized the present abbot and correctly mentioned his name; MTK showed the room where he meditated, and identified the things that he used. At the monastery, the child read the scriptures written in ancient Pali language and explained its meaning, which MTK could not have learnt in his home.

People were so impressed by the sermons of MTK that they came by thousands to listen and see him. Eventually his fame reached the ears of the governor. The governor invited MTK to convince himself of MTK's extraordinary gifts and remembrance of his previous birth. Governor was very pleased with the masterful exposition of Buddhist tenets by MTK and gave him a hundred rupee note, which the boy could not accept, as MTK said he cannot sell Dharma. Governor was greatly touched by the little boy when MTK wanted to give him a gift. MTK opened his rosary from his wrist and gave it to the governor. Smilingly accepting the gift the governor said – "now you must tell me how to use this rosary". MTK explained in details that this is to meditate on three marks of existence – impermanence, suffering, and egolessness.

The boy spoke not like the one who was taught, to repeat words which he himself could not understand, on the contrary he spoke with such conviction and sincerity that the governor was profoundly impressed by this child. He asked MTK to go from one end of the country to other and preach to high and low and even to prisoners in the jail. Governor believed even the hardest criminals will melt in hearing his genuine faith and sincere goodwill. The boy did so and the prison doors were opened for him.

The case of the American boy Jay Greenberg (1991-) is similar to MTK. Jay was born in a family which did not have any musical background. However, Jay was not a Jatismara. But from age two he started showing talent in music. Some say he is the greatest musician to come in last 200 years. He wrote 5 symphonies by the time he was 13. At age 14 London Symphony Orchestra has recorded his music for Sony Company. His case was first aired on 60 minutes CBS TV program, in 2006 in USA [14]. Mozart was also a famous child prodigy, but he was born in a musical family. Those who speak fluently a foreign language, between ages 2-4, should also be considered under this category, although it has a special name - Xenoglossia.

III. Proof Of Reincarnation

In this section we discuss how a theory is established using research, verification, and investigation of all counter logic behind the theory.

3.1Definition of Proof

Our normal understanding of proof comes from the science and engineering concepts. Let us say that we want to prove that hydrogen and oxygen when combined properly will produce water. We prove this inside a chemistry laboratory. We take precisely known amounts of hydrogen and oxygen, mix them together in a test tube and then burn or give an electric spark [15] to ignite them to produce water. In our context we want to say that this is not really a proof; instead this is a demonstration of a theory.

We may want to say that the proof is the long process that required lot of research by many people over many years to find out that we needed hydrogen and oxygen. Then we did lot of trial and error to find out the exact amounts needed of them. Again after long investigation researchers have found that the items must be ignited by some means to combine them. We call this entire process as the proof. Once we have come to a definite answer to all our questions, then we repeated the test and documented the final steps. Now anyone can repeat those steps to demonstrate the theory.

Reincarnation also can be proven in the same way. In this case the laboratory will be the whole world. Similar amount of research needs to be done over long time and by many people to identify and short list very convincing cases of Jatismaras that cannot be explained by any other known processes. Then any one can take these final selected cases, carefully analyze them, document the results, and then publish them. This is basically what has been done by Professor Ian Stevenson [7] and his colleagues for over 40 years for more than 3000 cases all over the world.

But long before, Stevenson's proof, the reincarnation theory has been proven by local people and by their own methods of verification [12], which were similar to what Stevenson did. This proof is also very much like the experience of the family of James Leininger, the airplane pilot, as described earlier. Each family examined their own cases more thoroughly, than Stevenson did, over the entire 4-5 years of the child's early ages. Their effort was more rigorous and thorough than possibly anyone else can do, because the parents lived with the child. They have examined the details of every moment in the child's daily activities. This is how reincarnation was proven over and over again for more than several thousand years and all over the world. The parents believed, local community believed, and eventually the entire society, civilization, and the world believed.

Many say – those who believe in reincarnation will not require any proof and those who do not believe no amount of proof will convince them. But we are not professing on belief or faith in this paper. Faith and belief are not at all scientific. When we talk about a physics or chemistry problem we do not mention belief or faith. We just ask you to go to the lab and do the experiment on your own or read the details of the experiment from the literature.

For reincarnation the idea is same. You can go and perform the experiment on any of the established recent cases. That is, go to the town and talk to the boy and their parents, stay there for two three days, and convince yourself. Alternatively, read the details of any one of the cases investigated by Professor Stevenson. Dr. Stevenson has documented most thoroughly each of the cases he has investigated.

Note that, just because in science many people are doing the research, and the world is investing lot of money, you should not blindly believe in science. In fact we show later that all math and physics theories are wrong, and we should not trust them. The same concept applies for economics also, as discussed later, to show that money is free. There is no rationality in believing what everybody is doing as right. Before Galileo we all believed that sun was going round the earth, but his rationality proved it otherwise.

3.2 Counter Arguments

Dr. Stevenson has discussed many standard counter logics in his investigation, both in general and in more specific way for individual cases. Some of the commonly placed counter ideas he discussed are (1) Paranormal knowledge, like fraud (motives and opportunities), conspiracy, and financial interests etc. (2) Imposed identification on the child by someone else, most likely from family members. (3) Capacity of parents to impose ideas (4) Cryptomnesia, the child may have known a person and confused it with the previous family. (5) Genetic memory (6) Extrasensory perception and personation etc. Many

reincarnation cases were rejected outright by Stevenson because of lack of proper evidences. He investigated cases only after his colleagues have identified very strong cases with verifiable evidences.

The extensively large amount of detailed data, which the Jatismara child produces in many cases, convinces any skeptic about the truth of reincarnation. It is said that god is in the details. And it is the details along with their precisions that are most important. As we discuss later, the simultaneity law is an important foundation. The reincarnation cases for the children develop over a period of 3-4 years, involving millions of bits and pieces of data, including body language, trigger moments, emotions, which are all linked simultaneously. Most scientists ignore such details and analyze things in isolation in their laboratories, and with adults. Many of these scientists probably did not even encounter a live case of a child. Most of them are also biased with a faith that humans are mortal [16]. As we show later that science has an important role in preventing the discovery of truth.

Carol [17, pp.171-204] has identified a few general signs for detecting reincarnation symptoms presented by a child. (a) Matter-of-fact tone: These are some spontaneous statements made by the child in some very casual way, particularly in the western societies. The way the child says these statements is important. (b) Consistency over time: The basic story remains consistent every time the child discusses the subject. The time gap may be long, more than one year. Although, as Dr. Stevenson points out that the stories may become hazy or sharp with many details, as happens with our own old memories of present life. (c) Knowledge beyond experience: These are obviously detectable by parents. These general observations by Carol are very difficult to counter. Those who are involved in the cases, like parents, teachers, and other adults immediately recognize that they are facts and not fantasies or conspiracies.

The cases of birth marks and scholastic types, along with information related to common type, cannot be explained without the idea of reincarnation. There are yogis who can even predict long before birth, that a baby will be born with specific birth marks to a specific parent at a specific location [13].

IV. Consequences And Benefits

The examples given above prove the law of reincarnation. There are thousands of such proven cases throughout the history of mankind and all over the world including west. These cases also give another proof of existence of soul as discussed before. The existence of soul opens a completely new dimension in our life, philosophy, medicine, education, and the design of societies. Our humanity during the last fifteen hundred years ignored the concept of soul. But now once we understand reincarnation as a fact, we see the existence of a new kind of object in nature, the soul. So far we were concerned with physical objects only, living and nonliving; and we also considered physical forces like, light, sound, mechanical forces etc. But now we have another object which is non-physical. Examples show that this soul is not part of nature; does not follow the laws of nature, and in particular the soul never follows the death process, a fundamental law of nature. We cannot see it, like gravitational forces or magnetic forces, but we can feel its presence in our body, and we see its impact in the early childhood of every birth of human being. The recognition of this new object, the soul, can have tremendous impact in our life. In the following subsections we analyze some of these consequences.

4.1 The Human Soul

To justify the reincarnation examples mentioned above we need to introduce the concept of soul. This is the object that helps to carry experiences and information from our past life to our present life. This is a very important characteristic of our soul.

We know that nature has only two kinds of objects, a physical object which we can see, touch, and feel, it occupies some space. There is also an energy or force type objects, which we cannot see but we can feel it, we can see its effects. We also know that the energy object is always associated with a physical object. A light always emanates from a physical object like sun, or light bulb etc. Similarly heat or sound also is an effect due to some physical objects. Energy or force objects cannot exist without a physical material object. Thus in this sense we only have one kind of object in our natural universe, which is physical.

We also know that no physical or material object can carry any kind of information about our life from one birth to another birth. Our scientists have not found any such physical material. All the physical objects have been identified in the periodic table of chemistry. None of these physical elements can carry any information. These physical objects are not living objects. Thus the soul is neither force and energy type nor a material type object. But since it carries information, it must be something else; nobody knows what kind of object it is. It is for sure that such an object must exist to justify the physical phenomenon of reincarnation. It is quite possible that souls exist in the entire universe, in all stars and in all galaxies. It can take any kind of life form in any kind of environment. On earth it obviously can take forms of animals, plants, and bacteria also.

We also express our knowledge about our soul in many different ways when we talk. Most common such statements are the following: My heart says this, I have a gut feeling, my intuition is telling me something, I hear my inner voice, I hear messages, my conscience says etc. All these kind of statements are telling us that we are aware of the existence of something that is more than or beyond our physical body and brain. The word soul is considered same as spirit in this paper. In a similar way we do not also distinguish between mind and soul. Most important consequence of the reincarnation theory is that we are not our physical body. We are our soul. The person we are talking with is a soul; the person who is talking is also a soul. It is this soul that reincarnates and not our body. We must not confuse our physical body with our soul. This physical body includes our brain also. We can make a fundamental change in our life style if we can constantly remember that we are not our physical body, our brain, or our mind.

4.2 We are different

Reincarnation law shows that we came to this world many times in the past. We were born in many different places, countries, to many families, and in many races. In some incarnations we were males and in some other we were females. Thus our souls do not have sex, race, and nationality. Since we are souls and not our bodies, then our bodies should not have any nationality also. In fact all yogis consider them as persons without any boundary. The examples show that the experiences of these past lives are still with us, and are helping to make an individual to progress and also the society to progress. We are building on them in each life. Many people refer to this as karma. Note that karma means work, not just in past life, but in present life also.

There were many wars in the world, based on nationality, race, religion, and of course wealth and moneypower. Indian ancient books like Ramayana and Mahabharata present two great wars. In Ramayana, two different races, human and monkey, joined forces against a monster race. This war therefore was not based on race, it was for Dharma, which means for justice, truth, duty, responsibility etc. The objective of both wars was for the same reason. Most important objective in those two wars was to restore and maintain the respect for woman. Thus if we understand reincarnation, if we understand soul, then we will never fight for manmade ideals like religion, nationality, or race. We will fight for god made or nature made objectives, for truth, responsibility, humanity, and equality.

If you throw a stone you can see its trajectory. You can see how the stone moves, where it came from, and where it is going. A soul also has a similar trajectory, but it is distributed over space and time. We cannot see or feel about its entire trajectory. The reincarnation examples show that this concept of trajectory is valid in real life. Our present life is only a small part of this trajectory. Thus all of us are in a long journey and for eternity with different trajectories. We inherit this trajectory; our present life is defined by experiences gained from this trajectory.

Since in every life we were born in different families, in different economic and social conditions, and in different times, we are all different. Every person is different. This universal thought should be taken into consideration in the design of our society, work force, education, medicine, legal and political systems. This is considered and used by many hypnotherapeutic practitioners, but the scope should be expanded in all aspects of our life. Every person should be treated in an unique way designed specifically for that person. This philosophy, if implemented correctly, will change our society completely. We should not treat everybody as equal; however, we must give equal opportunity and freedom to everybody. Just because we cannot remember our past lives, we should not treat others badly.

For the same reason, there cannot be anything good or bad in nature. They are just different. Everything is part of nature and is following the laws of nature. Apple is good and orange is bad cannot be true. Similarly Mr. X is good and Mr. Y is bad cannot also be true. We have gone through different trajectories of incarnations, so we are different. Death is an universal truth, and thus death cannot be bad also. Different person will die at different age and for different reason.

4.3 Body constructions

Birth mark cases show that human body is constructed by the soul, while the baby is inside mother's womb. If there was gunshot wound in the previous life then it can appear at same places in the new born baby. This discovery has tremendous consequences in our medicine, life, and philosophy. It is quite possible that everything in the normal body is also constructed individually in an unique way by its soul. An example has been discussed in [1] indicating that past life photograph matches very closely with present life. Thus the looks of a person may not depend on parents. The same can be said about, intelligence, diseases, medicine effects etc. Thus this law of reincarnation has a profound impact on the understanding of human life and then effectively using our people for proper design of our society including its philosophy.

Teaching such concepts will also make all parents aware of their babies past lives. Now most of us ignore past life. But asking some basic questions, at the age when the baby starts talking, we may be able to find information about past life. All pediatricians can be trained to detect birth marks and ask such questions to all of their child patients. This information can be used not only for health problems but for many social and philosophical problems also.

Many present-life diseases are due to past life accidents, sickness or diseases. A little boy had eczema at the wrist; he used to scratch under certain mental conditions causing hand to bleed. Once it was discovered that he was wounded by a gun shot in military battle field in his past life, he not only recovered from the phobia, but his eczema also completely vanished [17, pp. 4-22]. There is another such example, cyst in throat, in the video by BBC [16], as discussed later.

4.4 We were there

The reincarnation law says we were there before; we were there where Jesus Christ was, we were there when Prophet Muhammad was, Buddha was. We did not die in all the wars; we are back here again and probably fighting another war, or maybe trying to prevent another war. The case of Leininger [8], discussed in the example section, confirms that we were there in all places, we never die, and we come back to our earth to serve our society and each other. All the Jews who were killed in WWII are still here, they may not be Jews in this life but are not dead; all other millions who were killed in WWII are also here.

If death of somebody or some object brings good for greater benefit of the society, then death or killing is definitely a good thing to happen. Death is not bad at all because it is a law of nature. Since destiny, as we show later, is driving all of us, how can death and wars be bad? There is no need to feel bad or sad about our death. That is because death process is certain for everybody. Those who have born will die one day. According to reincarnation law they will be born again. This certainty and truth should remove sorrow and sadness from our life. Constantly remembering reincarnation law will give us peace in our mind all the time. This can be achieved by teaching reincarnation law starting from our high schools.

All the memories of our past lives are also with us and we are enjoying our companies with all the long history of each other. Many of us remember the past during our child hood days, but most do not. That does not mean that our soul forgot everything. Similarly, we all know our past lives, but it is known to our souls and not by our mind. However the past life experiences and memories are working in all our present actions. A person with yoga skills can tell us everything about our past lives. In many cases hypnosis can also reveal our past experiences and knowledge [1].

Understanding of such concepts, which is a consequence of reincarnation law, has a profound impact in the philosophy of our society and it can change our life style. Imagine what will happen to our next generation of people if we teach these subjects to our high school students.

4.5 Past life regression

Past life regression (PLR) therapy is now a well established method of treatment in Psychiatric branch of medical science. In this approach a patient is usually placed in a hypnosis environment and regressed backward in time slowly to past life. Some doctors do not use hypnotic method, yet take the patient consciously to past life memories. A good literature survey on the methodologies is presented in the Master's thesis [5]. Some doctors claim that this method proves the validity of reincarnation law.

It has been found that many chronic migraine headache cases for many adults are related to past life problems. In one such case [18] all normal medical treatments, over long period of time, failed to cure the patient. Accidentally the patient discovered the PLR technique and made an appointment for hypnosis. It was found out that she was raped, had a baby, and then died in an accident where she got wounded in her head. Once she discovered all the details she was completely cured automatically.

In a similar incident a child started growing a large cyst in his throat [16]. Doctors performed the operation but it grew again. One day the boy told his mother how he died in his past life due to a gunshot wound on his neck in a military battle field. Once the details were discussed with the boy, the cyst and the growth in the throat vanished completely. The normal medical doctors could not explain but had to accept it as a miracle. This case does not come under birth mark type; however it is similar to migraine headache problem. It is quite possible that a detail medical examination of the physical body would reveal an internal birth mark in both cases.

4.6 Yogis and Meditation

Yoga and meditations are well known in eastern countries. Many people from the west have gone to India and Tibet to learn and practice yoga meditation. Some people renounce their societies and live in forests, mountains, and caves in Himalayas to learn and practice the yoga mediation. The life stories of such yogis have been published in many books; see for example [1, 13, 19]. Reincarnation and the soul theory are the foundation of such practices. The major objective of such yogic meditation is to connect to your soul, called self realization, or swaroop darshan in Sanskrit. With this method they achieve powers to serve the people who desire their help.

These yogis can perform many miracles using their yogic power that modern technology cannot implement and explain. One such recent example is given by the video [20], which shows: a yogi lies down inside fire, an interview with the yogi, and also some results of scientific investigations. Some of the yogic powers, mentioned in the above three books are: they can (a) heal any sick person without any medication, (b) physically appear anywhere at any time, (c) simultaneously exists at multiple places; (d) view and describe about past, present, and future of any person, at any place, (e) mind read of any person of any language, (f) cast off their own body, enter a younger dead body and continue to relive, (g) extend their life to any length of time according to their desires, (h) stop the snow avalanche and rescue people [13, p. 124] etc. Their miracles are well known in the western world also and have been documented by western people [21].

The foundation of yoga principle is based on the existence of soul and its incarnations. If we understand this universal truth then we can design our education system to learn the yoga meditation technology to make our society much better. Our many health problems can be solved without any kind of modern medications which have so many side effects. Our general and mental health can also be significantly improved using such meditation procedures.

The book [1, p. 114] has documented one case of yoga meditation skill that can help to communicate with another person in a different country without any knowledge of the person. While living in Tibet, Govinda wanted to know about his mother's condition in Germany. A Tibetan yogi within few minutes brought the details about his mother. Two weeks later Govinda received a mail from his mother confirming the exact same information. It is therefore quite logical that we are also connected by our souls all the time with all persons. Our society will completely change if we teach our kids in their high schools how to achieve such yogic power and control our lives.

4.7 Tracking Incarnations

Using very sophisticated software, globalized computer network, and with integration of medical and other databases collected over many generations, it will be possible to track and identify reincarnation of all human beings. The modern technology, like the one, we are using now for tracking terrorists, can be used for finding past life persons. The kind of data items that maybe included are [22]: photographs at different ages, skin, hair color, land, climate, ethnicity, normal food, kitchen utensils, clothing, footwear, time of death, age, death experience etc. Pediatricians can be trained, across all hospitals, to enter their information in the database.

At this time these past life identifications are done only by people who have acquired special skills in yogic meditation [1]. Tibetans have well developed methods for finding their famous lamas after reincarnations, and providing

such children the opportunities, so that they can help the Tibetan society in later days. But this is managed using yogic power, which cannot be achieved by everyone. Such identification skills have been discussed in [13, 19] also. It will be good to take help from such yogis to design and verify the database search algorithms and identification results.

V. Laws Of Nature

Reincarnation law has significant impact on other laws of nature that we have studied in physics. It also has impact on the characteristics of our work or karma and the understanding of our destiny. Again, we emphasize that reincarnation, karma, and destiny have nothing to do with philosophy, religion, and god. We discuss the following laws: global plan, universal truth, death process, simultaneity, conservation, action reaction, destiny, and selfless karma. Since they are all laws of nature, they cannot be treated in isolation, they are all integrated inside nature. Reincarnation law plays an important role in integrating them both over space and over time.

5.1 Global Plan

There exists a global plan in our planet and our activities are part of that plan. Our galaxy is a giant spiraling structure with its associated motions in space. In one of its branches is our solar system. Our solar system is moving along with this huge galaxy. The sun cannot go anywhere on its own; it must follow the course dictated by the global plan of this galaxy. While staying on earth we do not see the definition of our galaxy. As we go away from earth, in the sky, the global plan of the galaxy begins to unravel its mystery, structure, and the journey. From this far away point in space we can get the glimpse [23] of the future path or destiny of our earth.

If we look inside a corporation we find a global plan that governs all activities of all the employees. When we start a new project in the company, many employees sit together in a conference and create a global plan for the project. They together decide the things to be done, assign a time schedule for each activity, assign people working on such activities, define how people will interface in creating their individual assignments etc. Once the plan is precisely drawn everyone knows exactly what they will do in the next day for several months, until the project is completed. During this period no one has any freedom to change their work plan, and why they would try to change, they would not, because they jointly created the plan. This corporation is also linked with other corporations in the same industry. Going farther outwards we see that the entire economy is working in a coordinated way under a global plan.

Same is true for our society. This global plan is created by the action-reaction law that started long time back and is still continuing and will continue forever. The reincarnation law says that we were there before. We came to this earth many times in the past and will continue to come again and again. The simultaneity law is also involved in this global plan. Things are happening because of simultaneous action and reaction of many people over global space and global time. These simultaneity, action-reaction, and reincarnation laws together create this global plan. Together they are generating all the activities in this universe. If we move far away, and look at the global history of our political and economical systems for past few centuries, then we will be able to see this global plan and then we can estimate its possible future.

At the individual level money plays an important role in placing us inside the global plan. The supply of money is controlled by the Central Bank (CB) as discussed later. There is a huge Money Power (MP) associated with the CB. It is the same money that controls all activities of this world. It is a very coherent and unified force. Using the money supply the CB can remote control us. By terminating us from our jobs, life can be completely changed. Thus we are all forced to participate in the global plan created by the CB and MP. Thus our destiny is intimately tied with this global plan. It is interesting to observe that CB was evolving over centuries, and incarnation after incarnation new souls entered and left the CB and MP, and yet none in CB and MP did try to change its role. This probably shows that CB and MP did not enter its death process yet.

Unfortunately, because of the complexity of action-reaction law, lack of knowledge of our past life activities, and the simultaneity law we cannot precisely estimate the future. When we come to any point in the future time then we can look back and see the global plan in the events of the past. Thus the existence of the plan is very definite but the prediction is not realistically definite. This observation is not just for our societies, it can be observed in our personal life also. Any event that appears meaningless or random now will appear meaningful and reasonable at some future time, when taken in global context.

If we look at things in local time, in local region, using local concepts and philosophy, we will see only local activities and it will appear like noise, random, and with no plan or purpose. The global plan can be understood well if we view the entire world and over long period of time covering 3-4 centuries, just like the galaxy example. A meaningful unified theory can be detected in the global plan only when all major as well as all minor events of the world history can be explained using this unified theory. Sometimes whistleblowers, like [24, 25], come out to reveal the inner workings of the power structures (CB and MP) giving us a great deal of the global view. These people were actually hired to reveal the secrets of power structures.

5.2 Universal Truth

The truth is always universal and unique in nature. There cannot be multiple truths on any subject, in the sense that the truth is constant over time and over space. Thus it cannot be true that reincarnation only happens in the east and is not happening in the west. It must be happening everywhere and for all time. There are ample documentations of reincarnations for all countries in the world. Reincarnation law is not based on religion, race, or nationality. Thus the reincarnation law

cannot be invalid for Christian and Muslim religions and valid only for Buddhists. This is because reincarnation is a law of nature and therefore is an unique universal truth.

But humans will never be able to find the universal truth. Because of the simultaneity law and the reincarnation law, every event is a result of actions of many people from many different places and over many incarnations. It is not possible for an ordinary human being to know all the information. This information space is a multidimensional space, and every individual lives only in one of its very small subspaces. A part cannot know the whole. The global plan cannot be visible from local space time state. Universal truth and the global plan are thus intimately related.

Only yogis can know the universal truth. Only with the help of yogic power a human can directly communicate with the soul of anybody and acquire all information it wants. Only such meditation and yogic power allows one to discover the mystery of soul and other characteristic of the universe. It is quite a miracle that yogis around the globe discovered the reincarnation law more than ten thousand years before. This fact alone should convince us about the claims of yogic power. There are many examples of controlling the soul by such yogis [1, 13, 19]. Through their meditation process they can present themselves in multiple places, heal any kind of diseases, cast-off human body to die, or enter a dead body and make it alive. These powers cannot be understood by any other means. These experiences of humans show that ordinary person cannot find the universal truth. We show later that math and science cannot also find the unique universal truth.

Observe that in one sense we have captured a very important universal truth. Consider a digital microprocessor. It is an electronic integrated circuit that can perform miracles. It can solve all problems of the world. You give any problem, or any complex algorithm, a person will be able to convert it into C-programming language or native assembly language, and execute it on the microprocessor. This microprocessor does not know what it is solving, it is only executing its own CPU logic one by one in sequence, but you are seeing that it is solving your problem. Thus a microprocessor has captured the universal truth behind all our engineering and other kinds of problems of our modern society. A microprocessor proves the existence of unique universal truth behind all our analytical thoughts.

The universal truth is always eternal. It always appears in all occasions. It cannot be suppressed. In our context the universal truths are: the reincarnation law, simultaneity law, the action-reaction law, the conservation law, and birth and death processes etc. Any process that tries to suppress the universal truth will die sooner than later. One universal truth we always know: that is death process for all objects. We all know one day we all will die. This is true for our economic and political systems also.

5.3 Death Process

Everything in nature goes through a birth process, a maturity process, and then to a death process. All these processes are a chain of action and reaction processes. A society is born; it develops into a matured system, and then dies. Roman Empire in Europe and Mughal Empire in India are such examples. Similarly an economic system, like imperialism, was born, matured to a worldwide system, and then finally died also. The scheme is true for all living objects including human beings. Our scientists have discovered that the stars are also born, remain active for a period, and then explode to die.

Reincarnation law however says that the souls do not die; it takes rebirth and goes through the cycle again. In each cycle it makes some progress towards its ultimate objective and then leaves the body again. The law of conservation then says that the soul cannot die, only human body dies. Thus the soul is eternal. The death process is true for all things in nature at the atomic and energy level. They just take different form in the next birth. Thus the soul does not belong to nature, it is outside of nature, or it has a separate existence, because it violates the death process. In Sanskrit the soul is called Purusha and the nature is called Prakriti. Soul's separate existence is conceived in Samkhya Karika, a scientific theory of soul, and is a part of Vedic scripture, as we discuss later.

Before death process begins everything starts deteriorating, fails to operate normally, and then eventually the whole system dies. Before our death, we may find that heart fails, lung fails, or brain fails. These failures are not bad things, because death is a law of nature. A man has to die. How a person will die, and when he will die only a yogi can tell. It is a very common statement that the seed of destruction is planted at the time of birth. This is true for all objects and systems, including economic systems.

Since death is an universal truth, and destiny is also an universal truth, killing somebody cannot be bad. This is because killing is a result of long chain of action and reaction of many people over many different times. Thus there are always reasons behind every death, which are consequences of laws of nature. The concept of reincarnation, the eternal existence of soul, and the separate identity of soul outside of nature, change our understanding of birth and death process. This expands our view of life to global space and global time.

5.4 Simultaneity Law

This law says that everything in nature is interconnected over global space and over global time. We are not isolated. We cannot do anything all by ourselves. Everything happens because of simultaneous interactions of all the people in this world over all past and present times. We can see it clearly as a result of globalization of our economy. We are all simultaneously influenced by the environment of the earth. Earthquake, tsunami, environmental pollution, financial recessions, all simultaneously affect us over all time including future time. We call the result of this law as the global space time (GST) effect.

Simultaneity law is very much evident inside a corporation. There we are all working together to create a product, like an automobile. Every project is precisely planned, all our activities are carefully designed and assigned to individual workers, and there are target dates for every milestone. We all know what exactly we will be doing tomorrow. All work

activities must match with every other activity, any error will cause a disruption. Many corporations are globally distributed, thus all our activities are also globally connected and simultaneously, with a global plan for the corporation.

Reincarnation examples show that my experience and knowledge of present life are derived from my past lives, that is, we are all connected via our actions of many previous lives. What I will be doing now will depend on what I did, and how I did, in my previous life. Since reincarnation is a law of nature, this is true for all humans, eastern or western. This law expands the simultaneity law over our past lives. Note that the simultaneity law is not just a feature of modern times and modern societies. It was in existence for more than thousands of years.

Thus the simultaneity law can naturally be modeled by an infinite set of simultaneous equations in infinite number of variables. Since infinity is not there in nature, in reality it will be a very large number. Since everything is changing over time these equations must be dynamic and therefore can be represented by a differential equation. A conventional linear state equation model of the type shown in (1) below can give a better view of the global plan defined by the simultaneity law. In the right hand side of (1) $\{x_i\}$ are the objects and $\{a_j x_i\}$ can be considered as actions on those objects. Since the model represents the entire universe, which is a closed system, there is no control variable in (1).

In the expression (1) if we take a local view, defined by the highlighted variables, we will never be able to understand the global view which is defined by all the variables.

$$\begin{array}{lcccccccc}
\dot{x}_1 & = & a_{11}x_1 & +a_{12}x_2 & +a_{13}x_3 & \cdots & +a_{1,15}x_{15} & +a_{1,16}x_{16} & \cdots \\
\dot{x}_2 & = & a_{21}x_1 & +a_{22}x_2 & +a_{23}x_3 & \cdots & +a_{2,15}x_{15} & +a_{2,16}x_{16} & \cdots \\
. & = & . & . & . & \cdots & . & . & \cdots \\
. & = & . & . & . & \cdots & . & . & \cdots \\
\dot{x}_{71} & = & a_{71,1}x_1 & +a_{71,2}x_2 & +a_{71,3}x_3 & & +a_{71,15}x_{15} & +a_{71,16}x_{16} & \cdots \\
. & = & . & . & . & \cdots & . & . & \cdots \\
. & = & . & . & . & \cdots & . & . & \cdots \\
\dot{x}_{251} & = & a_{251,1}x_1 & +a_{251,2}x_2 & +a_{251,3}x_3 & & +a_{251,15}x_{15} & +a_{251,16}x_{16} & \cdots \\
. & = & . & . & . & \cdots & . & . & \cdots \\
. & = & . & . & . & \cdots & . & . & \cdots
\end{array} \qquad (1)$$

Observe that reincarnation law also indicates simultaneity law. Since souls can be born in any place and in any country, a person born in one economic and cultural environment can be born in next life in another country and environment. This process infuses experiences of one country into another country, one culture into another culture, thus making simultaneous progress of all people according to a global plan.

5.5 Conservation Law

The law of conservation (LOC) of mass and energy are two important laws of nature. It has been shown [26] that this is the only meaningful law of nature; all other laws of physics are either equivalent to or can be derived from this law. The law says that mass and energy cannot be created or destroyed. Thus the sigma of all masses is a constant; the same is true for energy. They can only be transformed or transferred. Thus to produce a car we must use materials and energy from nature. It cannot be created out of nothing. We call it sigma law also. Sigma law can be stated using the following sigma notation:

$$\sum_{i=1}^{N} x_i = 0 \qquad (2)$$

Here the set $\{x_i\}$ represents any physical variable. If you use any consistent set of physical variables, with proper units and dimensions, then you will always find that the above sum in the left hand side of (2) will be zero. It can become a given constant, but the constant can be absorbed in the left hand side. The variables, for example, can be forces, energies, or masses etc. Thus (2) is a balancing equation, things are balanced in nature. Observe that equation (1) is nothing but a series of sigma laws of type in (2).

According to this law any win-win situation is not possible. Everything must be a win-lose system. In every apparently win-win situation a detailed analysis will always reveal a third party who will be the loser, because we are all simultaneously interconnected. A win-win will violate the balance in (2). This law also says that we cannot invent anything, we can only discover. Something new cannot happen; a nonexistent object cannot become existent. It is against the sigma law (2). The wheels, engines, chassis were all there we just put them together to create a vehicle. Even many forms of vehicles were already there too. The same is true for all kinds of products that we have created; math and science are no exceptions also.

Thus "I did it" is meaningless and is against the laws of nature. According to LOC things were already there; I could not have created it. Thus patent laws violate this law of nature. In many cases the idea of "I did it" may not also be valid, due to reincarnation, in the sense that may be I started working on the subject in my previous life along with many other people and I completed the task in the present life working with some other people. Thus the law of conservation leads to the egoless or selfless karma. A computer tracking system, discussed before, will be able to reveal such past life connections with our work of the present lives. The tracking system database therefore must contain work details of all persons for more than a century.

5.6 Action Reaction Law

The action-reaction law or the Newton's third law is another important law of nature. It can be found in [27, p.120] and has been explained in the following way. In an isolated environment, the forces always occur in pairs or that a single isolated force cannot exist. Any one of these two forces can be called the action force, and the other one then can be called the reaction force. The reaction force is equal in magnitude of the action force and of opposite in direction and can be written as in (3):

$$F_1 + F_2 = 0 \tag{3}$$

Because of global space time (GST) or the simultaneity law, for every action there will always be more than one reaction $\{F_2, F_3, \ldots F_N\}$. It is thus not possible to create an isolated system and produce a single reaction. However, the summation of all reactions must still be equal to the original action that produced all the reactions. Therefore in real life we should have (4):

$$F_1 = -(F_2 + F_3 + \cdots + F_N) \;\; or \;\; \sum_{i=1}^{N} F_i = 0 \tag{4}$$

Expression (4) shows that the Newton's third law is a sigma law or a law of conservation.

We should recognize that all human actions satisfy this law also. Our hands create physical forces, our ears receive physical sound wave actions; we see energy of natural lights through our eyes. Thus humans are integrated with this physical world. Inside our bodies also this same action-reaction law works. We can think and imagine, but all our actions are guided by this action-reaction law of nature. Because of reincarnation law we are connected with our past life actions also via the chain of actions and reactions that started in our past lives. In this chain of actions and reactions I was there many times from many places and from many past lives. Thus it will be meaningless to associate me with an action at present life.

In a corporation, we work on projects, where we decide our activities jointly, define our interfaces and interactions, and produce actions simultaneously and interactively to complete the tasks. Nothing is done by a single person in any corporation. Thus here again we see that, "I did it" – is not meaningful. Thus our ego, our selfishness, considered as foundation of capitalism, are against the laws of nature. In fact, because of reincarnation law, there is no "I". "I" was there for all past times.

5.7 Destiny Law

Destiny idea follows clearly and in a straight forward way from the action reaction law. As we have mentioned, this law says that for every action there is an equal and opposite reaction. This reaction, according to the law is supposed to happen instantaneously. But in nature nothing happens like that, everything takes some time. Thus if an action F1 happens at time t, then its reaction F2 will happen at dt time later, where dt is a very small time, can be called observational delay, measurement delay, or reaction time etc. Thus F2 will happen at time t+dt. We know that this F2 will be equal and opposite of F1, thus we can write F2 = -F1. Since we know F1, we know F2 also. Thus future is clearly known, this is future because t+dt is future time. Thus the action reaction law clearly states the destiny is precisely defined and can be found if we know the present.

However, as we have mentioned, action reaction law has an assumption of isolated environment, which cannot be true because of the simultaneity law. We are all tightly integrated in our world with our actions and reactions. This integration is not just in present life, because of reincarnation law we were connected in our past lives also. The past life actions are working in present life too. Thus for any action there will be more than one reactions at any future time t+dt. So the number of reactions, N in (4), will be very large, and the share of any action among all the reactions will be very difficult to find out. But theoretically we understand that it can be found out, that is, the action reaction law is valid. This also follows from the conservation law, because action reaction law is a law of conservation or a sigma law, as expressed by (2).

Note that at time t+dt many other new reactions will also interfere with the object, beside the reactions originated by F1. Thus all objects must be considered simultaneously to find the total reaction on any object. It must be understood clearly, that because of simultaneity law I do not create my destiny. My destiny is created by the actions of many people working together, including past life activities with many people. Thus destiny is tied with the global plan of the society. The notion that I create my destiny, I create my karma, I am independent are not correct and goes against the simultaneity law and reincarnation law of nature. We are not isolated individuals, we are together, and are highly integrated through our activities. Thus it is not my destiny, it is our destiny.

Thus destiny is defined by the simultaneity law expressed by (1). We can think of equation (1) as representing a large set spring-mass system. That is, assume that there are many objects like solid moving masses, and they are all interconnected by springs, and all are hanging in space. If any one of the masses moves then all other masses will move also, because of the interconnecting springs. I can think myself as one of the masses. I am constantly in touch with everybody via these springs. If any one takes any action I get immediate reaction from these springs. Thus my activities are not controlled by me; it is controlled by the global set of simultaneous activities defined by other masses in the expression (1). I am part of nature via (1), and I am forced to act by actions of all others via (1), I do not have any independence from (1).

The idea of destiny is the opposite of free will. That is, we cannot have free will. The simultaneity law says we are not free, we are working together. Our every present action depends on our previous actions and the actions of many other people. This works for every small detail of our activities. If I am used to drink both coffee and tea, then at break time whether I will take coffee or tea is not dependent on my free will. It will depend on what I have taken last time, how long before I took it, how is the situation of the coffee pot, if there is enough hot water, who else is there in the coffee room, etc.

There are many factors, including my own factors, and what others have done at the coffee room, will govern what I will drink now. A careful analysis will always show that everything is linked together simultaneously and instantaneously. The things happen so quickly inside our brain that most of the time we fail to recognize that we considered all the factors already, before we pour the coffee in our cups. Thus I do not create my destiny; it is created by many events and by many people working simultaneously, not only in this life but also by many people in many past lives. There is a global plan, and we are all following that plan and helplessly. The word helplessly (Avasah in Sanskrit) is important and is clearly pointed out in Gita (verse 3:5).

Einstein believed in precise destiny [28]. He said god does not play dice with the world. This destiny is also true according to Newton's theory as we explained above. The literature on the theory of relativity also talks about this global plan. It has been written in a physics book [29, p. 46] "Events do not happen; they are just there, and we come across them". Note that a simple logic will show that we cannot sit idle and let the destiny take us to the desired place. If it is not written in our destiny, we cannot sit idle. Moreover, the reincarnation examples show that we come to this world for a specific purpose, then why would I sit idle, why would I change my previous plan. Moreover, I am not my body, I am my soul. When I say I will sit idle, actually it means I am confusing my body with my soul. According to the spring mass analogy, I am constantly connected with everybody, and therefore I am moving all the time, and cannot stay idle.

The idea of destiny is really very simple. It simply means that there is a reason for everything. Whatever is happening now, there were reasons behind them in the past. Or in other words, present evolves from the past. This last statement is also same as the well known statement – as you sow so you reap. Thus destiny is very real and a trivial concept. Consider freewill – I want do something now, this clearly means - I have an idea and I want to try it – this idea becomes my reason or the cause for my action. The idea came first. Therefore it is not freewill anymore. Thus freewill is not really free, it is linked to the idea that I got minutes before, which is the reason, and therefore it is destiny.

In most cases we are not alone, it is not just my past activities, it is the past activities of many people. Corporation events, described earlier, are very good examples of daily destiny. Notice that it automatically means that I do not have any freedom while I am inside a corporation. This is also very obvious, because my daily life has been planned by me and jointly with others. We feel naturally very happy while we are in a corporation and know what we will do today. We just go, do our work, and come back home happily, knowing that we have executed our responsibility for today. Thus going with the flow, or obeying the nature made us happy. On the other hand if we had to make new changes, or plan a new work, and we had to choose, it would give us lot of stress. Thus inherently we do not like freewill, we like to go with nature and follow the destiny. Thus destiny is not a restriction; it is a blessing for us.

The idea of destiny also has some immediate consequences. Nothing can be good or bad in nature, because everything is planned. Similarly nothing can be improved in life after life according to my wishes. The universe is under a global plan. We are all here for a specific purpose. It is just like we are all here in a corporation, for a specific purpose: to create the product the corporation is manufacturing. All souls have same intelligence, they are all interconnected together. They are constantly in touch with each other. The only goal in every life cycle is physical death after we finish the project. Souls do not and cannot die or evolve. We cannot have god, because we cannot have freewill to meditate and find god. Everything is planned; if meditation is not planned for me I cannot do so. Thus god cannot appear and rescue me from my destiny cycles. Swami Vivekananda [30] says down with gods, down with God himself, I am all the God that ever existed, speak no more of God, I am the infinite.

A very thorough and systematic mathematical modeling method for the global plan is described in the paper [26]. It eventually leads to the derivation of equation (1) described earlier. But it must be recognized that practically it will be impossible to find exactly what will happen using even a very large computer. But the existence, not determination, of precise destiny can be proven using mathematics and the laws of nature. As we discussed, there are yoga mediation methods that can be used to find the future. This approach requires a completely different skill set.

Once we have the equations, like in (1), then we can imagine their solutions. The mathematical theory of differential equations ensures the existence of a solution under fairly realistic conditions. It has also been shown that the solution is unique under a given set of initial conditions. The theory also says that the solution can be extended in both directions of the initial time t_0, that is, from minus infinity to plus infinity on time scale. Thus the solutions can in theory, predict the past and the future. The solution of (1) represents the unique destiny of the entire universe or the global plan.

Many people suggest that uncertainty principle of quantum mechanics shows that the concept of destiny is not correct. But one should not rely on such principles, because physics and mathematics are based on many assumptions. As discussed later in another following section, nature cannot accept assumptions, and therefore the uncertainty principle cannot be correct. A detailed and thorough proof that uncertainty principle violates the laws of nature has been explored in [31]. More specifically, the uncertainty principle is based on Fourier Transform, which makes infinite time as an assumption. But infinity is not meaningful in nature. Replacing infinity by any finite value changes the uncertainty to certainty for all space time issues.

5.8 Selfless Karma

The idea of selfless karma or desire less work automatically comes from the simultaneity and reincarnation law. The idea says that we should all work with full honesty, sincerity, and devotion but never work for the result that we want. The reason is that a person does not and cannot know the result. Since everything is happening because of simultaneous effort of many people from many locations and over many time periods, including our past lives, we do not know what result to expect. All results are dependent on all efforts of many people. Nothing is isolated, humans are also not isolated, every

individual is a product of many past incarnations, thus future or the results will never be known using our simple crude knowledge of this life at this moment and at this location. A local view will always confuse us. Thus only way to create a satisfactory result out of our actions is to perform selfless work all along. All other efforts will violate the universal laws of nature. Only people with yogic skills can know such results. Using yogic skills it is possible to get a universal vision which allows yogis to see the universal truth. A highly sophisticated computer network, which tracks everything over many generations, may be able to predict correct and universal outcomes.

Thus the selfish work is bound to destroy our expectations, our peace in life, and the society in general. Since we are part of an evolving global plan, (defined by the simultaneity and reincarnation laws), which is not known to us, we cannot even know what we are working for. An employee can be laid off from his job, because the present system of capitalism is not under his control. Some CEO somewhere may be planning to sell the company for some other reasons. A student can get admission in a good school unexpectedly, maybe because the reviewer was a coworker of the student in their past lives, and thus helped the student to launch a great future career. We can never know how things happen in nature. But the action-reaction law, the simultaneity law, and the reincarnation law tell us that there is a reason for everything, and there is no randomness in our life. Interestingly, it seems Gita does not explain why results are not known, although selfless karma idea is originated in Gita. However, the reasons beyond our knowledge are discussed in Ramayan.

We should distinguish between Bible and Christianity, Quran and Islam, Vedas and Hinduism. These two groups, scriptures and religions, are two different things. It is like a knife. A knife can be used for cutting foods for cooking them, but it can also be used for killing people. Knife is a technology, it is a great invention. But how we use it depends on our society. Same is true for all scriptures for all religions. The religions should not therefore be confused with scriptures. Most importantly religions are dependent on money and money power. In the following few sections we briefly survey how reincarnation is treated in scriptures and also by corresponding religions.

VI. Reincarnation In Bible

A significant volume of public literature is available that presents existence of reincarnation in Bible. The book [32, p. 73] says there are many mentions in the Bible that can only be adequately explained in the light of reality of reincarnation. Smith says these can hardly be seen if Bible is read in a literalistic, dogmatic, and traditional way. The examples of burning bush, Cain, and Job when understood and taken collectively, according to Smith, establish the foundation of reincarnation in the Bible. He shows "how the Bible reveals reincarnation and its essential counterpart, the karma of humanity and of the individual soul".

In John 3: 1-12, there is one of the most concrete references to reincarnation. Here Christ the Master states, "Marvel not that I said unto thee you must be born again. The wind blows where it lists, and you hear the sound thereof, but cannot tell from where it comes, and where it goes: so is every one that is born of the Spirit" [33]. The last part of the sentence is a very clear indication of cycles of birth. The paper says there are at least thirty references in the Bible that directly or indirectly confirm the continuity of life. Robinson explains [33], how the commonly used statement against reincarnation, from Hebrews 9:27, in which Paul is the speaker, "And as it is appointed unto man once to die, but after that the judgment...", when placed in proper context will in fact corroborate reincarnation.

The book [34] provides another aspect of reincarnation in Bible. Most famous father of church, Origen (185-253 AD), undisputedly taught preexistence of soul. However, Origen's more than 2000 writings were nearly all burnt in the 6th century, so that researchers cannot today judge it from his original texts. Along with Origen many other Greek fathers made positive remarks about reincarnation. Rufinus (345-410 AD) translated some of the texts of Origen and openly admitted in correcting them so as not to run into conflict with Dogma. [34, p. 54] confirms the idea of power struggle in our life – "The Church accuses the reincarnation doctrine of teaching a path of self-redemption. A rivalry mentality of the Dogma seems to come through here, which doesn't want to permit any way to God, which isn't approved by the power structure of the Church".

As we have mentioned it is quite possible, like birthmark and birth defect cases, every aspect of our physical body is created by our soul, while in mother's womb, independent of any other conditions. Thus it is quite possible that the case of the blind person discussed in the Bible is also a birth defect case of reincarnation. Everybody is reincarnated; we just do not know, and may never know to what extent the body is reconstructed. John 9:2-3 declares: His disciples asked Him, 'Rabbi, who sinned, this man or his parents, that he was born blind?' 'Neither this man nor his parents sinned,' said Jesus, 'but this happened so that the work of God might be displayed in his life.'

VII. Reincarnation In Quran

This author did not find any comprehensive research that investigates the idea of reincarnation in Quran, the way it has been done, for example by [32] on Bible. Research in analyzing every verse, with reincarnation in mind, in the context of the global philosophy of Quran, appears to be missing. Many authors say that the Arabs, before Mohammad, believed in Reincarnation. Had there not been in the heart of Islamism a strong germ of esoteric teachings, Sufism could never have sprung from it. Quran was written after the death of Mohammad [35]. Mohammad's sons also died before him. Sufism has deeper connection with Mohammad's daughter.

Mainstream Islam rejects the concept of reincarnation. Believing in reincarnation into this world, in such a way that it could be interpreted as a denial of resurrection, may constitutes apostasy in Islam. A very few Sufi groups believe in reincarnation claiming that this concept is included in, "How can you deny God, when you were dead and God gave you life? Then God will cause you to die, and then revive you, and then you will be returned to God" (Quran 2:28). The

mainstream Islam however rejects this understanding of the verse, claiming that it refers to the worldly human life and the consequent resurrection in the hereafter [36].

Spanish-born Sufi poet Ibn Arabi (1164-1240) commented: There is some difference of opinion among the Muslim learned men as regards the method of Resurrection. Some of them say that Resurrection will be by reincarnation and quote passages from the Quran and authenticated sayings of the Prophet in support of their contention [37].

Another verse has been pointed out in [38]: "Set forth to them the similitude of the life of this world. It is like the rain which we send down from the skies, the earth's vegetation absorbs it, but soon it becomes dry stubble, which the winds do scatter: It is Allah who prevails over all things", Quran 18:45. However, the book also says, there are other verses that contradict the above in the Quran. Hence, more orthodox Muslims strongly contest the Sufi view.

Besides Sufi communities, Druze and Alawi are two Islamic sects, most numerous in Lebanon, Syria, and Turkey; who recognize reincarnation concepts. There are many, among them, who are also skeptics about the phenomenon. At the same time [38] there are others who discuss stories and maintain openness about the phenomenon. Interestingly, on both ends of the spectrum there is a guardedness associated with the talk of reincarnation because of sensitivity to outside perceptions. The above paper [39] presents some audio taped details of real life reincarnation stories among Druze families.

VIII. Reincarnation In Hinduism

In this section, we call Indian scriptures as the subjects that originated from Shruti. Shruiti is a non-mechanical sound of nature that can be heard (or seen) only after attaining certain level of mind by extensive yoga meditation. According to Swami [40], all books written before Buddha originated as Shruti. As per recent discovery [41], the latest date of Mahabharat is before 7500 years. Thus Ramayan which predates Mahabahrat, and Mahabharat should be considered as Indian scriptures.

Samkhya Karika [42] provides the most brilliant scientific theory in the shruti collection of Vedic system. It is credited to Kapila muni. In Gita [43] verse (Gita 10:26) Krishna has been defined as – "… among perfected beings I am the sage Kapila". Mahabharat says [44, Vol. 10, p.8] –"There is no knowledge that is equal to this (Sankhyas). Do not yield to any kind of doubt. The knowledge which is described in the system of the Sankhyas is regarded as the highest." Vivekananda [45], a famous Indian philosopher of modern time, says the following – "This wonderful man, the most ancient of philosophers, is mentioned even in the shruti - O lord, thou who produced the sage Kapila in the Beginning".

According to Samkhya Karika, the human body is associated with three kinds of objects (1) the soul (2) the subtle body and (3) the gross body. We can see and feel only the gross body. We cannot see the other two. Only through extensive yoga meditation one can acquire the knowledge of the other two objects. The soul never reincarnates, the subtle body is everlasting and incarnates, and the gross body is perishable. The subtle body consists of Intelligence (Mahat), I-Principle (Ahankar), eleven sense organs, and five primary elements (tanmatras). However the soul is intimately tied with other two objects. The soul is like perfume on a garment; and garment is the subtle body [42].

It is the subtle body that reincarnates after death, as we can read in Samkhya verse (SK:40) – "The mergent subtle body, produced primordially, unconfined, constant, composed of the tattavas beginning with Mahat and ending with tanmatras, transmigrates, free from experience, and tinged with dispositions". The translator of Samkhya uses the word transmigration instead of reincarnation. But Samkhya does not say that humans can take birth as non-humans.

Creation happens, according to Samkhya Karia, when the soul (Purusa) interacts with nature (Prakriti). At this time nature creates the subtle body components (tattavas) in the following order: Intelligence (Mahat), then I-Principle (Ahankar), then 11 sense organs, and finally five primary elements (tanmatras). The subtle body is so subtle that it can pass through the mountains [42]. The soul never reincarnates, is stated in (SK: 62) – "Thus, verily, Purusa is never bound, nor is he released, nor does he migrate. It is the Prakriti, being the support of manifold creation that migrates, is bound and is released". Thus subtle body is considered as part of nature, however, the soul remains identified with the subtle body for eternity.

The well known Hindu scripture Gita basically explains the Samkhya Karika in its own simpler way, as a dialogue between two persons Krishna and Arjun, so that the common people can understand the concept of reincarnation. Presenting theories in the form of dialogue is an important method for presenting complicated idea. Using FAQ (frequently asked questions) in modern websites essentially is a similar concept. The Sanskrit word Samkhya has been used in verse (Gita 5:4)- "Only the ignorant speak of devotional service (karma yoga) as being different from analytical study of the material world (Sankhya). Those who are actually learned say that he who applies himself well to one of these paths achieves the results of both" [43].

The verse (Gita 2:20) reconfirms, as stated in Samkhya, that soul does not reincarnate – "For the soul there is neither birth nor death at any time. He has not into being, does not come into being, and will not come into being. He is unborn, eternal, ever existing and primeval. He is not slain when the body is slain".

Gita says there is no discontinuity in characteristics of the subtle body; although from reincarnation examples we can see that there can be large break in time and space between two births. Thus the life continues from the end of one birth, to the next birth, without interruption of continuity of the subtle body. The verse (Gita 8:6) confirms "Whatever state of being one remembers when he quits his body, O son of Kunti, that state he will attain without fail". There are many real life examples of reincarnation which reflect concept of continuity in the above verse.

The ideas behind subtle body, like the concepts of intelligence, I-principle, and sense organs are buried in the verse (Gita 5:23)- "Before giving up this present body, if one is able to tolerate the urges of the material senses and check the force of desire and anger, he is well situated and is happy in this world". If the reverse happens, then the imprint of the gross body will be placed on the subtle body, creating the possibility of birth marks. This explains that although 20,000 people die every

year in USA due to gunshot wounds, but only a very small fraction of them talk about their past life wounds in the present body.

Both Ramayan and Mahabharat give at least one example of reincarnation in their stories. In Ramayana we see [46, pp.1607-1610] that Sita, the main female character, is the reincarnation of Vedavati; and in Mahabharat [44, Vol.5, p. 266] we find Shikhandin reincarnated as a man from her previous life as woman named Amba.

It should be recognized that besides reincarnation law, Ramayan and Mahabharat also talk about the other laws of nature like, cause and effect, destiny, theory of karma, law of conservation, simultaneity law over multiple life spans etc.

IX. Discussions

People have raised the issue that:

If reincarnation is a law of nature, then why is it not catching on with the people? (5)

The answer to question (5) is quite complex. However, its answers are both Yes and No type. We discuss them in this section, in some short details.

The answer to (5) is yes, because reincarnation theory is becoming popular, and various surveys show that nearly 20% [47] of the populations of various countries in the west believe in reincarnation. Moreover many Christians do not know that reincarnation was edited out from Bible around 375AD. If this fact becomes known then their believe system will change. Many books have come out recently about reincarnation. Carol [17] has become quite well known in USA for her research and books on this subject. She has documented a large number of reincarnation case histories on children of USA. There are many people who have started giving lectures on related subjects; many organizations have come up in the Yoga community who also talk about the related subjects. The word Karma and even Nishkam (selfless) Karma have become reasonably popular in English vocabulary. These days about 30% of populations in USA cremate their dead bodies [48], the idea of which originates in reincarnation.

Reincarnation has been used to make money also. Both USA and India have made many films based on soul theory and reincarnation. Academy award winning Indian director Satyajit Ray has made a film: The golden fortress (Sonar Kella), in 1974 based on past life memory of a child. A film on past life romance based on a novel by Indian Nobel Laureate in literature Rabindra Nath Tagore called Hungry Stone (Khudito Pasan) in 1960 has been made. Disney channel movie [49], Wendy Wu: Homecoming warrior, based on reincarnation broke records in UK and Europe in 2006. The 1998 academy award winning film: What dreams may come, was not a box office hit but was based on soul world. Such films, based on reincarnation and soul theory, have the potentials of breaking all barriers of race, nationality, and religion and creating a harmonious real world based on laws of nature.

The experience of reincarnation, although a global phenomenon, somehow has become tied with India and Hinduism. Fifty years back India was a poor country, so no one wanted to recognize its impact in the world. Today India is rich again, and it will begin to influence the world thoughts gradually. Moreover Internet technology will also help to propagate the concept. Very soon, may be within 50 years, reincarnation will become known to everybody and more than 50% in the west will start believing in it.

And the No answer to the question (5) is because of two important forces, money and science, that work against the reincarnation law of nature. We discuss the underlying problem briefly in the subsections below. It has to do with Money Power (MP) and Science Power. The MP case is quite obvious but the science case is very deep rooted, trivial also, and all engineers know about it. The subjects discussed below are well known to 1% of the community, but the vast majority of the population is kept under secret. A little investigative research, however, will always reveal the real universal truth.

9.1 Money Power

In this subsection we discuss the concept of money power, the owners of this power, its remote control capability, its pervasive characteristics, and how helpless we are under its control.

Objective of Money Power (MP)

Money is the most important control variable in our society. The same money is used everywhere in the world. It is used in our education, business, research, health care, manufacturing of food, philosophy, and religion. No one can escape this remote control capability of the money power (MP). The fundamental control objective of money is that no one should know or find out the truth of anything – including reincarnation and MP. As Carroll [24, p. 465], a mentor of US President Bill Clinton, says Britain has two groups: classes and masses. In his book he said education for classes has three negatives and one of them is that it must not find the truth. It appears that the same philosophy has now spread all over the world for all groups. We show with examples that, it is indeed the case in our life.

Central Bank (CB)

Most of us do not know that the source of money is the central bank (CB). In USA it is the Federal Reserve Bank (Fed). CB is a privately owned bank and is a very highly secretive organization. In some countries CB may be government owned, however, the money supply and control function of CB is still in private hands. Only CB can print money, and give it to anyone it wants, by any amount, and without any transparency and accountability. In 2008 the Bloomberg News sued the

Federal Reserve claiming that the Fed paid secretly $12.8 trillion dollars for bailout money [50]. The GDP for USA was $14.2 trillion at that time. Thus money supply is unlimited and free for the CB.

Money is not an object of nature. Money is not the paper or the coin, it is the value associated with it. Thus we cannot see, touch, and feel anything about money. So money, not being an object of nature, cannot follow the laws of nature too. Therefore money has to be false, free, and abundant. Unless we understand this real nature of money, it will be difficult to understand economy and the money power.

A little thinking will establish that money has to be free, because everything in nature is given to us as free. How can then something have a price? Thus we have distorted our society, created false money, and then using this false money the CB is controlling every activity of everybody. None of us can do anything against the objectives of the CB, and we all know this very well. That is why the Nobel Laureate in economics, Milton Friedman, said: "One unsolved economic problem of the day is how to get rid of the Federal Reserve" [51]. So naturally the goal of CB will be to prevent the discovery of truth. That is, if people find the real truth of any subject, then eventually people will discover the real truth about CB, which must be prevented. However, as mentioned before, 1% of the population always knows all the universal truths.

A past chairman of the Fed, [52] said no government has any power over this bank. CB is very powerful. It controls our government, military, CIA, FBI, Police force. CB is the King of our time. It is the most powerful king that the world has ever seen in its entire history. It rules the whole world using its MP. At one time, during imperialism, the world used to be controlled by the philosophy and the objective of the king. Now it is controlled by the philosophy and objective of the CB. The government cannot control the CB; the CB controls the government by controlling the supply of money to the government. More technical details of these ideas, facts, data, references, and information from publicly available and well authenticated research are collected and provided in the economics paper [53].

CB and Global Plan

It should be recognized that CB has done an extremely good job all over the world. Whatever good things have happened, today in our world has happened because of the CB. All wars were financed by banks and therefore by the CB, including the WW2. Today two billion people of India are free because of WW2. US presidential candidate Patrick [54, p.295] wrote - "As it was, Britain was dragged into an unnecessary war, which cost her nearly 400,000 dead, bankruptcy and the dissolution of the British empire." CB helped to destroy slavery from USA, apartheid from South Africa. Today we do not see any king anywhere. Most of the dictators are also gone. After implementing globalization by USA, national boundaries are vanishing, which is an ideal concept, derived from the law of reincarnation, and which as mentioned before says: souls do not have nationality.

After the 9-11 attack in New York, USA started the Afghanistan and Iraq Wars. These two wars created the immediate opportunity to install the CB in Afghanistan and Iraq. Only two more countries, Iran and North Korea, do not have western style CB. Once they are taken over, CB will have the full control over the world, and will truly become the global king. After that is achieved, and the world is stabilized for some length of time, it will be worth seeing what CB has in its global plan. According to simultaneity law this global plan has been created by many people from many different corners of the society, however, basically under the supervision of the CB. We must take a global view to understand the CB.

If money is removed from the world by CB, then that move will bring heaven on earth. Because of the modern networked computerized technology, it will be possible to create a moneyless economy [55], which will run this exact same economy we have now, in the exact same way, without any kind of money, and yet will provide the lifestyle anyone wants. In the meantime however, the world is suffering significantly due to poverty, and will continue to suffer. In the following subsections we track the root causes for this.

Printing Money

Assume that the total material wealth of a nation (GDP) is equivalent to a pot of gold. Similarly assume that the total money available (M3) is a bag of dollar bills. This bag of money has an one to one relationship with this pot of gold. This bag of money was used to create that pot of gold. By the law of conservation (LOC) this pot of gold cannot grow. Therefore this bag of money cannot grow either, because this is equivalent to that pot of gold and is attached to it by the LOC.

As pointed out by the Bloomberg report [50], we know that the Fed can print another bag of money, out of thin air. This extra bag doubles the price of the pot of gold causing inflation. If this money is allocated only to the top fifth of the population then their share of the pot of gold will increase, changing the wealth distribution. According to the LOC, since the gold cannot increase, the share of the bottom fifth will then naturally decrease causing transfer of wealth. This transfer of wealth happens not only because the money share decreases for the bottom fifth, the price of gold also increases, and thus reducing their purchasing power.

Transfer of wealth

Profiting is one of the pillars in the foundation of capitalism headed by the CB. Let us first examine how profiting is against the law of nature and how it helps to transfer your wealth. Consider a company that manufactures writing pens at a total cost of $5 per pen. Now assume that the company sells it at $15 per pen making a profit of $10 per pen. Thus the cost of the pen for the CEO of the company is $5 but for you and me it is $15. Therefore every pen is taking away an extra $10 from

all of us. This process of profiting helps to take money away from the people and to accumulate it in the hands of a very small group of people causing inflation and transfer of wealth. The interest charging process is essentially the same activity also. These capabilities of CB violate of the law of conservation, which as we have discussed, says there is no win-win situation possible. By law of conservation the money and the material wealth or GDP are tied together by an one-to-one relation. Thus accumulating paper money is equivalent to transferring material wealth.

Both profiting and interest charging were immoral according to major religions. But now because of MP it is not only legal it is encouraged also [56]. Similarly, creating recessions are major ways to transfer wealth from bottom fifth to upper fifth of the population. Many people will become unemployed in recessions, there will be no jobs, and unemployed will lose their properties, which will be purchased by rich people at low price, causing large scale transfer of wealth. Thus the activities of CB implemented via capitalism like: profiting, interest charging, giving higher salary to a small group, creating recessions, printing free money, etc. are designed to create classes and masses or rich and poor.

Reincarnation

Capitalism measures people using money. Since money is false, this merit system has to be false also. In business two jobs are never equal and so no two jobs can be compared. Therefore two persons working on those two jobs cannot be compared also. Two persons have entirely different life trajectories based on past life reincarnations. Since past life experiences are playing important role in our present lives, as shown by examples of reincarnations, we cannot compare two persons using only present life. Thus recognition of reincarnation will create fundamental problems in the merit system promoted by money power.

The theory of capitalism requires "you only have one life to live". You will be judged and paid according to your achievements in this one and only one life. So, you make money anyway you can to live better. In Wall Street it is called IBGYBG, I will be gone you will be gone [56]. So remain quiet, obey the business, take money, and help CB. All these principles of capitalism like: - I control my life, I have free will, I am the boss etc. - are against the law of reincarnation. Thus reincarnation creates contradictions for capitalism. Therefore naturally the CB will try to make people go against reincarnation. The discovery of truth behind reincarnation must be suppressed.

Nishkam Karma

Karma means work and Nishkam means selfless work. The objective of any human being should be to perform his work in a selfless manner. Only then it will be possible to provide best performance to the humanity. Any amount of selfishness will hinder the search of true knowledge and will prevent proper application of that knowledge for producing high quality work. In most of our activities time is used as a tool to prevent us from performing nishkam karma. In USA it is a very common statement that – we never find time to make things right the first time, but we always have enough time to fix the problems created during first time. Thus time is an artificial constraint, which prevents discovery of truth using perfect and nishkam karma.

The way of capitalism is to make more and more profit. Central bank will give you more and more money if you make more and more profit. Thus exploit people, product, and services as much as you can to make profit. This is promotion of selfishness. Thus capitalism inherently prevents manufacturing of quality products; a fact which we see abundantly around us. In addition this more and more money makes us loyal to the CB. And we become part of money power. This also creates a larger and larger group of masses and smaller and smaller group of classes. These activities are against the objective of yoga, meditation, nishkam karma, and reincarnation; which are all derived from the laws of nature. The laws of nature represent the universal truth. However, they shake the foundation of capitalism, and destroy the money power. Both of which are controlled and managed by the CB.

Suppress the Truth

Keynes [57, p. 235-236], a father of economic theories, said – "By a continuing process of inflation, governments can confiscate, secretly and unobserved, an important part of the wealth of their citizens. By this method they not only confiscate, but they confiscate arbitrarily; and while the process impoverishes many, it actually enriches some. … The process engages all the hidden forces of economic law on the side of destruction and it does it in a manner which not one man in a million is able to diagnose". We should recognize that the government is controlled by the CB. The government is not an independent body; it cannot function without money supply, which is managed by the CB. Note that, the above quotation confirms the idea of – do not find the truth – only one in a million may know. For the survival of CB, all truth must remain suppressed and should not be discovered. Reincarnation law cannot be an exception.

If you pick any modern macroeconomics text book published in USA, you will find that it never mentions that (a) CB is a private bank and the source of MP (b) It cannot be controlled by government (c) CB controls the government by controlling the supply of money (d) CB is not transparent, not responsible to anybody (e) Money is free for CB and its supply is abundant.

Thus no economics student, including professors, will ever discover the true nature of CB, and money power, without ever taking a special research and investigation. The truth is always unique and universal. That means, something that is true in USA but is false in China cannot be an universal truth. Similarly, the concept that was true thousand years back all over the world but is not true now also cannot be an universal truth. Only all laws of nature are unique universal truth all over the world and for all time. Anything that violates the laws of nature must be false and should be removed from the design of society.

9.2 Science Power

Science is also a major force against reincarnation. People believe that science is correct, and think that reincarnation therefore does not have any scientific basis. However, we show here with some examples and logic that science is wrong, it does not and cannot work, and therefore there is no concept like scientific basis. Money Power (MP) cannot allow science to find any truth. The CB has heavily invested in math and science and has created the science power to keep people away from real truth. As we have mentioned money is false; how can then a false thing be used to find truth? You cannot.

Are scientists against reincarnation theory? Actually any scientists will never be against it. By training a scientist must be an open minded person. Since, Professor Stevenson [7] has documented reincarnation in a very scientific way; the scientists can now read and understand the proof of reincarnation. These documents were not there before, so they were silent about the theory of reincarnation.

As a matter of fact, it is not necessary to understand science, to know that it is wrong. We can easily verify that it has to be wrong, from a philosophical point of view also. You have to accept only one truth: all math and science theories have assumptions. And it is obvious that nature does not and cannot make any assumptions. Therefore math and science are contradictory to nature, and so they are all false. However, we give one example to illustrate the details. A careful observation will show that assumptions do not make science and math approximate; they make them outright wrong as we show here.

Consider the example of Newton's first law [27, p.115], a very well known and popular law that we have studied in our high schools. This law has an assumption that says – "in the absence of any external forces". Let us investigate this assumption; if this assumption is wrong then we can say that the law must be wrong too. Clearly this assumption cannot be true, because there are always gravitational forces due to sun, earth, moon and many other heavenly objects of nature. There is no place in near earth and in deep space where there is no gravitation. Since earth is rotating, there is also a rotational force called Coriolis force. Thus the above assumption is wrong.

Obviously, nature does not and cannot make any assumptions in describing its laws. The nature must be taken as is. Therefore the nature's laws of motion cannot also have any assumptions. Thus the Newton's first law cannot be correct, because it comes with an assumption. Newton started with something that was misleading and confused all of us for centuries. The following statements, confirming our assertion, can be found in a physics textbook, [58, p. 8], about the Newton's first law: "We could hardly sustain that this principle (First law) is a strict experimental result. On the one hand it is not evident how to recognize whether a body is free of forces or not. Even if a unique body in the universe were thought, it is undoubted that its movement could not be rectilinear and uniform in every reference system". It is very easy to verify that if you leave a ball in deep space, it will not remain stationary as predicted by the first law. The ball will start moving and will change its speed as the time varying gravitational force changes. Thus the assumption did not make the law approximate, it made it wrong.

Every theory of physics and mathematics has an assumption about nature. Since nature cannot make any assumptions, all of these theories are wrong. We have explained it in the case of Newton's first law as an example. Many such examples are described in the paper [59]. This example confirms the theory that: education should not find the truth and is consistent with the objective of money power. Moreover, it is not possible for humans to understand nature. Humans are created by nature. Creation cannot know or understand the creator. For similar reasons, our computers cannot know humans, for example. At some point in the chain of questions on every subject, we have to accept the laws of nature without any explanation.

Consider an example from math: replacing infinity assumption by a large number does not make math approximate, but makes it completely wrong, consider the well known mathematical theory of Laplace Transform (LT) of a unit step function [59]. If you assume infinity in the definition of LT, then we get 1/s as its transform; which has a pole at s=0. But if we replace infinity by any finite value T, large or small, a little calculation will show the transform as $(1-e^{-sT})/s$, which has no poles at origin. Thus the entire characteristics of the LT will change for finite time systems. A similar change will happen for Fourier Transform also, making uncertainty principle of quantum mechanics as false.

The major problem of science is that it is not required to work. It works only on paper and pencil. When science is used in engineering we find that it does not work. This is because engineering, which uses natural components and natural materials, cannot make assumptions also, and must automatically follow natural laws. Engineers add lot of patches, kludges, and redundancies, to make the science and math work [59]. When you add patches, then the science is not a theory anymore, it is a patch work. Because engineering cannot make assumptions, engineering automatically eliminates all assumptions from science, making science invalid, because these theories work only under their assumptions. Science is used by CB to maintain the power of money. In this sense science indirectly prevents recognition or discovery of reincarnation law and all associated truths.

Many of our famous inventors, who changed the world, like Benjamin Franklin, Thomas Edison, Wright Brothers, Bill Gates, Steve Jobs, were not even formally educated. Thus science education is not necessary, that is because they cannot be used in engineering and are all wrong as illustrated with the examples above. We should not throw away reincarnation by saying it does not have a scientific basis, because there is no such thing as scientific basis. Science and education are controlled by money power. Therefore science carries the same objectives of the central bank – should not find the truth.

[1, p. 161] says reincarnation is not based on faith or belief system, it is an experience of the entire humanity. He asks more penetrating questions about science, for example, do we really know what electricity is. In reality we do not know. The law of conservation, which is a law of science, says that nothing can be destroyed or created. Since we know soul exists

when we are alive, therefore after death it cannot be destroyed, and similarly if soul does not exists, then at birth it cannot be created also. Therefore existence of soul at any time indicates reincarnation. Reincarnation is the only way to explain the natural phenomenon described by the examples given in this paper.

X. Conclusions

We have discussed three important types of reincarnation with real life examples. It is clear that birth defects type examples give a trivial proof of reincarnation. These examples cannot be denied by any logic. Then we explored scientific views and their links to the proof of reincarnation law. The paper explains how reincarnation law interacts with other laws of nature and creates the universal truth and our global plan. Some ideas on how our society can benefit from reincarnation are discussed. Discovery of some important research papers have shown how major religions like Christianity and Islam treat reincarnation. Some historical and original thoughts on reincarnation from Hinduism are also presented. They are a small fraction of the analytical foundations of reincarnation theory. The paper finally points out why and how our society is designed to suppress all truths including reincarnation.

XI. Acknowledgements

This paper is the result of several discussions by the author with many people and over a long period of time. The author wishes to acknowledge their valuable contributions and give sincere thanks to Dr. Sam Mohanta, Dr. Sukumar Sikdar, Tapan Majumdar, Sam Chakraborty, and Prof. Nirode Mohanty, Prof. Kalyan Datta, and Prof. Mrinal Kanti Ganguli. They not only contributed in thoughts, but provided many triggers that generated investigations and useful results. I must give sincere thanks to Dr. Nibir Datta, a close friend and a colleague, for his active participation in many discussions on various subjects of this paper. His many negative comments have motivated the author in many positive directions. Many times his single word or a sentence has significantly changed the contents of this research.

REFERENCES

[1] L. Govinda, The way of the white clouds, Boston, Shambhala, 1988, Pages 207.
[2] R. Almeder, Reincarnation Evidence: Stevenson's Research, Video, 2008, available from: http://www.youtube.com/watch?v=hZhMDU9GcVg
[3] C. Filice, The moral case for reincarnation, Religious Studies, 42, Cambridge University Press, Philosophy Department, State University of New York Geneseo, Geneseo, NY, 2006.
[4] M. Secrest, Omni magazine interview with Dr. Ian Stevenson, 1988, available from: http://reluctant-messenger.com/reincarnation-proof.htm
[5] C. Lightbourn, Past Life Therapy: An Effective Psychotherapeutic Approach, Master Thesis, A Research Paper, University of Wisconsin,Stout, 2006.
[6] S. Krishnanda, The philosophy, psychology and practice of yoga, The Divine Life Society, Sivananda Ashram, Rishikesh, India, 1983.
[7] I. Stevenson, Twenty cases suggestive of reincarnation, Ian Stevenson, Univ. press of Virginia, Charlottesville, Second Edition, 1974.
[8] Primetime, Parents Think Boy Is Reincarnated Pilot, ABC News, June 30, 2005, available from: http://abcnews.go.com/Primetime/Technology/story?id=894217&page=1
[9] YouTube, Reincarnation- past life evidence (P 1), 2007, available from: http://www.youtube.com/watch?v=_EWwzFwUOxA
[10] I. Stevenson, Birthmarks and Birth Defects Corresponding to Wounds on Deceased Persons, J. Scientific Exploration, Vol 7, No. 4, 1993, pp. 403-410.
[11] S.K. Pasricha, J. Keil, J.B. Tucker, and I. Stevenson, Some Bodily Malformations Attributed to Previous Lives, Journal of Scientific Exploration, Vol. 19, No. 3, 2005, pp. 359-383.
[12] S. Sivananda, What becomes of the soul after death, Divine life society publication, WWW edition, 1999.
[13] S. Rama, Living with the Himalayan Masters, Himalayan institute press, 2007, 153 pages.
[14] CBS, Bluejay spreads his wings, 60 Minutes, February, 2009, available from: http://www.cbsnews.com/stories/2006/11/22/60minutes/main2205521.shtml?tag=currentVideoInfo;videoMetaInfo
[15] Hydrogen, 2011, available from: http://en.wikipedia.org/wiki/Hydrogen
[16] BBC, Supernatural Science - Previous Lives (English), 2011, http://www.youtube.com/watch?v=iq64XvwqzyQ
[17] C. Bowman, Children's Past Lives, ISBN 0-553-57485-X, 1998
[18] I. Hickman, Past life regression - a case of migraines, 1959, http://www.deeptrancenow.com/exc2_migraines.htm
[19] P. Yogananda, Autobiography of a yogi, Self-realization fellowship publisher, Los Angeles, CA, USA, 1979.
[20] 3D Max Media, 2011, YouTube, The Fire Yogi http://www.youtube.com/watch?v=aj7iqdj1wT8
[21] Telegraph, The True Story of Sadhu Haridas, a 19th Century Yogi Phenomenon, London Telegraph,August 22, 1880. http://www.martialdevelopment.com/blog/yogi-stops-heart-for-six-weeks/
[22] H. Wambach, Reliving Past Lives, New York, Harper & Row, 1978.
[23] Gallow, Travel at Speed of Light, Uploaded by gallowspole2002bd on May 5, 2010, http://www.youtube.com/watch?v=9EXxzfjwC1A
[24] C. Quigley, Tragedy and Hope: A History of the World in Our Time, GSG and Associates, 1975.
[25] A.C. Sutton, Wall street and the Bolshevik revolution, 2001, from: http://vho.org/aaargh/fran/livres5/suttonhitler.pdf
[26] S. Das, Conservation laws of nature, Journal of Applied Global Research, Vol. 5, Issue 12, 2012
[27] R.A. Serway & J.W. Jewett, Physics, for scientists and engineers with modern physics, 6th edition, Thomson, California, 2004.
[28] Kaku, Why Quantum Physics Ends the Free Will Debate, 2011, available from:

http://www.youtube.com/watch?v=lFLR5vNKiSw&feature=related
[29] A.S. Eddington, Space time and gravitation, Cambridge university press, 1920.
[30] S. Vivekananda, Soul and God, Lecture, San Francisco, March 23, 1900, http://www.vivekananda.net/booksbyswami/completeworks/CV1/Lectures/19_SoulandGod.html
[31] S. Das, Assumptions in Quantum Mechanics, International Journal of Theoretical and Mathematical Physics, Scientific & Academic Publishing, Vol. 3, No. 2, 2013, pp 53-68.
[32] E.R. Smith, The soul's long journey, how the bible reveals reincarnation, Steiner books, 2003.
[33] L.W. Robinson, Reincarnation and the scriptures, Vol IV, No. 25, The Searchlight, Virginia Beach, Virginia, 1952.
[34] J.E. Sigdell, Reincarnation, Christianity and the Dogma of the Church, Unmasking the Myth that the Reincarnation Doctrine would be Unchristian, Ibera, Vienna, 2001.
[35] T. Pascal, Reincarnation - A Study in Human Evolution, Theosophical publishing society, London, 1910.
[36] M. Marathakam, Reincarnation, the art of transmigration, from the Web, ND.
[37] J. Hall, Reincarnation in world thought, from Web, ND.
[38] Rumi, The secret meaning, Rumi's spiritual lessons on Sufism, 5th edition, 2011.
[39] A. Bennett, Reincarnation, sect unity, and identity among the druze, Ethnology, Vol. 45, No. 2, 2006, pp. 87-104.
[40] S. Purnatmananda, Core messages of Vedanta, Lecture (in Bengali), Udbodhan, September, 2012, pp. 656-666.
[41] G. Hancock, Underworld: Flooded kingdoms of the Ice age, February, 2011. http://www.youtube.com/watch?v=nQZFS9Hij0M
[42] S. Virupakshananda, Samkhya Karika of Isvara Krsna, Ramakrishna Math, Madras, India, 1995.
[43] A.C.B.S. Prabhupada, Bhagavad-Gita, as it is, Bhaktivedanta book trust, USA, 1994.
[44] P.C. Roy, The Mahabharata of Krishna-Dwaipayana Vyasa, Bhishma parva, Vols. 1-10, Translated into English prose from the original Sanskrit text, Oriental publishing, Calcutta, ND.
[45] S. Vivekananda, Practical Vedanta, 12. A study of Sankhya philosophy, Lecture delivered in London, 1896.
[46] M.M. Dutta, The Ramayana, Uttarakandam, Translated into English prose from the original Sanskrit of Valmiki, Vol. 4, Calcutta, 1894.
[47] Wikipedia, Reincarnation, May, 2012, http://en.wikipedia.org/wiki/Reincarnation#Reincarnation_in_the_West
[48] L. Miller, We are all Hindus now, Newsweek Magazine, Aug 14, 2009, http://www.thedailybeast.com/newsweek/2009/08/14/we-are-all-hindus-now.html
[49] Wendy, Wendy Wu: Homecoming Warrior, Disney channel original movie, 2006, http://en.wikipedia.org/wiki/Wendy_Wu:_Homecoming_Warrior
[50] M. Pittman & B. Ivry, Financial Rescue Nears GDP as Pledges Top $12.8 Trillion (Update1), Bloomberg, March 31, 2009.
[51] D. Levy, "Interview with Milton Friedman", The federal reserve bank of Minneapolis, June 01, 1992, http://www.minneapolisfed.org/publications_papers/pub_display.cfm?id=3748
[52] A. Greenspan, Video, Let Greenspan tell you what fed is, Sept 06, 2009, available from: http://www.youtube.com/watch?v=qIQTu7kOT_8&NR=1
[53] S. Das, Federal Reserve's Plan to Transfer Wealth, Conference proceedings, Northeast business and economic association, Philadelphia, Pennsylvania, USA, Nov 3-5, 2011, pp. 564-570.
[54] P. Buchanan, Churchill, Hitler, and the Unnecessary War**:** How Britain Lost Its Empire and the West Lost the World, Crown Publishers, NY, 2008, 518 pages.
[55] S. Das, "Moneyless economy", The business review, Cambridge, Vol. 20, No. 1, Summer, 2012, pp. 17-25.
[56] J. Crotty, The Bonus-Driven Rainmaker Financial Firm: How These Firms Enrich Top Employees, Destroy Shareholder Value and Create Systemic Financial Instability, Political economy research institute, University of Massachusetts, Amherst, 2010.
[57] M.J. Keynes, The economic consequences of the peace, Harcourt, Brace and Howe, New York, 1920.
[58] R. Ferraro, Einstein's Space-time, Springer, 2007.
[59] S. Das, "Rethinking embedded system design", International Journal of Engineering (IJE), Volume (6), Issue (2), 2012, pp 70-85.

International Journal of Modern Engineering Research (IJMER)
www.ijmer.com Vol.3, Issue.2, March-April. 2013 pp-1212-1219 ISSN: 2249-6645

Proteus Based Simulation of PV Inverter for Rural Electrical Service

Mohammed Shoaib, [1] Prof V. Nagaraj[2]
[1]*Department Of Electrical &Electronics engineering,*
[2]*Assoc.Prof. (Senior Scale), Manipal Institute of Technology, Manipal University, Manipal, India*

Abstract: *In many remote or underdeveloped areas, direct access to an electric grid is impossible and a photovoltaic inverter system would make life much simpler and more convenient. With this in mind, this paper aims to design, and simulate PV inverter in proteus professional software. This inverter system could be used as backup power during outages, battery charging, or for typical household applications for rural especially. The principle is to adapt the output voltage of the solar module to the battery by using the technique of pulse width modulation (PWM). The sinusoidal pulse width modulated (PWM) waveform is generated from inverter in laboratory by 16 bit microprocessor through program developed using a novel technique of direct modulation strategy .The key features of the system are a true 50Hz, 230Vsinusoidal voltage output, a wide input range, and a power output of up to 350 watts. The overall goal is to design this system while minimizing component costs.. In addition, inverters in the lower price range typically lack most of the features. solar home lighting systems mostly comprises of solar panel, solar charger, battery & a inverter, The main motivation of this paper or the uniqueness of this project is to combine both the solar charger as well as inverter together to ATMEGA 32 RISC based which works up to 16MIBS which reduces the cost as well as the system becomes compact.*

Keywords: *Pv, Pwm, Mcu, Proteus, Dpwm, Pwm Charger.*

I. Introduction

India s off-grid solar (PV) market has three major segments: captive power plants (where the majority of generation is consumed at the source), telecom towers, and rural electrification. The market potential for these PV segments has created an off grid solar market in India. India like other developing countries has made tremendous progress in producing energy in agriculture sectors. However, it lags behind in meeting the entire energy demand in remote rural and its nearby suburban or urban areas. As a result, our country is facing acute shortage of power especially in those village areas where utility grids are either not available or its further extension is not possible due to costly affair. Even in the sub-urban or urban area of these villages where utility grids are available, only 20% electricity is available for end users and so they lack such basics of human need as lighting, irrigation, communication, primary health care facility, safe drinking water, education etc. Renewable energy is the only feasible option to electrify these villages and its surrounding areas.

Along with increases of demand for the new energy, and the key technologies of use new energy sources is how to integrate new energy into electrical energy. In this paper high computing speed, low-power single chip MCU ATMEGA 32 is used as the control chip, improve the inverter efficiency. This article also describes the structure of the inverter, control methods, focuses on software design and finally summarized.

The primary function of a charge controller in a stand-alone PV system is to maintain the battery at highest possible state of charge while protecting it from overcharge by the array and from over discharge by the loads [1]. Although some PV systems can be effectively designed without the use of charge control, any system that has unpredictable loads, user intervention, optimized or undersized battery storage (to minimize initial cost) typically requires a battery charge controller. The algorithm or control strategy of a battery charge controller determines the effectiveness of battery charging and PV array utilization, and ultimately the ability of the system to meet the load demands. Additional features such as temperature compensation, alarms, meters, remote voltage sense loads and special algorithms can enhance the ability of a charge controller to maintain the health and extend the lifetime of a battery, as well as providing an indication of operational status to the system caretaker.

Important functions of battery charge controllers and system controls are to [2]:

- Prevent Battery Overcharge*:* to limit the energy supplied to the battery by the PV array when the battery becomes fully charged.
- Prevent Battery Over discharge: to disconnect the battery from electrical loads when the battery reaches low state of charge.
- Provide Load Control Functions*:* to automatically connect and disconnect an electrical load at a specified time, for example operating a lighting load from sunset to sunrise.
- A series charge controller or series regulator disables further current flow into batteries when they are full. A shunt charge controller or shunt regulator diverts excess electricity to an auxiliary or "shunt" load, such as an electric water heater, when batteries are full.

Simple charge controllers stop charging a battery when they exceed a set high voltage level, and re-enable charging when battery voltage drops back below that level. Pulse width modulation (PWM) [2] and maximum power point tracker (MPPT) technologies are more electronically sophisticated, adjusting charging rates depending on the battery's level, to allow charging closer to its maximum capacity. Charge controllers may also monitor battery temperature to prevent overheating. Some charge controller systems also display data; transmit data to remote displays, and data logging to track electric flow over time [4].

II. System Block Diagram

2.1Inverter Drive circuit and Filter circuit design.

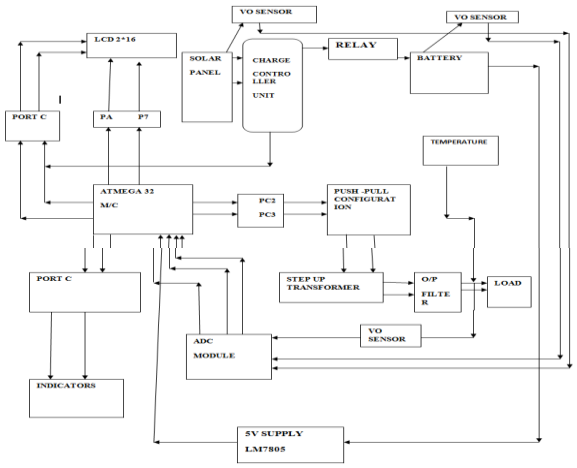

Figure: 1

ATMega32 microcontroller: It acts as the heart of the system. It controls and monitors entire system. The main function of this microcontroller is to generate SPWM signals. These signals are given to Half-bridge switches to convert dc voltage to ac voltage. Microcontroller also takes care of the protection. It protects the load from over voltage, under voltage.This system includes a feedback network where at the output AC is converted to DC using bridge rectifier and is properly isolated using an npn based opto coupler and a voltage divider circuit which is fed back to adc module of MCU and output voltage is regulated by controlling the duty cycle of the DPWM.

In the present work sinusoidal pulse width modulation (SPWM) technique is used to control the switches of the Halfe-bridge. This technique is widely used in inverter to digitize the power so that a sequence of voltage pulses can be generated by the on and off of the power switches. The pulse width modulation inverter has been the main choice in power electronics, because of its circuit simplicity and rugged control scheme.

After analysis and comparison, the part of the contra variance use half-bridge inverter circuit, Inverter Bridge is composed of FET IRF3205, using 2n3906 and 2 Bc547 as a driver circuit. Single-chip generated PWM signal, go though 2n3906 to control the inverter switching devices IRF3205 the shutdown of conduction, then inverter can produce sine wave outputs. But the sine wave contains many high-order harmonic generation, required the LC filter circuit to be smooth, non-standard high-order harmonic generation of sine wave. The size of capacitance and inductance values required theoretical calculations and the actual debugging to determine. In this design, we take C = 100uF, L = 40uH.

2.2 Pwm Control

A software program has been developed to generate sinusoidal pulses for N numbers in a half cycle using direct modulation strategy (DPWM) whose widths are proportional to amplitude of sine wave at sampled points (Fig.2). Mathematically the pulse width and corresponding notch width are expressed by (1) and (2) respectively as:

Pulse width (Pi)
*= K Pwm x 2 Sin (2i - 1) π / (2*N) . (1)*
Where,
i = 1, 2, 3,…..N
K = Voltage Factor (0 –1)
P wm = (D – G) * 2
D = 180 / (2*N)
G = Minimum Gap between pulses (say 1degree) at K=1
N = Number of PWM pulses in Half sine wave (180 degree i.e. = 10 ms)

Notch width (Ti) = 2D - [1/2(Pi – 1 + Pi)]. (2)

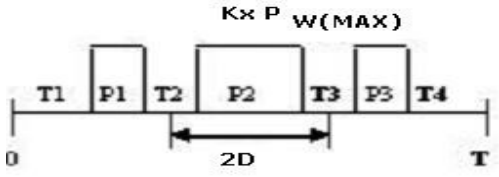

Figure 2: Programmable DPWM sinusoidal

Modulated (N = 3) half sine wave of 50 Hz . Y axis = Amplitude (5V), X axis = Total time (T) in half cycle i.e 180 degree =10ms.

III. System Software Design

3.1proteus Introduction

Proteus supports multiple mainstream microcontroller system simulation, such as 51 series, AVR series, PIC12 PIC16 series, PIC18 series, Z80 series, HC11 series, series, 68,000 series, etc. And provide software debugging function and its periphery connection device of RAM, ROM, keyboard, motor, LED, LCD, AD/DA, partial SPI device.

With the development of science and technology, the computer simulation technology has become an important sector of many design method of early. It is designed to be flexible, results, the process of unity. It can make the design time is shortened, cost reduction, also can reduce the risk of engineering. Believe in microcontroller application of PROTEUS can also have extensive application.

3.2Target specifications

3.2.1 Inverter specifications.

Frequency	50 Hz +/- 2Hz
Efficiency	>80 %
Output	350 watts, 12VDC ~ 220 V +/- 5
Harmonics	<5 %
spwm	Sine wave inverter
Mobility	Portable, microcontroller based
Protection circuits	yes

Table1

3.2.2 Solar charge controller specification:

- Prevents battery from being overcharged and damaged by the solar panel
- Compatible with 12 volt battery bank
- Overload, short circuit, and reverse polarity protected.
- LED's indicate charging status.

3.3 Simulation Results

3.3.1 pv inverter simulation

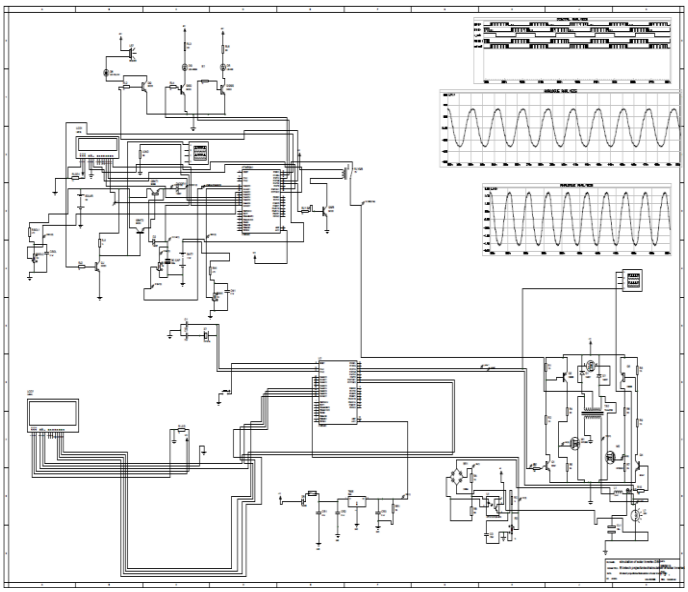

Figure 3: (Schematic of Proposed PV Inverter with battery charger.)

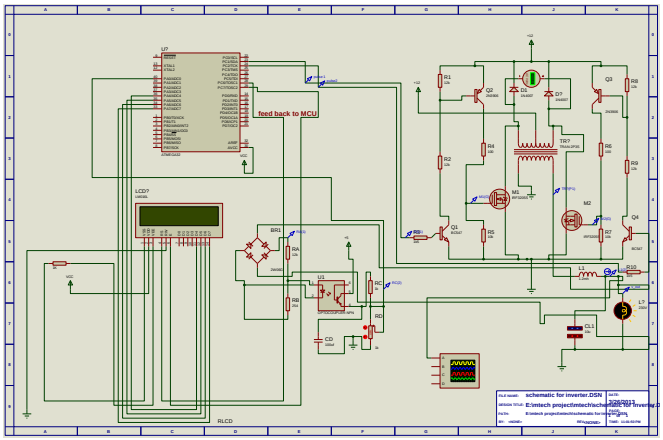

Fig4. (Schematic of inverter)

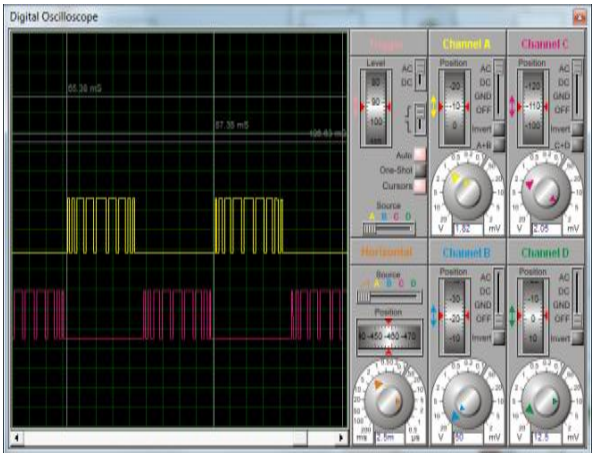

Fig5. (Pulse train drawing the mosfet T=20 ms, T_{ON}=10ms &T_{OFF}=10ms)

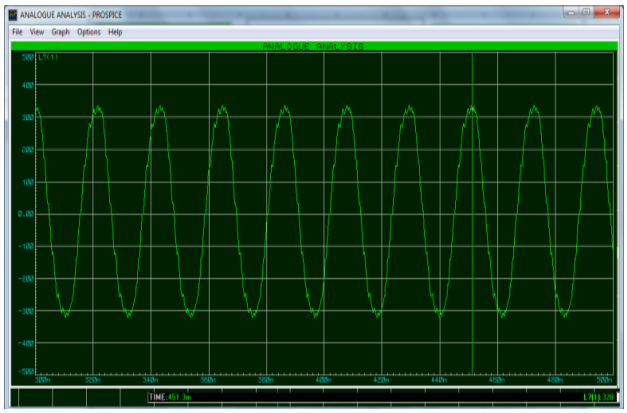

Fig6. (Output voltage waveform as per simulated resultsV_O=228 Volts).

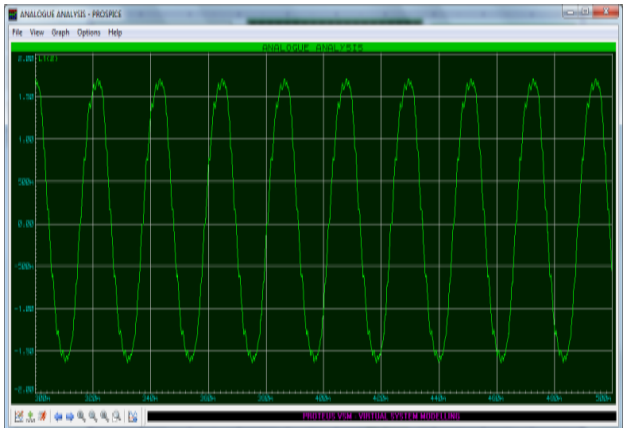

Fig7. (Current wave form as per simulated results I_O=1.7 Amps).

3.4 simulation of PWM charge controller

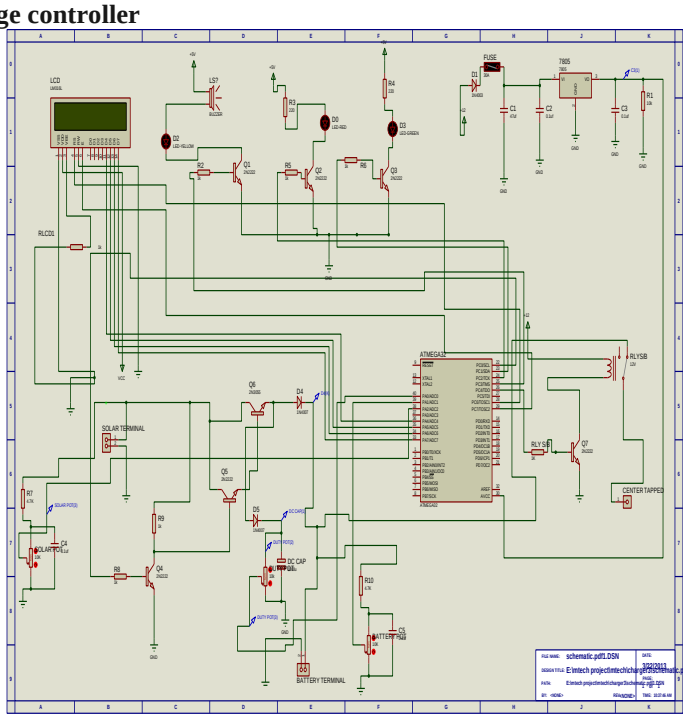

Figure 8(schematic of pwm based charge controller)

Solar Charge controller is a device, which controls the battery charging from solar cell and also controls the battery drain by load. The simple Solar Charge controller checks the battery whether it requires charging and if yes it checks the availability of solar power and starts charging the battery. Whenever controller found that the battery has reached the full charging voltage lavels, it then stops the charging from solar cell. On the other hand, when it found no solar power available then it assumes that it is night time and switch on the load. It keeps on the load until the battery reached to its minimum voltage levels to prevent the battery dip-discharge. Simultaneously Charge controller also gives the indications like battery dip-discharge, load on, charging on etc

OPERATION OF SYSTEM: Pulse Width Modulation (PWM) is the most effective means to achieve constant voltage battery charging by switching the solar system controller's power devices. When in PWM regulation, the current from the solar array tapers according to the battery's condition and recharging needs. In the fig 8 solar charge is controlled by controlling the duty cycle ,such that an optimum 13.75 volts is fed to battery for charging purpose.2N3055 NPN power transistor , Packaged in a TO-3 case style, it is a 15 amp, 60 volt is used as switching device Initially 50 %duty cycle is fed in MCU using PORT C0. As the solar voltage is unregulated the voltage is controlled by adjusting the duty cycle .Two reference voltage is fed in MCU, whenever solar voltage is < reference voltage V_1 (>> Pwm), similarly vice versa.

3.4 Simulation Results for PV Charger

The proposed charge controller is simulated by using Proreus ISIS 7 Professional for five cases listed in table 1 and the simulation results shown in figures 8-12.

Test no	Solar voltage	Battery voltage	Duty cycle%
1	18	11.0	96%
2	16	11.0	99%
3	10	12.0	35%
4	17	13.5	0%

Table 2

3.4.1Algorithm for Charge Controller

As microcontroller software works as sequential basis, it will perform these steps Sequentially.

1. Power On, RESET
2. Define Input / Output of the ports
3. Setup ADC for measurement
4. Start ADC Module
5. Measure ADC2, ADC3, ADC4, ADC5. ADC2 for 'Solar Voltage', ADC3 for 'Battery High Set', ADC4 for 'Battery Low Set' and ADC5 for 'Battery Voltage'
6. If 'Battery Voltage' < 'Battery High Set' and 'Solar Voltage' > 'Battery Voltage' then

a. Switch ON Battery Charging
b. Switch ON Charging LED
c. Switch OFF Battery High LED

7. If 'Battery Voltage' > or = 'Battery High Set' then
   a. Switch OFF Battery Charging
   b. Switch OFF Charging LED
   c. Switch ON Battery High LED
8. If 'Solar Voltage' < 'Battery Voltage' then
   a. Switch OFF Battery Charging
   b. Switch OFF Charging LED
   c. Switch ON Load
9. If 'Battery Voltage' < or = 'Battery Low Set' then
   a. Switch OFF Load
   b. Switch ON Battery Low LED
10. If 'Battery Voltage' > 'Battery Low Set' then
    a. Switch OFF battery Low LED
11. Go to Step 5.

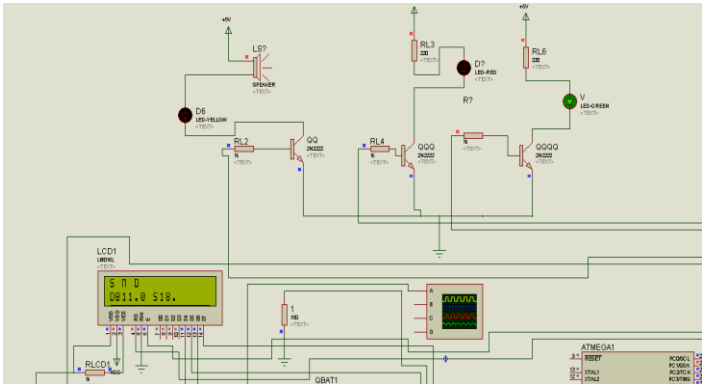

Figure: 9. (the above schematic refers to step no 6 of the algorithm).

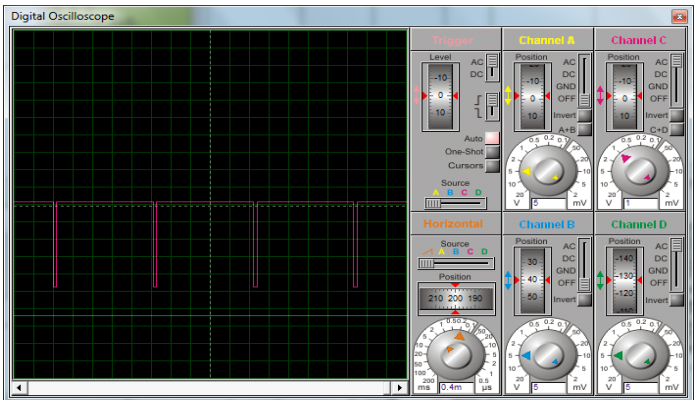

Figure: 10. Simulation Result for Test number 1(channel c represents the output of the MCU PWM signal)

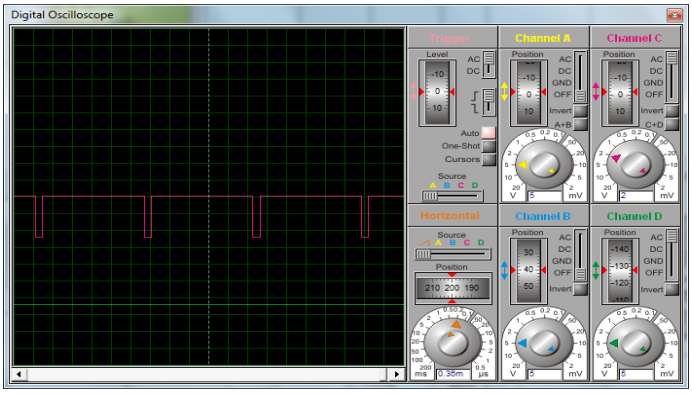

Figure: 11. Simulation Result for Test number 2(channel c represents the output of the MCU PWM signal).

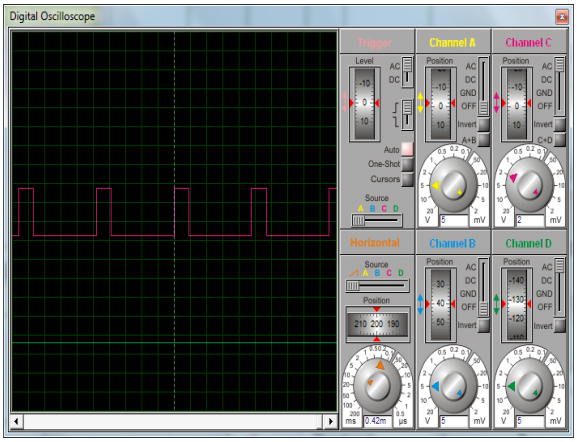

Figure: 12. Simulation Result for Test number 3(channel crepresents the output of the MCU PWM signal)

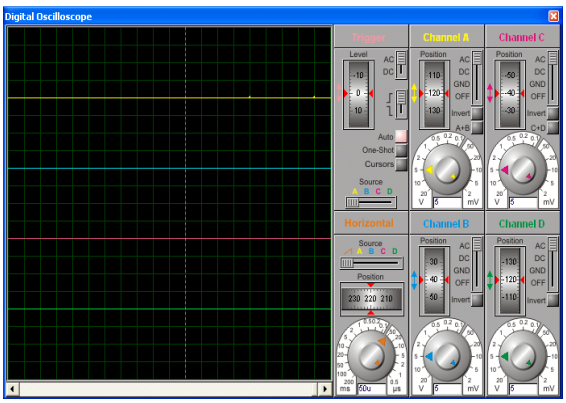

Figure: 13. Simulation Result for Test number 4(channel crepresents the output of the MCU PWM signal)

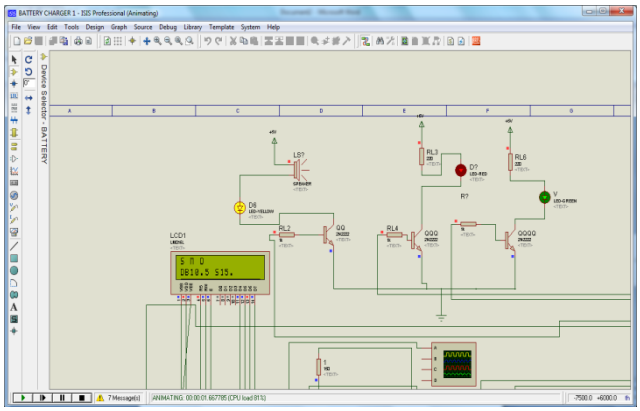

Figure13. (The above schematic refers to step no9 of the algorithm)

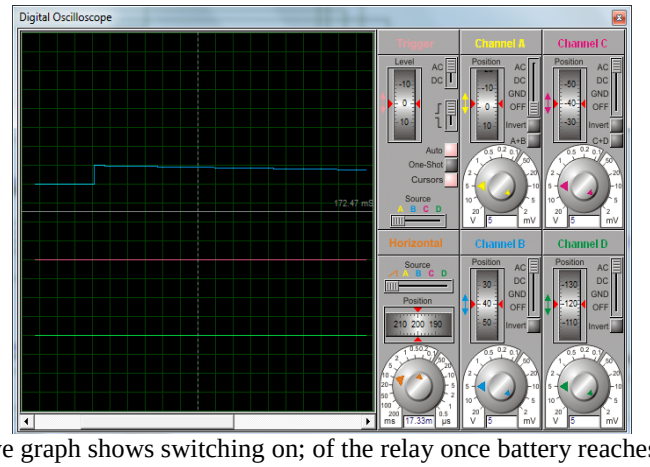

Figure14. (The above graph shows switching on; of the relay once battery reaches its low set point).

IV. Conclusion

The article is being simulated in the Proteus software, the hardware must be tested accordingly, Proteus not only make many MCU visualize, but also can visualize many MCU examples. Which is 80–90 % similar to real operating device? The above system does not require carrier signal or a comparator circuit as usually require in conventional triangular PWM generator circuit and thus reduces the cost as well as complexity in producing PWM base drive signals.

V. Acknowledgment

The authors pay their sincere gratitude to the Mr I.B rao the MD of power one Microsystems & the Management of Power one Microsystems ,Bangalore for funding this technical work.. The author also extends their heartily thanks to R&D Engineer Mr M. M. Venkateswaran & Mr Valache Siddalingappa, for their valuable time and effort for scrutinizing the design of the project.

References

[1] G.J. Vander et al, "150W Inverter – an optimal design for use in solar home system", International Symposium on Industrial Electronics, Proceedings ofISIE, 1998, Vol. 1, pp 57-62.
[2] B. Lindgrin, "A 110 W inverter for photovoltaic application", Published in International Journal of Renewable Energy Engineering, April 2002.
[3] S. Martínez, M. Castro, R. Antoranz, and F. Aldana, "Off-line uninterruptible power supply with zero transfer time using integrated magnetics," IEEE Trans. Ind. Electron, vol. 36, no. 3, pp. 441–445, Aug. 1989.
[4] M. T. Tsai and C. H. Liu, "Design and implementation of a cost-effective quasi line-interactive UPS with novel topology," IEEE Trans. Power Electron., vol. 18, no. 4, pp. 1002–1011, Jul 2003
[5] Adel Nasiri, Zhong Nie, Stoyan B. Bekiarov, and Ali Emadi, " An On-Line UPS System With Power Factor Correction and Electric Isolation Using BIFRED Converter" IEEE transaction on Industrial Electronics, vol, 55.no.2,pp. 722 - 730 ,February 2008.
[6] Ross, J., Markvart, T., and He, W.: „Modelling Battery charger Regulation for a Stand-alone Photovoltaic System" , Sol. Energy, 2000, 69, (3), pp. 181–190

ABOUT THE AUTHORS

MD SHOAIB has obtained his B.Tech degree in EEE from New Horizon College of engineering and currently pursuing his MTECH in power electronics system and control in Manipal University .His area of interest is power converters and embedded systems.

V.NAGARAJ has has obtained his ME in power systems from Mysore university, and He has 34years of teaching experience. He has published 2 research papers at national level. His area of teaching is Applications of soft computing systems to power Systems

International Journal of Modern Engineering Research (IJMER)
www.ijmer.com Vol.3, Issue.2, March-April. 2013 pp-1220-1228 ISSN: 2249-6645

Influence of grain refiner addition and heat treatment on the mechanical properties of Al-Si alloy

Anil Kumar. T, [1] Gajanan.Anne, [2] Dr N.D.Prasanna[3]
[1]*Asst. Professor, Dept of Mechanical Engg, M. S. Ramaiah Institute of Technology, Bangalore-54*
[2]*IV[th] sem M. Tech (MSE), Dept of Mechanical Engg, M. S. Ramaiah Institute of Technology, Bangalore-54*
[3]*Professor, Dept of Mechanical Engg, M. S. Ramaiah Institute of Technology, Bangalore-54*

Abstract: *In the present investigation, an attempt is made to study the effect of addition of grain refinement on Al-Si alloy, when it is subjected to the combined grain refiner addition (Al-5T-1B) and subjected to mechanical vibration and heat treatment. The material is tested for hardness property and dry sliding wear properties. The results of the present investigation indicate that there is a considerable improvement in the hardness valves, microstructure and resistance for wear.*

Keywords: *Aluminium-silicon alloys, Grain refinement, Heat treatment, Microstructure, Vibration*.

I. Introduction

Al-Si casting alloys play an important role in the field of cast aluminum alloys. They have been widely used in automobile, aerospace and engineering industries due to their excellent castability, weld ability, high corrosion resistance, thermal conductivity, ductility property, good mach inability etc. Many investigators (1) have reported the mechanism of grain refinement, and the development and usage of grain refiners (2). By refining the grain structure, improvement in some of the properties of castings is highlighted (3). Grain refinement involves the suppression of columnar and twinned columnar grains to produce equiaxed grain structure (4). The T6 heat treatment is associated with the decrease of secondary dendrite arm spacing, spheroidization of fine eutectic silicon and precipitation hardening. (5)The various techniques developed to achieve grain refinement of aluminum alloys are:

- Mechanical agitation of the molten alloy
- Rapid cooling
- Addition of grain refiners or master alloys to the melt
- Heat treatment

II. Experimental Details

2.1 Details of alloy

The alloy selected for the study is Al-Si alloy. The composition of the alloy was determined by subjecting the alloy to chemical test by optical emission spectrometer and the results of same is shown in table below.

Elements	Cu	Mg	Si	Fe	Mn	Ni	Zn	Pb	Sn	Ti	Al
%By Wt	0.04	0.41	6.82	0.34	Max0.03	0.02	Max0.07	Max0.01	Max0.03	0.08	Rem

Table 1: Composition of Al-Si alloy

2.2 Details of grain refiner

The refiner selected for the study was Al-5%Ti-1B.
Quantity of Al-Si alloy melted = 3.92kg
Percentage grain refiner addition = 2%
Weight of grain refiner to be added = (4000*0.02) = 80gms

2.3 Details of the permanent mould

Permanent mould made of EN 19 steel coated with mould coat and preheated to 300^0C was used in the present investigation. The details of the mould used is shown in figure-1

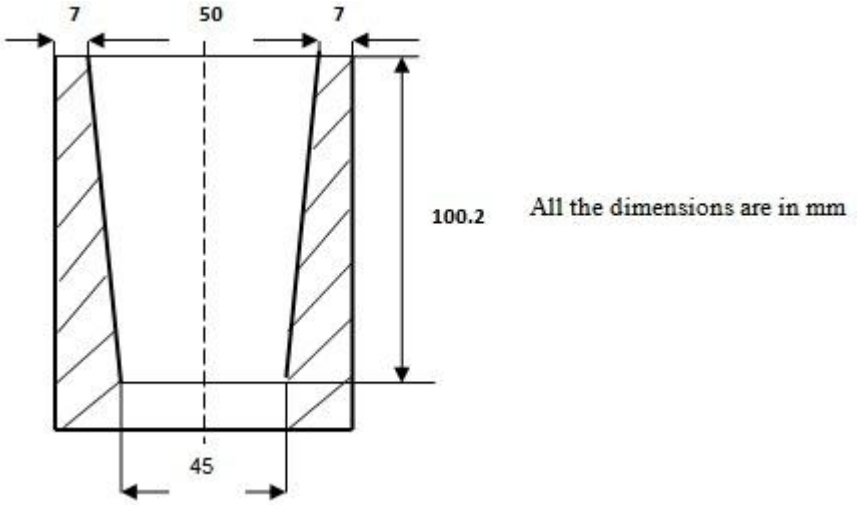

Fig.1 Details of the mould

2.4 Vibration set up

The detail of the vibration set up used in the present investigation to generate vibrations is illustrated in the block diagram.

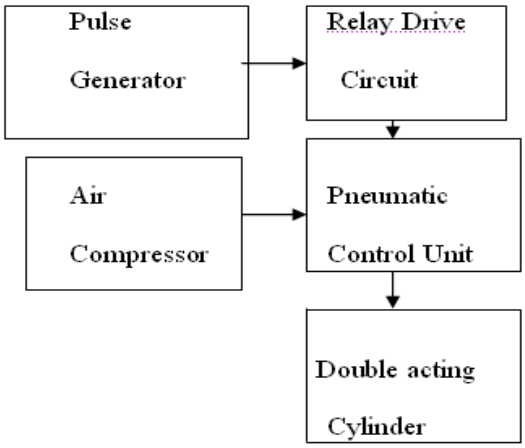

Fig: 2 Pneumatic vibration apparatus (Block diagram)

2.5 Specification of the set up

1. Switching mode power supply adapter: I/P: 100-240V,O/P: 12V, 1A The function of the above adapter is to convert A.C supply of 240V to D.C supply of 12 V.

2. Square Wave Pulse Generator: Figure: 3 show the photograph of the square wave pulse generator. This is used to supply current. The tests can be carried out by varying frequencies and amplitudes. Frequency Range: 1Hz to 1MHz, Amplitude: 0-5 V

Fig: 3 Square wave Pulse Generator

The tests were conducted by increasing (varying) the frequency levels and keeping amplitude constant. This will affect the rate of the movement of the piston in the cylinder. i.e it increases the rate of piston movement in turn results in the increase of vibration rate of the die (into which treated molten alloy is transferred).

3. **Relay Drive Circuit**: This essentially consists of a switching type NPN transistor (2N-3035)

Fig4: Relay Drive Circuit

This relay drive circuit is used to switch on and off the power supply to the solenoid controlled pneumatic control valve.

4. Pneumatic control unit: A single solenoid pilot operated valve with spring return mechanism was used. This unit operates in the pressure range 2-10 bar.

Figure5: Pneumatic control unit

The air flow can be controlled using solenoid controlled valves. Solenoid controlled valve is shown in Figure5a. The top of the valve body of the pneumatic control unit has two ports that is connected to a double acting pneumatic cylinder. The bottom of the valve body has a single pressure line (connected to air compressor) in the center with two exhausts at its sides. The solenoid is mounted on one side. When actuated (when the relay drive circuit switches to ON condition) it will drive the central spool towards the solenoid coil. In this position the air flows through the center port P to port A. Port A being connected to the bottom of the pneumatic cylinder results in making the die to move up. Presently air retained in the other side of piston is made to flow out of the cylinder through the port B and port R2.

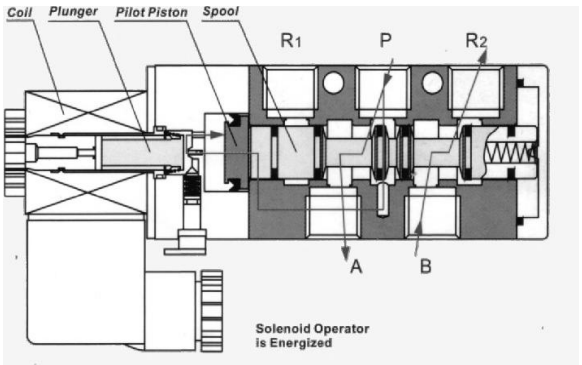

Figure 5a: Single solenoid control valve

When deactivated (when the relay drive circuit switches to OFF condition) there will be no current flow to the solenoid coil hence due to the spring action central spool will move away from the solenoid coil as shown in the figure 5b. Due to this, air flows through the center port P to port B. Port B being connected to the top of the pneumatic cylinder results in making the die to move down. Air retained in the other side of piston is made to flow out of the cylinder through the port A and port R1.

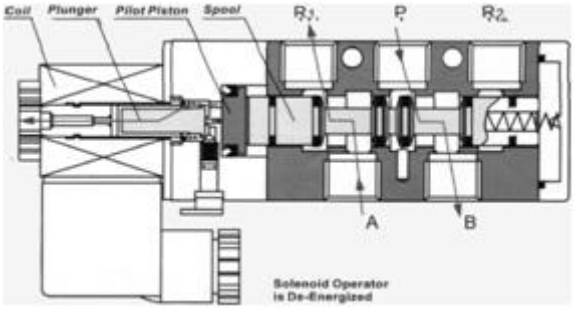

Figure 5b: Single solenoid control valve

Double Acting Pneumatic Cylinder

Details of the double acting pneumatic cylinder is shown in figure: 6
Maximum Stroke Length of the piston being 120mm.
Diameter of the piston: 30mm
Diameter of the piston rod: 12mm

Figure 6: Double Acting Pneumatic Cylinder

Experiments were conducted by varying the frequency of power supply and varying the rate of vibrations (keeping its amplitude constant.

2.6 Melting and treatment of the alloy

Melting was carried out in an electrical resistance furnace graphite crucible coated with mould coat dried and preheated was placed in the furnace. Ingot was transferred into the crucible. The furnace was started to melt the alloy. When the metal attained the molten condition (temperature was 750C) degassing was carried out using hexachloroethane degassing tablets. The dross was skimmed off and the clean molten metal was transferred into the mould. Following treatment of the molten alloy were carried out in different stages:

- Without addition of refiner and without mechanical vibration.
- By inducing the mechanical vibration to the molten metal without addition of refiner.
- By addition of refiner and by inducing of mechanical vibration to the molten metal.

The duration of inducing the mechanical vibration into the molten metal was maintained for 180 seconds till the alloy solidified. The intensity of the vibration was varied by increasing the frequency of vibration 4 to 10Hz by keeping amplitude of vibration to 3mm. After solidification and cooling to the room temperature the cast samples were ejected out from the mould. The cast samples were machined as per the required dimensions to carry out different tests and all the samples were subjected to a T6 heat treatment.

2.7 T6 Heat treatment

The heat treatment allows dissolving Mg2Si, homogenizing the solid solution and spherodise the eutectic silicon. The solution treatment was carried out at 540C for 6h followed by quenching immediately in the hot water and then artificial aging at 170 C for duration of 5h, followed by air cooling.

2.8 Microstructure examination

The of Microstructure examination forms important part of the investigation This helps in characterization of composition structure and properties of the material. Steps involving in the preparation of specimen for microstructure examination are: Sectioning, Grinding, Polishing, Etching.

2.9 Hardness measurements

Hardness measurements were carried out using a Brinell hardness tester. An average of three hardness measurements across the section was considered for the analysis.

III. Wear Test

The wear test were carried out using the pin on disk type wear testing machine.

Procedure employed:

- The surface of the disc was cleaned with acetone to remove dust, dirt present on the surface.
- The specimen was initially weighed and it was fixed in the holder provided and locked by tightening the screw.
- Motor was switched on and speed was adjusted to the required valve.
- Apply the weight on the hanger.
- The test was conducted for 5, 10,15mins duration of time. At the end of each time motor was switched off; specimen removed from the holder was cleaned and weighed precisely in the electronic balance.
- Weight loss was considered for wear analysis(i.e. the difference between the initial and final weight)

Formulae used for finding weight loss and wear rate is as shown below
Weight loss (W_L) = Initial weight – Final weight = $W_1 – W_2$ grams

- Rubbing Velocity (V) = $(2\pi rN)/60,000$
  r = Track radius in mm
  N = RPM of disc
- Wear rate = Weight loss/Distance traveled = $W_L/ 2\pi rN$ gm/m.

Test parameters:

- Disc diameter: 380mm
- Diameter of specimen (d) : 6mm
- Length of the specimen : 28mm
- Speeds studied: 400 rpm, 800 rpm, 1200 rpm
- Track radius : 40mm
- Load applied: 20N
- Duration of tests: 5min, 10min, 15min.

IV. Results and Discussion

The results of the investigation carried out on the grain refinement of Al-Si alloy subjected to mechanical vibration with and without the addition of refiner and T6 heat treatment discussed under the following headings.

- Hardness test
- Microstructure examination
- Dry sliding wear test.

4.1 Hardness test

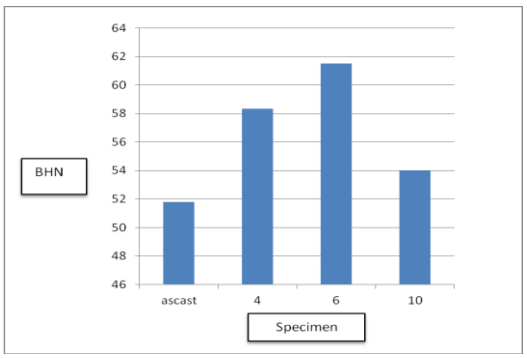

Fig7: shows the variation of hardness valves for different condition

It is observed that the frequency of vibration affects the value of hardness of the alloy. It is seen that the maximum hardness value (61.5BHN) is noticed for the alloy subjected to 6Hz frequency. Ascast specimen exhibits least hardness value (51.8 BHN).The study indicate that vibration has an influence on the hardness values of the specimen.

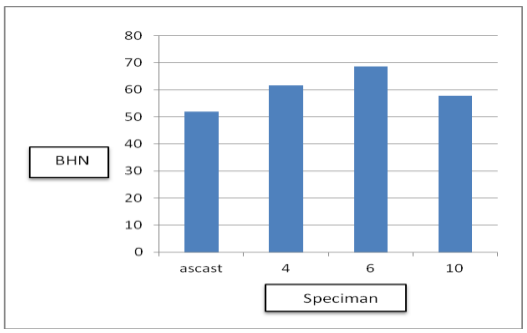

Fig8 : shows the variation of hardness valves with different conditions (with grain refiner addition and heat treatment)

It seen that maximum value of BHN is observed in the 6Hz specimen subjected to the combined effect of frequency for vibration and with grain refiner addition. An increase of 32.6% in hardness is seen with the specimen subjected to combined grain refiner addition and vibration as comparison with ascast condition.

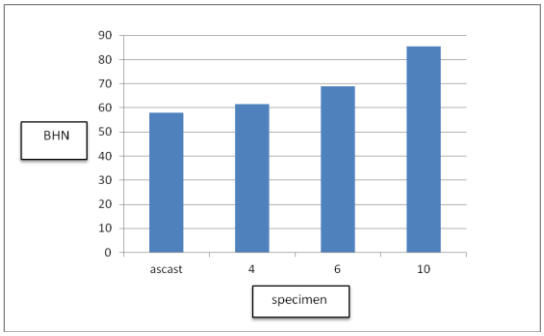

Fig9 **:** Effect of combined effect of grain refiner and vibration and T6 Heat treatment with 5h artificial aging

The figure 9 indicates that maximum value of BHN is observed in 10Hz specimen subjected to the combined effect of frequency for vibration and with grain refiner addition along with T6 heat treatment for the period of 5h of artificial aging. An increase of 47.7% is seen with the specimen subjected to combined grain refiner addition and vibration and heat treatment as comparison with ascast condition.

4.2 Microstructure examination

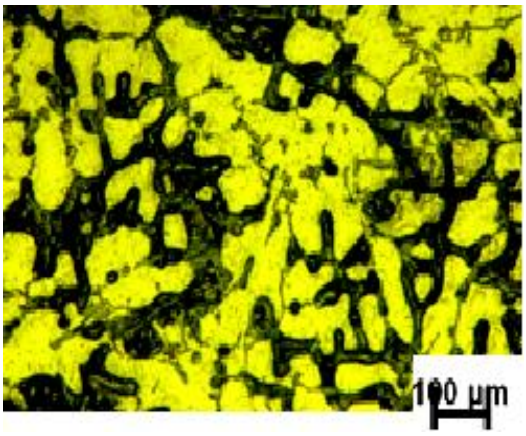

Fig10: Ascast Al-Si alloy

Figure-10 shows the structure of the ascast Al-Si alloy (without refiner addition and without the inducing vibration) It is observed that the structure of alloy is comprised of coarse aluminum matrix, which is strengthened by Si precipitates, and a dispersion of eutectic silicon particles and intermetallics. The secondary dendrites arm spacing (SDAS) was found to be 68.03µm calculated by linear intercept method.

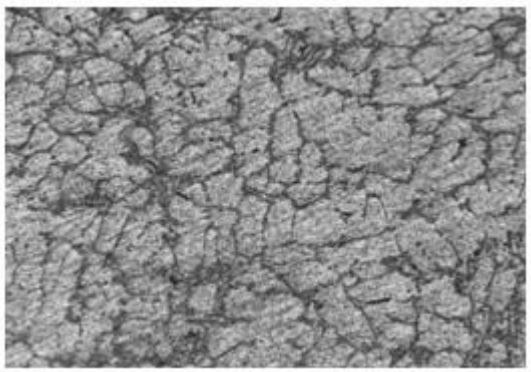

Fig11: 4Hz vibration without grain refiner

Fig12: 6Hz vibration without grain refiners

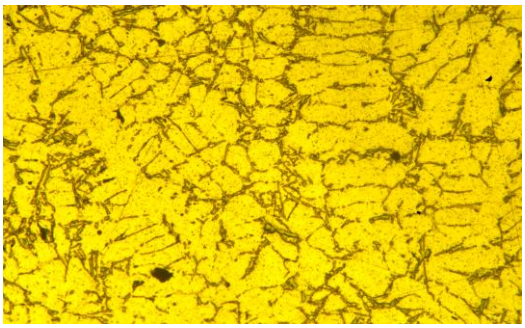

Fig13: 10Hz vibration without grain refiner

Fig11, 12 and 13 shows the photo micrograph of the specimen subjected to vibration frequency of 6 and 10Hz respectively. It can be seen that, the grain size is reduced and close grain structure is observed compared to the ascast structure. (SDAS of 4Hz, 6Hz and 10Hz are found was 39.3, 36.92 and 53.8µm respectively)

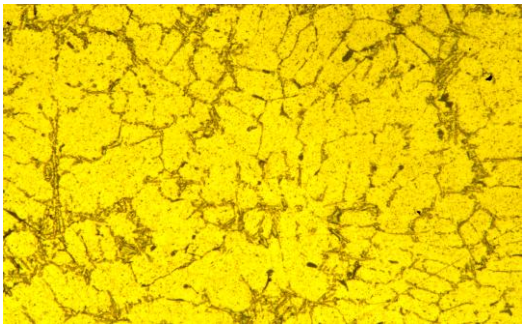

Fig14: 6Hz vibration with 2% grain refiner

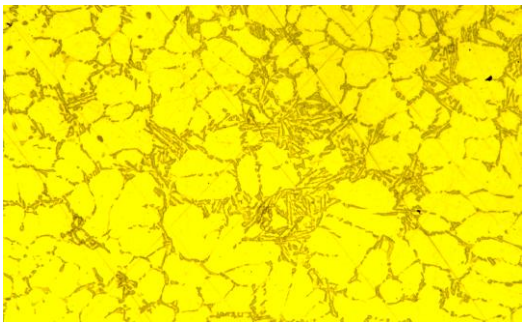

Fig15: 10 Hz vibration with 2% grain refiner

Figure14&15 shows the photo micrograph of the specimen subjected to an addition of 2% grain refiner and vibration frequency of 6 and 10Hz. It can be seen that, the grain size is reduced and close grain structure is observed. The SDAS of 6 and 10Hz was found to be 36.92 and 53.8µm respectively.

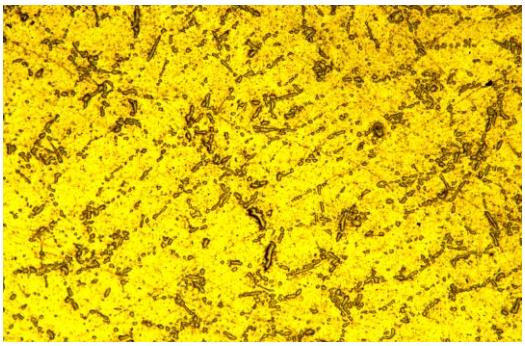

Fig16: 4 Hz vibration with 2% GR with T6 HT

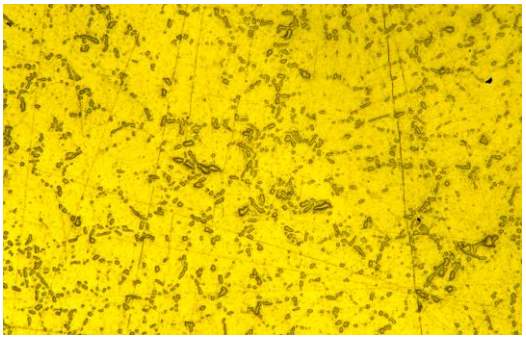

Fig17: 6Hz vibration with 2% GR with T6HT

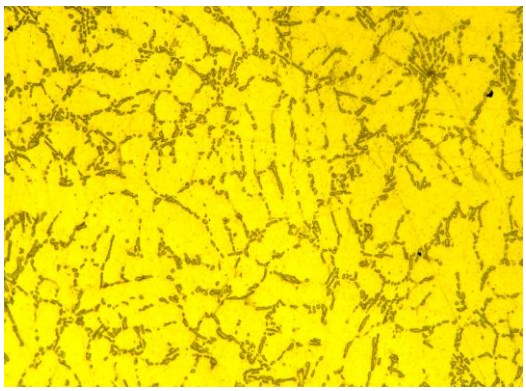

Fig18: 10Hz vibration with 2% GR withT6 HT

Figure16, 17&18 shows the photo micrograph of the specimen subjected to an addition of 2% grain refiner and vibration frequency of 4, 6 and 10Hz withT6 heat treatment and 5h of artificial ageing. It can be seen that, the 10Hz vibration with 2% grain refiner with T6 heat treatment gives higher BHN because of equeaxied grains. (The SDAS of 4, 6 and 10Hz are found to be 41.4, 39.5, 35.6μm respectively)

4.3 Dry sliding wear test.

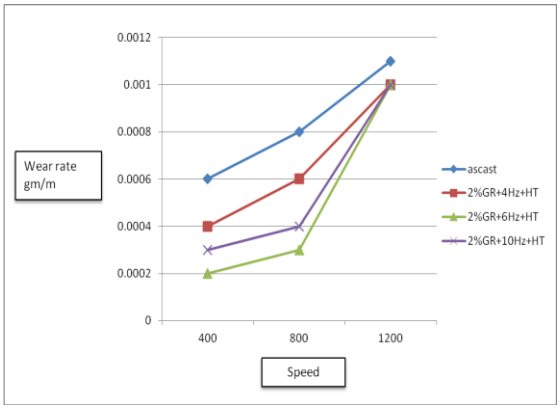

Fig19: wear rate versus speed

It can be seen from the figure19 that with increase in speed, the wear rate also increases. The maximum wear rate is seen in the as-cast specimen. There was a 10% improvement in the resistance for wear upon the alloy subjected to mechanical vibration with addition of grain refiner and T6 heat treatment and 5hours of artificial ageing.

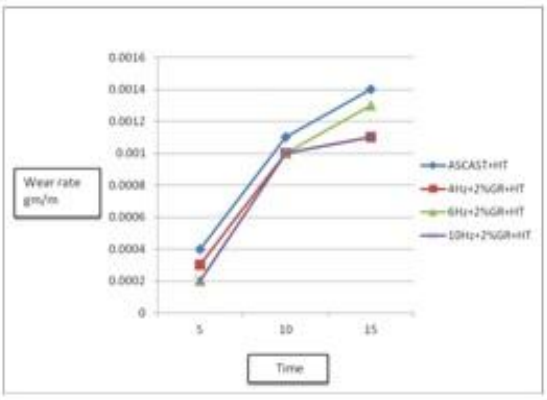

Fig20: wear rate versus time (1200rpm).

It can be seen from the figure that with increase in time, the wear rate also increases. The maximum wear rate is seen in the as-cast specimen. There was a 21.4 % improvement in the resistance for wear upon the alloy subjected to mechanical vibration with addition of grain refiner and T6 heat treatment.

V. Conclusions

From the investigation carried out on Al-Si alloy castings subjected to combination of vibration and grain refiner with T6 heat treatment, the following observations can be made.

5.1 Microstructure examination

Coarse acicular silicon particles are seen distributed along primary aluminum dendrite boundaries. Grain structure gets reduced and a closed structure is observed when the alloy is subjected to combination of vibration and grain refiner addition with T6 Heat treatment.

5.2 Mechanical properties

Hardness values get improved upon subjecting the castings to grain refinement and vibration with T6 Heat treatment (5h of artificial aging). The maximum hardness value of 85.54 BHN is observed in the specimen when it is subjected to combination grain refiner with vibration and T6 heat treatment. (An increase of 47.7% in hardness values is observed). This indicates that vibration has an influence on the mechanical properties of the Al-Si alloy castings.

5.3 Wear behavior

There was a considerable improvement in the resistance for wear upon the alloy subjected to mechanical vibration with addition of grain refiner and T6 heat treatment. There was a 21.4 % improvement in the resistance for wear upon the alloy subjected to mechanical vibration with addition of grain refiner and T6 heat treatment.

VI. Acknowledgement

Authors express their sincere gratitude to the management, principal, HOD, Mechanical Engineering department, M.S.R.I.T. Bangalore for the support and the encouragement.

References

[1] T.M. Chandrashekharaiah, S.A. Kori. Effect of grain refinement and modification on the dry sliding wear behaviour of eutectic Al–Si alloys. Tribology International 42 (2009) 59– 65
[2] S.A.Kori , Performance of Al-Ti, Al-B and Al-Ti-B master alloys on the grain refinement of Al-7Si alloy, Proceedings of the national conference on advances in materials and their processing (AMTP)-2003 Dec 2003, P154-162
[3] Cook, P.S.Cooper and M.A.Kearns, Benefits of Master alloy melt treatments in the alumeinum foundry industry
[4] N.H.S.Swamy, M.A.Joseph, N.M.Nagarajan, M.K.Muralidhara and H.Sundaramurthy, Effect of mould vibration and heat treatment parameters on microstructure and mechanical properties of cast A356 alloy, Indian Foundry Journal, Vol 54, No 1, Jan 2008, P 119-125
[5] Man Zhu, Zengyun Jian, Gencang Yang, Yaohe Zhou, Effect of T6 heat treatment on the microstructure, tensile properties, and fracture behavior of the modified A356 alloys

International Journal of Modern Engineering Research (IJMER)
www.ijmer.com Vol.3, Issue.2, March-April. 2013 pp-1229-1237 ISSN: 2249-6645

Numerical Characterization of the Pores and the Determination of the Point Of Crack Initiation in Some Cast Aluminum Alloys

Durowoju, M.O
Mechanical Engineering Department, Ladoke Akintola University of Technology Ogbomoso, Oyo State Nigeria

Abstract: *Porosity is a major defect in cast aluminum alloys affecting in particular, the fatigue strength. In this work, fractal analysis of the pores in the microstructure of cast aluminum alloys were done to provide information linking their composition and processing to the crack initiation.*

Two cast alloys: Al – 20%wtSi and Al – 20%wtCu, were used and the types of pores were studied in the as-cast samples. The shapes of the pores along with the percentage porosity in each of the microstructures were also evaluated. The Multi-Stage Random Sampling (MRS) and Spatial Point Pattern (SPP) Methods were used to determine the distribution of the pores and the point of crack initiation.

Fractal analysis showed that all the pores were shrinkage pores with $\beta<0.3$ and D approaching 2. The MRS and SPP methods revealed that crack initiation for eventual failure will start in the worst pore found in the lower right region of as-cast Al-20%wtSi because it has the value of D= 1.2846 and lowest sphericity β =0.0011.

This work has shown the effectiveness of using the fractal analysis, the MRS and the SPP methods for the characterization of the pores in the microstructure of cast aluminium alloys.

Keywords: *Fractal Analysis, Pores, MRS and SPP methods*

I. Introduction

For alloys and composite materials containing regular microstructures, a prediction of mechanical properties can be made by a quantitative measurement of features such as grain size, particle size, and spacing. This however is not the case where an irregular microstructure is involved because of the difficulty in the numerical characterization of the structure. For irregular microstructures, the application of fractal geometry offers a method by which both the individual particle shape and the mode of the distribution of the particles can be fully described in a numerical manner (1).

A Study carried out to evaluate the dependence of surface fractal dimension of Al_2O_3-SiO_2 composite membranes on chemical composition and sintering temperature (2) has shown that all composite membranes have rough surfaces with fractal dimensions ranging from 2 to 3. As SiO_2 content increases and sintering temperature rises from 200 to 600^0C, the fractal dimension increases. However, at 800^oC, the surface fractal dimension decreases. The computer aided stereo matching method on metals and ceramics was used to reconstruct the three-dimensional images of fracture surfaces formed by different mechanisms (3). An extensive experimental investigation of the scaling properties of fracture surfaces in heterogeneous materials was done (4). It was discovered that all the surfaces of the materials (silica glass, aluminum alloy, mortar and wood) investigated far from crack initiation point, are self –affine. In addition, it was observed that the Hurst exponent measured along the crack direction is found to be different from the one measured along the propagation direction. Furthermore, ductile fracture surface had the larger fractal dimension compared with the brittle type fracture surface.
The measurement of the porosity in aluminum cast alloys using fractal analysis was done (5). They observed that fractal analysis can be applied to the porosity measurement to describe the shapes of the pores in the aluminum silicon cast alloys using two dimensionless parameters, roughness, D and sphericity, β.

Spatial data analysis was used to study the distribution of micro porosity in 7050-T7451 aluminum plate alloys (6) and it was observed that the micro porosity was not randomly distributed throughout the sample. Similarly, another study on the distribution of micro porosity in an A356 aluminum alloy plate casting was done (7). From the study, it was concluded that the porosity was not randomly distributed but clustered, and that the clustering tendency was relatively constant throughout the casting. The patterns observed in the porosity distribution maps shown in Figure 1 was used to categorize the pores into random, regular, clustered, and clustered with random background (8). In the present work, the intention is to use the fractal analysis to characterize the pores in Al – 20%wtSi, and Al – 20%wtCu cast aluminum alloys and to identify the points of crack initiation using MRS and SPP methods.

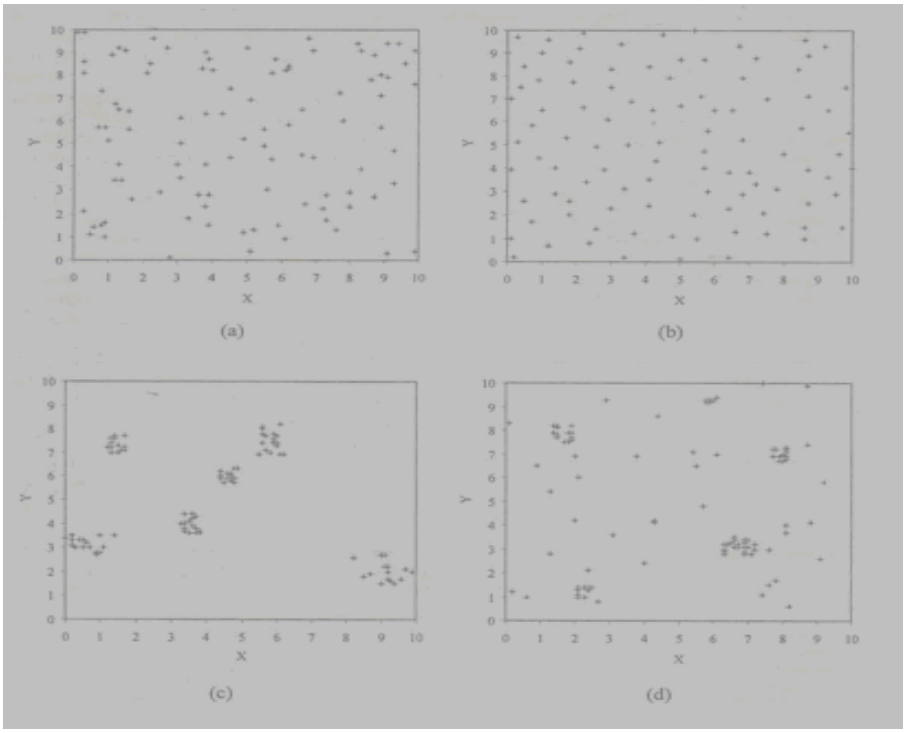

Fig. 1: The four common types of spatial point patterns (a) random, (b) regular, (c) clustered, (d) clustered superimposed on random background**.**

II. Materials and Methods

1kg (80% by proportion) of commercial aluminum (99.7% pure, by weight) and 250g each (20% by proportion) of Si and Cu, obtained from the Federal Institute of Industrial Research Oshodi (FIIRO), were prepared for the casting. Due to closeness in melting temperatures, pot A which contains Al+Si, with its contents was lowered into the furnace and the mixture melted.

In pot B, the alloying element Cu was first charged in the pot because of its high melting point of about 1108^{o}C. When the melting point was attained, the base metal Aluminum with melting point of 660^{o}C was added.

The molten alloys were poured into the prepared mould after cooling for three minutes (to avoid splashing). The two resulting cast samples in rod forms were removed from the mould after three hours (to allow for effective cooling).

Application of fractals

Fractal geometry was developed (10). Its principle is universal in any measurement and has been previously used to numerically describe complex microstructures including graphite flakes and nodules (1, 11, 12, 13, and 14). The Mathematical basis for measuring chaotic objects with the power law modified is adopted in this work. The basic equation is as follows:

$$P = P_E \delta^{D-1} \qquad \text{Eq 1}$$

$$\left(1 < D < 2 \text{ and } \delta_m < \delta < \delta_M\right) \qquad \text{Eq 1}$$

Where P_E is the measured perimeter, P is the true perimeter, δ is the yardstick,

From this expression, it can be deduced that the true perimeter is actually a function of the yardstick for measurement. The smaller the yardstick used, the more accurate the measurement. The fractal dimension, D, therefore describes the complexity of the contour of an object. It can be more practically called its roughness (5).

When $\delta < \delta_m$, the measurement is not sensitive to the yardstick chosen, therefore giving a smaller value of the slope, while when $\delta > \delta_M$, the size of the yardstick exceeds that of the individual feature being measured so that the measurement loses meaning because the object falls below the resolution limit of the yardstick used for measurement (1). Sphericity, β, another dimensionless number, is used together with the fractal dimension, D; to describe the shape of the pores formed (5). It can be expressed as

$$\beta = 4\pi A_T / P^2 \qquad \text{Eq 2}$$

$$\left(0 < \beta < 1 \text{ and } 1 < D < 2\right)$$

Substituting equation (Eq 1) in (Eq 2) gives

$$\beta = \left(4\pi A_T / P_E^2\right)\delta^{2(1-D)} \qquad \text{Eq 3}$$

$$\left(0 < \beta < 1 \text{ and } 1 < D < 2\right)$$

Where A_T is the total pore area
When $\beta = 1$ and $D = 1$, a perfect circular shape is formed by the pore in the microstructure.
As β decreases, the shapes become more elongated showing a departure from perfect sphere.
The locations of $1 < D < 2$ represent less regular shapes.

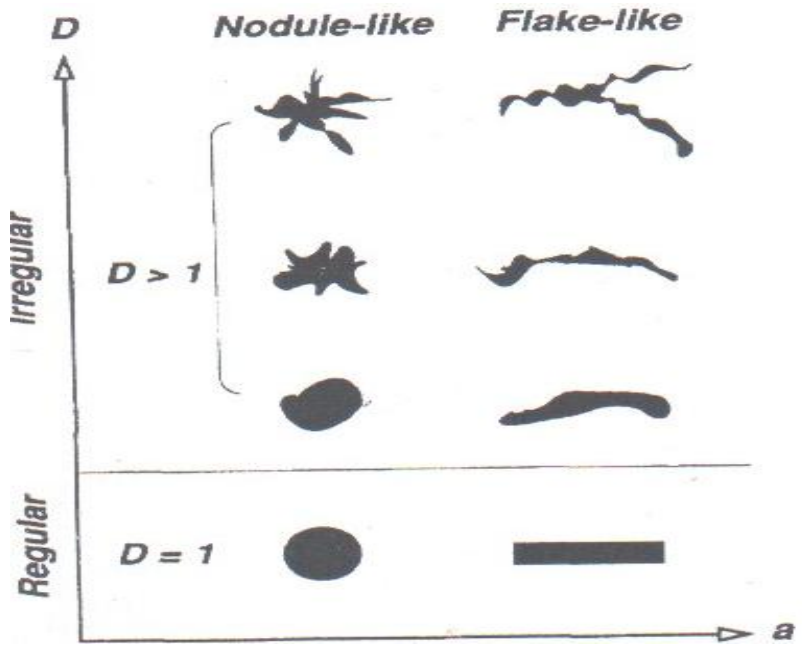

Fig. 2: Illustration of development of irregular shapes based upon Euclidean circle or rectangle. All the shapes have the same area. Source: Lu and Hellawell, (1994) (1)

Where **a** is the Shape Factor.

In Figure 2 the more complex shapes for each individual island present increasing ranges of local curvature and the fractal dimension, D, increases. By definition, the shape factors also change, as they do for Euclidean shapes, but not in a readily calculated manner, because the shape factor (**a)** is now a function of D.

Area of a pixel or yardstick = L x B
Area of the total pore A_T = Area of yardstick x Number of yardsticks
To calculate the perimeter *P* of the pore, the Slit Island Method (SIM)
(15) Introduced by Mandelbrot (1983) was used. It is expressed as:

$$\log_e P = 0.5 D \log_e A_T \qquad \text{Eq 4}$$

$$\log_e P = \log_e A_T^{D/2}$$

$$P = A_T^{D/2}$$

The Computer Program

Using the equations (Eq 1)-(Eq 4), an interactive Matlab program was developed to obtain the numerical values of the fractal dimension *D* and the sphericity β. To develop the program the box counting method was used with a counter incorporated into the program and the small boxes or pixels occupied by the pore outlines are counted. In all four pixels (2x2pixels, 4x4pixels, 8x8pixels and 16x16pixels) and four grid sizes (200x200, 100x100, 50x50 and 25x25) were selected. The selections were made for better resolution and to obtain accurate values. A flowchart showing the various stages and the subroutines in the computer program was drawn as shown in Fig.3.

MRS and SPP Methods.

The first stage involves the division of the microstructures into four quadrants (lower left, upper left, lower right, and upper right) as shown in Figure 4. The second stage is the random selection of two pores from each quadrant while the third stage is the purposive selection (purposive sampling) of the "worst" and the "best" pores from the eight pores selected from each microstructure. The fourth stage is the categorization of the porosity distribution map into random, regular, clustered, and clustered with random background. Fifth stage is the discrimination between the shrinkage and the gaseous pores. In this stage, the patterns described in stage four are associated with different types of porosity.

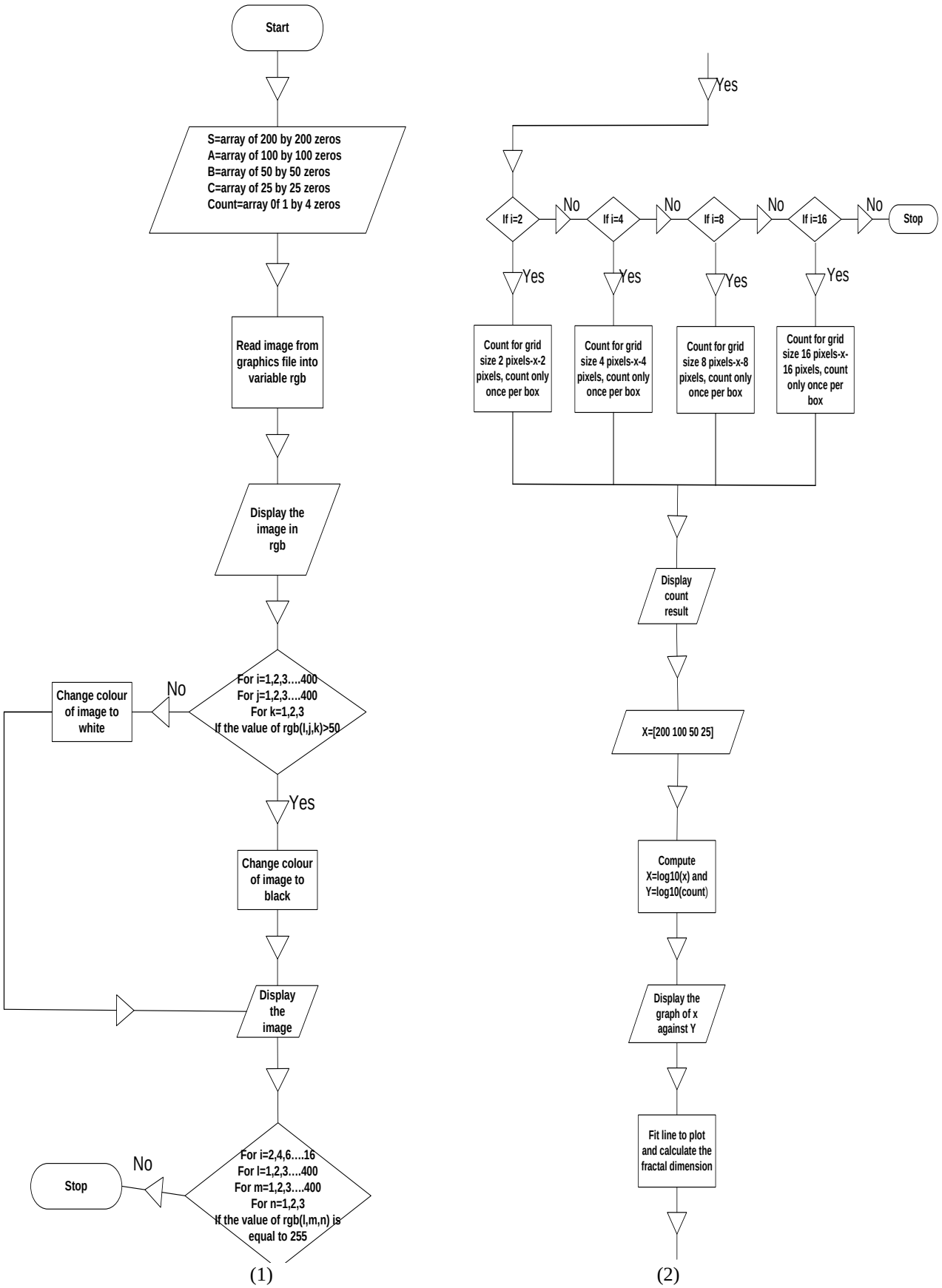
Start
S=array of 200 by 200 zeros
A=array of 100 by 100 zeros
B=array of 50 by 50 zeros
C=array of 25 by 25 zeros
Count=array 0f 1 by 4 zeros
Read image from graphics file into variable rgb
Display the image in rgb
For i=1,2,3....400
For j=1,2,3....400
For k=1,2,3
If the value of rgb(I,j,k)>50
No
Change colour of image to white
Yes
Change colour of image to black
Display the image
For i=2,4,6....16
For I=1,2,3....400
For m=1,2,3....400
For n=1,2,3
If the value of rgb(I,m,n) is equal to 255
No
Stop
(1)
Yes
If i=2
No
If i=4
No
If i=8
No
If i=16
No
Stop
Yes
Yes
Yes
Yes
Count for grid size 2 pixels-x-2 pixels, count only once per box
Count for grid size 4 pixels-x-4 pixels, count only once per box
Count for grid size 8 pixels-x-8 pixels, count only once per box
Count for grid size 16 pixels-x-16 pixels, count only once per box
Display count result
X=[200 100 50 25]
Compute X=log10(x) and Y=log10(count)
Display the graph of x against Y
Fit line to plot and calculate the fractal dimension
(2)

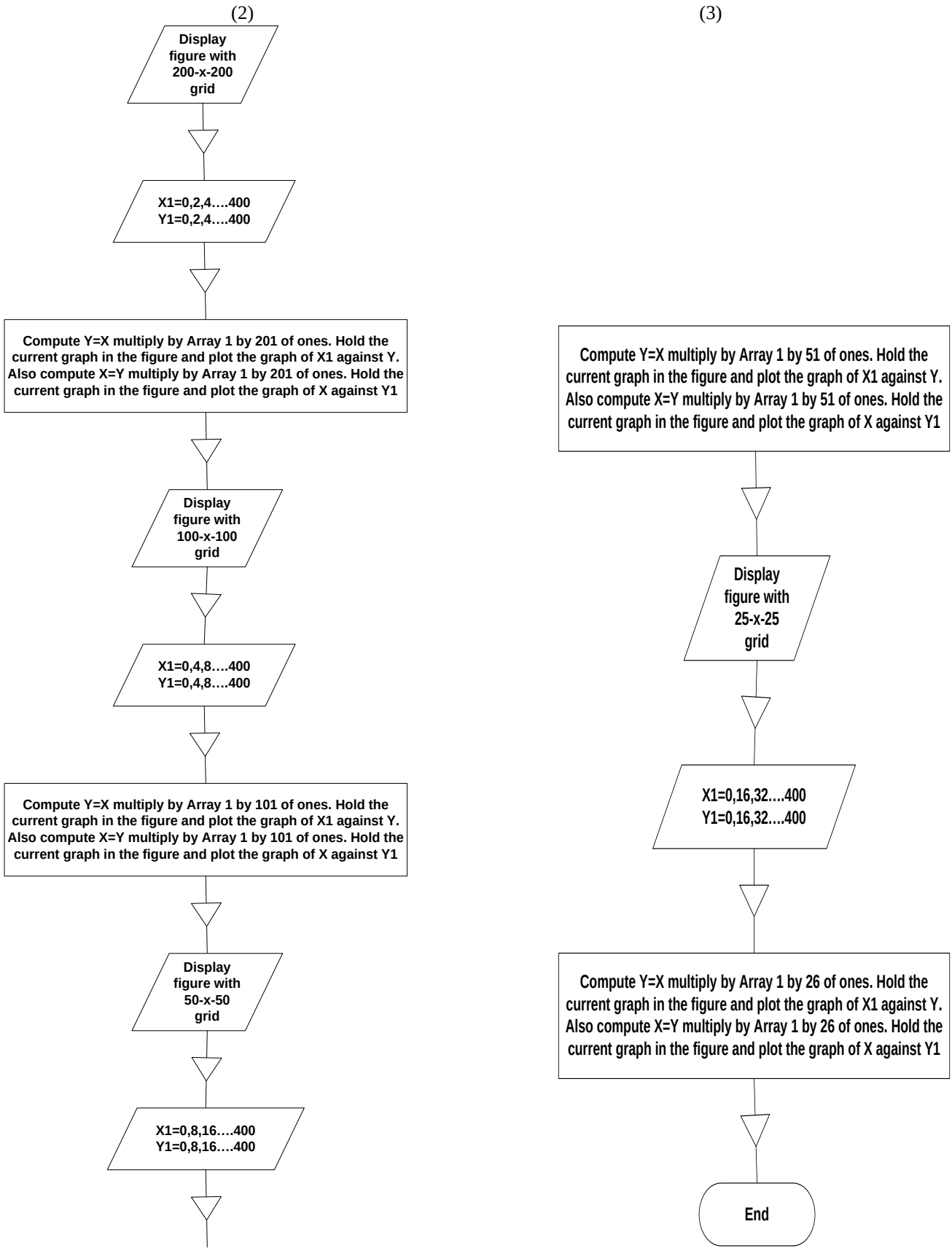

Fig.3: Flow chart of the computer program

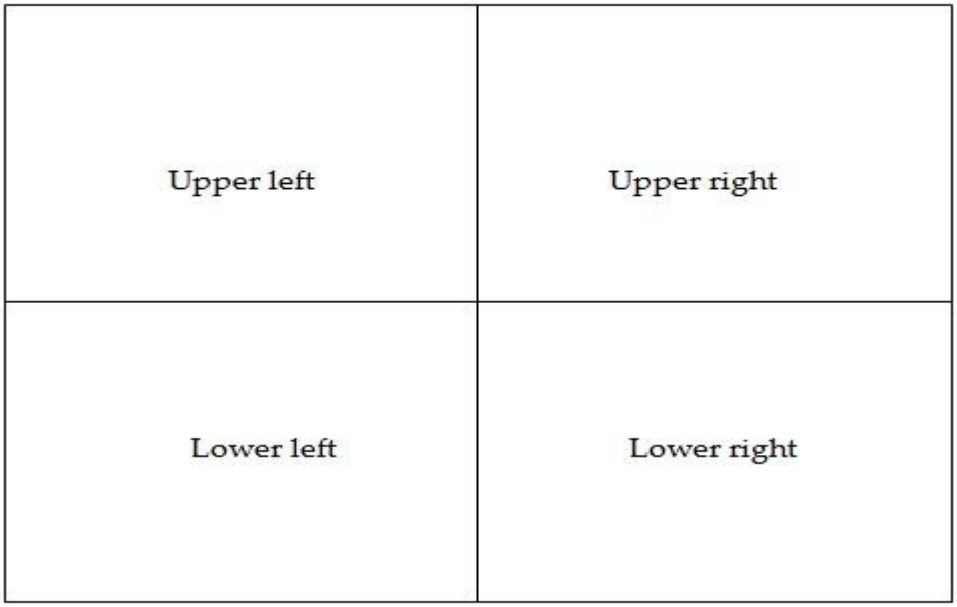

Fig. 4: The Multi-Stage Random Sampling Method of Dividing a Microstructure into four Quadrants.

III. Results and Discussions

Figure 5 shows the microstructures of the two alloy samples used in this work and the isolation of the pores in these samples. The shapes of the pores observed in the microstructures are summarized in Table 1 while the samples of the pores in the microstructures are shown in Figure 6. The pores are all-irregular in shape and are either nodule-like or flake-like.

It was observed that, for the as-cast samples, the predominant pores in Al-20%wtCu are the nodule-like pores while the flake-like pores dominate in Al-20%wtSi (see Table 1). The formation of the nodule-like or flake-like shape is due to the nucleation and growth kinetics usually compounded by composition variations and the concentration of elements such as copper, zinc, magnesium, and silicon in the samples.

Table 1: Shapes of the pores and the dominating shapes in the microstructures of as-cast samples

Cast Samples	Shapes of the Pores	
	Major Pores	Minor Pores
Al-20%wtCu	Nodule-Like	Flake-like
Al-20%wtSi	Flake-like	Nodule-Like

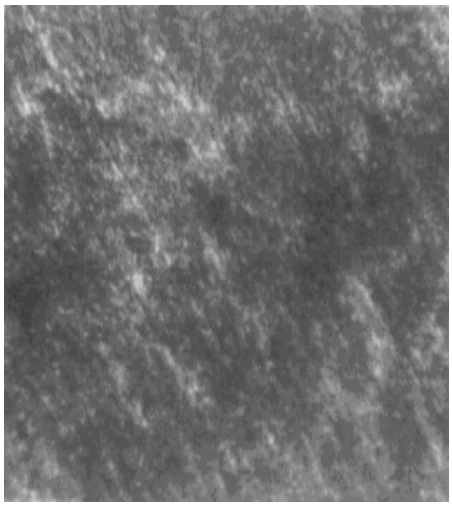

a: Al-20%wtCu

b:Isolation of the pores in Al-20%Cu

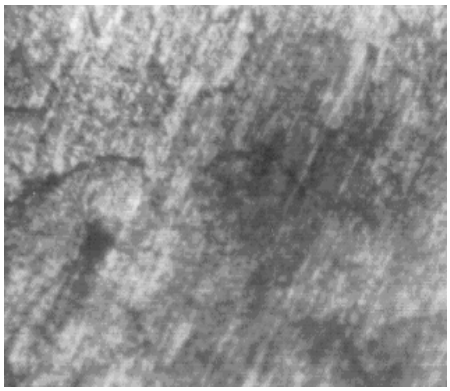

c: Al-20%wtSi

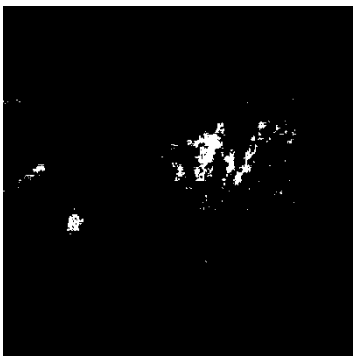

d: Isolation of the pores in Al-20%Si

Fig. 5: Microstructures of as-cast aluminum alloys

Legend:
Dark spot … pore
Grey spot … intermetallic particle
White spot…... Al-matrix

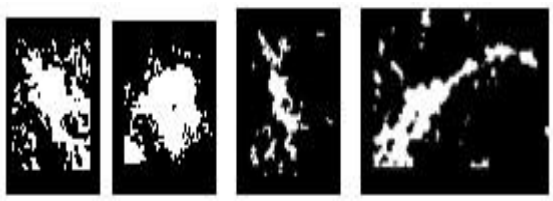

Fig. 6: Samples of pores from the microstructures

PERCENTAGE POROSITY

The percentage porosity, ratio of the pore area to the total area, in each of the as-cast sample, is illustrated in Table 2. It was observed that for the as-cast samples, Al-20%wtSi has the highest number with percentage porosity of 9.92% while Al-20%wtCu has the lowest number with percentage porosity of 4.48%. This is because of the different composition and concentration of the alloying elements. The large atomic radius of Copper compared to that of Silicon ease the formation of pores in the interstitial spaces created in Al-20%wtSi. Copper has atomic radius of 1.57Å, while Silicon has 1.46Å.

Table 2: Percentage Porosity

	As-Cast
Al-20%wtCu	4.48%
Al-20%wtSi	9.92%

Fractal analysis, MRS and SPP Methods

Table 3 presents the fractal dimension, sphericity and pore location for as-cast Al-20%wtCu alloy. The porosity distribution map (Figure 7) gives the "best" of the pores observed as the pore with D =1.0028 and β = 0.0459 while the "worst" of the pores is that with D =1.0678 and β = 0.0135 corresponding to pores numbers N8 and N7 respectively. Using spatial point data analysis, the pores in Figure 7 have regular spatial point pattern and the porosity distribution map represents gas porosity because gas pores are found at a distance from their immediate neighbours due to depletion of hydrogen gas in the area surrounding each pore.

Table 3: Values of fractal dimension D, and sphericity □, for (Al-20%wtCu) As- Cast Alloys

S/n	Alloys	Fractal Dimension D	Sphericity □	Pore Location
N1	Al-20%wtCu1	1.0462	0.0242	Upper right
N2	Al-20%wtCu2	1.0218	0.0266	Upper right
N3	Al-20%wtCu3	1.0966	0.0827	Upper left
N4	Al-20%wtCu4	1.0346	0.0228	Upper left
N5	Al-20%wtCu5	1.0080	0.0195	Lower left
N6	Al-20%wtCu6	1.0574	0.0250	Lower left
N7	Al-20%wtCu7	1.0676	0.0135	Lower right
N8	Al-20%wtCu8	1.0028	0.0459	Lower right

It can be deduced from Table 4 (for Al-20%wtSi alloy as-cast) and the porosity distribution map (Figure 8), that the "best" of the pores observed is the pore with D =1.0847 and β = 0.0579 while the "worst" of the pores is that with D = 1.2846 and β = 0.0011 corresponding to pores numbers N6 and N2 respectively. Figure 8 also has pores with random spatial point pattern because of the closeness of the pores to their immediate neighbours. The porosity distribution map therefore represents gas porosity. The implication of having only regular and random spatial point patterns, representing gas porosity in as-cast samples, is that the pores cannot easily link the nearest neighbour therefore making crack initiation difficult. Another implication is that if failure of the material will occur it will start at the locations with the worst pore shapes.

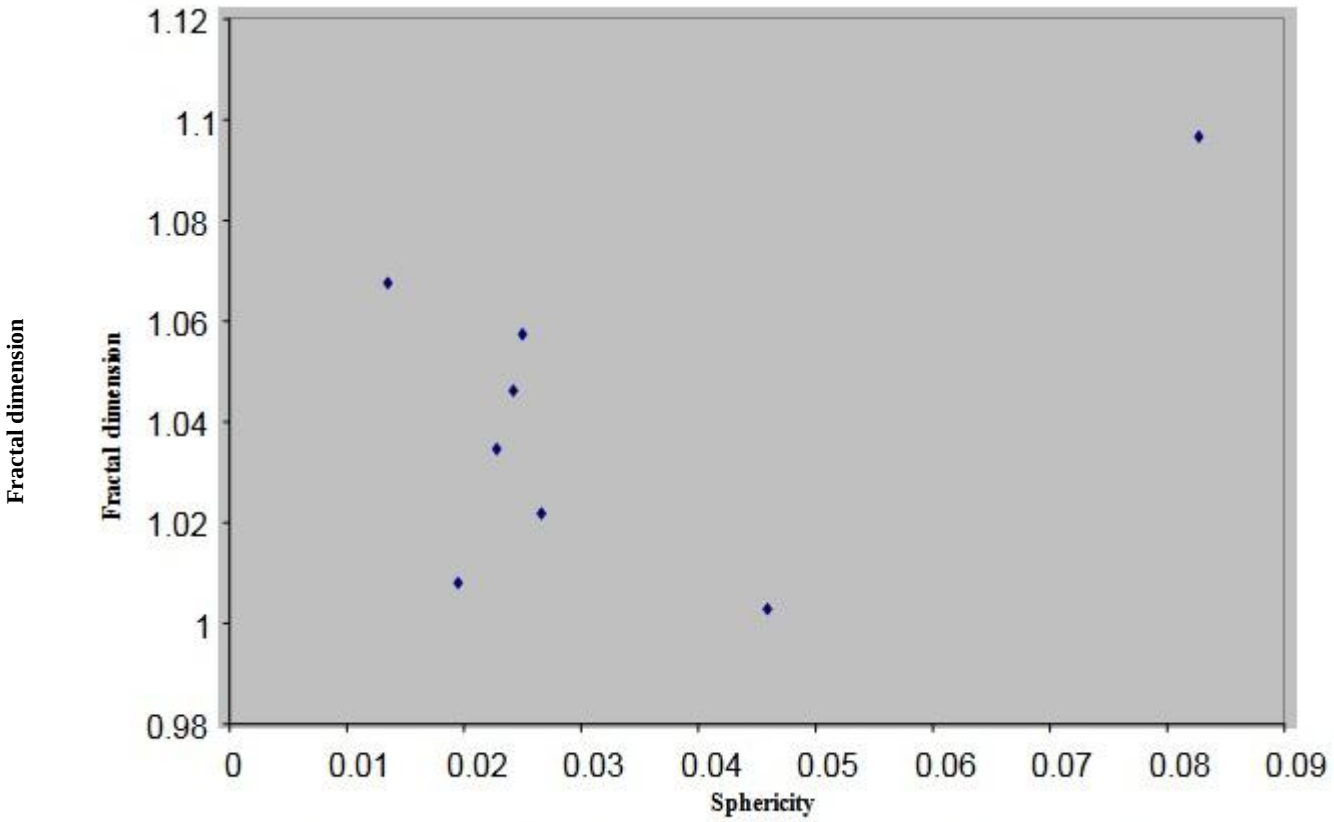

Fig. 7: Porosity distribution map for Al-20%wtCu As-cast Sample

Table 4: Values of fractal dimension D, and sphericity □, for (Al-20%wtSi) As-cast Alloys

S/N	Alloys	Fractal Dimension D	Sphericity □	Pore Location
N1	Al-20%wtSi1	1.0510	0.0348	Upper right
N2	Al-20%wtSi2	1.2846	0.0011	Upper right
N3	Al-20%wtSi3	1.1087	0.0074	Upper left
N4	Al-20%wtSi4	1.1278	0.0104	Upper left
N5	Al-20%wtSi5	1.1633	0.0057	Lower left
N6	Al-20%wtSi6	1.0847	0.0579	Lower right
N7	Al-20%wtSi7	1.0440	0.0114	Lower right
N8	Al-20%wtSi8	1.1253	0.0126	Lower left

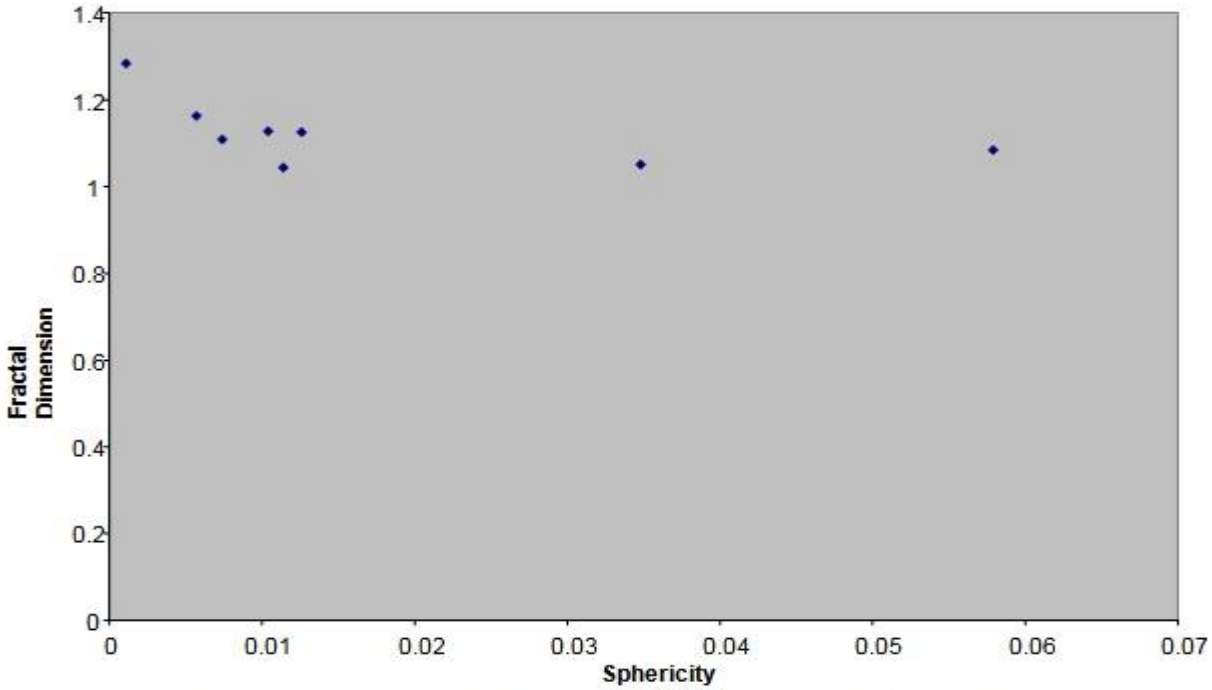

Fig.8: Porosity Distribution Map for Al-20%wtSi As-cast Sample

IV. Conclusions

- The noodle-like pores are the major pores in as-cast Al-20%wtCu while the flake-like pores are the major pores in Al-20%wtSi.
- The MRS and SPP methods revealed that if crack initiation will occur it will start in:
- Lower right region of as-cast Al-20%wtCu because it contains the "worst" pore shape with D = 1.0676 and β = 0.0135.
- Upper right region of as-cast Al-20%wtSi because it contains the "worst" pore shape with D = 1.2846 and β = 0.0011.

References

[1] Lu, S.Z and Hellawell, A. (1994) "An Application of Fractal Geometry to Complex Microstructures: Numerical Characterization of Graphite in Cast Irons", Acta Metall., Vol.42 pp. 4035-4047.
[2] Wei, Q., and Wang, D. (2003); "Pore Surface Fractal Dimension of Sol-Gel-Derived Al_2O_3-SiO_2 Membranes" Material Letters, Vol.57, pp.2015-2020.
[3] Tanaka, M.,Kimura, Y., Kayama, A., Kato, R., and Taguchi, J. (2004) " Fractal Analysis of Three-Dimensional Fracture Surfaces in Metals and Ceramics" ISIJ International, Vol. 44 No. 7 pp1250-1257.
[4] Ponson, L., Bonamy D., Auradon H., Mourot G., Morel S., Bouchaud E., Guillot C., and Hulin J.P.(2006)"Anisotropic Self – Affine Properties of Experimental Fracture Surfaces" International Journal of Fracture Vol.140 No.1-4 pp .27-37.
[5] Huang, Y. J., and Lu S.Z. (2002) "A Measurement of The Porosity in Aluminum cast Alloys Using Fractal Analysis" Proceeding of 2nd International Aluminum Casting Technology Symposium, ASME, Houston U.S.A.
[6] Zhang, J., Przystupa, M. A. and Luevano, A. J. (1998); "Characterization of Pore and Constituent Particle Populations in 7050-T7451 aluminum Plate Alloys" Metallurgical Transaction Vol.29A pp. 727-737.
[7] Tewari, A., Dighe, M., and Gokhale, A.M. (1998) "Quantitative Characterization of Spatial Arrangement of Micro pores in Cast Microstructures" Material Characterization.Vol.40 pp119-132.
[8] Anson, J. P., and Gruzleski, J. E. (1999) "The Quantitative Discrimination between Shrinkage and Gas Porosity Using Spatial Data Analysis" Materials Characterization .Vol.43 pp 319-335.
[9] Mandelbrot, B., B. (1983) "The Fractal Geometry of Nature", Freeman Publishers, London.
[10] Lu, S.Z and Hellawell, A. (1995[a]) "Fractal Analysis of Complex Microstructures in Materials", Proc. of MC95 International Metallographic Conference, May 10-12, Colmar, France, ASM pp. 119.
[11] Lu, S.Z and Hellawell, A. (1995[b]) "Modification of Aluminium-Silicon Alloys: Microstructural Change, Thermal Analysis and Mechanism", Journal of Materials, Vol.47 pp. 38-40.
[12] Lu, S.Z and Hellawell, A. (1995[c]); "Using Fractal Analysis to Describe Irregular Microstructures", Journal of Materials, Vol.47 pp. 14-17.
[13] Lu, S.Z and Hellawell, A. (1999); "A Fractal Method of Modularity Measurement in Ductile Iron", American Foundry Society Transaction, Vol. 107 No. 99-195, pp. 757-162
[14] Bigeralle, M. and Iost, A. (2006) "Perimeter Analysis of the Von Koch Island, Application to the Evolution of Grain Boundaries during Heating" Journal of Material Science. Vol. 41, pp. 2509-2516.

International Journal of Modern Engineering Research (IJMER)
www.ijmer.com Vol.3, Issue.2, March-April. 2013 pp-1238-1244 ISSN: 2249-6645

Design and Simulation by Photovoltaic System with Tapped Topology

Juan C. Yris, [1.4] Hugo Calleja G, [2] Leobardo H. Gonzalez, [3] José A. Olmos[1]
[1](Universidad Juárez Autónoma de Tabasco, Villahermosa, Tabasco, México)
[2] (Centro de Nacional de Investigación y Desarrollo Tecnológico, Cuernavaca, Morelos. México)
[3] (ESIME-C Instituto Politécnico Nacional, México, D.F)
[4](Instituto Tecnológico Superior de Comalcalco, Tabasco, México)

Abstract: *The concept of AC Module is typically applied to transform DC in AC. As a novel solution, center tapped topology is proposed for design of inverter into a Module Integrated Converter (MIC). Main contribution of converter with tapped inductor topology is to generate a bigger AC voltage to output, depending on the duty cycle and turn ratio of tapped inductor. The topology chose is convenient because is small, simple and cheap. To achieve a sinusoidal signal output the inverter is controlled with Sine Pulse Width Modulation (SPWM). The novel converter proposed and its control system is evaluated by means of the electronic simulator. The simulation results obtained is appreciated that the proposed converter working in a photovoltaic system increases the voltage gain, increases the efficiency and reduced the harmonic distortion with respect to traditional converters.*

Keywords: *Photovoltaic System, tapped Inductor, Module Integrated Converter.*

I. INTRODUCTION

Traditionally, Photovoltaic systems (PV) installed around the world are grouped in on-grid and off-grid. The first developed presented greater growth worldwide [1]. They are distinguished by the absence of a storage device, such as battery. One of its main features is the possibility of improving the quality of service of the energy supplied by the electrical-grid. There are three configurations of installation of PV systems that can to be connected to the electrical-grid, are: central inverter, string inverter and multi-string inverter [2], [3], [4], [5], [6], [7]. An improvement that is achieved in PV system consists on the implementation of a PV module with a DC-AC converter small or Module Integrated Converter, MIC, the union of this two is called "AC Module". The AC module easily connects to the electrical-grid under the operate mode of plug and play. It is suitable for use in powers of 40 to 200W and supports multiple connections in domestic applications with a maximum theoretical power of 2 kW [8]. Its advantages are: small size, modular and low cost. The main limitation of AC module is that MIC power will be equal to the delivered power by the PV module. To improve the delivered power the converter requires an element that elevates the voltage, such as: Low Frequency Transformer (LFT), High Frequency Transformer (HFT) and Without Isolation (WI).

The MIC with a conventional inverter uses a LFT in order to obtain electrical isolation between the PV module and the electrical-grid, as well as raise the low voltage supplied by the DC-AC converter (Fig.1). Its advantage is to have a simple system and with the disadvantage that it is very heavy. This limits the system to reduce size and weight.

One solution to solve the problem of MIC with a heavy transformer is to use a DC-DC converter with a transformer smaller operating at high frequency (Fig. 2). However, requires two different control circuits with switching processes and losses higher due to the cascade connection of two power stages.

Another option for high performance is to remove the LFT or HFT (WI), with them the weight is reduced, the price down, the size is smaller, the arrangement is simple and to obtain a 2% decrease in losses related to HFT [9] this topology is recommended for power less than 1 kW (Fig. 3).

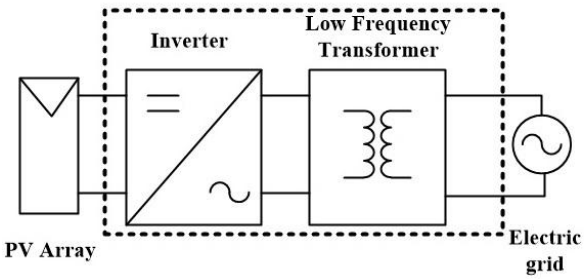

Fig. 1. MIC with LFT.

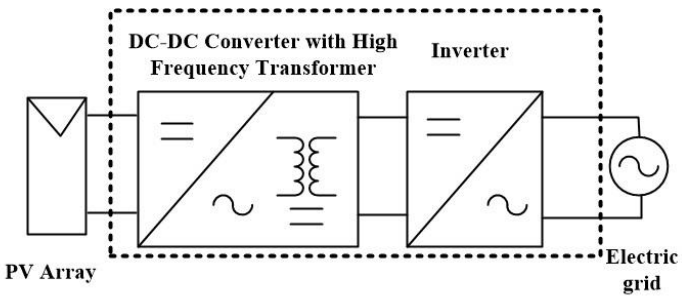

Fig. 2. MIC with HFT.

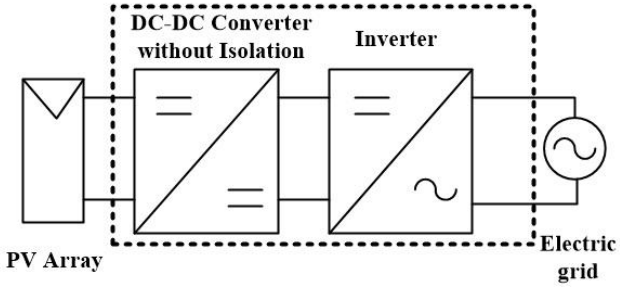

Fig. 3. MIC without isolation.

In [10] is presented a converter with the characteristics that must submit as: being small, light-weight and efficient, its disadvantage is having a low voltage gain. Therefore, it is necessary to develop a DC-DC converter without isolation with high gain, in order to generate voltage quality in the electrical-grid from a single PV Module (Mark, Conergy C1251P) [11], with typical output voltage of 14V to 17V, so it is necessary to have a MIC with a large gain to inverter. To do this, it is established that, it must have a minimum voltage to the inverter input of 180V. To obtain this high voltage is necessary to have a converter with the ability to raise the voltage, and then you must have a maximum gain of 12.85 for a voltage of $14V_{DC}$ and a minimum gain of 10.58 in the case of $17V_{DC}$. It should be mentioned that the maximum gains obtained in the traditional conditioner without isolation converters reported do not cover the above needs [12-17].

II. SELECTION OF PROPOSED TOPOLOGY BY DESIGN OF MIC

The MIC is divided into several stages of conversion [18]. When the converter is a single stage there are two built-in functions: firstly developed the conversion of DC-DC with voltage gain and second is developed the inverter (Fig. 4). For its domestic implementation, is required that the MIC has low weight, high efficiency, high gain and high power density.

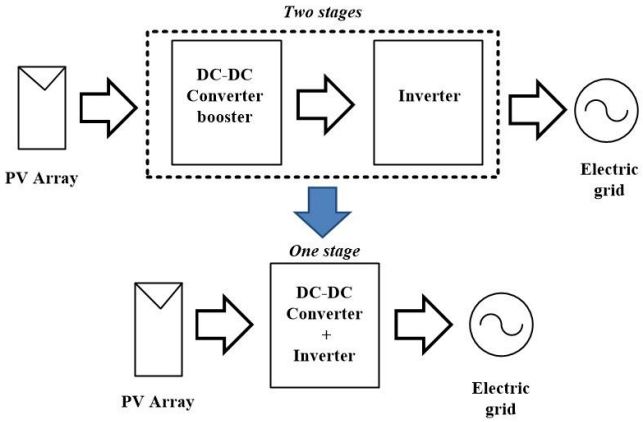

Fig. 4. MIC with reduction stages.

The trend in PV conditioners consisting principally of a single stage, with range of efficiency from 87% to 93.26%, range of switching frequency from 9.6 kHz to 70 kHz. Here are the three alternatives with the best performance gain by inverter without isolation.

The first inverter analyzed was proposed by Cáceres *et al*. [12]. It consists of two DC-DC converters type boost, operating in a complementary mode. However, it has the following disadvantages: low gain, all its transistors operate at High Frequency with hard switching technique, the switching loss increases and the system is susceptible to generation electromagnetic interference.

The second inverter analyzed was proposed by Kusakawa *et al*. [13], this converter operates with PWM signal and hard switching technique and control on both sides: on one hand you have the DC-DC conversion and on the other hand the inverter, it eliminates asymmetry problems. Furthermore, this inverter is appropriate for small power. Its disadvantage is having a single inductor **L** to provide the energy for each half cycle of the output voltage; this increases the losses due to heating.

The third inverter analyzed was proposed by Jain *et al* [14]. The converter has as function boost and inverts the waveform of the input voltage. This converter operates with two transistors which operate at high frequency and two transistors which operate at low frequency. Its reported efficiency is 87% due to losses in the inductors, works in Discontinuous Conduction Mode operation (DCM) and has implemented tracking Maximum Power Point MPP [19].

According to Table 1, the idea development by Jain presents better characteristics as: its higher gain, fewer components, lower inductance and capacitance and low switching frequency. Based on the reported characteristics by Jain, this proposal is more viable for the purpose of study, which is connected to the electrical-grid a MIC-PV. However, its gain of 3.6 is not adequate, requires a voltage conversion of 10.58 (minimum). The technique to use to obtain VAC is a differential connection of the load across the outputs of two converters, Fig.5. Where the converter 1 will produces V1 and

converter 2 will produces V2, the load voltage VO will be given by Vo= V1-V2. While V1 and V2 may both be individually positive, the voltage across the load can be positive or negative. The converter 1 will operate the positive half cycle of the AC signal and the converter 2 will operate in the negative half cycle.

Table 1. Comparative analysis of inverter without isolation

Name	Boost	Boost	Buck/Boost
Proposal	Cáceres	Kusak	Jain
Power	500	50	300
Gain	3.3	3.5	3.6
Efficiency (%)	-	87	87
Frequency (kHz)	30	70	10
THD (%)	4.74	3.67	5
# Components	12	13	11
# Capacitor (uF)	2 (40)	2 (-)	1 (4.4)
# Inductor (mH)	2 (800)	1	2 (3.25)
Reference year	1999	2001	2007

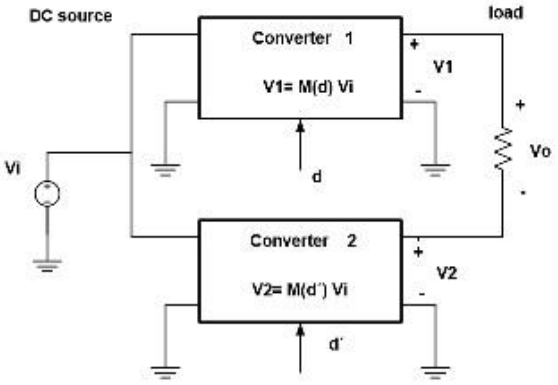

Fig 5. Differential connection of the inverter

III. SELECTION OF DC-CD CONVERTER

Of the various existing options to elevation the voltage, there are three viable alternatives for DC/DC converter. In the Table II are represents the most important characteristics of the three converters above. In it, we can see what is interesting to explore the tapped-inductor scheme, which while not a new technique has been recently taken [28-31], in order to obtain higher gain than for traditional converter To develop a DC-DC converter without isolation we have two options practices: a) traditional with ground output and b) modified without ground output [32]. In the arrangement of a differential output inverter is necessary that the inverter has without ground output. This characteristic only presented the family the boost converters. This configuration allows a greater gain than conventional converter. The relationship between the number of turns of primary (Np) and number of turns of secondary (N_S) of tapped-inductor is designated by the letter N (Fig.6).

The variant of converter that presents a better performance when working in two modes of driving is TIST-BB converter. Which has the advantage of having a duty cycle greater than the others, this is important for control l, because during the operating cycle of the converter to change the DCM to MCC, through the Case Critical CC.

Table II. - Comparative analysis with the values reported for DC-DC converters without isolation,

Table II. Comparative analysis with the value reported for DC-DC converters without isolation

Type	Proposal	Gain	Efficiency (%)	Fs (kHz)
Coupled Inductor	Zhao[20]	7.9	90,100	NR
	Tseng[21]	3.9	93,35	38
	Liang[22]	4.0	90,35	40
	Malo[23]	6.0	87,100	20
Coupled Inductor and Multiplier	Back[24]	8.3	NR,300	20
Tapped Inductor	Cheng[25]	10	NR	NR
	Grant[26]	12	NR	NR
	Fohringer[27]	5	NR,80	NR

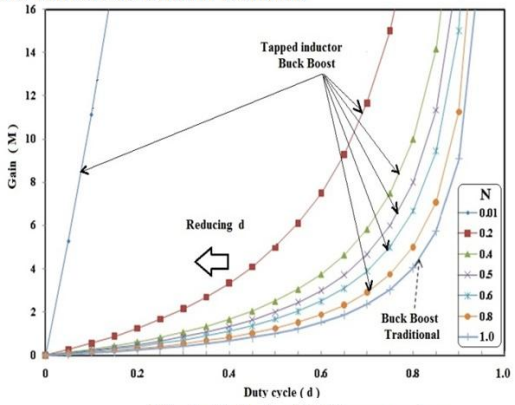

Fig 6. Gain in CCM converters

Develop variants of Boost Buck (BB) converters modified and are classified according to the bypass element connected as: Switch to Tap (**ST**), Diode to Tap (DT), and Rail to Tap (RT), see Fig 7.

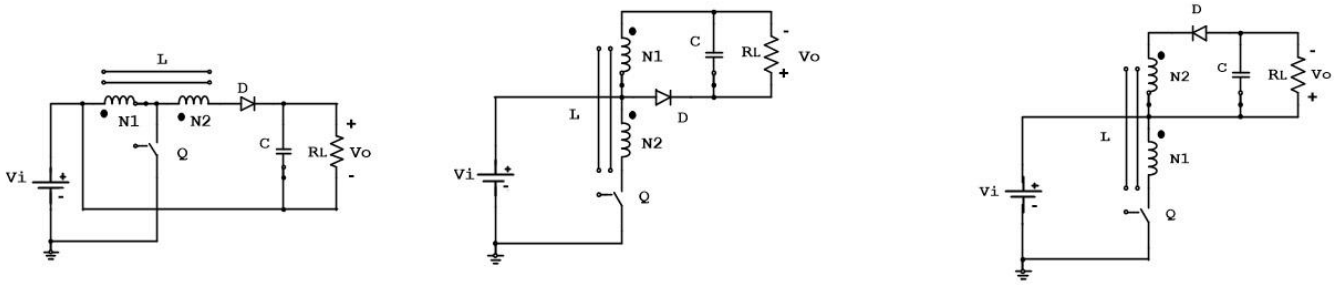

Fig. 7. a) Tap-Switch, ST b) Tap-Diode, DT c) Rail-Tap, RT.

The MIC selected consists of two DC-DC converters of the family TIST-BB, without isolation and with output without grounded (Fig. 8). The conversion of DC-AC is carried through four MOSFET and two diodes. Where two transistors work at Low Frequency (LF) and others two transistors work at High Frequency (HF) together alternately.

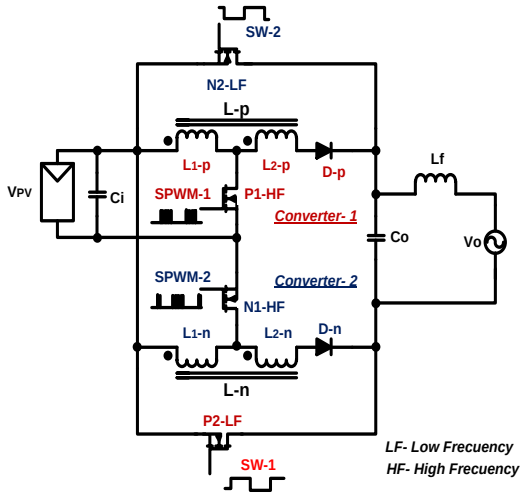

Fig. 8. Elements that switch at different frequencies TIST-BB.

The Table III shows the switching sequence of semiconductor devices for the positive cycle and negative cycle, corresponding to Figure 8.

Table III. Sequence of operation of TIST-BB

Half cycle of the form of AC wave		Positive		Negative	
Control	Devices	1p	2p	1n	2n
SPWM-1	P1-HF	on	off	off	off
SPWM-2	N1-HF	on	on	off	off
	D-p	off	on	off	off
SW-1	P2-LF	off	off	on	off
SW-2	N2-LF	off	off	on	on
	D-n	off	off	off	on

Table IV. Converter design specifications

Symbol	*Description*	*Value*
V_i	Input voltage.	14 V_{DC}
V_o	Output voltage.	200 V_{DC}
P_m	Maximum power.	80 W
ΔV_o	AC output voltage.	10 V
ΔI_L	AC current in the inductor	10 %
f_s	Switching frequency	20 kHz

Table V. Magnitudes of the parameters of the DC/DC converter.

Symbol	*Description*	*Value*
M	Voltage gain of the converter.	14.285
N	Relationship between the primary and secondary	0.5
d	Duty cycle.	0.877
L	Total inductance.	94.55 µH
I_{L1pk}	Primary inductor peak current.	12.98 A
$R_c(d)$	Critical resistance as a function of duty cycle.	500 Ω
$k_c(d)$	Critical factor k as a function of duty cycle.	0.00756
C	Capacitor DC / DC converter.	27.67µF

Table VI. Magnitudes of the parameters of the conditioner

Symbol	*Description*	*Value*
M	Voltage gain of the conditioner	14.285
N	Relationship between the primary and secondary windings	0.5
m_a	Modulation index	0.877
L	Total inductance	94.55 µH
Co	Output capacitor conditioner	0.44 µF

IV. SIMULATION OF MIC

In Fig. 9 show the waveforms of currents and voltages in the MOSFET and diode, obtained from the PSpice simulator. For Vi equal to 14VDC, according to design, we obtain a theoretical value of ILpk=12.98A, the simulator gives a value of 12A. In Fig. 10 are shows the diverse driving modes, DCM, CC and CCM? These changes in driving modes increased flows in the power devices. Thus, also increases the voltage and current at the converter output TIST-BB.

The maximum efficiency is equal to 92% which corresponds to input voltage Vi= 17VDC see Fig. 11. The performance efficiency has approximately linear behavior. The average efficiency for a 40W power converter is 79% for input voltage range between 14 to 17 VDC, see Fig. 12. In the converter DC/DC, as power is increased also increases the duty cycle for each value of input voltage in linear form. For example, when working an output power of 80W and d = 0.88 is achieved with input voltage equal to 180 with a input voltage of 14VDC.

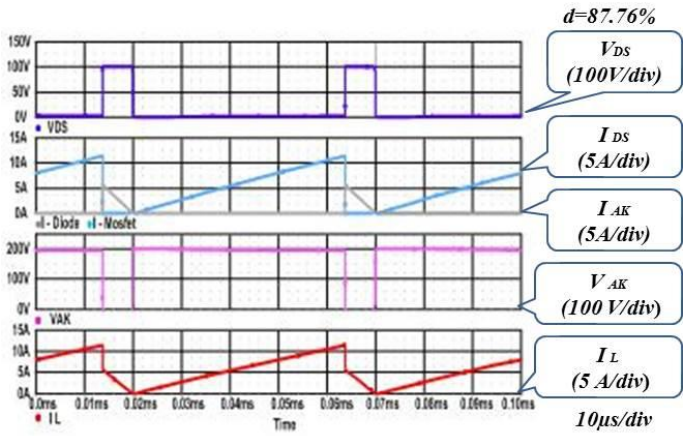

Fig. 9. Results of simulation of design prototype.

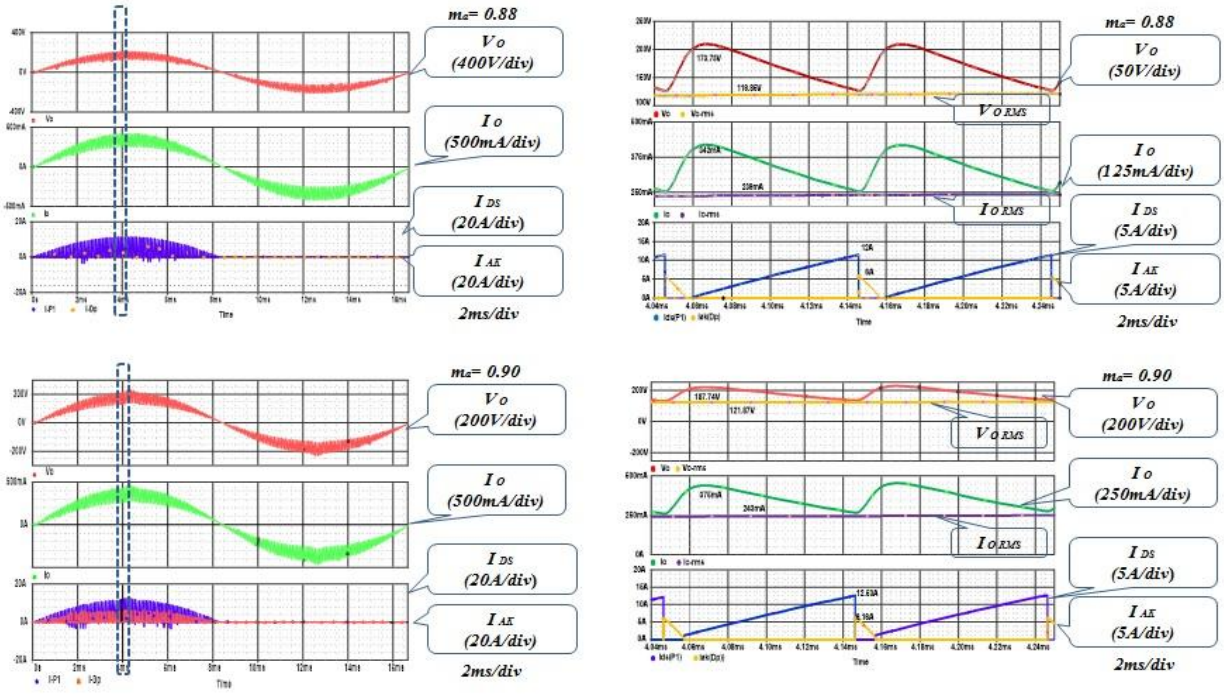

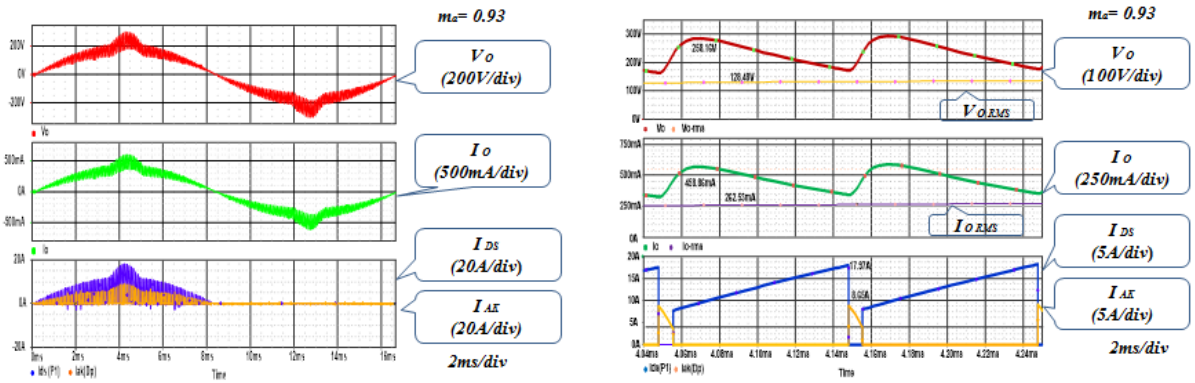

Fig. 10. Results obtained from the simulation by changing the modulation index (m_a), Po = 50W and Vi= 14V_{DC}: waveforms left and right side of an extreme extension to 90 degrees.

The stress in the switching devices are large, with greater detail, a comparison is made between the magnitudes of the results obtained using the simulator (Fig. 13 and 14). To quantify the efficiency, it is appreciated that there is a close to linear performance, where the greater efficiency corresponds to the low output power and less efficiency for the high input voltage.

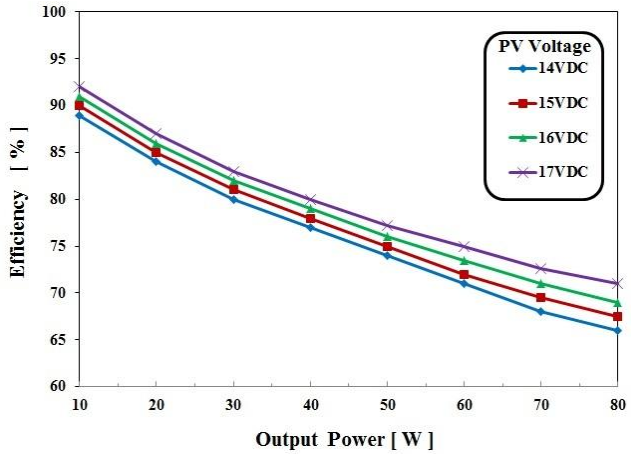

Fig. 11.Describes the performance efficiency against.

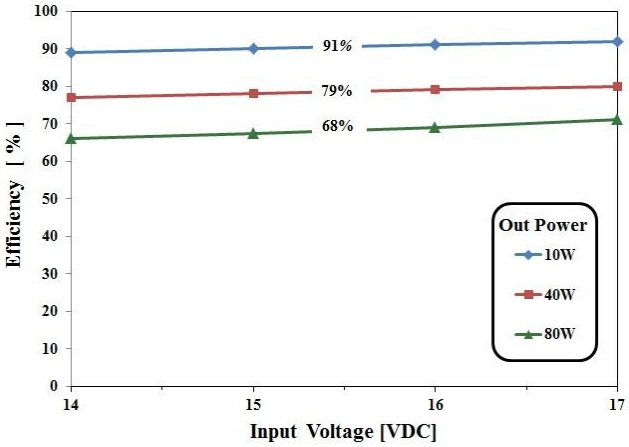

Fig. 12. Shows the average efficiency versus PV voltage.

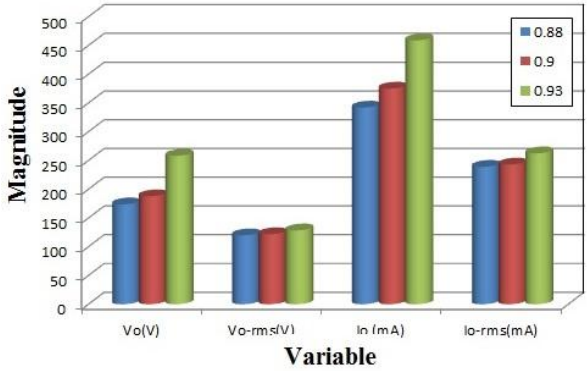

Fig. 13.MIC output variable.

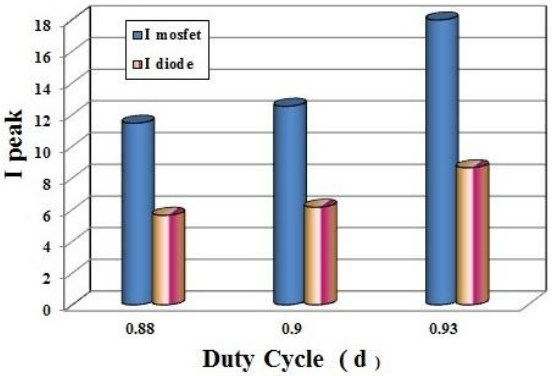

Fig. 14. Stress MIC devices.

V. CONCLUSION

We make an analysis for different types of converters with applications in photovoltaic systems, this analysis allow compare quantitatively and qualitatively between Continuous Conduction Mode (CCM) and Discontinuous Conduction Mode (DCM).

To verify the design methodology, we calculated a converter to the obtained design equations and evaluated in simulation. The results obtained in the simulation are satisfactory; taking up the factor N determines the relationship between the currents IL1 and IL2. In practice, the shunt inductor presents losses of two types: (1) in the copper losses and (2) magnetic core losses. This causes the decrease of the efficiency of MIC in direct proportion to the voltage reduction in the PV module. It confirms that an increase in index "*m*" cause an increase in the voltage and current, both to output, as in the switching devices. It was possible to fulfill the objective of developing a MIC converter capable of raising the direct voltage

input to an appropriate voltage in the mains. The design methodology allows obtain a prototype MIC with built simple, compact and lightweight. We conclude that the proposed MIC can be implemented in micro networks, under the concept of "AC Module"

REFERENCES

[1] Report IEA-PVPS T5-01: Utility Aspects of Grid Connected Photovoltaic Power Systems; 4. AC-MODULE, pp. 4-19.
[2] S.B Kjaer, J.K. Pedersen, F. Blaabjerg, "A review of single-phase grid-connected inverters for photovoltaic modules", IEEE Transactions on Industry Applications, Vol. 41, Issue 5, pp. 1292–1306, October 2005.
[3] J. M. A. Myrzik, M. Calais, "String and module integrated inverters for single-phase grid connected photovoltaic systems", IEEE Power Tech Conference Proceedings, Bologna, Vol. 2, pp. 8, 23-26, June 2003.
[4] M. Byung-Duk, L. Long-Pil, K. Jong-Hyun, K. Tae-Jin, Y. Dong-Wook, R. Kang-Ryoul, K. Jeong-Joong, S. Eui-Ho, "A Novel Grid-Connected PV PCS with New High Efficiency Converter", Journal of Power Electronics, Vol. 8, No. 4, pp. 309-316, October 2008.
[5] C. Gyu-Ha, K. Hong-Sung, H. Hye-Seong, J. Byong-Hwan, C. Young-Ho, K. Jae-Chul, "Utility Interactive PV Systems with Power Shaping Function for Increasing Peak Power Cut Effect", Journal of Power Electronics, Vol. 8, No. 4, pp. 371-380, October 2008.
[6] L. Jong-Pil, M. Byung-Duk, K. Tae-Jin, Y. Dong-Wook, Y. Ji-Yoon, "Input-Series-Output-Parallel Connected DC/DC Converter for a Photovoltaic PCS with High Efficiency under a Wide Load Range", Journal of Power Electronics, Vol. 10, No. 1, pp. 9-13, January 2010.
[7] C. Woo-Young, C. Jae-Yeon, "High-Efficiency Power Conditioning System for Grid-Connected Photovoltaic Modules", Journal of Power Electronics, Vol. 11, No. 4, pp. 561-567, July 2011.
[8] F. Blaabjerg, F. Iov, R. Teodorescu, "Power Electronics in Renewable Energy Systems"; 12th International Power Electronics and Motion Control Conference, pp. 1–17, August 2006.
[9] Chin Quin Yu, Mohan Ned, West Rick and Bonn Russell, "Status and Needs of Power Electronics for Photovoltaic Inverters", Sandia report SAND 2002-1535, pp. ii–iv. June 2002.
[10] S. B. Kjaer, J. K. Pedersen, F. Blaabjerg; "Power inverter topologies for photovoltaic modules-a review", Industry Applications Conference, Vol. 2, pp. 782-788, 13-18 October 2002.
[11] CONERGY, Photovoltaic C125PI-TD-MEX-0602, www.conergy.com.mx.
[12] R. O. Caceres, I. Barbi, "A boost DC-AC converter: analysis, design, and experimentation", IEEE Transactions on Power Electronics, Vol. 14, Issue 1, pp. 134–141, January 1999.
[13] H. Kusakawa, H. Nagayoshi; K. Kamisako, K. Kurahaura, "Further improvement of a transformerless voltage-boosting inverter for ac modules", Solar Energy Material and Solar Cells, Vol. 67, pp. 379-387, March 2001.
[14] N, Kasa, T. Iida, "Flyback type inverter for small scale photovoltaic power system", 28th Annual Conference of the Industrial Electronics Society IECON, Vol. 2, pp.1089-1094, 2002.
[15] W. Chien-Ming, C. Huang-Jen, "A novel single-stage half-bridge series-resonant buck-boost inverter", The Fifth International Conference on Power Electronics and Drive Systems, PEDS, Vol. 2, pp. 1307-1312, November 2003.
[16] W. Chien-Ming; "A Novel Single-Stage Series-Resonant Buck–Boost Inverter, IEEE Transactions on Industrial Electronics", Vol. 52, Issue 4, pp. 1099–1108, August 2005.
[17] S. Jain, V. Agarwal, "A Single-Stage Grid Connected Inverter Topology for Solar PV Systems with Maximum Power Point Tracking", IEEE Transactions on Power Electronics, Vol. 22, Issue 5, pp. 1928–1940, Sep. 2007.
[18] S. Saha, N. Matsui, V.P. Sudarsingh, "Design of a low power utility interactive photovoltaic inverter"; International Conference on Power Electronic Drives and Energy Systems for Industrial Growth, Vol. 1, pp.481–4871, 1998.
[19] T. Esram, P.L. Chapman, "Comparison of Photovoltaic Array Maximum Power Point Tracking Techniques"; IEEE Transaction on Energy Conversion, Vol. 22, Issue 2, pp. 439–449, June 2007.
[20] Z. Qun, F. C. Lee, "High performance coupled-inductor DC-DC converters", Eighteenth Annual Applied Power Electronics Conference and Exposition, Vol. 1, pp. 109-1139, 2003
[21] K. C. Tseng, T. J. Liang, "Novel high-efficiency step-up converter"; IEE Proceedings Electric Power Applications, Vol. 151, Issue 2, pp. 182–190, March 2004.
[22] T. J. Liang, K. C. Tseng; "Analysis of integrated boost-flyback step-up converter"; IEE Proceedings Electric Power Applications, Vol. 152, Issue 2, pp. 217–225, March 2005.
[23] S. Malo, R. Grino, "Output Voltage Regulation of a High-Efficiency High Step-Up DC-DC Power Converter"; IEEE International Symposium Industrial Electronics, ISIE 2007. pp. 854–859, June 2007.
[24] B. Ju-Won, R. Myung-Hyo, K. Tae-Jin, Y. Dong-Wook, K. Jong-Soo, "High boost converter using voltage multiplier"; 31st Annual Conference on Industrial Electronics Society, IECON 2005, pp. 567-5726, November 2005.
[25] K. W. E Cheng, "Tapped inductor for switched-mode power converters"; Power Electronics systems and Applications; ICPESA '06, pp. 14–20, 2006.
[26] D. A. Grant, Y. Darroman, J. Suter, "Synthesis of Tapped-Inductor Switched-Mode Converters"; IEEE Transactions on Power Electronics, Vol. 22, Issue 5, pp. 1964–1969, 2007.
[27] J. P. Fohringer, F. A. Himmelstoss, "Analysis of a boost converter with tapped inductor and reduced voltage stress across the buffer capacitor"; IEEE International Conference Industrial Technology ICIT, pp. 126–131, December 2006.
[28] S. V. Araujo, P. Zacharias, B. Sahan, R. P. Torrico Bascope, F. Antunes, V. Araújo, S. Z. Peter; R. Bascope-Torrico; A. Fernando L.M; "Analysis and proposition of a PV module integrated converter with high voltage gain capability in a non-isolated topology"; 7th International conference on Power Electronics EXCO Daegu, Korea, pp. 511-517, October 2007.
[29] S. V. Araùjo, P. Zacharias, B. Sahan, "Novel Grid-Connected Non-Isolated Converters for Photovoltaic Systems with Grounded Generator"; 39th IEEE Annual Power Electronics Specialists Conference, PESC, pp. 58-65, June 2008.
[30] H. Cheng, K. M. Smedley, A. Abramovitz; "A Wide-Input-Wide-Output (WIWO) DC –DC Converter"; IEEE Transactions on Power Electronics, Vol. 25, No.2, pp. 280-289, February 2010.
[31] B. Yang, W. Li, Y. Zhao, X. He, "Design and Analysis of a Grid-Connected Photovoltaic Power System"; IEEE Transactions on Power Electronic, Vol. 25 No.4, pp. 992-1000, April 2010.
[32] L. F. Lin, Advance DC/DC converters-power electronic and applications series; CRC Press LLC .www.crcpress.com.

International Journal of Modern Engineering Research (IJMER)
www.ijmer.com Vol.3, Issue.2, March-April. 2013 pp-1245-1252 ISSN: 2249-6645

Anomaly Detection Using Generic Machine Learning Approach With a Case Study of Awareness

Goverdhan Reddy Jidiga, [1] Dr. P Sammulal[2]
[1]*Research Scholar, JNTU & Lecturer in CSE, Department of Technical Education, Govt. of Andhra Pradesh, India*
[2]*Senior Assistant Professor, JNTUCEJ, JNT University Hyderabad, Andhra Pradesh, India*

Abstract: *Security of computer systems and information in flow is essential to acceptance for every network user utilities Now the standalone computer and internets are exposed to an increasing number of security threats with new types of attacks continuously appearing. For this to develop a robust, flexible and adaptive security oriented approaches is a severe challenge. In this context, anomaly based intrusion detection technique is an advanced accurate technique to protect data stored at target systems and while flow in the networks against malicious activities. Anomaly detection is an area of information security that has received much attention in recent years. So in this paper we are going to elaborate a latest techniques available in machine learning approach applied to anomaly detection which are used to thwarts the latest attacks like cyber based attacks and malware infections. Finally a case study is discussed on latest cyber attacks phased by top web domains and countries in the world motivated by a traditional security ethic are called E-Awareness.*

Keywords: *Anomaly, Cyber attacks, Machine learning, Malware, Phishing,*

I. INTRODUCTION

Every day the cyber criminals are invading countless homes and offices across the nation not by breaking down windows and doors, but by breaking into laptops, personal computers, and wireless devices via hacks and bits of malicious code. For this billions of dollars are lost every year repairing systems hit by such attacks. Some take down vital systems, disrupting and sometimes disabling the work of hospitals, banks, other services around the world. Today, these computer intrusion cases like counterterrorism, counterintelligence, and criminals are the paramount priorities of our cyber program because of their potential relationship to national security. The solutions are there, but not terminate permanently so only case that gather vital intelligence that helps us identify the cyber crimes that are most dangerous to our national security and to our economy.

Anomaly detection is type of Intrusion detection and the Intrusion detection [29] defined as the process of monitoring the anomaly based events occurring in a computer system or network and analyzing them for signs of intrusions, defined as attempts to bypass the standard security mechanisms of a clean computer or network that are compromise the confidentiality of the valuable data, data integrity, availability and access control of information sources as well as resources. Intrusion detection system (IDS) [15] is a combination of software and hardware that attempts to perform intrusion detection protection to normal users and system resources from information security threats. Computer security analysts use intrusion detection systems to assist them in maintaining computer system security. There were numerous attacks on software systems result in a process execution or human coding mistakes deviating from its normal behavior[2] , all these prominent examples include a malware related code injection attacks on internet server's processes and with resulting from buffer overflow and format string vulnerabilities. Up to now we have seen significant amount of research to detect such attacks through monitoring the behavior of the suspected process and comparing that behavior to a model [3] consist of normal behavior collected from past experiences. These are also called anomaly detection techniques because in compare to signature based detection which deviates from the normal behavior are taken as indications of anomalies.

II. ANOMALY DETECTION

2.1 Introduction

In this the basic unit of finding abnormal behavior is identified as an anomaly. Anomaly [8, 29] is a pattern in the data that does not conform to the expected behavior, depending on the nature of input data collected from profiles that represent normal behavior of users, applications, hosts, networks, and detecting attacks as significant deviations from this profile. Anomaly detection is monitors program executions and detects anomalous program behaviors through reverse analysis of executable program including a critical behavior monitoring points can be extracted from binary code sequences [2] and memory space. Most of the available intrusion detection systems are predominantly signature based, so such systems are not used to find the frequent rule based attacks, unknown attacks and updates. The existing systems even if it is designed by traditional and advanced anomaly detection techniques are not observing real world anomalies like emerging cyber threats, cyber intrusions, credit card frauds...etc. The anomalies occur relatively infrequently and their consequences can be quite dramatic, negative sense in the running of applications

2.2 Why Anomaly Detection

The security breaches are very common now in the society and organizations fail to take effective measures, with the legal action by authorities over breaches of and devastating damage to brands, reputation and customer confidence. When it comes to new technologies organizations have needed to move quickly, but they are not responding fast. Now smart

phones and latest gadgets were primarily used by everyone, so in the same way risks related to mobile devices, social media and in critical infrastructure are worst[21]. The business and personal use they have forced organizations to urgently implement policies that address the risks associated with an evolving array of emerging technologies.

Also the organizations are protecting how they guard to their data of the employees and their customers like service based organizations in the world phasing number of problems from attacks and threats with latest criminal mind showing their illegal operations. Today cyber attacks are common in the public banking sector, health organizations, defense, and service sector , so organizations are need to give training and guidelines, policy adjustments, stepping up awareness programs. So our aim is to prepare for an effective solutions working online and on the fly counter action is required to avoid the cyber criminals, viruses, malware and botnets shown. The security teams and experts must work round the clock to actively manage the risks created by threats in different top rated domains like business, online-shopping, social media including comprehensive policies and effective security controls. Now experts need to not only consider how they can occur and use powerful analytics to detect security events but also realize to aware of dynamic threats caused by malicious events.

Area/ Domain / Threat (Anomaly)	Stable Computers	Networks &Comm'n	Banking Sector	Health and Insurance	Social Network'g	Service sector orgs	Defense	World Economic	Supply-Chain Marketing	Cloud Computing	ICT/IT Sector
Cyber fraud	•	✓	✓	✓	✓	✓	✓	✓	✓	•	o
Malware	✓	✓	✓	✓	✓	✓	✓	✓	✓	✓	✓
Insecure API	•	✓	✓	✓	•	✓	✓	•	•	✓	✓
Wanted assaults	✓	✓	✓	✓	✓	✓	✓	o	•	o	✓
Organized crime	•	✓	✓	✓	✓	✓	✓	•	✓	✓	✓
Cyber war	•	✓	•	•	✓	✓	✓	✓	o	o	•
Cyber spying	✓	✓	✓	✓	✓	✓	✓	•	o	✓	✓
Nation states	•	✓	✓	•	✓	•	✓	✓	•	•	o
Big Data	•	•	o	✓	o	•	•	•	•	✓	o
Program source threats	✓	✓	•	•	✓	✓	•	•	•	✓	✓
Hacking as a service	•	✓	✓	✓	✓	✓	✓	o	✓	•	✓
Device Target (BYOD)	✓	✓	•	✓	✓	o	•	•	•	•	✓
Social Crime	•	✓	✓	✓	✓	✓	✓	✓	✓	✓	✓
Hactivism	✓	✓	✓	✓	✓	✓	✓	✓	✓	•	•
Fake certificates	•	✓	✓	✓	✓	✓	✓	•	✓	✓	•
Mobile Malware	✓	✓	•	•	•	✓	•	•	•	•	✓
Ransomware	✓	✓	✓	✓	✓	✓	o	✓	✓	o	✓
Cyber Miasma	•	•	•	•	•	•	•	✓	•	•	✓

• Low o Medium ✓ High

Fig.1. Threats Vs Area/Domain in 2012

According to information security survey [21, 22, 23] up to 2012 the threats and malware infections on the top list found in the world is classified according to area or domain as following Figure-1. In this there are many critical infrastructure top web domains are affected by different threats and their impact low, medium, and high. To overcome these threats we use the anomaly detection with usage of machine learning approaches [29]. The main uses for Anomaly Detection are detect precedent attack behavior, zero day attack detection, intrusion model, insider threat detection, situational awareness and validate or assist with signature data. The major advantages of anomaly detection are network intrusion detection, insurance or credit card fraud detection, healthcare informatics or medical diagnostics, industrial spoil detection, video surveillance or image processing, novel topic detection in text mining and so on. Anomaly detection (AD) systems have some advantages [27, 29]. First AD have the capability to detect insider attacks like someone using a stolen account starts performing actions that are outside the normal user profile, an anomaly detection system generates an alarm. Second, AD is based on customized profiles, it is very difficult for an attacker to know with certainty what activity it can carry out without setting off an alarm. Third, an anomaly detection system has the ability to detect previously unknown attacks.

III. RELATED WORK

Most of the anomaly intrusion detection systems are signature based and fundamental statistics or knowledge based, but these are all suitable in some applications and not suitable today in advanced technical concepts. Now we discussed some related work on old and new one is based on machine learning discussed in next paragraph. Anderson is the first person elaborated the intrusion concept in security and he developed model [1] threats are classified as external penetrations, internal penetrations, and misfeasance. The Anderson model [5] is good initially, but now it is not suitable. Denning proposed several models for Intrusion Detection System (IDS) development based on statistics, Markov chains, time-series, etc [4]. In Denning model, user's behavior that deviates sufficiently from the normal behavior is considered anomalous. Stanford Research Institute developed an Intrusion Detection Expert System (IDES) that continuously monitored user behavior and detected suspicious events. Later SRI developed an improved version of IDES called the Next-Generation Intrusion Detection Expert System (NIDES) [05] that could operate in real time for continuous monitoring of user activity. NIDES enable the system to compare the current activities of the user/system/network with the audited intrusion detection variables stored in the profile and then raise an alarm if the current activity is sufficiently far from the stored audited activity. A statistical anomaly based IDS were proposed by Haystack [29], which used both user and group based anomaly detection

strategies. In this system, a range of values were considered normal for each attribute and during a session if an attribute fell outside the normal range then an alarm raised. It was designed to detect six types of intrusions: attempted break-ins by unauthorized users, masquerade attacks, penetration of the security control system, leakage, denial of service, and malicious use. SNORT is an open source network intrusion detection and prevention system (NIDPS) developed by Sourcefire. In 1996, Forrest proposed an analogy between the human immune system and intrusion detection that involved analyzing a program's system call sequences to build a normal profile [10], if the sequences deviated from the normal sequence profile then it considered as an attack. The system they developed was only used offline using previously collected data and used a quite simple table-lookup algorithm to learn the profiles of programs.

Machine learning based work: In 2000, Valdes [11] developed an anomaly based intrusion detection system that employed naïve Bayesian network to perform intrusion detecting on traffic bursts. In 2003, Kruegel [26] proposed a multisensory fusion approach using Bayesian classifier for classification and suppression of false alarms that the outputs of different IDS sensors were aggregated to produce single alarm. In the same year, Shyu [12] proposed an anomaly based intrusion detection scheme using principal components analysis (PCA), where PCA was applied to reduce the dimensionality of the audit data and arrive at a classifier that is a function of the principal components. In [19,20] proposed an anomaly based intrusion detection using hidden Markov models that computes the sample likelihood of an observed sequence using the forward or backward algorithm for identifying anomalous behavior from normal behaviors. Lee [7, 13] proposed classification based anomaly detection using inductive rules to characterize sequences occurring in normal data. In 2000, Dickerson [14] developed the Fuzzy Intrusion Recognition Engine using fuzzy logic that process the network input data and generate fuzzy sets. So therefore, the primary and most important challenge is we needs to be develop the on the fly countermeasures and effective strategies to reduce the high rate of false alarms.

IV. MACHINE LEARNING

In this paper we concentrated on machine learning techniques , because machine learning approaches use strong statistical foundations to enhancing the dynamic and accurate learning that gives better accuracy, small false alarm rates, learned detectors use a more compact representation, possible performance improvements, ability to detect novelty, protection against zero-day exploits, faster incident response times.etc. Machine Learning systems [17, 27] offer unparallel flexibility in dealing with evolving input in a variety of applications, such as intrusion detection systems and spam e-mail filtering. However, machine learning algorithms themselves can be a target of attack by a malicious adversary. In the machine learning different novel contributions of techniques include taxonomy of different types of attacks on systems, a variety of defenses against those attacks.

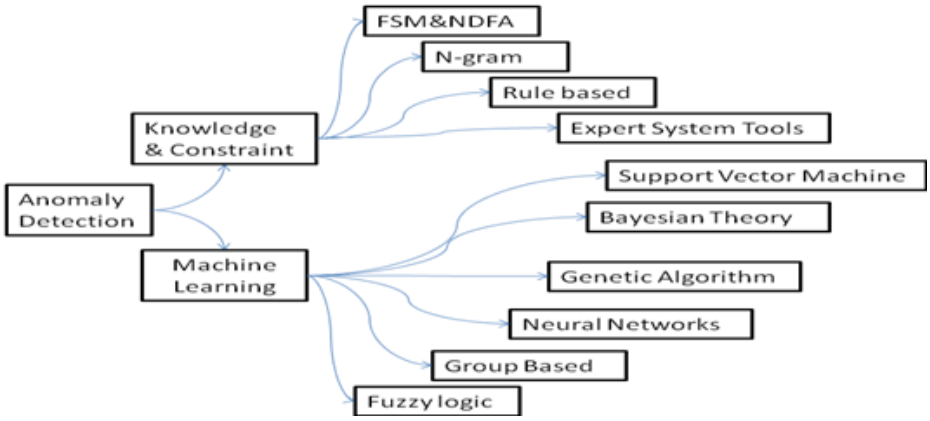

Fig.2. Taxonomy of Anomaly Detection based on Machine learning.

In the fig.2 the anomaly detection taxonomy[8,15] is given, it is based on classification of anomaly detection which is purely based foundational work done past authors of intrusion detection systems models and today performance based machine learning approaches. In this taxonomy the anomaly detection is based on machine learning and data mining approaches. The machine learning approaches use strong statistical foundations to enhancing the dynamic and accurate learning that gives better accuracy, small false alarm rates.

4.1 Proposed Model

In fig.3 the machine learning based AD (Anomaly Detection) is used and prototype is given with preprocessing data. In AD (Anomaly Detection) prototype model the audit data collection module is used in the data collection phase. The data collected in this phase is analyzed by the anomaly detection algorithm to find traces of suspicious activity. The source of the data can be host/network activity logs, command-based logs, application-based logs, etc. audit data in intrusion detection systems store the audit data either indefinitely or for a sufficiently long time for later reference. The volume of data is often exceedingly large, so persistent database is maintained.

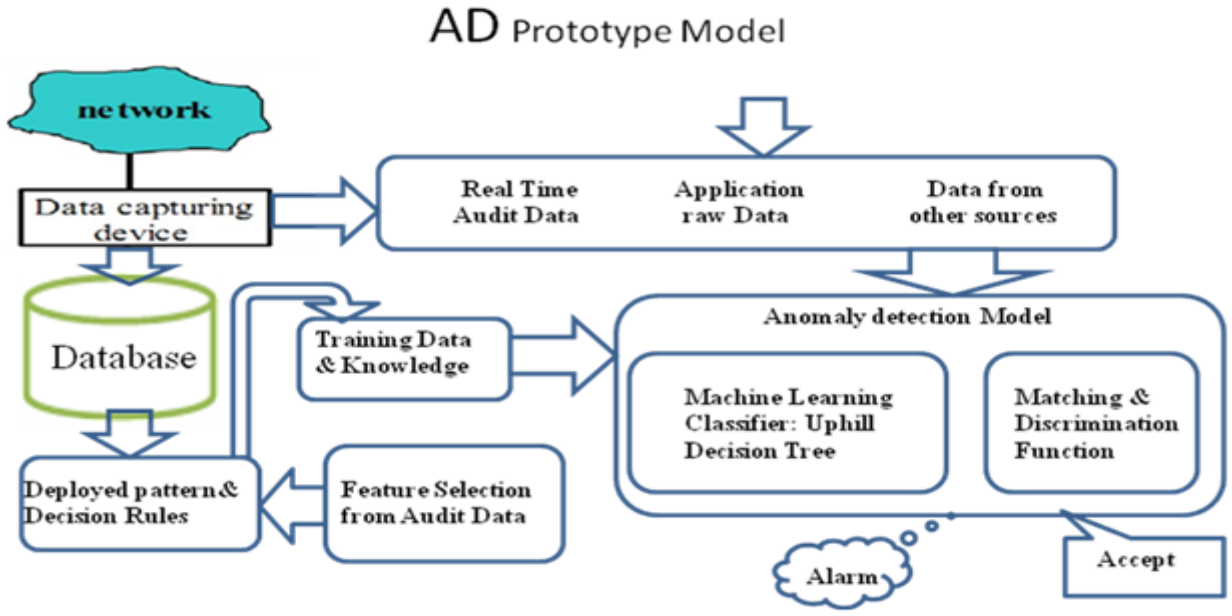

Fig.3. Anomaly Detection (AD) Prototype Model with Machine learning.

In Anomaly detection model the processing is here the algorithms to detect suspicious activities are implemented. Algorithms for the analysis and detection of intrusions have been traditionally classified into three broad categories: signature (or misuse) detection, anomaly detection and hybrid (or compound) detection. The configuration data is extracted from network database and user deployed rules framed from information that is pertinent to the operation of the intrusion detection system itself such as information on how and when to collect audit data, how to respond to intrusions, etc. Due to the complex and dynamic properties of intrusion behaviors, machine learning and data mining methods have been generally employed to optimize the performance of intrusion detection systems to finding specific point anomalies or range anomalies at moment of time. We give an efficient algorithm for provably learning uphill decision tree with extension adornments of existing multi-way decision tree algorithm. In fig.3 the machine learning is decision tree algorithm is considered first and later it is extended to uphill decision tree also called regression tree. The processing element must frequently store intermediate results such as information about partially fulfilled anomalies. The model contains a logic taken from uphill decision tree detect the anomalies by raising notified alarms.

4.2 Proposed Machine Learning Algorithm : A Uphill Decision Tree (UDT)

The Decision tree (DT) learning [18, 29] is a type of machine learning algorithm used in many application of information security in previous research. The decision tree (DT) is very powerful and popular data mining algorithm for decision-making and classification problems. It has been using in many real life applications like medical diagnosis, radar signal classification, weather prediction, credit approval, and fraud detection etc. DT can be constructed from large volume of dataset with many attributes, because the tree size is independent of the dataset size. A decision tree has three main components: nodes, leaves, and edges. Each node is labeled with an attribute by which the data is to be partitioned. Each node has a number of edges, which are labeled according to possible values of the attribute. An edge connects either two nodes or a node and a leaf. Today it is olden and not effecting in current cyber attacks. So the extension of this is an uphill decision tree.

A decision tree with real values at the leaves is called an uphill decision tree if the values on the leaves are non-decreasing in order from left to right. An Uphill decision tree is similarly a tree structured solution in which a constant or a relatively simple regression model is fitted to the data in each partition. In this algorithm we considered the data collected for e-mail to filtering whether it is phishing or spam.

Phishing [21] is a type of Internet fraud deployed to steal confidential financial information that includes theft of net banking passwords, corporate secrets, credit card numbers, financial status, bank account details and other valuable information and spam is anonymous, unsolicited bulk email diverting the cybercitizen's minds to use their services and products etc. phishing is also type of spam.

The total number of phishing emails and spam are increasing day to day, up to 2012 the top domains and areas in the world suffering with cyber threats like DOS, DDOS,SQL Injection, spamming attacks , phishing attacks and others. In that most of them are spam , phishing attacks affected on online banking, Online purchasing (PayPal, Amazon, eBay, etc.), Social media (Face book, Twitter, blogs, etc.) in all corners.

The semantics of e-mail are like domain, class, frequency, link, URL, IP address, script, validation, port address, dot, images, no. of ports valid or not, link valid or not, mismatching ..Etc available. Based on that we can estimate that the mail or websites are legitimate or phishing by using a pre determined set of rules designed in the construction of uphill decision tree.

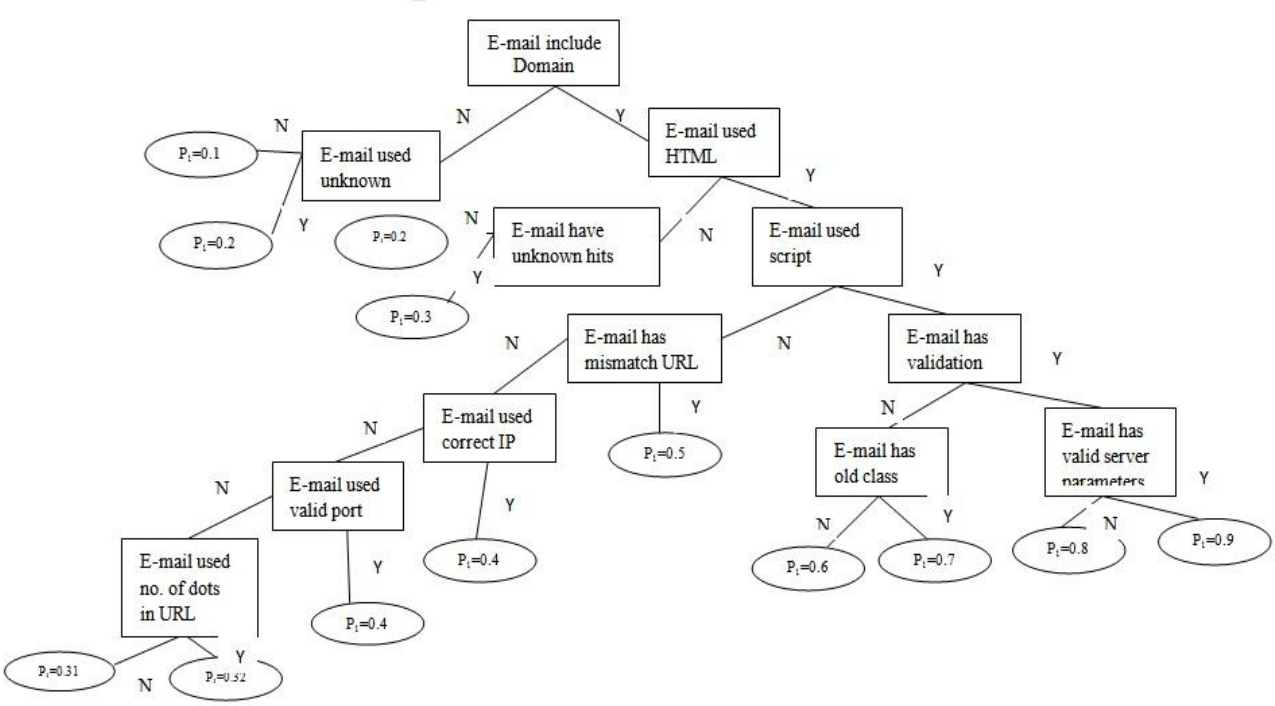

Fig.4. Uphill Decision Tree for e-mail verification to estimate the Phishing attack.

In fig.4 we have applied a concept of uphill decision tree (statistics are assumptions only) for e-mail verification whether the e-mail is come from legitimate organizations or not. The mail semantics are compiled by tree one by one and find the some unknown semantics are encountered that we compare with original semantics of e-mail.
In this we take an example-1 of e-mails is registrar@jntuh.ac.in, from jntuh.ac.in/new/academic/contacts_us.html, in JNTU.

Here if (domain=TRUE&e-mail-has=HTML&script=Java_script&Validation=TRUE&server=authenticate)
Then P (e-mail Semantics) = "90%". (This value depending on other semantics also)

In this e-mail, if all semantics are correct and verified by decision tree including URL, no. of dots in URL, IP address and port of application then we can probably identify that mail come from authorized party.

Example-2: VISA card related mail from VISA organization contains unknown hits like "dear valued customer" shown in fig.5, But in original mail from bank is not contains semantics like "dear valued customer".

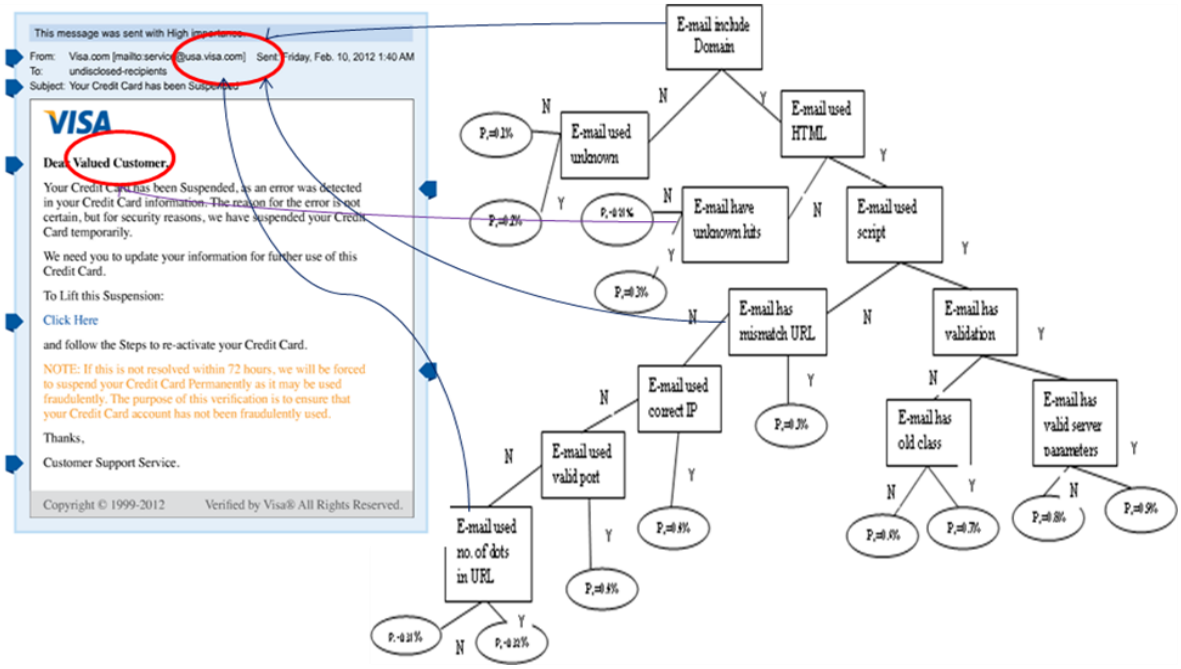

Fig.5. Phishing attack based e-mail verification came from VISA

Here if (domain=TRUE &e-mail-has="unknown hits") then P (e-mail Semantics) = "20%". (This value depending on other semantics also)

In this e-mail, first semantic is correct and verified by decision tree and semantic at node-3 has unknown hits may not included in semantics of VISA mail including URL, no. of dots in URL, IP address and port of application then we can probably identify that mail come from unauthorized party.

4.3 Ethical Solution to Phishing : E-Awareness and Case Study

The basic E-security awareness [23] is a process of keeping people in continuous attention of security to save information. In the abstract we clearly mentioned e-awareness also a part information security ethics to thwart a most vulnerabilities as "security awareness is better than prevention and prevention is better than detection". This was an ethic concept applied in all kinds of human life applications to survive in the nature. The people who are expert in security aspects to thwart the security deficiencies, eligible to train all users of information technology to identify and report the all kind of suspicious activities in their electronic environment. Now it is essential that each of us take responsibility and understand our role in securing cyberspace.

ACM Report[28] given the countermeasures on phishing is creating awareness and train end users to proactively recognize and avoid phishing attacks (ethical and very popular approach).The solutions are motivating people to be secure, micro games designed to teach people about phishing and embedded training.

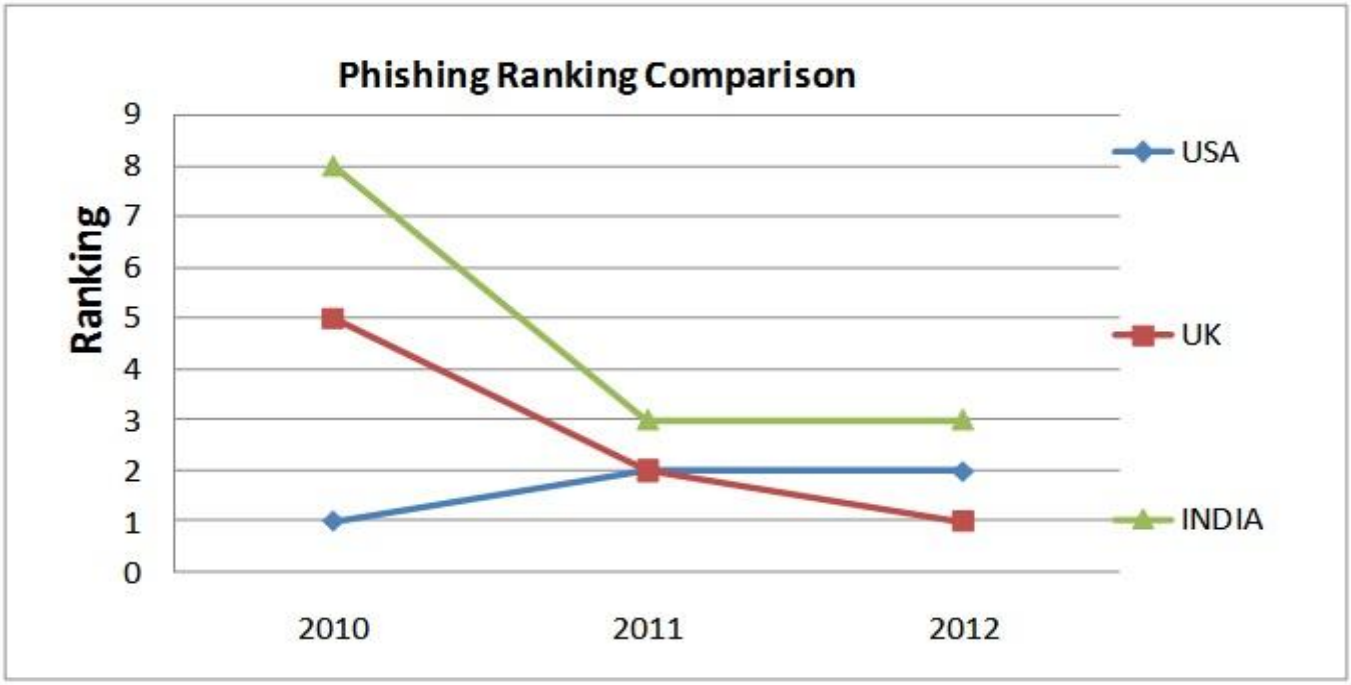

Fig.6. Phishing attack Ranking

From 2010 to 2013 USA ranking is going to down shown in fig.6, because the public and private partnership security awareness months [21, 23, 24] programs conducted by hundreds of organizations like

1) National Cyber-Security Alliance, FBI
2) U.S. Department of Homeland Security
3) DHS with RSA-EMC, Google, McAfee, Microsoft, Symantec, ADP, AT&T, Cisco, IBM
4) CERT, FTC, NCL.

The DHS of USA taking an active involvement in the control of all types of cyber threats by creating awareness, responsibility, co-operation, policy enforcement, and also motivating people to learn ethics.

The reasons to reduce the phishing in USA:

1) They are conducting fast track E-security awareness programs by monthly in different states.
2) Most of government and private organizations believing that "Awareness is only an impressive and vital element of the phishing combat".
3) USA promoting awareness, education, research on addressing the latest challenges well in advance.
4) Regular recommendations to update policies, guidelines, and risk assessment.
5) USA anti phishing group suggesting to use look ahead technology to avoid loss.
6) Respond rate is high due to education and motivation.
7) In 2012 USA conducted 120 awareness programs conducted approximately.
8) Regular alerts and reports.

The reasons to increase the phishing attacks in UK:

1) UK banking and financial institution customers use heavy online money transactions.
2) 84% people of UK using internet daily at least once and create breaches.
3) In UK most of the people use the mobile internet transaction leads to increasing phishing and also malware infection.
4) Insider impersonation of the organization.
5) Lack of coordination among the consumers and financial institutions to report latest trends in phishing.
6) Latest brands in the market

What are the reasons for increasing phishing and spam [22] in India are :

1) Lack of awareness, education and responsibility.
2) Lack of use of new technology and using of poor technology.
3) High unemployment, illiterate, ignorance, population and competition in the market.
4) Lack of government support, policy constraints, coordination, law.
5) Greediness in earning of easy money.
6) May fast economy development and technology using.
7) Use of pirated software.
8) Rate of using internet.
9) Huge growth in the usage of Mobiles.
10) System sharing.

V. CONCLUSION

In this paper we accepted only a machine learning approach to anomaly detection and applying to phishing attacks. Now phishing will persist in any electronic medium pursue a problem that can never truly be solved. In this nest better we can work on always to preventing, detecting, and responding to this e-awareness. Finally in this paper we present a case study on phishing attack based on the awareness model and today the machine learning is only approach encouraged by well known scientists in the field of security. So this will give concepts and motivates to you a do further research and also hope that this work to be true at our knowledge.

REFERENCES

[1] J.P.Anderson,"Computer security threat monitoring and surveillance," James P Anderson Co.,Fort Washington,Pennsylvania, USA, Technical Report 98–17, April 1980.

[2] H. H. Feng, Oleg M. Kolesnikov, P. Fogla, Wenke Lee, and Weibo Gong, "Anomaly Detection Using Call Stack Information"IEEE Symposium on Security and Privacy'2003, CA, Issue Date: 11-14 May2003 pp: 62-75 ISSN: 1081-6011 Print ISBN: 0-7695-1940-7.

[3] D. Wagner and D. Dean, "Intrusion Detection via Static Analysis", IEEE Symposium on Security and Privacy, Oakland, CA, 2001.

[4] D. E. Denning "An intrusion detection model" In IEEE Transactions on Software Engineering, CA,1987. IEEE Computer Society Press.

[5] D. Anderson, T . Frivold, and A.V aldes."Next-generation intrusion detection expert system (NIDES): A summary" Technical Report SRI–CSL–95–07,Computer Science Laboratory,SRI International, May 1995.

[6] Mukkamala,J.Gagnon,andS. Jajodia."Integrating data mining techniques with intrusion detection methods" Research Advances in Information Systems Security, Kluwer Publishers, Boston, MA. 33-46,2000.

[7] W.Lee, ChanP.K, Eskin, E WeiFan, Miller M. S.Zhang "Realtime datamining based intrusion detection" IEEE DARPA information Conference 2001,DISCEX'01,Proceedings IssueDate: 2001 page(s):89-100vol.1 12 Jun2001-14 Jun 2001 Print ISBN:0-7695-1212-7.

[8] S.Axelsson,"Intrusion Detection Systems: A Survey and Taxonomy," Chalmers University, Technical Report 99-15,March 2000.

[9] S.E.Smaha,"Haystack:An Intrusion Detection System," in IEEE Fourth Aerospace Computer Security Applications Conference, Orlando, FL, 1988, pp. 37 – 44.

[10] S. Forrest, S. A. Hofmeyr, A. Somayaji, and T. A. Longstaff, "A Sense of Self for Unix Processes," in IEEE Symposium on Research in Security and Privacy, Oakland, CA, USA, 1996, pp. 120--128.

[11] A. Valdes and K. Skinner, "Adaptive Model-based Monitoring for Cyber Attack Detection," in Recent Advances in Intrusion Detection Toulouse, France, 2000, pp. 80-92.

[12] M.L.Shyu,S.C.Chen,K.Sarinnapakorn, and L.Chang,"A Novel Anomaly Detection Scheme Based on Principal Component Classifier," in IEEE Foundations and New Directions of DataMining Workshop, Florida, USA, 2003, pp. 172-179.

[13] W. Lee and S. J. Stolfo, "Data mining approaches for intrusion detection," in 7th USENIX Security Symposium (SECURITY-98), Berkeley, CA, USA, 1998, pp. 79--94.

[14] J.E.Dickerson and J.A.Dickerson,"Fuzzy network profiling for intrusion detection",in 19th Intern'l Conference of the North American Fuzzy Information Processing Society(NAFIPS),Atlanta, 2000, pp. 301 – 306.

[15] L.Ertoz, E.Eilertson, A.Lazarevic, P.N. Tan, V. Kumar, J. Srivastava, and P. Dokas, "The MINDS - Minnesota Intrusion Detection System", in Next Generation Data Mining Boston: MIT Press, 2004.

[16] S.Mukkamala, G.I.Janoski, and A.H.Sung."Intrusion Detection Using Support Vector Machines",Proceedings of the High Performance Computing Symposium- HPC 2002, pp 178-183, San Diego, April 2002.

[17] T. Lane and C. E. Brodley. "An Application of Machine Learning to Anomaly Detection", Proceedings of the 20th National Information Systems Security Conference, pp 366-377, Baltimore, MD. Oct. 1997.

[18] Quinlan, J. Ross, "Induction of Decision Trees," Machine Learning, 1:81{106, 1986. Reprinted in Shavlik, J. and Dietterich, T.,Readings in Machine Learning, San Francisco: Morgan Kaufmann, 1990, pp. 57-69.

[19] Ghahramani Z,"An introduction to hidden markov models and bayesian networks". HMM: applications in computer vision, pages 9–42, 2002.

[20] HaiTao H,XiaoNan L,"A novel HMM-based approach to anomaly detection", Journal of Information and Computational Science 1 (3) (2004) 91–94.

[21] http://www.antiphishing.org/

[22] http://india.emc.com

[23] http://www.rsa.com

[24] http://www.cisco.com

[25] A. Ghosh and A. Schwartzbard, " A study in using neural networks for anomaly and misuse detection", 8th USENIX Security Symposium, pp. 141-151, 1999.

[26] C. Kruegel, D. Mutz, W. Robertson, and F. Valeur, "Bayesian Event Classification for Intrusion Detection," in 19th Annual Computer Security Applications Conference, Las Vegas, NV, 2003.

[27] L.Breiman,"Random Forests,"Machine Learning,vol. 45, pp. 5-32, 2001.

[28] By Jason Hong, "article on The State of Phishing Attacks" Communications of the ACM, Vol. 55 No. 1, Pages 74-81.

[29] A. Patcha, J-M. Park, "An Overview of Anomaly Detection Techniques: Existing Solutions and Latest Technological Trends", Computer Networks(2007)

[30] M. Roesch, "Snort - Lightweight Intrusion Detection for Networks " in Proceedings of the 13th USENIX conference on System administration Seattle, Washington 1999 pp. 229-238.

International Journal of Modern Engineering Research (IJMER)
www.ijmer.com Vol.3, Issue.2, March-April. 2013 pp-1253-1255 ISSN: 2249-6645

Cyclic Deformation of Hastelloy and Inconel Alloys and Slip Bands Formation

Aezeden Mohamed
Faculty of Engineering and Applied Science, Memorial University, St. John's, NL, Canada

Abstract: *Hastelloy C22 and Inconel 600 and 601 alloys specimens were cyclically deformed. Specimens were sectioned and investigated. Results indicated that the grain structure of Hastelloy C22 revealed planar slip bands, whereas Inconel 600 and 601 showed slip bands having triangular ribbon morphology. The triangular ribbon bands were more distinct in Inconel 601 than in Inconel 600.*

Keywords: *Hastelloy, Inconel, planar bands, triangular ribbon bands, cyclic deformation.*

I. INTRODUCTION

Slip bands are very common features in fatigued alloys such as aluminum alloy and nickel alloys [1,2], the formation of which has been attributed to their low stacking-fault energy (SFE). Low SFE leads to the formation of wide and extended dislocations, with reduced ability of screw dislocations to cross-slip onto other slip planes.

The occurrence of slip bands in materials depends on their stacking-fault energy. However, several authors [3–5] have demonstrated that reduced stacking-fault energy may not be the reason for the manifestation of deformation as slip banding in some solid solutions. They suggested that carbon content plays a great role in determining the nature of bands in nickel alloys [3-5] and other precipitation hardened alloys. The precipitates within the matrix sheared due to dislocations movement [5-8]. Normally, precipitation-hardened alloys show wavy bands in a way similar to that exhibited by single-phase alloys with high stacking-fault energy. Clavel and Pineau suggested that that the formation of slip bands was the prime factor for initiating nucleation which leads to fracture in nickel-based alloys. They also studied cyclic deformation of supper alloy IN718 concluded that the precipitates were slipped during cyclic deformation. Worthem [9] also observed a set of groups of deformation slip bands during cyclic deformation of IN718. Therefore, although slip bands have been observed due to SFE by several investigators [6–8], there seems to be no study on the investigated the effect of carbon content on slip bands of Hastelloy C22, Inconel 600, and Inconel 601. In the present study, scanning electron microscope (SEM) was employed to investigate the morphology of slip bands formed in these alloys during cyclic deformation.

II. MATERIALS AND EXPERIMENTAL PROCEDURES

To investigate the morphology of slip bands in Ni-based alloys, round bars of Hastelloy C22, Inconel 600 and Inconel 601 were machined into standard fatigue specimens. Their chemical compositions are given in Table 1. Prior to tension-tension fatigue testing, the machined samples were subjected to heat treatment at 1000ºC for 1 hour followed by air cooling to ensure an equiaxed microstructure and therefore reproducible mechanical properties. Fatigue testing was conducted at room temperature under the same test parameter using INSTRON1332 testing machine which was connected to INSTRON8500 programmable control unit with a frequency of 10 Hz. All tests were conducted at room temperature. After fatigue failure, discs were cut from regions immediately adjacent to the fracture surface and perpendicular to the loading axis using an electrical discharge machine (EDM). They were subsequently polished to high smoothness and etched using modified Kalling's II reagent.

Table 1: Chemical compositions of three Ni-based alloys (wt.%).

Alloy	Ni	Cr	Fe	Mo	C
Hastelloy C22	Bal.	21.42	2.95	13.67	0.003
Inconel 600	Bal.	15.77	8.58	-	0.05
Imconel 601	Bal.	22.14	16.09	-	0.3

III. RESULTS

The morphologies of the slip bands formed in the cyclically deformed specimens of the Hastelloy C22, Inconel 600 and Inconel 601 alloys are shown in "Fig. 1", "Fig. 2", and "Fig. 3", respectively. Slip bands was observed on the surfaces of all specimens tested, but the appearance of slip bands in the specimens of the three alloy specimens was different with respect to slip band density. The activation of multiple planar bands in Hastelloy C22 is shown in "Fig.1", where the slip bands formed in two directions within the grain. This suggests that cyclical deformation of Hastelloy C22 with straight grain boundary structure exhibited slip bands similar to those found in materials with low stacking fault energy. Two groups of parallel slip bands, with one group inclined at approximately 70° to the other, were found is the deformed alloy. This suggests that Hastelloy C22 experienced higher plastic deformation and longer fatigue life as compared to Inconel 600 and Inconel 601.

The morphology of slip bands formed in Inconel 600 and Inconel 601, as shown in "Fig. 2" and "Fig.3", is different from that of C22. The bands formed in these materials are in the form of triangular ribbons within the grain. The bands morphology may therefore be dependent on their carbon contents is responsible for the type of carbides morphology as shown on Table 1.

Although slip bands are generally straight and continuous, some interruptions, kinks and divergences in slip bands may be readily visible at high magnifications as shown in "Fig.1".

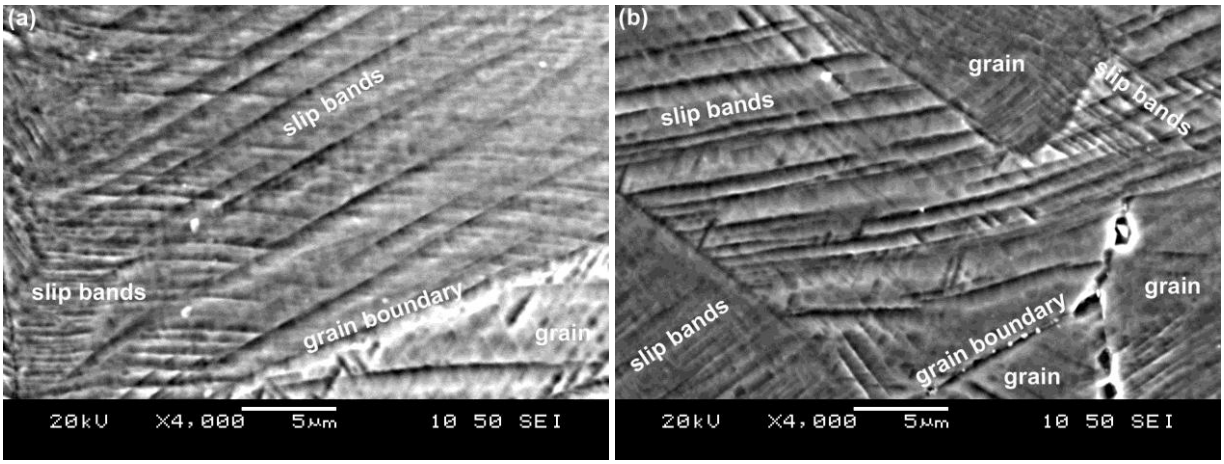

Figure 1: Scanning electron micrograps of Hastelloy C22 specimens showing planar bands fatigued at (a) 500 MPa and $7x10^6$ cycles, (b) 550MPa and $3x10^6$ cycles.

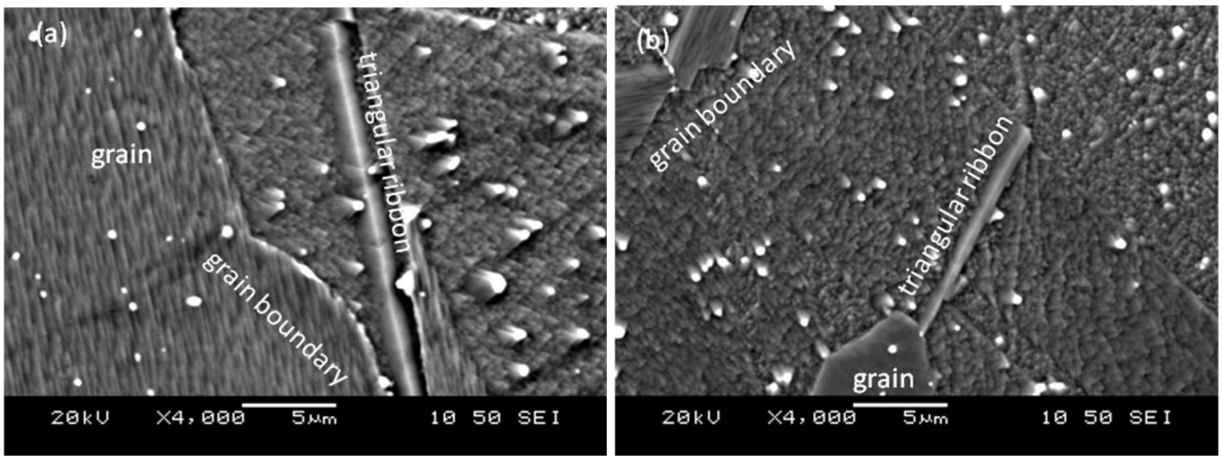

Figure 2: Scanning electron micrographs of Inconel 600 specimens showing short triangular ribbon-type slip bands fatigued at (a) 500MPa and $7x10^5$ cycles, (b) 550MPa and $3x10^5$cycles.

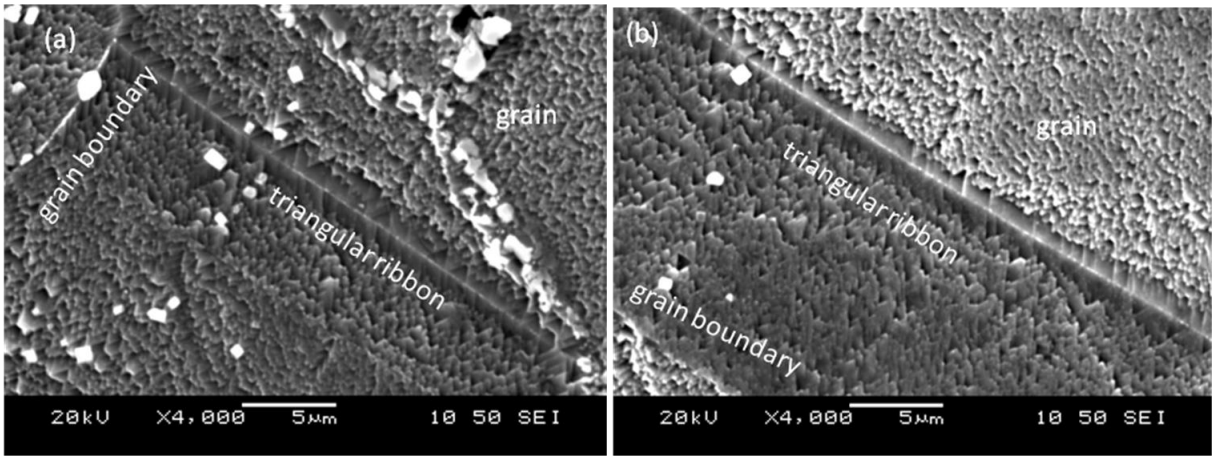

Figure 3: Scanning electron micrographs of Inconel 601 specimens showing long triangular ribbon bands fatigued at (a) 500MPa, and $430x10^3$ cycles, (b) 550MPa and $3x10^5$cycles.

IV. DISCUSSION

It is well accepted that slip bands produced by cyclic deformation can manifest as orientated distribution of defects such as dislocations. These defects would affect the deformation behavior of the grain structure greatly, causing deformation to take place readily along the slip planes. A strong evidence for the occurrence of slip nucleated in grain boundaries was shown in copper by Vinogradov [10]. Therefore, it is reasonable to suggest that the formation of slip bands in the three Ni-based alloys tested in the present study resulted from the grain boundary as shown in "Fig. 1", "Fig. 2", and "Fig. 3".
In the case of a complete stress-strain cycle slip bands may disappear totally leaving few slip bands in the specimen surface. However, some micro structural changes do take place internally owing to plastic incompatibility, especially at triple junctions and grain boundaries, resulting in the formation of void-type defects along the slip plane and grain boundary. With further cycling, the concentration of this type of defects would increase gradually. It is also likely that coalescence of defects and formation of voids would occur due to further plastic deformation. At the same time micro cracks would appear at the surface because fatigue damage usually occurs more easily on surfaces. Further cycling would not only promote void formation, but it will increase the level of plastic deformation; when the plastic deformation reaches a threshold value, the material cracks and eventually fractures. This would result in the formation of deformation steps during cyclic deformation resulting in a net displacement in the surface after cyclic deformation this was more pronounced in alloy C22 as shown in "Fig.1".

Accumulation of cyclic plastic deformation would eventually bring about the formation of slip bands as shown in "Fig.1", "Fig. 2" and "Fig. 3". It is shown clearly in the present paper that there is a direct connection between morphology of slip bands and morphology of grain boundary, which, dependent on the amount of carbides formed on grain boundary. It can be seen that the higher the carbon content of the alloy, the greater is the chance to nucleate triangular ribbon-type slip bands at the grain boundary. However, the slip bands morphology factors responsible for cyclic deformation are still open questions and need further investigations.

V. CONCLUSION

The current study briefly investigated the morphologies of slip bands in Hastelloy, and in Inconel alloys cyclically deformed. Results, revealed that planar type slip bands in Hastelloy C22, whereas triangular ribbon type slip bands in Inconel 600 and Inconel 601 alloys. The triangular ribbon bands were more distinct in Inconel 601 than in Inconel 600. The formation and morphology of the two types of slip bands may be attributed to the carbon content of the alloys.

REFERENCES

[1] P. Lukas, L. Kunz, and J. Krejci, Fatigue behaviour of single crystals of a Cu22%Zn alloy, Material Science Engineering A., A 158 (2), 1992, 177–183.
[2] Y. F,Li, and C. Laird, Cyclic response and dislocation structures of AISI 316L stainless steel, Materials Science and Engineering A, 186 (1-2), 1994, 87-103.
[3] L. Xiao, and Y. Umakoshi, Cyclic deformation behaviour and dislocation structure of Ti5 at. % Al single crystals oriented for double prism slip, Philosophical Magazine A,, 82, (12), 2002, 2379-2396.
[4] V. Gerold, H.P. Karnthaler, On the Origin of Planar Slip in FCC Alloys, Acta Metallurgica, 37 (8), 1989, 2177-2183.
[5] S. Heino, B. Karlsson, Cyclic deformation and fatigue behaviour of 7Mo–0.5N super austenitic stainless steel slip characteristics and development of dislocation structures, Acta Materialia, 49, (2), 2001, 353-363.
[6] H. F. Merrick, Effect of heat treatment on the structure and properties of extruded P/M alloy 718, Metallurgical and Materials Transactions A, 7, (4), 1976, 505-514.
[7] H. F. Merrick, The low cycle fatigue of three wrought nickel-base alloys, Metallurgical Transactions A, 5, (4), 1974, 891-897.
[8] M. Clavel, and A. Pineau, Frequency and wave-form effects on the fatigue crack growth behavior of alloy 718 at 298K and 823K, Metallurgical Transactions A, 9A, (4), 1978, 471-480.
[9] D. W. Worthem, and I. M. Robertson, I.M., F. A. Leckie, D. F. Socie, and C. J. Altstetter, Inhomogeneous deformation in INCONEL 718 during monotonic and cyclic loadings, Metallurgical transactions. A, 21 A, (12), 1990, 3215-3220.
[10] A. Vinogradov, S. Hashimoto, V. Patlan, and K. Kitagawa, Atomic force microscopic study on surface morphology of ultra-fine grained materials after tensile testing, ^{12}th International Conference on the Strength of Materials ICSMA-12, Materials Science and Engineering A, 319-321, 2001, 862-866.

International Journal of Modern Engineering Research (IJMER)
www.ijmer.com Vol.3, Issue.2, March-April. 2013 pp-1256-1262 ISSN: 2249-6645

Effective Positive Negative Association Rule Mining Using Improved Frequent Pattern

Ruchi Bhargava, [1] Prof. Shrikant Lade[2]
[1]*I. T. Dept. RKDF, Bhopal, INDIA*
[2]*Department of Information Technology, RGPV Bhopal*

Abstract: *Association Rule is an important tool for today data mining technique. But this work only concern with positive rule generation till now. This paper gives study for generating negative and positive rule generation as demand of modern data mining techniques requirements. Here also gives detail of "A method for generating all positive and negative Association Rules" (PNAR). PNAR help to generates all unseen comparative association rules which are useful for interesting pattern finding. This work focus on determine positive and negative rules, generation of candidate set is key issue in these techniques. This paper also discussed existing techniques, such as frequent pattern growth (FP-growth) method it's a most efficient and scalable approach for rules generation. This method can generate rules without candidate ser generation. This main problem in FP tree growth is large number of conditional FP tree. This algorithm able to generates all positive and negative association rule mining. We also proposed new positive and negative association rule mining algorithm using improved frequent pattern tree for better and efficient association rules.*

Keywords: *FP tree, association rules, Classification.*

I. INTRODUCTION

Data mining is the task to mining the useful meaningful information from data warehouse. It is the source of inexplicit, purely valid, and potentially useful and important knowledge from large volumes of natural data [7].

Data mining is the process of extracting implicit, previously unknown, and potentially useful information from large quantities of data. Through the accretion of current data with historical data, enterprises find themselves in possession of larger data sets in electronic form than at any time heretofore. Various techniques have been employed to convert the data into information, including clustering, classification, regression, association rule induction, sequencing discovery, and so forth. In general, an association rule represents a relationship between two sets of items in the same database. It can be written in the form $X \rightarrow Y$, where X and Y are item sets (i.e., values from stipulated domains) and $X \cap Y = \emptyset$. The left-hand side (LHS) of the rule is called the antecedent, while the right-hand side (RHS) is called the consequence.

The selected knowledge must be not only precise but also readable, comprehensible and ease of understanding. There are a many of data mining task such as ARs, sequential patterns, Classification, clustering, time series, etc., and there have been lots of techniques and algorithms for these tasks and different types of data in data mining. When the data consist continuous values, it becomes hard to mine the data and some special techniques need to be prepared. Association rule basically use for finding out the useful patterns, relation between items found in the database of transactions. For example, consider the sales database of a Music CD store, where the records represent customers and the attributes represent Music CD. The mined patterns are the set of Music CDs most frequently bought together by the customer. An example could be that, 70% of the people who buy old song cds also buy guzzle cds. The store can use this information for future sales, self restore of records etc. There are many application areas for association rule mining techniques, which include catalog design, store layout, customer segmentation, and telecommunication alarm diagnosis and so on.

1.1 Applications of Association Rule Mining In E-Commerce

In this section we survey the articles that implemented association rule mining in e-commerce.

1.1.1 Web Personalization

Personalization is the use of customer information for delivering a customized solution to that customer thus satisfying personal needs [8]. In the e-commerce environment the available choices for the visiting customers are more. The search cost and time increase due to this overload. Personalization can aid the customer in decision making process. Personalization can also communicate appropriate messages to the right customers on the basis of customer profiles. Typical stages in personalization are discussed by Murthi & sarkar [8]. Common way to incorporate personalization in firm's interaction with customers is through the use of recommender system.

1.1.2 Recommender systems

Customers like to have a recommender system by which customer can see the feedback from other users who already purchased the products. E-commerce makes use of recommender system to not only show feedback from other users but also suggest interesting and useful products to customers. Geyer et al [9] describes a recommender system that uses association rules derived from past purchases, for making recommendations to new anonymous customers. Diverse recommendation systems are proposed for different business which guides the customers to find products they would like to purchase. Most of them are based on either content filtering or collaborative filtering. Content based filtering (CBF)

approach recommends products to target customers according to the preferences of their neighbors. The collaborative filtering (CF) approach recommends products to object customers based on their past preferences. The draw backs in these traditional approaches are rectified and an personalized system was proposed by Yiyang zhang e al[10]. Zhang Xizheng[11] propose a personalized recommendation system using association rule mining and classification. Set of association rules are mined from customer requirements database using Apriori algorithm and then he apply CBA-CB algorithm to produce best rules out of whole set of rules.

1.1.3 Cross selling analysis

The association rule mining is a powerful tool to realize cross selling. Cross selling is a marketing strategy to sell a new product or service to the customer who already used the products of the same enterprise. To introduce a new product or service to a new customer and an old customer, the old customer is more likely to accept it and the success rate is higher. Cross selling is a marketing method which can improve customer value, for the more the relations between the enterprise and the customer, the more dependent the customer will be on the enterprise, and the higher the loyalty will be. Xiao-li Yin [12] discusses how the banks analyze the association relations between the deal activities and other properties like customer age, gender, education, occupation, etc, and can get the result which bank services or financial products the customer will be interested in.

1.1.4 Purchasing and traveling behavior of customers.

In e-commerce environment finding association rules between purchasing items is very important. There are many algorithms devised in this field. Path traversal pattern mining is the technique that finds most of the navigation behaviors of customers in the e-commerce environment. This information can be used to improve the website design and performance. Navigational suggestions can also be suggested to customers using this information. Many works are carried out in this field [13]. Yeu-shi-lee et al [14] propose an algorithm IPA that considers both purchasing behavior and travelling patterns of customer at the same time.

II. RELATED WORK

Paper [1] presents an efficient algorithm (PNAR) for mining both positive and negative association rules in databases. The algorithm extends traditional association rules to include negative association rules. When mining negative association rules, author use same minimum support threshold to mine frequent negative itemsets. With a Yule's Correlation Coefficient measure and pruning strategies, the algorithm can find all valid association rules quickly and overcome some limitations of the previous mining methods.

Traditional algorithms for mining association rules are built on the binary attributes databases, which has three limitations [2]. Firstly, it cannot concern quantitative attributes; secondly, only the positive association rules are discovered; thirdly, it treat each item with the same frequency although different item may have different frequency.

Mining the negative patterns has also attracted the attention of researchers in this area. The aim of paper [3] is to develop a new model for mining interesting negative and positive association rules out of a transactional data set. The proposed model in [3] is integration between two algorithms, the Positive Negative Association Rule (PNAR) algorithm and the Interesting Multiple Level Minimum Supports (IMLMS) algorithm, to propose a new approach (PNAR_IMLMS) for mining both negative and positive association rules from the interesting frequent and infrequent itemsets mined by the IMLMS model.

Against the above shortcomings, paper [4] proposes an FP-tree-based algorithm MMFI optimized with array and matrix for mining the maximal frequent itemsets. It not only reduces the quantity of the FP-trees constructed, but also saves the time in traversing the FP-trees. Paper [5] introduced the concept of weighted dual confidence, a new algorithm which can mine effective weighted rules is proposed in this paper, which is on the basis of the dual confidence association rules used in algorithm. The case studies show that the algorithm can reduce the large number of meaningless association rules and mine interesting negative association rules in real life.

In practical applications, the occurrence frequency of each itemset is different. Author set different minimum support for itemsets. In association rule mining, if the given minimum support is too high, then the items with low frequency of appearance couldn't be mined. Otherwise, if the given minimum support is too low, then combination explosion may occur. Authors support the technique that allows the users to specify multiple minimum supports to reflect the natures of the itemsets and their varied frequencies in the database. It is very effective for large databases touse algorithm of association rules based on multiple supports. The existing algorithms are mostly mining positive and negative association rules from frequent itemsets. But the negative association rules from infrequent itemsets are ignored. Furthermore, Authors set different weighted values for items according to the importance of each item. Based on the above three factors, an algorithm for mining weighted negative association rules from infrequent itemsets based on multiple supports(WNAIIMS) is proposed in paper [6].

III. PROBLEM STATEMENT

The search for exception rules will be based on the knowledge about strong association rules in the database. An example: we discover a strong association rule in the database, for instance shares of companies X and Y most times go up together X=>Y. Then those cases when shares of the companies X and Y do not go up together, X=>~Y or ~X=>Y, we call exceptions when satisfying the exceptionality measure explained in the next section. An algorithm for mining exception rules based on the knowledge about association rules will be proposed in the following sections.

We explain a few terms that will be used along the paper. Itemset is a set of database items. Association rule is an implication of the form X=>Y, where X and Y are database itemsets. The rule X => Y has support s, if s% of all transactions contain both X and Y. The rule X => Y has confidence c, if c% of transactions that contain X, also contain Y.

In association rules mining user-specified minimum confidence (minconf), minimum support (minsup) are given. Association rules with support>=minsup and confidence>=minconf are referred to as strong rules. Itemsets that have support at least equal to minsup are called frequent itemsets. Negative itemsets are itemsets that contain both items and their negations (for example XY~Z). ~Z means negation of the item Z (absence of the item Z in the database record).

Negative association rule is an implication of the form X=>~Y, ~X=>Y, ~X=>~Y, where X and Y are database items, ~X, ~Y are negations of database items. Examples of negative association rules could be Meat=>~Fish, which implies that when customers purchase meat at the supermarket they do not buy fish at the same time, or ~Sunny=>Windy, which means no sunshine implies wind, or ~Oil Stock=>~Petrol Stock, which says if the price the oil shares is falling, petrol shares price will be falling too.

IV. FP-TREE (FREQUENT PATTERN TREE)

FP-tree structure for the first time proposed for store information on frequent items, thus transforming the issue of mining frequent itemsets into that of mining FP-trees. In an FP-tree, every node is composed of three domains: an item name, designated as item name, a node count, designated as count, and a link, designated as node link; besides, in order to facilitate the traversing of the FP-trees, an item header table is created to make every time point to its presence in the tree through a node link, and the header table is made up of two domains: an item name, designated as item name, and a node link head, designated as head, and the head points to the first node in the FP-tree with the same name with it.

A tree structure in which all items are arranged in descending order of their frequency or support count. After constructing the tree, the frequent items can be mined using FP-growth.

4.1Creation of FP-Tree

4.1.1 First Iteration

Consider a transactional database which consists of set of transactions with their transaction id and list of items in the transaction. Then scan the entire database. Collect the count of the items present in the database. Then sort the items in decreasing order based on their frequencies (no. of occurrences).

4.1.2 Second Iteration

Now, once again scan the transactional database. The FP-tree is constructed as follows. Start with an empty root node. Add the transactions one after another as prefix subtrees of the root node. Repeat this process until all the transactions have been included in the FP-tree. Then construct a header table which consists of the items, counts and their head-of-node links. Consider the transactional database shown in Table 1 with 5 transactions.

TABLE I. EXAMPLE OF TRANSACTIONAL DATABASE

Tran. ID	Items
T1	A,B,D,E
T2	A,C,D
T3	E,F,H,I
T4	A,B
T5	C,E,F

The frequent itemlist for the above database is given in Table 2.

TABLE II. FREQUENT ITEM LIST FOR THE TRANSACTIONAL DATABASE IN TABLE1

Items	Count
A	3
B	2
C	2
D	2
E	3
F	2
H	1
I	1

The items that does not meet the minimum threshold has been eliminated. The frequent item list that support the minimum support threshold is given in Table 3.

TABLE III. FREQUENT ITEM LIST FOR THE TRANSACTIONAL DATABASE THAT SUPPORT MINIMUM THRESHOLD

Items	Count
A	3
E	3
B	2
C	2
D	2
F	2

The transactional database according to the frequent item list is given in Table 4.

TABLE IV. SORTED AND ELIMINATED TRANSACTIONS OF THE DATABASE IN TABLE 1

Tran. ID	Items
T1	A,E,B,D
T2	A,C,D
T3	E,F
T4	A,B
T5	E,C,F

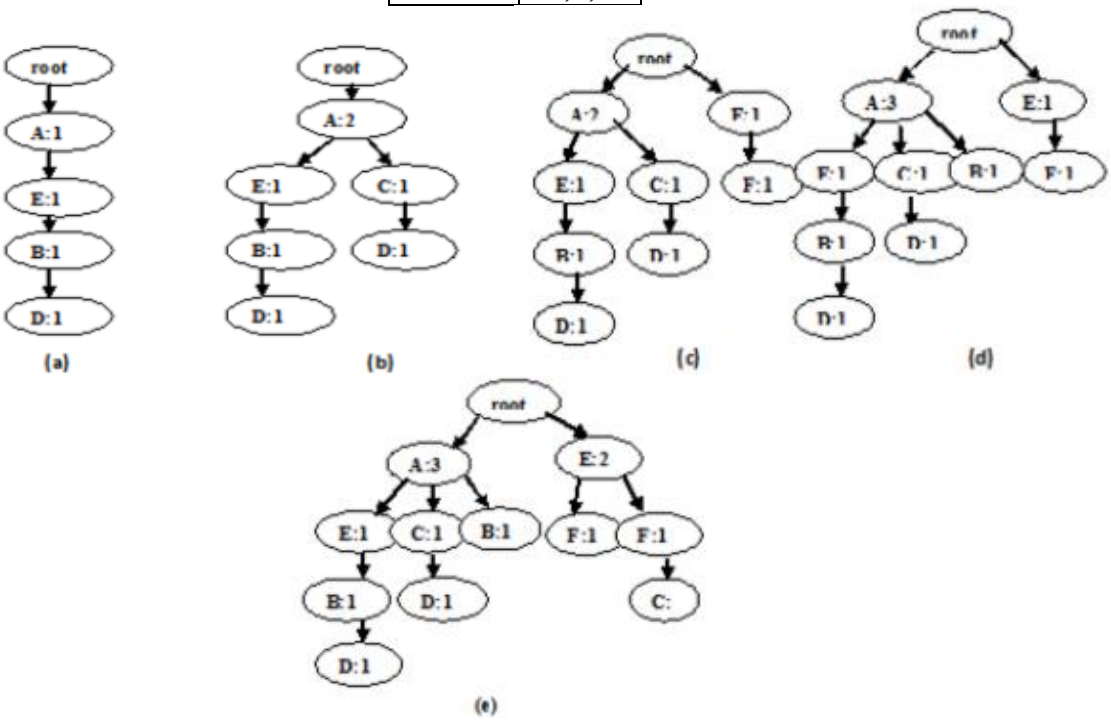

Fig. 1. Steps in Creating the FP-Tree.

4.2 Finding Frequent Patterns from FP-Tree

After the construction of FP-tree, the frequent patterns can be mined using a iterative approach FP-growth. This approach looks up the header table shown above and selects the item that supports the minimum support. It removes the infrequent items from the prefix-path of a existing node and the remaining items are considered as the frequent itemsets of the specified item.

Consider the item D. Its prefix paths are {((A, E, B): 1), ((A, C):1)}. After removing the infrequent items, (A: 2). so the frequent item set for D is A.

4.3 Advantages and Disadvantages

This method is advantageous because, it doesn't generate any candidate items. It is disadvantageous because, it suffers from the issues of spacial and temporal locality issues.

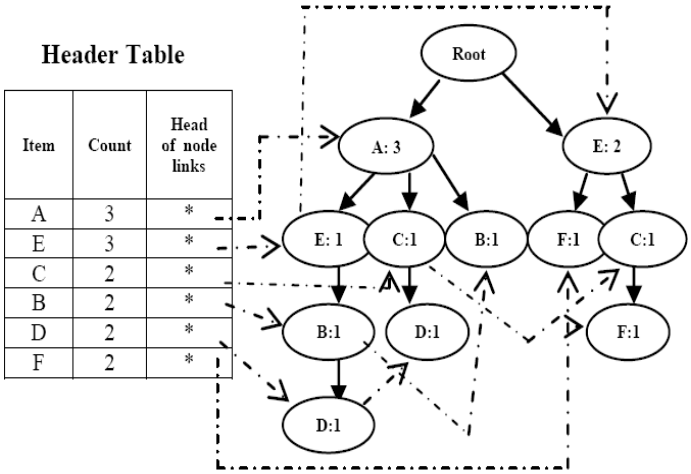

Fig. 2. FP-Tree with Header Table.

V. PROPOSED WORK

5.1 Positive and Negative Association rules

Corresponding to a positive association rule such as A=> B, there are three possible negative association rules, A=>~B, ~A=>B and ~A=>~B. For a negative association rule A=>~B and a certain transaction T, if A $\subseteq$ T and ~B $\not\subset$ T, we say that the transaction T supports A=>~B. Assume there is a negative association rule such as ({i1}, ~{ i2 , i3}), which means that if i1 is in a transaction T, i2 and i3 would not appeared in the transaction T at same time, but there is a possibility that one of the i2 and i3 is in transaction T. To discover negative association rule, we need to consider all of the possible itemsets in transaction databases. If A=>~B is a negative association rule, it will hold that sup (A∪~B)>= minsup. A higher value for minsup possibly means sup (A∪ B) <minsup, i.e., (A, B) is infrequent sequence. However, there are too many infrequent sequences in database. If A is a frequent item set while B is a infrequent itemset with support 1, we will have: sup (A)>=minsup, sup (B) =0, sup (A∪~B) = sup (A)>=minsup. Therefore, it seems that A=>~B is a negative association rule. In fact, this kind of sequences is rather prevalent in real database, for example, a set of the goods rarely bought by customers in supermarket is an infrequent itemset. In practice, since the task of data mining is to find all kinds of valuable correlations, we usually more focus on the correlations between the well-sold goods, which are based on the frequent sequence. In other word, if A->~B, ~A=>B and ~A=>~B are negative association rules, A and B would be frequent sequence. In generally speaking, we only focus on the frequent sequence whether the association rules are positive or negative.

In order to find valuable association rules, Piatetsky- Shapiro had put forward an interestingness measurement of association rules [15]. If sup (X∪Y) = sup (X) × sup(Y), X=>Y is considered as uninteresting rules. In other words, we can say that as the association rule X=>Y is interesting only if sup(X∪Y) = sup (X) × sup (Y) is no less than a specified minimum interesting value, mininterest. Similarly, we adopt the same method to measure the interesting of negative association rules.

Definition 1: an interesting negative association rule
A=>~B as:
(1) A ∩ B =ϕ;
(2) Sup (A)>=minsup, sup (B) >= minsup, sup(A∪~B) >= minsup;
(3) Sup (A∪~B) = sup (A) × sup (~B)>= mininterest.

Noted it need to satisfy condition sup (B)>=minsup since we are only interested in frequent itemset in association rules. By the same way we can define conditions of negative association rules forms as ~A=>B and ~A=>~B If A=>~B is a negative association rule, A∪B will be an interesting infrequent itemset. If i is an interesting infrequent itemset, there exists at least one expression, i=A∪B, which makes one of A=>~B, ~A=>B and ~A=>~B be interesting negative association rule hold.

5.2 PNAR Algorithm

As mentioned before, the process of mining both positive and negative association rules can be decomposed into the following three sub problems, in a similar way to mining positive rules only.

1) Generate the set PL of frequent itemsets and the set NL of infrequent itemsets.
2) Extract positive rules of the form A=>B in PL.
3) Extract negative rules of the forms A=>¬B and ¬A=>B in NL.

Noted it need to satisfy condition sup (B)>=minsup since we are only interested in frequent itemset in association rules. By the same way we can define conditions of negative association rules forms as ~A=>B and ~A=>~B If A=>~B is a negative association rule, A∪B will be an interesting infrequent itemset. If i is an interesting infrequent itemset, there exists at least one expression, i=A∪B, which makes one of A=>~B, ~A=>B and ~A=>~B be interesting negative association rule hold.

5.2.1 Algorithm for PNAR

As mentioned before, the process of mining both positive and negative association rules can be decomposed into the following three sub problems, in a similar way to mining positive rules only.

(1) Generate the set PL of frequent itemsets and the set NL of infrequent itemsets.
(2) Extract positive rules of the form A=>B in PL.
(3) Extract negative rules of the forms A=>¬B and ¬A=>B in NL.

Let DB be a database, and ms, mc, dms and dmc given by the user. Our algorithm for extracting both positive and negative association rules with a correlation coefficient measure and pruning strategies is designed as follows:

5.2.2 Algorithm: Positive and Negative Association Rules

Input: TDB-Transactional Database
MS-Minimum Support
MC-Minimum Confidence

Output: Positive and Negative Association Rules

Method:

```
1. P←ø, N←ø
2. Find F1← Set of frequent 1- itemsets
3. For (k=2; Fk-1! = ø; k++)
4. {
5.     Ck= Fk-1 join Fk-1
6.     // Prune using improve FP-Tree
7.     For each i ε Ck, any subset of i is not in
Fk-1 then Ck = CK - { i }
8.     For each i ε Ck find Support (i)
9.     For each A, B (A U B= i)
10.    {
11.       QA, B= Association (A, B);
12.       If Q>0
13.       If (supp (A→B)>=MS &&conf (A→B)>=MC) then
14.             P←P U {A→B}
15.       If Q<0
16.       {
17.             If (supp (A→¬B)>=MS&&conf (A→¬B)>=MC)
          Then
18.       N←N U {A→¬B}
19.       If (supp (¬A→B)>=MS&&conf (¬A→B)>=MC)
          Then
20.       N←N U {¬A→B}
21.       }
22.    }
23.}
24. AR← P U N
```

Pnar generates not only all positive association rules in PL, but also negative association rules in NL. When mining negative association rules, we use same threshold to improve the usability of the frequent negative itemsets. With a Yule's correlation coefficient measure and pruning strategies, the algorithm can find all valid association rules quickly. An example of mining positive and negative itemsets is given below for illustrative purposes.

VI. CONCLUSION

This paper gives overall review for association rules generation and positive negative rules finding from large data. A new algorithm is presented to generate all positive and negative class association rules using improved FP-tree and to build an accurate classification. The scheme has several features:

1. Its classification is performed based on positive and negative class association rules, which leads to better overall classification accuracy;
2. It prunes contradictory positive and negative class association rules effectively based on correlation between itemsets.
3. An improved FP tree applies for mining association rules. This algorithm mines all possible frequent item set without generating the conditional FP tree. It also provides the frequency of frequent items, which is used to estimate the desired association rules.

This proposed method expected that the algorithm would be highly effective at classification and has better average classification accuracy and efficiency. In future this algorithm is performed for various large dataset and measurements will be taken for proof effectiveness of proposed algorithm.

REFERENCES

[1] CH.Sandeep Kumar K.Srinivas Peddi Kishor T.Bhaskar, "An Alternative Approach to Mine Association Rules", Page 420-424, 2011 IEEE.

[2] Weimin Ouyang, "Mining Positive and Negative Fuzzy Association Rules with Multiple Minimum Supports", International Conference on Systems and Informatics (ICSAI 2012), 2012, IEEE.

[3] Idheba Mohamad Ali O. Swesi, Azuraliza Abu Bakar, Anis Suhailis Abdul Kadir, "Mining Positive and Negative Association Rules from Interesting Frequent and Infrequent Itemsets", 9th International Conference on Fuzzy Systems and Knowledge Discovery (FSKD 2012), 2012, IEEE.

[4] PENG Hui-ling, SHU Yun-xing, "A New FP-tree-based Algorithm MMFI for Mining the Maximal Frequent Itemsets", Page 61-64, 2012 IEEE.

[5] Yihua Zhong, Yuxin Liao, "Research of Mining Effective and Weighted Association Rules Based on Dual Confidence", Fourth International Conference on Computational and Information Sciences, 2012, IEEE.

[6] He Jiang, Xiumei Luan, Xiangjun Dong, "Mining Weighted Negative Association Rules from Infrequent Itemsets Based on Multiple Supports", International Conference on Industrial Control and Electronics Engineering, 2012, IEEE.

[7] Olafsson Sigurdur, Li Xiaonan, and Wu Shuning.Operations research and data mining, in: European Journal of Operational Research 187 (2008) pp: 1429–1448.

[8] Murthi B P S, Sarkar S 2003."The role of management sciences in research on personalilzation. Manage. Sci 49:1344-1362

[9] Liu Guo-rong, Zhang Xi-zheng, "Collaborative Filtering Based Recommendation system for Product bundling", Proceeding of ICMSE'06, Lille, France, pp.251-254, 2006.

[10] Zhan Xizheng "Building personalized recommendation system in E-commerce using Association rule-based mining and classification". Proceedings of 8th ACIS international conference on software engineering, Artificial intelligence, Networking and parallel/Distributed computing, 2007.

[11] Xiao-li Yin and Xu-sheng Fang," Data Mining Technology Application in Bank CRM", Economic Research Guide, 2009, pp. 112-113.

[12] M. S. Chen, J. S. Park and P. S. Yu. "Efficient Data Mining for Path Traversal Patterns in a Web Environment." IEEE Transaction on Knowledge and Data Engineering, Vol. 10, No. 2, pp. 209-221, 1998.

[13] S. J. Yen. "An Efficient Approach for Analyzing User Behaviors in a Web-Based Training Environment. "International Journal of Distance Education Technologies, Vol. 1, No. 4, pp.55-71, 2003.

[14] Hong Yu, Xiao lei Huang, Xiaorong Hu, Changxuan Wan, "Knowledge management in E-commerce: A data mining perspective", proceedings of international conference on Management of e-commerce and e-government, 2009.

[15] Liu, B., Hsu, W., and Ma, Y. Mining Association Rules with Multiple Minimum Supports. SIGKDD Explorations, 1999, pp.337-341.